

ENCYCLOPEDIA OF

---

# **POLYMER SCIENCE AND TECHNOLOGY**

**Fourth Edition**

**VOLUME 9**

---

COPYRIGHTED MATERIAL

## *EDITORIAL STAFF*

---

Executive Editor: **Arza Seidel**

Development Editor: **Mihai Peterca**

Production Manager: **Shirley Thomas**

Production Editor: **Kristen Parrish**



ENCYCLOPEDIA OF

---

**POLYMER SCIENCE  
AND TECHNOLOGY**

Fourth Edition

**VOLUME 9**

---

**WILEY**

Copyright © 2014 by John Wiley & Sons, Inc. All rights reserved.

Published by John Wiley & Sons, Inc., Hoboken, New Jersey.  
Published simultaneously in Canada.

No part of this publication may be reproduced, stored in a retrieval system, or transmitted in any form or by any means, electronic, mechanical, photocopying, recording, scanning, or otherwise, except as permitted under Section 107 or 108 of the 1976 United States Copyright Act, without either the prior written permission of the Publisher, or authorization through payment of the appropriate per-copy fee to the Copyright Clearance Center, Inc., 222 Rosewood Drive, Danvers, MA 01923, 978-750-8400, fax 978-646-8600, or on the web at [www.copyright.com](http://www.copyright.com). Requests to the Publisher for permission should be addressed to the Permissions Department, John Wiley & Sons, Inc., 111 River Street, Hoboken, NJ 07030, (201) 748-6011, fax (201) 748-6008.

**Limit of Liability/Disclaimer of Warranty:** While the publisher and author have used their best efforts in preparing this book, they make no representations or warranties with respect to the accuracy or completeness of the contents of this book and specifically disclaim any implied warranties of merchantability or fitness for a particular purpose. No warranty may be created or extended by sales representatives or written sales materials. The advice and strategies contained herein may not be suitable for your situation. You should consult with a professional where appropriate. Neither the publisher nor author shall be liable for any loss of profit or any other commercial damages, including but not limited to special, incidental, consequential, or other damages.

For general information on our other products and services please contact our Customer Care Department within the U.S. at 877-762-2974, outside the U.S. at 317-572-3993 or fax 317-572-4002.

Wiley also publishes its books in a variety of electronic formats. Some content that appears in print, however, may not be available in electronic format.

***Library of Congress Cataloging-in-Publication Data:***

Encyclopedia of polymer science and technology. – Fourth edition.

pages cm

An earlier edition was published under the title: Encyclopedia of polymer science and engineering.

Includes bibliographical references and index.

ISBN 978-1-118-63389-2 (volume 1: cloth)

1. Plastics–Encyclopedias.

2. Polymers–Encyclopedias.

3. Polymerization–Encyclopedias.

TP1110.E53 2014

668.903–dc23

2013037237

Printed in the United States of America.

10 9 8 7 6 5 4 3 2 1

# CONTENTS

---

NETWORKS, ELASTOMERIC, 1	
NEUTRON SCATTERING, 46	
NOMENCLATURE OF POLYMERS, 69	
NONDESTRUCTIVE TESTING, 101	
NONLINEAR OPTICAL PROPERTIES, 123	
NONWOVEN FABRICS, SPUNBONDED, 177	
NONWOVEN FABRICS, STAPLE FIBERS, 213	
NUCLEAR MAGNETIC RESONANCE, 237	
N-VINYLAMIDE POLYMERS, 315	
OLEFIN FIBERS, 345	
OPTICAL FIBERS, 367	
OPTICAL PROPERTIES, 386	
OXETANE POLYMERS, 413	
OXIDATIVE POLYMERIZATION, 432	
OXYGEN SCAVENGING SYSTEMS, 456	
PACKAGING MATERIAL, MOLECULAR WEIGHT, 466	
PACKAGING, FLEXIBLE, 469	
PELLETIZING, 479	
PERFLUORINATED POLYMERS, PERFLUORINATED ETHYLENE– PROPYLENE COPOLYMERS, 487	
PERFLUORINATED POLYMERS, POLYTETRAFLUOROETHYLENE, 502	
PERFLUORINATED POLYMERS, TETRAFLUOROETHYLENE–ETHYLENE COPOLYMERS, 526	
PERFLUORINATED POLYMERS, TETRAFLUOROETHYLENE– PERFLUORODIOXOLE COPOLYMERS, 542	
PERFLUORINATED POLYMERS, TETRAFLUOROETHYLENE– PERFLUOROVINYL ETHER COPOLYMERS, 547	
PHASE TRANSFORMATION, 560	
PHENOLIC RESINS, 578	
PHOSGENE, 623	
PHOSPHOLIPID POLYMERS, 635	
PHOSPHORUS-CONTAINING POLYMERS AND OLIGOMERS, 659	
PHOTOPOLYMERIZATION, CATIONIC, 695	
PHOTOPOLYMERIZATION, FREE RADICAL, 718	
PHOTOREFRACTION, 748	
PIEZOELECTRIC POLYMERS, 776	



# CONTRIBUTORS TO VOLUME 9

---

**James H. Andrews**, *Youngstown State University, Youngstown, Ohio*, Nonlinear Optical Properties; Photorefraction

**Kurt Binder**, *Institut für Physik, Johannes Gutenberg Universität, Mainz, Germany*, Phase Transformation

**B. Blümich**, *Institut für Technische Chemie und Makromolekulare Chemie, Rheinisch-Westfälische Technische Hochschule, Worringerweg, Aachen, Germany*, Nuclear Magnetic Resonance

**Paul D. Brothers**, *E. I. du Pont de Nemours & Co., Inc., Wilmington, Delaware*, Perfluorinated Polymers, Tetrafluoroethylene–Ethylene Copolymers; Perfluorinated Polymers, Tetrafluoroethylene–Perfluorodioxole Copolymers; Perfluorinated Polymers, Tetrafluoroethylene–Perfluorovinyl Ether Copolymers; Perfluorinated Polymers, Perfluorinated Ethylene–Propylene Copolymers; Perfluorinated Polymers, Polytetrafluoroethylene

**Andreas J. Brunner**, *Center for Nondestructive Testing, EMPA, Swiss Federal Laboratories for Materials Testing and Research, Dübendorf, Switzerland*, Nondestructive Testing

**Ying Cai**, *University of Iowa, Iowa City, Iowa*, Photopolymerization, Free Radical

**Roger Chapman**, *Texon UK Limited, Leicester, United Kingdom*, Nonwoven Fabrics, Staple Fibers

**Kay Cooksey**, *Clemson University Clemson, South Carolina, East Lansing, Michigan*, Oxygen Scavenging Systems

**Mark D. Dadmun**, *University of Tennessee, Knoxville, Tennessee*, Neutron Scattering

**D. E. Demco**, *Institut für Technische Chemie und Makromolekulare Chemie, Rheinisch-Westfälische Technische Hochschule, Worringerweg, Aachen, Germany*, Nuclear Magnetic Resonance

**M. P. Dreyfuss**, *Michigan Molecular Institute*, Oxetane Polymers

**P. Dreyfuss**, *Michigan Molecular Institute*, Oxetane Polymers

**Kenneth L. Dunlap**, *Bayer Corporation, New Martinsville, West Virginia*, Phosgene

**B. Erman**, *Department of Chemical and Biological Engineering, Koc University, Sariyer, Istanbul, Turkey*, Networks, Elastomeric

**Vassilios Galiatsatos**, *Equistar Chemicals, L.P., Cincinnati, Ohio*, Optical Properties

**Erik Grann Gammelgaard**, *FiberVisions, Varde, Denmark*, Olefin Fibers

**Subhash V. Gangal**, *E. I. du Pont de Nemours & Co., Inc., Wilmington, Delaware*, Perfluorinated Polymers, Tetrafluoroethylene–Ethylene Copolymers; Perfluorinated Polymers, Tetrafluoroethylene–Perfluorodioxole Copolymers; Perfluorinated Polymers, Tetrafluoroethylene–Perfluorovinyl Ether Copolymers; Perfluorinated Polymers, Perfluorinated Ethylene–Propylene Copolymers; Perfluorinated Polymers, Polytetrafluoroethylene

viii      **CONTRIBUTORS**

- Kimberly A. Guzan**, *Youngstown State University, Youngstown, Ohio*, Nonlinear Optical Properties
- Erwin Hack**, *Center for Nondestructive Testing, EMPA, Swiss Federal Laboratories for Materials Testing and Research, Dübendorf, Switzerland*, Nondestructive Testing
- J. S. Harrison**, *NASA Langley Research Center, Hampton, Virginia*, Piezoelectric Polymers
- Hideyuki Higashimura**, *Sumitomo Chemical Company Ltd., Tsukuba, Japan*, Oxidative Polymerization
- Kazuhiko Ishihara**, *The University of Tokyo, Tokyo, Japan*, Phospholipid Polymers
- Julie L. P. Jessop**, *University of Iowa, Iowa City, Iowa*, Photopolymerization, Free Radical
- Shiro Kobayashi**, *Kyoto University, Kyoto, Japan*, Oxidative Polymerization
- Kotaro Koike**, *Keio Photonics Research Institute, Keio University, Kawasaki, Japan; Polymer Research Institute, Polytechnic Institute of New York University, Brooklyn, New York*, Optical Fibers
- Yasuhiro Koike**, *Keio Photonics Research Institute, Keio University, Kawasaki, Japan*, Optical Fibers
- Peter W. Kopf**, *TIAX, LLC, Cambridge, Massachusetts*, Phenolic Resins
- Sergei V. Levchik**, *Israel Chemical Ltd. – Industrial Products, Tel Aviv, Israel*, Phosphorus-Containing Polymers and Oligomers
- Robert B. Login**, *Sybron Chemicals Inc.*, N-Vinylamide Polymers
- J. E. Mark**, *Department of Chemistry and the Polymer Research Center, University of Cincinnati, Cincinnati, Ohio*, Networks, Elastomeric
- Marcus Müller**, *Institut für Physik, Johannes Gutenberg Universität, Mainz, Germany*, Phase Transformation
- Jürg Neuenschwander**, *Center for Nondestructive Testing, EMPA, Swiss Federal Laboratories for Materials Testing and Research, Dübendorf, Switzerland*, Nondestructive Testing
- Z. Ounaies**, *Virginia Commonwealth University, Richmond, Virginia*, Piezoelectric Polymers
- J. L. Schultz**, *Wilmington, Delaware*, Nomenclature of Polymers
- Alec B. Scranton**, *University of Iowa, Iowa City, Iowa*, Photopolymerization, Cationic
- Vishal Sipani**, *University of Iowa, Iowa City, Iowa*, Photopolymerization, Cationic
- Ronald S. Smorada**, *Versacore Industrial Corporation, Kennett Square, Pennsylvania*, Nonwoven Fabrics, Spunbonded
- D. B. Todd**, *Baker Perkins, Inc.*, Pelletizing
- Edward D. Weil**, *Polytechnic Institute of NYU, Brooklyn, New York*, Phosphorus-Containing Polymers and Oligomers
- E. S. Wilks**, *Hockessin, Delaware*, Nomenclature of Polymers
- Jeffrey J. Wooster**, *The Dow Chemical Company, Freeport, Texas*, Packaging, Flexible
- Carl J. Wust**, *FiberVisions, Covington, Georgia*, Olefin Fibers

**Kit L. Yam**, *Rutgers University, New Brunswick, New Jersey*, Packaging Material,  
Molecular Weight

**Karen Zrebiec**, *Youngstown State University, Youngstown, Ohio*, Photorefrac-  
tion





## **NETWORKS, ELASTOMERIC**

### **Introduction**

The most striking features of a rubber-like material are its ability to undergo very large deformations with essentially complete recoverability. In order for a material to exhibit such unusual behavior, it must consist of relatively long polymeric chains that have a high degree of flexibility and mobility, and are joined into a network structure. The requirement of flexibility and mobility is associated with the very high deformability. As a result of an externally imposed stress, the long chains may alter their configurations which takes place relatively rapidly due to their high mobilities (1–13). The requirement of linking the chains into a network structure is associated with the solid-like features, where the chains are prevented from flowing relative to each other under external stresses. As a result, a typical rubber or elastomer may be stretched up to about 10 times of its original length. Upon removal of the external force, it rapidly recovers its original dimensions, with essentially no residual or nonrecoverable strain. As a result of these unique mechanical properties, elastomers find important usages ranging from automobile tires to heart valves, to gaskets in jet planes and space vehicles (14,15).

The above-mentioned general features of elastomeric materials have long been known and, in fact, the area of rubber-like elasticity has had one of the longest and most distinguished histories in all of polymer science (1,2,16). For example, quantitative measurements of the mechanical and thermodynamic properties of natural rubber and other elastomers go back to 1805, and some of the earliest studies have been carried out by such luminaries as Joule and Maxwell. Also, the earliest molecular theories for polymer properties of any kind were, in fact, addressed to the phenomenon of rubber-like elasticity.

### **Some Rubber-Like Materials**

The rubber-like materials described in this section are so designated since they exhibit the high deformability and recoverability so reminiscent of natural rubber

itself (2,17). They are thus frequently called “rubbers,” and the terms rubber-like materials, rubbers, and elastomers are used essentially interchangeably in the literature. Since high flexibility and mobility are required for rubber-like elasticity, elastomers generally do not contain stiffening groups such as ring structures and bulky side chains (2,13). These characteristics are evidenced by the low glass transition temperatures  $T_g$  exhibited by these materials. These polymers also tend to have low melting points, if any, but some do undergo crystallization upon sufficiently large deformations. Examples of typical elastomers, which do undergo strain-induced crystallization, include natural rubber, butyl rubber, and high *cis*-polybutadiene, with recent attention focusing on copolymers of high *trans*-polybutadiene (18). In contrast, poly(dimethylsiloxane) (PDMS)  $[-Si(CH_3)_2O-]$ , poly(ethyl acrylate), styrene-butadiene copolymer, and ethylene-propylene copolymer generally do not undergo strain-induced crystallization.

Some polymers are not elastomeric under normal conditions but can be made so by raising the temperature or adding a diluent (“plasticizer”). Polyethylene is in this category because of its high degree of crystallinity. Polystyrene, poly(vinyl chloride), and the biopolymer elastin are also of this type, but because of their relatively high glass transition temperatures also require plasticization to be elastomeric (13).

A final class of polymers is inherently nonelastomeric. Examples are polymeric sulfur, because of its chains are too unstable, poly(*p*-phenylene) because its chains are too rigid, and thermosetting resins because their chains are too short (13).

There is much current interest in hydrogels, particularly those robust enough to be used in biomedical applications.

## Preparation and Structure of Networks

Networks are formed by joining individual chains into a three-dimensional structure. The conventional method of network formation is by random cross-linking with a suitable cross-linking agent. More modern techniques involve end linking in order to obtain better controlled and characterized networks. Polymerization into a cross-linked system by adding a small amount of multifunctional reactants into the polymerizing system or by joining the chains by physical forces such as hydrogen bonding is also utilized.

**Random Chemical Cross-Linking.** In random cross-linking, chemical reactions are used that attack a pair of chains, at essentially random locations (1,13). Examples are the addition of sulfur atoms to the double bonds of diene elastomers and the attack of free radicals from peroxide thermolyses or high-energy radiation on side chains (frequently unsaturated) or on the chain backbone itself.

The cross-links formed in this way are generally highly stable. These networks, however, still present the problem that the cross-linking reaction used is highly uncontrolled in that it is not known how many cross-links are introduced or where they lie along the chain trajectories. It is thus very difficult to use these networks for quantitative purposes such as the development of structure-property relationships. Obtaining independent measures of their degree of cross-linking (as represented directly by the number density of cross-links or the

number density of network chains, or inversely by the average molecular weight  $M_c$  between the cross-links that mark off a network chain) is virtually impossible (13).

**Highly Specific Chemical End Linking.** If networks are formed by end-linking functionally terminated chains instead of haphazardly joining chain segments at random, then the nature of this very specific chemical reaction provides the desired structural information (6,13,19–28). Thus, the functionality of the cross-links is the same as that of the end linking agent, and the molecular weight  $M_c$  between cross-links and its distribution are the same as those of the starting chains prior to their being end linked.

Because of their known structures, such end-linked elastomers are now the preferred materials for the quantitative characterization of rubber-like elasticity. In addition, bimodal networks prepared by these end-linking techniques have very good ultimate properties, and there is currently much interest in preparing and characterizing such networks (13,22,25,29–33) and developing theoretical interpretations for their properties (34–37). Both subjects are discussed below.

**Polymerizations with Multifunctional Monomers.** Another way of making a network is by a copolymerization in which at least one of the comonomers has a functionality  $\phi$  of 3 or larger. This is one of the oldest ways of preparing networks but has been used mostly to prepare materials so heavily cross-linked as to be relatively hard thermosets rather than highly deformable elastomers (13,38). Some work in this area involves the use of sol fractions and statistical arguments to obtain information on the structures of the sol phases and gel (elastomeric) phases (39–43).

**Physical Aggregation.** Preparation of elastomeric networks is also possible by causing physical aggregation of some of the chain segments (3,13). Examples are the adsorption of chain segments onto filler particles, formation of polymer microcrystallites, condensation of ionic side chains onto metal ions, chelation of ligand side chains to metal ions, and microphase separation of glassy end blocks in an elastomeric triblock copolymer (44). These materials are now not much used in quantitative studies of rubber-like elasticity. The nature and extent of the cross-linking can change with the temperature, the presence of diluent, and degree of deformation in an uncontrolled manner, and the “cross-links” are frequently so large as to complicate greatly the theoretical analysis of any experimental results.

## Networks Prepared under Unusual Conditions

Several indirect approaches are undertaken in preparing networks of simpler topology with reduced degrees of network chain entangling (4). Some of the techniques employed involve (i) separating the chains prior to their cross-linking by either dissolution (45) or stretching (46), (ii) simultaneously forming two different but interpenetrating systems, (iii) trapping cyclics into the network, (iv) simultaneously cross-linking one component highly and the other lightly, and (v) using platelets as junctions.

**Cross-Linking in Solution.** This approach (5) did produce elastomers that had fewer entanglements, as indicated by the observation that such networks came to elastic equilibrium much more rapidly than elastomers

cross-linked in the dry state. When a network is cross-linked in solution and the solvent then removed, the chains collapse in such a way that there is reduced overlap in their configurational domains. It is primarily in this regard—namely, decreased chain-cross-link entangling—that solution cross-linked samples have simpler topologies.

These elastomers also exhibited stress-strain isotherms in elongation that were closer in form to those expected from the simplest molecular theories of rubber-like elasticity. Specifically, there were large decreases in the Mooney-Rivlin  $2C_2$  correction constant.

In these procedures, removal of the solvent has the additional effect of putting the chains into a “supercontracted” state (5). Experiments on strain-induced crystallization carried out on such solution cross-linked elastomers indicated that the decreased entangling was less important than the supercontraction of the chains, in that crystallization required larger values of the elongation than was the case for the usual elastomers cross-linked in the dry state (47). More recent work in this area has focused on the unusually high extensibilities of such elastomers (48).

One novel approach involves the use of collapsed cross-link regions that can unfold under stress, and then refold reversibly upon retraction of the elastomer (49). This is essentially biomimicry of some body tissues, such as the muscle protein titin, in which such behavior gives these biomaterials an impressive combination of deformability and strength.

**Cross-Linking in the Deformed State.** In this approach, a first network is generally introduced in the undeformed state, the resulting elastomer is elongated, and a second series of cross-links is introduced in the stretched state. Release of the stress permits the network to retract, but the second network of this “double-network” structure prevents retraction down to the original dimensions. The most interesting feature of the retracted network is the fact that it is anisotropic in structure and properties.

In some cases, double networks have shown increases in orientability and strain-induced crystallization (50) and improved fatigue resistance (51). In fact, some results show that there may be less of a compromise between failure properties in general and the modulus (52), which may be due in part to the decreased hysteresis observed for some of these elastomers. Theoretical treatment of such materials goes back to 1960 (53), and research has continued on them up to the present time (51,54–56). Better molecular understandings of these observations are being sought with, for example, extensive studies of residual strains and birefringence (55).

**Interpenetrating Networks.** If two types of chains have different end groups, then it is possible to end link them simultaneously into two networks that *interpenetrate* one another (57). Such a network could, for example, be made by reacting hydroxyl-terminated PDMS chains with tetraethoxysilane (in a condensation reaction), while reacting vinyl-terminated PDMS chains mixed into them with a multifunctional silane (in an addition reaction) (58). Interpenetrating networks can be very unusual with regard to both equilibrium and dynamic mechanical properties (59). For example, such materials can have considerable toughness and unusual damping characteristics.

**Slide Ring Gels.** Slide ring gels are topological networks with some similarities to linear rotaxane assemblies (60,61). In these gels, a number of cyclic

molecules are threaded onto a linear polymer chain and then trapped by placing bulky capping groups at the two ends of the chain. Some of the cyclics are then fused together to form mobile cross-links. In the case of two fused cyclics, the result is a figure-eight structure:  $\infty$  (62–66). These cross-links are called slide rings, and act like pulleys for the chains threading through them. The sliding is thought to thus equalize any network tensions, cooperatively. This gives the gels unusual mechanical properties, in particular very high deformabilities and degrees of swelling. There has been considerable interest in the theoretical treatment of such materials (67,68).

**Double Networks.** Double networks belong to a class of hydrogels that consist of two independently cross-linked networks, one consisting of a rigid polyelectrolyte and the other a flexible uncharged polymer. (69–73) The term “double networks” is an unfortunate choice of terminology since this name has long been applied to the completely different elastomeric materials described above as networks in which some of the cross-links are introduced in the deformed state.

Double networks are used as water-swollen gels and exhibit the best mechanical properties when the first network is highly cross-linked and the second only lightly cross-linked. The molar ratio of the second component to the first should be a factor as high as 10 or more, which makes them rather different from most interpenetrating networks (IPNs) (57). The enhanced mechanical properties of these double-network hydrogels are thought to be a result of the second network preventing cracks from growing to the point of producing catastrophic failure of the material. More specifically, this dissipation of crack energy may be facilitated by the second network appearing as clusters in voids occurring in what is apparently an inhomogeneous matrix of the first network. There is expected to be considerable entangling of the two types of chains in these domains. In some cases, a third component is used to form a triple network with, for example, uncross-linked polymer being added to reduce surface friction (74). Considerable modeling has been carried out to better understand the properties of these double network hydrogels (75–77).

**Nanocomposite Gels.** Nanocomposite gels use exfoliated platelets of clay as the cross-linking junctions (78–81). Ends of the polymer chains absorb strongly on the surfaces of the platelets and enough of the chains attach to *different* platelets to provide the bridges that constitute a network structure. The fact that the cross-links are planar sheets of considerable dimensions and junction functionality somehow yields unusual mechanical properties, including very good toughness.

## Network Structure

The elastic activity of a network depends directly on the molecular structure. Perfect networks with no dangling chains, which are connected to the network structure at one end only and no loops where the two ends of a chain terminate at the same junction, serve as suitable references. The structure of a perfect network may be defined by two variables, the cycle rank  $\xi$  and the average junction functionality  $\phi$  (3,13). Cycle rank is defined as the number of network chains that must be cut in order to reduce it to a tree (82), which is a giant molecule

containing no closed structures or cycles. The number of junctions  $\mu$ , the number of chains  $\nu$ , and the molecular weight  $M_c$ , of chains between two junctions, may be obtained from  $\xi$  and  $\phi$  by the following three relations (6):

$$\nu = \xi / (1 - 2/\phi) \quad (1)$$

$$\mu = 2\nu / \phi \quad (2)$$

$$M_c = \frac{(1 - 2/\phi)\rho N_A}{\xi N_0} \quad (3)$$

where  $\rho$  is the density,  $V_0$  is the reference volume of the network, and  $N_A$  is Avogadro's number. The number of junctions,  $\mu$ , and the number of chains,  $\nu$ , are typically given as number *densities*, by dividing them by the volume of the unswollen network. They are the standard two direct measures of the degree of cross-linking. The molecular weight  $M_c$ , of the network chains between two cross-links, is an inverse measure, and typically has a value ranging from 5,000 to 15,000 g/mol. This corresponds to using approximately one of a hundred repeat units for a cross-link (13).

## Effects of Network Structure on Elastomeric Properties

**Effects of Chain Length.** The length of a network chain between two cross-links decreases with increasing number of cross-links as can be seen from equations (1) and (3). As will be elaborated further in the following sections, the modulus of a network varies inversely with chain length (5,13).

**Effects of Chain Length Distribution.** Elastomeric networks are generally prepared in an uncontrolled manner such as peroxide curing (1,2). In such cross-linking, segments close together in space are linked irrespective of their locations along the chain trajectories. This results in a highly random network structure in which the distribution of chain lengths between cross-links is essentially unknown. New synthetic techniques are now available, however, for the preparation of "model" polymer networks of known structure. More specifically, if networks are formed by end-linking functionally terminated chains of known length distribution instead of haphazardly joining chain segments at random, then the nature of this very specific chemical reaction provides the desired structural information (5,13,26,83). Thus, characterizing the uncross-linked chains with respect to molecular weight  $M_n$  and molecular weight distribution, and then carrying out the specified reaction to completion gives elastomers in which the network chains have these characteristics, in particular a molecular weight  $M_c$  between cross-links equal to  $M_n$ , a network chain-length distribution the same as that of the starting chains, and cross-links having the functionality of the end-linking agent. A widely investigated system is end-linked PDMS using tetraethyl orthosilicate. The reaction is shown in Figure 1 (83–85). One reason for this choice is the fact that the polymer is readily available with either hydroxyl or vinyl end groups, and the reactions these groups participate in are relatively free of complicating side reactions. In the application of interest here, a mixture of two

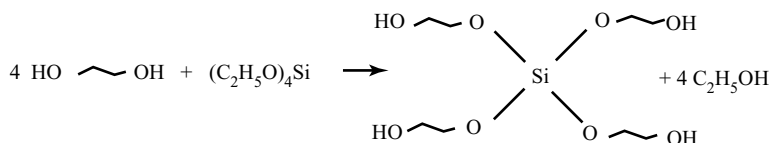


**Fig. 1.** End linking by a condensation reaction between hydroxyl groups at the ends of a polymer chain and the alkoxy groups on a tetrafunctional end-linking agent.

hydroxyl-terminated polymers is being cross-linked, one consisting of very short chains and the other, of much longer chains. An alternative approach involves the addition reaction between vinyl groups at the ends of a polymer chain and the active hydrogen atoms on silicon atoms in the  $[-\text{Si}(\text{CH}_3)\text{HO}-]$  repeat units in an oligomeric poly(methyl hydrogen siloxane). These ideas can obviously be extended to higher modalities (trimodal, etc).

The most novel elastomer of known structure has a *multimodal* distribution of network chain lengths. In the *bimodal* case, it consists of a combination of unusually short network chains (molecular weights of a few hundred) and the much longer chains typically associated with elastomeric behavior (molecular weights of ten or twenty thousand). One use of elastomers having such a bimodal distribution is possibly to improve the ultimate properties of an elastomer.

“Bimodal” elastomers prepared by these end-linking techniques have very good ultimate properties (5,13,83,84,86). In addition to this experimental work, there are now theoretical studies addressing the novel mechanical properties of bimodal elastomers (13).

The distribution of network chain lengths in a bimodal elastomer can be extremely unusual, in that there is simultaneously a large *number* fraction of short chains and a large *weight* fraction of long chains.

Although there have been attempts to evaluate the mechanical properties of trimodal elastomers, this has not been done in any organized manner. The basic problem is the large number of variables involved, specifically three molecular weights and two independent composition variables (mol fractions); this makes it practically impossible to do an exhaustive series of relevant experiments. For this reason, mechanical property experiments that have been carried out have generally involved arbitrarily chosen molecular weights and compositions (87, 88). Not surprisingly, only modest improvements have been obtained over the bimodal materials in these cases.

Some recent computational studies (36,89) suggest that a trimodal network prepared by incorporating small numbers of very long chains into a bimodal network of long and short chains could have significantly improved ultimate properties.

**Effects of Junction Functionality.** End linking of chains with linkers of a known functionality is used to control the structure in this way. Increasing the junction functionality decreases the fluctuation amplitudes of the junctions in the undeformed state. A network with suppressed junctions behaves close to an affine network under deformation. However, the affinity diminishes under increasing extension. Trifunctional and tetrafunctional PDMS networks prepared in this way have been used to test the molecular theories of rubber

elasticity with regard to the increase in nonaffineness of the network deformation with increasing elongation (90). The ratio  $2C_2/2C_1$  (which is a measure of the increasing nonaffineness as the elongation increases) decreases with the increase in cross-link functionality (91). This is due to the fact that cross-links connecting four chains are more constrained than those connecting only three. There is therefore less of a decrease in modulus brought about by the fluctuations which are enhanced at high deformation and give the deformation its nonaffine character. The decrease in  $2C_2/2C_1$  with the decrease in network chain molecular weight is due to the fact that there is less configurational interpenetration in the case of short network chains. This decreases the firmness with which the cross-links are embedded and thus the deformation is already highly nonaffine even at relatively small deformations.

**Effects of Entanglements.** An increase in the functionality of junctions suppresses their fluctuations and therefore fluctuations in chain dimensions are decreased. Also, the entanglements along the chains that come from the neighboring chains may further act as if they were additional (albeit temporary) junctions. Consequently, the modulus of such networks may exceed that of an affine network.

The idea of entanglement effects on network modulus originates from the trapped-entanglement concept of Langley (92), and Graessley (93,94) stating that some fraction of the entanglements, which are present in the bulk polymer before cross-linking, become permanently trapped by the cross-linking process and acts as additional cross-links. These trapped entanglements, unlike the chemical cross-links, have some freedom, and the two chains forming the entanglement may slide relative to one other. The two chains may therefore be regarded to be attached to each other by means of a fictitious "slip-link." An excellent review article on this topic is by Heinrich and co-workers (95).

Model networks may also be used to provide a direct test of molecular predictions of the modulus of a network of known degree of cross-linking. Some experiments on model networks (5,96,97) have given values of the elastic modulus in good agreement with theory. Others (20,98,99) have given values significantly larger than predicted (5,13), and the increases in modulus have been attributed to contributions from "permanent" chain entanglements. There are disagreements, and the issue has not yet been resolved. Since the relationship of modulus to structure is of such fundamental importance, there has been a great deal of research activity in this area.

**Effect of Dangling Chains.** Since dangling chains represent imperfections in a network structure, their presence should have a detrimental effect on ultimate properties such as the tensile strength, as gauged by the stress at rupture. This expectation was confirmed by an extensive series of results obtained on PDMS networks which had been tetrafunctionally cross-linked using a variety of techniques.

Additional, more quantitative information has been obtained using the very specific chemical reactions used to form ideal elastomers, but now modified to prepare intentionally nonideal networks containing known numbers and lengths of dangling chain irregularities (100). If more chain ends are present than reactive groups on the end-linking molecules, then dangling ends will be produced and their number is directly determined by the extent of the stoichiometric



imbalance. Their lengths, however, are of necessity the same as those of the elastically effective chains. This constraint can be removed by separately preparing monofunctionally terminated chains of any desired lengths and then attaching them as parts of the network.

Values of the ultimate strength of the networks containing the dangling ends were found to be lower than those of the more nearly perfect networks, with the largest differences occurring at high proportions of dangling ends (low  $2C_1$ ), as expected (101). The values of the maximum extensibility showed a similar dependence, as expected.

**Effect of Trapped Cyclics in Networks.** If cyclic molecules are present during the end linking of chains, some of them will be trapped because of having been threaded by the linear chains prior to the latter being chemically bonded into the network structure (5,102). The fraction trapped is readily estimated from solvent extraction studies. Some typical results, in terms of the fraction trapped as a function of degree of polymerization of the cyclic (103), showed that, as expected, very small cyclics do not get trapped at all, but almost all of the largest cyclics do.

These cyclics can change the properties of the network in which they are "incarcerated." For example, when PDMS cyclics are trapped in a thermoplastic material, they can act as a plasticizer that is in a sense intermediate to the usual external (dissolved) and internal (copolymerized) varieties. Interesting changes in mechanical properties have been observed in materials of this type (104).

It may also be possible to use this technique to prepare networks having no cross-links whatsoever (105). Mixing linear chains with large amounts of cyclic are then difunctionally end linking them could give sufficient cyclic interlinking to yield an "olympic" or "chain-mail" network (106,107). Computer simulations (108) could be particularly useful with regard to establishing the conditions most likely to produce such novel structures.

## Effects of Structure on Ultimate Properties

Of particular interest here are the upturns in the elastic modulus frequently exhibited by unfilled elastomers at very high elongations (13,109,110), and the commercially important increases in ultimate strength associated with them. This increase is important since it corresponds to a significant toughening of the elastomer. Its molecular origin, however, had been the source of some controversy. It had been widely attributed to the "limited extensibility" of the network chains. However, the increases in modulus had generally been observed only in networks that could undergo strain-induced crystallization, which could account for the increase in modulus, primarily because the crystallites thus formed would act as additional cross-links in the network.

This type of reinforcement resulting from strain-induced crystallization was identified by the fact that the higher the temperature, the lower the extent of crystallization and the worse the ultimate properties. The effects of the increase in swelling were found to parallel those for increase in temperature, as was expected, since diluent also suppresses network crystallization (111). On the other

hand, in those cases where the upturns are due to limited chain extensibility, the increase in temperature has relatively little effect on the upturns (5).

Attempts to observe upturns from non-Gaussian effects in noncrystallizable networks were observed by the use of some of end-linked, noncrystallizable model PDMS networks described above. These networks have high extensibilities, presumably because of their very low incidence of dangling chain network irregularities. They have particularly high extensibilities when they are prepared from a mixture of very short chains (around a few hundred  $\text{g mol}^{-1}$ ) with relatively long chains (around 18,000  $\text{g mol}^{-1}$ ), giving the already mentioned bimodal distributions of network chain lengths (22). Apparently, the very short chains in such networks are important because of their limited extensibilities, and the relatively long chains because of their ability to retard the rupture process. Stress-strain measurements on such bimodal PDMS networks exhibited upturns in modulus that were much less pronounced than those in crystallizable polymer networks. Furthermore, they are independent of temperature and are not diminished by incorporation of solvent. These characteristics are what is to be expected in the case of limited chain extensibility (13,112). Thus these results permit interpretation of properties such as the elongation at the upturn in the modulus and the elongation at rupture ("maximum extensibility").

In the case of elastomers capable of undergoing strain-induced crystallization, such as *cis*-1,4-polybutadiene networks (113), the higher the temperature, the lower the extent of crystallization and, correspondingly, the lower the ultimate properties. The effects of the increase in swelling parallel those for the increase in temperature, since diluent also suppresses network crystallization. For noncrystallizable networks, however, neither change is very important (114).

The weakest link theory (115) states that the shortest chains in a network are primarily responsible to elastomer rupture, and this idea was tested by preparing end-linked networks containing increasing amounts of short chains (13,116). Remarkably, these elastomers showed no significant decreases in ultimate properties with these increases in the numbers of short chains, in striking disagreement with the suggested mode of elastomer failure. Networks are apparently much more resourceful than given credit for in this theory. Apparently, the strain is continually being reapportioned during the deformation, in such a way that the much more easily deformed long chains bear most of the burden of the deformation. The flaw in the weakest link theory is thus the implicit assumption that all parts of the network deform in exactly the same way, that is, "affinely," whereas the deformation is actually markedly nonaffine (5,13).

The weakest link issue having been resolved, it became of interest to see what would happen in the case of bimodal networks having such overwhelming numbers of short chains that they could not be ignored in the network's response. As described below, there is a synergistic effect leading to mechanical properties that are better than those obtainable from the usual unimodal distributions!

Such bimodal distributions of network chain lengths have been shown to give significant improvements in mechanical properties. This is illustrated in Figure 2 (117), in which data on PDMS networks are plotted in such a way that the area under a stress-strain isotherm corresponds to the energy required to rupture the network. If the network is all short chains, it is brittle, which means that the maximum extensibility is very small. If the network is all long chains,

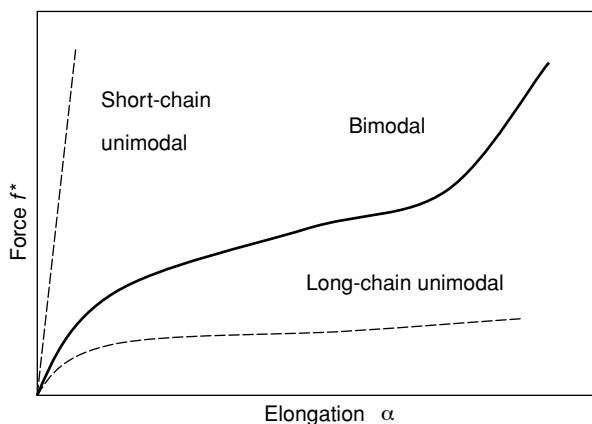


**Fig. 2.** Typical dependence of nominal stress against elongation for two unimodal networks having either all short chains or all long chains, and a bimodal network having some of both.

the ultimate strength is very low. In neither case is the material a tough elastomer. As can readily be seen from the figure, the bimodal networks are much improved elastomers in that they can have a high ultimate strength without the usual decrease in maximum extensibility. Apparently, the observed increases in modulus are due to the limited chain extensibility of the short chains, with the long chains serving to retard the rupture process.

## Elasticity Experiments

**Mechanical Properties.** Mechanical properties determine the unique usefulness of elastomeric materials and have been studied extensively (1,2,5,118–123). The relationship of primary interest is the stress–strain isotherm. Most experimental work is performed under simple elongation, largely because of the simplicity of the techniques involved. Measurements to determine the stress–strain isotherm under simple tension are typically carried out to the rupture point of a sample, thus yielding as well the two ultimate properties of the elastomer, namely its ultimate strength and maximum extensibility. In addition to providing practical information, such results are also much used to obtain estimates of the degree of cross-linking, and to test and compare the predictions of the various molecular theories. Results obtained with other deformations (2,6,124–134), such as biaxial extension, compression, shear, and torsion are, however, particularly valuable for gauging the generality of a particular theory.

**Elongation Results.** Experimental results for elongation of unswollen and swollen networks are represented in a manner consistent with the Mooney-Rivlin equation (2,135–140)

$$[f^*] = 2C_1 + 2C_2\alpha^{-1} \quad (4)$$

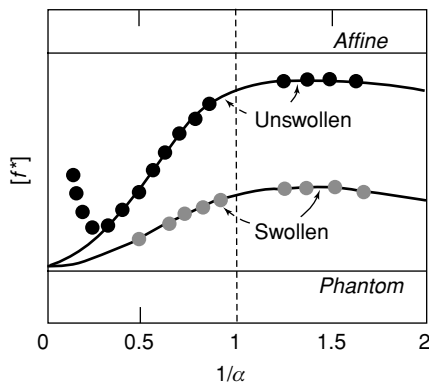


**Fig. 3.** Reduced stress as a function of reciprocal extension ratio. The upper and lower horizontal lines represent results from affine and phantom network models, respectively. Circles show representative data from experiments, and the curves are from the constrained junction theory.

where  $2C_1$  and  $2C_2$  are constants independent of elongation  $\alpha$ . A typical Mooney–Rivlin plot is presented in Figure 3. Typically, the reduced force in simple tension exhibits a drop represented by the nonzero slope  $2C_2$ . At high elongations, experimental data show an upturn, thus deviating significantly from the Mooney–Rivlin plot. Also, compression data depart significantly from the simple Mooney–Rivlin plot (5,13).

**Results in Other Mechanical Deformations.** There are numerous other deformations of interest, including compression, biaxial extension, shear, and torsion (2,141).

The equation of state for compression ( $\alpha < 1$ ) is the same as that for elongation ( $\alpha > 1$ ), and the equations for the other deformations may all be derived by proper specifications of the deformation ratios (1,2). Some of these deformations are considerably more difficult to study than simple elongation and, unfortunately, have therefore not been as extensively investigated.

Some measurements in biaxial extension have involved the direct stretching of a sample sheet in two perpendicular directions within its plane, by two independently variable amounts. In the equibiaxial case, the deformation is equivalent to compression. A good account of such experimental results (142) has been given by the simple molecular theory, with improvements at lower extensions upon use of the constrained-junction theory (5,13).

Biaxial extension studies can also be carried out by the inflation of sheets of the elastomer (2). Such results on unimodal and bimodal networks of PDMS (129) show upturns in the modulus at high biaxial extensions, as expected. Also of interest, however, are the pronounced maxima preceding the upturns. This represents a challenging feature to be explained by molecular theories addressed to bimodal elastomeric networks in general. Equibiaxial extension results have also been obtained on unimodal and bimodal networks of PDMS (132). Upturns in the modulus were found to occur at high biaxial extensions, as expected.

In shear measurements on some unimodal and bimodal networks of PDMS (143), the bimodal PDMS networks showed large upturns in the pure-shear

modulus at high strains, which were similar to those reported for elongation and biaxial extension. Very little work has been done on elastomers in torsion (twisting a cylindrical sample around its long axis). The same types of bimodal PDMS networks showed rather different behavior in torsion (134). Specifically, no unambiguous upturns in modulus were observed at large deformations. It has not yet been established whether this is due to the inability, to date, of reaching sufficiently large torsions, or whether this is some inherent difference in this type of deformation. There are also some torsion results on stress-strain behavior and network thermoelasticity (2).

Tear tests have been carried out on bimodal PDMS elastomers (144–147), using the standard “trouser-leg” method. Tear energies were found to be considerably increased by the use of a bimodal distribution, with documentation of the effects of compositional changes and changes in the ratio of molecular weights of the short and long chains. The increase in tear energy did not seem to depend on tear rate (144), an important observation that seems to suggest that viscoelastic effects are not of paramount importance in explaining the observed improvements.

Some Rheovibron viscoelasticity results have been reported for bimodal PDMS networks (148). To provide guidance for the desired interpretations, measurements were first carried out on unimodal networks consisting of the types of chains used in combination in the bimodal networks. One of the important results was documentation of the dependence of crystallinity on the network chain-length distribution.

Some measurements have been made on permanent set for PDMS networks in compressive cyclic deformations (149). There appeared to be less permanent set or creep in the case of the bimodal elastomers. This is consistent in a general way with some early results for polyurethane elastomers (150). Specifically, cyclic elongation measurements on unimodal and bimodal networks indicated that the bimodal ones survived many more cycles before the occurrence of failure from fatigue. The number of cycles to failure is approximately an order of magnitude higher for the bimodal network, at the same value of the modulus (5)!

In addition to mechanical properties, some important nonmechanical properties are mentioned in the following sections.

**Swelling.** In a swelling experiment, the network is typically placed into an excess of solvent, which it imbibes until the dilational stretching of the chains prevents further absorption (1–3,5,13,151). This equilibrium extent of swelling can be interpreted to yield the degree of cross-linking of the network, provided the polymer-solvent interaction parameter  $\chi$  (1) is known. Conversely, if the degree of cross-linking is known from an independent experiment, then the interaction parameter can be determined. Most studies of networks in swelling equilibrium give values for the cross-link density or related quantities that are in satisfactory agreement with those obtained from mechanical property measurements (1,2). More specifically, estimates in cross-link densities agree within the limits of the accuracy of the swelling measurements and the accompanying theory, and in particular within the uncertainties occasioned by unanticipated changes in the modulus with deformation (5,13).

A more interesting area involving some swollen networks or “gels” is their abrupt collapse (decrease in volume) upon relatively minor changes in

temperature, pH, solvent composition, etc (5,118,152,153). Although the collapse is quite slow in large, monolithic pieces of gel, it is rapid enough in fibers and films to make the phenomenon interesting with regard to the construction of switches and related devices.

**Sorption and Extraction of Diluents.** In these experiments, the rate at which a suitable diluent is absorbed into a network of known and controlled “pore size” and the rate at which it can subsequently be extracted are determined (151,154). Of obvious interest is the dependence of the extraction efficiency on the molecular weight  $M_c$  of the network chains (as a measure of pore size), the molecular weight  $M_d$  of the diluent, the structure of the diluent (linear, branched, or cyclic), and whether or not the diluent had been present during the end-linking process.

One way of obtaining a network swollen with diluent is to form the network in a first step, and then absorb an unreactive diluent into it. Alternatively, the same diluent can be mixed into the reactive chains prior to their being end linked into a network structure. In either case, oligomeric and polymeric diluents are of greatest interest, and they must be functionally inactive for them to “reptate” through the network rather than being bonded to it. Both types of networks can then be extracted to determine the ease with which the various diluents can be removed, as a function of  $M_d$  and  $M_c$ .

The efficiency of diluent removal was found to decrease with the increase in  $M_d$  and with the decrease in  $M_c$ , as expected. High molecular weight diluents are extremely hard to remove at values of  $M_c$  of interest in the preparation of model networks, a circumstance complicating the analysis of soluble polymer fractions in terms of degrees of perfection of the network structure. The diluents added after the end linking were the more easily removed, possibly because they were less entangled with the network structure, and this could correspond to differences in chain conformations of the diluent.

There is a complication, however, which can occur in the case of networks of polar polymers at relatively high degrees of swelling (13,112). The observation is that different solvents, at the same degree of swelling, can have significantly different effects on the elastic force. This is apparently due to a “specific solvent effect” on the unperturbed dimensions, which appear in the various molecular forms on the elastic equations of state. The effect is not yet well understood. It is apparently partly due to the effect of the solvent’s dielectric constant on the Coulombic interactions between parts of a chain, but probably also to solvent-polymer segment interactions that change the conformational preferences of the chain backbone (155).

**Optical and Spectroscopic Properties.** An example of a relevant optical property is the birefringence of a deformed polymer network (2,6,156–159). This strain-induced birefringence can be used to characterize chain segmental orientation, both Gaussian and non-Gaussian elasticity, crystallization and other types of chain ordering, and short-range correlations (2,3,13). Birefringence measurements have been shown to be very sensitive to bimodality, and have therefore also been used to characterize non-Gaussian effects resulting from it in PDMS bimodal elastomers (5,159,160). Relevant here is the effect of strain on the stress-optical coefficient (defined as the ratio of the birefringence to the stress) (157). There was found to be a large decrease in this coefficient over a relatively small

range in elongation, presumably from the limited extensibility of the short chains in the bimodal structure. It is therefore a sensitive way of characterizing non-Gaussian effects in network deformations. Other optical and spectroscopic techniques are also important, particularly with regard to segmental orientation. Some examples are fluorescence polarization (161,162), deuterium NMR (163–165), and polarized and two-dimensional infrared spectroscopy (166–168).

**Scattering.** The technique of this type of greatest utility in the study of elastomers is small-angle neutron scattering; for example, from deuterated chains in a nondeuterated host (169–171). One application has been the determination of the degree of randomness of the chain configurations in the undeformed state, an issue of great importance with regard to the basic postulates of elasticity theory. More specifically, such measurements have supported the major assumption that the network chains display their dimensions as “unperturbed” (1), by excluded-volume effects. Of even greater importance is determination of the manner in which the dimensions of the chains follow the macroscopic dimensions of the sample. Experiments to date indicate the dimensions do not simply parallel the changes in the macroscopic dimensions of the samples, as is assumed in the “affine” theory (13), of rubber-like elasticity described below. This relationship between the microscopic and macroscopic worlds is one of the central problems in rubber-like elasticity, and more experimental results clarifying it will surely be forthcoming.

Some small-angle X-ray scattering techniques have also been applied to elastomers, an example being the characterization of fillers incorporated into elastomers to improve their mechanical properties (172,173).

## Elasticity Theories

In this section, the expressions for the elastic free energy for different theoretical models are reviewed. In later sections, the force deformation relations for these model are derived. Simplest molecular theories of rubber-like elasticity are based on the Gaussian network chains. These theories are referred to as the Gaussian networks. The probability  $W(r)$  that the distance between the two ends of a network chain is given by the Gaussian function (1,13)

$$W(r) = \left( \frac{3}{2\pi \langle r^2 \rangle_0} \right)^{3/2} \exp \left( - \frac{3r^2}{2\langle r^2 \rangle_0} \right) \quad (5)$$

Here,  $\langle r^2 \rangle_0$  represents average of the squared end-to-end vectors, and the subscript zero indicated that the chain is in the unperturbed or the so-called theta state (1). It is now well established that chains in the bulk undiluted state are in this unperturbed state. For chains having fewer than 50 bonds, such as the short chains in a bimodal network, for example, the distribution departs markedly from the Gaussian limit (34). Here we discuss molecular theories of networks that are based on the Gaussian picture of the individual network chain are discussed.

The elastic free energy,  $A_{\text{el}}$ , of a Gaussian chain is related to the probability distribution  $W(r)$  by the thermodynamic expression (13)

$$A_{\text{el}} = C(T) - kT \ln W(r) \quad (6)$$

where  $C(T)$  is a function only of temperature  $T$ , and  $k$  is the Boltzmann constant. Substituting equation (5) into equation (6) leads to

$$A_{\text{el}} = A^*(T) + \left( \frac{3kT}{2\langle r^2 \rangle_0} \right) r^2 \quad (7)$$

where  $A^*(T)$  is a function of temperature alone. Equation (7) represents the elastic free energy of a single Gaussian chain with ends fixed at a separation  $r$ . The average force required to keep the two ends at this separation is obtained from the thermodynamic expression (13,174)

$$f = \left( \frac{\partial A_{\text{el}}}{\partial r} \right)_T = \left( \frac{3kT}{\langle r^2 \rangle_0} \right) r \quad (8)$$

where the second equality is obtained by using equation (7). The subscript  $T$  denotes differentiation at fixed temperature.

Equation (8) shows that the single chain behaves like a linear spring, obeying Hooke's law with a spring constant equal to  $3kT/\langle r^2 \rangle_0$ .

This approach is directly extendable to the chains making up a network structure because the total elastic free energy of the network is the sum of the elastic free energies of individual chains. Specifically, the difference in the total elastic free energy  $\Delta A_{\text{el}}$  of the network in the deformed and undeformed states is obtained by summing equation (7) over the  $\nu$  chains of the network (1,2,5,13):

$$\Delta A_{\text{el}} = \frac{3kT}{2\langle r^2 \rangle_0} \sum_{\nu} (r^2 - \langle r^2 \rangle_0) \quad (9)$$

$$= \frac{3kT}{2} \left( \frac{r^2}{\langle r^2 \rangle_0} - 1 \right) \quad (10)$$

where  $\langle r^2 \rangle = \Sigma r^2/\nu$  is the average square end-to-end vectors of chains in the deformed network. Substituting

$$\langle r^2 \rangle = \langle x^2 \rangle + \langle y^2 \rangle + \langle z^2 \rangle \quad (11)$$

into equation (10) and using the fact that chain dimensions are isotropic in the undeformed state, that is,

$$\begin{aligned} \langle r^2 \rangle_0 &= \langle x^2 \rangle_0 + \langle y^2 \rangle_0 + \langle z^2 \rangle_0 \\ &= 3\langle x^2 \rangle_0 = 3\langle y^2 \rangle_0 = 3\langle z^2 \rangle_0 \end{aligned} \quad (12)$$



yields

$$\Delta A_{el} = \frac{v k T}{2} \left[ \frac{\langle x^2 \rangle}{\langle x^2 \rangle_0} + \frac{\langle y^2 \rangle}{\langle y^2 \rangle_0} + \frac{\langle z^2 \rangle}{\langle z^2 \rangle_0} - 3 \right] \quad (13)$$

The  $x$ ,  $y$ , and  $z$  coordinates appearing in the above equations represent laboratory-fixed coordinates.

The ratios of mean-squared dimensions appearing in equation (13) are microscopic quantities. To express the elastic free energy of a network in terms of the macroscopic state of deformation, an assumption has to be made relating microscopic chain dimensions to macroscopic deformation.

The relationship of chain dimensions to macroscopic state of deformation has been the focus of a wide body of research. Two classical theories, the affine and the phantom network models, that relate the microscopic deformation to the macroscopic one are described first. More recent theories are then discussed.

**The Two Classical Theories.** The classical theories comprising the phantom and the affine network models were introduced between 1941 and 1943. The term “classical” is used in describing the phantom and affine models because of their conceptual simplicity and their status as suitable reference systems for all later treatments of the molecular theory. Below, the characteristic features of the classical theories are outlined.

**The Affine Network Model.** One of the earlier assumptions regarding microscopic deformation in networks is that the junction points in the networks move affinely with macroscopic deformation. The affine network model was developed by Kuhn, Wall, and Flory (1,175,176). According to the model, chain end-to-end vectors deform affinely, which gives

$$\Delta A_{el,affine} = \frac{1}{2} v k t (\lambda_x^2 + \lambda_y^2 + \lambda_z^2 - 3) \quad (14)$$

where the  $\lambda$ s are *macroscopic* deformation ratios along the three coordinate axes.

Theoretical developments after 1975 have not supported the affine network model (82,177–182), mainly because the assumption of embedding each junction securely into the continuum of the network volume was judged to be unrealistic. Even more important, neutron scattering results (5,183–185) provide clear evidence for junction fluctuations of the nature assumed in the phantom network model described below.

**The Phantom Network Model.** The theory of James and Guth, which has subsequently been termed the “phantom network theory,” was first outlined in two papers (186,187), followed by a mathematically more rigorous treatment (188–190). More recent work has been carried out by Duiser and Staverman (191), Eichinger (192), Graessley (193,194), Flory (82), Pearson (195), and Kloczkowski and co-workers (196,197). The most important physical feature is the occurrence of junction fluctuations, which occur asymmetrically in an elongated network in such a manner that the network chains sense less of a deformation than that imposed macroscopically. As a result, the modulus predicted in this theory is substantially less than that predicted in the affine theory.

The relations resulting from the phantom network model, and their derivations, are given elsewhere (5,13,82). The final result of relevance here is

$$\Delta A_{\text{el, phantom}} = \frac{1}{2} \xi kT (\lambda_x^2 + \lambda_y^2 + \lambda_z^2 - 3) \quad (15)$$

The elastic free energies for the affine and the phantom network models differ only in the front factor, that is, the factor  $(1/2) \xi kT$  appearing in equation (15) replaces the front factor  $(1/2) \nu kT$  in equation (14).

The affine and the phantom network models, based on the Gaussian chain, act as the two limiting idealized models of amorphous networks in the absence of intermolecular interactions such as interactions between network chains. Expressions for the elastic free energy of more realistic models than the affine and the phantom network models are given in the following sections.

**Extension of the Classical Models to Non-Gaussian Chains.** The affine and the phantom network models are based on the Gaussian distribution of end-to-end distances of the network chains. This distribution, however, is not suitable for very short chains, or for any chains stretched to near the limits of their extensibility (2,13,34,91,198,199). In these cases, the modulus shows a marked upturn at high elongations, a result that may be of practical as well as fundamental importance.

As a result of the non-Gaussian behavior of network chains, the distribution  $W(r)$  given by equation (5) is modified as

$$W(r) = \left( \frac{A\beta}{r l^2} \right) (\beta^{-1} \sinh \beta)^n \exp \left( -\frac{\beta r}{l} \right) \quad (16)$$

where  $A$  is a constant that normalizes the distribution,  $n$  is the number of repeat units of a network chain,  $l$  is the length of each repeat unit, and  $\beta$  is the inverse Langevin function  $\beta = L^* \left( \frac{r}{\langle r^2 \rangle_0^{1/2}} \right)$ , which is expressed in series as

$$\beta = 3\rho + \frac{9}{5}\rho^3 + \frac{297}{175}\rho^5 + \dots \quad (17)$$

where  $\rho = \frac{r}{\langle r^2 \rangle_0^{1/2}}$ . Equation (16) now takes the form (2)

$$W(r) = \frac{3A}{\langle r^2 \rangle_0 l} \left[ 1 + \frac{3}{5}\rho^2 + \frac{99}{175}\rho^4 + \dots \right] \exp \left\{ -\frac{3}{2\langle r^2 \rangle} r^2 \left[ 1 + \frac{3}{10}\rho^2 \frac{33}{175}\rho^4 + \dots \right] \right\} \quad (18)$$

With this modified distribution of the end-to-end vector of a network chain, the evaluation of the elastic free energy follows the same lines as given above for the affine model. When the chains are sufficiently long, the parameter  $\rho \rightarrow 0$ , and the Gaussian affine model is obtained.

**Modern Theories.** The term “modern” refers to theories of rubber-like elasticity introduced after 1975 mainly to account for the disagreement between experiment and the predictions of the phantom or affine network models. All

the theories in this category may essentially be regarded as corrections to the phantom network model. Corrections come in the form of contributions of entanglements to the elastic free energy.

*The Constrained-Junction Theory.* The constrained-junction model assumes that the fluctuations of junctions are diminished below those of the phantom network due to the presence of entanglements. It is based on initial work carried out by Ronca and Allegra (177), and subsequently developed by Flory and Erman (3,5,178,182). These studies have shown that the fluctuations in a phantom network are substantial. For a tetrafunctional network, the mean-square fluctuations of junctions amount to as much as half of the mean-square end-to-end vector of the network chains. According to the model, each junction fluctuates in a domain whose size is dictated by the strength of the constraints acting on it. Such constraints are illustrated in the upper portion of Figure 4. If the junction is highly constrained, the size becomes small. The strength of the constraints is measured by a parameter  $\kappa$ , defined as

$$\kappa = \frac{\langle(\Delta R)^2\rangle}{\langle(\Delta s)^2\rangle} \quad (19)$$

where  $\langle(\Delta R)^2\rangle$  and  $\langle(\Delta s)^2\rangle$  denote, respectively, the mean-square dimension of junction fluctuations in the phantom network and in the entanglement domain. If the range of fluctuations decreases to zero due to entanglements,  $\kappa$  becomes infinitely large. If the effect of entanglements is nil, then the junction is unconstrained and can move in an indefinite space, and  $\kappa = 0$ . The elastic free energy of the constrained junction model is given by the expression

$$\Delta A_{el} = \frac{1}{2}\xi kT \left( \sum_{t=1}^3 (\lambda_t^2 - 1) + \frac{\mu}{\xi} \sum_{t=1}^3 [B_t + D_t - \ln(1 + B_t) - \ln(1 + D_t)] \right) \quad (20)$$

where

$$B_t = \kappa^2 \frac{\lambda_t^2 - 1}{(\lambda_t^2 + \kappa)^2} \quad D_t = \lambda_t^2 B_t / \kappa \quad (21)$$

This theory has been shown to give results that agree quantitatively with stress-strain swelling data (200), birefringence (201,202), and segmental orientation (162,203), in uniaxially stretched networks and with experimental data obtained in shear and multiaxial states of stress (204).

The Ronca-Allegra theory (177), and Flory-Erman theory (3,178,182) are both based on the idea that effects of constraints are local and decrease with increasing strain and swelling. The basic difference between the two theories is that in the Ronca-Allegra theory the fluctuations of junctions become exactly affine as the undeformed state is approached, whereas in the Flory theory they are close to but below those of the affine state.

*The Constrained-Chain Theory.* This refinement of the constrained-junction model is based on reexamination of the constraint problem and evaluation of some neutron scattering estimates of actual junction fluctuations

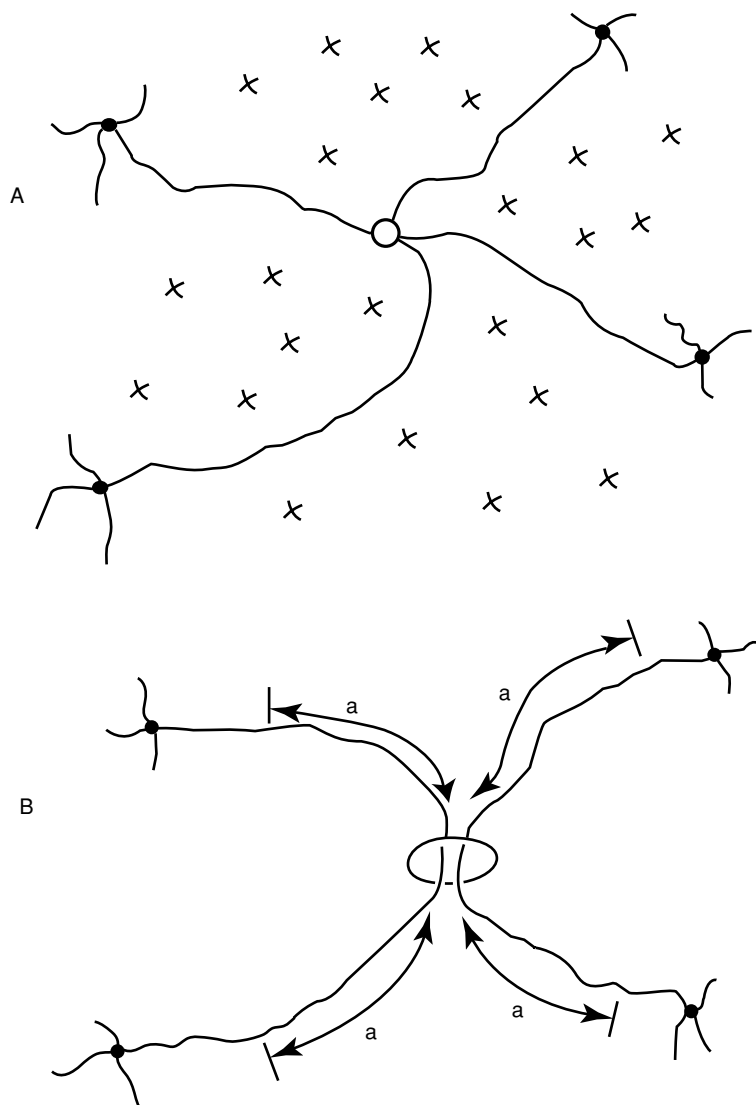


**Fig. 4.** (A) A central tetrafunctional junction surrounded by four other topologically neighboring junctions and a number of spatially neighboring junctions. (B) Schematic drawing of a slip link, with its possible motions along the network chains specified by the distances  $a$ , and its locking into position as a cross-link.

(183–185). It was concluded that the suppression of the fluctuations was overestimated in the theory, presumably because the entire effect of the interchain interactions was arbitrarily placed on the junctions. The theory was therefore revised to make it more realistic by placing the effects of the constraints on the centers of mass of the network chains (205–207). This modification also provided improved agreement between theory and experiment.

*The Diffused-Constraints Theory.* This theory attempts at even greater realism, by distributing the constraints continuously along the network chains. In its application to stress-strain isotherms in elongation (208), it has the advantage of having only a single constraint parameter and the values it exhibits upon comparing theory and experiment seem more reasonable than in the earlier models. Applications to strain birefringence (209), on the other hand, yield values of the birefringence that are much larger than those in the constrained-junction and constrained-chain theories.

*Network Models Based on the Edwards Approach.* The above theories on the effects of constraints on fluctuations start from a detailed molecular model of the real network (3,210). The fundamental postulate of the theory states that only strain-dependent contributions to the elastic free energy are of importance, and that these contributions vanish at infinitely large extensions or swelling. Contributions from trapped entanglements, for example, are categorically eliminated when this postulate is accepted. According to this approach, whether the trapped entanglements contribute to stress can only be determined by experiments. A complete statistical mechanical theory that does not depend on physical assumptions of the type stated above has been outlined by Freed (211), and a mathematical theory of elasticity of networks with internal constraints has been worked out by Edwards and collaborators (212–216). According to these theories, a set of internal constraints, including knots and entanglements, are assumed to be fixed during the formation of the network. These constraints are conserved under deformation, thus contributing to the elastic properties.

Edwards and colleagues formulated the contributions from entanglements by two different models, (i) the tube model and (ii) the slip-link model. In the tube model (217), the topological contributions are applied to every monomer of the network chain, confining its fluctuations to a tube. This potential is independent of network deformation. In a more recent work (218), the strength of tube constraints was made proportional to deformation. This model is referred to as the “Nonaffine Tube Model”.

In the slip-link model (219–221), the chain length along the contour of the tube has been replaced by a the slip-link. This is illustrated in the lower portion of Figure 4. In tube models, the intermolecular potential acting on a given network chain is formed collectively by many neighboring chains. In slip-link models each entanglement is formed by a pair of chains. Thus, according to the mechanism in the slip-link theory, a link joins two different chains which may slide a distance  $a$  along the contour of the chains. The effect of entanglements enters as further contributions and is proportional to the number of slip links. The slip-link and constraint models have been compared by Vilgis and Erman (222).

Recently, Rubinstein and Panyukov (223) reviewed the constraint models and proposed a “slip-tube” model by combining the ideas of the tube and slip-link models.

## Computer Simulations

In addition to the analytical formulations outlined in the preceding sections, rubber elasticity has been widely studied by computer simulations. The major applications of computer simulations are either in the form of Monte Carlo or

molecular dynamics simulations. Simulations either characterize the detailed statistical properties of single chains that constitute the building blocks of rubbers, or collective statistical properties of networks.

**Single Chain Simulations.** Monte Carlo simulations have been used to calculate thermoelastic results through the temperature coefficient of the unperturbed dimensions (224). In the case of networks of the protein elastin, such results were used to evaluate alternative theories for the molecular deformation mechanism for this bioelastomer (225).

Stress-strain isotherms have also been calculated with this approach. Examples are unimodal networks of polyethylene and poly(dimethylsiloxane) (226), polymeric sulfur and selenium (227), short *n*-alkane chains (228), natural rubber (229), several polyoxides (230,231), and elastin (232), and bimodal networks of poly(dimethylsiloxane) (233). It is possible to include excluded volume effects (1), in such simulations (234). In the case of the partially helical polymer polyoxymethylene, the simulations were used to resolve the overall distributions into contributions from unbroken rods, once-broken rods, twice-broken rods, etc. (231). It was also shown how applying stresses to the ends of chains of this type can be used to bias the distributions in the direction of increased helical content and increased average end-to-end distances (231). In this sense, imposition of a stress has the same effect on the helix-coil equilibrium as a decrease in the temperature (6).

The trapping process of cyclics in networks has been simulated using Monte Carlo methods based on a rotational isomeric state model for the cyclic chains (103). The first step was generation of a sufficient number of cyclic chains having the known geometric features and conformational preferences, and the desired degree of polymerization. In the present application, a chain having an end-to-end distance less than a threshold value was considered to be a cyclic. The coordinates of each "cyclic" chain thus generated were stored for detailed examination of the chain's configurational characteristics, in particular the size of the "hole" it would present to a threading linear chain. The trapping process was simulated using a torus centered around each repeat unit in the cyclic (103). Any torus found to be "empty" was considered to provide a pathway for a chain of specified diameter to pass through, threading it and then incarcerating it once the end-linking process has been completed. The simulation results thus obtained gave a good representation of the experimental trapping efficiencies.

**Chains in Networks.** One of the first studies of chains in networks is by Gao and Weiner (235) where they performed extended simulations of short chains with fixed (affinely moving) end-to-end vectors. The first extensive molecular dynamics simulations of realistic networks were performed by Kremer and collaborators (236). These calculations were based on a molecular dynamics method that has been applied to study entanglement effects in polymer melts (237). The networks obtained by cross-linking the melts were then used to study the effect of entanglements on the motion of the cross-links and the moduli of the networks. The moduli calculated without any adjustable parameters were close to the phantom network model for short chains, and supported the Edwards tube model for long ones. Similar molecular dynamics analyses were used to understand the role of entanglements in deformed networks in subsequent studies (238-240).

## Phenomenological Theory

The phenomenological approach to elasticity theory does not consider the molecular constitution of networks. It is based on continuum mechanics and symmetry arguments rather than on molecular concepts (2,241–243). It attempts to fit stress–strain data with a minimum number of parameters, which are then used to predict other mechanical properties of the same material.

The elastic free energy given by the elementary and the more advanced theories in this area are symmetric functions of the three extension ratios  $\lambda_x$ ,  $\lambda_y$  and  $\lambda_z$ . One may also express the dependence of the elastic free energy on strain in terms of three other variables, which are in turn functions of  $\lambda_x$ ,  $\lambda_y$  and  $\lambda_z$ . In phenomenological theories of continuum mechanics, where only the observed behavior of the material is of concern rather than the molecular mechanism, these three functions are chosen to be

$$\begin{aligned} I_1 &= \lambda_1^2 + \lambda_2^2 + \lambda_3^2 \\ I_2 &= \lambda_1^2 \lambda_2^2 + \lambda_1^2 \lambda_3^2 + \lambda_1^2 \lambda_3^2 \\ I_3 &= \lambda_1^2 \lambda_2^2 \lambda_3^2 \end{aligned} \quad (22)$$

Here,  $I_1$ ,  $I_2$ , and  $I_3$  are referred to as the three strain invariants. The term invariant designates the property in which the value of the expression is independent of the choice of the coordinate frame. The elastic free energies of the phantom and the affine network models now take the simple form

$$\Delta A_{\text{el}} = FkT(I_1 - 3) \quad (23)$$

where  $F$  equates to  $\xi/2$  and  $\nu/2$  for the phantom and the affine network models, respectively. In general, the elastic free energy of the network is expressed as

$$\Delta A_{\text{el}} = \Delta A_{\text{el}}(I_1, I_2, I_3) \quad (24)$$

The most general form of the elastic free energy may be written as a power series

$$\Delta A_{\text{el}} = \sum_{i,j,k=0}^{\infty} C_{ijk}(I_1 - 3)^i(I_2 - 3)^j(I_3 - 1)^k \quad (25)$$

where  $C_{ijk}$  are the phenomenological coefficients. The simple cases of the phantom and affine networks is obtained as the first term of the series

$$\Delta A_{\text{el}} = C_{100}(I_1 - 3) \quad (26)$$

The elastic free energy of the so-called Mooney–Rivlin solid is obtained from equation (26) as

$$\Delta A_{\text{el}} = C_{100}(I_1 - 3) + C_{010}(I_2 - 3) \quad (27)$$

where  $C_{100}$  and  $C_{010}$  corresponds to  $2C_1$  and  $2C_2$  of the Mooney–Rivlin form, respectively. This form of the elastic free energy has been used widely in the

treatment of data from simple tension experiments on elastomers. It should be noted, however, that while the Mooney–Rivlin expression represents the behavior of rubbers under tension satisfactorily, it fails utterly in compression (6).

### Stress–Strain Relationships

Here, the stress–strain relations, or the equations of state, of networks is described by considering the homogeneous deformation of a cube of sides  $L_0$  in the reference state and  $L_x$ ,  $L_y$ , and  $L_z$  in the deformed state (6). More general states of deformation are discussed in several textbooks (2,5,13). The reference state is defined as the state in which the network has been formed. The deformation ratios are defined as the ratio of the final to the reference state, such as  $\lambda_x = L_x/L_0$ , etc. The state of the network during formation is of particular importance in obtaining the correct expression for the stress. If the network is prepared in the presence of a diluent, the reference volume  $V_0 = L_0^3$  equals the sum of the dry volume  $V_d$  of bulk polymer, and the volume of solvent  $V_s$ .

Also,  $\lambda_x = \alpha_x(v_{2c}/v_2)$ , where  $\alpha_x$  represents the ratio of the length along the  $x$  direction in the deformed state to that in the swollen but undistorted state, with similar definitions for the  $y$  and  $z$  directions. The quantity  $v_{2c}$  is the volume fraction of polymer during network formation and  $v_2$  is that during the experiment (and is assumed to remain constant during network deformation). This approximation fails, obviously, if the sample is highly compressed, or if the deformation is carried out while the sample is immersed in the solvent. The volume of a dry network remains approximately constant during deformation. This condition is that of incompressibility, which approximately hold for rubbers. The incompressibility condition is given in terms of deformation components by

$$\alpha_x \alpha_y \alpha_z = 1 \quad (28)$$

and

$$\lambda_x \lambda_y \lambda_z = V/V_0 \quad (29)$$

The equation of state relating the components of the true stress tensor  $t_i$  to deformation is given for an incompressible material by the thermodynamic relation

$$t_i = \frac{2}{V} \lambda_2^i \frac{\partial \Delta A_{el}}{\partial \lambda_2^i} \quad i = 1, 2, 3 \quad (30)$$

where the  $i$ th component  $t_i$  of the true stress tensor is defined as the force along the  $i$ th coordinate direction per unit deformed area. It should be noted that the three components  $t_i$  ( $i = 1, 2, 3$ ) constitute the diagonal elements of the stress tensor  $\mathbf{t}$ , corresponding to the normal stresses acting on the three faces of the prism. The off-diagonal components correspond to shear stresses. In the particular case when the shear stresses equate to zero, the normal stresses are referred to as the principal stresses. In the following sections, only simple tension or compression, which is the simplest state of principal stresses, is considered. The reader is referred to the literature (2,5,13) for applications to other states of stress.



Equation (30) allows the derivation of the three principal stresses from the elastic free energy of the network. This free energy follows either from the molecular theories discussed above or from the phenomenological formulation.

The quantity of greatest interest is the reduced stress  $[f^*]$ , defined by

$$[f^*] \equiv \frac{f v_2^{1/3}}{A_d(\alpha - \alpha^{-2})} \quad (31)$$

For uniaxial deformation,  $\lambda_1 = \lambda$ ,  $\lambda_2 = \lambda_3 = \lambda^{-1/2}$ , and the force  $f$  is obtained by differentiating the elastic free energy according to equation (30) with respect to  $\lambda$ . For the affine and phantom network models, the force is obtained as

$$f = 2 \frac{F k T}{L_0} \left( \lambda - \frac{1}{\lambda^2} \right) \quad (32)$$

where  $F$  equates to  $\xi/2$  and  $\nu/2$  for the phantom and the affine network models, respectively. For the constrained-junction model, the uniaxial force  $f$  is obtained by differentiating equation (20) according to equation (30):

$$f = \left( \frac{\xi k T}{L_0} \right) \left( \lambda - \frac{1}{\lambda^2} \right) \left[ 1 + \frac{\lambda K(\lambda) - \lambda^{-2} K(\lambda^{-1})}{\lambda - \lambda^{-2}} \right] \quad (33)$$

where  $L_0$  is the length of the sample, and

$$K(\lambda) = B \left[ \frac{B}{B + 1} + \kappa_0^{-1} \frac{\lambda^2 B + B}{B + \kappa_0 \lambda^{-2}} \right] B = B \left[ \frac{1}{\lambda^2 - 1} - \frac{1}{\lambda^2 + \kappa_0} \right] \quad (34)$$

The reduced force from equation (31) becomes (6,13)

$$[f^*] = \left( \frac{\xi k T}{V_d} \right) v_2^{1/3} \left[ 1 + \frac{\mu}{\xi} \frac{\alpha K(\lambda_x) - \alpha^{-2} K(\lambda_y^{-1})}{\alpha - \alpha^{-2}} \right] \quad (35)$$

The reduced force may be interpreted as the shear modulus of the network (13). According to equation (35), the reduced force consists of a term due to contributions from the phantom network and another from the constraints. The contribution of constraints, proportional to the term  $\mu/\xi$  in the brackets in equation (35), decreases as the network is stretched or swollen, an important feature in comparisons of theory and experiment.

## Swelling and Gel Collapse

As stated above, swelling of a network in a well-characterized solvent is a convenient means of obtaining information on the structure of networks, or conversely, of characterizing the polymer-solvent interactions when the network structure is known. In recent years, much emphasis has been placed on swelling of networks

and their phase transitions under different activities of the network–solvent system. Large-scale volume transitions triggered by small changes in environmental variables directed attention to possible uses of swollen gels in the field of responsive materials technologies. The transition involves the gel exuding solvent, for example, upon decrease in temperature. The resulting shrinkage (“syneresis”) is widely known as “gel collapse.” The presence of charges on network chains facilitates the volume phase transitions in swollen gels.

The change in free energy of a network upon swelling is taken as the sum of the change in the elastic free energy,  $\Delta A_{\text{el}}$ , and the change in free energy of mixing,  $\Delta A_{\text{mix}}$  and the contributions from ionic groups  $\Delta A_i$ :

$$\Delta A = \Delta A_{\text{el}} + \Delta A_{\text{mix}} + \Delta A_i \quad (36)$$

where  $\Delta A_{\text{el}}$  may be taken as any of the expressions resulting from a model,  $\Delta A_{\text{mix}}$  is the free energy of mixing and  $\Delta A_i$  is the contribution of the ionic groups on the chains. The total chemical potential  $\Delta\mu_1$  of solvent in the swollen network is obtained for the constrained-junction model as

$$\frac{\Delta\mu_1}{RT} = \ln(1 - v_2) + v_2 + \chi v_2^2 + \frac{1}{\lambda} \frac{\rho V_1}{M_c} \left[ 1 + \frac{\mu}{\xi} K(\lambda^2) \right] - i v \left( \frac{V_1}{V_0 N_A} \right) \left( \frac{v_2}{v_{20}} \right) \quad (37)$$

where  $v_2$  is the volume fraction of polymer,  $\chi$  is the Flory interaction parameter,  $V_1$  is the molar volume of solvent,  $M_c$  is the molecular weight of a network chain, and  $\lambda$  is the extension ratio, defined for the swelling case as

$$\lambda = \left( \frac{V}{V_0} \right)^{1/3} = \left( \frac{n_1 V_1 + x V_1 n_2}{V_0} \right) \quad (38)$$

Here,  $x$  is the number of repeat units in one network chain,  $n_1$  is the number of solvent molecules,  $n_2$  is the total number of network chains in the system,  $i$  is the number of ionic groups on the chains,  $v$  is the number of chains, and  $v_{20}$  is the volume fraction of chains during the formation of the network.

Equating the chemical potential to zero gives a relationship between the equilibrium degree of swelling and the molecular weight  $M_c$ . The relation for  $M_{c,\text{ph}}$  is obtained for a tetrafunctional phantom network model as

$$M_{c,\text{ph}} = - \frac{\frac{1}{2} \rho V_1 \left( \frac{v_2}{v_{20}} \right)^{1/3}}{\ln(1 - v_2) + v_2 + \chi v_2^2 - i v \left( \frac{V_1}{V_0 N_A} \right) \left( \frac{v_2}{v_{20}} \right)} \quad (39)$$

where  $v_2$  denotes the equilibrium degree of swelling.

For the affine network model, the molecular weight between cross-links  $M_{c,\text{af}}$  is obtained as

$$M_{c,\text{af}} = - \frac{\rho V_1 \left( v_2^{1/3} - \frac{v_2}{2v_{20}} \right)}{\ln(1 - v_2) + v_2 + \chi v_2^2 - i v \left( \frac{V_1}{V_0 N_A} \right) \left( \frac{v_2}{v_{20}} \right)} \quad (40)$$

Equations (39) and (40) form the basis of determining the molecular weights of network chains (1). Equation (40) is the celebrated Flory–Rehner expression, improved by the incorporation of ionic group effects and the degree of swelling during network formation. The behavior of a swollen network is found to obey the constrained junction model (200), which predicts results between those of the phantom network model given by equation (39) and the affine network model given by equation (40). Alternatively, the chemical potential expression may be solved for  $v_2$ , leading to a value for the degree of swelling of the network. The result shows that the degree of swelling increases as the chain length between cross-links increases. The dominant forces that operate in swollen uncharged gels are van der Waals forces, hydrogen bonds, hydrophobic forces, and forces resulting from chain entropy.

For known network structure, equation (39) or (40) may be solved for the polymer–solvent interaction parameter  $\chi$ . Indeed, swelling serves as a convenient means of determining values of the  $\chi$  parameter.

When the network chains contain ionic groups, there will be additional forces that affect their swelling properties. Translational entropy of counterions, Coulomb interactions, and ion pair multiplets are forces that lead to interesting phenomena in ion-containing gels. These phenomena were studied in detail by Khokhlov and collaborators (244–248). The free energy of the networks used by this group is

$$\Delta A = \Delta A_{\text{mix}} + \Delta A_{\text{el}} + \Delta A_{\text{trans}} + \Delta A_{\text{coulomb}} \quad (41)$$

where  $\Delta A_{\text{trans}}$  and  $\Delta A_{\text{Coulomb}}$  are the contributions to the elastic free energy of the networks from the translational entropy of the counterions and the free energy of Coulomb interactions. Several interesting features of gels are obtained through the use of equation (41). A network chain of a polyampholyte gel contains both positive and negative charges. The liquid phase in the swollen polyampholyte gel may contain additional counterions. The theoretical and experimental literature on such gels was reviewed recently by Nisato and Candau (248). In ion-containing gels, when ion-containing groups are fully dissociated the gel swells excessively, because of the tendency of the free counterions to occupy as much space as possible. In the other extreme case, called the ionomer regime, counterions are condensed on oppositely charged monomer units, forming ion pairs followed by formation of multiplets. This decreases the osmotic pressure of the gel and results in its collapse. The conditions for ion pair formation and physical and chemical factors leading to gel swelling and collapse have been discussed by Philippova and co-workers (245).

## Theory vs. Experiment

The constrained-junction theory successfully describes most of the features of numerous investigations that have been made on stress–strain relationships involving a variety of types of deformations (1–3,13,220,249–252). Specifically, the decrease in modulus [ $f^*$ ] with the increase in elongation is viewed as the deformations becoming more nonaffine as the stretching of the network chains

decreases chain-junction entangling; this in turn increases junction fluctuations. The observation that the decrease in  $[f^*]$  is less in the case of swollen networks results from the swelling diluent decreasing some of this entangling even at low elongations. The observation that the isotherms become approximately horizontal in compression is also successfully predicted by the theory (13,253). The upturn in  $[f^*]$  at very high elongations is a non-Gaussian effect not accounted for in the theory and must be treated separately. Interpretation of the upturn in  $[f^*]$  in terms of the limited extensibility of the network chains first requires demonstration that reinforcement from strain-induced crystallization is not a significant part of the effect (254). Failure to test for this by swelling or the increase in temperature has caused a great deal of confusion in the literature.

Experiment and theory are in at least approximate agreement regarding swelling, in that estimates of degree of cross-linking from equilibrium swelling are generally in fair agreement with values obtained from mechanical properties (1,2,255).

A major unresolved issue concerns the observation that the swelling or dilation modulus frequently goes through an unanticipated maximum with the increase in degree of swelling (256–259). Modifications of existing theories to reproduce this feature quantitatively have not been very successful. In a worst-case scenario, this discrepancy could undermine one of the crucial assumptions in swelling theory, namely that the mixing and elastic contributions to the swelling free energy are separable and simply additive (257).

The reduced birefringence shows some properties that parallel the reduced stress or modulus. In other respects, however, it can be quite different, showing for example significant increases with the increase in degree of swelling. Nonetheless, experimental results and those from the constrained-junction theory seem to be in at least fair agreement (201,202).

Experimental results on the elongation and swelling dependence of the reduced orientation seem to be well reproduced by theory (162,203). Preparing networks by cross-linking a polymer in solution (260) can give very useful orientation results, but it is essential in such cases to account for changes in reference state in the interpretation of the data (261).

The most important elasticity result of this type is obtained by small-angle neutron scattering. In particular, such studies yield information on how the radius of gyration of the network chains transforms with elongation (13). Preliminary comparisons between theory and experiment are quite encouraging (262), but many issues remain unresolved in this relatively new approach to characterizing elastomeric behavior.

## Liquid-Crystalline Elastomers

**Introduction.** In the case of polymers, liquid crystallinity (“mesomorphism”) frequently occurs in very stiff chains such as the Kevlars and other aromatic polyamides (263). It can also occur with flexible chains, and it is these flexible chains in the elastomeric state that are relevant here. Some reasons why such liquid-crystalline elastomers are of particular interest is the fact that (*i*) they can be extensively deformed, (*ii*) the deformation produces alignment of the chains,

and (iii) alignment of the chains is central to the formation of liquid-crystalline phases (13).

A liquid-crystalline phase lies between the limits of completely ordered (crystalline) and completely disordered (isotropic) phases. In the case of *nematic* phases, the disorder that gives rise to the liquidity or fluidity is the sliding of chain segments relative to one another, to place them out of register. There are also a variety of *smectic* liquid-crystalline phases (264), in which layers of molecules or chain sequences occur in layers that are disordered relative to one another. In contrast, *cholesteric* phases have layers of nematic arrangements that are stacked in rotated arrangements, and a similar stacking occurs in the case of the *discotics* (13).

There can be liquid-crystalline arrangements that involve the side chains attached to the chain backbones. The three possibilities are groups that can form liquid-crystalline phases occurring in the backbone (265), in the side chains, and in both (in what's called "combined" structures). Polymer chains that are very stiff can also appear in *rigid-rod networks*. Such networks deform in response to a stress by rearranging these rigid chains relative to one another instead of usual unwinding a flexible chain from a compact state to one that is more extended in the direction of the strain.

**Main-Chain Liquid-Crystalline Elastomers.** The polymer in this category that has been the most studied is poly(diethylsiloxane) (PDES)  $[-\text{Si}(\text{OC}_2\text{H}_5)_2\text{O}-]$ . Of greatest interest has been its formation of a mesophase that is nematic, and relevant studies have focused on a wide range of properties. For example, stretching a PDES elastomer aligns its chains in a way that changes the temperature range over which the liquid-crystalline phase is stable (266). Several symmetric polysiloxane elastomers having longer side chains also show liquid-crystalline behavior, and these range from poly(di-*n*-propylsiloxane) to poly(di-*n*-decylsiloxane). The temperatures at which the liquid-crystallinity disappears (the "isotropization temperatures") show a very interesting monotonic increase with the increase in the number of methylene groups in the side chains (267). Beyond poly(di-*n*-decylsiloxane) complications arise, probably because the side chains are sufficiently long to crystallize themselves. Some polysiloxanes with cyclic groups in the backbone also form mesophases (268), as do some of the polyphosphazenes (269).

The property these materials exhibit of greatest relevance here is their stress-strain isotherms. Some obtained for PDES (270) as a function of degree of mesomorphic structure are shown schematically in Figure 5. The curves exhibit yield points similar to those shown by partially crystalline polymers, and the overall shapes of the curve differ greatly with the increase in the amounts of mesophase present, either present initially or induced by the deformation. As is generally the case, formation of a second phase leads to irreversibility in the stress-strain isotherms.

**Side-Chain Liquid-Crystalline Elastomers.** Of considerable interest is the orientation of the mesogenic groups and the chain backbones to which they are attached. Frequently studied backbones include siloxanes and acrylates, but a variety of other structures have also been studied, including amphiphilics (13). The side chains in these structures can rearrange into positions either parallel or perpendicular to the deformed chain backbone (271). The outcome depends

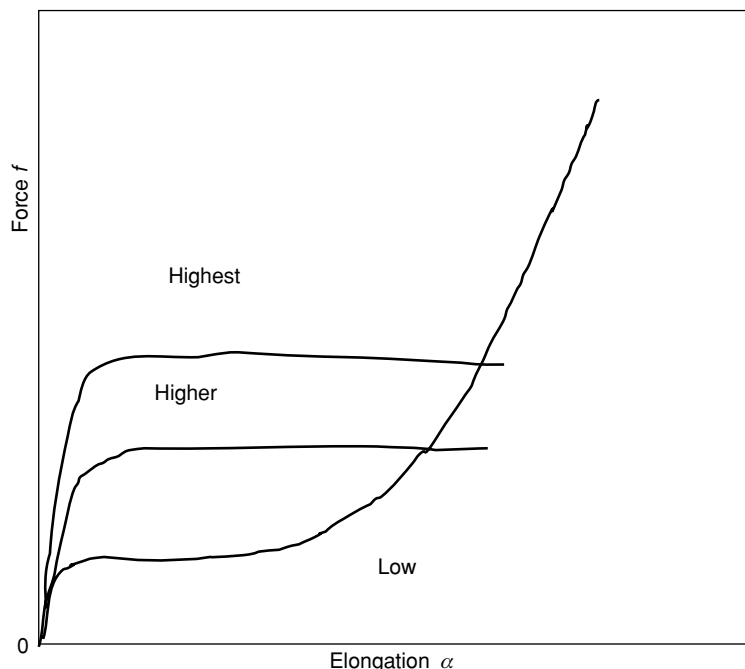


**Fig. 5.** Sketch showing stress-strain isotherms for a main-chain liquid-crystalline elastomer such as poly(diethylsiloxane), as a function of the amount of mesophase present.

particularly on the nature and length of the flexible spacer connecting the mesogenic groups to the chain backbone. As expected, the physical properties can become strongly anisotropic.

Some liquid-crystalline materials of this type could be oriented by imposing an electric or magnetic field (272). The chains could also be aligned when these liquid-crystalline elastomers, are deformed (generally in elongation but also in some cases in compression), and then cross-linked into network structures. The mesogenic behavior of such networks obviously depends strongly on their structures, in particular the degree of cross-linking, and composition (in the case of copolymers). The phase transitions exhibited also depend significantly on spacer length, with closer coupling between the mesogenic groups and the polymer backbone tending to make the system more sensitive to mechanical deformations (273).

The thermoelastic behavior of these materials has also been reported (274). Such experiments resolve the nematic-to-isotropic transition into entropic and enthalpic contributions and provides values of the corresponding energetic and entropic parts of the elastic force (275).

Considerably less work has been done on discotic liquid-crystalline elastomers, and the same seems to be true for smectic elastomers even though some of them have the additional interesting property of being chiral (276)! Some liquid-crystalline elastomers are ferroelectric (possess spontaneous electric polarization) or piezoelectric (become electrically polarized when mechanically strained, and become mechanically strained when exposed to an electric field) (277).

Finally, some liquid-crystalline elastomers exhibit interesting photonic effects such as nonlinear optical properties (278).

**Theory.** The unusual properties cited above have been the focus of numerous theoretical investigations (279,280). The simplest physical picture of nematic elasticity can be visualized by the lattice theory, in which semiflexible chains are assumed to be embedded in an isotropic lattice of solvent molecules. For example, calculations based on a lattice model (279) show an abrupt jump in the segmental orientation function at a finite elongation, and this corresponds to the isotropic-nematic transition. Below the transition, the sample behaves close to isotropic Gaussian elasticity. At a fixed uniaxial force, the transition is marked by a sudden elongation, resulting from the abrupt alignment of the segments along the direction of the force during the transition. Above the transition point, the segments are highly oriented along the direction of stretch, and the network becomes nematic, and its elastomeric behavior changes correspondingly.

## Bioelastomers

There are a number of cross-linked proteins that are elastomeric, and investigation of their properties may be used to obtain insights into elastic behavior in general. For example, elastin (118,281–284), which occurs in mammals, illustrates the relevance of several molecular characteristics to the achievement of rubber-like properties. First, a high degree of chain flexibility is achieved in elastin by its chemically irregular structure, and by choices of side groups that are almost invariably very small. Since strong intermolecular interactions are generally not conducive to good elastomeric properties, the choices of side chains are also almost always restricted to nonpolar groups. Finally, elastin has a glass-transition temperature of approximately 200°C in the dry state, which means it would be elastomeric only above this temperature. Nature, however, apparently also knows about “plasticizers.” Elastin, as used in the body, is invariably swollen with sufficient aqueous solutions to bring its glass transition temperature below the operating temperature of the body.

Elastin chains are cross-linked *in vivo* in a highly specific manner, using techniques very unlike those usually used to cure commercial elastomers (5,13,285). The cross-linking occurs through lysine repeat units, the number and placement of which along the chains are carefully controlled in the synthesis of elastin in the ribosomes. An analogous reaction has been carried out commercially on perfluoroelastomers, which are usually very difficult to cross-link because of their inertness. Nitrile side groups placed along the chains are trimerized to triazine, thus giving similarly stable, aromatic cross-links (5,13).

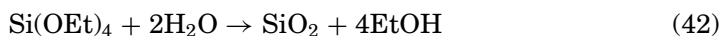
Another bioelastomer, found in some insects, is resilin (286). It is an unusual material because it is thought to have a relatively high efficiency in storing elastic energy (ie, very small losses due to viscous effects). A molecular understanding of this very attractive property could obviously have considerable practical as well as fundamental importance.

## Filled Elastomers

**Introduction.** Elastomers, particularly those that cannot undergo strain-induced crystallization, are generally compounded with a reinforcing filler. The two most important examples are the addition of carbon black to natural rubber and to some synthetic elastomers (287), and silica to polysiloxane ("silicone") rubbers and other elastomers (288,289). The advantages obtained include improved abrasion resistance, tear strength, and tensile strength. Disadvantages include increases in hysteresis (and thus heat buildup) and compression set (permanent deformation). The mechanism of the reinforcement obtained is only poorly understood in molecular terms. Some elucidation might be obtained by incorporating the fillers in a more carefully controlled manner, particularly using sol-gel technology (13,85), as described below.

### Sol-Gel Generation of Ceramic-Like Phases.

**Chemistry.** In the most important example, hydrolysis of an alkoxy silane such as tetraethoxysilane or tetraethylorthosilicate (TEOS),



is used to precipitate very small, well-dispersed particles of silica into a polymeric material (5,13,85,290,291). A variety of substances, generally bases, catalyze this reaction, which occurs quite readily near room temperature. Another example would be the catalyzed hydrolysis of a titanate, in the *in situ* precipitation of titania. Silica, titania, and related ceramic-like fillers thus produced within an elastomer have been shown to give good reinforcement in a variety of deformations.

**Methods for Carrying Out Sol-Gel Reactions within Elastomers.** The most common approach is to generate the filler after curing. In this technique, the polymer is first cured or vulcanized into a network structure using any of the well-known cross-linking techniques. The network is then swelled with the organosilane or related molecule to be hydrolyzed, after which it is exposed to water at room temperature, in the presence of a catalyst, for a few hours. The swollen sample can be either placed directly into an excess of water containing the catalyst, or merely exposed to the vapors from the catalyst-water solution. Drying the sample then gives an elastomer that is filled, and thus reinforced, with the ceramic particles resulting from the hydrolysis reaction.

The polymer used typically has end groups, such as hydroxyls, that can participate in the hydrolysis-condensation reactions (5,9,292). Such end groups provide better bonding between the two rather disparate phases, but bonding agents may also be introduced for this purpose (293). It is thus possible to mix hydroxyl-terminated chains (such as those of PDMS) with excess TEOS, which then serves simultaneously to tetrafunctionally end link the PDMS into a network structure and to act as the source of silica upon hydrolysis (5).

In the previous two techniques, removal of the unreacted TEOS and the ROH alcohol by-product causes a significant decrease in volume (294), which could be disadvantageous in some applications. One way of overcoming this problem is by precipitating the particles into a polymer that is inert under the hydrolysis conditions, for example, vinyl-terminated PDMS. After removal of volatiles,



the elastomer in this mixture can be subsequently cross-linked, with only the usual, very small volume changes occurring in any curing process.

**Approximately Spherical Particles and Their Reinforcing Properties.** Because of the nature of the *in situ* precipitation, the particles are well dispersed and are essentially unagglomerated (as demonstrated by electron microscopy). The mechanism for their growth seems to involve simple homogeneous nucleation, and since the particles are separated by polymer, they do not have the opportunity to coalesce. The particles are typically relatively monodisperse, with most of them having diameters in the range 100–200 Å. A variety of catalysts work well in the typical hydrolysis reactions used, including acids, bases, and salts (295). Basic catalysts give precipitated phases that are generally well-defined particles, whereas the acidic catalysts give more poorly defined, diffuse particles (296).

The reinforcing ability of such *in situ* generated particles has been amply demonstrated for a variety of deformations, including uniaxial extension (simple elongation), biaxial extension (compression), shear, and torsion (5,13). In the case of uniaxial extension, the modulus [ $f^*$ ] frequently increases by more than an order of magnitude, with the isotherms generally showing the upturns at high elongations that are the signature of good reinforcement (133,297). Some typical results in elongation and biaxial extension are shown schematically in Figure 6. As is generally the case in filled elastomers, there is considerable irreversibility in the isotherms, which is thought to be primarily due to some irrecoverable sliding of the chains over the surfaces of the filler particles upon being strained.

Some fillers other than silica, for example titania, do give stress-strain isotherms that are reversible, indicating interesting differences in surface chemistry, including increased ability of the chains to slide along the particle surfaces (298).

These *in situ* generated silica fillers also give increased resistance to creep or compression set in cyclic deformations (149). The *in situ* filled PDMS samples showed very little compression set, and these samples also exhibited increased thermal stability (299).

The low-temperature properties of some of these peculiarly filled materials have also been studied by calorimetric techniques. Of particular interest is the way in which reinforcing particles can affect the crystallization of a polysiloxane, both in the undeformed state and at high elongations (300). Finally, a number of studies using X-ray and neutron scattering (171,301) have also been carried out on filled elastomers (13,302). The results on the nature of the particles are generally consistent with those obtained by electron microscopy.

**Fillers with Controlled Interfaces.** By choosing the appropriate chemical structures, chains that span filler particles in PDMS-based composites can be designed so that they are either durable, are breakable irreversibly, or are breakable reversibly (303,304).

**Silicification and Biosilicification.** There has been some interest in generating silica-like particles using templates, as is done by nature in biosilicification processes (305). Various particle shapes have been obtained; platelet forms would be of particular interest with regard to their abilities to provide reinforcement and decrease permeability, as occurs with the layered fillers described below.

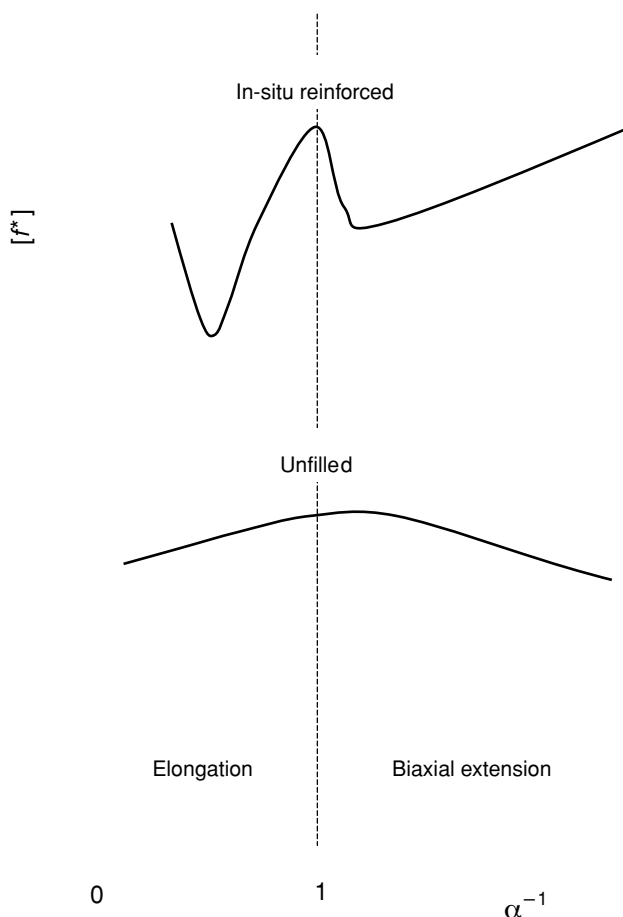


**Fig. 6.** Stress-strain isotherms for *in situ* reinforced elastomers in elongation (region to the left of the vertical dashed line, with  $\alpha^{-1} < 1$ ), and in biaxial extension (compression) (to the right, with  $\alpha^{-1} > 1$ ).

### Other Inorganic Particles.

**Polyhedral Oligomeric Silsesquioxanes.** These fillers are cage-like silicon-oxygen structures, and have been called the smallest possible silica particles (306–310). The most common structure has eight silicon atoms, each carrying a single organic group. The particles on which none of the groups are functionally reactive can be simply blended into elastomers such as PDMS using the usual mixing or compounding techniques. In this case, the inert groups are chosen to improve miscibility with the elastomeric host matrix. Polyhedral oligomeric silsesquioxanes molecules having one reactive functional group can be attached to a polymer as side chains. Those with two reactive groups can be incorporated into polymer backbones by copolymerization, and those with more than two can be used for forming cross-links, thus generating network structures.

**Porous Particles.** Some fillers such as zeolites are sufficiently porous to accommodate monomers, which can then be polymerized. This threads the chains through the cavities, with unusually intimate interactions between the reinforcing phase and the host elastomeric matrix (311–313). Unusually good reinforcement is generally obtained. Also, because of the constraints imposed by the cavity walls, these confined polymers frequently show no glass transition temperatures or melting points (27,314). PDMS chains have also been threaded through cyclodextrins, to form pseudo-rotaxanes (315).

**Layered Fillers.** Exfoliating layered particles such as the clays, mica, or graphite are being used to provide very effective reinforcement of elastomers at loading levels much smaller than in the case of solid particles such as carbon black and silica (316–320). Other properties can also be substantially improved, including increased resistance to solvents and reduced permeability and flammability.

**Miscellaneous Fillers.** There are a variety of miscellaneous fillers that are of interest for reinforcing elastomers. Examples are ground-up silica xerogels (321), carbon-coated silica (322), and functionalized silica particles (323,324).

### **Organic Particles.**

**Glassy Particles Deformable into Ellipsoidal Shapes.** It is also possible to obtain reinforcement of an elastomer by polymerizing a monomer such as styrene to yield hard glassy domains within the elastomer (325). Roughly spherical polystyrene (PS) particles are formed, and good reinforcement is obtained. It is possible to improve bonding onto the filler particles, for example, by including some trifunctional  $R'Si(OC_2H_5)_3$  in the hydrolysis (where  $R'$  is an unsaturated group). The  $R'$  groups on the particle surfaces then participate in the polymerization, thereby bonding the elastomer chains to the reinforcing particles.

The PS domains have a relatively low glass transition temperature ( $T_g \approx 100^\circ\text{C}$ ) (326) and are totally amorphous. Thus, it is possible to convert the essentially spherical PS particles into ellipsoids (5,327,328). First, the PS-elastomer composite is raised to a temperature well above the  $T_g$  of PS. The composite is then deformed, and cooled while in the stretched state. The particles in it are thereby deformed into ellipsoids, and retain this shape when cooled. Uniaxial deformations of the composite give prolate (needle-shaped) ellipsoids, and biaxial deformations give oblate (disk-shaped) ellipsoids (329). In these anisotropic materials, elongation moduli in the direction of the stretching were found to be significantly larger than those of the untreated PS-elastomer composite, whereas in the perpendicular direction they were significantly lower. Such differences were to be expected from the anisotropic nature of the systems. In the case of nonspherical particles in general, degrees of orientation are also of considerable importance. One interest here is the anisotropic reinforcements such particles provide, and there have been simulations to better understand the mechanical properties of such composites (330). Of, course, the ellipsoidal particles can be removed by dissolving away the polymer matrix and then redispersed randomly into another elastomer prior to its cross-linking.

**Nanotubes.** Carbon nanotubes are also of considerable interest with regard to both reinforcement and possible increases in electrical conductivity (306,309,331–333). There is considerable interest in characterizing the flexibility

of these nanotubes, in minimizing their tendencies to aggregate, and in maximizing their miscibilities with inorganic as well as organic polymers.

**Metal Particles.** Incorporating reinforcing particles that respond to a magnetic field is important with regard to aligning even spherical particles to improve mechanical properties anisotropically (334–336). Considerable anisotropy in structure and mechanical properties can be obtained (335). Specifically, the reinforcement is found to be significantly higher in the direction parallel to the magnetic lines of force.

**Simulations on Fillers.** Monte Carlo computer simulations have been carried out on a variety of filled elastomers (337–339) in an attempt to obtain a better molecular interpretation of how such dispersed phases reinforce elastomers. The approach taken enabled estimation of the effect of the excluded volume of the filler particles on the network chains and on the elastic properties of the networks. In the first step, distribution functions for the end-to-end vectors of the chains were obtained by applying Monte Carlo methods to rotational isomeric state representations of the chains (226). Conformations of chains that overlapped with any filler particle during the simulation were rejected. The resulting perturbed distributions were then used in the three-chain elasticity model (2) to obtain the desired stress–strain isotherms in elongation. These isotherms showed substantial increases in stress and modulus with the increase in filler content and elongation that are in at least qualitative agreement with the experiment.

In the case of nonspherical filler particles, it has been possible to simulate the anisotropic reinforcement obtained, for various types of particle orientations (330,340). Different types and degrees of particle agglomeration can also be investigated.

## BIBLIOGRAPHY

“Networks” in *EPSE*, 2nd ed., Vol. 10, pp. 95–112, by Paul J. Flory, Stanford University.

## CITED PUBLICATIONS

1. P. J. Flory, *Principles of Polymer Chemistry*, Cornell University Press, Ithaca, NY, 1953.
2. L. R. G. Treloar, *The Physics of Rubber Elasticity*, 3rd ed., Clarendon Press, Oxford, UK, 1975.
3. B. Erman and J. E. Mark, *Ann. Rev. Phys. Chem.* **40**, 351–374 (1989).
4. J. E. Mark, *New J. Chem.* **17**, 703–709 (1993).
5. B. Erman and J. E. Mark, *Structures and Properties of Rubberlike Networks*, Oxford University Press, New York, 1997.
6. J. E. Mark and B. Erman, in R. F. T. Stepto, ed., *Polymer Networks*, Blackie Academic, Chapman & Hall, Glasgow, UK, 1998.
7. J. E. Mark, in C. D. Craver and C. E. Carraher, Jr., eds., *Applied Polymer Science—21st Century*, American Chemical Society, Washington, DC, 2000, pp. 209–229.
8. J. E. Mark, *J. Chem. Educ.* **79**, 1437–1443 (2002).
9. J. E. Mark, *Prog. Polym. Sci.* **28**, 1205–1221 (2003).
10. J. E. Mark, *J. Phys. Chem., Part B* **107**, 903–913 (2003).

11. J. E. Mark, K. L. Ngai, W. W. Graessley, L. Mandelkern, E. T. Samulski, J. L. Koenig, and G. D. Wignall, *Physical Properties of Polymers*, 3rd ed., Cambridge University Press, Cambridge, UK, 2004.
12. J. E. Mark and B. Erman, eds., *Science and Technology of Rubber*, Elsevier, Amsterdam, 2005.
13. J. E. Mark and B. Erman, *Rubberlike Elasticity. A Molecular Primer*, 2nd ed., Cambridge University Press, Cambridge, UK, 2007.
14. A. N. Gent, ed., *Engineering with Rubber. How to Design Rubber Components*, Hanser Publishers, New York, 1992.
15. J. E. Mark, B. Erman, and F. R. Eirich, eds., *Science and Technology of Rubber*, Elsevier, Amsterdam, 2005.
16. H. Morawetz, *Polymers: The Origins and Growth of a Science*, Wiley-Interscience, New York, 1985.
17. J. E. Mark, in K. Fitzsimons, ed., *New Book of Knowledge*, Grolier, Scholastic Library Publishing, Danbury, CT, 2005, pp. 344–348.
18. D. Zhou and J. E. Mark, *J. Macromol. Sci.—Pure Appl. Sci.* **41**, 1221–1232 (2004).
19. J. E. Mark, *J. Inorg. Organomet. Polym.* **4**, 31 (1994).
20. A. N. Gent, G. L. Liu, and M. Mazurek, *J. Polym. Sci., Polym. Phys. Ed.* **32**, 271 (1994).
21. M. Shibayama, H. Takahashi, H. Yamaguchi, S. Sakurai, and S. Nomura, *Polymer* **35**, 2944 (1994).
22. J. E. Mark, *Acc. Chem. Res.* **27**, 271 (1994).
23. H. L. Trautenberg, J.-U. Sommer, and D. Goritz, *J. Chem. Soc. Faraday Trans.* **91**, 2649 (1995).
24. G. J. J. Out, A. A. Turetskii, M. Snijder, M. Moller, and V. S. Papkov, *Polymer* **36**, 3213 (1995).
25. S. Besbes, L. Bokobza, L. Monnerie, I. Bahar, and B. Erman, *Macromolecules* **28**, 231 (1995).
26. R. C. Hedden, H. Saxena, and C. Cohen, *Macromolecules* **33**, 8676–8684 (2000).
27. J. E. Mark, *Macromol. Symp.*, Kyoto issue **201**, 77–83 (2003).
28. J. E. Mark, *Molec. Cryst. Liq. Cryst.*, Bucharest Meeting **417**, 75–86 (2004).
29. C. M. Roland and G. S. Buckley, *Rubber Chem. Technol.* **64**, 74 (1991).
30. H. Oikawa, *Polymer* **33**, 1116 (1992).
31. E. E. Hamurcu and B. M. Baysal, *Polymer* **34**, 5163 (1993).
32. P. R. Subramanian and V. Galiatsatos, *Macromol. Symp.* **76**, 233 (1993).
33. M. A. Sharaf, J. E. Mark, and A. A.-R. Al-Ghazal, *J. Appl. Polym. Sci. Symp.* **55**, 139 (1994).
34. B. Erman and J. E. Mark, *J. Chem. Phys.* **89**, 3314–3316 (1988).
35. A. Kloczkowski, J. E. Mark, and B. Erman, *Macromolecules* **24**, 3266–3275 (1991).
36. G. Sakrak, I. Bahar, and B. Erman, *Macromol. Theory Simul.* **3**, 151–161 (1994).
37. I. Bahar, B. Erman, L. Bokobza, and L. Monnerie, *Macromolecules* **28**, 225 (1995).
38. S. S. Labana and R. A. Dickie, eds., *Characterization of Highly Cross-Linked Polymers*, American Chemical Society, Washington, DC, 1984.
39. K. Dusek, *Adv. Polym. Sci.* **78**, 1 (1986).
40. D. R. Miller and C. W. Macosko, *J. Polym. Sci., Polym. Phys. Ed.* **25**, 2441 (1987).
41. R. F. T. Stepto and B. E. Eichinger, in J. E. Mark and B. Erman, eds., *Elastomeric Polymer Networks*, Prentice-Hall, Englewood Cliffs, NJ, 1992.
42. I. Bahar, B. Erman, and B. Baysal, *Macromolecules* **19**, 1703 (1986).
43. B. Erman and B. Baysal, *Macromolecules* **18**, 1696 (1985).
44. G. Holden, N. R. Legge, R. Quirk, and H. E. Schroeder, eds., *Thermoplastic Elastomers*, Hanser Publishers, Munich, W. Germany, 1996.
45. R. M. Johnson and J. E. Mark, *Macromolecules* **5**, 41–45 (1972).

46. A. Greene, K. J. Smith, Jr., and A. Ciferri, *Trans. Faraday Soc.* **61**, 2772 (1965).
47. J. Premachandra, C. Kumudinie, and J. E. Mark, *J. Macromol. Sci., Pure Appl. Chem.* **39**, 301–320 (2002).
48. K. Urayama and S. Kohjiya, *Eur. Phys. J. B* **2**, 75–78 (1998).
49. A. M. Kushner, V. Gabuchian, E. G. Johnson, and Z. Guan, *J. Am. Chem. Soc.* **129**, 14110–14111 (2007).
50. C. M. Roland and M. L. Warzel, *Rubber Chem. Technol.* **63**, 285–297 (1990).
51. P. G. Santangelo and C. M. Roland, *Rubber Chem. Technol.* **76**, 892–898 (2003).
52. P. G. Santangelo and C. M. Roland, *Rubber Chem. Technol.* **68**, 124–131 (1995).
53. P. J. Flory, *Trans. Faraday Soc.* **56**, 722–743 (1960).
54. S. Kaang, D. Gong, and C. Nah, *J. Appl. Polym. Sci.* **66**, 917–924 (1997).
55. P. H. Mott and C. M. Roland, *Macromolecules* **33**, 4132–4137 (2000).
56. J. Wang, G. R. Hamed, K. Umetsu, and C. M. Roland, *Rubber Chem. Technol.* **78**, 76–83 (2005).
57. L. H. Sperling, *Interpenetrating Polymer Networks and Related Materials*, Plenum Press, New York, 1981.
58. J. E. Mark and Y.-P. Ning, *Polym. Eng. Sci.* **25**, 824–827 (1985).
59. S. H. Yoo, C. Cohen, and C.-Y. Hui, *Polymer* **47**, 6226–6235 (2006).
60. H. W. Gibson, M. C. Bheda, and P. T. Engen, *Prog. Polym. Sci.* **19**, 843–945 (1994).
61. J.-P. Sauvage and C. Dietrich-Buchecker, eds. *Molecular Catenanes, Rotaxanes and Knots*, Wiley-VCH, Weinheim, Germany, 1999.
62. Y. Okumura and K. Ito, *Adv. Mater.* **13**, 485–487 (2001).
63. T. Karino, Y. Okumura, K. Ito, and M. Shibayama, *Macromolecules* **37**, 6177–6182 (2004).
64. S. Granick and M. Rubinstein, *Nature Materials* **63**, 586–587 (2004).
65. G. Fleury, G. Schlatter, C. Brochon, and G. Hadziioannou, *Polymer* **46**, 8494–8501 (2005).
66. K. Ito, *Polym. J.* **39**, 489–499 (2007).
67. W. W. Graessley and D. S. Pearson, *J. Chem. Phys.* **66**, 3363–3370 (1977).
68. P.-G. de Gennes, *Physica A* **271**, 231–237 (1999).
69. J. P. Gong, Y. Katsuyama, T. Kurokawa, and Y. Osada, *Adv. Mater.* **15**, 1155–1158 (2003).
70. J. P. Gong, *Soft Matter* **2**, 544–552 (2006).
71. T. Tominaga, V. R. Tirumala, E. K. Lin, J. P. Gong, H. Furukawa, Y. Osada, and W.-L. Wu, *Polymer* **48**, 7449–7454 (2007).
72. M. Huang, H. Furukawa, Y. Tanaka, T. Nakajima, Y. Osada, and J. P. Gong, *Macromolecules* **40**, 6658–6664 (2007).
73. R. E. Webber, C. Creton, H. R. Brown, and J. P. Gong, *Macromolecules* **40**, 2919–2927 (2007).
74. D. Kaneko, T. Tada, T. Kurokawa, J. P. Gong, and Y. Osada, *Adv. Mater.* **17**, 535–538 (2005).
75. S. S. Jang, W. A. Goddard, III, M. Yashaar, and S. Kalani, *J. Phys. Chem. B* **111**, 1729–1737 (2007).
76. S. S. Jang, W. A. Goddard, III, M. Yashaar, S. Kalani, D. Myung, and C. W. Frank, *J. Phys. Chem. B* **111**, 14440–14440 (2007).
77. H. R. Brown, *Macromolecules* **40**, 3815–3818 (2007).
78. K. Haraguchi and H.-J. Li, *Macromolecules* **39**, 1898–1903 (2006).
79. K. Haraguchi and T. Takehisa, *Adv. Mater.* **14**, 1120–1124 (2002).
80. K. Haraguchi, *Macromol. Symp.* **256**, 120–130 (2007).
81. M. Shibayama, S. Miyazaki, H. Endo, T. Karino, and K. Haraguchi, *Macromol. Symp.* **256**, 131–136 (2007).
82. P. J. Flory, *Proc. R. Soc. London A* **351**, 351 (1976).

83. J. E. Mark, *Acct. Chem. Res.* **37**, 946–953 (2004).
84. J. E. Mark, *Macromol. Symp.*, St. Petersburg issue **191**, 121–130 (2003).
85. J. E. Mark, H. R. Allcock, and R. West, *Inorganic Polymers*, 2nd ed., Oxford University Press, New York, 2005.
86. J. E. Mark, *Rubber Chem. Technol.* **72**, 465–483 (1999).
87. T. Madkour and J. E. Mark, *J. Macromol. Sci., Macromol. Reports A* **31**, 153–160 (1994).
88. G. T. Burns, unpublished results, Dow Corning Corporation (1995).
89. B. Erman and J. E. Mark, *Macromolecules* **31**, 3099–3103 (1998).
90. J. E. Mark, R. R. Rahalkar, and J. L. Sullivan, *J. Chem. Phys.* **70**, 1794 (1979).
91. J. E. Mark, in J. E. Mark, A. Eisenberg, W. W. Graessley, L. Mandelkern, E. T. Samulski, J. L. Koenig, and G. D. Wignall, eds., *Physical Properties of Polymers*, American Chemical Society, Washington, DC, 1993, pp. 3.
92. N. R. Langley, *Macromolecules* **1**, 348 (1968).
93. W. W. Graessley, *Adv. Polym. Sci.* **16**, 1 (1974).
94. W. W. Graessley, *Adv. Polym. Sci.* **47**, 67 (1982).
95. G. Heinrich, E. Straube, and G. Helmis, *Adv. Polym. Sci.* **85**, 33 (1988).
96. B. E. Eichinger and O. Akgiray, in E. A. Colbourne, ed., *Computer Simulation of Polymers*, Longman, White Plains, NY, 1994, pp. 263–302.
97. M. A. Sharaf and J. E. Mark, *J. Polym. Sci., Polym. Phys. Ed.* **33**, 1151 (1995).
98. S. Venkatraman, *J. Appl. Polym. Sci.* **48**, 1383 (1993).
99. W. W. Graessley, *Polymeric Liquids and Networks. Structure and Properties*, Garland Science, New York, 2003.
100. J. E. Mark, in J. M. Zeigler and F. W. G. Fearon, eds., *Silicon-Based Polymer Science. A Comprehensive Resource*, American Chemical Society, Washington, DC, 1990, Vol. **224**, pp. 47–68.
101. A. L. Andradý, M. A. Llorente, M. A. Sharaf, R. R. Rahalkar, J. E. Mark, J. L. Sullivan, C. U. Yu, and J. R. Falender, *J. Appl. Polym. Sci.* **26**, 1829–1836 (1981).
102. S. J. Clarson, J. E. Mark, and J. A. Semlyen, *Polym. Commun.* **28**, 151–153 (1987).
103. L. C. DeBolt and J. E. Mark, *Macromolecules* **20**, 2369–2374 (1987).
104. W. Huang, H. L. Frisch, Y. Hua, and J. A. Semlyen, *J. Polym. Sci., Polym. Chem. Ed.* **26**, 1807 (1990).
105. Z. Rigbi and J. E. Mark, *J. Polym. Sci., Polym. Phys. Ed.* **24**, 443–449 (1986).
106. P. G. de Gennes, *Scaling Concepts in Polymer Physics*, Cornell University Press, Ithaca, NY, 1979.
107. L. Garrido, J. E. Mark, S. J. Clarson, and J. A. Semlyen, *Polym. Commun.* **26**, 53–55 (1985).
108. K. Iwata and T. Ohtsuki, *J. Polym. Sci., Polym. Phys. Ed.* **31**, 441 (1993).
109. J. E. Mark, *J. Chem. Educ.* **58**, 898 (1981).
110. J. E. Mark, A. Eisenberg, W. W. Graessley, L. Mandelkern, E. T. Samulski, J. L. Koenig, and G. D. Wignall, *Physical Properties of Polymers*, 2nd ed., American Chemical Society, Washington, DC, 1993.
111. L. Mandelkern, *Crystallization of Polymers*, Cambridge University Press, Cambridge, UK, 2003.
112. J. E. Mark, A. Eisenberg, W. W. Graessley, L. Mandelkern, and J. L. Koenig, *Physical Properties of Polymers*, 1st ed., American Chemical Society, Washington, DC, 1984.
113. T.-K. Su and J. E. Mark, *Macromolecules* **10**, 120–125 (1977).
114. D. S. Chiu and J. E. Mark, *Coll. Polym. Sci.* **225**, 644 (1977).
115. F. Bueche, *Physical Properties of Polymers*, Wiley-Interscience, New York, 1962.
116. J. E. Mark, *Makromol. Chem. Suppl.* **2**, 87 (1979).
117. M. A. Llorente, A. L. Andradý, and J. E. Mark, *J. Polym. Sci., Polym. Phys. Ed.* **19**, 621 (1981).

118. J. E. Mark and B. Erman, *Rubberlike Elasticity. A Molecular Primer*, Wiley-Interscience, New York, 1988.
119. A. Baumgartner and C. E. Picot, eds., *Molecular Basis of Polymer Networks, Springer Proceedings in Physics*, Vol. 42, Springer-Verlag, Berlin, 1989.
120. J. E. Mark and B. Erman, eds., *Elastomeric Polymer Networks*, Prentice-Hall, Englewood Cliffs, NJ, 1992.
121. *Polymer Networks*, Preprints, San Diego '92, edited by B. E. Eichinger (1993), Vol. 76.
122. J. E. Mark, B. Erman, and F. R. Eirich, eds., *Science and Technology of Rubber*, Academic Press, New York, 1994.
123. W. Brostow, J. Kubat, and M. M. Kubat, in J. E. Mark, ed., *Physical Properties of Polymers Handbook*, Springer-Verlag, New York, 1996, pp. 313–334.
124. A. N. Gent and T. H. Kuan, *J. Polym. Sci., Polym. Phys. Ed.* **11**, 1723–1733 (1973).
125. A. N. Gent and T. H. Kuan, *J. Polym. Sci., Polym. Phys. Ed.* **12**, 633–634 (1974).
126. M. A. Mohsin, J. P. Berry, and L. R. G. Treloar, *Brit. Polym. J.* **18**, 145–150 (1986).
127. M. A. Mohsin and L. R. G. Treloar, *Polymer* **28**, 1893–1898 (1987).
128. P. Xu and J. E. Mark, *Rubber Chem. Technol.* **63**, 276–284 (1990).
129. P. Xu and J. E. Mark, *J. Polym. Sci., Polym. Phys. Ed.* **29**, 355–358 (1991).
130. P. Xu and J. E. Mark, *Makromol. Chem.* **192**, 567–578 (1991).
131. S. Wang, P. Xu, and J. E. Mark, *Rubber Chem. Technol.* **64**, 746–759 (1991).
132. P. Xu and J. E. Mark, *Polymer* **33**, 1843–1848 (1992).
133. J. E. Mark, S. Wang, P. Xu, and J. Wen, in R. H. Baney, L. R. Gilliom, S.-I. Hirano, and H. K. Schmidt, eds., *Submicron Multiphase Materials*, Materials Research Society, Pittsburgh, PA, 1992, Vol. 274, pp. 77–84.
134. J. Wen and J. E. Mark, *Polym. J.* **26**, 151–157 (1994).
135. M. Mooney, *J. Appl. Phys.* **11**, 582 (1940).
136. M. Mooney, *J. Appl. Phys.* **19**, 434 (1948).
137. R. S. Rivlin, *Philos. Trans. R. Soc., A* **240**, 459 (1948).
138. R. S. Rivlin, *Philos. Trans. R. Soc., A* **240**, 491 (1948).
139. R. S. Rivlin, *Philos. Trans. R. Soc., A* **240**, 509 (1948).
140. R. S. Rivlin, *Philos. Trans. R. Soc., A* **241**, 379 (1948).
141. J. E. Mark and B. Erman, in W. Brostow, ed., *Performance of Plastics*, Hanser, Cincinnati, OH, 2001, pp. 401–428.
142. Y. Obata, S. Kawabata, and H. Kawai, *J. Polym. Sci., Part A-2* **8**, 903–919 (1970).
143. S. Wang and J. E. Mark, *J. Polym. Sci., Polym. Phys. Ed.* **30**, 801–807 (1992).
144. L. C. Yanyo and F. N. Kelley, *Rubber Chem. Technol.* **60**, 78–88 (1987).
145. T. L. Smith, B. Haidar, and J. L. Hedrick, *Rubber Chem. Technol.* **63**, 256–264 (1990).
146. G. B. Shah, *Macromol. Chem. Phys.* **197**, 2201–2208 (1996).
147. G. B. Shah, *J. Appl. Polym. Sci.* **94**, 1719–1722 (2004).
148. A. L. Andradý, M. A. Llorente, and J. E. Mark, *Polym. Bull.* **26**, 357 (1991).
149. J. Wen, J. E. Mark, and J. J. Fitzgerald, *J. Macromol. Sci., Macromol. Rep. A* **31**, 429–438 (1994).
150. Y. Kaneko, Y. Watanabe, T. Okamoto, Y. Iseda, and T. Matsunaga, *J. Appl. Polym. Sci.* **25**, 2467–2478 (1980).
151. J. Mazan, B. Leclerc, N. Galandrin, and G. Couarraze, *Eur. Polym. J.* **31**, 803–807 (1995).
152. T. Tanaka, *Phys. Rev. Lett.* **40**, 820 (1978).
153. T. Tanaka, *Sci. Am.* **244** (1), 124 (1981).
154. J. E. Mark, *J. Appl. Polym. Sci., Symp.* **44**, 209–216 (1989).
155. C. U. Yu and J. E. Mark, *Macromolecules* **7**, 229–232 (1974).
156. V. Galiatsatos and J. E. Mark, *Polym. Bull.* **17**, 197 (1987).
157. V. Galiatsatos and J. E. Mark, *Macromolecules* **20**, 2631 (1987).



158. V. Galiatsatos and J. E. Mark, in J. M. Zeigler and F. W. G. Fearon, eds., *Advances in Silicon-Based Polymer Science. A Comprehensive Resource*, Vol. 224. American Chemical Society, Washington, DC, 1990.
159. V. Galiatsatos, R. O. Neaffer, S. Sen, and B. J. Sherman, in J. E. Mark, ed., *Physical Properties of Polymers Handbook*, Springer-Verlag, New York, 1996, pp. 535–543.
160. E. Riande and E. Saiz, *Dipole Moments and Birefringence of Polymers*, Prentice-Hall, Englewood Cliffs, NJ, 1992.
161. L. Monnerie, *Faraday Symp. Chem. Soc.* **18**, 1 (1983).
162. J. P. Queslel, B. Erman, and L. Monnerie, *Macromolecules* **18**, 1991 (1985).
163. H. W. Spiess, *Angew. Makromol. Chem.* **202/302**, 133 (1992).
164. P. Jezzard, C. J. Wiggins, T. A. Carpenter, L. D. Hall, P. Jackson, N. J. Clayden, and N. J. Walton, *Adv. Mater.* **4**, 82 (1992).
165. A. E. Tonelli, in J. E. Mark, ed., *Physical Properties of Polymers Handbook*, Springer-Verlag, New York, 1996, pp. 271–289.
166. I. Noda, A. E. Dowrey, and C. Marcott, *Macromol. Symp.* **72**, 121 (1993).
167. I. Noda, A. E. Dowrey, and C. Marcott, *Polym. News* **18**, 167 (1993).
168. I. Noda, A. E. Dowrey, and C. Marcott, in J. E. Mark, ed., *Physical Properties of Polymers Handbook*, Springer-Verlag, New York, 1996, pp. 291–298.
169. J. S. Higgins and H. Benoit, *Neutron Scattering from Polymers*, Clarendon Press, Oxford, UK, 1994.
170. G. D. Wignall, in J. E. Mark, ed., *Physical Properties of Polymers Handbook*, Springer-Verlag New York, Inc., New York, 1996, pp. 299–310.
171. G. D. Wignall, in J. E. Mark, ed., *Physical Properties of Polymers Handbook*, 2nd ed., Springer-Verlag New York, Inc., New York, 2007, pp. 407–420.
172. M. R. Landry, B. K. Coltrain, C. J. T. Landry, and J. M. O'Reilly, *J. Polym. Sci., Polym. Phys. Ed.* **33**, 637–655 (1995).
173. D. W. Schaefer and C. Chen, *Rubber Chem. Technol.* **75**, 773–793 (2002).
174. H. B. Callen, *Thermodynamics and an Introduction to Thermostatistics*, Wiley, New York, 2000.
175. W. Kuhn, *J. Polym. Sci.* **1**, 380 (1946).
176. F. T. Wall and P. J. Flory, *J. Chem. Phys.* **19**, 1435–1439 (1951).
177. G. Ronca and G. Allegra, *J. Chem. Phys.* **63**, 4990 (1975).
178. P. J. Flory, *J. Phys. Chem.* **66**, 5720–5729 (1977).
179. P. J. Flory, in E. M. Pearce and J. R. Schaefgen, eds., *Contemporary Topics in Polymer Chemistry*, Plenum Press, New York, 1977, Vol. 2.
180. P. J. Flory, *Polymer* **20**, 1317 (1979).
181. P. J. Flory, *Polym. J.* **17**, 1–12 (1985).
182. P. J. Flory and B. Erman, *Macromolecules* **15**, 800 (1982).
183. R. Oeser, B. Ewen, D. Richter, and B. Farago, *Phys. Rev. Lett.* **60**, 1041 (1988).
184. B. Ewen and D. Richter, in A. Baumgartner and C. E. Picot, eds., *Molecular Basis of Polymer Networks*, 1989, Vol. 42, pp. 82.
185. B. Ewen and D. Richter, in J. E. Mark and B. Erman, eds., *Elastomeric Polymer Networks*, Prentice-Hall, Englewood Cliffs, NJ, 1992, pp. 220–234.
186. E. Guth and H. M. James, *Ind. Eng. Chem.* **33**, 624 (1941).
187. H. M. James and E. Guth, *Ind. Eng. Chem.* **34**, 1365 (1942).
188. H. M. James, *J. Chem. Phys.* **15**, 651 (1947).
189. H. M. James and E. Guth, *J. Chem. Phys.* **15**, 669 (1947).
190. H. M. James and E. Guth, *J. Chem. Phys.* **21**, 1039 (1953).
191. J. A. Duiser and A. J. Staverman, in J. A. Prins, ed., *Physics of Non-Crystalline Solids*, North-Holland, Amsterdam, 1965.
192. B. E. Eichinger, *Macromolecules* **5**, 496–505 (1972).
193. W. W. Graessley, *Macromolecules* **8**, 186 (1975).

194. W. W. Graessley, *Macromolecules* **8**, 865 (1975).
195. D. S. Pearson, *Macromolecules* **10**, 696 (1977).
196. A. Kloczkowski, J. E. Mark, and B. Erman, *Macromolecules* **22**, 1423–1432 (1989).
197. B. Erman, A. Kloczkowski, and J. E. Mark, *Macromolecules* **22**, 1432–1437 (1989).
198. K. Nagai, *J. Chem. Phys.* **39**, 924 (1963).
199. J. P. Queslel and J. E. Mark, in R. A. Meyers, ed., *Encyclopedia of Polymer Science and Engineering*, 2nd edition, Wiley-Interscience, New York, 1986, pp. 365.
200. B. Erman and P. J. Flory, *Macromolecules* **15**, 806 (1982).
201. B. Erman and P. J. Flory, *Macromolecules* **16**, 1601 (1983).
202. B. Erman and P. J. Flory, *Macromolecules* **16**, 1607 (1983).
203. B. Erman and L. Monnerie, *Macromolecules* **18**, 1985 (1985).
204. B. Erman, *J. Polym. Sci., Polym. Phys. Ed.* **19**, 829 (1981).
205. B. Erman and L. Monnerie, *Macromolecules* **22**, 3342–3348 (1989).
206. F. Fontaine, C. Noel, L. Monnerie, and B. Erman, *Macromolecules* **22**, 3352 (1989).
207. B. Erman and L. Monnerie, *Macromolecules* **25**, 4456 (1992).
208. A. Kloczkowski, J. E. Mark, and B. Erman, *Macromolecules* **28**, 5089–5096 (1995).
209. A. Kloczkowski, J. E. Mark, and B. Erman, *Comput. Polym. Sci.* **5**, 37–45 (1995).
210. B. Erman and J. E. Mark, in J. E. Mark, B. Erman, and F. R. Eirich, eds., *Science and Technology of Rubber*, Academic Press, San Diego, CA, 1994, pp. 189–210.
211. K. Freed, *J. Chem. Phys.* **55**, 5588 (1971).
212. S. F. Edwards, *J. Phys. A, Gen Phys.* **1**, 15 (1968).
213. S. F. Edwards and K. F. Freed, *J. Phys. C* **3**, 739, 750, 760 (1970).
214. S. F. Edwards, in A. J. Chompff and S. Newman, eds., *Polymer Networks: Structural and Mechanical Properties*, Plenum Press, New York, 1971.
215. S. F. Edwards, *Brit. Polym. J.* **3**, 140 (1971).
216. R. T. Deam and S. F. Edwards, *Philos. Trans. R. Soc. London, A* **280**, 317 (1976).
217. S. F. Edwards, *Proc. Phys. Soc. (London)* **92**, 9 (1967).
218. M. Rubinstein and S. V. Panyukov, *Macromolecules* **30**, 8036 (1997).
219. R. C. Ball, M. Doi, and S. F. Edwards, *Polymer* **22**, 1010 (1981).
220. S. F. Edwards and T. A. Vilgis, *Polymer* **27**, 483 (1986).
221. S. F. Edwards and T. A. Vilgis, *Rep. Prog. Phys.* **51**, 243 (1988).
222. T. A. Vilgis and B. Erman, *Macromolecules* **26**, 6657 (1993).
223. M. Rubinstein and S. Panyukov, *Macromolecules* **35**, 6670–6686 (2002).
224. P. J. Flory, *Statistical Mechanics of Chain Molecules*, Interscience, New York, 1969.
225. L. C. DeBolt and J. E. Mark, *Polymer* **28**, 416 (1987).
226. J. E. Mark and J. G. Curro, *J. Chem. Phys.* **79**, 5705–5709 (1983).
227. J. E. Mark and J. G. Curro, *J. Chem. Phys.* **80**, 5262–5265 (1984).
228. J. E. Mark and J. G. Curro, *J. Chem. Phys.* **81**, 6408 (1984).
229. J. E. Mark and J. G. Curro, *J. Polym. Sci., Polym. Phys. Ed.* **23**, 2629 (1985).
230. J. G. Curro and J. E. Mark, *J. Chem. Phys.* **82**, 3820 (1985).
231. J. G. Curro, K. S. Schweizer, D. Adolf, and J. E. Mark, *Macromolecules* **19**, 1739 (1986).
232. L. C. DeBolt and J. E. Mark, *J. Polym. Sci., Polym. Phys. Ed.* **26**, 865–874 (1988).
233. J. G. Curro and J. E. Mark, *J. Chem. Phys.* **80**, 4521–4525 (1984).
234. P. Cifra and T. Bleha, *J. Chem. Soc., Faraday Trans.* **91**, 2465 (1995).
235. J. Gao and J. H. Weiner, *Macromolecules* **27**, 1201 (1994).
236. E. R. Duering, K. Kremer, and G. S. Grest, *J. Chem. Phys.* **101**, 8169–8192 (1994).
237. K. Kremer and G. S. Grest, *J. Chem. Soc., Faraday Trans.* **88**, 1707 (1992).
238. R. Everaers and K. Kremer, *Macromolecules* **28**, 7291 (1995).
239. R. Everaers and K. Kremer, *Phys. Rev. E* **53**, R37–R40 (1996).
240. R. Everaers and K. Kremer, *Macromolecules* **28**, 7291–7294 (1996).

- 241. R. W. Ogden, in H. G. Hopkins and M. J. Sewell, eds., *Mechanics of Solids*, Vol. 28, Academic Press, New York, 1982, pp. 499.
- 242. R. W. Ogden, *Rubber Chem. Technol.* **59**, 361 (1986).
- 243. R. W. Ogden, *Polymer* **28**, 379 (1987).
- 244. A. R. Khokhlov, in K. Dusek, ed., *Responsive Gels: Volume Transitions I.*, Springer-Verlag, Berlin, 1992, p. 125.
- 245. O. E. Philippova, T. G. Pieper, N. L. Sitnikova, S. G. Starodoubtsev, A. R. Khokhlov, and H. G. Kilian, *Macromolecules* **28**, 3925 (1995).
- 246. A. R. Khokhlov and O. E. Philippova, in S. E. Webber, P. Munk, Z. Tuzar, eds., *Solvents and Self-Organization of Polymers*, Kluwer Academic Publishers, Dordrecht, The Netherlands, 1996, p. 197.
- 247. A. R. Khokhlov and O. E. Philippova, in Y. Osada and A. R. Khokhlov, eds., *Polymer Gels and Networks*, Marcel Dekker, New York, 2002, p. 163.
- 248. G. Nisato and S. J. Candau, in Y. Osada and A. R. Khokhlov, eds., *Polymer Gels and Networks*, Marcel Dekker, New York, 2002, p. 131.
- 249. H. Pak and P. J. Flory, *J. Polym. Sci., Polym. Phys. Ed.* **17**, 1845–1854 (1979).
- 250. M. Gottlieb and R. J. Gaylord, *Polymer* **24**, 1644 (1983).
- 251. R. W. Brotzman and J. E. Mark, *Macromolecules* **19**, 667 (1986).
- 252. M. G. Brereton and P. G. Klein, *Polymer* **29**, 970 (1988).
- 253. B. E. Eichinger, *Ann. Rev. Phys. Chem.* **34**, 359 (1983).
- 254. J. E. Mark, *Polym. Eng. Sci.* **19**, 409–413 (1979).
- 255. Z. Tan, R. Jaeger, and G. J. Vancso, *Polymer* **35**, 3230 (1994).
- 256. M. Gottlieb and R. J. Gaylord, *Macromolecules* **17**, 2024 (1984).
- 257. N. A. Neuberger and B. E. Eichinger, *Macromolecules* **21**, 3060 (1988).
- 258. G. B. McKenna and J. M. Crissman, in J. Kahovec, ed., *Macromolecules 92*, VSP, Utrecht, The Netherlands, 1993, p. 67.
- 259. F. Horkay and G. B. McKenna, in J. E. Mark, ed., *Physical Properties of Polymers Handbook*, Springer-Verlag, Berlin, 1996, pp. 379–398.
- 260. A. Dubault, B. Deloche, and J. Herz, *Macromolecules* **20**, 2096 (1987).
- 261. B. Erman and J. E. Mark, *Macromolecules* **22**, 480 (1989).
- 262. B. Erman, *Macromolecules* **20**, 1917 (1987).
- 263. A. M. Donald and A. H. Windle, *Liquid-Crystalline Polymers*, Cambridge University Press, Cambridge, UK, 1992.
- 264. D. Kramer and H. Finkelmann, *Macromol. Rapid Commun.* **28**, 2318–2324 (2007).
- 265. P. Beyer, E. M. Terentjev, and R. Zentel, *Macromol. Rapid Commun.* **28**, 1485–1490 (2007).
- 266. Y. K. Godovsky and L. A. Valetskaya, *Polym. Bull.* **27**, 221–226 (1991).
- 267. Y. K. Godovsky, N. N. Makarova, V. S. Papkov, and N. N. Kuzmin, *Makromol. Chem.* **6**, 443–450 (1985).
- 268. Y. K. Godovsky, S. I. Belousov, N. N. Makarova, G. Brezesinski, H. Mohwald, T. R. Jensen, and K. Kjaer, *Nonlinear Opt. Quantum Opt.* **31**, 31–44 (2004).
- 269. M. Kojima, J. H. Magill, U. Franz, M. L. White, and K. Matyjaszewski, *Makromol. Chem. Phys.* **196**, 1739–1749 (1995).
- 270. V. S. Papkov, A. A. Turetskii, G. J. J. Out, and M. Moller, *Int. J. Polym. Matet.* **51**, 369–391 (2002).
- 271. R. Zentel and M. Benalia, *Makromol. Chem.* **188**, 665–674 (1987).
- 272. H. Finkelmann, H.-J. Kock, W. Gleim, and G. Rehage, *Makromol. Rapid Commun.* **5**, 287–293 (1984).
- 273. W. Kaufhold, H. Finkelmann, and H. R. Brand, *Makromol. Chem.* **192**, 2555–2579 (1991).
- 274. R. V. Talroze, T. I. Gubina, V. P. Shibaev, and N. A. Plate, *Makromol. Rapid Commun.* **11**, 67–71 (1990).

275. D. K. Shenoy, D. L. Thomsen, P. Keller, and B. R. Ratna, *J. Phys. Chem.* **107**, 13755–13757 (2003).
276. K. Semmler and H. Finkelmann, *Makromol. Chem. Phys.* **196**, 3197–3208 (1995).
277. J. H. Wendorff, *Angew. Chem., Int. Ed. Eng.* **30**, 405–406 (1991).
278. M. Warner and E. M. Terentjev, *Macromol. Symp.* **200**, 81–92 (2003).
279. B. Erman, I. Bahar, A. Kloczkowski, and J. E. Mark, *Macromolecules* **23**, 5335 (1990).
280. M. Warner and E. M. Terentjev, *Liquid Crystal Elastomers*, Oxford University Press, New York, 2003.
281. R. Ross and P. Bornstein, *Sci. Am.* **224**, 44–50 (1971).
282. C. A. J. Hoeve and P. J. Flory, *Biopolymers* **13**, 677–686 (1974).
283. L. B. Sandberg, W. R. Gray, and C. Franzblau, eds., *Elastin and Elastic Tissue*, Plenum Press, New York, 1977.
284. A. L. Andradý and J. E. Mark, *Biopolymers* **19**, 849–855 (1980).
285. J. M. Gosline, in J. F. V. Vincent and J. D. Currey, eds., *The Mechanical Properties of Biological Materials*, Cambridge University Press, Cambridge, UK, 1980, pp. 331–357.
286. M. Jensen and T. Weis-Fogh, *Philos. Trans. R. Soc. London, B.* **245**, 137 (1962).
287. J. Donnet and E. Custodero, in J. E. Mark and B. Erman, eds., *Science and Technology of Rubber*, Elsevier, Amsterdam, 2005, pp. 367–400.
288. E. L. Warrick, O. R. Pierce, K. E. Polmanteer, and J. C. Saam, *Rubber Chem. Technol.* **52**, 437–525 (1979).
289. B. Rodgers, ed., *Rubber Compounding. Chemistry and Applications*, Marcel Dekker, Inc., New York, 2004.
290. A. I. Nakatani, R. J. Hjelm, M. Gerspacher, and R. Krishnamoorti, eds., *Filled and Nanocomposite Polymer Materials*, Materials Research Society, Warrendale, PA, 2001, Vol. 661.
291. G. Kickelbick, in G. Kickelbick, ed., *Hybrid Materials. Synthesis, Characterization, and Applications*, Wiley-VCH Verlag, Weinheim, Germany, 2007, pp. 1–48.
292. J. E. Mark, *Acc. Chem. Res.* **39**, 881–888 (2006).
293. Z. Ahmad, S. Wang, and J. E. Mark, in A. K. Cheetham, C. J. Brinker, M. L. Mecartney, and C. Sanchez, eds., *Better Ceramics Through Chemistry VI*, Materials Research Society, Pittsburgh, 1994, Vol. 346, p. 127.
294. B. M. Novak, *Adv. Mater.* **5**, 422–433 (1993).
295. C.-Y. Jiang and J. E. Mark, *Makromol. Chem.* **185**, 2609 (1984).
296. K. D. Keefer, in J. M. Zeigler and F. W. G. Fearon, eds., *Silicon-Based Polymer Science. A Comprehensive Resource*, American Chemical Society, Washington, DC, 1990, Vol. 224, pp. 227–240.
297. J. E. Mark and Y.-P. Ning, *Polym. Bull.* **12**, 413–417 (1984).
298. S.-B. Wang and J. E. Mark, *Polym. Bull.* **17**, 271–277 (1987).
299. G. B. Sohoni and J. E. Mark, *J. Appl. Polym. Sci.* **45**, 1763 (1992).
300. M. I. Aranguren, *Polymer* **39**, 4897–4903 (1998).
301. G. D. Wignall, in J. E. Mark, K. L. Ngai, W. W. Graessley, L. Mandelkern, E. T. Samulski, J. L. Koenig, and G. D. Wignall, eds., *Physical Properties of Polymers*, 3rd ed., Cambridge University Press, Cambridge, UK, 2004, pp. 424–511.
302. D. W. Schaefer, J. E. Mark, D. W. McCarthy, L. Jian, C.-C. Sun, and B. Farago, in D. W. Schaefer and J. E. Mark, eds., *Polymer-Based Molecular Composites*, Materials Research Society, Pittsburgh, 1990, Vol. 171, pp. 57–63.
303. D. W. Schaefer, B. T. N. Vu, and J. E. Mark, *Rubber Chem. Technol.* **75**, 795–810 (2002).
304. B. T. N. Vu, J. E. Mark, and D. W. Schaefer, *Compos. Interfaces* **10**, 451–473 (2003).
305. S. V. Patwardhan, V. P. Taori, M. Hassan, N. R. Agashe, J. E. Franklin, G. Beaucage, J. E. Mark, and S. J. Clarson, *Eur. Polym. J.* **42**, 167–178 (2006).

306. J. D. Lichtenhan, J. Schwab, and W. A. Reinert, Sr., *Chem. Innov.* **31**, 3–5 (2001).
307. R. M. Laine, J. Choi, and I. Lee, *Adv. Mater.* **13**, 800–803 (2001).
308. D. A. Loy, C. R. Baugher, D. A. Schnieder, A. Sanchez, and F. Gonzalez, *Polym. Preprints* **42**, 180–181 (2001).
309. T. S. Haddad, A. Lee, and S. H. Phillips, *Polym. Preprints* **42**, 88–89 (2001).
310. G. Pan, in J. E. Mark, ed., *Physical Properties of Polymers Handbook*, Springer-Verlag, New York, 2006.
311. H. L. Frisch and J. E. Mark, *Chem. Mater.* **8**, 1735–1738 (1996).
312. J. E. Mark, in J.-P. Sauvage and C. Dietrich-Buchecker, eds., *Molecular Catenanes, Rotaxanes and Knots*, Wiley-VCH, Weinheim, Germany, 1999, pp. 223–246.
313. G. Kickelbick, *Prog. Polym. Sci.* **28**, 83–114 (2003).
314. G. S. Sur, H. Sun, T. J. Lee, S. G. Lyu, and J. E. Mark, *Coll. Polym. Sci.* **281**, 1040–1045 (2003).
315. H. Okumura, M. Okada, Y. Kawaguchi, and A. Harada, *Macromolecules* **33**, 4297–4298 (2000).
316. E. P. Giannelis, R. Krishnamoorti, and E. Manias, *Adv. Polym. Sci.* **138**, 107–147 (1999).
317. R. A. Vaia and E. P. Giannelis, *MRS Bull.* **26** (5), 394–401 (2001).
318. T. J. Pinnavaia and G. Beall, eds., *Polymer-Clay Nanocomposites*, Wiley, New York, 2001.
319. Y. T. Vu, J. E. Mark, L. H. Pham, and M. Engelhardt, *J. Appl. Polym. Sci.* **82**, 1391–1403 (2001).
320. W. Zhou, J. E. Mark, M. R. Unroe, and F. E. Arnold, *J. Macromol. Sci.—Pure Appl. Chem. A* **38**, 1–9 (2001).
321. Q. Q. Deng, J. R. Hahn, J. Stasser, J. D. Preston, and G. T. Burns, *Rubber Chem. Technol.* **73**, 647–665 (2000).
322. D. Kohls, G. Beaucage, S. E. Pratsinis, H. Kammler, and G. Skillas, in R. J. Hjelm, A. I. Nakatani, M. Gerspacher, and R. Krishnamoorti, eds., *Filled and Nanocomposite Polymer Materials*, Materials Research Society, Warrendale, PA, 2001, Vol. 661.
323. P. Espiard, A. Guyot, and J. E. Mark, *J. Inorg. Organomet. Polym.* **5**, 391–407 (1995).
324. J.-L. Luna-Xavier, E. Bourgeat-Lami, and A. Guyot, *Coll. Polym. Sci.* **279**, 947–958 (2001).
325. F.-S. Fu and J. E. Mark, *J. Appl. Polym. Sci.* **37**, 2757–2768 (1989).
326. J. E. Mark, ed., *Physical Properties of Polymers Handbook*, Springer-Verlag, New York, 2007.
327. S. Wang and J. E. Mark, *Macromolecules* **23**, 4288–4291 (1990).
328. C. C. Ho, M. J. Hill, and J. A. Odell, *Polymer* **34**, 2019 (1993).
329. S. Wang, P. Xu, and J. E. Mark, *Macromolecules* **24**, 6037–6039 (1991).
330. M. A. Sharaf and J. E. Mark, *Polymer* **45**, 3943–3952 (2004).
331. J. Pyun, K. Matyjaszewski, T. Kowalewski, P. T. Mather, and S. B. Chun, Abstracts, Chicago Am. Chem. Soc. Meeting (2001).
332. J. Choi, J. Harcup, A. F. Yee, Q. Zhu, and R. M. Laine, *J. Am. Chem. Soc.* **123**, 11420–11430 (2001).
333. R. Tamaki, J. Choi, and R. M. Laine, *Chem. Mater.* **15**, 793–797 (2003).
334. Z. Rigbi and J. E. Mark, *J. Polym. Sci., Polym. Phys. Ed.* **23**, 1267–1269 (1985).
335. G. B. Sohoni and J. E. Mark, *J. Appl. Polym. Sci.* **34**, 2853–2859 (1987).
336. P. Calvert and A. Broad, in K. L. Mittal, ed., *Polymers in Information Storage Technology*, Plenum Press, New York, 1991, pp. 257–272.
337. J. E. Mark, Preprints, 2001 International Conference on Computational Nanoscience, Hilton Head Island, SC, 2001.
338. J. E. Mark, *Makromol. Symp.* **171**, 1–9 (2001).

339. J. E. Mark, R. Abou-Hussein, T. Z. Sen, and A. Kloczkowski, *Polymer* **46**, 8894–8904 (2005).
340. M. A. Sharaf and J. E. Mark, *Polymer* **43**, 643–652 (2002).

J. E. MARK

Department of Chemistry and the Polymer  
Research Center, University of Cincinnati

B. ERMAN

Department of Chemical and Biological  
Engineering, Koc University

## NEUTRON SCATTERING

### Introduction

“Scattering” to most polymer scientists means light scattering, and the extent of their experience with the experiment is often the description in a course of how light scattering can be used to determine the molecular weight and radius of gyration of a polymer in solution, as well as the second virial coefficient of the solution, by measuring the scattered light intensity from a series of dilute solutions for multiple angles. (1–4) This data is then plotted as a Zimm plot to obtain the desired characteristics of the polymer chain and solution. Or maybe the polymer scientist is interested in the crystal structure of a commercial polymer and uses X-ray diffraction to provide details of the local ordering of the pertinent long-chain molecule. (5–7) The X-ray scatterer may not see the correlation between the diffraction peaks and the information in the Zimm plot, but there is one. The angular dependence of scattered radiation provides direct information on the spatial distribution and microscopic structure of the scattering particles, whether in light scattering, X-ray diffraction, or neutron scattering experiments. For X-ray diffraction this information is on the order of angstroms and provides the arrangement of atoms on an ordered lattice, while (small-angle) light scattering provides data on the average size of a complete polymer chain on a length scale of a few to tens of nanometers.

In fact, scattering is a powerful analytical method that can be utilized to determine the structure and dynamics of a range of “soft” materials (colloids, polymers, proteins, etc) using X-rays, light, and neutrons. Moreover, the fundamental physics of the correlation between the angular dependence of the scattered intensity to the microscopic structure of the scattering particle is identical for all types of radiation; it is only the manner in which the data is treated and analyzed to provide information on the structure that makes them appear different. A given analysis can be used with any type of radiation; the same analyses that are used in X-ray diffraction are used in neutron diffraction, and can be used in light-diffraction experiments, if it will provide important data on the ordering of the particles that are diffracting (scattering) the incoming radiation. Small-angle X-ray, neutron, and light-scattering experiments are commonly reported in

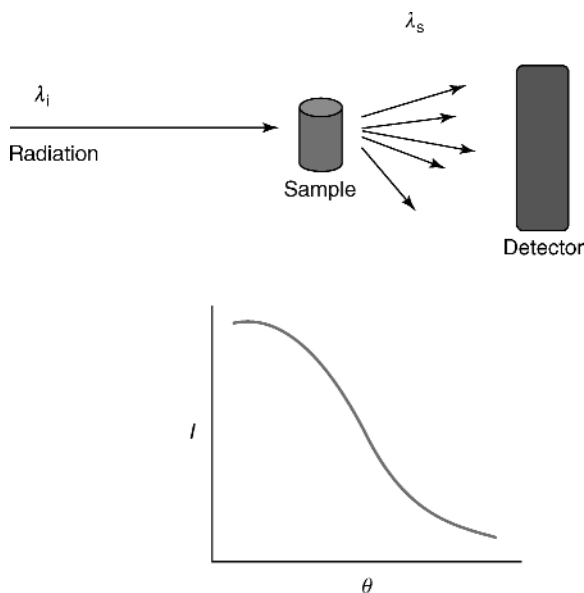


**Fig. 1.** (a) Schematic of an experiment to determine the angular dependence of the scattering of an incident radiation by a sample; (b) Typical intensity of scattered radiation vs scattering angle plot.

journals, with similar analyses and types of results. The primary difference is the type of radiation that shines on the sample and its interaction with the scattering particle.

## The Scattering Experiment

Differences among radiation types can best be explained through a discussion of the scattering experiment itself. A scattering experiment can be depicted as in Figure 1, where the radiation shines on the sample, interacts with the sample, and is scattered in all directions. The intensity of the scattered radiation ( $I$ ) is then measured at a detector for multiple angles ( $\theta$ ) and can be plotted as shown in the  $I$  vs  $\theta$  plot in Figure 1. For most geometries and samples, the scattering intensity is a maximum at zero angle and drops with increasing angle. In this diagram the wavelength of the incident radiation ( $\lambda_i$ ) and the wavelength of the scattered radiation ( $\lambda_s$ ) are equal, and thus this is an elastic scattering event. The angular dependence of the scattering intensity can then be analyzed to provide information on the size, shape, and orientation of the scattering particle in the sample. This type of experiment is often termed a *static* scattering experiment as the information garnered is related to the static structure of the scattering particle, not its dynamics.

However, in order to obtain a useful  $I$  vs  $\theta$  curve, a number of specific criteria must be met. Two of the most important criteria are that the measurement be

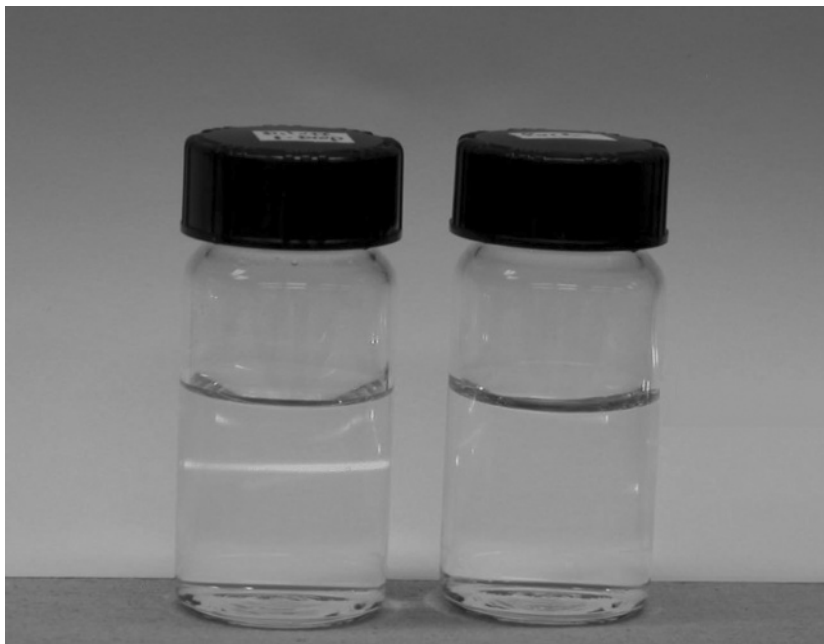


**Fig. 2.** Illustration of scattering power. The left vial contains polystyrene spheres that have a different refractive index than water, which provides contrast that results in scattering of the laser that is observable by the human eye.

taken in the correct angular range and that there be sufficient contrast in the sample for scattering to occur.

The correct angular range and sufficient contrast in the sample depends intimately on the type of radiation that is used in the scattering experiment, and a more detailed discussion of the scattering process is necessary to clarify this point.

Consider two vials, one that contains pure solvent and another that contains a solution with particles that may scatter light. Figure 2 shows a beam of light from a laser pointer shining through two vials, where the right-hand one is pure water and the left is a 0.0002% solution of polystyrene (PS) microspheres ( $0.4\ \mu\text{m}$ ) in water. Notice how the laser light is strongly scattered by the solution, but not the pure solvent. That is because the solution contains PS particles that have a different refractive index than the water solvent that it is immersed in. This difference in the refractive index of the solute (PS,  $n = 1.59$ ) and the solvent (water,  $n = 1.33$ ) provides the contrast that is needed to observe scattering. Notice that in the pure water, there is no portion of the sample that has a different refractive index than the rest of the sample, and thus there is no observable scattering because there is no contrast. It is important to emphasize that it is possible to have a solution, but still not have sufficient contrast between the solvent and solute to observe scattering. For instance, if you have a solution where the solute and solvent have refractive indices that are identical, there will be no portion of the sample that has a different refractive index than the rest of the sample, and



therefore there is no significant scattering. This phenomenon is termed *contrast matching* and is utilized in some scattering experiments to extract the scattering from a single component in a multicomponent sample.

This concept of “contrast” also holds true for the scattering of X-rays and neutrons by a polymer solution. However, when X-rays are being scattered by a particle, the X-rays interact with electrons of an atom and thus the intensity of scattering from a given atom depends on the electron density of that atom, not the refractive index. The electron density increases with atomic number on the periodic chart. Thus, for a polymer solution to strongly scatter X-rays, the electron density of the polymer and solvent must be significantly different. Finally, when neutrons are scattered, the neutrons interact with the nucleus of the atom and thus the intensity of the scattered radiation depends on the structure of the nucleus. This scattering power is quantified by the scattering length density  $b$  of a given atom and can vary by isotope. Therefore, to observe significant scattering from a polymer in solution, the scattering length density of the polymer must differ from that of the solvent. This has dramatic consequences for studying polymers and other soft matter by neutron scattering, as the scattering length densities of hydrogen and deuterium are significantly different. Thus, by changing the level of deuteration of a polymer (or solvent), the contrast (and thus amount of scattering) of a polymer in solution can be tuned without dramatically altering the thermodynamics of the mixture. (8–10)

This control of contrast in polymer mixtures by selective deuteration results in a unique and powerful aspect of neutron scattering in studying polymer systems; by the dispersion of a deuterated polymer chain in a matrix of identical hydrogenated chains, neutron scattering can be used to examine the structure and dynamics of a polymer in the melt or concentrated solution. This ability to “highlight” a single molecule in a matrix of identical polymer chains is illustrated in Figure 3. In Figure 3a, groups of polymer chains are shown, all drawn the same color. Because there is no contrast between the various chains, it is difficult to pick out one single chain. In Figure 3b, the color of one of the chains has been changed slightly, modeling the system where the scattering length density of one chain is slightly different than that of the matrix. Although this chain may now be observable, it is still difficult to examine. Finally in Figure 3c, a single chain is much darker than the remainder and is easy to pick out from the matrix and examine precisely. This picture illustrates the system where that chain is deuterated while the matrix of chains remains protonated with respect to neutron scattering. This one chain stands out as different from the matrix and can be selectively studied by neutron scattering.

The other criterion that is required to successfully utilize scattering to study polymer systems involves completing a scattering experiment in the correct angular range to extract useful information concerning the structure of the scattering particle from the angular dependence of the scattering intensity. This can best be exemplified in Figure 4, which shows the resultant  $I$  vs  $\theta$  plots for scattering experiments that are completed in the wrong angular range. The  $I$  vs  $\theta$  plot shown in Figure 4a shows a quick drop in intensity at low angle and very little scattering at higher angles. This type of curve is the result of measuring over too wide of an angular range so that the important information in the small-angle region is not resolved. Alternatively, Figure 4b shows a modest drop in intensity with angle,



(a)



(b)



(c)

**Fig. 3.** Illustration of contrast. Figure **a** contains 10 polymer chains, where each chain is the same color, and thus there is no contrast between chains and it is difficult to differentiate one chain from the rest. Figure **b** contains the same 10 chains, but one has a slightly different color than the remaining chains, and thus this chain may be examined with difficulty. Figure **c** contains the same 10 chains, where one is now much darker than the remaining chains, providing a mechanism to clearly study this chain.

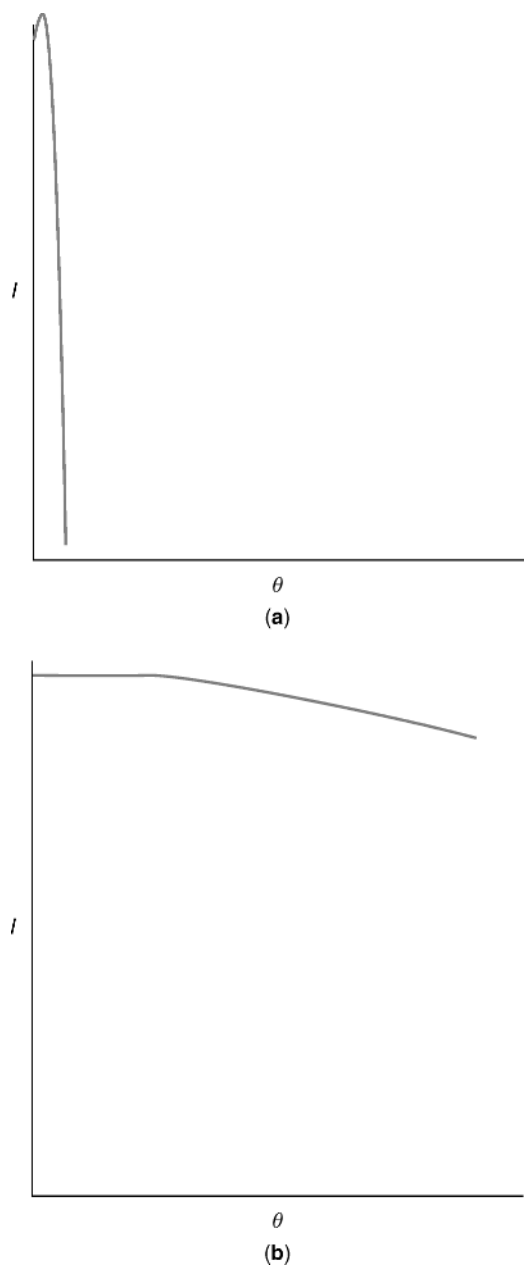


**Fig. 4.** Examples of the measured angular dependence of the scattering intensity for poorly designed experiments. The angular range in (a) is too broad, while the experiment shown in (b) is the result of an experiment where the angular range is too narrow.

but no significant change in scattering intensity over the angular range of the scattering. In this case, the angular range is too small and there is insufficient data to quantify the drop in intensity with angle that can provide information on the structure and size of the scattering particle.

The quantification of this “correct” angular range requirement provides a correlation of the length scales that can be studied by radiation of a given wavelength. At small angles, the length scale that is measured,  $d$ , is approximately  $\lambda/\theta$ , where  $\lambda$  is the wavelength of the radiation and  $\theta$  is the scattering angle. This approximation demonstrates that neutrons are indeed ideal to examine the structure of proteins and polymers; for cold neutrons,  $\lambda = 0.5 - 1.5$  nm, and small-angle scattering instruments provide a range of  $\theta$  that allows the observation of the structure of soft matter over length scales ranging from 1 to 100 nm, perfect to determine the structure of a macromolecule from the local to global length scales.

**Scattering with Neutrons.** Thus, observing the scattering of neutrons by a polymeric system is a very powerful tool to determine the structure and dynamics of polymers over the correct length scales, primarily because of the ability to tune the contrast between components by selectively deuterating the particles (or portions of particles) that are of interest. Additionally, neutrons offer further benefits, including their ability to penetrate matter. Because the neutrons interact with the nucleus of an atom, a large portion of the neutrons that impact a sample will be transmitted through it without absorption or scattering. One useful result of this is that the sample holder can be quite large and complex as the neutrons are then able to penetrate a large sample holder and scatter from the sample. Thus, it is possible to complete neutron-scattering experiments from a broad range of sample environments including *in situ* steady shear (11–13), high pressure (14,15), oscillatory shear (16), and even when the sample is an aerosol (17,18).

However, there are some drawbacks to using neutron scattering. Most notably, the production of neutrons is a very costly process, as the neutrons are most often produced for scattering experiments by nuclear fission in a nuclear reactor or by spallation. *Spallation* is the process where energetic subatomic particles, such as protons, strike a target and eject particles, including many neutrons from the nuclei of the atoms in the target. These neutrons then serve as the source of the radiation for the neutron-scattering experiments. In either case, the cost of a nuclear reactor or spallation source is beyond most companies or laboratories and thus is in the domain of government agencies. Thus, there exist a handful of facilities in the United States, with more spread out around the world, where a polymer scientist can complete neutron-scattering experiments, and their completion requires the time and expense of travel. Additionally, the current flux of neutrons requires significant sample size (usually,  $\sim 0.1$ – $1.0$  g), with larger sizes needed for exotic sample environments, such as a shear cell. This may be a particular problem for biological and exotic samples, where it is difficult to create more than a few milligrams of a given material. However, the Spallation Neutron source that is currently being built in Oak Ridge, Tennessee, will provide much greater intensity of neutrons on the sample, and thus allow faster measurements on smaller samples.

Even given these limitations, neutron scattering is a unique and very powerful technique that can provide information on the microscopic structure and dynamics of a polymeric material that is not obtainable by any other method. For instance, no other method provides a direct measure of the size of a polymer chain in the melt that is available by measuring the scattered intensity of

neutrons from a blend of deuterated and protonated versions of the same polymer. Similarly, the shape and thermodynamic interactions of polymers in concentrated mixtures are most effectively monitored by carefully designed neutron-scattering experiments, some of which will be described in detail later in the article.

## Structure from the Scattering Curve

There are a number of excellent reviews that detail the relationship between the angular dependence of the scattering intensity to the density distribution of the scattering system, and that will not be duplicated here (19,20). Rather, the methods to extract the structural information of the scattering system from the scattering pattern will be emphasized.

Classical scattering theory shows that the coherent scattering from a one-component system is proportional to the Fourier transform of the density correlation function,  $C(\mathbf{r})$ , of the particles in the system (19,21,22):

$$\left(\frac{\partial\sigma}{\partial\Omega}\right) \propto \int_V \exp(-i\mathbf{q}\cdot\mathbf{r})C(\mathbf{r})d\mathbf{r} \quad (1)$$

where  $(\frac{\partial\sigma}{\partial\Omega})$  is the number of scattered neutrons per second per solid angle  $\partial\Omega$  in the neutron-scattering experiment. For simplicity, this quantity will be replaced by  $I(q)$  in the remainder of this article. In equation 1,  $\mathbf{q}$  is the scattering or momentum transfer vector, and has a magnitude  $|\mathbf{q}| = q = 4\pi/\lambda \sin(\theta/2)$ , where  $\lambda$  is the wavelength of the scattered radiation and  $\theta$  is the scattering angle.

In a multicomponent system, such as a mixture of two constituents (component 1 and component 2), the scattering intensity now has contributions from correlations among particles of type 1, correlations among particles of type 2, and correlations between type 1 and type 2 particles, resulting in a scattering intensity  $I(q)$  that can be described as

$$I(q) = b_1^2 S_{11}(q) + b_2^2 S_{22}(q) + 2b_1 b_2 S_{12}(q) \quad (2)$$

where  $b_i$  is the scattering length of component  $i$  and  $S_{ij}$  is the partial structure factor that describes the contribution to the scattering of the correlations between components  $i$  and  $j$  and is

$$S_{ij} = \int_V \int_{V'} \langle n_i(\mathbf{r}) n_j(\mathbf{r}') \rangle \exp[-i\mathbf{q}\cdot(\mathbf{r}' - \mathbf{r})] d\mathbf{r} d\mathbf{r}' \quad (3)$$

where  $n_i(\mathbf{r})$  is the local density of component  $i$  at point  $\mathbf{r}$  and  $\langle \dots \rangle$  denotes an average over the scattering volume. Note that comparing equation 1 and equation 3, the density distribution function of the scattering particles  $C(\mathbf{r}') = \langle n_i(\mathbf{r}) n_j(\mathbf{r}') \rangle$  where  $\mathbf{r}' = \mathbf{r} - \mathbf{r}'$ . Thus, the partial structure factor is the Fourier transform of the density distribution of the scattering particles, and if it can be extracted from the measured scattering intensity, it will provide information on

the structure of the scattering particles; ie,  $S_{11}(q)$  will provide information on the spatial distribution of the particles of type 1.

At first glance, the sum of three partial structure factors appears to add significant complexity to analyzing the  $I(q)$  to determine the correlation between measured scattering patterns and structure of the scattering sample. However, it is relatively straightforward to show that, for two scattering particles of equal volumes,  $S_{11}(q) = S_{22}(q) = -\frac{1}{2} S_{12}(q)$ , which simplifies equation 2 to (23,24)

$$I(q) = (b_1 - b_2)^2 S_{11}(q) = (b_1 - b_2)^2 S_{22}(q) = -(b_1 - b_2)^2 S_{12}(q) \quad (4)$$

Thus, the angular dependence of the scattering intensity of a binary mixture can be analyzed as the Fourier transform of the density correlation function of any of the scattering particles scaled by the square of the difference in scattering lengths of the two components.

Let us assume that component 1 is a polymer and component 2 is a solvent. The requirement that the scattering particles (1 and 2) have equal volume for equation 4 to be valid requires that "particle 1" be equivalent to a section of the polymer chain that is the same volume as the solvent. Approximating this as a monomer segment of the polymer chain leads to an interesting result. Equation 4 tells us that  $I(q) = (b_1 - b_2)^2 S_{11}(q)$ ; therefore the scattering pattern from a polymer/solvent mixture will provide a direct measure of the spatial distribution of the monomers (as they have been defined as the scattering particles of type 1). Moreover, if the polymer molecules are sufficiently dilute to be independent of each other, the  $q$  dependence of the scattering pattern is the Fourier transform of the spatial distribution of the monomers in a single-particle chain. This quantity is known as the *Particle Form Factor* of the polymer chain,  $P(q)$ , and Debye has shown that the Fourier transform of a Gaussian segment distribution, known as the *Debye Function*, is (25)

$$P(q) = 2 \frac{[v^2 - 1 + \exp(-v)^2]}{v^4} \quad (5)$$

where  $v = qR_g$ , and  $R_g$  is the radius of gyration of the polymer molecule. Thus, by fitting the experimentally determined scattering pattern to equation 5, the radius of gyration and random coil nature of the polymer chain can be determined.

If the polymer molecules are not dilute, then a term for the *intermolecular* correlation between monomer segments [ $Q(q)$ ] also contributes to the scattering pattern and must be accounted for in any subsequent data analysis. Fortunately, when analyzing the scattering pattern of a mixture of two identical polymers, where one is deuterated and the other is not,  $Q(q)$  can be related to the single particle form factor  $P(q)$ , and thus the scattering intensity pattern,  $I(q)$ , from this type of mixture can be directly correlated to the single-particle form factor,  $P(q)$ . Therefore the scattering from a mixture of deuterated and protonated identical polymers *at any concentration* can be readily analyzed to provide information on the structure of a polymer chain in the melt (23,24)

$$I(q) = (b_d - b_h)^2 x(1-x) N z^2 P(q) \quad (6)$$

where  $b_d$  is the scattering length of the deuterated polymer,  $b_h$  is the scattering length of the protonated polymer,  $x$  is the volume fraction of deuterated polymer,  $N$  is the total number of polymer molecules, and  $z$  is the number of monomer segments in the polymers.

Thus, from a practical standpoint, the scattering intensity of neutrons from a polymeric system as a function of angle can be measured. This scattering pattern is the Fourier transform of the density distribution of the scattering particles and, therefore, can be analyzed to provide information on the spatial distribution of the scattering particles. More specifically, in dilute mixtures or when a deuterated polymer is dispersed in its protonated counterpart, the size ( $R_g$ ) and structure (does it obey the Gaussian distribution and is thus a random coil?) of the polymer chain can be readily determined from this scattering intensity pattern. Other single-particle form factors can also be used to model scattering data, such as that for a rigid rod, hollow sphere, or cylinder (26,27), which can provide size and structural information on other objects beyond random coils. For instance, the packing of a thermotropic, semiflexible liquid crystalline polymer has been shown to pack into a cylindrical conformation by fitting the resultant neutron scattering to the single particle form factor of a cylinder, where the radius and length of the cylinder are readily obtained from the fit (28).

Moreover, it is not difficult to design other experiments and apply broader analysis techniques to the measured  $I(q)$  to provide information on the structure and thermodynamics of polymeric systems beyond the conformation of a polymer chain in the melt. Rather than describe the exact conditions and analyses for each of these opportunities, the remainder of this article will detail specific examples that describe efforts to examine particular structural aspects of polymeric systems with small-angle neutron scattering.

## The Conformation of a Polymer Chain in the Melt

The most well-known examples of neutron-scattering experiments were completed in the early 1970s to unequivocally determine the conformation of a polymer chain in the melt. Over 20 years earlier, Flory had predicted that a polymer chain that is dispersed in a matrix of identical polymer chains would follow random walk statistics (29) rather than the more obvious self-avoiding walk statistics that polymers are known to adopt in a good solvent. Unfortunately, there were no available techniques at the time to determine the conformational statistics of a single chain in the melt to test this prediction. However, the advent of neutron scattering provided a mechanism to determine the structure of a single polymer chain in the melt by selectively deuterating one molecule, dispersing it in a matrix of nearly identical protonated polymers, and examining it.

The design of these experiments was straightforward; the researchers dispersed protonated poly(methyl methacrylate) in deuterated poly(methyl methacrylate) at a level of a few percent and analyzed the resulting neutron-scattering intensity patterns to determine the radius of gyration of the polymer as well as the second virial coefficient of this solution. These results show that the polymer attains the same radius of gyration as that measured in a theta solvent and that the second virial coefficient of this mixture is zero (30–32). Similar

**Table 1. Conformation of Polymer Chain in the Melt and in a  $\theta$  Solvent**

Polymer	State	Bulk	In $\theta$ solvent
		$R_g^a/M_w^{0.5}, \text{\AA}/(\text{g/mol})^{0.5}$	$R_g^a/M_w^{0.5}, \text{\AA}/(\text{g/mol})^{0.5}$
Atactic poly(methyl methacrylate)	Glass	0.25–0.27	0.25
Isotactic poly(methyl methacrylate)	Glass	0.30	0.28
Syndiotactic poly(methyl methacrylate)	Glass	0.29	0.24
Polybutadiene	Melt	0.35	0.34–0.42
Atactic polystyrene	Glass	0.265–0.28	0.27–0.28
Atactic polystyrene	Melt	0.275	0.27–0.28
Poly(vinyl chloride)	Glass	0.40	0.37
Polyisobutylene	Melt	0.31	0.30
Poly(ethylene terephthalate)	Glass	0.39	0.42
Polyethylene	Melt	0.45–0.46	0.45

<sup>a</sup>To convert  $\text{\AA}$  to nm, divide by 10.

experiments on mixtures of protonated polystyrene and deuterated polystyrene were completed that provided information on the scaling relationship between the radius of gyration and molecular weight for this polymer (33,34). All of these experiments demonstrated that the  $R_g$  scales as  $M^{0.5}$  in the melt and obeys the Debye function down to a length scale of 1 nm, as would be expected from random walk statistics and was predicted by Flory.

In fact, further experiments over the years have shown that the  $R_g$  scales as  $M_w^{0.5}$  for a range of polymers in the melt or glassy state with the proportionality constant equal to that which is observed in a theta solvent, verifying that flexible polymer chains in the melt attain a configuration that is accurately modeled as random coil. These results are tabulated in Table 1, where the data are taken from Reference 19 9 (see also CONFORMATIONS AND CONFIGURATION).

## The Location of End Groups in Dendrimers

Dendrimers are highly branched polymers that can be synthesized by the consecutive addition of multifunctional monomers to a multifunctional core to form a tree-like structure (35,36), where an illustration of a dendrimer formed from trifunctional monomers is presented in Figure 5 (see DENDRONIZED POLYMERS). These macromolecules have recently attracted significant attention as possible sensors, drug carriers, lubricants, and surface-active agents. As the molecule is synthesized and becomes larger, more active sites remain at the outer edge of the molecules with each successive generation. As the number of active growth sites increases with size, the mass of the molecule increases exponentially with the number of generations. Clearly, the packing of each new generation becomes more dense, until the density saturates and the size of the molecule reaches a maximum.



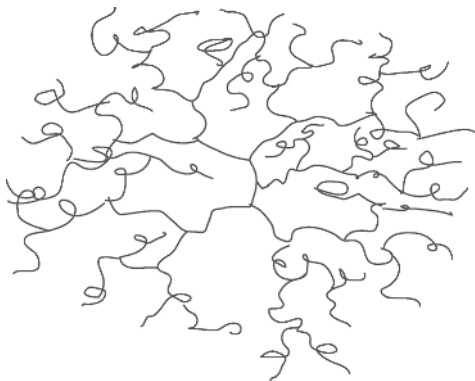


**Fig. 5.** Illustration of a dendrimer that is formed from trifunctional monomers, grown to the fourth generation.

The density profile of these unique structures has been the subject of much investigation. DeGennes first predicted that the dendrimer will have a density minimum at the center of the molecule, increase with radius, and reach a maximum at the outer edge of the spherical molecule (37). This structure provides a cavity in the center of the molecule that would provide an ideal structure for its use as a carrier. However, further theoretical and simulation studies have suggested that the molecule is not hollow, but has a density maximum at the center that decreases with radius (38–40).

Small-angle X-ray scattering and other studies have not clarified the radial structure of these intriguing molecules (41,42); however, a recent study of the radial density profile by small-angle neutron scattering has provided a clearer picture of its structure (43). Lindner and co-workers have used contrast variation small angle neutron scattering to unequivocally show that these molecules have a density maximum at the center, and a density profile that decreases with radius.

The specifics of this set of experiments take advantage of the ability to control the contrast between the dendrimer and the solvent by varying the extent of deuteration of the solvent, which is accomplished by mixing deuterated dimethyl acetamide (DMA-D<sub>9</sub>) and protonated dimethyl acetamide (DMA-H<sub>9</sub>). These researchers determined the scattering pattern of a fifth-generation dendrimer dissolved in DMA at various concentrations and varying ratios of DMA-D<sub>9</sub> to DMA-H<sub>9</sub>. The authors analyze this data to extract the portion of the scattering that is due solely to the shape of the dendrimer [ $I_s(q)$ ] from the measured scattering intensity which also contains contributions due to inhomogeneities of the dendritic structure, which may result from imperfections in the structure and the fact that the building blocks of the dendrimer may not all have the same structure (and thus scattering length). This careful analysis provides a measure of the average scattering length density of the dendrimer, which provides an exact measure of the molecular weight of the dendrimer. A comparison of this value to the ideal fifth-generation dendrimer indicates that the structure is not perfect.

Finally, the authors extract the radial density profile of the dendrimer from  $I_s(q)$  by its Fourier inversion to show that the density of the dendrimer is a

maximum at the center that decreases smoothly to the outer edge. Moreover, the results demonstrate that the dendrimer radius extends to 6 nm and is thus a fluctuating, not a dense, structure. This analysis is further verified by comparing the scattering intensity [ $I_s(q)$ ] to the Fourier transform of this density distribution and to the Fourier transform of the homogeneous sphere, where this comparison shows a clear coincidence to the experimentally determined density profile and clear deviations from that of the homogeneous sphere.

Thus the ability to systematically vary the contrast between the solute and solvent by mixing deuterated and protonated solvents provides a mechanism to unequivocally extract the scattering from the solute, and thus determine the structure of that solute. These results show that the end groups of this dendrimer are not confined to the outer layer of this centrosymmetric structure, which would result in a core-shell density profile. Rather, the end groups are distributed throughout the volume of the macromolecule. This information will have significant impact on the utilization of these novel macromolecules and their use in the design of molecular scale sensors, drug carriers, and lubricants.

### The Radius of Gyration of Polymers in Ultrathin Films

It is well known that confining a polymer molecule to a thin film or near a surface lowers its configurational entropy. This confinement may also alter the configuration of the polymer, which may impact its adhesive and thermal properties, among others. One can easily imagine that a polymer chain that is confined to a thin film that is on the order of (or less than) its radius of gyration may be flattened. Moreover, as devices become smaller, polymers are often utilized in applications where the confinement of the polymer chain is significant. Thus, the alteration of the configuration of a polymer chain by confinement is of importance to their use in micro- and nanoscale devices. It is, therefore, important to understand how confinement alters the size and shape of a polymer chain, with the expectation that this data can provide fundamental information to predict, understand, and control the properties of polymers in these environments.

As polymers in miniature devices are mostly melts, neutron scattering becomes an ideal experimental technique to provide this information. Clearly, by dispersing a fraction of deuterated polymer in a protonated thin film of the polymer, SANS can be used to determine the radius of gyration of a polymer confined to the film, as a function of film thickness, in a similar way to the bulk measurements in the 1970s that verified the random coil nature of the polymer chain in the melt (30,32,33). However, the relatively low intensity of neutrons that strike the sample in a scattering experiment introduces a complication into this planned experiment. In a scattering experiment, the intensity of scattered radiation is proportional to the amount of sample in the beam. In a bulk SANS experiment, a sample usually contains on the order of 0.1–0.5 g to optimize the signal to noise. However, with a radius of a neutron beam that is on the order of a centimeter, a thin film of polymer that is only as thick as the radius of gyration of a polymer will only provide 0.000785 mg of sample in the beam, clearly an amount that is insufficient to provide adequate signal-to-noise ratio to accurately determine the radius of gyration of a polymer. Researchers who have completed such a study

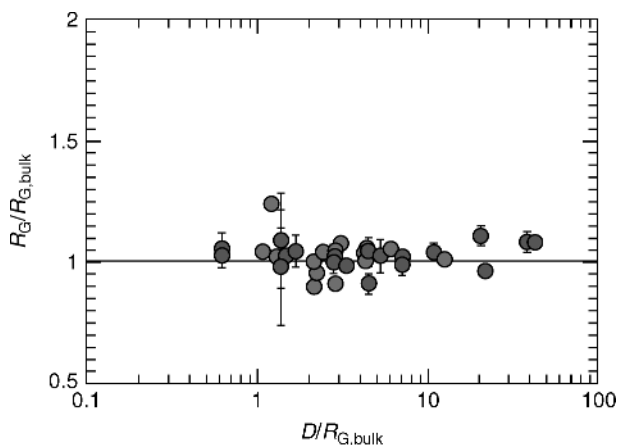


**Fig. 6.** The radius of gyration of deuterated polystyrene in a thin film normalized to its radius of gyration in the bulk as a function of film thickness that is also normalized to the radius of gyration of the polymer in the bulk. ●  $M_w = 270$  K, ○  $M_w = 650$  K. Reprinted with permission from Ref. 44. Copyright (2001) American Chemical Society.

overcame this obstacle by simultaneously scattering from multiple, identical thin films, thus effectively increasing the sample size (44,45).

The authors of this study measured the neutron-scattering intensity of isotopic blends that contain 25 wt% deuterated polystyrene and 75 wt% protonated polystyrene in thin films that vary in thickness ( $D$ ) from 1  $\mu\text{m}$  down to 10 nm. These thicknesses correspond to  $D/R_{g,\text{bulk}}$  that range from 50 to 0.5. The samples were annealed at high temperature and quenched to ensure that the samples were at equilibrium. The data were analyzed by accounting for scattering from interfacial roughness in the form of capillary waves and incoherent scattering to extract the scattering due to the dispersion of the deuterated polymers in the protonated matrix  $I_s(q)$ . This scattering,  $I_s(q)$ , was then analyzed using the RPA model and the Kratky approach ( $q^2 I$  vs  $q^2$ ) to determine the radius of gyration of the deuterated polymers and test the Gaussian nature of the confined chains, respectively. The  $R_g$  results are shown in Figure 6, which shows that the size of the polymer chain in the plane of the surface does not change from that of the chain in the bulk, even when the thickness of the film is less than the  $R_g$  of the bulk chain. The data also verify that the chains do retain their Gaussian character for all film thicknesses studied. This result agrees with recent simulation and theoretical studies and will have implications on the properties and dynamics of a polymer chain in confined geometries.

## Polymer Blends

**The Spinodal Decomposition Process in Polymer Blends.** For many mixtures, there exists a temperature range where the system will remain miscible for all compositions, while a change in temperature will alter the balance of the enthalpy and entropy of mixing to create a thermodynamic state where the most stable system is one where two phases coexist and the mixture, therefore,

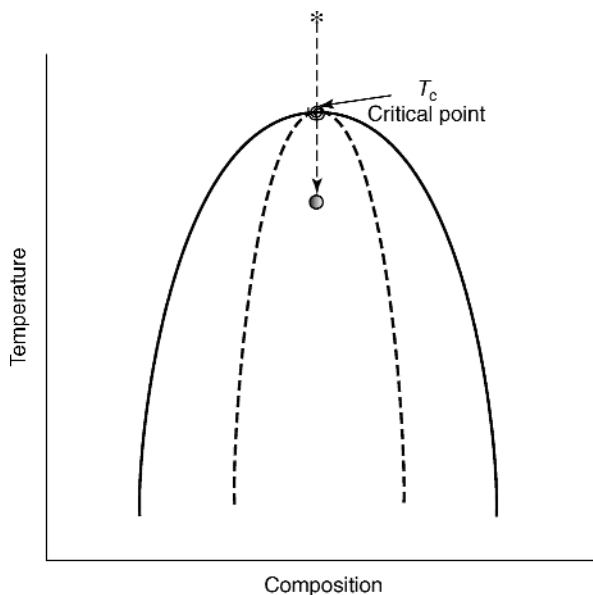


**Fig. 7.** Representative phase diagram of a binary mixture of two molecules that have similar sizes.

phase separates. This situation is illustrated in Figure 7, which shows the phase diagram of a regular solution (46). When below the critical temperature, the outer line of this phase diagram denotes the compositions of the two phases that coexist at a given temperature. Therefore, for this system, it is possible to design a temperature program where the system is brought from the one-phase state at high temperature to a phase-separated system at low temperature.

In fact, the kinetics of the process by which the system goes from a homogeneous, one-phase system to the final equilibrium state of two coexisting phases is extremely important to both industrial and academic researchers. From an industrial standpoint, understanding and control of the morphology of the phase-separated system can provide a mechanism to create new materials with novel properties. From an academic point of view, the self-assembling process of the phase separation and resultant morphologies provide insight into nonequilibrium thermodynamics. Of particular interest, a more complete understanding of the kinetics of spinodal decomposition as a phase separation process has been an area of intense study (47–51).

It is known from thermodynamics that in the region of the phase diagram below the spinodal line (dotted line in Figure 7) that a one-phase system is absolutely unstable and the system will phase separate spontaneously via the spinodal decomposition mechanism (SD). Moreover, the time evolution of the change in concentration is well described in the early stages of SD by the theory first presented by Cahn for small molecules (52,53). This theory predicts that there exists a dominant length scale for the phase separation process that does not change with time in this early stage and that the amplitude of the concentration fluctuations  $[\Delta\phi(\mathbf{r},t)]$  that occur on this length scale grows exponentially with time.

Unfortunately, these predictions were difficult to observe in small molecular mixtures, as the time scale of the early stage is too brief (ie  $<1$  s) for experimental measurements. However, because polymers are larger and slower, the time scale over which this early stage lasts is minutes, providing sufficient time to monitor the time dependence of the growth of the concentration fluctuations to test this theory. Moreover, small-angle neutron scattering is an ideal tool to monitor these changes, as the scattering intensity  $[I(q)]$  of the mixture provides direct information on the distribution of the scattering particles, and thus can be used to observe the variation of the spatial distribution of the concentration fluctuations as a function of time.

Time-resolved small-angle neutron scattering has, thus, been used to determine the coarsening kinetics of spinodal decomposition in polymer blends. Blends systems that have been investigated include mixtures of hydrogenated and deuterated polybutadiene as well as deuterated polystyrene and poly(vinyl methyl ether) (49–51) where the deuteration of one component in the blend provides the necessary contrast to complete the experiments. In these experiments, the researchers create a polymer blend that is initially in the one phase-region (\* in Fig. 7). This mixture is then quickly brought to a temperature in the phase-separated regime, below the spinodal decomposition line (o in Fig. 7), and subsequently the scattering intensity  $[I(q)]$  for the system as a function of time is measured. The resultant scattering patterns can then be fit to the Fourier transform of the theoretically predicted concentration fluctuation distribution (47), which provides a direct mechanism to test the theories of the kinetics of spinodal decomposition.

These results confirm that  $\Delta\phi(\mathbf{r},t)$  grows exponentially with time while the characteristic length scale  $\mathbf{r}$  remains constant in the early stage (54). Further experiments have documented that at later times, in the intermediate stage of SD, the phase-separated morphology coarsens with time, resulting in a nonexponential growth of  $\Delta\phi(\mathbf{r},t)$  and an increase in  $\mathbf{r}$  with time. At even later times, in the late stage of the SD process, the interface between the separate domains narrows and  $\Delta\phi(\mathbf{r},t)$  reaches an equilibrium value, which is defined by the specifics of the phase diagram. These domains can coarsen further (though more slowly than earlier stages) and thus, the length scale of the domains,  $\mathbf{r}$ , continues to grow slowly.

Thus, the ability of small-angle neutron scattering to tune the contrast of the phase separating blends combined with its ability to examine the correct length scales of this phase separation process make SANS an ideal technique to determine the kinetics of the concentration fluctuation growth during spinodal decomposition. Moreover, the results show that the linearized Cahn–Hilliard–Cook theory of SD (52,53,55) accurately describes the early stage of spinodal decomposition, and that the intermediate and late stage kinetics obey universal kinetics.

**The Crossover from Mean-Field to Ising Behavior in Critical Polymer Blends.** Polymer systems have long been known to follow mean-field behavior at most temperatures, as long-range fluctuations are readily damped because of their slow relaxation processes and intimate mixing of chains (56,57). However, it is expected from critical theory that as a mean field system approaches a critical point, fluctuations will become more prevalent and impact the structure of the

system. The increased importance of the fluctuations results in a polymer mixture transitioning to behave as a non-mean-field (Ising) system (58). The point where this transition occurs is known as the *Ginzburg criterion* (59). This transition from mean-field to non-mean-field behavior can be determined by monitoring the temperature dependence of concentration fluctuation size ( $\xi$ ), where it is expected that  $\xi \sim (T - T_c)^{-\nu}$  and  $\nu = 0.5$  for a system that obeys mean-field behavior and  $\nu = 0.63$  for an Ising type system.

As neutron scattering measures the fluctuation in the scattering length density of a system, it is an ideal tool to monitor the presence and growth of concentration fluctuations in a polymer/polymer mixture. In fact, the inverse of the zero-angle scattering,  $I^{-1}(q=0)$ , is proportional to the second derivative of the free energy of the mixture with respect to the blend concentration, which is the osmotic compressibility of a mixture. Theories of cooperative phenomena show that  $I^{-1}(q=0) \sim (T - T_c)^{-2\nu}$  (60) and thus the determination of  $I^{-1}(q)$  extrapolated to  $q=0$  for a polymer blend at a series of temperatures near  $T_c$  will provide a method to verify the existence of this crossover and its influence on the mixing behavior of two polymers (61,62).

To test this prediction of the crossover from mean-field to Ising-type behavior, very precise small-angle neutron scattering measurements were completed on blends of deuterated polystyrene (d-PS) and poly(vinyl methyl ether) (PVME) at the critical concentration for a series of temperatures as the one-phase mixture approaches the temperature of phase separation (ie, the critical point  $T_c$  in Fig. 7) (61). The data were analyzed by fitting the measured  $I(q)$  to the random phase approximation to estimate  $I(q=0)$  for each temperature, where the temperature is controlled to  $\pm 0.01$  K.

Far away from the critical temperature, Schwahn and co-workers found that the inverse of the scattering intensity at zero angle,  $I^{-1}(q=0)$ , scales with  $(T_c - T)$  where  $T$  is the temperature at which the scattering is measured, as would be expected from a mean-field system. However, as the temperature approached the critical temperature,  $I^{-1}(q=0)$  diverges from a linear relationship with  $(T_c - T)$  within 3 K of  $T_c$ . Moreover, in this narrow region near the critical point,  $I^{-1}(0)$  scales as  $(T_c - T)^{1.26}$  as one would expect from a system that obeys Ising-type behavior. This transition is shown in Figure 8, taken from Reference 61.

This result emphasizes that mean-field theory is a very accurate model to describe the behavior of polymer systems for most of the phase diagram, except in a narrow window near the critical temperature and concentration. This implies that concentration fluctuations do not significantly influence the phase behavior of polymers, whereas for small molecule mixtures, it is known that composition fluctuations can influence the system throughout the phase diagram of the mixture and neutron scattering is an instrumental technique in defining these differences.

## Flow-Induced Structure in Polymers

In order to create a useful polymeric product, the material will have to undergo some level of processing where a shear flow is applied to a polymer melt or solution to create the desired shape. However, it is well known that the application

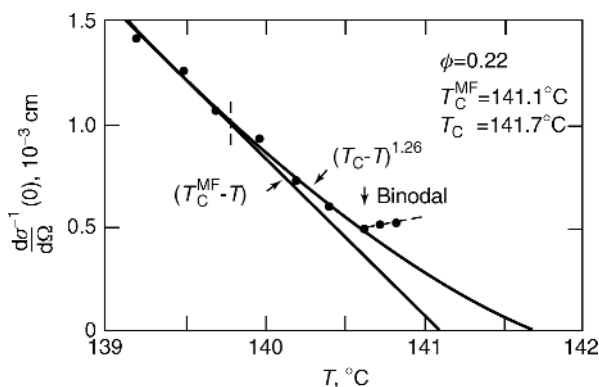


**Fig. 8.** The inverse of the zero-angle scattering of a polymer blend (d-PS/PVME) as it approaches the phase separation temperature. Note the deviation from mean-field behavior just below 140  $^{\circ}\text{C}$ . Reprinted with permission from Ref. 61. Copyright (1987) by the American Physical Society.

of a shear field onto a polymer melt or solution can modify its structure (63). One interesting phenomenon that has been observed is the enhancement of concentration fluctuations by the application of a shear field. In other words, a polymer solution that is miscible at rest appears to phase separate when it is sheared. This phenomenon has been well studied, but is not completely understood (64–67).

As neutron scattering provides information on the spatial distribution of concentration fluctuations by virtue of its ability to provide direct evidence of the spatial distribution of the scattering particles, it is an ideal technique to examine the changes that occur during this phenomenon on length scales ranging from the monomeric level to that of many chains. Moreover, if combined with light scattering, which provides information on larger length scales than that of neutrons, an understanding of the development and deformation of the concentration fluctuations as a function of parameters such as shear rate and temperature over length scales ranging from submolecular to micrometers can be found. There exist a number of articles describing the monitoring of the structures that are induced in polymer blends, phase-separated block copolymer, liquid crystalline polymer solutions and melts, and polymer solutions by an applied shear field; but to exemplify the utility of this technique, the work of Hashimoto and Lindner on the impact of temperature and shear rate on the enhancement and deformation of concentration fluctuations in polystyrene/dioctyl phthalate solutions (PS/DOP) using neutron- and light-scattering experiments will be discussed (68).

In this work, the investigators measured the scattering patterns of PS/DOP while they were being sheared. This requires that a sample holder be designed whereby the material can be constantly sheared during the time that the scattering pattern is collected. A geometry that has provided significant success at collecting the scattering of polymer systems *in situ*, during shear flow, is a couette cell as shown in Figure 9. In this cell, an outer cup is made out of a material that is relatively transparent to neutrons, such as quartz. This cup then contains a stator that fits symmetrically into the cup, but leaves a thin annulus between the cup and the stator into which the polymer melt or solution can be filled (11). It is

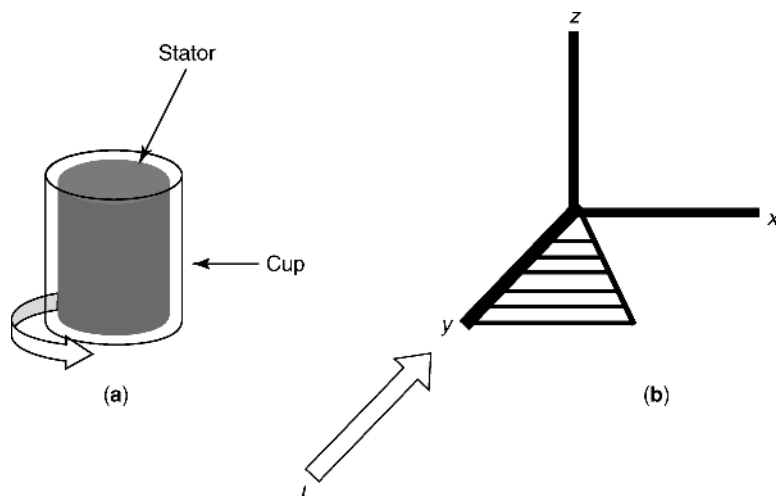


**Fig. 9.** (a) Diagrammatic representation of a couette shear cell. (b) The resultant geometry of the shear field, where the  $x$ -axis is the flow direction, the  $y$ -axis is the shear gradient and the  $z$ -axis is the vorticity direction. Note that the incident radiation is also along the  $y$ -axis, and the measured scattering intensity is in the flow–vorticity plane.

important that the stator also be manufactured from a material that allows large transmission of neutrons. Stators have been successfully made from quartz and oxygen free copper, where the copper provides better heat transport and higher use temperatures, and thus provides the ability to measure shear effects on bulk polymer materials as well as solutions.

The SALS and SANS data were combined to provide information on the structure of the concentration fluctuations on length scales ranging from tens of angstroms to 10 microns. The authors were able to fit the data to model the scattering from the structure of the thermal concentration fluctuations as well as the contributions from the demixed phases. The scattering pattern was, thus, fit to the sum of an Ornstein–Zernike function (to model thermal fluctuations) and a modified squared Lorentzian function (to model the demixed phases). From these fits, the authors were able to provide quantitative information regarding the size and shape of the demixing domains as a function of temperature, shear rate, and polymer molecular weight. Moreover, the results provide a data set that can be used to test current and pioneering theoretical models of this phenomenon and find that earlier theoretical treatments do not agree well with this broad set of results. The results, however, do appear to agree with more recent theoretical models and thus provide critical insight into the physics of this unique phenomenon.

Thus, the combination of neutron scattering and light scattering is a valuable tool set that allows these researchers to monitor the structures that exist in the phase-separating mixture on a broad range of length scales. It is only with the information of the structure of this polymer solution over these length scales that allows the researchers to critically evaluate theoretical models of shear-induced phase separation in polymer mixtures.



## Structure of Proteins by Contrast Variation

The mechanism by which biological enzymes become active, bind with substrates, and affect a catalytic reaction is of broad interest. Specific details on how the enzymes coordinate and interact with regulators are of particular importance in understanding enzymatic activity. For instance, calmodulin is a receptor for calcium that is responsible for binding of  $\text{Ca}^{2+}$  in calcium-dependent regulation of cellular processes via interactions with enzymes (69). A model system for this regulation of enzymatic activity is the calcium/calmodulin activation of myosin light chain kinase (MLCK) (70,71). MLCK contains a catalytic cleft that is normally inhibited by a regulatory sequence within the MLCK. The binding of the  $\text{Ca}^{2+}$ /calmodulin (CaM) to the MLCK activates the catalytic cleft, and enables target enzyme recognition and substrate binding. However, the specific structural mechanism by which the CaM complex activates the catalytic cleft was not verified until Trehwella and co-workers utilized small-angle neutron scattering experiments with contrast variation to elucidate the change in structure of the CaM complex and MLCK upon binding that results in the activation of the catalytic cleft. (72,73)

In these experiments (73), the authors determined the scattering patterns for CaM–MLCK (in which the CaM is deuterated) complexes in  $\text{H}_2\text{O}/\text{D}_2\text{O}$  mixtures that were 0, 20, 75, 82, and 85%  $\text{D}_2\text{O}$ . This range of mixtures provided the needed information to extract the individual shape functions of the MLCK and CaM structures at various stages of the binding process. This is accomplished by analyzing the measured scattering function  $I(q, \Delta b_c, \Delta b_K)$  with the following equation

$$I(q, \Delta b_c, \Delta b_K) = \Delta b_c^2 I_c(q) + \Delta b_c \Delta b_K I_{CK}(q) + \Delta b_K^2 I_K(q) \quad (7)$$

where subscripts c and K denote deuterated CaM and MLCK, respectively,  $\Delta b_i$  is the contrast between the scattering length density of component  $i$  and solvent ( $b_i - b_s$ ) and  $I_c(q)$ ,  $I_K(q)$ , and  $I_{CK}(q)$  denote the contribution to the total scattering from the structure of the CaM, the structure of the MLCK, and the correlation between the structures of CaM and MLCK, respectively. Note that by completing the experiments for a series of  $\text{D}_2\text{O}/\text{H}_2\text{O}$  mixtures, a series of equations that fit equation 7 are created, and the scattering from each individual structure [ $I_c(q)$  and  $I_K(q)$ ] can be extracted and analyzed.

The authors do precisely that: they fit the resulting individual form factors to those of two ellipsoids that provide information on the size, shape, and relative dispositions of the CaM and MLCK. This information provides a very precise picture of how the two molecular components come together, interact, and activate the catalytic cleft of the MLCK, which is illustrated in Figure 10 (from Reference 73). The scattering results indicate that a regulatory sequence within the MLCK keeps its catalytic cleft open. The binding of  $\text{Ca}^{2+}$  to CaM opens hydrophobic clefts in the CaM. Upon binding of the CaM with MLCK, the hydrophobic clefts on the CaM interact with hydrophobic residues of the MLCK sequence, which induces movement of the MLCK regulatory sequence away from its catalytic cleft, relieving the MLCK auto-inhibition and providing an activated structure that can now bind with substrates and thus enable enzymatic activity.

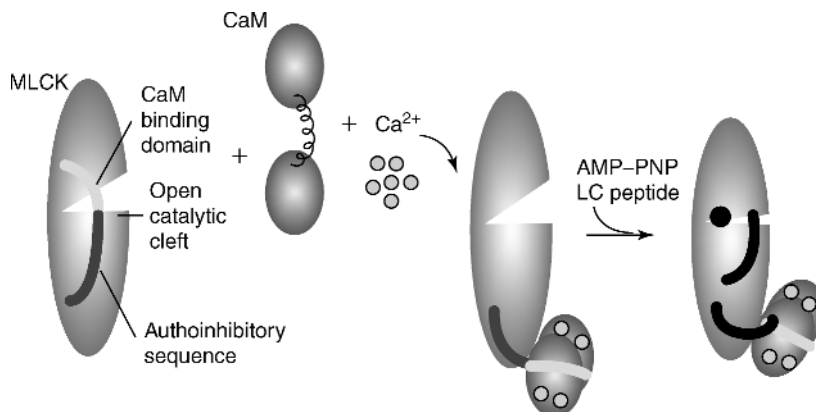


**Fig. 10.** Diagram that depicts the interaction of CaM to MLCK that results in the activation of the catalytic cleft of MLCK to enzymatic activity. Reprinted with permission from Ref. 73. Copyright (1998) American Chemical Society.

This example further demonstrates the power of neutron scattering to extract structural information of individual components in a complex system by use of the contrast variation method. Contrast variation provides an additional sample preparation technique that allows the extraction of the scattering of a single component in a multicomponent mixture and broadens the utility of neutron scattering into fields such as the study of biological complexes and the structure of diblock copolymers (74).

## BIBLIOGRAPHY

"Neutron Scattering" in *EPSE* 2nd ed., Vol. 10, pp. 112–184, by G. D. Wignall, Oak Ridge National Laboratory; in *EPST* 3rd ed., Vol. 10, pp. 502–524, by M. D. Dadmun, University of Tennessee.

## CITED PUBLICATIONS

1. P. C. Painter and M. M. Coleman, *Fundamentals of Polymer Science, An Introductory Text*, Technomic Press, Lancaster, Pa., 1997.
2. P. C. Hiemenz, *Polymer Chemistry, The Basic Concepts*, Marcel Dekker, New York, 1984.
3. A. Rudin, *The Elements of Polymer Science*, Academic Press, New York, 1999.
4. L. H. Sperling, *Introduction to Physical Polymer Science*, Wiley-Interscience, New York, 1992.
5. B. D. Cullity, *Elements of X-ray Diffraction*, Addison Wesley, Reading, Mass., 1978.
6. A. Guinier, *X-Ray Diffraction in Crystals, Imperfect Crystals, and Amorphous Bodies*, Freeman, San Francisco, 1963.
7. M. Kakudo and N. Kasai, *X-Ray Diffraction by Polymers*, Elsevier, Amsterdam, 1972.
8. F. S. Bates, G. D. Wignall, and W. C. Koehler, *Phys. Rev. Lett.* **55**, 2425 (1985).
9. F. S. Bates, L. J. Fetters, and G. D. Wignall, *Macromolecules* **21**, 1086 (1988).

10. F. S. Bates, M. Muthukumar, G. D. Wignall, and L. J. Fetters, *J. Chem. Phys.* **89**, 535 (1988).
11. A. I. Nakatani, H. Kim, and C. C. Han, *J. Res. Natl. Inst. Stand. Tech.* **95**, 7 (1990).
12. F. A. Morrison, J. W. Mays, M. Muthukumar, A. I. Nakatani, and C. C. Han, *Macromolecules* **26**, 5271 (1993).
13. M. D. Dadmun and C. C. Han, *Macromolecules* **27**, 7522 (1994).
14. B. Hammouda, N. P. Balsara, and A. A. Lefebvre, *Macromolecules* **30**, 5572 (1997).
15. A. A. Lefebvre, J. H. Lee, N. P. Balsara, and B. Hammouda, *Macromolecules* **33**, 7977 (2000).
16. K. A. Koppi, M. Tirrell, and F. S. Bates, *Phys. Rev. Lett.* **70**, 1449 (1993).
17. B. E. Wyslouzil, J. L. Cheung, G. Wilemski, and R. Strey, *Phys. Rev. Lett.* **79**, 431 (1997).
18. C. H. Heath, K. A. Streletzky, B. E. Wyslouzil, J. Wolk, and R. Strey, *J. Chem. Phys.* **118**, 5465 (2003).
19. J. S. Higgins and H. C. Benoit, *Polymers and Neutron Scattering*, Oxford University Press, Oxford, 1994.
20. R. J. Roe, *Methods of X-ray and Neutron Scattering in Polymer Science*, Oxford University Press, Oxford, 2000.
21. G. E. Bacon, *Neutron Diffraction*, Oxford University Press, Oxford, 1975.
22. G. L. Squires, *Introduction to the Theory of Thermal Neutron Scattering*, Cambridge University Press, Cambridge, (1978).
23. M. Daoud, J. P. Cotton, B. Farnoux, G. Jannink, G. Sarma, and H. Benoit, *Macromolecules* **8**, 804 (1975).
24. A. Akcasu, G. C. Summerfield, S. N. Jahshan, C. C. Han, C. Y. Kim, and H. Yu, *J. Polym. Sci., Polym. Phys.* **18**, 863 (1980).
25. P. J. Debye, *J. Appl. Phys.* **15**, 338 (1944).
26. T. Neugebauer, *Annalen der Physik* **42**, 509 (1943).
27. A. Guinier and G. Fournet, *Small Angle Scattering of X-Rays*, John Wiley and Sons, Inc., New York, 1955.
28. F. Hardouin, G. Sigaud, M. F. Achard, A. Brulet, J. P. Cotton, D. Y. Yoon, V. Percec, and M. Kawasumi, *Macromolecules* **28**, 5427 (1995).
29. P. J. Flory, *J. Chem. Phys.* **17**, 303 (1949).
30. R. G. Kirste, W. A. Kruse, and J. Schelten, *J. Makromol. Chem.* **162**, 299 (1973).
31. R. G. Kirste, W. A. Kruse, and J. Schelten, *Angew. Chem. Int. Ed.* **12**, 431 (1973).
32. J. Schelten, W. A. Kruse, and R. G. Kirste, *Kolloid Z. Z. Polym.* **251**, 919 (1973).
33. D. G. H. Ballard, G. D. Wignall, and J. Schelten, *Eur. Polym. J.* **10**, 861 (1974).
34. J. M. Guenet, C. Picot, and H. Benoit, *Macromolecules* **12**, 86 (1979).
35. D. A. Tomalia, A. Naylor, and W. A. Goddard, *Angew. Chem. Int. Ed.* **29**, 138 (1990).
36. G. R. Newkome, C. N. Moorefield, and F. Vögtle, *Dendritic Molecules*, VCH, Weinheim, Germany, 1996.
37. P. G. DeGennes and H. Hervet, *J. Phys. (Paris)* **44**, L351 (1983).
38. R. L. Lescanec and M. Muthukumar, *Macromolecules* **23**, 2280 (1990).
39. M. Murat and G. S. Grest, *Macromolecules* **29**, 1278 (1996).
40. D. Boris and M. Rubinstein, *Macromolecules* **29**, 7251 (1996).
41. T. J. Prosa, B. J. Bauer, E. J. Amis, D. A. Tomalia, and R. Scherrenburg, *J. Polym. Sci., Part B: Polym. Phys.* **35**, 2913 (1997).
42. R. Scherrenburg, B. Coussens, P. van Vliet, G. Edouard, J. Brackman, E. de Brabander, and K. Mortensen, *Macromolecules* **31**, 456 (1998).
43. D. Pötschke, M. Baullauff, P. Lindner, M. Fischer, and F. Vögtle, *Macromolecules* **32**, 4079 (1999).

44. R. L. Jones, S. K. Kumar, D. L. Ho, R. M. Briber, and T. P. Russell, *Macromolecules* **34**, 559 (2001).
45. R. L. Jones, S. K. Kumar, D. L. Ho, R. M. Briber, and T. P. Russell, *Nature* **400**, 146 (1999).
46. J. Hildebrand, *J. Am. Chem. Soc.* **51**, 66 (1929).
47. T. Hashimoto, *Phase Transitions* **12**, 47 (1988).
48. H. L. Snyder and P. Meakin, *J. Chem. Phys.* **79**, 5588 (1983).
49. T. Hashimoto, M. Itakura, and N. Shimizu, *J. Chem. Phys.* **85**, 6773 (1986).
50. T. Sato and C. C. Han, *J. Chem. Phys.* **88**, 2057 (1988).
51. F. S. Bates and P. Wiltzius, *J. Chem. Phys.* **91**, 3528 (1989).
52. J. W. Cahn, *Acta Metall.* **9**, 795 (1961).
53. J. W. Cahn, *J. Chem. Phys.* **42**, 93 (1965).
54. H. Jinnai, H. Hasegawa, T. Hashimoto, and C. C. Han, *J. Chem. Phys.* **99**, 4845 (1993).
55. H. E. Cook, *Acta Metall.* **18**, 287 (1970).
56. M. Kurata, *Thermodynamics of Polymer Solutions*, MMI Press, New York, 1982.
57. P. G. deGennes, *Scaling Concepts in Polymer Physics*, Cornell University Press, Ithaca, N.Y., 1979.
58. K. Binder, *Phys. Rev. A* **29**, 341 (1984).
59. V. L. Ginzburg, *Sov. Phys. Solid State* **2**, 1824 (1960).
60. H. E. Stanley, *Introduction to Phase Transitions and Critical Phenomena*, Oxford University Press, Oxford, 1971.
61. D. Schwahn, K. Mortensen, and H. Yee-Madeira, *Phys. Rev. Lett.* **58**, 1544 (1987).
62. F. S. Bates, J. H. Rosedale, P. Stepanek, T. P. Lodge, P. Wiltzius, G. H. Fredrickson, and R. P. Hjelm, *Phys. Rev. Lett.* **65**, 1893 (1990).
63. A. I. Nakatani and M. D. Dadmun, eds., *Flow-Induced Structure in Polymers*, ACS Symposium Series 597, American Chemical Society, Washington, D.C. 1995.
64. E. Helfand and G. H. Fredrickson, *Phys. Rev. Lett.* **62**, 2468 (1989).
65. S. T. Milner, *Phys. Rev. E* **48**, 3674 (1993).
66. A. Onuki, *J. Phys.: Condens. Matter* **9**, 6119 (1997).
67. A. Onuki, R. Yamamoto, and T. Taniguchi, *J. Phys. II* **7**, 295 (1997).
68. S. Saito, T. Hashimoto, I. Morfin, P. Lindner, and F. Boue, *Macromolecules* **35**, 445 (2002).
69. J. T. Stull, in P. Cohen and B. C. Klee, eds., *Molecular Aspects of Cellular Regulation*, Elsevier, Amsterdam, 1988.
70. B. E. Kemp, M. W. Parker, S. H. Hu, T. Tiganis, and C. House, *Trends Biochem. Sci.* **19**, 440 (1994).
71. J. K. Krueer, R. C. Padre, and J. T. Stull, *J. Biol. Chem.* **270**, 16848 (1995).
72. D. B. Heidorn, P. A. Seeger, S. E. Rokop, D. K. Blumenthal, A. R. Means, H. Crespi, and J. Trewhella, *Biochemistry* **28**, 6757 (1989).
73. J. K. Kreuger, G. Zhi, J. T. Stull, and J. Trewhella, *Biochemistry* **37**, 13997 (1998).
74. L. Ionescu, C. Picot, R. Duplessix, M. Duval, H. Benoit, J. P. Lingelser, and Y. Gallot, *J. Polym. Sci.: Polym. Phys. Ed.* **19**, 1033 (1981).

MARK D. DADMUN  
University of Tennessee

## NOMENCLATURE OF POLYMERS

Nomenclature, as used in this article, refers to the naming of polymeric materials. The nomenclature of scientific communication is emphasized, although there is generally little reason for differences between scientific and other, eg, commercial, usages.

### Overview

Since the publication of the first edition of this encyclopedia, the International Union of Pure and Applied Chemistry (IUPAC) established the Commission on Macromolecular Nomenclature, which was, for the duration of its existence, the leading nomenclature body in the field of polymers. Between its inception in 1968 and the end of 2001, when the IUPAC underwent a major reorganization to a project-driven organization, the Commission promulgated a series of definitions and recommendations that established polymer nomenclature on a much more systematic basis than had previously been the case. The Commission developed a set of definitions for many of the basic terms dealing with polymer molecules, assemblies of polymer molecules, polymer solutions, polymer crystals, polymer melts and solids, polymerization reactions, etc. It also extended existing nomenclature to more complicated cases, such as double-strand (ladder and spiro) polymers. Completion of this work was accomplished by the early 1990s. Table 1 lists the Commission publications on polymer nomenclature.

Polymer naming and terminology became largely systematized and, following the IUPAC practice in other fields of chemistry, a compendium of polymer nomenclature recommendations was published in 1991 (32).

For 2002 and subsequent years, the IUPAC Macromolecular Division established the Subcommittee on Macromolecular Terminology, which has already embarked on the projects listed in Table 2.

The IUPAC has prepared an electronic *Guide to Macromolecular Terminology and Nomenclature* (35); Chapter 8 is entitled Macromolecular Nomenclature.

The International Standardization Organization (ISO), primarily through its Technical Committee TC/61 Plastics, and various national nomenclature bodies (such as that of the American Chemical Society) are also helping to shape the field.

Chemical Abstracts Service (CAS) is also an authority on polymer nomenclature. CAS publishes *Chemical Abstracts*, which is available both in printed format and electronically via STN<sup>®</sup> International, Scientific and Technical Information Network. The *Chemical Abstracts* Registry file provides many examples of CAS polymer nomenclature principles, which are published as Section 222 of Appendix IV in every edition of the *CA Index Guide* (36).

**Basic Definitions.** No nomenclature document was more fundamental to polymer science than the one which set forth definitions of basic terms. First published by the IUPAC Commission in 1974 (5), this document defined 53 terms, including polymer, constitutional unit, monomer, polymerization, regular polymer, tactic polymer, block polymer, graft polymer, monomeric unit, degree of polymerization, addition polymerization, condensation polymerization, homopolymer, copolymer, bipolymer, terpolymer, copolymerization, and many

**Table 1. Commission Publications on Polymer Nomenclature**

Title	Comment	Ref.
Report on Nomenclature in the Field of Macromolecules (1952)	Obsolete	1
Report on Nomenclature Dealing with Steric Regularity in High Polymers (1962)	Superseded by Ref. 3	2
Report on Nomenclature Dealing with Steric Regularity in High Polymers (1966)	Superseded by Ref. 10	3
Report of the Committee on Nomenclature of the International Commission on Macromolecules (1968)	Obsolete	4
Basic Definitions of Terms Relating to Polymers (1974)	Superseded by Ref. 22	5
List of Standard Abbreviations (Symbols) for Synthetic Polymers and Polymer Materials (1974)	Superseded by Ref. 7	6
Use of Abbreviations for Names of Polymeric Substances (1986)		7
Nomenclature of Regular Single-Strand Organic Polymers (1975)	Superseded by Ref. 29	8
Stereochemical Definitions and Notations Relating to Polymers (1980)	Provisional Recommendations 1980	9,10
Nomenclature for Regular Single-Strand and Quasi-Single-Strand Inorganic and Coordination Polymers (1984)	Provisional Recommendations 1984	11
	Recommendations 1984	12
Note on the Terminology for Molar Masses in Polymer Science (1984)		13
Source-Based Nomenclature for Copolymers (1985)		14
Definitions of Terms Relating to Individual Macromolecules, Their Assemblies, and Dilute Polymer Solutions (1988)		15
Definitions of Terms Relating to Crystalline Polymers (1988)		16
A Classification of Linear Single-Strand Polymers (1988)		17
Nomenclature of Regular Double-Strand (Ladder and Spiro) Organic Polymers (1993)		18
Structure-Based Nomenclature for Irregular Single-Strand Organic Polymers (1994)		19
Graphic Representations (Chemical Formulae) of Macromolecules (1994)		20
Basic Classification and Definitions of Polymerization Reactions (1994)		21
Glossary of Basic Terms in Polymer Science (1996)		22

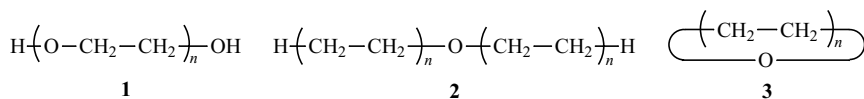
*(Continued)*

**Table 1. (Continued)**

Title	Comment	Ref.
Definitions of Terms Relating to Degradation, Aging, and Related Chemical Transformations of Polymers (1996)		23
Source-Based Nomenclature for Non-Linear Macromolecules and Macromolecular Assemblies (1997)		24
Definitions of Terms Relating to the Non-Ultimate Mechanical Properties of Polymers (1998)		25
Definitions of Basic Terms Relating to Low-Molar-Mass and Polymer Liquid Crystals (2001)		26
Generic Source-Based Nomenclature for Polymers (2001)		27
Definitions Relating to Stereochemically Asymmetric Polymerizations (2002)		28
Nomenclature of Regular Single-Strand Organic Polymers (2002)		29
Definitions of Terms Relating to Reactions of Polymers and Functional Polymers (2004)		30
Definitions of Terms Related to Polymer Blends, Composites, and Multiphase Polymeric Materials (2004)		31

others. Both structure-based and process-based definitions were given. In 1996, these recommendations were revised, enlarged, and updated (22). The new glossary, which provides a total of 135 terms, deals with three major groups of terms relating to molecules and molecular structure, substances, and reactions. These definitions are essential to any systematic polymer nomenclature, and the reader is strongly encouraged to consult the full document.

**The Principle of Source-Based Nomenclature.** Traditionally, polymers have been named by attaching the prefix “poly” to the name of the real or assumed monomer (the “source”) from which it is derived. Thus, polystyrene is the polymer made from styrene. When the name of the monomer comprises two or more words, parentheses should be used (7), as in poly(vinyl acetate), poly(methyl methacrylate), etc. Failure to use parentheses can lead to ambiguity: polychlorostyrene can be the name of either a polychlorinated (monomeric) styrene or of a polymer derived from chlorostyrene; polyethylene oxide can refer to either the polymer **1**, the polymer **2**, or the macrocycle **3**.



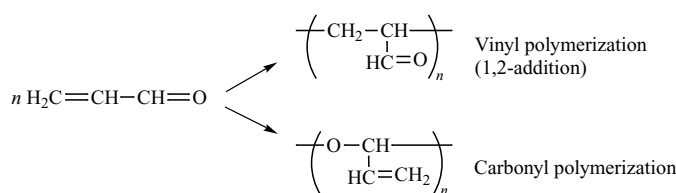
These problems are easily overcome with parentheses: names such as poly(chloro)styrene, poly(chlorostyrene), and poly(ethylene oxide) clearly indicate the part of the name to which the prefix “poly” refers. The omission of parentheses is, unfortunately, still common in the literature.

**Table 2. Subcommittee Projects on Polymer Nomenclature and Terminology<sup>a</sup>**

Title	Anticipated completion date
<i>Compendium of Macromolecular Terminology and Nomenclature</i> (The Purple Book), 2nd ed.	2005
Definitions of terms relating to the structure and processing of inorganic and polymeric gels and networks, and inorganic polymeric materials	2006
Glossary of class names of polymers based on their chemical structure and molecular architecture	2006 or 2007
Kinetics, thermodynamics, and mechanisms of polymerizations	2005 or 2006
Nomenclature for chemically modified polymers	2006 or 2007
Nomenclature for macromolecular rotaxanes	2006 or 2007
Nomenclature for rotaxanes	2006
Source-based nomenclature for organic homopolymers and copolymers	2007 or 2008
Terminology and nomenclature of macromolecules with cyclic structures	2006
Terminology and structure-based nomenclature of dendritic and hyperbranched polymers	2006 or 2007
Terminology of polymers with ionizable groups and polymers containing ions	2005 or 2006

<sup>a</sup>An italicized title indicates a book; the other items listed will be published as recommendations in *Pure and Applied Chemistry*.

The principal deficiency of source-based nomenclature is that the chemical structure of the monomeric unit in a polymer is not identical with that of the monomer (eg,  $-\text{CHX}-\text{CH}_2-$  versus  $\text{CHX}=\text{CH}_2$ ); thus, a “polymonomer” name is actually a misnomer. The structure of the constitutional repeating unit may also not be implied in this scheme; for example, the name polyacrolein does not indicate whether the vinyl or the aldehyde group has polymerized.



Depending on the polymerization conditions, different types of polymerization can take place with many other monomers. Furthermore, a name such as poly(vinyl alcohol) refers to a hypothetical source, since this polymer is obtained by hydrolysis of poly(vinyl acetate).

Despite these serious deficiencies, source-based nomenclature is still firmly entrenched in the industrial literature and, to a lesser extent, in scientific communication. It originated at a time when polymer science was less developed and the structure of most polymers was ill-defined. The significant advances made during the last 50 years on the structure determination of polymers are gradually shifting the emphasis of polymer nomenclature away from starting materials and toward the structure of the macromolecules.



**The Principle of Structure-Based Nomenclature.** Structure-based nomenclature is based on a method of naming the sequence of constitutional or structural units that represent the ideal, and sometimes the actual, repeating pattern of the structure of a typical macromolecule in a polymer. The name has no direct relation to the structure of the (co)monomer(s) used to synthesize the polymer. Details are given below in both the IUPAC Nomenclature and Chemical Abstracts Nomenclature sections entitled “Structure-Based Nomenclature.”

## IUPAC Nomenclature

### Source-Based Nomenclature.

*Homopolymers.* Although source-based names are usually simpler and less rigorous than structure-based names, historically the Commission has not systematically recommended source-based names for homopolymers because it considered that the more rigorous structure-based names were more appropriate for scientific communications (27). This rationale was based upon two specific points:

- (1) A homopolymer that can be represented by a source-based name can usually be given a completely unambiguous structure-based representation, and such a representation should therefore be ideally accompanied by a structure-based name. A source-based name was therefore deemed redundant.
- (2) There are cases in which the simplicity of source-based nomenclature leads to ambiguous names for homopolymers. Two examples illustrate this point:
  - i. A source-based name such as poly(buta-1,3-diene) or polybutadiene does not indicate whether the structure is 1,2-, 1,4-*cis*-, or 1,4-*trans*-.
  - ii. The polyacrolein example cited above.

Despite the Commission's long-standing position, the scientific community has continued to use source-based nomenclature for homopolymers such as polystyrene and poly(vinyl acetate) because of their simplicity, convenience, and obvious relationship with the monomers from which the homopolymers were prepared. The Commission therefore decided to recommend source-based nomenclature as an alternative official nomenclature for homopolymers in a 2001 publication (27). Consequently, both source-based and structure-based names are now available for most polymers. The names of monomers in the source-based names may be trivial or semisystematic, if well established by usage, not necessarily only those retained in the 1993 *A Guide to IUPAC Nomenclature of Organic Compounds* (33).

The broad principle is to write the source-based name of a homopolymer by combining the prefix “poly” with the name of the monomer. When the latter consists of more than one word, or any ambiguity is anticipated, the name of the monomer is parenthesized.

The same publication (27) recommended generic source-based nomenclature, which comprises the optional addition of a polymer class name to the

source-based name of the polymer. The addition is recommended only to avoid ambiguity or to add clarification.

*Example.* The source-based name poly(vinyloxirane) is ambiguous; ambiguity about the structure is removed by writing either polyalkylene:vinyloxirane to

accompany the structure-based representation  $\begin{array}{c} \text{---}(\text{CH}-\text{CH}_2)\text{---} \\ \diagup \quad \diagdown \\ \text{O} \end{array}$  or polyether:vinyloxirane to accompany the structure-based representation  $\begin{array}{c} \text{---}(\text{O}-\text{CH}-\text{CH}_2)\text{---} \\ | \\ \text{CH}=\text{CH}_2 \end{array}$ .

**Copolymers.** Copolymers are polymers that are derived from more than one species of monomer (22). Similarly to homopolymers, source-based nomenclature has been applied to copolymers (14). The principal problem in this scheme is to define the kind of arrangement in which various types of monomeric units are related to each other. Seven types of separate arrangements have been defined, which are shown in Table 3, where A, B, and C represent the names of monomers. The monomer names are linked through an italicized qualifier used as either a connective (infix), such as “-co-,” to form the name of the copolymer, as in poly(styrene-co-acrylonitrile), or a prefix, such as “co.” The order of citation of the monomers is arbitrary.

An equally acceptable alternative scheme, shown in the last column of Table 3, utilizes the prefix “copoly” followed by citation of the names of the monomers used, separated from each other by a solidus (oblique stroke). Parentheses are also needed. For example, copoly(styrene/butadiene) denotes an unspecified copolymer of styrene and butadiene. The other connectives in Table 3 are placed *before* such names to provide additional structural information, as in *ran*-copoly(ethylene/vinyl acetate) or *alt*-copoly(styrene/maleic anhydride). It is unnecessary to use parentheses to enclose names of monomers comprising more than one word, eg, vinyl acetate, maleic anhydride, methyl acrylate, etc; the names of the polymers, as written here, are unambiguous.

The names of copolymers, derived either from the main scheme or the alternative, can be further modified to indicate various structural features. For example, the chemical nature of end groups can be specified as  $\alpha$ -X- $\omega$ -Y-poly(A-*alt*-B), as in  $\alpha$ -butyl- $\omega$ -carboxy-*block*-copoly(styrene/butadiene).

Subscripts placed immediately after the formula of the monomeric unit or the block designate the degree of polymerization or repetition. On the other hand, mass and mole fractions and relative molecular masses, which in most cases are average quantities, are expressed by placing corresponding figures after the complete name of the copolymer. The order of citation is as for the monomeric species in the name. Unknown quantities are designated by *a*, *b*, etc. Table 4 gives some examples.

The complete document (14) should be consulted for names of more complex copolymers, eg, those having a multiplicity of grafts or having chains radiating from a central atom.

The utility of generic source-based nomenclature (27) can also be illustrated for source-based names of copolymers. As for homopolymers, the addition of a polymer class name is recommended only to avoid ambiguity or to add clarification.

*Example.* The source-based name poly[(benzene-1,2:4,5-tetracarboxylic dianhydride)-*alt*-4,4'-oxydianiline] is ambiguous; ambiguity about the

**Table 3. IUPAC Nomenclature of Copolymers<sup>a</sup>**

Type	Arrangement of monomeric units	Representation	Example	
			Connective	Alternative name
Unspecified	Unknown or unspecified	(A-co-B)	-co-	Copoly(styrene/methyl methacrylate)
Statistical	Obeys known statistical laws	(A-stat-B-stat-C)	-stat-	stat-Copoly(styrene/acrylonitrile-butadiene)
Random	Obeys Bernoullian statistics	(A-ran-B)	-ran-	ran-Copoly(ethylene/vinyl acetate)
Alternating	Alternating sequence	(AB) <sub>n</sub>	-alt-	alt-Copoly(ethylene glycol/terephthalic acid)
Periodic	Periodic with respect to at least three monomeric units	(ABC) <sub>n</sub> (ABB) <sub>n</sub> (AABB) <sub>n</sub> (ABAC) <sub>n</sub>	-per-	per-Copoly(formaldehyde/ethylene oxide/ethylene oxide)
Block	Linear arrangement of blocks	—AAAA—BBBB—	-block- <sup>b</sup>	block-Copoly(styrene/butadiene)
Graft	Polymeric side chain different from main chain <sup>c</sup>	—AAAAA—   B   B   B   B	-graft- <sup>d</sup>	graft-Copoly(butadiene/styrene)

<sup>a</sup>Main system described in IUPAC document (14); an alternative scheme is described in the text.

<sup>b</sup>The connective -b- has also been used.

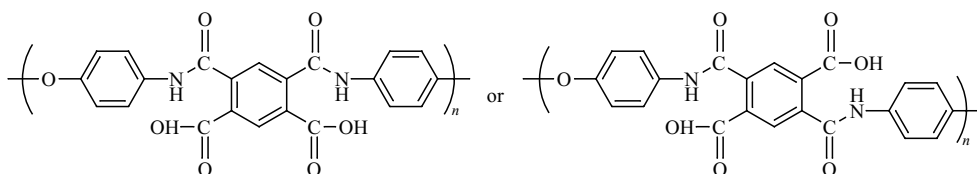
<sup>c</sup>Main chain (or backbone) is specified first in the name.

<sup>d</sup>The connective -g- has also been used.

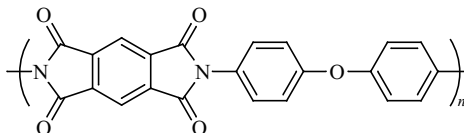
Table 4. Examples of the IUPAC Nomenclature Formats for Copolymers

Description	Nomenclature formats
A block copolymer containing 75 mass% of polybutadiene and 25 mass% of polystyrene	Polybutadiene- <i>block</i> -polystyrene (0.75:0.25 <i>w</i> ) or <i>block</i> -copoly(butadiene/styrene) (75:25 mass %)
A graft copolymer, comprising a polyisoprene backbone grafted with isoprene and acrylonitrile units in an unspecified arrangement that contains 85 mol % of isoprene units and 15 mol% of acrylonitrile units	Polyisoprene- <i>graft</i> -poly(isoprene-co-acrylonitrile) (0.85:0.15 <i>x</i> ) or <i>graft</i> -copoly[isoprene/(isoprene; acrylonitrile)] (85:15 mol%)
A graft copolymer comprising 75 mass% of polybutadiene with a relative molecular mass of 90,000 as the backbone, and 25 mass% of polystyrene in grafted chains with a relative molecular mass of 30,000	Polybutadiene- <i>graft</i> -polystyrene (75:25 mass%; 90 000:30 000 $M_r$ )
A graft copolymer in which the polybutadiene backbone has a degree of polymerization (DP) of 1,700 and the polystyrene grafts have an unknown DP	<i>graft</i> -copoly(butadiene/styrene) (1700: <i>a</i> DP)

structure is removed by writing poly(amide-acid):[(benzene-1,2:4,5-tetracarboxylic dianhydride)-*alt*-4,4'-oxydianiline] to accompany the structure-based representation



and polyimide:[(benzene-1,2:4,5-tetracarboxylic dianhydride)-*alt*-4,4'-oxydianiline] to accompany the structure-based representation.



In 1997, the principles of source-based nomenclature for regular copolymers were extended to nonlinear macromolecules and macromolecular assemblies (24), which are classified according to the following terms: cyclic, branched (long- and short-branched), micronetwork, network, blend, semiinterpenetrating polymer network, interpenetrating polymer network, and polymer-polymer complex. The range of italicized qualifiers, listed as connectives in Table 3 for regular copolymers, was extended by addition of new qualifiers such as “*blend*,” “*comb*,” “*star*,” or “*net*.” Table 5 lists the new qualifiers, together with examples of their

use. Quantitative characteristics of a macromolecule or an assembly of macromolecules, such as mass and mole fractions or percentages as well as the degrees of polymerization and molar masses, may be expressed by placing corresponding figures after the complete name. The complete document (24) should be consulted for details and more examples.

### Structure-Based Nomenclature.

**Regular Single-Strand Organic Polymers.** For organic polymers that are regular (ie, have only one species of constitutional repeating unit in a single sequential arrangement) and comprise only single strands, the IUPAC has promulgated a structure-based system of naming polymers (29). Originally devised by the Nomenclature Committee of the American Chemical Society Polymer Division (36), the system consists of naming a polymer as “poly(constitutional repeating unit),” wherein the repeating unit is named as a bivalent organic group according to the usual nomenclature rules for organic chemistry. It is important to note that, in structure-based nomenclature, the name of the constitutional repeating unit has no direct relationship to the source from which the unit was prepared. The name is simply that of the identifiable constitutional repeating unit in the polymer, and locants for unsaturation, substituents, etc are dictated by the *structure* of the unit.

The steps involved in naming the constitutional repeating unit (CRU) are (1) identification of the unit (taking into account the kinds of atoms in the main chain and the location of substituents), (2) orientation of the unit; and (3) naming of the unit. The CRUs are named systematically according to the IUPAC-recommended nomenclature of organic compounds (33). Examples of names for some common polymers are given in Table 6. Note that, in this system, parentheses, brackets, braces, or a combination of these, are always used to enclose the CRU. For organic names, the IUPAC uses parentheses for the innermost set, then brackets, then braces, thus: {[(. . .)]}. If further nesting is required, this cycle is repeated: {[(. . .)]}, [{[(. . .)]}], {[{[(. . .)]}]}, etc.

Structure-based nomenclature can be utilized to name polymers of great complexity, provided only that they be regular and single stranded. Among these are polymers the constitutional repeating units of which consist, themselves, of a series of smaller subunits, polymers with hetero atoms or heterocyclic ring systems in the main chain, and polymers with substituents on acyclic or cyclic subunits of constitutional repeating units. It should be noted that structure-based nomenclature is also applicable to copolymers having a regular structure, regardless of the starting materials used, eg, poly(oxyethyleneoxyterephthaloyl) for poly(ethylene terephthalate) (14).

The basic principles of structure-based nomenclature have been extended beyond regular, single-strand organic polymers (29) to single-strand and quasi-single-strand inorganic and coordination polymers (12), double-strand (ladder and spiro) polymers (18), irregular single-strand organic polymers (19), and other complex systems. Work in this field is continuing.

Structure-based nomenclature has gained wide acceptance in the scientific literature, eg, in *Chemical Abstracts*, because it overcomes many of the deficiencies of source-based nomenclature.

**Inorganic and Coordination Polymers.** The nomenclature of regular single-strand inorganic and coordination polymers (12) is governed by the same fundamental principles as those for single-strand organic polymers. The name

**Table 5. IUPAC Source-Based Nomenclature for Nonlinear Macromolecules and Macromolecular Assemblies**

Macromolecule or assembly	Italicized qualifier	Examples	Comments
Cyclic	<i>cyclo</i>	<i>cyclo</i> -Poly(dimethylsiloxane)	
Branched, unspecified		<i>cyclo</i> -Poly(styrene- <i>stat</i> - $\alpha$ -methylstyrene)	
	<i>branch</i>	<i>branch</i> -Polystyrene- <i>v</i> -divinylbenzene	Polystyrene crosslinked with divinylbenzene, insufficient to cause a network to form
Short-chain branched	<i>sh-branch</i>	<i>sh-branch</i> -Polyethylene	
Long-chain branched	<i>l-branch</i>	<i>l-branch</i> -Poly(ethyl acrylate)- <i>v</i> -(ethylene dimethacrylate)	
Branched with branch points of functionality <i>f</i>	<i>f-branch</i> ( <i>f</i> is given a numerical value)		
Comb(like)	<i>comb</i>	<i>comb</i> -Poly(styrene- <i>stat</i> -acrylonitrile)	Both the main chain and side chains are statistical copolymer chains of styrene and acrylonitrile
Star		Polystyrene- <i>comb</i> -polyacrylonitrile <sup>a</sup>	Main chains of styrene homopolymer; side chains of acrylonitrile homopolymer <sup>b</sup>
	<i>star</i>	Polystyrene- <i>comb</i> -[polyacrylonitrile; poly(methyl methacrylate)] <sup>a</sup> <i>star</i> -(PolyA; polyB; polyC)	A variegated star copolymer molecule consisting of arm(s) of polyA, arm(s) of polyB, and arm(s) of polyC
		<i>star</i> -(PolyA- <i>block</i> -polyB- <i>block</i> -polyC)	Star copolymer molecule, each arm of which consists of the same block-copolymer chain

Star with $f$ arms		<i>star</i> -[Polystyrene- <i>block</i> -poly(methyl methacrylate)]	Each arm of the star macromolecule is a block copolymer chain with a polystyrene block attached to the central unit
	$f$ - <i>star</i> ( $f$ is given a numerical value)	4- <i>star</i> -Polystyrene	
		3- <i>star</i> -Polystyrene- $\nu$ -methyltrichlorosilane <i>star</i> -(Polyacrylonitrile; polystyrene) ( $M_r$ 100,000:20,000)	Star macromolecule consisting of arms of polyacrylonitrile of a total $M_r = 100,000$ and arms of polystyrene of a total $M_r = 20,000$
		6- <i>star</i> -(Polyacrylonitrile ( $f$ 3); polystyrene ( $f$ 3)) ( $M_r$ (arm) 50,000:10,000)	A six-armed star macromolecule consisting of three arms of polyacrylonitrile, each of $M_r = 50,000$ , and three arms of polystyrene, each of $M_r = 10,000$
Network		<i>net</i> -Polybutadiene	
	<i>net</i>	<i>net</i> -Poly(phenol-co-formaldehyde) <i>net</i> -Polybutadiene- $\nu$ -sulfur	Polybutadiene vulcanized with sulfur
		<i>net</i> -Polystyrene- $\nu$ -divinylbenzene	Polystyrene crosslinked with divinylbenzene to form a network
		<i>net</i> -Poly[(hexane-1,6-diyl diisocyanate)- <i>alt</i> -glycerol] <i>net</i> -Poly[styrene- <i>alt</i> -(maleic anhydride)]- $\nu$ -(ethylene glycol)	Alternating copolymer of styrene and maleic anhydride crosslinked with ethylene glycol to form a network

(Continued)

**Table 5. (Continued)**

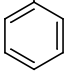
Macromolecule or assembly	Italicized qualifier	Examples	Comments
		Poly[(ethylene glycol)- <i>alt</i> -(maleic anhydride)]- <i>net</i> -oligostyrene	Unsaturated polyester cured with styrene
		Poly(methyl methacrylate)- <i>net</i> -poly(ethylene oxide)	
		[Poly(butyl vinyl ether)- <i>v</i> -(2-vinylloxyethyl methacrylate)]- <i>net</i> -[poly(methyl methacrylate)- <i>v</i> -(2-vinylloxyethyl methacrylate)]	Poly(butyl vinyl ether) and poly(methyl methacrylate) chains crosslinked mutually with 2-vinylloxyethyl methacrylate to form a network
Micronetwork	<i>μ-net</i>	<i>μ-net</i> -Poly[styrene- <i>stat</i> -(vinyl cinnamate)]	Crosslinked copolymeric micronetwork
Polymer blend	<i>blend</i>	Polystyrene- <i>blend</i> -poly(2,6-dimethylphenol) ( <i>net</i> -Polystyrene)- <i>blend</i> -( <i>net</i> -Polybutadiene) ( <i>net</i> -Polybutadiene)- <i>ipn</i> -( <i>net</i> -polystyrene)	Blend of two networks IPN of two networks
Interpenetrating polymer network	<i>ipn</i>	[ <i>net</i> -Poly(styrene- <i>stat</i> -butadiene)]- <i>ipn</i> -[ <i>net</i> -Poly(ethyl acrylate)]	IPN of two networks
Semi-interpenetrating polymer network	<i>sipn</i>	( <i>net</i> -Polystyrene)- <i>sipn</i> -poly(vinyl chloride)	SIPN of a polystyrene network and a linear poly(vinyl chloride)
Polymer-polymer complex	<i>compl</i>	Poly(acrylic acid)- <i>compl</i> -poly(4-vinylpyridine)	Complex of two species of linear macromolecules
		Poly[(methyl methacrylate)- <i>stat</i> -(methacrylic acid)]- <i>compl</i> -poly( <i>N</i> -vinyl-2-pyrrolidone)	Complex of statistical copolymer and homopolymer molecules

<sup>a</sup>In naming nonlinear copolymer molecules having linear subchains of two or more types, the italicized connective for the skeletal structure is placed between the source-based names of the types of constituent linear subchains. In the case of branched and comb-like macromolecules, the linear chain named before the connective is that which forms the main chain, whereas that (those) named after the connective forms (form) the side chain(s). The names of different species of side chain are separated by semicolons. In the case of variegated star macromolecules, the prefix is placed before the name of the macromolecule with the different species of arms separated by semicolons.

<sup>b</sup>Equivalent to polystyrene-*graft*-polyacrylonitrile; -*graft*- is recommended for these cases. However, *comb* as a prefix cannot be replaced by *graft*.



**Table 6. Examples of Structure-Based and Source-Based Names for some Common Polymers<sup>a</sup>**

Structure	Structure-based name	Source-based or trivial name
$\left(\text{CH}_2-\text{CH}_2\right)_n$	Poly(methylene)	Polyethylene
$\left(\text{CH}-\text{CH}_2\right)_n$   CH <sub>3</sub>	Poly(1-methylethylene)	Polypropene; polypropylene
$\left(\text{C}(\text{CH}_3)_2-\text{CH}_2\right)_n$	Poly(1,1-dimethylethylene)	Polyisobutylene
$\left(\text{C}=\text{CH}-\text{CH}_2-\text{CH}_2\right)_n$   CH <sub>3</sub>	Poly(1-methylbut-1-ene-1,4-diyl)	Polyisoprene
$\left(\text{CH}-\text{CH}_2\right)_n$   	Poly(1-phenylethylene)	Polystyrene
$\left(\text{CH}-\text{CH}_2\right)_n$   Cl	Poly(1-chloroethylene)	Poly(vinyl chloride)
$\left(\text{CH}-\text{CH}_2\right)_n$   CN	Poly(1-cyanoethylene)	Polyacrylonitrile
$\left(\text{CH}-\text{CH}_2\right)_n$   OCOCH <sub>3</sub>	Poly(1-acetoxyethylene)	Poly(vinyl acetate)
$\left(\text{CF}_2-\text{CH}_2\right)_n$	Poly(1,1-difluoroethylene)	Poly(vinylidene fluoride)
$\left(\text{CF}_2-\text{CF}_2\right)_n$	Poly(difluoromethylene)	Polytetrafluoroethylene
$\left(\text{CH}_2-\text{CH}(\text{OCH}_2\text{CH}_2\text{CH}_3)-\text{CH}_2\right)_n$   OCH <sub>2</sub> CH <sub>2</sub> CH <sub>3</sub>	Poly[(2-propyl-1,3-dioxane-4,6-diyl)methylene]	Poly(vinyl butyral)
$\left(\text{C}(\text{CH}_3)(\text{COOCH}_3)-\text{CH}_2\right)_n$	Poly[1-(methoxycarbonyl)-1-methylethylene]	Poly(methyl methacrylate)
$\left(\text{O}-\text{CH}_2-\text{CH}_2\right)_n$	Poly(oxyethylene)	Poly(ethylene oxide)
$\left(\text{O}-\text{C}_6\text{H}_4\right)_n$	Poly(oxy-1,4-phenylene)	Poly(phenylene oxide)
$\left(\text{O}-\text{CH}_2-\text{CH}_2-\text{O}-\text{C}(=\text{O})-\text{C}_6\text{H}_4-\text{C}(=\text{O})\right)_n$	Poly(oxyethyleneoxyterephthaloyl)	Poly(ethylene terephthalate)

(Continued)

Table 6. (Continued)

Structure	Structure-based name	Source-based or trivial name
$\left[ \text{NH}-\underset{\text{O}}{\underset{\parallel}{\text{C}}}-(\text{CH}_2)_4-\underset{\text{O}}{\underset{\parallel}{\text{C}}}-\text{NH}-(\text{CH}_2)_6 \right]_n$	Poly(iminoadipoyl-iminohexane-1,6-diyl)	Poly[hexamethylenediamine- <i>alt</i> -(adipic acid)] or poly(hexamethylene adipamide)
$\left( \text{CH}=\underset{\text{O}}{\underset{\parallel}{\text{C}}}-\text{O}-\underset{\text{O}}{\underset{\parallel}{\text{C}}}=\text{CH}-\underset{\text{C}_6\text{H}_5}{\text{CH}}-\text{CH}_2 \right)_n$	Poly[(2,5-dioxotetrahydrofuran-3,4-diyl)-(1-phenylethylene)]	Poly(maleic anhydride- <i>alt</i> -styrene)

<sup>a</sup>Ref. 29.Table 7. Examples of Inorganic and Coordination Polymers<sup>a</sup>

Name	Structure
<i>catena</i> -Poly[dimethyltin]	$\left( \begin{array}{c} \text{CH}_3 \\   \\ \text{---} \text{Sn} \text{---} \\   \\ \text{CH}_3 \end{array} \right)_n$
<i>catena</i> -Poly[titanium-tri- $\mu$ -chloro]	$\left( \begin{array}{c} \text{---} \text{Ti} \text{---} \\ \diagup \quad \diagdown \\ \text{Cl} \quad \text{Cl} \\ \diagdown \quad \diagup \\ \text{---} \end{array} \right)_n$
<i>catena</i> -Poly[nitrogen- $\mu$ -thio]	$\text{---} \text{N} \text{---} \text{S} \text{---}$
<i>catena</i> -Poly[silver- $\mu$ -(cyano- <i>N</i> :C)]	$\left( \text{---} \text{Ag} \text{---} \text{NC} \right)_n$
<i>catena</i> -Poly[(diphenylsilicon)- $\mu$ -oxo]	$\left( \begin{array}{c} \text{C}_6\text{H}_5 \\   \\ \text{---} \text{Si} \text{---} \text{O} \text{---} \\   \\ \text{C}_6\text{H}_5 \end{array} \right)_n$
$\alpha$ -Ammine- $\omega$ -(amminedichlorozinc)- <i>catena</i> -poly[(amminechlorozinc)- $\mu$ -chloro]	$\text{H}_3\text{N} \left( \begin{array}{c} \text{NH}_3 \\   \\ \text{---} \text{Zn} \text{---} \text{Cl} \\   \\ \text{Cl} \end{array} \right)_n \text{---} \begin{array}{c} \text{NH}_3 \\   \\ \text{---} \text{Zn} \text{---} \text{Cl} \\   \\ \text{Cl} \end{array}$

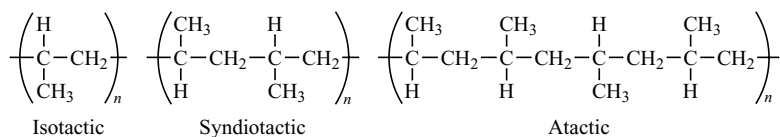
<sup>a</sup>If named according to the rules for linear organic polymers (29), the polymers on lines 1 and 5 would be oriented and named poly(dimethylstannanediyl) and poly[oxy(diphenylsilanediyl)], respectively.

of such a polymer is that of the smallest constitutional repeating unit prefixed by the terms “poly,” “*catena*” (for linear chains) or other structural indicator, and designations for end groups. The structural units are named by the nomenclature rules for inorganic and coordination chemistry. Table 7 lists some examples.

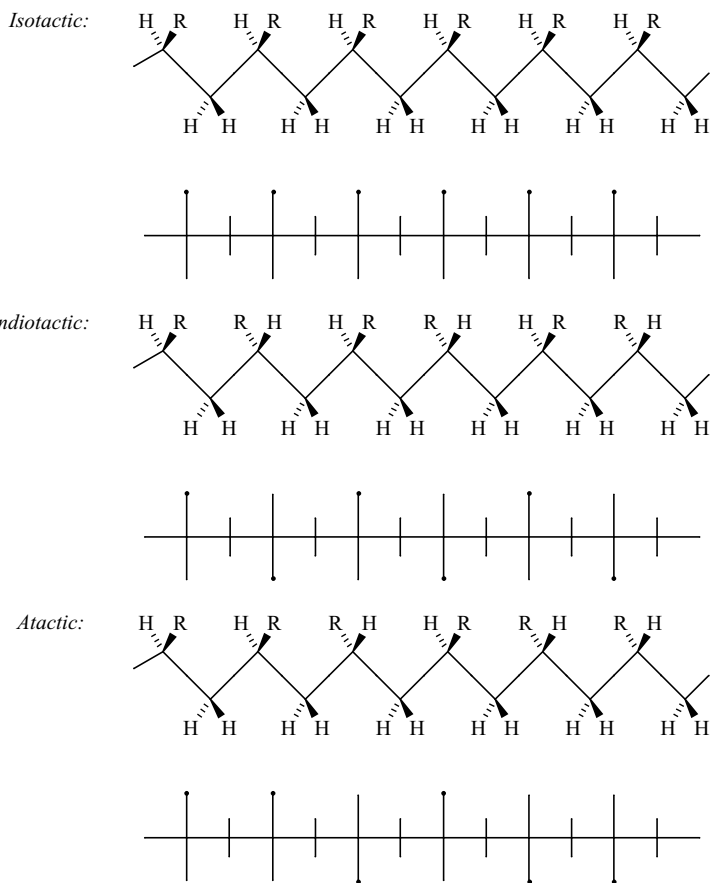
**Stereochemical Definitions and Notations.** Structure-based nomenclature of regular polymers (10) can denote stereochemical features if the repeating unit used is the configurational base unit, ie, a constitutional repeating unit

having one or more sites of defined stereoisomerism in the main chain of a polymer molecule (22). Structure-based names are then derived in the usual fashion. The various stereochemical features that are possible in a polymer must be defined.

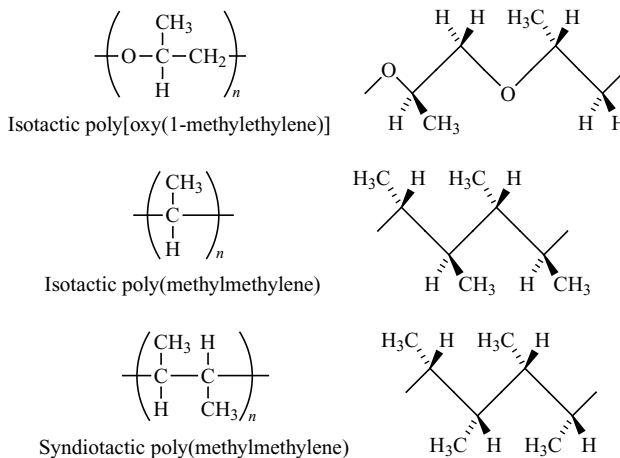
The pioneering work of Natta and co-workers introduced the concept of tacticity, ie, the orderliness of the succession of configurational repeating units in the main chain of a polymer. For example, in polypropene (polypropylene), possible steric arrangements are (shown in Fischer projections displayed horizontally):



An isotactic polymer has only one species of configurational base unit in a single sequential arrangement, and a syndiotactic polymer shows an alternation of configurational base units that are enantiomeric, whereas in an atactic polymer the molecules have equal numbers of the possible configurational base units in a random sequence distribution. This can be generalized as follows:



Further examples of tactic polymers are



The published IUPAC document (10) should be consulted for more information.

*Regular Double-Strand (Ladder and Spiro) Organic Polymers.* Structure-based and source-based nomenclature rules have been extended to regular double-strand (ladder and spiro) organic polymers (18). A double-strand polymer is defined as a polymer, the molecules of which are formed by an uninterrupted sequence of rings with adjacent rings having one atom in common (spiro polymer) or two or more atoms in common (ladder polymer).

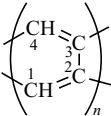
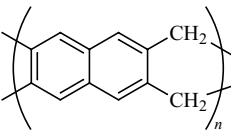
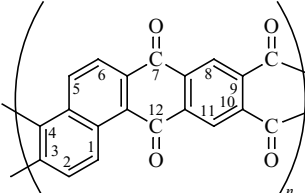
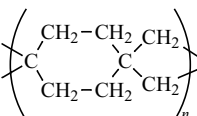
The structure-based nomenclature rests upon the selection of a preferred CRU (22,29) of which the polymer is a multiple; the name of the polymer is the name of this repeating unit prefixed by "poly." The unit itself is named wherever possible according to the established principles of organic nomenclature (33). For double-strand polymers, this unit usually is a tetravalent group denoting attachment to four atoms. Since some of these attachments may be double bonds, the unit may be hexavalent or octavalent. Table 8 lists some examples.

As in linear, single-strand polymers, substituents that are clearly part of the constitutional repeating unit are denoted by means of prefixes affixed to the name of the subunit to which they are bound.

End groups are specified by prefixes cited in front of the name of the polymer. The ends designated by  $\alpha$  and  $\alpha'$  are those attached to the left side of the constitutional repeating unit as drawn; the end groups attached to the right side are designated by  $\omega$  and  $\omega'$ . End groups are named by the nomenclature rules for organic compounds (33). The designations and names of the end groups proceed in a clockwise direction starting from the lower left:  $\alpha, \alpha', \omega, \omega'$ . Table 9 lists two examples with substituents (lines 1 and 2) and one with both substituents and end groups (line 3).

Source-based nomenclature identifies the starting monomer(s) from which the double-strand polymer is prepared with addition of an appropriate prefix

**Table 8. Examples of Structure-Based Nomenclature for Regular Double-Strand (Ladder and Spiro) Organic Polymers**

Name	Structure
Poly(buta-1,3-diene-1,4:3,2-tetrayl)	
Poly(naphthalene-2,3:6,7-tetrayl-6,7-dimethylene)	
Poly[(7,12-dihydro-7,12-dioxobenzo[α]anthracene-3,4:9,10-tetrayl)-9,10-dicarbonyl]	
Poly(cyclohexane-1,1:4,4-tetrayl-4,4-dimethylene)	

“*ladder*–” or “*spiro*–.” Examples are

- (1) *ladder*-poly(1,4-diphenyldiacetylene)
- (2) *ladder*-poly(2,5-dichloro-3,6-dihydroxy-*p*-benzoquinone)
- (3) *ladder*-poly[(pyromellitic dianhydride)-*alt*-(1,2,5,6-tetraaminoanthraquinone)]
- (4) *spiro*-poly[dispiro[3.1.3.1]decane-2,8-bis(carbonyl chloride)]

The rules are complex, and the published IUPAC document (18) should be consulted for more information.

**Irregular Single-Strand Organic Polymers.** Irregular single-strand organic polymers are single-strand organic polymers that can be described by the repetition of more than one type of constitutional unit or that comprise constitutional units not all connected identically with respect to directional sense. A new system (19) names irregular polymers for which the source-based system is inadequate, eg, polymers that have undergone partial chemical modification, homopolymers having both head-to-tail and head-to-head arrangements of monomeric units, and polymers derived from a single monomer that can provide more than one kind of monomeric unit.

**Table 9. Examples of Nomenclature for Regular Double-Strand (Ladder and Spiro) Organic Polymers with Substituents and End Groups**

Name	Structure
Poly[(1,4-dimethyl-7-azabicyclo[2.2.1]heptane-2,3:5,6-tetrayl)-5,6-dicarbonyl]	
Poly(2,4-dimethyl-1,3,5-trioxa-2,4-disilapentane-1,5:4,2-tetrayl) <sup>a</sup>	
$\alpha\alpha'$ -Dihydro- $\omega,\omega'$ -dihydroxypoly(2,4-diphenyl-1,3,5-trioxa-2,4-disilapentane-1,5:4,2-tetrayl) <sup>a</sup>	

<sup>a</sup>The CRU is named using replacement nomenclature ("a" nomenclature) (18,33).

The new system also provides a structure-based alternative to source-based nomenclature for copolymers. Irregular polymers, oligomers, or blocks are named by placing the prefix "poly" before the structure-based names of the constitutional units; the latter are collectively enclosed in parentheses, with the names of the component constitutional units separated by solidi (oblique strokes).

Block copolymers are named by using dashes (double-length hyphens) for the bonding of blocks with each other and with junction units. With graft and star polymers, the grafts or the arms, respectively, are considered to be substituents to the main chain, and the structure is named in the same way as a regular or irregular polymer. Table 10 lists some examples.

The published IUPAC document (19) should be consulted for more information.

## Chemical Abstracts Nomenclature

Chemical Abstracts Service is the publisher of *Chemical Abstracts* and corresponding products and services, which are available in the following formats:

**Table 10. Examples of Nomenclature for Irregular Single-Strand Organic Polymers**

Characteristics	Name	Structure <sup>a</sup>
A statistical copolymer comprising units derived from 1-phenylethene and 1-chloroethene joined head-to-tail	Poly(1-chloroethylene/1-phenylethylene)	$\left( \begin{array}{c} \text{---CH---CH}_2\text{---} \\   \quad   \\ \text{Cl} \quad \text{C}_6\text{H}_5 \end{array} \right)_n$
An irregular polymer derived from 1-chloroethene, the units of which are linked both head-to-tail and head-to-head	Poly(1-chloroethylene/2-chloroethylene)	$\left( \begin{array}{c} \text{---CH---CH}_2\text{---} \\   \quad   \\ \text{Cl} \quad \text{Cl} \end{array} \right)_n$
A modified (chlorinated) poly(methylene)	Poly(chloromethylene/dichloromethylene/methylene)	$\left( \begin{array}{c} \text{Cl} \\   \\ \text{---CH---} \\   \\ \text{Cl} \end{array} \right)_n$
A modified (partially hydrolyzed) head-to-tail poly(1-acetoxyethylene)	Poly(1-acetoxyethylene/1-hydroxyethylene)	$\left( \begin{array}{c} \text{---CH---CH}_2\text{---} \\   \quad   \\ \text{OCOCH}_3 \quad \text{OH} \end{array} \right)_n$
A triblock copolymer consisting of a sequence of three blocks joined directly or through unspecified junction units	Poly(oxy-1,4-phenylene)—poly(2-cyanoethylene)—poly(ethyleneoxy)	$\left( \text{---O---} \langle \text{benzene ring} \rangle \text{---} \right)_p \left( \text{---CH}_2\text{---CH---} \right)_q \left( \text{---CH}_2\text{---CH}_2\text{---O---} \right)_r$
A diblock copolymer in which the blocks are joined by a specific junction unit	Poly(ethyleneoxy)—dimethylsilanediyl—poly(1-chloroethylene)	$\left( \text{---CH}_2\text{---CH}_2\text{---O---} \right)_p \text{---} \left( \begin{array}{c} \text{CH}_3 \\   \\ \text{---Si---} \\   \\ \text{CH}_3 \end{array} \right)_q \left( \text{---CH---CH}_2\text{---} \right)_q$

(Continued)

**Table 10. (Continued)**

Characteristics	Name	Structure <sup>a</sup>
A graft copolymer with many of one type of graft unit	Poly[methylene/poly(2-phenylethylene)methylene]	$\left[ \text{---CH}_2\text{---} / \text{---CH---} \left( \text{CH}_2\text{---CH---} \right)_p \right]_n$ $\left[ \text{---O---} \text{C}_6\text{H}_5 \right]_n$
A poly(oxyphenylene) with a poly(2-chloro-ethylene) block grafted through a carbonyloxy group (a junction unit) to the 2-position in some of the rings	Poly{oxy-1,4-phenylene/oxy-2-[poly(2-chloroethylene)carbonyloxy]-1,4-phenylene}	$\left[ \text{---O---} \text{C}_6\text{H}_4 \text{---} \text{O---} \text{C}(=\text{O})\text{---} \left( \text{CH}_2\text{---CH---} \right)_p \text{Cl} \right]_n$
A four-armed star polymer comprising silane substituted with different polymer blocks	Bis[poly(but-2-ene-1,4-diyl)][poly(1-phenylethylene)][poly(2-phenylethylene)]silane	$\left( \text{CH}_2\text{---CH=CH---CH}_2 \right)_p \text{Si} \left( \text{CH}_2\text{---CH=CH---CH}_2 \right)_q \left( \text{CH}_2\text{---CH=CH---CH}_2 \right)_r$ $\left( \text{CH}_2\text{---CH=CH---CH}_2 \right)_p$ $\left( \text{CH}_2\text{---CH=CH---CH}_2 \right)_q$ $\left( \text{CH}_2\text{---CH=CH---CH}_2 \right)_r$

<sup>a</sup>The dashes at each end of the formulas on lines 1, 2, 3, 4, 7, and 8 are drawn fully inside the enclosing marks, because they do not necessarily denote terminal chemical bonds of the macromolecules.



printed, microform, online databases, CD-ROM, World Wide Web. Polymers selected for inclusion in the CAS Chemical Registry System and the *CA Chemical Substance Indexes* are indexed in following two ways:

- (1) in terms of the component monomer(s) from which they are prepared;
- (2) in terms of the structural representation of the polymer formed.

CAS has published its own set of principles governing how each type of polymer is registered and named (36). Specific polymers are named on the basis of the monomers from which they are formed and/or on the basis of their structure, as represented by a structural repeating unit (SRU). Since original documents sometimes provide insufficient structural information to allow generation of the SRU name, the method most frequently used for describing polymeric substances is by citation of the component monomers. However, a few commercial polymers, including poly(ethylene terephthalate) (PET), nylon 66, and nylon 6, each of which has a large number of index entries, are exceptions; they are indexed *only* at the SRU-based systematic polymer name.

CAS chemical nomenclature is in general agreement with the IUPAC recommendations. However, there is one important difference. For any given chemical substance, the IUPAC nomenclature guidelines always lead to an unambiguous name, but not necessarily to only one name. In most communications about chemical substances, this approach causes few problems, but where a formal, rigidly controlled index is needed, such as the *CA Chemical Substance Indexes*, it is insufficiently rigorous. CA Index names must be unique, unambiguous, completely reproducible, and written in a way that brings together alphabetically all structurally related substances (36). CAS recognizes that a unique name is required for indexing purposes and for substance identification, but it is not expected that the highly structured CA Index names would be used in normal communications among authors or lecturers, or in industry and in the primary publications.

The more fully systematic IUPAC rules were adapted for the highly ordered alphabetical CA indexes. Most common names and special rules for some classes of substances were discontinued in 1972. Names used in the previous CA indexes as well as trivial names used in the literature have been retained as cross-references in the *CA Index Guide* and in the CAS database, and are available for polymer searching and retrieval. For each identifiable substance, a rigid order of precedence of chemical functions and compound classes is followed to determine first the preferred "index heading parent," and then a single preferred name.

Systematic names of chemical substances in the indexes are arranged in inverted format as follows. The *index heading parent* (usually the basic skeleton name with a locant and suffix that denotes the principal function), a comma, any *substituents*, and any *modification* (derivative of the principal function). Table 11 lists some common monomers, with both common names and CA Index names.

Similarly, many commonly named multiplying and substituent groups have their systematic equivalents in CA Indexes. Table 12 lists some examples.

**Table 11. Examples of Common Monomers with Common Names and CA Index Names**

Common name	CA Index name
Acrylamide	2-Propenamide
Acrylic acid	2-Propenoic acid
Acrylonitrile	2-Propenenitrile
Adipic acid	Hexanedioic acid
<i>p</i> -Aminobenzoic acid	Benzoic acid, 4-amino-
Bisphenol A	Phenol, 4,4'-(1-methylethylidene)bis-
Butadiene	1,3-Butadiene
Butylene glycol	1,4-Butanediol
$\epsilon$ -Caprolactam	2 <i>H</i> -Azepine-2-one, hexahydro-
$\epsilon$ -Caprolactone	2-Oxepanone
Dimethyl terephthalate	1,4-Benzenedicarboxylic acid, dimethyl ester
Ethylene	Ethene
Ethylene glycol	1,2-Ethanediol
Ethylene oxide	Oxirane
Fumaric acid	2-Butenedioic acid (2 <i>E</i> )- <sup>a</sup>
Glycolic acid	Acetic acid, hydroxy-
Hexafluoropropylene	1-Propene, 1,1,2,3,3,3-hexafluoro-
Hexamethylenediamine	1,6-Hexanediamine
Hydroquinone	1,4-Benzenediol
<i>p</i> -Hydroxybenzoic acid	Benzoic acid, 4-hydroxy-
Isobutylene	1-Propene, 2-methyl-
Isophthalic acid	1,3-Benzenedicarboxylic acid
Isoprene	1,3-Butadiene, 2-methyl-
Lactic acid	Propanoic acid, 2-hydroxy-
Maleic acid	2-Butenedioic acid (2 <i>Z</i> )- <sup>a</sup>
Maleic anhydride	2,5-Furandione
Melamine	1,3,5-Triazine-2,4,6-triamine
Methacrylic acid	2-Propenoic acid, 2-methyl-
Methyl acrylate	2-Propenoic acid, methyl ester
Methyl methacrylate	2-Propenoic acid, 2-methyl-, methyl ester
4,4'-Methylenedianiline	Benzenamine, 4,4'-methylenebis-
Methylenedi- <i>p</i> -phenylene diisocyanate	Benzene, 1,1'-methylenebis[4-isocyanato-
4,4'-Oxydianiline	Benzenamine, 4,4'-oxybis-
<i>m</i> -Phenylenediamine	1,3-Benzenediamine
<i>p</i> -Phenylenediamine	1,4-Benzenediamine
Phthalic anhydride	1,3-Isobenzofurandione
Propylene	1-Propene
Propylene oxide	Oxirane, methyl-
Pyromellitic dianhydride	1 <i>H</i> ,3 <i>H</i> -Benzo[1,2- <i>c</i> :4,5- <i>c'</i> ]difuran-1,3,5,7-tetrone
Styrene	Benzene, ethenyl-
Terephthalic acid	1,4-Benzenedicarboxylic acid
2,4-Toluene diisocyanate	Benzene, 2,4-diisocyanato-1-methyl-
Vinyl acetate	Acetic acid ethenyl ester <sup>a</sup>
Vinyl alcohol	Ethenol
Vinyl chloride	Ethene, chloro-
Vinyl fluoride	Ethene, fluoro-
Vinylidene chloride	Ethene, 1,1-dichloro-
Vinylidene fluoride	Ethene, 1,1-difluoro-

<sup>a</sup>No typical comma between the parts of the name is present, because of a special formatting rule for large, subdivided index headings.

**Table 12. Examples of Multiplying and Substituent Groups with Common Names and CA Equivalents**

Common name	CA equivalent	Common name	CA equivalent
Adipoyl	1,6-Dioxo-1,6-hexanediyl	Allyl	2-Propenyl
<i>sec</i> -Butyl	1-Methylpropyl	<i>tert</i> -Butyl	1,1-Dimethylethyl
Ethylene	1,2-Ethanediyl	Hexamethylene	1,6-Hexanediyl
Isobutyl	2-Methylpropyl	Isophthaloyl	Carbonyl-1,3-phenylenecarbonyl
Isopropyl	1-Methylethyl	<i>p</i> -Phenylene	1,4-Phenylene
Succinyl	1,4-Dioxo-1,4-butanediyl	Terephthaloyl	Carbonyl-1,4-phenylenecarbonyl
Vinyl	Ethenyl	Vinylene	1,2-Ethenediyl

**Table 13. Examples of Common Names and Their CA Index Name Equivalents**

Common name	CA Index name	Molecular formula
Poly( <i>p</i> -aminobenzoic acid)	Benzoic acid, 4-amino-, homopolymer	(C <sub>7</sub> H <sub>7</sub> NO <sub>2</sub> ) <sub>x</sub>
Poly(methyl methacrylate)	2-Propenoic acid, 2-methyl-, methyl ester, homopolymer	(C <sub>5</sub> H <sub>8</sub> O <sub>2</sub> ) <sub>x</sub>
Polystyrene	Benzene, ethenyl-, homopolymer	(C <sub>8</sub> H <sub>8</sub> ) <sub>x</sub>
Poly(vinylidene fluoride)	Ethene, 1,1-difluoro-, homopolymer	(C <sub>2</sub> H <sub>2</sub> F <sub>2</sub> ) <sub>x</sub>

### Source-Based Nomenclature.

**Homopolymers.** The CA Index name is written by citation of the name of the monomer, and the term “homopolymer” is cited in the *modification*. Table 13 lists some examples.

**Copolymers.** The CA Index name is written by citation of the name of the senior comonomer, in inverted format, followed by a comma. The modification contains the expression “polymer with B, C, D, . . . and Z” where B, C, D, . . . , and Z are the names of the other comonomers, alphabetized, and in uninverted format, and also stereochemical and structural terms such as *isotactic*, *syndiotactic*, *alternating*, *block*, or *graft* whenever applicable. The senior comonomer is chosen by a set of principles that include a strict order of precedence of chemical functions and compound classes (36). The format is A, polymer with B, C, D, . . . , and Z in which A, B, C, D, . . . , and Z are the comonomers.

Before 2002, for most records, in addition to the CA Index names, systematic Index names were generated for each comonomer. Thus, for a copolymer containing *n* comonomers, a total of (*n* – 1) additional Index names, each beginning with the name of a different comonomer in the copolymer, were created. This practice was discontinued in 2002. Examples are

- (1) CA Index name: 1-Propene, polymer with ethene
- (2) Other CA names: Ethene, polymer with 1-propene
- (3) CA Index name: 2-Propenoic acid, 2-methyl-, polymer with ethene, 1-propene and 2-propenoic acid

**Table 14. Examples of Post-Treated Polymers**

Post-treated polymer <sup>a</sup>	CA Index name
Acrylic acid-methyl methacrylate copolymer esterified to an unknown degree to methyl acrylate	2-Propenoic acid, 2-methyl-, methyl ester, polymer with 2-propenoic acid, methyl ester <sup>b</sup>
Acrylic acid-styrene copolymer esterified to an unknown degree to methyl acrylate	2-Propenoic acid, polymer with ethenylbenzene, methyl ester
Ethylene-methacrylic acid copolymer neutralized to an unknown degree to sodium methacrylate	2-Propenoic acid, 2-methyl-, polymer with ethene, sodium salt <sup>c</sup>
Isophthalic acid-ethylene glycol copolymer post-treated to form the diallyl ester	1,3-Benzenedicarboxylic acid, polymer with 1,2-ethanediol, di-2-propenyl ester

<sup>a</sup>The degree of modification (esterification for lines 1 and 2, neutralization for line 3) is not part of the chemical record.

<sup>b</sup>Notice the difference in word order between the CA Index name of this modified copolymer and that of the unmodified methyl acrylate-methyl methacrylate copolymer, in which the second comonomer name is written in uninverted format: 2-propenoic acid, 2-methyl-, methyl ester, polymer with methyl 2-propenoate.

<sup>c</sup>Notice the difference in word order between the CA Index name of this modified copolymer and that of the unmodified ethylene-sodium methacrylate copolymer: 2-propenoic acid, 2-methyl-, sodium salt, polymer with ethene.

- (4) Other CA names: 1-Propene, polymer with ethene, 2-methyl-2-propenoic acid and 2-propenoic acid
- 2-Propenoic acid, polymer with ethene, 2-methyl-2-propenoic acid and 1-propene
  - Ethene, polymer with 2-methyl-2-propenoic acid, 1-propene and 2-propenoic acid

The CA Index name of a post-treated (modified) polymer is written by citation of the name of the polymer, inverted as described above; the *modification* segment of the name indicates how the polymer was post-treated. Post-treated polymers fall into two subcategories.

For esters, ethers, and salts of homopolymers and copolymers, this information is associated with the CA Index name and is part of a unique CAS Registry record. Table 14 lists some examples.

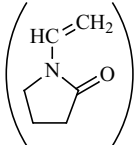
For other types of post-treated homopolymers and copolymers, such as those that have been aminated, chlorinated, hydrolyzed, etc, this type of information is present in the index entry only when associated with a specific document. CAS Registry numbers are not assigned to such post-treated polymers except for use in certain regulatory inventories, such as those mandated by the Toxic Substances Control Act. Table 15 lists some examples.

Telomers are named as copolymers with the term “telomer with” cited in the *modification* under either the monomer (taxogen) or the chain-transfer agent (telogen), depending on which is the senior component. Table 16 lists some examples.

**Table 15. Examples of Post-Treated Polymers (Halogenated or Chlorosulfonated to an Unknown Degree)**

Post-treated polymer	CA Index entry
Post-brominated polystyrene	Benzene, ethenyl-, homopolymer, brominated
Post-chlorosulfonated polyethylene (chlorosulfonation introduces both —Cl and —SO <sub>2</sub> Cl groups)	Ethene, homopolymer, chlorinated, chlorosulfonated

**Table 16. Examples of Telomers**

Telomer	CA Index name	Molecular formula structure representation
Vinylpyrrolidone homopolymer terminated with 3-mercaptopropionic acid	Propanoic acid, 3-mercapto-, telomer with 1-ethenyl-2- pyrrolidinone	$(C_6H_9NO)_x \cdot C_3H_6O_2S$  $\cdot HS-CH_2-CH_2-CO_2H$
Acrylic acid-vinyl chloride copolymer terminated with carbon tetrachloride	2-Propenoic acid, telomer with chloroethene and tetra- chloromethane	$(C_3H_4O_2 \cdot C_2H_3Cl)_x \cdot CCl_4$ $(H_2C=CH-CO_2H \cdot H_2C=CH-Cl)_x \cdot CCl_4$

There is no provision for structuring and naming end groups in source-based representations, except for ester-terminated polymers (see Table 14) and mixed polyalkylene glycols (see below).

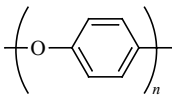
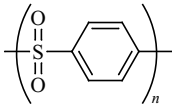
**Structure-Based Nomenclature.** When the regular structure of a polymer is well documented, or can be confidently assumed, in addition to the main entry with a source-based name, a *supplementary* entry is made for the SRU and its accompanying systematic structure-based name.

Assumptions are made for

- polyamides formed from a diamine and a dibasic acid, ester, or dihalide; from an amino acid, ester, or halide; from a lactam;
- polycarbonates formed from a dihydric alcohol or phenol and carbonic acid, ester, or dihalide;
- polyesters formed from a dihydric alcohol or phenol and a dibasic acid, anhydride, ester, or dihalide; from a hydroxy acid, ester, or halide; from a lactone;
- polyurethanes formed from a diisocyanate and a dihydric alcohol or phenol.

The SRU is named by citation of one or more multivalent radicals of regular substitutive nomenclature. The CAS SRU is equivalent to the IUPAC CRU. CAS

Table 17. Examples of Structure-Based Representations

Common name	CA Index name	Molecular formula structure representation
Poly(ethylene terephthalate)	Poly(oxy-1,2-ethanediylloxycarbonyl-1,4-phenylenecarbonyl)	$(C_{10}H_8O_4)_n$ (See Table 6 for structure)
Nylon 66	Poly[imino(1,6-dioxo-1,6-hexanediyl)imino-1,6-hexanediyl]	$(C_{12}H_{22}N_2O_2)_n$ (See Table 6 for structure)
Nylon 6	Poly[imino(1-oxo-1,6-hexanediyl)]	$(C_6H_{11}NO)_n$ $\left[ \text{NH}-\overset{\text{O}}{\underset{\text{O}}{\parallel}}\text{C}-(\text{CH}_2)_5 \right]_n$
Poly( <i>p</i> -phenylene oxide)	Poly(oxy-1,4-phenylene)	$(C_6H_4O)_n$ 
Poly( <i>p</i> -phenylene sulfone)	Poly(sulfonyl-1,4-phenylene)	$(C_6H_4O_2S)_n$ 

and the IUPAC are in virtually perfect agreement with regard to the guidelines for identification and orientation of repeating units; the guidelines are given in the IUPAC section entitled "Structure-Based Nomenclature."

The CA Index name of a structure-based representation is written by citation of the name of the SRU, parenthesized and preceded by the prefix "poly." Table 17 lists some examples.

Poly(alkylene glycols) and their ethers and esters are indexed as SRUs; end groups, when known, are added as *substituents* after the name of the repeating unit. Table 18 lists some examples.

Because the fragment sequences are unknown, mixed glycols such as "polyethylene-polypropylene glycol" or "polyethylene-polytetramethylene glycol" are structured and named as copolymers of the respective monomers:

- (1) CA Index name: Oxirane, methyl-, polymer with oxirane
- (2) CA Index name: Furan, tetrahydro-, polymer with oxirane

Ethers (end groups) of such mixed polyalkylene glycols are named analogously to the post-treated (modified) polymers:

- (1) CA Index name: Oxetane, polymer with methyloxirane, dipropyl ether

**Table 18. Examples of Poly(alkylene glycols)**

Common name	CA Index name <sup>a</sup>	Molecular formula structure representation
Polyethylene glycol	Poly(oxy-1,2-ethanediyl), $\alpha$ -hydro- $\omega$ -hydroxy-	$(\text{C}_2\text{H}_4\text{O})_n\text{H}_2\text{O}$ $\text{H}-\left(\text{O}-\text{CH}_2-\text{CH}_2\right)_n\text{OH}$
Polyethylene glycol monomethyl ether	Poly(oxy-1,2-ethanediyl), $\alpha$ -methyl- $\omega$ -hydroxy-	$(\text{C}_2\text{H}_4\text{O})_n\text{CH}_3\text{O}$ $\text{H}_3\text{C}-\left(\text{O}-\text{CH}_2-\text{CH}_2\right)_n\text{OH}$
Polybutylene glycol diacetate	Poly(oxy-1,4-butanediyl), $\alpha$ -acetyl- $\omega$ -(acetyloxy)-	$(\text{C}_4\text{H}_8\text{O})_n\text{C}_4\text{H}_6\text{O}_3$ $\text{H}_3\text{C}-\overset{\text{O}}{\underset{\text{  }}{\text{C}}}-\left[\text{O}-\left(\text{CH}_2\right)_4\right]_n-\text{O}-\overset{\text{O}}{\underset{\text{  }}{\text{C}}}-\text{CH}_3$

<sup>a</sup>End group citation order is governed by a set of rules (36), not by alphabetization.

Wiley's *Polymer Handbook* (4th ed.) contains a comprehensive chapter on "Chemical Abstracts Registry Numbers and Online Database Searching for Polymer Literature" (38), which contains examples of CA Index names for over 500 homopolymers and copolymers.

## Trade Names and Abbreviations

Because the systematic names of polymers can be cumbersome, trade names and abbreviations are frequently used as a shortcut in industrial literature and oral communication. For example, the simple generic name nylon-66, in which the first number refers to the number of carbon atoms of the diamine component and the second number to that of the diacid component used to form the polyamide, appears often in the literature in lieu of systematic names such as poly(iminoadipoyliminohehexane-1,6-diyl) (structure-based name) or poly[hexamethylenediamine-*alt*-(adipic acid)] (source-based name). Useful compilations of trade names for polymers can be found in References (39–46) and (50–56).

Perhaps the most widely used shortcut is the use of abbreviations for common industrial polymeric materials. The IUPAC recognizes that there may be advantages in some cases to the use of abbreviations, but urges that each abbreviation be fully defined the first time it appears in the text and that no abbreviation be used in titles of publications. Because of the inherent difficulties in assigning systematic and unique abbreviations to polymeric structures, only a short list has the IUPAC's official sanction (7). This list, published in 1987, will be updated in 2006. ISO published a more extensive list in 2001 (47), and in the mid-1980s the American Chemical Society's Polymer Nomenclature Committee compiled a master-list of all known abbreviations in the polymer field (48). The *Polymer Handbook* (49) contains an extensive list. A selection of abbreviations and acronyms from these sources is reproduced in Table 19.

Table 19. List of Abbreviations and Acronyms for Polymers

Abbreviation	Polymer
ABS <sup>a</sup>	Poly(acrylonitrile/butadiene/styrene)
AEPDS <sup>a</sup>	Poly[acrylonitrile/(ethylene/propylene/diene)/styrene] (generic)
AMMA <sup>a</sup>	Poly[acrylonitrile/(methyl methacrylate)]
ASA <sup>a</sup>	Poly(acrylonitrile/styrene/acrylate)
CA <sup>a</sup>	Cellulose acetate
CAB <sup>a</sup>	Cellulose acetate butyrate
CAP <sup>a</sup>	Cellulose acetate propionate
CF <sup>a</sup>	Poly(cresol/formaldehyde)
CMC <sup>a</sup>	Carboxymethylcellulose
CN <sup>a</sup>	Cellulose nitrate
CP <sup>a</sup>	Cellulose propionate
CPE <sup>b</sup>	Chlorinated polyethylene
E/P <sup>a</sup>	Poly(ethylene/propene)
EC <sup>a</sup>	Ethylcellulose
EEAK <sup>a</sup>	Poly(ethylene/ethyl acrylate)
EP <sup>a</sup>	Epoxide resin; epoxy (generic)
EVAC <sup>a</sup>	Poly(ethylene/vinyl acetate)
FEP <sup>a</sup>	Poly[perfluoro(ethylene/propene)]; poly(tetrafluoroethylene/ hexafluoropropene)
MF <sup>a</sup>	Melamine/formaldehyde resin
MP <sup>a</sup>	Melamine/phenol resin
PA <sup>a</sup>	Polyamide (generic)
PAC <sup>b</sup>	Polyacrylonitrile
PAN <sup>a,c</sup>	Polyacrylonitrile
PAPI; PMPP <sup>i</sup>	Polymethylenepolyphenylene isocyanate
PBAK <sup>a</sup>	Poly(butyl acrylate)
PB <sup>a</sup>	Poly(1-butene)
PBI <sup>b</sup>	Polybenzimidazole (generic)
PBT <sup>a</sup>	Poly(butylene terephthalate)
PC <sup>b</sup>	Polyacrylonitrile
PC <sup>a,b,d</sup>	Polycarbonate
PCF <sup>b</sup>	Poly(chlorotrifluoroethylene)
PCO <sup>b</sup>	Polycarbonate
PCTFE <sup>a,c</sup>	Poly(chlorotrifluoroethylene)
PDAP <sup>a</sup>	Poly(diallyl phthalate)
PDMS <sup>b</sup>	Poly(dimethylsiloxane)
PE <sup>a,b,c</sup>	Polyethylene
PE <sup>b</sup>	Polyester (generic)
PEA <sup>b</sup>	Poly(ethyl acrylate)
PEC <sup>b</sup>	Chlorinated polyethylene
PE-C <sup>a</sup>	Chlorinated polyethylene
PEEK <sup>a,b,e</sup>	Polyetheretherketone
PEG <sup>b</sup>	Poly(ethylene glycol)
PEKK <sup>b,f</sup>	Polyetherketoneketone
PEO <sup>b,c</sup>	Poly(ethylene oxide)
PEOX <sup>a,b</sup>	Poly(ethylene oxide)

(Continued)



Table 19. (Continued)

Abbreviation	Polymer
PEOX <sup>a,b</sup>	Poly(ethylene oxide)
PET <sup>a,b</sup>	Poly(ethylene terephthalate)
PETP <sup>b,c</sup>	Poly(ethylene terephthalate)
PF <sup>a</sup>	Phenol/formaldehyde resin
PFA <sup>a,b</sup>	Perfluoroalkoxy resins <sup>g</sup> (generic)
PIB <sup>a,b,c</sup>	Polyisobutene; polyisobutylene
PMMA <sup>a,b,c</sup>	Poly(methyl methacrylate)
PMP <sup>a,b</sup>	Poly(4-methyl-1-pentene)
POM <sup>a,b,c</sup>	Poly(oxymethylene); polyformaldehyde; polyacetal
POP <sup>b</sup>	Poly(oxy-1,4-phenylene); poly(1,4-phenylene oxide)
PP <sup>a,b,c</sup>	Polypropene; polypropylene
PPO <sup>® b</sup>	Poly(oxy-1,4-phenylene); poly(1,4-phenylene oxide)
PPS <sup>a,b</sup>	Poly(sulfanediyl-1,4-phenylene); poly(thio-1,4-phenylene); poly(1,4-phenylene sulfide)
PS <sup>a,b,c</sup>	Polystyrene
PTFE <sup>a,b,c</sup>	Poly(tetrafluoroethylene)
PTMEG <sup>b</sup>	Poly(tetramethylene ether glycol); poly(tetrahydrofuran)
PU <sup>b</sup>	Polyurethane (generic)
PUA <sup>b</sup>	Polyurea (generic)
PUR <sup>a,b</sup>	Polyurethane (generic)
PVA <sup>b</sup>	Poly(vinyl acetate)
PVA <sup>b</sup>	Poly(vinyl alcohol)
PVAC <sup>a,b,c</sup>	Poly(vinyl acetate)
PVAL <sup>a,b,c</sup>	Poly(vinyl alcohol)
PVB <sup>a</sup>	Poly(vinyl butyral) <sup>h</sup>
PVC <sup>a,b,c</sup>	Poly(vinyl chloride)
PVDC <sup>a,b,c</sup>	Poly(vinylidene dichloride)
PVDF <sup>a,b,c</sup>	Poly(vinylidene difluoride)
PVF <sup>a,b,c</sup>	Poly(vinyl fluoride)
PVFM <sup>a</sup>	Poly(vinyl formal) <sup>i</sup>
PVK <sup>a</sup>	Poly(vinylcarbazole); poly( <i>N</i> -vinylcarbazole)
PVME <sup>b</sup>	Poly(vinyl methyl ether)
PVOH <sup>b</sup>	Poly(vinyl alcohol)
PVP <sup>a,b</sup>	Poly(vinylpyrrolidinone); poly( <i>N</i> -vinylpyrrolidone)
SB <sup>a</sup>	Poly(styrene/butadiene)
SMS <sup>a,b</sup>	Poly(styrene/ $\alpha$ -methylstyrene)
SI <sup>a</sup>	Silicone (generic)
SIS <sup>b</sup>	Poly(styrene/isoprene/styrene)
UF <sup>a</sup>	Urea/formaldehyde resin
UP <sup>a</sup>	Unsaturated polyester (generic)
VC/E <sup>b</sup>	Poly[(vinyl chloride)/ethylene]
VCE <sup>a</sup>	Poly[(vinyl chloride)/ethylene]
VC/E/VAC <sup>b</sup>	Poly[(vinyl chloride)/ethylene/(vinyl acetate)]
VCEVAC <sup>a</sup>	Poly[(vinyl chloride)/ethylene/(vinyl acetate)]
VC/E/MA <sup>b</sup>	Poly[(vinyl chloride)/ethylene/(methyl acrylate)]
VC/EMA <sup>a</sup>	Poly[(vinyl chloride)/ethylene/(methyl acrylate)]
VC/MA <sup>b</sup>	Poly[(vinyl chloride)/(methyl acrylate)]

(Continued)

Table 19. (Continued)

Abbreviation	Polymer
VCMAK <sup>a</sup>	Poly[(vinyl chloride)/(methyl acrylate)]
VC/MMA <sup>b</sup>	Poly[(vinyl chloride)/(methyl methacrylate)]
VCMMA <sup>a</sup>	Poly[(vinyl chloride)/(methyl methacrylate)]
VC/VAC <sup>b</sup>	Poly[(vinyl chloride)/(vinyl acetate)]
VCVAC <sup>a</sup>	Poly[(vinyl chloride)/(vinyl acetate)]
VCVDC <sup>a</sup>	Poly[(vinyl chloride)/(vinylidene chloride)]

<sup>a</sup>Ref. 47.<sup>b</sup>Ref. 49.<sup>c</sup>Ref. 7.<sup>d</sup>“PC” usually means poly[oxycarbonyloxy-1,4-phenylene(dimethyl)methylene]-1,4-phenylene], but it can also mean “polycarbonates” in a generic sense.<sup>e</sup>Structure-based name poly(oxy-1,4-phenyleneoxy-1,4-phenylenecarbonyl-1,4-phenylene).<sup>f</sup>Structure-based name poly(oxy-1,4-phenylenecarbonyl-1,4-phenylenecarbonyl-1,4-phenylene).<sup>g</sup>Copolymers of tetrafluoroethylene with perfluorinated alkyl vinyl ethers.<sup>h</sup>Predominantly poly(vinyl acetate) hydrolyzed to poly(vinyl alcohol) and then cyclized by reaction with butanal (butyraldehyde). Depending upon the degree of hydrolysis, some residual monomeric units of vinyl acetate may be present. See Table 6 for idealized, completely cyclized polymer.<sup>i</sup>Predominantly poly(vinyl acetate) hydrolyzed to poly(vinyl alcohol) and then cyclized by reaction with formaldehyde. Depending upon the degree of hydrolysis, some residual monomeric units of vinyl acetate may be present.

## BIBLIOGRAPHY

“Nomenclature” in *EPST* 1st ed., Vol. 9, pp. 336–344, by Robert B. Fox. U.S. Naval Research Laboratory, and Chairman (1963–1967), Polymer Nomenclature Committee of the American Chemical Society; in *EPSE* 2nd ed., Vol. 10, pp. 191–204, by Norbert M. Bikales, National Science Foundation, and Secretary (1978–1987), IUPAC Commission on Macromolecular Nomenclature; in *EPST* 3rd ed., Vol. 7, pp. 262–292, by J. L. Schultz and E. S. Wilks, E. I. Du Pont de Nemours.

## IUPAC INDIVIDUAL RECOMMENDATIONS

1. Report on Nomenclature in the Field of Macromolecules. *J. Polym. Sci.* **8**, 257–277 (1952). Obsolete.
2. Report on Nomenclature Dealing with Steric Regularity in High Polymers. *J. Polym. Sci.* **56**, 153–161 (1962). Superseded by Ref. 3.
3. Report on Nomenclature Dealing with Steric Regularity in High Polymers. *Pure Appl. Chem.* **12**, 643–656 (1966). Superseded by Ref. 10.
4. Report of the Committee on Nomenclature of the International Commission on Macromolecules. *J. Polym. Sci., Part B: Polym. Phys.* **6**, 257–260 (1968). Obsolete.
5. Basic Definitions of Terms Relating to Polymers 1974. *Pure Appl. Chem.* **40**, 477–491 (1974). Reprinted as Chapter 1 of Ref. 32. Superseded by Ref. 22.
6. List of Standard Abbreviations (Symbols) for Synthetic Polymers and Polymer Materials 1974. *Pure Appl. Chem.* **40**, 473–476 (1974). Superseded by Ref. 7.
7. Use of Abbreviations for Names of Polymeric Substances (Recommendations 1986). *Pure Appl. Chem.* **59**, 691–693 (1987). Reprinted as Chapt. 9 of Ref. 32.

8. Nomenclature of Regular Single-Strand Organic Polymers (Rules Approved 1975). *Pure Appl. Chem.* **48**, 373–385 (1976). Reprinted as Chapt. 5 of Ref. 32.
9. Stereochemical Definitions and Notations Relating to Polymers (Provisional). *Pure Appl. Chem.* **51**, 1101–1121 (1979). Superseded by Ref. 10.
10. Stereochemical Definitions and Notations Relating to Polymers (Recommendations 1980). *Pure Appl. Chem.* **53**, 733–752 (1981). Reprinted as Chapt. 2 of Ref. 32.
11. Nomenclature for Regular Single-Strand and Quasi-Single-Strand Inorganic and Coordination Polymers (Provisional). *Pure Appl. Chem.* **53**, 2283–2302 (1981). Superseded by Ref. 12.
12. Nomenclature for Regular Single-Strand and Quasi-Single-Strand Inorganic and Coordination Polymers (Recommendations 1984). *Pure Appl. Chem.* **57**, 149–168 (1985). Reprinted as Chapt. 6 of Ref. 32 and as Chapt. II-7 of Ref. 34.
13. Note on the Terminology for Molar Masses in Polymer Science. *Makromol. Chem.* 185 (appendix to no. 1) (1984); *J. Polym. Sci., Polym. Lett. Ed.* **22**, 57 (1984); *J. Colloid Interface Sci.* **101**, 277 (1984); *J. Macromol. Sci., Chem.* **A21**, 903–904 (1984); *Br. Polym. J.* **17**, 92 (1985).
14. Source-Based Nomenclature for Copolymers (Recommendations 1985). *Pure Appl. Chem.* **57**, 1427–1440 (1985). Reprinted as Chapt. 7 of Ref. 32.
15. Definitions of Terms Relating to Individual Macromolecules, Their Assemblies, and Dilute Polymer Solutions (Recommendations 1988). *Pure Appl. Chem.* **61**, 211–241 (1989). Reprinted as Chapt. 3 of Ref. 32.
16. Definitions of Terms Relating to Crystalline Polymers (Recommendations 1988). *Pure Appl. Chem.* **61**, 769–785 (1989). Reprinted as Chapt. 4 of Ref. 32.
17. A Classification of Linear Single-Strand Polymers (Recommendations 1988). *Pure Appl. Chem.* **61**, 243–254 (1989). Reprinted as Chapt. 8 of Ref. 32.
18. Nomenclature of Regular Double-Strand (Ladder and Spiro) Organic Polymers (IUPAC Recommendations 1993). *Pure Appl. Chem.* **65**, 1561–1580 (1993).
19. Structure-Based Nomenclature for Irregular Single-Strand Organic Polymers (IUPAC Recommendations 1994). *Pure Appl. Chem.* **66**, 873–889 (1994).
20. Graphic Representations (Chemical Formulae) of Macromolecules (IUPAC Recommendations 1994). *Pure Appl. Chem.* **66**, 2469–2482 (1994).
21. Basic Classification and Definitions of Polymerization Reactions (IUPAC Recommendations 1994). *Pure Appl. Chem.* **66**, 2483–2486 (1994).
22. Glossary of Basic Terms in Polymer Science (IUPAC Recommendations 1996). *Pure Appl. Chem.* **68**, 2287–2311 (1996).
23. Definitions of Terms Relating to Degradation, Aging, and Related Chemical Transformations of Polymers (IUPAC Recommendations 1996). *Pure Appl. Chem.* **68**, 2313–2323 (1996).
24. Source-Based Nomenclature for Non-Linear Macromolecules and Macromolecular Assemblies (IUPAC Recommendations 1997). *Pure Appl. Chem.* **69**, 2511–2521 (1997).
25. Definitions of Terms Relating to the Non-Ultimate Mechanical Properties of Polymers (IUPAC Recommendations 1998). *Pure Appl. Chem.* **70**, 701–754 (1998).
26. Definitions of Basic Terms Relating to Low-Molar-Mass and Polymer Liquid Crystals (IUPAC Recommendations 2001). *Pure Appl. Chem.* **73**, 845–895 (2001).
27. Generic Source-Based Nomenclature for Polymers (IUPAC Recommendations 2001). *Pure Appl. Chem.* **73**, 1511–1519 (2001). Available on the world-wide web at <http://www.iupac.org/publications/pac/2001/pdf/7309x1511.pdf>. Errata: *Pure Appl. Chem.* **74**, 2019 (2002).
28. Definitions Relating to Stereochemically Asymmetric Polymerizations (IUPAC Recommendations 2002). *Pure Appl. Chem.* **74**, 915–922 (2002).
29. Nomenclature of Regular Single-Strand Organic Polymers (IUPAC Recommendations 2002). *Pure Appl. Chem.* **74**, 1921–1956 (2002).

30. Definitions of Terms Relating to Reactions of Polymers and Functional Polymers (IUPAC Recommendations 2003). *Pure Appl. Chem.* **76**, 889–906 (2004).
31. Definitions of Terms Related to Polymer Blends, Composites, and Multiphase Polymeric Materials (IUPAC Recommendations 2004). *Pure Appl. Chem.* **76**, 1985–2007 (2004).

## IUPAC BOOKS

32. W. V. Metanomski, ed., *Compendium of Macromolecular Nomenclature* (The Purple Book), Blackwell Scientific Publications, Oxford, 1991.
33. R. Panico, W. H. Powell, and J.-C. Richer, eds., *A Guide to IUPAC Nomenclature of Organic Compounds (Recommendations 1993)* (The Blue Book), Blackwell Scientific Publications, Oxford, 1993. Errata: *Pure Appl. Chem.* **71**, 1327–1330 (1999).
34. J. A. McCleverty and N. G. Connelly, eds., *Nomenclature of Inorganic Chemistry II. Recommendations 2000* (The Red Book II), Royal Society of Chemistry, Cambridge, 2001.
35. E. S. Wilks, ed., *Guide to Macromolecular Terminology and Nomenclature* (2005). Chaps. 3–8 of this Guide are being made available on the world wide web at: <http://www.iupac.org/publications/guide401/index.html> during 2005. Chaps. 1 and 2 will be added as they become available.

## OTHER PUBLICATIONS

36. Chemical Abstracts *CA Index Guide*, Appendix IV. Chemical Abstracts Service, Columbus, OH, 2002. See especially Section 222 for polymer indexing principles. Reprints of Appendix IV are available gratis under the title “*Naming and Indexing of Chemical Substances for Chemical Abstracts*.” Inquiries should be addressed to Marketing Communications, Chemical Abstracts Service, P. O. Box 3012, Columbus, OH 43210-0012.
37. Nomenclature Committee, Division of Polymer Chemistry, American Chemical Society. A Structure-Based Nomenclature for Linear Polymers. *Macromolecules* **1**, 193–198 (1968).
38. M. Johnson and E. A. Grulke. Chemical Abstracts Registry Numbers and Online Database Searching for Polymer Literature, in J. Brandrup, E. H. Immergut, and E. A. Grulke, eds., *Polymer Handbook*, 4th ed. John Wiley & Sons, New York, 1999, Vol. VIII, pp. 25–52.
39. M. Ash and I. Ash, *Encyclopedia of Plastics, Polymers, and Resins*, Chemical Publishing, New York, 1982.
40. H.-G. Elias and R. A. Pethrick, eds., *Polymer Yearbook*, Harwood Academic Publishers, New York, 1984, p. 113.
41. L. A. Utracki. *Polymer Alloys and Blends: Thermodynamics and Rheology*, Carl Hanser Verlag, Munich, 1989 (distributed in USA by Oxford University Press, New York).
42. M. Hough, ed., *The Plastics Compendium: Volume 1—Key Properties and Sources*, RAPRA Technology Ltd., Shawbury, Shrewsbury, Shropshire, UK, 1995.
43. S. Allen, ed., *New Trade Names in the Rubber and Plastics Industries*, RAPRA Technology Ltd., Shawbury, Shrewsbury, Shropshire, UK, 1996.
44. F. W. Billmeyer, *Textbook of Polymer Science*, 3rd ed. John Wiley and Sons, New York, 1984.
45. M. Ash and I. Ash, *Chemical Tradename Dictionary*. VCH Publishers, New York, 1993.
46. A. Masterson and M. Miller, eds., *Rubber Directory and Buyer's Guide*, 23rd ed, Rubber and Plastics News, Akron, OH, 1999.

47. *Plastics—Symbols and Abbreviated Terms—Part 1: Basic Polymers and Their Special Characteristics, International Standard ISO 1043-2001*, The International Standardization Organization, Geneva, Switzerland, 2001.
48. Nomenclature Committee, Division of Polymer Chemistry, American Chemical Society. Abbreviations for Thermoplastics, Thermosets, Fibers, Elastomers, and Additives. *Polym. News* **9**, 101–110 (1983); **10**, 169–172 (1985).
49. H.-G. Elias, Abbreviations for Thermoplastics, Thermosets, Fibers, Elastomers, and Additives, in J. Brandrup, E. H. Immergut, and E. A. Grulke, eds., *Polymer Handbook*, 4th ed. John Wiley & Sons, New York, 1999, Vol. VIII, pp. 1–24.

## WORLD-WIDE WEB (INTERNET) RESOURCES

50. Polymer Trade Names. <http://www.polymerweb.com/> or especially <http://www.polymerweb.com/misc/tradenam.html>, <http://www.plasticsusa.com/tradenam.html>, and <http://www.indianplasticportal.com/tradenames.html>
51. Index of Polymer Trade Names (2nd ed.) (A listing of 35,000 trade names, available as printed handbook or CD-ROM). WILEY-VCH, Weinheim, or WILEY-VCH, New York. <http://www.fiz-chemie.de/katalog/polymers/>
52. Matweb Material Property Data (American Precision Products); data on 29,500 substances, including polymers. [www.matweb.com](http://www.matweb.com) or <http://www.matweb.com/index.asp?ckck=1>, <http://www.matweb.com/search/SearchTradeName.asp>, and <http://www.matweb.com/polymertradenam.htm>
53. Polymer Doctor Trade Name Directory. [http://www.polymerdoctor.com/fine/plsql/tradenam\\_link\\_new](http://www.polymerdoctor.com/fine/plsql/tradenam_link_new)
54. Polymer information resources in the Chemistry Library. <http://www.lib.duke.edu/chem/polyinfo.htm>
55. Plastics, Polymer Tradenames, and Suppliers. <http://www.theotherpages.org/tradname.html>
56. Plastics Technology Online. <http://www.plasticstechnology.com/> To access the Materials Database, see <http://66.192.79.234/>

J. L. SCHULTZ  
Wilmington, Delaware  
E. S. WILKS  
Hockessin, Delaware

## NONDESTRUCTIVE TESTING

### Introduction

*Polymers* are macromolecules that contain repetitive, regular or irregular arrangements of organic molecular groups, ie, carbon atoms covalently bonded with other carbon and/or heteroatoms. Technical polymers usually contain additives, fillers, and pigments. Polymer–matrix composites (PMC) contain at least a second, insoluble phase, frequently in the form of fibers or particles. The structure and morphology of polymers and PMC can be quite complex; see, eg, AMORPHOUS POLYMERS, SEMICRYSTALLINE POLYMERS, MORPHOLOGY, ADDITIVES, VISCOELASTICITY,

PHASE TRANSFORMATION, and Reference 1. Properties of polymers and PMC that may be relevant for nondestructive testing (NDT) are as follows: (1) (pronounced) temperature dependence, viscoelastic behavior, and, in some cases, specific transition temperatures; (2) limited thermal stability, upper limit set by incipient decomposition or melting; (3) relatively low density; (4) transparency, semitransparency, or opaqueness with respect to the visible part of the electromagnetic spectrum; (5) electrical insulation and relatively low electrical conductivity for specially formulated compositions; and (6) possible changes in volume, properties, and, in some cases, even chemical reactions induced by absorption or diffusion of media.

The literature on NDT of polymers and PMC comprises the classes shown in Table 1. References illustrate the available range of literature or a specific topic. Omission or inclusion of a reference does not imply a rating by the authors. The amount of information available in electronic format only is steadily increasing, eg, References 2–8, and many journals feature electronic on-line editions. Electronic database searches are sensitive to spelling, eg, “non-destructive” yields 27, and “nondestructive” 384, active standards of the American Society for Testing and Materials International. Most NDT methods apply to various material classes. Those documents that explicitly mention polymers or PMC deal with effects specific to certain materials, eg, the Felicity effect in PMC (9), or with polymer products used in large quantities (10–14). Standards tend to lag behind technical developments, as discussed for acoustic emission (15), but similar arguments hold for other NDT methods.

*Nondestructive testing* (NDT) is the development and application of technical methods for the detection, location, measurement, and evaluation of discontinuities, defects and other imperfections, the assessment of integrity, the assessment of properties and composition, or the measurement of geometrical characters without impairing the intended use or application of the test object (31).

*Composites* are a combination of at least two materials, insoluble in one another, combined to yield a material with certain properties not possessed by the constituents (32). In PMC, polymers form a continuous constituent, called *matrix*, in which the other phase(s) are embedded (see COMPOSITE MATERIALS).

The distinction between “natural” and “synthetic” polymers or PMC (eg, natural versus synthetic rubber, plastics versus biopolymers, wood versus fiber-reinforced composites) is of limited relevance for the application of NDT methods.

**Classes of Nondestructive Test Methods.** NDT methods are classified according to the physical principle or effect that constitutes their base (26), corresponding to the probe-type or energy source (Table 2, the list of methods is incomplete). Each NDT method can be characterized by its type of (1) probe or energy source, (2) interaction with the test object, (3) signal detection, (4) signal recording, and (5) signal interpretation (26). Other categories for grouping NDT methods are, eg, (1) “imaging” versus “nonimaging” methods, (2) “volume” versus “local” method, (3) noncontact versus contacting methods, (4) *in situ* versus *ex situ* or “field” versus “laboratory” testing, (5) real-time versus post-test indication and (6) “small” or “specific” specimen size versus full-scale testing.

**Table 1. Classes of Literature on NDT of Polymers and PMC**

Source type	Sample references	Remarks
Handbooks	(16–26)	Some volumes available in 3rd edition, others in preparation; 3rd edition also available in electronic format on compact disc with supplemental information
Monographs	(27,28)	
Normative codes and standards	(9–14)	Few codes and standards are explicitly on NDT applied to polymers and PMC, but most NDT codes and standards are applicable to polymers and PMC, except when explicitly stating another class of materials; up-to-date information can be obtained on the Web sites of standards-issuing organizations, eg (2–5)
Guidelines (without normative character)	(29,30)	A few guidelines are explicitly on NDT applied to polymers and PMC, but most NDT guidelines apply to polymers and PMC, except when stating explicitly another class of materials
Journals	Electronic journals Class A (6,7) Class B (8)	Literature on NDT of polymers and PMC comprises two classes (see Bibliography for examples): A. journals dealing with NDT B. journals dealing with polymers and PMC
Conference proceedings	Class A Class B	Conferences again comprise two classes: A. general or topical (on specific NDT methods and/or applications) NDT conferences B. conferences on polymers and PMC  Information on many conferences is available on the Internet, eg, through links on the Web sites of national NDT societies <sup>a</sup>
Technical documents	Equipment descriptions, technical manuals, application notes	Provided, eg, by equipment manufacturers or test agencies
Educational documents	Lecture notes, training manuals	Provided, eg, by lecturers, national NDT societies, NDT training and certification agencies

<sup>a</sup>Web sites of most national NDT societies can be found at [www.icndt.org/directory.htm](http://www.icndt.org/directory.htm) (however, some listings may not be up-to-date).

**Table 2. Classes of NDT Methods**

Class	Methods (examples)	Remarks
Mechanical	E-modulus measurement Vibration analysis Modal analysis Scanning probe microscopy	Mostly indirect indications of defects
Optical	Visual inspection Optical microscopy Brillouin scattering Photoelasticity Projection moiré Shearography Optical holography	Using visible part of electromagnetic spectrum (wavelength roughly between 400 and 700 nm)
Penetrating radiation	X-ray radiography X-ray tomography $\gamma$ -ray radiography Neutron radiography Neutron scattering Electron microscopy	Electromagnetic (wavelengths below about 1 nm) and particle radiation
Electromagnetic	Dielectric spectroscopy Resistance measurement Eddy-current testing	X-ray and $\gamma$ -ray classified among penetrating radiation
Sonic/ultrasonic	Tap testing Acoustic emission Acousto-ultrasonics Ultrasonics Acoustic microscopy	
Thermal/infrared	Thermography	Infrared spectrometry is classified among chemical/analytical
Chemical/analytical	Infrared spectrometry Raman spectrometry Ultraviolet spectrometry X-ray spectrometry Magnetic resonance imaging	

### Mechanical Test Methods

Determination of mechanical properties is one, although indirect, way of finding indications of defects (see MECHANICAL PERFORMANCE OF PLASTICS). The elastic modulus of polymers and PMC depends, among others, on porosity or



microcrack content. Quantitative evaluation requires comparison with specimens with known content from destructive analysis or others (33). Qualitative, relative comparison is feasible, but still requires careful conditioning, since mechanical properties depend on humidity content and temperature. The tensile elastic modulus of samples from one batch typically yields standard deviations of 3–5% for carbon fiber-reinforced polymers (CFRP) and of 5–7% for glass fiber-reinforced polymers (GFRP). Values around 2% have been obtained for high quality CFRP laminates.

Dynamic Mechanical Analysis (qv) (DMA) or dynamic thermal mechanical analysis (DTMA) indicate damage in polymers or PMC (34), and aging effects in polymers by a shift in the transition temperature (35). Limitations are the volume of the test chamber or the required specimen shape.

*Compliance*, ie, the displacement-to-load ratio, is used in fracture mechanics tests to determine crack length or to monitor crack growth (36).

Vibration or modal analysis yield indications of defects in structural elements or parts when excited by suitable loads (37) (also see Sonic and Ultrasonic Test Methods). The literature mainly describes applications to PMC laminates, aiming at detecting critical delaminations (38). A relative comparison for a specific element with time, loading, or exposure may be sufficient to find indications of a defect or of a change in the behavior of the structure. Comparison with finite element calculations is one approach for quantitative evaluation (39). Recent research on monitoring of PMC elements or structures also investigates the use of piezoelectric sensors for detection of delaminations by external excitation (40).

Scanning probe microscopy of polymers (listing of web sites on Atomic Force and Scanning Probe Microscopy, with images, is available at <http://www.ou.edu/research/electron/www-vl/afm.shtml>) and PMC (41,42), beside images indicating possible defects, yields mechanical properties, eg, force-stiffness relations (43), and quantitative surface roughness or corrugation relating to tribology (44), on a microscopic scale.

## Optical Test Methods

Optical test methods use the visible part of the electromagnetic spectrum; ie, they comprise a subset of the electromagnetic test methods.

Visual inspection by eye is certainly the oldest method and is widely used, but subject to physiological limitations. Optical and electronic equipment, eg, endoscopes originally developed for medical applications, and electronic image recording and processing have become standard tools for visual inspection.

Composition and/or morphology of many polymers and PMC limit NDT visual inspection to surface and near-surface features. Transparent polymers and semitransparent PMC allow for the detection of inhomogeneities, such as voids, pores, or cracks, as well as qualitative or semiquantitative estimates of fiber volume fraction and/or fiber alignment. Light sources enhance sensitivity in visual through-thickness and surface inspection.

Standards for visual inspection of polymer products are in preparation (12). Evaluation requires experience and is operator-dependent. Indications can be documented with photography. Digital photography or digitization of photographs allow for image processing and automated image analysis.

Conventional dye penetrant testing for surface crack detection in PMC is described in older literature (45), but is now rarely used, except for highlighting cracks in PMC after destructive sectioning (46).

Optical microscopy has also profited from recent advances. Scanning near field optical microscopy (SNOM) (47) (SNOM images of polymers and other materials are available at, eg, <http://wwwex.physik.uni-ulm.de/SNOMWeb/>), eg, reaches spatial resolution at the molecular level when using fluorescent molecules, competing with the scanning probe methods (48). The limitations are typical specimen size and scanning area.

Using coherent or structured light to illuminate the test object can reveal information that is not accessible to visual inspection (25,49,50). Commonly, a film or camera is used to record this information.

Interferometric methods use laser illumination to measure surface deformations under thermal, mechanical, vibration, or pressure loading (51). By virtue of the high sensitivity of a few tens of nanometer, inhomogeneities in the interference fringe pattern due to cracks, delaminations, or material inhomogeneities can be revealed using small loads. Because the laser light is only used to record the information, care must be taken to set up the appropriate loading scheme that enhances the type of defect to be found. Well-known methods in composite testing, especially for aerospace and spacecraft applications, are electronic or digital speckle pattern (correlation) interferometry (ESPI or DSPI) (52–55) and shearography, also termed shearing speckle pattern interferometry (SSPI) (56). The methods are used to find indications of delaminations, voids, and cracks. Quantitative evaluation of deformation and strain is also important (57) and can be used to measure stress concentrations, vibration modes (58,59), or material parameters. By nature, the techniques discussed are surface techniques and therefore most appropriate for surface or close-to-surface defects. However, when combined with transient loads, some information on the depth of a flaw can be gained (60).

(Digital) holographic interferometry (61) basically yields the same information as DSPI, but is limited because it requires a development step (photographic processing or numerical reconstruction) before indicating the load effect on the object.

Limitations of the interferometric techniques are due to the required mechanical stability of the measurement head relative to the object of better than 1  $\mu\text{m}$ . Safety regulations for using high power lasers also have to be observed.

Structured light methods comprise shadow moiré, projection moiré, and fringe projection (25,62). They use a structured intensity pattern, most commonly a set of parallel fringes, to illuminate the object. A camera records the fringes on the object surface from a triangulation angle. In moiré methods (63) fine pitch gratings can be used, because the imaged fringes are demodulated by a reference grating in front of the camera before recording. Moiré methods are usually used to measure deformations or to compare the shape of objects, eg, in production control, with a resolution of roughly 1/10,000 of the field of view (64–66). The

physics of fringe projection is basically the same (67), but the fringes are directly recorded by the camera. Hence, the pitch of the grating is limited by the camera resolution.

By using a sequence of ever coarser gratings and a calibrated setup, the absolute shape of an object is acquired with a resolution of roughly 1/1,000 of the field of view (68).

## Penetrating Radiation Test Methods

*Penetrating radiation* comprises electromagnetic radiation in the wavelength range below about 1 nm (roughly equivalent to 1 keV energy) or particle radiation. The former is generated in the electronic shell of atoms (X-rays) or by processes in the atomic nuclei ( $\gamma$ -rays). Particle radiation can be generated with particle accelerators, sometimes requiring special targets. Neutrons, eg, come from a spallation source (69) or a nuclear reactor. X-rays are produced by electron beam impact on targets in evacuated tubes or in accelerators by *Bremsstrahlung*, the “braking” radiation emitted by accelerated, charged particles. Ultraviolet and low energy X-ray radiation of high intensity from synchrotrons is used for analysis (70) and processing (71) of polymers and PMC. A list of currently operational synchrotron sources is available, eg, at [http://www.src.wisc.edu/community/sr\\_sources.html](http://www.src.wisc.edu/community/sr_sources.html).

Polymers and PMC are of relatively low density and hence do not absorb X-rays or  $\gamma$ -rays efficiently. “Low” energy radiation (typically 10–40 keV) yields enhanced contrast for X-ray radiology or radiography of polymers and PMC due to the nonlinear shape of the absorption versus energy curve (72). Higher energy  $\gamma$ - and X-ray sources are hence less suitable.

Contrast can be enhanced by X-ray contrast agents or X-ray dye penetrants (73). These consist of high density materials, eg, liquid halogen compounds (ZnI, methylenediiodide, or diiodobutane) and are different from the dye penetrants used in visual penetrant testing. Test objects are immersed or the contrast agent is injected into, eg, cracks or delaminations extending to the surface of the test object. Any pore, void, crack, or delamination not extending to the surface hence escapes detection. Sufficient wetting between contrast agent and material is important for complete penetration. Even then, a minimum amount of contrast agent is necessary to obtain detectable contrast. Many commercial contrast agents (1) are toxic or carcinogenic requiring appropriate safety measures, (2) are volatile to some degree, limiting immersion time and imaging duration, (3) are of limited shelf life, and (4) raise concerns about inducing deleterious effects (73). There is at least one documented case of suspected dye penetrant induced microcracking in PMC (74).

Penetration and absorption of the electromagnetic or particle radiation results in energy deposition (heating) and implantation of beam particles. Energy deposition and particle irradiation may affect the microstructure and induce breaking or formation of new molecular bonds. Examples are gamma radiation effects (75) and cross-linking in polyethylene by electron irradiation (71). The intensity needed for cross-linking usually exceeds that obtained from NDT beam sources.

Conventional X-ray tubes with an energy range from 10 to 450 keV have a typical source diameter (focal spot) of a few millimeters. Microfocal X-ray sources (76) with a source diameter of about 5 to 10  $\mu\text{m}$  allow for magnification in X-ray radiography by projection imaging (test object close to source, imaging system at a distance). The small source size limits the blur due to geometrical projection with conventional X-ray sources. Energy—microfocal X-ray sources operate up to about 200 keV—and intensity limit the maximum distance between source and imaging system. Magnification can be up to 100 times, but frequently the size of details to be imaged or the maximum size of the imaging system set lower limits.

At energies below 40 keV, X-ray absorption in air is a major limitation, and replacing air by low density helium has been recommended (77). This requires a special enclosure for X-ray source and imaging system, often limiting the size of the test object. *X-ray beam hardening* (78), ie, the preferential absorption of low energy X-rays in the test object, also occurs in polymers and PMC, but to a lesser extent than in denser materials.

Low X-ray intensity yields longer exposure times; for a 1-mm thick CFRP plate a G2 class X-ray film (79) (ie, a D4 class film at that time), 17–18 keV X-ray energy, 1000 mm imaging system–focus distance, and a focus–object distance of 150 mm, resulted in an exposure of about 600 s (80).

X-ray image intensifiers converting the incident X-rays into an image on a scintillating screen allow time-resolved X-ray imaging when recorded with a video camera. Crack initiation in PMC, eg, was investigated with a microfocal X-ray source and X-ray image intensifier with 25-Hz video imaging at magnifications between 5 and 10 times (81). Digitized frames of the video recording can be electronically processed and analyzed. Conventional or X-ray film still images can also be digitized for electronic processing (82).

X-ray radiography is moving from X-ray film to computed radiography (CR). Reusable imaging plates with 25 or 50  $\mu\text{m}$  resolution are commercially available. Manufacturers data sheets indicate that up to 1000 record–erase cycles can be performed (83). Special electronic filters may improve detection of indications. Electronic image recording and storage allow for easy processing and electronic data transmission. However, long-term storage and readability of the records may pose problems in the future. Development of standards in CR is under way (84, 85).

X-ray Compton back-scattering can yield indications of delaminations in PMC without the use of contrast agents, ie, including those that do not extend to the surface. The basis is a special source–detector arrangement (86).

X-ray laminography was developed for investigating specific layers of fiber-reinforced laminate sheets by multiple exposure on the same film. Recently, it has been developed into a computer tomography (CT) method (87), but is rarely used.

X-ray CT with commercial CT equipment or synchrotron radiation (70) is increasingly used in research and development, and industrial use is incipient. X-ray micro-CT yields spatial resolution of around 10–20  $\mu\text{m}$  for microfocal (76) and down to 1–2  $\mu\text{m}$  for synchrotron X-ray sources (88). These resolutions require “small” test objects, around a few cubic decimeters in the microfocal and a few cubic centimeters in the synchrotron X-ray source.

X-ray refraction, based on small angle X-ray scattering (SAXS), may prove useful in the detection of microdamage in PMC, such as crack growth (89) and fiber debonding (90). SAXS images of polymer nanocomposites are shown in Reference 91. Near-edge X-ray absorption fine structure (NEXAFS) and related X-ray techniques provide information on composition and morphology of polymers on a microscopic scale (see X-RAY MICROSCOPY).

Neutrons find various applications in the characterization of polymers and PMC (92). Neutron scattering experiments investigate structure and behavior of polymers at the atomic level (93). Neutron absorption as a function of the atomic number of the elements differs from that of X-rays, and the power of neutron radiography (94) for polymers and PMC, even combined with metals, is illustrated at, eg, <http://neutra.web.psi.ch/gallery/index.html>. Currently operational neutron radiography sources are listed at [www.anlw.anl.gov/nr/oldindex.htm](http://www.anlw.anl.gov/nr/oldindex.htm).

Positron annihilation spectroscopy (PAS) is used in research on free volume (95) or on aging effects in polymers (96), and muon spin resonance with muon beams (97) yields information on dynamic processes in polymers (98), but specimen size may be limited.

Electron microscopy is one example of electron beam analysis of polymers and PMC. Beam charging effects occur in most polymers and PMC (99), unless when coated with a thin conductive layer (carbon, gold, or platinum). Environmental scanning electron microscopes (ESEM) do not require such coatings (100). Size and shape of the test object and possible electron beam heating effects then decide whether the method is NDT.

## Electromagnetic Test Methods

Many polymers and most PMC show no or only comparatively low electrical conductivity, which limits application of electromagnetic test methods. One of the main exceptions is CFRP. The continuous network of carbon fibers in CFRP allows for electrical resistance measurements, eg, based on the four-probe method. Electrical potential (101) or resistance methods are used in fracture mechanics to detect delaminations (102) and to monitor damage in CFRP (103). Whether the application of electrodes is nondestructive depends on the intended use.

Electrical conductivity measurements have also been developed as tomography (104). Eddy-current testing (ET) of CFRP laminates is feasible (105). ET is noncontact and NDT, as long as thermal effects from resistive heating and energy dissipation are sufficiently small. Superconducting quantum interference devices (SQUID) have been used for ET to detect damage in CFRP (106). However, SQUID may soon be replaced by sensors based on giant magnetoresistance (GMR) or giant magnetoimpedance (GMI) effects (107).

Dielectric measurements are performed on polymers and PMC for research and industrial applications, specifically to find materials with low dielectric losses (108) (see DIELECTRIC RELAXATION).

*Fractoluminescence* (109), ie, the emission of visible light, and electromagnetic emission from fracture of polymers or PMC (110) have not yet been investigated as NDT tools. Microwave testing is applicable to nonconducting materials (111) and used, eg, for exciting ultrasonic waves in PMC (112) or the

characterization of anisotropic materials, such as short fiber–reinforced injection molded parts (113). The energy deposition due to microwave radiation, on the other hand, is applied in processing of polymers and PMC (114).

## Sonic and Ultrasonic Test Methods

Sonic and ultrasonic test methods use elastic waves propagating in solid or fluid media and are classified into “active” and “passive” methods. The former requires emission of waves into the test object; the latter, waves emitted by the material itself.

Tap testing a PMC structure by hand or by a suitable instrument, an experienced operator can tell whether the structure is sufficiently defect-free (115).

Acoustic emission (AE) analysis is an example of a passive method (21). Beside piezoceramic lead zirconate titanate (PZT) sensors, thin piezoelectric poly(vinylidene fluoride) (PVDF) films (116) and noncontact interferometry (117) also sense the rapid, transient elastic waves generated inside most materials. Composites (118) made from PZT fibers have recently been characterized as AE sensors (119). AE of polymers and PMC is affected by (1) relatively large signal attenuation limiting the maximum distance between sensor and signal source, and mainly in PMC; (2) anisotropy, limiting location accuracy; and (3) several source mechanisms that can act simultaneously. In PMC, the so-called Felicity effect ie, the appearance of AE activity at the same sensitivity but lower load levels than previously attained (31), forms the base of commercial AE applications in integrity assessment of PMC structures (9).

Quantitative AE analysis for characterizing damage accumulation in PMC is described in Reference 120, approaches for signal analysis and identification of mechanisms in Reference 121, and a practical AE application to automotive composites in Reference 122.

Ultrasonic waves (typically in the MHz range) can be excited by piezoelectric transducers coupled to the test object. Electromagnetic acoustic transducers (EMAT) (123) cannot be used for ultrasonics of polymers and PMC; alternatives are discussed in Reference 124. The waves propagate and are scattered and attenuated in the material. The signal can be detected in either reflection or transmission mode (by the transducer emitting the ultrasonic pulse for reflection or by additional transducers at other locations in transmission). Acousto-ultrasonics (AU) (11) records low frequency guided waves (typically 30–500 kHz) emitted at another location to detect changes in the test objects, eg, in carbon–carbon composites (125). Recently developed stacked transducers look promising for low frequency applications (126).

Ultrasonic A-, B-, and C-scans (23) can be obtained from polymers and PMC. Isotropic or anisotropic elastic constants, attenuation, and phase transitions are detected in detailed A-scan data analysis (127,128). Ultrasonics is also used for process monitoring in manufacturing of polymeric or PMC parts (129).

Ultrasonic C-scan is standard for quality inspection of PMC plates (28), but the large signal attenuation with penetration depth limits this to “thin” plates.

Lower frequency waves, eg, 0.5 MHz, yield larger penetration for equivalent attenuation, but the longer wavelengths limit the spatial resolution (eg, 6 mm for 0.5 MHz at 3000 m/s).

Another limitation is posed by the shadowing effect in PMC. The delamination closest to the transducer will reflect the ultrasonic pulse to such an extent that delaminations below will be masked, unless their lateral size is larger. Even C-scans taken on both sides do not necessarily guarantee detection of delaminations in all layers. In the reflection mode, repeat echoes from multiple reflections have to be distinguished from “real” indications, especially in relatively thin PMC shells.

The shape of certain structures, eg, shells or thin rods with small radii of curvature, limits the application of ultrasonics, but there is equipment that allows three-dimensional movement of the transducer (130).

The standard coupling via immersion in water or use of water jets may be prohibited, since many polymers and PMC change mechanical properties or chemical composition due to penetration of water (swelling, softening, leaching of components, hydrolysis). If immersion in water is used, formation of gas-bubbles from dissolved air has to be prevented. Gel-like coupling agents may leave stains on the surface, but now wheel array sensors for dry coupling (131,132) are available, eg, for the inspection of aerospace structures (133). Air-coupled ultrasonics also offer an alternative (131,134,135). Ultrasonic pulses in polymers and PMC can also be generated by laser (136,137), but this may lead to heating effects. Ultrasonic imaging is widely used for electronic components, where indications of defects (delaminations, cracks, pores) in the epoxy packaging have to be detected (138).

Ultrasonic computer tomography (CT) of polymers is feasible (139).

Recently, phased-array technology (140) has become a novel ultrasonic scanning technique. Multielement transducers in conjunction with high speed electronics allow for electronic focusing and steering of the ultrasonic beam. Since no mechanical movement is involved, the “scanning speed” can be enhanced, enabling imaging for on-line control of manufacturing (141,142).

Ultrasonic transducers can excite various wave modes, eg, guided Lamb waves that may be suitable for specific applications (143). Ultrasonic excitation is also used to detect the so-called acoustic nonlinearity associated with defects, eg, in PMC (144,145). The combination of recording guided ultrasonic waves with numerical back-calculation of wave propagation for detecting indications of defects in PMC pipes also looks promising (146). Surface-bonded fiber optics can detect ultrasonic waves via interferometric techniques (147). Beyond frequencies of 1 GHz, ultrasonics is called *acoustic microscopy*; for details, the reader is referred to Reference 148. This technique can be applied to polymers or PMC (149), specifically to polymeric microelectronics packaging (150).

## Thermal and Infrared Test Methods

Thermal and infrared methods can also be classified as passive or active (see THERMAL ANALYSIS). *Passive thermography*, ie, recording the temperature

distribution, is rarely used for detecting indications, but probably found useful in polymer and PMC process monitoring (151). The emissivity of the specimen and other factors have to be considered for accurate measurements (152).

Active thermography requires the application of a stimulus (thermal heat), either as single pulse (153) or continuously varying with time (154). The pulse, typically from flash lights, its duration, and intensity, as well as direction (surface or back side of test object) will affect the detectability of the indications (155). Surface finish or paint coats may affect the absorption of the pulse. In CFRP, excitation by short ultrasonic pulses (156) and noncontact eddy currents is also feasible.

In lock-in thermography (154), the selected frequency of the heat “wave” to which the detector is tuned (locked) is important. *Heat waves* are diffusion waves that yield a quadratic dependence on time for the observation of indications at a certain depth of the test object. For thin-walled PMC shells (a few millimeters) this does not constitute a severe limitation (157). Limited operating temperature, pronounced temperature-dependent properties, and thermal degradation may pose limits on the application of active thermography to polymers and PMC. A recent example of a possible application of active thermography in PMC is the determination of the fiber orientation of CFRP (158) that, in the future, may replace the conventional destructive methods.

## Chemical and Analytical Test Methods

Chemical analysis of polymers typically deals with monomers or functional groups rather than constituent atoms. Thermal infrared and laser optical Raman spectrometry are the typical tools (36) (see TEST METHODS; VIBRATIONAL SPECTROSCOPY), but frequently, specific specimen size or form is required. For physical properties, mechanical and sonic/ultrasonic NDT methods are available (see above). Molecular mass distribution and related properties of polymers, or fiber or particle volume fraction and distribution for PMC, are usually determined destructively (see TEST METHODS).

## Detection, Sizing, and Evaluation of Indications with Nondestructive Test Methods

**Basic Approaches.** The morphology of polymers and PMC comprises several levels, each with specific defects. In NDT, a defect is an aggregate of or a single imperfection or discontinuity that exceeds specified acceptance criteria. These criteria may depend on and vary with location, size, or orientation of the indication. The indications can further be (1) relevant, (2) nonrelevant, or (3) false (31). Hence, not all detected indications are “defects.”

Locating the indication is frequently performed with “imaging” methods that also image reference points on the test object. Some nonimaging methods



also yield information on location, eg, from source location algorithms in acoustic emission analysis (21).

Locating is a prerequisite for *sizing*, ie, the determination of geometrical dimensions required by specified size criteria. This relates to the spatial resolution of the NDT method. For nonimaging methods, sizing may be replaced, eg, in acoustic emission by defect severity evaluation (159). Principles, limitations, and accuracy of defect location and sizing in polymers and PMC with specific NDT methods are described in (16–26).

Defect types frequently relate to the mechanism causing the indication. Many NDT methods have an intrinsic sensitivity for specific types of indications. Examples are (1) ultrasonic C-scans sensitive to boundaries between materials of different acoustic impedance (eg, voids, delaminations), (2) X-ray radiography sensitive to variations in density (eg, inclusion of foreign objects, voids), and (3) acoustic emission sensitive to microscopic stress release (eg, crack growth).

**Determination of Structural Integrity with Nondestructive Test Methods.** Some commercial NDT applications, mainly on PMC, do not aim at detection and evaluation of individual indications, but rather at the so-called structural integrity. Most technical structures contain flaws that may evolve into defects that accumulate and grow with time. Structural integrity analysis evaluates test objects with respect to critical defect accumulation, beyond which further use may lead to catastrophic failure. A prime method for determination of the integrity of PMC structures is acoustic emission analysis (9,21). Driven in part by economic considerations, predicting the remaining service-life is increasing in importance. NDT monitoring is hence expected to contribute to, or to be incorporated into, service-life engineering approaches to design.

**Smart Monitoring of Polymer–Matrix Composites Elements.** The increasing use of PMC in structural elements or as reinforcement or for repair may, at least in critical applications, require periodic inspection or even continuous monitoring. Intermittent or continuous, smart monitoring of PMC aims at automatic detection of specified defects. One research direction develops intelligent materials or structures that sense indications, assess their significance, eg, with computer-based evaluation or expert systems (160), and, if considered significant, take appropriate corrective measures. A full review of smart monitoring of PMC structures is beyond the scope of this article, but a few examples will illustrate this active research area.

Fiber optics based monitoring of PMC includes, eg, strain (161), temperature, acoustic emission signals, and other measurements (162). Electromagnetic resistance measurements yield information on strain changes and defect accumulation (101–104). Even carbon nanotubes are now investigated as strain sensors in PMC (163). Piezoelectric thin wafers or plates (164) or active fiber composites made from piezoelectric fibers (165) also yield, eg, strain and acoustic emission signals. The performance of fiber optics and piezoelectric sensors for detection of microdamage in CFRP is compared in Reference 166.

Another area receiving increasing attention recently is the application of electroactive polymers in actuators and sensors (167). Quite likely, this could lead to new approaches for NDT of polymers and PMC in the context of smart monitoring of structural elements.

## Special Applications of Nondestructive Test Methods

**Determination of Geometry or Size and Reverse Engineering.** So far, determination of geometrical characteristics has only been discussed with respect to defect location and sizing. However, NDT also comprises determining geometrical characteristics of test objects per se (31). Determination of size and shape, with calipers by hand, with gauges, or with computer-controlled tactile coordinate-measuring machines, is a routine quality assurance procedure, but noncontact methods are also used (168). Size and shape of the test object may pose some limitations. Another example is wall thickness measurements with dedicated ultrasonic thickness gauges (169). As discussed above, the maximum thickness is limited by the frequency-dependent, attenuating properties of polymers and PMC. Requirements on spatial resolution, eg, for test objects where the wall thickness varies over distances that are short compared with the size of the probe, pose another limitation. CT offers another approach for determining geometrical characteristics, X-ray CT being most widely used. CT based on other probe types (see Table 2), eg, ultrasonics (139), magnetic resonance imaging (MRI), also called Nuclear Magnetic Resonance (NMR) imaging (170) (see NUCLEAR MAGNETIC RESONANCE), optical coherence tomography (mainly applicable to GFRP but with limited penetration in CFRP and not suitable for aramide fiber-reinforced PMC) (171), thermal impedance tomography (172), and positron emission tomography (173) are feasible as well.

The driving force behind the development of industrial CT has been and still is the medical field; new methods and improvements are likely to originate there (174). Spatial resolution in X-ray CT depends on the type of X-ray source and on the size and shape of the test object (76,88). X-ray and MRI CT, however, yield more than geometrical characteristics; the data can be converted into distributions of, eg, density, elemental composition (175), or even velocity (176). Three-dimensional CT representations of the geometry, converted into computer-aided design (CAD)-compatible files (177), are used for quality control by comparing with CAD design data for deviations from specification and tolerances, or for computer-aided manufacturing, such as rapid prototyping or reverse engineering (178,179).

**Nondestructive Testing of Adhesive Joints.** Many commercially available adhesives are based on polymers. NDT of adhesive joints (180) poses challenges because of (1) the small size of possibly deleterious defects (eg, porosity), (2) the thinness of the adhesive layers, and (3) sometimes, the size, shape, and material of the adherends. Acousto-ultrasonics (181) and various types of ultrasonics (182,183) are applicable to adhesive joints. Ultrasonics can be combined with noncontact optical methods (184) and pulsed thermography (185). However, the assessment of the “quality” or of the quantitative strength of the adhesive bond based on the NDT data often proves difficult.

**Process Monitoring and Process Control with Nondestructive Test Methods.** NDT plays an important role in quality assurance for products from all classes of materials and is increasingly used in process monitoring and control. NDT monitoring of polymers and PMC comprises, eg, cure monitoring of molding with thermography (151), infrared methods (186), fiber optics (187), dielectric

spectroscopy (188), or ultrasonics (129). Phased-array ultrasonics may be used for on-line manufacturing control (142). NDT process control requires sufficiently fast data analysis and feedback into the process management or steering facility. Some approaches for smart monitoring of PMC, eg, AE, show potential for NDT process control.

Cost may limit process control to either crucial or most effective parameters, eg, pressure and temperature in extrusion (189). Process simulation for optimization of parameters (190) prior to process implementation is also a cost-effective tool.

## Summary and Outlook

Beside technical aspects mentioned above, there are additional considerations for selecting NDT methods for a specific purpose. Cost, frequently, is decisive and major cost factors are (1) test duration, including time used for setup and post-test analysis and assessment; (2) type of equipment, its sophistication, calibration, and maintenance (compatibility with previous records from periodic inspection may require costly maintenance of aging equipment); (3) equipment operator, specifically operator training and certification (191); (4) accreditation of test agency; (5) qualification or validation of the NDT method (192); and (6) accuracy and precision estimates required by test standards or quality management systems.

NDT may hence be effective and economic in scientific research, product or process development, manufacturing process control, quality assurance, and in-service monitoring of crucial or high performance rather than mass produced, low cost polymer and PMC products.

Size and shape of the test object relative to the required spatial and, sometimes, temporal resolution may significantly influence the choice of the NDT method. "Small" objects are readily tested with commercial equipment, while "large" objects may require portable equipment or robots, special test rigs, or several operators. "Single shot" imaging, if satisfying the specification, is to be preferred over scanning, where test duration mainly depends on scan time, ie, scan step to scan area ratio. The shape of test objects may preclude the use of imaging methods, eg, because of hidden areas or uneven spatial resolution. Large size combined with high spatial and/or temporal resolution increases the amount of data and duration of analysis.

Five trends seem to govern the development of NDT, namely, (1) increasing sensitivity, (2) increasing spatial resolution, (3) decreasing test and analysis duration, (4) increasing automation of testing, analysis, and evaluation, and (5) increasing use of so-called real-time NDT methods (80). The increase in computing power at constant or even lower cost, frequently projected to follow an exponential growth, called *Moore's law* (<http://www.intel.com/research/silicon/mooreslaw.htm>), is still defying predictions that computer technology will reach physical limits. Hence, the last three trends may continue, while the first two may reach physical or economic limits sooner.

Applying a combination of NDT methods is advisable in many cases. A useful guiding principle is to choose NDT methods that yield complementary information, eg, based on different probe types (Table 2). One example is acoustic emission monitoring with high sensitivity for potentially critical areas, followed by high spatial resolution inspection of such areas by, eg, ultrasonic or X-ray methods to quantitatively locate and size the indication.

The general problem of selecting the “optimum” NDT method for polymers and PMC requires consideration and balancing of several aspects. These are (1) requirements on type and size of indications that have to be detected with specified confidence compared to size and shape of the test object; (2) technical feasibility of the test method, including behavior of the material under the applied stimulus; (3) availability of the test method; (4) (eventually) formal requirements, eg, operator certification, test facility accreditation, test method validation; (5) (eventually) compatibility with previous measurements; and (6) overall cost. It would be of interest to have more quantitatively evaluated, comparative tests applying different NDT methods to specimens with simulated, known defects (80) or to real test objects. A comparative study of the cost of different NDT methods for polymer and PMC would also be welcome.

## BIBLIOGRAPHY

### CITED PUBLICATIONS

1. M. Stamm and B. Carlowitz, *Ullmann's Encyclopedia of Industrial Chemistry*, Wiley-VCH Verlag GmbH, Weinheim, Germany, 2002.
2. International Organization for Standardization Web site: <http://www.iso.ch>.
3. Comité Européen de Normalisation Web site: <http://www.cenorm.be>.
4. International Electrotechnical Commission Web site: <http://www.iec.ch>.
5. American Society for Testing and Materials International Web site: <http://www.astm.org>.
6. *J. ASTM Int.* Electronic journal starting Jan. 2004, see Ref. 5.
7. *NDT.net*. Electronic journal available at <http://www.ndt.net>.
8. *e-polymers*. Electronic journal available at <http://www.e-polymers.org>.
9. ASTM E1067, Standard Practice for Acoustic Emission Examination of Fiberglass Reinforced Plastic Resin (FRP) Tanks/Vessels, *Annual Book of ASTM Standards*, Vol. 03.03, American Society for Testing and Materials International, West Conshohocken, Pa., 2004.
10. ASTM E1118, Standard Practice for Acoustic Emission Examination of Reinforced Thermosetting Resin Pipe (RTRP), *Annual Book of ASTM Standards*, Vol. 03.03, American Society for Testing and Materials International, West Conshohocken, Pa., 2004.
11. ASTM E1736, Standard Practice for Acousto-Ultrasonic Assessment of Filament-Wound Pressure Vessels, *Annual Book of ASTM Standards*, Vol. 03.03, American Society for Testing and Materials International, West Conshohocken, Pa., 2004.
12. EN 13100-1, *Nondestructive testing of welded joints of thermoplastics semi-finished products*, Part 1: Visual examination.
13. prEN 13100-2, *Nondestructive testing of welded joints of thermoplastics semi-finished products*, Part 2: X-ray radiographic testing.

14. prEN 13100-3, *Nondestructive testing of welded joints of thermoplastics semi-finished products*, Part 3: Ultrasonic testing.
15. A. J. Brunner and J. Bohse, *NDT.net* 7(9), 10 (2002).
16. C. N. Jackson, C. N. Sherlock, and P. O. Moore, eds., *Nondestructive Testing Handbook, Vol. 1: Leak Testing*, 3rd ed., American Society for Nondestructive Testing, Columbus, Ohio, 1998.
17. N. Tracy and P. O. Moore, eds., *Nondestructive Testing Handbook, Vol. 2: Liquid Penetrant Testing*, 3rd ed., American Society for Nondestructive Testing, Columbus, Ohio, 1999.
18. X. P. V. Maldague and P. O. Moore, eds., *Nondestructive Testing Handbook, Vol. 3: Infrared and Thermal Testing*, 3rd ed., American Society for Nondestructive Testing, Columbus, Ohio, 2001.
19. R. H. Bossi, F. A. Iddings, G. C. Wheeler, and P. O. Moore, eds., *Nondestructive Testing Handbook, Vol. 4: Radiographic Testing*, 3rd ed., American Society for Nondestructive Testing, Columbus, Ohio, 2002.
20. S. S. Udpa and P. O. McIntire, eds., *Nondestructive Testing Handbook, Vol. 4: Electromagnetic Testing*, 3rd ed., American Society for Nondestructive Testing, Columbus, Ohio, 2004.
21. R. K. Miller and P. McIntire, eds., *Nondestructive Testing Handbook, Vol. 5: Acoustic Emission Testing*, 2nd ed., American Society for Nondestructive Testing, Columbus, Ohio, 1987.
22. Th. J. Schmidt, K. Skeie, and P. McIntire, eds., *Nondestructive Testing Handbook, Vol. 6: Magnetic Particle Testing*, 2nd ed., American Society for Nondestructive Testing, Columbus, Ohio, 1989.
23. A. S. Birks, R. E. Green Jr., and P. McIntire, eds., *Nondestructive Testing Handbook, Vol. 7: Ultrasonic Testing*, 2nd ed., American Society for Nondestructive Testing, Columbus, Ohio, 1991.
24. M. W. Allgaier, S. Ness, P. McIntire, and P. O. Moore, eds., *Nondestructive Testing Handbook, Vol. 8: Visual and Optical Testing*, 2nd ed., American Society for Nondestructive Testing, Columbus, Ohio, 1993.
25. R. K. Stanley, P. O. Moore, and P. McIntire, eds., *Nondestructive Testing Handbook, Vol. 9: Special Nondestructive Testing Methods*, 2nd ed., American Society for Nondestructive Testing, Columbus, Ohio, 1995.
26. S. Ness, C. N. Sherlock, P. O. Moore, and P. McIntire, eds., *Nondestructive Testing Handbook, Vol. 10: Nondestructive Testing Overview*, 2nd ed., American Society for Nondestructive Testing, Columbus, Ohio, 1996.
27. J. Summerscales, ed., *Non-Destructive Testing of Fibre-Reinforced Plastics Composites*, Vol. 1, Elsevier Science, Ltd., Oxford, 1987.
28. J. Summerscales, ed., *Non-Destructive Testing of Fibre-Reinforced Plastics Composites*, Vol. 2, Elsevier Science, Ltd., Oxford, 1990.
29. Committee on Acoustic Emission from Reinforced Plastics, CARP of the Society of Plastics Industries, *J. Acoustic Emission* 11(3), C1–C24 (1993).
30. ASTM E1495, Standard Guide for Acousto-Ultrasonic Assessment of Composites, Laminates, and Bonded Joints, *Annual Book of ASTM Standards*, Vol. 03.03, American Society for Testing and Materials International, West Conshohocken, Pa., 2004.
31. ASTM E1316, Standard Terminology for Nondestructive Examinations, *Annual Book of ASTM Standards*, Vol. 03.03, American Society for Testing and Materials International, West Conshohocken, Pa., 2004.
32. ASTM D3878, Standard Terminology for Composite Materials, *Annual Book of ASTM Standards*, Vol. 15.03, American Society for Testing and Materials International, West Conshohocken, Pa., 2004.

33. ASTM WK581, Standard Guide for Assessing the Porosity of Polymeric Scaffolds for Use in Tissue-Engineered Medical Products, New Work Item, ASTM Subcommittee F04.42, see information in Ref. 5.
34. D. S. Jones, *Int. J. Pharm.* **179**, 167–178 (1999).
35. C. Saron and M. I. Felisberti, *Mater. Sci. Eng. A* **370**, 293–301 (2004).
36. P. Davies, A. J. Brunner, and B. R. K. Blackman, *Appl. Compos. Mater.* **5**(6), 354–364 (1998).
37. S. S. Kessler, S. M. Spearing, M. J. Atalla, C. E. S. Cesnik, and C. Soutis, *Compos., Part B: Eng.* **33**, 87–95 (2002).
38. S. Vanlanduit and P. Guillaume, *Mech. Systems Signal Process.* **18**, 79–88 (2004).
39. J. Cugnoni, Th. Gmür, and A. Schorderet, *Compos., Part A: Appl. Sci. Manuf.* **35**(7/8), 977–987 (2004).
40. P. Tan and L. Tong, *J. Compos. Mater.* **38**(4), 321–325 (2004).
41. D. W. Bonnell, *Scanning Probe Microscopy and Spectroscopy, Theory, Techniques, and Applications*, 2nd ed., Wiley-VCH, New York, 2001.
42. B. D. Ratner and V. V. Tsukruk, eds., *Scanning Probe Microscopy of Polymers* (ACS Symposium Series 694), American Chemical Society Division of Polymer Chemistry, Calif. ACS Meeting, Orlando, 1996.
43. R. J. Colton, D. R. Baselt, Y. F. Dufrène, J.-B.D. Green, and G. U. Lee, *Curr. Opin. Chem. Biol.* **1**, 370–377 (1997).
44. G. V. Dedkov, *Phys. Status Solidi A* **179**, 3–75 (2000).
45. R. Vipond and C. J. Daniels, *Composites* **16**(1), 14–18 (1985).
46. S. A. Hitchen and S. L. Ogil, *Compos. Sci. Technol.* **47**(3), 239–244 (1993).
47. K. D. Jandt, *Mater. Sci. Eng. R* **21**, 221–295 (1998).
48. J. Michaelis, C. Hettich, J. Mlynek, and V. Sandoghdar, *Nature* **405**, 325–328 (2000).
49. P. K. Rastogi and D. Inaudi, eds., *Trends in Optical Non-destructive Testing and Inspection*, Elsevier, Amsterdam, 2000.
50. P. K. Rastogi, ed., *Optical Measurement Techniques and Applications*, Artech House, London, 1997.
51. R. Jones and C. Wykes, *Holographic and Speckle Interferometry*, 2nd ed., Cambridge University Press, Cambridge, 1989.
52. M. V. Rao, R. Samuel, and A. Ananthan, *Opt. Lasers Eng.* **40**, 563–571 (2003).
53. G. Georgeson, *Proc. Int. Soc. Opt. Eng. SPIE* **4704**, 104–115 (2002).
54. M. O. W. Richardson, Z.-Y. Zhang, M. Wisheart, J. R. Tyrer, and J. Petzing, *Compos., Part A: Appl. Sci. Manuf.* **29**(7), 721–729 (1998).
55. W. C. Wang, C. H. Day, C. H. Hwang, and T. B. Chiou, *Res. Nondestr. Eval.* **10**(1), 1–15 (1998).
56. H. O. Nyongesa, A. W. Otieno, and P. L. Rosin, *Compos. Struct.* **54**(2/3), 313–318 (2001).
57. V. Shchepinov and V. Pisarev, eds., *Strain and Stress Analysis by Holographic and Speckle Interferometry*, John Wiley & Sons, Inc., New York, 1996.
58. M. Whelan, *Key Eng. Mater.* **167/168**, 122–31 (1999).
59. M. Roesel, K. Herstrass, and P. Bajons, *Ultrasonics* **41**, 663–669 (2003).
60. A. Davila, P. D. Ruiz, G. H. Kaufmann, and J. M. Huntley, *Opt. Lasers Eng.* **40**, 447–458 (2003).
61. T. Kreis, *Holographic Interferometry*, Akademie Verlag, Berlin, 1996.
62. M. Heredia-Ortiz and E.-A. Patterson, *Strain* **39**(3), 95–100 (2003).
63. O. Kafri and I. Glatt, *The Physics of Moiré Metrology*, John Wiley & Sons, Inc., New York, 1990.
64. H. R. Meyer-Piening, M. Farshad, B. Geier, and R. Zimmermann, *Compos. Struct.* **53**(4), 427–35 (2001).

65. A. H. Fagg, B. Hales, and H. P. Stahl, *Proc. Int. Soc. Opt. Eng. SPIE* **1779**, 68–72 (1992).
66. T. M. Wang, I. M. Daniel, and J. T. Gotro, *J. Compos. Mater.* **26**(6), 883–899 (1992).
67. P. Tataschiere and E. K. Hack, *Opt. Eng.* **34**(7), 1887–1898 (1995).
68. W. Osten, *Opt. Eng.* **39**(1), 232–243 (2000).
69. G. S. Bauer, *Nucl. Instrum. Methods Phys. Res. Sect. B* **139**, 65–71 (1998).
70. R. J. Cernik and P. Barnes, *Radiat. Phys. Chem.* **45**(3), 445–457 (1995).
71. R. L. Clough, *Nucl. Instrum. Methods Phys. Res. Sect. B* **185**, 8–33 (2001).
72. R. C. Barry and R. A. Betz, *Mater. Eval.* **49**, 474–477 (1991).
73. G. Sala, *Compos., Part B: Eng.* **31**, 357–373 (2000).
74. A. Paige Clifton Furrow, D. A. Dillard, T. L. St. Clair, J. Hinkley, *J. Compos. Mater.* **32**, 31–48 (1998).
75. J. C. M. Suarez and R. S. de Biasi, *Polym. Degrad. Stab.* **82**(2), 221–227 (2003).
76. R. V. Ely, ed., *Microfocal Radiography*, Academic Press, London, U.K., 1980.
77. I. Rudich, L. Lesensky, and F. Kapelewski, *Mater. Eval.* **44**, 1158–1184 (1986).
78. R. Ferreira de Paiva, J. Lynch, E. Rosenberg, and M. Bisiaux, *NDT&E Int.* **31**(1), 17–22 (1998).
79. EN 584-1, Non-destructive testing—Industrial radiographic film—Part 1: Classification of film systems for industrial radiography, Comité Européen de Normalisation, 1994.
80. A. J. Brunner and J. Neuenschwander, in C. A. Mota Soares, C. M. Mota Soares, and M. J. M. Freitas, eds., *Mechanics of Composite Materials and Structures* (NATO Science Series E: Applied Science 361), Kluwer Academic Publishers, Boston, Mass., 1999, pp. 261–278.
81. A. J. Brunner, *Comput. Methods Appl. Mech. Eng.* **185**(2/4), 161–172 (2000).
82. M. K. Choong, M. Bister, P. Sathyamoorthy, Zaharah, H. Y. Boey, and Y. C. Wong, *Int. Congr. Ser.* **1256**, 285–291 (2003).
83. U. Ewert, Y. Onel, U. Zscherpel, J. Stade, and P. Willems, in *Proceedings of the 7th European Conference on Nondestructive Testing*, Vol. 3, 2004, pp. 2725–2732.
84. ASTM WK670, Test Method for Classification of Computed Radiology Systems, New Work Item, ASTM Subcommittee E07.01, see information in Ref. 5.
85. ASTM WK4511, Standard Practice for the Qualification of Computed Radiography Systems, New Work Item, ASTM Subcommittee E07.01, see information in Ref. 5.
86. J. Kosanetzky, G. Harding, H. H. Fischer, and A. Meyer, *Proceedings of the 4th European Conference on Nondestructive Testing*, Pergamon Press, New York, 1988, pp. 2118–2132.
87. S. Gondrom, J. Zhou, M. Maisl, H. Reiter, M. Kröning, and W. Arnold, *Nucl. Eng. Des.* **190**, 141–147 (1999).
88. B. Müller, F. Beckmann, M. Huser, F. Maspero, G. Székely, K. Ruffieux, Ph. Thurner, and E. Wintermantel, *Biomol. Eng.* **19**, 73–78 (2002).
89. K.-W. Harbich, M. P. Hentschel, and J. Schors, *NDT&E Int.* **34**, 297–302 (2001).
90. M. P. Hentschel, K.-W. Harbich, and A. Lange, *NDT&E Int.* **27**(5), 275–280 (1994).
91. S. S. Ray and M. Okamoto, *Prog. Polym. Sci.* **28**, 1539–1641 (2003).
92. M. W. Johnson, *Appl. Radiat. Isot.* **46**(6/7), 673–680 (1995).
93. R.-J. Roe, *Methods of X-Ray and Neutron Scattering in Polymer Science* (Topics in Polymer Science Series), Oxford University Press, New York, 2000.
94. S. Fujine, K. Yoneda, K. Yoshii, M. Kamata, M. Tamaki, K. Ohkubo, Y. Ikeda, and H. Kobayashi, *Nucl. Instrum. Methods Phys. Res., Sect. A* **424**, 190–199 (1999).
95. D. Fink, M. Müller, S. Ghosh, K. K. Dwivedi, J. Vacik, V. Hnatowicz, J. Cervena, Y. Kobayashi, and K. Hirata, *Nucl. Instrum. Methods Phys. Res., Sect. B* **156**, 170–176 (1999).

96. D. M. Bigg, *Polym. Eng. Sci.* **36**(6), 737–743 (1996).
97. H. Daniel, *Nucl. Instrum. Methods Phys. Res., Sect. B* **68**, 459–467 (1992).
98. F. L. Pratt, S. J. Blundell, Th. Jestädt, B. W. Lovett, A. Husmann, I. M. Marshall, W. Hayes, A. Monkman, I. Watanabe, K. Nagamine, R. E. Martin, and A. B. Holmes, *Physica B* **289/290**, 625–630 (2000).
99. G. Czeremuszkin, M. Latrèche, and M. R. Wertheimer, *Nucl. Instrum. Methods Phys. Res., Sect. B* **185**, 88–99 (2001).
100. C. M. Ramsdale, I. C. Bache, J. D. MacKenzie, D. S. Thomas, A. C. Arias, A. M. Donald, R. H. Friend, and N. C. Greenham, *Physica E* **14**, 268–271 (2002).
101. A. Todoroki, H. Kobayashi, and K. Matuura, *JSME Int. J. Ser. A* **38**(4), 524–530 (1995).
102. A. Todoroki and Y. Tanaka, *Compos. Sci. Technol.* **62**(5), 629–639 (2002).
103. D. D. L. Chung and S. K. Wang, *Polym. Polym. Compos.* **11**(7), 515–525 (2003).
104. R. Schueler, S. P. Joshi, and K. Schulte, *Compos. Sci. Technol.* **61**(6), 921–930 (2001).
105. G. Mook, R. Lange, and O. Koeser, *Compos. Sci. Technol.* **61**(6), 865–873 (2001).
106. Y. Hatsukade, N. Kasai, M. Kurosawa, R. Kawai, H. Takashima, F. Kojima, and A. Ishiyama, *Physica C* **372–376**, 267–270 (2002).
107. A. E. Mahdi, L. Panina, and D. Mapps, *Sens. Actuators, A* **105**, 271–285 (2003).
108. M. Bini, R. Olmi, A. Ignesti, J. Abusleme, M. Bassi, and A. Sanguineti, *Mater. Res. Innovations* **8**(1), 23–26 (2004).
109. L. M. Sweeting, *ChemMatters* **8**(3), 10–12 (1990).
110. C. Sklarczyk, S. Winkler, and B. Thielicke, *Materialwissenschaft und Werkstofftechnik* **27**, 559–566 (1996) (in German).
111. W. Saleh, N. Qaddoumi, and M. Abu-Khousa, *Compos. Struct.* **62**(3/4), 403–407 (2003).
112. E. Guilliorit, B. Hosten, C. Bacon, and D. E. Chimenti, *Ultrasonics* **41**, 97–103 (2003).
113. L. Diener, *Rev. Prog. Quant. Nondestr. Eval.* **14**, 615 (1995).
114. S. Zhou and M. C. Hawley, *Compos. Struct.* **61**, 303–309 (2003).
115. D. K. Hsu, D. J. Barnard, and J. J. Peters, *Proc. Int. Soc. Opt. Eng. SPIE* **4336**, 100–107 (2001).
116. R. Stiffer and E. G. Henneke, *Mater. Eval.* **41**, 956–960 (1983).
117. M. Enoki, M. Watanabe, P. Chivavibul, and T. Kishi, *Sci. Technol. Adv. Mater.* **1**, 157–165 (2000).
118. A. Bent and N. W. Hagood, *J. Intell. Mater. Syst. Struct.* **8**(11), 903–919 (1997).
119. M. Barbezat, A. J. Brunner, P. Flüeler, C. Huber, and X. Kornmann, *Sens. Actuators, A* **114**(1), 13–20 (2004).
120. R. A. Nordstrom, A. J. Brunner, and P. Flüeler, *J. Acoustic Emission* **13**(3/4), 67–77 (1995).
121. J. Bohse, *Compos. Sci. Technol.* **60**(8), 1213–1226 (2000).
122. N. Sato and T. Kurauchi, *Res. Nondestr. Eval.* **9**, 119–136 (1997).
123. S. Dixon and S. B. Palmer, *Ultrasonics* **42**(10), 1123–1136 (2004).
124. W. M. D. Wright, D. A. Hutchins, A. Gachagan, and G. Hayward, *Ultrasonics* **34**, 825–833 (1996).
125. P. K. Raju and U. K. Vaidya, *Polym. Compos.* **17**(2), 275–287 (1996).
126. A. Cochran, P. Reynolds, and G. Hayward, *Ultrasonics* **36**, 969–977 (1998).
127. S. Baudouin and B. Hosten, *Ultrasonics* **34**(2–5), 379–382 (1996).
128. K. Matsushige, N. Hiramatsu, and H. Okabe, *Adv. Polym. Sci.* **125**, 147–186 (1996).
129. M. Rath, J. Döring, W. Stark, and G. Hinrichsen, *NDT&E Int.* **33**(2), 123–130 (2000).
130. D. J. Cotter, J. E. Michaels, T. E. Michaels, I. V. Ivakhnenko, and D. Kass, in *Proceedings of the 15th World Conference on Non-Destructive Testing*, Paper No. 216, 2000; available in Ref. 7.



131. D. J. Cotter, T. E. Michaels, J. E. Michaels, D. Kass, M. E. Stanton, I. V. Kosenko, and F. H. C. Hotchkiss, in *Proceedings of the 15th World Conference on Non-Destructive Testing*, Paper No. 215, 2000; available in Ref. 7.
132. S. J. Bourne, M. Newborough, and D. J. Highgate, *INSIGHT* **43**(1), 26–28 (2001).
133. C. J. Brotherhood, B. W. Drinkwater, and R. J. Freemantle, *INSIGHT* **45**(11), 729–734 (2003).
134. J. Buckley, in *Proceedings of the 15th World Conference on Non-Destructive Testing*, Paper No. 507, 2000; available in Ref. 7.
135. A. Neild, D. A. Hutchins, and D. R. Billson, *Ultrasonics* **42**(1–9), 859–864 (2004).
136. F. H. Chang, T. E. Drake, M. A. Osterkamp, R. S. Prowant, J. P. Monchalain, R. Heon, P. Bouchard, C. Padioleau, D. A. Froom, W. Frazier, and J. P. Barton, *Rev. Prog. Quant. Nondestr. Eval.* **12A**, 611–616 (1993).
137. J. P. Monchalain, *Rev. Prog. Quantitative Nondestr. Eval.* **23A**, 3–31 (2004).
138. G. Pfannschmidt, in A. Briggs and W. Arnold, eds., *Advances in Acoustic Microscopy*, Vol. 2, 1996, pp. 1–38.
139. T. H. Gan, D. A. Hutchins, D. R. Billson, and F. C. Wong, *Res. Nondestr. Eval.* **13**, 131–152 (2001).
140. X. E. Gros, N. B. Cameron, and M. King, *INSIGHT* **44**(11), 673–6768 (2002).
141. M. Lethiecq, C. Pejot, M. Berson, P. Guillemet, and A. Roncin, *NDT&E Int.* **27**(6), 311–315 (1994).
142. J. Neuenschwander, B. Blau, I. L. Horvath, T. Lüthi, and H. Marti, *IEEE Trans. Appl. Supercond.* **12**, 1199–1202 (2002).
143. M. Castaings and B. Hosten, *NDT&E Int.* **34**(4), 249–258 (2001).
144. D. Donskoy, A. Sutin, and A. Ekimov, *NDT&E Int.* **34**, 231–238 (2001).
145. N. Krohn, R. Stoessel, and G. Busse, *Ultrasonics* **40**, 633–637 (2002).
146. T. Leutenegger and J. Dual, *Ultrasonics* **41**(10), 811–822 (2004).
147. T. S. Jang, S. S. Lee, and Y. G. Kim, *Ultrasonics* **42**(1–9), 837–841 (2004).
148. A. Briggs, *Acoustic Microscopy*, Clarendon Press, Oxford, 1992.
149. F. Lisy, A. Hiltner, E. Baer, J. L. Katz, and A. Meunier, *J. Appl. Polym. Sci.* **52**(2), 329–352 (1994).
150. J. Yang, *Microelectron. Reliability* **36**(9), 1291–1295 (1996).
151. A. R. Greenberg, S. S. Shojaie, W. B. Krantz, and S. B. Tantekin-Ersolmaz, *J. Membr. Sci.* **107**, 249–261 (1995).
152. M. Honner, P. Litoš, and M. Švantner, *Infrared Phys. Technol.* **45**, 131–142 (2004).
153. S. M. Shepard, J. R. Lhota, T. Ahmed, and Y. L. Hou, *SAMPE J.* **39**(5), 53–59 (2003).
154. D. Wu and G. Busse, *Revue Générale de Thermique* **37**, 693–703 (1998).
155. G. Giorleo and C. Meola, *NDT&E Int.* **35**, 287–292 (2002).
156. A. Mian, X. Han, S. Islam, and G. Newaz, *Compos. Sci. Technol.* **64**, 657–666 (2004).
157. H. Berglind and A. Dillenz, *NDT&E Int.* **36**, 395–399 (2003).
158. W. Karpen, D. Wu, and G. Busse, *Res. Nondestr. Eval.* **11**, 179–197 (1999).
159. B. R. A. Wood and R. W. Harris, *Int. J. Pressure Vessels Piping* **77**, 125–132 (2000).
160. S. N. Dwivedi and A. Sharan, *J. Mater. Process. Technol.* **141**, 155–162 (2003).
161. P. M. Nellen, R. Brönnimann, A. Frank, P. Mauron, and U. Sennhauser, *Proc. Int. Soc. Opt. Eng. SPIE* **3860**, 44–54 (1999).
162. P. Clark, J. Boriniski, M. Gunther, S. Poland, D. Wigent, and S. Watkins, *Smart Mater. Bull.* **2001**(6), 8–11 (2001).
163. A. H. Barber, Q. Zhao, H. D. Wagner, and C. A. Baillie, *Compos. Sci. Technol.* **64**, 1915–1919 (2004).
164. G. Mook, J. Pohl, and F. Michel, *Smart Mater. Struct.* **12**, 997–1004 (2003).
165. X. Kornmann, C. Huber, M. Barbezat, and A. J. Brunner, in *Proceedings of the 11th European Conference on Composite Materials*, 2004, p. 9, Paper B047.

166. J.-M. Park, S.-I. Lee, O.-Y. Kwon, H.-S. Choi, and J.-H. Lee, *Compos. Part A: Appl. Sci. Manuf.* **34**, 203–216 (2003).
167. Y. Bar-Cohen, ed., *Proc. Int. Soc. Opt. Eng. SPIE* 5385, 2004.
168. W. Li and P. Gu, *Computer-Aided Des.* **36**, 1395–1417 (2004).
169. prEN 1427 Non-Destructive Testing—Ultrasonic Thickness Measurement, Comité Européen de Normalisation, Brussels, Belgium, Oct. 2003.
170. D. E. Demco and B. Blümich, *Curr. Opin. Solid State Mater. Sci.* **5**, 195–202 (2001).
171. J. P. Dunkers, F. R. Phelan, D. P. Sanders, M. J. Everett, W. H. Green, D. L. Hunston, and R. S. Parnas, *Opt. Lasers Eng.* **35**, 135–147 (2001).
172. R. Smallwood, P. Metzgerall, D. Hose, M. Delves, H. Pollock, A. Hammiche, C. Hodges, V. Mathot, and P. Willcocks, *Thermochim. acta* **385**, 19–32 (2002).
173. C. Degueldre, H. Pleinert, P. Maguire, E. Lehmann, J. Missimer, J. Hammer, K. Leenders, H. Böck, and D. Townsend, *Earth Planet. Sci. Lett.* **140**, 213–225 (1996).
174. G. Sakas, *Comput. Graphics* **26**, 577–587 (2002).
175. D. H. Phillips and J. J. Lannutti, *NDT&E Int.* **30**(6), 339–350 (1997).
176. R. Kimmich, A. Klemm, and M. Weber, *Magnetic Resonance Imaging* **19**, 353–361 (2001).
177. A. F. Obrist, A. Flisch, and J. Hofmann, *NDT&E Int.* **37**(5), 373–380 (2004).
178. X. Yan and P. Gu, *Computer-Aided Des.* **28**(4), 307–318 (1996).
179. B. Schillinger, W. Blümlhuber, A. Fent, and M. Wegner, *Nucl. Instrum. Methods Phys. Res., Sect. A* **424**, 58–65 (1999).
180. R. D. Adams and B. W. Drinkwater, *NDT&E Int.* **30**(2), 93–98 (1997).
181. O.-Y. Kwon, T.-H. Kim, and K.-J. Lee, *Proceedings 15th World Conference on Non-Destructive Testing*, Paper No. 473, 2000; available in Ref. 7.
182. C. J. Brotherhood, B. W. Drinkwater, and S. Dixon, *Ultrasonics* **41**(7), 521–529 (2003).
183. A. M. Robinson, B. W. Drinkwater, and J. Allin, *NDT&E Int.* **36**, 27–36 (2003).
184. F. Lanza di Scalea, M. Bonomo, D. Tuzzeo, *Res. Nondestr. Eval.* **13**, 153–171 (2001).
185. J. A. Schroeder, T. Ahmed, B. Chaudhry, and S. Shepard, *Compos. Part A: Appl. Sci. Manuf.* **33**, 1511–1517 (2002).
186. J. Mijović and S. Andjelić, *Polymer* **37**(8), 1295–1303 (1996).
187. C. Li, M. Cao, R. Wang, Z. Wang, Y. Qiao, L. Wan, Q. Tian, H. Liu, D. Zhang, T. Liang, and C. Tang, *Compos. Sci. Technol.* **63**, 1749–1758 (2003).
188. J.-M. Gonnnet, J. Guillet, C. Raveyre, G. Assezat, R. Fulchiron, and G. Seytre, *Polym. Eng. Sci.* **42**(6), 1171–1180 (2002).
189. S. A. Nield, H. M. Budman, and C. Tzoganakis, *Control Eng. Practice* **8**, 911–920 (2000).
190. A. Gokce, K.-T. Hsiao, and S. G. Advani, *Compos. Part A: Appl. Sci. Manuf.* **33**, 1263–1272 (2002).
191. EN 473, Nondestructive Testing: Qualification and Certification of NDT Personnel—General Principles, Comité Européen de Normalisation, Brussels, Belgium, Oct. 2000.
192. prCEN/TR 14748, Non-Destructive Testing—Methodology for Qualification of Non-destructive Tests, Comité Européen de Normalisation, Brussels, Belgium, Aug. 2003.

ANDREAS J. BRUNNER

ERWIN HACK

JÜRGEN NEUENSCHWANDER

Center for Nondestructive Testing, EMPA,  
Swiss Federal Laboratories for  
Materials Testing and Research

## NONLINEAR OPTICAL PROPERTIES

### Introduction

This article introduces the field of nonlinear optics and the electronic nonlinear optical (NLO) response of polymers and polymer composites. Both second- and third-order NLO phenomena are included, with primary emphasis on harmonic generation, the intensity-dependent refractive index, and nonlinear (multiphoton) absorption effects. The beginning sections introduce the phenomena and explain how the order of the nonlinearity can be understood from a series expansion of the polarization in powers of the electric-field. In addition to listing the variety of nonlinear optical phenomena and some applications, some of the advantages of polymeric materials for NLO applications are also surveyed.

Structure-property relationships that are important to the NLO response are explored in later sections. The approach taken in this article is to work backwards from the bulk effects, described first, to their origin at the molecular level. Thus, Section 5 describes the connection between the constituent molecular NLO hyperpolarizabilities and the macroscopic NLO response. Topics include local field effects, orientation of molecules and polymers, methods of incorporating NLO chromophores into polymers, and limitations on the application of simple summative models. Particular molecular properties that determine the microscopic NLO response are discussed and a few distinct models and parameters useful for optimizing second-order and third-order material properties are provided. The emphasis is on understanding the influence of  $\pi$ -electrons and electron delocalization, as well as on the nature and scaling of polymer repeat units for third-order materials. Also briefly reviewed are several categories of polymer structures that have been studied, and their advantages and disadvantages for NLO applications. Finally, major test methods for measuring the NLO properties of materials are surveyed.

The research literature on nonlinear optics and NLO polymers is vast, whereas this article is, of necessity, intended to serve primarily as a starting point for further investigation. Major topics of related NLO research are left to other articles in this book and to the reading list and bibliography. The reading list at the end of this article recommends books, proceedings, and special journal issues devoted to nonlinear optics and the NLO properties of molecular organic materials and polymers. (See, especially, References 1–7). The article is also focused primarily on all-optical nonlinearities. See article ELECTROOPTICAL APPLICATIONS for a discussion of the changes in the optical response of polymers due to an applied AC or DC electric-field from the so-called Pockels or Kerr effects. Nonlinearities arising primarily from vibrational or rotational/orientational motion (8) are not considered here. Also omitted are the unique NLO properties of many specialized classes of polymers, such as liquid crystalline polymers (see LIQUID CRYSTALLINE POLYMERS, MAIN-CHAIN), organometallic polymers (see METAL-CONTAINING POLYMERS), chiral and biological polymers, and magneto-optical polymers. Similarly, promising studies of polymer-based nanoscale structures, the optical properties of conducting polymers (9) and their application to the development of electroluminescent polymers for organic light-emitting diodes (LEDs) and lasers are outside the scope of this article (see LIGHT-EMITTING DIODES).

## Overview of Nonlinear Susceptibilities

**Linear and Nonlinear Optics Compared.** A simple comparison with the characteristics of linear optics illustrates some of the unique phenomena associated with nonlinear optics. Light bends (refracts) at an optical interface between two media because of the change in speed of propagation of light, as described by each media's refractive index. In linear optics, the refractive index  $n$  of the material does not change with the intensity of the light at ordinary light levels. (Otherwise one would need different power eyeglasses for low levels of light and for bright sunshine.) Also, the light transmitted by a linear transparent material does not change frequency upon passing through it. An incident red light emerges red. For both linear and nonlinear optics, media are dispersive, so that the index of refraction changes with the frequency of the light, and a medium may absorb visible light at some frequencies, giving the material a distinctive color. If the optical properties are linear, however, both the dispersion and the relative fraction of power absorbed are independent of the intensity of the light.

If the incident light is sufficiently intense, as in a laser, these simple linear relationships are no longer sufficient to describe the optical response of so-called nonlinear media (or any media, for that matter, if the measurement is precise enough or the intensity is high enough and the material is not destroyed in the process). When the optical properties of the material become nonlinear, the refractive index may change with the intensity of the incident light, thereby changing the optical path length and the focusing properties of an optical element made from that material. In addition, the presence of one beam may amplify another or change its polarization when the beams overlap in the medium, as in an optical switch. Also, the material's absorption (the imaginary part of the index of refraction) may vary with incident intensity. For example, in an optical limiter, the material may appear to be transparent to low levels of light, but a sufficiently intense beam will trigger significant absorption. Conversely, the absorption of a so-called saturable absorber decreases as the intensity of the light increases. Finally, the frequency response of the medium may also be altered when nonlinear effects become apparent. For example, an intense infrared laser may produce a significant visible frequency component upon passing through a material, through harmonic generation, or through another frequency conversion process.

**Anharmonic Oscillator Model.** At the microscopic level, materials respond to light (or more specifically to the oscillations of the electric-field of the light) through the back-and-forth movement of charges. As an example of how the nonlinear displacement of the charge affects the detected response, it is helpful to view the effects of the oscillating optical electric-field on a material using an anharmonic oscillator model (10). Ignoring the vector nature of the field for the present, the force on the electron in an electric-field  $E$  is simply  $F_e = eE$ , where  $e$  is the electron charge. For linear media, the restoring force on the electrons in the presence of the optical field is directly proportional to the electron displacement  $x$  from equilibrium, just like the restoring force for a simple spring,  $F_{\text{restore}} = -kx = -m\omega_0^2x$ , where  $k$  is the spring constant,  $\omega_0$  the resonant frequency, and  $m$  the mass. The resulting equation of motion for the electron, ignoring damping of the oscillations, is then simply  $eE - m\omega_0^2x = m\frac{d^2x}{dt^2}$ . The solution to this equation in

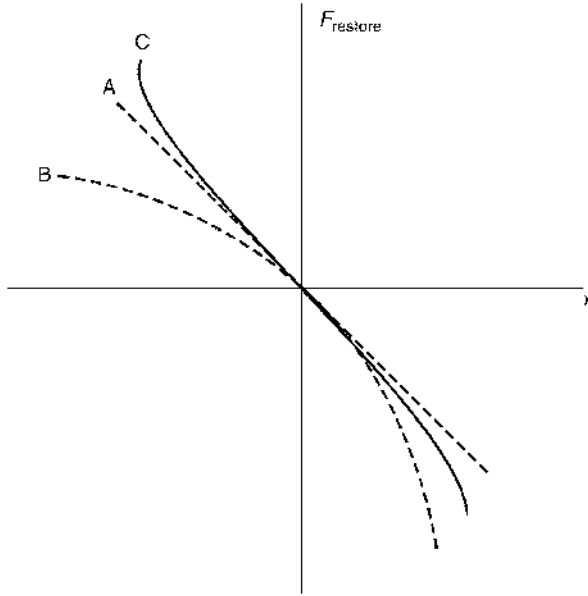


**Fig. 1.** Examples of restoring forces  $F_{\text{restore}}$  as functions of  $x$  for (A) a linear restoring force, (B) a restoring force with a quadratic nonlinear term, and (C) a restoring force with a cubic nonlinear term.

the case of a monochromatic optical field oscillating at  $\omega$  ( $E = E_0 \cos \omega t$ ) is

$$x = -\frac{e}{m} \frac{E}{(\omega_0^2 - \omega^2)} \quad (1)$$

As the pull of the applied field becomes stronger, however, the electron's spring-like response becomes distorted. The restoring force must include additional, nonlinear terms proportional to the square of the displacement for second-order processes ( $F_{\text{restore}} = -kx - ax^2$ ) or the cube of the displacement for third-order processes ( $F_{\text{restore}} = -kx - bx^3$ ). (Coefficients  $a$  and  $b$  may be positive or negative. Figure 1 shows examples of quadratic and cubic nonlinear restoring forces for positive coefficients.) The solution to the equation of motion in the case of an anharmonic restoring force is not possible in closed form, but the solution can be expressed as a series expansion,  $x = x_1 + x_2 + x_3 + \dots$ , where  $x_1$  is the solution without any anharmonic term in the restoring force (given by equation 1). Given a single monochromatic incident optical field as a driving force for the oscillator, again expressed as  $E = E_0 \cos \omega t$ , the simplest nonlinear contributions turn out to be proportional to the square  $x_2 \sim E_0^2 \cos^2 \omega t$  and the cube  $x_3 \sim E_0^3 \cos^3 \omega t$  of the incident field (11). Application of simple trigonometric identities to the expressions for  $x_2$  and  $x_3$  reveals typical resulting phenomena. Using the identity  $\cos^2 \omega t = \frac{1}{2} + \frac{1}{2} \cos 2\omega t$ , the  $\cos^2 \omega t$  term may be expressed as a combination of a second-harmonic response ( $2\omega = \omega + \omega$ ) and a constant DC field response called optical rectification ( $0 = \omega - \omega$ ). The expansion  $\cos^3 \omega t = \frac{3}{4} \cos \omega t + \frac{1}{4} \cos 3\omega t$  similarly leads to a third harmonic response ( $3\omega = \omega + \omega + \omega$ ) and a

response at the incident frequency ( $\omega = \omega + \omega - \omega$ ). The latter is responsible for the intensity-dependent refractive index change in the material (12).

**Nonlinear Susceptibilities.** Nonlinear optical effects are formally understood through the series expansion of the  $i$ th component of the polarization (average dipole moment per unit volume)  $\mathbf{P}$  of a material in powers of the electric-field in the medium  $\mathbf{E}$  (typically on the order of  $10^6$  V/m or greater for nonlinear effects to appear), as in (13)

$$\begin{aligned} P_i^\omega = P_i + \varepsilon_0 [ & \chi_{ij}^{(1)}(-\omega; \omega) E_j^\omega + \chi_{ijk}^{(2)}(-\omega; \omega_1, \omega_2) E_j^{\omega_1} E_k^{\omega_2} \\ & + \chi_{ijkl}^{(3)}(-\omega; \omega_1, \omega_2, \omega_3) E_j^{\omega_1} E_k^{\omega_2} E_l^{\omega_3} + \dots ] \end{aligned} \quad (2)$$

where summation over repeated coordinate indices ( $i, j, k$ ) is assumed,  $\varepsilon_0$  is the permittivity of free space, and the frequency dependence will vary with the NLO process under investigation. [Equation 2 expresses the components of the polarization in the frequency domain, which is the customary approach appropriate for monochromatic or nearly monochromatic fields. In some cases, such as recent research using ultrashort pulses, an analogous and more general time-domain expansion may be preferable (14).] The resultant response frequency  $\omega$  is a combination (sum and/or difference) of the incident frequencies  $\omega_n$ . The negative sign is included as a reminder that photon energy (and momentum) is conserved in these parametric processes. Thus, the sum of the frequencies given within each of the parentheses equals zero. The first term on the right,  $P_i$ , represents the permanent dipole moment per unit volume in the material. The second term provides the linear contribution to the refractive index (and, if  $\chi^{(1)}$  is complex, the absorption coefficient) through the usual second-rank tensor for the linear susceptibility  $\chi^{(1)}$ . (Recall, in the case of linear homogeneous, isotropic, transparent media, the index of refraction is related to  $\chi^{(1)}$  by  $n = \sqrt{1 + \chi^{(1)}}$ .) The remaining terms are responsible for the NLO properties of the material, primarily through the second- and third-order susceptibility tensors,  $\chi^{(2)}$  and  $\chi^{(3)}$ . Although including an arbitrarily large number of terms in the expansion of the polarization in equation 2 is possible, categorizing nonlinear phenomena as either second-order or third-order, using just the terms explicitly shown in equation 2, is practically sufficient. Higher order terms are usually of greatly diminished strength (15).

**Centrosymmetric vs Noncentrosymmetric Bulk Media.** The distinction between second- and third-order nonlinearities is particularly important for the design of NLO materials for different applications. The terms with even powers in the series expansion of the polarization (eq. 2) are identically zero for centrosymmetric materials. Only noncentrosymmetric materials can exhibit second-order ( $\chi^{(2)}$ ) NLO properties, such as second harmonic generation. [All materials, however, are noncentrosymmetric at their surfaces, and researchers have used surface techniques, such as surface second-harmonic generation, to study centrosymmetric materials (16). For recent reviews, see Reference 17.] The presence of second-order effects depends on the asymmetry both of the individual molecules and on the arrangement of those molecules. The requisite asymmetry is not found naturally in bulk amorphous polymers. The amorphous nature of most polymers requires special preparation to produce the requisite asymmetry, such as

electric-field poling (18), a liquid crystalline phase (19), self-assembly (20), or film formation techniques, as in a Langmuir–Blodgett film (21,22). Most of these techniques are used to align dipolar donor–acceptor groups that are either dissolved in a guest–host system or attached to a polymer to produce macroscopic asymmetry, as discussed in Section 5.4 on incorporating chromophores into polymers. These film preparation techniques and the material properties based on them are beyond the scope of this article, but the references above provide starting points for further investigation. (see also LANGMUIR-BLODGETT FILMS; LIQUID CRYSTALLINE POLYMERS, MAIN-CHAIN). Polymer orientation is also discussed at length in the article Electrooptical Applications (qv) because the second-order susceptibility is critical to linear electrooptic devices.

**Nonlinear Susceptibility Tensor Elements.** In general, the nonlinear susceptibilities,  $\chi^{(2)}$  and  $\chi^{(3)}$ , are complex third- and fourth- rank tensors and, therefore, are comprised of  $3^3$  and  $3^4$  different complex numbers, respectively. Fortunately, various symmetries significantly restrict the number of independent tensor elements. Kleinman showed that in certain circumstances, the susceptibility tensor elements are identical for rearrangements of the tensor indices (23). For second-harmonic generation in lossless media, for example, Kleinman's symmetry reduces the number of elements of  $\chi^{(2)}$  to 10. In this case, an abbreviated notation has been introduced,  $d_{il} = \frac{1}{2} \chi_{ijk}^{(2)}$ , where  $l$  represents the six permuted combinations of the  $jk$  indices ( $l = 1, 2, 3, 4, 5$ , and  $6$ , corresponding to the respective index combinations  $11, 22, 33, 23 = 32, 13 = 31$ , and  $12 = 21$ ), and the  $ijk$  indices can be freely permuted (10). Thus, for example,  $2d_{13} = \chi_{133}^{(2)} = \chi_{313}^{(2)} = \chi_{331}^{(2)} = 2d_{35}$  and  $2d_{33} = \chi_{333}^{(2)}$ . For cylindrically symmetric materials (a poled polymer, for example) only two tensor elements are important: the element  $d_{33}$ , which describes interactions parallel to the dipolar axis, and the element  $d_{31}$ , which describes interactions perpendicular to the dipolar axis (24).

For centrosymmetric materials, such as amorphous polymers, the lowest order nonzero nonlinear susceptibility is  $\chi^{(3)}$ . For an isotropic polymer, the number of independent  $\chi_{ijkl}^{(3)}$  elements is only three, generally, because no direction can be preferred over any other and each direction must appear at least twice (leading to  $\chi_{1111}^{(3)} = \chi_{1122}^{(3)} + \chi_{1212}^{(3)} + \chi_{1221}^{(3)}$ ) [It should be noted that an isotropic solution of chiral molecules will exhibit second-order nonlinearities, but not second-harmonic generation (25)]. For third-harmonic generation, the susceptibility elements simplify to only one ( $\chi_{1122}^{(3)} = \chi_{1212}^{(3)} = \chi_{1221}^{(3)}$ ), and for the nonlinear refractive index, the number of elements needed is only two ( $\chi_{1122}^{(3)} = \chi_{1212}^{(3)}$ ). Furthermore, the nature of the physical mechanism leading to the nonlinear refractive index can sometimes be determined from the ratio of the elements. For example, the relation  $\chi_{1122}^{(3)} = \chi_{1221}^{(3)}$  applies if the refractive index change is only due to the nonresonant electronic response of the charges, but  $\chi_{1221}^{(3)} = 6\chi_{1122}^{(3)}$  applies if the refractive index change is due to molecular reorientation (26). Fortunately, in many cases it is not necessary to specify individual tensor elements. Unless otherwise stated, the effective nonlinear susceptibility appropriate for the geometry of the material and configuration of the experiment should be assumed.

**Problems With Conventions, Reference Standards, and Units.** The expression for the relationship between the response and the input fields given by equation 2 is not the only expression commonly used in the literature. Variations

include expanding the polarization in a Taylor series instead of a power series (27), and defining the relationship between the field and the polarization differently (28). Differences between conventions often make it difficult to compare bulk nonlinear susceptibilities and the related molecular susceptibilities (or hyperpolarizabilities) obtained by different experimental methods and by different researchers (29). A more complete theoretical discussion of the problem of comparing conventions as well as the inconsistent use of reference standards for NLO process can be found in Reference 28. For purposes of this article, trends in structure-property relationships will be emphasized, rather than precise values of the NLO coefficients measured. Nonetheless, typical SI values for  $\chi^{(2)}$  are  $10^{-12} - 10^{-9}$  m/V and for  $\chi^{(3)}$  are  $10^{-22} - 10^{-18}$  m<sup>2</sup>/V<sup>2</sup>. Dramatic variations in these values are possible, particularly near a resonance where thermal effects and saturated absorption also contribute to the NLO response. Slower, nonelectronic effects, such as reorientation and electrostriction, also can increase the effective nonlinear susceptibility by orders of magnitude (30). The permittivity factor  $\epsilon_0$  in equation 2 is appropriate for SI units. Most researchers publish results in electrostatic units (esu), however, sometimes without even specifying the fundamental dimensions to which these units refer. Conversion to SI is a straightforward, though not always obvious process. For example, a typical polymer  $\chi^{(3)}$  value of  $10^{-12}$  esu =  $10^{-12}$  cm<sup>2</sup>/statvolt<sup>2</sup> converts to  $4\pi/9 \times 10^{-20}$  m<sup>2</sup>/V<sup>2</sup> in SI units, whereas a typical poled polymer  $\chi^{(2)}$  value of  $10^{-8}$  esu =  $10^{-8}$  cm/statvolt becomes  $4\pi/3$  pm/V in SI. A detailed discussion of the unit conversion process can be found in Reference 31, with the caveat that different conversions are required between SI and esu depending upon the choice of convention for the series expansion of the polarization (28). For example, many authors choose to omit the factor of  $4\pi$  in the conversion (32).

## Nonlinear Phenomena

This section surveys the most widely studied phenomena included among NLO effects that arise due to the electronic contributions to the real and imaginary parts of  $\chi^{(2)}$  and  $\chi^{(3)}$ . This review will be primarily concerned with phenomena related to harmonic generation, the intensity-dependent refractive index, and multiphoton absorption.

**Parametric Processes.** Parametric processes are those in which photon energy is conserved while the light propagates through the medium. Parametric phenomena of particular interest for devices due to the real part of the nonlinear susceptibility tensors include

- (1) second-harmonic generation (SHG) given by

$$P_i^{2\omega} = \frac{1}{2} \epsilon_0 \chi_{ijk}^{(2)}(-2\omega; \omega, \omega) E_j^\omega E_k^\omega \quad (3)$$

- (2) third-harmonic generation (THG) given by

$$P_i^{3\omega} = \frac{1}{4} \epsilon_0 \chi_{ijkl}^{(3)}(-3\omega; \omega, \omega, \omega) E_j^\omega E_k^\omega E_l^\omega, \quad (4)$$



- (3) degenerate four-wave mixing, (DFWM or the all-optical Kerr effect, OKE) given by

$$P_i^\omega = \frac{3}{4} \varepsilon_0 \chi_{ijkl}^{(3)}(-\omega; \omega, \omega, -\omega) E_j^\omega E_k^\omega E_l^{-\omega} \quad (5)$$

In each case above, the fractional prefactor accounts for the indistinguishability (degeneracy) of the frequencies of the incident fields so that different expressions yield the same susceptibilities in the zero-frequency limit. This convention is common, but not universally adopted (33).

**Harmonic Generation.** Nonlinear frequency conversion, especially harmonic generation, is important for the development of sources of coherent light at frequencies not otherwise accessible by efficient lasers, in particular the blue, violet, and UV frequencies needed for dense data storage. Harmonic generation is also useful for nonlinear spectroscopic studies, which probe excited states in materials (34).

For harmonic conversion, the conversion efficiency (the ratio of harmonic to fundamental power,  $\eta$ ) is largely determined by the size of the effective nonlinearity, the input power  $P_\omega$ , the interaction length  $l$ , and the ability to phase-match the spatial frequencies of the second harmonic and the fundamental light (35). For purposes of illustration, in the limit where only a small fraction of the power is converted and the index of refraction,  $n_\omega$ , in the material is assumed to be real (lossless) and isotropic, the conversion efficiency can be expressed as (36)

$$\eta = \frac{128\pi^5 (\chi_{\text{eff}}^{(2)})^2 l^2 P_\omega}{n_{2\omega} n_\omega^2 \lambda^2 c} \left( \frac{\sin \Delta\varphi/2}{\Delta\varphi/2} \right)^2 \quad (6)$$

Here,  $\Delta\varphi = \pi l/\lambda (n_{2\omega} - n_\omega)$  is the phase shift between the propagating fundamental and the generated harmonic light,  $\lambda$  is the wavelength in free space, and  $c$  is the speed of light. If  $\Delta\varphi = 0$ , then the factor  $(\sin(\Delta\varphi/2)/\Delta\varphi/2)$  in equation 6 takes on its maximum value 1. If the indices of refraction at the second harmonic ( $n_{2\omega}$ ) and the fundamental ( $n_\omega$ ) are not equal, however, the resulting efficiency oscillates with rapidly diminishing peaks as the interaction length increases. The process of minimizing  $\Delta\phi$  by making the *effective* refractive indices the same for the fundamental and harmonic light is called *phase-matching*. Techniques for phase-matching are discussed in later in connection with the discussion of using harmonic generation as a technique for characterizing the NLO properties of a polymeric material and for device applications. Poled polymers, have been studied extensively for use in second harmonic generation and other frequency conversion devices.

**Degenerate Four-Wave Mixing.** DFWM involves input and output light all at the same frequency. When applied to a single input beam, this effect is responsible for applications such as self-focusing and defocusing due to differences in intensity across the beam profile. When two distinct input beams overlap in a sample, another effect of DFWM may be the transfer of energy between the beams, which is useful for many applications such as single-frequency, all-optical switching (37).

DFWM is best understood in terms of an intensity-dependent refractive index. The two lowest order terms in the refractive index expansion for isotropic media may be written simply as

$$n = n_0 + n_2 I \quad (7)$$

where  $I$  is the incident intensity,  $n_0$  is the usual linear index (as seen for lower light levels), and

$$n_2 = \frac{3}{4\epsilon_0 c n_0^2} \text{Re}[\chi^{(3)}] \quad (8)$$

The key parameter in optical switching is the intensity-dependent phase-shift (as might appear between the arms of a Mach–Zehnder interferometer (38) or in a directional coupler (39), for example) given by

$$\Delta\varphi(\lambda, L) = \frac{2\pi L n_2 I}{\lambda} \quad (9)$$

where  $L$  is the interaction length, and  $n_2$  also depends upon the wavelength  $\lambda$  (40). Phase shifts of  $\pi$  or greater are required for most devices, though some applications require only a shift of  $\pi/2$  (41).

**Sum and Difference Frequencies; Nondegenerate Four-Wave Mixing.** In addition to the phenomena described above, interesting NLO phenomena may also result from a combination of monochromatic fields of different frequencies, as in sum ( $\omega = \omega_1 + \omega_2$ ) and difference ( $\omega = \omega_1 - \omega_2$ ) frequency generation in second-order processes, or nondegenerate four-wave mixing, a third-order process in which the detected frequency may be any combination of the input frequencies (for example,  $\omega = 2\omega_1 - \omega_2$  or  $\omega = \omega_1 + 2\omega_2$ ). These phenomena have historically been of less importance for polymer device applications, though commercial applications for optical parametric generation using inorganic crystals, such as  $\beta$ -barium borate are well developed. Finally, third-order, nondegenerate, four-wave mixing may also involve the use of light of one frequency to cause a change in the refractive index of the medium that is experienced by a second beam at a different frequency ( $\omega = \omega_1 - \omega_1 + \omega_2$ ) (42,43).

**Resonant Nonlinear Phenomena.** The susceptibility tensors  $\chi^{(2)}$  and  $\chi^{(3)}$  may be complex, indicating the presence of multiphoton resonances and nonlinear absorption effects. The effects of nonlinear absorption are of significant interest in polymer device applications and are typically expressed in a power series in the incident intensity with the transmitted intensity  $I_1$  given by (44)

$$\frac{dI_1}{dz} = -\alpha^{(1)} I_1 - \alpha^{(2)} I_1 I_2 - \alpha^{(3)} I_1 I_2 I_3 - \dots \quad (10)$$

where the light propagates in the  $z$ -direction and the different subscripts 1, 2, 3 allow for light of different wavelengths to impact the transmission at wavelength 1. The two-photon absorption coefficient  $\alpha^{(2)}$  is related to the imaginary part of

the complex third-order susceptibility for an isotropic medium by

$$\alpha^{(2)} = \frac{3\omega}{2\varepsilon_0 c^2 n_0^2} \text{Im}[\chi^{(3)}] \quad (11)$$

One figure of merit for all-optical switching is the relative two-photon absorption that accompanies an intensity-dependent change in refractive index. The quantity  $2\alpha^{(2)}\lambda/n_2$  must be less than unity for switching to be possible (45).

In some resonant phenomena, such as saturated absorption, the use of a power series as shown in equation 10 may be inappropriate because of the contributions from higher order processes. For a dye in a solid polymer matrix, the intensity-dependent absorption coefficient, based on inhomogeneous broadening of the absorption, is often expressed in terms of the saturation intensity  $I_s$  at which the population of excited states in the dye from decay processes matches the decay rate from the excited states (46):

$$\alpha(I) = \frac{\alpha^{(1)}}{(I + I_s)^{\frac{1}{2}}} \quad (12)$$

Multiphoton absorption is already widely used for spectroscopic analysis. As discussed later in this article, linear absorption spectra of centrosymmetric molecules only give transitions between states of opposite parity. Two-photon absorption is capable of providing information about transitions between states of the same parity, or so-called two-photon states. In addition, even in noncentrosymmetric materials, two-photon absorption can probe the bulk properties of the medium at frequencies near the linear absorption band where a linear probe may be absorbed at the material surface (44). Two-photon absorption promises to be useful for ultrafast optical limiters, which protect against damage due to high power laser pulses. Polymers containing metal centers or carbon-60 (fullerene) have been especially interesting for this application (47–49). Multiphoton absorption effects are also being investigated currently for their application to laser mode locking, optical pulse shaping, and other beam processing applications (50).

### Other Effects.

**Combination with Static Fields.** A common technique, useful for optoelectronic devices, is to combine a monochromatic optical field with a DC or quasi-static field. This combination can lead to refractive index and absorption changes (linear or quadratic electrooptic effects and electroabsorption), or to electric-field induced second-harmonic generation (EFISH or DC-SHG,  $2\omega = \omega + \omega + 0$ ) in a quasi-third-order process. In EFISH, the DC field orients the molecular dipole moments to enable or enhance the second-harmonic response of the material to the applied laser frequency. The combination of a DC field component with a single optical field is referred to as the linear electrooptic (Pockels) effect ( $\omega = \omega + 0$ ), or the quadratic electrooptic (Kerr) effect ( $\omega = \omega + 0 + 0$ ). These electrooptic effects are discussed extensively in the article Electrooptical Applications (qv). EFISH is discussed in this article, however, for the important role that it has played in the characterization of nonlinear optical materials for other applications.

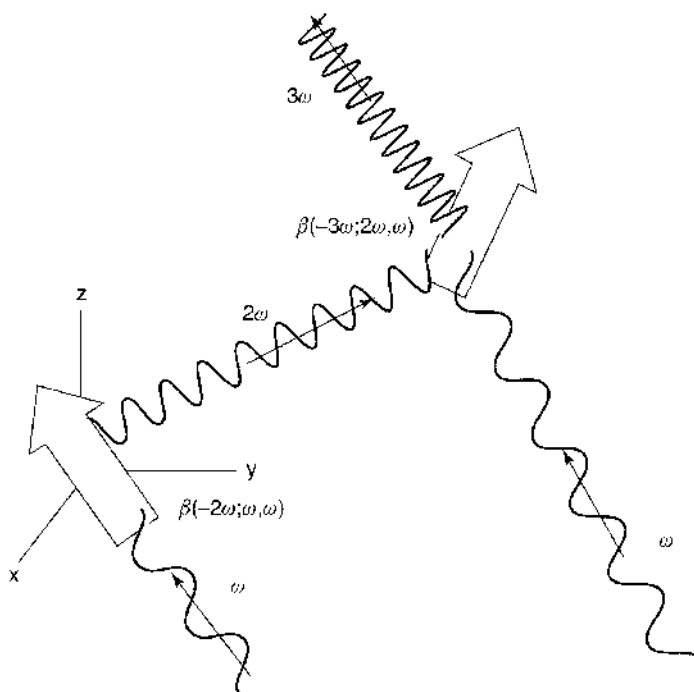


**Fig. 2.** Schematic showing a cascaded optical nonlinearity in which the second harmonic generated at one molecule combines with the fundamental by sum frequency generation at a nearby molecule to result in a third harmonic generated through a cascade of second-order processes.

*Cascading.* In most cases, the distinction between second- and third-order nonlinearities is evident from the different phenomena each produce. That distinction blurs, however, when one considers the cascading of second-order effects to produce third-order nonlinear phenomena (51). In a cascaded process, the nonlinear optical field generated as a second-order response at one place combines anew with the incident field in a subsequent second-order process. Figure 2 shows a schematic of this effect at the molecular level where second-order effects in noncentrosymmetric molecules combine to yield a third-order response that may be difficult to separate from a pure third-order process. This form of cascading is complicated by the near-field relationships that appear in the interaction between molecules, but analysis of cascaded phenomena is of interest, because it provides a way to explore local fields and the correlations between orientations of dipoles in a centrosymmetric material (52).

Another form of cascading takes advantage of nonlocal, phase-matched cascading of successive  $\chi^{(2)}$  processes to produce third-order nonlinear phase shifts (53). These cascading effects have been investigated for their ability to lead to large intensity-dependent refractive indices in poled waveguide materials (54). For example, two successive second-order effects, such as second-harmonic generation, followed by down conversion ( $\omega = 2\omega - \omega$ ), or optical rectification, followed by the linear electrooptic effect, lead to an intensity-dependent refractive index based on successive  $\chi^{(2)}:\chi^{(2)}$  interactions (55). The interested reader is

referred to the references for a more complete discussion of the enhancements that have been achieved through cascaded nonlinearities.

**Nonlinear Light Scattering.** Other forms of frequency conversion processes and nonlinear spectral broadening are possible through nonlinear light scattering. When the scattering is due to fluctuations in the molecular susceptibility, the result provides yet another method for investigating NLO properties referred to as hyper-Rayleigh scattering (HRS) (56,57). A brief description of HRS is included later because of its growing use in measuring optical nonlinearities of organic chromophores incorporated into NLO polymers, especially octupolar molecules and conducting solutions, not amenable to investigation through EFISH. Other nonlinear optical scattering processes are generally beyond the scope of this article, but are mentioned here for completeness. Stimulated Raman scattering and coherent anti-Stokes Raman spectroscopy (CARS), for example, involve light scattering from optical phonons and are widely used to convert available laser output frequencies to a variety of infrared, visible or even ultra-violet wavelengths, via so-called Stokes and anti-Stokes shifts (58,59). Stimulated Brillouin scattering involves light scattering from sound waves, a photon/acoustic phonon interaction through electrostriction (60). Rayleigh scattering leads to frequency shifts from inhomogeneities in the material and is called Rayleigh wing-scattering if due to fluctuations in the orientation of anisotropic molecules (61).

## Advantages of NLO Polymers

Optical second-harmonic generation (SHG) in an organic material was first reported in 1964 (62). The first measurements of the third-order NLO response of a polymer were performed on polydiacetylene crystalline polymers by Sauteret and co-workers in 1976 (63). Interest in polymeric second-order materials increased dramatically in the early 1980s when Meredith and co-workers performed the first studies on dye-doped glass-forming systems (64) and Singer and co-workers developed the process of electric-field poling to lock in the orientation of the chromophores in a guest-host system (65).

**Why Polymers?** Though most current commercial NLO applications use inorganic crystals and semiconductors, polymeric materials have been found to offer many advantages over their inorganic counterparts. These advantages include fast (subpicosecond) response times for nonresonant electronic effects, high optical damage thresholds, large susceptibilities combined with low dielectric constants, ease of processability as thin films or as fibers, ability to be integrated into silicon-based semiconductor structures or onto almost any substrate through spin-coating or other film deposition techniques, and, most importantly, compositional flexibility, which allows their physical and chemical properties to be tailored for specific end use applications through custom-functional design. These advantages, in turn, lead to large figures of merit for device applications. Disadvantages to be overcome, however, include lower thermal stability at high and low temperatures, lower mechanical strength, and, in some cases, higher linear optical absorption and scattering.

Generally, the suitability of a material for device applications requires a balance between optical nonlinearity, thermal and chemical stability, optical losses, and processability. Tradeoffs are to be expected as higher nonlinearities near

resonance, for example, lead to increased absorption losses. For third-order materials, the all-optical device applications are especially diverse and promising. These devices include all-optical switches (66), logic gates, optical memories, optical limiters, light modulators, ultrafast shutters, directional couplers (67), nonlinear amplifiers (68), and phase conjugators (69). The application of polymers to waveguide devices is a very important area of applied research, though the details are beyond the scope of this article. Polymer fibers have also been studied for their ability to provide high quality long-length interaction for nonlinear effects with low losses and large bandwidth (70–72). Though no devices have yet been put into mass production (41), the basic figures of merit for switching device applications have been met by several materials and methods, including polydiacetylene waveguides (38) and poly(methyl methacrylate) fibers (73), and through the use of cascaded nonlinearities (74).

### Connecting Macroscopic Properties to Microscopic Unit Properties

The foregoing sections described how various NLO phenomena can be understood in terms of the nonlinear susceptibilities. In this section, those susceptibilities are described in terms of the polarizabilities and hyperpolarizabilities, which characterize the separation of charge due to the electric-field at the molecular level. Major factors considered in bridging between the microscopic and the macroscopic properties include (1) local field effects, (2) orientation effects, (3) methods for incorporating NLO chromophores into a polymer to optimize the bulk properties, and (4) limits to the optimization of bulk properties through additive effects of the microscopic response.

**Relating Macroscopic and Molecular Properties.** For many organic/polymeric materials, the bulk polarization is best understood through averaging of the molecular polarizabilities of the weakly-interacting constituent materials. The molecular polarizability is expressed in a series expansion, similar to equation 2 for the polarization, (28)

$$p_I^\omega = \mu_I + \alpha_{ij}(-\omega; \omega) F_J^\omega + \beta_{ijk}(-\omega; \omega_1, \omega_2) F_J^{\omega_1} F_K^{\omega_2} + \gamma_{ijkl}(-\omega; \omega_1, \omega_2, \omega_3) F_J^{\omega_1} F_K^{\omega_2} F_L^{\omega_3} + \dots \quad (13)$$

where  $\mathbf{F}$  represents the *local* electric-field at the molecule. It is helpful to note the terminology differences between the macroscopic and molecular levels. Upper case subscripts are used to distinguish the molecular coordinate system from the laboratory coordinate system in which the macroscopic properties are measured.  $\mu$  is the permanent dipole moment of the molecule.  $\alpha$  is the linear polarizability tensor (not the absorption coefficient found in equation 10). The  $\chi^{(2)}$  and  $\chi^{(3)}$  tensors are referred to as *second-* and *third-order* susceptibilities; the corresponding molecular level tensors,  $\beta$  and  $\gamma$ , are called the *first* and *second* hyperpolarizabilities. Values for  $\beta$  and  $\gamma$  are usually given in esu, where a typical chromophore value for  $\beta$  of  $10^{-30}$  esu =  $10^{-30}$  cm<sup>4</sup>/statvolt becomes  $4.2 \times 10^{-40}$  m<sup>4</sup>/V in SI units and a value for  $\gamma$  of  $10^{-33}$  esu =  $10^{-33}$  cm<sup>5</sup>/statvolt<sup>2</sup> becomes  $1.4 \times 10^{-47}$

$\text{m}^5/\text{V}^2$  in SI (28). The reader is warned, however, that different unit conventions, and different conversion factors, are also used (75).

**Local Fields.** Relating the macroscopic nonlinear susceptibilities to the hyperpolarizabilities requires (1) incorporating the effects of the local fields at the molecules, and (2) averaging over the arrangement of molecules in the bulk. In general, finding the relationship between the local field in equation 13 and the macroscopic field found in equation 2 is a highly nonlinear and difficult problem (the “local field problem”) (49). (Analysis in the case of monomolecular films is simpler because local field corrections are less important and the materials are highly oriented (76)). The local field  $\mathbf{F}$  acting on the molecule is the vector sum of the applied field and the polarization field. The polarization field is the difference between the field due to nearest neighbor molecules and the collective field of a large number of molecules in a carefully defined volume around the molecule. The local field problem is solved satisfactorily for homogeneous materials by approximating the polarization by the linear term in the series expansion of equation 2 and assuming that the molecule exists in a spherical cavity in a homogenous media (77). This method of analysis, first described by Lorentz, leads to the so-called Lorentz local field factors,  $f_\omega = (n_\omega^2 + 2)/3$ , where  $n_\omega$  is the linear index of refraction of the medium at frequency  $\omega$ . (If static fields are involved, an Onsager local field treatment provides a first approximation to a more detailed treatment. In this case, the relevant local field factor becomes  $f_0 = [\varepsilon(n^2 + 3)]/(n^2 + 2\varepsilon)$  where  $\varepsilon$  represents the relative permittivity (78)). Thus, for homogeneous isotropic media and optical fields only,

$$\chi^{(2)}(-\omega; \omega_1, \omega_2) = N/\varepsilon_0 \times f_\omega f_{\omega_2} f_{\omega_1} \times \langle \beta(-\omega; \omega_1, \omega_2) \rangle \quad (14)$$

$$\chi^{(3)}(-\omega; \omega_1, \omega_2, \omega_3) = N/\varepsilon_0 \times f_\omega f_{\omega_3} f_{\omega_2} f_{\omega_1} \times \langle \gamma(-\omega; \omega_1, \omega_2, \omega_3) \rangle \quad (15)$$

with  $N$  being the number density of the molecules and  $\langle \rangle$  representing orientational averaging, which is discussed in the following section.

The local field effects for *composite* materials require more detailed analysis and can lead to a significant enhancement of the NLO response. For example, a promising method for enhancing the nonlinearity by several orders of magnitude through local field effects is to embed either finely distributed or fractal clusters of metal particles (79) in a polymer matrix.

**Orientational Averaging.** In general, orientational averaging requires careful consideration of the tensor nature of the hyperpolarizabilities and susceptibilities, and an appropriate choice of distribution functions for the geometries of the molecules involved and their arrangement in the bulk. The orientational averaging of  $\gamma$  (or  $\beta$ ) is given formally by the integration of  $\gamma$  (or  $\beta$ ), weighted by an appropriate distribution function for the range of orientations, over the appropriate range of angular orientations (79)

$$\langle \gamma \rangle = \frac{\int G(\Omega) \gamma(\Omega) d\Omega}{\int G(\Omega) d\Omega} \quad (16)$$

In the case of an isotropic polymer, the weighting function  $G(\Omega)$  is a constant for all orientations. See also Reference 80 for a discussion of theoretical

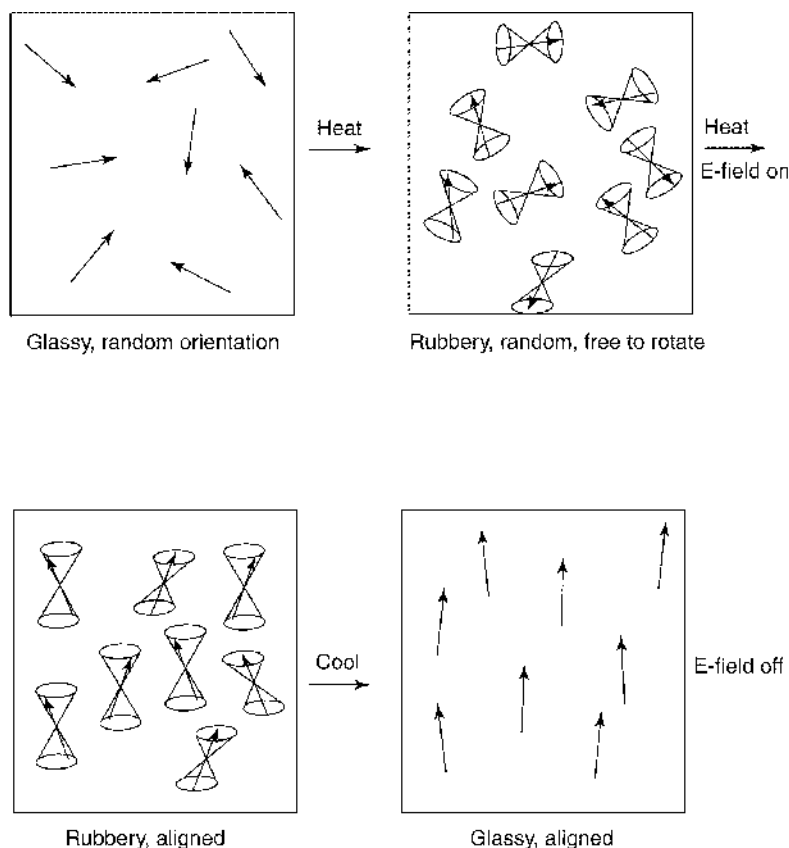


**Fig. 3.** Illustration of the electric-field poling process where the arrows represent the dipole moment orientation for NLO chromophores dissolved in a polymer matrix. (First appearing in Reference 81. Reprinted with permission.)

models used to calculate the appropriate order parameters used to perform the orientational averaging for  $\beta$ .

**Electric-Field Poling for Second-Order NLO Polymers.** As previously discussed, only noncentrosymmetric media have nonzero  $\chi^{(2)}$  values. Similarly, the molecular constituents of the media must have nonzero  $\beta$ . Moreover, in amorphous polymers, the bulk is centrosymmetric with  $\chi^{(2)} = 0$ , even if  $\beta$  is nonzero, due to the random orientation of the molecules. Thus, it is necessary to align the polar constituents in the polymer in order to generate second-harmonic or produce other  $\chi^{(2)}$  effects (though second-harmonic generation through hyper-Rayleigh scattering is still possible). Alignment is usually accomplished through electric-field poling, as illustrated in Figure 3. Poling involves heating the polymer, with the NLO chromophore incorporated into it, to a temperature above the temperature at which the polymer becomes rubbery, called the glass-transition temperature,  $T_g$  (see GLASS TRANSITION). At and above  $T_g$ , the dipoles can be aligned simply by the application of an external electric (poling) field, typically on the order of 100 MV/m. With the poling field maintained, the polymer is cooled



back to room temperature, locking in the polar alignment (at least temporarily). See Reference (78) for a more complete description of the poling process and its implications for orientational averaging and long-term thermal stability. The foregoing section assumes that  $T_g$  is lower than the chromophore decomposition temperature. Hybrid pressure poling and all-optical poling methods are also in use. These utilize other optical effects such as photoisomerization to assist the poling process (82).

For an isotropic, poled polymer film of essentially one-dimensional NLO molecules, the orientational average is expressed in terms of the average angle between the ground-state dipole moments of the chromophores and the direction in the film they would be pointing if perfectly aligned (83). For a polymer film in which the nonlinear component or moiety is rotationally symmetric about the film normal ( $z$ -axis), the only two nonzero susceptibility components can be determined from the angle ( $\theta$ ) between the film normal and the molecular  $Z$ -axis, (84)

$$\chi_{zzz}^{(2)} = N\beta_{zzz}^* \langle \cos^3 \theta \rangle \quad \chi_{xxz}^{(2)} = \frac{1}{2} N\beta_{xxz}^* \langle \cos \theta \sin^2 \theta \rangle \quad (17)$$

where \* indicates that appropriate local field corrections are already incorporated into the hyperpolarizabilities. For poled polymer materials, the orientational averages shown in equation 17 are determined thermodynamically by the coupling between the poling field  $E_p$  and the nonzero molecular dipole moment  $\mu$ . (The ground state dipole moment can be determined from measurements of the permittivity and refractive index as a function of concentration (85)). The only two tensor components of  $\chi^2$  can then be expressed simply as

$$\chi_{zzz}^{(2)} = N\beta^* \frac{\mu^* E_p}{5\epsilon_0 kT} \quad \chi_{xxz}^{(2)} = N\beta^* \frac{\mu^* E_p}{15\epsilon_0 kT} \quad (18)$$

where  $kT$  is the Boltzman energy. When poling is needed to induce polar order, the molecular figure of merit is the  $\mu\beta$  product. Nonresonant values of  $\mu\beta$  as great as  $10 \times 10^{-45}$  esu have been reported for 3-phenyl-5-isoxazolone, for example (86). In the absence of dipolar interactions, such as assemblies of octupolar multidimensional molecules, a more complicated analysis is required. In these cases, the desired alignment may be a highly ordered octupolar state without dipolar interactions (87). A later section briefly discusses polymeric materials with multidimensional constituents.

Maintaining polar order in a poled polymer is of great importance for second-order applications (88,89). The dielectric relaxation process leading to decay in the orientation of ordered polymers has been studied extensively and is the subject of another article (see DIELECTRIC RELAXATION). Several models that describe the chromophore reorientation for NLO materials have been proposed, including the Kohlrausch–Williams–Watts (KWW) model (90,91), biexponential and triexponential decay models (92), time-dependent Debye relaxation time models (93), and the Liu–Ramkrishna–Lackritz (LRL) model (94). For further information on these and other issues relating to dielectric relaxation in poled polymers, see also Reference 95.

One more example of the difficulties that can arise in comparing the hyperpolarizabilities and bulk susceptibilities is seen in the case of EFISH. Although EFISH is a macroscopic third-order process, the microscopic–macroscopic transition for EFISH is expressed as

$$\chi_{ijkl}^{(3)}(-2\omega; \omega, \omega, 0) = N[\langle \gamma_{IJKL}^*(-2\omega; \omega, \omega, 0) \rangle_{ijkl} + \langle \mu_I^*(-0; 0) \beta_{Jkl}^*(-2\omega; \omega, \omega) \rangle_{ijkl}] \quad (19)$$

The second term on the right side of equation 19 ultimately determines the usefulness of the molecule when incorporated into a polymer for second-order applications (96). A DC field aligns the dipole moment  $\mu$  so that the first hyperpolarizability,  $\beta$ , can contribute to the bulk response. A similar expression is applied to poled polymers (24). The assumption that  $\gamma$  is negligible compared to  $\beta$  is usually valid for nonlinear chromophores, but not for extended  $\pi$ -electron donor–acceptor systems because  $\gamma$  increases with conjugation length faster than  $\beta$  (97).

**Orientational Effects in Third-Order Polymers.** Bulk asymmetry is not required for a third-order NLO response, but orientation of polymer chains remains an important factor even if  $\beta = 0$ . For one-dimensional,  $\pi$ -electron conjugated polymers, the largest contribution to the NLO response occurs for light polarized parallel to the direction of the conjugated chain. Therefore, alignment of polymer chains, which restricts electron delocalization to one-dimension, enhances the magnitude of the NLO response of the polymer. Polymers with high levels of anisotropy exhibit significantly larger NLO response when the applied electric-field is polarized in a direction parallel to the chain orientation. The NLO response of an unoriented film of linear chain molecules has been shown to be one-fifth the NLO response of oriented film when the electric-field is applied parallel to the molecules (98). The implication is that processing polymers on a microscopic level is one method of enhancing the third order response of the polymer. A common method used to align polymer chains is stretch orientation of thin films (99). See also Reference 79 for an example of the application of the orientational averaging process to third-order materials.

**Incorporating Chromophores into Polymers.** The dominant approach used to enhance the second-order NLO response of organic materials is to incorporate optimized chromophores into a polymer matrix. The method used for incorporating the chromophore varies. The choice of polymer depends upon linear optical and other properties that make the polymer suitable for devices (81).

**Guest–Host Polymers.** The simplest, but not optimal, approach to incorporating NLO chromophores into a polymer is to dissolve the dye molecules into the polymer in a guest–host solid solution system (see Fig. 4a). (Poly (methyl methacrylate) has been one of the most commonly used polymers for this purpose for its ease of processability.) There are several significant drawbacks, however, to using a guest–host system. (1) The amount of dye that can be dissolved is usually very limited. (2) The glass transition temperature drops with increased doping due to plasticization. (3) The chromophore tends to leave the polymer at elevated temperatures. (4) Finally, the alignment of the molecular dipoles is less stable, so that a poled guest–host system is unlikely to retain its orientation for

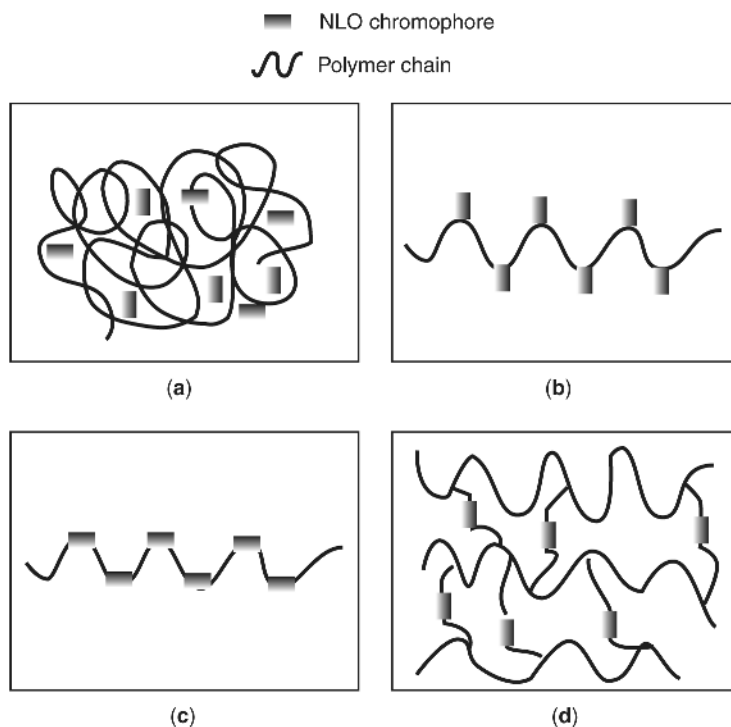


**Fig. 4.** Schematic of methods for incorporating NLO chromophores into a polymer, including (a) guest–host system, (b) side-chain functionalized system, (c) main-chain functionalized system, and (d) cross-linking system.

long periods (24). Methods to overcome these limitations include using high glass-transition temperature polymers, such as polyimides or polyetherketones, doped with relatively miscible chromophores (100,101).

**Side-Chain Polymers.** Though more challenging to produce than a guest–host system, a side-chain functionalized system in which at least one end of each of the chromophores is attached as a side chain to the polymer backbone, avoids some of the limitations of the guest–host system (see Fig. 4b). The resultant polymer retains the nonlinearity of the dopant molecules and permits greater chromophore concentration for a larger NLO response. Still, packing problems may appear if the chromophore concentration becomes too high. Attaching the chromophore as a side chain causes the orientational stability and other thermal properties of the system to depend more on the thermal properties of the polymer. For example, a polyimide with a high  $T_g$  is better able to preserve the polar order of the chromophore if the chromophore is incorporated as a side chain, rather than a simple solute (102).

**Main-Chain Polymers.** Main-chain polymers incorporate the chromophore directly into the chain by linking both ends of the chromophore, in either head-to-tail (isoregic) or head-to-head (syndioregic) configuration or some combination. Though a main chain configuration should add stability, establishing polar order in these polymers is not always obvious. The syndioregic configuration offers the

possibility of folding the polymer like an accordion so that the chromophores will align (103) (see Figure 4c).

**Cross-Linked Polymers.** Perhaps the greatest promise for long-term stability in molecular materials comes from cross-linked polymers (see Fig. 4d). Cross-linking must be performed during poling, but can be accomplished with guest–host (104), side-chain, or main-chain systems. The cross-linking must be done carefully to avoid the introduction of defects. One promising approach is the use of interpenetrating polymer networks (105).

**Limitations to Relating the Polymer Response to Molecular and Oligomeric Properties.** In many cases, the NLO response of the polymer can be derived entirely from the response of the molecular NLO chromophore units and their concentration in the polymer as a medium. The assumption that the system is weakly interacting is justified if the nonlinearity is a linear function of molecular concentration (106,107). For large concentrations of molecules in a polymer matrix, the assumption of a weakly interacting system may break down, however, as dimerization or aggregation become important (108).

**Oligomers.** Similarly, the third-order NLO properties of  $\pi$ -conjugated polymers are often extrapolated from oligomeric structure studies. Effective conjugation length scaling laws and band gap narrowing are examples of properties that have been investigated in terms of the oligomeric unit (109,110). Unfortunately, some aspects of a polymeric system cannot be modeled by smaller molecules, and extending oligomeric structure–property relationships to polymeric materials can be problematic. For instance, saturation effects in electron delocalization become apparent as conjugated chains become very long. Also, it is known that the excited state structure of a polymer may differ from its corresponding oligomer (111), and the effect that substitution may have on a polymer is not reflected by substitution on its related oligomeric or polyeneic structure (112). Many other issues that surround the extension of oligomer structure–property relationships to polymer relationships have been considered and much literature is available on the topic (113). With these caveats in mind, the next section discusses the electronic character of constituent NLO materials for the purpose of understanding the origin of the hyperpolarizabilities.

## Structure–Property Relationships: Understanding Constituent NLO Properties

How macroscopic NLO properties of a material are determined from the response of its microscopic constituents was shown in the previous section. The origin of the NLO properties of these constituents is discussed here. A fundamental theoretical problem is to calculate the NLO response directly from the electronic configuration of the molecules. This section explores the molecular parameters that contribute to large hyperpolarizabilities. Particular emphasis is on sum rule calculations and essential states models as guides to obtaining the optimal NLO response.

The discussion necessarily divides into separate consideration of the structure–property relationships for the molecular constituents, which particularly impact the  $\chi^{(2)}$  response, and the nature of the supramolecular and

polymeric effects, especially relevant to  $\chi^{(3)}$  materials. Fundamental factors affecting each are discussed, including symmetry, donor–acceptor groups and charge transfer, conjugation or  $\pi$ -electron delocalization length, the nature of the  $\pi$ -electron bonding sequence, bond length alternation (or bond order alternation), aromaticity, multidimensionality, and the substitution of alternate atoms into the conjugated structure.

**Brief Overview of Quantum Calculations.** Most organic and polymeric systems, unlike inorganic systems, owe their nonlinear response to virtual electron excitations occurring in the individual molecular or monomeric units. A complete theoretical understanding of the NLO response requires extensive quantum mechanical calculations, which encompass every structural aspect of the system. These aspects include the positions and electron configuration of each atom, the nature of the bonds between atoms, and the full electronic energy band structure, including all interactions. The linear and nonlinear properties can be deduced from the wavefunction of the system, which is the solution to the Schrodinger equation  $H\Psi = E\Psi$ , where  $H$  is the suitably chosen Hamiltonian operator including interactions among all the charges and  $E$  is the energy of the system. The molecular orbital (MO) approach expands the wavefunction in a self-consistent set of basis functions with appropriate configuration interactions (CI), using a linear combination of atomic orbitals (114). The number of CI integrals to be calculated increases as the fourth power or higher of the number of basis functions in the molecule, so that calculations even for small molecules can be time-consuming (115).

At least three different approaches are used to calculate the nonlinear response from quantum chemical considerations (40,116). In so-called “derivative” techniques, the polarizability and hyperpolarizabilities are found by taking derivatives of the dipole moment components with respect to the various electric-field components.

$$\begin{aligned}\alpha_{ij} &= \frac{\partial \mu_i}{\partial E_j} \\ \beta_{ijk} &= \frac{\partial^2 \mu_i}{\partial E_j \partial E_k} \\ \gamma_{ijkl} &= \frac{\partial^3 \mu_i}{\partial E_j \partial E_k \partial E_l}\end{aligned}\tag{20}$$

These derivatives are evaluated using so-called coupled Hartree–Fock techniques and either static or oscillating fields (117). A second approach is to model the nonlinear media as a set of coupled anharmonic oscillators, with resonant frequencies corresponding to excited state transition frequencies. The strength of the coupling is a function of the proximity of the external field frequency to the resonant frequency of the oscillator.

A third approach, the one most important for the current discussions, is to treat the electric-field as a source of perturbation of the total molecular energy using real and virtual excited state transitions. This approach uses electronic wave functions either for all of the electrons of the molecule (ab initio calculations)

or for only the valence electrons (so-called semiempirical theories). Semiempirical Hamiltonians may ignore electron interactions completely (Huckel theory). They may assume one  $\pi$ -orbital per carbon and assume no overlap between adjacent electron orbitals (Pariser–Parr–Pople or PPP). Or, they may include both the  $\sigma$  and  $\pi$  electrons and either no overlap (so-called complete neglect of differential overlap or CNDO), or only include overlap between orbitals on the same atom (intermediate neglect of differential overlap or INDO). The goal of each of these techniques is to compute the energy levels, transition moments, and dipole moment differences for essential energy states of a molecule (118). These parameters are used in a sum-over-states perturbation approach to determine the hyperpolarizabilities. See, for example, References (40,119–121). An advantage of the perturbation approach is the explicit appearance of the frequency response and the role that different excited states play in the frequency response.

### **Sum-Over-Essential States Models for Molecular Materials.**

*The Two-Level Model for  $\beta$ .* For NLO organic chromophores (dyes) used to provide a large second-order nonlinear response, the sum-over-states approach has proven to be a particularly valuable predictor of  $\beta$  and its spectral dispersion. In the sum-over-states approach, hyperpolarizabilities may be calculated in theory by including contributions from virtual and real transitions to and from *all* of the excited states or energy levels of the molecules. In practice, however, only a few states are expected to contribute measurably. The key to using this approach for optimizing  $\beta$  (or  $\gamma$ ) is to identify and characterize the contributions of the most important excited states of the molecule in the spectral region of interest. In fact,  $\beta$  is often well understood by truncating the sum to include only the ground state and *one* excited state, a so-called two-level model. The energy difference between these two states is sometimes called the optical gap, and the nature and location of the transition (gap) between the two states is particularly important for its dominant role in the linear absorption spectrum. The two-level model yields a simple formula for  $\beta$  in the case of second-harmonic generation (122):

$$\beta_{\text{two-level}} = \frac{3}{2\hbar^2} \frac{\omega^2 |\mu_{01}^2| \Delta\mu_{10}}{[\omega_{10}^2 - \omega^2][\omega_{10}^2 - 4\omega^2]} \quad (21)$$

where  $\hbar\omega_{10}$  is the energy difference between the ground and excited state,  $\mu_{01}$  is the transition dipole moment between the two states, “0” (the ground state) and “1” (the excited state), and  $\Delta\mu_{10} = \mu_{11} - \mu_{00}$  is the difference between dipole moments of these two states. The transition dipole moment  $\mu_{01}$  can be determined by numerical integration of the absorption spectra. The ground state dipole moment  $\mu_{00}$  is determined through concentration-dependent measurements of the relative permittivity and refractive index. The excited state dipole moment  $\mu_{11}$  is typically found by analysis of spectral shifts in the absorption band due to changes in the local electric-field (electrochromism or solvatochromism) (85).

The two-level model justifies the dominant approach for optimization of the second-order NLO response, which is to couple the largest transition moment with the largest dipole moment difference. This combination of a large transition moment and large dipole moment difference is usually accompanied by a sharp absorption peak. A general rule-of-thumb, which has been adopted by many

researchers into second-order molecular materials is summed up by the adage, “Redder is better.” In effect, the lower the energy of the dominant absorption peak of the chromophore, the greater is the nonlinear response. (Interestingly, some highly nonlinear organic chromophores such as Foron brilliant blue and squaraine dyes (123,124) have sharp absorption peaks shifted so far into the visible so as to absorb the red wavelengths, yet transmit higher energy blue wavelengths, prompting the enigmatic description that such chromophores “are so red, they’re blue!”)

The two-level model has guided researchers in finding optimal chromophores for nonlinear polymers ever since the original work by Oudar and Chemla in the early 1970’s (125). More recent theoretical analysis by Kuzyk of sum-rule-restricted off-resonance contributions to the optical nonlinearity shows that a full quantum sum-rule analysis provides a physical limit to the maximum diagonal tensor component, *off resonance*, for both  $\beta$  (126), and  $\gamma$  (127). This study indicates that the key to increasing  $\beta$  and  $\gamma$  is to design molecules that have *one* dominant excited state at an energy close to the ground state with as many double (or triple) bonds (delocalized electrons) as possible. Molecules with a single dominant excited state are, therefore, particularly well-suited to a two-level model analysis. Kuzyk has also extended this work to off-diagonal tensor components to show that the maximum off-diagonal components can be no larger than the largest possible diagonal component (128). (The off-diagonal components for a particular molecule, however, may be larger than the available diagonal components for that molecule (25)).

**Donor–Acceptor Groups.** The difference between the ground state and excited state dipole moments,  $\Delta\mu_{01}$ , is important in designing optimal second-order NLO chromophores because  $\Delta\mu_{01}$  quantifies the ability of the electrons in the molecule to shift preferentially in one direction along the molecule with the application of an oscillating electric-field. To impart such a bias, initial studies used aromatic and long-chain  $\pi$ -electron systems with an electron donating group at one end and an accepting group at the other. A prototypical dye molecule with these features, dimethylaminonitrostilbene (DANS), is shown in Figure 5. Recall that the dipole moment is simply a measure of the separation of a unit charge along the length of the molecule. The effect of substitution of different electron donor and acceptor groups has been the subject of extensive study, and tables of values for different groups can be found in References 129 and 130.

**Nature of  $\pi$ -Electron Bonding, Aromaticity, and Bond Length Alternation.** A comparison between the ground and excited state structures in Figure 5 introduces another line of inquiry for optimizing  $\beta$ . In the charge-transfer (CT) excited state, the charge configuration will change from the aromatic structure of Figure 5a to the more quinonal (and zwitterionic) structure represented in Figure 5b. In this case, the CT state has lost “aromaticity,” as can be seen by the loss of conjugation in the rings. Marder and co-workers have studied CT processes and found that a larger effective donor–acceptor strength will often result from a degenerate ground state in which the  $\pi$ -electrons are optimally delocalized along the chain. In this case, the CT state gains aromaticity and the  $\Delta\mu_{01}$  factor will be negative, leading to a negative  $\beta$  off-resonance (131).

The relative contributions to the ground-state energy of different electron configurations (as those shown in Figs. 5a and 5b can be described by the

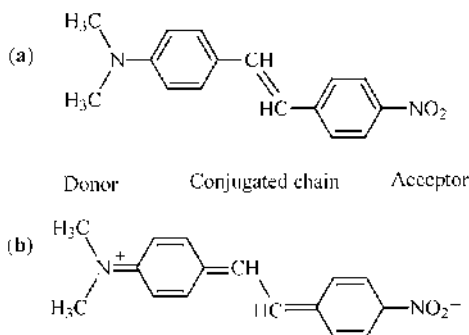


**Fig. 5.** Typical linear donor–acceptor chromophore (DANS) (a) ground state and (b) first excited state structures.

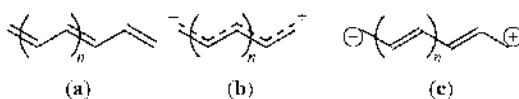


**Fig. 6.** The nature of  $\pi$ -electron bonding varies between the (a) polyene, (b) cyanine, and (c) zwitterionic limits.

tendency of the ground state to exhibit pronounced bond length alternation (BLA). In general, BLA refers to the difference in the bond lengths between adjacent carbon atoms within the backbone chain of the molecule. (Similarly, bond order alternation refers to the extent of alternating single, double, or triple bonds along the backbone, where single bonds are longest and triple shortest.) The nature of the  $\pi$ -electron bonding can be seen also in Figure 6, which illustrates the difference between polyene, cyanine, and zwitterionic forms for the conjugated chain. The polyene and zwitterionic structures show significant bond length alternation, while the cyanine shows none (131). Tuning between these forms is possible through changing solvent polarity and the strength of the donor and acceptor end groups (118).

Studies by Meyers and co-workers have shown that the NLO response of many strong donor-acceptor molecules suffer from too much bond length alternation (on the order of 0.01 nm), which inhibits charge transfer in the excited state (132).  $\beta$  is zero in the cyanine limit, however, when there is no bond length alternation. Interestingly,  $\beta$  peaks with opposite sign when the BLA is either intermediate between the polyene/cyanine structure or intermediate between a cyanine/zwitterionic structure ( $\text{BLA} \sim \pm 0.004$  nm) (133). One important result from these studies is that the relative amount of charge separation is a function not only of the end groups involved, but also of the molecular environment due to solvatochromic effects (118). For a more extensive discussion of the balance of factors represented in the two-level model and techniques for optimizing  $\beta$ , see also Reference 134. A discussion of methods for determining the dependence of  $\beta$  on other parameters may also be found in Reference 135.

**Conjugation Length.** The dominant characteristics for second-order materials are  $\pi$ -electron delocalization and strong acceptor–donor dipolar charge



transfer. Thus, the distance and magnitude of the charge transfer of the  $\pi$ -electrons in the excited state determines the magnitude of  $\beta$ .  $\beta$  increases with charge separation (electron delocalization) only if strong coupling through the conjugated bridge unit between the donor and the acceptor ends is preserved. Studies of the conjugation length dependence of  $\beta$  have shown an initial increase as the third power in that length, at least for the first 12  $\pi$ -electrons or more (136). However, studies have demonstrated that the donor-acceptor interaction stops increasing after a certain chain length, limiting the electron delocalization, and the result is an observable saturation effect (137,138). Unfortunately, increased conjugation length correlates with increased absorption, leading to reduced linear optical transparency. The significance of conjugation length is also explored further below in connection with third-order materials.

*The Two-Level Model for  $\gamma$  and Its Limitations.* Generally, essential-states-model calculations have been very successful in explaining and predicting the second-order response of noncentrosymmetric materials, but considerable work remains for understanding third-order materials. As a starting point, consider again the two-level model, which can be expressed for third-harmonic generation as (139)

$$\gamma_{\text{two-level}} = \frac{\mu_{01}^2}{4\hbar^3} [\Delta\mu_{10}^2 D_{111} - \mu_{01}^2 D_{11}] \quad (22)$$

The dependence on the energy difference between the ground state and excited state and the incident photon energy is given by the denominator “ $D$ ” factors (omitting resonance damping effects near the excited state transition energies)

$$D_{111} = [(\omega_{10} - 3\omega)(\omega_{10} - 2\omega)(\omega_{10} - \omega)]^{-1} + [(\omega_{10} + \omega)(\omega_{10} - 2\omega)(\omega_{10} - \omega)]^{-1} \\ + [(\omega_{10} + \omega)(\omega_{10} + 2\omega)(\omega_{10} - \omega)]^{-1} + [(\omega_{10} + \omega)(\omega_{10} + 2\omega)(\omega_{10} + 3\omega)]^{-1}$$

and

$$D_{11} = [(\omega_{10} - \omega)^2(\omega_{10} - 3\omega)]^{-1} + [(\omega_{10} + \omega)(\omega_{10} - \omega)^2]^{-1} \\ + [(\omega_{10} + \omega)^2(\omega_{10} - \omega)]^{-1} + [(\omega_{10} + \omega)^2(\omega_{10} + 3\omega)]^{-1} \quad (23)$$

A major difference between  $\beta_{\text{two-level}}$  and  $\gamma_{\text{two-level}}$  is the presence of two competing terms in equation 22. (Only the second term will contribute, however, with a centrosymmetric material, yielding a negative  $\gamma$  if  $D_{111}$  and  $D_{11}$  are positive, as they must be below resonance.) Competition between the two terms of the model results for noncentrosymmetric molecules. Fundamental calculations by Kuzyk show that the maximum theoretical result for noncentrosymmetric molecules is positive and four times the value in the centrosymmetric case (127).

*Two-Photon Resonant Enhancement.* The frequency dependence of the essential states models is also important as indicated by the potential for resonant enhancement in the denominators “ $D$ ” of the sum-over-states (with appropriate damping effects not indicated in eq. 23). Generally, it is undesirable to operate near a resonance with either the fundamental input frequency  $\omega$  or the desired harmonic output. When  $2\omega$  approaches  $\omega_{10}$ , however, an important intermediate

two-photon resonance is evident from the second  $D_{111}$  term. In this case, resonant enhancement appears without undesirable absorption effects. The  $(\omega_{10}-2\omega)$  denominator term also appears in expressions for other types of frequency conversion and even the nonlinear refractive index. Intermediate resonant enhancement applies not only to the two-level model. Absorption and/or resonant enhancement are possible whenever there are real energy levels close to the one, two, or three photon transitions (140).

*Bond Length Alternation Revisited.* Meyers and co-workers have also theoretically examined simple donor-acceptor polyenes by applying an external, static homogeneous electric-field to tune to different degrees of bond length alternation and mimic the effects of varying solvent polarity. Their studies indicate that for highly bond-length alternated molecules, such as polyenes, the off-resonant  $\gamma$  is positive, but, as the bond alternation is decreased,  $\gamma$  changes sign and peaks negatively in the cyanine limit (133).

*Extension to Multilevel Models for Constituent Materials.*

*Symmetry and Excited States.* It should be emphasized that Kuzyk's sum-rule calculations, which highlight the importance of the energy difference between the ground and the first excited states, only provide upper bounds on the values of  $\beta$  and  $\gamma$ . Predicting actual values require more complex relationships. Similarly, the two-level model has been shown to be inadequate even as a starting point for many materials, (139,141) failing to account even for the sign of  $\gamma$ . For example, measurements, as well as full quantum chemical calculations, show that centrosymmetric polyene-like molecular materials show a positive off-resonant nonlinearity. The two-level model predicts only negative  $\gamma$  off-resonance for centrosymmetric systems (142). In contrast, linear cyanines have been modeled theoretically in detail by Pierce, who found that, below resonance,  $\gamma < 0$  for all-trans linear centrosymmetric cyanines. His calculations, as well as several experimental studies, however, show that the two-level model is still inadequate for these molecules and higher lying two-photon states must be included (143,144).

To understand the effects of additional states beyond the two-level model in centrosymmetric molecular materials, it is helpful to analyze symmetry conditions that dictate allowable transitions between states. Because the ground state (also called the 1Ag state) is of Ag symmetry, the lowest optically allowed one-photon transition is to the 1Bu state (of opposite symmetry), which is the lowest lying one-photon excited state in the linear absorption spectrum. The 1Bu state is not necessarily the lowest lying excited state, however. One fundamental difference between centrosymmetric polyenes and cyanines is the location of another excited state, the lowest lying two-photon state or 2Ag state. Studies show that the 2Ag state lies energetically below the linear absorption peak (1Bu state) for polyenes, but above the peak for cyanines. Electron correlations that lower the 2Ag state below the 1Bu state create a nonradiative decay pathway for the 1Bu state and can significantly detract from the nonlinear response (145).

*Excited-State Enhancements.* Several studies also consider further enhancements that may be possible if starting from an excited state (146). By optically pumping to increase the population of an excited state, Heflin and co-workers observed a two-order magnitude enhancement (147). The reasons for this increase can be seen again from the terms of the two-level model in equations 21 and 22. By starting from an excited state, one can take advantage of larger

optical transition moments  $\mu_{nm}$ , where  $n$  and  $m$  are both excited states, and smaller energy differences,  $\hbar\omega_{nm}$ , between the populated excited state  $n$  and the excited state  $m$ .

**Some Structure–Property Relationships for Third-Order Polymers and Macromolecules.** The preferred approach for developing dipolar second-order materials has been to find optimized chromophores and incorporate these into a polymer with appropriate functionalization. For third-order applications chromophore doping is sometimes used, but is not necessary as the conjugated polymer itself contributes significantly to the NLO response. Third-order materials more often focus on the polymer matrix itself as a system for maximizing extended  $\pi$ -electron conjugation, though researchers have probed third-order phenomena through the use of smaller, simpler monomers and oligomers. Polymers systems are more difficult to probe because of their size and complexity. Optimization parameters include conjugation length (limited by significant saturation effects, and optimizing interaction among the electrons through chain conformation) and the introduction of spacers and donor–acceptor groups, sometimes leading to increased dimensionality of the polymer system.

*Conjugation Length and Saturation Effects.* The effective conjugation length of a polymer heavily influences the size of the third-order NLO response (148). The free-electron model of Rustagi and Ducuing showed that  $\gamma$  increases exponentially with the number of repeat units in the chain ( $L$ ) by,  $\gamma \sim L^n$ , where  $n = 5$  for short chains (149). Experimental studies agree (150), in general, with this relationship, though the scaling exponent varies in the range of  $n \sim 3$ –5.4 (151). The scaling exponent  $n$  is dependant upon factors such as the chemical structure of the material and substituent groups. For instance, ( $n \sim 2.5$ ) was reported by Samuel and co-workers for unsubstituted polyacetylene (152), and various substituted polyacetylenes values of  $n$  between 2.3 and 4.6 were reported by Neher and co-workers (153). The effect of electron correlations on the scaling has also been investigated, but is beyond the scope of this article. See, for example, Reference 154.

Oligomeric studies have also shown, however, that the NLO response of a conjugated polymer can become quickly saturated as the quantity of repeat units in the chain is increased beyond a certain, critical value. For example, very long chain polyene oligomers showed a saturation of  $\gamma$  at 60 double bonds (155), and poly(triacetylene) oligomers showed saturation of NLO values at 10 repeat units (110). Another study by Yang and co-workers provided evidence that suggested that the exponential scaling factor  $n$  in longer conjugated chains actually becomes dependant upon the number of repeat units ( $L$ ) in the chain (156). This function,  $n(L)$ , can be used to gain a more detailed understanding of the phenomena that occurs during the transition from a very short chain oligomer to a very long chain oligomer and ultimately a polymer.

*Donor–Acceptor Groups, Spacers, and Planar Structure for Third-Order Polymers.* A rigid planar structure in a polymeric material increases the third-order nonlinear optical response by maximizing the overlap area of the  $\pi$ -electron orbitals, thereby enhancing electron delocalization (157). Electron donor–acceptor groups are sometimes incorporated in conjugated, third-order polymer systems to enhance electron delocalization. As with second-order NLO chromophores, these “push–pull” groups can be added as end groups, or can be

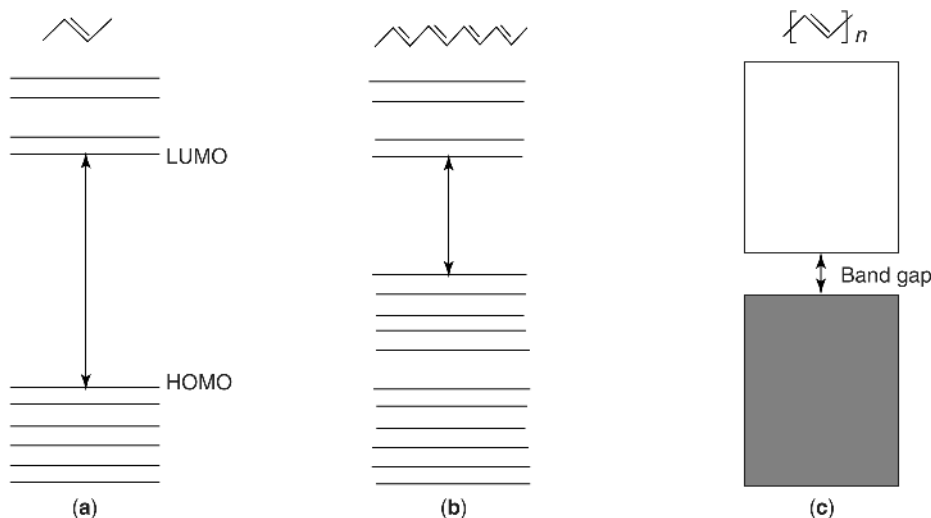


**Fig. 7.** Electronic effects upon increasing the number of repeat units in a conjugated chain. In a very long chain, discrete energy levels are replaced by valence and conduction bands, and as the conjugation length is increased, the band gap is typically reduced. (a)  $\pi$ -conjugated chain with few repeat units, (b)  $\pi$ -conjugated chain with increased number of repeat units, and (c)  $\pi$ -conjugated polymer chain.

inserted directly into the conjugated backbone structure. A recent study by Gubler and co-workers showed that inserting various spacer groups in the conjugated pathway of a polyene molecule increased  $\gamma$  for the molecule due to increased electron delocalization (158). The relationship between the presence of spacers and the maintenance of a rigid planar structure can be complicated. In the Gubler study, when the polyene to which spacers were added was polymerized, the third-order response of related polymeric materials did not maintain the increased NLO response of the polyenes. This loss in scaling was attributed to a decrease in electron delocalization due to a loss of planar structure that occurred in the polymer sample as a result of the interchain spacers. Other studies have also indicated that the planarity of the polymer is a dominating factor in deciding the third-order nonlinear response of the polymer (159). Further investigation of the effect of the spacers and the effect of the substitution on third-order materials is needed.

**Band Gap.** A common model for characterizing the effects of excited states for extended polymer systems is to consider the so-called band gap in the polymer.  $\pi$ -Conjugated polymers are sometimes considered organic semiconductors because the energies of their electrons exist in energy bands rather than discrete energy levels. The transition of the electronic structure (of a growing  $\pi$ -conjugated chain), from energy levels to energy bands, occurs as monomer units are added to a growing chain (see Fig. 7). As units are added, the number of valence and conduction energy bands increases as does the amount of electron delocalization. When the chain is sufficiently long, the energy levels are forced together so closely that energy bands are formed and discrete energy levels no longer exist.

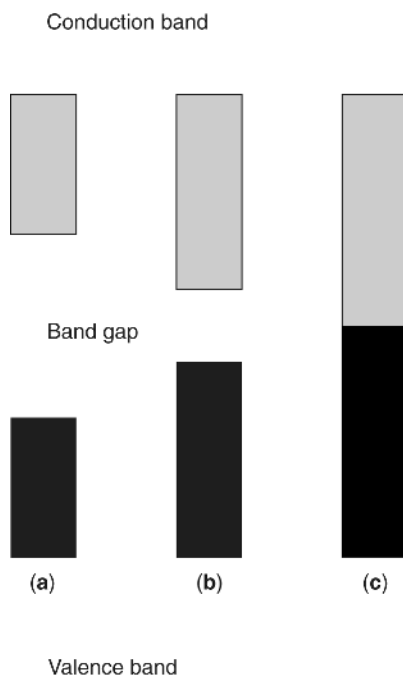


**Fig. 8.** Band gaps in (a) an insulator, where the gap is large and electrons are unable to pass from valence band to conduction band; (b) a semiconductor, where electrons with sufficient energy are able to pass from the valence to the conduction band; and (c) a conductor, where no band gap exists.

The band gap is considered to be the energy difference that exists between the highest occupied molecular orbital (HOMO) in the ground state and the lowest unoccupied molecular orbital (LUMO) in the excited state. Theoretically, the *band gap* is defined as the amount of energy required for an electron to transition from the ground state to the first dipole-allowed (one-photon) excited state. Experimentally, the band gap of a  $\pi$ -conjugated material is quantified by measuring by the longest wavelength electronic absorption maximum ( $\lambda_{\text{max}}$ ) (160). In general, reducing the band gap causes an increase in electron delocalization along a conjugated chain and therefore an increase in the third-order NLO response.

Much research in third-order  $\pi$ -conjugated materials is driven towards reducing the band gap to a semiconductor (161) or even intrinsically conducting status, as illustrated in Figure 8 (162). Two important approaches to minimizing the band gap of  $\pi$ -conjugated materials are minimizing BLA and incorporating donor–acceptor groups (163). Polyacetylene, for instance, would have a zero band gap (and be a intrinsically conducting polymer) if the adjacent carbons atoms along the chain were all equidistant; in other words, if the BLA value were zero. This is not the case, however, due to the alternating single and double bonds along the PA chain. Therefore PA has a finite band gap. Consider a thiophene monomer, which can have either an aromatic or quinoid structure. The structure that is exclusively quinoid has a relatively large band gap because the bonds

between the thiophene repeat units are completely double bond in nature. Similarly, the linkages between the aromatic repeat units are fully single bond in character. The ideal strategy in reducing the band gap of a polythiophene is synthesizing a structure in which the quinoid and aromatic structures balance in such a way that the BLA is effectively zero.

The excited states in semiconducting materials can be viewed as containing electrons and “holes” (vacancies left by the absence of an electron), which are formed from the ground state by promoting electrons from filled (valence band) orbitals to the empty (conduction band) orbitals. In the free charge continuum, these electrons and holes are uncorrelated, meaning that the knowledge of the position of either an electron or a hole does not yield any information about the location of the other. Any state that lies below the band edge of the continuum is known as an excitonic state. In these states, the motion of the electron and hole are correlated, and the combination is referred to as an “exciton.” At energies close to a one-photon resonance, double-excited states or “biexcitons” can play a major role in the two-photon absorption spectrum (164).

**Multidimensional Molecular Materials.** Current trends in the field have shifted away from quasi-one-dimensional or dipolar intermolecular charge transfer materials, and towards inherently two- or three-dimensional and octupolar molecules (165). The hyperpolarizabilities of these molecules do not follow the rules of Kleinman symmetry referred to earlier. The electrons move in at least two dimensions, allowing for polarization-independent applications (25). A main advantage of pushing beyond traditional one-dimensional materials is that alignment of nondipolar materials enables high density packing arrangements not feasible in the presence of dipolar interactions (166). The scope of materials that can be utilized is also much increased. Materials studied include tight-packing donor–acceptor–donor  $\Lambda$ -shaped molecules, stretchable chains to induce axial nonpolar alignment (87), and a variety of chiral shapes, including chiral bulk materials made from achiral molecules arranged in a chiral fashion, such as a threefold propeller-like arrangement (167).

Second-order studies have also begun to focus on large-scale dendritic structures for which large  $\beta$  are seen in HRS measurements without the need for bulk alignment (168,169). Functionalized dendrimers have been also investigated recently for second- and third-order applications. In these large structures, the nonlinear chromophore is placed in the core, along a branch, or at the ends of the dendrimeric structure depending on the application (170). Phthalocyanines and organometallics are interesting second- and third-order nonlinear materials, in part due to their generally high chemical and thermal stability. The  $\pi$ -electron behavior in the molecule is altered by the presence of a metal in the conjugated structure. Ligand-metal bonding leads to transfer of electron density between the metal atom and the ligand systems, causing the electron orbitals of the metal and the ligands to overlap, leading to large hyperpolarizabilities. This class of materials includes polysilanes, metalloporphyrin complexes and metallophthalocyanines (171).

**Polymer Structures for NLO Applications.** Polymers with  $\pi$ -electron conjugated backbones are favored and widely researched candidates for third-order NLO studies (172–176). The broad categories of  $\pi$ -electron conjugated polymers considered for third-order include linearly conjugated polymers such as

**Table 1. Representative Nonresonant Enhanced  $\chi^3$  Values for Prominent Third-Order  $\pi$ -Conjugated Polymeric Materials**

Polymer <sup>a</sup>	Structure	$\chi^3$ (esu) $\times 10^{-12}$	Technique	Wavelength, $\mu\text{m}$	Reference
PDA	<b>1</b> ( $R' = R'' = \text{H}$ )	1.4	THG	1.907	181,182
PDA-PTS	<sup>b</sup>	160	THG	2.62	59
PDA-4-BCMU	<sup>c</sup>	49	THG	1.064	183
<i>trans</i> -PA	<b>2</b>	1300	THG	1.907	184,185
PAZ	<b>3</b>	8	THG	1.5	186,187
PI	<b>4</b>	1.2	DFWM	.602	188,189
PQ	<b>5</b>	2.2	THG	2.38	190,191
PPV	<b>6</b>	7.8	THG	1.85	192,193
PT	<b>7</b>	30	DFWM	1.604	194,195
PBZO	<b>8</b>	8.1	THG	2.4	196,197
PBZT	<b>9</b>	8	DFWM	.602	197,198
BBL	<b>10</b>	15	DFWM	1.604	197,199
BBB	<b>11</b>	5.5	DFWM	1.604	197,200

<sup>a</sup>PDA: polydiacetylene; BMCU: butoxycarbonylmethylurathane group; PTS: *para*-toluene sulfonate; *trans*-PA: *trans*-polyacetylene; PAZ: polyazine; PI: polyimide; PQ: polyquinoline; PPV: poly(*p*-phenylene vinylene); PT: polythiophene; PBZO: poly(*p*-phenylene benzobisoxazole); PBZT: poly(*p*-phenylene benzobisthiazole); BBL and BBB: benzimidazophenanthroline-type heteroaromatic ladder polymer.

<sup>b</sup>PDA structure (**1**):  $R' = R'' = \text{CH}_2\text{—O—SO}_2\text{—C}_6\text{H}_4\text{CH}_3$

<sup>c</sup>PDA structure (**1**):  $R' = R'' = (\text{CH}_2)_3\text{—O—CO—NH—CH}_2\text{—COO—C}_4\text{H}_9$

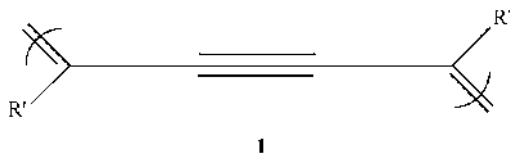
polyacetylene (PA), polydiacetylene (PDA), polyazines (PAZ), and linear polyimides (PI); polyheterocyclic polymers such as polypyrrole (Ppy) (177), heterocyclic polyimides, polyquinoline (PQ) (178) polythiophene (PT), polyvinylenes (PV), and polyanilines (PANI) (179); rigid-rod polymers Rigid-Rod Polymers (qv) such as poly(*p*-phenylene benzobisoxazole) (PBZO) and poly(*p*-phenylene benzobisthiazole) (PBZT); and benzimidaxobenzophenanthroline-type (BBB or BBL) ladder polymers. Though localized  $\sigma$ -bonds in carbon chains generally contribute little to the nonlinear response, silicon-based polymers, polysilanes (180), have been studied for their advantages as a third-order material. These polymers are  $\sigma$ -electron conjugated, and therefore maintain the fundamental electron delocalization required for large third-order NLO response. A short survey of some of the more widely studied of these basic polymeric structures, follows; see also Table 1.

**Polydiacetylene—First NLO Polymer Research.** Polydiacetylene (**1**) was the first polymer to be investigated for third-order NLO properties. In the late 1970s, Sauteret and co-workers published the first documentation of a large third-order NLO response in a single *p*-toluene sulfate crystal of polydiacetylene (63). The crystal displayed a fast response time ( $10^{-14}$  s), a high NLO response (on the order of  $10^{-11}$  esu), and a high laser damage threshold (50 Gw/cm<sup>2</sup> with picosecond response times for a single crystal). Subsequent reports have given third-order susceptibility values ranging over several orders of magnitude (201–203). Influencing factors are chemical structure, resonance enhancement, and measurement techniques.

Polydiacetylenes are linear polymers with highly conjugated  $\pi$ -electron backbones (see DIACETYLENE AND TRIACETYLENE POLYMERS). They can be synthesized via a solid-state polymerization reaction, namely a 1,4-topochemical polymerization of diacetylene monomeric units (204–206). This synthesis mechanism is unique because the polymer product retains the crystalline structure of its monomeric precursors, whereas most polymers have a predominately amorphous structure and limited regions of crystallinity. This type of polymerization has been achieved for polydiacetylene thin films (207,208), Langmuir–Blodgett films (209–211) monolayers (212), single crystals (62), and solutions (213,214). The crystalline structure offers enhanced third-order NLO properties due to high levels of anisotropy (215), but preparation of crystals with high optical quality can be difficult.

One of the most promising of all materials studied for third-order applications is the polydiacetylene, poly(diacetylene *para*-toluene-sulfonate), commonly referred to as PTS. PTS is thermally stable to  $\sim 180^\circ\text{C}$ , and so less prone to optically induced thermal effects. It can be processed into waveguide structures for device applications and is one of the very few materials that have been shown to meet the standard figures of merit for optical switching devices (38).

Polydiacetylene has been useful in probing third-order phenomena for several reasons. Its centrosymmetric structure excludes second-order NLO effects. Also, polydiacetylenes exhibit chromism in response to such external influences as temperature and solvents (216). Thermochromic and solvatochromic properties have been used to probe third-order effects as a function of conjugation (217). The high degree of structural control that is possible through side-chain substitution allows a wide variety of polydiacetylene polymers to be synthesized (216). It is common to substitute a long alkyl chain as one side group and a carboxylic group as the second. Undergoing this type of substitution allows the polymer to be processed as a Langmuir–Blodgett film. Butoxycarbonylmethylurathane (BCMU)-type polydiacetylenes (**1**) have side groups  $R_1 = R_2 = -(\text{CH}_2)_3-\text{O}-\text{CO}-\text{NH}-\text{CH}_2-\text{COO}-\text{C}_n\text{H}_{2n+1}$  widely studied due to their high solubility in aqueous and nonaqueous solvents, the planar structure, and alternation of color observable with change in conjugation (218–220). Many other polydiacetylene-type polymers have been investigated for their third-order NLO properties (181). Future efforts will likely include methodologies such as engineering diacetylene monomers to obtain polymers with enhanced optical properties and processability, and synthesizing a polydiacetylene with a ladder polymer structure (221).

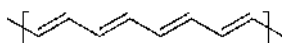


**Polyacetylenes.** Another widely-studied class of linear conjugated polymer are polyacetylenes, (222) which exist in both the *trans* and *cis* isomeric states. The *trans* isomer (**2**) exhibits cubic susceptibility values an order of magnitude greater than the *cis* isomer, over the entire range of the optical spectrum



(223). This phenomenon has been attributed to the twofold degenerate ground state (224). A ground state is degenerate if the single and double bonds along the chain can be interchanged with no change in corresponding conformational energy. Soliton formation is unique to structures that have degenerate ground states (225). Within the class of NLO  $\pi$ -conjugated polymers, soliton formation is common in *trans*-polyacetylene and some forms of polyaniline (the reduced leucoemeraldine-base or LB (226), and the fully oxidized form, polypernigraniline (227)). In a nondegenerate ground state, exchanging of single and double bonds results in a higher and a lower energy configuration (228,229). Solitons form on a chain when the ground state has twofold degeneracy, which means that two energetically equivalent conformations are possible. A region of degeneracy is formed on the same chain and is separated by a transition region (which is the soliton) in which the BLA decreases and ultimately becomes zero at the center. One energy level is formed directly in the center of the band gap. Soliton movement is not analogous to that of polaron (discussed below under Polyazines) in that a soliton is a topological defect that cannot pass from chain to chain or through another soliton on the same chain.

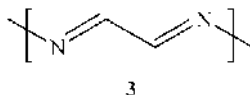
Polyacetylenes have very good mechanical properties and high electrical conductivity values, as compared to other conducting polymers. (Although electrical conductivity is not directly linked to NLO activity, a polymer with high electrical conductivity and large NLO response could be a promising candidate for device applications.) Polyacetylene is an air-sensitive and insoluble polymer (230). Attempts have been made to alter the polymer to afford increased solubility and environmental stability (222). A graft copolymer of polyacetylene and poly(methyl methacrylate), for example, has displayed enhanced solubility and stability (231). Substituting a phenyl ring onto polyacetylene offers increased stability. This polymer, poly(phenyl acetylene), has a lesser NLO response as compared to polyacetylene. One method used to increase the NLO response of poly(phenyl acetylene) is further substitution on the phenyl ring itself (232) (see ACETYLENIC POLYMERS, SUBSTITUTED).



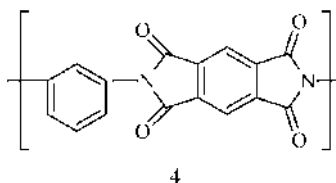
2

**Polyazines.** Polyazines (3) are one-dimensional  $\pi$ -conjugated, arylene-type polymers that are isoelectric to polyacetylene. The differentiating factor is that polyazines have nitrogen atoms substituted into the backbone structure, whereas polyacetylene backbone contains carbon atoms exclusively. Polyazine, like most conjugated polymers, has a nondegenerate ground state, which means that, unlike *trans*-polyacetylene, no solitons will be present in the polymer. It is thought, however, that polyazines contain polaron and bipolaron defects. Polaron-type excitations are common to  $\pi$ -conjugated chains and can be formed by adding an electron (or an electron hole) to a conjugated chain, leading to changes in chain conformation, energy levels, and electron delocalization. (See Reference 233 for a comprehensive discussion of excited states in conjugated polymers.) Incorporating nitrogen increases the environmental stability and optical transparency of polyazine polymers. The chief advantages of polyazines are extreme architectural

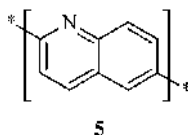
flexibility, environmental stability, and solubility; and the characteristic disadvantage is the high optical absorption. Compensation for absorption is possible, however, through chemical modification.



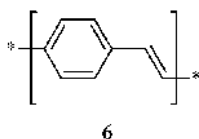
**Polyimides.** Polyimides (4) contain carbon–nitrogen double bonds. Linearly conjugated polyimides exist as both thermoplastics and thermosets. High mechanical strength, good insulating properties, processability from a soluble precursor, long-term chemical and orientational stability, and high thermal stability are among the characteristics that make polyimides a useful contender for optical applications (234). Heterocyclic polyimides have also been investigated due to increase in electron delocalization inherent to the ring structure. Polyimides (qv) are commonly synthesized under severe reaction conditions which limits the ability to chemically modify the polymer (by either NLO chromophore addition or other NLO enhancing substituents) (235).



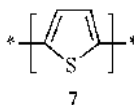
**Polyquinolines.** The high mechanical strength, solubility in organic solvents, ability to be easily processed into thin films with desirable optical properties (such as low optical loss), and thermal stability (at temperatures as high as 600°C) make polyquinolines good candidates for device application studies. Polyquinolines (5) are commonly used as the host in guest host polymer systems, and are therefore the subject of much second-order poling research (236). They have also been studied as NLO chromophore functionalized polymers (235). In addition to good end use and processability properties, polyquinolines also have large third-order susceptibilities because of the electron delocalization occurring between carbon–nitrogen double bonds. One recent study reported off-resonant  $\chi^{(3)}$  values as large as  $1.1 \times 10^{-10}$  esu for a polyquinoline copolymer with fluorene chromophores [the chromophores were incorporated to increase planarity and rigidity of the polymer which enhances the third-order NLO response (237)].



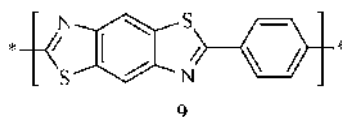
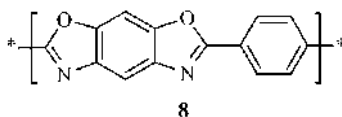
**Polyvinylenes.** Polyvinylenes, particularly poly(*p*-phenylenevinylene) (qv) (238,239), have been studied for their large  $\chi^{(3)}$  values on the order of magnitude of  $10^{-11}$  esu (but varying over several orders of magnitude) (240). Polyvinylenes (**6**) can be prepared via a soluble precursor, which is of interest for device applications because the polymer solution can be easily processed and then converted, via thermal polymerization, to its finalized solid-state form (241). Good optical quality thin films have been achieved, which exhibit high mechanical strength, large optical damage thresholds, high electrical conductivity values upon doping, and a high degree of orientational anisotropy (242). For dipolar polymers, a high degree of anisotropy increases the third-order NLO response under conditions where the incident polarization is directed parallel to the polymer backbone (243).



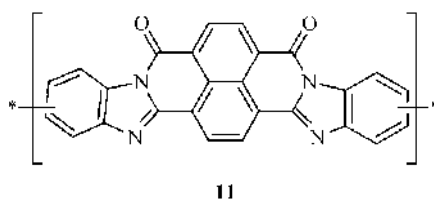
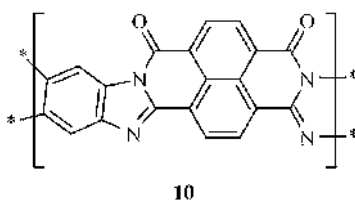
**Polythiophenes.** Polythiophenes (**7**) are polyheterocyclic polymers that have a thiophene ring as a repeating backbone unit. Polythiophenes exhibit high electrical conductivity values, yet offer increased environmental stability (244) as compared to polyacetylenes (see ELECTRICALLY ACTIVE POLYMERS). Doping polythiophenes changes their electrical conductivity, but the third-order response of the polymer has been reported to be the same in doped and undoped samples, suggesting that electrical conductivity and NLO response originate from dissimilar origins (245). They are intensely colored materials due to high optical absorptions, and have large resonant third-order responses (246). Polythiophenes are not soluble in organic solvents. Successful efforts to countermand this disadvantage include incorporating methyl methacrylate units in the main chain via copolymerization (247), and substitution of an alkyl chain at the 3-position on the thiophene ring of the polymer (248).



**Rigid Rod Polymers.** One class of rigid polymers that has been commonly studied for its optical, as well as electrical, properties is poly(*p*-phenylenebenzazoles) (PBX). The rigid rod structure of these polymers provides excellent mechanical strength and thermal and thermo-oxidative stability, and they are classed as high performance polymers (249). Two PBX-type polymers that have been of particular interest to NLO applications are poly(*p*-phenylenebenzobisoxazole) (**8**) (PBZO or PBO) and poly(*p*-phenylenebenzobisthiazole) (**9**) (PBZT or PBT) (251). The backbones of these polymers are uniquely conjugated, collinear, and coplanar, which makes intramolecular charge mobility possible, and allows for a large third-order NLO response (see ELECTROOPTICAL APPLICATIONS).



**Heteroaromatic Ladder Polymers.** BBB and BBL are benzimidazophenanthroline ladder polymers which lend themselves to third-order NLOs through their planar conformation, quasi-two-dimensional structure, and to end use applications through their mechanical and thermal stability and electrical properties (252). BBL and BBB are very similar in their repeat unit structure; the manner in which the monomer units are linked together, however, is different. BBL (**10**) has a full-ladder structure, which means that the monomeric units are linked by two covalent bonds, whereas BBB (**11**) has a semi ladder structure because its monomer units are linked by a single covalent bond. As a result, the  $\chi^{(3)}$  of BBL is about three times larger than that of BBB. BBL has a larger NLO response due to the increased planarity of the full-ladder structure of the polymer.



## Measurement Techniques and Devices

For every nonlinear optical effect, one would expect that there is a measurement technique to characterize it. Not all of NLO effects, however, are subject to measurements that are convenient or informative for comparative purposes or device applications. This section highlights a few of the more common test methods for NLO organic molecules and polymers, and provides references for more detailed explanations of these techniques. Significant omissions here are techniques based

on the linear and quadratic electrooptic effect, which are discussed in the article ELECTROOPTICAL APPLICATIONS.

Just as there are two broad categories of nonlinear effects, (1) changes in the frequency of the output, and (2) changes in the refractive index or absorption, so also there are two types of measurements that are typically performed to quantify these effects. The first type includes measurements based on frequency mixing where the input and detected frequencies differ, as in harmonic generation, non-degenerate four-wave mixing, and hyper-Rayleigh scattering. The second type measures changes in the refractive index through birefringence, diffraction, or other methods, as in the optical Kerr effect and degenerate four-wave mixing. Both types of measurements can be adapted to spectral studies and determination of the real and the imaginary parts of the nonlinear susceptibilities, and, in turn, the related hyperpolarizabilities.

The nonlinear susceptibility can be determined either through absolute or relative methods (253). Absolute measurements are very difficult to implement, however, because they require an accurate determination of the incident and harmonic powers. Even for standard reference materials with relatively large nonlinearities, inconsistent reporting and disagreement over the appropriate values has complicated comparisons (28). Whether the standard values can be agreed upon or not, determination of the susceptibilities relative to common accepted standards is the favored approach for reporting nonlinearities of new materials.

**Frequency Mixing Techniques: Harmonic Generation, Hyper-Rayleigh Scattering, and Nondegenerate Four-Wave Mixing.** A major advantage of frequency mixing techniques is their ability to distinguish electronic contributions to the nonlinear susceptibility from contributions due to vibrational, orientational, and thermal effects, and to distinguish resonant and non-resonant electronic motions. The price paid for this advantage is the requirement of very high powered lasers, especially for third harmonic and other third-order effects, and the need for careful filtering and weak-signal detection of non-phase-matched outputs.

**Harmonic Generation.** In a typical relative measurement involving harmonic generation, the input laser radiation is split into two beams, one incident upon the sample to be measured and the second on a suitable reference standard, such as quartz glass for second-harmonic generation or BK-7 glass for third-harmonic generation, or carbon disulfide for other third-order processes. By simultaneously measuring the harmonic response of both the sample and the reference, the effects of laser fluctuations in power are greatly diminished. After suitable spectral filtering of the output beams to detect only the harmonic (typically using photomultiplier tubes or avalanche photodiodes), the harmonics from the previously characterized reference and the sample are compared.

Simply placing the source and reference in the laser's path is not sufficient, however, to ensure a useful relative measurement. The magnitude of the harmonic response is a function of the path length in the material, and harmonic intensity generated fluctuates through the mismatch in propagation phase between the fundamental and the harmonic wave. The typical sample is not "phase-matched" in that the harmonic and fundamental do not propagate at the same speed through the sample. In second-harmonic generation, the coherence length is the spatial period of the oscillation in the output and, thus, a measure of the

effective length in the material for efficiently generating second harmonic. The coherence length of the output in this case is defined as

$$\ell_{\text{coh}} = \frac{\pi}{\Delta k} \quad \Delta k = \frac{2\omega(n_{2\omega} - n_{\omega})}{c} \quad (24)$$

where  $n_{\omega}$  is the refractive index at  $\omega$ . The coherence length for a polymer is typically on the order of 20  $\mu\text{m}$  (254). For samples approaching that thickness or greater, the optical path length through the material must be systematically altered during measurement either by translating a wedge-shaped sample and reference through the beam during measurement, or by rotating the sample and reference each about an axis through and perpendicular to the beam path. The resulting interference patterns (sometimes called Maker fringes (255)) are then analyzed in terms of both their magnitudes and their periodicity to determine the nonlinear susceptibility (256). The second harmonic output, for example, is given by

$$I_{2\omega} \propto \frac{|\chi^{(2)}(-2\omega; \omega, \omega)|^2 (I_{\omega})^2 L^2}{\lambda_{2\omega}^2 n_{\omega}^2 n_{2\omega} \varepsilon_0^2} \frac{\sin^2(2\pi L/\ell_{\text{coh}})}{2\pi L/\ell_{\text{coh}}} \quad (25)$$

where  $I_{\omega}$  is the incident intensity and  $L$  is the interaction length (thickness) in the sample. The accuracy and interpretation of these measurements depends also on careful measurements of the linear optical properties and geometries of the samples and setup, including the effects of multiple reflections at the interfaces (257). Significant birefringence and/or absorption further complicate the analysis, (258) but also provide information about the imaginary parts of the nonlinear susceptibilities.

*Phase-Matching.* As indicated previously, due to spectral dispersion,  $n_{2\omega}$  and  $n_{\omega}$  are generally not equal in an isotropic material. In regions of ordinary dispersion, for example, the refractive index at the second harmonic is always greater than the refractive index of the fundamental for two beams of the same polarization propagating in the same direction. Second-order materials are *not* isotropic, however, so that the natural birefringence of these materials (that is, the different refractive indices for different light polarizations) can be used to achieve a reasonable degree of phase matching. The nature of the birefringence of a material depends upon its crystal class. Poled polymers, being cylindrically symmetric about the polar axis, are classed as  $\infty mm$  materials because they have a unique axis “3” in the poling direction about which there is an infinite-fold rotation, and an infinity of mirror planes (259,260). In a positive uniaxial crystal, for example, as well as some poled polymers (261), the index of refraction,  $n_0$ , for light polarized perpendicular to the plane of incidence and so also perpendicular to poling direction (a so-called ordinary ray) is smaller than that for light having a component parallel to the optic axis or poling direction (an extraordinary ray with index  $n_e$ ). For a negative uniaxial crystal, the relative values of the extraordinary indices are smaller than the ordinary index.

For poled polymers, if light is polarized along the poling axis, it will couple more strongly to the charge-transfer axis, which should have a larger polarizability and hence larger refractive index. So  $n_e$  should be greater than  $n_0$  leading to

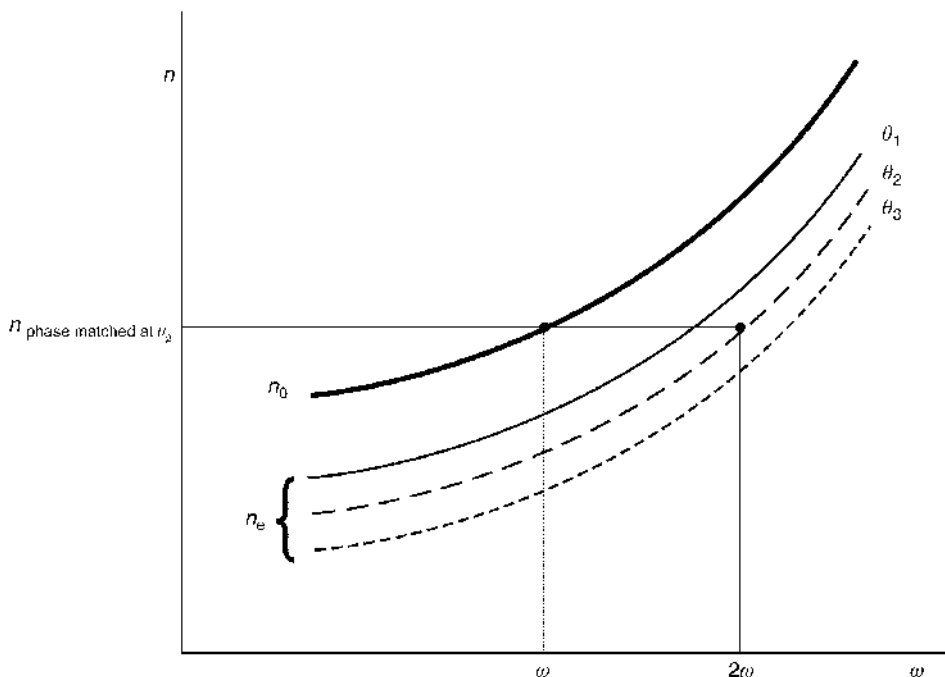


**Fig. 9.** Sample ordinary and extraordinary dispersion curves in the normal dispersion regime for a negative birefringent material for which the possible extraordinary indices are smaller than the ordinary indices. For the frequencies shown, the phase-matching condition is met for the second harmonic when the light propagates at  $\theta_2$  with respect to the optic axis.

a positive uniaxial material. For polymers like polyimides, however, it is possible that the index for the polymer dominates, and polyimides molecules tend to lie in the plane of the film. So in general, the birefringence of the polymer would tend to give a larger index in the plane, and the molecule would tend to give a larger index perpendicular to the plane of the film. Depending on the concentrations and polarizabilities, the overall birefringence could have either sign (K. D. Singer, private communication).

Because both the extraordinary ray and the optic axis are in the plane of incidence, the index of refraction seen by the extraordinary ray depends upon the angle of incidence. Thus, a common method for achieving phase-matching, called “Type I” phase-matching as shown in Figure 9, is to find the angle at which the index of refraction of the fundamental extraordinary ray,  $n_e(\theta)$ , at  $\omega$  equals that of the harmonic ordinary ray,  $n_0$ , at  $2\omega$ . Another common method, called “Type II,” is for the fundamental to consist of two orthogonal polarizations that average to the same index of refraction as that experienced by the harmonic. For further details, See Reference 262. A significant drawback of these methods is that the different indices of refraction for the orthogonal polarizations also lead to different angles of refraction for the fundamental and harmonic rays. Thus, the interaction length is further constrained by the walk-off of the rays from one another due to

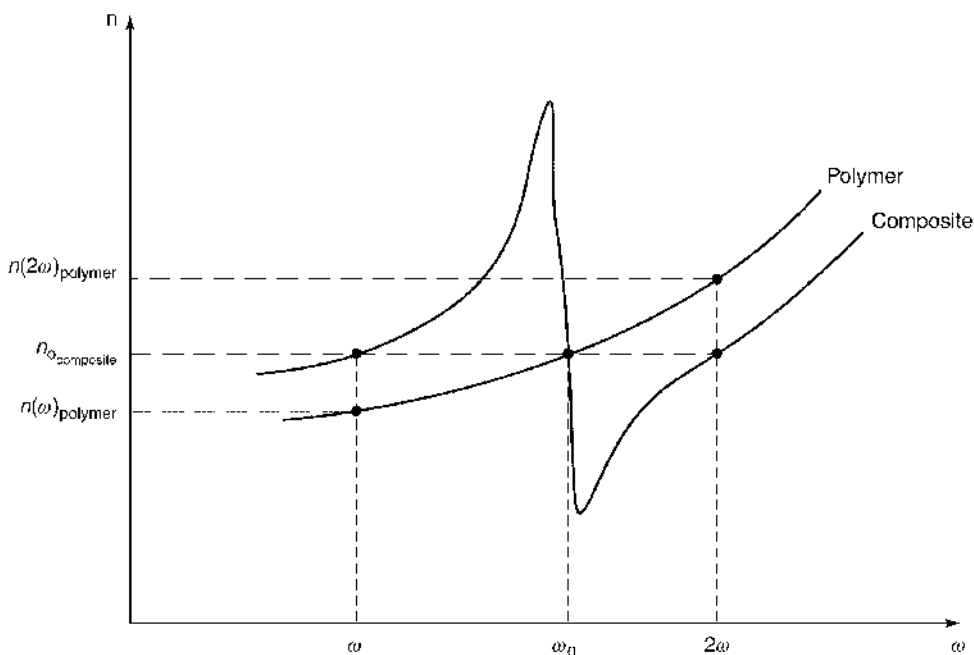


**Fig. 10.** An example of anomalous dispersion phase-matching in which the dopant molecule exhibits a strong absorption at frequency  $\omega_0$  between the fundamental ( $\omega$ ) and harmonic ( $2\omega$ ), leading to a lower index of refraction at the harmonic. The dopant is added to a polymer exhibiting normal dispersion resulting in a composite with equal refractive indices at the fundamental and harmonic,  $n_0$ .

birefringence. If can arrange that the angle for optimal phase-matching is  $90^\circ$  (as might be seen in a single-mode guided wave), then there will be no walk-off.

Another method for phase-matching, which does not require that the rays have different polarization directions and so avoids the problem of walk-off, is to arrange the harmonic conversion frequencies and material properties so that the device operates in a spectral region where there is an absorption peak at frequencies between the fundamental and the harmonic. In this case, a region of anomalous dispersion where the index of refraction is a decreasing function of frequency, accompanies the presence of the intermediate absorption. By carefully combining materials, so that the resulting composite has the same index of refraction at both the fundamental and harmonic, phase-matching results for that pair of frequencies (263) (see Fig. 10).

In integrated optics devices, phase matching must occur in a waveguide structure. The quantized effective indices of refraction vary for different modes of propagation in the waveguide, and the dispersion in the effective mode index of refraction is generally greater than that of the bulk index of refraction. Phase-matching may be achieved by propagating the fundamental in one mode and polarization and the harmonic in a different mode or different polarization. The details of this procedure can be found in Reference 264. A major drawback of phase-matching in different modes in a waveguide is that light rays propagating



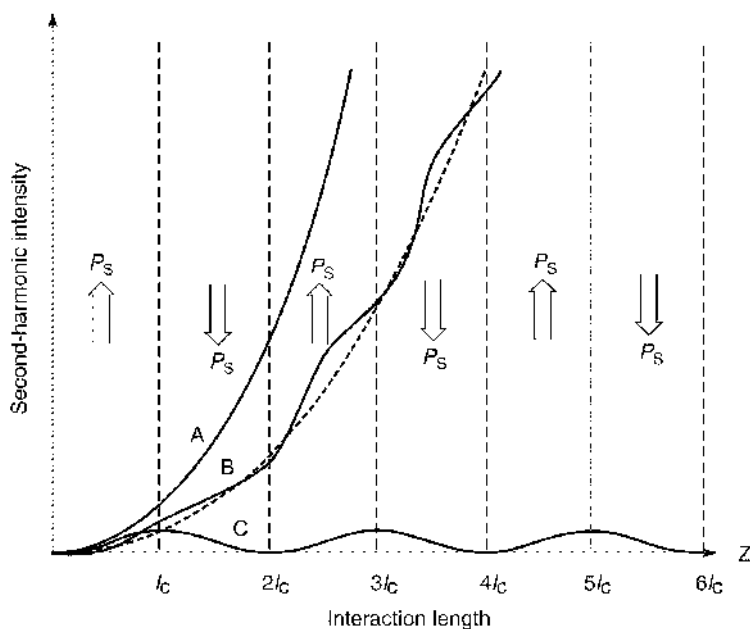


**Fig. 11.** Variation of second-harmonic intensity as a function of interaction length represented for (A) a phase-matched system, (B) a periodically poled system for which the poling field, and therefore the nonlinearity, changes direction every coherence length, and (C) a non-phase-matched process for which the power flows back from the harmonic completely back to the fundamental during every other coherence length of interaction. (From Reference 6, p. 262. Reprinted with permission.)

in different modes do not necessarily overlap well in the waveguide, limiting their interaction.

Phase-matching in a waveguide is also accomplished by spatial periodic poling (so-called quasi-phase-matching), where the direction of poling is either reversed or polar order is inhibited in the waveguide at regular intervals so that the length of each interaction region is at or shorter than the coherence length (the length over which the phase-mismatch begins to decrease the harmonic output.) Figure 11 illustrates this process by showing the growth in second-harmonic intensity as a function of interaction length. This method has also been applied to cascaded nonlinearities where it induces effective cubic nonlinearities (265).

**Electric-Field-Induced Second Harmonic Generation.** As previously discussed, in almost all cases the bulk NLO second-order response can be understood through summation over molecular nonlinearities of the constituents. Thus, the key measurements for optimizing polymeric NLO materials are aimed at characterizing their molecular constituents. The wedged cell technique described above has been applied to liquids containing dissolved organic chromophores, through electric-field-induced second harmonic generation. The major additional factor in this case is that solutions of polar molecules lack the requisite bulk asymmetry needed for second harmonic generation. To align the dipoles and break the symmetry, a large, but usually very short, DC voltage is applied across the solution

just as the beam passes through it (266). (The relationship between the  $\chi^{(3)}$  value obtained through this measurement and the molecular properties of the dipoles is given by equation 19).

**Hyper-Rayleigh Scattering.** EFISH cannot be used, however, on ionic or conductive solutions, due to the need for a large DC field, or on molecules that have no dipole moment, but only have an octupolar moment. Instead, researchers often prefer to use hyper-Rayleigh scattering (HRS) to make measurements, which can be used for all types of molecules, including multidimensional structures, chiral molecules, and stretched polymers (56,267). In the HRS technique, the nonlinear response of the sample is measured from the *scattered* second harmonic, rather than second harmonic transmitted through the sample, again by comparison to a known reference. Careful comparisons between the EFISH and HRS response, including spectral dispersion of each, have shown the consistency of these two methods (268). Ostroverkhova and co-workers have shown that with measurements based on just two different polarizations, the full hyper-Rayleigh scattering tensor can be expressed in terms of its rotationally invariant components for  $\beta$ , and that figures of merit corresponding to each of the rotationally invariant tensors can be determined (269). The range of information that can be obtained by HRS is expanded by varying the polarization of the detected light, including circular and elliptical polarizations, (270) and by varying the angle at which the scattered light is measured to determine the relative tensor components to the susceptibility. HRS measurements are complicated by the need to account for solvent effects and background fluorescence. The  $\beta$  values obtained are combinations of  $\beta$ -tensor components.

### Measuring Nonlinear Refractive Index Changes.

**Z-Scan.** Z-scan is one of the simpler methods to implement and rapidly measure both the nonlinear refractive index and the nonlinear absorption in a solid, liquid, or solution (271). Many different variations on the basic idea behind z-scan exist and interpretation of the results of a z-scan measurement can be complicated. The most common z-scan technique, illustrated in Figure 12, involves focusing a laser beam on a point in space and translating the sample through the focal point for a distance a few times greater than the diffraction length,  $Z_0 = \pi w_0^2/\lambda$  (where  $w_0$  is the focal spot half-width at  $1/e^2$  of the maximum irradiance and  $\lambda$  is the laser wavelength). The detector is placed behind a fixed aperture on the other side of the sample for measuring the transmitted light in the far-field. As the location of the sample changes, so does the amount of transmission through the aperture according to the placement of the sample in the path, the thickness of the sample and its index of refraction, and, most importantly, the changes in the sample's refractive index with intensity. As the sample approaches the focal point from the far side of the aperture, the light through the aperture is diminished by a self-focusing nonlinearity ( $\Delta n > 0$ ). The sample acts so as to enhance the focusing power of the lens, thus taking the focal point away from the aperture and reducing transmission through the aperture to the detector. As the sample passes through the focal point, the situation is reversed and the same positive  $\Delta n$  in the sample will tend to reduce the divergence of the light, increasing the transmission through the aperture. For  $\Delta n < 0$  and self-defocusing, the result is reversed in that the transmission through the aperture is increased when the

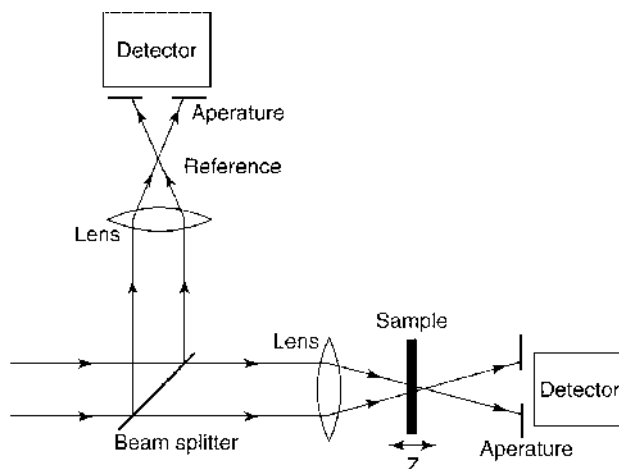


**Fig. 12.** Schematic for z-scan technique. By varying the placement of the sample along the optic axis, the amount of light being detected through the aperture changes due to the intensity-dependent refractive index of the sample.

sample is on the far side of focal point and decreased on the near side from the aperture (272).

Interpretation of the resulting normalized transmittance can yield both the nonlinear refractive index (based on the change in optical path length) and the nonlinear absorption coefficient (based on the change in absorption by the sample). The results depend upon knowing the laser beams spatial and temporal profile, power content, and stability. One disadvantage of the technique is that it cannot be used to identify the origin of the nonlinearity, as it treats nonlinearities arising from electronic processes the same as orientational and other processes by giving only time-averaged results. Thus, the results must be interpreted based on the theoretical origin of the nonlinearity. Furthermore, the z-scan technique is more difficult to apply with thick samples where the nonlinearity may cause changes in the beam profile through diffraction or self-focusing inside the sample.

Many parameters for and variations on z-scan must be omitted here, but some of the variations include (1) open aperture z-scans, (273) where all the transmitted light is collected in order to determine two-photon absorption effects, (2) eclipsing z-scan (EZ-scan), (274) which replaces the aperture with a block and collects the light at the outer edges, (3) excite-probe and two-color z-scans, (275) which use two collinear beams that differ in either polarization or wavelength and can be time-resolved, and (4) non-Gaussian beam or top-hat beam z-scans, (276) which use a beam with a steeper curvature gradient spatial profile to increase the z-scan's sensitivity.

**Optical Kerr Effect.** Another important method used to characterize polymers is the optical Kerr effect (OKE). The optical Kerr effect differs from the quadratic electrooptic effect in that the birefringence effects are induced solely by an optical field (37). In this measurement, an intense linearly polarized pump pulse induces birefringence in the nonlinear sample through an

intensity-dependent refractive index change. The sample is placed between crossed polarizers and a weak, typically tunable, continuous wave (cw) probe laser (usually at a different wavelength and polarized at  $45^\circ$  to the pump pulse) overlaps the pumped region. The increased transmission of the probe beam when the pump pulse arrives is proportional to  $(\chi_{\text{eff}}^{(3)})^2$ , a combination of elements of the  $\chi^{(1)}$  tensor. Many variations on this technique have been used including (1) use of a pulsed probe beam to reduce the effects of stray probe light, (277) (2) use of a nonlinear mixing crystal, after the analyzer in which a portion of the pump beam is frequency mixed with the probe to enhance the signal to noise ratio by creating an optical gate for the probe coincident with the pump pulse, (278) (3) use of an optical heterodyne technique in which a slightly uncrossed analyzer polarization allows for interference between the optical Kerr effect signal and the unaltered probe beam, (279) and (4) use of circularly and elliptically polarized pump beams tuned near a Raman active vibration in the sample to determine the Raman spectrum and  $\chi_{\text{eff}}^{(3)}$  simultaneously (called the Raman-induced optical Kerr effect) (280). OKE measurements using pulsed probes and time-domain studies are especially helpful for characterizing molecular mechanisms contributing to the effect (281). The optical Kerr effect is especially significant in characterizing polymers for applications such as ultrafast light gates or optical shutters.

**Degenerate Four-Wave Mixing.** A slightly more complex configuration for studying real third-order nonlinearities is one in which a single laser beam is split into two or more beams, which are then crossed at the sample, leading to intensity-dependent diffraction. There are two common geometries of this so-called degenerate four-wave mixing (DFWM) (1) backward or phase conjugate scattering and (2) forward scattering. In the former case, shown in Figure 13, two counter propagating pump beams will be incident on the sample with approximately equal intensities, and a third, probe beam, will cross these at the sample. The result of the nonlinear interaction is a backward scattering of the probe beam. The backward scattered beam is the phase conjugate of the probe and the ratio of the phase conjugate reflectivity to the incident probe intensity yields  $\chi_{\text{eff}}^{(3)}$ , as a function of the sample length, absorption, and field amplitudes on both sides of the sample (37).

In the forward scattering, or two-wave mixing geometry, two strong pump beams with wave vectors  $\mathbf{k}_1$  and  $\mathbf{k}_2$  cross to generate a diffracted beam that conserves momentum with the wave vector direction  $2\mathbf{k}_1 + \mathbf{k}_2$ . By varying the delay between the two beams arrival, real-time studies of grating dynamics can be used to distinguish nonresonant electronic nonlinearities. DFWM is a favored technique for studying photorefractive in NLO polymers and other materials.

**Nonlinear Absorption.** In theory, any of the above measurement techniques could be applied to materials in the presence of nonlinear absorption and interpreted to provide the two-photon absorption coefficient  $\alpha^{(2)}$  or the two-photon cross-section  $\sigma^{(2)}$ . The study of multiphoton absorption is, of course, inherently spectroscopic, probing the multiphoton resonances that impact various nonlinear phenomena. Third-harmonic generation in thin films has been used to characterize the phase of the complex  $\chi^{(3)}$  and thus  $\alpha^{(2)}$ , but the experimental technique requires additional steps and interpretation may be complicated by excited state absorption and three-photon resonances (282). The presence of an imaginary

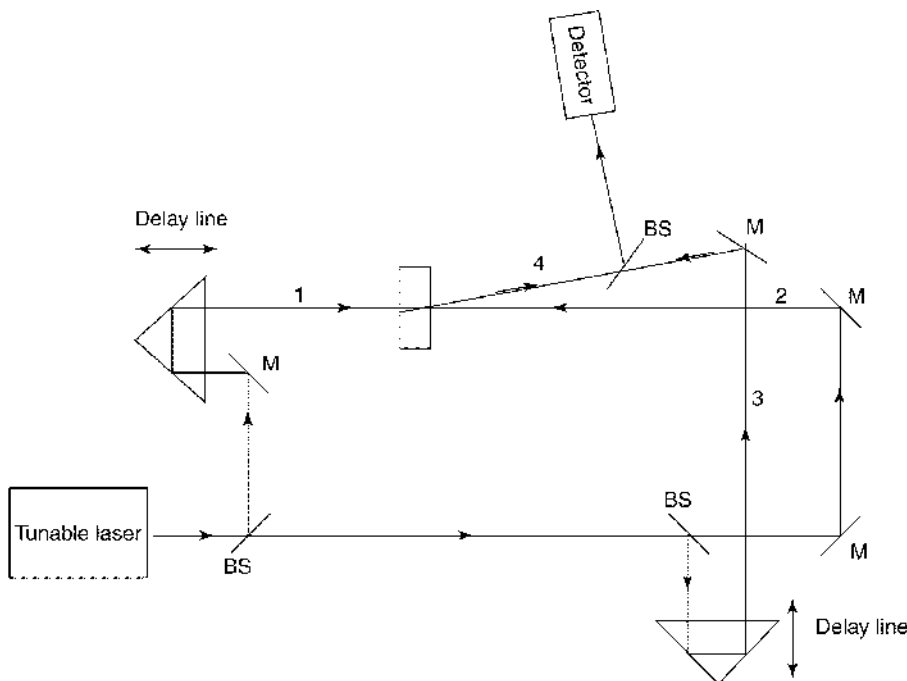


**Fig. 13.** Schematic for backward scattered (phase conjugate) degenerate four-wave mixing. (BS = beam splitter; M = mirror.) The pump beams (1) and (2) are collinear and counterpropagating. The probe beam (3) when incident on the sample leads to the creation of the phase conjugate beam (4), which is detected and compared to a suitable reference. The delay lines are included so that the timing of pulsed light arriving at the sample via paths (1), (2), and (3) can be varied.

component of  $\chi^{(3)}$  significantly complicates DFWM measurements by adding additional phase grating components to the phase conjugate beam, including thermal gratings. Separation of the different contributions to the imaginary part of  $\chi^{(3)}$  has been accomplished by time-resolved (283) and picosecond time-scale (284) measurements.

If the primary aim is to characterize the nonlinear absorption, several direct techniques are more easily implemented or interpreted. Conceptually, the simplest technique is to measure the transmitted intensity as a function of the incident intensity on the sample. Separating the linear and nonlinear contributions depends upon the spatial and temporal characteristics of the laser, however, as well as the thickness  $L$  and reflectivity  $R$  of the sample surfaces. For example, if the laser provides a CW beam of uniform spatial intensity, normally incident on a sample, the transmission  $T$  may be expressed as a product  $T = T_L T_{NL}$  of the linear transmission  $T_L = (1 - R^2) e^{-\alpha^{(1)}L}$  and a nonlinear factor  $T_{NL} = 1/(1 + f)$  where

$$f = \frac{\alpha^{(2)}(1 - R)I_1(1 - e^{-\alpha^{(1)}L})}{\alpha^{(1)}} \quad (26)$$

Of course, the illumination is more commonly of nonuniform spatial and temporal quality, leading to more complicated expressions for  $T_{NL}$  (44). Instead, it may be easier to use relative measures of nonlinear absorption by splitting the beam between the sample and a reference, such as ZnSe (285).

Another technique is to use a z-scan setup with an open aperture so that the change in collected light as the sample is translated through the focal point is determined solely by the relative absorption in the sample rather than the focusing or defocusing effects of the sample. This technique includes both two-photon effects and excited-state absorption. Van Stryland and co-workers have shown that the two effects can be separated by comparing the absorption for equal incident energies, but different powers, by adjusting the pulse duration. The two-photon absorption depends upon the intensity, whereas the excited-state absorption depends upon the fluence of the pulse (286).

Many other techniques have been used in addition to those discussed. For example, additional absorption techniques, generally beyond the scope of this article include two-photon luminescence (287), thermal lensing (288), photoacoustic techniques (289), and white-light continuum spectroscopy (290). For further information, the reader is referred particularly to Reference 1.

## BIBLIOGRAPHY

"Nonlinear Optical Properties" in *EPST* 3rd ed., Vol. 10, pp. 525–578, by J. H. Andrews and K. A. Guzan, Youngstown State University.

## CITED PUBLICATIONS

1. M. G. Kuzyk and C. W. Dirk, eds. *Characterization Techniques and Tabulations for Organic Nonlinear Optical Materials*, Marcel Dekker, Inc., New York, 1998.
2. H. S. Nalwa, ed., *Handbook of Advanced Electronic and Photonic Materials and Devices, Vol. 9: Nonlinear Optical Materials*, Academic Press, San Diego, Calif., 2001.
3. J. Zyss, ed., *Molecular Nonlinear Optics: Materials, Physics, and Devices*, Academic Press, San Diego, Calif., 1994.
4. H. S. Nalwa, ed., *Handbook of Organic Conductive Molecules and Polymers*, Vol. 4, John Wiley & Sons, Inc., New York, 1997.
5. G. A. Lindsay and K. D. Singer, eds., *Polymers for Second-Order Nonlinear Optics* (ACS Symposium Series 601), American Chemical Society, Washington, D.C., 1995.
6. P. N. Prasad and D. J. Williams, *Introduction to Nonlinear Optical Effects in Molecules and Polymers*, John Wiley & Sons, Inc., New York, 1991.
7. H. S. Nalwa and S. Miyata, eds., *Nonlinear Optics of Organic Molecules and Polymers*, CRC Press, Boca Raton, Fla., 1997.
8. D. M. Bishop, *Rev. Mod. Phys.* **62**, 343–374 (1990).
9. F. Hide, M. A. Diaz-Garcia, B. J. Schwartz, M. R. Andersson, Q. Pei, and A. J. Heeger, *Science* **273**, 1833 (1996).
10. R. W. Boyd, *Nonlinear Optics*, 2nd ed., Academic Press, Inc., San Diego, Calif., 2002, Chapt. 1.
11. Ref. 6, p. 20.
12. M. Pope and C. E. Swenberg, *Electronic Processes in Organic Crystals and Polymers*, 2nd ed., Oxford University Press, New York, 1999.
13. Y. R. Shen, *The Principles of Nonlinear Optics*, John Wiley & Sons, Inc., New York, 1984.

14. P. N. Butcher and D. Cotter, *The Elements of Nonlinear Optics*, Cambridge University Press, Cambridge, 1990, p. 28.
15. A. A. Said, C. Wamsley, D. J. Hagan, E. W. Van Stryland, B. A. Reinhardt, P. Roderer, and A. G. Dillard, *Chem Phys. Lett.* **228**, 646–650 (1995); K. Yang, J. Kumar, D.-C. Lee, D. J. Sandman, and S. Tripathy, *Opt. Lett.* **25**, 1186–1188 (2000).
16. Y. R. Shen, *Nature* **337**, 519–525 (1989).
17. K. B. Eisenthal, *Chem. Rev.* **96**, 1343–1360 (1996); R. M. Corn and D. A. Higgins, *Chem. Rev.* **94**, 107–126 (1994).
18. K. D. Singer, M. G. Kuzyk, R. B. Comizzoli, H. E. Katz, M. L. Schilling, J. E. Sohn, and S. J. Lalama, *Appl. Phys. Lett.* **53**, 1800–1802 (1988).
19. I. C. Khoo, *Liquid Crystals: Physical Properties and Nonlinear Optical Phenomena*, Wiley-Interscience, New York, 1994.
20. Y. Liu, R. O. Claus, D. Marciu, C. Figura, and J. R. Heflin, in B. Kippelen, H. S. Lackritz, and R. O. Claus, eds., *Organic Nonlinear Optical Materials and Devices*, Materials Research Society, Warrendale, Pa., 1999, pp. 29–32. Symposium Proceedings, Vol. 561.
21. A. Ulman, *An Introduction to Ultrathin Organic Films*, Academic Press, New York, 1991.
22. D. M. Nguyen, T. M. Mayer, S. F. Hubbard, K. D. Singer, J. A. Mann Jr., and J. B. Lando, *Macromolecules* **30**, 6150–6157 (1997).
23. D. A. Kleinman, *Phys. Rev.* **126**, 1977–1979 (1962).
24. G. A. Lindsay, in Ref. 5, pp. 1–19.
25. V. Ostroverkhova, O. Ostroverkhova, R. G. Petschek, K. D. Singer, L. Sukhomlinova, and R. J. Twieg, *IEEE J. Quantum Electron.* **7**, 781–792 (2001).
26. Ref. 10, pp. 193–209.
27. D. M. Bishop, *Rev. Mod. Phys.* **62**, 343–374 (1990).
28. R. F. Shi, and A. F. Garito, in Ref. 1, Chapt. 1, pp. 1–36.
29. D. M. Burland, C. A. Walsh, F. Kajzar, and C. Sentein, *J. Opt. Soc. Am., B* **8**, 2269–2281 (1991).
30. Ref. 10, p. 193.
31. I. M. Skinner and S. J. Garth, *Am. J. Phys.* **58**, 177–181 (1990).
32. Ref. 12, p. 1145.
33. J. R. Heflin, Y. M. Cai, and A. F. Garito, *J. Opt. Soc. Am B* **8**, 2132–2147 (1991).
34. S. Mukamel, *Principles of Nonlinear Optical Spectroscopy*, Oxford University Press, New York, 1995.
35. K. D. Singer, S. F. Hubbard, A. Schober, L. M. Hayden, and K. Johnson, in Ref. 1, pp. 311–514.
36. Ref. 6, p. 89.
37. R. A. Norwood, in Ref. 1, Chapt. 4, pp. 693–765.
38. M. Thakur and D. M. Kroi, *Appl. Phys. Lett.* **56**, 1213–1215 (1990).
39. G. Assanto, G. Stegeman, M. Sheik-Bahae, and E. Van Stryland, *Appl. Phys. Lett.* **62**, 1323–1325 (1993).
40. J. L. Bredas, C. Adant, P. Tackx, and A. Persoons, *Chem. Rev.* **94**, 243–278 (1994).
41. G. I. Stegeman and A. Miller, in J. E. Midwinter, ed., *Photonics in Switching*, Vol. 1, Academic Press, San Diego, Calif., 1993, pp. 81–145.
42. R. Adair, L. L. Chase, and S. Payne, *J. Opt. Soc. Am. B* **4**, 875–881 (1987).
43. M. D. Levenson, *Introduction to Nonlinear Spectroscopy*, Academic Press, New York, 1982.
44. S. Kershaw, in Ref. 1, Chapt. 7, pp. 515–654.
45. V. Mizrahi, K. W. DeLong, G. I. Stegman, M. A. Saifi, and M. J. Andrejco, *Opt. Lett.* **14**, 1140–1142 (1989).

46. K. K. Sharma, K. D. Rao, and G. R. Kumar, *Opt. Quantum Electron* **26**, 1–23 (1994).
47. S. R. Mishra and S. C. Mehnendale, in Ref. 2, Chapt. 8 pp. 347–367.
48. R. Crane, K. Lewis, E. Van Stryland, and M. Khoshnevisan, eds., *Materials for Optical Limiting*, Mater. Res. Soc. Proc., Vol. 374, 1995.
49. J. Venturini, E. Koudoumas, S. Couris, J. M. Janot, P. Seta, C. Mathis, and S. Leach, *J. Mater. Chem.* **12**, 2071–2076, (2002).
50. J. W. Perry, in Ref. 7, pp. 813–860.
51. G. R. Meredith, *J. Chem. Phys.* **77**, 5863–5873 (1982).
52. J. H. Andrews, K. L. Kowalski, and K. D. Singer, *Phys. Rev. A* **46**, 4172–4184 (1992).
53. G. I. Stegeman, *Quantum Semiclass. Opt.* **9**, 139–153 (1997); G. I. Stegeman, D. J. Hagan, and L. Torner, *Opt. Quantum Electron.* **28**, 1691 (1996).
54. D. Y. Kim, W. E. Torruellas, J. Kang, C. Bosshard, G. I. Stegeman, P. Vidakovic, J. Zyss, W. E. Moerner, R. Twieg, and G. Bjorklund, *Opt. Lett.* **19**, 868–70 (1994); Y. Ueno, G. I. Stegeman, and K. Tajima, *Jpn. J. Appl. Phys., Part 2 Lett.* **36**, 613–615 (1997).
55. J. B. Khurgin, A. Obeidat, S. J. Lee, and Y. J. Ding, *J. Opt. Soc. Am. B* **14**, 1977–1983 (1997).
56. G. J. T. Heeskin, A. G. T. Ruiter, N. F. van Hulst, and B. Bolger, *Phys. Rev. Lett.* **71**, 999–1002 (1995).
57. K. Clays and A. Persoons, in H. S. Nalwa, ed., *Handbook of Advanced Electronic and Photonic Materials and Devices, Vol. 9: Nonlinear Optical Materials*, Academic Press, San Diego, Calif., 2001, pp. 229–265.
58. E. P. C. Lai and H. S. Ghaziaskar, *Appl. Spectrosc.* **48**, 1011–1014 (1994); H. S. Ghaziaskar, W. M. Mullett and E. P. C. Lai, *Vib. Spectrosc.* **5**, 337–344 (1993).
59. S. J. Cyvin, J. E. Rauch, and J. C. Decius, *J. Chem. Phys.* **43**, 4083–4095 (1965).
60. S. Y. Lehman, L. E. Mcneil, and R. J. Albalak, *J. Polym. Sci., Part B: Polym. Phys.* **38**, 2170–2178 (2000); J. K. Kruger, J. Embs, J. Brierley, and R. Jimenez, *J. Phys. D: Appl. Phys.* **31**, 1913–1917 (1998).
61. I. W. Shepherd, *Rep. Prog. Phys.* **38**, 565–620 (1975); R. Y. Chiao, P. L. Kelley, and E. Garmire, *Phys. Rev. Lett.* **17**, 1158–1161 (1966).
62. P. M. Rentzepis and Y. H. Pao, *Appl. Phys. Lett.* **5**, 156–158 (1964).
63. C. Sauteret, J. P. Hermann, R. Frey, F. Rradere, J. Ducing, R. H. Baughman, and R. R. Chance, *Phys. Rev. Lett.* **36**, 956–959 (1976).
64. G. R. Meredith, J. G. VanDusen, and D. J. Williams, *Macromolecules* **15**, 1385–1389 (1982).
65. K. D. Singer, J. E. Sohn, and S. L. Lalama, *Appl. Phys. Lett.* **49**, 248–250 (1986).
66. D. J. Welker and M. G. Kuzyk, *Appl. Phys. Lett.* **69**, 1835–1836 (1996).
67. S. R. Vigil, Z. Zhou, B. K. Canfield, J. Tostenrude, and M. G. Kuzyk, *J. Opt. Soc. Am. B* **15**, 895–900 (1998).
68. T. Tagaya, Y. Koike, T. Kinoshita, E. Nihei, T. Yamamoto, and K. Sasaki, *Appl. Phys. Lett.* **63**, 883–884 (1993).
69. H. Watanabe, T. Omatsu, T. Hirose, A. Hasegawa, and M. Tateda, *Opt. Lett.* **24**, 1620–1622 (1999).
70. Y. Ohtsuka, E. Nihei, and Y. Koike, *Appl. Phys. Lett.* **57**, 120–122 (1990).
71. R. F. Shi, C. Koeppen, G. Jiang, J. Wang, and A. F. Garito, *Appl. Phys. Lett.* **71**, 3625–3627 (1997).
72. M. G. Kuzyk, ed., *Proc. SPIE* **3473**, 1–151 (1998). Session 2 papers.
73. M. G. Kuzyk, D. W. Garvey, S. R. Vigil, and D. J. Welker, *Chem. Phys.* **245**, 533–544 (1999).
74. Y. Baek, R. Schiek, G. I. Stegeman, G. Krijnen, I. Baumann, and W. Sohler, *Appl. Phys. Lett.* **68**, 2055–2057 (1996).



75. K. D. Singer, S. F. Hubbard, A. Schober, L. M. Hayden, and K. Johnson, in Ref. 1, pp. 311–514.
76. T. F. Heinz, H. W. K. Tom, and Y. R. Shen, *Phys. Rev. A* **28**, 1883–1885 (1983).
77. J. D. Jackson, *Classical Electrodynamics*, 2nd ed., John Wiley & Sons, Inc., New York, 1975.
78. K. D. Singer and J. H. Andrews, in J. Zyss ed., *Molecular Nonlinear Optics: Materials Physics, and Devices*, Academic Press, San Diego, Calif., 1994, pp. 245–298.
79. M. G. Kuzyk, in Ref. 1, pp. 111–220.
80. K. D. Singer, M. G. Kuzyk, and J. E. Sohn, *J. Opt. Soc. Am. B* **4**, 968–976 (1987).
81. R. D. Small, K. D. Singer, J. E. Sohn, M. G. Kuzyk, and S. J. Lalama, *Proc. SPIE* **682**, 160–169 (1986).
82. A.-C. Etile, C. Fiorini, F. Charra, and J.-M. Nunzi, *Phys. Rev. A* **56**, 3888–3896 (1997); J. Si, J. Qiu, and K. Hirao, *J. Appl. Phys.* **90**, 4895–4899 (2001).
83. F. Ghebremichael, M. G. Kuzyk, K. D. Singer, and J. H. Andrews, *J. Opt. Soc. Am. B* **15**, 2294–2297 (1998).
84. T. F. Heinz, H. W. K. Tom, and Y. R. Shen, *Phys. Rev. A* **28**, 1883 (1983).
85. F. Wurthner, F. Effenberger, R. Wortmann, and P. Kramer, *Chem. Phys.* **173**, 305–314 (1993).
86. S. R. Marder, L. T. Cheng, B. G. Tiemann, A. C. Friedli, M. Blanchard-Desce, J. W. Perry, and J. Skindhøj, *Science* **263**, 511–514 (1994).
87. V. Ostroverkhov, K. D. Singer, and R. G. Petschek, *J. Opt. Soc. Am. B* **18**, 1858–1865 (2001).
88. C. P. J. M. van der Vorst, and S. J. Picken, *J. Opt. Soc. Am. B* **7**, 320–325 (1990).
89. H. S. Lackritz and J. M. Torkelson, in J. Zyss ed., *Molecular Nonlinear Optics: Materials Physics, and Devices*, Academic Press, San Diego, Calif., 1994, Chapt. 8, pp. 339–377.
90. G. Williams and D. C. Watts, *Trans. Faraday Soc.* **66**, 80 (1970); M. L. Williams, R. F. Landel, and J. P. Ferry, *J. Am. Chem. Soc.* **77**, 3701–3707 (1955).
91. A. Dhinojwala, G. K. Wong, and J. M. Torkelson, *J. Chem. Phys.* **100**, 6046–6054 (1994).
92. H. L. Hampsch, J. Yang, G. K. Wong, and J. M. Torkelson, *Macromol.* **23**, 3640–3647 (1990).
93. T. Goodson and C. H. Wang, *J. Phys. Chem.* **100**, 13920–13926 (1996).
94. L. Liu, D. Ramkrishna, and H. S. Lackritz, *Macromolecules* **27**, 5987–5999 (1994).
95. Y. S. Fu, M. H. Ostrowski, and H. S. Lackritz, in J. P. Runt and J. J. Fitzgerald, eds., *Dielectric Spectroscopy of Polymeric Materials*, Oxford University Press, Oxford, 1997, Chapt. 14.
96. M. Barzoukas, D. Josse, P. Fremaux, J. Zyss, J. F. Nicoud, and J. O. Morely, *J. Opt. Soc. Am. B* **4**, 977–986 (1987).
97. D. M. Burland, C. A. Walsh, F. Kajzar, and C. Sentein, *J. Opt. Soc. Am. B* **8**, 2269–2281 (1991).
98. M. Sinclair, D. Moses, K. Akagi, and A. J. Heeger, *Phys. Rev. B* **38**, 10724–10733 (1987).
99. C. C. Fay, D. M. Stoakley, and A. K. Clair, *High Performance Polym.* **11**, 145–156 (1999).
100. A. J. Beuhler, D. A. Wargowski, K. D. Singer, and T. Kowalczyk, *IEEE Trans. Comp. Pack. Manuf. Technol. B* **18**, 232 (1995).
101. W. Shi, Y. J. Ding, X. Mu, C. Fang, Q. Pan, and Q. Gu, *J. Opt. Soc. Am. B* **19**, 215–221 (2002).
102. W. Sotoyama, S. Tatsuura, and T. Yoshimura, *Appl. Phys. Lett.* **64**, 2197–2199 (1994).
103. J. D. Stenger-Smith, R. A. Henry, A. P. Chafin, and L. H. Merwin, in Ref. 5, pp. 1–19.

104. T. C. Kowalczyk, T. Z. Kosc, K. D. Singer, A. J. Beuhler, D. A. Wargowski, P. A. Cahill, C. H. Seager, and M. B. Meinhardt, in Ref. 5, pp. 381–400.
105. S. Marturunkakul, J. I. Chen, L. Li, X. L. Jiang, R. J. Jeng, S. K. Sengupta, J. Kumar, and S. K. Tripathy, in Ref. 5, pp. 198–204.
106. R. Tykwinski, U. Gubler, R. Martin, F. Diederich, Ch. Bosshard, and P. Günter, *J. Phys. Chem. B* **102**, 4451–4465 (1998).
107. U. Gubler, *Third Order Nonlinear Optical Effects in Polymers*, Ph. D. dissertation, Swiss Fed. Inst. Tech., Zurich, 2000. Available at <http://ecollection.ethbib.ethz.ch/cgi-bin/show.pl?type=diss&nr=13605> (Accessed September 12, 2003).
108. G. J. Ashwell, P. Leeson, G. S. Bahra, and C. R. Brown, *J. Opt. Soc. Am. B* **15**, 484–488 (1998).
109. Y. Aoki, T. Tada, and Y. Orimoto, *Phys. Rev. B* **66**, 1931041–1931044 (2002).
110. R. E. Martin, U. Gubler, J. Cornil, M. Balakina, C. Boudon, Ch. Bosshard, J.-P. Gisselbrecht, F. Diederich, P. Günter, M. Gross, and J.-L. Brédas, *Chem.—Eur. J.* **6**, 3622–3635 (2000).
111. J. Seixas de Malo, L. M. Silva, and L. G. Arnaut, *J. Chem. Phys.* **111**, 5427–5433 (1999).
112. Ref. 4, p. 339.
113. E. H. Sargent, M. D'Iorio, J. Zyss, C. Andraud, and P. W. E. Smith, eds., in *J. Opt. A: Pure Appl. Opt.* **4**, 593–671 (2002).
114. M. A. Pasquinelli, *An Effective Particle Approach to the Photophysics of Conjugated Polymers*, Ph.D. dissertation, Carnegie-Mellon University, January, 2002. Available at [www.chem.cmu.edu/groups/yaron/pdf/pasquinellithesis.pdf](http://www.chem.cmu.edu/groups/yaron/pdf/pasquinellithesis.pdf). Accessed September 12, 2003.
115. D. P. Shelton and J. E. Rice, *Chem. Rev.* **94**, 3–30 (1994).
116. J. M. Andre, J. Delhalle, and J. L. Bredas, *Quantum Chemistry Aided Design of Organic Polymers. An Introduction to the Quantum Chemistry of Polymers and Its Applications*, World Scientific, Singapore, 1991.
117. S. P. Karna, G. B. Talapatra, W. M. K. P. Wijekoon, and P. N. Prasad, *Phys. Rev. A* **45**, 2763–2770 (1992).
118. I. D. L. Albert, T. J. Marks, and M. A. Ratner, in Ref. 1, pp. 37–110.
119. B. J. Orr and J. F. Ward, *Mol. Phys.* **20**, 513–526 (1971).
120. W. Liptay, in E. C. Lim, ed., *Excited States*, Academic Press, New York, 1974.
121. B. Champagne and B. Kirtman, in Ref. 2.
122. J. Zyss and J. L. Oudar, *Phys. Rev. A* **26**, 2028–2048 (1982).
123. C. W. Dirk, L. T. Cheng, and M. G. Kuzyk, *Int. J. Quantum Chem.* **43**, 27–36 (1992).
124. H. Ikeda, T. Sakai, and K. Kawasaki, *Chem. Phys. Lett.* **179**, 551–554 (1991).
125. J. L. Oudar and D. S. Chemla, *J. Chem. Phys.* **66**, 2664–2668 (1977).
126. M. G. Kuzyk, *Phys. Rev. Lett.* **85**, 1218–1221 (2000).
127. M. G. Kuzyk, *Opt. Lett.* **25**, 1183–1185 (2000); errata in *Opt. Lett.* **28**, 135 (2003).
128. M. G. Kuzyk, *IEEE J. Quantum Electron.* **7**, 774–780 (2001).
129. K. D. Singer, S. F. Hubbard, A. Schober, L. M. Hayden, and K. Johnson, in Ref. 1, pp. 311–514.
130. H. S. Nalwa, T. Watanabe, and S. Miyata, in Ref. 7, pp. 89–350.
131. S. R. Marder, B. Kippelen, A. K.-Y. Jen, and N. Peyghambarian, *Nature* **388**, 845–851 (1997).
132. S. R. Marder, C. B. Gorman, F. Meyers, J. W. Perry, G. Bourhill, J. L. Bredas, and B. M. Pierce, *Science* **265**, 632–635 (1994).
133. F. Meyers, S. R. Marder, B. M. Pierce, and J. L. Bredas, *J. Am. Chem. Soc.* **116**, 10703–10714 (1994).
134. S. R. Marder, D. N. Beratan, and L. Cheng, *Science* **252**, 103–106 (1991).

135. K. D. Singer, H. E. Katz, J. E. Sohn, C. W. Dirk, L. A. King, and H. M. Gordon, *J. Opt. Soc. Am. B* **6**, 1339–1350 (1989).
136. L. T. Cheng, W. Tam, S. R. Marder, A. E. Stiegman, G. Rikken, and C. W. Spangler, *J. Phys. Chem.* **95**, 10643–10652 (1991).
137. V. Alain, *J. Phys. Chem.* **95**, 10643–10652 (1991).
138. V. Alain, L. Thouin, M. Blanchard-Desce, U. Gubler, C. Bosshard, P. Gunter, J. Muller, A. Fort, and M. Barzoukas, *Adv. Mater.* **11**, 1210–1214 (1999).
139. M. G. Kuzyk and C. W. Dirk, *Phys. Rev. A* **41**, 5098–5109 (1990).
140. Z. G. Soos and D. Mukhopadhyay, *J. Chem. Phys.* **101**, 5155 (1994).
141. J. H. Andrews, J. D. V. Khaydarov, K. D. Singer, D. L. Hull, K. C. Chuang, *J. Opt. Soc. Am. B* **12**, 2360–2371 (1995).
142. S. Mazumdar and F. Guo, *J. Chem. Phys.* **100**, 1665–1672 (1994).
143. B. M. Pierce, *Proc. SPIE*. **1560**, pp. 148–161 (1991).
144. K. S. Mathias, M. G. Kuzyk, C. W. Dirk, A. Tan, S. Martinez, and G. Gampos, *J. Opt. Soc. Am. B* **15** 871–883 (1998).
145. J. W. Wu, J. R. Heflin, R. A. Norwood, K. Y. Wong, O. Zamani-Khamiri, A. F. Garito, P. Kalyanaraman, and J. Sounik, *J. Opt. Soc. Am. B* **6**, 707–720 (1989).
146. J. R. Heflin, D. C. Rodenberger, R. F. Shi, M. Wu, N. Q. Wang, Y. M. Cai, A. F. Garito, *Phys. Rev. A* **45**, 4233–4236 (2002).
147. D. C. Rodenberger, J. R. Heflin, and A. F. Garito, *Nature* **359**, 309–311 (1992).
148. M. T. Zhao, M. Samoc, P. H. Singh, P. N. Prasad, *J. Chem Phys.* **93**, 7916–7920 (1989).
149. Ref. 12, p. 1148.
150. Ref. 6, p. 235.
151. R. R. Tykwinski, U. Gubler, R. E. Martin, F. Diederich, C. Bosshard, and P. Gunter, *J. Phys. Chem. B*. **102**, 4451–4465 (1998).
152. I. D. W. Samuel, I. Ledoux, C. Dhenaut, J. Zyss, H. H. Fox, R. R. Schrock, and J. Sibley, *Science* **256**, 1070–1072 (1994).
153. D. Neher, A. Kaltbeitzel, A. Wolf, C. Bubeck, G. C. Wegner, *J. Phys. D: Appl. Phys.* **24**, 1193–1202 (1991).
154. C. Q. Wu, *Cond. Mat.* **23**, 1–22 (1992). Also available at [http://arxiv.org/PS\\_cache/cond-mat/pdf/9210/9210022.pdf](http://arxiv.org/PS_cache/cond-mat/pdf/9210/9210022.pdf).
155. I. Ledoux, I. D. W. Samuel, J. Zyss, S. N. Aliraki, F. J. Schattenmann, R. R. Schock, and R. J. Silbey, *Chem. Phys.* **245**, 1–16 (1999).
156. H. Meier, D. Ickenroth, U. Stalmach, K. Koynov, A. Bahtiar, and C. Bubeck, *Eur. J. Org. Chem.* **2001**, 4431–4443 (2001).
157. J.-T. Lin, J.-H. Sheu, and S.-L. Lee, *Chem. Phys. Lett.* **345**, 228–234 (2001).
158. U. Gubler, S. Concilio, Ch. Bosshard, I. Biaggio, P. Gunter, R. E. Martin, M. J. Edelmann, J. A. Wytko, and F. Diederich, *Appl. Phys. Lett.* **81**, 2322–2324 (2002).
159. X. Zhan, Y. Liu, D. Zhu, W. Huang, and Q. Gong, *J. Chem. Phys. B* **106**, 1884–1888 (2002).
160. J. Ma, S. Li, and Y. Jiang, *Macromolecules* **35**, 1109–1115 (2002).
161. D.-H. Hwang, J.-H. Chang, H.-K. Shim, and T. Zyung, *Synth. Met.* **119**, 393–394 (2001).
162. M. Jayakannan, P. A. van Hal, and R. Janssen, *J. Poly. Sci. A*. **40**, 251–261 (2002).
163. H. A. M. van Mullekom, J. A. J. M. Vekemans, E. E. Havinga, and E. W. Meijer, *Mater. Sci. Eng: R.-Rep.* **32**, 1–40 (2001).
164. V. A. Shakin and S. Abe, *Phys. Rev. B* **50**, 4306–4315 (1994).
165. J. Zyss and S. Brasselet, *C. R. Acad. Sci.* **4**, 601–608 (2000).
166. D. Beljonne, W. Wenseleers, E. Zojer, Z. Shuai, H. Vogel, S. Pond, J. Perry, S. Marder, and J. Bredas, *Adv. Funct. Mater.* **12**, 631–641 (2002).
167. S. Van Elshocht, T. Verbiest, M. Kauranen, L. Ma, H. Cheng, K. Musick, L. Pu, and A. Persoons, *Chem. Phys. Lett.* **309**, 315–320 (1999).

168. S. Mukamel, *Nature* **388**, 425–427 (1997).
169. M. Kauranen, T. Verbiest, C. Boutton, M. N. Teerenstra, K. Clays, A. J. Schouten, R. J. M. Nolte, and A. Persoons, *Science* **270**, 966–969 (1995).
170. H. Ma and A. K.-Y. Jen, *Jen, Adv. Mater.* **13**, 1201–1205 (2001).
171. K. S. Suslick, N. A. Rakow, M. E. Kosal, and J.-H. Chou, *J. Porphyrins and Phthalocyanines* **4**, 407–413 (2000).
172. W. R. Salaneck, I. Lundström, and B. Rånby, eds., *Conjugated Polymers and Related Materials: Interconnection of Chemical and Electronic Structure*, Oxford University Press, Oxford, 1993.
173. G. Zerbi, ed., *Organic Materials for Photonics*, North-Holland, Amsterdam, 1993.
174. J. L. Brédas and R. Sibley, eds., *Conjugated Polymers*, Kluwer, Dordrecht, Netherlands, 1991.
175. J. Messier, F. Kajzar, and P. Prasad, eds., *Organic Molecules for Nonlinear Optics and Photonics*, Vol. 94 of NATO Advanced Study Institute, Series E, Applied Sciences, Kluwer, Dordrecht, the Netherlands, 1991.
176. Ref. 4, p. 309.
177. Y. Matsuzaki, M. Nakano, K. Yamaguchi, K. Tanaka, and T. Yamabe, *Chem. Phys. Lett.* **263**, 119–125 (1996).
178. A. K. Agrawal, S. Jenekhe, H. Vanherzeele, and J. S. Meth, *J. Phys. Chem.* **96**, 2837–2843 (1992).
179. J. A. Osahemi, S. Jenekhe, H. Vanherzeele, S. Meth, Y. Sun, and A. G. MacMiarmid, *J. Phys. Chem.* **96**, 2830–2836 (1992).
180. E. A. Perpète, J.-M. André, and B. Champagne, *J. Chem. Phys.* **109**, 4624–4637 (1998).
181. Ref. 7, pp. 648–649.
182. K. Kubodera and T. Kaino, in T. Kobayashi, ed., *Springer Proceedings in Physics*, Vol. 36, Springer, Berlin, 1989, p. 163.
183. C. Hsu, Y. Kawabe, Z. Ho, N. Ppeyghambarian, J. N. Polky, W. Krug, E. Miao, *J. Appl. Phys. Lett.* **67**, 7199–7203 (1990).
184. F. Kajzar, S. Etemad, G. L. Baker, and J. Messier, *Solid State Commun.* **63**, 1113–1117 (1987).
185. Ref. 7, p. 665.
186. H. S. Nalwa, A. Kakuta, A. Mukoh, *J. Appl. Phys.* **73**, 4743–4745 (1993).
187. Ref. 7, p. 704.
188. Ref. 7, p. 715.
189. R. O. Ebewele, *Polymer Science and Technology*, CRC Press, New York, 2002, p. 442.
190. Ref. 7, p. 700.
191. Ref. 7, p. 702.
192. T. Kaino, K. Kubodera, S. Tomaru, T. Kurihara, S. Saito, T. Tsutsui, S. Tokito, *Electron Lett.* **23**, 1095 (1987).
193. Ref. 6, p. 235.
194. D. D. C. Bradley, Y. Mori, *Jn. J. Appl. Phys.* **28**, 74 (1989).
195. Ref. 7, p. 688.
196. S. A. Jenekhe, J. A. Osaheni, J. S. Meth, and H. Vanherzeele, *Chem. Mater.* **4**, 683–687 (1992).
197. Ref. 7, p. 697.
198. Ref. 7, p. 699.
199. J. R. Lindle, F. J. Bartoli, C. A. Hoffman, O. K. Kim, Y. S. Lee, J. S. Shirk, and Z. H. Kafafi, *Appl. Phys. Lett.* **56**, 712–714 (1990).
200. Ref. 4, p. 336.
201. Ref. 7, pp. 658–660.
202. Ref. 4, p. 322.

203. Ref. 6, p. 232.
204. D. Sandman, I. Kim, J. M. Njus, D. Lee, A. Cholli, and S. Sahoo, *Macromol. Symp.* **192**, 99–113 (2003).
205. G. Wegner, *Naturforsch Z, B* **24**, 824 (1969).
206. M. Schott and G. Wegner, in D. S. Chemla and J. Zyss, eds., *Nonlinear Optical Properties of Organic Molecules and Crystals*, Vol. 2, Academic Press, New York, 1987, pp. 3–46.
207. J. LeMoigne, M. Moroni, H. Coles, A. Thierry, and F. Kajzar, *Mater. Res. Soc. Symp. Proc.* **247**, 65 (1992).
208. T. Kanetake, K. Ishikawa, T. Hasewaga, T. Koda, K. Takeda, M. Hasewaga, K. Kubodera, and H. Kobayashi, *Appl. Phys. Lett.* **54**, 2287–2289 (1989).
209. P. A. Chollet, F. Kajzar, and J. Messier, *Synth. Met.* **18**, 459–464 (1987).
210. F. Kajzar and J. Messier, *Thin Solid Films* **132**, 11–19 (1985).
211. E. Geiger, P. Hug, and A. Keller, *Macromol. Chem. Phys.* **203**, 2422–2431 (2002).
212. M. D. Mowery, M. Cai, H. Menzel, and C. E. Evans, *J. Vac. Sci. Technol., A* **17**, 2136–2141 (1999).
213. M. Chandross, Y. Shimoi, and S. Mazumdar, *Synth. Met.* **85**, 1001–1006 (1997).
214. A. Sarkar, S. Okada, H. Matsuda, and H. Nakanishi, *Polym. Bull.* **41**, 425–431 (1998).
215. C. C. Hsu, Y. Kawabe, Z. Z. Ho, N. Peyghambarain, J. M. Polky, W. Krug, and E. Miao, *J. Appl. Phys.* **67**, 7199–7203 (1990).
216. Ref. 7, p. 648.
217. Ref. 6, p. 234.
218. C. C. Hsu, Y. Kawabe, Z. Z. Ho, N. Peyghambarain, J. N. Polky, W. Krug, and E. Miao, *J. Appl. Phys.* **67**, 7199–7203 (1990).
219. S. Okada, T. Doi, A. Mito, K. Hayamizu, A. Ticktin, H. Matsuda, N. Kikuchi, A. Masaki, N. Minami, K. Haas, and H. Nakanishi, *Nonlinear Opt.* **8**, 121 (1994).
220. Ref. 6, p. 235.
221. A. Sarkar, S. Okada, H. Matsuzawa, H. Matsuda, and H. Nakanishi, *J. Mater. Chem.* **10**, 819–828 (2000).
222. A. S. M. Karim, R. Nomura, H. Kajii, R. Hidayat, K. Yoshino, and T. Masuda, *J. Polym. Sci. Part A: Polym. Chem.* **38**, 4717–4723 (2000).
223. Ref. 7, p. 666.
224. Ref. 7, p. 664.
225. M. V. Mostovoy, M. T. Figge, J. Knoester, *Europhys. Lett.* **38**, 687–692 (1997).
226. J. M. Grindler, A. P. Epstein, *Phys. Rev. B* **41**, 10674–10684 (1990).
227. M. C. dos Santos, J. L. Bredas, *Phys. Rev. Lett.* **62**, 2499–2505 (1989).
228. Ref. 4, p. 336.
229. A. J. Heeger, S. Kivelson, J. R. Schrieffer, and W.-P. Su, *Rev. Mod. Phys.* **60**, 781–850 (1988).
230. G. Costa, in G. Allen, ed., *Comprehensive Polymer Science*, Oxford University Press, New York, 1989, Chapt. 9, p. 155.
231. Ref. 6, p. 238.
232. D. Neher, A. Wolf, M. Leclerc, A. Kaltbeizel, C. Bubeck, G. Wegner, *Synth. Met.* **37**, 249–253 (1990).
233. Y. Furukawa, N. S. Sariciftci, eds., in *Primary Photoexcitations in Conjugated Polymers*, World Scientific, Singapore, 1997, Chapt. 17, pp. 511–519. Available at [http://www.ipc.uni\\_linz.acat/publ/book/Chapter17.pdf](http://www.ipc.uni_linz.acat/publ/book/Chapter17.pdf). Accessed August 27 2003.
234. K. Y. Kim, S. Jang, F. W. Harris, *Macromolecules* **34**, 8925–8933 (2001).
235. A. K.-Y. Jen, X. Wu, and H. Ma, *Chem. Mater.* **10**, 471–473 (1998).
236. Y. M. Cal and A. K.-Y. Jen, *Appl. Phys. Lett.* **67**, 299–301 (1995).

237. X. W. Zhan, Y. Q. Liu, D. B. Zhu, G. Xu, X. C. Liu, P. X. Ye, *Appl. Phys. A* **77**, 375–378 (2003).
238. M. Guohong, L. Guo, J. Mi, Y. Lui, Q. Shixiong, J. Liu, G. He, and Y. Li, *Physica B* **305**, 147–154 (2001).
239. D. R. Gagnon, J. D. Capistran, F. E. Karasz, R. W. Lenz, S. Antoun, *Polymer* **28**, 567–573 (1987).
240. Ref. 7, p. 684.
241. A. Samoc, M. Samoc, M. Woodruff, and B. Luther-Davies, in D. L. Wise, D. J. Trantolo, G. E. Wnek, T. M. Cooper, and J. D. Gresser, eds., *Photonic Polymer Systems*, Marcel Dekker, Inc., New York, 1998, pp. 373–436.
242. R. Riehn, A. Charas, J. Morgado, F. Cacialli, *Appl. Phys. Lett.* **82**, 526–528 (2003).
243. McBranch, M. Sinclair, A. J. Heeger, A. O. Patil, S. Shi, S. Askari, and F. Wudl, *Synth. Met.* **29**, 85–90 (1989).
244. E. Ando, S. Onodera, M. Iino, O. Ito, *Carbon* **39**, 101–108 (2001).
245. T. Kaino, K. Kubodera, T. Kobayashi, S. Kurihara, T. Sato, T. Tsutsui, S. Takito, and H. Murata, *Appl. Phys. Lett.* **53**, 2002–2004 (1988).
246. H. S. Nalwa, *J. Appl. Phys. D.* **23**, 745–747 (1990).
247. H. S. Nalwa, *Thin Solid Films* **225**, 175–181 (1993).
248. Ref. 4, p. 687.
249. Z. Wu, F. Li, L. Huang, Y. Shi, X. Jin, S. Fang, K. Chuang, R. E. Lyon, F. W. Harris, and S. Z. D. Cheng, *J. Therm. Anal. Calorimetry* **59**, 361–373 (2000).
250. S. A. Jenekhe, J. A. Osaheni, J. S. Meth, H. Vanherzeele, *Chem. Mater.* **4**, 683–687 (1992); H. Vanherzeele, J. S. Meth, S. Jenekhe, M. F. Roberts, *J. Opt. Soc. Am. B* **9**, 524–533 (1992).
251. R. J. Gehr, G. L. Fischer, R. W. Boyd, J. E. Sipe, *Phys. Rev. A* **53**, 2792–2798 (1995).
252. J. R. Lindle, F. J. Bartolli, C. A. Hoffman, O.-K. Kim, Y. S. Lee, J. S. Shirk, Z. H. Kafafi, *Appl. Phys. Lett.* **56**, 712–714 (1989).
253. K. D. Singer, S. F. Hubbard, A. Schober, L. M. Hayden, and K. Johnson, in Ref. 1, pp. 311–514.
254. M. G. Kuzyk, R. C. Moore, and L. A. King, *J. Opt. Soc. Am. B* **7**, 64–72 (1990).
255. P. D. Maker, R. W. Terhune, M. Nisenhoff, and C. M. Savage, *Phys. Rev. Lett.* **8**, 21–22 (1962).
256. J. Jerphagnon and S. K. Kurtz, *J. Appl. Phys.* **41**, 1667–1681 (1970).
257. D. Neher, A. Wolf, C. Bubek, and G. Wegner, *Chem. Phys. Lett.* **163**, 116 (1989).
258. W. N. Herman and L. M. Hayden, *J. Opt. Soc. Am. B* **12**, 416–427 (1995).
259. K. D. Singer, M. G. Kuzyk, and J. E. Sohn, *J. Opt. Soc. Am. B* **4**, 968–976 (1987).
260. K. D. Singer and J. H. Andrews, in J. Zyss, ed., *Molecular Nonlinear Optics: Materials Physics, and Devices*, Academic Press, San Diego, Calif., 1994, p. 254.
261. D. Jungbauer, I. Teraoka, D. Y. Yoon, B. Reck, J. D. Swalen, R. Tieg, and C. G. Willson, *J. Appl. Phys.* **69**, 8011–8017 (1991).
262. Ref. 6, Chapt. 5.
263. T. Dai, K. D. Singer, R. J. Twieg, and T. C. Kowalczyk, *J. Opt. Soc. Am. B* **17**, 412–421 (2000).
264. G. I. Stegeman and R. H. Stolen, *J. Opt. Soc. Am. B* **6**, 652–662 (1989).
265. C. Balslev Clausen, O. Bang, and Y. S. Kivshar, *Phys. Rev. Lett.* **78**, 4749–4752 (1997).
266. K. D. Singer and A. F. Garito, *J. Chem. Phys.* **75**, 3572 (1981).
267. V. Ostroverkhov, O. Ostroverkhova, R. G. Petschek, K. D. Singer, L. Sukhomlinova, R. J. Twieg, S.-X. Wang, and L. C. Chien, *Chem. Phys.* **257**, 263–274 (2000).
268. S. F. Hubbard, R. G. Petschek, and K. D. Singer, *Opt. Lett.* **21**, 1774–1776 (1996).
269. S. F. Hubbard, R. G. Petschek, K. D. Singer, N. D'Sidocky, C. Hudson, L. C. Chien, C. C. Henderson, and P. A. Cahill, *J. Opt. Soc. Am. B* **15**, 289–301 (1998); V.

- Ostroverkhov, R. G. Petschek, K. D. Singer, L. Sukhomlinova, R. J. Twieg, S.-X. Wang, and L. C. Chien, *J. Opt. Soc. Am. B* **17**, 1531–1542 (2000).
270. P. Kaatz and D. P. Shelton, *J. Chem. Phys.* **105**, 3918–3929 (1996).
271. M. Sheik-Bahae, A. A. Said, and E. W. Van Stryland, *Opt. Lett.* **14**, 955–957 (1989).
272. E. W. Van Stryland and M. Sheik-Bahae, in Ref. 1, pp. 655–692.
273. M. Sheik-Bahae, A. A. Said, T. H. Wei, D. J. Hagan, and E. W. Van Stryland, *J. Quantum Electron.* **26**, 760–769 (1990).
274. T. Xia, D. J. Hagan, M. Sheik-Bahae, and E. W. Van Stryland, *Opt. Lett.* **19**, 317–319 (1994).
275. M. Sheik-Bahae, J. Wang, J. R. DeSalvo, D. J. Hagan, and E. W. Van Stryland, *Opt. Lett.* **17**, 258–260 (1992).
276. W. Zhao and P. Palffy-Muhoray, *Appl. Phys. Lett.* **65**, 673–675 (1994).
277. L. Yang, R. Dorsinville, P. P. Ho, W. K. Zou, N. L. Yang, and R. R. Alfano, *Appl. Phys. Lett.* **53**, 2009–2010 (1988).
278. M. G. Kuzyk, R. A. Norwood, J. W. Wu, and A. F. Garito, *J. Opt. Soc. Am. B* **6**, 154–164 (1989).
279. B. Blaszcak, *Opt. Commun.* **58**, 439–443 (1986).
280. D. Heiman, R. W. Hellwarth, M. D. Levenson, and G. Martin, *Phys. Rev. Lett.* **36**, 189–192 (1976).
281. M. J. Feldstein, P. Vohringer, and N. F. Scherer, *J. Opt. Soc. Am. B* **12**, 1500 (1995).
282. T. Hasegawa, Y. Iwasa, H. Kishida, T. Koda, Y. Tokura, H. Tachibana, and Y. Kawabata, *Phys. Rev. B* **45**, 6317–6320 (1992).
283. R. L. Sutherland, E. Rea, V. Natarajan, T. Pottenger, and P. A. Fleitz, *J. Chem. Phys.* **98**, 2593–2603 (1993).
284. M. Zhao, Y. Cui, M. Samoc, P. N. Prasad, M. R. Unroe, and B. A. Reinhardt, *J. Chem. Phys.* **95**, 3991–4001 (1991).
285. E. W. Van Stryland, M. A. Woodall, H. Vanherzeele, and M. J. Soileau, *Opt. Lett.* **10**, 490–492 (1985).
286. T. H. Wei, D. J. Hagan, M. J. Spence, E. W. Van Stryland, J. W. Perry, and D. R. Coulter, *Appl. Phys. B* **54**, 46–51 (1992).
287. C. H. Chen and M. P. McCann, *Opt. Commun.* **63**, 335–338 (1987).
288. P. Foggi, P. R. Salvi, R. Bini, and E. Castellucci, *J. Mol. Struct.* **175**, 147–152 (1988).
289. R. Philip, P. Sathy, V. P. N. Nampoori, J. Philip, and C. P. G. Vallabhan, *J. Phys. B* **25**, 155–161 (1992).
290. R. A. Negres, J. M. Hales, A. Kobaykov, D. J. Hagan, and E. W. VanStryland, *Opt. Lett.* **27**, 270–272 (2002).

## READING LIST

With respect to polymeric and organic molecular materials, there are several monographs and numerous collections of research works to consider. Annual proceedings presenting current research were published through 1997 by the Society of Photo-optical Instrumentation Engineers (SPIE) under the title *Nonlinear Optical Properties of Organic Materials*, Vols. I–X. Since 2001, this series has been superceded by the annual series *Linear and Nonlinear Optics of Organic Materials*, Vols. I–III, currently edited by M. Kuzyk. Additional recent relevant proceedings from SPIE include:

M. G. Kuzyk, *Third Order Nonlinear Optical Materials*, 3473 SPIE, Bellingham, Wash., 1998.

M. Eich, *Organic Nonlinear Optical Materials*, 3796 SPIE, Bellingham, Wash., 1999.

The proceedings of the October 2003 annual meeting, entitled *Organic Materials and Nanotechnology*, CDS 100 SPIE, Bellingham, Wash., 2004, promise to provide an up-to-date account of research in that field.

Noteworthy collections and monographs include:

K.-S. Lee, ed., *Polymers for Photonics Applications, Vol. 1: Advances in Polymer Science*, Vol. 158, Springer, Berlin, 2002.

H. S. Nalwa, ed., *Supramolecular Photosensitive and Electroactive Materials*, Academic Press, San Diego, Calif., 2001.

H. S. Nalwa, ed., *Handbook of Advanced Electronic and Photonic Materials and Devices, Vol. 9: Nonlinear Optical Materials*, Academic Press, San Diego, Calif., 2001.

M. Pope and C. E. Swenberg, *Electronic Processes in Organic Crystals and Polymers*, 2nd ed., Oxford University Press, New York, 1999.

H. S. Nalwa, ed., *Handbook of Organic Conductive Molecules and Polymers*, CRC Press, Inc., Boca Raton, 1997.

M. G. Kuzyk and C. W. Dirk, eds., *Characterization Techniques and Tabulations for Organic Nonlinear Optical Materials*, Marcel Dekker, Inc., New York, 1998.

S. Miyata, and H. Sasabe, eds., *Poled Polymers and Their Applications to SHG and EO Devices*, Gordon and Breach, Queensland, Australia, 1997.

H. S. Nalwa and S. Miyata, eds., *Nonlinear Optics of Organic Molecules and Polymers*, CRC Press, Boca Raton, Fla., 1997.

G. A. Lindsay And K. D. Singer, ed., *Polymers for Second-Order Nonlinear Optics* (ACS Symposium Series No. 601), American Chemical Society, Washington, D.C., 1995.

S. Mukamel, *Principles of Nonlinear Optical Spectroscopy*, Oxford University Press, New York, 1995.

J. Zyss, ed., *Molecular Nonlinear Optics: Materials, Physics, and Devices*, Academic Press, Inc., San Diego, Calif., 1994; and its predecessor volumes D. S. Chemla and J. Zyss, *Nonlinear Optical Properties of Organic Molecules and Crystals*, Vols. 1 and 2, Academic Press, Inc., San Diego, Calif., 1987.

L. A. Hornak, ed., *Polymers for Lightwave and Integrated Optics*, Marcel Dekker, Inc., New York, 1992.

P. N. Prasad and D. J. Williams, *Introduction to Nonlinear Optical Effects in Molecules and Polymers*, John Wiley & Sons, Inc., New York, 1991.

S. Miyata and H. Sasabe, *Light Wave Manipulation using Organic Nonlinear Optical Materials*, Gordon and Breach, Amsterdam, 2000.

Ch. Bosshard, K. Sutter, Ph. Pretre, J. Hullinger, M. Florsheimer, P. Kantz, and P. Gunter, in A. F. Garito and F. Kajzar, eds., *Advances in Nonlinear Optics, Vol. 1: Organic Nonlinear Optical Materials*, Gordon and Breach, Basel, Switzerland, 1995.

Because the field of nonlinear optical properties of polymers is cross-disciplinary among optical sciences, material sciences, polymer chemistry, and other disciplines, important research is published in a wide variety of journals, including those of the Materials Research Society (MRS), the Optical Society of America (OSA), the Institute of Physics (IOP), the American Chemical Society (ACS), the American Physical Society (APS), and the IEEE Lasers and Electro-Optics Society. Particularly noteworthy are the special issues on organic materials for nonlinear optics and photonics, including:

N. Peyghambarian and S. Marder, eds., *IEEE Selected Top. Quantum. Electron.* **7**, 757–863 (2001).

C. Hooker, W. R. Burghardt, and J. M. Torkelson, eds., *Chem. Phys.* **245**, 1–568 (1999).

M. G. Kuzyk, K. D. Singer, and R. J. Twieg, eds., *J. Opt. Soc. Am. B.* **15**(1, 2), 254–488 and 724–932 (1998).

J. Michl, ed., *Chem. Rev.* **94**(1), 1–278 (1994).

Finally, the following texts provide a broad selection of views on the field of nonlinear optics.

R. W. Boyd, *Nonlinear Optics*, 2nd ed., Academic Press, San Diego, Calif., 2002.

G. S. He and S. H. Liu, *Physics of Nonlinear Optics*, World Scientific, Singapore, 1999.



- E. G. Sauter, *Nonlinear Optics*, John Wiley & Sons, Inc., New York, 1996.  
R. L. Sutherland, *Handbook of Nonlinear Optics*, Marcel Dekker, Inc., New York, 1996.  
P. N. Butcher and D. Cotter, *The Elements of Nonlinear Optics*, Cambridge University Press, New York, 1990.  
Y. R. Shen, *The Principles of Nonlinear Optics*, John Wiley & Sons, Inc., New York, 1984.  
N. Bloembergen, *Nonlinear Optics*, W. A. Benjamin, New York, 1965.

JAMES H. ANDREWS  
KIMBERLY A. GUZAN  
Youngstown State University

## NONWOVEN FABRICS, SPUNBONDED

### Introduction

In 2001, the global production of spunbonded fabrics reached a record 1,400,000 t with an annual growth rate of between 6 and 8% (1). There are approximately 260 individual production lines in operation throughout the world. Spunbonded fabrics are distinguished from other nonwoven fabrics in their one-step manufacturing process which provides either a complete chemical-to-fabric or polymer-to-fabric process. Although the use of monomers as part of the in-line process is no longer in commercial use, in either instance the manufacturing process integrates the spinning, laydown, consolidation, and bonding of continuous filaments to form a fabric. Commercialization of this process dates to the early 1960s in the United States and Western Europe (2,3) and in the early 1970s in Japan (4). Many of the first plants constructed are still in operation attesting to the usefulness of the method. New production plants continue to be built (1,5) to supply the growing demand (Table 1).

The large investment required for a turnkey spunbonded plant (\$15–50 million, 2002 U.S. dollars) is offset by their high productivity. Spunbonded production was originally limited to western Europe, the United States, and Japan, but has since spread to virtually all areas of the world. Production lines, mainly nonproprietary, have been installed throughout Asia, South America, and the Middle East, areas and countries that previously did not participate in the technology. Considerable ownership changes occurred in the United States and Europe as the strategies of companies committed to the technology evolved (6).

Early marketing efforts for spunbonded fabrics centered on their substitution for existing (ie, woven) textile fabrics. Generally, success was achieved in areas where only functionality was important. Extremely slow progress has occurred in areas where textile-like aesthetics are required. Only in the area of disposable protective clothing has success been achieved for the garment market. Nevertheless, spunbonded fabrics are recognized as a unique class of materials within the general category of nonwoven fabrics (see NONWOVEN FABRICS, STAPLE FIBERS).

**Table 1. Spunbond Producers by Region**

Company	Polymer base <sup>a</sup>	Technology base
<b>North America</b>		
Ahlstrom	PP	Nordson
American Nonwovens	PP	Ason Neumag
Avgol	PP	Reifenhauser
BBA Nonwovens	PET	via DuPont <sup>b</sup>
	PP	via duPont <sup>c</sup>
		Self-developed
		Reifenhauser
Colbond	PET/PA	via Akzo <sup>d</sup>
DuPont	HDPE, PET	Self-developed <sup>e</sup>
First Quality	PP	Reifenhauser
Freudenberg	PET	Self-developed <sup>f</sup>
Johns Manville	PET	via Hoechst <sup>g</sup>
Kimberly-Clark	PP	Self-developed
PGI Nonwovens	PP	Reifenhauser
		STP Impianti
Texbond	PP	STP Impianti
Western Nonwovens	PA	via Monsanto <sup>h</sup>
<b>Europe</b>		
BP	PP	Reifenhauser
BBA Nonwovens	PP	Reifenhauser
		Lurgi
		Self-developed
NWI (Cartiere Mirano)	PP	NWT
Colbond	PET, PET/PA	via Akzo <sup>d</sup>
Don & Low	PP	Reifenhauser
DuPont	HDPE	Self-developed <sup>e</sup>
	PP	Self-developed <sup>c</sup>
Fibertex	PP	Reifenhauser
Freudenberg	PET	Self-developed <sup>f</sup>
Johns Manville	PET	via Hoechst <sup>g</sup>
Pegas	PP	Reifenhauser
Politex-Freudenberg	PET	Self-developed
Polyfelt	PP	Lurgi
Tenotex	PP	Self-developed
Texbond	PP	STP Impianti
		Self-developed
Terram BBA	PP/PE	via ICI
<b>South America</b>		
Bidim BBA	PET	via Rhone Poulenc
Companhia Providencia	PP	Reifenhauser
Kami	PP	Reifenhauser
Fitesa	PP	STP Impianti
PGI	PP	Reifenhauser
<b>Japan</b>		
Asahi	PP, PET, Cupra	Self-developed
Chisso	PP, PP/PE	Reifenhauser
Idemitsu	PP	Reifenhauser

**Table 1. (Continued)**

Company	Polymer base <sup>a</sup>	Technology base
Futamura	Rayon	Self-developed
Mitsui	PP	Self-developed
		Reifenhauser
OJI Paper	PP	Reifenhauser
Teijin	PET, PP	Self-developed
Toray	PET	Self-developed
Toyobo	PET	Self-developed
Unitika	PET, PA	Self-developed
Other Areas		
Avgol (Israel)	PP	Reifenhauser
Cheil (S. Korea)	PP	Reifenhauser
Freudenberg (Taiwan)	PET	Self-developed <sup>f</sup>
Hanil (S. Korea)	PP/PET	Kobelco
IndoSyntec (Indonesia)	PET	NWT
Kaymac Industries	PET	via Rhone Poulenc
Kimberly-Clark (Australia)	PP	Self-developed
Kolon (S. Korea)	PP/PET	Self-developed
Nan Ya (Taiwan)	PP	Lurgi & Reifenhauser
PGI (China)	PP	Reifenhauser
SAAF (Saudi Arabia)	PP	Reifenhauser
Spuntec (S. Africa)	PP	Reifenhauser
Thai Tusco (Indonesia)	PP/PET	via Unitika
Yuhan-Kimberly (S. Korea)	PP	Self-developed

<sup>a</sup>PP = polypropene; PET = poly(ethylene terephthalate); PA = ; HD PE = high density polyethylene.

<sup>b</sup>Reemay process.

<sup>c</sup>Typar process.

<sup>d</sup>Split process.

<sup>e</sup>Flashspun Tyvek process (HDPE).

<sup>f</sup>Lutradur process.

<sup>g</sup>Began with RhonePoulenc license.

<sup>h</sup>Cerex process.

The area of largest growth for spunbonded fabrics continues to be disposable diaper coverstock, that accounts for approximately 70% of the U.S. coverstock market. Forecasts for the future growth of spunbonded fabrics continue to be favorable as consumption in both durable and disposable areas continues to grow. Growth is forecast to generally exceed the growth of all nonwovens, which itself is expected to grow at 3–6% per annum (1,6). In addition to diaper coverstock and hygiene, growth is anticipated in geotextiles, roofing, carpet backing, medical wrap, and durable paper applications such as envelopes (6).

New plant construction will bring increased capacity to levels of regional overcapacity, which will force producers to export large quantities of product to keep supply and demand in balance. Considerable consolidation of ownership has occurred during the last five years and the investment and output for each new line has grown enormously. New production lines can produce up to 1 billion m<sup>2</sup> of coverstock per year more than doubling the annual output of lines built

only 5 years ago. Environmental issues have had relatively little effect on either production or products. Consumers prefer the convenience of disposable diapers, and studies have shown that diapers are still a relatively small contributor to landfill space.

Although producers have benefited from the generally stable prices for crude oil, a sudden increase in these prices or decrease in availability of resin feedstocks would adversely impact both profitability and growth. Producers who have not upgraded to newer, faster, and more efficient lines have experienced low or negative profitability. There appear to be no new fiber technologies that would radically change the manner in which spunbonded structures are produced. Any serious challenges to existing markets will likely come from film, airlay, or advances in alternative technologies within a specific market segment.

### General Characteristics

Spunbonded fabrics are filament sheets made through an integrated process of spinning, attenuation, deposition, bonding, and winding into roll goods. The fabrics are made up to 5.2 m wide and usually not  $> 3.0$  m in order to facilitate productivity. Fiber sizes range from 0.1 to 50 dtex although a range of 2–20 dtex is most common. A combination of thickness, fiber fineness (denier), and number of fibers per unit area determines the fabric basis weight which ranges from 8–800 g/m<sup>2</sup>; 13–180 g/m<sup>2</sup> is typical. Average basis weights in hygiene have fallen by 20% or more because of improvements in process technology.

Most spunbonded processes yield a sheet having planar–isotropic properties owing to the random laydown of the fibers (Table 2). Unlike woven fabrics, spunbonded sheets are generally nondirectional and can be cut and used without concern for higher stretching in the bias direction or unraveling at the edges. It is possible to produce nonisotropic properties by controlling the orientation of the fibers in the web during laydown. Although it is not readily apparent, most sheets are layered or shingled structures with the number of layers increasing with higher basis weights for a given product. Fabric thickness varies from 0.1 to 4.0 mm; the range 0.15–1.5 mm represents the majority of fabrics in demand. The method of bonding greatly affects the thickness of the sheets, as well as other characteristics. Fiber webs bonded by thermal calendering are thinner than the same web that has been needle-punched, because calendering compresses the structure through pressure, whereas needle-punching moves fibers from the  $x$ – $y$  plane of the fabric into the  $z$  (thickness) direction.

The structure of traditional woven and knit fabrics permits the fibers to readily move within the fabric when in-plane shear forces are applied, resulting in a fabric that readily conforms in three dimensions. Because calender bonding of a spun web causes some of the fibers to fuse together, thus giving the sheet integrity, the structure has a relatively stiff hand or drape compared to traditional textile fabrics. This is a result of the immobilization of fibers in the areas of fiber-to-fiber fusion. The immobilization may be moderated by limiting the bonds to very small areas (points) or by entangling the fibers mechanically or hydraulically. Saturation bonding of spun webs with chemical binders such as acrylic emulsions can bond the structure throughout and result in very stiff

Table 2. Physical Properties of Spunbonded Products

Product	Basis weight, g/m <sup>2</sup>	Thickness, mm	Tensile strength, <sup>a</sup> N <sup>b</sup>	Tear strength, <sup>a</sup> N <sup>b</sup>	Mullen burst, kPa <sup>c</sup>	Bonding method
Accord	69		144 MD 175 XD	36 MD 40 XD	323	Point thermal
Bidim	150		495	280	1545	Needle-punch
Cerex	34	0.14	135 MD 90 XD	40 MD 32 XD	240	Chemically induced area
Colback	100	0.6	300 <sup>d</sup>	120		Area thermal (sheath-core)
Corovin	75		130	15		Point thermal
Lutradur	84	0.44	225 MD 297 XD	85 MD 90 XD	598	Copolymer area thermal
Polyfelt	137		585	225	1445	Needle-punch
Reemay	68	0.29	225 MD	45 MD	330	copolymer
			180 XD	50 XD		area thermal
Terram	137	0.7	850	250	1100	Area thermal (sheath-core)
Trevira	155		630 MD	270 MD	1512	Needle-punch
			495 XD	248 XD		
Typar	103	0.305	540 MD	207 MD		Undrawn segments
			495 XD	235 XD	825	Area thermal
Tyvek	54	0.15	4.6 <sup>e</sup> MD	4.5 MD		Area and point thermal
			5.1 <sup>e</sup> XD	4.5 XD		

<sup>a</sup>MD = Machine direction; XD = cross-direction.

<sup>b</sup>Unless otherwise noted. To convert N to pound-force, divide by 4.448.

<sup>c</sup>To convert kPa to psi, multiply by 0.145.

<sup>d</sup>300 N/5 cm = 34.5 ppi.

<sup>e</sup>N/mm; to convert N/mm to ppi, divide by 0.175.

**Table 3. Fibers for Spunbonded Nonwoven Fabrics**

Fiber type	Breaking tenacity, N/tex <sup>a</sup>	Elongation, %	Specific gravity	Moisture regain, <sup>b</sup> %	Approximate melt point, °C
Polyester	0.17–0.84	12–150	1.38	0.4	248–260
Nylon-6,6	0.26–0.88	12–70	1.14	4.0	248–260
Polypropylene	0.22–0.48	20–100	0.91	~0.0	162–171

<sup>a</sup>To convert N/tex to gf/den, multiply by 11.3.

<sup>b</sup>At 21°C and 65% rh.

sheets. This technique is used to provide thermal and mechanical dimensional stability to certain structures whereby the emulsion binder functions as a non-thermoplastic component within the thermoplastic matrix.

Other approaches include powder bonding, although this method may be more suitable for bonding nonwoven fabrics made from staple fibers (7,8) (see NONWOVEN FABRICS, STAPLE FIBERS).

The method of fabric manufacture dictates many of the characteristics of the sheet, but intrinsic properties are firmly established by the base polymer selected. Properties such as fiber density, temperature resistance, chemical and light stability, ease of coloration, surface energies, and others are a function of the base polymer. Thus, because nylon absorbs more moisture than polypropylene, spunbonded fabrics made from nylon are more water-absorbent than fabrics of polypropylene.

The majority of spunbonded fabrics are based on either isotactic polypropylene or polyester (Table 1). Small quantities are made from nylon-6,6 and an increasing tonnage from (flashspun) high density polyethylene. Table 3 illustrates the basic characteristics of fibers made from different base polymers. Although some interest has been seen in the use of linear low density polyethylene (LLDPE) as a base polymer, largely because of potential increases in the softness of the final fabric (9), economic factors continue to favor polypropylene (see PROPYLENE POLYMERS (PP)). Bicomponent technology will allow polyethylene to be used in a more economical way by directing it only to the surfaces where it brings a useful property.

Isotactic polypropylene is the most widely used polymer in spunbonded production because it is the least expensive fiber-forming polymer that provides the highest yield (fiber per weight) and covering power owing to its low density. Isotactic polypropylene is only ca 70% the density of most types of polyesters, and thus equivalent yields of fiber require a greater weight of more expensive polyester. Large advances have been made in the manufacture of polypropylene resins and additives since the first spunbonded polypropylene fabrics were commercialized in the 1960s. Unstabilized polypropylene fibers are readily degraded by ultraviolet UV light, but dramatic improvements in additives permit years of outdoor exposure to occur before fiber properties are significantly affected. Metallocene polypropylene resins are the latest major resin improvement available for spun bonding.

Polypropylene fibers are neither dyeable by conventional methods nor readily stained because dye receptor sites do not naturally exist along the molecular

backbone. However, some spunbonded polypropylene fabrics are colored by the addition of a pigment to the polymer melt, wherein the pigment becomes encased within the fiber interior. Advantages to this method include higher resistance to fading and bleeding and ease of reproducibility of color shades from lot to lot. A key disadvantage is the generation of small to large quantities of off-quality production during the transitions into and out of a particular color, and coloration normally occurs only on low output lines. A delustering pigment, eg  $\text{TiO}_2$ , is often added to polypropylene as it almost always is with the manufacture of nylon fibers.

Most off-quality or scrap polypropylene fibers may be repelletized and blended in small percentages with virgin polymer to produce first-grade spunbonded fabrics. The economics are of great importance in a process where high yields are required in order to be competitive. Some manufacturing equipment directly recycles edge-trim back into an extruder, where it is blended back into the polymer melt (see OLEFIN FIBERS).

Polyester fiber has several performance advantages versus polypropylene, although it is less economical. Polyester can produce higher tensile strength and modulus fabrics that are dimensionally stable at higher temperatures than polypropylene. This is of importance in selected applications such as roofing, automotive carpet backing, and dryer sheets. Polyester fabrics are easily dyed and printed with conventional equipment which is of extreme importance in apparel and face fabrics, although of lesser importance in most spunbonded applications (see POLYESTERS, FIBERS).

Spunbonded fabrics have been made from both nylon-6 and nylon-6,6 polymers. Because nylon is more costly and highly energy-intensive, it is less economical than either polyethylene or polypropylene. Although a considerable body of knowledge exists in the preparation of nylon polymers, such as end group control, it has been of little advantage in spunbonded fabric production. Historically, nylon-6,6 spunbonded fabrics have been commercially produced at weights as low as  $10 \text{ g/m}^2$  with excellent cover and strength, but recently this has been achieved with polypropylene as well. Unlike the olefins and polyesters, fabrics made from nylon absorb water quite readily through hydrogen bonding between the amide group and water molecules (see POLYAMIDES, FIBERS).

Traditional melt spun methods have not utilized polyethylene as the base polymer because the resin is more expensive and the physical properties obtained have been lower compared to those obtained with polypropylene. Advances in polyethylene technology have resulted in the commercialization of new spunbonded structures having characteristics, such as softness, not attainable with polypropylene. Although fiber-grade polyethylene resin was announced in late 1986, it has seen limited acceptance because of higher costs and continuing improvements in polypropylene resin technology (see ETHYLENE POLYMERS).

Flashspun high density polyethylene fabrics have been commercial since the early 1960s; however, this is a proprietary and radically different process of manufacturing a spunbonded fabric, more technically challenging to produce, and highly capital-intensive. Today, there is only one manufacturer of flashspun fabrics, although they are produced in both Europe and the United States.

Some fabrics are composed of combinations of polymers where a lower melting polymer functions as the binder element. The binder element may be a

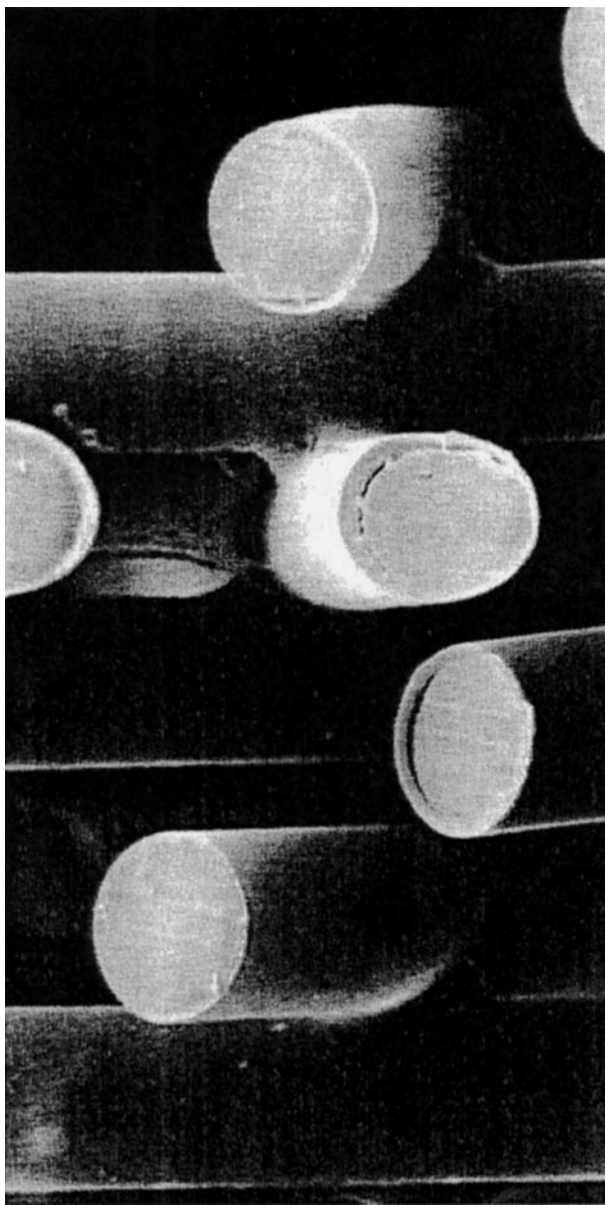


**Fig. 1.** Microstereo view of the cross-section of skin core filaments.

separate fiber interspersed with higher melting fibers (10), or the two polymers may be combined in one fiber type (11). In the latter case, the so-called bicomponent fiber may have the lower melting portion as a sheath covering a core of the higher melting polymer (Fig. 1). Bicomponent fibers can also be spun, whereby the two polymers are extruded side by side. The polymer composition of the binder element in such structures may be either polyethylene, nylon-6, and polyester copolymers typically modified by lowering the terephthalic acid content



by substitution with isophthalic acid. Great advances have been made in bicomponent spinning and a large variety of intrafiber structures can be easily produced from turnkey spinbeams (Fig. 2) (12). Bicomponent webs can be subjected to mechanical stresses such as water jet impact which causes the individual filament to fracture into its components yielding a new number of filaments equal to the number of components or segments created in the filament during spinning. Thus, a single filament containing 16 pie segments will fracture into 16 smaller wedge-shaped filaments.

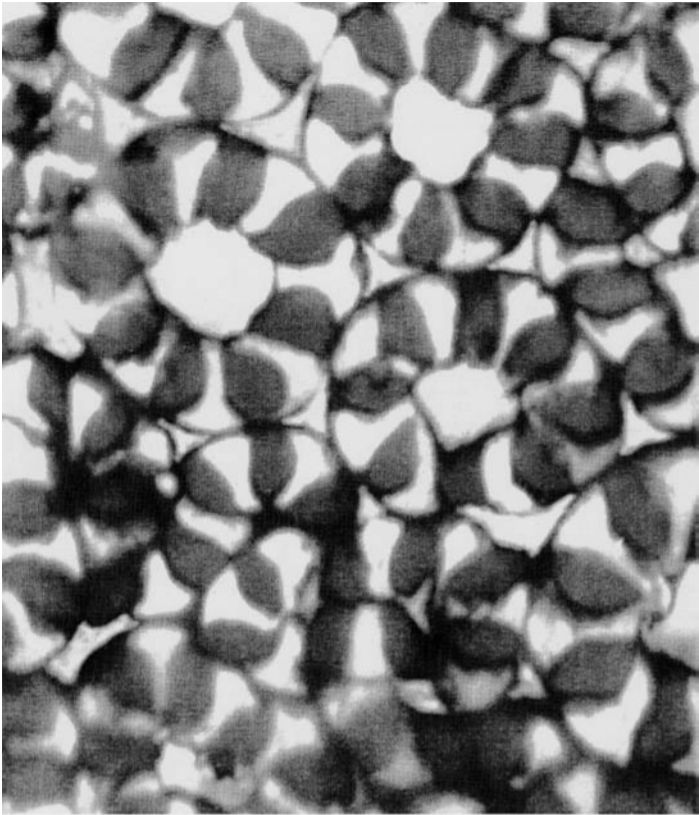
Spunbonded fabrics with elastomeric properties are now commercial. One type of structure has been commercialized in Japan on the basis of thermoplastic polyurethanes, but the process is more similar to melt blowing than spun bonding (13). This represented the first commercial production of such fabrics, although spunbonded urethane fabrics have been previously discussed (14). A more economical approach using polypropylene has recently become commercial and is used in medical and hygienic applications (15). High costs and inferior performance versus woven fabrics continue to exclude these fabrics from the huge apparel markets. Elastomeric fabrics may also be created using the meltblown process for specialty applications.

There is an almost unlimited number of ways to characterize spunbonded fabrics. Many tests in use were originally developed for the characterization of textiles and paper products. When taken together, properties such as tensile, tear, and burst strength; toughness; elongation to break; basis weight; thickness; air porosity; dimensional stability; and resistance to heat and chemicals are often sufficient to uniquely describe one product. The reason is that these properties reflect both the fabric composition and its structure, the latter being defined by a manufacturing process unique to that fabric. Compare, eg, the differing shapes of the generic stress-strain curves of thermally bonded and needle-punch bonded fabrics (Fig. 3). The shape of each curve is largely a function of the freedom of the filaments to move when the fabric is placed under stress, and is thus a function of fabric structure.

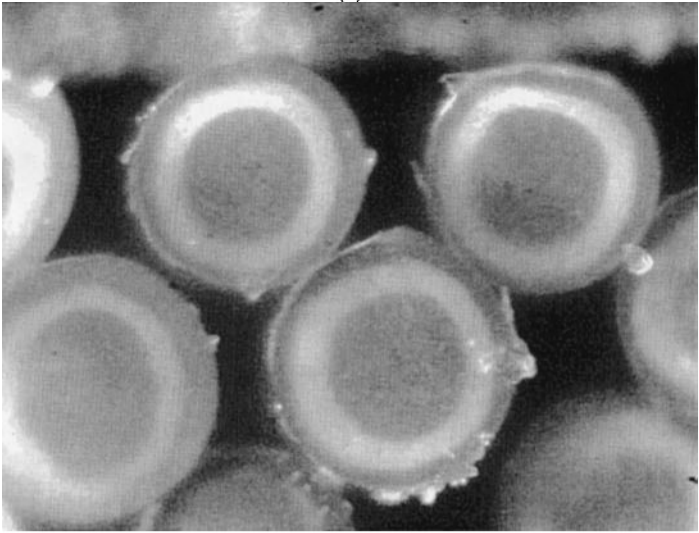
Diverse applications for the fabric sometimes demand specialized tests, such as for moisture vapor, liquid transport barrier to fluids, coefficient of friction, seam strength, resistance to sunlight, oxidation and burning, and/or comparative aesthetic properties. Most properties can be determined using standardized test procedures that have been published as nonwoven standards. Test methods adopted in the USA are published by INDA, while those adopted in Europe are published by EDANA. A comparison of typical physical properties for selected spunbonded products is shown in Table (2).

## Spinning and Web Formation

Spunbonded fabric production couples the fiber spinning operation with the formation and consolidation of the web in order to maximize productivity. It is the coupling of these processes that distinguishes the spunbonded process from traditional methods of fabric formation where fiber is first spun and collected, then formed into a fabric by a separate process such as weaving or carded into a web. If the bonding device is placed in line with spinning and web formation, the web



(a)



(b)

**Fig. 2.** Bicomponent filament structures. (a) Hollowpie; (b) sheathcore—large. Courtesy Hills Inc..

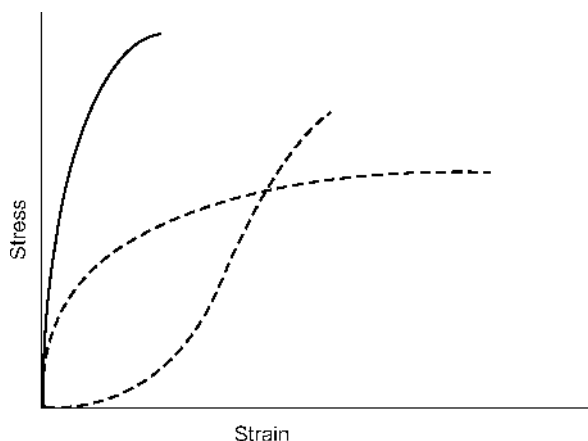


**Fig. 3.** Typical stress-strain curves of nonwoven fabrics, where (—) is woven; (---), thermally bonded nonwoven; and (- - -), needle-punched nonwoven.

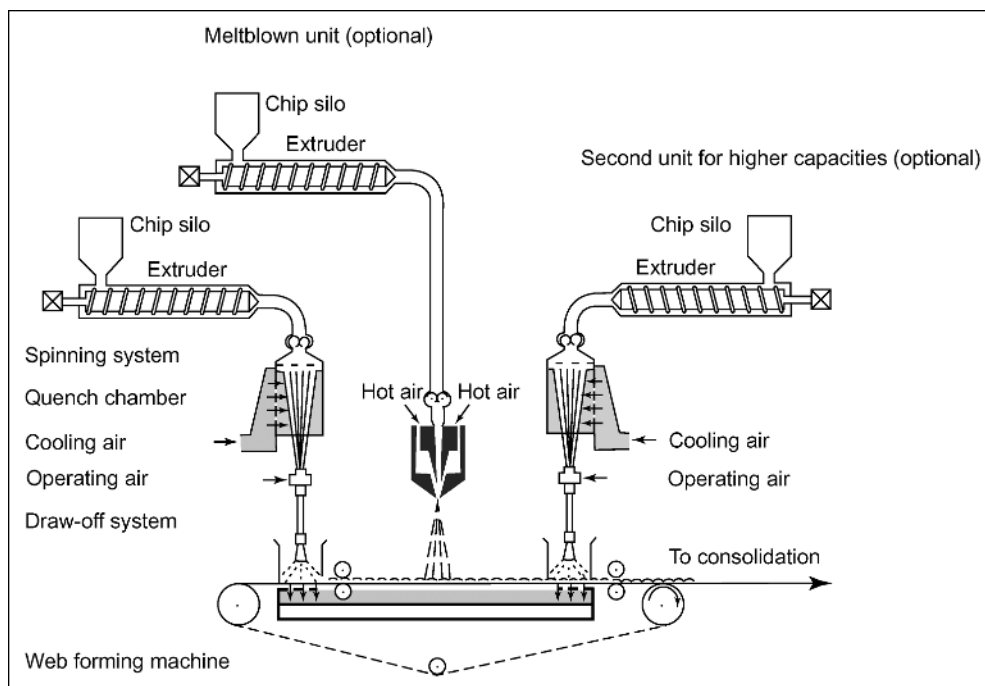


**Fig. 4.** Typical multibeam spunbonded process (3).

is converted into bonded fabric in one step (Fig. 4). In some arrangements, the web is bonded off-line in a separate step which appears at first to be less efficient; however, this offers the advantage of being more flexible if more than one type of bonding is to be performed on the web being produced. Some specialty processes also separate the spinning and the laydown steps which adds cost but provides high control on the fiber properties and ensures few breaks in laydown.

The basic spinning process is similar to the production of continuous filament yarns and utilizes similar extruder conditions for a given polymer (16). Fibers are formed as the molten polymer exits the 500 or more tiny holes (ca 0.2 mm) of each spinnerette, where it is immediately quenched by chilled air. Since a key objective of the process is to produce a relatively wide (eg, 3–4 m) web, individual spinnerettes are placed side by side in order that sufficient fibers be generated across the width. This entire grouping of spinnerettes is often called a block or bank, and in commercial production it is common for between two and four blocks, but as many as eight, to be used in tandem in order to increase the coverage and uniformity of laydown of the fibers in the web.

Most spunbond machinery producers now utilize large rectilinear spinplates in lieu of multiple small individual spinnerettes. In effect, the spinning plate is slightly wider than the desired web, and a continuous curtain of filaments is formed providing uniformity from point to point relative to multiple side-by-side spinnerettes in a block. Each spinbeam can contain up to 30,000 holes and it is common for multiple spinbeams to be used in tandem to further improve uniformity and increase throughput.

Prior to deposition on a moving belt or screen, the molten polymer threads from a spinnerette must be attenuated to orient the molecular chains of the fibers in order to increase fiber strength and decrease extendibility. This is accomplished by hauling the plastic fibers off immediately after they have exited the spinnerette. In practice, this is done by accelerating the fibers either mechanically (17) or pneumatically (17–19). In older processes, the fibers are pneumatically accelerated in multiple filament bundles; however, most new installations accelerate an entire beam or curtain of filaments (20–22).

In traditional textile spinning, some orientation of fibers is achieved by winding up the filaments at a rate of 3000–5000 m/min to produce the so-called partially oriented yarns (POYs) (23). The POYs can then be mechanically drawn in a separate step to achieve maximum strength. In spunbonded production, filament bundles are partially oriented by being pneumatically accelerated at speeds of 6000 m/min or greater (19,24). Accelerating the filaments at such great speeds not only achieves a partial orientation but results in extremely high rates for web formation, particularly for lightweight structures (eg, 15 g/m<sup>2</sup>). The formation of wide webs at high speeds results in a high efficiency of manufacture. Newer processes have been commercialized, that can accelerate filaments at speeds up to 8000 m/min and simultaneously create very small fiber deniers with high throughput (25).

For many applications this partial degree of orientation imparts a sufficient increase in strength and decrease in extendibility to make the final bonded fabric perfectly functional; eg, diaper coverstock. However, some applications, such as geotextiles and primary carpet backing, demand that the filaments achieve a very high tensile strength and low degree of extension. This requires subsequent additional attenuation, such as the mechanical drawing of filaments, a process usually accomplished over heated rolls with a typical draw ratio of ca 3.5:1 (17). After drawing, the filaments are pneumatically deposited onto a moving belt or screen. Because drawing rolls cannot normally dispatch filaments as fast as pneumatic jets, the web-forming process is usually less rapid, although the resulting web has greater physical strength.

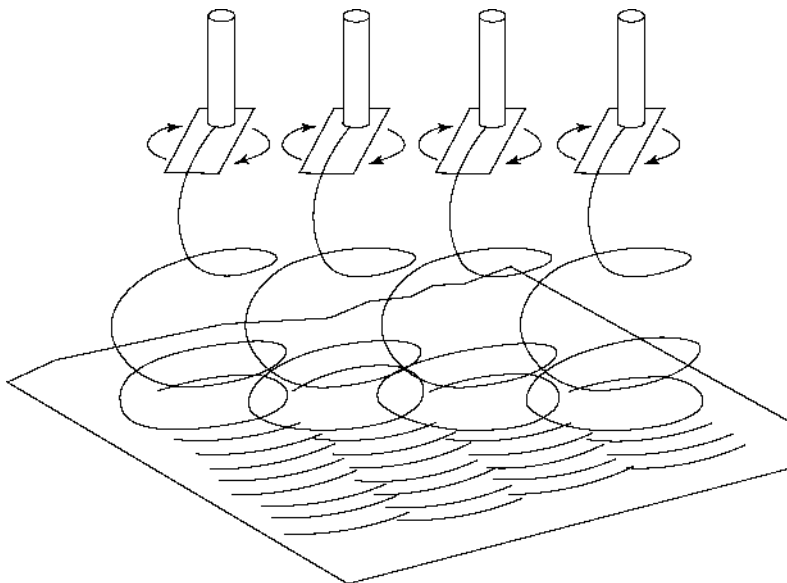


**Fig. 5.** Deflector plane for separation of filaments.

The pneumatic deposition of the filament bundles onto the moving belt results in formation of the web. A pneumatic gun uses high pressure air to move the filaments through a constricted area of lower pressure but higher velocity, as in a venturi tube. Pneumatic jets used in spunbonded production have been described (17,24). Unfortunately, the excellent filament uniformity coming out of the spinnerette is lost when the filaments are consolidated going through a gun.

In order for the web to achieve maximum uniformity and cover, it is imperative that the individual filaments be separate from each other prior to reaching the belt. Failure to sufficiently separate individual filaments results in the appearance of “ropes” in the web. One method used to effect this state of separation is to induce an electrostatic charge onto the bundle while still under tension and prior to pneumatic deposition. The charge may be induced either triboelectrically or more typically by applying a high voltage charge to the filaments (26). The level of electrostatic charge on the filaments must be at least  $30,000 \text{ esu/m}^2$  of filament surface area (16) to be effective. After deposition onto the moving belt, it is necessary to discharge the filaments; this is usually accomplished by bringing the filaments in contact with a conductive grounded surface. In some cases, the deposition belt is made of conductive wire and connected to ground. The electrostatic repulsion method has the advantage of being relatively simple and reliable. Producing webs by spinning rectilinearly arranged filaments through a so-called slot jet reduces or eliminates the need for such bundle-separating devices (20,21), because the filament bundles are not collapsed en route to the belt as they are in a pneumatic gun.

Other routes to achieving filament separation have been described and rely on mechanical or aerodynamic forces to affect separation. Figure 5 illustrates one method that utilizes a rotating deflector plane to force the filaments apart

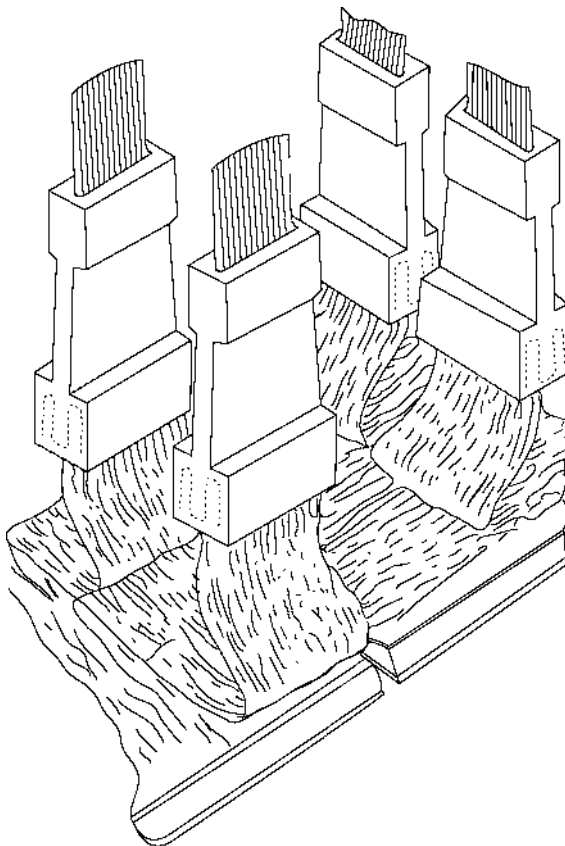


**Fig. 6.** Web production with predominantly machine and cross-machine direction.

while depositing the opened filaments in overlapping loops (27). After the splayed filaments fall to the deposition surface or forming screen, a suction from below the disposition surface holds the fiber mass in place.

For many applications, it is acceptable or desirable to lay down the filaments in a random fashion without orienting the filament bundles with respect to the direction of the laydown belt (24). However, it is sometimes desirable to control the directionality of the splayed filaments on the laydown belt in order to achieve a particular characteristic in the final fabric. Directionality can be controlled by traversing the filament bundles either mechanically (19,27) or aerodynamically (17,28) as they travel downward toward the collecting belt. The aerodynamic method consists of supplying alternating pulses of air on either side of the filaments as they emerge from the pneumatic jet. By properly arranging the spinnerette blocks and the directing jets, laydown can be achieved predominately in the desired direction. Figure 6 illustrates the production of a web with predominately machine and cross-machine direction filament laydown (17). It is possible to generate highly ordered laydown patterns by oscillating filament bundles between closely spaced plates to achieve a high degree of parallelism.

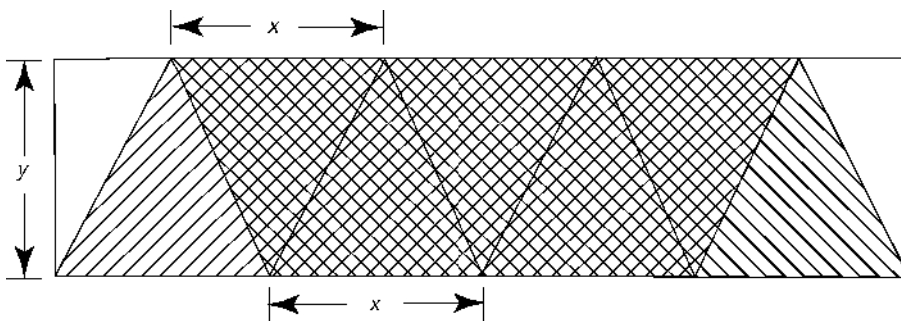


Fig. 7. Laydown pattern diagram.

If the laydown belt is moving and filaments are rapidly traversed across this direction of motion, the filaments are deposited in a zigzag or sine wave pattern on the surface of the moving belt. The effect of the traverse motion on the coverage and uniformity of the web have been described mathematically (29). The relationships between the collecting belt speed, period of traverse, and the width of filament curtain being traversed determine the appearance of the formed web upon the laydown belt. Figure 7 illustrates the laydown for a process where the collecting belt travels a distance equal to the width of the filament curtain,  $x$ , during one complete period of traverse across a belt width  $y$ . If the belt speed is  $v_b$  and the traverse speed is  $v_t$ , the number of layers deposited,  $z$ , is calculated by the formula,  $z = (x \cdot v_t)(y \cdot v_b)$ . It can be seen that if the traverse speed is twice the belt speed and if  $x$  and  $y$  are equal, then a double coverage will occur over all areas of the belt.

The alternative to the use of multiple spinnerettes per bank, and now the most widely utilized process, is the so-called curtain spin process, which utilizes a single plate of the width of the desired web which has been drilled with holes for fiber formation. The advantage to this approach is that it results in a uniform distribution of filaments within the curtain of continuous fibers produced from the spinning plate. The use of the single uniform distribution of filaments within the curtain of continuous fibers is produced from the spinning plate. The use of the single spinning plate automatically places the fibers in a uniformly distributed array and thereby presents a curtain of high uniformity filaments to the fiber attenuation mechanism. Care must be taken to keep individual filaments from sticking while they are still plastic, which is normally in the quench or cooling area between the spin plate and the laydown jet.

By comparison, the multiple spinnerette per bank process requires additional effort prior to laydown in order to compensate for the gaps between the individual spinnerettes. Failure to present a uniformly distributed filament array to the laydown screen will result in spot-to-spot variations in fiber density and a web that has the appearance of blotch.

In general, once the curtain of filaments has been produced, it is necessary to attenuate the filaments in order to provide strength and resistance to deformation. The most commonly practiced approach is to utilize a single slot, which is at least the width of the curtain, at a point below the spinning plate and above the

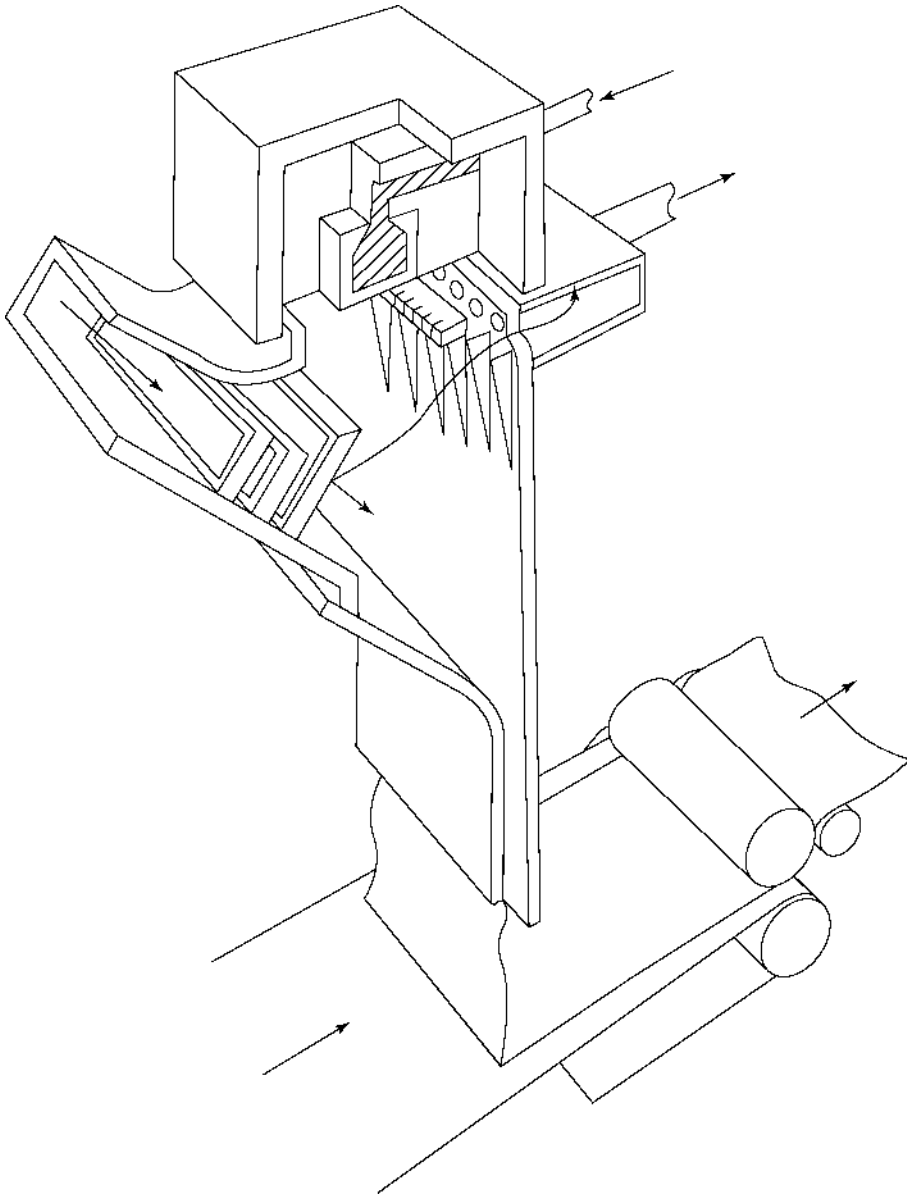


**Fig. 8.** Curtain spinning process (22).

laydown screen. There are three practical approaches taken. The first utilizes the injection of low pressure air at a point above the slot so that the fibers attain sufficient acceleration in the slot to provide adequate draw (21) (Fig. 8). The second utilizes a low pressure vacuum below a venturi to provide the pressure differential required for sufficient acceleration and resulting attenuation (30). The third utilizes an acceleration slot immediately below the spin plate with little or no quench or cooling of the filaments (25).



One of the limitations of the curtain-slot draw process has been that the amount of fiber attenuation is constrained because of the short distance generally allowed between the spinnerette and the venturi slot, and the use of relatively low pressure air for drawing so as not to induce high turbulence in the area of the laydown. In order to adapt this concept for the production of polyester fabrics that inherently require much higher fiber acceleration to attain the desired polyester fiber properties, a new process has been commercialized (25).

## Bonding

Many methods can be used to bind the fibers in the spun web. Although most procedures were originally developed for use with nonwoven staple fibers, three were adapted for use with continuous filaments: mechanical needling, thermal, and chemical/binder. Thermal and chemical-binder methods may bond the web by fusion or adhesion of fibers using either large or small regions, generally referred to as area bonding and point bonding, respectively. Point bonding results in the fusion of fibers at discrete points with fibers remaining relatively free in between the point bonds. Other methods that are used with staple fiber webs, but which are not routinely used with continuous filament webs, are stitchbonding (29,31), ultrasonic fusing (8,32), and hydraulic entanglement (33). Hydraulic entanglement is currently being developed as a high speed bonding process for spunlaid webs as a way to achieve superior softness. It has the potential to produce the most radically different continuous filament structures; however, it has the disadvantage of being a more costly and complex bonding process.

Of the three standard bonding methods used in spunbonded manufacturing, mechanical needling, also called needle punching or needle bonding, is the simplest and least expensive. Although it is the oldest process, it continues to be widely used. Significant improvements in throughput and flexibility have resulted in the sales growth of needle-bonded fabrics, particularly for geotextiles (qv) and roofing. An excellent review of mechanical needling technology has been published (29).

In the needle-punching process, a continuous filament web is subjected to barbed needles which are rapidly passed through the plane of the moving spun web (see NONWOVEN FABRICS, STAPLE FIBERS). The needles pass in and out of the web at frequencies exceeding 3,000 strokes/min that can result in as many as 500 penetrations/cm<sup>2</sup> depending on the needle density and the line speed, which can be as high as 150 m/min (34). The effect of this operation is to interlace the fibers and thus bond the structure together, relying only on the mechanical entanglement and fiber-to-fiber friction. The fabric produced tends to be more conformable and bulky than fabrics bonded by thermal or chemical/binder methods. Because the fibers have freedom to move over each other, the fabric is easily deformed and exhibits a low initial modulus (Fig. 2).

The principal variables in needle-punching are the needle design, punch density, and depth of punch. Considerable research has been conducted on the shape and design of the needles and how this affects the interlacing of the fibers (29). Needling produces a fabric that is 100% fiber with no points or areas of fusion or melting, thus it is easily adapted to most fiber webs and requires less

precise control than thermal bonding. In addition it is the only bonding method suitable for the production of spunbonded fabrics of very high basis weights, eg, 800 g/m<sup>2</sup>. It is, however, only suitable for the production of uniform fabrics greater than ca 80 g/m<sup>2</sup> because needling tends to concentrate fibers in areas resulting in loss of visual uniformity at lower weights.

Unlike mechanical needling, both thermal and chemical/binder bonding depend on fiber-to-fiber attachment as the means of establishing fabric integrity. It is the degree and extent of attachment that determines many of the fabric qualities, most notably the hand or softness. Because point bonding can be accomplished using as little as 10% bonding area, (ie, 90% unbonded area), such fabrics are considerably softer than area-bonded structures. Fiber mobility is retained, in part or in total, outside the areas of the point bonds. Thermal bonding is far more common than chemical-binder bonding and is generally more economical because the latter method adds the cost of resin and still requires a thermal curing treatment as the final step. Both area and point thermal bonding are rapid processes having line speeds in excess of 300 m/min and up to 800 m/min during production of lightweight fabrics.

Area thermal bonding can be accomplished by passing the spun web through a source of heat, usually steam or hot air. Prior to entering the bonding area, the spun web may be consolidated by passing it under compressional restraint through a heated prebonding area which adds integrity to the web (10). While in the bonder, the consolidated web is exposed to hot air or pressurized steam that causes fusion to occur between some, but not all, of the fiber crossover points. Complete fusion leads to a paper-like structure with low resistance to tearing. The spun web may contain small percentages, typically 5–30%, of a lower melting fiber (10), or the filaments may contain undrawn segments that are lower melting than the drawn or matrix segment (28). Heterofilament structures utilize a lower melting covering (sheath) on the outside of the filaments to effect fusion. Both polyethylene and nylon-6 have been used as the lower melting sheath in commercial spunbonded products.

The use of steam is generally limited to polypropylene and polyethylene fusion because impractical pressures are required to reach the temperature levels (eg, >200°C) required for bonding polyesters. In general, greater temperature control is required for area bonding polypropylene than for other polymers because the temperature difference between the matrix and binder fibers can be only 3°C (28).

Whereas thermal area bonding uses temperature as the variable to a great degree and relies on sophisticated web structures containing binder fibers, thermal point bonding utilizes both temperature and pressure to affect fiber-to-fiber fusion. Thus it is a simpler approach to bonding because it does not require the web to contain lower melting fibers or segments and is less demanding of the technology required to produce the web. Point bonding is usually accomplished by passing a web, previously consolidated or compacted with either heated or unheated press rolls, through heated nip rolls, one of which contains a raised pattern on its surface (Fig. 9). When bonding, polypropylene roll temperatures generally do not exceed 170°C; however, pressures on the raised points are quite high, preferably 138–310 MPa (20,000–45,000 psi) (35). The degree of bonding between the points can be controlled by varying the ratio of heights of the raised

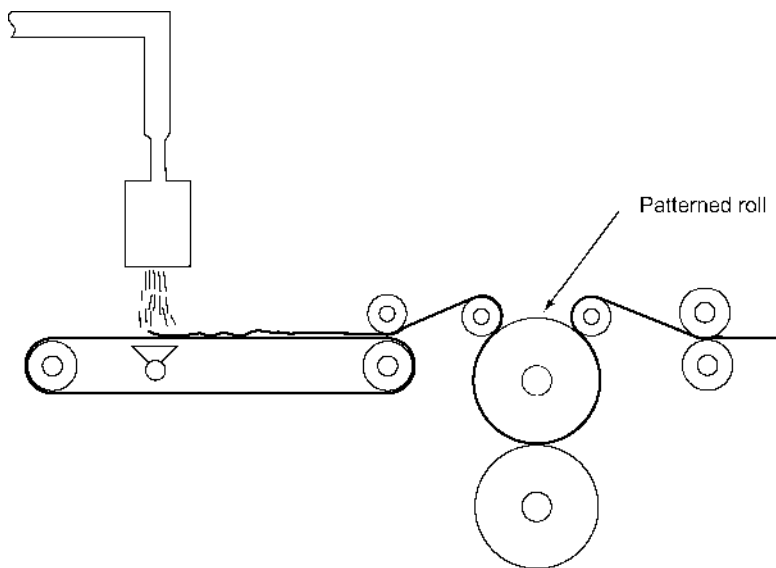


**Fig. 9.** Pattern bonding roll at the end of a spun bonding line.

points to the depth of the web (36). Typically only 10–25% of the surface available for bonding is converted to fused, compacted areas of bonding.

Optimum conditions of pressure and temperature are dependent on many variables including, but not limited to, the nature of the web, line speed, and engraved pattern. Optimized conditions are best obtained through detailed investigations and much experience. Even subtle changes in any of these variables can result in significant changes in the properties of the finished fabric (7,8). New designs for bonding calenders continue to refine the process (37).

Because engraved point bonding rolls can be as wide as 5 m, the problem of maintaining uniform pressure across the width must be addressed. Small differences in pressure across the width can produce an unacceptably variable product. Hydraulic pressure is applied at the ends to the roll causing a slight deflection that results in less pressure being applied in the center compared to the ends. A number of solutions to this problem have been devised (37), including cambering wherein the roll diameter decreases slightly from the center to the ends and mechanical means such as pressurizing the external shell of one of the two nip rollers.

Chemical–binder bonding is used less frequently than thermal bonding in the production of spunbonded fabrics, and in a shift over the past decade the same is also true for staple fiber nonwovens. Resin binders are occasionally used with spunbonded webs to achieve special characteristics that are unattainable thermally (38). In a typical case, acrylic resin(s) are applied to saturate the web, excess resin is removed by nip rolls, and the wet web is passed through a drying oven to remove excess water and cure the resin which tends to concentrate at fiber–fiber junctions. By curing the resin, a thermoset binder conveys high thermal dimensional stability to the web for applications such as roofing.

Resin binders may alternatively be applied in discreet points in a pattern so as to immobilize fewer fibers and produce a softer fabric; however, it is difficult to accurately control the diffusion of the resin, and the drying step requirements make it less attractive than thermal bonding.

Chemical bonding with hydrogen chloride gas has been used with spun webs of nylon-6,6 to commercially produce spunbonded nylon fabrics (39). In this bonding process, the activating hydrogen chloride gas is passed over web fibers held in close contact by tension. The hydrogen chloride disrupts hydrogen bonds between the polymer chains and forms a complex with the amide group. When the gas is desorbed the process reverses, this time with new hydrogen bonds formed between polymer chains in different fibers. This basic method has been further refined to permit only the formation of pattern bonds, whereby fiber mobility is retained between the bonded areas yielding a softer hand to the bonded fabric (40).

Bonding a web by any means allows for certain generalizations. If the web is highly bonded, most of the fibers are bonded to another fiber. The resulting structure is relatively stiff, paper-like, and has higher tensile and modulus but lower resistance to tear propagation. On the other hand, if the web is only slightly bonded fewer fiber-to-fiber bonds are present and the structure is more conformable with lower tensile and modulus but higher resistance to tear propagation due to bunching of filaments. Additionally, webs that are only slightly bonded exhibit low surface abrasion resistance. In comparing area to point bonding, greater varieties of structures are achievable through point bonding because of the various bonding roll patterns available. The expense associated with the manufacture of the pattern roll generally dictates the careful selection of the pattern, however.

## Meltblown Fabrics

Meltblown fabrics differ from the traditional spunbonded fabrics by having lower fiber denier (fineness) and by usually being composed of discontinuous filaments. Although meltblown fabrics are not generally referred to as spunbonded, the integration of spinning, attenuation (although slight), laydown, and bonding during the production of meltblown webs describes a process traditionally defined as spun bonding. The inherent fiber entanglement often makes additional bonding unnecessary, however. Fibers produced by melt blowing are very fine, having typical diameters of 3  $\mu\text{m}$  (41,42), smaller by nearly an order of magnitude than traditional spunbonded fibers. The fibers are extremely fine and largely unoriented, causing the webs to be quite weak and easily distorted. Most thermoplastic polymers have been meltblown, but the majority of commercial products are produced from high melt flow grade polypropylene.

In the manufacture of meltblown fabrics, a special die is used in which heated, pressurized air attenuates the molten polymer filament as it exits the orifice of the dye or nozzle (Fig. 10). Air temperatures range from 260 to 480°C with sonic velocity flow rates (43).

The rapidly moving hot air greatly attenuates the fibers as they exit from the orifices to create their small diameters. The fibers are relatively weak and

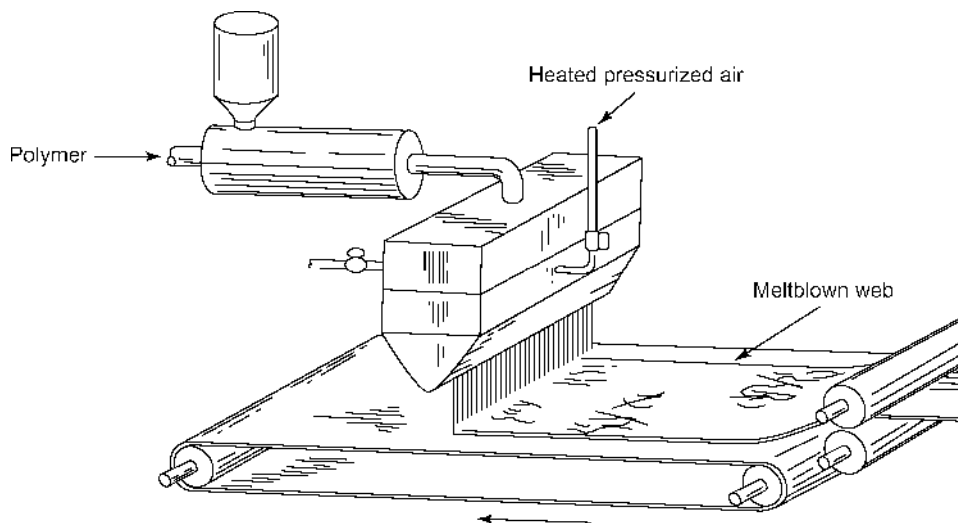


**Fig. 10.** Schematic of the meltdown process.

deposited on the forming screen as a random entangled web that may be thermally point bonded to improve strength and appearance. The web may also be deposited onto a conventional spun web, then thermally bonded. Sandwich structures, called SMS, are routinely created with the meltblown web in the middle between two conventional spunbonded webs (44). Other materials, eg, cellulose, have been blended into the meltblown filament stream to yield a meltblown structure with a unique combination of properties (45). Mixtures of meltblown and crimped bulking fibers have been sold as thin thermal insulation for use in outdoor clothing and gear (46). Meltblown technology has also been adapted to produce nontraditional spunbonded fabrics, such as elastomeric webs (47).

The great quantity of very fine fibers in a meltblown web creates several unique properties such as large surface areas and small ( $<1\ \mu\text{m}$ ) pore sizes. These have been used in creating new structures for hospital gowns, sterile wrap, incontinence devices, oil spill absorbers, battery separators, and special requirement filters. During the last decade, meltblown technology has experienced large growth mainly in the form of SMS or SMMS sandwich structures in hygiene (6).

## Flashspun Fabrics

The process of producing spunbonded webs by flash spinning is a radical departure from the conventional melt spinning approach. In melt spinning, a molten polymer is typically extruded through a spin plate containing  $\sim 20,000$  tiny holes. This produces a fiber curtain containing  $\sim 20,000$  fibers, each typically  $15\text{--}50\ \mu\text{m}$  in diameter. The fibers are kept separate from each other until the bonding operation connects some or all of them.

By contrast, flash spinning begins with a 10–15% polymer solution prepared by dissolving a solid polymer, such as high density polyethylene, with a suitable solvent, such as pentane, trichlorofluoromethane, or methylene chloride

(48). The solution is heated to approximately 200°C, pressurized to ~4.5 MPa (653 psi), and the pressurized vessel is connected to a spinnerette containing a single hole. When the pressurized solution is permitted to expand rapidly through the hole, the low boiling solvent is instantaneously flashed off leaving behind a three-dimensional film-fibril network referred to as a plexifilament. The three-dimensionality results from the cross-linking interconnection of the fine fibers which produces a film thickness of 4  $\mu\text{m}$  or less (48). Thus many individual but interconnected fibers are created from a single-hole spinnerette.

It is believed that bubbles form rapidly as the pressurized solution undergoes depressurization during spinning and the bubbles may grow and rupture, thus forming the plexifilamentary network (48). Gases that are effectively insoluble in the solvent may be added to the pressurized solution in order to facilitate high rates of bubble nucleation.

When a multiplicity of single-hole spinnerettes are assembled across a width, the plexifilaments produced can form a wide web that can be thermally bonded to produce a flat sheet structure (49). The web-forming procedure is ameliorated by use of a baffle that deflects the stream of plexifilaments after exiting the spinnerette.

Unlike fine fibers prepared by melt blowing, the plexifilaments from flash spinning are substantially oriented and possess relatively high tenacities [0.08 N/tex ( $>1\text{g} \cdot \text{f/den}$ )]. The plexifilaments scatter light effectively as a result of high surface areas (ca 2  $\text{m}^2/\text{g}$ ) and thus form opaque webs. In addition, the fineness of the plexifilament fibrils also results in a web structure of exceptional softness. Webs are either area or point bonded to yield paper- or cloth-like aesthetics, respectively. The paper-like sheets are used as durable papers and may be printed using conventional inks (qv) and printing equipment, whereas the point-bonded structures are very soft and find use in disposable protective clothing.

Flash spinning is the most complex and sophisticated method for manufacturing spunbonded fabrics. A single production line can require an investment of nearly \$200 million, and serious safety issues must be addressed in the plant's design and operation. Although the process has been in use since 1962, the need to spin heated and pressurized solutions under precise conditions has resulted in only one company (DuPont) practicing the technology as a route to these unique spunbonded products. A second producer (Asahi) stopped producing in Japan some years ago after forming a marketing joint venture with Du Pont. Hydrocarbon solvents are now being used for the process since chlorofluorocarbons, the traditional solvents, are restricted because of environmental regulations (50).

The physical properties of flashspun fabrics are unique and not attainable via the melt-spun spunbond process. Even bicomponent melt spinning cannot produce similar structures. As a result the profitability of a flashspun operation is very high when the capacity of a line is fully utilized.

## Test Methods

Spunbonded fabrics are characterized by standardized test procedures originally developed for textile fabrics and paper products. The Association of the Nonwoven Fabrics Industry (INDA) has published a list of test procedures (Table 4) (51) which are routinely used in determining specific physical characteristics of

Table 4. INDA Test Methods<sup>a</sup>

Property	Description	IST number
Absorbency	Amount of liquid absorbed and speed of absorption	10.1-3
Abrasion	Resistance of nonwovens to being worn away	20.1-5
Bursting strength	Force to rupture nonwoven under water pressure	30.1
Electrostatic properties	Amt of charge that can build up on a sample	40.1-2
Optical properties	Opacity: resistance to light being passed brightness: whiteness	60.1-2
Permeability	Ease of air or water vapor passage under pressure	70.1-2
Repellency	Resistance of nonwovens to wetting and penetration after exposure to water, salt solutions, alcohol, and hydrocarbon solvents and oils	80.1-9
Bacterial	Resistance of a nonwoven to penetration by bacteria in a salt solution under water pressure	
Stiffness		
Cantilever	Tendency for a nonlimp nonwoven to droop as it is pushed over the edge of a surface	90.1
Curly	Ability of a heavy, stiff nonwoven to push a pendulum aside as it is moved past it	90.2
Handle-O-Meter	ability of a soft, lightweight nonwoven to flex and not drag as it is pushed through an opening	90.3
Tear	Resistance of a nonwoven to continue to tear after being cut and pulled from both sides	100.1-3
Breaking load and elongation	Force to break a nonwoven when it is pulled from both ends; extent of stretching before breaking	110.1-4
Seam breaking	Force needed to break a seam holding two pieces of nonwoven together when the sample is pulled from both ends	
Bond strength of laminates	Force to separate a nonwoven from another material after they have been laminated together	
Internal bond strength	Force to pull a nonwoven fabric into two plies	120.1-2
Thickness	How thick a nonwoven is when it is held between a weight and a surface	140.1
Coefficient of friction	Drag when a nonwoven is slid over itself or over a polished surface	150.1
Dry cleaning and laundering	Shrinkage, loss of strength, ability to be peeled apart experienced by a single fabric or laminate	
Linting	Extent of particles loosened from nonwoven as it is bent and flexed in air stream	160.1
Extraction	Amt of material leached out of nonwoven after exposure to hot solvents	190.1

<sup>a</sup>Ref. 53.

spunbonded and other nonwoven fabrics. Analogous test methods are published in Europe by EDANA, the European Association of Nonwoven Fabrics. INDA and EDANA are working together to develop and publish harmonized international test procedures. Many tests are established for the evaluation of nonstrength-related properties such as washability, stiffness, and softness. Great strides have been made in the test methodology used to evaluate the hand of materials for textile applications such as clothing. A methodology and equipment, permitting quantitative evaluation of fabric hand, have been developed (52).

As applications are developed, the need for new end use specific test methods grows. Geotextile uses are a good example of how a large new application requires the design of new test methods (54). In addition to break, stretch, tear, and burst resistances described in Table 4, geotextile fabrics are tested for puncture, maximum opening size, permittivity, and asphalt retention, according to IST 180.1–9. The puncture test notes the resistance to being punctured by a probe with either a flat or spherical tip. Maximum opening measures the largest size glass beads that can pass through a fabric, thereby reflecting the size of soil particles that can be stopped by a geotextile. Permittivity is how fast water, at a given pressure, passes through a geotextile. Asphalt retention is judged by how much asphalt cement is left in a geotextile after it is dipped in the cement and allowed to drain, and what change in area the geotextile undergoes.

Long-term applications also demand test methodology on the aging characteristics of spunbonded fabrics. Roofing applications, for example, require that the saturated fabrics retain their strength for many years despite a hostile environment. By heating the fabric at several different temperatures higher than the expected nominal conditions, and measuring the time it takes to observe a significant property change, for instance loss of 50% tensile strength, effects can be plotted to permit some extrapolation back to expected nominal conditions (55). The importance of aging tests will increase as more long-term applications are developed for synthetic fabrics. The Swedish Building Institute has developed heat aging tests and standards for films and fabrics used in building construction. Canada has established a number of longevity and performance test procedures for construction fabrics, such as housewrap.

In medical applications, many test procedures have been developed for screening the efficiency of fabrics to block the passage of viruses, blood-borne pathogens, etc. Spunbonded SMS sandwich fabrics are widely used as protective gowns in hospital operating rooms because of their combination of barrier and comfort.

Overall, the test methods published by INDA (Table (4)) continue to be the general tests used to characterize fabrics; however, specific market applications often generate special test procedures to fulfill unique needs.

## **Applications for Spunbonded Fabrics**

Uses for spunbonded fabrics have traditionally been segmented into durable and disposable categories. In the early 1970s, consumption of spunbondeds was predominately for durable uses such as carpet backing, furniture, bedding, and geotextiles. By 1980, however, disposable applications accounted for an increasingly



large percentage because of the acceptance of lightweight (eg, 17 g/m<sup>2</sup>) spunbonded polypropylene fabrics as a coverstock for diapers and incontinence devices (6). In the 1990s, the use of new diaper and training pants designs have increased the demand for lightweight fabrics far beyond earlier predictions.

Both the durable and disposable markets for spunbondeds have experienced dramatic growth (~6% per year). Disposable applications utilize the vast majority of the yardage produced although only ~50% on a tonnage basis (56). Significant areas of durable growth have been in the building and construction industries where spunbondeds are used in geotextiles, roofing membranes, and Housewrap. Growth has also been achieved in primary carpet backing in automotive carpets and carpet tiles, where moldability and high dimensional stability, respectively, were achieved through the use of polyester spunbonds.

With the possible exception of Housewrap, however, there have been virtually no new markets established as a result of the special characteristics of spunbonded fabrics. Growth has come about in an evolutionary fashion where spunbonded fabrics were substituted for woven fabrics, other nonwoven fabrics (including knits), paper or film in previously existing applications, or where the cost–property relationship has permitted an extension of an existing application, such as the redesign of diapers. The principal contributions that spunbondeds have made in these markets generally have been attractive economics, or improved processibility and performance in the final product. This combination has greatly accelerated the use of the products within an application and consequently contributed to the growth of specific markets. General market opportunities for nonwovens have been reviewed (6,7,56).

Of the four basic polymer types available in spunbonded form (ie, polypropylene, polyethylene, polyester, and nylon), both polyester and nylon are more costly polymer forms than either of the olefins. It is possible for this cost advantage to be offset by other factors, such as production of the fabric in lighter unit weight, but in general olefin-based products have an economic advantage for an equivalent weight fabric. In addition, the lower density of olefinic polymers provides a greater “yield” of more fibers per unit area, which provides better cover and performance. In some applications, however, this advantage is moot if the olefin-based product cannot perform properly. An example of this is in roofing membranes where a key requirement is dimensional stability to hot bitumen at temperatures approaching 200°C, which is above the melting point of both polypropylene and polyethylene but well within the performance limits of polyester. To a great extent this one property, ie, higher temperature resistance, largely differentiates the opportunities for polyester spunbondeds versus olefinic counterparts. Although polyester fibers exhibit higher modulus and more flexible dyeing, these properties seem to be of little advantage in the markets for spunbonded fabrics.

**Spunbonded Markets: Durable Applications.** A summary of late 1990s markets for nonwoven fabrics in the United States and western Europe is shown in Figures 11, 12, and 13. Approximately 37% of total global nonwoven production for 2001 was estimated as being spunbonded (1). In North America this represents 550,000 t of spunbonded production with volume growth of 8.5% per year for the period 1996–2001 (1). The principal durable applications center around construction and automotive applications although there are other smaller areas.

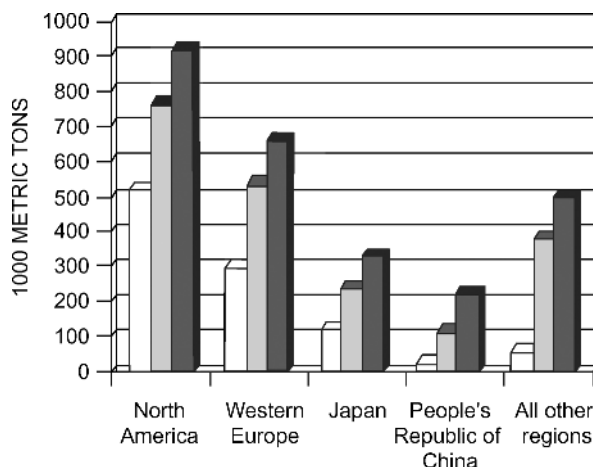


**Fig. 11.** Global demand forecast for nonwoven fabrics. □ 1988; ■ 1996; ■ 2001 (57).

One of the first durable applications was the use of spunbonded polypropylene in primary carpet backing. First introduced in the mid-1960s as a replacement for woven jute, it is still used in specialty carpets and holds a unique position in applications that require isotropic planar properties for dimensional stability such as printed or patterned carpets. The finer fiber versus woven ribbons or jute also allows tufting needles to penetrate with little deflection where fine-gauge tufting is desired. Finally, because the spunbonded backing is bonded at many fiber junctions, it offers the advantage of maintaining clean edges after cutting or trimming, making it attractive for use in small rugs where the unraveling feature of woven ribbon backings can be a concern. Although the first spunbonded primary carpet backing was made from polypropylene, other spunbonded products based on polyester and polyester-nylon were later commercialized as tuftable carpet backing products, mainly for automotive uses.

An extremely successful application for spunbonded fabrics is in the area of furniture, bedding, and home furnishings. In furniture construction the use of lower cost spunbonded fabrics has become routine, whereas in the 1970s woven sheeting dominated the market. Spunbondeds are used in hidden areas requiring high strength and support in chairs, sofas, and other seating. The bottoms of chairs are often covered with dust covers made of spunbonded fabrics because of the nonfraying characteristics, high porosity, excellent cover, and low cost. An inherent resistance to rot and mildew versus natural fabrics also adds to the popularity of spunbonded fabrics in home uses.

In bedding, spunbondeds are used as spring insulators, spring wrapping in mattress construction, dust covers under box springs, and facing cloth for quilting. Home furnishing uses include mattress pad covers where the spunbonded fabric serves as the top and bottom of a sandwich structure with a middle layer of fiberfill and fastened by ultrasonic quilting. Draperies also have used spunbonded fabrics wherein the lightweight fabric serves as a stitching medium for use with stitchbonding equipment. Spunbonded fabrics are also used in blinds, both vertical and horizontal, wherein the fabric, which must be extremely

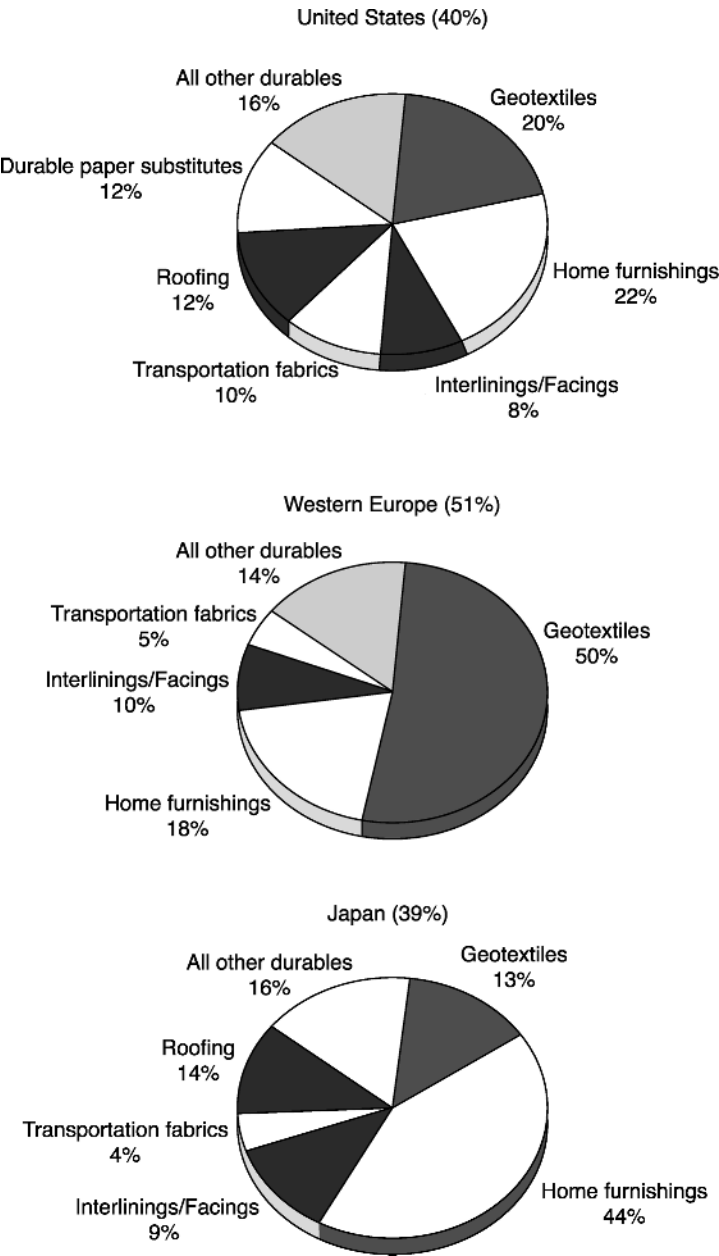


**Fig. 12.** Durable nonwovens market demand by applications and region (58).

uniform, may be saturated with colored resins to form opaque and optionally pleatable blinds.

A high growth application for spunbonded fabrics is the air infiltration barrier whereby the penultimate vertical surfaces of old or newly constructed houses are covered with a layer of spunbonded fabric followed by the application

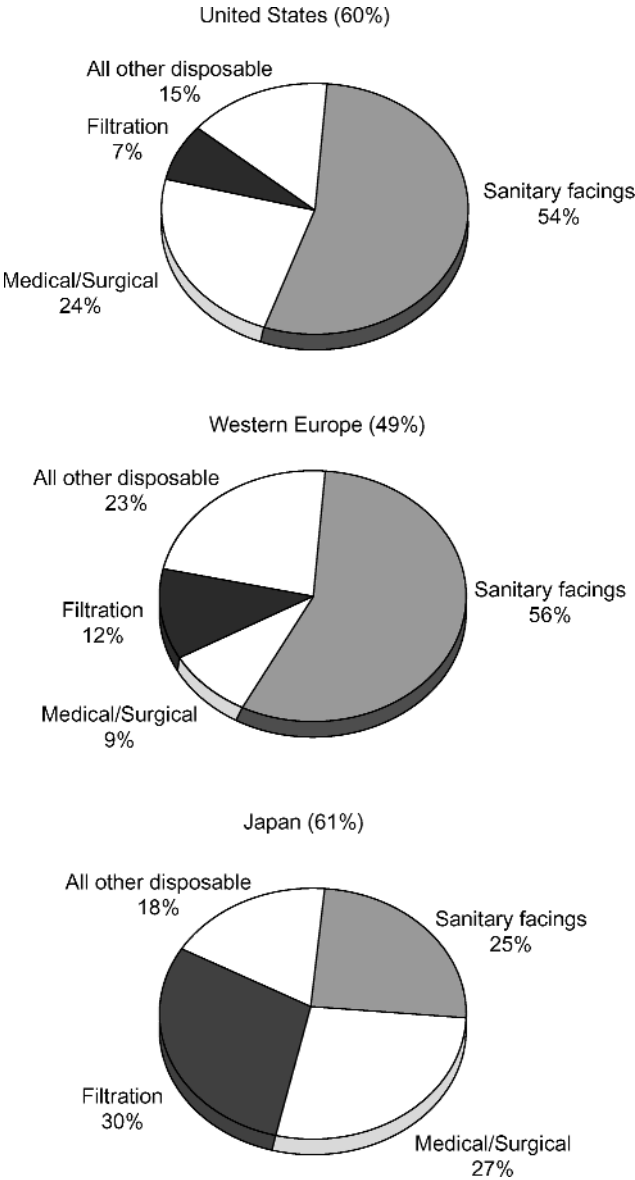


**Fig. 13.** Disposable nonwovens market demand by applications and region (59).

of the ultimate external sheathing such as siding or masonry. The objective is to construct a barrier to the infiltration of air into the wall cavity and to the insides of homes, thus lowering the cost of heating and cooling. Tests conducted by the National Bureau of Standards and the National Association of Homebuilders confirmed the effectiveness of the air infiltration barrier concept as a means of lowering the cost of heating a home (60). Certain spunbonded fabrics are well suited for this application because they possess a unique combination of

properties required for functionality. These include resistance to the penetration of liquid water and low porosity to air currents, but with a simultaneously high transport of moisture vapor. In a winter climate, warm moist air from inside the house can penetrate through the wall cavity and to the outside. If the air barrier material is not sufficiently permeable to moisture vapor, condensation can occur inside the wall cavity where damage from moisture can occur. In addition, the effective R-value of the insulation (eg, fiber glass) inside the wall cavity is diminished by the presence of liquid and solid water. Trapped moisture in wall cavities provides an opportunity for the growth of molds, a growing concern in warm moist climates. The combination of water and air current resistance combined with breathability to moisture vapor and high tensile and tear strength is a difficult combination of properties to assemble. Spunbonded technology can provide these characteristics in economical form.

Uses for nonwovens in automobiles have grown from a rather modest beginning in the 1970s to a position of significance (58). Although needle-punched nonwoven fabrics have been used in large-area applications, such as backing for vinyl seats and landau tops, spunbonded fabrics have, historically, been utilized in lower volume applications such as labels for seat belts, spring insulators, listings in seats, and as coated fabrics for ducting. Spunbonded polyester has become accepted as a tuftable backing in molded carpets where the use of spunbonded backing allows for greater molding precision, improved dimensional stability, and resistance to puncture. Newer applications include headliners, which are often complex composites that can be molded into sophisticated shapes. Lightweight spunbonds are used as sound insulators in between dashboard components, and as the base fabric in interior door panels and sun visors.

Material acceptance in roofing applications has changed significantly since the mid-1970s, particularly for spunbonded fabrics. The market opportunity is extremely large and is thought to exceed  $1.86 \times 10^8 \text{ m}^2$  for commercial buildings (flat roofing) in the United States alone. Much of the development for roofing applications was done in Europe and slowly became accepted in the United States. Although fiber glass fabrics have been the largest volume nonwoven consumed in roofing, spunbonded polyester and polypropylene have made considerable penetration (61). A significant difference between glass and polyester is the ability of polyester to flex and stretch without damage to the filaments. Because rooftops are known to expand and contract with seasonal changes, fabrics of polyester are less susceptible to damage from sudden temperature fluctuations which induce rapid dimensional changes.

Spunbonded polyester is basically a carrier for bituminous waterproofing membrane. Here spunbonded fabric is saturated with bitumen and serves to provide integrity and dimensional stability to the bitumen. As bitumen coatings modified with elastomeric polymers, such as atactic polypropylene (APP) or sequenced butadiene-styrene (SBS), became accepted as improvements over unmodified bitumen, changes occurred in the installation and manufacture of membranes. Historically, built-up roofs were made *in situ* by mopping hot bitumen into organic felts that had been placed on the roof decking. In the 1990s, the roof membrane was manufactured under tightly controlled conditions in a factory distant from the site of application. The spunbonded fabric is typically saturated with modified bitumen by dipping into tanks of hot bitumen which are heated up to

200°C. Excess bitumen is metered off and the cooled surfaces are coated with a release material such as talc to prevent blocking together on the roll. The composite is packaged into rolls approximately 1 m wide and 50 m long. The rolls are then shipped to the job site and applied to the flat roof surface by slowly unrolling while heating the underside to tackiness with a propane torch to enable it to adhere to the roof deck. Adjacent rolls are lap seamed to provide for watertightness across the roll width of the roof. Spunbonded polyester is also used in the so-called cold roof method, typically used for roof maintenance. In this method, a cold mastic is applied over a fiber glass base sheet, followed by more mastic, another layer of polyester, more mastic, and a final topcoat.

In Europe, particularly France and Germany, bitumen-coated spunbonded polypropylene fabrics are widely accepted as rooflinings under concrete, clay, or ceramic tiles for pitched-roof construction. In this use, the spunbonded fabric is a critical element of the membrane because the rooflining is draped between roof rafters and depends on the strength of the spunbonded for self-support during the life of the roof. The bitumen coating renders the spunbonded waterproof and allows it to shed any water that might leak between the tiles during snow and rainstorms. Spunbonded fabrics coated with nonbituminous materials such as acrylics have also been used in Europe. Rooflinings represent a considerable opportunity for spunbonded fabrics in Europe and in the sunbelt areas of the United States.

Nonwoven fabrics have played an important part in the development of geotextile applications. Needle-punch fabrics manufactured from either staple fibers or spunbonded continuous filaments have found worldwide acceptance on the basis of field performance. In 2000, it is estimated that North America consumed approximately 300 million m<sup>2</sup> of geotextiles (62).

Many fabric manufacturers have dedicated considerable effort to the marketing of their products in order to participate in this growth area. Geotextile fabrics function by being porous to water but not to the fines of the soil, thereby permitting them to effectively separate or partition soil fines from other elements. The net effect is keeping the soil from eroding or moving position. For example, in the construction of a new road the geotextile can separate the subsoil from the gravel or aggregate. By maintaining this separation, the aggregate is not driven into the subsoil base by the weight of vehicles nor are soil fines pumped up into the aggregate since the geotextile filters out their passage. However, water is freely transported through the fabric, enabling proper drainage without buildup of hydrostatic pressures. Thus the road resists rutting and sustains the weight of traffic more effectively while permitting proper drainage of water through the fabric. In drainage ditches, perforated drainage pipes are often wrapped with a geotextile prior to installation to prevent them from becoming clogged.

Spunbonded fabrics are effective filters in that they are layered structures of relatively fine fibers, the three-dimensional structure of which creates a tortuous path. Even relatively thin spunbonded fabrics (eg, 0.2–0.25 mm) present a significant challenge to the passage of soil fines and are suitable for use in some filtration applications. The porosity of geotextile fabrics is classified by means of several procedures such as flux (volume flow/area per time) and equivalent opening size (EOS), which is a measure of the apparent pore size of the openings in the fabric. The flux measures the porosity to liquid water, and the EOS measures

the porosity to solid particles of a known diameter. Literature is available on limitations of particular styles of fabrics within an application.

Growing university research ensures that users and specifiers will continue to become more sophisticated in their methodology and more demanding of manufacturers. Excellent textbooks are available for both students and practicing engineers (53,63).

A growing use for spunbond fabrics is in landscaping where lightweight (eg, 70–100 gsm) fabrics are sold as landscape fabrics for weed control. Typically these fabrics are placed in landscape beds over the soil and covered with stones or mulch where they resist the emergence of weeds from the soil while allowing water to drain through into the soil. They will not, however, prevent seed germination in the mulch, and they should be viewed as only a partial solution for weed control.

Other durable applications such as interlinings and coating/laminating substrates do not appear to offer much near-term opportunity for growth for spunbonded fabrics. In interlinings, however, spunlaced nonwovens have received wider acceptance because of the outstanding drape and softness, previously unavailable from any other fabric.

Spunbonded fabrics have a relatively small percentage of the coated fabric market which is dominated by other nonwovens. Needle-punched nonwovens offer more of the bulk and resiliency required for functionality in automotive and furniture seating.

Many filtration requirements are fulfilled by spunbonded structures, and a growing but technically complex market has developed since the 1970s (64). Applications include pool and spa, air particulate, coolant, milk, and sediment for household water.

A recent development is the automatic shaping of heavyweight spunbonded and needlepunched fabrics into three-dimensional honeycomb-shaped structures that allows, for the first time, the use of spunbonded fabrics as a three-dimensional solid object (65). This platform process opens up vast new applications previously unreachable by the two dimensional nature of these fabrics. Spunbond fabrics can be automatically converted into products as diverse as mattresses, sandwich panels, air-flow straighteners, sand walls for temporary dikes, and drainage containment blocks. There is high interest in third world areas for the very inexpensive mattresses that can be produced from spunbond lines already in place in these areas. This process holds promise to open up large new markets for existing spunbonded fabrics.

**Spunbonded Markets: Disposable Applications.** The outlook for spunbonded disposable applications indicates a 5–7% compounded annual growth forecast (1,6). Spunbonded plant capacity installed or announced since the 1980s has been aimed at satisfying increased demand largely for disposable applications. Key markets are components for baby diapers, training pants, incontinence devices, surgical gowns and drapes, medical sterilization wrap, protective clothing, and envelopes (see Fig 13, Ref. 69).

The use of spunbonded fabrics as coverstock for diapers and incontinence devices has grown dramatically since 1980, and by 1995 consumption exceeded 2 billion m<sup>2</sup> in the United States and is forecast to reach 3.5 billion within five years (67). A coverstock functions as a one-way medium through which urine is

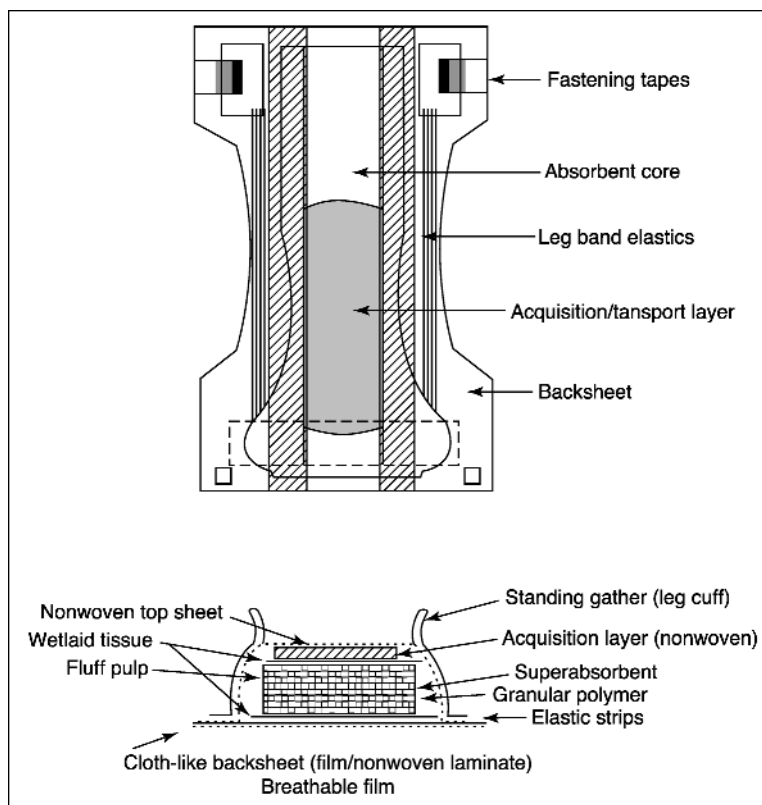


**Fig. 14.** Components of a modern disposable diaper (56).

transported into the absorbent core. The laminar structural feature of the coverstock helps keep the skin of the user dry and comfortable. Figure 14 shows the uses of nonwovens in a premium price diaper (68). Although  $17 \text{ g/m}^2$  spunbonded polyester was originally used in diaper coverstock, it has been supplanted entirely by 15–17 gsm weight spunbonded polypropylene.

Changes in diaper design have made disposable diapers among the most highly engineered disposable products in the world, and involve not only coverstock but the nature of the absorbent layer and design of the diaper itself. The use of form-fitting legs with leg cuffs for leak protection, as well as refastenable closures, has accelerated the acceptance of disposable diapers for both infants and adults. Spunbonded fabrics are used in several major components of the diaper, including coverstock, leg cuffs, and backsheet (68). Spunbonded coverstock is also widely used in feminine napkins and, to a limited extent, in tampons. The conversion of eastern European countries to market economies has created increasing demand for disposable diapers and consequently spunbonded polypropylene coverstock. Other areas of the world showing higher penetration of disposable diapers are South America and China.

The uses of spunbonded fabrics as fabrics in diapers and other personal absorbent devices will most likely remain unchallenged for the near term.



Virtually any other nonwoven production method appears to be at a cost disadvantage opposite spunbonded polypropylene. Perforated films lack tactile feel and are largely limited to use in feminine napkins. There have been composite products developed from meltblown and spunbonded combinations, generally where improved hydrophobicity is desired. These products can be produced on-line at relatively low additional cost and offer high value to diaper manufacturers.

In medical applications, great progress has been made in the substitution of traditional reusable woven materials with higher performing spunbondeds (69). Historically, flashspunbonded polyethylene was the first 100% spunbonded to find limited acceptance in medical uses such as disposable operating room gowns, shoe covers, and sterilizable packaging. Other spunbonded fabrics of polypropylene or nylon found some acceptance as cellulosic composites with the lightweight spunbonded serving to add physical strength to the composite. Over the last decade, composite structures of spunbond-meltblown-spunbond polypropylene (SMS) have gained wide acceptance in operating room gowns and sterilizable (CSR) wrap. Structures made of spunlaced polyester-cellulose are also widely used but have lost market share to SMS because of the higher barrier of SMS.

Operating room gowns worn by members of the surgical team place very high demands on fabric properties. Key requirements include breathability for comfort, low noise, absolute barrier to fluid penetration, low particle generation (linting), sterilizability, and impermeability to bacteria and viral particles. Woven cotton fabric gowns were worn for many years but had to be reused because of high cost. This required the added expense of laundering the garments and the need to decide when each garment was no longer suitable for use in the operating room. Several studies comparing disposable and reusable fabrics have been conducted in an attempt to correlate the effect of fabric linting with post-operative infections. Although no correlation has yet been established, some studies have demonstrated that single-use fabrics generate significantly fewer particles than cotton fabrics (70). Other studies have indicated that the rate of postoperative wound infection is reduced with the use of high barrier spunbonded olefin gowns and drapes. Concern for viral transmission (eg, AIDS) has increased the demand for disposable, higher barrier fabrics without loss of comfort.

Medical devices or trays of devices are often sterilized after the nonsterile device is sealed in a package. A part of this package, such as the lid, is made from flashspun or spunbonded/meltblown fabric because it possesses the unique property of permitting the sterilizing gas of ethylene oxide to pass through while remaining impenetrable to bacteria. These fabrics are manufactured to tightly controlled standards to ensure the highest resistance to bacterial/viral penetration. The superiority of a spunbonded fabric to the alternative coated papers has been reviewed (71).

Spunbonded fabrics have been utilized as shoe covers in the operating room. The covers are usually sewn with an elastic band at the top to allow them to be held snugly in place. The fabric requirements are toughness, some porosity for comfort, nonlinting, resistance to slippage, and a nonstatic characteristic. In order to achieve the last property, the fabric is usually treated with an antistatic coating. Failure to use a nonstatic fabric may cause sparks to be generated in the operating room environment, which could damage sensitive electronic devices or lead to fire. Other medical applications for spunbonded fabrics include

head covers, face masks, drapes, and other uses requiring breathable/barrier properties.

A large-volume area for spunbonded fabrics is the disposable protective clothing market (72). To a great extent the demand for high performance disposable protective clothing has tracked high technology manufacturing, environmental demands, and more recently the concern from biological or chemical terrorism. The manufacture of particulate sensitive electronic components, such as silicon chip integrated circuits, resulted in the construction of clean rooms where the generation of any particulate was in part controlled through the use of nonlinting yet comfortable clothing made from spunbonded fabrics. Because the spunbonded fabrics are made of continuous filaments, practically no linting results. At the same time the structure allows the passage of moisture and air, thus helping the wearer to remain comfortable. The spunbonded garment is worn over other clothing; therefore the maximum pore size must be sufficiently small to prevent the passage of lint and other particles through the garment and into the clean room.

The 1980s saw the beginning of the removal of large quantities of asbestos (qv) from schools and buildings, creating the need for clothing which could not be penetrated by small asbestos fibrils, yet inexpensive enough to permit daily disposal. Certain spunbonded and spunbond/meltblown laminate fabrics demonstrate excellent resistance to asbestos penetration from particles as small as  $0.5\ \mu\text{m}$ .

Similarly the handling of hazardous materials has prompted the need for affordable, disposable protective clothing. Once exposed to toxic waste, pesticides, or radioactive materials, the clothing itself is transformed into a hazardous material and must be disposed of to prevent spreading of contamination. Garments that demand the utmost in protection at the lowest price are often made by extrusion coating, laminating spunbonded fabrics with polyethylene, or laminating the fabric to poly(vinylidene chloride) film.

Packaging applications for spunbonded fabrics are for the most part a specialty area in which paper products or plastic films do not adequately perform. One of the largest packaging applications for spunbonded fabric is high performance envelopes. Although lightweight tear- and puncture-resistant envelopes are not in demand by individual consumers, both large and small businesses have found spunbonded envelopes to outperform those made from conventional paper products. The lighter weight of the spunbonded envelope allows for postal savings, and some corporations specializing in overnight delivery have successfully used spunbonded envelopes with excellent results. Coated spunbonded fabrics are used as the outerwrap of coils of steel and aluminum where they outperform alternative materials such as films and papers.

A significant percentage of U.S. synthetic staple fiber production is packaged in bales of extrusion coated spunbonded fabrics, so treated to render the fabric impervious. Synthetic fibers have been shipped worldwide in this manner with great success.

Although other nonwoven processes such as spunlacing have experienced large growth in disposable wipes, spunbonded fabrics have not participated in this segment generally because some cellulosic fibers are required in the wipe and spun bonding cannot readily utilize such fibers.

A reverse-wipe application is seen in the clothes dryer fabric softener sheet wherein the spunbonded fabric is coated with a complex combination of wax, surfactants, and perfumes which are released into the environment of a hot clothes dryer to soften and perfume the clothes, as well as provide an antistatic quality. The spunbonded sheet, which must be made of polyester or nylon for temperature resistance, provides a simple and cost-effective medium to store the chemical compounds prior to release in the dryer.

There are many other smaller specialty disposable applications for spunbonded fabrics which vary widely from country to country. These applications include candy wrapping, agricultural coverings, wall covering, and packaging.

## BIBLIOGRAPHY

"Nonwoven Fabrics, Spunbonded" in *EPSE* 2nd ed., Vol. 10, pp. 227–253, by Ronald L. Smorada, Reemay, Inc.; in *EPST* 3rd ed., Vol. 10, pp. 578–614, by R. S. Smorada, Versacore Industrial Corporation.

## CITED PUBLICATIONS

1. T. Wirtz, in *12th Annual TANDEC Conference*, Nov. 19–21, 2002, Knoxville, Tenn.
2. R. L. Smorada, *INDA J. Nonwovens Res.* **3**(4) (Fall 1991).
3. D. T. Ward, *ITB Nonwovens Ind. Text.* 27–33 (Feb. 1998).
4. K. Ohmura, *Nonwovens Ind.* **36** (Nov. 1999).
5. K. Ohmura, *Nonwovens Ind.* **26** (July 2002).
6. J. R. Starr, *Nonwovens World* 68–73 (Feb.–Mar. 1999).
7. *Nonwovens World* **5**(1), 16 (Jan. 1990).
8. *Nonwovens Ind.* **24**(10), 54–63 (Oct. 1993).
9. *Guide to Nonwoven Fabrics*, INDA, Cary, N.C., p. 24.
10. U.S. Pat. 3,989,788 (Nov. 2, 1976), L. L. Estes, A. F. Fridrichsen, and V. S. Koshkin (to Du Pont).
11. Brit. Pat. 1,157,437 (July 9, 1969), B. L. Davies (to ICI Ltd.).
12. J. Hagwood, in *12th Annual TANDEC Conference*, Nov. 19–21, 2002, Knoxville, Tenn.
13. Y. Ogawa, *Spunbonded Technology Today 2*, Miller-Freeman, San Francisco, 1992, p. 123.
14. U.S. Pat. 3,439,085 (Apr. 15, 1969), L. Hartmann (to C. Freudenberg).
15. U.S. Pat. 6,225,243 (May 1, 2001), J. Austin (to BBA Nonwovens).
16. U.S. Pat. 3,338,992 (Aug. 29, 1967), G. A. Kinney (to E. I. du Pont de Nemours & Co., Inc.).
17. U.S. Pat. 3,991,244 (Nov. 9, 1976), S. C. Debbas (to E. I. du Pont de Nemours & Co., Inc.).
18. Brit. Pat. 1,436,545 (May 19, 1976), J. Brock (to ICI Ltd.).
19. U.S. Pat. 4,017,580 (Apr. 12, 1977), J. Barbey (to Rhône-Poulenc).
20. U.S. Pat. 3,502,763 (Mar. 24, 1970), L. Hartmann (to C. Freudenberg).
21. U.S. Pat. 4,405,297 (Sept. 20, 1983), D. W. Appel and M. T. Morman (to Kimberly-Clark Corp.).
22. U.S. Pat. 5,545,371 (Aug. 13, 1996), F. Lu (to Ason Engineering Inc.).
23. U.S. Pat. 3,771,307 (Nov. 13, 1973), D. G. Petrille (to E. I. du Pont de Nemours & Co., Inc.).
24. U.S. Pat. 3,692,618 (Sept. 19, 1972), O. Dorschner, F. Carduck, and C. Storkebaum (to Metallgesellschaft AG).
25. U.S. Pat. 6,183,684 (Feb. 6, 2001), F. Lu (to Ason Engineering Inc.).

26. U.S. Pat. 5,225,018 (July 6, 1993), L. M. Zeldin, R. E. Lamkin, and J. E. Werner (to Fiberweb North America).
27. U.S. Pat. 4,163,305 (Aug. 7, 1979), V. Semjonow and J. Foedrowitz (to Hoechst AG).
28. U.S. Pat. 3,322,607 (May 30, 1967), S. L. Jung (to E. I. du Pont de Nemours & Co., Inc.).
29. H. Külter, in J. Lunenschloss and W. Albrecht, eds., *Non-Woven Bonded Fabrics*, Ellis Horwood Ltd., Chichester, U.K., 1985, p. 178.
30. U.S. Pat. 4,813,864 (Mar. 21, 1989), H. Balk (to Reifenhauser GmbH).
31. R. G. Mansfield, *Textile World* (June 2002).
32. J. Neuwirth, *Nonwovens World* 136–139, April–May 2002.
33. K. Völker, *Nonwovens World* 97–103, Apr.–May 2002.
34. K. Bitz, *Nonwovens Ind.* 45–50 (Feb. 2002).
35. U.S. Pat. 3,855,046 (Dec. 17, 1974), P. B. Hansen and L. B. Pennings (to Kimberly-Clark Corp.).
36. U.S. Pat. 3,855,045 (Dec. 17, 1974), R. J. Brock (to Kimberly-Clark Corp.).
37. I. H. Doring, *Ind. Text.* 51–52 (Dec. 2000).
38. U.S. Pat. 4,125,663 (Nov. 14, 1978), P. Eckhart (to Hoechst AG).
39. U.S. Pat. 3,542,615 (Nov. 24, 1970), E. J. Dobo, D. W. Kim, and W. C. Mallonee (to Monsanto Corp.).
40. U.S. Pat. 3,322,607 (May 30, 1967), S. L. Jung (to E. I. du Pont de Nemours & Co., Inc.).
41. J. R. Collier and co-workers, in *12th Annual International TANDEC Conference*, Nov. 19–21, Knoxville, Tenn.
42. E. Schwartz, in *32nd Clemson Nonwovens Fabrics Forum*, June 25–28, 2001, Clemson Univ., Clemson, S.C.
43. U.S. Pat. 3,972,759 (Aug. 3, 1976), R. R. Buntin (to Exxon).
44. U.S. Pat. 4,374,888 (Feb. 22, 1983), S. R. Bornslaeger (to Kimberly-Clark Corp.).
45. U.S. Pat. 4,100,324 (July 11, 1978), R. A. Anderson, R. C. Sokolowski, and K. W. Ostermeier (to Kimberly-Clark Corp.).
46. U.S. Pat. 4,118,531 (Oct. 3, 1978), E. R. Hauser (to 3M Co.).
47. Y. Ogawa, *Nonwovens World* 79–81 (May–June 1986).
48. U.S. Pat. 3,081,519 (Mar. 19, 1963), H. Blades and J. R. White (to E. I. du Pont de Nemours & Co., Inc.).
49. U.S. Pat. 3,442,740 (May 6, 1969), J. C. David (to E. I. du Pont de Nemours & Co., Inc.).
50. U.S. Pat. 5,081,177 (Jan. 14, 1992), H. Shin (to E. I. du Pont de Nemours & Co., Inc.).
51. *Nonwoven Fabrics Handbook*, INDA, Cary, N.C., pp. 77–79.
52. S. Kawabata, *The Standardization and Analysis of Hand Evaluation*, 2nd ed., Textile Machinery Society of Japan, Osaka, Japan, 1980.
53. *Standard Test Methods Manual*, INDA, Cary, N.C., pp. 168–177.
54. R. M. Koerner, *Designing with Geosynthetics*, 4th ed., Prentice-Hall, Englewood Cliffs, N.J., 1999, pp. 93–146.
55. Ref. 54, p. 137.
56. K. Shariq, *Nonwovens World* 90–96 (Winter 1998).
57. Ref. 56, p. 90.
58. Ref. 56, p. 94.
59. Ref. 56, p. 93.
60. *Du Pont Tyvek Literature*, Bulletin E-60658.
61. C. E. Frei, *Nonwovens Ind.* 56–60 (Oct. 1999).
62. C. E. Pelc, *Nonwovens Ind.* p. 42 (Oct. 2000).
63. A. A. Balkema, in R. Veldhuijzen Van Zanten, ed., *Geotextiles and Geomembranes in Civil Engineering*, Rotterdam/Boston, Mass., 1986.
64. C. E. Pelc, *Nonwovens Ind.* pp. 30–36 (Nov. 2000).

65. R. L. Smorada, *Nonwovens World* pp. 49–52 (Feb.–Mar. 2002).
66. D. K. Smith, *Nonwovens World* pp. 64–70 (Winter 1998).
67. P. Hannah, *Nonwovens World* pp. 79–86 (Winter 1998).
68. C. White, *Nonwovens Ind.* pp. 26–39 (Jan. 1999).
69. D. K. Lickfield, *Technical Text. Technol.* pp. 18–20 (Mar. 2003).
70. S. P. Scheinberg, J. H. O'Toole, and S. K. Rudys, *Partic. Microbiol. Cont.* (July/Aug. 1983).
71. Th. Mengen and A. Jordy, in *8th Symposium of the Austrian Society for Hygiene, Microbiology and Preventative Medicine*, Vienna, Austria, 1984.
72. A. Teng, *Nonwovens Ind.* pp. 38–44 (Mar. 2003).
73. Arthur D. Little Report C87352 (May 1982).

RONALD S. SMORADA  
Versacore Industrial Corporation

## NONWOVEN FABRICS, STAPLE FIBERS

### Introduction

A nonwoven fabric is a textile structure made from fibers, without a yarn being first made; knitted and woven fabrics, require yarns. A nonwoven fabric normally comprises a network of fibers or continuous filament yarns strengthened by mechanical, chemical, or thermally interlocking processes. Examples are bonding with binders such as latex polymers, needling, hydroentanglement, and stitch-bonding.

**History.** Johnson and Johnson became involved in nonwovens in the 1930s (1). After 10 years of experimentation its nonwovens department became part of Chicopee Manufacturing Corp. Viscose rayon was used to make a wide range of products including bedpads, surgical towels, disposable diapers, sanitary napkins, and wiping cloths. In the 1970s water jets were being used to bond fibers together to make surgical gauze.

Other companies with an early involvement in developing nonwovens to replace textiles include Avondale Mills, Kimberly-Clark, The Kendall Co., and the West Point Manufacturing Co. Freudenberg started trying to make a leather substitute in the 1930s (2).

The spunbond process transforms polymer directly to fabric by extruding filaments, orienting them as bundles or groupings, layering them on a conveying screen, and interlocking them by thermal fusion, mechanical entanglement, chemical binders, or combinations of these. The technology was developed by Freudenberg and DuPont in the 1950s (see NONWOVEN FABRICS, SPUNBONDED).

Meltblown fabrics are also made directly from thermoplastic resins. Polymer granules are melted and extruded. As soon as the melt passes through the extrusion orifice, it is blown with air at high temperature. The airstreams attenuate the molten polymer and solidify it into a random array of very fine fibers. The fibers are then separated from the air stream as a randomly entangled web and

compressed between heated rolls. The combination of fine-diameter fibers, random entanglement, and close packing results in a fabric structure with a large surface area and many small pores.

After the development of spunbonded and meltblown processes, combined systems such as SMS (spunbonded/meltblown/spunbonded) were developed to combine the benefits of each fabric type. In the late 1990s bicomponent spunbonded technology was introduced.

**Definitions.** The Textile Institute defines nonwovens as “textile structures made directly from fibre rather than yarn. These fabrics are normally made from continuous filaments or from fibre webs or batts strengthened by bonding using various techniques: these include adhesive bonding, mechanical interlocking by needling or fluid jet entanglement, thermal bonding and stitch bonding.”

The ISO 9092 definition is as follows: “A manufactured sheet, web or batt of directionally or randomly orientated fibres, bonded by friction, and/or cohesion and/or adhesion, excluding paper and products which are woven, knitted, tufted, stitch-bonded incorporating binding yarns or filaments, or felted by wet-milling, whether or not additionally needled. The fibres may be of natural or manufactured origin. They may be staple or continuous filaments or be formed in situ.” Various notes are included in this definition including clarification on the difference between a wet-laid nonwoven and a wet-laid paper—in essence, the difference depends on the presence of a substantial proportion of fibers.

Nonwoven structures need not be considered as substitutes for knitted or woven fabrics—they are a class in their own, enabling a unique range of engineered properties and aesthetics to be achieved.

## Nonwoven Processes

The basic concept employed in making a nonwoven fabric is to transform fiber-based materials into two-dimensional sheet structures with fabric-like properties. These are flexibility, porosity, and mechanical integrity. Their manufacturing processes can be split into four groups: dry-laid webs, extrusion-formed webs, wet-laid webs, and web-bonding.

**Dry-Laid Processes.** These include mechanical, eg carded, and aerodynamic, eg air-laid routes. Dry-laid nonwovens are made with staple fiber processing machinery such as cards and garnetts, which are designed to manipulate staple fibers in the dry state. Also included in this category are nonwovens made from filaments in the form of tow, and fabrics composed of staple fibers and stitching filaments or yarns, ie, stitchbonded nonwovens.

**Extrusion-Formed Webs.** Examples include spunbonded and meltblown. Extrusion technology is used to produce spunbond, meltblown and porous-film nonwovens. These fabrics are made with machinery associated with polymer extrusion methods such as melt-spinning, film casting and extrusion coating (see EXTRUSION).

**Wet-Laid Processes.** Papermaking technology is used to process wood pulp fibers, synthetic fibers longer than wood pulp, and other fibers that differ in other ways from pulps. Included in this category are methods for producing dry-laid pulp and wet-laid nonwovens. These fabrics are made with machinery

associated with pulp fiberizing, such as hammer mills, and paperforming, ie slurry pumping onto continuous screens which are designed to manipulate short fibers in a fluid.

**Web-Bonding Processes.** These can be split into chemical and physical. Chemical bonding refers to the use of water-based and solvent-based polymers to bind together the fibrous webs. These binders can be applied by saturation (impregnation), spraying, printing, or application as a foam. Physical bonding processes include thermal processes such as calendering and hot air bonding, and mechanical processes such as needling and hydroentangling.

The various nonwoven processes and the fabrics made from each have a number of common characteristics. In general, textile technology-based processes provide maximum product versatility, because most textile fibers and bonding systems can be utilized and conventional textile web processing equipment can be readily adapted at minimal cost. Extrusion technology-based processes provide somewhat less versatility in product properties, but yield fabric structures with exceptional strength-to-weight ratios, as is the case with spunbonds; high surface area-to-weight characteristics, a benefit of using meltblown technology; or high property uniformity per unit weight, as is the case with textured films, at modest cost.

Paper technology-based nonwoven processes provide the least product versatility and require a high investment at the outset, but yield outstandingly uniform products at exceptional speeds. Hybrid processes provide combined technological advantages for specific applications.

## Fibers for Nonwovens

Nonwoven fabrics made directly from polymers are discussed elsewhere. The properties of nonwoven fabrics are highly influenced by the properties of their constituent fibers.

Technically, a fiber is a material characterized by fineness, flexibility, and by having a high ratio of length to thickness. Textile fibers also exhibit sufficient strength and extensibility, elasticity, flexibility, and temperature stability to endure the environments in which they are to be used. They can be divided into continuous filaments or staple forms. Staple fibers range in length from about 2 to 20 mm. Fibers with thicknesses greater than about 100  $\mu\text{m}$  are generally considered coarse bristles; fibers with lengths less than a centimeter are generally not processed on textile-based processing machinery.

Typical textile fibers used, for example, in a needle-punched filter fabric, are a blend of 3.3 and 6.6 dtex polyester staple fibers. These are about 5 cm long, have diameters ranging from 18 to 25  $\mu\text{m}$ , linear density of 350–650 mg per 1000 m and length-to-width ratios in the order of 1000 to 1.

Virtually all fibers (an important exception is glass fibers) are composed of long-chain molecules or polymers arranged along the fiber axis. Essential requirements for fiber formation include long-chain molecules with no bulky side groups, strong main-chain bonding, parallel arrangement of polymer chains, and chain-to-chain attraction or bonding. Basic phases in the fiber formation process are obtaining a suitable polymeric material, converting the material to liquid

**Table 1. Properties of Some Commercially Available Textile Fibers**

Fiber	Density, g/mL	Modulus, N/tex <sup>a</sup>	Tenacity, N/tex <sup>a</sup>	Elongation, %	Regain, %	T <sub>m</sub> , °C
Cotton	1.52	4.85	0.26–0.44	7	7	
Jute	1.52	17.2	0.44–0.52	2	12	
Wool	1.31	2.38	0.08–0.17	40	13	
Rayon	1.54	4.85–7.5	0.8–0.44	8–20	11	177
Acetate	1.32	3.53	0.11	25–45	6.5	260
Nylon	1.14	2.65	0.44–0.79	15–50	3–5	260
Polyester	1.38	4.41–8.38	0.35–0.71	15–50	0.4	254
Acrylic	1.16	6.44	0.17–0.26	20–30	1–1.5	
Polypropylene	0.91	7.76	0.26–2.64	20	0.01–0.1	177
Nomex <sup>b</sup>	1.38	8.83	0.35–0.44	20–30	4	371
Kevlar <sup>b</sup>	1.44	42.34	0.79–1.14	1.5–4	5	482
Sulfur	1.37	2.65–3.53	0.26–0.35	25–35	0.6	285
Glass	2.56	30.89	0.79–1.76	2–5	0	1482

<sup>a</sup>To covert N/tex to g/den, multiply by 11.33.

<sup>b</sup>Polyamides.

form, solidifying the material into fiber dimensions, and treating the fiber to bring about desired properties. These four phases are present in the formation of natural as well as manufactured synthetic fibers, the principal differences being the amount of time and energy required.

A selection of fiber properties is given in Table 1. In general, fiber diameters range from 5 to over 40  $\mu\text{m}$  for natural fibers, and from less than 10  $\mu\text{m}$  (microfibers) upwards for manufactured fibers.

Almost all the fibers used in nonwovens are synthetic. The split is approximately as follows: Polypropylene 63%; polyester 23%; viscose rayon 7%; acrylic 2%; polyamide 2%; other 3%; (see PROPYLENE POLYMERS (PP); OLEFIN FIBERS; POLYESTERS, FIBERS; CELLULOSE FIBERS, REGENERATED; ACRYLIC FIBERS; POLYAMIDES, FIBERS).

With the increasing need to reduce cost and achieve sustainability, there has been a growth in interest in using recycled fibers, eg, from polyester bottles.

## Web Formation

Web formation, the second phase in manufacturing nonwoven fabrics, transforms fibers or filaments from linear elements into planar arrays in the form of preferentially arranged layers of lofty and loosely held fiber networks termed webs, batts, or sheets. Mechanical and fluid means are used to achieve the fiber arrangement. Basic fabric parameters established at web formation, in addition to fiber orientation, are the unfinished product weight per unit area and the manufactured width. In all nonwoven manufacturing systems, the fiber material is deposited or laid on a forming or conveying surface. The physical environment at this phase is dry when textile technology is used, wet when papermaking technology is used, and molten when extrusion technology is used.



Webs are prepared by opening, blending, and carding.

**Opening and Blending.** A bale of fibers needs to be broken apart and the closely packed fibers in the tufts need separating before further processing can be carried out. This is an important first stage to forming a web—once the web has been formed it cannot be made more even by further processing, and any irregularities will adversely affect product performance. So it is important to open the fiber tufts, remove any contamination, and even out bale-to-bale variation before further processing.

**Textile Carding.** Carding is the process of disentangling, cleaning, and intermixing fibers to make a web for further processing into a nonwoven. The aim is to take a mass of fiber tufts and produce a uniform, clean web. The process predominantly aligns the fibers which are held together as a web by slight mechanical entanglement and fiber–fiber friction. The main type of card is a roller card. The carding action is the combing or working of fibers between the points of saw-tooth wire clothing on a series of interworking card rollers. Short fibers and foreign bodies are removed, the fiber tufts are opened, and the fibers are arranged more or less parallel. The carding or parallelization of fibers occurs when one of the surfaces moves at a speed greater than the other. Fibers are removed, or “stripped,” when the points are arranged in the same direction and the more quickly moving surface removes or transfers the fibers from the more slowly moving surface.

Woollen cards, for example, were designed to process a rather wide range of fiber lengths ( $<1\text{--}20\text{ cm}$ ) and diameters ( $<20\text{--}50\text{ }\mu\text{m}$ ) with additional objectives of removing contaminants, mixing fibers, preserving fiber length, extracting as few fibers as possible, and delivering as many as 100 slivers. Conventional woollen cards, consequently, consist of a series of relatively wide and large cylinders to achieve productivity and accommodate fiber length requirements; multiple rolls to work and mix fibers on the large cylinders; and smaller cylinders and rolls to take fibers to and transfer them from each working area.

Cotton cards, on the other hand, were designed to process shorter fibers (15–30 mm) and a more narrow range of fiber diameters (15–30  $\mu\text{ms}$ ). Additional requirements include eliminating very short fiber segments and extracting nonfibrous material such as seed coat particles and leaf fragments. A traditional cotton card consists of a roll-to-plate mat feeding assembly, a fiber-from-mat separating roll (lickerin), one large cylinder and several curvilinear surfaces (revolving flats) between which the carding action takes place, a smaller cylinder which removes fibers (doffs) from the carding cylinder, and a web-condensing and sliver-coiling assembly.

When short (35–50 mm) synthetic fibers are processed on cotton cards, the flats are often replaced with stationary granular surfaces in order to minimize the fiber extraction and damage. Fibers up to 150 mm in length are processed on cotton cards with workers and strippers (Fig. 1).

Garnetts were designed to thoroughly disentangle textile fibers which were reclaimed from various fiber or textile manufacturing operations or regenerated from threads and rags. Garnetts are compact, versatile, and highly productive. Most have a feeding section, a gentle opening section, a working section consisting of one to four cylinders with or without a worker and stripper rolls, and one to four doffers.

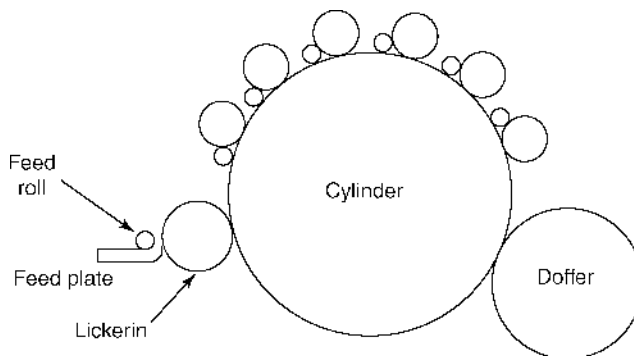


**Fig. 1.** Cotton card with workers and strippers (doffers).

The choice between using a cotton card, a woollen card, or a garnett depended on fiber dimensions. Woollen cards were used for long, coarse fibers, cotton cards for finer, shorter fibers, and garnetts for fibers having a wide range of dimensions.

**Nonwoven Cards.** Modern, high speed cards designed to produce nonwoven webs show evidence of either a cotton or wool fiber-processing heritage and have processing rate capabilities comparable to those of garnetts. Contemporary nonwoven cards are available up to 5 m and are configured with one or more main cylinders, roller or stationary tops, one or two doffers, or various combinations of these principal components.

Single-cylinder cards are usually used for products requiring machine-direction or parallel-fiber orientation. Double-cylinder cards, frequently called tandem cards, are basically two single-cylinder cards linked together by a section of stripper and feed rolls to transport and feed the web from the first working area to the second. The coupling of two carding units in tandem distributes the working area and permits greater fiber throughput at web quality levels comparable to slower single-cylinder machines.

Roller-top cards have five to seven sets of workers and strippers to mix and card the fibers carried on the cylinder. The multiple transferring action and re-introduction of new groupings of fibers to the carding zones provides a doubling effect which enhances web uniformity. Stationary-top cards have strips of metallic clothing mounted on plates positioned concavely around the upper periphery of the cylinder. The additional carding surfaces thus established provide expanded fiber alignment with minimum fiber extraction.

Double-doffer cards are generally used to conserve manufacturing space or optimize throughput while maintaining web quality. The double-doffer configuration splits the web, which essentially doubles the output of lightweight structures or yields an additional doubling action for heavier ones (Fig. 2).

## Web Layering

Forming fibers into a web on a carding or garnetting machine takes place at the doffer. The web forms as the doffer strips and accumulates fibers from the

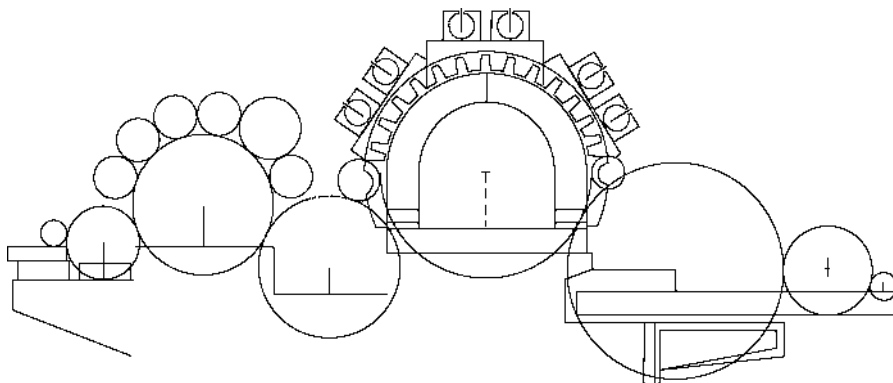


**Fig. 2.** Contemporary nonwoven card configuration.

cylinder. The number of fibers accumulated and the mass of each fiber determine the weight of the web. For a given fiber orientation, web weight per unit area is limited by the ratio of the surface speed of the cylinder to the surface speed of the doffer. This is typically 10–15. The result is that cotton cards give up to  $10 \text{ g/m}^2$  per doffer, woollen cards up to  $25 \text{ g/m}^2$ , and garnetts up to  $50 \text{ g/m}^2$ .

Nonwoven fabrics are made in weights ranging from less than 10 to several hundred grams per square meter, and fiber orientations ranging from parallel to random. Webs can be built up or layered to achieve the desired weight. This can be done by folding from one machine, collection from multiple forming machines, or cross-lapping.

Web folders or straight plaiters are used with cotton cards to produce surgical waddings, and with woollen cards and garnetts to produce padding and cushion filler. The resulting batt is limited in width to the width of the forming machine. Delivery is in the form of individual stacks of parallel fiber layers. Layering of webs from two or more cards or garnetts arranged in tandem onto a conveying apron or screen provides continuous delivery. Tandemly arranged, roller-top cotton carding lines are used to form webs for diaper and feminine pad facings, interlinings, and wipes. In this instance, web weight is controlled by the number of cards included and finite adjustment of cylinder or doffer speed ratios. Density gradient and multifiber laminate webs can be formed by processing fibers of different sizes and chemical types on individual cards in the line. Web characteristics include a high degree of fiber parallelization and increased uniformity due to the doubling effect of layering.

Parallel laid webs can only be the width of the card web and they remain anisotropic; cross-laid webs can be wider and more uniform.

Cross-lapping is essentially the plaiting or folding of a fiber web onto a conveying device placed at an angle of  $90^\circ$  to the forming unit. Delivery is continuous and fiber orientation is biaxial. In addition to being a means of determining a range of product weights, cross-lapping is also a means of determining a range of product widths. Additives, such as binder and particulate matter, can also be deposited onto individual web layers at the lapping stage.

Cross-lapping can be achieved by doffing webs onto reciprocating floor aprons, inclined aprons (camel back) reciprocating onto stationary floor aprons or conveyors, or runout (horizontal) apron folders reciprocating onto stationary floor aprons or conveyors. Cross-lapped web widths may range from several centimeters to several meters. Cross-lapped webs are used in the production of highloft and needled structures.

**Web Spreading and Web Drafting.** Spreading layers of parallel fiber webs is a means of simultaneously increasing web width, decreasing web weight, and altering fiber orientation. Controlled stretching or drafting web layers is a means of simultaneously increasing web throughput, decreasing web weight, and altering fiber orientation.

Spreading devices typically consist of modules of bowed rolls of increasingly wider widths operating at speeds slightly greater than the conveying speed of the input web. Fibers move longitudinally but mostly horizontally past one another, resulting in a lateral stretching or drafting of the web and overall repositioning of individual fibers. Width increases of 50–250% are common. Web-drafting devices consist of a series of top-and-bottom roll sets of the same width operating at successively increasing speeds. When heavy cross-lapped layers are drafted, a more isotropic arrangement of fibers is achieved. Draft ratios of six and higher are practiced in some nonwoven operations. Web drafters are also used as a means for in-line weight control.

**Random Cards.** Fiber orientation ratios as low as 3:1 can be achieved on cards by expanding the condensing action at doffing through the addition of scrambling or randomizing rolls operating at successively slower surface speeds. Proper selection of clothing wire and speed ratios can yield webs with increased *z*-direction fiber orientation, resulting in increased thickness and loft; throughput speed, however, is decreased. Cards specifically designed to produce random webs at contemporary throughputs are configured with several small cylinders that hurl the fibers onto adjacent doffers or cylinders, which in turn transfer the fibers centrifugally onto subsequent cylinders. Figure 3a shows the roll arrangement for lightweight nonwovens and Figure 3b for heavier weight nonwovens.

**Aerodynamic Web Formation.** Heavy webs, especially of coarse fibers, cannot easily be made on a mechanical system such as carding. Air-laying is the preferred manufacturing route. By this means it is possible to make a heavy fabric as a single layer, unlike carding or folding for which the layers can split. The principle is that the fibers are well-opened before being directed by air currents onto a collector which can be a flat conveyor or a drum. In principle a better balance of properties in the CD and MD directions should be possible, with a significant proportion of fiber elements in the thickness direction.

Air-laid nonwovens can be grouped into two categories: those formed from natural or synthetic textile fibers and those formed from natural or synthetic pulps. The basic elements are a preformed feed mat, a feeding arrangement, a fiber separation device, an air-generating means, an air-regulation means, and a fiber collection or condensing means.

As fibers in the feed mat pass between the feed roll and feed plate, they are separated by metallic wire teeth on the lickerin roll and carried to an air venturi where they are stripped and tumbled until they strike a moving, perforated collection surface (Fig. 4). At the collection surface, the airborne fibers

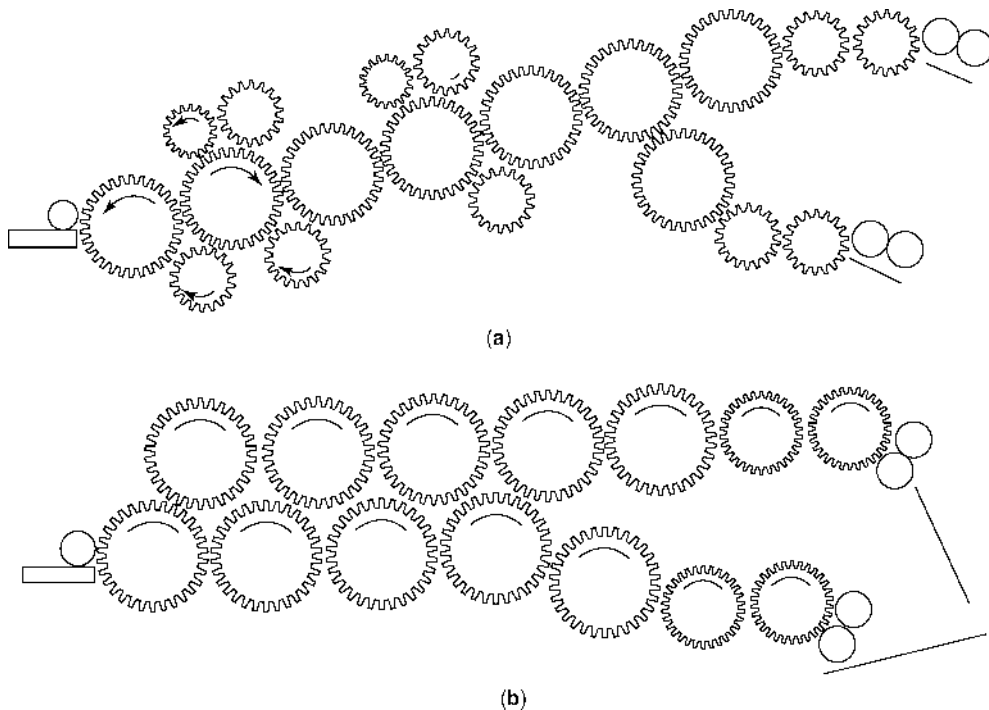


**Fig. 3.** Random card roll arrangements designed for (a) lightweight nonwovens and (b) highloft nonwovens.

follow paths of least resistance and accumulate in a self-levelling manner while the air passes through perforations. Fiber orientation in the web is isotropic in layers corresponding to the number of fibers transferred from the wire teeth to the air-transportation zone, the intensity of the air, and the speed of the collection surface.

Other configurations include a standard roller card with a series of workers and clearers to open the fiber, with various arrangements of air distribution, eg overpressure or under pressure to direct the fibers and lay them on the perforated collector.

Three-dimensional webs can be made on air-forming machines, provided the fibers used are relatively short and stiff and the webs made are of relatively low density. Air-forming machines allow for production of web thicknesses up to several centimeters, and weights ranging from 30 to 3000 g/m<sup>2</sup> at widths from one to several meters.

Textile fibers can be air-formed directly into end-use configuration by including a shaped condensing surface or, as in the production of pillows, an air-permeable screen drum or belt. Aerodynamic web formation is a suitable means of processing brittle fibers such as glass and ceramics.

Fibers of different diameters, lengths, shapes, and densities break up when processed together in air streams. This fractionation results in the formation of

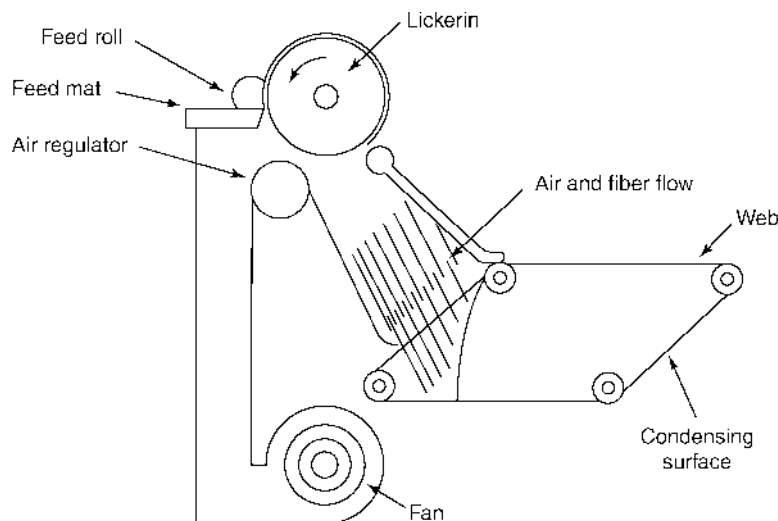


**Fig. 4.** Aerodynamic web formation.

webs with different top and bottom surface characteristics, as well as varying density and porosity gradients. Such structures have been used in filtration.

**Short Fiber Systems.** The web formation phase of the papermaking process occurs between the headbox and the forming wire. In this area, the fibers, suspended in a dilute water slurry, are deposited on a moving screen which permits the water to pass and the fibers to collect. Traditional papers use a variety of wood pulps or other short cellulosic fibers which pack together to form relatively dense, nonporous, self-adhered sheets. The use of textile fibers, instead of cellulose-based materials, with papermaking machinery distinguishes wet-laid nonwoven manufacturing from traditional paper manufacturing. Both manufacturing methods, however, transport the fibers in a water slurry. The use of papermaking fibers on air-laid nonwoven machinery bridges a gap between textile and paper systems. In both technologies, the transport medium is a fluid: water in wet-laid nonwovens and air in dry-laid pulps.

**Dry-Laid Pulp.** A principal objective of using air to form webs from natural and synthetic fiber pulps is to produce relatively lofty, porous structures from short fibers, without using water. Air or dry-laid pulp machinery can be imagined as a series of forming-unit modules. Each module consists of two to four perforated drums through which airborne fibers are circulated and further agitated by mechanical beaters placed in close proximity to the inner drum surfaces. As the fibers circulate and separate by the force of the air and the sweeping action of the beaters, they are pulled through the drum perforations by a vacuum onto a condensing conveyor.

Air-laid pulp-forming lines generally consist of three or more forming heads in tandem. Web weights range 70–2000 g/m<sup>2</sup> at throughputs of about 1000 kg/h.

**Wet-Laid Web Formation.** In the wet-lay or wet-forming process, fibers are suspended in water, brought to a forming unit where the water is drained

off through a forming screen, and the fibers are deposited on the screen wire. A principal objective of wet-laid nonwoven manufacture is to produce structures with textile characteristics, primarily flexibility and strength, at papermaking speeds. This can be done by incorporating textile fibers at web formation.

In general, however, it is difficult to incorporate textile fibers because they do not readily wet out, are difficult to disperse, and tend to tangle with one another. Consequently, large amounts of water are needed to keep the fibers in suspension. Also, if the slurry is not handled properly, the fibers tangle and cause poor sheet formation. This can be overcome by increasing the slurry dilution and controlling fiber orientation.

Forming machine designs that have been commercially successful include the inclined-wire fourdrinier and the cylinder former. Inclining the forming wire and suction boxes on a fourdrinier machine to an angle of  $5^{\circ}$ – $30^{\circ}$  expands the forming area, which in turn decreases the flow requirements for web formation, increases drainage, and aligns fibers along the machine direction. The cylinder former configuration also provides an expanded forming area. Another benefit of this design is that higher vacuum pressures can be used, which results in the ability to produce both heavy and dense as well as light and relatively impermeable structures.

## Web Consolidation

Nonwoven bonding processes interlock webs or layers of fibers, filaments, or yarns by mechanical, chemical, or thermal means. The extent of bonding is a significant factor in determining fabric strength, flexibility, porosity, density, loft, and thickness. Bonding is normally a sequential operation performed in tandem with web formation but it is also carried out as a separate and distinct operation.

In some fabric constructions, more than one bonding process is used, for example, sometimes a needled fabric is thermally bonded and then chemically bonded with the aim of achieving high stiffness.

**Needle-Punching.** In this method, fiber webs are mechanically interlocked by physically moving some of the fibers or elements of the length of some fibers from a near-horizontal to a near-vertical position. This is achieved by intermittently passing an array of barbed needles into the web to move groups of fibers, and then withdrawing the needles without significantly disturbing the newly-positioned fibers. The degree of interlocking depends on the extent to which the needles penetrate the web (depth of penetration), the needling density (penetrations per unit area of fabric), and the number of groups of fibers or fiber elements which are repositioned per penetration. The latter depends on the design of the needles used.

The basic parts of a needloom are the web-feeding mechanism, the needle beam which comprises a needleboard which holds the needles, a stripper plate, a bed plate, and a fabric take-up mechanism. (Fig. 5).

The fiber web, sometimes carried or reinforced by a scrim or other fabric, is guided between bed and stripper plates, which have openings corresponding to the arrangement of needles in the needle board. During the downstroke of

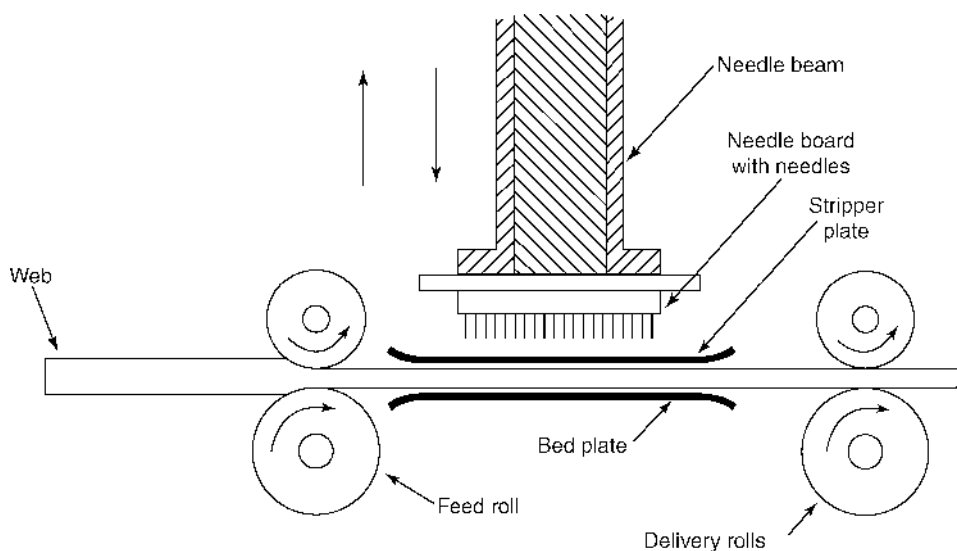


**Fig. 5.** Basic elements of a needle-punch machine.

the needle beam, each barb carries groups of fibers, corresponding in number to the number of needles and number of barbs per needle, into subsequent web layers to a distance corresponding to the penetration depth. During the upstroke of the needle beam, the fibers are released from the barbs, and interlocking is accomplished. At the end of the upstroke, the fabric is advanced by the take-up, and the cycle is repeated. Needling density is determined by both the distance advanced and the number of penetrations per stroke.

The development of a mechanical process for producing felt is dated to 1820 and has been attributed to J.R. Williams (3). The transition from interlocking fibers by working the scales on adjacent fiber surfaces against one another to working the fibers by a scaled external member in the form of a barbed penetrating device took place during the last quarter of the nineteenth century. This transition was made possible by the development of the mechanisms and machinery to produce needled nonwovens in a factory environment.

Needle looms are produced in widths ranging from several centimeters to several meters. Virtually all needle looms employ reciprocating motion to provide the penetration action. The most common needle loom configuration is the single upper-board, downstroke arrangement. Other arrangements include double upper-board, single upper- and lower-board, and double upper- and lower-board. To achieve high penetration densities on both sides of a fabric, needle looms of differing configurations are often placed in tandem.

Needle looms with low density boards are used to lightly consolidate webs and are termed pre-needlers or tackers. Machines with multiple or high density needle capabilities are referred to as consolidation or finishing needle looms. Machines designed to produce patterned or raised surfaces are termed structuring looms and are used as a mechanical finishing process.



Fabric weights range from 50 to 5000 g/m<sup>2</sup>, and needling densities range from fewer than a hundred to several thousand penetrations per square centimeter.

Most needled fabric is made in flat form; however, tubular fabric, ranging in diameter from a few millimeters to papermakers' felt dimensions, can be made on some machines.

Needled nonwovens are sometimes mistaken for fabrics which have been felted or fabrics made directly from fibers which have been interlocked by a combination of mechanical work, chemical action, moisture, and heat. Fabrics which have been felted are generally composed of yarns spun from wool fibers and have undergone a controlled shrinkage by subjection to the fulling process, a mechanical beating in the presence of lubricating agents. Fabrics made directly from fibers which have been interlocked by a combination of mechanical work, chemical action, moisture, and heat are felts. Felts are generally composed of wool or fur fibers and are physically held together by the interlocking of scales on individual fibers. Fiber interlocking in a felt is achieved by a process called *hardening*, which consists of passing fiber webs between oscillating and vibrating plates in the presence of steam. Following hardening, the felt is subjected to a fulling process. Felt density, stiffness, and tenacity are dependent on web weight and extent of hardening and fulling.

On the other hand, a needled felt is a fabric composed of natural, synthetic, or a combination of natural and synthetic fibers physically interlocked by the action of a needle loom with or without combination of other textile fabrics and with or without suitable combination of mechanical work, chemical action, moisture, and heat, but without weaving, knitting, stitching, thermal bonding, or adhesives (4).

Early needle-punched nonwovens were made from coarse animal hair and vegetable fibers and were used as carpet underlays and padding for mattresses and furniture. By the late 1950s needled synthetic products were being introduced for home furnishings and apparel. Several attempts were made to make synthetic leather in the 1960s, with the needled fabric as a substrate.

The main applications of needle-punched fabrics are automotive, geotextiles, footwear components, insulation, and roofing substrates.

**Stitchbonding.** This is a mechanical bonding method that uses knitting elements, with or without yarn, to interlock fiber webs. Sometimes called stitchthrough or web knitting, this technology was developed in eastern Europe in the late 1940s. Maliwatt and Arachne machines use yarn; Malivlies and Arabeva machines use modified knitting needles to interlock the fibers. Both families of machines operate essentially on the same principle, but differ in the positioning of the knitting elements, direction of web passage, and type of needles used.

The sequence of operations for a web-consolidation cycle on an Arachne machine is as follows. The web is guided upward and positioned between the web-holder table and knock-over table and penetrated by the needle. After passing through the web, the hook of the needle is provided with a yarn properly placed by the closing motion of the yarn guide. When the needle reaches the end of the upward stroke, the yarn is pulled through the previously formed loop, the loop is cast off, the fabric is advanced, and the cycle is repeated. Similar functions are served by the Arachne web-holder table and the needle loom bed plate, the Arachne

knock-over table and the needle loom stripper plate, and the Arachne knitting needle and the needle loom needle. Thus, when yarn is eliminated, stitchbonding and needle-felting methods interlock fibers similarly.

Stitchbonded fabrics are used in home furnishings, footwear, filtration, and coating.

**Hydroentanglement.** This is a generic term for a nonwoven process that can be used for web consolidation, fabric surface-texturing purposes, or both. The mechanism is one of fiber rearrangement within a preformed web by means of fluid forces. When used for bonding, hydroentanglement repositions individual fibers into configurations that result in frictional interlocking. When used as a surface-texturing means, hydroentanglement repositions fibers into open-patterned arrangements.

Also termed spunlaced or jet-laced nonwovens, fabrics of this type have been sold commercially since the early 1970s and have been successfully used in applications such as interlinings, wipes, wound dressings, and surgical gowns. The earliest hydroentangled fabrics were lightweight but now weights of up to 400 g/m<sup>2</sup> are possible.

The hydroentanglement process, as illustrated by DuPont patent drawings (5), involves subjecting the web and its conveying device to increasingly higher pressure jets of water. When the water jet strikes the web, it moves individual fibers away from the high points of the conveying means and is deflected by the conveying surface. As a result, voids are created in the web, and fibers intermingle. Whether the fabric surface is visibly smooth or openly patterned depends on the wire design or surface geometry. When highly interlocked, mechanically bonded (spunlace) structures are desired, high water pressure and plain mesh wire are used. The resulting fabric surface is comparatively smooth and the overall structure is relatively strong because of a large amount of individual fiber entanglement. When open-surface (apertured) structures are desired, lower water pressure and conveying wire combinations or surfaces with preferred patterning configurations and depths are used, and a fabric surface with an overall aperture geometry reflective of wire or surface contour is established. A wide variety of aperture shapes and lines are possible. Individual aperture shape or hole clarity is a function of fiber dimensions, jetting pressure, and wire interlacing or embossment shape and height.

**Chemical Bonding.** Sometimes called resin bonding, chemical bonding is a general term describing the technologies employed to interlock fibers by the application and curing of a chemical binder. The chemical binder most frequently used to bond nonwovens is waterborne latex. Most latex binders are made from vinyl polymers, such as vinyl acetate, vinyl chloride, styrene, butadiene, acrylic, or combinations thereof. The monomer is polymerized in water, and the polymeric material takes the form of suspended (emulsified) particles. Thus the emulsion polymerization of vinyl acetate yields a vinyl acetate polymer binder and the copolymerization of styrene and butadiene yields styrene-butadiene copolymer (qv) or styrene-butadiene rubber (SBR) binder.

Latexes (or latices) are widely used as nonwoven binders because they are versatile, can be easily applied, and are effective adhesives. The chemical composition of the monomer determines stiffness and softness properties, strength,

water affinity, elasticity, and durability. The type and nature of functional side groups determine solvent resistance, adhesive characteristics, and cross-linking nature. The type and quantity of surfactant used influence the polymerization process and application method. The ability to incorporate additives such as colorants, water repellents, bacteriostats, flame retardants, wetting agents, and lubricants expands this versatility even further (see LATEX TECHNOLOGY).

Chemical binders are applied to webs in amounts ranging from about 5 to 60 wt%. In some instances when clays or other weight additives are included, addition levels can approach or even exceed the weight of the web. Waterborne binders are applied by spray, saturation, print, and foam methods. A general objective of each method is to apply the binder material in a manner sufficient to interlock the fibers and provide chemical and mechanical properties sufficient for the intended use of the fabric.

Spray bonding is used for fabric applications which require the maintenance of high loft or bulk, such as fiberfill. The binder is atomized by air pressure, hydraulic pressure, or centrifugal force, and is applied to the upper surfaces of the web in droplet form using a system of nozzles. To apply binder to the lower surface, the web direction is reversed on a second conveyor and the web passes under a second spray station. After each spraying, the web is passed through a heating zone to remove water. The binder is cured, or cross-linked, upon passage through a third heating zone. Drying and curing is frequently done in a three-pass oven. Binder addition levels commonly range from 30 to 60% of the fiber weight.

Saturation bonding (sometimes simply called "impregnation") is used in conjunction with processes that require rapid binder addition, such as card-bond systems, and for fabric applications that require strength and maximum fiber encapsulation, such as carrier fabrics or some shoe stiffeners. Fiber encapsulation is achieved by totally immersing the web in a binder bath or by flooding the web as it enters the nip point of a set of pressure rolls. Excess binder is removed by vacuum or roll pressure. There are three variations of saturation bonding: screen, dip-squeeze, and size-press. Screen saturation is used for medium weight nonwovens, such as interlinings. Dip-squeeze saturation is used for web structures with sufficient strength to withstand immersion without support. Size-press saturation is used in high speed processes, such as wet-laid nonwovens. Through-air ovens or perforated drum dryers are used to remove water and cure the resin. Binder addition levels range from 20 to 60% of fiber weight.

In print bonding, binder is applied in predetermined areas or patterns. This method is used for fabric applications that require some areas of the fabric to be binder-free, such as wipes and coverstocks. Many lightweight nonwovens are print-bonded. Printing patterns are designed to enhance strength, fluid transport, softness, hand, and drape. Print bonding is most often carried out with gravure rolls arranged as shown in Figure 6a. Binder addition levels are dependent on both engraved area and depth, and the binder-solids level. Increased pattern versatility can be achieved by using rotary-screen rolls arranged as shown in Figure 6b. Drying and curing are carried out on heated drums or steam-heated cans.

Foam bonding is used when low water and high binder-solids concentration levels are desired. The basic concept involves using air as well as water as the

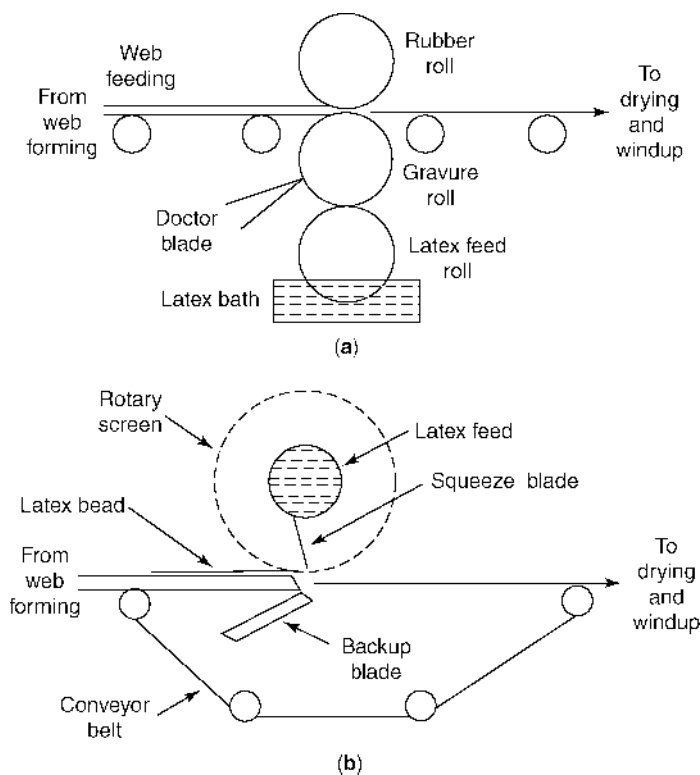


**Fig. 6.** Print bonding methods where (a) is gravure and (b) is rotary-screen printing.

binder carrier medium. Foam-bonded nonwovens generally require less drying and curing energy because less water is used. The foam is generated by concurrently aerating and mechanically agitating the binder compound. Air/binder dilutions (blow ratios) range from 5 to 25. The addition of a stabilizing agent to the binder solution causes the foam to resist collapse during application and curing, and yields a fabric with enhanced loft, hand, and resilience.

Nonstabilized foams are referred to as froths; froth-bonded fabrics are similar in properties to some saturation-bonded nonwovens. Typical foams used as nonwoven binder solutions have a consistency similar to shaving cream. Application methods include knife-edge layering onto a horizontal web surface followed by vacuum penetration, and saturation and penetration of a vertical web surface using a horizontal-nip pad. Drying and curing are carried out in ovens, drum dryers, or steam cans.

**Thermal Bonding.** In thermal bonding, heat energy is used to activate an adhesive, which in turn flows to fiber intersections and interlocks the fibers upon cooling. The adhesive may be individual fibers, portions of individual fibers, or powders. Advantages of thermal bonding include low cost and the wide availability of binder materials and machines. The use of thermal bonding is increasing and replacing chemical bonding in medium weight nonwovens.

Thermal bonding is achieved as the result of a sequence of three events: heating, flowing, and cooling. The adhesive component, distributed in a nonwoven web in the form of a unicomponent fiber, bicomponent fiber, or powder particle, is subjected to heat. For binder fibers and powders, initial heat softens the binder surface and expands its contact area with other fibers; additional heat induces binder flow, resulting in molten binder–fiber wetting and broader binder-to-fiber contact. As the adhesive approaches its melting point, its surface softens, and contact areas with more stable fibers expand further to form potential bonding sites. Upon melting, the adhesive, now in liquid form, becomes attached to a network fiber. It then flows along the network fiber into a crossing of two or more fibers, or forms an adhesive bead. Upon cooling, the adhesive solidifies and forms a bond at each fiber contact.

In addition to the melt-flow properties of the adhesive, bond strength is a function of the percentage of fiber surface area joined or shared at fiber intersections, the heating and cooling times, and bonding temperature. Bond effectiveness is also dependent on binder distribution and binder concentration. Fabric strength, resilience, softness, and drape are affected by bond strength, bond position, and total bonded area. A properly produced thermal-bonded nonwoven can approach the idealized nonwoven structure, namely, one in which individual fibers are connected at crossings with each other.

Three basic methods of heating are used for thermal bonding: conduction, radiation, and convection. Conduction technologies include fixed contact with a heated surface and ultrasonic welding. Direct contact heating is done with heated calender rolls. For area or surface glazing, smooth rolls are used. For point bonding, patterned or embossed rolls are used. Thermal calendering is most efficient in terms of heat loss, but heavy roll pressures tend to destroy fabric loft.

For fabrics containing a significant proportion of thermoplastic material which is usually thermoplastic fibers but could be powder, bonding, including in patterns, can be done ultrasonically. An illustration of the basic elements of an ultrasonic bonding unit is given in Figure 7. In this bonding method, a web is placed between a high frequency oscillator or horn, and a patterned roll. As the waves pass through the web and are concentrated on the raised points of the patterned roll, sound energy heats the fibers. If they are thermoplastic, they will soften and start to melt, bonding the fabric together in patterns corresponding to those on the surface of the roll.

Radiation heating concentrates fiber bonding on the surface. For lofty or thick structures, this effect yields a bond intensity gradient throughout the fabric thickness. Radiant heating systems are used mostly for applications which require instant heating and concentrated heating zones. Convection heating methods pass heated air through the nonwoven web and are used to bond many medium and heavy weight nonwovens. Two common commercial configurations are multizone through-air ovens and compact through-air ovens. Multizone ovens transport the nonwoven web through heating and cooling zones on a flat conveyor, with production speed and dwell time requirements being accommodated by increasing oven length. Compact through-air ovens use felt or perforated belts to guide the webs around perforated drums. In these systems, hot air is recirculated through the fabric, drum, and heat exchanger by low speed radial fans. The belt

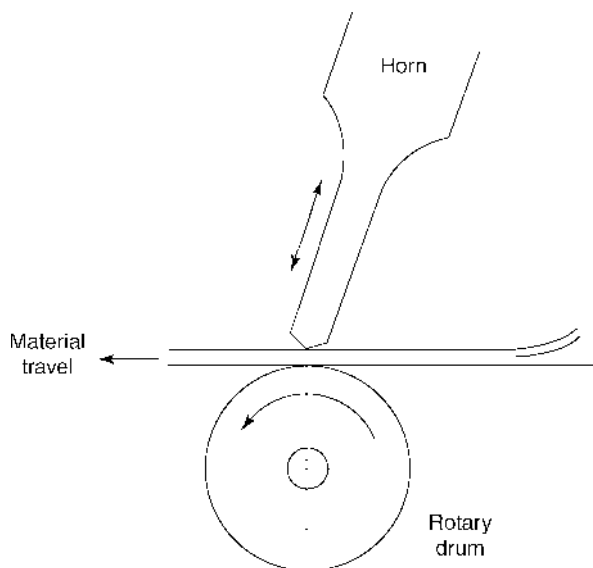


**Fig. 7.** Basic elements of ultrasonic bonding.

guide conveyor serves to stabilize the nonwoven batt during heating, and also controls fabric loft and shrinkage.

From an energy standpoint, modern thermal bonding, ie web consolidation with no heat requirement for water removal, is very efficient. Manufacturing lines for thermal-bonded nonwovens also require less floor space and operate at higher production rates. Thermal-bonded nonwovens are generally softer and drier, have greater strength per unit weight, and are absorbent and porous because of smaller bonding points.

Thermal bonding also provides the opportunity to design fabrics which are more easily recyclable than chemically bonded fabrics.

## Finishing

Commercial nonwoven fabrics are transported from the manufacturing plant to the customer in the form of rolls of varying dimensions to accommodate the fabric end-use application or subsequent conversion processes. Slitting and winding are finishing processes common to all nonwoven manufacturing methods. Roll width is determined at the slitting operation, and roll length is determined at the winding operation.

The fabric may also be given one or more of a number of other finishing treatments, either in tandem with web formation and bonding or off-line as a separate operation, as a means of enhancing fabric performance or aesthetic properties. Performance properties include functional characteristics such as moisture transport, absorbency, or repellency, flame retardancy, electrical

conductivity, abrasion resistance, and frictional behavior. Aesthetic properties include appearance, surface texture, and smell.

Generally, nonwoven finishing processes can be categorized as either chemical, mechanical, or thermomechanical. Chemical finishing involves the application of chemical coatings to fabric surfaces or the impregnation of fabrics with chemical additives or fillers. Mechanical finishing involves altering the texture of fabric surfaces by physically reorienting or shaping fibers on or near the fabric surface. Thermomechanical finishing involves altering fabric dimensions or physical properties through the use of heat and pressure.

Finishing may also be viewed as another means for providing nonwovens with additional application-dependent chemical and/or physical properties. Finishing processes bring about value-added fabrics with technically sophisticated properties for specific end-use applications.

**Chemical Finishing.** For many nonwovens, chemical finishing is an extension of the binder application process through the use of technology associated with fabric coating. In most instances, the coating process is applied to enhance the properties of the nonwoven; however, in some applications, the nonwoven is used as a carrier to transmit the properties of the coating material. The coating may be applied as a continuous covering or as a pattern; it is most frequently applied in aqueous solution form. With many nonwoven substrates, special care must be taken because of the delicate nature of the structure itself or the arrangement of fibers on or near the fabric surface.

A number of different methods are used to coat nonwovens depending on the viscosity requirements of the coating material and the amount and location of coating desired. Knife-over-roll (blade coating), reverse-roll, air-knife, wire-wound rod, transfer-roll, rotary screen, and slot-die methods are used to apply continuous coatings to single surfaces. Double-surface coating of relatively nonporous nonwovens with high viscosity materials can be achieved by using dip saturators or size presses with gapped or low pressure squeeze rolls. Impregnation of substantially porous nonwovens can be achieved by using the same equipment at higher roll pressures. Patterned coatings or decorative printing can be achieved with the use of gravure rolls or rotary screens. Likewise, fabrics can be impregnated with different impregnants either side, using rotary screens followed by a pair of nip rolls.

Transfer roll, rotary screen, saturation, size press, and gravure apparatus are similar to those used for resin bonding. Reverse-roll coaters are similar in configuration to gravure print-bonding apparatus, but differ in the surface patterning and direction of rotation of the applicator roll. The amount of material applied when using this method is controlled by adjusting the relative speeds of the applicator roll and the rate of fabric passage through the coating system.

In knife-over-roll or blade coating, the coating material is placed on the fabric surface behind a knife, or doctor blade, and metered according to the gap set between the blade and the fabric surface. This method is used to apply thick coatings of highly viscous materials such as pastes, plastisols, or foams.

Air-knife coating is a high speed process used to apply continuous coatings of relatively low viscosity materials onto nonwovens with irregular surfaces. The principal components of this system are illustrated in Figure 8. Following an initial application, the coating material is metered by air impingement.

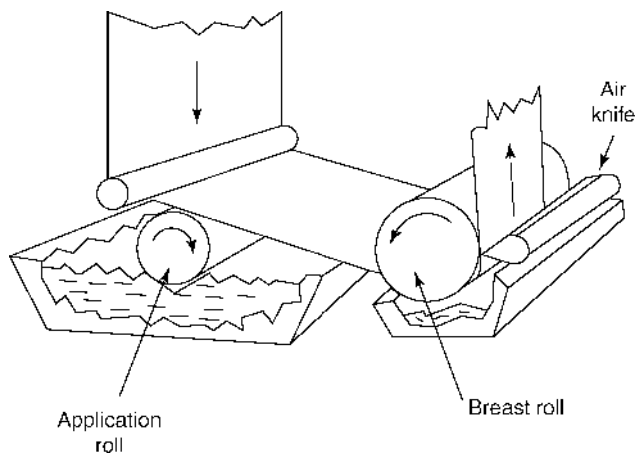


**Fig. 8.** Components of an air-knife coating apparatus.

Wire-bar (Mayer) coating is used to uniformly coat lightweight material applications. As in air-knife coating, the material is applied initially at a first station, but in this system, the coating material is metered and levelled by a wire-wound rod. Coating weight and uniformity are controlled by changing wire thickness and pitch on the metering rod.

Transfer-roll or flexographic coating is used to apply continuous coatings of low or medium viscosity materials at high speeds. This system is particularly suitable for coating stiff or irregularly surfaced nonwovens and for applying abrasives. With high viscosity materials and appropriately designed gravure rolls, flexographic coaters can be used as pattern applicators for decorative prints.

Rotary-screen coating is also used to apply either continuous or discontinuous coatings to nonwovens. The screen is a sleeve, perforated according to a mesh size which corresponds to the size and number of hole per unit area of surface. A material supply tube and squeegee blade are fitted inside the screen. The coating material, in the form of a paste or foam, is forced by the blade through the perforations of the rotating screen onto the nonwoven. For a given coating material, coating weight and penetration are controlled by varying mesh size and squeegee pressure. Patterned coatings or printed designs can be achieved by blocking out selected perforations.

Slot-die or extrusion coating involves the application of molten polymer resin through a slot die directly onto the surface of a nonwoven. Upon extrusion, the resin is smoothed and quenched by a cooling roll. Coating weight is controlled by slot size and extrusion rate. In a variant of this method, nonwoven fabrics are combined with an extruded film just after the die and before the roll-stack. The fabrics can be subsequently chemically bonded to give a sandwich structure. Such products are used as waterproof insales in shoes.

Various chemical finishes can be applied by impregnation, spraying, etc. These include softeners, flame retardants, and antistatic, antisoil, water-repellent, and antibacteria finishes.



Finally dyeing and printing can be included as examples of chemical finishing of nonwovens.

**Mechanical and Thermomechanical Methods.** These methods provide nonwovens with patterned surface structures, enhance the surface texture of nonwovens, or both. Patterned surfaces may be established by embossing, by compressive shrinkage, and for needle-felted nonwovens, by creating loops or pile. Surface textures, ranging from flat and smooth to raised and levelled, may be created or altered by calendering, sueding, napping, polishing, brushing, or shearing. In general, mechanical finishing processes operate at speeds slower than web-consolidation processes and, consequently, are carried out off-line or as a separate batch process.

Smooth surfaces are normally established by calendering, a process which subjects the fabric at the nip point(s) of two or more rolls to the influence of controlled time, temperature and pressure. When calendering is used as a thermal-bonding process, the rolls are of the same dimension and composition and are independently driven. However, when calendering is used as a fabric finishing operation, the rolls are frequently of different dimensions and composition and are not always independently driven.

Specific terms have been designated according to the function and composition of various rolls. Steel rolls that impose pressure, transmit heat, and emboss a pattern onto the fabric are known as pattern rolls. Flexible surface rolls that transport the fabric and permit pressure transmission to the fabric are termed bowl rolls or bowls. Bowl rolls are usually larger in diameter than pattern rolls. The material used to make these types of rolls is chosen according to the depth of surface smoothness to be placed on the fabric being calendered, and must be compatible with the pattern roll.

Calender designations include embossing calenders, friction calenders, and compaction calenders. Most embossing calenders are fitted with a main pattern roll and either one or two bowl rolls which are positively driven by the pattern roll through interconnecting gearing. In friction calendering, the rubbing action is accomplished by operating the pattern rolls at higher rates than their bowl counterparts. Compaction calendering establishes desired fabric thicknesses or calliper through adjustable gapping or roll spacing.

Sueding is a mechanical finishing process in which fibers on the surface of a fabric are cut by the abrasive action of a sanding roll operating at relatively high speed. The cut fibers are oriented in the direction of the sand roll rotation and protrude about a millimeter from the surface. The primary components of a sueding machine are the guiding system, sanding roll, support roll, and roll spacing structure and control. Sueding is sometimes used to reduce the gauge and raise the surface of synthetic leather materials.

The napping process mechanically raises fibers to the surface of a lubricated fabric by withdrawing the fibers from the interior of the fabric. A planetary napping machine configuration is shown in Figure 9; basic components include a series of working rolls wound with hooked wire and a fabric guiding system. The working rolls are operated in a direction opposite the fabric and at surface speeds greater than the fabric passage speed. The napping action takes place as the wires of the working rolls penetrate the fabric, withdraw fibers, and form a nap of raised fibers on the surface of the fabric. Depending on wire design, wire

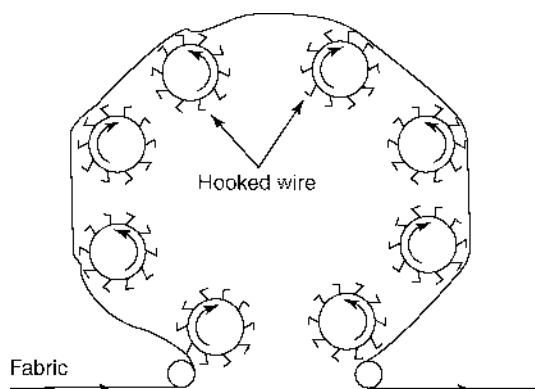


**Fig. 9.** Planetary napping machine configuration.

wrapping pattern, roll arrangement, number of rolls, and relative roll rotation and direction, nappers can be used to produce a wide range of either loop or velour surface effects.

Polishing is a thermomechanical process that aligns the pile of a raised fabric surface. Polishing machine components include a guiding system consisting of a tension blanket and a spirally grooved heated cylinder. The mechanical action of the rotating edge of the roll groove against the tensioned fabric surface results in a static charging of the pile fibers, which in turn aligns the fibers in a parallel orientation. Rotation of the spiral roll in the direction that momentarily entraps fibers in the grooves results in a raised, parallel pile surface. Rotation of the spiral roll in the opposite direction results in a flat, parallel pile surface.

Brushing is a mechanical finishing process that lifts fibers to the fabric surface and aligns the raised fibers along the machine direction of the fabric. Brushing machinery is similar in configuration to both sueding and napping machinery, but the composition of the working roll is different. Straight-wire clothing is used in brushing machine rolls. As the working roll rotates against the fabric surface, the straight wire withdraws and orients the fibers along the direction of fabric passage through the machine. The length of fiber withdrawn is determined by the gap adjustment between the working and support rolls.

Shearing cuts raised fibers to uniform heights. Fabric shearing generally follows a brushing operation and consists of subjecting the fabric surface to a series of spirally wound shearing blades rotating over a stationary ledger blade. The working elements of a shearing machine are similar in configuration to a reel-type lawn mower. In operation, the fabric is guided under the shear blades while the pile is held in a raised position by vacuum. As the fabric passes a shearing point, the raised fibers strike the ledger blade and are cut by the rotating shear blades. Cut pile height is controlled by adjustment of the distance between the fabric guide and the rotating blades.

Tumbling can be used to soften chemically bonded fabrics—this technology was developed for leather and involves breaking of internal bonds in the structure to provide increased softness and suppleness.

The addition of some shrinkage fibers enables the fabric to be shrunk by heating to an appropriate temperature. This technique is often used to increase the density of a needled fabric and is employed in the manufacture of synthetic leather—after needling, the fabric is shrunk and then chemically bonded.

Another process commonly used in synthetic leather manufacture is splitting. A thick and dense, chemically bonded needlefelt is split up to six times to provide material for shoe-linings, handbags, etc.

## Production

Total consumption of nonwovens in 2001 was around 3 million tons and was thought to be growing to about 4 million tons by 2005. Ninety-nine percent of all nonwovens are made from synthetic fibers. Polypropylene predominates (63%), with polyester being second (23%) and viscose rayon third (7%).

The United States continues to be the major nonwoven producer (37%), then Western Europe (29%), followed by Japan (8%) and China (6%). Production in China is growing quickly—especially in spunbonded and spunlace fabrics.

Production according to manufacturing technology is approximately as follows: highloft 26%, spunbonded 17%, needlepunched 10%, bonded pulp 8%, thermal-bonded carded webs 7%, hybrids 7%, resin-bonded carded webs 6%, spunlace 5%, wet-laid 5%, meltblown 4%, and the rest 5%.

The majority of card-resin-bonded and card-thermal-bonded fabrics are used as coverstock; interlinings, wipes, and carrier sheets account for most of the remainder. More than half the highloft volume is used in furniture and sleeping applications; filtration, apparel, insulation, healthcare, with geotextiles accounting for most of the remainder. Stitchbonded fabrics are used in bedding, shoe linings, and a variety of coated products. Needle-punch fabrics are used in automotive, geotextiles, filtration, bedding, and home furnishing applications.

The major use for spunlace fabrics is in medical products; other applications include wipes, industrial apparel, interlinings, absorbent components, filtration, and coating. Medical applications account for about a third of all wet-laid nonwovens. Most bonded pulp fabrics are used as wipes or as absorbent components.

Spunbondeds are commonly used for coverstock, geotextiles, roofing substrates, carpet-backing, medical products, filtration, furniture, and packaging. Meltblown fabrics, because of their relatively fine fiber structure, is commonly used in filtration, sorbents, wipes, and sanitary products.

## Applications

Nonwoven goods applications split into disposables and durables, with disposables being the major share.

Coverstock is the nonwoven fabric placed on the user's side of sanitary absorbent products such as baby diapers, nappy liners, adult diapers, incontinence products, and feminine hygiene products. Medical and surgical products include protective wrap for hospital items which are distributed through the central supply room; surgical drapes, packs, and gowns; other protective products such as

face masks, caps, aprons, bibs, and shoe covers; absorbent products such as surgical dressings and sponges; and other hospital products such as isolation gowns, examination gowns, sheets, shrouds, underpads, and bedding.

Nonwoven wipes includes products for babies and adults, the food service and electronics industries, medical and clean room applications, dusters, shoe cleaning cloths and hand towels. Nonwoven fabrics are used to filter air, water, petroleum, food, and beverages. Nonwovens loaded with abrasives, cleansers, or finishes are used in a wide range of products for cleaning and scouring. Also, many protective garments are made from nonwoven fabrics.

Durable products include geotextiles, for example, to stabilize earth works, roads, landscaping, etc. In agriculture, nonwovens are used as protective or capillary mats, shading, and windbreaks.

In aircraft, nonwovens are used as reinforcement media in composites and lightweight insulation. In electronic components, nonwovens are used as battery separators, and in cable insulation—nonwovens of superabsorbent fiber have been used as cablewrap to protect the core from the ingress of water. Vehicle applications include moldable carpet backings, headlinings, and interior trim. In building construction, nonwovens are used for roofing, insulation, and water-impermeable wrappings. In furniture and bedding, nonwovens are used as decking and ticking, quilt backings, carpet backings, underlays, wallcoverings, and padding. In shoes, chemically bonded nonwovens are used as shoe stiffeners and insoles. Uppers and linings are made from synthetic leather which comprises chemically bonded nonwovens made from microfibers.

## BIBLIOGRAPHY

“Nonwoven Fabrics, Survey” in *EPSE* 2nd ed., Vol. 10, pp. 204–227, by A. Drelich, Chicopee; “Nonwoven Fabrics, Staple Fibers” in *EPST* 3rd ed., Vol. 10, pp. 614–637, by R. Chapman, Texon UK Limited.

## CITED PUBLICATIONS

1. R. Johnson, *Robert Johnson Talks It Over*, Johnson & Johnson, New Brunswick, N.J., 1949.
2. J. N. Balboni, in *INDA-TEC'93*, INDA, Cary, N.C., 1993.
3. E. A. Vaughn, *J. Nonwovens Res.* **4**, 1 (1992).
4. ASTM Designation D2475-77, American Society for Testing and Materials, Philadelphia, Pa.
5. U.S. Pat. 3,485,706 (Dec. 23, 1969), F. J. Evans (to E. I. du Pont de Nemours & Co., Inc.).

ROGER CHAPMAN  
Texon UK Limited

## NUCLEAR MAGNETIC RESONANCE

### Introduction

An important objective in materials science is the establishment of relationships between the microscopic structure or molecular dynamics and the resulting macroscopic properties. Once established, this knowledge then allows the design of improved materials. Thus, the availability of powerful analytical tools such as NMR spectroscopy (1–13) is one of the key issues in polymer science. Its unique chemical selectivity and high flexibility allows one to study structure, chain conformation and molecular dynamics in much detail and depth. NMR in its different variants provides information from the molecular to the macroscopic length scale and on molecular motions from 1 to  $10^{10}$  Hz. It can be applied to crystalline as well as to amorphous samples which is of particular importance for the study of polymers. Moreover, NMR can be conveniently applied to polymers since they contain predominantly nuclei that are NMR sensitive such as  $^1\text{H}$  and  $^{13}\text{C}$ .

Although well established for liquid-like samples such as macromolecules in solutions (14,15), the applications of NMR to solid or solid-like polymers is more demanding because of the presence of anisotropic interactions that complicate the analysis of the results. Several techniques for the removal of these interactions have thus been developed and are nowadays in a state where they could be routinely applied. Nonaveraged anisotropic interactions on the other hand provide valuable information that is lost in the solution state. Thus, while it is often necessary to remove the anisotropic interactions, in many cases one would simultaneously like to preserve them in order to exploit their information content.

This is where two-dimensional (2D) spectroscopy comes into play (1), for instance, by correlating one-dimension where the anisotropic interactions are preserved with a (high resolution) dimension where they are removed. Multidimensional NMR spectroscopy proves to be a powerful method to reveal structural and dynamical information at the molecular level in elastomers (16). Residual dipolar couplings can be measured site-selectively and correlated with the cross-link density and mechanical stress. The local segmental order and information on local molecular motions can also be obtained with newly developed 2D NMR methods (16). The information at the molecular level can be correlated with macroscopic properties of elastomers and provides the basis for a better design of material properties for specific applications.

From the viewpoint of NMR, elastomers, and other viscoelastic polymers above their glass-transition temperature exhibit both, solid-like and liquid-like features (12). Whereas the segmental motions give rise to the liquid-like behavior, the presence of permanent or nonpermanent cross-links leads to residual dipolar couplings, that is responsible for the solid-like properties. This promises that both properties can be exploited, but the application of 2D techniques to viscoelastic materials has to deal with the difficulties related to both, rigid and mobile samples (16). Compared with the wealth of applications in solution and in the solid state, NMR has not been widely applied to viscoelastic polymers, although it can provide information on such important areas as the chain dynamics in elastomers, the local structure, residual couplings (induced by chemical cross-links

and topological constraints), dynamic order parameters, internuclear distances, intermolecular interactions (which are important for instance for the miscibility), the effects of fillers on molecular motions, and segmental orientation under mechanical stress and others.

NMR imaging finds most of its applications in medical diagnostics of humans and pathology studies of animal models (17–22). The success of the method is based on noninvasiveness of the nuclear magnetic resonance and the unsurpassed soft-matter contrast, which is hard to achieve with competitive methods like X-ray or computer tomography. The same advantages can be exploited in imaging studies related to materials science (19,22). Here, an important class of soft-matter materials is given by synthetic polymers above the glass transition temperature. Apart from Semicrystalline Polymers (qv) like polyethylene, polypropylene, some polyamides, and polymer melts, elastomers constitute the most striking class of synthetic soft matter with a modulus similar to many biological tissues. Applications of imaging for which nondestructiveness or contrast are essential, are competitive with other imaging techniques in the information gained and the cost of the experiment. Such applications to elastomers concern distributions in temperature, stress, cross-link density, modulus, and the dynamics of fluid absorption and swelling.

The nucleus imaged most often is the proton. The reason is not only sensitivity but also the weak dipolar couplings between protons in a chemical group and between different chemical groups which dominate the signal decay by relaxation. These dipolar couplings are motionally averaged by the often fast but nearly always anisotropic motion of intercross-link chains. This motion and consequently the value of the residual dipolar couplings are affected by chain stiffness, cross-link density, chain orientation, temperature, and additives, etc. Given that the residual dipolar interactions are too strong to obtain chemical-shift resolution without sample spinning or multipulse techniques, relaxation techniques that probe different time regimes of molecular motion provide the primary access to contrast in imaging of elastomers.

After a brief introduction of the basic principles of NMR, the one-dimensional (1D) and two-dimensional (2D) methods that have been applied to viscoelastic materials will be reviewed. NMR imaging which can be considered as a special form of multidimensional NMR will be introduced by discussing principles and image contrast. Illustrative examples of NMR imaging to elastomer materials are given.

## Basic Principles of NMR

**Magnetic Resonance Phenomenon.** Magnetic resonance is a branch of spectroscopy that detects the quantum-mechanical transitions induced by electromagnetic radiation in a system of discrete energy levels of electron or nuclei placed in a static magnetic field. Nuclear magnetic resonance (NMR) employs electromagnetic waves in the radio-frequency range between 900 MHz and 2 kHz.

Nuclear magnetic resonance is one of the most powerful method for structural and dynamics investigation on matter in different states of aggregation. This is due to the following features: (1) The interaction of nuclear magnetic

moments are very weak compared with the thermal energy, therefore, we deal with nuclear paramagnetism. Moreover, the energy delivered by the radio-frequency generator are much larger compared with the strength of these inter-nuclear couplings. That leads to the possibility to manipulate these interactions in a specific way and to simplify the spectral response. (2) The radio-frequency photons have much lower energy compared with the energy of chemical bonds. Therefore, the interaction of electromagnetic radiation with the matter, especially, biomolecules is nonionising. (3) The number of radio-frequency photons with a specific frequency is very large. Hence, the phase of the associated electromagnetic wave is very well defined. The high degree of coherence of radio-frequency radiation is essential for implementation of NMR experiments including magnetic resonance imaging (MRI).

The appearance of NMR spectra, and consequently the molecular structure they are able to provide, arises from the discrete nature of the energy levels pertaining to a nuclear spin system. The energy levels are mainly a result of the Zeeman interaction  $-\vec{\mu} \cdot \vec{B}_0$  between the static magnetic field of induction  $\vec{B}_0$  and nuclear magnetic moment  $\vec{\mu}$ . The quantum-mechanical quantity called spin momentum  $\vec{I}$  is related to magnetic moment by  $\vec{\mu} = \gamma \hbar \vec{I}$ , where  $\gamma$  is the magnetogyric ratio and  $\hbar$  is the Planck constant divided by  $2\pi$ .

In the absence of the magnetic field the nuclear spin states are degenerated (see Fig. 1a). The application of a static magnetic field  $\vec{B}_0$  induces a magnetic interaction described by the Zeeman Hamiltonian  $H = -\vec{\mu} \cdot \vec{B}_0$ . Taking the magnetic field orientation to be along the z-direction we get

$$H = -\gamma \hbar B_0 I_z \quad (1)$$

The eigenvalues  $E_m$  of this Hamiltonian can be evaluated from the Schrödinger equation

$$H|m\rangle = -\gamma \hbar B_0 m|m\rangle \quad (2)$$

where  $|m\rangle$  is the eigenstate corresponding to the eigenvalue  $E_m = -\gamma \hbar B_0 m$ . The magnetic quantum number is  $m$  where  $m = I, I-1, \dots, -I$ . Therefore, the equidistant energy differences are for the single-quantum transitions  $\Delta m = \pm 1$  given by

$$\Delta E = \hbar \omega_0 \quad (3)$$

where the Larmor frequency is  $\nu_0 = \nu_L = \omega_0/2\pi$ . Energy level diagrams of a spin  $I = 1/2$  and  $I = 1$  are shown in Figure 1.

Another important ingredient for a magnetic resonance experiment is represented by the presence of the radio-frequency (rf) field. Only the magnetic component of the electromagnetic field, ie,  $\vec{B}_1(t) = \vec{B}_{10} \cos(2\pi \nu t)$  interacts with the magnetic moment of the nuclei. The amplitude of the rf field is  $\vec{B}_{10}$  and  $\nu$  is the carrier frequency. This field is produced by a rf coil and leads to a perturbation Hamiltonian

$$H_p = -\gamma \hbar \vec{B}_{10} \cdot \vec{I} \cos(2\pi \nu t) \quad (4)$$

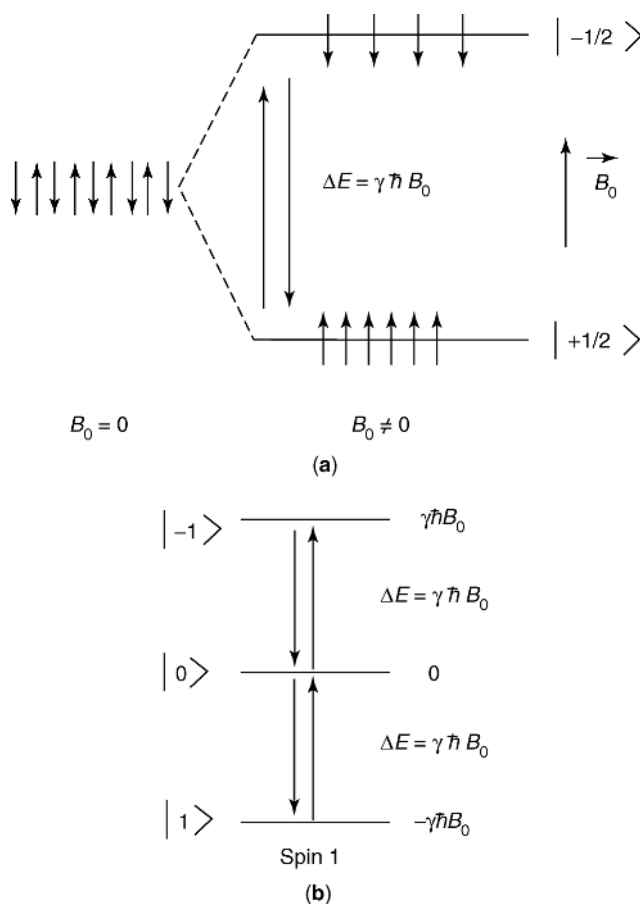


**Fig. 1.** (a) Energy levels diagram and allowed transitions of an ensemble of spins with  $I = 1/2$  in the absence and the presence of  $\vec{B}_0$ . The small arrows indicate the orientation of nuclear spins relative to  $\vec{B}_0$ . (b) Energy diagram and allowed single-quantum transitions for spins with  $I = 1$ .

From time-dependent perturbation theory of quantum-mechanics, it can be stated that a transition between two states  $|\psi\rangle$  and  $|\phi\rangle$  is allowed provided that  $\langle\psi|H_p|\phi\rangle \neq 0$ . This takes place if  $\nu \approx \nu_0$  (ie, the resonance condition) and the alternative magnetic field  $\vec{B}_1(t)$  is polarized perpendicularly to the static magnetic field  $\vec{B}_0$ . Concerning a spin  $I = 1$  (Fig. 1b), similar calculations show that only the single-quantum transitions  $|0\rangle \rightarrow |1\rangle$  and  $|-1\rangle \rightarrow |0\rangle$  (and those in the opposite directions) are allowed in the first approximation and occur at the same frequency, given by equation 3.

Quantitative spin system evolution in the presence of the interspin couplings has to be described in the language of quantum-mechanics. This is a reflection of the quantum-mechanical nature of the spins and the fact that the spin couplings via propagator operators encode NMR observables. Nevertheless, the description of nuclear magnetization relaxation processes is done by a



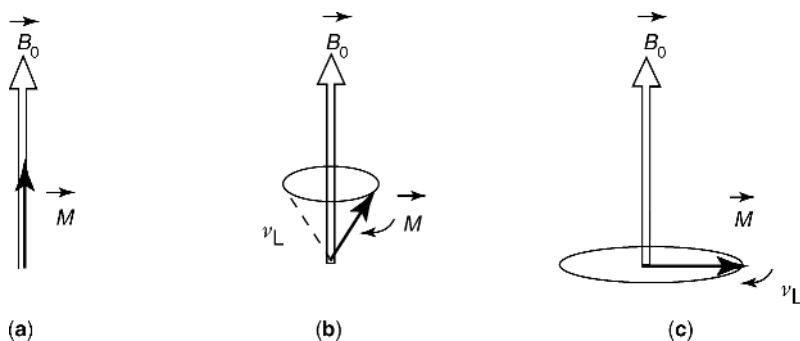


**Fig. 2.** (a) At thermal equilibrium, the nuclear magnetization  $\vec{M}$  is collinear with  $\vec{B}_0$ . (b) Under the action of an electromagnetic perturbation  $\vec{M}$  is displaced from equilibrium position. It starts undergoing precessional motion around  $\vec{B}_0$  at the Larmor frequency  $\nu_L = \nu_0$ . (c) After the action of a  $90^\circ$  rf pulse the magnetization  $\vec{M}$  is brought in a transverse plane to  $\vec{B}_0$ .

semiclassical approach where the thermal bath is described classically and the spin system by a quantum-mechanical formalism.

In general, the NMR experiments are performed at high temperatures employing a large number of spins. These features lead to the possibility to treat classically some aspects of the experiments. The excess of spins oriented along the static magnetic field  $\vec{B}_0$  with respect of those oriented in the opposite direction (cf Fig. 1a) results in a macroscopic nuclear magnetization  $\vec{M}$  aligned along the static magnetic field, which is called equilibrium magnetization (cf Fig. 2a). It can be displaced from this equilibrium by an appropriate perturbation, for instance, by a rf excitation. It is then subject to a precessional motion around  $\vec{B}_0$  with the Larmor frequency  $\nu_L$  (Fig. 2b). The electromagnetic perturbation which brings  $\vec{M}$  into a plane perpendicular to  $\vec{B}_0$  allows the observation of the Larmor precession through an electromotive force which occurs in a coil whose axis is contained in that plane (Fig. 2c). This can be done by rotation of the nuclear magnetization using a resonant  $90^\circ$  rf pulse. The nuclear magnetization  $M$  can be oriented antiparallel to  $\vec{B}_0$  by the action of  $180^\circ$  pulse. The majority of NMR experiments used pulse sequences composed of  $90^\circ$  and  $180^\circ$  rf pulses.

**Magnetic and Electric Spin Interactions.** The nuclear spins can experience various external and internal interactions. These interactions can have magnetic or electric origin. The external interactions are, in general, represented by the Zeeman interactions with static and rf magnetic fields and the gradients of these fields.

The chemical shielding, dipole-dipole, spin-spin indirect coupling or  $J$ -coupling, spin-rotation, and hyperfine couplings represent the major internal magnetic interactions. The quadrupolar interaction has an electrostatic character. All these interactions have a tensorial character, ie, are function on the orientation of the principal axes of the tensor relative to the direction of  $\vec{B}_0$ . They are relevant for solid polymers below and around the glass transition temperatures. For polymer in solution or for soft polymers fast molecular motions average these anisotropic interactions to isotropic or residual values which can be zero. Detailed

description of the properties of these spin interactions can be found in References 1–9.

In the studies of elastomers by NMR experiments dipolar and quadrupolar interactions have been mainly used. The presence of the high magnetic field already imposes a manipulation of the spin system which separates certain parts of the spin interaction Hamiltonian. This process is called truncation and the secular dipolar Hamiltonian of two spins  $I$  and  $S$  has the general form

$$H_d^{(0)} = - \left( \frac{\mu_0}{4\pi} \right) \frac{\gamma_I \gamma_S}{r^3} \frac{1}{2} (3 \cos^2 \theta_{IS} - 1) (3I_z S_z - \vec{I} \cdot \vec{S}) \quad (5)$$

The factor  $\mu_0/4\pi$ , where  $\mu_0$  is the magnetic susceptibility of vacuum has been introduced in conformity with MKSA units. The magnetogyric ratios are  $\gamma_I$  and  $\gamma_S$ . The spin operators are denoted by  $\vec{I}$  and  $\vec{S}$ . The space encoded part of the dipolar Hamiltonian depends on the distance  $r$  of spins  $I$  and  $S$  and the angle  $\theta_{IS}$  between  $\vec{r}$  and  $\vec{B}_0$ . The anisotropic segmental motions average the space part of  $H_d^{(0)}$  to a residual value.

Finally, the truncated form of the axially symmetric quadrupolar Hamiltonian for nuclei with spin  $I$  larger than 1/2 can be expressed as

$$H_Q^{(0)} = C_Q [3I_z^2 - \vec{I}^2] \quad (6)$$

The quadrupolar coupling  $C_Q$  is defined by

$$C_Q = \frac{eQV_{ZZ}}{4hI(2I-1)} \quad (7)$$

where  $eQ$  is the quadrupolar moment of a specific isotope and  $V_{ZZ}$  is the Z component of the electric field tensor at the position of the nucleus. In the presence of anisotropic molecular motions, the electric field gradient tensor is averaged to a residual value.

The spin interactions can be classified as inhomogeneous and homogeneous (4). The NMR spectrum generated by the inhomogeneous spin interaction which is linear in the spin operator  $I_z$ , is a sum of independent individual lines. A selective rf irradiation can saturate only a group of spins producing a hole in the spectrum. For homogeneous lines the NMR spectrum is a sum of individual lines with no shift with respect to each other. The spin interactions bilinear in the spin operators generate these spectra. The excitation of the spectrum with a selective pulse will affect all the spectral frequencies.

**Magnetization Relaxation.** One of the important sources of information about molecular motions is related to the relaxation of the longitudinal ( $M_z$ ) and transverse ( $M_x$  and  $M_y$ ) components of the macroscopic nuclear magnetization. The molecular motions modulate the spin interactions that lead to the exchange of energy between the nuclear energy levels and the lattice or thermal bath represented by the molecular degree of freedom. This process is described by a time constant  $T_1$  the so-called longitudinal relaxation time. The dephasing of the transverse magnetization components  $M_x$  and  $M_y$ , which is related to the increase

of the entropy of the spin system is described by the transverse relaxation time  $T_2$ .

The molecular motions responsible for the relaxation include: (1) overall translational or rotational motions, (2) local motions such as internal rotations around C—C bonds or molecular axis of symmetry or segmental motions of polymer chains, and (3) exchange between two different distinct chemical sites within the same molecule or different molecules.

In the simplest assumption, the time evolution of the nuclear magnetization under relaxation processes can be described by the Bloch equations (see (19), and references therein)

$$\begin{aligned}\frac{dM_{x,y}(t)}{dt} &= -\frac{M_{x,y}(t)}{T_2} \\ \frac{dM_z(t)}{dt} &= -\frac{M_z(t) - M_0}{T_1}\end{aligned}\quad (8)$$

where  $M_0$  is the magnetization of the spin system in the thermodynamic equilibrium. The time evolution of  $\vec{M}(t)$  vector under relaxation processes described by equation 8 is given by exponential functions. This approximation is not valid in many cases for polymer or other macromolecular systems where complex relaxation mechanisms are present (23,24). In such cases, a complete treatment requires additional relaxation parameters such as cross-relaxation or cross-correlation rates (1,23–25). Such a situation occurs whenever two spins A and X interact by a random fluctuating spin interactions. For this cross-relaxation process A spins magnetizations induces a modification of X magnetization which add up to the specific evolution of X magnetization. More formally, this coupling can be expressed via the Solomon equations (see for instance, Reference 25) which contain besides the longitudinal relaxation rates of spins A and X also cross-relaxation rate which reflects the coupling between the A and X spin magnetizations. Several two-dimensional NMR experiments (see below) can measure cross-relaxation rates that enhance our knowledge about molecular motions in complex systems (1,25).

The longitudinal magnetization relaxation can be measured using different methods (5,18,19,25) based on the scheme:

#### Initial perturbation – Evolution ( $\tau$ ) – Detection

The initial perturbation brings the spin system in a state on nonequilibrium and can be represented by an inversion pulse of  $180^\circ$  (ie,  $M_z(0) \rightarrow -M_0$ ) or a saturation train of  $90^\circ$  pulses (ie,  $M_z(0) = 0$ ). The detection is performed by a standard  $90^\circ$  pulse under low or high resolution conditions.

The transverse relaxation measurements are performed using a Hahn echo (see below) or Carr–Purcell–Meiboom–Gill (CPMG) pulse sequences (18,19). The first method uses the pulse scheme:  $90_x^\circ - \tau - 180_{x,y}^\circ - \tau$  – Hahn echo and measure the time evolution of the amplitude of the Hahn echo as a function of echo time  $2\tau$ . CPMG scheme,  $90_x^\circ - [\tau - 180_y^\circ - \tau - \text{Hahn echo}]_N$  allows measuring the transverse magnetization decay in a single scan using a train of  $N$  Hahn echoes.

The mechanisms of relaxation are produced by local magnetic fields originating from randomly fluctuating spin interactions like homonuclear or heteronuclear dipolar, quadrupolar or chemical shielding interactions. They would induce quantum-mechanical transitions in the Zeeman energy levels manifold whose effect would be to take the nuclear magnetization back to the equilibrium configuration. When performing a spectra decomposition of these fluctuating local fields  $\tilde{h}(t)$  (which are in general, tensorial quantities), we can find a nonzero component frequencies equal to those of the various transitions which can exist within the Zeeman energy level diagram. Efficiency of the local magnetic fields to induce transitions can be appreciated by the quantities named spectral densities of the form

$$J_i(\omega) = \int_0^\infty \overline{h_i(t)h_i(0)} \exp(-i\omega t) dt \quad (9)$$

where  $h_i(t)$  is the random fluctuating  $i$  component of local fields. The bar denotes an average over the ensemble of spin systems. On the other hand, a quantum-mechanical transition can be induced by a fluctuating local field at the condition that a certain degree of coherence is present. The autocorrelation function  $C(t) = \overline{h_i(t)h_i(0)}$  is indicative of this coherence that essentially persists for a time equal with the correlation time  $\tau_c$ . A more general correlation function is represented by space-time autocorrelation function  $C(\vec{x}, t)$ , where  $\vec{x}$  is a general spatial coordinate meant to represent translational or rotational coordinates. These correlation functions will turn out to be necessary in the context of characterization of two-dimensional (2D) exchange spectra (2). Moreover, a three-dimensional (3D) spectrum, being a three-time distribution, contains information that cannot be directly retrieved from the 2D spectrum. The detailed information on the nature of the nonexponential loss of correlation in polymers obtained from reduced four-dimensional (4D) exchange spectrum is also not accessible in the corresponding one-dimensional relaxation measurements and the 2D exchange spectrum (2).

Molecular processes with a single correlation time are rarely found in partially or strongly disordered solids like semicrystalline or amorphous polymers. A distribution of the correlation times  $g(\tau)$  has to be introduced in order to evaluate the correlation function (2), ie,

$$C(t) = \int_0^\infty \exp\left\{-\frac{t}{\tau}\right\} g(\tau) d\tau \quad (10)$$

Such distribution has been shown to span several orders of magnitude for instance in the case of local motions in the glassy state. Instead of the distribution function, other fitting functions for correlation function  $C(t)$  are considered. One of these functions is the stretched exponential Kohlraush-Williams-Watts function  $\exp\{-(t/\tau_{\text{kww}})^\beta\}$  that has been found to fit the data quite universally (2).

**Spin Coherences.** In all NMR experiments the spin system evolves under internal and external spin interactions. For isolated spins, the spin dynamics can be described in terms of the motion of classical magnetization vectors. Many structural and molecular dynamics problems in NMR involve couples spins. In

this case, it is necessary to recourse to a quantum—mechanical formalism where a density operator describes the state of the system (1).

The density operator  $\rho(t)$  is a generalized wave function which describes a so-called mixed state. This state corresponds to a statistical ensemble of quantum-mechanical objects, which in our case is a collection of nuclei with magnetic moments. Therefore, the statistics specific of these objects and the statistics of an ensemble are simultaneously present.

The equation of motion for the density operator is given by Liouville–von-Neumann equation

$$i \frac{\partial \rho(t)}{\partial t} = [H(t), \rho(t)] \quad (11)$$

where  $H(t)$  is the Hamiltonian or total energy operator of the system expressed in angular frequency units, which may itself be time dependent. In general, equation 11 does not have an exact solution. Several mathematical methods have been applied to obtain an approximate solution for  $\rho(t)$  one of the most efficient and accurate being the Floquet technique (1). The dynamics of the spin system detected via an observable  $\langle O(t) \rangle$  described by a quantum-mechanical operator  $O$  can be evaluated by

$$\langle O(t) \rangle = \text{Tr}\{O\rho(t)\} \quad (12)$$

Thus, the expectation value is found by evaluating the trace of the product of the observable operator and the density operator.

A particularly simple interpretation of the density matrix is possible in the eigenbase of the Hamiltonian  $H$ . The diagonal element  $\rho_{rr}$  is equal to the probability that the spin system is found in the eigenstate  $|r\rangle$ . The population of state  $|r\rangle$  is  $P_r$  and therefore,  $\rho_{rr} = P_r$ . The off-diagonal element is defined by

$$\rho_{rs} = \langle r | \rho(t) | s \rangle = \overline{c_r(t)c_s^*(t)} \quad (13)$$

where the bar indicates an ensemble average. These elements describe a “coherent superposition” of eigenstates  $c_r(t)|r\rangle + c_s(t)|s\rangle$  in the sense that the time dependence and the phase of the various members of the ensemble are correlated with respect to  $|r\rangle$  and  $|s\rangle$ . Such a coherent superposition is simply called “coherences”. A spin coherence can be associated with a transition between two eigenvalues specified by the eigenstates  $|r\rangle$  and  $|s\rangle$ . If the two states span an allowed transitions with a difference in magnetic quantum numbers  $\Delta M_{rs} = M_r - M_s = \pm 1$ , the coherences  $\rho_{rs}$  is related to the NMR observables represented by the transverse magnetization components  $M_x^{(rs)} \pm iM_y^{(rs)}$ . In general, a matrix element of the density operator  $\rho_{rs}$  represents  $p$ -quantum coherence for which  $p = M_r - M_s$ , which, for  $p \neq \pm 1$ , does not lead to observable magnetization and can only be detected indirectly by two-dimensional spectroscopy (1,26).

The density operator  $\rho(t)$  has been formulated for the entire quantum-mechanical system. For magnetic resonance applications, it is usually sufficient to calculate expectation values of a restricted set of operators which act exclusively on nuclear variables. The remaining degrees of freedom are referred to

as “lattice”. The reduced spin density operator is defined by  $\sigma(t) = \text{Tr}_1\{\rho(t)\}$ , where  $\text{Tr}_1$  denotes a partial trace over the lattice variables. The reduced density operator can be represented as a vector in a Liouville space of dimension  $n^2$ , ie,

$$\sigma(t) = \sum_r^{1,n^2} b_r(t) B_r \quad (14)$$

where  $n$  is the dimension of the Hilbert space of all admissible state functions and  $\{B_r\}$  is a complete set of orthogonal base operators. A proper selection of this base is often essential to ease the solution of a particular spin dynamics problem. For instance, for systems with spins  $I_k = 1/2$  the product of the Cartesian spin operators is a convenient base operators (1,27). As an example, the complete set of product operators  $\{B_r\}$  for two  $J$  or dipolar coupled nuclei with spin  $I = 1/2$  consists of  $2^{2 \times 2} = 16$  operators, ie,

$$\frac{1}{2} E \text{ (E is the unity operator), } I_{ix}, I_{iy}, I_{iz}$$

$$2I_{ix}I_{jx}, 2I_{iy}I_{jy}, 2I_{iz}I_{jz}, 2I_{ix}I_{jy}, 2I_{ix}I_{jz}, \text{ for } i, j = 1, 2 \quad (15)$$

The spin modes described by the product operators of equation 15 are the matrix elements of the density operator

$$\rho = \begin{pmatrix} P_1 & \text{SQ} & \text{SQ} & \text{DQ} \\ \text{SQ} & P_2 & \text{ZQ} & \text{SQ} \\ \text{SQ} & \text{ZQ} & P_3 & \text{SQ} \\ \text{DQ} & \text{SQ} & \text{SQ} & P_4 \end{pmatrix} \quad (16)$$

The above product operators can be detected by a proper design NMR experiment (1,26) and reflect different features of the spin systems related to the structure, spin interaction topology, and molecular dynamics. The most popular spin modes are represented by single-quantum coherences (SQ) of spin  $i$ ,  $I_{ix}$  and  $I_{iy}$  that are related to  $x$ - and  $y$ -magnetizations, respectively. Two-spin coherences of spin  $i$  and  $j$  consist of superposition of  $p = 0$  (zero-quantum (ZQ)) and  $p = \pm 2$  (double-quantum (DQ)) quantum coherences. The former is insensitive to the inhomogeneity of the magnetic field and the latter is reflecting the existence of spin couplings. Not only the existence of  $J$ - or dipolar couplings can be detected by editing DQ coherences but also the strength of these couplings can be measured including internuclear distances and dihedral angles (27–29).

**Spin-Echoes.** The evolution of spin coherences under nonfluctuating spin interactions is a reversible process. The strength and sign of the spin Hamiltonians can be manipulated by rf pulses and/or sample rotation such that the evolution of the spin system during a period of time is refocused during the spin system evolution at a latter time.

The spin interactions described by inhomogeneous or homogeneous spin Hamiltonians lead to inhomogeneous and homogeneous spin-echoes. If a linear superposition of both types of spin Hamiltonians is present, a mixed spin-echo

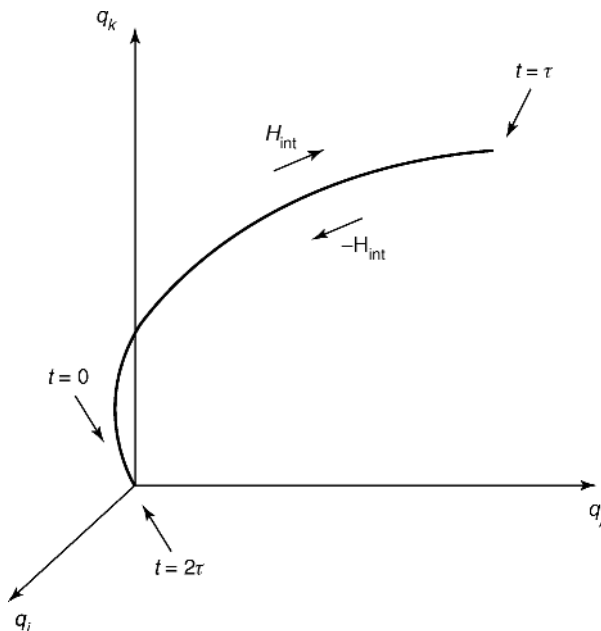


**Fig. 3.** Evolution of the quantum-mechanical state of a spin system in a Liouville space. The evolution from the initial time  $t = 0$  to an intermediate time  $t = \tau$  takes place under a Hamiltonian  $H_{\text{int}}$  which describes internal and external spin interactions. At this time, a pulse sequence change the sign of the spin Hamiltonian. The spin system evolves on the same generalized trajectory and after total evolution time  $t = 2\tau$  the initial state is refocused under a spin echo.

can be generated. The most common used inhomogeneous echoes are: Hahn (30), stimulated (30), and gradient echoes (5,18). Solid (31) and magic (32–34) echoes are the most familiar types of homogeneous echoes.

In order to understand how a spin echo can be produced, we shall consider a spin system composed of  $N$  nuclei, which interact, or not between themselves. The quantum-mechanical state of such a system can be described by a linear superposition of spin coherences represented by a vector evolving in a Liouville space of dimension  $2^{2N}$  (cf Fig. 3). In this abstract space, the state of the spin system at time  $t = 0$  is represented by a configurational point. This state corresponds in many cases to the single-quantum coherences excited after a  $90^\circ$  rf pulse. The spin system evolves in laboratory or rotating reference frames for a time  $\tau$ , evolution described by the propagator operator  $E_{\text{evolution}} = \exp\{-iH_{\text{int}}\tau\}$ , where  $H_{\text{int}}$  is the spin-interaction Hamiltonian. At the end of this evolution period, a pulse or a complex pulse sequence is applied which change the sign of the Hamiltonian  $H_{\text{int}}$ . During the refocusing period of duration  $\tau$  the evolution operator is now  $E_{\text{refocusing}} = \exp\{-i(-H_{\text{int}})\tau\}$ . This is formally equivalent with a time reversal, ie,  $\tau \rightarrow -\tau$ . For the full evolution period  $2\tau$ , the propagator is  $E_{\text{evolution}} E_{\text{refocusing}} = E$ , where  $E$  is the unity operator and the spin system is reaching the initial state. Hence, a spin echo was generated with an amplitude identical with the free induction decay as long as the magnetization relaxation processes are neglected.

The pulse sequence used for generation of inhomogeneous spin-echo of the Hahn type is shown in Fig. 4a. The spin systems for which this echo can be produced are characterized by the Hamiltonian  $H_{\text{int}} = -\delta I_z$ , where  $\delta$  describes the inhomogeneity of the magnetic fields or chemical shift distributions. By the action of refocusing  $180^\circ_y$  pulses, the spin operator  $I_z$  becomes  $-I_z$  and the spin Hamiltonian changes the sign, ie,  $H_{\text{int}} = -H_{\text{int}}$ . If the transverse magnetization relaxation is neglected, the amplitude of the Hahn echo is equal with the amplitude of the free induction decay generated after  $90^\circ_x$  preparation pulse (cf Fig. 4a). The relaxation encoding is given by the factor  $\exp\{-2\tau/T_2\}$ , where  $T_2$  is the transverse relaxation time. The Hahn echo represents an important tool for measuring residual dipolar couplings, correlation function of molecular motions, and encoding of spatial information and mass transport. If the  $180^\circ_x$  pulse is split in two  $90^\circ_x$  pulses separated by a time  $\tau_2$  (cf Fig. 4b), a stimulated echo is produced at time  $\tau_1$  after the action of the last pulse. This spin-echo has under ideal conditions the amplitude half of the amplitude of FID and the lifetime is much longer compared with that of the Hahn echo. Therefore, it is an ideal instrument for measuring self-diffusion coefficients.

The scheme used for gradient echo is presented in Figure 4c. The evolution of the single-quantum excited by a preparation  $90^\circ_x$  pulse under a field gradient  $G_z$  is refocused by the filed gradient with the opposite direction  $-G_z$ . The amplitude of the echo is affected by the presence of the magnetic field gradients inside the sample. This effect is exploited for enhancement of the contrast in MRI.

In many rigid or soft polymers, the protons are dipolar coupled in a complex network. The dipolar Hamiltonian is bilinear in spin operators representing a homogenous interaction. Pulse sequences can be designed that change the sign of the dipolar Hamiltonian  $H_d$ , ie,  $H_d \rightarrow -kH_d$ , where  $k$  is a scaling factor. An example of such a homogeneous spin-echo is given by magic echo for which  $k = 1/2$  (cf Fig. 5b). The most simple homogeneous spin echo is represented by solid echo (Fig. 5a). For a spin system composed of spin-1/2 pairs the spin evolution is fully refocused by the solid echo. This is not the case for a multispin dipolar network. These echoes can be used for high resolution NMR spectroscopy of solids, measurement of residual spin interactions, and NMR imaging of rigid polymers.

**Two-dimensional Fourier Spectroscopy.** Two-dimensional (2D) spectroscopy is a general concept that can be applied to different branches of spectroscopy which make it possible to acquire more detailed information about the molecular system under investigation. Since the first proposal in the 1971 (35) and the first experimental realization in the 1974 (36–38) a large number of 2D NMR methods have been invented and applied (1) to solve structural and dynamical problems in physics, chemistry, biology, and medicine.

Several strategies can be employed for obtaining a 2D spectrum, which is a signal function  $S(\omega_1, \omega_2)$  of two independent frequency variables  $(\omega_1, \omega_2)$  (1). The most popular one is based on the 2D time-domain experiments. In this approach, a time-domain signal  $s(t_1, t_2)$  is obtained by incrementing the time interval  $t_1$  parametrically from experiment to experiment, and recording the free induction signal as a function of  $t_2$ . In a general case, for a 2D experiment, we distinguish four intervals:

$$[\text{Preparation } (t_p)] - [\text{Evolution } (t_1)] - [\text{Mixing } (t_m)] - [\text{Detection } (t_2)].$$



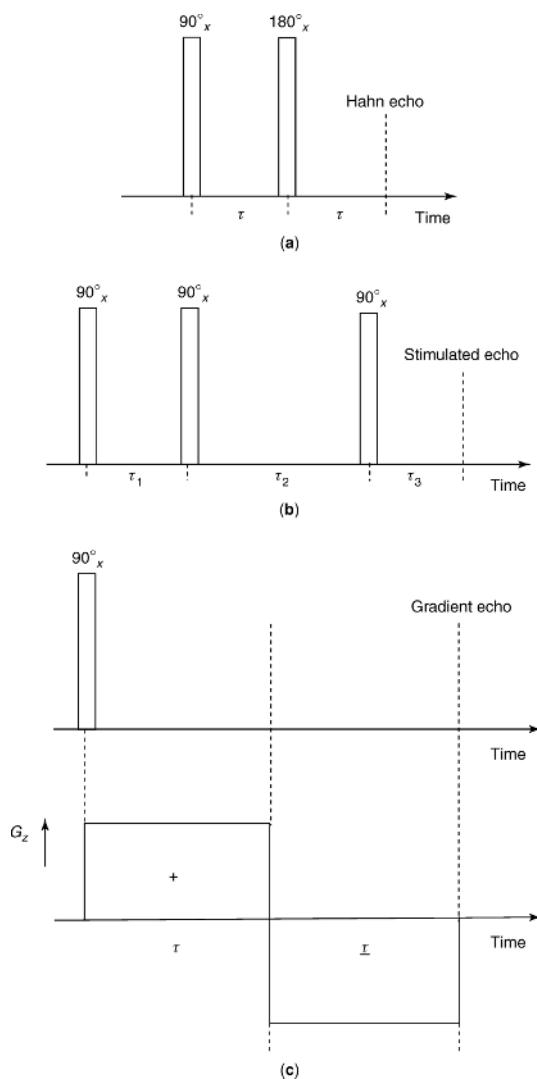


**Fig. 4.** Pulse sequences used for Hahn echo (a), stimulated echo (b), and gradient echo (c) are shown.

The four basic intervals have the following qualitative features: (1) *Preparation period*: In the course of this period of fixed length the spin system is prepared in a coherent nonequilibrium state. In the simplest experiments, the preparation period consists of a single rf pulse. However, this period can involve more sophisticated procedures like cross-polarization (39,40) and excitation of multiple-quantum coherences (1,41). (2) *Evolution period*: During this period, in general, the spin system evolves under a spin Hamiltonian, which may be modified by heteronuclear decoupling (42), sample spinning (43,44), or homonuclear decoupling pulse sequences (45,46). The evolution during this indirect dimension of the 2D experiment determines the frequencies in the  $\omega_1$ -domain. (3) *Mixing period*: This

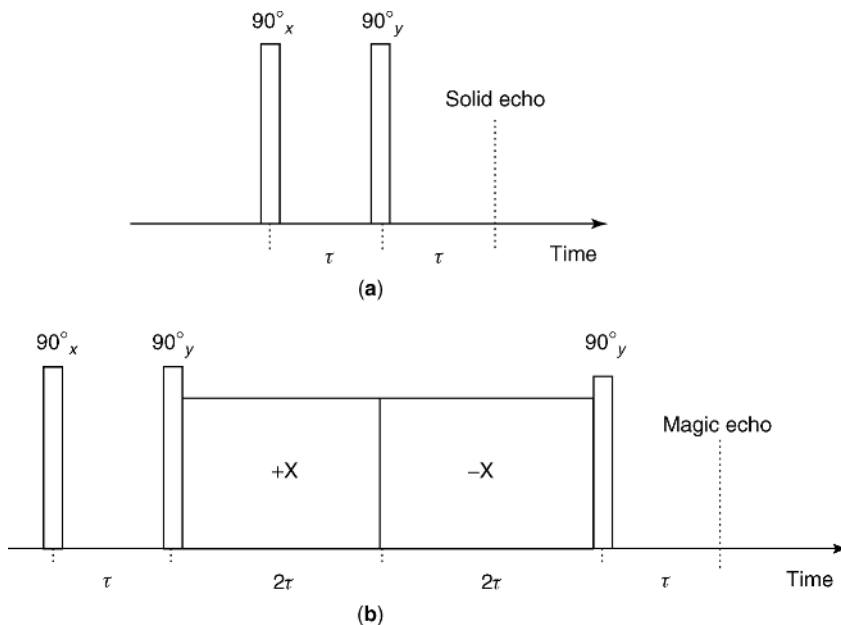


**Fig. 5.** Pulse sequences used for solid echo (a) and magic echo (b) are shown.

period may consists of one or more rf pulses, separated by intervals with fixed or variable durations. During the mixing period, transfer of coherences or polarization can take place. For instance, mixing process transforms single (SQ)-, multiple (MQ)- or zero-quantum (ZQ) coherences into observable transverse magnetization. In many cases, the 2D spectrum may be regarded as a visual representation of the pathways of the mixing process. (4) *Detection period*: In the course of the detection period, the SQ coherences evolution is measured as a function of time-domain variable  $t_2$ . The spin system can be manipulated by the action of coherent averaging pulse sequences and/or sample spinning, or by polarization transfer to nuclei with higher sensitivity. Finally, a complex 2D spectrum is obtain for the time-domain data by a complex 2D Fourier transformation defined by

$$S(\omega_1, \omega_2) = \int_{-\infty}^{\infty} dt_1 \exp\{-i\omega_1 t_1\} \int_{-\infty}^{\infty} dt_2 \exp\{-i\omega_2 t_2\} s(t_1, t_2) \quad (17)$$

The major advantages of 2D NMR spectroscopy are related to the assignment of complex spectra, of revealing the correlated transitions to establish  $J$ - or dipolar coupling topologies or for studying complex dynamic processes. These features lead to a classification of 2D spectroscopic experiments in three groups (1).

The interpretation of NMR spectra is often impeded by the complexity of overlapping resonances. When the interactions responsible for the multiplet structure are different such as chemical shielding, dipolar, or scalar couplings, it is often possible to render spectra more intelligible by *separating* various

interactions in orthogonal frequency domains. In the course of *2D separation* experiments the number of peaks is conserved.

The second group of 2D experiments is represented by *2D correlation* methods based on coherence transfer. These experiments allow interpretation of NMR spectra of networks of coupled spins by establishing the connectivities of nuclear spins coupled by *J* or dipolar interactions. The appearance of cross-peaks in 2D correlation spectra constitutes a proof of the existence of resolved scalar or dipolar couplings, and allows one to correlate the chemical shifts of coupled partners. These experiments are designed to correlate transitions of coupled spins by transferring magnetization of MQ coherences from one transition to another in the course of a suitable designed mixing process.

A third class of 2D time-domain experiments is concerned with studying *dynamic processes* such as cross-relaxation, nuclear Overhauser effects, chemical exchange, and magnetization exchange including spin diffusion (1,2). These methods have a number of advantages particularly when the system comprises an extended network of exchange processes that occur simultaneously. Moreover, the 2D methods are most useful for studying slow dynamic processes with rates that are too low to affect the lineshapes. The basic idea of 2D exchange spectroscopy is the “frequency labeling” of the longitudinal magnetization of various chemical sites before chemical or magnetization exchange takes place, such that after exchange the pathways of the magnetization can be traced back to their origins.

The magnetic resonance imaging (MRI) techniques used most frequently for applications to soft polymers are directly related to the multidimensional Fourier transform (5,18,19,47). Just like in 2D spectroscopy, the phase of the signal acquired during the detection period (time domain  $t_2$ ) is modulated by the coherence phases present in the evolution period ( $t_1$ ). The idea is that the accumulated signal phase is primarily a result of the applied gradient which induces a position encoding. A 2D Fourier transformation then produces a 2D image of the object.

## One-Dimensional NMR Studies of Molecular Motions and Dynamic Order

NMR methods can probe molecular dynamics in polymers on various time scales from relatively fast segmental motions (with correlation times of the order of  $10^{-10}$  s) down to slow motions in the  $10^{-3}$  s range or even slower (2–6,48). Dynamics in the range of around  $10^{-10}$  s can be investigated by  $T_1$  measurements that are sensitive to motions around the Larmor frequency. Particularly useful for such investigations is the field cycling technique, where the magnetic field and thus also the Larmor frequency  $\omega$  can be varied over several orders of magnitudes down to the 10 kHz regime. By acquiring  $T_1(\omega)$ , molecular dynamics can be probed over the corresponding range ((5), and references therein).

Slow motions can be studied using so-called longitudinal relaxation in the rotating frame ( $T_{1\rho}$ ) (5). In these experiments, a radio-frequency field (“spin-lock pulse”) with field strength of around 10–100 kHz plays the same role as the main magnetic field does for  $T_1$ . For instance, the changes in the phase structure under

mechanical deformation of thermoplastic elastomers have been investigated by  $T_{1\rho}$  measurements of  $^{13}\text{C}$  nuclei under MAS (49).

Transverse relaxation ( $T_2$ ) and lineshape analysis has also been the topic of many studies of molecular dynamics in viscoelastic media ((12,13,50,51), and references therein). It was found to be indicative of heterogeneities of molecular motions (12,13). Transverse relaxation curves therefore often turn out to be composed of a superposition of multiexponential and the Gaussian decays. Measurement of residual dipolar couplings, molecular motions, and other parameters have been performed by this relaxation technique on different nuclei like  $^1\text{H}$ ,  $^{13}\text{C}$ ,  $^{15}\text{N}$ ,  $^{31}\text{P}$ , and  $^{29}\text{Si}$  and could be related to material properties such as the cross-link density (12,13). In order to separate the liquid-like and solid-like contributions of the  $T_2$  decay, a linear combination of Hahn echoes and solid echoes have been used (52,53). While Hahn spin-echo amplitudes are encoded by irreversible dephasing due to molecular motions and by reversible residual dipolar couplings, only the first effect encodes the amplitudes of solid echo (actually mixed echo) to first approximation. The appropriate combination of these spin-echoes thus gives access to residual dipolar couplings and the fluctuation rate (52,53). The method was applied to measure the degree of segmental order induced in natural rubber upon stretching (53).

A powerful technique for the study of orientation and dynamics in viscoelastic media is lineshape analysis in deuterium NMR spectroscopy (2,50,51,53). Recent reviews on this topic were published (50,51). For instance, the average orientation of chain segments in elastomer networks upon macroscopic strain can be determined by this technique (54–60). For a nondeformed rubber, a single resonance line in the deuterium NMR spectrum is observed (57) while the spectrum splits into a well-defined doublet structure under uniaxial deformation. It was shown that the usual network constraint on the end-to-end vector determines the deuterium lineshape under deformation, while the interchain (excluded volume) interactions lead to splitting (57–60). Deuterium NMR is thus able to monitor the average segmental orientation due to the cross-links and mean field separately (60).

The network structure of unfilled and filled elastomers was probed by the analysis of the quadrupolar splitting in  $^2\text{H}$  solid echo spectra of uniaxially strained samples (55) (see Fig. 6). The local chain order at a given elongation is larger by a factor of 1.5–2 in the filled system. A decrease of local chain mobility in the absorption layer is observed under stress. The same method was applied to investigate molecular dynamic in thermoplastic elastomer based on hydrogen bonding complexes (61,62).

The 1D NMR techniques described above already allow a detailed investigation of polymer dynamics but they are mostly not selective in the sense that they do not provide information on the averaging of particular couplings. For the interpretation of some of the above results therefore a representative spin pair along the chain was assumed, thus neglecting local site-specific motions as well as the geometry of the bonds. This is where multidimensional NMR techniques come into play.

**Residual van Vleck Moments.** The difficulties related to these measurements are due to the small values of the residual spin couplings compared to those of other spin interactions, the many-body character of the dipolar couplings and

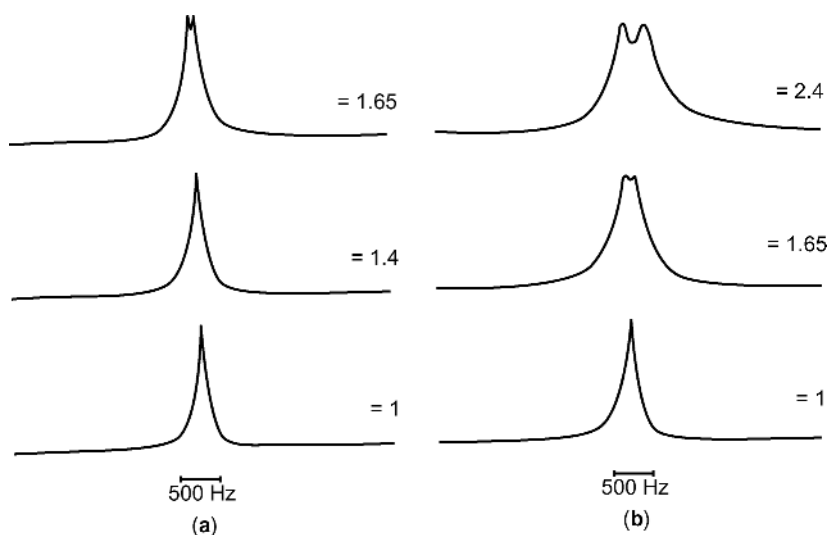


**Fig. 6.** Deuterium solid echo spectra of unfilled (a) and filled (b) poly[dimethylsiloxane] networks at 305 K with and without mechanical stress as given by the parameter  $\lambda$ . Reproduced from Ref. 55, with permission from Wiley-VCH.

the presence of molecular motions which produce a supplementary encoding of the spin system response.

One-dimensional (1D) NMR methods based on the dipolar correlation effect in combination with the Hahn and solid echoes (52,63), the stimulated echo (5), the magic echo (64), magnetization-exchange (65), and cross-relaxation dynamics (66) provide access only to the second van Vleck moment via a model which takes into account the solid-like and liquid-like contributions to the spin system response (67). Model free access is given by the analysis of multiple-quantum buildup (68) and decay (69) curves recorded in the initial regime of the excitation/reconversion periods.

In the following, we discuss a method to measure model free the residual dipolar van Vleck moments without contributions from inhomogeneous spin interactions originating from static magnetic field inhomogeneities, local susceptibility effects, and heteronuclear dipolar interactions (70). Moreover, in the first approximation this method is insensitive to the transverse relaxation produced by the fluctuating dipolar interactions.

**Principles of the Method.** The method is based on the mixed echo composed of the Hahn and the magic echo (33,71,72). The Hahn echo explores the magic echo shape generated by an accordion magic sandwich (cf Fig. 7).

One possibility to have the amplitude of the Hahn echo encoded by the homonuclear dipolar interactions is to employ a mismatched magic sandwich (MS), ie,  $90_x^\circ - (\tau + n\Delta) - 90_y^\circ - \text{Burst Pulse}_x (2\tau - n\Delta) - \text{Burst Pulse}_x (2\tau - n\Delta) - 90_y^\circ - (\tau + n\Delta) - \text{Mixed Echo}$  (see Fig. 7), where  $n$  is a positive and negative integer number and  $\Delta$  is the time decrement and increment, respectively. We call this mismatched MS composite pulse with variable  $n$  the *accordion magic sandwich* (hereafter the method will be called AIMS).

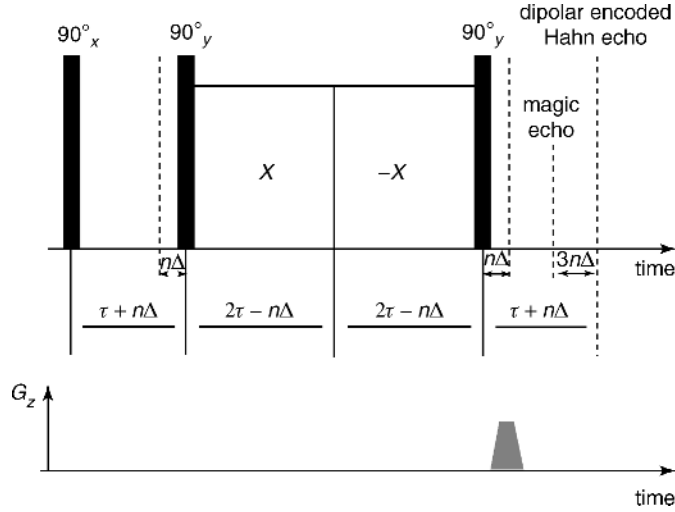


**Fig. 7.** AIMS pulse sequence used for generation of a mixed echo composed of a magic and a Hahn echo. A dephasing gradient pulse is applied at the end of the sequence. Reproduced from Ref. 70, with permission from Elsevier.

The spin system response to the AIMS sequence was evaluated in Reference 70 for a multispin dipolar network characteristic to elastomers and other soft polymers. It was shown that the normalized amplitude of the Hahn echo measured at time  $t = 6\tau$  is encoded only by the homonuclear dipolar couplings and relaxation, ie,

$$\frac{S(3n\Delta)}{S(0)} = \frac{\text{Tr} \left\{ I_y \exp \left\{ -i\hat{H}_d^{(0)}(3|n|\Delta) \right\} I_y \right\}}{\text{Tr} \{ I_y^2 \}} \exp \left\{ -2n\Delta \left( \frac{1}{T_2^*} - \frac{1}{T_{2\rho}^*} \right) \right\} \quad (18)$$

where  $T_2^*$  and  $T_{2\rho}^*$  are the effective transverse relaxation times in the laboratory and rotating frames, respectively. It is easy to see from the above equation that a combination of signals taken with  $+|n|$  and  $-|n|$  is given by

$$\frac{S(3|n|\Delta)S(-3|n|\Delta)}{S(0)^2} = G(3|n|\Delta)^2 \quad (19)$$

This composite NMR signal is not encoded by the transverse relaxation. The function  $G(t)$  describes the magic echo shape and is given by (4)

$$G(t) = \frac{\text{Tr} \left\{ I_y \exp \left\{ -i\hat{H}_d^{(0)} t \right\} I_y \right\}}{\text{Tr} \{ I_y^2 \}} \quad (20)$$

In the short-time limit, ie, for  $3|n|\Delta\omega_d \ll 1$ , we obtain from the above equations,

$$\frac{S(3|n|\Delta)S(-3|n|\Delta)}{S(0)^2} \cong 1 - \bar{M}_2(3|n|\Delta)^2 + \frac{1}{12}\bar{M}_4(3|n|\Delta)^4 - \dots \quad (21)$$

where  $\bar{M}_2$  and  $\bar{M}_4$  are the residual second and forth van Vleck moments, respectively (4).

In conclusion, the AIMS pulse sequence produces a disentanglement of the magic and Hahn echoes in time. The dipolar encoding of the signal occurs because the Hahn echo samples the magic echo shape.

**<sup>1</sup>H Residual van Vleck Second Moments of Cross-Linked Series of Natural Rubber.** Proton residual second and fourth van Vleck moments were measured by AIMS for the samples of cross-linked series of natural rubber (NR). The residual van Vleck moments  $\bar{M}_2$  and  $\bar{M}_4$  can be evaluated by the best fits of the composite signals with equation 21 and these results are shown in Figures 8a and 8b, respectively, for the whole NR series.

The measured values of  $\bar{M}_2$  are in good agreement with the values measured on the same series using the model dependent dipolar correlation function (64). The best fit of the dependence of  $\bar{M}_2$  and  $\bar{M}_4$  on shear modulus  $G$  is given by continuous lines in figures 9a and 9b. These are described, in general, by a polynomial  $\sum_1^m (-1)^p a_p G^p$  up to the powers four and eight in  $G$ , respectively. This polynomial dependence can be justified by considering high order corrections to a Gaussian distribution of the end-to-end vectors (68). The classical Gaussian distribution will lead only to dependences of powers two and four in  $G$  which are shown by the dashed lines in these figures. Nevertheless, in the case of samples with low values of the cross-link density the Gaussian approximation is able to describe the experimental data sufficiently well (see the insets of figures 8a and 8b). These results also show that high order van Vleck moments are more sensitive to cross-link density compared to the second van Vleck moment which is usually used.

The value of the ratio  $\bar{M}_4/\bar{M}_2^2$  on shear modulus is shown in figure 8c. The <sup>1</sup>H NMR absorption lineshape is quasi-Lorentzian for all samples but starts to deviate towards a Gaussian lineshape for higher values of the cross-link density.

**Residual Dipolar Couplings by <sup>1</sup>H Multiple-Quantum NMR.** The measurements of residual dipolar couplings in elastomer system is desirable, because they reflect the hindrance to molecular motions by the cross-linking, topological constraints, and the external factors like mechanical stress. Dipolar-encoded longitudinal magnetization (DELM) NMR decay curves, double-quantum (DQ) and triple-quantum (TQ) NMR buildup intensities for measuring the residual dipolar couplings and the associated dynamic order parameters were discussed in Reference 68. These methods allow measuring residual dipolar couplings model free and in the limit of short excitation time regime the effective dipolar network is simplified.

**Principles of the Method.** One of the important features of the MQ spectroscopy is the possibility to edit the strongest dipolar couplings. This feature is based on the fact that the efficiency of MQ pumping is a nonlinear function of the dipolar coupling strength. For instance, the pumping efficiencies of DQ and

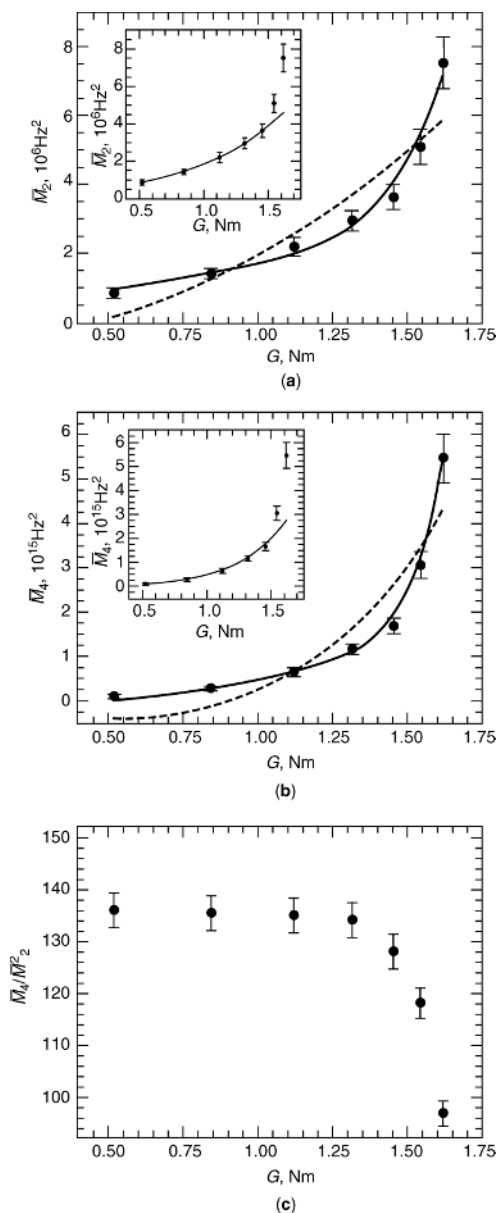


**Fig. 8.** Proton residual van Vleck moments  $\bar{M}_2$  (a),  $\bar{M}_4$  (b), and the ratio  $\bar{M}_4/\bar{M}_2^2$  (c) measured by AIMS for the samples of a series of cross-linked natural rubber versus the shear modulus  $G$ . Reproduced from Ref. 70, with permission from Elsevier.

TQ coherences in the initial excitation time regime are proportional to  $(D^{ij})^2$  and  $(D^{ij})^4$ , respectively, where  $D^{ij}$  is the dipolar strength between protons  $i$  and  $j$  (73–75). Therefore, we can estimate that the pumping efficiency of DQ coherences for methylene protons is about six times higher compared to that of methyl protons. The editing capabilities are expected to be even better for the intergroup dipolar



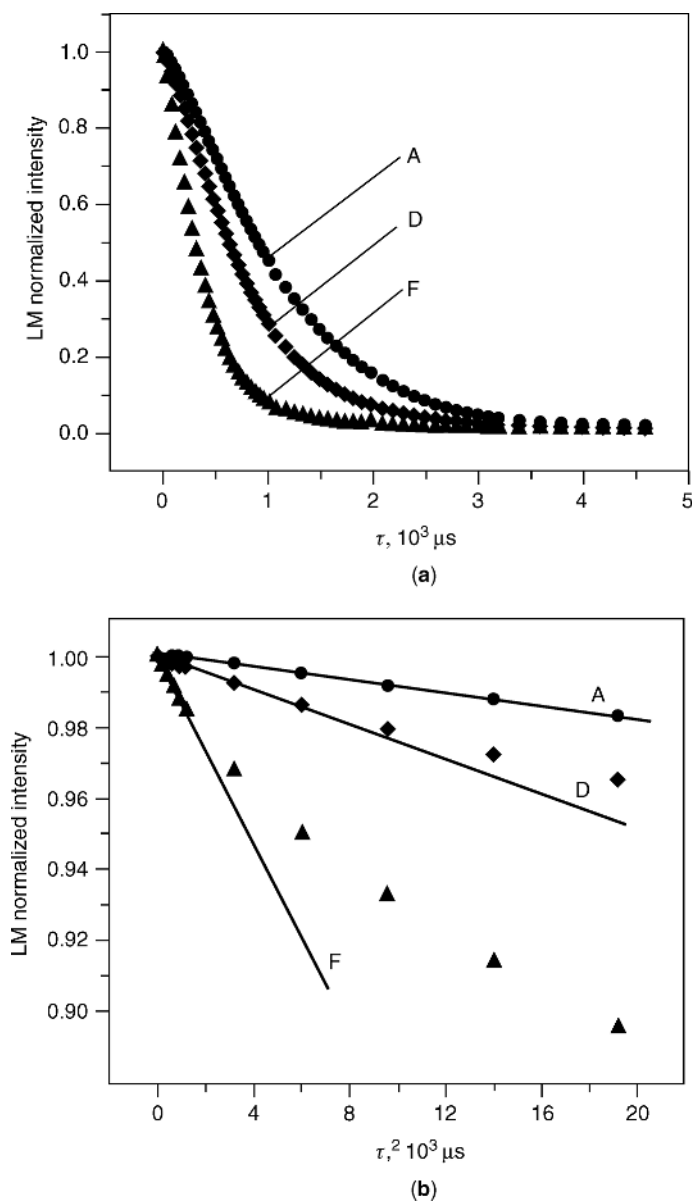


**Fig. 9.** (a) Proton dipolar-encoded longitudinal magnetization decay curves for a series of synthetic polyisoprene samples with different cross-link densities. (b) The initial time behavior of DELM decays exhibits a linear dependence in  $\tau^2$  (solid lines). Reproduced from Ref. 68, with permission from American Institute of Physics.

interactions. In the case of TQ coherences, the maximum pumping efficiency is expected for the methyl group.

The possibility to implement a MQ dipolar filter has already been demonstrated. For instance, by use of a  $^{13}\text{C}$ – $^{13}\text{C}$  DQ dipolar filter working in the initial

excitation time regime the signal of the crystalline domains in polyethylene could be enhanced (74). The possibility of functional group editing by MQ NMR methods is also supported by DQ experiments performed on static and rotating elastomers. The 2D  $^1\text{H}$  DQ MAS spectrum of polyisoprene (68) shows that for short excitation times the response of the methylene protons can be approximated well by an isolated spin pair. Moreover, the experiment shows that the DQ coherences at which methyl protons participate are mainly originating from the  $\text{CH}_3$  group. This also leads to the conclusion that TQ coherences excited in the initial time regime can be attributed mainly to the methyl groups. Weak dipolar coupling of  $\text{CH}_2$  and  $\text{CH}_3$  protons with CH protons is demonstrated (68). But, the contribution of the methine protons to the overall NMR signal is only about 12% so that these couplings are negligible in a good approximation.

The spin system response to the pulse sequence used for excitation of different multipolar spin states can be evaluated in the limit of short dipolar encoding time. For DELM, it is possible to write (68)

$$S_{\text{DELM}}(\tau) \approx 1 - \left\{ l_2 [D^{(2)} S_s^{(2)}]^2 + l_3 [D^{(3)} S_s^{(3)}]^2 + \text{intergroup} \right\} \tau^2 - \dots \quad (22)$$

$$\equiv 1 - [D_{\text{eff}}]^2 \tau^2 - \dots$$

where the numerical coefficients are  $l_2 = 21/80$ , and  $l_3 = 63/190$  and correspond to the  $\text{CH}_2$  and  $\text{CH}_3$  groups.  $D_{\text{eff}}$  is the effective residual dipolar coupling describing contributions from both  $\text{CH}_2$  and  $\text{CH}_3$  groups as well as intergroup residual dipolar couplings. Nevertheless, the residual dipolar couplings of methylene and methyl protons dominate the intergroup couplings and the slope of the LM decay curve versus the square of the excitation time  $\tau$  is given by a weighted sum of the squares of dynamic order parameters of  $\text{CH}_2$  and  $\text{CH}_3$  groups.

The DQ signal can be evaluated in a similar manner, and finally one can write

$$S_{\text{DQ}}(\tau) \approx \left( d_2 [D^{(2)} S_s^{(2)}]^2 + d_3 [D^{(3)} S_s^{(3)}]^2 + \text{intergroup} \right) \tau^2 + \dots \quad (23)$$

$$\equiv [D'_{\text{eff}}]^2 \tau^2 + \dots$$

where the numerical coefficients are  $d_2 = 21/40$  and  $d_3 = 9/200$ . An effective residual dipolar coupling  $D'_{\text{eff}}$  similar (but not identical) to  $D_{\text{eff}}$  for dipolar encoded longitudinal magnetization can be introduced describing DQ-edited residual dipolar couplings.

In the regime of short excitation times the TQ coherences are derived mainly from the methyl protons. The spin system response to the pulse sequence (68) for a proton triad rotating rapidly around the  $\text{C}_3$  axis in a static sample can be evaluated similar to the procedure used for DQ coherences. In the limit of short excitation times, the normalized TQ-filtered signal is given by

$$S_{\text{TQ}}(\tau) \approx \left( r_3 [D^{(3)} S_s^{(3)}]^4 + \text{intergroup} \right) \tau^4 + \dots \quad (24)$$

$$\equiv [D''_{\text{eff}}]^4 \tau^4 + \dots$$

where  $r_3 = 39/4$ . Again as above, an effective residual dipolar coupling  $D''_{\text{eff}}$  can be introduced for the full dipolar network. These effective residual dipolar couplings, introduced by the above equations, depend on the dipolar network edited by the experiments and it is therefore not easy to express them in terms of site-specific dynamic order parameters. Nevertheless,  $D''_{\text{eff}}$  is expected to be dominated by the methyl protons.

**Dynamic Order Parameters.** Dipolar-encoded longitudinal magnetization decay curves were measured for  $^1\text{H}$  in a series of cross-linked synthetic polyisoprene samples (68). The decays for three samples (A, D, and F with the cross-link density of 0.75, 5.0, and 15.0, respectively) are shown in Figure 9.

The decay curves show a dependence on the cross-link density. In the short-time regime, the dipolar-encoded LM decays display a linear dependence in  $\tau^2$ , in accordance with equation 22, (cf Fig. 9b). DQ buildup curves for the same samples are shown in figure 10 for the full range of excitation time  $\tau$ . Systematic dependence of the DQ-filtered signal intensity on the cross-link density is evidenced in Figure 10a. Based on equation 23, an initial dependence of the signal amplitude on  $\tau^2$  will be shown by the DQ signals with a slope related to the scaled dynamic order parameters of methylene and methyl protons (cf Fig. 10b). TQ buildup curves for protons in polyisoprene also show a clear dependence on the cross-link density similar to the case of the DQ buildup curves.

Within the limit of experimental errors scaled dynamic order parameters measured from the MQ experiments show a linear dependence on cross-link density (cf Fig. 11).

This is expected because the dynamic order parameters  $S_s^{(2)}$  and  $S_s^{(3)}$  are inversely proportional to the number  $N$  of statistical segments. The same dependence on  $N$  is expected for cross-link density as measured in parts per hundred of rubber (phr) of cross-linking agent. For the whole series, the dynamic order parameters of methyl protons are slightly larger than those of the methylene protons. This reflects the hindrance imposed to the motion of methyl groups attributed to backbone chain by the short-range interactions between segments belonging to different chains in comparison with the case of the methylene proton located along the polymer chain.

The values of the effective  $^1\text{H}$  residual dipolar couplings  $D_{\text{eff}}/2\pi$  measured from the initial decays of the LM are shown as a function of cross-link density in Figure 11b. In the good approximation, the dipolar couplings are linearly proportional to cross-link density. These quantities can also be evaluated from equations 23 and 24 by using the dynamic-order parameters measured site-selectively from DQ and TQ buildup curves. These  $D_{\text{eff}}/2\pi$  are plotted versus cross-linked density in Figure 11b, again showing a linear dependence on cross-linked density. They are systematically lower than the values measured from the LM decays. This fact can be due to the shorter time scale used for extraction of  $D_{\text{eff}}/2\pi$  from LM decays compared to that used in DQ and TQ buildup curves.

The dynamic order parameters determined by the above methods can be compared to those measured by other NMR techniques if the specific dynamic time scale is considered. It was shown that residual dipolar couplings measured in the initial time regime of the LM decays, DQ, and TQ buildup curves are more sensitive to cross-link density as compared to, for instance, transverse relaxation rates (68).

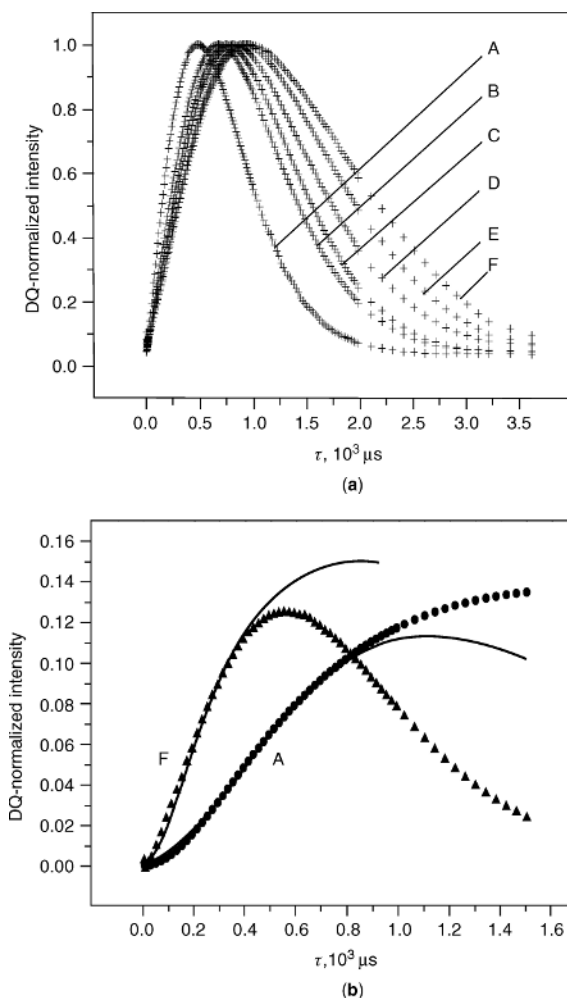


**Fig. 10.** Proton DQ buildup curves for a series of synthetic polyisoprene samples with different cross-link densities increasing from samples A to F. **(a)** The signal dependence on excitation and reversion times  $\tau$  for the full time domain. **(b)** The initial time regime of the DQ buildup curves for samples A and F together with the simulated curves including transverse relaxation (continuous lines). Reproduced from Ref. 68, with permission from American Institute of Physics.

The proposed methods are generally applicable to partially averaged proton dipolar interactions and can be applied for studying segmental order and its associated dynamics in a variety of polymer networks or entangled melts and solutions (transient networks) without the need for isotopic labeling, sample rotation, or the use of cross-polarization.

**Heterogeneity in Segmental Chain Order of Grafted Polymers.** Proton multiple-quantum NMR was also used for investigation of heterogeneity in segmental chain order of grafted polymers. The measurements were performed on a series of samples of poly(dimethylsiloxane) (PDMS) layers chemically

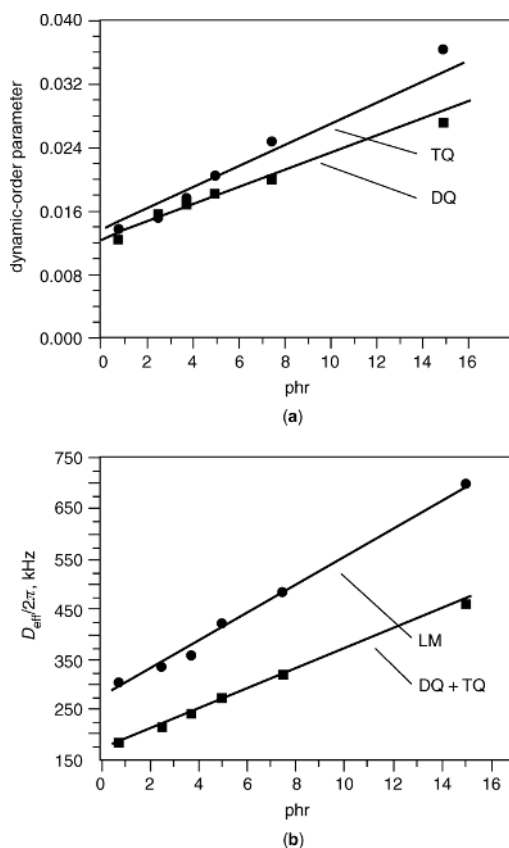


**Fig. 11.** (a) The dependence of dynamic-order parameters measured from DQ (squares) and TQ (circles) buildup curves on the cross-link density for synthetic polyisoprene. (b) The effective residual dipolar coupling  $D_{\text{eff}}$  (circles) measured from dipolar encoded longitudinal magnetization decays together with the  $D_{\text{eff}}$  values (squares) computed from dynamic-order parameters. A linear dependence on the cross-link density is evidenced in all cases (solid lines). Reproduced from Ref. 68, with permission from American Institute of Physics.

attached to the surface of hydrophilic silica (76). These grafted PDMS layers consists of partially immobilized chain segments at the PDMS–silica interface and mobile chain portions outside the interface which is probed by measurements of homonuclear double- and triple-quantum buildup curves. These curves reveal a bimodal distribution of the residual dipolar couplings along the PDMS chain (see Fig. 12).

The segmental orientation detected in the interface and mobile regions are related to the average chain length and reflects the competing effects of the surface-induced orientation and chain conformations.

The  $^1\text{H}$  DQ (and TQ) buildup curves were measured at two temperatures  $T = 298\text{ K}$  and  $T = 227\text{ K}$  for the three grafted PDMS samples with different chain lengths ( $N_t$ ) and the results are shown in Figure 12. The buildup curves display two maxima. The first maximum shows a relatively sharply defined value of

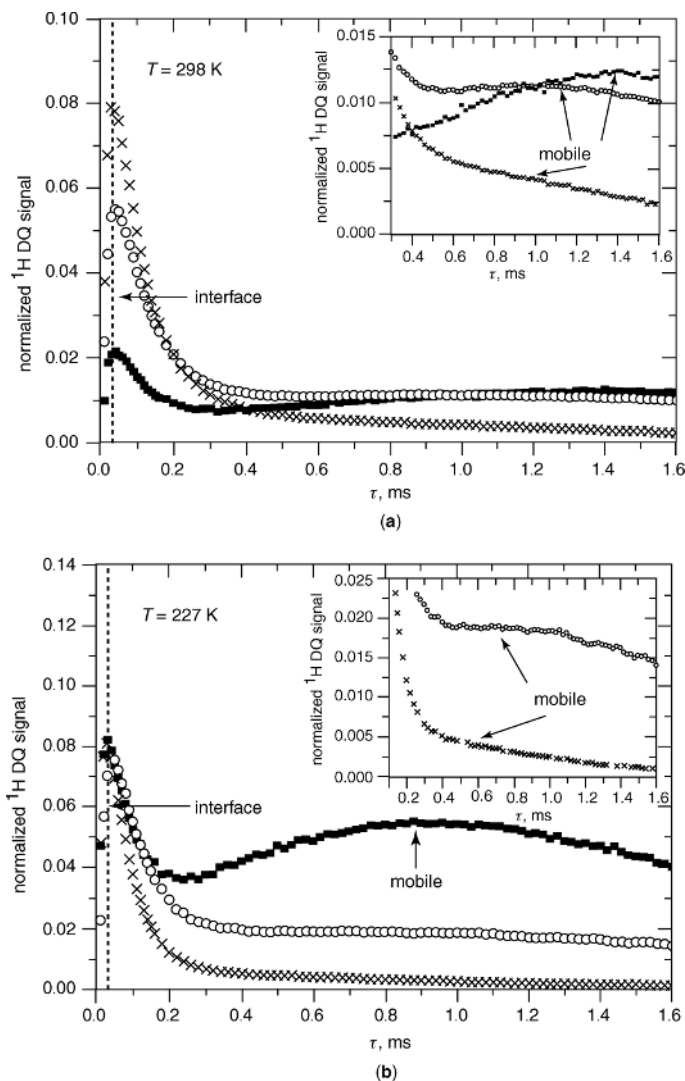


**Fig. 12.** Proton DQ buildup curves of grafted PDMS samples recorded at  $T = 298\text{ K}$  (a) and  $T = 227\text{ K}$  (b). (■) PDMS1, (○) PDMS2, and (×) PDMS3. The region of the DQ buildup curves after the first maximum is enlarged in the insets. Reproduced from Ref. 76, with permission from American Chemical Society.

the excitation and reconversion time  $\tau$ . The second maximum at longer  $\tau$  values are more difficult to identify in sample PDMS3 ( $N_t = 4.5$ ) and less pronounced in sample PDMS2 ( $N_t = 6.2$ ) due to the small amount of the mobile fraction and the broadness of the signal. Nevertheless, the second maximum is enhanced at lower temperature (cf Fig. 12b) due to reduced mobility and therefore increasing residual dipolar coupling. The maximum at short  $\tau$  values are due to the segments at the interface, and those present at longer  $\tau$  correspond to the mobile fractions of the grafted PDMS chains. The first maximum occurs at the same  $\tau$  value for

the three samples indicating the same chain immobilization in the interface of all three samples. The immobilizations are caused by a loss of conformation entropy due to chain anchoring to the silica surface and by excluded volume effects from the silica surface and neighboring chains. Thus, the averaged residual dipolar couplings of the interface have the same values independent of  $N_t$ . These results are both reflected in the  $^1\text{H}$  DQ as well as in the  $^1\text{H}$  TQ buildup curves (76).

The positions of the second maximum of the three samples are also indicative of the anisotropy of chain motions outside the interface. Assuming the same thickness of the interface in all three samples, we deduce that the fraction of the mobile chain fragments decreases from sample PDMS1 ( $N_t = 7.7$ ) to PDMS3 ( $N_t = 4.5$ ). This results in a shorter  $\tau$  value for the position of the second maximum for sample PDMS3 versus samples PDMS2 and PDMS1 that can be detected in the DQ as well as the TQ buildup curves (76).

A bimodal distribution of the segmental-chain orientation corresponding to the interface and the mobile regions of PDMS chains grafted onto silica was detected by  $^1\text{H}$  multiple-quantum NMR spectroscopy. The size of the interface is found to be independent of the total length of the PDMS chains. A broad distribution of segmental orientation prevails in the mobile region, and the segmental mobility is proportional to its fraction and therefore to the chain length. At lower temperatures, the mobility decreases until at  $T = 198$  K the whole chain appears to be immobile at the time scale of the NMR experiment of about  $10^{-5}$  s.

The measurements using transverse  $^1\text{H}$  relaxation shown that this quantity is also highly sensitive to the heterogeneous mobility of PDMS chains grafted onto a silica surface (77). This method allowed the distinction between a dense brush-like structure of the grafted layer containing chains of a fairly uniform length and a layer containing a significant fraction of long-chain loops outside the grafted layer. The mobility of the chain outside the interface was found to increase with increasing average length of the grafted chains in agreement with the measurements performed by MQ NMR (76).

**Local Segmental Anisotropy Induced by Mechanical Deformation.** A well-known consequence of the theory of rubber elasticity is bond orientation (78,79). Deformation of an elastomer induces anisotropy of the backbone bonds of the polymer coil. In recent NMR studies of rubber elasticity, the mechanism of deformation and the orientation of network chains have received increasing attention (50,51). The local segmental anisotropy induced by a uniaxial applied force in elastomers was also investigated by NMR in terms of  $^1\text{H}$  dipolar encoded longitudinal magnetization decays and double-quantum coherences buildup curves (80). These multipolar nuclear spin states were measured as a function of the angle  $\theta$  between the static magnetic field and the direction of the applied force. The experimentally determined angular dependence of the effective residual dipolar couplings shows a minimum around the magic angle. These NMR methods offer the possibility to investigate in great detail the mechanisms responsible for the induced local anisotropy in strained polymer networks without contributions from the dipolar correlation effect (*vide infra*) and without need for chain deuteration.

**Network Properties by Transverse Magnetization Relaxation.** The transverse relaxation reflects mainly the loss of quantum phase coherence of spins. The axial symmetry induced by the presence of static magnetic field is

of particular interest for observing the broad spectrum of relaxation rates related to the hierarchy of fluctuations, which affect any polymer chain in a melt or network (from about  $10^9 \text{ s}^{-1}$  down to less than  $1 \text{ s}^{-1}$ ). For protons attached to polymer chains, the irreversible dynamics of the longitudinal magnetization is sensitive to properties generated by the local viscosity, which governs the random rotations of monomeric units. With regard to the transverse magnetization, the relaxation process cannot be analyzed without considering the time interval allotted for the full random rotations of chemical units that is close to the time interval (about 1 s or more) required for the full renewal of the chain configurations. However, this is too long a process for inducing any magnetic relaxation mechanism; consequently, the transverse magnetization is sensitive to a part of the hierarchy of chain fluctuations, only. In other words, random motions of units are detected as nonisotropic rotations generated by the topological constraints and the irreversible dynamics of the transverse magnetization is thus governed by the nonzero average of the dipolar interactions. A solid-like behavior of the transverse relaxation is expected to be associated with the property of elasticity, provided the time scale of the renewal of configurations is longer than the NMR scale of observation. This effect is considerably enhanced when permanent networks are observed.

**Models for Transverse Relaxation.** The simplest model to describe chain statistics from the NMR point of view is a chain of freely jointed segments of fixed length (12). Such a chain may be rescaled in several hierarchical steps according to the time scale of the motions which takes place at different space scales, compared to the time scale defined by the NMR spin interactions. All intrachain motions are assumed to be fast enough to average elementary interactions, whereas junction average positions are static.

Let us consider a linear chain of  $N$  statistical segments, fixed at its extremities. An average orientation is induced along the chain by these constraints. To estimate the effect of this average orientation on NMR parameters, the simplest picture is to consider that each segment carries an isolated pair of spins, usually protons (two-spin approximation). Within this framework, the time evolution of the transverse magnetization  $M_{\vec{R}}(t)$  for a spin pair attached to a chain may be written in the very simple form

$$M_{\vec{R}}(t) = \text{Re} \left[ M_0 \exp \left\{ -\frac{t}{T_2} \right\} \exp \{ i \omega_{\vec{R}} t \} \right] \quad (25)$$

where  $M_{\vec{R}}(t)$  is the initial polarization,  $T_2$  is the transverse relaxation time related to the fluctuating part of the dipolar Hamiltonian, and  $\omega_{\vec{R}}$  is the residual dipolar interaction in angular frequency units. Other theories of transverse relaxation ((13), and references therein) are more complex than this simple approach. A polymer network is considerably disordered. To model this disorder, the end-to-end vector components  $\vec{R}(x, y, z)$  may be supposed to obey ideal, the Gaussian statistics, ie,

$$P(\vec{R}) = \left( \frac{3}{2\pi N a^2} \right)^{3/2} \exp \left\{ -\frac{3}{2} \frac{\vec{R}^2}{N a^2} \right\} \quad (26)$$



where  $a$  is the length of the statistical segment. The overall evolution of the complex transverse magnetization is then obtained by averaging equation 25 over end-to-end vector distribution. This yields (67)

$$M(t) = \text{Re} \left[ M_0 \left( 1 - \frac{2}{3} i D_{ij} N_e^{-1} t \right)^{-1/2} \left( 1 + \frac{1}{3} i D_{ij} N_e^{-1} t \right)^{-1} \exp \left\{ -\frac{t}{T_2} \right\} \right] \quad (27)$$

where  $D_{ij}$  is the dipolar coupling constant for a spin pair and  $N_e$  is the effective number of statistical segments. At short times, ie, for  $\Delta^2 N_e^{-1} t^2 \ll 1$  the transverse relaxation decay has a Gaussian behavior corresponding to the presence of the residual dipolar couplings.

Experimental transverse relaxation decays cannot be usually described from exponential time functions but integral treatments of these curves yield standard parameters equivalent to relaxation rates (81). Without entering into too many details, it may be worth noting that the integral treatment amount to calculating several moments of the function  $P(\vec{R})$ . The first and the third moments of the distribution function are obtained from the two following integral treatments of the experimental relaxation curves

$$A_1 = \int_0^\infty \frac{M(t)}{\sqrt{t}} dt, \text{ and } A_3 = \int_0^\infty \frac{dM(t)/dt}{\sqrt{t}} dt. \quad (28)$$

A NMR structural parameter  $\chi_c$  was introduced which is defined as  $\chi_c = A_3/A_1$ . The quantity  $1/\chi_c$  is proportional to the correlation length of segments between two consecutive nodes. Thermal behavior, swelling effects, NMR-vulcanization, and NMR-elasticity relationships can be derived using the  $\chi_c$  parameter ((81), and references therein). For instance, linear dependence of the NMR relaxation rate  $\chi_c$  on the modulus of elasticity  $E$  measured on randomly PDMS chains (82) are shown in Figure 13.

Segmental fluctuations involved in the linear mechanical response to a small strain are directly observed from the transverse magnetization relaxation, in the absence of any strain.

**Characterization of Polymer Networks by Transverse Relaxation.** The NMR transverse magnetisation relaxation experiments were extensively used for quantitative analysis of the density of chemical cross-links, temporary and trapped chain entanglements and physical network junctions which are formed in filled rubbers, semicrystalline and ionic containing elastomers, and for determination of the molecular-scale heterogeneity of polymer networks ((83), and reference therein).

Several types of heterogeneity may occur in rubbery materials: (1) molecular-scale heterogeneity, which is caused by the chemical heterogeneity of uncured elastomers, network defects, and heterogeneous distribution of network junctions on a molecular level; (2) morphological heterogeneity of rubbery compounds due to a spatially heterogeneous distribution of components and filler in the compound; (3) spatial heterogeneity due to a difference in curing conditions such as temperature and concentration of vulcanisation agents throughout the sample volume.

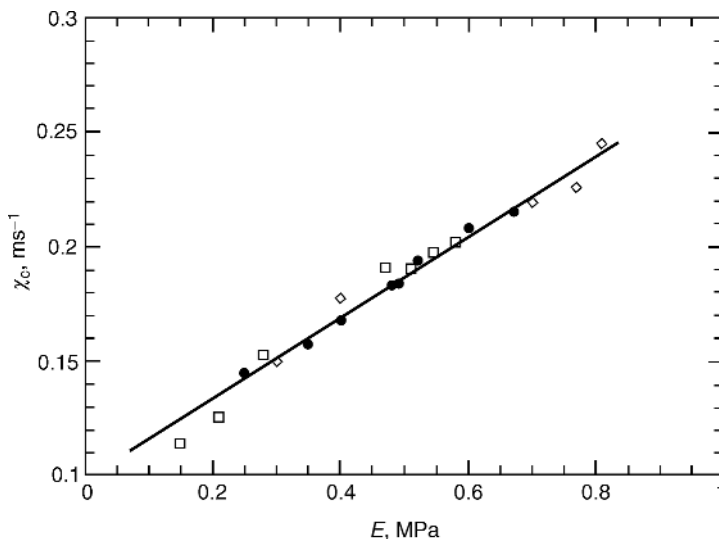


**Fig. 13.** Relaxation rate parameter  $\chi_c$  as a function of the Young modulus  $E$  for randomly cross-link PDMS chains. NMR measurements were performed without any sample deformation. Reproduced from Ref. 82, with permission from American Chemical Society.

A significant difference between the large spatial-scale mobility of network chains and that of network defects allows us to determine the degree of network heterogeneity. The most reliable data are obtained for swollen samples, because an increasing solvent content results in the disentanglement of network defects from network chains (84–86). The molecular mobility of network chains is consequently decoupled from that of network defects, resulting in a major distinction in the relaxation behavior.

One example is given by the monoexponential  $T_2$  decay of a cured acrylate that is splitted into two components upon swelling. This behavior is most clearly observable at high solvent concentrations (84,85). One component has short decay time  $T_2^s$ , which is comparable with that of the original sample. This component apparently derives from network chains. Starting at a low volume solvent content (see Fig. 14),  $V_s$ ,  $T_2^s$  shows an increase, which may be attributable to the following phenomena: (1) the disentanglement of network chains, (2) an increase in the frequency of the large spatial-scale chain motion, and (3) a slight decrease in the strength of the interchain proton dipole–dipole interactions. At  $V_s \approx 40$ –50 vol%,  $T_2^s$  reaches a maximum value. A value of  $T_2^s$  at the maximum,  $(T_2^s)^{\max}$ , is related to the molecular mass of the network chains between chemical cross-links and trapped chain entanglements. At higher values of  $V_s$ ,  $T_2^s$  decreases until the state of equilibrium swelling is reached. This decrease in  $T_2^s$  is thought to reflect the increase in the interchain proton dipole–dipole interactions as a result of the network chain elongation following a progressive increase in the solvent fraction in a swollen gel (12).

The long decay time ( $T_2^1$ ) of the other component is typical of semidiluted polymer solutions. A  $T_2^1$  value continuously increases with an increasing solvent content. This component is apparently originated from the relaxation of network

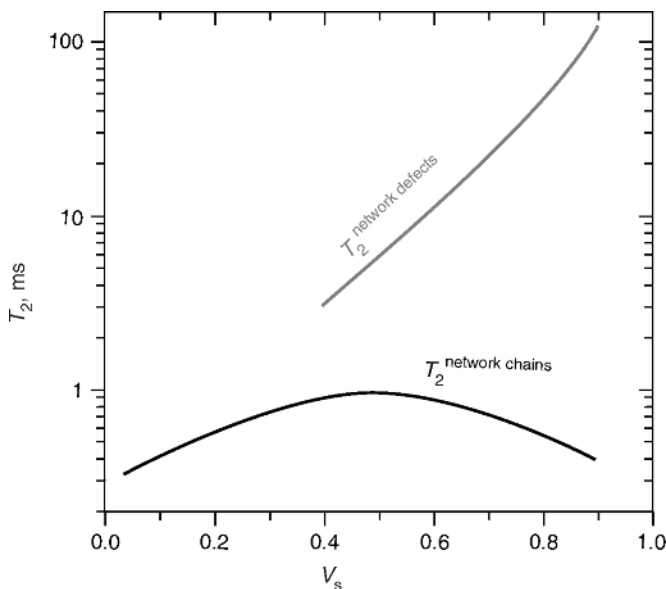


**Fig. 14.** The transverse relaxation time for a polymer network with defects against the volume fraction of a good solvent. Reproduced from Ref. 84, with permission from American Chemical Society.

defects which are disentangled from network chains in a swollen state. At the equilibrium swelling degree, the relative fraction of the  $T_2^1$  relaxation component could be used as a measure of the fraction of highly mobile network defects. The described behavior of  $T_2$  relaxation decay following a progressive increase in the solvent fraction is typical of networks containing a significant fraction of network defects.

Distinct  $T_2$  relaxation components with widely differing mean decay times suggest molecular or macroscopic heterogeneity of the material. In such cases, the submolecules concept can be used to describe the relaxation behavior (12). In a simplified interpretation, the overall  $T_2$  relaxation decay of a heterogeneous elastomer is the weighted sum of the decays originating from the submolecules, which are defined as the network chains that are formed by the chemical and physical junctions, and network defects, ie, chains that are not attached to the network, chain loops and dangling chain ends. The large spatial-scale mobility of these submolecules differs substantially, and so does their relaxation behavior. The relative contribution of the submolecules to the overall decay is proportional to the number of protons attached to these chain fragments.

A quantitative analysis of the shape of the decay curve is not always straightforward due to the complex origin of the relaxation function itself (12,81,87–89) and the structural heterogeneity of the long-chain molecules. Nevertheless, several examples of the detection of structural heterogeneity by  $T_2$  experiments have been published, for example the analysis of the gel/sol content in cured (90,91) and filled elastomers (85,86), the estimation of the fraction of chain-end blocks in linear and network elastomers (91,92), and the determination of a

distribution function for the molecular mass of network chains in cross-linked elastomers (93,94).

**Chain Orientation and Slow Dynamics by Dipolar Correlation Effect.** An important 1D NMR method used for investigating anisotropy of chain dynamics and segmental order in polymer networks is given by the decay of the solid echo (12,63), a combination of Hahn and solid echoes (52), and a normalized stimulated echo (95–97). For all these cases, the echo amplitude decays can be described by a residual dipolar or quadrupolar correlation function (DCF) (for an introduction, see Reference 5). This function describes the autocorrelation of dipolar or quadrupolar randomly fluctuating interactions around the residual nuclear spin interactions that have been preaveraged by the fast dynamics of the chains and functional groups. Measurement of the DCF together with a corresponding theoretical model reveals important information about local segmental order and slow-chain dynamics under various experimental conditions. The possibility to measure the DCF using a combination of a solid echo, a Hahn echo and the free induction decay of protons, and deuterons has been discussed in Reference 63. An improved method was introduced later by Callaghan and Samulski (52) which exploits the fact that Hahn echo refocuses chemical shielding interactions and magnetic field inhomogeneities. Moreover, the Hahn echo amplitude is encoded by the molecular motions and residual dipolar couplings. The fluctuation of the dipolar interactions encodes the amplitude of the solid echo (actually a mixed echo) to a first approximation. The appropriate combination of these echoes, thus, gives access to residual dipolar couplings and the fluctuation rates. From the viewpoint of the spin system response, the solid echo completely refocuses the evolution of coherences of quadrupolar nuclei of spin  $I = 1$  like  $^2\text{H}$  and of a pair of  $1/2$  spins other than the  $^1\text{H}$  multispin dipolar interactions. Therefore, the solid echo is strongly affected by the residual multispin interaction which makes the measurements of DCF inaccurate. Moreover, the time scale of the dipolar or quadrupolar interaction fluctuations is limited to the time of the solid echo decay which is shorter than the transverse magnetization relaxation time. A considerably longer NMR time-window is offered by the DCF recorded with a stimulated echo (95–97). However, the amplitude of the stimulated echo is smaller than that of the solid echo and is affected by the multispin residual dipolar couplings as well as by the fluctuating dipolar fields. Furthermore, the evolution of the chemical shift Hamiltonian before storage of the  $z$ -magnetization encodes the stimulated echo evolution. Moreover, magnetization exchange competes with the dipolar correlation effect.

In all the cases discussed above, only the response of the spin system composed of dipolar coupled spin- $1/2$  pairs was considered. Proton DQ-NMR spectroscopy on elastomers—static and spinning at the magic angle—proved that the consideration of isolated spin- $1/2$  pairs is a crude approximation (68). The dipolar couplings between the protons belonging to various functional groups are shown to be active in two-dimensional DQ-MAS spectra for high excitation/reconversion times (68,73).

Dipolar correlation function can be measured for a multispin dipolar coupled network, for example, for the protons in functional groups attached to polymer chains in elastomers by a mixed echo given by the combination of the magic and the Hahn echo. The magic echo refocuses the residual multispin dipolar Hamiltonian with high efficiency (71–73,98). In a good approximation, the amplitude of

the mixed echo is independent of residual (quasistatic) multispin couplings and inhomogeneous spin interactions including chemical shielding interaction. The following gives an evaluation of the dipolar correlation function describing slow chain motions within the limits of an exponential correlation function and a distribution of correlation times.

**Mixed Echo Decay.** The mixed echo amplitude decay can be expressed in terms of the autocorrelation function of the dipolar Hamiltonian (64). Transverse relaxation processes described by a single correlation time are rarely found in amorphous polymers including elastomers. If a normalized distribution of correlation times  $g(\tau_c)$  is introduced, then the mixed echo decay is given by (64)

$$S_{\text{ME}}(6\tau) \cong 1 - \bar{M}_2 \int_0^\infty \tau_c^2 \left\{ e^{-\frac{6\tau}{\tau_c}} - 3 e^{-\frac{5\tau}{\tau_c}} + \frac{9}{4} e^{-\frac{4\tau}{\tau_c}} + 3 e^{-\frac{\tau}{\tau_c}} + \frac{3\tau}{\tau_c} - \frac{13}{4} \right\} g(\tau_c) d\tau_c \quad (29)$$

where  $\tau_c$  is the correlation time. It is obvious from equation 29 that the measurement of DCF leads to a mixture of contributions from residual van Vleck second moment and the distribution function of correlation times that is model dependent.

A particularly simple form for the function  $g(\tau_c)$  is related to the log-Gaussian distribution (see for instance Reference 2), ie,

$$g(\tau_c) \equiv \frac{1}{\tau_c} F_G(\ln \tau_c) \quad (30)$$

where

$$F_G(\ln \tau_c) \equiv \frac{1}{\sigma_{\ln} \sqrt{2\pi}} \exp \left\{ -\frac{[\ln(\tau_c/\tau_{c0})]^2}{2\sigma_{\ln}^2} \right\} \quad (31)$$

The center of gravity of the correlation time distribution is given by  $\ln(\tau_{c0})$  and the width of the distribution is  $\Delta_{1/2} = 1.02 \sigma_{\ln}$ .

**Parameters of the Dipolar Correlation Function for a Cross-Linked Elastomer Series.** The mixed echo decays were measured for a series of cross-linked natural rubber (64). The model involving the distribution of correlation times (see eq. 29) was used to fit the mixed echo decay. The residual second van Vleck moments obtained from fits as a function of shear modulus  $G$ .

For ideal polymer coils, the most significant and distinctive property is the Gaussian distribution of the end-to-end distances. By considering the different segments of the freely jointed chain which are statistically independent and can be represented by a Markov chain, one can derive the correction to the Gaussian distribution of the end-to end distances (see Reference 99).

Using the corrected Gaussian distribution function one then gets (64)

$$\langle M_2 \rangle \propto \frac{5}{3} \frac{1}{N^2} - \frac{2}{3} \frac{1}{N^3}. \quad (32)$$

Within the limit of the approximation used, it is concluded that the residual second van Vleck moment scales with  $1/N^2$  for high numbers of statistical segments,

ie, for  $N \gg 1$ , which means for low cross-link densities. However, this regime is invalid for the series of cross-linked natural rubber investigated using DCF (64). The effective number of statistical segments  $N$  is defined by the number of segments  $N^{(0)}$  between physical cross-links or topological constraints and the number  $N^{(C)}$  of segments between chemical cross-links. If we assume that the contributions to the residual dipolar coupling are additive and topological constraints are independent of the degree of chemical cross-linking, we can write  $(N)^{-1} \approx (N^{(0)})^{-1} + (N^{(C)})^{-1}$ . In this case, one expects (cf equation 32) that  $\langle M_2 \rangle$  has a polynomial dependence on cross-link density or shear modulus.

Based on the dependence of the residual second moment on  $1/N$  given by equation 32, the measured  $\langle M_2 \rangle$  values can be fitted by a polynomial up to the forth power in the shear modulus  $G$ , ie,

$$\langle M_2 \rangle = a_0 - a_1 G + a_2 G^2 - a_3 G^3 + a_4 G^4 \quad (33)$$

This dependence is similar with that shown in Figure 8a measured using AIMS method (70). If only the first four values of  $\langle M_2 \rangle$  corresponding to an intermediate regime of cross-linking are considered, the  $G^2$  term dominates the dependence as it is expected from a Gaussian distribution of end-to-end vectors. The DCF measurements also reveal that the centre of gravity, as well as the logarithmic width of the distribution function of correlation time—which describes the slow motion of the network chains—scale with the cross-link density in a complex manner (64).

The development of NMR methods that allow accurate measurements of residual second van Vleck moments and the distribution of correlation times yields new tools to test polymer network theories that are more sophisticated than the theory of the freely jointed chain corresponding to a Markov chain.

## Viscoelastic Polymers by Two-Dimensional NMR Spectroscopy

The investigation of molecular dynamics and local segmental orientation by two-dimensional (2D) NMR spectroscopy has a number of advantages (1,2) particularly when dealing with complicated spin systems such as viscoelastic polymers. Below, we will discuss examples of such investigations, concentrating on techniques that are particularly sensitive to the viscoelastic regime that is, NMR techniques for measuring residual dipolar couplings and dynamic order parameters. Readers interested in a more general overview of multidimensional NMR of polymers are referred to references (2,3,6).

**Chain Orientation from 2D  $^1\text{H}$  Magnetization Exchange Spectroscopy.** Two-dimensional  $^1\text{H}$  magnetization-exchange spectroscopy and its reduced one-dimensional (1D) variant have been used to probe residual dipole–dipole couplings between different functional groups of a SBR sample, namely between the CH and  $\text{CH}_2$  groups of the butadiene units (65,100). The intergroup residual dipolar couplings can then be correlated with the shear modulus that is an independent measure of the cross-link density (65). Hence, the dynamic local-order parameter associated with the partially averaged

dipolar coupling can be evaluated taking the average over the relevant dynamic processes.

*Principle of the Method.* Following the general scheme of 2D NMR spectroscopy, an evolution period of duration  $t_1$  follows the excitation pulse. This interval ends with a flip-back pulse and the system is allowed to exchange during the mixing period  $t_m$ . After a third pulse the remaining signal is acquired during the detection interval  $t_2$  (1). The intensity of the cross-peaks in the resulting 2D spectra then reflects the degree of exchange between the corresponding groups. Since full 2D NMR spectroscopy is time-consuming, for quantitative evaluations also a reduced 1D form has been used. In this case, the time  $t_1$  is fixed and adjusted such that it acts as a chemical-shift filter (2) for one of the two butadiene lines in the static SBR spectrum. The reappearance of the filtered line with increasing mixing time is then a measure of the magnetization exchange between the protons of the CH and CH<sub>2</sub> groups. Note, that unlike the 500 MHz spectrum the styrene line and the CH line could not be distinguished in these experiments so that only the CH and CH<sub>2</sub> lines of the butadiene units are resolved. They are separated by about 3.35 ppm, corresponding to 1 kHz at the Larmor frequency of 300 MHz.

The theory needed for the evaluation of the exchange process was also developed (65,100). The model of the spin system used is depicted in Figure 15.

For short mixing times, the measurable exchange of <sup>1</sup>H longitudinal magnetization is predominantly determined by the protons belonging to nearest-neighbor CH and CH<sub>2</sub> groups. At longer mixing times on the other hand, a much larger spin system along the polymer chain must be considered, in principle. In Reference 100, however, it was shown that even in this case the intergroup residual dipolar coupling can be measured from the initial-time regime of the magnetization-exchange decay curve.

In the limit of short mixing times  $t_m$ , the initial decay rates for the CH line were found (65,100) to depend only on the intergroup residual dipolar coupling  $\bar{D}^{\text{CH}-\text{CH}_2}$  according to

$$\langle\langle I_z(t_m) \rangle\rangle = 1 - \frac{1}{2} \langle(\bar{D}^{\text{CH}-\text{CH}_2})^2\rangle t_m^2 \quad (34)$$

where  $\langle\langle I_z(t_m) \rangle\rangle$  is the observable for the CH protons (for the CH<sub>2</sub> protons the factor 1/2 must be substituted by 1/4 in equation 34). The symbol  $\langle \rangle$  represents the statistical ensemble average of the space part of the dipolar coupling in a disordered elastomer. Note, that from such measurements, the intergroup dipolar coupling  $\bar{D}^{\text{CH}-\text{CH}_2}$  can be determined which is largely parallel to the segment axis. That is, it is much more informative with respect to the detection of chain order and chain motion than intragroup couplings would be.

*Two-Dimensional <sup>1</sup>H Magnetization-Exchange Processes in Cross-Linked SBR.* From the point of view of molecular motion, cross-linked elastomers are highly heterogeneous systems and a solid-like behavior is present together with slow and fast motions of both chains segments and functional groups. Hence, the magnetization-exchange process is expected to be also heterogeneous, that is, driven by different mechanisms.

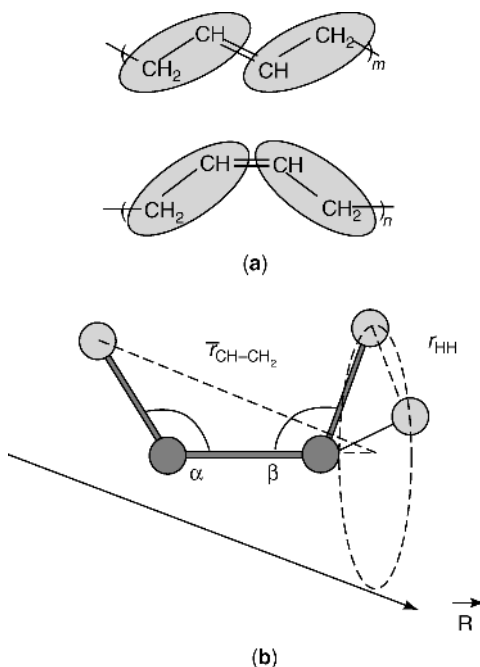


**Fig. 15.** (a) The monomer unit of *trans*- and *cis*-1,4-butadiene. The alternating sequence of  $\text{CH}-\text{CH}_2$  groups, for which the magnetization-exchange process is treated. (b) The geometry of the  $\text{CH}-\text{CH}_2$  spin system. The shaded circles represent protons and the black circles carbon atoms. The conformational jumps of the methylene protons lead to an average  $\text{CH}-\text{CH}_2$  proton distance  $\bar{r}_{\text{CH}-\text{CH}_2}$ . Reproduced from Ref. 65, with permission from American Institute of Physics.

In order to investigate this heterogeneity, a series of static 2D NMR experiments was performed on SBR for increasing mixing time (100). As already discussed above, the aromatic and the olefinic protons are not resolved under the applied experimental conditions as can be seen in the 2D spectra shown in Figure 16.

A remarkable feature of the diagonal 2D spectrum for short mixing times is that the width of the diagonal peaks perpendicular to the  $(\omega_1, \omega_2)$  diagonal is much smaller than the widths along the diagonal. This indicates that the  $^1\text{H}$  NMR spectrum is heterogeneously broadened (65). The width of each line along the diagonal reflects both the solid- and the liquid-like contributions, whereas the width perpendicular to the diagonal reflects selectively the liquid-like line width only. This feature is very pronounced for the CH diagonal peak and less for the  $\text{CH}_2$  diagonal peak because of the strong proton-proton coupling within the methylene group. A similar result was already found in a  $^{13}\text{C}$  magnetization-exchange experiment on natural rubber aimed to detect chain diffusion (101). While no chain diffusion was detected, the lines were also found to be spread out along the diagonal.

In the  $^1\text{H}$  magnetization-exchange experiment on SBR not much cross-peak signal is found for mixing times shorter than 2.5 ms (see Fig. 16a). This indicates



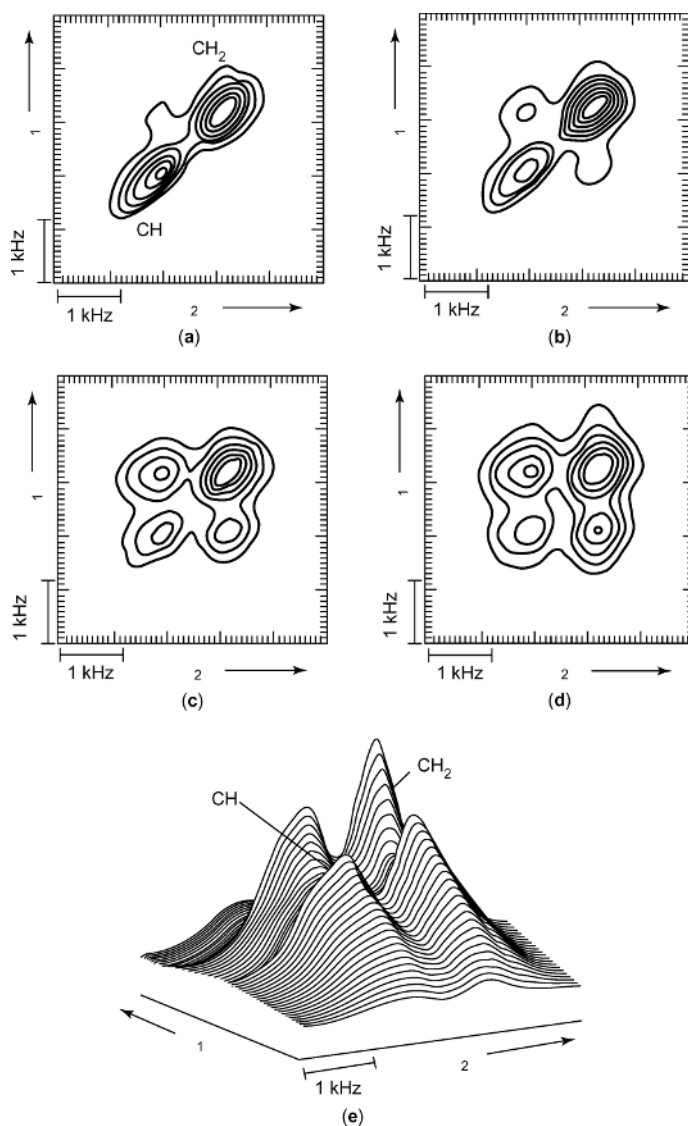


**Fig. 16.** Two-dimensional  $^1\text{H}$  magnetization-exchange spectra of a SBR recorded with different mixing times have been used:  $t_m = 2.5$  ms (a), 5 ms (b), 15 ms (c), and 30 ms (d). The 2D surface representation for  $t_m = 30$  ms in (e) shows that all cross-peaks are positive. Reproduced from Ref. 65, with permission from American Institute of Physics.

that within this time scale the CH and CH<sub>2</sub> functional groups can be considered in reasonable approximation to be isolated. The intergroup residual dipolar coupling leads to magnetization exchange for longer mixing times. Intense positive cross-peaks are thus present for  $t_m = 30$  ms (see Figs. 16d and 16e). Such positive cross-peaks can arise for two reasons: from the exchange process mediated by residual dipolar couplings and from cross-relaxation induced by segmental motions with correlation times  $\tau_c$  longer than  $\omega_0^{-1}$  (1).

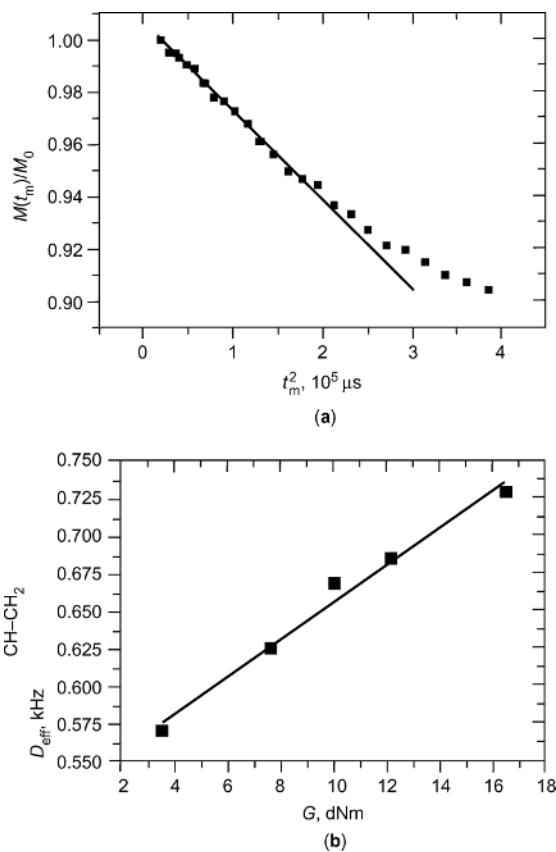


**Fig. 17.** (a) The initial decays of the proton magnetization for the exchange process  $\text{CH} \rightarrow \text{CH}_2$ . The initial part of the magnetization-exchange data (starting with  $t_m = 100 \mu s$ ) shows the predicted dependence in  $t_m^2$ . The effective  $\text{CH-CH}_2$  intergroup dipolar coupling constant  $D_{\text{eff}}^{\text{CH-CH}_2}$  can be evaluated by fitting the theoretical curve. (b)  $D_{\text{eff}}^{\text{CH-CH}_2}$  as a function of the shear modulus  $G$  for a series of differently cross-linked SBR samples. Reproduced from Ref. 65, with permission from American Institute of Physics.

**Proton Intergroup Residual Dipolar Couplings.** The residual dipolar couplings between the protons of the CH and the  $\text{CH}_2$  groups were determined from the  $t_m$  dependence of the peak intensities. The decay of the longitudinal magnetization  $M(t_m)$  of the diagonal signals (normalized to the value  $M_0$  that corresponds to zero mixing time) is recorded for short mixing times for the CH group. According to equation 34, the magnetization-exchange dynamics should show an initial quadratic dependence on  $t_m$ . This dependence is indeed found in the experiments and is shown in Figure 17a for SBR as an example.

From the slope of the initial magnetization decay, the values of the effective residual dipolar couplings  $D_{\text{eff}}^{\text{CH-CH}_2} = \langle (\bar{D}_{\text{eff}}^{\text{CH-CH}_2})^2 \rangle^{1/2}$  could be evaluated and it could be shown that these couplings scale with the cross-link density (65,100). The correlation of the coupling constant  $D_{\text{eff}}^{\text{CH-CH}_2}$  with the shear modulus  $G$  as an independent measure of the cross-link density demonstrates this behavior

(Fig. 17b). Note, however, that the line in Figure 17b does not cross the origin but provides a significant value for  $\bar{D}_{\text{eff}}^{\text{CH}-\text{CH}_2}$  at  $G = 0$ . This is not in contradiction with the applied model, but reflects the influence of local chain order (physical cross-links). From extrapolating to  $G = 0$  in Figure 17b, the intergroup residual coupling of an uncross-linked SBR melt was determined to be  $\bar{D}_{\text{eff}}^{\text{CH}-\text{CH}_2} \approx 533$  Hz. Using average internuclear distances and bond angles for SBR, one can extract the value for the dynamic-order parameter  $S_{\text{H}-\text{H}_2}$  of the  $\text{CH}-\text{CH}_2$  intergroup linkage  $\bar{r}_{\text{CH}-\text{CH}_2}$  according to  $\bar{D}_{\text{eff}}^{\text{CH}-\text{CH}_2} = D_{\text{rigid}}^{\text{CH}-\text{CH}_2} S_{\text{H}-\text{H}_2}$ . This yields  $S_{\text{H}-\text{H}_2} \approx 0.1$  and suggests an even higher value for the dynamic-order parameter for the corresponding carbon-carbon bond  $S_{\text{C}-\text{C}} \approx 0.13$ , since  $\bar{r}_{\text{CH}-\text{CH}_2}$  and  $\bar{r}_{\text{C}-\text{C}}$  forms an angle of  $24^\circ$ . Thus, even in polymer melts the chain motion can be largely anisotropic, as shown previously for poly(methacrylates) (102).

Magnetization-exchange NMR spectroscopy offers a convenient means for measuring the residual dipolar couplings between functional groups along the polymer chains. The intergroup dipolar coupling is remarkably high even in uncross-linked melts representing relatively high local segmental order. In cross-linked samples, it scales with the cross-link density as predicted by the scale-invariant model of residual dipolar couplings (12), emphasizing its relation to viscoelastic properties of the elastomers.

**Segmental Motions by 2D NOESY-MAS Spectroscopy.** In the previous paragraph, we have discussed the coherent magnetization-exchange process by  $^1\text{H}$  non vanishing average dipolar couplings. Under fast MAS conditions, however, the residual couplings responsible for the exchange are largely refocused for full rotor periods and cross-relaxation by the fluctuating part of the dipolar interaction predominates. This so-called nuclear Overhauser effect (NOE) (103) takes place if the spins system is not in internal equilibrium. It corresponds to relaxation between dipolar-coupled nuclei such as  $^{13}\text{C}$  and  $^1\text{H}$  or between different nonequivalent magnetically sites of the same type of nucleus. NOE spectroscopy (NOESY) is well known in liquid-state NMR where it is one of the standard 2D techniques to elucidate and assign structures of macromolecules in solution (1).

Following the success of the technique in solution state, NOESY has been also applied to polymers or viscoelastic materials (104–110). As in solution experiments, one takes advantage of the fluctuating part of the dipolar coupling to extract useful structural and dynamical information. Using this method, nuclear Overhauser enhancement factors have been measured in polyisoprene over a range of temperatures with static  $^{13}\text{C}$  NOE spectroscopy (104). A molecular-weight independent change of regime was observed at around  $60^\circ\text{C}$  for the backbone motion reflecting a loss of motional cooperativity with increasing temperature. Also the temperature-independent correlation time of the internal rotation of the methyl group could be inferred.

The polymer miscibility in polymer blends (PS/PVME) was probed by  $^{13}\text{C}$  NOE spectroscopy under MAS (105). This study takes advantage of the fact that cross-peaks appear only between spins that are neighbors of each other, thus establishing NOE as a probe for the degree of mixture on the molecular level. Additional information on the molecular structure of the blend could be obtained from the NOE growth rates. The results suggest that there exists a specific interaction between the phenyl ring of the PS and the PVME methyl group. In Reference 106

the same technique was applied for investigating methyl groups as a source of cross-relaxation in solid polymers such as polycarbonate or polystyrene.

Static  $^1\text{H}$  2D NOE spectroscopy was applied in a first experiment showing that the technique can be used to measure interchain interactions (107). This work was then continued by applying the technique under MAS to investigate the intermolecular interactions responsible for the miscibility in polybutadiene/polyisoprene blends above the glass-transition temperature (108). It could be shown that intermolecular association can be probed by this technique and the results reveal the existence of weak intermolecular interactions between the polyisoprene methyl group and the vinyl side chain of the polybutadiene.

**Segmental Motions of Elastomers.** NOESY experiment under MAS on protons was used to study molecular motions in technical relevant materials such as rubbers (109,110). For the evaluation of these parameters, it is necessary to understand the cross-relaxation process in the presence of anisotropic motions and under sample spinning. Such a treatment is provided in Reference 110 and the cross-relaxation rates were found to weakly depend on fast motions in the Larmor frequency range and strongly on slow motions of the order of the spinning frequency  $\nu_R$ . Explicit expressions for the  $\nu_R$  dependent cross-relaxation rates were derived for different motional models. Examples explicitly discussed were based on a heterogeneous distribution of correlation times (2,12,111) or on a multistep process in the most simple case assuming a bimodal distribution of correlation times (112–114).

The derived relationships were tested experimentally on a cross-linking series of styrene–butadiene rubbers and the cross-relaxation was studied as a function of the rotor frequency  $\nu_R$ . As an illustration of such measurements, Figure 18a shows a surface representation of the gradient-selected 2D NOESY spectrum of a SBR sample acquired with a mixing time of 2.7 ms at a rotor frequency of 8 kHz. The lines corresponding to the aliphatic, the olefinic, and the aromatic protons are well resolved and can be assigned as indicated. Already at short mixing times pronounced cross-peaks are visible, in particular between the olefinic CH and the  $\text{CH}_2$  group.

Figure 18b shows the decay curve of the diagonal peaks for mixing times up to 3 ms. Unlike in the magnetization-exchange case (65), the decay is found to be approximately linear in  $t_m$  in the short mixing time regime and exponential or biexponential for long times (110). A similar curve can be plotted for the increase of the cross-peaks. In order to investigate the effect of the sample spinning on the cross-relaxation rates, series of 2D NOESY-MAS spectra were acquired as a function of the rotor frequency. The rates evaluated from these series were found to decrease linearly with rotor frequency that is an indication that cross-relaxation in elastomers is dominated by slow motions in the 10 kHz regime rather than by motions in the Larmor frequency range as in case of liquids. The cross-relaxation rates at room temperature were found to depend moderately only on the cross-link density that is another indication that cross-relaxation is dominated by the  $\alpha$  process.

The experimental rates were analyzed in terms of the explicit expressions derived by the theoretical treatment (110). As expected for a statistical copolymer, segmental motions in the SBR samples cannot be described by a single correlation time (2). From  $T_1$  data that were also measured the correlation time

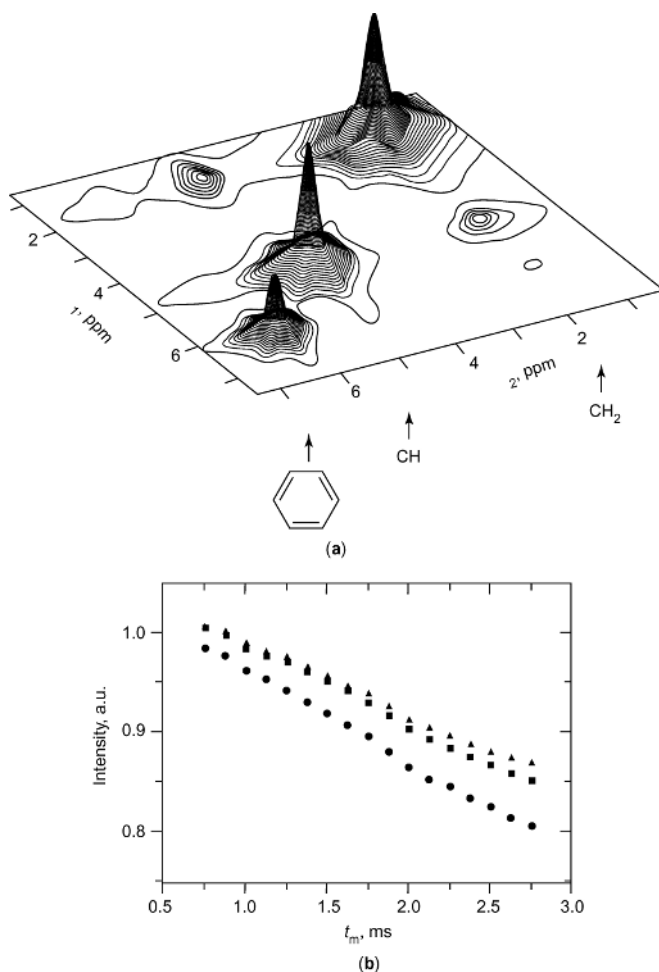


**Fig. 18.** (a) 2D  $^1\text{H}$ -NOESY surface spectrum of SBR acquired for a mixing time of 2.7 ms and under 8 kHz MAS. Already at this short mixing time pronounced cross-peaks are visible. (b) Short-time decay of the cross-peak intensity evaluated from a series of 2D spectra. Such curves can be analyzed providing information on internuclear distances and segmental dynamics (■) aromatic CH, (●) olefinic CH, (▲) CH. Reproduced from Ref. 110, with permission from Taylor & Francis Ltd.

should be in the range of  $10^{-8}$  s while the rotor frequency  $\nu_R$  dependence of the cross-relaxation rates requires a correlation time of  $10^{-5}$  s. So it is clear that at least two different correlation times are necessary to account for the experimental findings. The relaxation dispersion data  $T_1(\omega)$  ( $\omega$  being the Larmor frequency) (96), however, show no discontinuity that would indicate the presence of two distinct motional processes. Thus, the data were analyzed in terms of a broad distribution of correlation times for almost isotropic segmental motions ( $\alpha$  relaxation). With a simple log-Gaussian distribution function of reasonable parameters (110) it was found that one could account for both the  $T_1$  values and the  $\nu_R$ -dependent cross-relaxation rates. From the center of gravity of the distribution, the

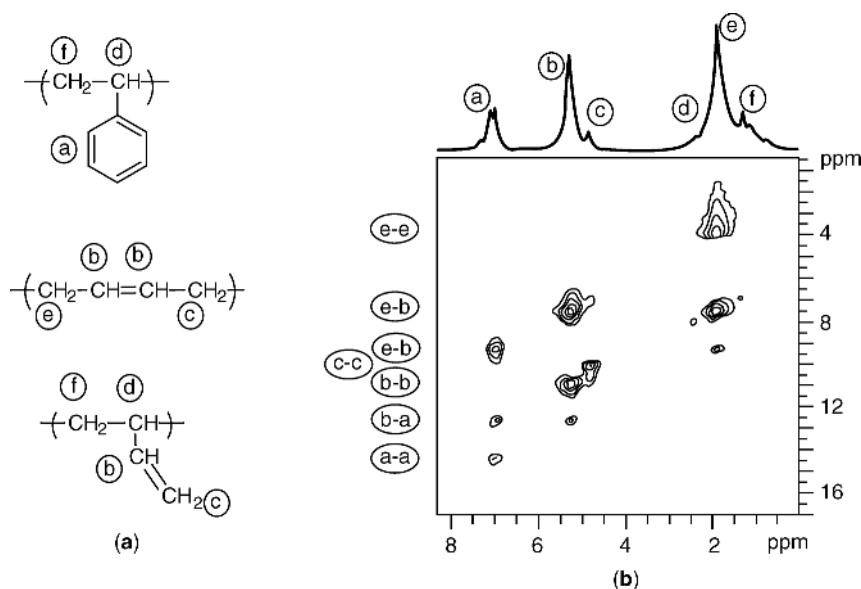


**Fig. 19.** Proton DQ MAS spectrum of a SBR sample with a low value of cross-link density (0.8–0.8 phr sulfur accelerator). The rotor frequency was 10 kHz and the  $t_1$  increment was 15  $\mu$ s. The diagonal peaks and the cross-peaks of the functional groups are assigned as indicated (compare (a) and (b)). Reproduced from Ref. 73, with permission Elsevier.

glass-transition temperature could be estimated as  $T_g = 230$  K using the well-known Williams–Landel–Ferry (WLF) equation (2). This value compares favorably with the known value of  $T_g = 220$  K for uncross-linked SBR-1500.

**Selective Residual Dipolar Couplings by  $^1H$  Multiple-Quantum NMR Spectroscopy.** Multiple-quantum MQ NMR spectroscopy is well established for structural studies of liquids and highly mobile solutes in liquid crystals (1, 26). In recent years, there has been a sustained effort to obtain homonuclear (73,115–119) and heteronuclear (120–122) high resolution MQ NMR spectra also for organic solids using fast MAS to increase resolution and sensitivity. Such MQ spectra proved to be valuable tools for determining dipolar connectivities between spin-1/2 nuclei (74,75,116). More quantitatively, dipolar couplings, internuclear distances, and molecular torsion angles can be measured by these techniques (74). For viscoelastic materials, it was recently shown that  $^1H$  high resolution MQ NMR spectroscopy offers the possibility to measure site-selective residual dipolar couplings between all resolved protons (73,119). The MQ technique thus is an attractive tool for studying structure and dynamics in polymer melts (119) and elastomers (68,73).

**Dipolar Connectivities from the High Resolution  $^1H$  DQ MAS Spectroscopy.** Figure 19 shows the  $^1H$  DQ spectrum of a cross-linked SBR sample that has been acquired at a spinning frequency of 10 kHz (73).

The peaks in the 2D DQ spectrum correspond to double-quantum coherences between two spins which must be relatively close neighbors in space in order to contribute significantly to the peak intensity as follows from the strong distance

sensitivity of the dipolar coupling. From the existence of the corresponding peaks therefore through space dipolar connectivities can be easily established.

The assignment of the peaks is shown along the  $\omega_1$  dimension by pairs of letters a–f (see Fig. 19a) which indicates the functional groups that are involved in the generation of the corresponding DQ peaks. From a simple qualitative inspection of the DQ spectrum, it can be seen that there are dipolar connectivities between practically all functional groups. The strongest DQ signals are found between protons of the polybutadiene groups, but also DQ peaks of considerable intensity are visible between the polybutadiene protons and the aromatic protons of the styrene units. This indicates a good mixture of the different functional groups on the nanometer length scale as is found for instance in the case of a statistical copolymer.

Another recent example of the use of  $^1\text{H}$  DQ MAS NMR spectroscopy is given by the study of molecular scale miscibility of poly(butylenes terephthalate)-*block*-poly(tetramethylene oxide) multiblock (PBT-*block*-PTMO) copolymers (123) by looking for correlation peaks between signals from the hard and soft blocks.

Previous  $^{13}\text{C}$  NMR MAS relaxation experiments revealed a large, bimodal-like heterogeneity of the PTMO chain mobility, which were explained by microphase separation of the amorphous phase into a highly mobile PTMO-rich phase and a less mobile PBT/PTMO mixed phase (PBT/PTMO interface) (124). However, the motional heterogeneity of the PTMO blocks can also originate from a dynamical interface due to anchoring of PTMO blocks to rigid PBT domains, which can cause apparent “two-phase” behavior. 2D NMR experiments can provide direct information on the molecular scale miscibility in polymeric materials.  $^1\text{H}$  DQ correlation spectroscopy under fast MAS using the back-to-back (BABA) sequence is used in the present study to determine the proximity of the PBT and PTMO chain units in the block copolymers.

The  $^1\text{H}$  MAS NMR spectrum of PBT-*block*-PTMO consists of resonances at 8.0, 4.4, 3.4, and 1.6 ppm that originate from the aromatic protons of PBT,  $\text{OCH}_2$  protons of PBT,  $\text{OCH}_2$  protons of PTMO, and the  $(\text{CH}_2)_2$  protons of PBT and PTMO, respectively. It is noted that the  $\text{OCH}_2$  protons of PBT and PTMO at the transition from PBT to PTMO blocks along the chain have slightly different chemical shifts, as measured by  $^1\text{H}$  solution NMR spectra, ie, 4.35 and 3.45 ppm for PBT and PTMO, respectively. However, these resonances are not resolved in the solid state NMR spectra. Figure 20 shows the phase-sensitive 2D spectrum of sample A1000/35 measured using the BABA sequence (123). The single-quantum (SQ) and double-quantum (DQ) dimensions are shown on the horizontal and vertical axes, respectively. The signals in the DQ dimension are situated at the sum of the frequencies of the two-coupled protons. Therefore, a DQ signal between two protons with identical chemical shifts will be on the diagonal, and signals between two protons with different chemical shifts will be off-diagonal giving rise to two signals equally spaced from the diagonal. One should note the different positions of off-diagonal signals are compared to COSY/NOESY spectra.

As expected, all resonances of PBT and PTMO blocks are present in the 2D spectrum, ie, all diagonal peaks and off-diagonal correlation peaks between the aromatic and the  $\text{OCH}_2$  protons of PBT as well as a correlation peak between the  $\text{CH}_2$  and  $\text{OCH}_2$  peaks of PTMO. Additionally, there is a correlation peak between

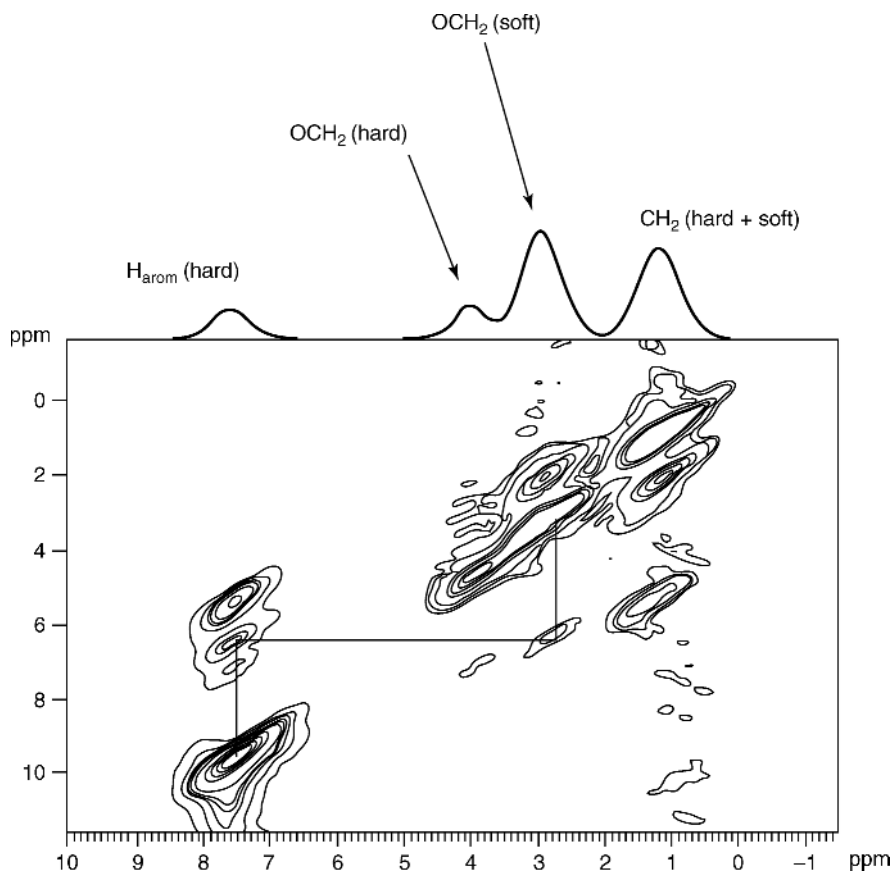


**Fig. 20.** Two-dimensional  $^1\text{H}$  DQ MAS spectrum for thermoplastic elastomers PBT-*block*-PTMO with a length of PTMO block of 1000 g/mol and amount of PTMO block of 35% in weight (sample A1000/35) showing the dipolar correlation between the resonances of PBT and PTMO chain units, as indicated by the lines connecting the peak positions. Reproduced from Ref. 123, with permission from American Chemical Society.

the aromatic protons from PBT and the  $\text{OCH}_2$  groups from PTMO, suggesting a close proximity of these two chain fragments. The signal is in fact much more intense than one would expect (1) from a small fraction (only 14%) of PTMO chain units that are located at the transition from PBT to PTMO blocks in a single chain and (2) from the rather long intrachain distance between aromatic PBT and the  $\text{OCH}_2$  protons of PTMO at the transition from the hard to the soft blocks along the chain. The correlation peak cannot be explained by spin diffusion during the 1ms  $z$ -magnetization delay after the reconversion period. Therefore, the DQ BABA MAS experiment is not affected essentially by the spin diffusion process and gives information about the molecular scale mixing. This correlation peak has to come primarily from intermolecular couplings between the PBT and PTMO protons of adjacent chains. In fact, it was shown that a DQ correlation signal arises at short recoupling times, which in our case, marks an interproton



distance below 0.5 nm. Therefore, this correlation peak can be unambiguously attributed to PBT and PTMO units in a mixed PBT/PTMO phase.

**Site-Selective Double-Quantum Buildup Curves and Correlation with Cross-Link Density.** A more quantitative evaluation of the DQ peak intensities is possible by acquiring the experimental DQ buildup curves for each of the peaks performing a series of DQ experiments with increasing excitation time. As an example, the buildup curves for the three main contributions are shown in Figure 21 for two SBR samples with different cross-link densities (73).

A fit of the experimental DQ buildup curves using a relationship derived in the spin-pair approximation allows the ratio of the corresponding residual dipolar couplings to be determined, ie,  $(\bar{D}^{\text{CH}_2\text{S}_s^{\text{CH}_2}}) : (\bar{D}^{\text{CH}_2\text{-CH}_s^{\text{CH}_2\text{-CH}}}) : (\bar{D}^{\text{CH-CH}_s^{\text{CH-CH}}})$ , where  $\bar{D}^{ij}$  represents a preaveraged dipolar coupling constant and  $S_s^{ij}$  the corresponding scaled dynamic-order parameter (73,119). The order parameter  $S_s^{\text{CH}_2\text{-CH}}$  (calibrated using a 1D MAS sideband pattern) is found to be close to the value  $S_s^{\text{CH}_2\text{-CH}} = 0.1$  that has been estimated for SBR samples by the magnetization-exchange experiments described above (65). The order parameter corresponding to the CH-CH coupling is even higher (73). This coupling provides the best measure for the chain dynamics since it is predominantly aligned along the segmental axis.

For investigating a series of samples with different cross-link densities, however, the procedure described above is very time-consuming. In this case, a somewhat less detailed 1D measurement of the integral DQ-filtered signal can be used to establish the relationship between the total DQ intensity and the cross-link density. The square root of the DQ intensity is found to be an approximately linear function of the cross-link density but, more important, the topological constraints that are already present in the melt are found to dominate the residual couplings (see also Reference 119). Hence, the technique is not so much a sensitive measure of the cross-link density but is a rather sensitive and selective probe for local dynamic chain order.

The strongest residual dipolar couplings were also edited in a nonrotating cross-linked polyisoprene series by exciting double- and triple-quantum coherences in the short time regime (68). From this, the dynamic order parameters of the methylene and methyl groups were estimated and correlated with the cross-link density. Essentially, the same behavior was found as for SBR.

**Residual Local Dipolar Fields by Heteronuclear Correlation Experiments.** The NMR spectrum of rare spins (eg  $^{13}\text{C}$ ) contains extremely useful information because of the usually high chemical-shift dispersion and the possibility to easily eliminate undesired spin interactions. It would thus be advantageous to combine this high resolution dimension with  $^1\text{H}$  spectroscopy in form of a heteronuclear correlation experiment (1). In the following, we will concentrate on the so-called wide-line separation (WISE) experiment (2,125-128), in which  $^1\text{H}$  broadline information is correlated with the  $^{13}\text{C}$  spectroscopic information. There are however also other possibilities for including heteronuclear information in a 2D experiment, for instance, 2D heteronuclear  $J$ -resolved spectroscopy which was applied for the investigation of filled natural rubber in Reference 101. It was concluded that there must be a high degree of motion in order to allow the scalar  $^{13}\text{C}$ - $^1\text{H}$  couplings to be revealed by magic-angle spinning alone.

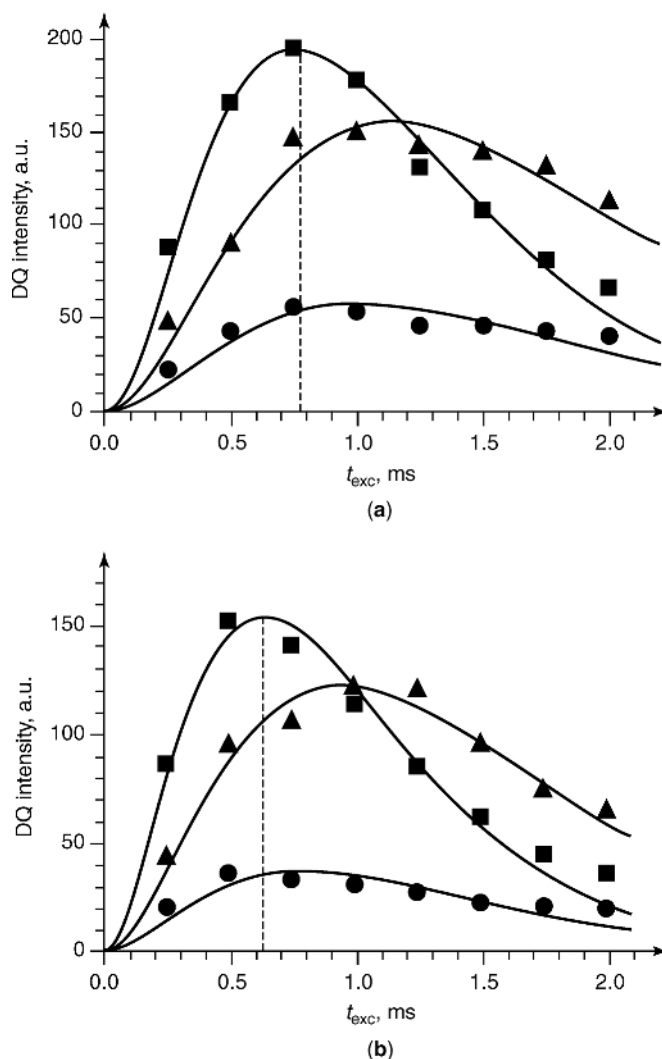


**Fig. 21.** Site-selective  $^1\text{H}$  DQ buildup curves for low (a) and high (b) cross-linked SBR samples. The DQ signals correspond to the  $-\text{CH}_2-$  (■),  $\text{CH}_2-\text{CH}-$  (▲) and  $\text{CH}=\text{CH}$  coherences (●). The vertical dashed lines mark the excitation times for the maximum signal for the methylene protons, which differs for the two cases. Reproduced from Ref. 123, with permission from Elsevier.

The  $^{13}\text{C}$  line width was found to be determined by susceptibility effects due to the presence of the filler.

While the (heteronuclear and homonuclear) residual dipolar couplings have to be eliminated in such  $J$ -resolved experiments, they are the main source of information in the WISE experiment described below. For the investigation of viscoelastic materials the experiment thus must be performed under static

conditions or under slow magic-angle spinning. The method is discussed in the previous section.

**<sup>13</sup>C-<sup>1</sup>H Local Residual Dipolar Couplings by WISE-MAS Experiments.**

For elastomers and rubbery-like materials well above the glass-transition temperature  $T_g$ , the high molecular mobility reduces the dipolar couplings dramatically. The WISE experiment allows one to investigate site-selectively residual dipolar interactions and thus molecular dynamics by editing the corresponding proton slices of the 2D data set.

In References 129 and 130 <sup>13</sup>C-edited <sup>1</sup>H transverse relaxation was investigated in a nonrotating SBR cross-linking series. A short contact time was used to avoid <sup>1</sup>H spin diffusion. As a consequence of this, only <sup>1</sup>H atoms directly bonded to <sup>13</sup>C atoms are observed and the <sup>1</sup>H transverse relaxation is thus found to be mainly governed by <sup>1</sup>H-<sup>13</sup>C heteronuclear couplings which makes analysis simple. The <sup>13</sup>C-edited <sup>1</sup>H transverse relaxation could be fitted with only one adjustable parameter, the effective number of statistical segments (129). This was invoked as a justification for the heterogeneous model used to describe transverse relaxation. Moreover, the effect of cross-linking could be investigated and it was shown that it affects the dynamics of all functional groups to the same extend (125).

A similar experiment has been performed in (125) but under MAS conditions. For a series of cross-linked natural rubber samples (A-F1), <sup>13</sup>C-edited <sup>1</sup>H spinning sidebands have been extracted from the 2D spectrum. These sideband patterns are encoded by the residual dipolar couplings of the corresponding functional groups and are presented in Figure 22.

For the experimental conditions given, the spectra are found to be dominated by heteronuclear dipolar interactions which leads to relatively narrow, well-separated dipolar spinning sidebands. The heteronuclear dipolar couplings could be evaluated by simulating the spectra on this basis (see right column in Figure 22). They were found to be between 0.9 and 1.5 kHz for the samples of the series (the intercross-link masses  $M_c$  were between 6700 and 11,000 g/mol). A practically identical envelope of the spinning-sidebands intensities in the indirect dimension is found for all functional groups. This indicates that the effective <sup>1</sup>H-<sup>13</sup>C vectors of different segments are affected in approximately the same way by internal motions.

Spin diffusion as an alternative explanation of this effect could be excluded by a similar experiment with additional <sup>13</sup>C decoupling during the evolution period  $t_1$  which eliminates the encoding by the heteronuclear dipolar couplings (125). Distinct features are then visible for the spinning sideband patterns of the CH<sub>3</sub>, CH<sub>2</sub> and CH groups (see Reference 125) proving that different functional groups are relatively isolated from each other on the time scale of the experiment as a consequence of the reduction of homonuclear dipolar interactions by high segmental mobility and magic-angle sample spinning. Therefore, the indirect detection of the spinning sideband patterns via cross-polarization <sup>13</sup>C spectroscopy allows for selective measurements of residual dipolar interactions on different functional groups (125).

**Deuterium NMR Studies on Thermoplastic Elastomers.** For the investigation of the molecular dynamics in polymers, deuterium solid-state nuclear magnetic resonance (<sup>2</sup>D-NMR) spectroscopy has been shown to be a

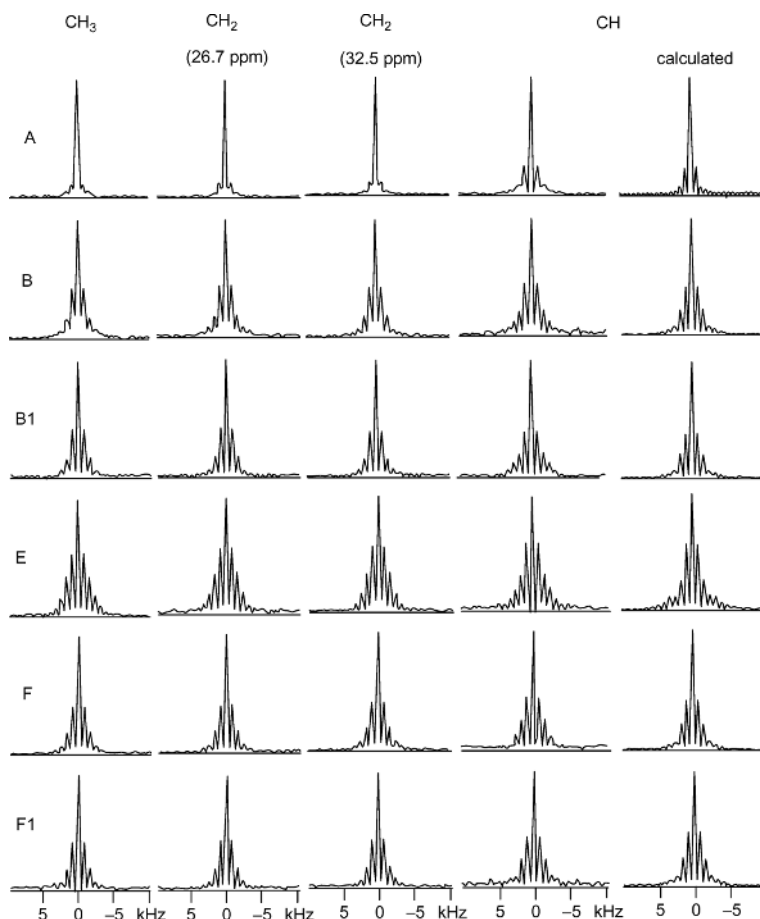


**Fig. 22.** Slices from a 2D experiment corresponding to  $^{13}\text{C}$ - $^1\text{H}$  WISE experiment performed on a series of cross-linked natural rubber samples A–F1 under magic-angle spinning. The slices reflecting proton sideband pattern for the different functional groups that are encoded by the  $^1\text{H}$  residual dipolar couplings. The distinct features of dipolar slices prove that the different functional groups may be considered as relatively isolated groups of spins on the time scale of the evolution and cross-polarization. Reproduced from Ref. 125, with permission from Rapra Technology.

powerful method (2). In the field of viscoelastic polymers, segmental dynamics of poly(urethanes) has been studied intensively by  $^2\text{D}$ -NMR (131,132). In addition to 1D NMR Spectroscopy, 2D NMR exchange spectroscopy was used to extend the time scale of molecular dynamics up to the order of milliseconds or even seconds. In combination with line-shape simulation, this technique allows one to obtain correlation times and correlation-time distributions of the molecular mobility as well as detailed information about the geometry of the motional process (2).

**Principles of the Method.** The scheme typically used for such 2D-exchange NMR experiments corresponds to that given in References 1 and 2, however, in case of deuterons often a solid echo sequence is used for detection instead of the

last pulse. During the mixing time  $t_m$  of the experiment, molecular reorientations are allowed to take place. If the molecular orientation of a C—<sup>2</sup>H bond has changed due to slow molecular motions, the signal continues to evolve with a new frequency. For reorientation about a well-defined angle  $\theta$ , the 2D exchange spectrum exhibits characteristic ridges in the form of ellipses that can be analyzed with respect to motions (for details about the analysis we refer to literature (2)).

**Local Motions and Segmental Orientation in Supramolecular Hydrogen Bond Assemblies.** In the field of viscoelastic materials, the technique has been mainly applied to thermoplastic elastomers. One interesting elastomer belonging to this class consists of polybutadiene chains functionalised by 4-(3,5-dioxo-1,2,4-triazolidin-4-yl) benzoic acid (U4A) units which act as effective junctions zones. The molecular dynamics of the phenyl rings of the U4A units has been probed by 1D and 2D <sup>2</sup>H-NMR (see Reference 133, and references therein). In this system, there are three spatially separated environments that are reflected in the mobility of the polar units. Phenyl rings which are incorporated in the structure are either rigid or undergo 180° phenyl flips. The small fraction of free functional groups move isotropically and their mobility is coupled to the dynamics of the polymer matrix. The 1D <sup>2</sup>H-NMR spectra can be described quantitatively assuming a distribution of correlation times over 2–3 decades and the geometry of the motional processes is defined by the environment in the clusters up to the order–disorder transition temperature. 2D spectra of the model compounds show an elliptical exchange patterns, indicating well-defined slow 180° phenyl flips on a time scale of 100 ms up to 3 s.

## Principles of NMR Imaging Methods

In polymers, the spatial distribution of the nuclei and the spin interactions as well as motions can be probed by NMR at different length scales using different strategies. The NMR techniques suitable for investigation of spatial structures are identified in Figure 23 together with the appropriate spatial resolution scale. In the nanoscale range, spectroscopic methods based on manipulation of spin interactions can measure internuclear distances and bond angles ((27), and references therein).

The field gradients are used for selection of the coherence pathways and encoding of molecular diffusion but many methods perform without the demand for field gradients. In the mesoscopic range, spin diffusion ((2), and references therein) can be used for measuring domain sizes and morphology. The domain of NMR imaging of polymers (134–138), which uses space encoding by field gradients can probe today only the macroscopically distributed heterogeneities, ie, in the order of 10–100  $\mu\text{m}$ .

In recent years, the field of spatially resolved magnetic resonance which includes imaging, microscopy, and volume localized spectroscopy of materials (5,18) has been advanced by the introduction of several new techniques and improvement of the existing ones designed to overcome, mainly, the dipolar interactions of abundant proton spins in rigid polymers that contribute to broadening of the NMR resonance lines. The well-known condition  $\Delta x = 2\pi \Delta\nu_{1/2}/(\gamma G_x)$  (see for instance, Reference 47) for the spatial resolution  $\Delta x^{-1}$  by frequency encoding,

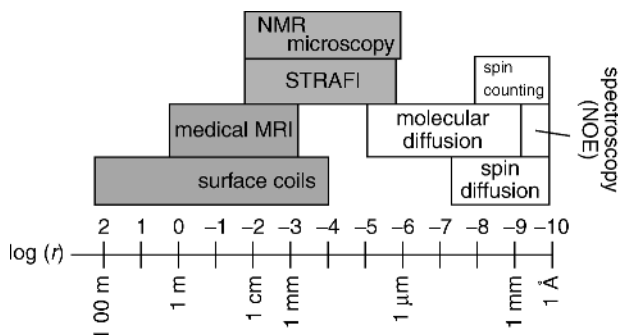


**Fig. 23.** Range of spatial resolution available from different NMR experiments that covers over ten orders of magnitude. The methods using direct space encoding by gradient are shaded, but all other spatial information can be included for creation of image contrast. Reproduced from Ref. 136, with permission from Wiley.

where  $\gamma$  is the magnetogiric ratio,  $\Delta\nu_{1/2}$  is the full width at half height of NMR spectrum and  $G_x$  is the field gradient strength in the  $x$ -direction, can define the strategies for improving the quality of NMR images. There are, in principle, two possibilities: either the gradient strength can be increased or the line width be reduced (47,139–141). This can be achieved by manipulation of the spin or the space part of the interaction Hamiltonian or both, or by dilution manipulations (4). Increasing the gradient, strength might seem the simpler approach. However, the difficulty of using a large gradient is that the receiver bandwidth must be increased to accommodate the spread in resonance frequencies and therefore more noise is introduced into the resultant image. The noise content is proportional to the square root of the receiver bandwidth, and hence the time to acquire a given quality image, in both resolution and sensitivity, depends on the line width.

Many solid-state imaging techniques use spin coherences refocused by *echoes* for different purposes: (1) To record very short free induction decays present, in general, for solids and/or in the presence of strong field gradients. (2) For space encoding during the echo time. (3) For line narrowing by homonuclear or heteronuclear dipolar decoupling. (4) Reconversion of multiple-quantum (MQ) coherences into detectable single-quantum coherences. The properties of the spin echoes that refocus inhomogeneous and homogeneous spin interactions have been discussed in the previous section. Also mixed echoes can be produced which eliminate all internal and external spin interactions. In the maximum of a mixed echo, each individual spin is fully isolated in the rotating reference frame in the absence of relaxation processes; a “time-suspension” process is taking place.

Methods of liquid-state imaging which can be applied, for instance, for analysis of elastomers or polymer swelling have been reviewed on several occasions (see for instance, References 19,47,135, and 139–141). Many of the methods used to record NMR images of solids can be combined with spectroscopic information. This unique feature and the richness in parameter contrast compensate for the relatively modest spatial resolution in many applications. If the spatial information is phase encoded, ie, indirectly detected, then the spectroscopic dimension

is scanned directly, in many cases, by means of spin-echoes and in the absence of gradients. This approach is referred to as spectral frequency encoding. On the other hand, the spectroscopic information can be phase encoded or detected indirectly in the same way as in conventional two-dimensional spectroscopy. This approach is referred to as spectral phase encoding.

**Spin System Response for a Heterogeneous Sample.** In the following, a heterogeneous sample having magnetically equivalent nuclei with magnetogyric ratio  $\gamma$  and the local spin density  $\rho(\vec{r})$  is considered. The space localized thermodynamic equilibrium magnetization corresponding to a voxel with coordinates  $(x, y, z)$  of the position vector  $\vec{r}$  is given by  $m_0(x, y, z) = C\rho(x, y, z)$ , where  $C$  is the Curie constant. In the rotating reference frame at the resonance frequency, the single-pulse NMR spin system response  $s(\vec{r}, t)$  can be expressed by the local free induction decay (FID)  $f(\vec{r}, t)$ ,

$$s(\vec{r}, t) = C\rho(\vec{r})f(\vec{r}, t) \quad (35)$$

Spatially resolved NMR is concerned with unraveling the spatial distribution of  $\rho(x, y, z)$  and measuring associated NMR parameters at individual “volume cells”, or voxels at space point specified by the vector  $\vec{r}$ . If many contiguous voxels are investigated on a plane, or if a projection is investigated, one refers to NMR *imaging*, if individual voxels are investigated one refers to volume-selective NMR.

The spin density distribution can be resolved by different techniques. The standard approach exploits the possibility of introducing space dependence to the resonance frequency  $\omega$  in each voxel by superposing a magnetic field gradient to a homogeneous magnetic field  $\vec{B}_0(0, 0, B_0)$  by the use of additional coils. In general, the field gradient is a Cartesian tensor with nine components related by the Maxwell equations. In the limit of large static magnetic field and small gradient, the gradient tensor can be reduced to a gradient vector  $\vec{G}$  for an approximate description of the imaging experiments with good accuracy. Then the resonance frequency becomes dependent on the space vector  $\vec{r}$ , ie,  $\omega(\vec{r}) = \gamma(B_0 + \vec{G} \cdot \vec{r}) = \omega_0 + \gamma\vec{G} \cdot \vec{r}$ , where the field gradient vector collects the derivatives of the magnetic field in the  $z$ -direction with respect to the space coordinates defined by the component of the field gradient:  $\vec{G}(\partial B_0/\partial x, \partial B_0/\partial y, \partial B_0/\partial z)$ .

The total time-dependent signal of an inhomogeneous object of volume  $V$  measured in a magnetic field gradient and in rotating frame at the angular frequency  $\omega_0$  is given by

$$S(t) \propto C \iiint_V \rho(x, y, z) f(x, y, z, t) \exp[i\gamma\vec{G} \cdot \vec{r}t] dx dy dz \quad (36)$$

In high magnetic field the spatial dependence of the Curie constant can be neglected in a good approximation.

In order to illustrate the basic concepts of space encoding time-dependent gradients  $\vec{G}(t)$  shall be admitted. The wave vector  $\vec{k}$  can be introduced which is

the Fourier conjugate to the space variable  $\vec{r}$ ,

$$\vec{k}(t) = \gamma \int_0^t \vec{G}(t') dt'. \quad (37)$$

In this notation, the single-pulse response signal in time-dependent main field gradients becomes

$$S(t) \propto C \iiint_V \rho(x, y, z) f(x, y, z, t) \exp[i\vec{k}(t) \cdot \vec{r}] dx dy dz. \quad (38)$$

This equation is the starting point for the discussion of spatial resolved NMR basic procedures.

**Spatial Resolution by Frequency Encoding.** The principle of the spatial resolution of NMR imaging by frequency encoding is discussed in the following in the presence of a pulsed uniform gradient, say  $G_x = \partial B_0 / \partial x$ . After the radio-frequency excitation pulse the quantity  $k_x(t)$  grows linearly with time according to equation 37, ie,  $k_x(t) = \gamma G_x t$ . Thus,  $\vec{k}$  space is sampled in the direction of  $k_x$ , and time  $t$  and  $k_x$  are equivalent variables. If  $t$  is replaced by  $k_x / (\gamma G_x)$  the spin system response given by equation 38 becomes

$$S(k_x / (\gamma G_x)) \propto C \iiint_V \rho(x, y, z) f(x, y, z, k_x / (\gamma G_x)) \exp[i\gamma k_x \cdot x] dx dy dz \quad (39)$$

The complex FID signal acquired in this way is composed of contributions evolving according to the local offset resonance frequency  $\gamma G_x x$  labeling the nuclei responsible for this local transverse magnetization, hence, the term frequency encoding. Note that this is the conventional way of encoding in the Fourier transform spectroscopy. However, in context with NMR imaging, signals are processed in terms of the wave numbers  $k_x$  rather than of offset frequencies. The Fourier transform over  $k_x$  produces the convolution of the Fourier transform of the functions  $\rho(x, y, z)$  and  $f(x, y, z, k_x / (\gamma G_x))$ . If  $f(x, y, z, k_x / (\gamma G_x)) \approx f(k_x / (\gamma G_x))$ , the Fourier transform of the FID is the space-dependent spectral response  $F(x)$  and the Fourier transform of the triple integral is a projection  $P(x) = \int \int \rho(x, y, z) dy dz$  of the spin density on the  $x$ -axis. Then, the Fourier transform of equation 39, can be written as

$$S(x) \propto C \int_{x_{\text{sample}}} F(x - x') P(x') dx' \quad (40)$$

where  $x_{\text{sample}}$  represents the sample size in the  $x$ -direction. A faithful representation of the spin-density projection  $P(x)$  would be obtained by this method of frequency encoding only if the spectrum  $F(x - x')$  is a Dirac function  $\delta(x - x')$ , or a narrow NMR absorption line like for liquid samples.

The above discussion is illustrated in Figure 24. If the samples are liquid, a narrow NMR absorption line is observed for both samples in a homogeneous magnetic field and a projection of the object along the  $x$ -axis is measured in the



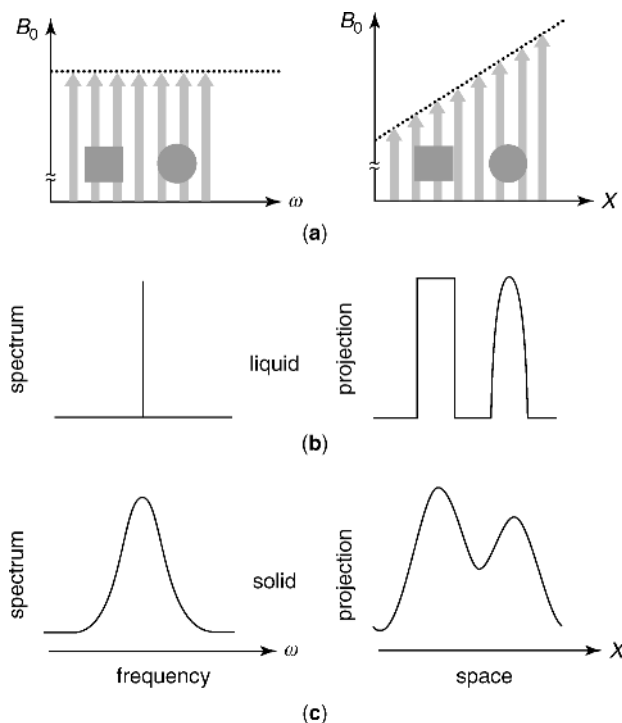


**Fig. 24.** Effect of field gradient on the NMR signal. The samples consists of a rectangular and a circular object. (a) Homogeneous magnetic field (left) and magnetic field with a linear space dependence (right). (b) Spectroscopic response for a liquid sample with a single, narrow line in the NMR spectrum. (c) Spectroscopic response for a solid sample with a single, broad line in the NMR spectrum. Reproduced from Ref. 136, with permission from Wiley.

presence of the field gradient  $G_x$ . The signal amplitude at each resonance frequency or space coordinate is determined by the number of spins that experience the same magnetic field strength. If the spectrum in a homogeneous field is broad like in the solid samples (bottom traces) then the convolution (cf eq. 40) of the projection of the spin density by the line shape becomes noticeable, and the spatial features are smeared out. Thus, the minimum distance  $\Delta x$  which can be resolved is defined by the ratio of the full width at half spectral intensity  $\Delta\omega_{1/2}$  of spectral features to the spread of the resonances introduced by the field gradient, ie,

$$\Delta x = \frac{\Delta\omega_{1/2}}{\gamma G_x} \quad (41)$$

Clearly, equation 41 indicates that when the line width increases, the gradient strength  $G_x$  also has to be increased, at least when the resolution  $\Delta x$  is to be kept constant.

**Spatial Resolution by Phase Encoding.** Broadening of the projection by the NMR spectrum (cf eq. 40) can be avoided if the spatial information is

detected indirectly in the fashion of the multidimensional Fourier NMR spectroscopy (1). For instance, a magnetic-field gradient  $G_y$  is switched on for an evolution time  $t_1$  following a radio-frequency excitation pulse, and the signal is acquired in a detection time  $t_2$  after the gradient has been switched off. For this 2D scheme, the NMR signal can be written as

$$S(t_1, t_2) \propto C f(t_1) f(t_2) \int_{y_{\text{sample}}} P(y) \exp\{i\gamma k_y y\} dy \quad (42)$$

where  $k_y = \gamma G_y t_1$  and  $P(y) = \int \int \rho(x, y, z) dx dz$ . It becomes clear that there are two ways to perform the experiment: either  $t_1$  is varied in the custom of 2D NMR spectroscopy, or  $t_1$  is kept constant and  $G_y$  is stepped in increments  $\Delta G_y$ . The first case bears no advantage compared to direct frequency encoding discussed above. As time  $t_1$  proceeds, not only does  $k_y$  increase, but also the free induction decay  $f(t_1)$  evolve and deteriorate the signal intensity and finally the spatial resolution. But, if  $t_1$  is kept constant  $f(t_1)$  has a fixed value, and the phase change of the signal in the evolution period depends only on the wave vector  $k_y$ . Thus, the spatial resolution achievable for phase encoding depends on the maximum gradient strength available and on the signal-to-noise ratio, because the signal strength decreases with increasing  $\vec{k}$ .

The digital resolution or the pixel resolution of an NMR image can be much higher than the actual space resolution. The digital resolution  $1/\Delta y$  of the NMR imaging in  $y$ -direction is determined by the maximum value of  $k_y$  or equivalently by the number  $n_y$  of complex signal values and the  $\vec{k}$  space sampling intervals  $\Delta k_y$ , ie,  $1/\Delta y = n_y \Delta k_y / (2\pi)$ . To avoid signal aliasing,  $k_y$  has to be stepped in small enough intervals so that the signal-phase increment  $y_{\text{max}} \Delta k_y$  for the maximum object coordinate  $y_{\text{max}}$  never exceeds  $2\pi$ .

**Sampling  $\vec{k}$  Space.** Different imaging schemes are often discriminated against the way  $\vec{k}$  space is sampled (for more details see Reference 19).

Two elementary 2D NMR imaging methods are illustrated in Figure 25: 2D Fourier imaging (2DFI, Fig. 25a) and back-projection imaging (BPI, Fig. 25b). Orthogonal gradients are switched subsequently in 2DFI and simultaneously in BPI. As a consequence,  $\vec{k}$  space is sampled in orthogonal coordinates for 2DFI. When applied simultaneously, the direction of the resulting gradient changes depending on the relative strengths of  $G_x$  and  $G_y$  gradients. In this way,  $\vec{k}$  space can be sampled in cylindrical coordinates in BPI. In either case, the image is obtained by the Fourier transformation of the  $\vec{k}$ -space data.

Often phase and frequency encoding are combined for acquisition of two-dimensional (2D) images (cf Fig. 25a, left). Then the gradient  $G_y$  is called the phase encoding gradient, and  $G_x$  is the frequency encoding gradient. This is one of the most used methods for recording images in elastomers materials that are soft solids with NMR line widths  $\Delta\nu_{1/2} \approx 100 \text{ Hz/1 kHz}$ .

**Contrast in NMR Imaging.** Compared with other image-forming methods, the NMR imaging is characterized by the abundance of parameters that can be exploited for producing contrast (142,143). Many features invisible to other image-forming techniques can thus be visualized with NMR. To exploit the diversity of contrast features, it is useful to optimize the imaging experiment for

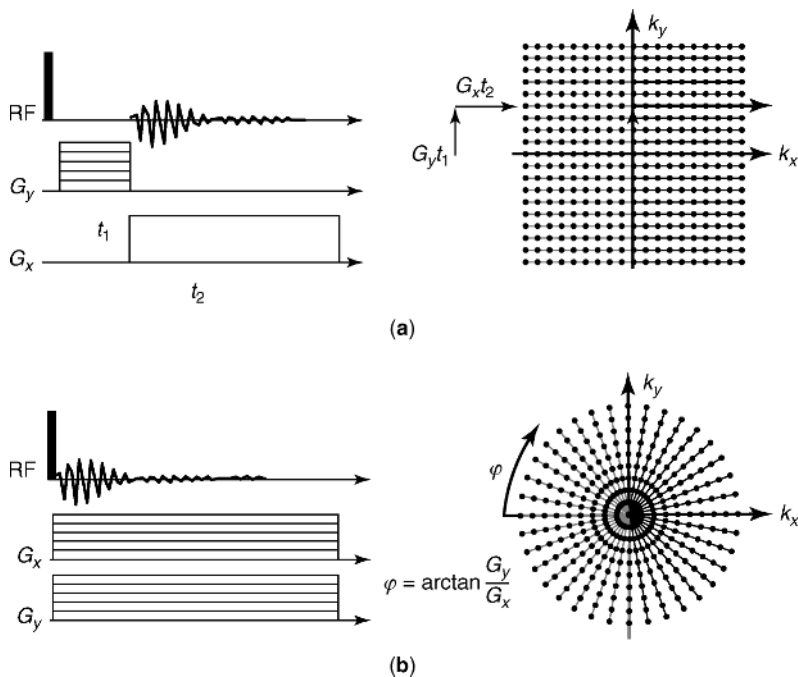


**Fig. 25.** Schemes for acquisition of 2D NMR images. Excitation and detection schemes (left) and maps in  $\vec{k}$  space, where NMR signals is acquired (right). Reproduced from Ref. 136, with permission from Wiley.

generation of maximum contrast. The local contrast  $C$  is defined as the relative difference in image intensities  $M$  of neighboring structures  $i$  and  $j$  (17)

$$C = \frac{|M(\vec{r}_i) - M(\vec{r}_j)|}{|M_{\max}|} \quad (43)$$

where  $|M_{\max}|$  is the absolute maximum of  $M(\vec{r}_i)$  and  $M(\vec{r}_j)$ , where  $\vec{r}_i$  and  $\vec{r}_j$  are the space coordinates of voxels  $i$  and  $j$  under consideration.

**Contrast Parameters and Material Properties.** The contrast parameters relevant for polymer characterization by NMR imaging are directly related to the spin density, static and fluctuating nuclear spin interactions, and to the mass transport parameters. Even if the above quantities can change on molecular or mesoscopic scale only the variation of them on the space domains larger than the resolution of image can be detected in NMR imaging. The residual dipolar and quadrupolar interactions are related to the NMR parameters like van Vleck moments (4) and relaxation times (144). The fluctuating part of spin interactions leads to a variety of contrast parameters of magnetization relaxation type like spin-lattice relaxation in the laboratory reference frame ( $T_1$ ), rotating frame ( $T_{1r}$ ), transverse relaxation ( $T_2$ ), solid echo or coherent averaging pulse sequences decay time ( $T_{2e}$ ) (4), and dipolar correlation decays (5). The relaxation NMR parameters are also related to the manipulation of sample by contrast agents like

paramagnetic relaxation agents, ferromagnetic particles (17), and hyperpolarized xenon (145,146).

The chemical shielding interaction leads to chemical contrast parameters related to the chemical composition as well as molecular orientation. Differences in magnetic susceptibility and the distribution of magnetic fields produced by electrical currents can be also detected via chemical shift (19).

The NMR quantities defining the contrast of NMR images depend on various macroscopic and microscopic physical and chemical parameters of the investigated samples that affect the nuclear spin interactions or molecular transport parameters. They can be classified as internal and external. Moreover, they can be state parameters that are stationary quantities like stress, strain, moduli of shear and compression, cross-link density, distribution and agglomeration of filler particles, molecular orientation, fibril orientation and domain size distribution, distribution of voids, and the temperature distribution. Transition parameters or kinetic parameters characterize the time evolution of the polymer system. They are determined in *in situ* NMR experiments or in stop-and-go experiments. Examples are characteristic times of chemical and physical aging (147,148) of vulcanization (149) and curing (150) processes of heat dissipation and fluid permeation (151,152).

Transition parameters can be determined directly from the analysis of the time evolution of changes in NMR images, but state parameters must be related to NMR parameters either by theory or calibration. Theories have been published that relate the cross-link density of unfilled and filled elastomers to the parameters of transverse relaxation parameters (153) and others relating dynamic storage modulus of polymers to the cross-polarization rate (154).

A simpler approach is based on empirical correlations between NMR parameters and sample properties, which often can be established by calibration of an NMR parameter against a material parameter (155,156). An example of stress-strain calibration is given in Figure 26 by calibration of  $T_2$  of filled poly(dimethyl siloxane) rubber against strain (153), (cf Fig. 26a). By use of the stress-strain curve (Fig. 26b) from mechanical measurements,  $T_2$  can be calibrated against stress (see Fig. 26c).

The procedure can be used to translate the spatially resolved NMR parameters  $T_2$  into values related to the strength of local stress.

Another possibility is given by the observation of the quadrupole splitting in deuteron NMR (155,157). For small strain, the splitting  $\Delta_Q$  is linearly proportional to  $\Lambda^2 - \Lambda^{-1}$  where  $\Lambda = \frac{L}{L_0}$  is the elongation ratio,  $L$  and  $L_0$  are the length of polymer band after stretching and in the relaxed state, respectively (see Fig. 27).

The rubber samples are prepared by swelling in a solution of deuterated spy molecules, these molecules follow the polymer network alignment under strain and the residual quadrupolar coupling that results from their anisotropic motion is observed either by spectroscopic imaging or by double-quantum imaging (158, 159). The above deuteration procedure leads to the modification of the network and to potential modulation of the NMR signal encoding by the self-diffusion of the incorporated oligomers.

The above adverse effects can be avoided if  $^1\text{H}$  residual dipolar couplings of elastomer chains (68) were used to generate contrast in NMR imaging of stretched samples. Dipolar contrast filters can be implemented based on dipolar

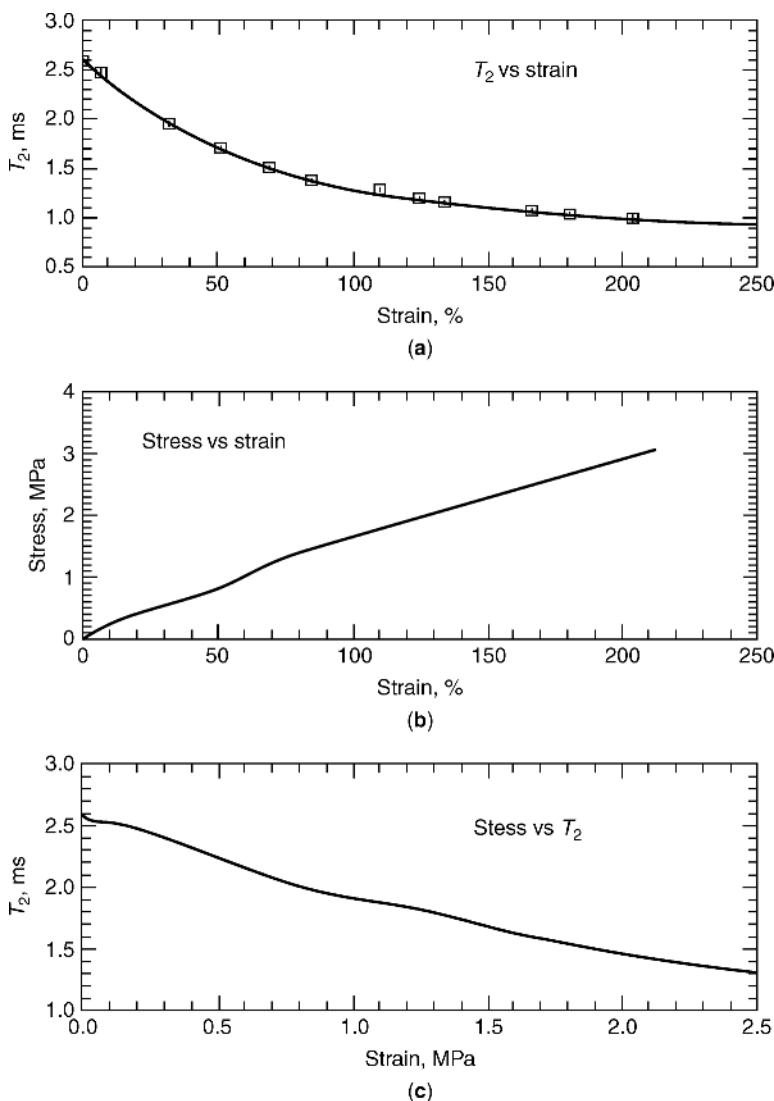


**Fig. 26.** Calibration of  $T_2$  values measured for different strain (a) of filled poly(dimethyl siloxane) against stress (c) by use of the mechanical stress-strain curve (b). Reproduced from Ref. 142, with permission from Wiley.

encoded longitudinal magnetization as well as double- and triple-quantum coherences (160,161). The associated contrast filter parameters were investigated by measurements of the line width in  $^1\text{H}$  multiple-quantum filtered spectra, the dipolar encoded longitudinal magnetization decay curves, and the double- and triple-quantum buildup curves as a function of the extension ratio for a natural rubber band. Together with stress-strain measurements, these results allow for correlation of  $^1\text{H}$  residual dipolar couplings with stress values in stretched natural rubber.

**Magnetization Filters.** The contrast generation in NMR imaging is directly related to the concept of magnetization or coherences filters. Various molecular

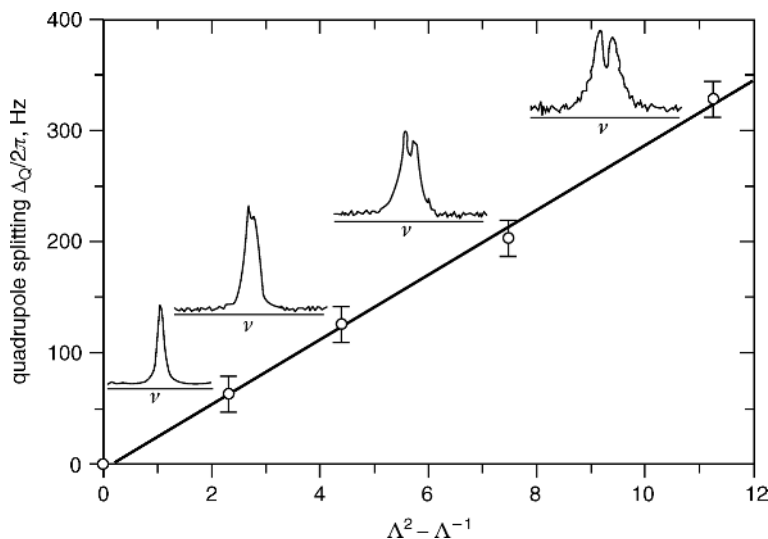


**Fig. 27.** Deuteron quadrupolar splitting of 1,4-tetra-deuterated butadiene oligomers from natural rubber bands for different strains. Reproduced from Ref. 142, with permission from Wiley.

(internal) or external parameter weights are introduced by the use of magnetization or coherences filters (Fig. 28), which block part of the incoming signal originating from the thermodynamic equilibrium magnetization.

As a result, there is a gain in selectivity of the output signal at the expense of a deterioration of signal-to-noise ratio.

A generic scheme for contrast optimisation in the Fourier NMR imaging is illustrated in Figure 28b, (142). In general, three periods are distinguished: a filter period, a space-encoding period, and a spectroscopy period. For image contrast other than the often-uninformative spin density, the space-encoding period must be combined either with a magnetization filter or with spectroscopic data acquisition or both. The signal detected after the action of the general pulse sequence designed to introduce image contrast can be written as (162)

$$S(\vec{k}) = \int \rho(\vec{r}) F_c(\{p\}, \vec{r}) \exp[-i2\pi \vec{k} \cdot \vec{r}] d\vec{r} \quad (44)$$

where the contrast parameter manifold is denoted by  $\{p\}$  and  $F_c(\{p\}, \vec{r})$  is the combined local contrast function. This function could be a product of several parameter contrast functions, such as

$$F_c(\{p\}, \vec{r}) \equiv F_c(T_1, \vec{r}) F_c(T_{1\rho}, \vec{r}) F_c(T_2, \vec{r}) F_c(\delta_i, \vec{r}) F_c(\vec{q}, \vec{r}) \dots \quad (45)$$

where for instance, the contrast factors in the right-hand side of equation 45 representing the effects of longitudinal ( $T_1$  and  $T_{1\rho}$ ) and transverse ( $T_2$ ) relaxation times, chemical shift ( $\delta$ ), and the effect of coherent and incoherent molecular translation motions described in the  $\vec{q}$  space (18).

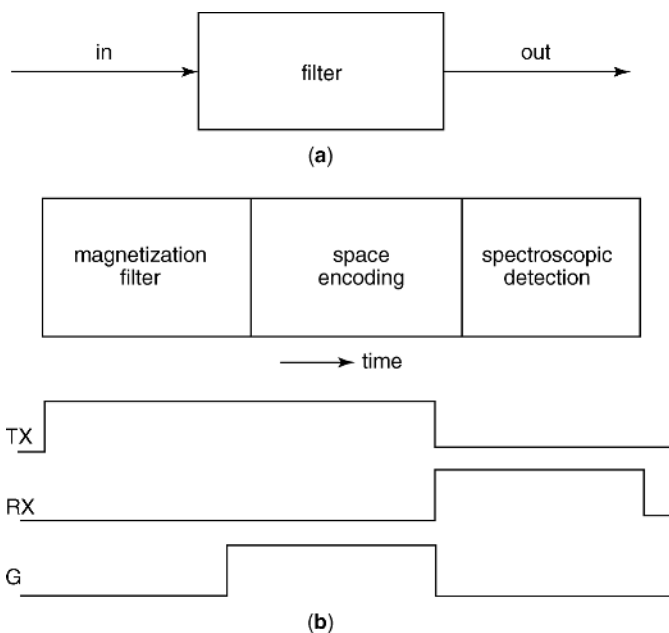


**Fig. 28.** (a) A magnetization filter blocks part of the incoming magnetization or spin coherences. (b) General scheme for generation of NMR image contrast. Initial nuclear magnetization is filtered by the radio-frequency irradiation of resonant nuclei (TX) before or also during space encoding period by magnetic-field gradients ( $\vec{G}$ ). In the absence of gradients, the NMR signal is detected (RX) for the extraction of spectroscopic information. Reproduced from Ref. 143, with permission from Wiley.

There are two basic approaches by which the image contrast can be studied. The first makes the pulse sequence sensitive to a particular contrast parameter  $p$  so that the image intensity bears or is weighted by the influence of that contrast. This approach offers the advantage of time efficiency but is only qualitative. The quantitative information can be obtained by the second approach that include inter alia two-image scheme (162). This method requires two imaging experiments under two contrast conditions. The final parameter map is computed from the two images, voxel by voxel, by means of some mathematical calculation, such as division.

The first approach is illustrated in Figure 29 for the simple case of spin-lock-filtered projections of a composite piece of rubber cut from the tread of a car tire. Such a filter imposes a  $T_{1\rho}$  weight on the spin density (cf Fig. 29a). From the space distributed magnetization decays, the parameter map of  $T_{1\rho}$  can be obtained (cf Fig. 29b) independent of spin densities.

An important class of magnetization filters are mobility filters which select magnetization based on the time scale of segmental motions ((19), and references therein). The parameters for discrimination are the amplitude and characteristic frequency or the correlation time  $\tau_c$  of molecular motions. The effect a filter exerts on a NMR signal can be represented by the filter transfer function. Examples are given in Figure 30 (163,164) with transfer function for filters, which select magnetization based on the time scale of molecular motion.

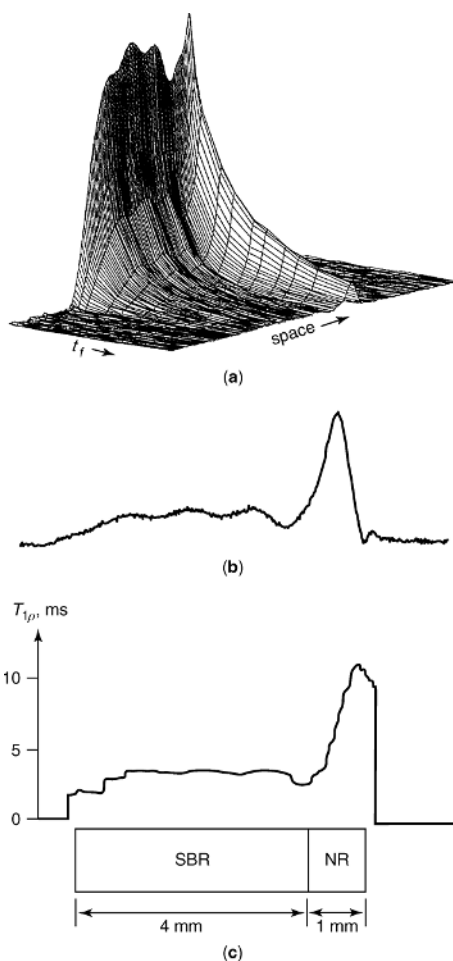


**Fig. 29.** Filter-weighted and spin-lattice relaxation in the rotating frame  $T_{1\rho}$  of an elastomer composite of SBR and natural rubber cut from the tread of a car tire. (a) A stack of one-dimensional  $^1\text{H}$  images with variable duration  $t_f$  of the spin-lock radio-frequency magnetic field. (b) A  $T_{1\rho}$  parameter map obtained from the decay shown in (a). Reproduced from Ref. 143, with permission from Wiley.

Depending on the time scale, different pulse sequences can be used. In the fast motion regime,  $T_1$  filters are applicable. Both saturation recovery and the stimulated echo can be used for this, but the transfer function of both filters is complementary. The spin-echo or Hahn echo filter has a transfer function similar to that of the saturation recovery filter, but because  $T_2$  processes are efficient at slower molecular motions, the filter cut off is shifted to longer correlation times. The dipolar filter exploits the strength of the dipolar couplings averaged by the molecular motions. The residual dipolar filters can use  $^1\text{H}$  double- and triple-quantum coherences (160,161) as well as  $^1\text{H}$ – $^1\text{H}$  magnetization exchange (165). Dipolar correlation effect detected via stimulated echo can be used for a mixed residual dipolar coupling/slow motion filter (166). Resolved splitting of the residual quadrupolar coupling of  $^2\text{H}$  of spy molecules has been used as



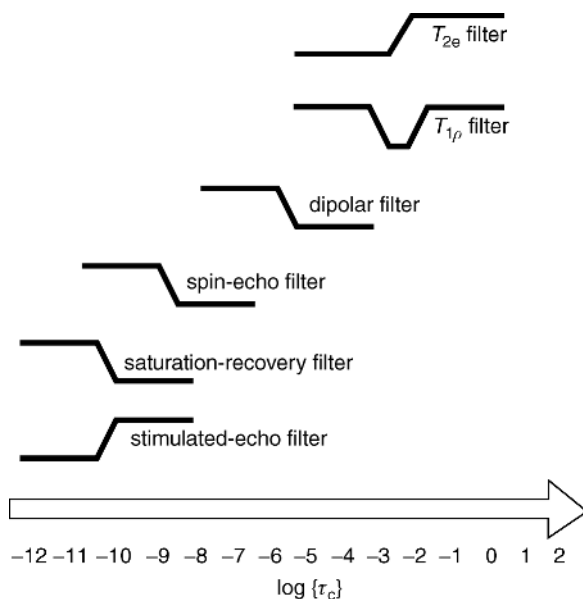


**Fig. 30.** Time scale of molecular motion and filter transfer functions of pulse sequences, which can be used for selecting magnetization according to the time scale of the molecular motion. Reproduced from Ref. 143, with permission from Wiley.

quadrupolar coupling filter (158,159). The spin-lattice relaxation in the rotating frame or  $T_{1\rho}$  filter is efficient at slow motions with correlation times of the order of the inverse of the angular frequency of the spin-lock radio-frequency pulse. The transverse magnetization decay for a train of solid echoes or magic echoes is characterized by the effective transverse relaxation time  $T_{2e}$  (68) a parameter sensitive to the slow segmental motion like  $T_{1\rho}$ .

The identification of material heterogeneities based on differences in molecular motion is an important feature of NMR imaging. The importance of slow molecular motion for image contrast is demonstrated in Figure 31 with relaxation time parameter images through a partially aged sheet of carbon-black-filled styrene-*co*-butadiene rubber (SBR) (147).

The one-dimensional space scale starts at the unaged center of the rubber sheet at  $\Delta r = 0$  and ends at the aged surface at  $\Delta r = 700 \mu\text{m}$ . Two curves are shown for each relaxation parameters as a function of space. The top curve is for unaged material and it varies little with space. The bottom curve is for the aged material. Both curves overlap in the center of the sheet and split toward the surface. The splitting is a direct measure of image contrast. The contrast is largest for those relaxation times that are sensitive to slow molecular motions. the contrast is largest for  $T_{2e}$  and  $T_{1\rho}$  images and almost zero for  $T_1$ .

## NMR Imaging of Elastomers

Potentially rather useful applications of NMR imaging are in elastomer industry. This section features some selected examples that illustrate the type of information obtained by imaging of elastomers. Such applications to elastomers

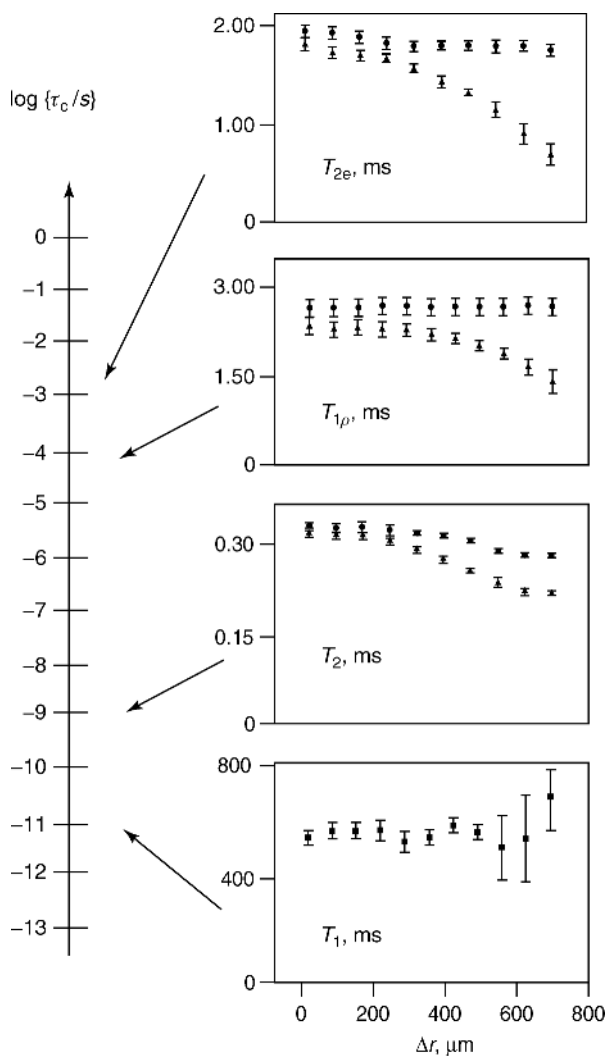


**Fig. 31.** Relaxation parameters  $T_1$ ,  $T_2$ ,  $T_{1\rho}$ , and  $T_{2e}$  for contrast in thermal oxidative aging of SBR. The insets depict the space distribution of relaxation times for a partially aged (lower curve) and an unaged (upper curve) rubber sheet. Reproduced from Ref. 147, with permission from Wiley.

concern distribution in temperature stress, cross-link density, modulus, and the dynamics of fluid absorption and swelling.

**Heterogeneities in Elastomers.** Heterogeneities in elastomers materials are related to the defects induced in the process of preparation. The processes that lead to the defects are as follows.

**Mixing Processes.** Technical elastomers are blends of up to about 30 different compounds like natural rubber, styrene–butadiene rubber, silicate and carbon-black fillers, and mobile components like oils and waxes. Improper mixing leads to inhomogeneities with corresponding variation in mechanical and thermal properties. An important source of heterogeneities of this type is represented by

filler clusters. Even the variance of the distribution statistics of active filler may lead to heterogeneities detected as an average over a volume cell or voxel with the spatial resolution of NMR imaging.

**Vulcanization.** Heterogeneous structures arise from effects of thermal conductivity, which lead to space-dependent temperature profile during the vulcanization process depending on the position of the heat source and on heat dissipation. As a result, inhomogeneous cross-link densities may be established (167). If the process of cross-linking is incomplete the defects represents by the free chains are also presents. The changes in segmental mobility from progress of the vulcanization reaction and from the associated sample temperature distribution can be monitored directly by the NMR imaging *in situ* (149). In the covulcanization of blends and sheets from different formulations, inhomogeneities in cross-link density max arise from differences in solubility and diffusion of curatives (168).

**Aging.** Aging processes are often induced by ultraviolet (UV) irradiation or other ionization radiations (169), exposure to heat and oxygen, and by biological mechanisms. Depending on the load applied, different aging processes are observed (170). The action of electromagnetic radiation with high energy of the associated photons as well as nuclear irradiation will produce chain scission with decrease in the cross-link density and associated increase in chain mobility. Thermal oxidative aging usually leads to the formation of hardened surface layers in natural rubber (NR) as well as synthetic rubber (styrene-*co*-butadiene rubber (SBR) (147,148,171–174). Typically, these layers approach a thickness of 200–300  $\mu\text{m}$  and inhibit progress of the aging process further into the bulk of thin sample. The material hardening is explained by an increase in cross-link density. In the absence of oxygen, chain scission may dominate at elevated temperatures with an associated increase in the segmental mobility. Other types of aging involve aggressive fluids and gases. In this context, a sample of degraded rubber hose gas been investigated (175), but also the degradation of polyethylene pipes and the enzymatic degradation of biologically synthesized polymers (176) have been studied through NMR imaging. Related investigations have been carried out on asphalts (177). Aging associated with swelling of the rubber particles has been observed in crumb-rubber modified asphalts (178).

**Mechanical Load.** Static mechanical load by strain leads to stretching of random-coil polymer chains in the direction of sample elongation and chain compression in the orthogonal directions. The value of the residual dipolar and quadrupolar couplings is increased by the mechanical load, and moreover, the distribution of the correlation times is also modified. Therefore, many NMR parameters sensitive to the residual dipolar couplings and slow motions can be used for characterization of the local strain–stress effects in heterogeneous elastomers (158,160,161,179). Dynamics mechanical load leads to sample heating where the temperature distribution in dynamic equilibrium is determined by the temperature-dependent loss-modulus and the thermal conductivity of the sample. Because transverse relaxation rate (approximated by the  $T_2$  relaxation) scales with the temperature for carbon filled SBR, a  $T_2$  map provides a temperature map of the sample. Such temperature maps have been measured for carbon-black filled SBR cylinders for different filler contents and mechanical load (180).

**NMR Images and Parameter Maps in Elastomers.** NMR of elastomers including NMR imaging appears to address one of the industrially most relevant

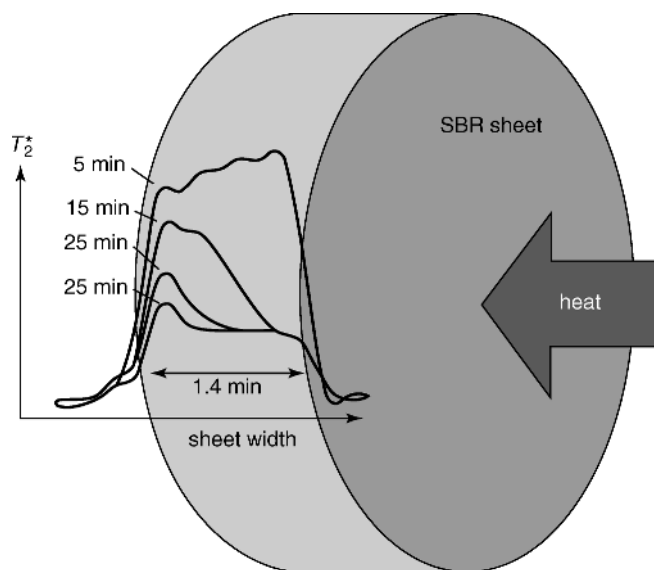


**Fig. 32.** Time-resolved  $T_2^*$  parameter one-dimensional images across a 1.4 mm thick sheet of SBR following the vulcanisation process. Reproduced from Ref. 149, with permission from Rapra Technology.

applications of NMR. Applications of the one- (1D) and two-dimensional (2D) NMR images and parameter maps for characterization of elastomer materials with heterogeneous mesoscopic and macroscopic structure will be reviewed in the following.

**Vulcanization and Covulcanization.** The main effect taking place during the vulcanization process is the space distribution in the cross-link density. One source of this variation is the spatial distribution of the rubber formulation, although short-scale variations are often smoothed by component diffusion during the vulcanization process. Differences on the millimeter scale can lead to interfacial structures.

Another source of variations in cross-link density on the millimeter scale is the curing process in combination with the sample geometry. Heat is supplied to the sample for a certain time and after vulcanization is removed from the sample in certain time. Near the heat source the cross-linking process induced by vulcanization is set in first and near the heat sink is sets in last. Depending on the time dependence of the heat from the source and sink, surface and the thermal properties of the sample, complicated time-dependent temperature profiles are established in the sample.

The vulcanization process has been followed across a thick disk from unfilled SBR by NMR imaging of the effective transverse signal decay (149). The measurements were carried out in a magnetic field slightly inhomogeneous from the construction of a special vulcanization probe and the effective transverse relaxation time  $T_2^*$  was measured (see Fig 32). Despite accelerated signal decay from the field inhomogeneities,  $T_2^*$  still turned out to be sensitive to chain mobility because of a sufficiently strong contribution from  $T_2$ .

A nonlinear relationship between the effective transverse relaxation rate  $1/T_2^*$  and the reduced shear modulus was found. Nevertheless, the relationship that low modulus corresponds to high  $T_2^*$  and high modulus to low  $T_2^*$  can be used to interpret the imaging data across the SBR sheet measured during the vulcanization process (see Fig. 32). Immediately after sample heating, chain mobility is high and so is  $T_2^*$ . With the formation of the cross-links chain mobility decreases and so does  $T_2^*$ . The vulcanization front is defined by the center of change in  $T_2^*$ . It can be seen to migrate through the thin sample on a time scale of about half an hour with the temperature in the range between 140 and 170°C across the sample. With increasing time the slope of the  $T_2^*$  curve flattens indicating a broadening of the reactive vulcanization zone.

Another example of spatial determination of the local cross-link density in inhomogeneous vulcanized elastomers by means of the spatially dependent  $T_2^*$  decay times was discussed on poly(isobutylene-*p*-methylstyrene-*p*-bromomethylstyrene) (PIB-PMS/BrPMS) (181). It was shown that by swelling the elastomers in the aprotic solvent  $\text{CCl}_4$ , the proton signal in the magnetic resonance images originates almost exclusively from the rubber methyl protons (182). This makes it possible to acquire selective images of the rubbery phase, which were demonstrated to be superior toward the visualization of the network homogeneity. Moreover, swelling of these elastomers in an appropriate solvent enhances the molecular chain mobility and reduces the proton line width to an extent acceptable for recording magnetic resonance images.

The gravimetric Flory–Rehner (183) experiments are combined with NMR imaging to study spatially dependent degree of cross-linking, in unfilled, 1,6-hexamethylenediamine-cured PIB-PMS/BrPMS terpolymers (181). Localized relaxometry reveals two proton  $T_2^*$  relaxation decay times in  $\text{CCl}_4$  swollen specimens: a fast decaying component reflecting the constrained chain segments near the cross-links and topological constraints ( $T_{2s}^*$ ) and a slow decaying component originating from less constrained, remote chains ( $T_{2l}^*$ ). On the basis of a linear relation between the bulk number-average molecular weight between effective cross-link ( $M_{n,\text{eff}}^{\text{bulk}}$ ) and the volume average  $T_2^*$ , magnetic resonance images allow the determination of the local cross-link density in inhomogeneous cross-link PIB terpolymer samples by means of the spatially-dependent effective transverse relaxation. The measurements of the localized  $T_{2s}^*$  and  $T_{2l}^*$  allow to deduce the localized molecular weight between the effective cross-links  $M_{n,\text{eff}}(\vec{r})$  for each region of interest labeled 1–10 in Fig. 33. This method reveals that the sample 1 exposes a very heterogeneous network structure as is illustrated by a large variation in the localized  $M_{n,\text{eff}}(\vec{r})$ . This indicates an unfavourable mixing. This in strong contrast to specimen 2, having a rather homogeneous network structure as is demonstrated by the small variation in  $M_{n,\text{eff}}(\vec{r})$  as a result of a uniform curing. The homogeneity of mixing and curing of the specimens 3 and 4 (cf Fig. 33) is somewhere in between. These results clearly demonstrate that NMR image is a useful technique to investigate the homogeneity of mixing and curing of elastomers.

During fabrication of elastomer products like car tires different elastomer formulations often need to be covulcanized. At the interface between an SBR and an NR layer, an interfacial layer with a modulus higher than either SBR and NR had been detected (145,171). In images detected using Hahn-echo method

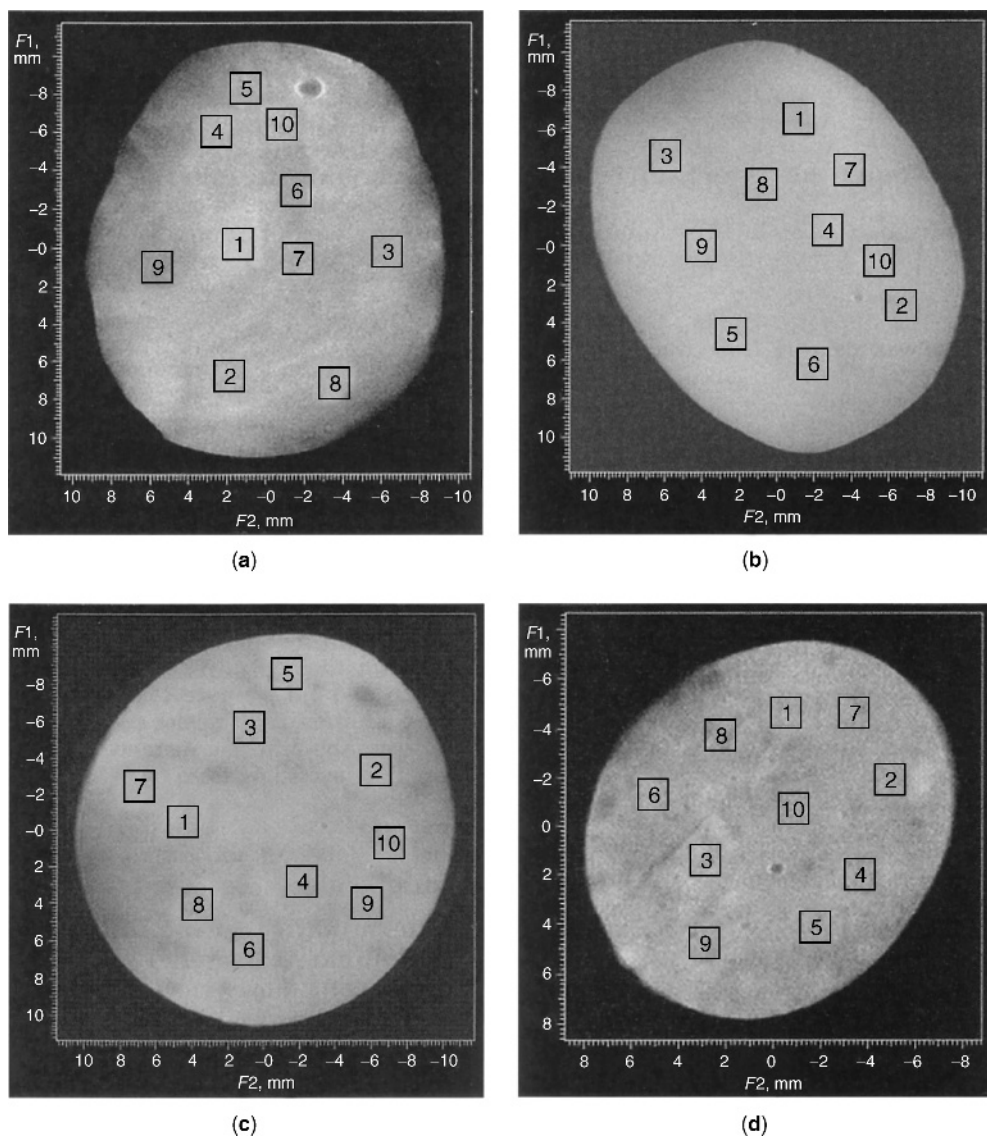


**Fig. 33.** Proton NMR images of unfilled polyisobutylene-based elastomers, cured with 1,6-hexamethylenediamine, after equilibrium swelling in  $\text{CCl}_4$ . The degree of cross-linking increases from samples 1 to 4. The regions of interest indicate the locations used to determine the local relaxation decay times. Reproduced from Ref. 181, with permission from American Chemical Society.

the interface is identified by a dark line paralleled to a slightly brighter line (see Fig. 34).

A mixture of spin density and relaxation forms contrast in the Hahn-echo image. Contrast in the quotient image is determined only by transverse relaxation. In this image, the interface appears abrupt and well defined. The image of the interface shows a transition from the hard SBR component to the soft NR

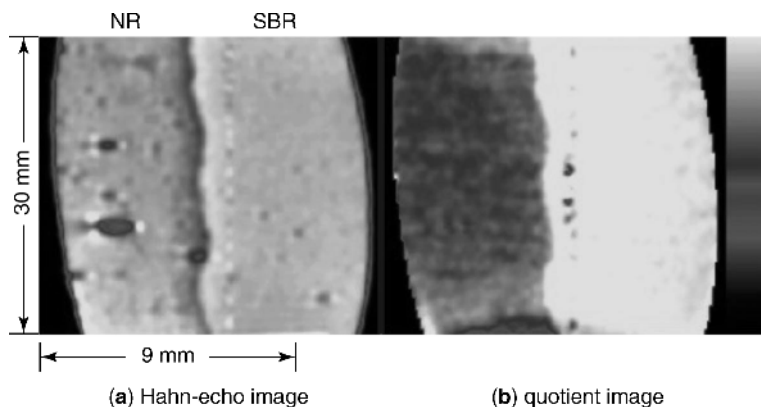


**Fig. 34.** Proton  $T_2^*$ -weighted Hahn-echo image (a) of an unfilled SBR/NR covulcanisate with dimensions  $9\text{ mm} \times 30\text{ mm}$ . The image has been acquired with an echo time of  $t_E = 3.3\text{ ms}$ . A quotient image (b) computed as the quotient of two Hahn-echo images acquired with different echo times of 4.2 and 3.4 ms. Reproduced from Ref. 145, with permission from Rapra Technology.

component with a width of the order of 0–5 mm (184,185). This is the space scale on which the modulus changes. The shape and dimension of the interface are defined by the concentration differences in the vulcanizing agents, which diffuse at elevated temperatures across the interface until their diffusion is hampered by their role in the vulcanization reaction. Thus, the interface arises from a delicate balance between diffusion, reaction, heat supply, and removal.

**Blending.** Interfaces similar to those encountered during covulcanization may arise in blends with incomplete mixing. In unvulcanized samples, heterogeneities from blending can be deduced by gradient echo imaging, where the contrast is enhanced by differences in magnetic susceptibility of the components (186). However, fine structures are usually homogenized during the vulcanization process. Larger structures survive, in particular, when one component had already been vulcanized.

An example of such a case is illustrated in Figure 35 by two orthogonal slices through a block of a vulcanised blend from a soft (bright) and a previously vulcanised hard (dark) component (141). In slice (a), the structures invoked by mixing of components appear coarse but random, but slice (b) reveals stream lines of material flow in the rolling mill.

The presence of carbon-black filler usually does not affect the NMR data in contrast to functionalized silicate filler. This is attributed to rapid transverse relaxation of network chain segments near carbon-black filler particles caused by paramagnetic centers in the filler. Thus, for the technologically important class of carbon-filled elastomers, NMR can provide the chemical cross-link density.

**Aging.** Aging of elastomers is a process that affects the mobility of intercross-link chains by packing, chain scission, and formation of new cross-links. Thermooxidative aging of many elastomers including SBR and NR leads to the formation of a brittle surface layer with reduced mobility that appears dark in  $^1\text{H}$  Hahn-echo images. Often this region is followed by a zone of brighter image intensity, which can be attributed to chain scission or the accumulation of low molecular-weight additives (148).

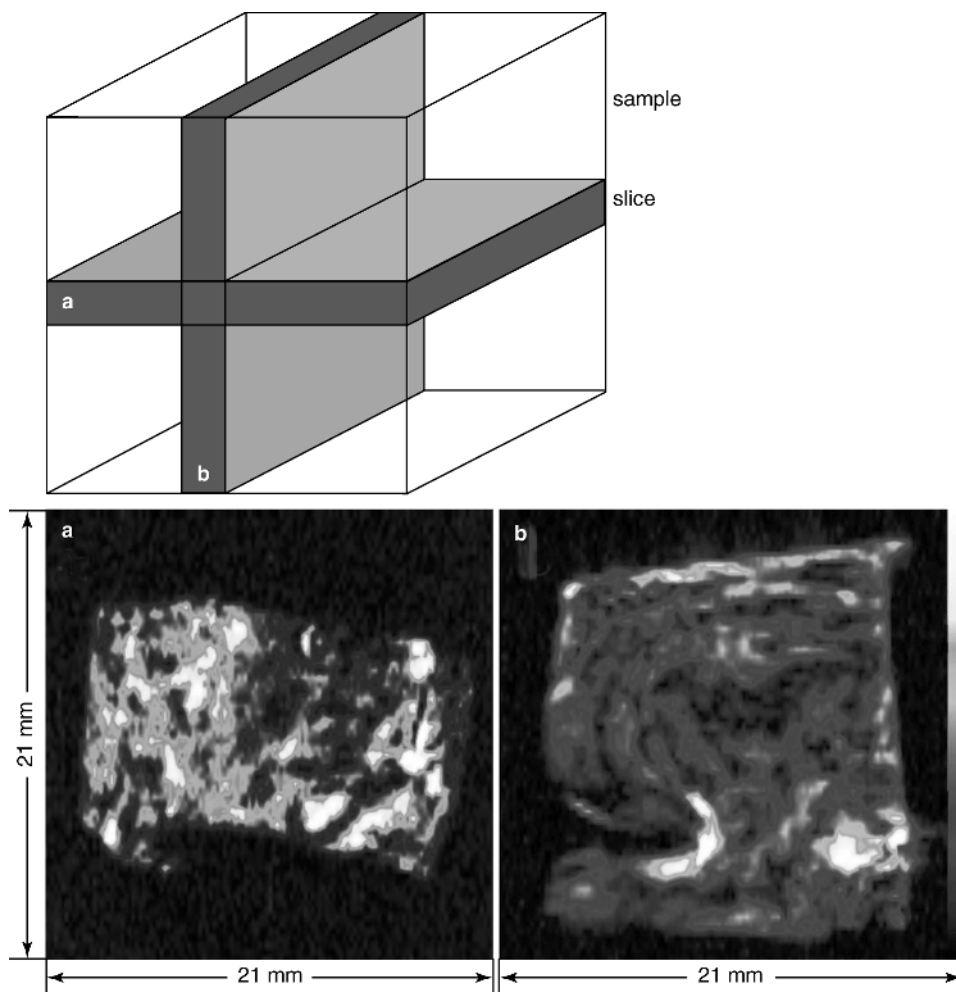


**Fig. 35.** (a) Proton  $T_2^*$ -weighted orthogonal slices of a carbon-black filled blend with a soft (bright) and a hard (dark) component. Insufficient blending in a rolling mill is visualized by the stream lines in slice (b). Reproduced from Ref. 145, with permission from Rapra Technology.

The time evolution of the thermooxidative aging in SBR has been studied by NMR imaging (see Ref. 145). In order to detect the aged surface layer with reduced signal intensity in Hahn-echo images, two aged sheets were stacked and the stack was imaged along its axis. In this way, the signal from the soft core delineated the hardened surface layers (cf Fig. 36).

**Sample Deformation.** Sample deformations modify the number of accessible conformations of intercross-link chains, so that they can be detected by analysis of relaxation and residual dipolar and quadrupolar couplings. For instance, dynamic mechanical load on elastomers is often exerted at small deformations and low deformation rates but over extended time periods. Then part of the mechanical energy is dissipated into heat depending on the value of the loss modulus. As a consequence, a temperature profile is established within the sample.



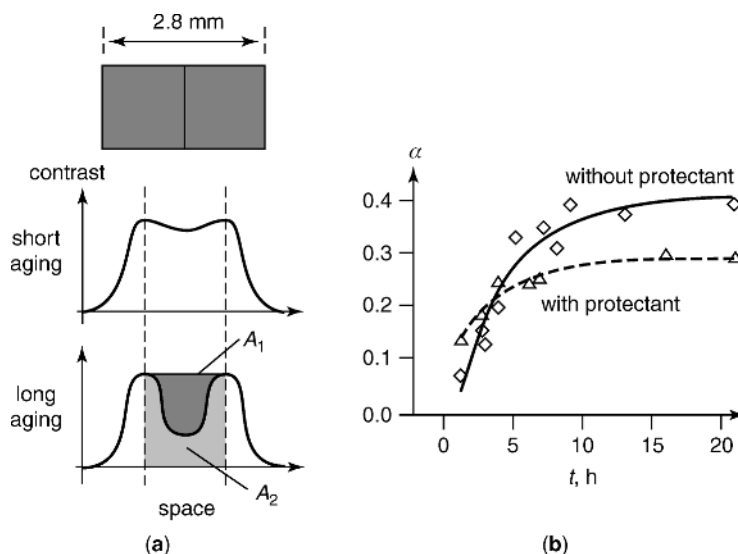


**Fig. 36.** Analysis of thermal oxidative aging by  $T_2^*$ -weighted Hahn-echo imaging. **(a)** Two SBR layers stacked after aging. The aged layer suffers a signal loss marked by the area  $A_1$ . The relative signal decrease defines the aging parameter  $\alpha$ . **(b)** The progress in aging can be followed by evaluating the aging parameter  $\alpha$  as a function of aging time  $t$ . Reproduced from Ref. 145, with permission from Rapra Technology.

Then the modulus varies across the sample depending on the temperature profile and properties determined for thick samples under dynamic load are average quantities.

The temperature profile associated with sample heating during weak dynamic shear deformation of carbon-black filled SBR cylinders of 10 mm diameter and 10 mm in height has been imaged by NMR by use of a specially designed probe (180).

The transverse relaxation time strongly depends on temperature (cf Fig. 37a), so that the temperature can be mapped by parameter imaging of  $T_2$ . Axial parameter projections have been acquired in dynamic equilibrium at a shear rate of 10 Hz and for carbon-black contents ranging from 10 to 70 phr. One-dimensional cross sections through those projections are depicted in Figure 37b. An increase of the temperature in the center of the sample is observed with increasing carbon-black contents which scales with the increasing loss modulus of the sample. The 70 phr sample is warmer by over 10°C in the center of the sample than the 10 phr sample.

**NMR Mobile Sensor for Quality Control of Elastomers.** Over the last few years, a mobile NMR surface scanner called NMR-MOUSE has been developed for the nondestructive investigation of arbitrarily large objects (187,188). The NMR-MOUSE is a palm-size NMR device which is built up from two permanent magnets. The magnets are mounted on an iron yoke with antiparallel polarization to form the classical horseshoe geometry. The main direction of the polarization magnetic field  $B_0$  is across the gap and the field strength decreases rapidly with increasing distance from the surface. The radio-frequency (rf) field  $B_1$  is generated by a surface coil which is mounted in the gap. The NMR-MOUSE

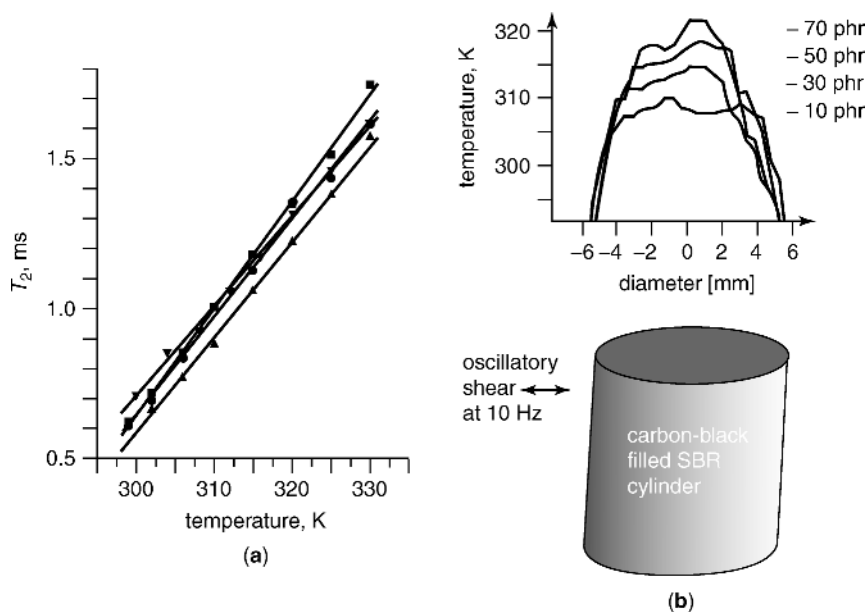


**Fig. 37.** Temperature profiles from  $T_2$  parameter images of SBR cylinders with different carbon-black filler contents undergoing oscillatory shear deformations. (a) Temperature calibration curves and (b) temperature profiles across the cylinders. (■) 10 phr (●) 30 phr, (▲) 50 phr, and (▼) 70 phr. The pixel resolution was  $0.4 \times 0.4 \text{ mm}^2$ . Reproduced from Ref. 180, with permission from Rapra Technology.

is characterized by strong inhomogeneities in the static and radio-frequency magnetic fields. Due to these fields inhomogeneities, NMR spectroscopy of the chemical shift is not possible, but magnetization relaxation times and parameters of translational motion can be measured by echo techniques (189–192). Moreover, the orientation dependence of NMR parameters can be easily investigated with the mobile NMR sensor for large samples on stretching devices (191).

Some selected applications of the NMR-MOUSE to elastomers are summarized in Figure 38 (193). In Figure 38a, transverse relaxation times have been measured for a series of carbon-filled NR samples with different curing times. Normalized values measured at high and homogeneous magnetic field (7 T, DMX 300) are compared to those measured with the NMR-MOUSE (0.5 T). Although the values differ because of different  $B_0$  field strengths, they closely follow the same trend. This confirms that relaxation measurements by the NMR-MOUSE are a valid alternative to relaxation measurements at homogeneous magnetic fields.

In Figure 38b, relaxation times are shown for a series unfilled SBR samples with variations in sulfur content. With increasing sulfur content the chemical cross-link density increases. Relaxation times are given for measurements with Hahn echoes and with solid echoes. The change in relaxation times and thus the sensitivity of the method is larger for the Hahn-echo measurements at small cross-link density and for the solid echo measurements at high cross-link density. Solid echoes reduce the signal attenuation from the dipole–dipole interaction

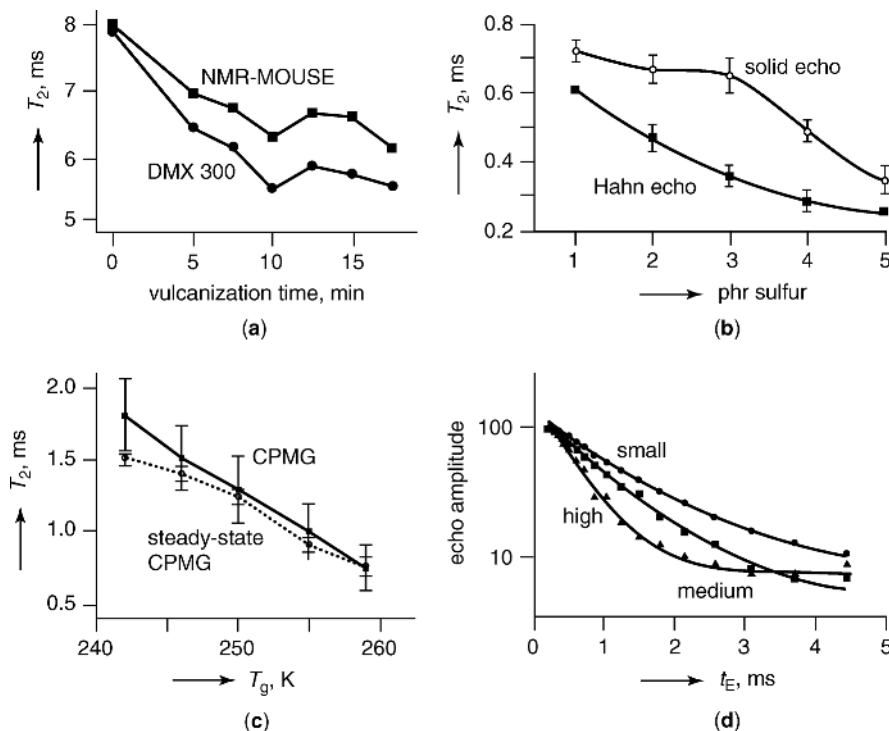


**Fig. 38.** Applications of the NMR-MOUSE to elastomer materials. **(a)** Values of  $^1\text{H}$   $T_2$  for a curing series of carbon-black filled NR. The measurements made with NMR-MOUSE are compared with the values obtained at 300 MHz in high homogeneous field. **(b)**  $T_2$  of a cross-link series of unfilled SBR with different sulfur contents. **(c)**  $T_2$  versus glass-transition temperature  $T_g$  of unfilled SBR by the CPMG and steady-state CPMG methods. **(d)** Normalized Hahn-echo decays for polybutadiene latex samples for small, medium, and large cross-link densities. Reproduced from Refs. 189 and 190, with permission from Rapra Technology.

between two spins in addition to producing a Hahn echo. At high cross-link density multicenter dipolar couplings become effective and the solid echo becomes less effective in reducing signal attenuation from dipolar interactions. The Hahn echo does not affect the dipole-dipole interaction at all. This explains the difference in contrast obtained with both methods.

A reduction in measurement time is gained when the measurements are performed in dynamic equilibrium between radio-frequency excitation and longitudinal relaxation (1). NMR methods which operate in this regime are referred to as steady-state methods. They deliver equivalent information compared to methods which demand complete relaxation to thermodynamic equilibrium between scans.  $T_2$  measurements performed with the CPMG and the steady-state CPMG method are depicted in Figure 38c and correlated with the glass-transition temperature  $T_g$  of unfilled SBR laboratory samples of different cross-link densities. The NMR measurements were done at room temperature, whereas  $T_g$  had been determined by temperature-dependent measurements of the dynamic-mechanical loss modulus (189,190). The correlation between both measurements

is not surprising, because both probe the network dynamics. These data demonstrate that in certain cases  $T_g$  can be determined locally and nondestructively on large samples at room temperature by the NMR-MOUSE.

The large magnetic-field gradients give rise to rapid signal loss from molecules with translational motion, so that signal from low molecular-weight fluids is suppressed at echo times  $t_E$  of the order of 1 ms and more. The signal detected at larger echo times is from larger molecules or particles. This effect of solvent suppression is exploited in the characterization of cross-link density in polybutadiene latex samples (see Fig. 38d). The signal decay for weak cross-link density is slow compared to that for large cross-link density. In summary, Figure 38 demonstrates that the NMR-MOUSE is a suitable device for determination of relative cross-link density in a number of different soft materials.

The possibility to excite and detect proton NMR double-quantum coherences in inhomogeneous static and radio-frequency magnetic fields was also investigated (194,195). For this purpose, specialized pulse sequences which partially refocus the strongly inhomogeneous evolution of the spin system and generate double-quantum buildup and decay curves were implemented on the NMR-MOUSE. It was shown that DQ decay curves have a better signal-to-noise ratio in the initial time regime compared to DQ buildup curves. The double-quantum buildup and decay curves were recorded for a series of cross-linked natural rubber samples. These curves give access to quantitative values of the ratio of proton total residual dipolar couplings that are in good agreement with those measured in homogeneous fields. A linear dependence of these ratios on the sulfur-accelerator content was reported.

The self-diffusion coefficient ( $D$ ) of swollen liquids in elastomers can be measured using NMR-MOUSE with a bar magnet (192). The method was shown to be particularly useful for measuring  $D$  of small penetrant molecules in elastomers without the need for measurements of the transverse relaxation rates. The self-diffusion coefficient of toluene in a series of cross-linked natural rubber samples was measured and correlated with the cross-link density.

The NMR-MOUSE is simple mobile NMR sensor suitable for operation in an industrial environment. Its use for quality control is demonstrated in Figure 39 by the  $T_2$  statistics measured at both sides of a conveyor belt with steel cords (193). The magnetic field  $B_0$  distortions from the steel cords were minimized by suitable orientation of the NMR-MOUSE with respect to the direction of the cords. The upper side of the belt exhibits a higher average  $T_2$  value than the lower side, which indicates lower cross-link density. In addition to that the variance of the measured values is larger for the lower side indicating a better quality material on the upper side.

Images can be obtained with the NMR-MOUSE by measuring voxels individually by lateral displacement of the device or a change of excitation frequency to shift the sensitive volume in depth (193). On the other hand, also pulsed magnetic field gradients can be employed for phase encoding of the space information. Frequency encoding is hampered by the nonlinear magnetic field profile together with the inaccessibility of the FID.

In direction parallel to the magnetic gap, the magnetic field gradient is weakest, and a sensitive volume of a centimeter and more in width can be excited by a short rf pulse. Solenoidal gradient coils can readily be incorporated into the gap and pulsed to produce antiparallel magnetic fields (196,197). Then a

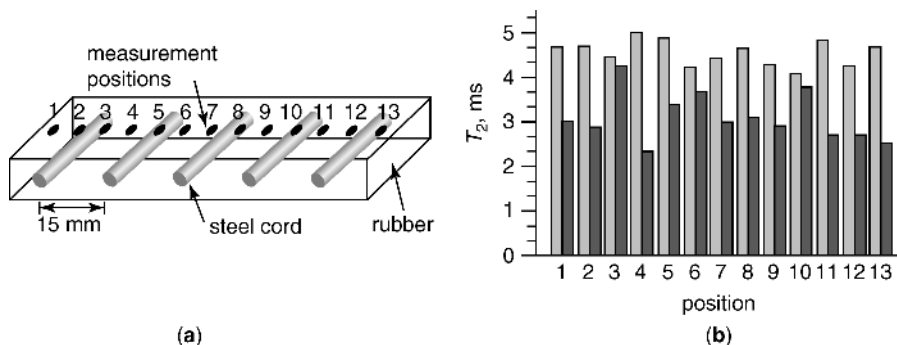


**Fig. 39.** Quality control of a conveyor-belt section with steel cords. (a) Position of measurement points. (b)  $T_2$  values for upper and lower sides determined with the CPMG pulse sequence (■) upper side and (■) lower side. Reproduced from Ref. 193, with permission from Rapra Technology.

gradient field is established along the gap and spatial resolution can be introduced into the measurement by phase-encoding techniques similar to single-point imaging. The effects of the background field inhomogeneity  $B_z - B_0$  and of chemical shift on the magnetization phase are balanced in the peak of the Hahn echo and the only phase evolution from the pulsed field gradient remains. By applying gradient pulses with different amplitudes,  $k$  space can be scanned in the direction along the gap, so that the Fourier transformation of the acquired signal produces a one-dimensional image (196). This measurement protocol has been applied in a study of a rubber sheet with parallel textile fibers. The fibers do not contribute to the detected signal, so that their positions can be located by the dips in the 1D profile.

Clearly, the basic imaging scheme can be extended to include relaxation-time contrast for discrimination of variations in cross-link density and strain, and the 1D MRI-MOUSE (magnetic resonance imaging MOUSE) can be extended with further gradient coils to permit imaging in three dimensions. Recently, a two-dimensional imaging with a single-sided NMR probe was reported (197). Numerous applications of the MRI-MOUSE can be envisioned in soft-matter analysis, in particular in those areas, where imaging with conventional equipment has proven to be successful and where smaller, less expensive, and mobile devices are in need.

## BIBLIOGRAPHY

"Nuclear Magnetic Resonance" in *EPST* 1st ed., Vol. 9, pp. 356–396, by F. A. Bovey, Bell Telephone Laboratories; in *EPSE* 2nd ed., Vol. 10, pp. 254–327, by F. A. Bovey and L. W. Jelinski, AT&T Bell Laboratories; in *EPST* 3rd ed., Vol. 10, pp. 637–717, by D. E. Demco and B. Blümich, Institut für Technische Chemie und Makromolekulare Chemie, Rheinisch-Westfälische Technische Hochschule.

## CITED PUBLICATIONS

1. R. R. Ernst, G. Bodenhausen, and A. Wokaun, *Principles of Nuclear Magnetic Resonance in One and Two Dimensions*, Clarendon Press, Oxford, 1987.

2. K. Schmidt-Rohr and H. W. Spiess, *Multidimensional Solid State NMR and Polymers*, Academic Press, New York, 1994.
3. V. J. McBrierty and K. J. Parker, *Nuclear Magnetic Resonance in Solid Polymers*, Cambridge University Press, Cambridge, 1993.
4. M. Mehring, *Principles of High Resolution NMR Spectroscopy in Solids*, 2nd ed., Springer, Berlin, 1983.
5. R. Kimmich, *NMR: Tomography, Diffusiometry, Relaxometry*, Springer, Berlin, 1997.
6. F. A. Bovey and P. A. Mireau, *NMR of Polymers*, Academic Press, San Diego, 1996.
7. F. Horii, in I. Ando and T. Asakura, eds., *Solid State NMR in Polymers*, Elsevier, Amsterdam, 1998.
8. H. W. Beckham and H. W. Spiess, *NMR Basic Princ. Prog.* **32**, 163 (1994).
9. H. W. Spiess, *Annu. Rep. NMR Spectrosc.* **34**, 1 (1997).
10. P. A. Mirau, S. A. Heffner, G. Kogler, and F. Bovey, *Polym. Int.* **26**, 29 (1991).
11. B. F. Chmelka, K. Schmidt-Rohr, and H. W. Spiess, in R. Tycko, ed., *Nuclear Magnetic Resonance Probes of Molecular Dynamics*, Kluwer Academic Publishers, the Netherlands, 1994, p. 113.
12. J.-P. Cohen Addad, *Prog. NMR Spectros.* **25**, 1 (1994).
13. V. D. Fedotov and H. Schneider, Structure and dynamics of bulk polymers by NMR method, *NMR, Basic Principles and Progress* Vol. 21, Springer, Berlin, 1989.
14. F. A. Bovey, *High Resolution NMR of Macromolecules*, Academic Press, New York, 1972.
15. J. N. S. Evans, *Biomolecular NMR Spectroscopy*, Oxford University Press, New York, 1995.
16. D. E. Demco, S. Hafner, and H. W. Spiess, Multidimensional NMR techniques for characterization of viscoelastic materials, in V. M. Litvinov and P. P. De, eds., *Handbook of Spectroscopy of Rubbery Materials*, Rapra Technology Ltd., Shawbury, 2002.
17. P. Mansfield and P. G. Morris, NMR imaging in biomedicine, *Advanced Magnetic Resonance*, Suppl. 2, Academic Press, New York, 1982.
18. P. T. Callaghan, *Principles of Nuclear Magnetic Resonance Microscopy*, Clarendon Press, Oxford, 1991.
19. B. Blümich, *NMR Imaging of Materials*, Clarendon Press, Oxford, 2000.
20. E. M. Haacke, R. W. Brown, M. R. Thompson, and R. Venkatesan, *Magnetic Resonance Imaging, Physical Principles and Sequence Design*, Wiley-Liss, New York, 1999.
21. M. T. Vlaardingerbroek and J. A. den Boer, *Magnetic Resonance Imaging*, 2nd ed., Springer, Berlin, 1999.
22. B. Blümich and D. E. Demco, NMR Imaging of Elastomers, in V. M. Litvinov, and P. P. De, eds., *Handbook of Spectroscopy of Rubbery Materials*, Rapra Technology Ltd., Shawbury, 2002.
23. J.-J. Delpuech, ed., *Dynamics of Solutions and Fluid Mixtures by NMR*, John Wiley & Sons, Ltd., Chichester, 1995.
24. R. Tycko, ed., *Nuclear Magnetic Resonance of Molecular Dynamics*, Kluwer Academic Publishers, Dordrecht, 1994.
25. D. Canet, *Nuclear Magnetic Resonance. Concepts and Methods*, John Wiley & Sons, Ltd., Chichester, 1996.
26. M. Munowitz and A. Pines, *Adv. Chem. Phys.* **66**, 1 (1987).
27. M. H. Levitt, *Spin Dynamics*, John Wiley & Sons, Ltd., Chichester, 2001, and references therein.
28. I. Schnell and H. W. Spiess, *J. Magn. Reson. Adv. Magn. Reson.* **151**, 153 (2001).
29. S. B. Brown and H. W. Spiess, *Chem. Rev.* **101**, 4125 (2001).
30. E. Hahn, *Phys. Rev.* **80**, 580 (1950).

31. J. G. Powles and P. Mansfield, *Phys. Lett.* **2**, 58 (1962).
32. H. Schneider and H. Schmiedel, *Phys. Lett.* **30A**, 298 (1969).
33. W.-K. Rhim, A. Pines, and J. S. Waugh, *Phys. Rev. B* **3**, 684 (1971).
34. D. E. Demco, *Phys. Lett.* **45A**, 113 (1973).
35. J. Jeener, Ampere International Summer School, Basko Polje, Yugoslavia, 1971.
36. R. R. Ernst, *Chemia* **29**, 179 (1975).
37. L. Müller, A. Kumar, and R. R. Ernst, *J. Chem. Phys.* **63**, 5490 (1975).
38. W. P. Aue, E. Bertholdi, and R. R. Ernst, *J. Chem. Phys.* **64**, 2229 (1976).
39. S. R. Hartmann and E. L. Hahn, *Phys. Rev.* **128**, 2042 (1962).
40. A. Pines, M. G. Gibby, and J. S. Waugh, *J. Chem. Phys.* **59**, 569 (1973).
41. M. Munowitz and A. Pines, *Adv. Chem. Phys.* **66**, 1 (1987).
42. R. Freeman, *Spin Choreography. Basic Steps in High Resolution NMR*, Spektrum, Oxford, 1997, and references therein.
43. E. R. Andrew, A. Bradbury, and R. G. Eades, *Nature* **182**, 1659 (1958).
44. I. J. Lowe, *Phys. Rev. Lett.* **2**, 285 (1959).
45. J. S. Waugh, L. M. Huber, and U. Haeberlen, *Phys. Rev. Lett.* **20**, 180 (1968).
46. P. Mansfield, M. J. Orchard, D. C. Stalker, and K. H. B. Richards, *Phys. Rev. B* **7**, 90 (1973).
47. P. Mansfield and P. G. Morris, NMR imaging in biomedicine, *Advanced Magnetic Resonance*, Suppl. 2, Academic Press, New York, 1982.
48. A. K. Whittaker, *Annu. Rep. NMR Spectrosc* **34**, 106 (1997).
49. A. Schmidt, W. S. Veeman, V. M. Litvinov, and W. Gabrielse, *Macromolecules* **31**, 1652 (1998).
50. B. Deloche and P. Sotta, in V. M. Litvinov and P. P. De, eds., *Handbook of Spectroscopy of Rubbery Materials*, Rapra Technology Ltd., Shawbury, 2002.
51. P. G. Klein and M. E. Ries, *Prog. NMR Spectrosc.* **42**, 31 (2003).
52. P. T. Callaghan and E. T. Samulski, *Macromolecules* **30**, 113 (1997).
53. R. Ball, P. T. Callaghan, and E. T. Samulski, *J. Chem. Phys.* **106**, 7352 (1997).
54. B. Deloch, A. Dubault, and D. Durand, *J. Polym. Sci., Part B: Polym. Phys.* **30**, 1419 (1992).
55. V. M. Litvinov and H. W. Spiess, *Makromol. Chem.* **193**, 1181 (1992).
56. P. Sotta and B. Deloch, *J. Chem. Phys.* **100**, 4591 (1994).
57. P. Sotta, *Macromolecules* **31**, 3872 (1998).
58. M. G. Brereton and E. R. Ries, *Macromolecules* **29**, 2644 (1996).
59. M. G. Brereton, *Macromolecules* **24**, 6160 (1991).
60. M. E. Ries, M. G. Brereton, P. K. Klein, I. M. Ward, P. Ekanayake, H. Menge, and H. Schneider, *Macromolecules* **32**, 4961 (1999).
61. A. Dardin, R. R. Stadler, C. Boeffel, and H. W. Spiess, *Makromol. Chem.* **194**, 3467 (1993).
62. A. Dardin, H. W. Spiess, R. R. Stadler, and E. T. Samulski, *Polym. Gel Networks* **5**, 37 (1997).
63. J. Collignon, H. Sillescu, and H. W. Spiess, *Colloid Polym. Sci.* **259**, 220 (1981).
64. R. Fechete, D. E. Demco, and B. Blümich, *J. Chem. Phys.* **118**, 2411 (2003).
65. D. E. Demco, S. Hafner, C. Fülber, R. Graf, and H. W. Spiess, *J. Chem. Phys.* **105**, 11285 (1996).
66. C. Fülber, D. E. Demco, O. Weintraub, and B. Blümich, *Macromol. Chem. Phys.* **197**, 581 (1996).
67. P. Sotta, C. Fülber, D. E. Demco, B. Blümich, and H. W. Spiess, *Macromolecules* **29**, 6222 (1996).
68. M. Schneider, L. Gasper, D. E. Demco, and B. Blümich, *J. Chem. Phys.* **111**, 402 (1999).
69. A. Wiesmath, C. Filip, D. E. Demco, and B. Blümich, *J. Magn. Reson.* **149**, 258 (2001).

70. D. E. Demco, R. Fechete, and B. Blümich, *Chem. Phys. Lett.* **375**, 406 (2003).
71. A. Pines, W.-K. Rhim, and J. S. Waugh, *J. Magn. Reson.* **6**, 457 (1972).
72. S. Matsui, *Chem. Phys. Lett.* **179**, 187 (1991).
73. R. Graf, D. E. Demco, S. Hafner, and H. W. Spiess, *Solid State Nucl. Magn. Reson.* **12**, 139 (1998).
74. R. Graf, D. E. Demco, S. Hafner, and H. W. Spiess, *J. Chem. Phys.* **106**, 885 (1997).
75. J. Gottwald, D. E. Demco, R. Graf, and H. W. Spiess, *Chem. Phys. Lett.* **243**, 314 (1995).
76. M. Wang, M. Bertmer, D. E. Demco, B. Blümich, V. M. Litvinov, and H. Barthel, *Macromolecules* **36**, 4411 (2003).
77. V. M. Litvinov, H. Barthel, and J. Weis, *Macromolecules* **35**, 4356 (2002).
78. L. R. G. Treloar, *The Physics of Rubber Elasticity*, Clarendon Press, Oxford, 1975.
79. B. Erman and J. Mark, *Structures and Properties of Rubberlike Networks*, Oxford University Press, Oxford, 1997.
80. R. Fechete, D. E. Demco, and B. Blümich, *Macromolecules* **35**, 6083 (2003).
81. J.-P. Cohen Addad, in V. M. Litvinov and P. P. De, eds., *Handbook of Spectroscopy of Rubbery Materials*, Rapra Technology Ltd., Shawbury, 2002, p. 291.
82. J.-P. Cohen Addad, B. Phan Thanh, and H. Montes, *Macromolecules* **30**, 4374 (1997).
83. V. M. Litvinov, in V. M. Litvinov and P. P. De, eds., *Handbook of Spectroscopy of Rubbery Materials*, Rapra Technology Ltd., Shawbury, 2002, p. 353.
84. V. M. Litvinov and A. A. Dias, *Macromolecules* **34**, 4051 (2001).
85. V. M. Litvinov and P. A. M. Steeman, *Macromolecules* **32**, 8476 (1999).
86. V. M. Litvinov, *Int. Polym. Sci. Technol.* **15**, T/28 (1988).
87. M. G. Brereton, *Macromolecules* **23**, 1119 (1990).
88. M. G. Brereton, *Macromolecules* **24**, 2068 (1991).
89. J. P. Cohen-Addad and O. Girard, *Macromolecules* **25**, 593 (1992).
90. T. P. Kulagina, V. M. Litvinov, and K. T. Summanen, *J. Polym. Sci., Part B: Polym. Phys.* **31**, 241 (1993).
91. H. W. Weber and R. Kimmich, *Macromolecules* **26**, 2597 (1993).
92. R. Kimmich, M. Köpf, and P. T. Callaghan, *J. Polym. Sci., Part B: Polym. Phys.* **29**, 1025 (1991).
93. G. I. Sandakov, V. P. Tarasov, N. N. Volkova, Y. A. Ol'khov, L. P. Smirnov, L. N. Erofeev, and A. K. Khitrin, *Vysokomol. Soedin., Ser. B* **31**, 821 (1989).
94. N. N. Volkova, G. I. Sandakov, A. I. Sosikov, Y. A. Ol'khov, L. P. Smirnov, and K. T. Summanen, *Polym. Sci. U.S.S.R.* **34**, 127 (1992).
95. R. Kimmich, E. Fischer, P. Callaghan, and N. Fatkullin, *J. Magn. Reson. A* **117**, 53 (1995).
96. E. Fischer, F. Grinberg, R. Kimmich, and S. Hafner, *J. Chem. Phys.* **109**, 846 (1998).
97. F. Grinberg, M. Garbarczyk, and W. Kuhn, *J. Chem. Phys.* **111**, 11222 (1999).
98. D. E. Demco, S. Hafner, and R. Kimmich, *J. Magn. Reson.* **96**, 307 (1992).
99. A. Y. Grosberg and A. R. Khokhlov, *Statistical Physics of Macromolecules*, American Institute of Physics, Woodbury, NY, 1994.
100. L. Gasper, D. E. Demco, and B. Blümich, *Solid State Nucl. Magn. Reson.* **14**, 105 (1999).
101. A. P. M. Kentgens, W. S. Veeman, and J. van Bree, *Macromolecules* **20**, 1234 (1987).
102. A. S. Kulik, D. Radloff, and H. W. Spiess, *Macromolecules* **27**, 433 (1994).
103. A. W. Overhauser, *Phys. Rev.* **92**, 411 (1953).
104. J. Denault and J. Prud'homme, *Macromolecules* **22**, 1307 (1989).
105. J. L. White and P. Mirau, *Macromolecules* **26**, 3049 (1993).
106. J. L. White, *Solid State NMR* **10**, 79 (1997).
107. P. Mirau, P. H. Tanaka, and F. Bovey, *Macromolecules* **21**, 2929 (1988).
108. S. A. Heffner and P. Mirau, *Macromolecules* **27**, 7283 (1994).



109. T. Fritzmanns, S. Hafner, D. E. Demco, H. W. Spiess, and F. H. Laukien, *J. Magn. Reson.* **134**, 355 (1998).
110. T. Fritzmanns, D. E. Demco, S. Hafner, and H. W. Spiess, *Mol. Phys.* **97**, 931 (1999).
111. E. Fischer, R. Kimmich, U. Beginn, M. Möller, and N. Fatkulin, *Phys. Rev. E* **59**, 4079 (1999).
112. G. Lipardi and A. Szabo, *J. Am. Chem. Soc.* **104**, 4546 (1982).
113. G. Lipardi and A. Szabo, *J. Am. Chem. Soc.* **104**, 4559 (1982).
114. G. Simon, K. Baumann, and W. Gronski, *Macromolecules* **25**, 3624 (1992).
115. H. Geen, J. J. Titman, J. Gottwald, and H. W. Spiess, *Chem. Phys. Lett.* **227**, 79 (1994).
116. M. Feike, D. E. Demco, R. Graf, J. Gottwald, S. Hafner, and H. W. Spiess, *J. Magn. Reson.* **122**, 241 (1996).
117. C. Filip, X. Filip, M. Bertmer, D. E. Demco, and B. Blümich, *J. Magn. Reson.* **150**, 184 (2001).
118. X. Feng, P. J. E. Verdegem, Y. K. Lee, D. Sandström, M. Edén, P. Bovee-Geurts, W. J. de Grip, J. Lugtenburg, H. J. M. de Groot, and M. H. Levitt, *J. Am. Chem. Soc.* **119**, 6853 (1997).
119. R. Graf, A. Heuer, and H. W. Spiess, *Phys. Rev. Lett.* **80**, 5738 (1998).
120. W. Sommer, J. Gottwald, D. E. Demco, and H. W. Spiess, *J. Magn. Reson. A* **112**, 131 (1995).
121. M. Hong, J. D. Gross, and R. G. Griffin, *J. Phys. Chem. B* **101**, 5869 (1997).
122. K. Saalwächter, R. Graf, D. E. Demco, and H. W. Spiess, *J. Magn. Reson.* **139**, 287 (1999).
123. V. M. Litvinov, M. Bertmer, L. Gasper, D. E. Demco, and B. Blümich, *Macromolecules* **36**, 7598 (2003).
124. W. Gabrielse, M. Suliman, and K. Dijkstra, *Macromolecules* **34**, 1685 (2001).
125. C. Malveau, P. Tekely, and D. Canet, *Solid State NMR* **7**, 271 (1997).
126. P. Tekely, D. Nicole, J. Brondeau, and J. J. Delpuech, *J. Phys. Chem.* **90**, 5608 (1986).
127. N. Zumbulyadis, *Phys. Rev. B* **33**, 6495 (1986).
128. K. Schmidt-Rohr, J. Clauss, and H. W. Spiess, *Macromolecules* **25**, 3273 (1992).
129. P. Sotta, C. Fülber, D. E. Demco, B. Blümich, and H. W. Spiess, *Macromolecules* **29**, 6222 (1996).
130. C. Fülber, D. E. Demco, O. Weintraub, and B. Blümich, *Macromol. Chem. Phys.* **197**, 581 (1996).
131. A. D. Meltzer, H. W. Spiess, C. D. Eisenbach, and H. Hayen, *Makromol. Chem. Rapid Commun.* **12**, 261 (1991).
132. J. A. Kornfield, H. W. Spiess, H. Nefzger, H. Hayen, and C. D. Eisenbach, *Macromolecules* **24**, 4787 (1991).
133. A. Dardin, C. Boeffel, H. W. Spiess, R. Stadler, and E. T. Samulski, *Acta Polym.* **46**, 291 (1995).
134. P. Blümli and B. Blümich, *Rubber Chem. Technol.* **70**, 469 (1997).
135. B. Blümich and D. E. Demco, in V. M. Litvinov and P. P. De, eds., *Spectroscopy of Rubbery Materials*, Rapra Technology Ltd., Shrewsbury, 2001.
136. D. E. Demco and B. Blümich, *Conc. Magn. Reson.* **10**, 19 (1997).
137. D. E. Demco and B. Blümich, *Conc. Magn. Reson.* **10**, 269 (1997).
138. D. G. Cory, *Annu. Rep. NMR Spectrosc.* **24**, 88 (1992).
139. P. Blümli and B. Blümich, *NMR Basic Princ. Prog.* **30**, 211 (1994).
140. J. H. Strange, *Phil. Trans. Soc. Lond. A* **333**, 427 (1990).
141. P. J. McDonald, *Prog. NMR Spectrosc.* **30**, 69 (1997).
142. B. Blümich, *Conc. Magn. Reson.* **10**, 19 (1998).
143. B. Blümich, *Conc. Magn. Reson.* **11**, 71 (1998).
144. A. Abragam, *Principles of Nuclear Magnetism*, Oxford Academic Press, London, 1961.
145. D. Raftery and B. F. Chmelka, *NMR Basis Princ. Prog.* **30**, 111 (1994).

146. D. E. Demco and B. Blümich, *Curr. Opp. Solid State Mater. Sci.* **5**, 195 (2001), and references therein.
147. C. Fülber, B. Blümich, K. Unseld, and V. Herrmann, *Kautsch. Gummi Kunstst.* **48**, 254 (1995).
148. P. Blümmler and B. Blümich, *Macromolecules* **24**, 2183 (1991).
149. C. Fülber, K. Unseld, V. Herrmann, K. H. Jakob, and B. Blümich, *Colloid Polym. Sci.* **274**, 191 (1996).
150. R. L. Armstrong, A. Tzalmona, M. Menzinger, A. Cross, and C. Lemaire, in B. Blümich and W. Kuhn, eds., *Magnetic Resonance Microscopy*, VCH, Weinheim, 1992, p. 309.
151. P. Mansfield, R. Bowtell, and S. Blackband, *J. Magn. Reson.* **99**, 507 (1992).
152. M. A. Rana and J. L. Koenig, *Macromolecules* **27**, 3727 (1994).
153. G. Simon and H. Schneider, *Macromol. Chem. Macromol. Symp.* **52**, 233 (1991).
154. A. A. Parker, J. J. Marcinko, P. Rinaldi, D. P. Hendrick, and W. Ritchey, *J. Appl. Polym.* **48**, 667 (1993).
155. P. Blümmler and B. Blümich, *Acta Polym.* **24**, 2183 (1991).
156. C. Schwarzbauer, J. Zange, H. Adolf, R. Deichmann, U. Nöth, and A. Haase, *J. Magn. Reson. B* **100**, 178 (1995).
157. P. Sotta, B. Deloche, J. Herz, A. Lapp, D. Durand, and J.-C. Rabadeux, *Macromolecules* **20**, 2769 (1987).
158. M. Klinkenberg, P. Blümmler, and B. Blümich, *Macromolecules* **30**, 1038 (1997).
159. M. Klinkenberg, P. Blümmler, and B. Blümich, *J. Magn. Reson. A* **119**, 197 (1996).
160. M. Schneider, D. E. Demco, and B. Blümich, *Macromolecules* **34**, 4019 (2001).
161. M. Schneider, D. E. Demco, and B. Blümich, *J. Magn. Reson.* **140**, 432 (1999).
162. Y. Xia, *Conc. Magn. Reson.* **8**, 205 (1996).
163. P. Blümmler and B. Blümich, *Magn. Reson. Imag.* **10**, 779 (1992).
164. B. Blümich and P. Blümmler, *Makromol. Chem.* **194**, 2133 (1993).
165. L. Gasper, D. E. Demco, and B. Blümich, *Solid State Nucl. Magn. Reson.* **14**, 105 (1999).
166. F. Grindberg, M. Heidenreich, and W. Kuhn, *J. Magn. Reson.* **159**, 87 (2002).
167. S. R. Smith and J. L. Koenig, *Macromolecules* **24**, 3498 (1991).
168. B. Klei and J. L. Koenig, *Acta Polym.* **48**, 199 (1997).
169. P. Palmas, R. Colson, L. Lemaire, and M. Sebbare, *Polymer* **44**, 4889 (2003).
170. P. Denner, B. Walker, and T. Willing, *Macromol. Symp.* **119**, 339 (1997).
171. P. Blümmler, B. Blümich, and H. Dümmler, *Kautsch. Gummi Kunstst.* **45**, 699 (1992).
172. M. Knörger, U. Heuert, H. Schneider, P. Barth, and W. Kuhn, *Polym. Bull.* **38**, 101 (1997).
173. M. Knörger, U. Heuert, H. Menge, and H. Schneider, *Angew. Makromol. Chem.* **261/262**, 123 (1998).
174. J. A. Chudek and G. Hunter, *J. Mater. Sci. Lett.* **11**, 222 (1992).
175. M. Sardashti, B. A. Baldwin, and D. J. O'Donnell, *J. Polym. Sci., B: Polym. Phys.* **33**, 571 (1995).
176. A. Spyros, R. Kimmich, B. H. Briese, and D. Jenddrossek, *Macromolecules* **30**, 8218 (1997).
177. F. P. Miknis, A. T. Pauli, L. C. Michon, and D. A. Netzel, *Fuel* **77**, 399 (1998).
178. F. P. Miknis and L. C. Michon, *Fuel* **77**, 393 (1998).
179. P. Blümmler and B. Blümich, *Acta Polym.* **44**, 125 (1993).
180. D. Hauck, P. Blümmler, and B. Blümich, *Macromol. Chem. Phys.* **198**, 2729 (1997).
181. P. Adriaenssens, A. Pollaris, M. Kelchtermans, and J. Gelan, *Macromolecules* **36**, 706 (2003).
182. P. Adriaenssens, A. Pollaris, D. Vanderzande, J. Gelan, J. L. White, A. J. Dias, and M. Kelchtermans, *Macromolecules* **32**, 4692 (1999).
183. P. J. Flory, *J. Chem. Phys.* **18**, 108 (1950).

184. P. Prado, L. Gasper, G. Fink, B. Blümich, V. Herrmann, K. Unseld, H-B. Fuchs, H. Möhler, and M. Rühl, *Macromol. Mater. Eng.* **274**, 13 (2000).
185. P. Prado, L. Gasper, G. Fink, and B. Blümich, *Appl. Magn. Reson.* **18**, 1 (2000).
186. P. Blümli, V. Litvinov, H. G. Dikland, and M. van Duin, *Kautsch. Gummi. Kunstst.* **51**, 865 (1998).
187. G. Eidmann, R. Salvesberg, P. Blümli, and B. Blümich, *J. Magn. Reson. A* **122**, 104 (1992).
188. F. Balibanu, K. Hailu, R. Eymael, D. E. Demco, and B. Blümich, *J. Magn. Reson.* **145**, 246 (2000).
189. G. Zimmer, A. Guthausen, and B. Blümich, *Solid State Nucl. Magn. Reson.* **12**, 183 (1998).
190. A. Guthausen, G. Zimmer, P. Blümli, and B. Blümich, *J. Magn. Reson.* **130**, 1 (1998).
191. K. Hailu, R. Fechet, D. E. Demco, and B. Blümich, *Solid State Nucl. Magn. Reson.* **22**, 327 (2002).
192. M. Klein, R. Fechet, D. E. Demco, and B. Blümich, *J. Magn. Reson.* **164**, 310 (2003).
193. B. Blümich and D. E. Demco, in V. M. Litvinov and P. P. De, eds., *Spectroscopy of Rubbery Materials*, Rapra Technology Ltd., Shrewsbury, 2001.
194. A. Wiesmath, C. Filip, D. E. Demco, and B. Blümich, *J. Magn. Reson.* **149**, 258 (2001).
195. A. Wiesmath, C. Filip, D. E. Demco, and B. Blümich, *J. Magn. Reson.* **154**, 60 (2002).
196. I. P. Prado and B. Blümich, *J. Magn. Reson.* **144**, 200 (2000).
197. F. Casanova and B. Blümich, *J. Magn. Reson.* **163**, 38 (2003).

D. E. DEMCO

B. BLÜMICH

Institut für Technische Chemie und Makromolekulare  
Chemie, Rheinisch-Westfälische Technische Hochschule

## N-VINYLAMIDE POLYMERS

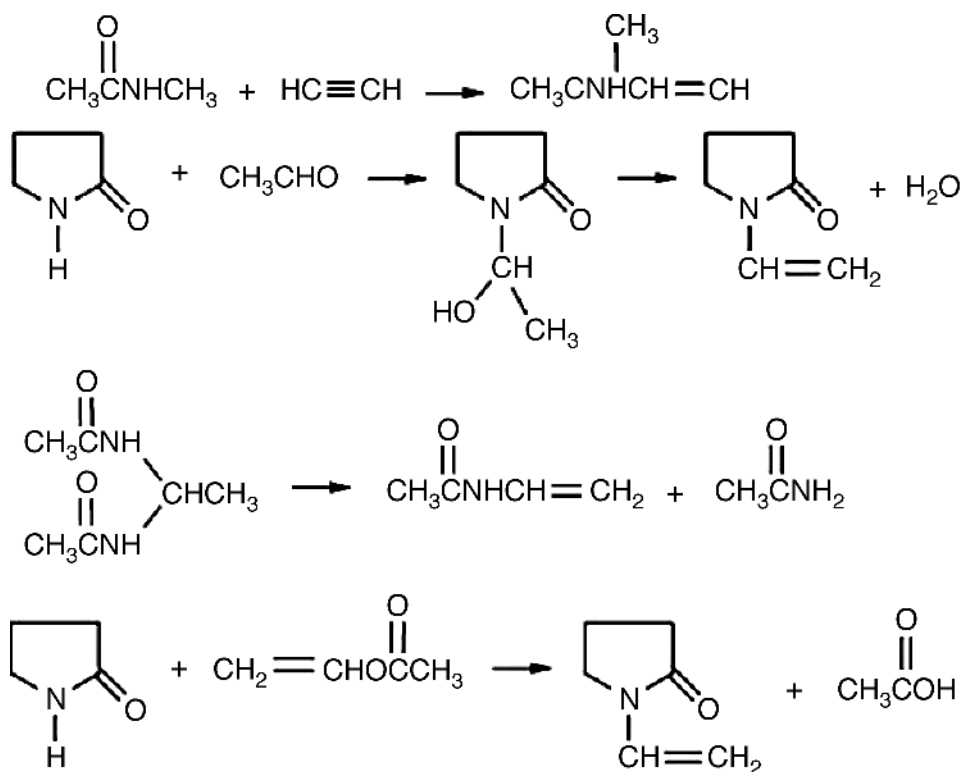
### Introduction

*N*-Vinylamide-based polymers, especially the *N*-vinyl lactams, such as poly(*N*-vinyl-2-pyrrolidinone) [9003-39-8] or simply polyvinylpyrrolidinone (PVP), continue to be of major importance to formulators of personal-care, pharmaceutical, agricultural, and industrial products because of desirable performance attributes and very low toxicity profiles. Because of hydrogen bonding of water to the amide group, many of the *N*-vinylamide homopolymers are water soluble or dispersible. Like proteins, they contain repeating (but pendant) amide (lactam) linkages and share several protein-like characteristics (1). Many studies have actually employed PVP as a substitute for proteins, eg, in simplifying the chemistry of the effects of radiation on polymers (2). Proteins are extremely complicated molecules with not only sequence distribution but tertiary bonding and structural complexity and it is an oversimplification to compare them to PVP, but the effects of radiation on PVP can be more readily studied. PVP can even be considered as a uniform synthetic protein-like analogue. By itself it does not enter into intermolecular hydrogen bonding, thus affording low viscosity concentrates, and

also, unlike the proteins, PVP is soluble in polar solvents like alcohol. But even given these differences, the chemistry of PVP, the most commercially successful polymer of the class, is in many respects similar to that of proteins because of amide linkages sharing with them complexation to large anions such as polyphenols, anionic dyes, and surfactants. In addition to the ability to complex, PVP and its analogues along with a large assortment of copolymers are excellent film formers. They exhibit the ability to interact with a variety of surfaces by hydrogen or electrostatic bonding, resulting in protective coatings and adhesive applications of commercial significance such as hair-spray fixatives, tablet binders, disintegrants, iodophors, antidye redeposition agents in detergents, protective colloids, dispersants, and solubilizers, among many others.

### Monomers

*N*-Vinylamides and *N*-vinylimides can be prepared by reaction of amides and imides with acetylene (3), by dehydration of hydroxyethyl derivatives (4), by pyrolysis of ethylidenebisamides (5), or by vinyl exchange (6), among other methods; the monomers are stable when properly stored.



Poly *N*-vinyl-2-pyrrolidinone (VP) [88-12-0] is of significant commercial importance and hence is the principal focus of this article. Vinylcaprolactam is available (BASF) and is growing in importance, and vinyl formamide is available as

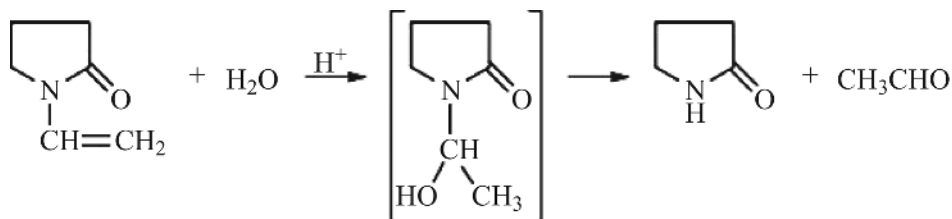
**Table 1. Physical Properties of Selected Vinylamides and Vinylimides**

Compound	CAS Registry Number	Bp, °C <sub>kPa</sub> <sup>a</sup>	Mp, °C
<i>N</i> -Vinylacetamide	[5202-78-8]	107–109	
<i>N,N</i> -Methylvinylacetamide	[3195-78-6]	70 <sub>3.3</sub>	
<i>N</i> -Vinylacetanilide	[4091-14-9]	102–105 <sub>0.13</sub>	52
<i>N</i> -Vinyl-2-piperidinone	[4370-23-4]	125–126 <sub>3.3</sub>	45
<i>N</i> -Vinylcaprolactam	[2235-00-9]	129–130 <sub>2.7</sub>	34.5
<i>N</i> -Vinylphthalimide	[3485-84-5]	128–130 <sub>3.3</sub>	86.5
<i>N</i> -Vinyl-2-oxazolidinone	[4271-26-5]	77–78 <sub>0.067</sub>	
<i>N</i> -Vinyl-5-methyl-2-oxazolidinone	[3395-98-0]	105–108 <sub>0.33</sub>	

<sup>a</sup>To convert kPa to mmHg, multiply by 7.5. Pressure = 101.3 kPa (760 mmHg) if not shown.

a developmental monomer (Air Products). Some physical properties are given in Table 1.

***N*-Vinyl-2-Pyrrolidinone.** Commonly called vinylpyrrolidinone or VP, *N*-vinyl-2-pyrrolidinone was developed in Germany at the beginning of World War II. It is a clear, colorless liquid that is miscible in all proportions with water and most organic solvents. It can polymerize slowly by itself but can be easily inhibited by small amounts of ammonia, sodium hydroxide (caustic pellets), or antioxidants such as *N,N'*-di-*sec*-butyl-*p*-phenylenediamine. It is stable in neutral or basic aqueous solution but readily hydrolyzed in the presence of acid to form 2-pyrrolidinone and acetaldehyde. Properties are given in Table 2.



Commercially available VP is usually over 99% pure but does contain several methyl-substituted homologues and 2-pyrrolidinone. Even at this high level of purity, further purification is required if reliable kinetic data concerning rates of polymerization are desired. This can be accomplished only by recrystallization, because distillation will not separate methyl-substituted isomers (7).

**Manufacture.** The principal manufacturers of *N*-vinyl-2-pyrrolidinone are ISP and BASF. Both consume most of their production captively as a monomer for the manufacture of PVP and copolymers. The vinylation of 2-pyrrolidinone is carried out under alkaline catalysis analogous to the vinylation of alcohols. 2-Pyrrolidinone is treated with ca 5% potassium hydroxide, then water and some pyrrolidinone are distilled at reduced pressure. A ca 1:1 mixture (by vol) of acetylene and nitrogen is heated at 150–160°C and ca 2 MPa (22 atm). Fresh 2-pyrrolidinone and catalyst are added continuously while product is withdrawn. Conversion is limited to ca 60% to avoid excessive formation of by-products. The *N*-vinyl-2-pyrrolidinone is distilled at 70–85°C at 670 Pa (5 mmHg) and the yield is 70–80% (8).

**Table 2. Properties of N-Vinyl-2-Pyrrolidinone (Commercial Production)**

Property	Value
Molecular wt.	111
Assay, %	98.5 <sup>a</sup>
Moisture content, %	0.2 <sup>b</sup>
Color (APHA)	100 <sup>b</sup>
Vapor pressure, Pa <sup>c</sup> at 17°C	
17°C	6.7
24°C	13.3
45°C	67
54°C	133
64°C	266
77°C	667
Boiling point at 400 mmHg	193
Freezing point	13.5
Flash point (open cup)	98.4
Fire point	100.5
Viscosity at 25°C, mPa·s (=cP)	2.07
Specific gravity (25/4°C)	1.04
Refractive index, $n_D^{25}$	1.511
Solubility	Completely miscible in water and most organic solvents, including methanol, ethyl acetate, methylene chloride, ethyl ether, and hydro-carbons in general
Ultraviolet spectrum	No significant absorption at wavelengths longer than 220 nm

<sup>a</sup>Value is minimum.<sup>b</sup>Value is maximum.<sup>c</sup>To convert Pa to mmHg, multiply by 0.0075.

**Shipment and Storage; Specifications.** N-Vinyl-2-pyrrolidinone is available in tank cars and tank trailers and in drums of various sizes. Shipping containers are normally steel or stainless steel. Tank cars are provided with heating coils to facilitate unloading in cold weather. Rubber, epoxy, and epoxy-phenolic coatings are attacked and must be avoided. Carbon steel has been successfully used for storage tanks, but stainless steel preserves product quality better. Aluminum and certain phenolic coatings are also satisfactory.

**Toxicity Data on N-Vinyl-2-Pyrrolidinone.** Results of a chronic inhalation study in rats warrant a review of industrial hygiene practices to assure that VP vapor concentrations are maintained at a safe level. One of the manufacturers, ISP, recommends that an appropriate workplace exposure limit be set at 0.1 ppm (vapor) (9). Additionally, normal hygienic practices and precautions are recommended, such as prompt removal from skin and avoidance of ingestion. In case of accidental eye contact, immediately flush with water for at least 15 min and seek medical attention. Refer to the manufacturers' Material Safety Data Sheets for more detailed information. Table 3 provides some toxicity data.

**Table 3. Summary of Toxicity Data for N-Vinyl-2-Pyrrolidinone**

Test	Result
Acute oral LD <sub>50</sub>	1.5 mL/kg (rats)
Acute dermal LD <sub>50</sub>	0.56 g/kg (rabbits)
Acute inhalation LC <sub>50</sub>	700 ± 100 ppm(rats)
Eye irritation	Severe (rabbits)
Primary irritation index (PII)	0.38 (rabbits)
Skin Repeated Insult Patch Test	Not a primary irritant or sensitizer (humans)
Subacute inhalation	No gross or clinical abnormal effects; subacute/chronic inflammation of respiratory tract at 16.5 and 66 ppm (rats)
Subchronic inhalation	Evidence of liver damage at 15, 45, and 120 ppm; no evidence of toxicity at 1 ppm (rats)
Chronic inhalation	Benign and malignant tumors of the nasal mucosa at the 10 and 20 ppm levels; liver tumors noted at 20 ppm
Mutagenicity	Negative in a battery of five assays

### Homopolymerization of N-Vinyl-2-Pyrrolidinone

VP was originally polymerized in bulk by heating in the presence of small amounts of hydrogen peroxide. This neat polymerization was a difficult process to work-up, requiring crushing of the solidified polymer mass and extraction with ether to remove unreacted monomer and by-products. However, it was important to the original application as a blood substitute because it afforded low molecular weight (10,11). Low molecular weight is necessary for excretion from the kidneys (12). Bulk polymerization favors the tendency of VP to undergo chain transfer to monomer. Neat VP polymerized with di-*tert*-butyl peroxalate in the presence of a nitroxide scavenger that exclusively traps carbon centered radicals generates considerable nonvinyl radicals by chain transfer (13,14). VP (and presumably PVP) can, under the right circumstances, undergo chain transfer, and this route is more prevalent as the concentration of monomer is increased.

Because VP and PVP are soluble in water, early workers realized that polymerization could be more easily controlled in such a high heat capacity solvent. In the presence of acid, VP readily hydrolyzes, and when initiated with hydrogen peroxide, the pH drops quickly into the acidic range. The problem this presents was solved by buffering with bases. Of all of the bases tried by the early German chemists, ammonia not only prevented hydrolysis by neutralizing acidic by-products, it accelerated the polymerization. The early workers found that with an optimized concentration of monomer and ammonia level, the molecular weight was reproducibly controlled by the hydrogen peroxide level. Even relatively high molecular weight could be achieved by small amounts of hydrogen peroxide, but such levels might easily be compromised by unproductive side reactions. High molecular weight homopolymers are more reliably produced by initiation with organic peroxides and azo initiators.

**Ammonia H<sub>2</sub>O<sub>2</sub> Initiation.** The lower molecular weight grades (K-15 and K-30) of PVP are prepared industrially with an ammonia/H<sub>2</sub>O<sub>2</sub> initiation system. Such products are the standards for the pharmaceutical industry and conform to the various national pharmacopeias. Several papers have appeared concerning the mechanism of this polymerization (15).

The proposed rate expression for the ammonia/H<sub>2</sub>O<sub>2</sub> process is as follows:

$$R_p = k[H_2O_2]^{1/2}[NH_3]^{1/4}[VP]^{3/2} \quad (1)$$

Comparing this to the theoretical expression based on the steady state approximation suggests that the mechanism is not straightforward:

$$R_p = k_p[M] \frac{(fkd[I])^{1/2}}{k_t} \quad (2)$$

Higher than first order for monomer, such as the 3/2 power suggests that VP is involved in initiation (16). If the efficiency of initiation is a function of the monomer concentration, then  $f = f^1[M]$ , and substituting in equation 2 gives

$$R_p = k_p[M]^{3/2} \frac{(f^1kd[I])^{1/2}}{k_t} \quad (3)$$

The  $[I]^{1/2}$  is reflected in  $[H_2O_2]^{1/2}$  but  $[NH_3]^{1/4}$  can be explained by the finding (17) that the rate of polymerization is proportional to  $[NH_4^+]^{1/2}$ . If the equilibrium expression for  $NH_3/[NH_4^+]$  is solved for  $[NH_4^+]$  and this expression substituted, the quarter power for ammonia is apparent.

Several papers (6,18) have appeared that attempt to reconcile the ability of H<sub>2</sub>O<sub>2</sub> to act as a rather strong transfer agent (hydrogen donor), generating the weakly initiating species HOO•, with its ability to act as a source of HO• hydroxy radicals that are known to be active vinyl initiators. Such studies demonstrate that HO• generated by photolysis behaves classically as an initiator for PVP (the rate is, as expected, first order in VP and half order in H<sub>2</sub>O<sub>2</sub>). Polymerization with 2,2'-azobisisobutyronitrile (AIBN) in the presence of H<sub>2</sub>O<sub>2</sub> demonstrates that H<sub>2</sub>O<sub>2</sub> in this case acts as a proton donor, reducing molecular weight, suggesting it also functions similarly during NH<sub>3</sub>/H<sub>2</sub>O<sub>2</sub> initiation. Even with other water-soluble initiators, VP behaves classically, with the rate expression being first order in monomer and half order in initiator (19,20). This would indicate that VP is a vinyl monomer with normal behavior and hence the H<sub>2</sub>O<sub>2</sub>/NH<sub>3</sub> initiation system is unusual. The evidence clearly demonstrates that it is a redox initiator system requiring trace amounts of cuprous or ferrous salt (21). Other bases such as NaOH or KOH can be employed to replace NH<sub>3</sub> if precautions are taken to sequester these metal ions, preventing them from being deactivated in the redox complex (22).

In one of the few published studies of H<sub>2</sub>O<sub>2</sub> initiation, it is shown that in the case of methacrylamide, the monomer participates in its own initiation by reacting with H<sub>2</sub>O<sub>2</sub>, forming an intermediate hydroperoxide (23). Subsequently, this hydroperoxide generates hydroxyl radicals capable of initiation. Like that of methacrylamide, VP polymerization is very sensitive to molecular oxygen reacting faster with it than propagation to polymer (18), and a similar reaction



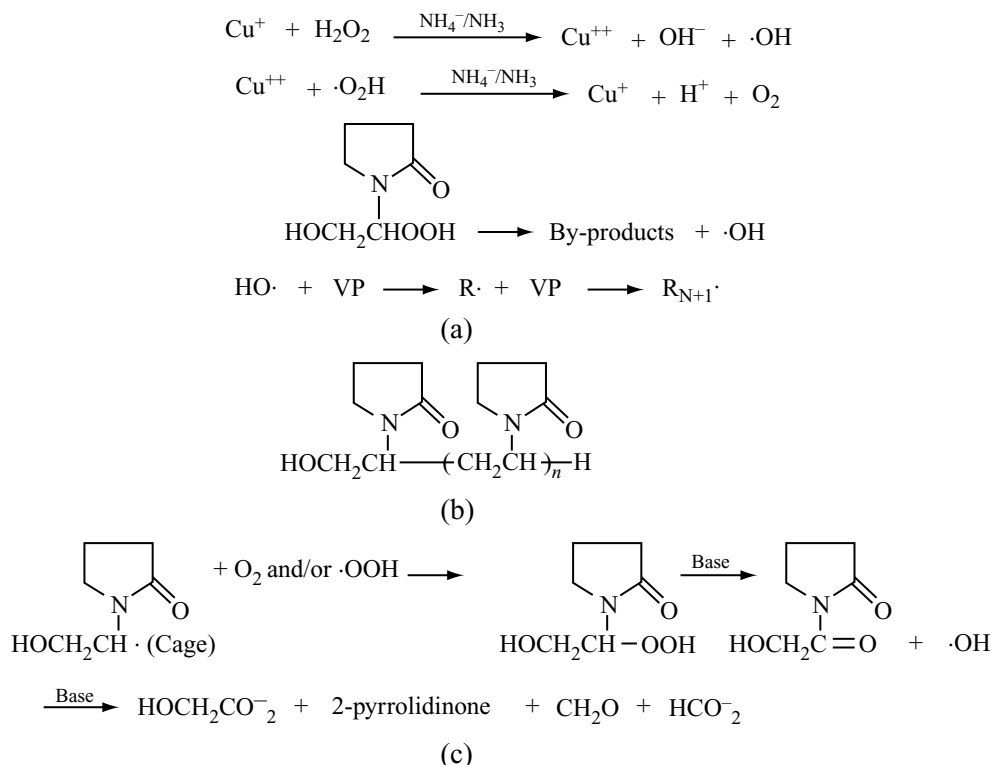


**Fig. 1.** Mechanism of  $\text{NH}_3/\text{H}_2\text{O}_2$  polymerization of VP: (a) initiation; (b) end groups; (c) 2-pyrrolidinone generation.

might be at work with VP that would be expected to generate an intermediate hydroperoxide capable of entering into a redox initiation system. The proposed mechanism would also explain the formation of 2-pyrrolidinone as a consequence of redox polymerization, dispelling the previous belief that 2-pyrrolidinone was a result of primary radical termination caused by reaction of hydroxyl radicals with the growing chain, followed by hydrolysis of the hemiacetal (24,25) subsequently formed. Hydroxyl radicals afford PVP with one hydroxyl per chain, correlating well with a mechanism that relies on hydroxyl radical initiation and strong  $\text{H}_2\text{O}_2$  chain transfer (26). In this case, one end of the polymer is not an aldehyde but rather a hydroxyl group, and no evidence for other than proton termination could be found, producing a methylene terminus at the other end of the polymer chain. Figure 1 illustrates the proposed mechanism and explains the formation of acidic by-products responsible for the acidic pH drift during polymerization.

### Organic Peroxides and Azo Initiation

The  $\text{H}_2\text{O}_2$ /ammonia initiation system is not employed commercially in the manufacture of higher molecular weight homologues; they are prepared with organic initiators. Such polymerizations follow simple chain theory and are usually performed in water commercially. The rate of polymerization is at a maximum in

aqueous media at pH 8–10 and at 75 wt% monomer (27,28). Polymerization rates follow the polarity and hydrogen bonding capability of the solvent (29). One possible explanation for this fact is that water is most capable of reducing the apparent negative charge on the beta carbon VP's vinyl group by hydrogen bonding to the pyrrolidinone carbonyl and polar interactions. Such a reduction permits the electron-rich radical terminus to more easily approach another VP and hence allows the acceleration (29). Alternatively, PVP may be somewhat more hydrophobic than VP forming associates ("micelles") capable of enhancing the rate of polymerization by concentrating monomer close to the reacting polymer terminus. This is the reason why even in relatively dilute aqueous solutions the rate can be substantial. The hydrophobic effect accounts for a higher VP concentration at the reactive polymer terminus (30).

**Cationic Polymerization.** VP polymerizes to low molecular weight (oligomers) with typical cationic initiators, such as boron trifluoride etherate (31). This reaction requires high concentrations, if not neat, of monomer and scrupulously anhydrous conditions for high yields; VP will readily hydrolyze to 2-pyrrolidinone and acetaldehyde even in the presence of trace moisture when catalyzed by strongly acidic reagents. Pyrrolidinone derivatives apparently complex and deactivate cationic polymerization catalysts and generally present an unfavorable environment for polymerization (32). Thus, initiating species are relatively short-lived and readily deactivated, or undergo chain transfer; hence, more than catalytic amounts of initiator are required for high yields.

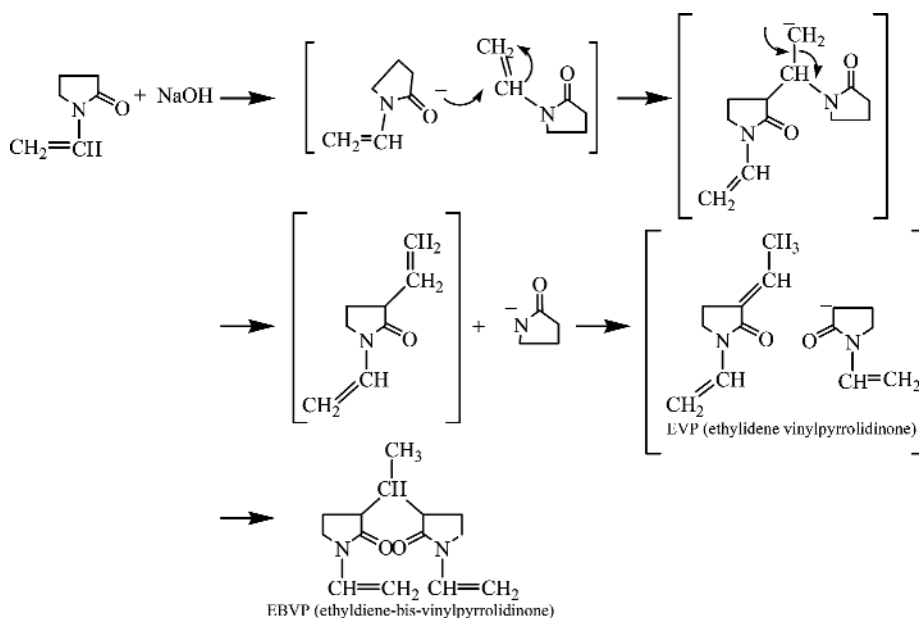
Interest has been rekindled in cationic polymerization by the discovery that carboxylic acid groups trapped in insoluble matrices like activated carbon or poly(glutamic acid) can generate higher mol wt. polymers (33–35). Additionally, oxoammonium salts (36) derived from 2,2,6,6-tetramethylpiperidine-1-oxyl (TEMPO) or anodic polymerization (37) on platinum electrode surfaces will also afford higher molecular weight polymers. Such cationically generated polymers would be expected to afford microstructure and greater tacticity because of the higher activation energy for inversion associated with a growing cationic terminus vs a growing free-radical terminus. Unfortunately, none of the above references present detailed polymer structural characterizations.

**Microstructure.** Interest in PVP microstructure and the potential for tacticity has been reviewed (38,39). PVP generated by free radicals has been shown to be atactic except when polymerization is conducted in water. In this case, some syndiotacticity is observed (39). In the presence of syndiotactic templates of poly(methacrylic acid) (or poly(MAA)), VP will apparently polymerize with syndiotactic microstructure, although proof is lacking (40–44). The reverse, polymerization of MAA in the presence of PVP, affords, as expected, atactic poly(MAA) (45,46).

Advances in VP cationic polymerization hold out the possibility of tacticity, and the study of this route to crystalline homologues continues to be of interest.

**Proliferous Polymerization.** Early attempts to polymerize VP anionically resulted in proliferous or "popcorn" polymerization (47). This was found to be a special form of free-radical addition polymerization, and not an example of anionic polymerization, as originally thought. VP contains a relatively acidic proton alpha to the pyrrolidinone carbonyl. In the presence of strong base such as

sodium hydroxide, VP forms crosslinkers *in situ*, probably by the following mechanism:



Both ethylidene vinyl pyrrolidinone (EVP) and ethylidene-bis-vinylpyrrolidinone (EBVP) are generated in about a 10:1 ratio, respectively (24). At the temperature required to generate these cross-linkers and when their concentration reaches some minimum level, usually a few percent, proliferous polymerization begins (48). The same situation can be reached by the addition of a suitable cross-linker (49). Although no initiator is required, the polymerization can be prevented in the presence of typical free-radical inhibitors or initiated by very small amounts of AIBN. Reviews indicate that the rate of polymerization accelerates because the initially formed cross-linked seeds swell to generate active sites by bond homolysis and that growing chains resist termination because of the rigid cross-linked structure. Very high conversions can be achieved and the resulting product, a granular "popcorn" mass, can be freed of residual monomer/soluble polymer by careful washing. Drying results in a free-flowing white powder (50).

Crospovidones are produced commercially by these two processes, ie, *in situ* generation of cross-linker or addition of divinylimidazoline, and they are indistinguishable by ir. Both types exhibit a  $T_g$  of 190–195°C, which is not that much above the 175°C of high molecular weight, soluble PVP (24). Proliferous polymers prepared with easily hydrolyzed cross-linker containing an imine linkage do not further swell even when the cross-links are hydrolyzed (49). In order to reach the low swell volume typical of these resins with a typical VP/cross-linker polymerized with free-radical initiator, sizeable amounts of cross-linker are actually required, resulting in much higher (240°C)  $T_g$ s. The crospovidones are therefore unusually high molecular weight, highly chain-entangled polymers having

covalent cross-links that most likely retard the termination reaction during polymerization and are not entirely responsible for the resulting mechanical properties, such as swell ratio. Even hydrolyzing such cross-links is not sufficient to cause dissolution.

The crospovidones are easily compressed when anhydrous but readily regain their form upon exposure to moisture. This is an ideal situation for use in pharmaceutical tablet disintegration and they have found commercial application in this technology. PVP strongly interacts with polyphenols, the crospovidones can readily remove them from beer, preventing subsequent interaction with beer proteins and the resulting formation of haze. The resin can be recovered and regenerated with dilute caustic.

### PVP Hydrogels

Cross-linked versions of Water-Soluble Polymers (qv) swollen in aqueous media are broadly referred to as Hydrogels (qv) and have a growing commercial utility in such applications as oxygen-permeable soft contact lenses (Table 4) and controlled-release pharmaceutical drug delivery devices (51). Cross-linked PVP and selected copolymers fit this definition and are of interest because of the following structure/performance characteristics:

Structure	Performance	Benefit
Nonionic	Compatibility with other ingredients	Stable formulation
Pyrrolidinone	Low toxicity	Nonirritating/nonthrombogenic
	Complexation actives/O <sub>2</sub>	Controlled release transport
	High $T_g$	Mechanical stability
Ethylene backbone	Hydrolytic stability	Storage stable
	Nonbiodegradable, hydrolytic stability	Resists biocontamination storage-stable
Cross-links	Swell volume/viscosity	Mechanical stability/diffusion control

Cross-linked PVP can be prepared by several routes other than proliferous polymerization PPVP (crospovidones). Although a hydrogel, the swell volume of this type of polymer cannot be controlled over a large increment because the granular particles cannot be formed into larger uniform assemblies. These limitations can be overcome by the polymerization of VP in the presence of a few percent of suitable cross-linker utilizing standard free-radical initiation by, for example, AIBN (52–54) or actinic radiation (gamma rays) (55,56). This results in a lightly cross-linked PVP. If the polymerization is carried out incorrectly, significant amounts of uncross-linked soluble polymer may be present that must be removed before a meaningful physical analysis such as swell ratio can be accomplished. The solution to this problem is to balance the reactivity ratios of the cross-linker and other comonomers with those of VP to obtain uniform copolymerization and cross-linking (57,58). Not only does this reduce the level of soluble uncross-linked polymer but affords crystal-clear hydrogels so important for

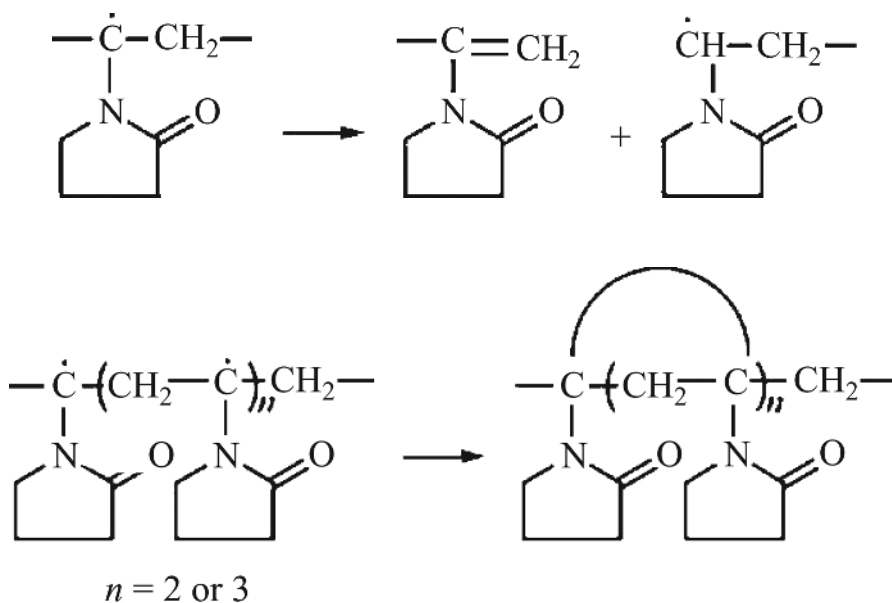
**Table 4. Generic Names of Polymeric Compositions Used in Soft Contact Lenses**

USAN Generic Name	Polymer composition <sup>a</sup>	Water, %	Trademarks	Manufacturer
Droxifilcon-A	Copolymer of HEMA and MA modified with poly(2-vinyl-pyrrolidone)	47	Accugel	Strieter Labs
Lidofilcon-B	Copolymer of MMA and 2-vinylpyrrolidone (VP)	79	Sauflon PW	American Medical Optics
Surfilcon-A	Copolymer of MMA, VP, and other methacrylates	74	Permaflex	Cooper Vision, Inc.
Tetrafilcon-A	Terpolymer of HEMA, MMA, and VP cross-linked with divinylbenzene	42.5	Aosoft Aquaflex	American Optical Corp., Cooper Vision, Inc.
Vifilcon-A	Copolymer of HEMA and MA with PVP cross-linked with EGDM	55	Softcon	American Optical Corp.

<sup>a</sup>HEMA, hydroxyethylmethacrylate; EGDM, ethyleneglycoldimethacrylate.

use in contact lenses. Allyl-substituted sugars used to generate cross-linked polyacrylic acid gels, carbomers, employed as thickeners in pharmaceutical formulations, have been shown to work well with VP (59).

Cross-linked PVP can also be obtained by cross-linking the preformed polymer chemically (with persulfates, hydrazine, or peroxides) or with actinic radiation (60). This approach requires a source of free radicals capable of hydrogen abstraction from one or another of the labile hydrogens attached alpha to the pyrrolidone carbonyl or lactam nitrogen. The subsequently formed PVP radical can combine with another such radical to form a cross-link or undergo side reactions such as scission or cyclization (61,62), thus:



If the starting PVP homopolymer is too low in molecular weight or too dilute, cyclization or cleavage is preferred (62,63). However, because of the high  $T_g$  of PVP, the backbone is sufficiently rigid to avoid reorientation during bond homolysis so that the same bond has a good chance of reforming; hence, PVP yields cross-linked structures in preference to cleavage (64) and PVP hydrogels formed by e-beam have become commercially important for use as conductive electrodes for medical applications (65).

### Poly(*N*-Vinyl-2-Pyrrolidinone)

Poly(*N*-vinyl-2-pyrrolidinone) (PVP) is undoubtedly the best characterized and most widely studied *N*-vinyl polymer. It derives its commercial success from its biological compatibility, low toxicity, film-forming and adhesive characteristics, unusual complexing ability, relatively inert behavior toward salts and acids, and thermal and hydrolytic stability.

First developed in Germany by I. G. Farben (W. Reppe) during the 1930s, PVP was subsequently widely used in Germany as a blood-plasma substitute and extender during World War II (66). In the United States, it has been manufactured since 1956 by ISP, and more recently by BASF.

**Molecular Weight and  $K$  Value.** Poly(*N*-vinyl-2-pyrrolidinone) is described in the *United States Pharmacopeia* (67) as consisting of linear *N*-vinyl-2-pyrrolidinone groups of varying degrees of polymerization. The molecular weights of PVP samples are determined by size-exclusion chromatography (sec), osmometry, ultracentrifugation, light scattering, and solution viscosity techniques. The most frequently employed method of determining and reporting the molecular weight of PVP samples utilizes the sec/low angle light-scattering (lalls) technique (68,69).

A frequently used and commonly recognized method of distinguishing between different molecular weight grades of PVP is the  $K$  value. Its nomenclature is accepted by the USP, FDA, and other authoritative bodies worldwide. The *Pharmacopeia* (USP) specifies that for very low molecular weight, a 5% solution whereas for very high molecular weight, a 0.1% solution be measured. All other molecular weights employ a 1% solution. The relative viscosity is obtained with an Ostwald-Fenske or Cannon-Fenske capillary viscometer, and the  $K$  value is derived from Fikentscher's equation (70).

$$\log \frac{\eta_{\text{rel}}}{c} = \frac{75K_o^2}{1+1.5K_o c} + K_o$$

where  $K = 1000K_o\eta_{\text{rel}}$  = relative viscosity, and  $c$  = concentration of the solution in g/100 mL. Solving directly for  $K$ , the Fikentscher equation is converted to

$$K = [300c \log Z + (c + 1.5c \log Z)^2 + 1.5c \log Z - c] / (0.15c + 0.0003c^2)$$

where  $Z = \eta_{\text{rel}}$ . Table 5 illustrates a correlation chart where the  $K$  value is simply read off from a knowledge of  $\eta_{\text{rel}}$ .

**Table 5.  $K_o$  Value vs Relative Viscosity at 1% Concentration (wt/vol)<sup>a</sup>**

$K$ value	Relative viscosity	$K$ value	Relative viscosity
20	1.120	60	2.031
25	1.175	65	2.258
30	1.243	70	2.527
35	1.325	75	2.846
40	1.423	80	3.225
45	1.539	85	3.678
50	1.677	90	4.219
55	1.839	95	4.870

<sup>a</sup>Ref. 68.**Table 6.  $K$  Value vs Weight-Average Molecular Weight for PVP<sup>a</sup>**

$K$ value	$\bar{M}_w$ , amu	$K$ value	$\bar{M}_w$ , amu
10	2,600	70	626,900
15	8,100	75	761,500
20	18,300	80	913,500
25	34,400	85	1,084,000
30	57,500	90	1,273,000
35	88,800	95	1,483,000
40	129,300	100	1,714,000
45	180,300	105	1,967,000
50	242,700	110	2,242,000
55	317,600	115	2,542,000
60	405,900	120	2,866,000
65	508,600		

<sup>a</sup>Ref. 68.

The intrinsic viscosity  $[\eta]$  may be approximated from the Fikentscher equation by

$$[\eta] = 2.303 (0.001K + 0.000075K^2)$$

where  $[\eta]$  = intrinsic viscosity and  $K = K$  value of sample.

Utilizing the Mark–Houwink equation (71)

$$[\eta] = K\bar{M}_v^a$$

it is possible to relate the viscosity-average molecular weight ( $\bar{M}_v$ ) to the  $K$  value.

For commercial grades of unfractionated PVP prepared by similar means (presumed to exhibit similar molecular weight distribution (MWD) and degree of branching), the following regression formula can be employed (68):

$$\log \text{mol wt.} = 2.82 \log K + 0.594$$

Table 6 indicates mol wt. vs  $K$  value obtained by this technique. Table 7 lists  $M_n$  obtained by osmometry methods. The specifications for Technical and Pharmaceutical grades are given in Tables 8 and 9.

**Table 7. Osmometry Molecular Weights for PVP<sup>a</sup>**

Sample	Technique	$\overline{M}_n$
K-90	Membrane osmometry	37,4000
K-60	Membrane osmometry	67,500
K-30	Vapor pressure osmometry	8,430
K-15	Vapor pressure osmometry	5,170

<sup>a</sup>Ref. 69.**Table 8. Specifications of Technical PVP Grades**

Designation	Form	<i>K</i> range	Water, %max	Ash, %max	$M_v(\times 10^{-3})^a$
K-15	Powder	13–19	5	0.02	10
K-15	Aqueous solution	13–19	72		10
K-30	Powder	26–34	5	0.02	40
K-60	Aqueous solution	50–62	55	0.02	220
K-90	Aqueous solution	80–100	80	0.02	630
K-90	Powder	88–100	5	0.02	630
K-120	Powder	115–125	5	0.02	1450

<sup>a</sup>Performed at 25°C, in H<sub>2</sub>O, using Mark–Houwink constants of  $K = 1.4 \times 10^{-4}$  and  $\alpha = 0.7$ .**Table 9. Specifications of Pharmaceutical PVP Grades (Povidone)**

Assay	Value <sup>a</sup>
<i>K</i> value	
10–15	85–115% of stated supplier's value
16–90	90–107% of stated supplier's value
Moisture, %	5
pH <sup>b</sup>	3.0–7.0
Residue on ignition, %	0.02
Aldehydes, % <sup>c</sup>	0.02
<i>N</i> -Vinyl-2-pyrrolidinone, %	0.20
Lead, ppm	10
Arsenic, ppm	1
Nitrogen, %	11.5–12.8

<sup>a</sup>All single values are maximum.<sup>b</sup>Of a 5% solution in distilled water.<sup>c</sup>Calculated as acetaldehyde.

**Glass-Transition Temperature.** The  $T_g$  of PVP is sensitive to residual moisture (72) and unreacted monomer. It is even sensitive to how the polymer was prepared, suggesting that MWD, branching, and cross-linking may play a part (73). Polymers presumably with the same molecular weight prepared by bulk polymerization exhibit lower  $T_g$ s compared to samples prepared by aqueous solution polymerization, lending credence to an example, in this case, of branching caused by chain transfer to monomer.

Molecular weight also plays a significant role in  $T_g$ , which increases to a limiting value of 180°C for high purity samples above K-90 in molecular weight.



**Table 10. Glass-Transition Temperatures of PVP**

Sample <sup>a</sup>	Measured <i>K</i> value	<i>T<sub>g</sub></i> , °C
Plasdone K-15	14.0	126
PVP K-15	14.9	130
Plasdone K-25	22.5	160
PVP K-30	27.5	163
Plasdone K-29/32	28.7	164
PVP K-60	55.5	170
PVP K-90	89.6	174

<sup>a</sup>Courtesy of ISP Corp.

The following equation applies:

$$T_g(\text{C}^\circ) = 175 - \frac{9685}{K^2}$$

and Table 10 illustrates this relationship with commercially available samples.

**Solubility.** One of PVP's more outstanding attributes is its solubility in both water and a variety of organic solvents. PVP is soluble in alcohols, acids, ethyl lactate, chlorinated hydrocarbons, amines, glycols, lactams, and nitroparaffins. Solubility means a minimum of 10 wt% PVP dissolves at room temperature (moisture content of PVP can influence solubility). PVP is insoluble in hydrocarbons, ethers, ethyl acetate, *sec*-butyl-4-acetate, 2-butanone, acetone, cyclohexanone, and chlorobenzene. Both solvent polarity and Hbonding strongly influence solubility (74).

**Swelling Behavior.** One way to visualize the interaction of solvents with PVP is to examine the effect the former have on lightly cross-linked PVP, as a model for the linear polymer (75).

Such gels can be prepared from a minimum of diallyl cross-linker and VP to afford products that are mechanically stable and easy to handle as hydrogels. Such samples must be extracted because soluble polymer competes for solvent, affording lower swell volumes than those expected. The extracted and dried samples are swollen to equilibrium in a variety of solvents (Table 11). Three groups of solvents can be distinguished: the first includes those in which the cross-linked polymer swells 15–25 times. VP, H<sub>2</sub>O, CH<sub>3</sub>OH, C<sub>2</sub>H<sub>5</sub>OH, benzylamine, and chloroform are examples. Swelling drops off with longer chain-length alcohols. Aromatic derivatives like benzyl alcohol and aniline afford similar swelling ratios to each other and to aliphatic analogues. This indicates that simple aromatic groups do not interact. When comparing volume instead of weight, water actually causes a 0.36% shrinkage of the gel. Water can therefore cross-link by hydrogen bonding to a limited but measurable extent. The second group consists of acetone, MEK, and dioxane solvents that not only increase the swell ratio (to a much lesser extent) but also increase the swell volume by 60–100%. The third group consists of hydrocarbons, benzene, carbon tetrachloride, isopropyl ether, and triethyl amine. In this case, they have little or no effect on swelling. The hallmark of this group is lack of hydrogen-bonding capability.

In water, the swell ratio actually decreases with temperature at a constant rate of  $-0.12\%/^\circ\text{C}$ . PVP gels therefore swell exothermically in water, and, as

**Table 11. Swelling of Cross-linked Polyvinylpyrrolidone in Various Liquids at 20°C<sup>a</sup>**

Liquid	Degree of swelling	Liquid	Degree of swelling
1-Propanol	25.6	Chloroform	16.7
Ethanol	24.8	Ethylenediamine	15.6
Isoamyl alcohol	24.8	Acetone	2.1
Methanol	24.0	Methyl ethyl ketone	2.0
Water	19.7	Cyclohexanone	1.9
Benzyl alcohol	19.5	Dioxane	1.6
<i>n</i> -Octanol	19.1	Trimethylamine	1.07
Benzylamine	17.1	Carbon tetrachloride	1.03
Prim-phenyl ethyl alcohol	16.9	Benzene	1.02
		Isopropyl ether	1.0

<sup>a</sup>Ref. 75.**Table 12. Temperature-Dependence of Degree of Swelling in Four Liquids<sup>a</sup>**

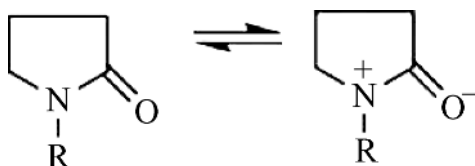
Liquid	Temperature, °C	Degree of swelling
Dioxane	20	1.57
	50	2.34
Methyl ethyl ketone	20	1.69
	50	2.86
Ethanol	20	18.3
	50	17.3
Chloroform	20	24.6
	50	24.0

<sup>a</sup>Ref. 75.

expected, heat reverses the process. Cooling back to a lower temperature results in the expected higher swell ratio being reestablished. Alcohols and other hydrogen bonding solvents cause the same effect but to a lesser extent. Nonhydrogen-bonding solvents actually cause an increase in swelling with temperature (Table 12).

**Rheology.** PVP solubility in water is limited only by the viscosity of the resulting solution. The heat of solution is  $-16.61\text{kJ/mol}$  ( $-3.97\text{ kcal/mol}$ ) (76); aqueous solutions are slightly acidic (pH 4–5). Figure 2 illustrates the kinematic viscosity of PVP in aqueous solution. The kinematic viscosity of PVP K-30 in various organic solvents is given in Table 13.

**Aqueous Solutions of PVP.** Although it is soluble in a variety of polar solvents, PVP has generated significant interest because of its aqueous solubility. Water can readily hydrogen bond to the polar, negatively charged pyrrolidinone carbonyl oxygen because pyrrolidinone, a five-membered planar lactam, affords maximum  $\pi$ ,  $\pi$ -orbital overlap. The canonical resonance forms highlight the potential for a partial negative charge to form on oxygen:



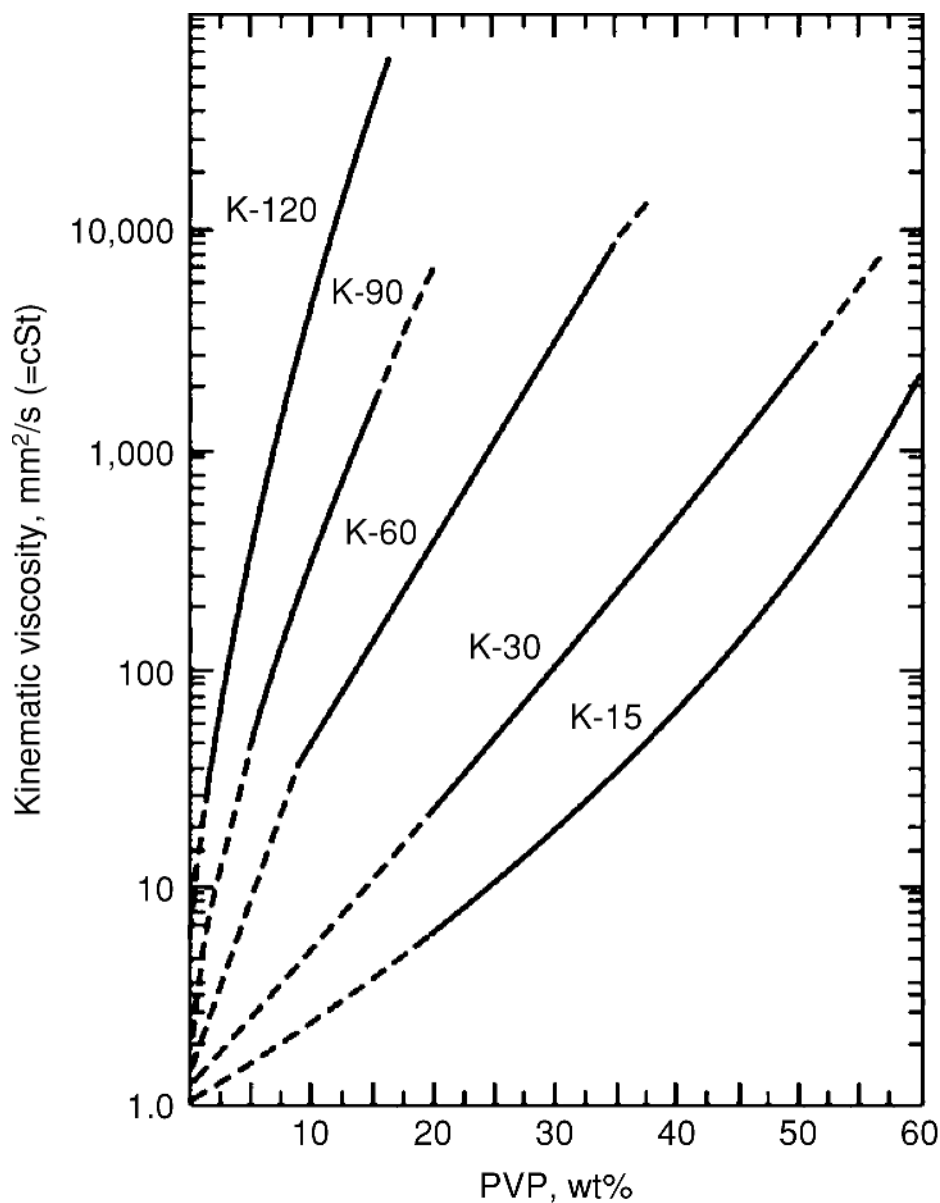


Fig. 2. Kinematic viscosity of PVP in aqueous solutions.

The partial charge on nitrogen is sterically shielded by the polymer backbone and the surrounding pyrrolidinone methylenes. Because of high dipole moment and polarity, PVP has a noticeable effect on water structure and various methods have been proposed to measure bound water (77). One study even illustrates the different categories of water generated by freezing aqueous PVP solutions (78). The results are summarized in Figure 3, and, as can be seen, PVP is hydrated with bound water that will not freeze (concentrated solutions >57% will not freeze). PVP is therefore used as a protectorate in cryobiology (79).

**Table 13. Kinematic Viscosity of PVP K-30 in Organic Solvents**

Solvent	Kinematic viscosity, <sup>a</sup> mm <sup>2</sup> /s (=cSt)	
	2% PVP	10% PVP
Acetic acid (glacial)	2	12
1,4-Butanediol	101	425
Butyrolactone	2	8
Cyclohexanol	80	376
Diacetone alcohol	5	22
Diethylene glycol	39	165
Ethanol (absolute)	2	6
Ethyl lactate	4	18
Ethylene glycol	24	95
Ethylene glycol monoethyl ether	3	12
Glycerol	1480	2046
2-Propanol	4	12
Methyl cyclohexanone	3	10
N-Methyl-2-pyrrolidone	2	8
Methylene dichloride	1	3
Monoethanolamine	27	83
Nitroethane	1	3
Nonylphenol	3300	
Propylene glycol	66	261
Triethanolamine	156	666

<sup>a</sup>Kinematic viscosity = absolute viscosity/density.

The actual amount and structure of this “bound” water have been the subject of debate (80), but the key factor is that in water, PVP and related polymers are water structure organizers, which is a lower entropy situation (81). Therefore, it is not unexpected that water would play a significant role in the homopolymerization of VP, because the polymer and its reactive terminus are more rigidly constrained in this solvent and termination  $k_t$  is reduced (82).

## Complexation

The combination of electrostatic interaction (induced dipole–dipole interaction) with an increase in entropy resulting from the discharge of bound water is fundamental to PVP's ability to complex with a variety of large anions.

Other factors that can stabilize such a forming complex are hydrophobic bonding by a variety of mechanisms (van der Waals, Debye, ion dipole, charge transfer, etc). Such forces complement the stronger hydrogen bonding and electrostatic interactions.

Approximately a minimum  $\bar{M}_n$  of 1–5000 is required before complexation is no longer dependent on molecular weight for small anions such as  $\text{KI}_3$  and 1-anilinonaphthalene-8-sulfonate (ANS) (83,84). The latter anion is a fluorescent probe that, when bound in hydrophobic environments, will display increased fluorescence and, as expected, shows this effect in the presence of aqueous PVP.

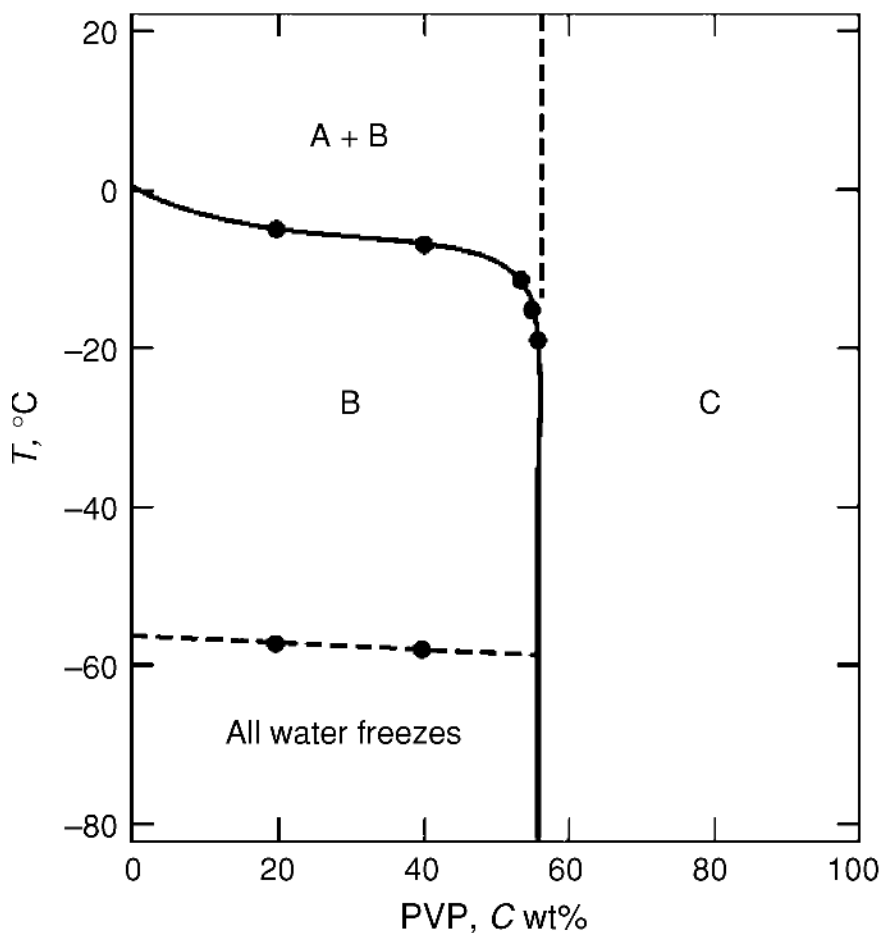


**Fig. 3.** Phase diagram for the three kinds of water in PVP aqueous solutions (78). A, freezable water; B, bound, nonfreezable water (six per repeat unit); C, nonfreezable water.

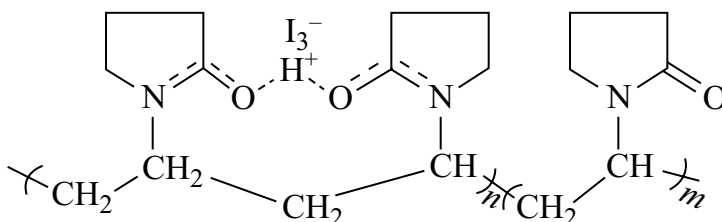
PVP, when complexed with  $\text{HI}_3$ , shrinks in size as it loses hydrodynamic volume, possibly because of interchain complexation. ANS, on the other hand, causes the polymer to swell by charge repulsion because it behaves like a typical polyelectrolyte (85).

**Adsorption Isotherms.** Equilibrium dialysis studies indicate around 10 repeat VP units (base moles) are required to form favorable complexes (86,87). This figure can rise to several hundred for methyl orange and other anions depending on structure (88,89).

Although hydrophobic bonding is well established as a significant force stabilizing such complexes, some work suggests that such generalizations do not apply to every case (89). However, a study of the complexes of PVP with tetraanionic porphyrins has shown that the reaction of porphyrin with cupric ion is slowed dramatically in the presence of PVP. This is interpreted as demonstrating the existence of hydrophobic pockets preventing a reaction that is clearly favored if

both species are in aqueous environments (90). Hydrophobic bonding has been illustrated by comparing competitive binding of butyl orange (BO) with 1-amino-4-methylamino anthraquinone-2-sulfonate (AQ) (91). The thermodynamic data for BO show that the binding process is athermal and stabilized entirely by the entropy term. On the other hand, AQ exhibits a large enthalpy and small entropy value and its binding is by the stronger and energetic interaction caused by hydrogen bonding (NH groups of AQ) and hydrophobic interaction of the polynuclear aromatic AQ; both structural features are missing from BO (91).

**Iodine Complexes.** The small molecule/PVP complex between iodine and PVP is probably the best-known example (92) and can be represented as follows:



It is widely employed as a disinfectant in medicine (povidone-iodine) because of its mildness, low toxicity, and water solubility. In actuality, the complex is based on  $\text{HI}_3$  since  $\text{HI}$  is formed *in situ* from iodine during the manufacturing process (93). According to the *U.S. Pharmacopeia*, povidone-iodine is a free flowing, brown powder that contains from 9 to 12% available iodine. It is soluble in water and lower alcohols. When dissolved in water, the uncomplexed free-iodine level is very low (Fig. 4) (94); however, the complexed iodine acts as a reservoir and by equilibrium replenishes the free iodine to the equilibrium level. This prevents free iodine from being deactivated because the free form is continually available at effective biocidal levels from this large reservoir (95). The structure of the complex has been studied and in essence is similar to the representation above (95,96). PVP will interact with other small anions and resembles serum albumin and other proteins in this regard (97). It can be "salted in" with anions such as  $\text{NaSCN}$  or "out" with  $\text{Na}_2\text{SO}_4$  much like water-soluble proteins (98).

**Phenolics.** PVP readily complexes phenolics of all types to some degree, the actual extent depending on structural features such as number and orientation of hydroxyls and electron density of the associated aromatic system. A model has been proposed (99). Complexation with phenolics can result in reduced PVP viscosity and even polymer-complex precipitation (100).

One practical result of this strong interaction is the employment of PVP to remove unwanted phenolics such as bitter tanins from beer and wine. This process is more easily carried out with insoluble crospovidone, which can be regenerated for reuse with dilute base (101). Soluble PVP has been employed to prevent photoyellowing of paper by complexing free-phenolic hydroxyl groups in lignin (102).

**Dyes.** PVP is currently (ca 1997) employed in a variety of antidye redeposition detergents as a result of its strong interaction with fugitive anionic dyes (103,104). This interaction depends on the structure of the dye. Cationic dyes

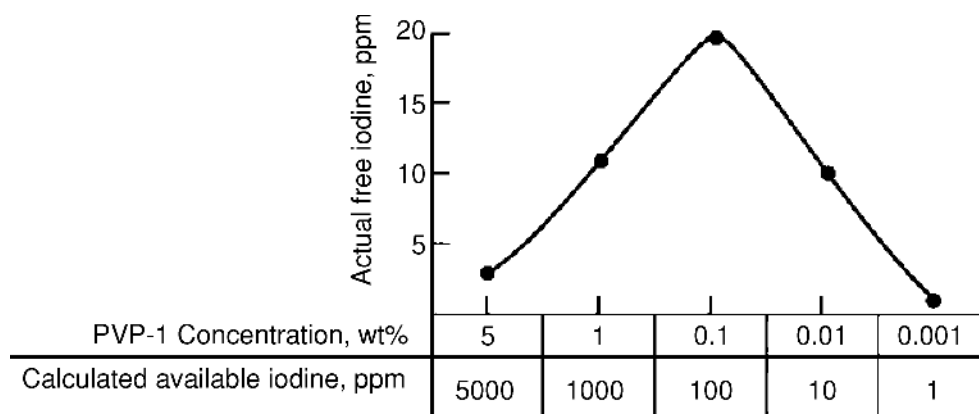


**Fig. 4.** Free iodine in povidone–iodine aqueous solutions (96).

complex only if they also contain hydrogen-bonding functionality. Anionic dyes complex more easily, depending on the number of anionic groups, size of the aromatic nucleolus, and number and orientation of phenolic hydroxyl groups, etc.

**Anionic Surfactants.** PVP also interacts with anionic detergents, another class of large anions (105). This interaction has generated considerable interest because addition of PVP results in the formation of micelles at lower concentration than the critical micelle concentration (CMC) of the free surfactant the mechanism is described as a “necklace” of hemimicelles along the polymer chain, the hemimicelles being surrounded to some extent with PVP (106). The effective lowering of the CMC increases the surfactant’s apparent activity at interfaces. PVP will increase foaming of anionic surfactants for this reason.

Because of this interaction, PVP has found application in surfactant formulations, where it functions as a steric stabilizer for example to generate uniform particle-size polystyrene emulsions (107–109). In a variety of formulations, a surfactant’s ability to emulsify is augmented by PVP’s ability to stabilize colloids sterically and to control rheology.

**Polymer/Polymer Complexes.** PVP complexes with other polymers capable of interacting by hydrogen bonding, ion dipole, or dispersion forces. For example mixing of PVP with poly(acrylic acid) (PAA) in aqueous solution results in immediate precipitation of an insoluble complex (110). Addition of base results in disruption of hydrogen bonding and dissolution (111–113). Complexes with a variety of polyacids (114) and polyphenols (115) have been reported. The interest in compatibility on a molecular level, an interesting phenomenon rarely found to exist between dissimilar polymers, is favored by the ability of PVP to form polymer/polymer complexes.

Practical applications have been reported for PVP/cellulosics (105,116,117) and PVP/polysulfones (118,119) in membrane separation technology, eg, in the manufacture of dialysis membranes. Electrically conductive polymers of polyaniline are rendered more soluble and hence easier to process by complexation with PVP (120). Addition of small amounts of PVP to nylon 66 and 610 causes

Table 14. VP Copolymerization Parameters<sup>a</sup>

Comonomer ( $M_2$ )	$r_1$	$r_2$	Reference
N-Vinyl caprolactam	2.80	1.70	125
Maleic anhydride	-0.027	0.074	126
Methyl methacrylate	0.01	4.04	127
Styrene	0.057	17.2	128
Vinyl acetate	3.40	0.195	128
Acrylic acid	0.100	0.880	129
Dimethylaminoethyl	0.07	4.7	130
Methacrylate	0.69	11.16	131

<sup>a</sup>Ref. 124.

significant morphological changes, resulting in fewer but more regular spherulites (121).

### Copolymerization

The  $Q$  and  $e$  values of VP are 0.088 and  $-1.62$ , respectively (122). This indicates resonance interaction of the double bond of the vinyl group with the electrons of the lactam nitrogen, whence the electronegative nature. With high  $e+$  monomers such as maleic anhydride, VP forms alternating copolymers, much as expected (123). With other monomers between these  $Q$  and  $e$  extremes a wide variety of possibilities exist. Table 14 lists reactivity ratios for important comonomers.

Copolymerizations can be conveniently carried out in aqueous solution or in a variety of solvents, depending on monomer/polymer solubilities. Various strategies have been employed to compensate for the divergence in reactivity ratios in order to form uniform (statistical) copolymers such as semibatch or mixed monomer feeds, the goal being to add the more reactive monomer at the rate at which it is being consumed (132). Clearly, if the difference in reactivity is too great, then the amount of more reactive monomer that can be uniformly incorporated is significantly reduced. Of the monomers listed, styrene fits this category (133).

**Poly(Vinylpyrrolidinone-co-Vinyl Acetate).** The first commercially successful class of VP copolymers, poly(vinylpyrrolidinone-co-vinyl acetate) is currently manufactured in sizeable quantities by both ISP and BASF. A wide variety of compositions and molecular weights are available as powders or as solutions in ethanol, isopropanol, or water (if soluble). Properties of some examples of this class of copolymers are listed in Table 15.

Although reactivity ratios indicate that VP is the more reactive monomer, reaction conditions such as solvent polarity, initiator type, percent conversion, and molecular weight of the growing radical can alter these ratios (135). Therefore, depending on polymerization conditions, copolymers produced by one manufacturer may not be identical to those of another, especially if the end use application of the resin is sensitive to monomer sequence distribution and MWD.

An important reason for the ongoing interest in these copolymers is that vinyl acetate reduces hydrophilicity so that applications that require less



**Table 15. Properties of PVP/VA Copolymers<sup>a</sup>**

	PVP-VA copolymer						
	E-735	E-635	E-535	E-335	I-735	I-535	I-335
Physical form at 25°C	Clear liquid				Light yellow liquid		
Solvent	SDA-40 anhydrous ethanol				2-propanol		
Solids after infrared drying, %	50 ± 2	50 ± 2	50 ± 2	50 ± 2	50 ± 2	50 ± 2	50 ± 2
Vinylpyrrolidinone-vinyl Acetate ratio	70:30	60:40	50:50	30:70	70:30	50:50	30:70
K value of 1% ethanol solution	30-50	30-50	30-50	25-35	30-40	25-35	20-30
Moisture as is, Karl Fischer, %max	0.5	0.5	0.5	0.5	0.5	0.5	0.5
Nitrogen, dry basis, Kjeldahl, %	8-9	7-8	5.8-6.8	3.1-4.1	8-9	5.9-6.9	3.9-4.9
Specific gravity at 25°C	0.955 ± 0.01						

<sup>a</sup>Ref. 134.

moisture-sensitive films such as those employed to set hair are less prone to plasticize and become tacky under high humidity conditions (136) (Fig. 5).

As shown in Figure 6, desirable fixative properties superior to PVP homopolymer can be specified by judicious selection of the amount of vinyl acetate. Hair sprays are limited in the molecular weight of the resin because if they are too high the resulting viscosity of the formulation will result in a poor (coarse) spray pattern. Increasing the VP/VA ratio causes properties to increase in the direction shown by the arrows.

Other applications for VP/VA copolymers are uses as water-soluble or re-moistenable hot-melt adhesives (137), pharmaceutical tablet coatings, binders, and controlled-release substrates.

**Tertiary Amine-Containing Copolymers.** Copolymers based on dimethylaminoethyl methacrylate (DMAEMA) in either free-amine form or quaternized with diethyl sulfate or methyl chloride have achieved commercial significance as fixatives in hair-styling formulations, especially in the well-publicized "mousses" or as hair-conditioning shampoo additives. This success has occurred because the cationic charge affords substantive resins that strongly adhere to the hair (138).

The most successful of these products contain high ratios of VP to DMAEMA and are partially quaternized with diethyl sulfate (Polyquaternium 11) (139-141). They afford very hard, clear, lustrous, nonflaking films on the hair that are easily removed by shampooing. More recently, copolymers with methylvinylimidazolium chloride (Polyquaternium 16) (142) or methacrylamidopropyltrimethyl ammonium chloride (MAPTAC) (Polyquaternium 28) have been introduced. Replacement of the ester group in DMAEMA with an amide analog as in Polyquaternium 28 results in a resin resistant to alkaline hydrolysis and hence greater

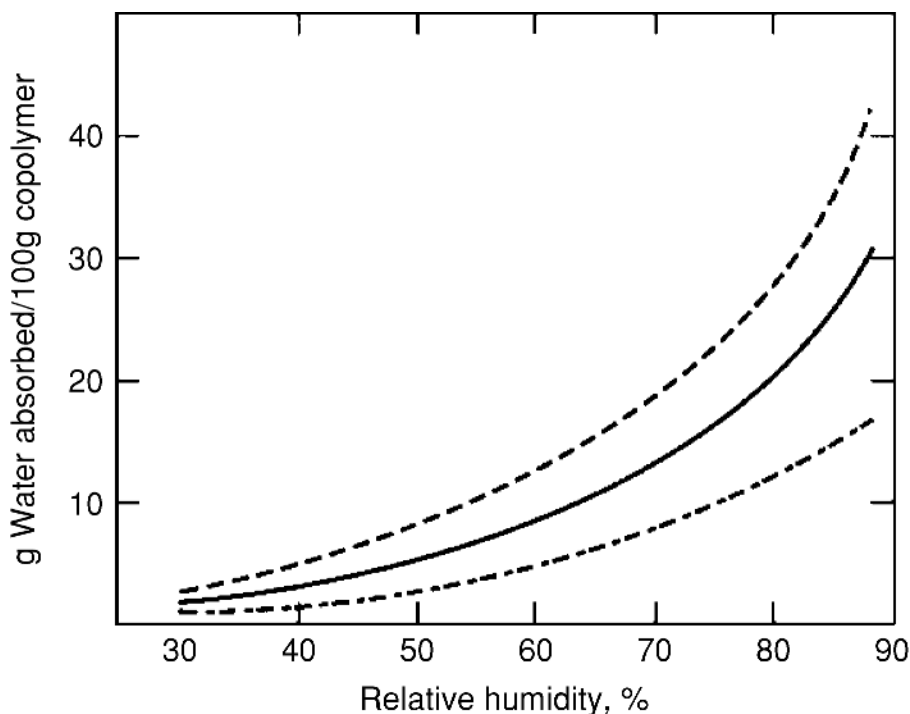


**Fig. 5.** Hydrophilicity of three wt% monomer ratios of PVP/VA: (---), 70/30; (—), 50/50; (— · —), 30/70.

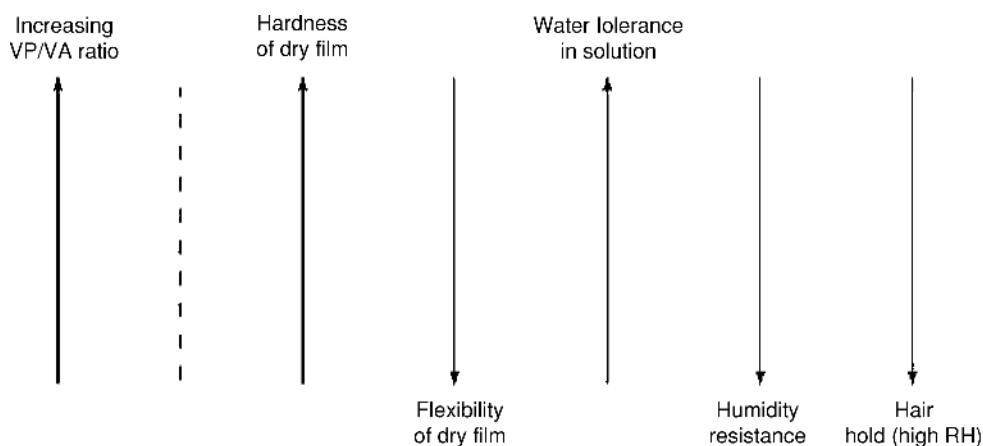


**Fig. 6.** Effect of VP/VA monomer ratio on properties of VP/VA copolymers.

utility in alkaline permanent wave and bleach formulations (see QUATERNARY AMMONIUM COMPOUNDS).

Unquaternized DMAEMA copolymers afford resins that are mildly cationic and less hygroscopic. They provide more moisture-resistant fixatives (143). Further refinements have been accomplished by adding a third comonomer such as

*N*-vinylcaprolactam (VCl). In this case, replacement of VP with VCl results in a terpolymer (VP/VCl/DMAEMA) with even greater high humidity moisture resistance and curl retention.

**Copolymers Containing Carboxylic Groups.** A new line of VP/acrylic acid copolymers in powdered form prepared by precipitation polymerization (144) from heptane have been introduced commercially (145). A wide variety of compositions and molecular weights are available, from 75/25 to 25/75 wt% VP/AA and from  $20 \times 10^3$  to  $250 \times 10^3$  molecular weights.

The copolymers are insoluble in water unless they are neutralized to some extent with base. They are soluble, however, in various ratios of alcohol and water, suggesting applications where delivery from hydroalcoholic solutions (146) but subsequent insolubility in water is desired, such as in low volatile organic compound (VOC) hair-fixative formulations or tablet coatings. Unneutralized, their  $T_g$ s are higher than expected, indicating interchain hydrogen bonding (147).

**Miscellaneous Copolymers.** VP has been employed as a termonomer with various acrylic monomer–monomer combinations, especially to afford resins useful as hair fixatives. Because of major differences in reactivity, VP can be copolymerized with alpha-olefins, but the products are actually PVP grafted with olefin or olefin oligomers (148,149). Likewise styrene can be polymerized in the presence of PVP and the resulting dispersion is unusually stable, suggesting that this added resistance to separation is caused by some grafting of styrene onto PVP (150). The literature contains innumerable references to other copolymers but at present (ca 1997), those reviewed in this article are the only ones known to have commercial significance.

## Applications

An overview of the various product categories is given in Table 16.

The Chemical Abstracts Services Registry Number and IUPAC nomenclature for PVP are [9003-39-8] and 1-ethenyl-2-pyrrolidinone homopolymer, respectively; however, it is known by a variety of approved names by foreign and domestic regulatory authorities. For example:

Name	Chemical name
Povidone	Poly( <i>N</i> -vinyl-2-pyrrolidinone)
Polyvidone	
Polyvidon	Poly( <i>N</i> -vinylbutyrolactam)
Polyvidonum	Poly(1-vinyl-2-pyrrolidinone)
	1-Vinyl-2-pyrrolidinone polymer
	Poly{1-(2-oxo-1-pyrrolinyl)ethylene}

Trade names for nonpharmaceutical grades are PVP, Peregol ST, Albigen A, and Luviskol; for pharmaceutical grades, Plasdone and Kollidon. The insoluble or crospovidones likewise exist as two grades: nonpharmaceutical are Polyclar and Divergan; pharmaceutical, Polyplasdone XL and Kollidon Cl.

Table 16. Properties and Applications of Commercial PVPs

Polymer	Mfr/Trade name	Grades	Properties/applications
<i>Homopolymers</i>			
PVP	ISP/PVP, Plasdone BASF/Luviskol, Kollidon	K-15 to K-120 K-12 to K-90	film former, adhesive, binder, com-plexant, stabilizer, crystallization inhibitor, dye scavenger, detoxi-cant, viscosity modifier
<i>Cross-linked</i>			
Proliferous polymerization	ISP/Polyclar, Polyplasdone BASF/Divergan	various (by particle size)various (by particle size)	pharmaceutical tablet disintegrant, adsorbent for polyphenols (tanins), beverage clarification
<i>Copolymers</i>			
PVP/VA	BASF/ISP/ PVP-VA copolymers	Various monomer ratios in ethanol, IPA or water in ethanol, IPA or water	Film forming adhesives for hairsprays, mousses, gels, shampoos, styling lotions, bio-adhesives, water-remoist-enable or removable adhesives
PVP/DMAEMA	ISP/copolymer	845/937/958	Mildly cationic, hair styling aids and conditioners, with strong hold; sub-stantive, lustrous film-formers
PVP/DMAEMA DES quaternary	ISP/Gafquat BASF/Luviquat	755N/734PQ11	Strongly cationic, substantive, mousse and gel hair fixative ingredients
PVP/imidazolinum quaternary	BASF/Luviquat FC		
PVP/styrene <sup>a</sup>	ISP/Polectron 430	30% VP	opacifier for personal care products; very stable styrene emulsion
PVP/alpha-olefins <sup>a</sup>	ISP/Ganex	Various (olefin chain length and monomer ratios)	surface active film formers; waterproofing of sunscreens
<i>Terpolymers</i>			
VP/VC/DMAEMA	ISP/Gaffix VC-713	VC-713	Cationic water-soluble hair styling aid hair fixatives
VP/tBMA/MA	BASF/Luviflex	Various	

<sup>a</sup>Graft copolymers.

## BIBLIOGRAPHY

"N-Vinyl Amide Polymers" in *EPST* 1st ed., Vol. 11, pp. 239–251, by Donald H. Lorenz, GAF Corporation; "N-Vinyl Amide Polymers" in *EPSE* 2nd ed., Vol. 17, pp. 198–257, by E.S. Barabas, GAF Chemicals Corporation.

## CITED PUBLICATIONS

1. P. Molyneux, in G. Starnsby, ed., *The Chemistry and Rheology of Water-Soluble Gums and Colloids*, S.C.I. Monograph No. 24, Society of Chemical Industries, London, 1966, p. 91.
2. A. Charlesby, *Radiat. Phys. Chem.* V **18**(1–2), 59 (1981).
3. W. Reppe and co-workers, *Justus Leibig's Ann. Chem.* **601**, 134 (1956).
4. J. Falbe and H. J. Schulze-Steinem, *Brennst. Chem.* **48**, 136 (1967).
5. D. J. Dawson, R. D. Gless, and R. E. Wingard Jr., *JACS* **98**, 5996 (1976).
6. T. M. Karaputudze and co-workers, *Vysokomol. Soedin., Ser. B.* **24**, 305 (1982).
7. C. Bramford, E. Schofield, and D. Michael, *Polymer* **26**, 946 (1985).
8. S. A. Miller, *Acetylene, Its Properties, Manufacture, and Uses*, Vol. **2**, Academic Press, New York, 1965, pp. 338–339.
9. *Vinylpyrrolidone (VP) Toxicity*, Update No. 2303-222R' 2M-292, ISP Corp., Wayne, N.J., 1992.
10. G. M. Kline, *Mod. Plastics* **22**, 157 (1945).
11. J. W. Copenhaver and M. H. Bigelow, *Acetylene and Carbon Monoxide Chemistry*, Reinhold Publishing Corp., New York, 1949.
12. B. V. Robinson and co-workers, *PVP, A Critical Review of the Kinetics and Toxicology of Polyvinylpyrrolidone (Povidone)*, Lewis, Chelsea, Mich., 1990.
13. J. W. Breitenbach, *J. Polym. Sci.* **23**, 949 (1957).
14. S. Bottle and co-workers, *Eur. Polym. J.* **23**, 671 (1989).
15. Y. E. Kirsh, *Polym. Sci.* **35**(2), 98 (1993).
16. G. Odian, *Principles of Polymerization*, 3rd ed., Wiley-Interscience, 1991, p. 217.
17. R. T. Woodhams, Ph.D. Dissertation, Polytechnic Institute of Brooklyn, Brooklyn, N.Y., 1954.
18. V. Shtamm and co-workers, *Zh. Fiz. Khim.* **55**, 2289 (1981).
19. M. V. Encinas, E. A. Lissit, and J. Quiroz, *Eur. Polym. J.* **28**, 471 (1992).
20. K. C. Gupta, *J. Appl. Polym. Sci.* **53**, 71 (1994).
21. W. Kern and H. Cherdron, *Houben Weyl, Methoden der Organische Chemie*, 4th ed., Vol. **14**, Verlag, Stuttgart, Germany, 1961, p. 1106.
22. Ger. Pat. DE 3,532,747 (1987), A. Nuber and co-workers (to BASF).
23. S. C. Ng, *Eur. Polym. J.* **18**, 917 (1982).
24. F. Haaf, A. Sanner, and F. Straub, *Polym. J.* **17**(1), 143 (1985).
25. V. V. Kopeikin, Y. G. Santuryan, and M. Y. Danilova, *Khim. Farm. Zh.* **22**, 1253 (1988).
26. I. G. Gulis and co-workers, *Khim. Farm. Zh.* **25**(9), 82 (1991).
27. E. Senogles and R. Thomas, *J. Polym. Sci. Polym. Symp.* **49**, 203 (1975).
28. E. Senogles and R. Thomas, *J. Polym. Sci. Polym. Lett. Ed.* **16**, 555 (1978).
29. T. M. Karaputadze, V. I. Shumskii, and Y. E. Kirsh, *Vysokomol. Soedin. Ser. A* **20**, 1854 (1978).
30. V. R. Gromov and co-workers, *Eur. Polym. J.* **27**, 505 (1991).
31. M. Biswas and P. K. Mishra, *Polymer* **16**, 621 (1970).
32. G. D. Jones, in P. H. Plesch, ed., *The Chemistry of Cationic Polymerization*, Macmillan, New York, 1963, p. 554, Chapt. 14.
33. N. Tsubokawa, N. Takeda, and A. Kanamaru, *J. Polym. Sci. Polym. Lett. Ed.* **18**, 625 (1980).

34. N. Tsubokawa, H. Maruyama, and Y. Sone, *J. Macromol. Sci. Chem. A* **25**(2), 171 (1988).
35. N. Tsubokawa and co-workers, *J. Polym. Sci. Polym. Chem. Ed.* **31**, 3193 (1993).
36. E. Yoshida and co-workers, *J. Polym. Sci. Polym. Chem. Ed.* **31**, 1505 (1993).
37. E. Leonard-Stibbe and co-workers, *J. Polym. Sci. Polym. Chem. Ed.* **32**, 1551 (1994).
38. H. N. Cheng, T. E. Smith, and D. M. Vitus, *J. Polym. Sci. Polym. Lett. Ed.* **19**, 29 (1981).
39. J. R. Ebdon, T. N. Hackerby, and E. Senogles, *Polymer* **24**, 339 (1983).
40. T. Bartels, Y. Y. Tan, and G. Challa, *J. Polym. Sci.* **15**, 341 (1977).
41. D. W. Koetsier, G. Challa, and Y. Y. Tan, *Polymer* **17**, 1709 (1980).
42. D. W. Koetsier, Y. Y. Tan, and G. Challa, *J. Polym. Sci.* **18**, 1933 (1980).
43. G. O. R. Alberda van Ekenstein, D. W. Koetsie, and Y. Y. Tan, *Eur. Polym. J.* **17**, 845 (1981).
44. V. S. Rajan and J. Ferguson, *Eur. Polym. J.* **18**, 633 (1982).
45. I. V. Kotlyarskii and co-workers, *Vysokomol. Soedin. Ser. A* **31**, 1893 (1989).
46. J. Matuszewska-Czerwink and S. Polowski, *Eur. Polym. J.* **26**, 549 (1990).
47. U.S. Pat. 2,938,017 (1960), F. Grosser (to AF).
48. U.S. Pat. 5,286,826 (Feb. 15, 1994), J. S. Shih and S. Y. Tseng (to ISP).
49. J. W. Breitenbach and H. Axmann, in N. Platzer, ed., *Polymerization Kinetics and Technology*, Chapt. 7 (Advances in Chemistry Series 128, ACS, 1973).
50. E. Barabas and C. Adeyeye, *Anal. Profiles Drug Subst. Excipients* **24**, 87–163 (1996).
51. B. I. Da Silveira, *Eur. Polym. J.* **29**, 1095 (1993).
52. J. W. Breitenbach, *J. Polym. Sci.* **23**, 949 (1957).
53. J. W. Breitenbach and E. Wolf, *Makromol. Chem.* **18/19**, 217 (1956).
54. J. W. Breitenbach and A. Schmidt, *Monatsh. Chem.* **85**(1), 52 (1954).
55. T. P. Davis and M. B. Huglin, *Makromol. Chem.* **191**, 331 (1990).
56. O. Guven and M. Sen, *Polymer* **32**(13), 2491 (1991).
57. M. B. Huglin and M. Zakaria, *Polymer* **25**, 797 (1984).
58. T. Davis, M. Huglin, and D. Yip, *Polymer* **29**, 701 (1988).
59. J. Shih, J. C. Chuang, and R. B. Login, *Polym. Mater. Sci. Eng.* **72**, 374 (1995).
60. C. C. Anderson, F. Rodriguez, and D. A. Thurston, *J. Appl. Polym. Sci.* **23**, 2453 (1979).
61. H. Tenhu and F. Sundholm, *Makromol. Chem.* **185**, 2011 (1984).
62. P. Alexander and A. Charlesby, *J. Polym. Sci.* **23**, 355 (1957).
63. A. Chapiro and C. Legris, *Eur. Polym. J.* **25**, 305 (1989).
64. J. E. Davis and E. Senogles, *Aust. J. Chem.* **34**, 1413 (1981).
65. U.S. Pat. 4,699,146 (Oct. 13, 1987), D. L. Sieverding (to Valley Lab).
66. J. W. Copenhaver and M. H. Bigelow, *Acetylene and Carbon Monoxide Chemistry*, Reinhold Publishing Corp., New York, 1969, pp. 67–74.
67. *USP 23*, The United States Pharmacopeial Convention, Inc., Rockville, Md., 1995.
68. C. Wu, in C. Wu, ed., *Handbook of Size Exclusion Chromatography*, Marcel Dekker, Inc., New York, 1995, Chapt. 12.
69. L. Senak, C. Wu, and E. Malawer, *J. Liq. Chrom.* **10**, 1127 (1987).
70. H. Fikentscher and K. Herrle, *Mod. Plast.* **23**, 157, 212, 214, 216, 218 (1945).
71. J. Brandrup and E. H. Immergut, eds., *Polymer Handbook*, 3rd ed., John Wiley & Sons, Inc., New York, p. VII 18.
72. Y. Y. Tan and G. Challa, *Polymer* **17**, 739 (1976).
73. D. T. Turner and A. Schartz, *Polymer* **26**, 757 (1985).
74. P. Molyneux, in F. Franks, ed., *Water: A Comprehensive Treatise*, Vol. **4**, New York, 1975, pp. 569–801, Chapt. 7.
75. J. W. Breitenbach and E. Wolf, *Makromol. Chem.* **18/19**, 217 (1956).
76. R. Meza and L. Gargallo, *Eur. Polym. J.* **13**, 235 (1977).
77. Y. E. Kirsh, *Prog. Polym. Sci.* **18**, 519–542 (1993).

78. N. Shinyashiki and co-workers, *J. Phys. Chem.* **98**, 13612 (1994).
79. S. K. Jain and G. P. Johari, *J. Phys. Chem.* **92**, 5851 (1988).
80. M. J. Blandamer and J. R. Membrey, *J. Chem. Soc. Perkin II* 1400 (1974).
81. V. V. Kobayakov and co-workers, *Vysokomol. Soedin. Ser. A* **23**(1), 150 (1981).
82. D. A. Topchiev, personal communication, 1995.
83. Y. E. Kirsh and co-workers, *Eur. Polym. J.* **15**, 223 (1979).
84. Y. E. Kirsh and co-workers, *Eur. Polym. J.* **18**, 639 (1983).
85. E. Killmann and R. Bittler, *J. Polym. Sci. Part C* **39**, 247 (1972).
86. B. P. Molyneux and H. P. Frank, *J. Am. Chem. Soc.* **83**, 3169 (1961).
87. H. P. Frank, S. Barkin, and F. R. Eirich, *J. Am. Chem. Soc.* **61**, 1375 (1957).
88. W. Scholtan, *Makromol. Chem.* **11**, 131 (1953).
89. R. L. Reeves, S. A. Harkaway, and A. R. Sochor, *J. Polym. Sci.* **19**, 2427 (1981).
90. F. M. El Torki and co-workers, *J. Phys. Chem.* **91**, 3686 (1987).
91. T. Takagishi and co-workers, *J. Polym. Sci.* **22**, 185 (1984).
92. W. Gottardi, in S. Block, ed., *Disinfection, Sterilization and Preservation*, Lea & Febiger, 1991, Chapt. 8.
93. H. Schenck, P. Simak, and E. Haedicke, *J. Pharm. Sci.* **68**, 1505 (1979).
94. J. L. Zamora, *Am. J. Surg.* **151**, 400 (1986).
95. D. Horn and W. Ditter, in G. Hierholzer and G. Gortz, eds., *PVP-Iodine in Surgical Medicine*, Springer, New York, 1984.
96. H. N. Cheng, T. E. Smith, and D. M. Vitus, *J. Polym. Sci. Polym. Phys. Ed.* **23**, 461 (1985).
97. L. Turker and co-workers, *Colloid Polym. Sci.* **268**, 337 (1990).
98. A. Guner and M. Ataman, *Colloid Polym. Sci.* **272**, 175 (1994).
99. P. Molyneux and S. Vekavakaynondha, *J. Chem. Soc., Faraday Trans. 1* **82**, 291 (1986).
100. P. Molyneux and S. Vekavakaynondha, *J. Chem. Soc., Faraday Trans. 1* **82**, 635 (1986).
101. D. Oechsle and B. Fussnegger, *Brauwelt* **41**, 1780 (1990).
102. M. Ratto and co-workers, *Tappi* **76**(6), 67 (1993).
103. J. C. Hornby, *Tappi* **88** (Jan., 1995).
104. H. U. Jager and W. Denzinger, *Tenside* **6**, 428 (1991).
105. M. Paillet and co-workers, *Colloid Polym. Sci.* **271**, 311 (1993).
106. Y. J. Nikas and Blankschtein, *Langmuir* **10**, 3512 (1994).
107. Y. Almog, S. Reich, and M. Levy, *Brit. Polym. J.* **14**, 131 (1982).
108. A. J. Paine, *J. Polym. Sci. Polym. Chem. Ed.* **28**, 2485 (1990).
109. C. M. Tseng and co-workers, *J. Polym. Sci. Polym. Chem. Ed.* **28**, 2569 (1990).
110. H. L. Chen and H. Morawetz, *Eur. Polym. J.* **19**, 923 (1983).
111. I. Iliopoulos and R. Audebert, *J. Polym. Sci. Polym. Lett. Ed.* **26**, 2093 (1988).
112. I. Iliopoulos, J. L. Halary, and R. Audebert, *J. Polym. Sci. Polym. Chem. Ed.* **26**, 275 (1988).
113. I. Iliopoulos and R. Audebert, *Eur. Polym. J.* **24**(2), 171 (1988).
114. K. R. Shah, *Polymer* **28**, 1212 (1987).
115. M. J. Fernandez-Berridi and co-workers, *Polymer* **31**(1), 38 (1993).
116. M. T. Qurashi, H. S. Blair, and S. J. Allen, *J. Appl. Polym. Sci.* **46**, 255, 263 (1992).
117. J. F. Masson and R. St. John Manley, *Macromolecules* **24**, 6670 (1991).
118. C. M. Tam, M. Dal-Cin, and M. D. Guiver, *J. Membr. Sci.* **78**, 123 (1993).
119. C. M. Tam and co-workers, *Desalination* **89**, 275 (1993).
120. W. B. Stockton and M. F. Rubner, *Polym. Prepr.* **19**, 319 (1978).
121. H. D. Keith, F. J. Padden Jr., and T. P. Russell, *Macromolecules* **22**, 666 (1989).
122. R. Z. Greenley, in J. Brandrup and E. H. Immergut, eds., *Polymer Handbook*, 4th ed., John Wiley & Sons, Inc., New York, p. 318, Chapt. II.

123. G. Georgiev, C. Konstantinov, and V. Kabaivanov, *Macromolecules* **25**, 6302 (1992).
124. Ref. 125, p. II, 247.
125. E. E. Skorikova and co-workers, *Vysokomol. Soedin., Ser. B* **27**, 869 (1985).
126. W. M. Culbertson, in J. I. Kroschwitz, ed., *Encyclopedia of Polymer Science and Engineering*, 2nd ed., Vol. **9**, John Wiley & Sons, Inc., NY, 1987, p. 240.
127. M. Orbay, R. Laible, and L. Dulong, *Makromol. Chem.* **47**, 183 (1982).
128. J. F. Bork and L. E. Coleman, *J. Polym. Sci.* **43**, 413 (1960).
129. Van Paesschen and G. Smets, *Bull. Soc. Chem. Belg.* **64**, 173 (1955).
130. A. Chapiro and L. D. Trung, *Eur. Polym. J.* **10**, 1103 (1974).
131. K. Deboudt, M. Delporte, and C. Loucheux, *Macromol. Chem. Phys.* **196**, 279 (1995).
132. K. Y. Choi, *J. Appl. Polym. Sci.* **37**, 1429 (1989).
133. M. B. Huglin and K. S. Khairou, *Eur. Polym. J.* **24**, 239 (1988).
134. PVP/VA brochure No. 2302-194, ISP, 1990.
135. Yu. D. Semchikov and co-workers, *Eur. Polym. J.* **26**, 889 (1990).
136. R. Y. Lochhead, *Cosmet. Toiletries* **103**, 23 (1988).
137. G. Russell, *Eur. Adhes. Sealants* (June, 1989).
138. J. Jachowicz, M. Berthiaume, and M. Garcia, *Colloid Polym. Sci.* **263**, 847 (1985).
139. U.S. Pat. 3,910,862 (1975), E. S. Barabas and M. M. Fern (to GAF).
140. U.S. Pat. 3,914,403 (1975), K. Valan (to GAF).
141. Bulletin No. QO394, *International Specialty Products*, 1994.
142. Ger. Pat. 4,138,763 (1991), H. Meyer and A. Sanner (BASF).
143. U.S. Pat. 4,223,009 (1980), P. M. Chakrabarti (to GAF).
144. U.S. Pat. 5,015,708 (1991), J. S. Shih, T. E. Smith, and R. B. Login (to GAF).
145. J. S. Shih, J. C. Chuang, and R. B. Login, Vol. 67, American Chemical Society, Division of Polymeric Materials (Fall, 1992), p. 226.
146. U.S. Pat. 5,219,906 (1993), J. S. Shih and T. E. Smith (to ISP).
147. J. C. Hornby, J. D. Pelesko, and D. Jon, *Soap/Cosmet. Specialt.* (June, 1993).
148. S. L. Kopolow, R. B. Login, and M. Tazi, in C. G. Gebelein, T. C. Cheng, and U. C. Yang, eds., *Cosmetic and Pharmaceutical Application of Polymers*, Plenum Publishing Co., New York, 1991.
149. *Ganex Bulletin* (2302-191 5M-989), ISP Corp., 1989.
150. *Polectron Emulsion Copolymers Bulletin* (2302-104), GAF Corp., 1984.

ROBERT B. LOGIN  
Sybron Chemicals Inc.



## OLEFIN FIBERS

### Introduction

Olefin fibers, also called polyolefin fibers, are defined as manufactured fibers in which the fiber-forming substance is a synthetic polymer of at least 85 wt% ethylene, propylene, or other olefin units (1). Several olefin polymers are capable of forming fibers, but only polypropylene [9003-07-0] (PP) and, to a much lesser extent, polyethylene [9002-88-4] (PE) are of practical importance. Olefin polymers are hydrophobic and resistant to most solvents. These properties impart resistance to staining but cause the polymers to be essentially undyeable in an unmodified form.

The first commercial application of olefin fibers was for automobile seat covers in the late 1940s. These fibers, made from low density polyethylene (LDPE) by melt extrusion, were not very successful. They lacked dimensional stability, abrasion resistance, resilience, and light stability. The success of olefin fibers began when high density polyethylene (HDPE) was introduced in the late 1950s (see ETHYLENE POLYMERS, HDPE). Yarns made from this highly crystalline, linear polyethylene have higher tenacity than yarns made from the less crystalline, branched form (LDPE) (see ETHYLENE POLYMERS, LDPE). Markets were developed for HDPE fiber in marine rope where water resistance and buoyancy are important. However, the fibers also possess a low melting point, lack resilience, and have poor light stability. These traits caused the polyethylene fibers to have limited applications.

Isotactic polypropylene, based on the stereospecific polymerization catalysts discovered by Ziegler and Natta, was introduced commercially in the United States in 1957. Commercial polypropylene fibers followed in 1961. The first market of significance, contract carpet, was based on a three-ply, crimper-textured yarn. It competed favorably against wool and rayon-wool blends because of its lighter weight, longer wear, and lower cost. In the mid-1960s, the discovery of improved light stabilizers led to the development of outdoor carpeting based on polypropylene. In 1967, woven carpet backing based on a film warp and fine-filament fill was produced. In the early 1970s, a bulked-continuous-filament

**Table 1. Physical Properties of Commercial Fibers<sup>a</sup>**

Polymer	Standard tenacity, GPa <sup>b</sup>	Breaking elongation, %	Modulus, GPa <sup>b</sup>	Density, kg/m <sup>3</sup>	Moisture regain <sup>c</sup>
Olefin	0.16–0.44	20–200	0.24–3.22	910	0.01
Polyester	0.37–0.73	13–40	2.1–3.7	1380	0.4
Carbon	3.1	1	227	1730	
Nylon	0.23–0.60	25–65	0.5–2.4	1130	4–5
Rayon	0.25–0.42	8–30	0.8–5.3	1500	11–13
Acetate	0.14–0.16	25–45	0.41–0.64	1320	6
Acrylic	0.22–0.27	35–55	0.51–1.02	1160	1.5
Glass	4.6	5.3–5.7	89	2490	
Aramid	2.8	2.5–4.0	113	1440	4.5–7
Fluorocarbon	0.18–0.74	5–140	0.18–1.48	2100	
Polybenzimidazole	0.33–0.38	25–30	1.14–1.52	1430	15

<sup>a</sup>Ref. 2.<sup>b</sup>To convert GPa to psi, multiply by 145,000.<sup>c</sup>At 21°C and 65% rh.

(BCF) yarn was introduced for woven, texturized upholstery. In the mid-1970s, further improvement in light stabilization of polypropylene led to a staple product for automotive interiors and nonwoven velours for floor and wall carpet tiles. In the early 1980s, polypropylene was introduced as a fine-filament staple for thermal bonded nonwovens.

The growth of polyolefin fibers continues. Advances in olefin polymerization provide a wide range of polymer properties to the fiber producer. Inroads into new markets are being made through improvements in stabilization, and new and improved methods of extrusion and production, including multicomponent extrusion and spunbonded and meltblown nonwovens.

## Properties

**Physical Properties.** Table 1 (2) shows that olefin fibers differ from other synthetic fibers in two important respects: (1) olefin fibers have very low moisture absorption and thus excellent stain resistance and almost equal wet and dry properties, and (2) the low density of olefin fibers allows a much lighter weight product at a specified size or coverage. Thus 1 kg of polypropylene fiber can produce a fabric, carpet, etc, with much more fiber per unit area than a kilogram of most other fibers.

**Tensile Strength.** Tensile properties of all polymers are a function of molecular weight, morphology, and testing conditions. The effect of temperature on the tensile properties of a typical polypropylene fiber is shown in Figure 1 (3). Tensile properties are also affected by strain rate, as shown in Figure 2 (3). Lower temperature and higher strain rate result in higher breaking stresses at lower elongations, consistent with the general viscoelastic behavior of polymeric materials. Similar effects are observed on other fiber tensile properties, such as tenacity or stress at break, energy to rupture, and extension at break (4). Under

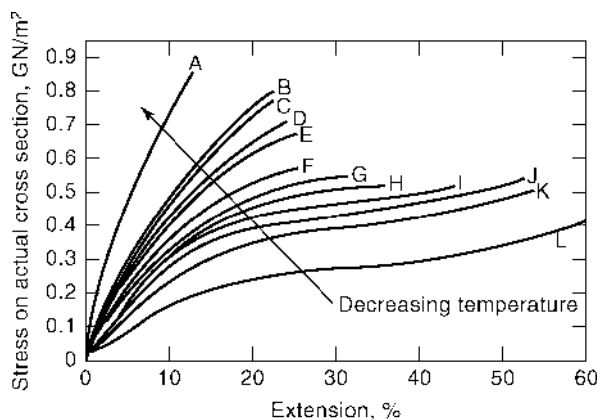


**Fig. 1.** Effect of temperature on tensile properties of polypropylene (3); strain rate =  $6.47 \times 10^{-4} \text{ s}^{-1}$ . In degrees Kelvin: A, 90; B, 200; C, 213; D, 227; E, 243; F, 257; G, 266; H, 273; I, 278; J, 283; K, 293; and L, 308 (broken at 74.8% extension,  $4.84 \times 10^8 \text{ N/m}^2$ ). To convert  $\text{GN/m}^2$  to  $\text{dyne/cm}^2$ , multiply by  $10^{10}$ .

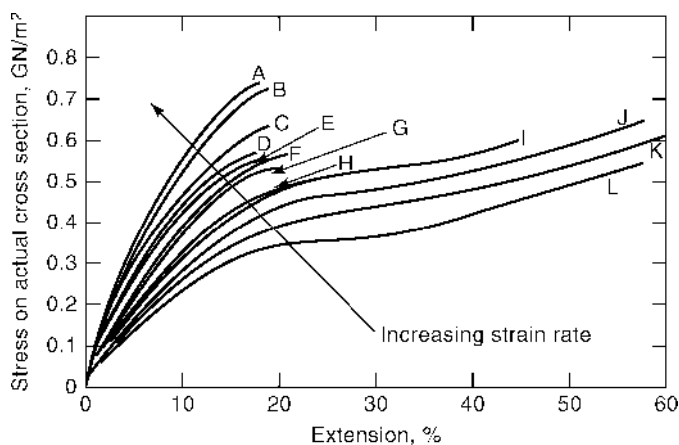


**Fig. 2.** Effect of strain rate on tensile properties of polypropylene at  $20^\circ\text{C}$  (3). In  $\text{s}^{-1}$ : A,  $4.9 \times 10^2$ ; B,  $2.48 \times 10^2$ ; C,  $1.26 \times 10^2$ ; D,  $6.3 \times 10^1$ ; E,  $3.2 \times 10^1$ ; F,  $2.87 \times 10^1$ ; G,  $2.3 \times 10^{-1}$ ; H,  $3.3 \times 10^{-2}$ ; I,  $1.33 \times 10^{-2}$ ; J,  $4.17 \times 10^{-3}$ ; K,  $1.67 \times 10^{-3}$ ; and L,  $3.3 \times 10^{-4}$ . To convert  $\text{GN/m}^2$  to  $\text{dyne/cm}^2$ , multiply by  $10^{10}$ .

the same spinning, processing, and testing conditions, higher molecular weight results in higher tensile strength. The effect of molecular weight distribution on tensile properties is complex because of the interaction with spinning conditions (4,5). In general, narrower molecular weight distributions result in higher breaking tenacity and lower elongation (4,6). The variation of tenacity and elongation with draw ratio for a given spun yarn correlates well with amorphous orientation (7,8). However, when different spun yarns are compared, neither average nor amorphous orientation completely explains these variations (9–11). Theory suggests that the number of tie molecules, both from molecules traversing the interlamellar region and especially those resulting from entanglements in the

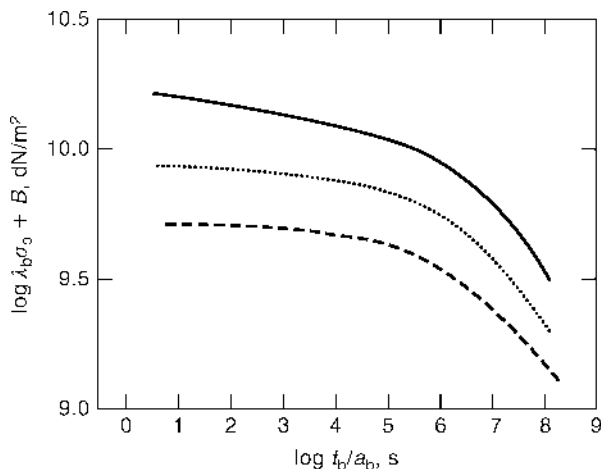


**Fig. 3.** Composite curve of true stress at break  $\lambda_b\sigma_b$  at 40°C vs reduced time to break  $t_b/a_b$  for polypropylene fibers of three draw ratios (15): (—),  $2.7 \times$  draw,  $B = 0$ ; (·····),  $3.5 \times$  draw,  $B = 0.2$  (---),  $4.5 \times$  draw,  $B = 0.4$ . Values of  $B$  are arbitrary.

interlamellar region, defines the range of tensile properties achievable using draw-induced orientation (12,13). Increased entanglements (more ties) result in higher tenacity and lower elongation.

**Creep, Stress Relaxation, and Elastic Recovery.** Olefin fibers exhibit creep, or time-dependent deformation under load, and undergo stress relaxation, or the spontaneous relief of internal stress. Because of the variety of molecular sizes and morphological states present in semicrystalline polymers, the creep and stress relaxation properties for materials such as polypropylene cannot be represented in one curve by using time-temperature superposition principles (14). However, given a spun yarn and thus a given structural state, curves for creep fracture (time to break under variable load) can be developed for different draw ratios, as shown in Figure 3 (15), indicating the importance of spun-yarn structure in a crystallizable polyolefin fiber. The same superposition can be carried out up to 110°C, where substantial reordering of polymer crystalline structure occurs (16).

High molecular weight and high orientation reduce creep. At a fixed molecular weight, the stress-relaxation modulus is higher for a highly crystalline sample prepared by slow cooling than for a smectic sample prepared by rapid quench (14). Annealing the smectic sample raises the relaxation modulus slightly, but not to the degree present in the fiber prepared by slow cooling.

Elastic recovery or resilience is the recovery of length upon release of stress after extension or compression. A fiber, fabric, or carpet must possess this property in order to spring back to its original shape after being crushed or wrinkled. Polyolefin fibers have poorer resilience than nylon; this is thought to be partially related to the creep properties of the polyolefins. Recovery from small strain cyclic loading is a function of temperature, as shown in Figure 4, and found to be a minimum for polypropylene at 10°C, near the glass-transition temperature  $T_g$  (17). The minimum for polyethylene is at 30°C, higher than the amorphous  $T_g$ . This

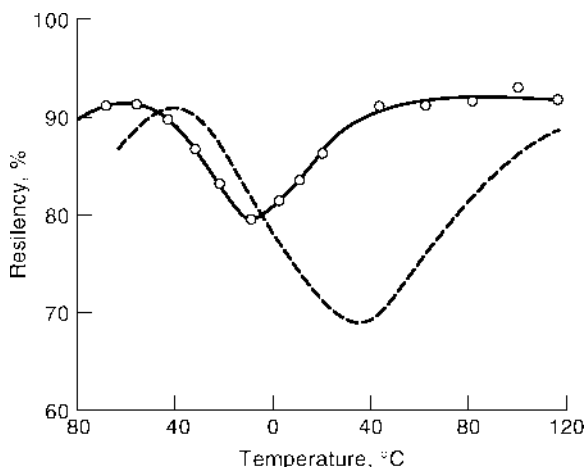


**Fig. 4.** Resiliency of polypropylene (—○—) and polyethylene (---), multifilament yarns as a function of temperature (17).

**Table 2. Thermal Properties of Olefins and Other Fiber-Forming Polymers**

Polymer <sup>a</sup>	$T_g$ , °C	$T_m$ , °C	Softening temperature, °C	Thermal degradation temperature, °C
High density polyethylene (HDPE)	-120	130	125	
i-Polypropylene (PP)	-20	165	160	290
i-Poly(1-butene)	-25	128		
i-Poly(3-methyl-1-butene)		315		
i-Poly(4-methyl-1-pentene)	18	250	244	
Poly(ethylene terephthalate) (PET)	70	265	235	400
Nylon-6,6	50	264	248	360

<sup>a</sup>i = isotactic.

minimum is thought to be associated with motions in the crystalline phase of the highly oriented crystalline structure (17).

**Chemical Properties.** The hydrocarbon nature of olefin fibers, lacking any polarity, imparts high hydrophobicity and, consequently, resistance to soiling or staining by polar materials, a property important in carpet and upholstery applications. Unlike the condensation polymer fibers, such as polyester and nylon, olefin fibers are resistant to acids and bases. At room temperature, polyolefins are resistant to most organic solvents, except for some swelling in chlorinated hydrocarbon solvents. At higher temperatures, polyolefins dissolve in aromatic or chlorinated aromatic solvents, and show some solubility in high boiling hydrocarbon solvents. At high temperatures, polyolefins are degraded by strong oxidizing acids.

**Thermal and Oxidative Stability.** The thermal transitions of several polyolefins are compared to other polymers in Table 2. In general, polyolefins undergo thermal transitions at much lower temperatures than condensation polymers, and thus the thermal and oxidative stability of polyolefin fibers are

**Table 3. Stabilization of Polypropylene Fiber by Polymeric HALS<sup>a</sup>**

HALS	Manufacturer	Carbon arc T50, h <sup>b</sup>	Florida T50, kJ/m <sup>2c,d</sup>
None		70	<105
Chimassorb 944	CIBA-GEIGY Corp.	300	293–418
Cyasorb 3346	American Cyanamid Co.	320	418
Spinuvex A-36	Montedison Corp.	370–400	293

<sup>a</sup>Test specimens were 0.5 tex (4.5 den) filaments containing 0.25% specified HALS (22).

<sup>b</sup>Hours to 50% retention of initial tensile strength under carbon arc exposure.

<sup>c</sup>kJ/m<sup>2</sup> to 50% retention of tensile strength; Florida under glass exposure.

<sup>d</sup>To convert kJ/m<sup>2</sup> to Langley, multiply by 239.

comparatively poor (18). They are highly sensitive to oxygen, which must be carefully controlled in all processing. The tertiary hydrogen in polypropylene imparts sensitivity to oxidative degradation by chain scission resulting in molecular weight degradation. Polyolefins are stabilized by hindered phenols or phosphites. Hindered phenol stabilizers provide moderate melt stability and good long-term heat aging, but undergo gas yellowing, which is a chemical reaction of phenolic compounds and nitrous oxide gases producing yellow-colored compounds. Typical sources of nitrous oxides are gas-fired heaters, dryers, and tenters, and propane-fueled lift trucks used in warehouses. Phosphites are good melt stabilizers and do not gas yellow, but have poor long-term heat aging. Preferred stabilizers are highly substituted phenols such as Cyanox 1790 and Irganox 1010, or phosphites such as Ultrinox 626 and Irgafos 168 (see ANTIOXIDANTS; HEAT STABILIZERS).

**Ultraviolet Degradation.** Polyolefins are subject to light-induced degradation (19); polyethylene is more resistant than polypropylene. Although the mechanism of UV degradation is different from thermal degradation, the resulting chain scission and molecular weight degradation is similar. In fiber applications, stabilization against light is necessary to prevent loss of properties. The stabilizer must be compatible, have low volatility, be resistant to light and thermal degradation itself, and must last over the lifetime of the fiber. Chemical and physical interactions with other additives must be avoided. Minimal odor and toxicity, colorlessness, resistance to gas yellowing, and low cost are additional requirements (see UV STABILIZERS).

Stabilizers that act as UV screens or energy quenchers are usually ineffective by themselves. Because polyolefins readily form hydroperoxides, the more effective light stabilizers are radical scavengers. Hindered amine light stabilizers (HALS) are favored, especially high molecular weight and polymeric amines that have lower mobility and less tendency to migrate to the surface of the fiber (20,21). This migration is commonly called *bloom*. Test results for some typical stabilizers are given in Table 3 (22).

**Flammability.** Flammability of polymeric materials is measured by many methods, most commonly by the limiting-oxygen-index test (ASTM D2863), which defines the minimum oxygen concentration necessary to support combustion, or the UL 94 vertical-burn test, which measures the burn length of a fabric. Most polyolefins can be made fire retardant using a stabilizer, usually a bromine-containing organic compound, and a synergist such as antimony oxide

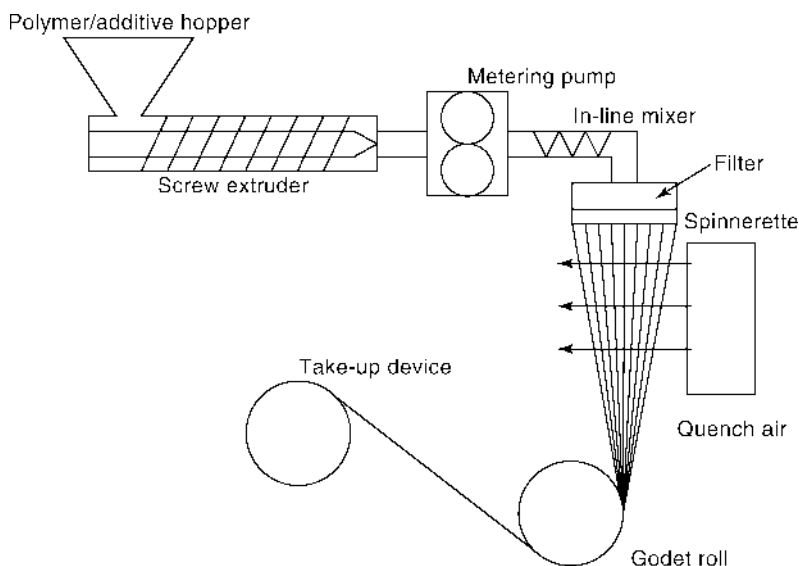


**Fig. 5.** Melt spinning process.

(23). However, the required loadings are usually too high for fibers to be spun. Fire-retardant polypropylene fibers exhibit reduced light and thermal resistance. Commercial fire-retardant polyolefin fibers have just recently been introduced, but as expected the fibers have limited light stability and poor luster. Where applications require fire retardancy, it is usually conferred by fabric finishes or incorporation of fire retardants in a latex, such as in latex-bonded nonwovens and latex-coated wovens.

**Dyeing Properties.** Because of their nonionic chemical nature, olefin fibers are difficult to dye. Oil-soluble dispersed dyes diffuse into polypropylene but readily bloom and rub off. In the first commercial dyeing of olefin fibers, nickel dyes such as UV-1084, also a light stabilizer, were used. The dyed fibers were colorfast but dull and hazy. A broad variety of polymeric dye-sites have been blended with polypropylene; nitrogen-containing copolymers are the most favored (24–26). A commercial acid-dyeable polypropylene fiber is prepared by blending the polypropylene with a basic amino-polyamide terpolymer (27). In apparel applications where dyeing is important, dyeable blends are expensive and create problems in spinning fine denier fibers. Hence, olefin fibers are usually colored by pigment blending during manufacture, called *solution dyeing* in the trade.

## Manufacture and Processing

Olefin fibers are manufactured commercially by melt spinning, similar to the methods employed for polyester and polyamide fibers (see POLYESTERS, FIBERS; POLYAMIDES, FIBERS). The basic process of melt spinning is illustrated in Figure 5. The polymer resin and ingredients, primarily stabilizers, pigments, and rheological modifiers, are fed into a screw extruder, melted, and extruded through

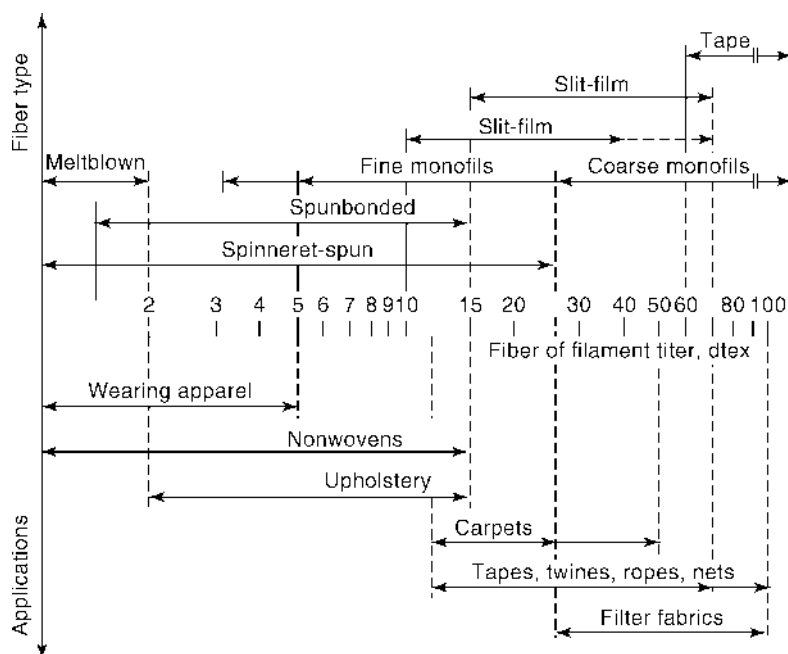


Fig. 6. Linear density of olefin fibers in various applications (29); dtex = 1.1 den.

fine diameter holes. The plate containing the holes is commonly called a *spinnerette*. A metering pump and a mixing device are usually installed in front of the spinneret to ensure uniform delivery and mixing to facilitate uniform draw-down at high speeds. In the traditional or long spinning process, the fiber is pulled through a long cooling stack-type quench chamber by a take-up device at speeds in the range of 50–2000 m/min and discontinuously routed to downstream finishing operations. In the short spinning process, filaments are cooled within a few centimeters of the spinneret at speeds of 50–150 m/min. Because of the lower speeds, fiber can be continuously routed to downstream finishing operations in a one-step process (28). Finishing operations include drawing the fiber to as much as six times its original length, heat treatment to relieve internal stresses, and texturizing processes, which are combinations of deformational and heat treatments. These treatments were developed to impart specific characteristics to the olefin fiber dependent on its end use. Commercial olefin fibers are produced in a broad range of linear densities, from 0.1 to 12 tex (1.1–110 den), to fit a variety of applications, as shown in Figure 6 (29).

**Extrusion.** Polymer resin and additives are melted and pumped through an extruder into a spinning pump. The pump meters the molten polymer through a filter system which removes particles from the molten polymer stream that might clog the capillaries of the spinneret or cause discontinuities in fine diameter fiber. These filters are typically either sand packs or metal screens. The polymer continues to a spinneret, where it is extruded through holes under pressure. These holes or capillaries define the size and shape of the extruded fiber. A spinneret may contain up to several thousand capillaries, typically 0.3–0.5 mm in



**Table 4. Molecular Weight Characterization Data for Polypropylene Samples<sup>a, b</sup>**

Code <sup>c</sup>	Melt flow rate <sup>d</sup>	$M_w \times 10^{-5}$	$M_w/M_n$	$M_z/M_w$	$M_v \times 10^{-5}$
High molecular weight polypropylene					
○ Narrow	4.2	2.84	6.4	2.59	2.40
△ Regular-broad	5.0	3.03	9.0	3.57	2.42
□ Broad-regular	3.7	3.39	7.7	3.54	2.71
Middle molecular weight polypropylene					
⊙ Narrow	11.6	2.32	4.7	2.81	1.92
▲ Regular	12.4	2.79	7.8	4.82	2.13
▣ Broad	11.0	2.68	9.0	4.46	2.07
Low molecular weight polypropylene					
⊕ Narrow	25.0	1.79	4.6	2.47	1.52
● Regular-narrow	23.0	2.02	6.7	3.18	1.66

<sup>a</sup>Ref. 30.<sup>b</sup>Figs. 7-9.<sup>c</sup>Narrow, regular, and broad refer to molecular weight distribution.<sup>d</sup>ASTM D1238 (Condition L; 230/2.16).

diameter. The length of the capillary is sized to the melt viscosity of the polymer. Typical length-to-diameter ratios of spinneret capillaries are 2:1 to 8:1. The spinneret holes can be arranged in a variety of hole spacings and patterns, including rectangular, round, and annular. Considerations include throughput rate, heat transfer required to quench the fiber, and fiber diameter.

The extrusion of olefin fibers is largely controlled by the polymer. Polyolefin melts are strongly viscoelastic, and melt extrusion of polyolefin fibers differs from that of polyesters and polyamides. Polyolefins are manufactured in a broad range of molecular weights and ratios of weight-average to number-average molecular weight ( $M_w/M_n$ ). Unlike the condensation polymers, which typically have molecular weights of 10,000–15,000 and  $M_w/M_n$  of approximately 2, polyolefins have weight-average molecular weights ranging from 50,000 to 1,000,000 and, as polymerized,  $M_w/M_n$  ranges from 4 to 15. Further control of molecular weight and distribution is obtained by chemical or thermal degradation. The full range of molecular weights used in olefin fiber manufacture is above 20,000, and  $M_w/M_n$  varies from 2 to 15. As molecular weight increases and molecular weight distribution broadens, the polymer melt becomes more pseudoplastic as indicated in Table 4 and shown in Figure 7 (30). In the sizing of extrusion equipment for olefin fiber production, the wide range of shear viscosities and thinning effects must be considered because these affect both power requirements and mixing efficiencies.

Fiber spinning is a uniaxial extension process, and the elongational viscosity behavior, which is the stress–strain relationship in uniaxial extension, is more important than the shear viscosity behavior. The narrower molecular weight distributions tend to be less thinning, and as shown in Figure 8 (30), elongational viscosity increases at higher extension rates. This leads to higher melt orientation, which in turn is reflected in higher spun fiber orientation, higher tenacity, and lower extensibility. In contrast, the broad molecular weight distributions tend to be more thinning and hence more prone to necking and fracture at high

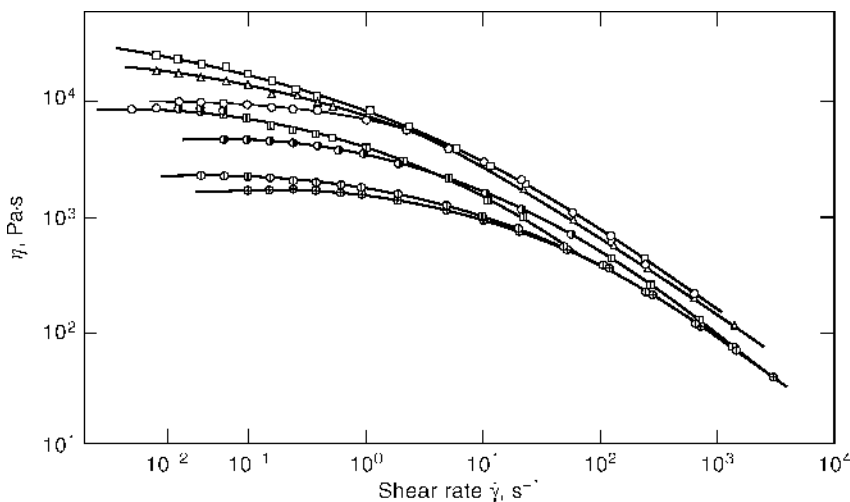


**Fig. 7.** Shear viscosity at 180°C of polypropylene of different molecular weight and distribution vs shear rate (30); see Table 4 for key.  $\text{Pa} \cdot \text{s} = 0.1 \text{ P}$ .

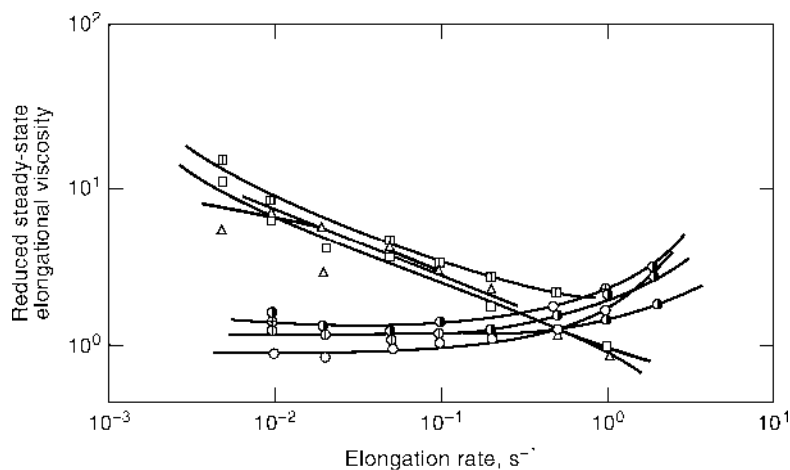


**Fig. 8.** Elongational viscosity at 180°C of polypropylene of different molecular weight and distribution (30); see Table 4 for key.

spinning speeds (30,31), but yield a less oriented, higher elongation spun fiber. The choice of an optimum molecular weight and molecular weight distribution is determined by the desired properties of the fiber and the process continuity on available equipment.

Because of the high melt viscosity of polyolefins, normal spinning melt temperatures are 240–310°C, which is 80–150°C above the crystalline melting point. Because of the high melt temperatures used for polyolefin fiber spinning, thermal stabilizers such as substituted hindered phenols are added. In the presence of pigments, the melt temperature must be carefully controlled to prevent color degradation and to obtain uniform color dispersion.

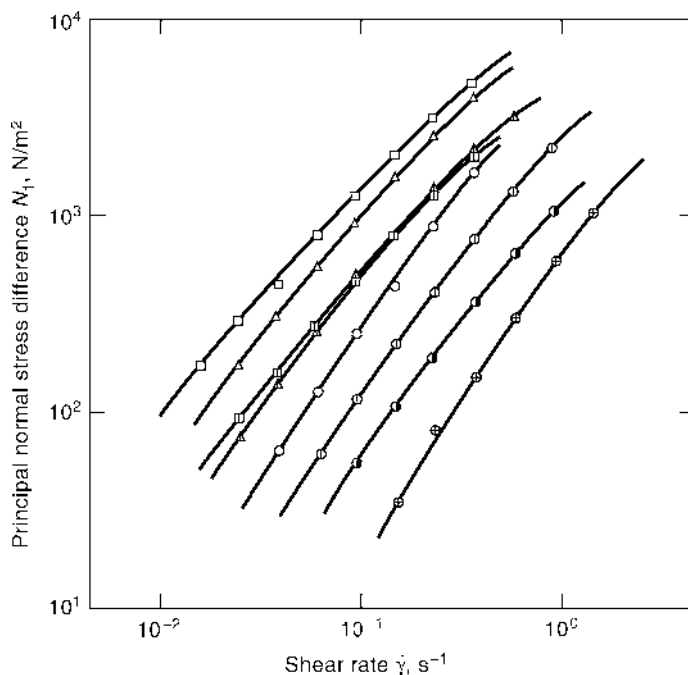


**Fig. 9.** First normal stress differences of polypropylene of different molecular weight and distribution (30); see Table 4 for key. To convert  $\text{N/m}^2$  to  $\text{dyne/cm}^2$ , multiply by 10.

Polyolefin melts have a high degree of viscoelastic memory or elasticity. First normal stress differences of polyolefins, a rheological measure of melt elasticity, are shown in Figure 9 (30). At a fixed molecular weight and shear rate, the first normal stress difference increases as  $M_w/M_n$  increases. The high shear rate obtained in fine capillaries, typically on the order of  $10^3$ – $10^4 \text{ s}^{-1}$ , coupled with the viscoelastic memory, causes the filament to swell (die swell or extrudate swell) upon leaving the capillary. On a molecular scale, the residence time in the region of die swell is sufficient to allow relaxation of any shear-induced orientation. However, high die swell significantly affects the drawdown or extension rate, leading to threadline breaks. Die swell can be reduced by lower molecular weight, narrower molecular weight distribution, or higher melt temperature.

**Quench.** Attempts have been made to model this nonisothermal process (32–35), but the complexity of the actual system makes quench design an art. Arrangements include straight-through, and outside-in and inside-out radial patterns (36). The optimum configuration depends on spinneret size, hole pattern, filament size, quench-chamber dimensions, take-up rate, and desired physical properties. Process continuity and final fiber properties are governed by the temperature profile and extension rate.

Polypropylene and other linear polyolefins crystallize more rapidly than most other crystallizable polymers. Unlike polyester, which is normally amorphous as spun, the fiber morphology of polyolefins is fixed in the spinning process; this limits the range of properties in subsequent drawing and annealing operations. In a low crystallinity state, sometimes called the paracrystalline or smectic

form, a large degree of local order still exists. It can be reached by extruding low molecular weight polyolefins, processing at low draw ratio, or by a rapid quench such as by using a cold water bath (37).

Quench is more commonly practiced commercially by a controlled air quench in which the rate of cooling is controlled by the velocity and temperature of the air. During normal cooling, crystallization occurs in the threadline. In-line X-ray scattering studies demonstrate that crystallization is extremely rapid; the full crystalline structure is almost completely developed in fractions of a second (38). Fiber spinning is an extensional process during which significant molecular orientation occurs. Under rapid crystallization, this orientation is fixed during the spinning process. Small-angle neutron-scattering studies of quiescent polypropylene crystallization show that the chain dimensions in both melt and crystallized forms are comparable (39). Although there may be significant relaxation of the amorphous region after spinning, the primary structure of the fiber is fixed during spinning and controls subsequent drawing and texturizing of the fiber. For fixed extrusion and take-up rates, a more rapid quench reduces the average melt-deformation temperature, increases relaxation times, and gives a more entangled melt when crystallization begins. The rapidly quenched fiber usually gives lower elongation and higher tenacity during subsequent draw (40). Using a very rapid quench, the melt may not be able to relax fast enough to sustain drawdown, resulting in melt fracture. Under conditions of a slow quench, the melt may totally relax, leading to ductile failure of the threadline.

A common measurement useful in predicting threadline behavior is fiber tension, frequently misnamed spinline stress. It is normally measured after the crystallization point in the threadline when the steady state is reached and the threadline is no longer deformed. Fiber tension increases as take-up velocity increases (38) and molecular weight increases. Tension decreases as temperature increases (41). Crystallinity increases slightly as fiber tension is increased (38). At low tension, the birefringence increases as tension is increased, leveling off at a spinline tension of 10 MPa (1450 psi) (38).

**Take-Up.** Take-up devices attenuate the spinline to the desired linear density and collect the spun yarn in a form suitable for further processing. A godet wheel is typically used to control the take-up velocity which varies from 1–2 m/s for heavy monofilaments to 10–33 m/s for fine yarns. The yarn can be stacked in cans, taken up on bobbins, or directly transferred to drawing and texturizing equipment.

In the spunbond process (Fig. 10), an aspiratory is used to draw the fibers in spinning and directly deposit them as a web of continuous, randomly oriented filaments onto a moving conveyor belt. In the meltblown process (Fig. 11), high velocity air is used to draw the extruded melt into fine-denier fibers that are laid down in a continuous web on a collector drum.

**Draw.** Polyolefin fibers are usually drawn to increase orientation and further modify the physical properties of the fiber. Linear density, necessary to control the textile properties, is more easily reduced during drawing than in spinning. The draw step can be accomplished in-line with spinning in a continuous spin-draw-texturing process (36,42) or in a second processing step. This second processing step allows simultaneous mixing of colors in a multi-ply continuous filament yarn for textiles. For staple fiber production, large bundles or tows

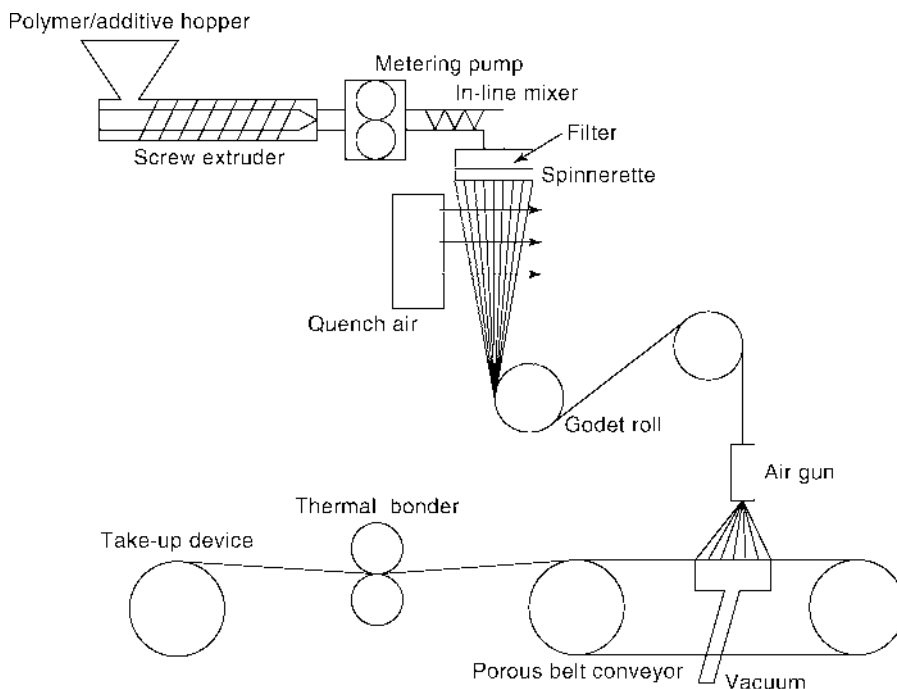


**Fig. 10.** Flow sheet for typical spunbond fabric manufacture.

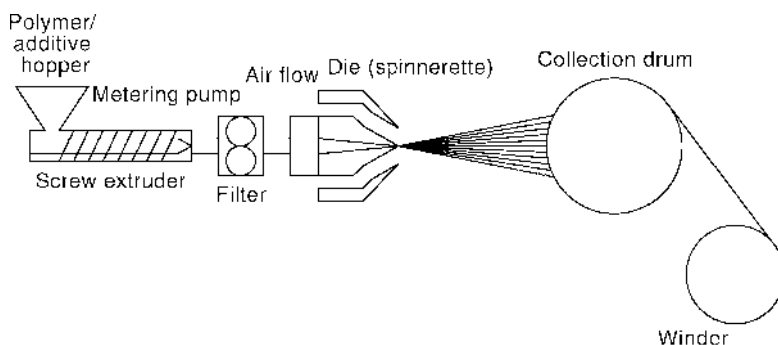


**Fig. 11.** Flow sheet for typical meltblown fabric manufacture.

consisting of up to a million or more filaments are stretched, texturized (crimped), and cut.

In secondary drawing operations, the aging properties of the spun yarn must be considered. Because polypropylene fibers have a low  $T_g$ , the spun yarn is restructured between spinning and drawing; this is more important as the smectic content is increased (43). The aging process depends on whether the yarn is stored on bobbins under tension or coiled in cans with no tension on the fiber. The aging of quick-quenched (smectic) polypropylene films has been studied (43). Stored at room temperature, the increase in yield stress is 5% in 24 hours. Similar data on

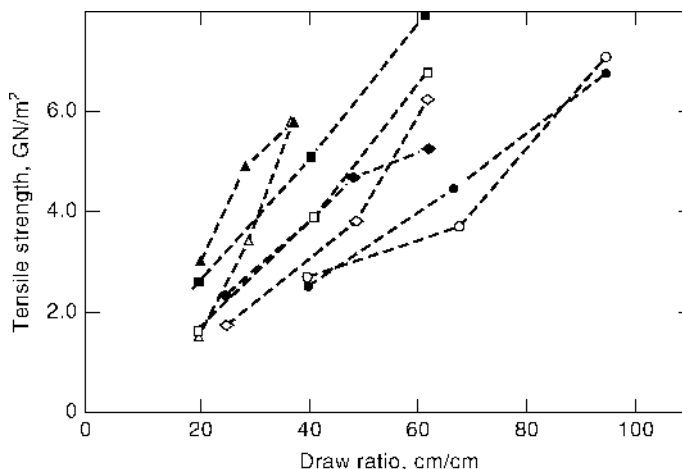


**Fig. 12.** Tensile strength vs draw ratio (6): 0.42 melt index spun at 50 m/min, ■, □; and 500 m/min, ▲, △; 12.0 melt index spun at 100 m/min, ●, ○; and 500 m/min, ◆, ◇. Open symbols = cold drawn and annealed at 140°C; filled symbols = drawn at 140°C. To convert GN/m<sup>2</sup> to dyne/cm<sup>2</sup>, multiply by 10<sup>10</sup>.

polypropylene spun fibers have not been published, but aging effects are similar. Drawn fiber properties, such as density, stress relaxation modulus, and heat of fusion, age because of collapse of excess free volume in the noncrystalline fraction (44).

The crystalline structure of the spun yarn affects the draw process. Monoclinic yarns tend to exhibit higher tenacity and lower elongation at low draw ratios than smectic yarns (6). They exhibit lower maximum draw ratios, undergo brittle fracture, and form microvoids (45) at significantly lower draw temperatures, which creates a chalky appearance. Studies of the effect of spun-yarn structure on drawing behavior show that the as-spun orientation and morphology determine fiber properties at a given draw ratio, as shown in Figure 12 (9,45,46). However, final fiber properties can be correlated with birefringence, a measure of the average orientation, as shown in Figure 13 (9,45). Fiber properties and amorphous orientation show good correlation in some studies (Fig. 14) (7,8), but in most studies the range of spun-yarn properties is limited. Such studies suggest that the deformation during draw primarily affects the interlamellar amorphous region at low draw ratio. At higher draw ratio, the crystalline structure is substantially disrupted.

**Texturing.** The final step in olefin fiber production is texturing; the method depends primarily on the application. For carpet and upholstery, the fiber is usually bulked, a procedure in which fiber is deformed by hot air or steam jet turbulence in a nozzle and deposited on a moving screen to cool. The fiber takes on a three-dimensional crimp that aids in developing bulk and coverage in the final fabric. Stuffer box crimping, a process in which heated tow is overfed into a restricted outlet box, imparts a two-dimensional sawtooth crimp commonly found in olefin staple used in carded nonwovens and upholstery yarns.

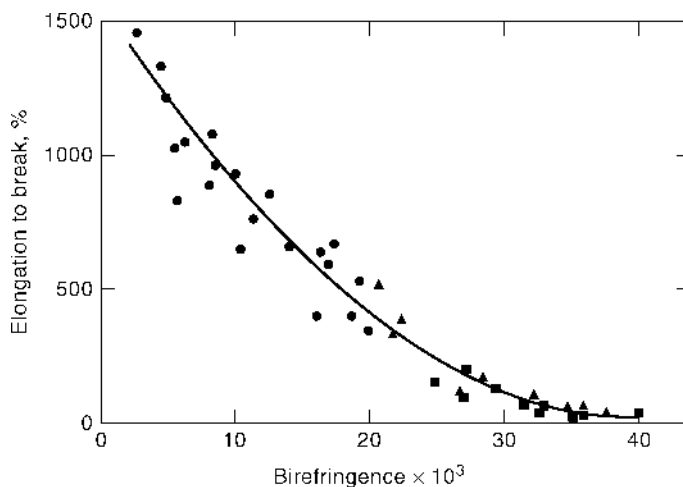


**Fig. 13.** Elongation to break as a function of birefringence for undrawn, hot-drawn, and cold-drawn annealed fibers (6): ●, undrawn; ▲, cold-drawn, annealed at 140°C; ■, hot-drawn at 140°C.

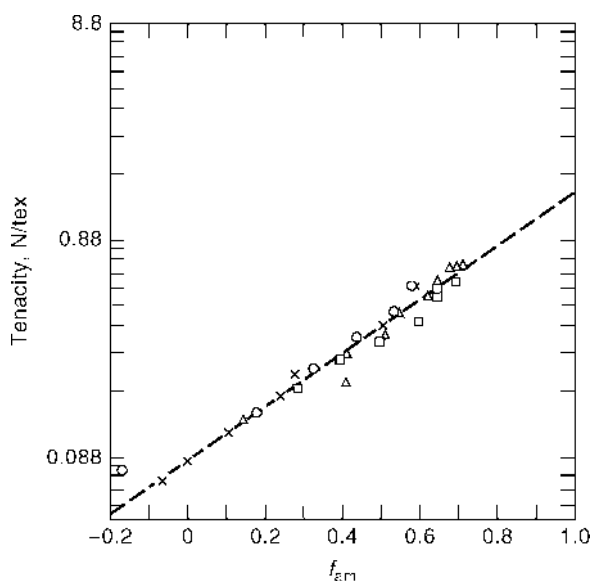


**Fig. 14.** Tenacity as a function of amorphous orientation ( $f_{am}$ ) for polypropylene fibers and films (7). Film drawn at 135°C (○), 110°C (×), and 90°C (□). Δ, Heat-set fiber. To convert N/tex to gf/den, multiply by 11.3. Tenacity<sub>max</sub> = 1.3 N/tex (15 gf/den).

**Slit-Film Fiber.** A substantial volume of olefin fiber is produced by slit-film or film-to-fiber technology (29). For producing filaments with high linear density, above 0.7 tex (6.6 den), the production economics are more favorable than monofilament spinning (29). The fibers are used primarily for carpet backing and rope or cordage applications. The processes used to make slit-film fibers are versatile and economical.

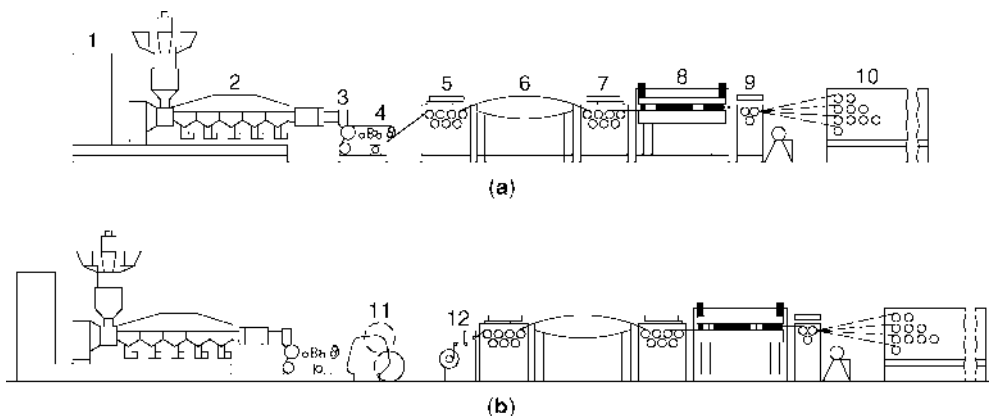


**Fig. 15.** Production lines for stretched film tape (29): (a) continuous production line for film tape; (b) discontinuous production lines for film and film tape. 1, Control cabinet; 2, extruder; 3, flat die; 4, chill roll; 5, septet (seven rolls); 6, hot plate; 7, septet (seven rolls); 8, heat-setting oven; 9, trio (three rolls); 10, bobbin winder; 11, film winder; and 12, film-unrolling stand.

The equipment for the slit-film fiber process is shown in Figure 15 (29). An olefin film is cast, and, as in melt spinning, the morphology and composition of the film determine the processing characteristics. Fibers may be produced by cutting or slitting the film, or by chemomechanical fibrillation. The film is fibrillated mechanically by rubbing or brushing. Immiscible polymers, such as polyethylene or polystyrene (PS), may be added to polypropylene to promote fibrillation. Many common fiber-texturing techniques such as stuffer-box, false-twist, or knife-edge treatments improve the textile characteristics of slit-film fibers.

Several more recent variations of the film-to-fiber approach result in direct conversion of film to fabric. The film may be embossed in a controlled pattern and subsequently drawn uniaxially or biaxially to produce a variety of nonwoven products (47). Addition of chemical blowing agents to the film causes fibrillation upon extrusion. Nonwovens can be formed directly from blown film using a unique radial die and control of the biaxial draw ratio (48) (see NONWOVEN FABRICS, STAPLE FIBERS).

**Bicomponent Fibers.** Polypropylene fibers have made substantial inroads into nonwoven markets because they are easily thermal bonded. Further enhancement in thermal bonding is obtained using bicomponent fibers (49). In these fibers, two incompatible polymers, such as polypropylene and polyethylene, polyester and polyethylene, or polyester and polypropylene, are spun together to give a fiber with a side-by-side or core-sheath arrangement of the two materials. The lower melting polymer can melt and form adhesive bonds to other fibers; the higher melting component causes the fiber to retain some of its textile characteristics.

Bicomponent fibers have also provided a route to self-texturing (self-crimping) fibers. The crimp results from the length differential developed during processing caused by differential shrinkage in the two polymers in side-by-side or eccentric core-sheath configurations (50).



Conventional spinning technology is limited in the production of very fine denier filaments because of spinning and mass uniformity problems as the melt drawdown is increased. Ultrafine filaments (microfibers) can be produced through bicomponent technology by extruding two or more components together as a single fiber and later separating the components through chemical or mechanical processes. Fibers of 0.1–0.001 tex ( $\sim 1$ –0.01 den) per filament can be produced (50,51).

**Meltblown, Spunbond, and Spurted Fibers.** A variety of directly formed nonwovens exhibiting excellent filtration characteristics are made by meltblown processes (52), producing very fine, submicrometer filaments. A simple schematic of the die is shown in Figure 11. A stream of high velocity hot air is directed on the molten polymer filaments as they are extruded from a spinneret. This air attenuates, entangles, and transports the fiber to a collection device. Because the fiber cannot be separated and wound for subsequent processing, a nonwoven web is directly formed. Mechanical integrity of the web is usually obtained by thermal bonding or needling, although other methods, such as latex bonding, can be used. Meltblown fabrics are made commercially from polypropylene and polyethylene. The webs are soft, breathable, and drapable (53–55).

In the spunbond process, the fiber is spun similarly to conventional melt spinning, but the fibers are attenuated by air drag applied at a distance from the spinneret (see NONWOVEN FABRICS). This allows a reasonably high level of filament orientation to be developed. The fibers are directly deposited onto a moving conveyor belt as a web of continuous randomly oriented filaments. As with meltblown webs, the fibers are usually thermal bonded or needled (53).

Pulp-like olefin fibers are produced by a high pressure spurling process developed by Hercules, Inc. and Solvay, Inc. Polypropylene or polyethylene is dissolved in volatile solvents at high temperature and pressure. After the solution is released, the solvent is volatilized, and the polymer expands into a highly fluffed, pulp-like product. Additives are included to modify the surface characteristics of the pulp. Uses include felted fabrics, substitution in whole or in part for wood pulp in papermaking, and replacement of asbestos in reinforcing applications (56).

**High Strength Fibers.** The properties of commercial olefin fibers are far inferior to those theoretically attainable. Theoretical and actual strengths of common commercial fibers are listed in Table 5 (57). A number of methods, including superdrawing (58), high pressure extrusion (59), spinning of liquid crystalline polymers or solutions (60), gel spinning (61–65), and hot drawing (66) produce higher strengths than those given in Table 5 for commercial fibers, but these methods are tedious and uneconomical for olefin fibers. A high modulus commercial polyethylene fiber with properties approaching those of aramid and graphite fibers (Table 6) (67) is prepared by gel spinning (68) (see CARBON FIBERS; POLYAMIDES, AROMATIC). Although most of these techniques produce substantial increases in modulus, higher tensile strengths are currently available only from gel spinning or dilute fibrillar crystal growth. Even using these techniques, the maximum strengths observed to date are only a fraction of the theoretical strengths.

**Hard-Elastic Fibers.** Hard-elastic fibers are prepared by annealing a moderately oriented spun yarn at high temperature under tension. They are

**Table 5. Theoretical and Actual Strengths of Commercial Fibers<sup>a</sup>**

Polymer	Density, kg/m <sup>3</sup>	Molecular area, nm <sup>2</sup>	Theoretical strength, GPa <sup>b</sup>	Strength of commercial fiber, GPa <sup>b</sup>
Polyethylene	960	0.193	31.6	0.76
Polypropylene	910	0.348	17.6	0.72
Nylon-6	1140	0.192	31.9	0.96
Polyoxymethylene	1410	0.185	32.9	
Poly(vinyl alcohol)	1280	0.228	26.7	1.08
Poly( <i>p</i> -benzamide)	1430	0.205	29.7	3.16
Poly(ethylene terephthalate)	1370	0.217	28.1	1.15
Poly(vinyl chloride)	1390	0.294	20.8	0.49
Rayon	1500	0.346	17.7	0.69
Poly(methyl methacrylate)	1190	0.667	9.2	

<sup>a</sup>Ref. 56.<sup>b</sup>To convert GPa to psi, multiply by 145,000.**Table 6. Properties of Commercial High Strength Fibers<sup>a</sup>**

Fiber	Density, kg/m <sup>3</sup>	Strength, GPa <sup>b</sup>	Modulus, GPa <sup>b</sup>	Elongation to break, %	Filament diameter, mm
Polyethylene	970	2.6	117	3.5	0.038
Aramid	1440	2.8	113	2.8	0.012
S-glass	2490	4.6	89	5.4	0.009
Graphite	1730	3.1	227	1.2	0.006
Steel whiskers	7860	2.3	207	1.3	0.250

<sup>a</sup>Ref. 66.<sup>b</sup>To convert GPa to psi, multiply by 145,000.

prepared from a variety of olefin polymers, acetal copolymers, and polypivalolactone (69,70). Whereas the strengths observed are comparable to those of highly drawn commercial fiber, in the range 0.52–0.61 N/tex (6–7 gf/den), the recovery from elongation is substantially better. Hard-elastic fibers typically exhibit 90% recovery from 50% elongation, whereas highly drawn, high tenacity commercial fibers exhibit only 50–75% recovery from 5% elongation. The mechanism of elastic recovery differs from the entropic models normally used to explain plastic properties. The hard elastic fibers are thought to deform through opening of the lamellae stacked structure, resulting in void formations; recovery is controlled by energy considerations. Although there are potential uses in applications involving substantial deformation, products such as stretch fabrics and hard-elastic fibers are not yet used commercially.

## Economic Aspects

Polyolefin fiber (from polypropylene or ethylene polymers) has continued to be one of the fastest growing segments of the synthetic fiber industry. Worldwide

production has been increasing at an annual rate of 6% since 1996 and reached 5.5 million ton in 1999. Polyolefin fibers account for 18% of the worldwide synthetic fibers market. Polypropylene fibers predominate and account for 89–95% of the polyolefin production in Western Europe and the United States. The remainder is manufactured from polyethylene. Polypropylene fibers account for 80% usage in Japan (71).

The principal use for polyolefin fibers is in consumer products. The primary use is the production of carpets and rugs, and includes backings. Polyolefins in the form of nonwoven fabrics is the second largest use.

Nonwoven fabrics continue to be the largest growing segment in the textile industry. In 2001, worldwide consumption was 3.5 billion ton valued at over \$14 billion. Between 1997 and 2001, world consumption grew at a rate of 11.2%/year. For much of the past decade, solid growth has occurred in industrialized nations. Double-digit growth is now seen in developing nations (primarily Asia). In 2001, developing countries consumed 39% of all nonwovens produced. Consumption is up from 11% in 1988. Use should continue to grow at the rate of 10–12% through 2006 (72).

Demand for nonwoven roll goods currently exceeds local capacity by 50%. Growth, particularly in China, has seen expansion of local manufacturing capabilities. In North America, Western Europe, and Japan, demand for nonwovens is expected to increase at 3–5%/year through 2006.

Industrial applications of polyolefin fibers include woven and nonwoven geotextiles, agricultural fabrics, construction sheeting, automobile fabrics, filtration media, rope/twine, woven bags, narrow-woven web and tapes, tents, and tarpaulins. Geosynthetic fabrics will continue to be a growing market for polypropylene nonwovens.

## Applications

Olefin fibers are used for a variety of purposes from home furnishings to industrial applications. These include carpets, upholstery, drapery, rope, geotextiles, and both disposable and nondisposable nonwovens. Fiber mechanical properties, relative chemical inertness, low moisture absorption, and low density contribute to desirable product properties. Olefin fiber use in apparel has been restricted by low melting temperatures, which make machine drying and ironing of polyethylene and polypropylene fabrics difficult or impossible. However, this market is increasing as manufacturers take advantage of the wicking properties (moisture transport) as in lightweight sportswear (73).

Polypropylene fibers are used in every aspect of carpet construction from face fiber to primary and secondary backings. Polypropylene's advantages over jute as carpet backing are dimensional stability and minimal moisture absorption. Drawbacks include difficulty in dyeing and higher cost. Bulked-continuous-filament (BCF) carpet yarns provide face fiber with improved crimp and elasticity. BCF carpet yarns are especially important in contract carpets, characterized by low dense loops, where easy cleaning is an advantage.

Olefin fiber is an important material for nonwovens (74). The geotextile market is still small, despite expectations that polypropylene is to be the

principal fiber in such applications. Disposable nonwoven applications include hygienic coverstock, sanitary wipes, and medical roll goods. The two competing processes for the coverstock market are thermal-bonded carded staple and spunbond, both of which have displaced latex-bonded polyester because of improved strength, softness, and inertness.

A special use for meltblown olefin fiber is in filtration media such as surgical masks and industrial filters (75). The high surface area of these ultrafine filament fibers permits preparation of nonwoven filters with effective pore sizes as small as 0.5  $\mu\text{m}$ .

Other applications, including rope, cordage, outdoor furniture webbing, bags, and synthetic turf, make up the remaining segments of the olefin fiber market. Spunbond polyethylene is used in packaging applications requiring high strength and low weight. Specialty olefin fibers are employed in asphalt and concrete reinforcement (76–79). Hollow fibers have been tested in several filtration applications (80,81). Ultrafine fibers are used in synthetic leather, silk-like fabrics, and special filters (50,51). These fibers are also used in sports outerwear, where the tight weaves produce fabrics that are windproof and waterproof, but are able to pass vapors from perspiration and thus keep the wearer cool and dry (51). If the economics of the high modulus olefin fibers becomes more favorable, substantial markets could be developed in reinforced composites such as boat hulls (67).

## BIBLIOGRAPHY

"Olefin Fibers" in *EPST* 1st ed., Vol. 9, pp. 403–440, by Victor L. Erlich, Reeves Brothers, Inc.; in *EPSE* 2nd ed., Vol. 10, pp. 373–395, by L. M. Landoll, Hercules, Inc.; in *EPST* 3rd ed., Vol. 10, pp. 718–739, by C. J. Wust and E. G. Gammelgaard, FiberVisions.

## CITED PUBLICATIONS

1. The Textile Fiber Products Identification Act, Public Law 85–897, Washington, D.C. (Sept. 1958).
2. *Text. World* **134**, 49 (Nov. 1984).
3. I. M. Hall, *J. Polym. Sci.* **54**, 505 (1961).
4. F. Lu and J. E. Spruiell, *J. Appl. Polym. Sci.* **34**, 1521 (1987).
5. J. E. Flood and S. A. Nulf, *Polym. Eng. Sci.* **30**, 1504 (1990).
6. H. S. Brown, T. L. Nemzek, and C. W. Schroeder, paper presented at *The 1983 Fiber Producer Conference*, Greenville, S.C., Apr. 13, 1983, sponsored by Fiber World, Bril-liam Publishing Co., Atlanta, Ga.
7. R. J. Samuels, *Structural Polymer Properties*, Wiley-Interscience, New York, 1974.
8. F. Geleji and co-workers, *J. Polym. Sci. Polym. Symp.* **58**, 253 (1977).
9. H. P. Nadella, J. E. Spruiell, and J. L. White, *J. Appl. Polym. Sci.* **22**, 3121 (1978).
10. A. J. de Vries, *Pure Appl. Chem.* **53**, 1011 (1981).
11. A. J. de Vries, *Pure Appl. Chem.* **54**, 647 (1982).
12. D. T. Grubb, *J. Polym. Sci., Polym. Phys. Ed.* **21**, 165 (1983).
13. D. Thirion and J. F. Tassin, *J. Polym. Sci., Polym. Phys. Ed.* **21**, 2097 (1983).
14. G. Attalla, I. B. Guanella, and R. E. Cohen, *Polym. Eng. Sci.* **23**, 883 (1983).
15. A. Takaku, *J. Appl. Polym. Sci.* **26**, 3565 (1981).

16. A. Takaku, *J. Appl. Polym. Sci.* **25**, 1861 (1980).
17. G. M. Bryant, *Text. Res. J.* **37**, 552 (1967).
18. L. Reich and S. S. Stivala, *Rev. Macromol. Chem.* **1**, 249 (1966).
19. D. J. Carlsson and D. M. Wiles, *J. Macromol. Sci. Rev., Macromol. Chem.* **14**, 65 (1976).
20. D. J. Carlsson, A. Garton, and D. M. Wiles, in G. Scott, ed., *Developments in Polymer Stabilisation*, Applied Science Publishers, London, 1979, p. 219.
21. F. Gugumaus, in Ref. 20, p. 261.
22. L. M. Landoll and A. C. Schmalz, private communication, Hercules Inc., Oxford, Ga., 1986.
23. J. Green, in M. Lewin, S. M. Atlas, and E. M. Pierce, eds., *Flame-Retardant Polymeric Materials*, Vol. 3, Plenum Press, New York, 1982, Chapt. 1.
24. U.S. Pat. 3,873,646 (Mar. 25, 1975), H. D. Irwin (to Lubrizol Corp.).
25. U.S. Pat. 3,653,803 (Apr. 4, 1972), H. C. Frederick (to E. I. du Pont de Nemours & Co., Inc.).
26. U.S. Pat. 3,639,513 (Feb. 1, 1972), K. Sadakata, Mitaka-shi, M. Sasaki, H. Masahiro, Yamaguchi-ken, Y. Nakamura, Y. Mikida, K. Ito, and K. Kimura (to Mitsubishi Rayon Co., Ltd.).
27. U.S. Pat. 3,433,853 (Mar. 18, 1969), R. H. Earle, A. C. Schmalz, and C. A. Soucek (to Hercules Inc.).
28. K. Hawn and R. Meriggi, *Nonwovens World* 44 (Sept. 1987).
29. H. Krassig, *J. Polym. Sci., Macromol. Rev.* **12**, 321 (1977).
30. W. Minoshima, J. L. White, and J. E. Spruiell, *Polym. Eng. Sci.* **20**, 1166 (1980).
31. O. Ishizuka and co-workers, *Sen-i Gakkaishi* **31**, T372 (1975).
32. S. Kase and T. Matsuo, *J. Polym. Sci., Part A* **3**, 2541 (1965).
33. S. Kase and T. Matsuo, *J. Appl. Polym. Sci.* **11**, 251 (1967).
34. C. D. Han and R. R. Lamonte, *Trans. Soc. Rheol.* **16**, 447 (1972).
35. R. R. Lamonte and C. D. Han, *J. Appl. Polym. Sci.* **16**, 3285 (1972).
36. F. Fourne, *IFJ* **3**, 30 (Aug., 1988).
37. C. Prost and co-workers, *Makromol. Chem., Macromol. Symp.* **23**, 173 (1989).
38. H. P. Nadella, H. M. Henson, J. E. Spruiell, and J. L. White, *J. Appl. Polym. Sci.* **21**, 3003 (1977).
39. D. G. H. Ballard and co-workers, *Polymer* **20**, 399 (1979); **23**, 1875 (1982).
40. W. C. Sheehan and T. B. Cole, *J. Appl. Polym. Sci.* **8**, 2359 (1964).
41. Ref. 20, p. 1541.
42. R. Wiedermann, *Chemiefasern Textilind.* **28/80**, 888 (1978).
43. D. M. Gezovich and P. H. Geil, *Polym. Eng. Sci.* **8**, 210 (1968).
44. C. P. Buckley and M. Habibullah, *J. Appl. Polym. Sci.* **26**, 2613 (1981).
45. H. Bodaghi, J. E. Spruiell, and J. L. White, *Intern. Polym. Processing* **III**, 100 (1988).
46. A. Garten and co-workers, *J. Polym. Sci., Polym. Phys. Ed.* **15**, 2013 (1977).
47. U.S. Pat. 3,137,746 (June 16, 1964), D. E. Seymour and D. J. Ketteridge (to Smith and Nephew, Ltd.).
48. U.S. Pat. 4,085,175 (Apr. 18, 1978), H. W. Keuchel (to PNC Corp.).
49. *Text. Month* 10 (Aug. 1983).
50. D. O. Taurat, *IFJ* **3**, 24 (May 1988).
51. W. R. Baker, *IFJ* **7**, 7 (Apr. 1992).
52. R. R. Buntin and D. T. Lohkamp, *TAPPI* **56**, 74 (1973).
53. J. Zhou and J. E. Spruiell, *Nonwovens—An Advanced Tutorial*, TAPPI Press, Atlanta, Ga., 1989.
54. L. C. Wadsworth and A. M. Jones, Paper presented at *INDA/TEC, The International Nonwovens Technological Conference*, Philadelphia, Pa., June 2–6, 1986.

55. A. M. Jones and L. C. Wadsworth, Paper presented at *TAPPI 1986 Nonwovens Conference*, Atlanta, Ga., Apr. 21–24, 1986.
56. T. W. Rave, *Chemtech* **15**, 54 (Jan. 1985).
57. T. Ohta, *Polym. Eng. Sci.* **23**, 697 (1983).
58. M. Kamezawa, K. Yamada, and M. Takayanagi, *J. Appl. Polym. Sci.* **24**, 1227 (1979).
59. H. H. Chuah and R. S. Porter, *J. Polym. Sci., Polym. Phys. Ed.* **22**, 1353 (1984).
60. J. L. White and J. F. Fellers, *J. Appl. Polym. Sci., Appl. Polym. Symp.* **33**, 137 (1978).
61. P. Smith and P. J. Lemstra, *Makromol. Chem.* **180**, 2983 (1979).
62. P. Smith and P. J. Lemstra, *J. Mater. Sci.* **15**, 505 (1980).
63. P. Smith and P. J. Lemstra, *Polymer* **21**, 1341 (1980).
64. B. Kalb and A. J. Pennings, *Polymer* **21**, 3 (1980).
65. B. Kalb and A. J. Pennings, *J. Mater. Sci.* **15**, 2584 (1980).
66. A. F. Wills, G. Capaccio, and I. M. Ward, *J. Polym. Sci., Polym. Phys. Ed.* **18**, 493 (1980).
67. R. C. Winckelhofer, Paper presented at *TAPPI 1985 Nonwovens Symposium*, Myrtle Beach, S.C., Apr. 21–25, 1985.
68. U.S. Pat. 4,413,110 (Nov. 1, 1983), S. Kavesh and D. C. Prevorsek (to Allied-Signal Inc.).
69. R. J. Samuels, *J. Polym. Sci., Polym. Phys. Ed.* **17**, 535 (1979).
70. S. L. Cannon, G. B. McKenna, and W. O. Statton, *J. Polym. Sci., Macromol. Rev.* **11**, 209 (1976).
71. B. Davenport, W. Cox, F. Dubois, and M. Yoneyama, *Chemical Economics Handbook*, SRI International, Menlo Park, Calif., Nov. 2000.
72. B. F. Hadjuk, T. Sasano, and S. Schlag, *Chemical Economics Handbook*, SRI International, Menlo Park, Calif., Jan. 2003.
73. *Am. Tex.* **13**, 44 (Dec. 1984).
74. R. G. Mansfield, *Nonwovens Ind.* **16**, 26 (Feb. 1985).
75. W. Shoemaker, *Nonwovens Ind.* **15**, 52 (Oct. 1984).
76. D. J. Hannant, *Fiber Cements and Fiber Concretes*, John Wiley & Sons, Inc., New York, 1978.
77. *Nonwovens Rept.* **87**, 1 (July 1978).
78. U.S. Pat. 4,492,781 (Jan. 8, 1985), F. J. Duszak, J. P. Modrak, and D. Deaver (to Hercules Inc.).
79. J. P. Modrak, Paper presented at *19th Paving Conference and Symposium*, Albuquerque, N. Mex., Jan. 12, 1982.
80. A. G. Bondarenko and co-workers, *Fibre Chem.* **14**, 246 (May–June 1982).
81. *Daily News Record* **11**, 12 (May 4, 1981).

CARL J. WUST  
ERIK GRANN GAMMELGAARD  
FiberVisions

## OPTICAL FIBERS

### Introduction

More than half a century ago, in the 1950s, when researchers began seriously exploring the possibilities of optical fibers, few would have believed that within a few decades, optical fibers would revolutionize our lives, leading to dramatic changes in the way we communicate. Glass optical fibers (GOFs), which were first developed in the 1960s, exhibited significant propagation losses above 1000 dB/km; the transmission distance was severely limited. The first breakthrough in fiber optics was brought by Kao and Hockham in 1966 (1). He theorized that by using a fiber of the purest glass, it would be possible to transmit light signals more than 100 km, in contrast to fibers available in the 1960s that could only realize a distance of 20 m. Just 4 years later, in 1970, the first ultrapure fiber with an attenuation of 20 dB/km was successfully fabricated (2). Others soon followed, and losses were pushed down to the theoretical limit (0.2 dB/km) (3–5). A first-generation fiber-optic communication system was successfully deployed in 1976, and since then GOFs have steadily connected the world. Today, more than a billion kilometers of GOFs have been placed underground and in oceans, enabling global broadband communication media such as the Internet.

We believe that the next big step in optical fiber technology will be polymer optical fibers (POFs). In advanced countries, “fiber-to-the-home” (FTTH) services that interconnect homes with a GOF backbone are well established. However, intrabuilding networks such as home networks have yet to be adequately developed. With the increase in the number and use of home PCs, high-definition (three-dimensional) TVs, smartphones, tablet devices, and intelligent home appliances, the demand has increased for optical datalink connections not only up to the end-users’ buildings but also within them (6). Surprisingly, the entire length of all terminal networks accounts for 95% of that of all optical networks. In such short-distance applications, from optical local area networks (LANs) for homes and offices to high-speed backplanes, the extremely low attenuation of a single-mode GOF is unnecessary. Instead, simpler and less expensive components, greater flexibility, and higher reliability against bending, shocks, and vibrations are considerably more valuable properties. Naturally, polymers are overwhelmingly superior to glasses in all of these requirements.

However, for POFs, which have been overshadowed by the success of GOFs in previous decades, the road has never been smooth. In particular, many studies have sought to reduce fiber attenuation as had been done for GOFs. To be used as the core base material, polymers must ultimately be transparent even though hundreds times higher attenuations than GOFs are allowed for the short-range networks. Given its amorphous structure and easy processing via a free-radical bulk polymerization that requires no metal catalysts and avoids contaminants, poly(methyl methacrylate) (PMMA) has mainly been utilized for POFs (7). Coupled with low material costs, its adequate thermal stability and excellent corrosion resistance have also made PMMA the representative material for POF. However, even with highly purified PMMA-based POFs, the intrinsic problem of attenuation caused by C–H molecular vibrations remained unresolved. Furthermore, POFs with a large core and modal dispersion had severe limitations in

bandwidth. In this article, we begin with a brief explanation of optical fibers and proceed to describe technical developments that have solved the abovementioned problems and propelled POFs into the main stream of modern short networking applications.

## Basic Concept and Classification of Optical Fibers

The principle of light propagation through POFs is the same as that for GOFs. POFs are basically composed of two coaxial layers: the core and the cladding. The core is the inner part of the fiber that guides light, whereas the cladding completely surrounds the core. The refractive index of the core is slightly higher than that of the cladding. Hence, when the incident angle of the light input to the core is greater than the critical angle, the input is confined to the core region because of total internal reflection at the interface between the different dielectric materials comprising each layer. Although this simple concept is a useful approximation of light guidance in many kinds of fibers, it does not provide a full explanation. Light is really an electromagnetic wave with a frequency in the optical range. An optical fiber guides the waves in distinct patterns called modes, which describe the distribution of light energy across the waveguide. Commonly used optical fibers can be separated into two classes based on their modal properties: single- and multimode fibers. Single-mode fibers are step-index (SI) fibers, whereas multimode fibers can be divided into SI and graded-index (GI) fibers. SI and GI refer to patterns of variation in the refractive index with the radial distance from the fiber axis. Figure 1 schematically shows these three types of fibers: (a) the single-mode fiber, (b) the SI multimode fiber, and (c) the GI multimode fiber.

The information-carrying capacity of an optical fiber is determined by its impulse response. The impulse response and hence bandwidth are largely determined by the modal properties of the fiber. Given that single-mode transmission avoids modal dispersion and other effects that occur with multimode transmission, single-mode fibers with core diameters of 5–10  $\mu\text{m}$  can carry signals at considerably higher speeds than multimode fibers (8,9). Modal dispersion can be understood by referring to the SI multimode fiber (Fig. 1b), where different rays are shown to travel along paths with different lengths. Even if they are coincident at the input end and travel at the same speed within the fiber, these rays disperse at the output end because of their different path lengths. As a result, the impulse signal broadens. This becomes a serious restriction on the transmission speed because pulses that overlap can interfere with each other, making it impossible to receive the signal. On the other hand, GI guides have less modal dispersion and greater transmission capacity than SI guides. The refractive index of the core in GI multimode fibers is not constant, but decreases gradually from its maximum at the core center to its minimum at the core/cladding boundary. From Figure 1c, it is easy to understand qualitatively why the modal dispersion decreases for GI fibers. As in the case of SI fibers, the path is longer for more oblique rays (higher order mode). However, the ray velocity changes along the path because of variations in the refractive index. The speed of light in a material,  $v$ , is equal to the velocity of light in vacuum,  $c$ , divided by the refractive index, that is,  $v = c/n$ . More specifically, ray propagation along the fiber axis takes the shortest path but has



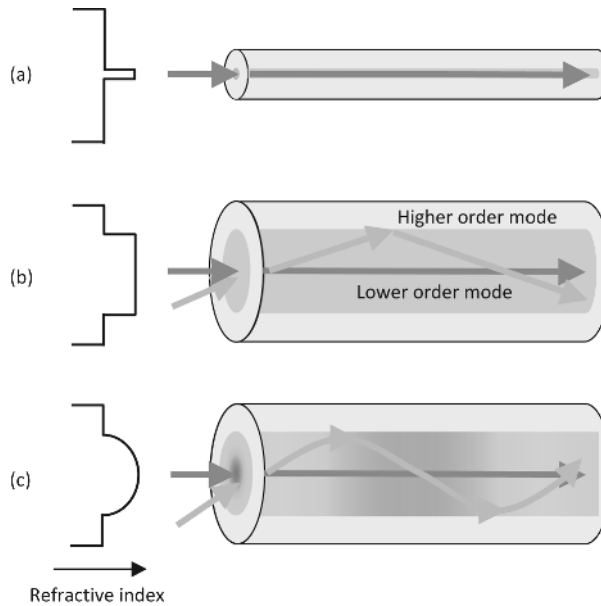


**Fig. 1.** Ray trajectories through basic types of optical fibers: (a) single-mode fiber, (b) step-index multimode fiber, and (c) graded-index multimode fiber. Reprinted from Koike, Y.; Koike, K., *J. Polym. Sci., Part B: Polym. Phys.* 2011, 49, 2–17, with permission of the John Wiley & Sons.

the slowest speed since the index is largest along this path. Oblique rays have a large part of their path in a lower refractive index medium in which they travel faster. The difference in the refractive index is small but sufficient to compensate for the time delay. By carefully controlling the refractive index profile in the core region, the modal dispersion can be drastically reduced.

Currently, most GOFs are fabricated with single-mode structures and are commonly used in long-distance applications such as core and metropolitan networks. With respect to coupling loss, the small core of single-mode fibers is a serious disadvantage; the smaller the core diameter, the harder it is to couple light into the fiber. Hence, GI multimode-type fibers were also extensively studied and deployed in some telecommunication applications up until the mid-1980s (10–13). However, as single-mode GOFs were far superior in both attenuation and bandwidth, they gradually shifted to short-length applications such as storage area networks. Coupling light into a single-mode fiber inevitably requires considerably tighter tolerances than doing so into the larger cores of a multimode fiber. However, such tighter tolerances were achieved; nowadays, the single-mode GOF has become the standard choice for virtually all kinds of telecommunications that involve high bitrates or span distances longer than a couple of kilometers.

On the other hand, POFs have attracted attention as optimal candidates for short-distance networks such as intrabuilding networks (7). Optical fibers must be able to connect various devices in the individual rooms of a building; hence, they must be flexible, easy to bend, and connected at several points. Predictably, the single-mode GOF is unsuited for this application given its brittleness and

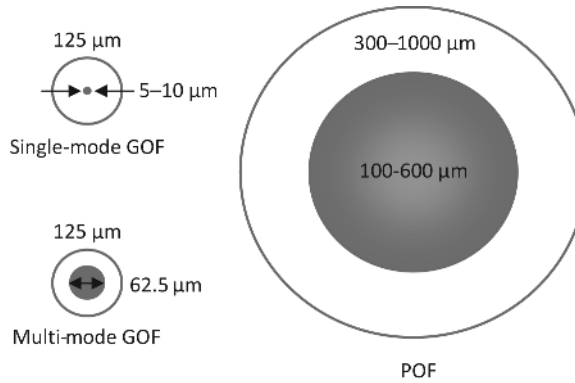


**Fig. 2.** Cross-sectional views of representative optical fibers.

small core. In contrast, POFs can be enlarged to approximately 1 mm in diameter without losing flexibility or ease of fiber alignment (Fig. 2). Therefore, apart from a few exceptions (14–16), a great deal of effort has been focused on developing multimode POFs with large diameters.

## The Advent of POFs and Analyses of Attenuation

**The First POFs.** The first POF, CROFON, which was invented in the mid 1960s by Du Pont, was a multimode fiber with an SI profile in the core region. Compared to GOFs, the SI POF was also advantageous in terms of mass production. The first commercialized SI POF was ESKA, which was introduced by Mitsubishi Rayon in 1975; subsequently, Asahi Chemical and Toray also entered the market. However, the first fibers were insufficiently transparent to be used as an intrabuilding communication medium and their application was severely limited to extremely short-range areas such as light guides, illuminations, audio datalinks, and sensors.

**Analyses of Attenuation.** Fiber attenuation limits how far a signal can propagate in the fiber before the optical power becomes too weak to be detected. The oldest and most common approach for determining fiber attenuation is measuring the optical power transmitted through long and short lengths of the same fiber using identical input couplings, a method known as the cutback technique. First, the optical power at the output (or far end) of the fiber is measured. Subsequently, the fiber is cut off a few meters from the light source and the output power at this near end is measured without disturbing the input. When  $P_{\text{out}}$  and  $P_{\text{in}}$  represent the output powers of the far and near ends of the fiber, respectively, the attenuation  $\alpha$ , which is normally expressed in decibels, is defined as follows:

$$\alpha(\text{dB/km}) = -\frac{10}{L} \log_{10} \left( \frac{P_{\text{out}}}{P_{\text{in}}} \right) \quad (1)$$

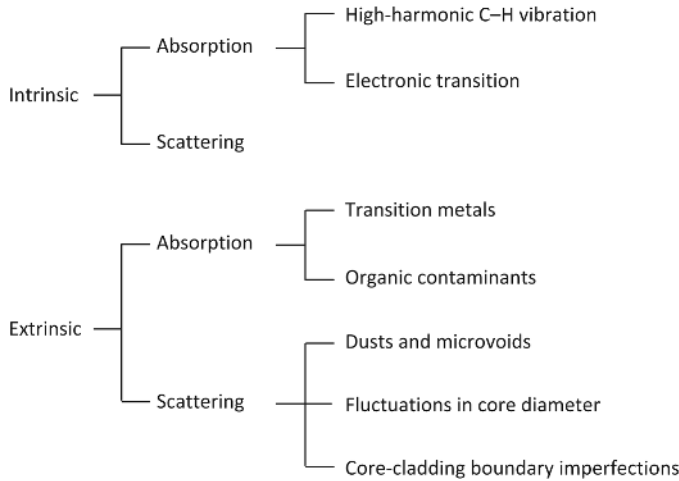


**Fig. 3.** Classification of intrinsic and extrinsic factors affecting the POF attenuation.

where  $L$  (in kilometers) is the distance between the two measurement points. The attenuation of the first prototype was more than 1000 dB/km, and many researchers have attempted to reduce the attenuation. Although the various mechanisms contributing to losses in POFs are basically similar to those in GOFs, their relative magnitudes differ. Figure 3 shows the loss factors for POFs, which are divided into intrinsic and extrinsic factors. These are further classified into absorption and scattering losses.

**Absorption Loss.** Every material absorbs light energy, whose amount depends on the wavelength and material. Intrinsic absorption loss in POFs is caused by electronic transitions and molecular vibrations. Electronic transition absorption results from transitions between electronic energy levels of bonds within the materials; the absorption of photons causes an upward transition, which leads to excitation of the electronic state. Typically, electronic transition peaks appear in the ultraviolet wavelength region, and their absorption tails influence the transmission losses in POFs. The relationship between the electronic transition loss  $\alpha_e$  (in dB/km) and the wavelength of incident light  $\lambda$  (in nm) can be expressed by using Urbach's rule (17):

$$\alpha_e = A \exp(B/\lambda) \quad (2)$$

where  $A$  and  $B$  are substance-specific constants. In the case of PMMA,  $A$  and  $B$  have been clarified to be  $1.58 \times 10^{-12}$  and  $1.15 \times 10^4$ , respectively (18). Hence, the  $\alpha_e$  value of PMMA is less than 1 dB/km at 500 nm. On the other hand, poly(styrene) (PS) and poly(carbonate) (PC), which are also universal polymers for POFs, exhibit considerably larger absorption losses (Fig. 4) (18,19). This is because of the  $\pi - \pi^*$  transition of the phenyl groups in PS and PC. The energy band gap between the  $\pi$  and  $\pi^*$  levels is close to photon energy of visible light. The tails are drastically shifted to longer wavelengths as the conjugation length increases.

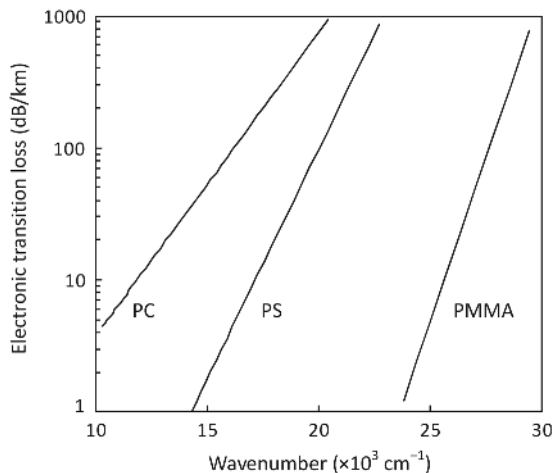


**Fig. 4.** Electronic transition loss of PMMA, PS, and PC. Reprinted from Koike, Y.; Koike, K., *J. Polym. Sci., Part B: Polym. Phys.* 2011, 49, 2–17, with permission from the John Wiley & Sons.

The effect of molecular vibrational absorptions becomes strong at wavelengths in the visible-to-infrared region. In the case of PMMA, which shows negligibly small electronic transition absorption, this molecular vibration is the predominant factor contributing to fiber attenuation. Groh approximated the attenuation by the overtone vibrational absorptions of the C–H and C–X bonds as follows (20):

$$\alpha_v = 3.2 \times 10^8 \frac{\rho N_{CX}}{M} \left( \frac{E_v^{CX}}{E_1^{CH}} \right) \quad (3)$$

where  $\alpha_v$  (in dB/km) is the attenuation,  $\rho$  (in g/cm<sup>3</sup>) the polymer density,  $M$  (in g/mol) the molecular weight of the monomer unit,  $N_{CX}$  the number of C–X bonds per monomer, and  $E_v^{CX}/E_1^{CH}$  the vibration energy ratio of each bond to the fundamental frequency of the C–H bond. Figure 5 shows the spectral overtone positions and normalized integral band strengths for the C–H, C–D, and C–F vibrations. If we set  $\rho = 1.19$  g/cm<sup>3</sup>,  $M = 100$  g/mol, and  $N_{CH} = 8$  as the PMMA values, it follows from equation 3 that  $E_v^{CH}/E_1^{CH} = 3.3 \times 10^{-8}$  corresponds to an attenuation of 1 dB/km. In the visible-to-near infrared region, the overtones for C–D and C–F are several orders of magnitude lower than the overtone for C–H. This implies that fiber attenuation can be reduced drastically by substituting the hydrogen atoms for heavier atoms such as deuterium and fluorine with lower energy absorption bands.

**Scattering Loss.** Scattering losses in polymers arise from microscopic variations in material density. The isotropic light scattering loss  $\alpha_s$  (in dB/km) in POFs can be experimentally estimated by measuring the static light scattering

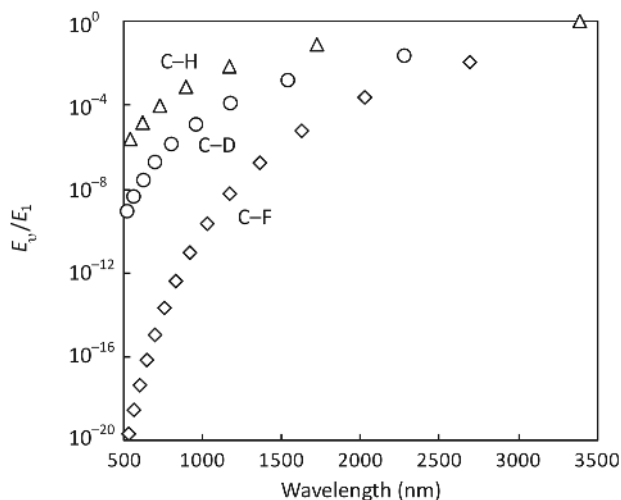


**Fig. 5.** Calculated spectral overtone positions and normalized integral band strengths for different C–X vibrations. Reprinted from Koike, Y.; Koike, K., *J. Polym. Sci., Part B: Polym. Phys.* 2011, 49, 2–17, with permission of the John Wiley & Sons.

of the polymer rod and is calculated by using the following equation (21):

$$\alpha_s = 4.342 \times 10^5 \pi \int_0^\pi (1 + \cos^2 \theta) V_V^{\text{iso}} \sin \theta \, d\theta \quad (4)$$

$$V_V^{\text{iso}} = V_V - \frac{4}{3} H_V \quad (5)$$

where  $V$  and  $H$  denote vertical and horizontal polarizations, respectively. The symbol  $A$  and the subscript  $B$  in the expression for a scattering component,  $A_B$ , represent the directions of the polarizing phase of a scattered light and an incident light, respectively.  $\theta$  is the scattering angle in relation to the direction of the incident ray. By using Einstein's fluctuation theory, the intensity of the isotropic light scattering  $V_V^{\text{iso}}$  from thermally induced density fluctuations in a structureless liquid is expressed by (22)

$$V_V^{\text{iso}} = \frac{\pi^2}{9\lambda_0^4} (n^2 - 1)^2 (n^2 + 2)^2 kT\beta. \quad (6)$$

where  $\lambda_0$  is the wavelength of light in vacuum,  $n$  the refractive index,  $k$  the Boltzmann constant,  $T$  the absolute temperature, and  $\beta$  the isothermal compressibility.

Through analyses of light scattering in several optical polymers such as PMMA (23), PS (24), and PC (25), this equation has proven to be suitable for amorphous polymers with heterogeneous structures small in size relative to the wavelength of the incident light. In particular, PMMA, which has the lowest scattering loss among such polymers, has received considerable attention. Using published data of  $\beta = 3.55 \times 10^{-11} \text{ cm}^2/\text{dyn}$  at around  $T_g$  for bulk PMMA (26) and

assuming freezing conditions, the value of  $V_V^{\text{iso}}$  at room temperature and a wavelength of 633 nm is  $2.61 \times 10^{-6} \text{ cm}^{-1}$ . As a result, the theoretical light scattering loss can be estimated from the  $V_V^{\text{iso}}$  value as 9.5 dB/km by using equation 4; this is almost identical to the experimental value of 9.7 dB/km (23).

**Low-Loss Step-Index Polymer Optical Fibers.** Through the analyses of each factor of fiber attenuation described above, the limitations of POFs based on several materials and their theoretical groundings have been steadily clarified. Meanwhile, it has been shown that the major factors causing high attenuation were not intrinsic but rather extrinsic—those such as contaminants becoming mixed into the polymer during the fiber fabrication process. By preparing the fiber in an all-closed system from monomer distillation to fiber drawing, low-loss POFs with losses near theoretical limits were fabricated. In 1981, Kaino reported a PS-based SI POF with an attenuation of 114 dB/km at 670 nm (27), and in the following year his group also succeeded in obtaining a PMMA-based SI POF with an attenuation of 55 dB/km at 568 nm (28).

## Graded-Index Technologies for Faster Transmission

**Bandwidth and Modal Dispersion.** After the studies on transparency, a high-speed optical network based on POFs became realistic. However, the SI POF requiring the excitation of several tens of thousands of modes for transmission had a limitation in bandwidth. The large core increases modal dispersion and drastically degrades the bandwidth to approximately several hundred megahertz over 100 m. The concept of fiber bandwidth originates from the general theory of time-invariant linear systems. If the optical fiber can be treated as a linear system, its input and output powers in the time domain are described simply as follows:

$$p_{\text{out}}(t) = h(t) * p_{\text{in}}(t). \quad (7)$$

The output pulse response  $p_{\text{out}}(t)$  of the fiber can be calculated through the convolution of the input pulse  $p_{\text{in}}(t)$  and the impulse response function  $h(t)$  of the fiber. The optical bandwidth of the fiber is defined by the Fourier-transformed  $H(f)$ . This is normally done in terms of the  $-3$  dB bandwidth, which is the modulation frequency at which the optical power of  $H(f)$  falls to one half the value of the zero frequency modulation. The larger the  $-3$  dB bandwidth  $f_{-3\text{dB}}$ , the narrower the output pulse and the higher the possible transmission capacity. Typically, modal dispersion is the dominant factor degrading the bandwidth for multimode optical fibers. However, as mentioned above, it can be minimized by forming a quadratic refractive index profile in the core region and by controlling the propagation speed of each mode. This method was first developed by Nishizawa and co-workers for glass fibers (10,13), and subsequently, it was adapted to POFs.

**Development of Graded-Index Polymer Optical Fibers.** The first GI POF was reported in 1982 (29). Initially, the GI profile was formed by copolymerizing two or three kinds of monomers with different refractive indices and monomer reactivity ratios (30). In this system, several properties such as

attenuation, bandwidth, refractive index profile, and numerical aperture were limited by the differences in the refractive indices and reactivity ratios between the monomers. To solve the problem, a simpler method of forming the GI profile—the low molecular doping method—was developed in 1994 (31). By adding a dopant with a higher refractive index than the base polymer and forming a concentration distribution in the radial direction, it became easy to control the refractive index profile. Furthermore, this groundbreaking method enabled the reliable fabrication of low-loss GI POFs. Since the first GI POF was reported, various methods for forming a GI profile have been proposed (32–34). Among these, here we discuss two major techniques using the low molecular doping method.

**Interfacial-Gel Polymerization Technique.** In this method, a rod with a GI profile called a “preform” is first prepared, after which the preform is heat drawn to the GI POF. The interfacial-gel polymerization technique (35) refers to the method used to form a parabolic refractive index profile in the core region. In this section, we use a typical system as an example. The base polymer of the core and cladding layers is PMMA and the low –molecular weight dopant is diphenyl sulfide (DPS). First, a glass tube charged with MMA monomer mixtures including benzoyl peroxide and *n*-butyl mercaptan as the initiator and chain transfer agent, respectively, is rotated on its axis at 3000 rpm in an oven at 70°C for 3–6 h. The MMA monomer comes to coat the inner wall of the glass tube because of centrifugal force and is gradually polymerized (Fig. 6a). After heat treatment at 90°C for 24 h, the polymer tube based on PMMA is obtained as the cladding layer of the GI preform. The tube is then filled with a core solution containing a mixture of MMA monomers as well as DPS, di-*tert*-butyl peroxide, and *n*-lauryl mercaptan as the dopant, initiator, and chain transfer agent, respectively. The tube filled with the mixture is heated in an oil bath at 120°C for 48 h under a nitrogen pressure (Fig. 6b). Finally, the preform is heat drawn to the fiber at 220–250 °C (Fig. 6c).

The mechanism for forming a GI profile is described in Figure 7. At the beginning of core polymerization, the inner wall of the PMMA tube becomes slightly swollen by the monomer–dopant mixture to form a polymer gel phase. The reaction rate of polymerization is generally faster in the gel phase than in the monomer mixture because of the gel effect, and the polymer phase grows from the inner wall of the tube to the core center. During the growth process, the MMA monomer can diffuse into the gel phase more easily than the dopant molecules because the molecular volume of the dopant, which contains benzene rings, is larger than that of the monomer. Hence, the dopant is concentrated in the middle region to form a quadratic refractive index profile.

The interfacial-gel polymerization technique has been particularly common in acrylic GI POF studies and has enabled the precise control of the refractive index profile, leading to a maximally high bandwidth (36). However, this batch process requires many complicated procedures. Furthermore, the fiber length obtained at any one time is completely dependent on the preform size. This is a serious limitation in terms of fabrication costs.

**Coextrusion Process.** To realize mass production, a new process for GI POF fabrication called coextrusion has been investigated (37,38). In this process, polymers doped with low –molecular weight dopants and homogeneous polymers are first prepared as the base materials of the core and cladding layers,

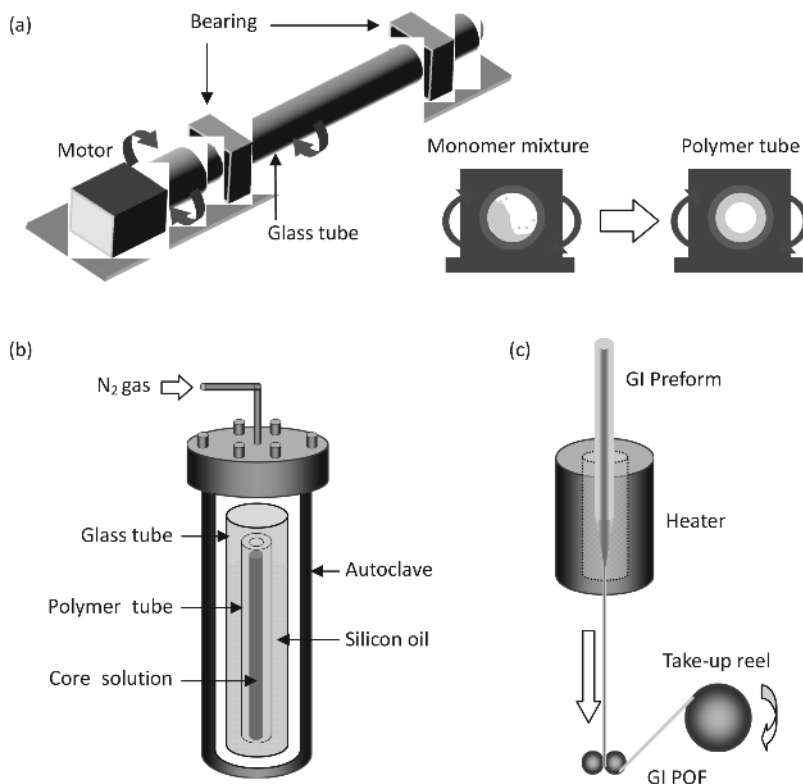


**Fig. 6.** Fabrication process of GI POFs by the preform method: (a) preparation of polymer tube, (b) core polymerization, and (c) heat drawing. Reprinted from Koike, Y.; Koike, K., *J. Polym. Sci., Part B: Polym. Phys.* 2011, 49, 2–17, with the permission of the John Wiley & Sons.

respectively. In PMMA–DPS systems, polymerizations are performed at 90°C for 24 h. The bulk polymers are then further heated at 110°C for 48 h. The two materials are melted in their respective extrusion sections at 210–250°C and compounded in a die to fabricate a POF with a concentric circular core/cladding structure. At this point, the fiber does not have a GI distribution. However, by heating the fiber in the diffusion section, a radial concentration profile of low-molecular weight dopant is formed as a result of molecular diffusion. Finally, the GI POF is obtained by winding it onto a take-up reel. The operational procedure of coextrusion is illustrated in Figure 8. This process is very simple, and hence GI POFs are expected to be manufactured continuously at a relatively low cost.

In previous studies, it was presumed that a GI POF fabricated by this process would have a refractive index distribution with a tail at the core/cladding boundary, not as steep as that prepared by the conventional batch process. Therefore, the bandwidth of the GI POF obtained by dopant diffusion coextrusion would be inferior to that obtained by the batch process. However, contrary to this



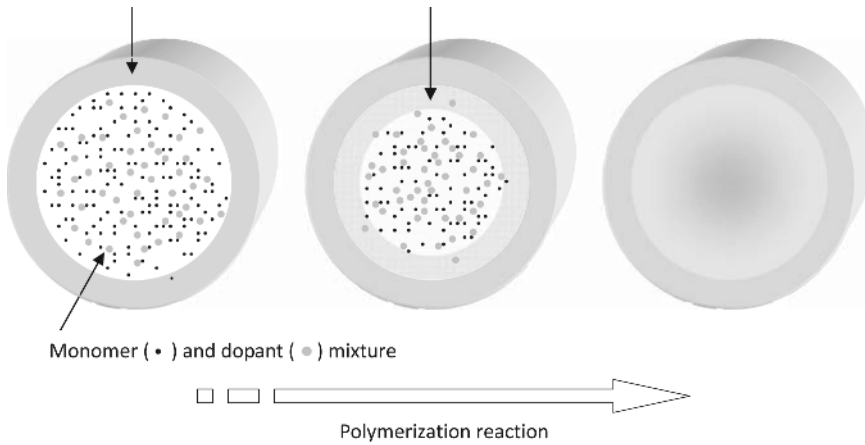


**Fig. 7.** Formation process of GI distribution by the interfacial-gel polymerization technique. Reprinted from Koike, Y.; Koike, K., *J. Polym. Sci., Part B: Polym. Phys.* 2011, 49, 2–17, with permission of the John Wiley & Sons.

expectation, a GI POF without any tail prepared by the process was reported in 2007 (38). If low molecular weight molecules diffuse in a radial direction, their diffusion can be expressed by Fick's diffusion equation:

$$\frac{\partial C}{\partial t} = \frac{1}{r} \frac{\partial}{\partial r} \left( Dr \frac{\partial C}{\partial r} \right) \quad (8)$$

where  $C$  is the concentration of low-weight molecules,  $t$  the diffusion time,  $r$  the distance from the fiber center, and  $D$  the mutual diffusion coefficient of low-weight molecules. The concentration profile calculated using equation 8 has a gradual shape around the diffusion front because  $D$  is almost constant in general systems. However, in the polymer–dopant system, the plasticization that occurs as a result of adding the dopant into the polymer matrix must be considered. As the dopant concentration increases, the  $T_g$ , which determines the mobility and diffusivity of the dopant, decreases linearly. In other words, diffusion within the diffusion section of the coextrusion equipment obeys Fick's law with a diffusion coefficient that varies as a function of dopant concentration. Figure 9 shows the comparison of the refractive index profiles of experimental and simulated data. The simulation was performed with a diffusion coefficient calculated from the results of a one-dimensional diffusion experiment. The polymer matrix and dopant are PMMA and DPS, respectively. The experimental and simulated data show good agreement, indicating a high possibility that a high-bandwidth GI POF can be prepared by the dopant diffusion coextrusion process. Currently, this continuous fabrication method is well established and is employed for some commercially available GI POFs.

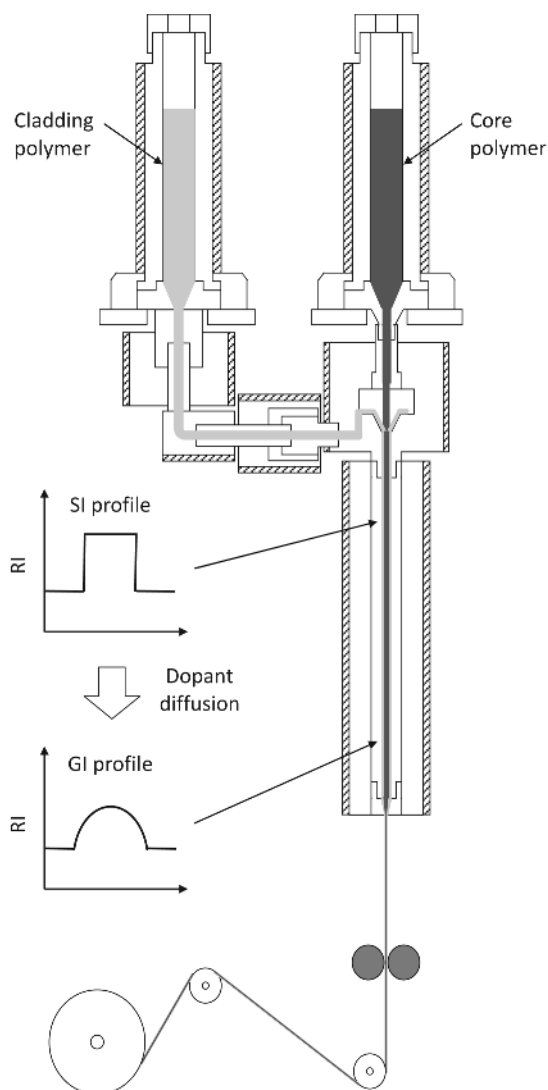


**Fig. 8.** Schematic diagram of GI POF fabrication by the coextrusion procedure. Reprinted from Koike, K.; Koike, K., in *Advanced Photonics Polymer: Materials and Applications*, 2011, pp. 21–27, with permission of the CMC, Tokyo, Japan.

### Fluoro Materials for Advanced Polymer Optical Fibers

With various improvements in the fabrication process enabling the avoidance of contaminants and the formation of GI profiles, low-loss and high-bandwidth POFs have become leading candidates for short-range networks. Since the first SI POF was commercialized, most POFs have been manufactured using PMMA, a mass-produced commercially available polymer that demonstrates high light transmittance and provides excellent corrosion resistance to both chemicals and weather. These properties, coupled with low manufacturing costs and easy

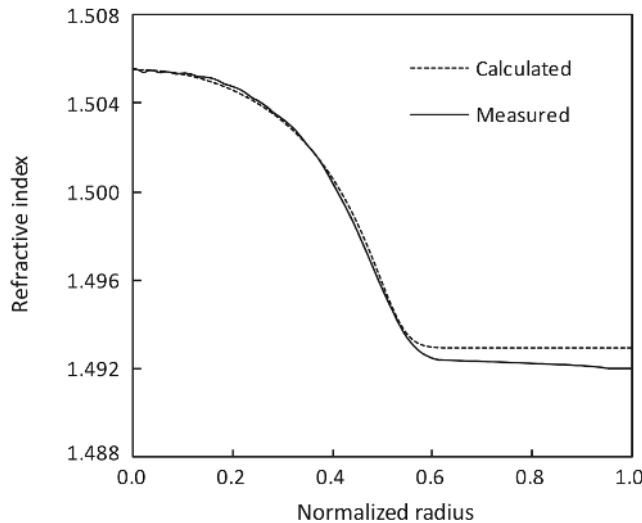


**Fig. 9.** Refractive index profiles. A broken line indicates the refractive index profile calculated from equation 8 using the measured dependence of the mutual diffusion coefficient for a PMMA–DPS system. A solid line indicates the measured refractive index profile for a PMMA–DPS-based GI POF fabricated by the coextrusion method. Reprinted from—Ref. (38), permission of the IEEE.

processing, have made PMMA a valuable substitute for glass in optical fibers. However, the performances can be further improved by modifying the base material.

**Partially Fluorinated Polymers.** The high attenuation of conventional POFs is dominated by C–H overtone stretches and combinations of stretch and deformations. Hence, the most effective method to obtain a low-loss POF is substituting hydrogen with heavier atoms such as fluorine, as is shown in Figure 5. However, if vinyl monomers such as MMA are perfluorinated, the polymerization rate drastically decreases. Boutevin studied various partially fluorinated polymers, which are easily prepared by free-radical polymerization and calculated the influence of the molar number of C–H bonds per unit volume (39). The contribution of the fluorine substituent is considerably larger than expected from the chemical structure. For instance, poly(2,2,2-trifluoroethyl methacrylate) (poly(TFEMA))-based GI POF provides a surprisingly low attenuation—71 dB/km at 650 nm (40)—relative to that for PMMA-based GI POF. Although the number of C–H bonds per monomer unit between TFEMA and MMA differs by only 1, the trifluoroethyl group of TFEMA possesses a large volume, and the number of C–H bonds per unit volume in poly(TFEMA) is only 64% of that in PMMA. However, the long side chain not only reduces fiber attenuation but also lowers  $T_g$ .

Recently, a novel GI POF based on a partially fluorinated copolymer with a lower attenuation and higher  $T_g$  than those of PMMA-based GI POF was reported (41). In this study, a copolymer of MMA and pentafluorophenyl methacrylate (PFPMA) was employed as the core polymer. In general, copolymers tend to have extremely high scattering losses because of their large heterogeneous

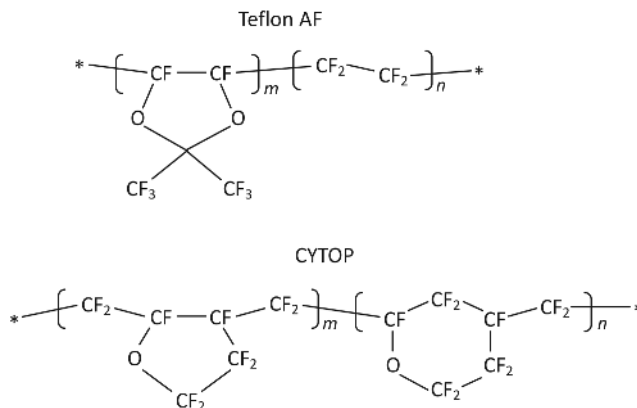


**Fig. 10.** Chemical structures of Teflon AF and CYTOP.

structure and corresponding heterogeneity of the refractive index; consequently, they have not been leading candidates for POF base materials. In this copolymeric system, however, the increase in scattering loss is negligibly small since the refractive indices of both homopolymers are almost identical (PMMA:  $n_D = 1.4914$ , poly(PFPMA):  $n_D = 1.4873$ ). Moreover, the number of C—H bonds per unit volume in poly(PFPMA) compared with that in PMMA is only 34%; hence, smaller absorption losses and lower attenuation than those for PMMA can be obtained by copolymerization. When the core composition is 65/35 = MMA/PFPMA (mol%), the attenuations are 172–185 dB/km at 670–680 nm, and  $T_g$  of the fiber is more than 90°C, ensuring long-term usage in home environments.

**Perfluorinated Polymers.** For further reduction of fiber attenuation, perfluorinated polymers have also been intensively investigated. Compared to a large number of radically polymerizable hydrocarbon monomers, only a few classes of perfluoromonomers can homopolymerize under normal conditions via the free-radical mechanism. The most typical example of a perfluoromonomer that can be prepared via free-radical polymerization is tetrafluoroethylene (TFE), developed by DuPont in 1938. As is well known, poly(TFE) (TEFLON) is opaque despite a lack of C—H bonds. In general, perfluorinated resins are rigid and easily form partially crystalline structures (42). Hence, light is scattered at the boundary between the amorphous and crystalline phases, causing haziness. To avoid the crystalline form, an effective method is to introduce aliphatic rings into the main chain, which becomes twisted and incapable of forming a crystalline structure. The most famous examples of amorphous perfluorinated polymers are Teflon AF and CYTOP, which were developed by DuPont and AGC, respectively. Their chemical structures are shown in Figure 10. Both have excellent clarity, solubility in fluorinated solvents, thermal and chemical durability, high electrical isolation, low water absorption, and low dielectric properties. In particular, their high transparencies arise from cyclic structures existing in the polymer main chains. Teflon AF is a copolymer of perfluoro-2,2-dimethyl-1,3-dioxole (PDD), which possesses a cyclic structure in its monomer unit, and TFE. On the other hand, CYTOP is a homopolymer of perfluoro(4-vinyl-1-butene) (BVE)

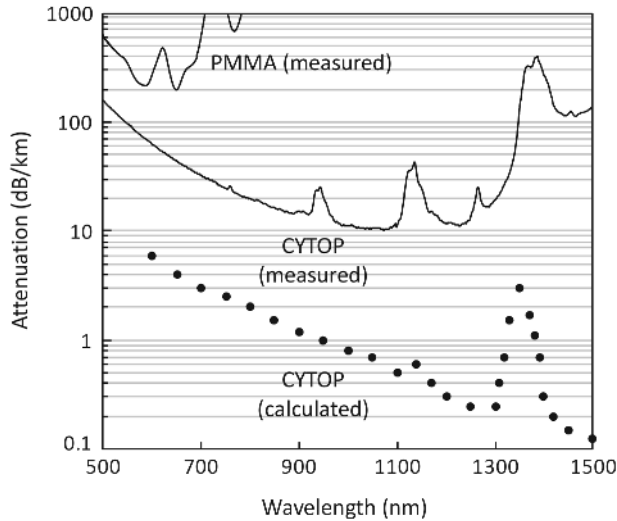


**Fig. 11.** Comparison of attenuation spectra between PMMA, and CYTOP-based GI POFs. Reprinted from—Ref. (36), with permission of IEEE.

and cyclopolymerization yields the cyclic structures (penta- and hexacyclic) on the polymer chain (43).

Although both have sufficient properties as the core material, Teflon AF has mainly been utilized as the cladding layer of optical fibers or waveguides because of its extremely low refractive index ( $n_D = 1.29$ ). Given that this value is lower than even that of water, liquid-core optical fibers have been studied for other purposes such as Raman spectroscopy analysis (44). In 2000, AGC commercialized the first CYTOP-based GI POF (Lucina), which has been adopted by condominiums, hospitals, data centers, and other facilities in Japan. Figure 11 is a comparison of the attenuation spectra for PMMA- and CYTOP-based GI POFs. CYTOP molecules consist solely of C—C, C—F, and C—O bonds. The wavelengths of the fundamental stretching vibrations of these atomic bonds are relatively long; therefore, vibrational absorption loss of CYTOP at the region of the light source wavelength is negligibly small. In addition, it has a fairly low-light scattering property because of the low refractive index ( $n_D = 1.34$ ) (see eq. 6). The attenuation of CYTOP-based GI POF is approximately 10 dB/km at 1.0  $\mu\text{m}$ . Given that the theoretical limit of attenuation is 0.7 dB/km at this wavelength (45), it is expected that the attenuation can be lowered further by preventing contamination during the fabrication process.

In fact, the excellent low-loss characteristic of CYTOP-based GI POF is far beyond the requirement of short-range networks. However, its real uniqueness is the low material dispersion derived from the low refractive index. The bandwidth of multimode optical fibers that excite many modes is predominantly influenced by modal dispersion. However, once the modal dispersion is reduced by forming a GI profile, the influence of material dispersion on bandwidth can no longer be ignored. Material dispersion is induced by the wavelength dependence of the refractive index of the fiber material and the finite spectral width of the light source.

The refractive index profiles of GI POFs can be approximated by the following power law (46):

$$\begin{aligned} n(r) &= n_1[1 - 2\Delta(r/R)^g]^{1/2}, \quad 0 \leq r \leq R \\ &= n_1(1 - 2\Delta)^{1/2}, \quad R < r \end{aligned} \quad (9)$$

where  $n(r)$  is the refractive index  $n$  at radius  $r$  of the fiber,  $n_1$  the refractive index at the core center,  $n_2$  the refractive index of the cladding,  $R$  the core diameter,  $g$  the refractive index profile coefficient, and  $\Delta$  the relative index difference defined as follows:

$$\Delta = \frac{n_1^2 - n_2^2}{2n_1^2} \cong \frac{n_1 - n_2}{n_1}. \quad (10)$$

The crucial factor defining the refractive index profile in GI POFs is the coefficient  $g$ , and the optimum value for maximizing the bandwidth can be determined from the modal and material dispersions (47,48). From analyses using the Wentzel–Kramers–Brillouin method, the modal dispersion  $\sigma_{\text{inter}}$ , material dispersion  $\sigma_{\text{intra}}$ , and total dispersion  $\sigma_{\text{total}}$  can be expressed as follows:

$$\begin{aligned} \sigma_{\text{inter}} &= \frac{Ln\Delta}{2c} \frac{g}{g+1} \left( \frac{g+2}{3g+2} \right)^{1/2} \\ &\quad \left[ S_1^2 + \frac{4S_1S_2\Delta(g+1)}{2g+1} + \frac{4S_2^2\Delta^2(2g+2)^2}{(5g+2)(3g+2)} \right]^{1/2} \end{aligned} \quad (11)$$

$$\begin{aligned} S_1 &= \frac{g-2-\varepsilon}{g+2}, \quad S_2 = \frac{3g-2-2\varepsilon}{2(g+2)}, \\ \varepsilon &= \frac{-2n_1}{n} \frac{\lambda d\Delta}{\Delta d\lambda}, \quad n = n_1 - \lambda \frac{dn_1}{d\lambda} \end{aligned} \quad (12)$$

$$\begin{aligned} \sigma_{\text{intra}} &= \frac{L\sigma_s}{\lambda} \left[ \left( -\lambda^2 \frac{d^2n_1}{d\lambda^2} \right)^2 - 2\lambda^2 \frac{d^2n_1}{d\lambda^2} (n\Delta) S_1 \left( \frac{2g}{2g+2} \right) \right. \\ &\quad \left. + (n\Delta)^2 \left( \frac{g-2-\varepsilon}{g+2} \right)^2 \frac{2g}{3g+2} \right]^{1/2} \end{aligned} \quad (13)$$

$$\sigma_{\text{total}} = \sqrt{\sigma_{\text{inter}}^2 + \sigma_{\text{intra}}^2} \quad (14)$$

where the spectral width  $\sigma_s$  is the wavelength dispersion of the input pulse,  $c$  the velocity of light,  $\lambda$  the wavelength of light, and  $L$  the transmission distance. Figure 12 shows a comparison of material dispersions among PMMA, CYTOP, and silica glass. The material dispersion of CYTOP is even lower than that of silica glass. The theoretical dependence of the bandwidth of the CYTOP-based GI POF and a multimode GOF on wavelength is shown in Figure 13. CYTOP-based GI POFs are predicted to have a higher bandwidth than multimode GOFs. Indeed, in 1999, AGC and Bell Laboratories reported an experimental transmission at 11 Gbps over 100 m using CYTOP-based GI POFs (49). Furthermore,

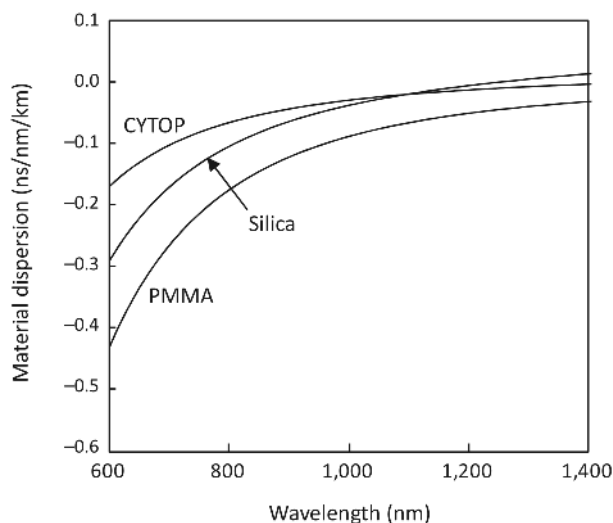


**Fig. 12.** Comparison of the material dispersion of fiber materials for CYTOP, PMMA, and silica. Reprinted from Ref. (36), with permission of IEEE.

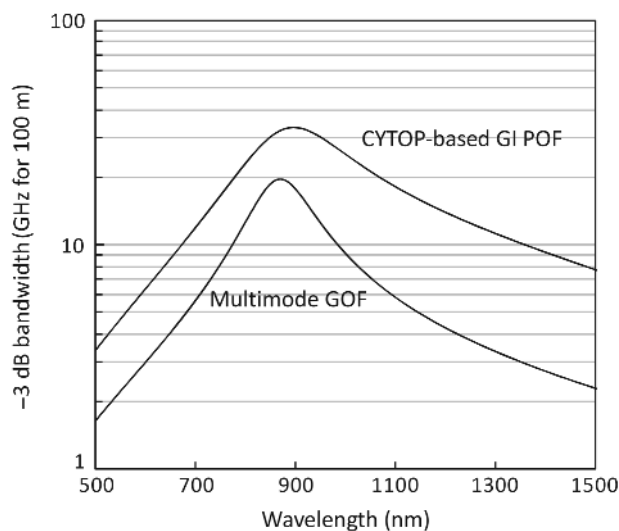


**Fig. 13.** Dependence of the theoretical  $-3$  dB bandwidth on wavelength in the CYTOP-based GI POF link as compared with that in multimode GOF ( $\sigma_s = 1.0$  nm). Bandwidth is calculated based on the assumption that each fiber has an optimal refractive index profile at 850 nm. Reprinted from Ref. (36), with permission of the IEEE.

CYTOP-based GI POFs capable of 40 Gbps transmission over 100 m were subsequently reported in 2007 (50) and 2008 (51,52). These are highly significant results that demonstrate that POFs can achieve a higher bandwidth than multimode GOFs.

Recently, demands for the replacement of electrical with optical signals are rapidly increasing for not only in-home networks but also those of shorter reach, such as in-device and on-board networks. In these areas, the required bit

rate is forecasted to be tens of gigabits per second in the next decade. Although multimode GI GOFs are currently considered for the transmission medium, the above data show that POFs can offer better performance even in such extremely high-speed connections. Moreover, POFs can also provide ease of handling and flexibility in wiring design with its features of plastic-specific robustness. In 2010, AGC released another CYTOP-based GI POF called Fontex. By employing a double cladding structure—a thin layer with considerably lower refractive index is placed around the first cladding—the bending loss was further reduced while high-speed capacity was maintained (53), thereby enabling various wiring designs to become possible. In addition, the continuous fabrication of GI POF has also been established by the coextrusion process.

## Conclusion

This article reviewed the status of POF developments in the past half century that have focused on loss reduction and bandwidth enhancement. Today, optical fibers are ubiquitous and can be encountered anywhere—in networks such as submarine links, long-distance terrestrial networks, metropolitan and access loops, and FTTH drop architectures. However, they are still not used in buildings. Currently, several technologies are available for broadband intrabuilding networking. In particular, coaxial cables, twisted-pair cables, and wireless LANs are being intensively investigated. However, from the standpoints of transmission speed, reliability, ease of handling, and safety, GI POFs appear to be the best solution. Furthermore, POFs are now ready for use in not only intrabuilding networking but also device and storage interconnections where data transmissions more than 40 Gbps will be required in the near future. POFs are no longer just alternatives to GOFs; their advantages for short-range networks are obvious. In the future beyond FTTH services, there awaits a world in which all information will be directly transferred by light signals, bringing us back to real-time face-to-face communications with large screens and clear motion pictures. We believe that POF technologies will contribute in no small way to accelerate this paradigm shift.

## Acknowledgments

This research is partly supported by the Japan Society for the Promotion of Science (JSPS) through its “Funding Program for World-Leading Innovative R&D on Science and Technology (FIRST Program).”

## BIBLIOGRAPHY

### CITED PUBLICATIONS

1. C. K. Kao and A. G. Hockham, *Proc. IEEE* **113**, 1151–1158 (1996).
2. F. P. Kapron, D. B. Keck, and R. D. Maurer, *Appl. Phys. Lett.* **17**, 423–425 (1970).
3. T. Izawa, N. Shibata, and A. Takeda, *Appl. Phys. Lett.* **31**, 33–35 (1977).
4. T. Miya, Y. Terunuma, T. Hosaka, and T. Miyashita, *Electron. Lett.* **15**, 106–108 (1979).



5. K. Nagayama, M. Matsui, M. Kakui, T. Saitoh, K. Kawasaki, H. Takamizawa, Y. Ooga, I. Tsuchiya, and Y. Chigusa, *SEI Tech. Rev.* **57**, 3–6 (2004).
6. P. Chanclou, Z. Belfqih, B. Charbonnier, T. Duong, F. Frank, N. Genay, M. Huchard, P. Guignard, L. Guillo, B. Landousies, A. Pizzinat, H. Ramanitra, F. Saliou, S. Durel, P. Urvoas, M. Ouzzif, and J. L. Masson, *C. R. Physique* **9**, 935–946 (2008).
7. C. Emslie, *J. Mater. Sci.* **23**, 2281–2293 (1988).
8. K. I. White and B. P. Nelson, *Electron. Lett.* **15**, 394–395 (1979).
9. H. Tsuchiya and N. Imoto, *Electron. Lett.* **15**, 476–478 (1979).
10. JP Pat. 4,629,291 (1964), J. Nishizawa and I. Sasaki.
11. S. E. Miller, *Bell Syst. Tech. J.* **44**, 2017–2063 (1965).
12. T. Uchida, M. Furukawa, I. Kitano, K. Koizumi, and H. Matsumura, *IEEE J. Quantum Electron.* **6**, 606–612 (1970).
13. J. Nishizawa and A. Otsuka, *Appl. Phys. Lett.* **21**, 48–50 (1972).
14. M. A. Eijkelenborg, M. Large, A. Argyros, J. Zagari, S. Manos, N. A. Issa, I. Bassett, S. Fleming, R. C. McPhedran, C. M. Sterke, and N. Nicorovici, *Opt. Exp.* **9**, 319–327 (2001).
15. K. Kalli, H. L. Dobb, D. J. Webb, K. Carroll, M. Komodromos, C. Themistos, G. D. Peng, Q. Fang, and I. W. Boyd, *Opt. Exp.* **32**, 214–216 (2007).
16. D. Kong and L. Wang, *Opt. Lett.* **34**, 2435–2437 (2009).
17. F. Urbach, *Phys. Rev.* **92**, 1324 (1953).
18. T. Kaino, M. Fujiki, and K. Jinguji, *Rev. ECL* **32**, 478–488 (1984).
19. T. Yamashita and K. Kamada, *Jpn. J. Appl. Phys.* **32**, 2681–2686 (1993).
20. W. Groh and A. Zimmerman, *Macromolecules* **24**, 6660–6663 (1991).
21. M. Dettenmaier and E. W. Fischer, *Makromol. Chem.* **177**, 1185–1197 (1976).
22. A. Einstein, *Ann. Phys.* **33**, 1275–1298 (1910).
23. Y. Koike, N. Tanio, and Y. Ohtsuka, *Macromolecules* **22**, 1367–1373 (1989).
24. T. Kaino, M. Fujiki, S. Oikawa, and S. Nara, *Appl. Opt.* **20**, 2886–2888 (1981).
25. T. Yamashita and K. Kamada, *Jpn. J. Appl. Phys.* **32**, 1730–1735 (1993).
26. S. Matsuoka and H. E. Bair, *J. Appl. Phys.* **48**, 4058–4062 (1977).
27. T. Kaino, M. Fujiki, and S. Nara, *J. Appl. Phys.* **52**, 7061–7063 (1981).
28. T. Kaino, K. Jinguji, and S. Nara, *Appl. Phys. Lett.* **42**, 567–569 (1983).
29. Y. Koike, Y. Kimoto, and Y. Ohtsuka, *Appl. Opt.* **21**, 1057–1062 (1982).
30. Y. Koike, H. Hatanaka, and Y. Ohtsuka, *Appl. Opt.* **23**, 1779–1783 (1984).
31. U.S. Pat. 5,541,247, Jpn. Pat. 3,332,922, Eur. Pat. 0,566,744, KR Pat. 170,358, CA Pat. 2,098,604 (originally filed in 1991), Y. Koike.
32. B. C. Ho, J. H. Chen, W. C. Chen, Y. H. Chang, S. Y. Yang, J. J. Chen, and T. W. Tseng, *Polym. J.* **27**, 310–313 (1995).
33. I.-S. Sohn and C.-W. Park, *Ind. Eng. Chem. Res.* **40**, 3740–3748 (2001).
34. A. G. Villegas, M. A. Ocampo, G. Luna-Barcenas, and E. Saldivar-Guerra, *Macromol. Symp.* **283–284**, 336–341 (2009).
35. Y. Koike, T. Ishigure, and E. Nihei, *J. Lightw. Technol.* **13**, 1475–1489 (1995).
36. Y. Koike and T. Ishigure, *J. Lightw. Technol.* **24**, 4541–4553 (2006).
37. U.S. Pat. 5,783,636 (1998), Y. Koike and M. Naritomi.
38. M. Asai, R. Hirose, A. Kondo, and Y. Koike, *J. Lightw. Technol.* **25**, 3062–3067 (2007).
39. B. Boutevin, A. Rousseau, and D. Boscz, *J. Polym. Sci. Part A: Polym. Chem.* **30**, 1279–1286 (1992).
40. K. Koike and Y. Koike, *J. Lightw. Technol.* **27**, 41–46 (2009).
41. K. Koike, T. Kado, Z. Satoh, Y. Okamoto, and Y. Koike, *Polymer* **51**, 1377–1385 (2010).
42. E. Giannetti, *Polym. Int.* **50**, 10–26 (2001).
43. K. Yamamoto and G. Ogawa, *J. Fluorine Chem.* **126**, 1403–1408 (2005).
44. R. Altkorn, I. Koev, R. P. Van Duyne, and M. Litorja, *Appl. Opt.* **36**, 8992–8998 (1997).
45. N. Tanio and Y. Koike, *Polym. J.* **32**, 43–50 (2000).

- 46. R. Olshansky and D. B. Keck, *Appl. Opt.* **15**, 483–491 (1976).
- 47. L. G. Cohen, *Appl. Opt.* **15**, 1808–1814 (1976).
- 48. J. W. Fleming, *J. Am. Ceram. Soc.* **59**, 503–507 (1976).
- 49. G. Giaretta, M. Wegmueller, and R. V. Yelamarty, PD-14, Proceeding of the Optical Fiber Communication Conference. San diego, CA, USA 21–26 Feb, 1999.
- 50. A. Polley, K. Balemarchy, and S. E. Ralph, CWM5, Proceeding of the OSA/CLEO, Baltimore, MD, USA 6–11 May, 2007.
- 51. A. Polley and S. E. Ralph, OWB2, Proceeding of the OFC/NFOEC, San diego, CA, USA 24–28 Feb, 2008.
- 52. S. R. Nuccio, L. Christen, X. Wu, S. Khaleghi, O. Yilmaz, A. E. Wilner, and Y. Koike, We. 2. A. 4, Proceeding of the ECOC, Bruxelles, Belgium 21–25 Sep, 2008.
- 53. T. Noda and Y. Koike, *Opt. Exp.* **18**, 3128–3136 (2010).

YASUHIRO KOIKE

Keio Photonics Research Institute  
Keio University, Kawasaki, Japan

KOTARO KOIKE

Keio Photonics Research Institute  
Keio University, Kawasaki, Japan  
Polymer Research Institute  
Polytechnic Institute of New York University  
Brooklyn, New York

## OPTICAL PROPERTIES

### Introduction

Three phenomena take place when light interacts with polymeric materials: absorption, scattering, and transmission through the bulk of the material. In the case of absorption, it is possible that emission may take place of some or all of the absorbed energy. In the case of scattering, the light vector changes direction. This change may happen either with a change in energy (inelastic scattering) or without (elastic scattering). The scattered intensity depends on the refractive index variation within the material. In the case of transmission, the light propagates through the material and its state of polarization may change.

Polymers have many important optical properties, such as refractivity, reflection, scattering, absorption, clarity, haze, birefringence, stress-optical coefficient, optical configuration parameter, yellowness index, transmission, gloss, surface texture, and color among others (1).

Market applications based on optical properties of polymers are countless. Polymer optical lenses, CDs, DVDs, and packaging applications for the medical, electronic, food, and cosmetic markets are just a small sampling where optical properties of polymers play a dominant role (see Fig. 1).

Optical computing, optoelectronics, and fiber optics are some other emerging high technology areas. Transitioning from traditional copper wire to fiber-optic cables for faster information transfer, light switches of very high speed, or



**Fig. 1.** Advances in our understanding of optical properties of polymers have led in advances such as optical storage media (picture from Bayer MaterialsScienceNafta.com at <http://www.bayermaterialsciencenafta.com>).

intensity modulators up to 40 GHz are areas of immense interest in today's market. Altering the frequency of light from red to blue for laser applications and the associated increase in the density of data stored on an optical disk because of the shorter wavelength of blue light has recently been accomplished. Polymers can play a vital role in developing new electro-optical devices, optical waveguides, display screens, optical integrated circuits, amplifiers, attenuators, and photonic switching systems.

The future of information technology requires processing at ultrahigh speeds and storage capacities that do not seem to have an upper limit. Photoresponsive polymer materials designed at the molecular level promise to deliver function and performance beyond those of the current materials (2). Photon-induced direct structuring of polymers has led to new applications at the interface with laser technology (3).

Applications in the biomedical and food-related areas are also very important. Contact lenses, medical tubing, and films for food packaging are just few examples. There is literally no area of our life that has not been positively affected by the usefulness of the optical properties of polymers.

### Basic Definitions and Computational Prediction of Fundamental Optical Properties of Polymers

Reliable prediction of optical properties allows a better, clearer understanding of the underlying structure–property relationships. This in turn opens new avenues for designing new polymers with desired optical properties. One may rely on *ab initio* (“from first principles”) and semiempirical models to study polymer fragments and monomers (4). Monte Carlo, molecular dynamics, and QSPR (quantitative structure–property relationships) techniques are also being extensively used to study single chains and multichain polymer systems in bulk and in solution (5). Here, we very briefly review the theory and qualitatively look at some of the available methods for predicting optical properties.

**Optical Polarizability and Its Anisotropy.** The polarizability,  $\alpha$ , the constant of proportionality between the induced dipole moment,  $\mu'$ , and the intensity

of the applied electric field,  $E$ , is of primary importance and is given by (6)

$$\mu' = \mu + \alpha E + 1/2\beta E^2 + 1/6\gamma E^3 + \dots \quad (1)$$

where  $\mu$  is the permanent dipole moment and the parameters  $\beta$  and  $\gamma$  in the nonlinear terms are the hyperpolarizabilities (see also under Nonlinear Optical Properties). Qualitatively, polarizability is the “ease” of the displacement of the electrons around the nuclei because of the presence of the field.

Application of perturbation theory allows the calculation of the electronic polarizability according to

$$\alpha = \frac{2}{3} \sum_n \frac{|\langle 0|\mu|n\rangle|^2}{E_n - E_0} \quad (2)$$

where the numerator is proportional to the square of the electric transition dipole moment  $\mu$  from the ground (eg, “0”) to the excited (eg,  $n$ ) states. Dynamic polarizabilities far from an absorption band may be calculated from

$$\alpha(\omega) = \frac{2}{3\hbar} \sum_n \frac{\omega_{n0} |\langle 0|\mu|n\rangle|^2}{\omega_{n0}^2 - \omega^2} \quad (3)$$

where  $\hbar = h/2\pi$  with  $h$  being the Planck’s constant and  $\omega$  the frequency.

It is common to divide the polarizability by the factor  $4\pi\epsilon_0$  to obtain what is called the “polarizability volume,” which typically has units of  $\text{\AA}^3$ . According to equation 1, if the two vector quantities  $\mu$  and  $E$  are not of the same direction, then  $\alpha$  must be a tensor. Generally for a molecule, one may write the polarizability tensor as (7)

$$\alpha = \begin{bmatrix} \alpha_{xx} & \alpha_{xy} & \alpha_{xz} \\ \alpha_{yx} & \alpha_{yy} & \alpha_{yz} \\ \alpha_{zx} & \alpha_{zx} & \alpha_{zz} \end{bmatrix} \quad (4)$$

from which through diagonalization one obtains

$$\alpha = \begin{bmatrix} \alpha_X & 0 & 0 \\ 0 & \alpha_Y & 0 \\ 0 & 0 & \alpha_Z \end{bmatrix} \quad (5)$$

where  $X$ ,  $Y$ , and  $Z$  are now the principal axes of the molecule. In the case of spherical symmetry,  $\alpha_X = \alpha_Y = \alpha_Z$ . Carbon tetrachloride, an optically isotropic solvent used routinely in depolarized Rayleigh scattering experiments, is a typical molecule with spherical symmetry. For cylindrical symmetry, it holds that  $\alpha_Y = \alpha_Z$ . This will be true, for example, for the bonds of a polymer chain that is being treated in the freely jointed chain limit.

The anisotropic part of the polarizability tensor is defined as

$$\hat{\alpha} = \alpha - \frac{1}{3} \text{Tr}(\hat{\alpha}\hat{\alpha}) E_3 \quad (6)$$

where  $E_3$  is the identity matrix of order 3. The quantity  $1/3 \text{Tr}(\hat{\alpha}\hat{\alpha})$  is equal to the mean polarizability, and  $\text{Tr}(\ )$  is the trace of the product matrix.

In some cases, it is convenient to employ the following two relationships:

$$\alpha_{||} = \alpha_X - \frac{\alpha_Y + \alpha_Z}{2} \quad (7)$$

and

$$\alpha_{\perp} = \alpha_Y - \alpha_Z \quad (8)$$

where the symbols  $\alpha_{||}$  and  $\alpha_{\perp}$  denote the longitudinal and transverse anisotropies of the polarizability, respectively.

***Ab Initio* and Semiempirical Approximations and Models.** The general formulas of *ab initio* methods can be used for calculations directly and without any approximation, only if the set of wavefunctions and eigenenergies is known with sufficient accuracy. This is true only in the case of the very simplest atoms and molecules. The “from first principles” approach is to calculate the wavefunctions by solving the Schrödinger equation exactly. For large molecules, such as polymer fragments and chains, it is currently impossible to produce a set of exact wavefunctions or to obtain sufficient spectroscopic data. Therefore, various assumptions are introduced to alleviate the complexity of the calculations; semiempirical models contain such assumptions which are beyond the scope of this chapter. However, one may rely on semiempirical quantum-mechanical methods to predict (at least qualitatively) properties of polymer chain fragments.

Optical properties, such as linear polarizabilities can be calculated by relying on the methods mentioned above. For nonlinear optical properties, there are several approximate methods available too. Some of the most basic ones are given below in a qualitative manner. For further reading a number of excellent books on the subject are suggested (8–10).

***Resonant Case.*** The greatest simplification of the general formulas for the susceptibilities (see under Nonlinear Properties) can be made in the case when the nonlinear process under study is resonantly enhanced. In this case, one aims to extract the significant resonant terms from the full expression for susceptibility,  $\chi^{(n)}$ , and then piece together the contributions from all the other levels into a negligible term. The resonant contribution may then be calculated using the best available wavefunctions for the resonant levels. One could also choose to use experimental data for the selected transition frequencies and oscillator strengths. In the case when one pair of levels provides the dominant resonant contribution, a two-level model is appropriate.

***Resonant Two-Level Atom Systems.*** The description of resonant optical processes is greatly simplified by focusing on the dominant resonant transition. The model is based on a concept of an ensemble consisting of many two-level atoms that are identical and noninteracting. By “two-level,” one refers to two energy eigenstates that are used to describe the atom. An alternative approach is to consider the eigenstates of the system and the optical field taken together (often called “dressed” atoms approach).

*Unsoeld Approximation and Charge Models.* In the case when all the combinations of optical frequencies involved are far removed from molecular resonances, the hyperpolarizabilities do not depend on the details of the energy structure but only on the chemical bonding. The hyperpolarizabilities depend on the detailed distribution of charges in the ground state *only*, together with statistical averages of the frequencies and oscillator strengths of transitions to the excited states.

For saturated molecules in which the electrons are localized in bonds, the moments can be estimated using the vector sum of the polarizabilities of the individual bonds, and the interaction between bonds is neglected (bond additivity scheme—see below for more on bond additivity).

*Sum Over States.* This method computes molecular orbitals, from which values for transition frequencies may be calculated. First the electronic ground state of the molecular system is determined, after which one may apply either the Hartree–Fock–Roothan method or the LCAO (linear combination of atomic orbitals) approximation. Then one accounts for correlations by configuration interaction calculations to form the lowest energy excited states and transition dipole moments of the molecule. Finally, transition frequencies and dipole moments are employed along with the formulas for the hyperpolarizabilities. The sum over states method needs as input, energies, and transition moments for excited states. It yields  $\beta(\omega)$  directly (eq. 1); identification of contributing excited states is important.

*Finite-Field Method.* This method relies on deriving the various terms in the power series for the static-induced molecular dipole moment in terms of derivatives with respect to the local field. Therefore, if the molecular dipole moment can be calculated as a function of local electric field  $E$  then  $\beta_{ijk}$  is obtained from the second derivative of this function at  $E = 0$ .

## The Local Field

The role of local field is very important in determining optical properties of polymers, both in solution and in the bulk (11). It becomes particularly critical in measurements where polarized light is involved. It is therefore reasonable to include a short description in this article.

In a vacuum, the electric field  $E$  is defined in terms of the force experienced by an infinitesimal test charge that can be placed at any point in space. However, this cannot be done within systems like a polymer melt or a polymer solution, since, by definition, the space where we would like to measure the field is already occupied by either a polymer fragment or a solvent molecule.

Typically, the standard definition of  $E$  at a point in a polymer system proceeds analogously to the procedure in vacuum except that one first creates a needle-shaped cavity oriented along the field direction. This definition has its own limitations: the shape of the cavity in which  $E$  is defined will probably be different from that of the definition; real charges will probably not have an appropriately shaped cavity around them. The actual field must be modified by allowance of the real shape of the molecule to which the charge belongs. The definition neglects the

fields due to the other charges that belong to the molecule under consideration.  $E$  is defined in the absence of the other charges that belong to the molecule. Even if the interaction of these charges is already taken into account in the quantum-mechanical calculation of the molecular states in vacuum, there are contributions mediated through material outside the cavity that must be included.

Lorenz–Lorentz theory addressed the issue by extending the approach of Clausius–Mossotti to optical frequency fields (12,13). This extension relies on a spherical cavity (compare with the need for a needle-shaped cavity) and takes into account the effect of other charges. The only thorny issue is that a spherical cavity is not the best choice for anisotropic molecules. Nevertheless, the Lorenz–Lorentz approach has been widely used in studying optical properties of polymers (14). The expression of the local field is given by

$$L = \frac{n^2 + 2}{3} E \quad (9)$$

Using the molecular shape as a guide to develop the anisotropic cavity field may be a more realistic way of dealing with the issue. Boundary conditions could be a needle-shaped cavity and a disk-shaped one.

For polarized measurements, the relationship between refractive index and absorbance is critical. Directional absorbance changes lead to birefringence, which in turn will affect strongly the nature of polarized light. The Kramers–Kronig relations come into play for cases like this one (15). They relate the complete electromagnetic absorption spectrum of a material to its refractive index at all frequencies and vice versa. A form of the relation is

$$\Delta n = \frac{2.303Cc}{2\pi^2} P \int_0^\infty \frac{\varepsilon(v') dv'}{v'^2 - v^2} \quad (10)$$

$\Delta n$  is the contribution to the refractive index due to the solute whose concentration is  $C$  (mol/L),  $c$  is the speed of light, and  $\varepsilon(v')$  is the molar extinction coefficient.  $\Delta n$  is the difference between the refractive indices of the solution and the solvent.  $\Delta n$  is essentially the isotropic contribution to the refractive index by the solute whose absorption spectrum determines  $\varepsilon(v')$ . A common application of the Kramers–Kronig relation appears in light scattering, especially when one is interested in the effects of scattering on absorbance measurements.

## Refractive Index

According to the ISO definition (16), refractive index is the ratio of electromagnetic radiation *in vacuo* to the phase velocity of electromagnetic radiation of a specified frequency in the medium. The refractive index is always greater than unity, and it is dimensionless. For anisotropic materials, the state of polarization of the light and its direction must be defined relative to a reference axis in the sample.

The two experimental methods recommended by ISO-489 are the Abbe refractometer technique and the Becke line technique. The latter is more useful with powdered or granulated transparent material or even with small flakes

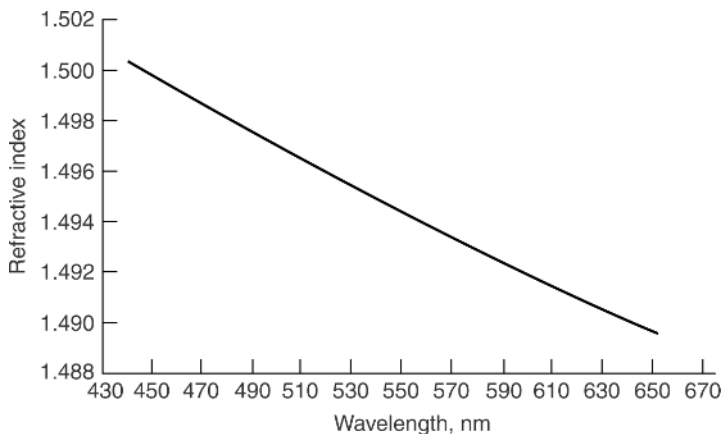


**Fig. 2.** Dispersion curve for an acrylic cast sheet. From Ref. 17.

of material taken from a larger sample. ASTM D542 method includes only the Abbe method, and it is widely used for the characterization of refractive index of polymers.

The refractive index decreases with increasing wavelength. The term *dispersion curve* refers to the graphical representation of that dependence (Fig. 2) (17).

One may estimate the refractive index in terms of the molar refraction  $R$ , which quantifies the intrinsic refractive power of the structural units constituting the polymer. According to References 18 and 19, the molar refraction  $R_{LL}$  is given as

$$n = \sqrt{\frac{(V + 2R_{LL})}{(V - R_{LL})}} \quad (11)$$

According to another definition, by Gladstone, molar refraction  $R_{GD}$  is given by

$$n = 1 + \frac{R_{GD}}{V} \quad (12)$$

The value of  $n$  increases with the refractive power of the polymer. There is no simple correlation between high mass density and high refractive index for all polymers. For example, the densities of many polymers containing aromatic rings are not especially high, but these polymers usually have high refractive indices.

Both the intrinsic refractivity and the density are key physical factors determining the refractive index.

Both  $R_{LL}$  and  $R_{GD}$  have relatively little dependence on temperature and crystallinity. On the other hand, the molar volume  $V$  changes drastically with both of those properties. In particular, volume increases with temperature while it decreases with increasing crystallinity. As a result, the refractive index decreases with increasing temperature and increases with crystallinity. The refractive index undergoes a change at the glass-transition temperature.



**Table 1. Refractive Indexes for Some Polymers**

Polymer	Refractive index	Temperature, °C
Nylon 6,6	1.566	See Ref. 21
Poly(butyl acrylate)	1.3900	25
Poly(methyl acrylate)	1.5750	25
PMMA	1.49	See Ref. 21
Poly(carbonate)	1.5570	25
Polyethylene (0.914 g/cc)	1.5050	25
Poly(tetrafluoroethylene)	1.555	20

The temperature dependence of  $n$  is quite similar for all polymers. An empirical rule for glassy polymers (20) is that  $n$  decreases by about from  $1 \times 10^{-4}$  to  $2 \times 10^{-4}$  per deg K increase of temperature. For isotropic amorphous polymers above  $T_g$  that value changes to about from  $3 \times 10^{-4}$  to  $5 \times 10^{-4}$  per deg K, at typical temperatures. Since  $n$  can never be less than unity, the rate of decrease with increasing temperature above  $T_g$  eventually levels off and asymptotically approaches zero. However, most polymers will degrade long before reaching temperatures high enough to for such a phenomenon be observed. Therefore, the empirical rule mentioned above is valid for (moderate) temperatures of practical interest.

Typically, one aims to predict the refractive index of the amorphous limit for a semicrystalline polymer. After that, the effect of crystallinity may be calculated by using either  $R_{LL}$  or  $R_{GD}$  combined with an estimate of the change in volume due to crystallization. A large collection of refractive index data on polymers may be found in *Physical Properties of Polymers Handbook* by the American Institute of Physics (21). A representative albeit necessarily short list is given below in Table 1.

Bicerano, in his book *Prediction of Polymer Properties*, proposes the following predictive equation for the refractive index at room temperature (22):

$$n = 1.885312 + 0.024558(17^0\chi^v - 20^0\chi - 12^1\chi^v - 9N_{\text{rot}} + N_{\text{ref}})/N \quad (13)$$

$\chi^0$ ,  $^0\chi^v$ , and  $^1\chi^v$  are the connectivity indices;  $N_{\text{rot}}$  and  $N_{\text{ref}}$  are correction factors that account for crystallinity and for contributions of certain atoms such as F, Si, and ring structures.

The graphical representation of the correlation is given in Figure 3.

**Specific Refractive Index Increments.** The rate of change of refractive index  $n$  of a dilute solution with changing polymer concentration  $C$  plays an important role in the extraction of information from light-scattering experiments, in particular for the determination of weight-average molecular weights (see Fig. 4). That change depends on the polymer type, solvent, and temperature (23).

$$\frac{dn}{dC} \approx \frac{(n_{\text{polymer}} - n_{\text{solvent}})}{\rho_{\text{polymer}}} \quad (14)$$

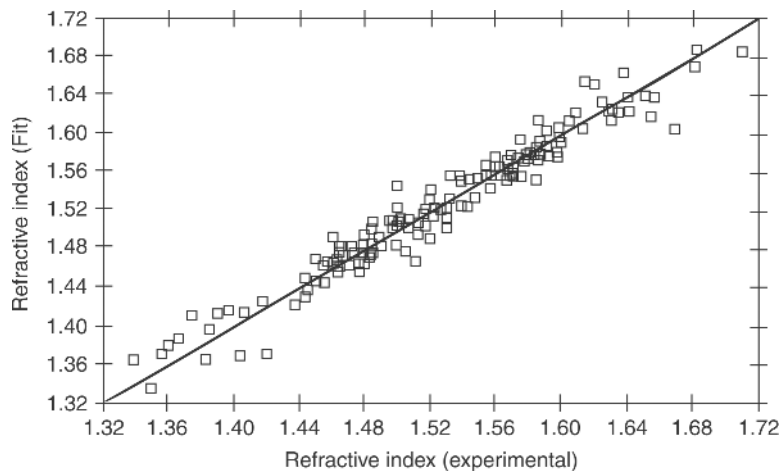


**Fig. 3.** Refractive index correlation for a series of polymers. Standard deviation: 0.0157; correlation coefficient: 0.9770. The line denotes  $y = x$ . From Ref. 22.

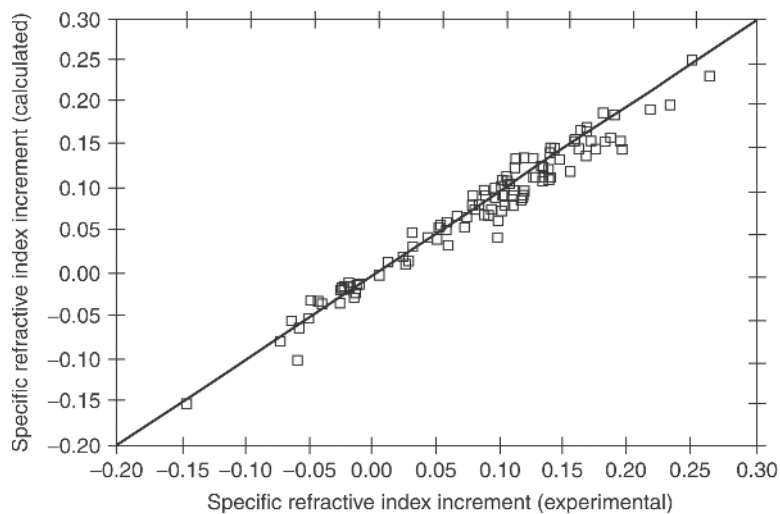


**Fig. 4.** Correlation for specific refractive index increments for a series of polymers. Standard deviation: 0.0158; Correlation coefficient: 0.9796. The line denotes  $y = x$ . From Ref. 22.

The correlation outlined above relies on values of refractive index and of density for the amorphous phase. All results are for room temperature.

**Refractive Index Fluctuations in Glassy Polymers.** Fluctuations in the refractive index within the bulk of a polymer can arise because of various optical inhomogeneities. Those fluctuations may be described by a radial correlation function, defined as

$$\gamma(r) = \frac{\langle \eta_i \eta_j \rangle_r}{\langle \eta^2 \rangle_{av}} \quad (15)$$

where  $\eta_j$  and  $\eta_i$  are the refractive indices at positions  $j$  and  $i$ , respectively, being at a distance  $r$  from each other. The brackets denote averages at all pairs of points at distance  $r$  apart.

At  $r = 0$ , the correlation function approaches unity. A common expression is

$$\gamma(r) = \exp(-r/a) \quad (16)$$

with constant  $\alpha$  being the correlation length. For PMMA, for example,  $\alpha$  is at 100–200 nm.

Fluctuation in the refractive index will affect the intensity of the scattered light. According to Debye and Bueche (24), the scattered intensity at an angle  $\theta$  to the incident beam has intensity  $I$ , given by

$$I \sim \langle \eta^2 \rangle_{\text{av}} \int_0^\infty \gamma(r) r^2 \frac{\sin Sr}{Sr} dr \quad (17)$$

with

$$S = 4\pi/\lambda \sin(\theta/2) \quad (18)$$

For PMMA, the root mean square refractive index fluctuation is around  $2 \times 10^{-4}$ . The larger the fluctuation magnitude, the larger is the scattering intensity. This is significant for applications such as fiber optics, where transmission distances are critical.

**Refractive Index and Orientation Fluctuations in Semicrystalline Polymers.** The crystalline regions in semicrystalline polymers are optically anisotropic. The simplest spherulite-based model for predicting light scattering is a sphere of radius  $r$  with a different polarizability in the radial direction  $\alpha_r$  than in the tangential direction  $\alpha_t$  (25). Assuming vertically polarized incident light, the intensities of the two scattered components (vertical and horizontal) are

$$I_{VV} \sim \cos^4 \mu_A (\alpha_t - \alpha_r)^2 + \dots \quad (19)$$

$$I_{HV} \sim \sin^2 \mu_A \cos^2 \mu_A (\alpha_t - \alpha_r)^2 \quad (20)$$

where  $\mu_A$  is the azimuthal angle in the scattering pattern. The HV component will have a maximum intensity in the  $\theta$  direction at

$$\sin\left(\frac{\theta_m}{2}\right) = \frac{1.025}{\pi} \left(\frac{\lambda}{r}\right) \quad (21)$$

Therefore, the scattering maximum moves to larger  $\theta$  values as the mean spherulite radius decreases. For unpolarized incident light, the scattering pattern becomes axially symmetric, with intensity independent of the angle  $\mu_A$ .

There is always a concern when one tries to simultaneously optimize properties such as transparency and toughness, because the requirements for those two in terms of particle size conflict with each other. For example, rubber-toughened

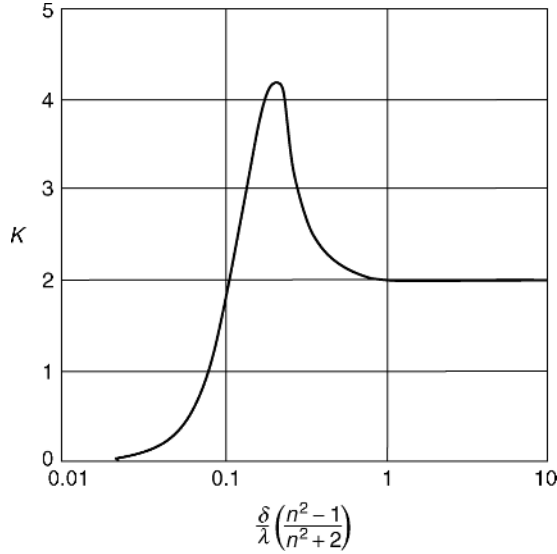


**Fig. 5.** Scattering coefficient  $K$  for a single sphere of relative refractive index  $n$  versus the ratio of the sphere diameter to the wavelength of the light. From Ref. 26.

ABS is opaque because the particle size of the rubber particles is kept at  $1 \mu\text{m}$  in order to optimize toughness.

Another example is that of polypropylene film produced on a cast film line. Its optical properties can change considerably by changing line conditions such as die temperature and chill roll temperature. Line speed affects cooling time and is therefore important too in affecting optical properties. All those conditions affect the development of the crystalline structure of the film, which in turn is related to its optical properties. Random copolymers of PP will have better optical properties than homopolymers, because of their inherently lower crystallinity.

**Particulate Scattering from Isolated Irregularities.** A model that addresses the issue of particulate scattering on the surface is the following: If the scattering centers are sufficiently separated from each other, the total scattering is the sum of those calculated individually from each particle. Mie light-scattering theory (26,27) uses spherical particles of diameter  $d$  and relative refractive index  $n$  (which is the ratio of the refractive index of the sphere to that of the matrix) (28).

The scattering efficiency factor  $K$  is defined as the total scattered energy divided by the energy incident on the surface of the particle. The size of the sphere will affect the values of  $K$  (Fig. 5). In general there are three regions of interest:

When the particle diameter is less than 10% of the wavelength of light, Rayleigh scattering is observed, in which the efficiency factor is given by

$$K = \frac{8}{3} \pi^4 \left( \frac{d}{\lambda} \right)^4 \left( \frac{n^2 - 1}{n^2 + 2} \right)^2 \quad (22)$$

When the diameter is of the same order of magnitude as the wavelength of light, a peak in the value of  $K$  is observed. When the diameter is larger the scattering efficiency is around 2.

**Internal Absorption.** Internal absorption causes the transmitted intensity  $I$  to fall exponentially as the path length  $L$  increases through the polymer:

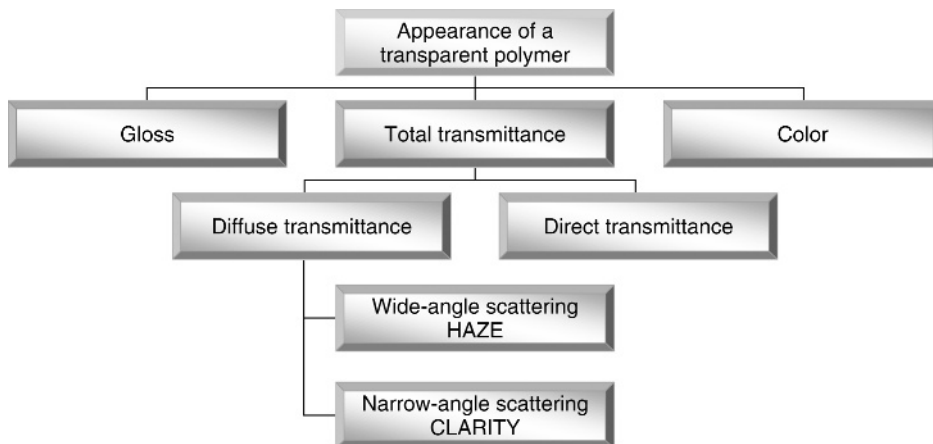
$$I = (1 - R)^2 I_0 e^{-AL} \quad (23)$$

$I_0$  is the incident intensity, and  $A$  is the attenuation coefficient. All polymers absorb strongly in the UV region.

### Transmission and Haze

The degree of optical transparency of a polymeric material is determined by its luminous transmittance, haze, and clarity. Total luminous transmittance is the ratio of the transmitted luminous flux to the incident luminous flux. Regular transmittance is the ratio of undiffused transmitted flux to incident flux. Typically, it encompasses the flux that deviates from the incident beam no more than  $2.5^\circ$ .

A breakdown of the factors affecting the appearance of a transparent polymer appears in the chart below:



The term “haze” is used to describe the slightly cloudy appearance of film material resulting from the forward scattering of light. ASTM D1003 defines “haze” as the “percentage of transmitted light which in passing through the specimen deviates from the incident beam by forward scattering.” For the purposes of this method, only light flux deviating more than  $2.5^\circ$  on the average is considered to be haze. Haze can be caused from a variety of sources found at the surface or in the bulk of the material. Some of them could be impurities, voids, bubbles, and filler particles. Regions of different refractive indices brought about by crystallization can also be a cause of haze. Surface roughness could also be a reason for haze. For example, abrasion and/or weathering will affect haze by altering the surface of a polymer sample.

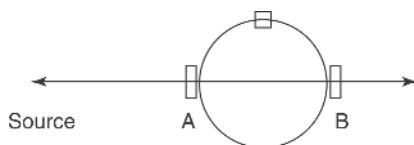


**Fig. 6.** Simple hazemeter schematic. From Ref. 29.

Haze characterizes the loss of contrast that results when objects are viewed through a scattering medium. The deterioration of contrast is mainly due to light scattered forward at large angles to the undeviated transmitted beam and is usually expressed through the forward-scattered fraction.

It is important to distinguish between surface and bulk scattering; for testing purposes, the former is minimized by wetting the surface with a liquid of similar refractive index. That way the two effects (surface vs bulk) can be decoupled. The “milk-like” appearance of translucent polymer samples viewed from the side on which light is incident is due to back scattering.

It is customary to calculate the total luminous transmittance of the sample,  $T_t$ , as well as haze,  $H$ . The ASTM method uses the following equations:

$$T_1 = 100 \left( \frac{T_2}{T_1} \right) \quad (24)$$

and

$$H = 100 \left[ \left( \frac{T_4}{T_2} \right) - \left( \frac{T_3}{T_1} \right) \right] \quad (25)$$

The various transmittances are defined as follows (29):

Measurement	Position A	Position B
$T_1$	No sample	White standard
$T_2$	Sample	White standard
$T_3$	No sample	Light trap
$T_4$	Sample	Light trap

A simple hazemeter schematic is shown in Figure 6.

ISO CD 14872, on the determination of haze of transparent material, specifies instrumentation similar but not identical to ASTM. While both methods require four measurements each, the sphere geometry employed is different.

Polymer morphology and its response to processing parameters will affect haze values. For example, polypropylene homopolymers have higher haze than random copolymers, with ethylene. A highly polished mold will produce much better optical quality samples than a nonpolished mold. The haze values of polypropylene copolymers, in cast film operations, will be affected by such parameters as die temperature, chill roll temperature, line output, and sample thickness.

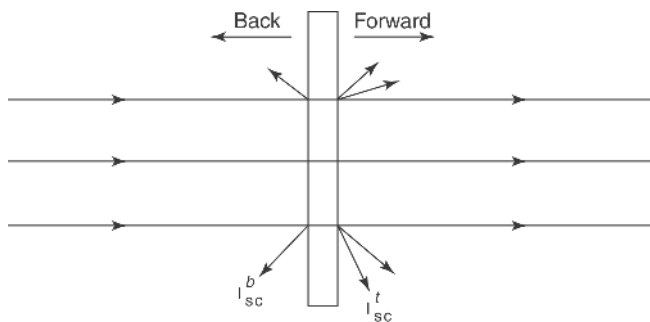


**Fig. 7.** Transmission of light through a sheet. From Ref. 30.

### Transparency and Clarity

Transparency is a property that depends mainly upon the optical homogeneity of the polymer both in the bulk and at the surface. The variation of the refractive index in the material has the following effects:

- (1) It produces changes in the phase and the amplitude of the light wave.
- (2) It removes from the incident wave part of its energy through scatter within a certain solid angle.

The first effect is responsible for the aberration of the image formed by the optical system, for example, films, sheets, or optical lens. Typically, loss of clarity is associated with the confusion in the image plane of two distinct points in the object plane.

The second effect is responsible for the deterioration of contrast of the formed image. The two effects are closely interrelated and together constitute the two different aspects of what is typically termed as “transparency.”

Consider a monochromatic parallel beam of unpolarized flux  $\phi$  incident perpendicularly on a polymer film immersed in a liquid of matching refractive index. A certain amount of the flux,  $\phi_{sc}$ , will be scattered in all directions; another part,  $\phi_{ab}$ , will be absorbed by the material. The remainder,  $\phi_{under}$ , will be transmitted without any deviation (Fig. 7) (30):

$$\phi_{under} = \phi - \phi_{ab} - \phi_{sc} \quad (26)$$

The specular transmittance  $T$  is defined as

$$T = \phi_{under}/\phi \quad (27)$$

$T$  is a function of the wavelength of the incident light and of the thickness of the sample. Immersion of the sample in a liquid of matching refractive index avoids having to take into account the reflective losses at the incident and emerging surfaces.

For materials of fairly high transparency, the relationship between specular transmittance and sample thickness  $Z$  is given by

$$T = \exp\{(-\sigma + K)Z\} \quad (28)$$

An expression based on the extinction index  $n''$  is

$$(\sigma + K) = (4\pi/\lambda)n'' \quad (29)$$

The sum  $\sigma + K$  is equivalent to the attenuation factor  $\alpha$ :

$$\alpha \simeq 54.6(n''/\lambda) \quad (30)$$

$\sigma$  is known as the scattering coefficient and is a measure of the amount of scattered light.  $K$  is the absorption coefficient and represents the amount of light absorbed. Both quantities have units of  $\text{m}^{-1}$ . Typically, for polymers,  $K$  is fairly small when compared to  $\alpha$ . Therefore, the attenuation coefficient may be taken to be equal to the scattering coefficient, which leads to the following expression for the total flux transmitted,  $\phi_T$ :

$$\phi_T = \phi_{\text{under}} + \phi_{\text{sc}} \quad (31)$$

Clarity is the ability of the sample to transmit the fine details of an object viewed through it. Maximum clarity is therefore achieved by minimizing the size of scattering centers as it is strongly related to the angular distribution of the scattering intensity. It is also affected by the distance between the object viewed and the sample (31).

Fresnel's law allows calculation of the maximum transparency  $\tau_i$  of a plastic material.

$$\tau_i = 1 - R_0 \quad (32)$$

with

$$R_0 = \frac{(n - 1)^2}{(n + 1)^2} \quad (33)$$

Maximum transparency of a polymer can range between 98% (for a refractive index of 1.33) and 92.8% (for a refractive index of 1.73). However, none of these values can be achieved in practice because there is always absorption and/or scattering of light by the sample.

For example, poly(methyl methacrylate) (PMMA), one of the most transparent plastics, never exceeds a transparency of around 93% for wavelengths between 430 and 1100 nm. In theory, however, PMMA could achieve a transparency of 96.1%. PMMA's transparency decreases above 1150 nm and below 380 nm.

Transparent polymers have values of  $\tau_i$  higher than 90%. On the other hand, polymers with  $\tau_i$  less than 90% appear clear as only thin films. These are called



translucent or contact-clear because films look clear when in contact with an object but hazy when viewed alone.

Clarity is negatively affected by light absorption and scattering. As we saw earlier, loss of contrast by forward scattering causes haze. The combined loss by scattering (both forward and backward) causes a “milk-like” appearance.

Local fluctuations of refractive index and/or orientation of anisotropic volume elements cause a polymer to be opaque. The various volume elements must be at least equal to the wavelength of the incident light. The clarity of the material can thus be increased considerably if elements such as microdomains are decreased. For example, spherulites are more homogeneous optically than lamellar structures of similar diameter.

Adjustment of refractive indices of phases within a polymer blend can somewhat improve the clarity of the polymer. For example, ABS-modified PVC has a milky/yellowish appearance if the ABS is dispersed in PVC. The blend looks bluish milky if PVC is dispersed in ABS. In general, if the dispersed materials have core-shell morphology then one can get transparent material if the mean refractive index of the core-shell particles matches that of the matrix.

Processing conditions strongly influence the morphology of polymers, thus affecting their transparency. For example, for injection/blow-molded PET, non-spherulitic structure and a limited range of crystal orientations can be achieved by (1) imparting crystallization at a low temperature upon heating from a glassy or partially disordered state, (2) cooling preforms very rapidly so they are glassy, and (3) subsequent reheating to 100°C, so very small crystals form. Biaxial stretching before the occurrence of crystallization results in the desired microstructure.

Minimization of the refractive index difference between the crystalline and amorphous phases will also yield in higher transparency of articles. For example, poly(4-methyl-1-pentene) will yield transparent injection-molded products because of the small difference in refractive index for the two phases.

The hiding power of a polymer surface is related to inhomogeneities (such as fillers or more than one phase) that cause strong reflections.

$$R_{0,h} = \frac{(n_1 - n_2)^2}{(n_1 + n_2)^2} \quad (34)$$

The refractive index of the polymer is given by  $n_1$  and that of the inhomogeneity (eg, filler) by  $n_2$ .

The hiding power of a polymer is also affected by light scattering. High filler concentrations lead to multiple scattering, which reduces the hiding power through reduction of the relative scattering intensity. If one wishes to increase the hiding power, one must look into increasing the backward scattering. Increasing the size of the filler particles would be one way to accomplish that. Typically though, one finds that the hiding power reaches a maximum at certain filler size and then it decreases.

ASTM D-1746 correlates see-through clarity with regular transmittance. However, the correlation is not very strong for highly diffusing materials. There is no method widely accepted for this property. The work of Webber is often cited as a popular approach (32).

## Reflection and Gloss

*Reflectivity* is defined as the ratio of the intensity of reflected to incident light. Both of these depend on the angles of incidence ( $\alpha$ ), and refraction ( $\beta$ ):

$$R = \frac{I_r}{I_0} = \frac{1}{2} \left[ \frac{\sin^2(\alpha - \beta)}{\sin^2(\alpha + \beta)} + \frac{\tan^2(\alpha - \beta)}{\tan^2(\alpha + \beta)} \right] \quad (35)$$

*Gloss* is the ratio of the reflectivity of a sample to the reflectivity of a standard.

The gloss increases with increasing refractive index and with angle of incidence. In the polymer film industry, three different angles are employed: 20°, 45°, and 60°. A test at an angle of 85° may also be performed in certain cases.

Gloss decreases when the sample has a rough surface because of the scattering. Optical inhomogeneities just below the surface also affect the values of gloss in a negative way.

Differences in local gloss on a surface cause “glitter” as a result of high directed light reflections. For example, polymer fibers show glitter if their cross-sections are triangular or trilobal.

Gloss can also be defined as the degree to which a surface simulates a perfect reflecting material in its capacity to reflect light. *Specular gloss* is the term used for the proportion of light reflected in the mirror direction. The typical standard for gloss is optically flat, black glass. However, the assigned values of gloss depend on the refractive index of the glass employed, so comparisons between tests must take that into account.

According to ASTM D523, an angle of 60° is recommended for general use, 20° for high gloss materials, and 85° for low gloss materials. ASTM D2457 suggests measurements at 20°, 45°, and 60°.

Polymer surface morphology will affect the value of gloss. Processing parameters as well as mold finish (for various molding operations) or chill roll finish (in cast film operations) will also affect gloss values. Typically, rubber-modified polyolefins have a lower gloss than highly crystalline polyolefins.

## Birefringence

Birefringence is the optical phenomenon in which a polymer sample exhibits different refractive indexes for light with plane polarization in two perpendicular directions. In other words, an unequal retardation of orthogonal components is observed. Crystalline phases in a polymer are birefringent. Birefringence may also be induced in the unordered phase by applying an orientation field, be that mechanical or electromagnetic. Orientation birefringence is a result of physical ordering of optically anisotropic elements along some preferential dimension. For uniaxially oriented samples, there will be two refraction indexes  $n_{\parallel}$  and  $n_{\perp}$  corresponding to the polarization of light parallel and perpendicular to the sample symmetry axis. In a Cartesian coordinate system, the birefringence for uniaxial symmetry will be given as

$$\Delta n = n_{\parallel} - n_{\perp} \quad (36)$$

Its individual components, along the axis, are given by

$$\Delta n_x = \Delta n_y \text{ and } \Delta n_z = 0 \quad (37)$$

A macroscopic, quantitative way to analyze birefringence is through Jones (33–40) and Mueller (41) calculus and the Poincare sphere (42). These tools are widely used in the optical industry and references on them abound. Another active field of birefringence applications is the combination of the technique with polymer rheology, called flow-birefringence (43,44).

### Birefringence of the Single-Chain and the Rotational Isomeric State Model

The optical behavior of a single isolated chain is central in building optical molecular theories for polymers. Application of the rotational isomeric state (RIS) model to strain-birefringence is a well-known technique that has been around for the last 30 years. We focus on the mechanics of calculating the optical configuration parameter of a chain. The optical-configuration parameter is central to the structure-property optical relationships in polymers. This will help us to better understand the optical behavior of polymer networks later on. Flory and Nagai have shown how to evaluate the optical-configuration parameter in terms of the RIS model, thereby obtaining the following equation (7,45,46):

$$\Delta\alpha_s = \frac{3}{2} \sum \frac{\langle r^T \hat{\alpha}_i r \rangle_0}{\langle r^2 \rangle_0} \quad (38)$$

where  $r^T$  is the transpose (ie, the row form) of the end-to-end vector  $r$  and  $\hat{\alpha}_i$  is the traceless tensor representing the anisotropy of the polarizability of bond  $i$  defined by

$$\hat{\alpha}_i = \alpha_i - \bar{\alpha}_i \mathbf{E}_3 \quad (39)$$

where  $\alpha_i$  is the polarizability tensor,  $\bar{\alpha}_i$  is the mean polarizability, and  $\mathbf{E}_3$  is the identity matrix of order 3. The angle brackets denote averages over the free unperturbed chain.

Application of the RIS model transforms the sum to a serial matrix multiplication scheme as follows:

$$\sum_{i=1}^n \langle r^T \alpha_i r \rangle_0 = 2Z^{-1} \mathbf{J}^* \left( \prod_{i=1}^n \mathbf{Q}_i \right) \mathbf{J} \quad (40)$$

The configuration partition function is denoted by  $Z$ . The matrix  $\mathbf{Q}_i$  is the generator matrix, for the quantity  $\langle r^T \alpha_i r \rangle_0$  and is a rather large expression. The interested reader is encouraged to consult Flory's work on the subject (7).

Matrix  $\mathbf{T}_i$  transforms a vector from its representation in local coordinate system  $i + 1$  into its representation in local coordinate system  $i$ . The row and

column operators  $J$  and  $J^*$  in equation 40 are given by the first and last columns, respectively, of the matrix  $\mathbf{Q}_i$ .

**Birefringence of Semicrystalline Polymers.** For semicrystalline polymers, the birefringence is the sum of the following terms:

$$\Delta n = v_c \Delta n_c + (1 - v_c) \Delta n_a + \Delta n_f \quad (41)$$

$v_c$  is the volume-fraction crystallinity determined from density measurements,  $\Delta n_c$  is the contribution to birefringence from the crystalline phase,  $\Delta n_a$  is the contribution of the amorphous phase, and  $\Delta n_f$  is the contribution from the boundaries between the two phases. An alternative expression, using the degree of crystallinity  $\chi_c$ , as it is determined from X-ray diffraction, is

$$\Delta n = \chi_c \Delta n_c + (1 - \chi_c) \Delta n_a + \Delta n_f \quad (42)$$

The value of  $\Delta n_f$  depends on the shape of the boundary between the phases as well as the difference in the average refractive indexes of the two phases. If that difference is small enough, one could neglect its contribution. One way to determine its value is to swell the oriented polymer in solvents of varying refractive index. The solvent should swell the amorphous phase only and alter its refractive index. Thus, the refractive index difference between the crystalline and the swollen amorphous phase may be altered (47).

Deformation birefringence arises as a result of an external deformation applied to the polymer sample. It could result from chain-packing changes or even bond-angle or bond-length deformations. Applying an external deformation is one way to make a normally optically isotropic sample optically anisotropic.

Deformation birefringence of a semicrystalline polymer is given by

$$\Delta n = v_c \Delta n_c^0 f_c + (1 - v_c) \Delta n_a^0 f_a + \Delta n_f \quad (43)$$

$\Delta n_c^0$  is the intrinsic birefringence of a crystalline phase, where the axis of the crystal is most nearly parallel to the chain axis.

The strain-induced birefringence in the amorphous region of a semicrystalline polymer disappears at the glass-transition temperature, as the chains assume isotropic configurations.

The deformation birefringence for graft or block copolymers is

$$\Delta n = v_A \Delta n_A^0 f_A + v_B \Delta n_B^0 f_B + \Delta n_f \quad (44)$$

The volume fractions of the individual components A and B are denoted by  $v_A$  and  $v_B$ . Their respective orientation functions are denoted by  $f_A$  and  $f_B$ .

**Birefringence of Polymer Networks.** Elastomeric polymer networks deserve special mention because their cross-linked structure gives them unique physical properties, unlike those of other polymers. Covalently bonded networks are insoluble in any solvent, even in those that dissolve their precursor polymers. Optical techniques such as strain-induced birefringence allow the development of structure-property relationships as well as the study of their optical

properties. Here we review some of the classical theories as well as some of the latest developments in the field.

*The Theory of Kuhn and Gr $\ddot{u}$ n.* The theory of birefringence of deformed elastomeric networks was developed by Kuhn and Gr $\ddot{u}$ n and by Treloar relying on the same procedure as that used for the development of the classical theories of rubber-like elasticity (48,49). The pioneering theory of Kuhn and Gr $\ddot{u}$ n is based on the affine network model: that is, upon the application of a macroscopic deformation, the components of the end-to-end vector for each network chain are assumed to change in the same ratio as that of the corresponding dimensions of the macroscopic sample.

Kuhn and Gr $\ddot{u}$ n proceeded to calculate the length of the deformed chain vector and its angular coordinates in terms of the original length and orientation and the macroscopic elongation of the sample. Their assumptions allow the calculation of the contribution of a given chain to the total polarizability referred parallel to the principal axes of strain. Integration over all network chains allows the determination of the total polarizability for the network.

The chain model adopted by Kuhn and Gr $\ddot{u}$ n is not based on the detailed chemical structure of the chain repeat units. Instead, the chain is composed of anisotropic “statistical segments” that become oriented as the network is deformed. Each segment is free to assume any orientation without any correlation to the orientation of the neighboring segments. The chain is considered to follow Gaussian statistics. Each link is assigned two polarizability components for light polarized parallel (symbol:  $\alpha_{\parallel}$ ) and perpendicular (symbol:  $\alpha_{\perp}$ ) to the segment axis. The difference in the refractive indexes is in general given by

$$n_i - n_j = \Delta n_0 \Psi_{ij} \quad i, j = 1, 2, \text{ or } 3 \quad (45)$$

where  $\Psi_{ij}$  is an orientation function depending on the angles  $\theta$  and  $\phi$ . The angle between the axis of the segment and the 3-direction is denoted by  $\theta$ . The angle between the projection of the segment on the 1,2-plane and the 3-axis is denoted by  $\phi$ . The Hermans orientation function is then given by

$$f = \frac{3\langle \cos^2 \theta \rangle - 1}{2} \quad (46)$$

where  $(\cos^2 \theta)$  is over the orientation of all segments.

On the basis of this model, Kuhn and Gr $\ddot{u}$ n developed the following expression for the stress-optical coefficient  $C$  for the case of uniaxial elongation:

$$C = \frac{\Delta n}{\tau} \frac{2\pi}{45kT} \frac{(\bar{n}^2 + 2)}{\bar{n}} \Delta \alpha_s \quad (47)$$

where  $\Delta n$  is the birefringence of the uniaxially stretched sample subjected to a stress  $\tau$  (per unit area in the stretched state),  $k$  is Boltzmann constant,  $T$  is the absolute temperature, and  $\bar{n}$  is the average refractive index of the network. The stress-optical coefficient is essentially the proportionality constant between the birefringence and the difference between the true stresses along the same axes. It is predicted to be independent of the degree of cross-linking and

proportional to the anisotropy of the statistical segment. Experimentally, it is found that this conclusion captures only part of the actual physics of the network. The anisotropy of the statistical segment  $\Delta\alpha_s$  is given by

$$\Delta\alpha_s = (\beta_1 - \beta_2)_s \quad (48)$$

where  $\beta_1$  and  $\beta_2$  are the polarizabilities parallel and perpendicular, respectively, to the axis of the segment.

One crucial assumption here is that the local field on a segment is given by the Lorentz–Lorenz equation, which implies that the environment of a segment is optically isotropic. (See also under Local Field). The treatment also involves the assumption of tensor additivity of polarizabilities of noninteracting segments (valence optical scheme or bond additivity scheme).

The anisotropy of a segment may be related to the anisotropy of the constituent bonds, again assuming polarizability additivity, by using

$$\Delta\alpha_s = \sum \{(\beta_1 - \beta_2)_i [3 \cos^2 \theta_i - 1] / 2\} \quad (49)$$

where  $\beta_{1i}$  and  $\beta_{2i}$  are the polarizabilities of the  $i$ th bond along and perpendicular to the bond axis, respectively, and  $\theta_i$  is the angle between the bond axis and the segment axis.

According to the theory, the orientation of the statistical links is predicted to be proportional to the stress difference,  $\tau_i - \tau_j$

$$\Psi_{ij} = \frac{1}{5} \frac{v_c}{v_L} (\alpha_i^2 - \alpha_j^2) = \frac{\tau_i - \tau_j}{5v_L kT} \quad (50)$$

where  $v_c$  is the number of network chains per unit volume and  $v_L$  is the number of statistical segments per unit volume.

**Birefringence of Phantom Networks.** This theory is the basis for all theories that deal with birefringence of elastomeric polymer networks. It is based on the phantom network model of rubber-like elasticity. This model considers the network consisting of “phantom” (ie, noninteracting) chains. Consider the instantaneous end-to-end distance  $r$  for the  $i$ th network chain at equilibrium and at fixed strain. For a perfect (ie, no-defects) phantom network, the birefringence induced because of a deformation is defined as (50)

$$\Delta n = \left( \frac{2\pi}{27} \right) \left( \frac{v}{V} \right) \left[ \frac{(n^2 + 2)^2}{n} \Gamma_2 \right] \left[ \Lambda_x^2 - \frac{(\Lambda_y^2 + \Lambda_z^2)}{2} \right] \quad (51)$$

$\Lambda_t^2$  are the components of the molecular deformation tensor, which is given by

$$\Lambda_t^2 = \left[ 1 - \frac{2}{\phi} \right] \lambda_t^2 + \frac{2}{\phi} \quad t = x, y, z \quad (52)$$

where  $\lambda_t^2$  are the components of the macroscopic deformation tensor.

As we saw previously, the quantity  $\Gamma_2$  is defined as

$$\Gamma_2 = \frac{9}{10} \sum_i \frac{\langle \mathbf{r}^T \hat{\mathbf{a}}_i \mathbf{r} \rangle_0}{\langle r^2 \rangle_0} \quad (53)$$

The summation is over all the units forming the chain.  $\hat{\mathbf{a}}_i$  is the anisotropic part of the polarizability tensor for the unit with index  $i$ .  $\mathbf{r}^T$  is the transpose vector of the end-to-end vector  $\mathbf{r}$ , and the subscript 0 signifies that the average is over all configurations of the free chain. It is assumed that the polarizability tensor for the chain with a given configuration is obtained as the sum of the polarizability tensors of the groups forming the chain.

The connection between the polarizability tensor and the parameter  $\Gamma_2$  given by

$$\left[ \alpha_{xx} - \frac{(\alpha_{yy} + \alpha_{zz})}{2} \right]_r = \Gamma_2 \frac{x^2 - [(y^2 + z^2)/2]}{\langle r^2 \rangle_0} \quad (54)$$

and  $\langle r^2 \rangle_0$  is the mean square end-to-end distance of a free chain.  $\alpha_{xx}$ ,  $\alpha_{yy}$ , and  $\alpha_{zz}$  are the  $x$ ,  $y$ , and  $z$  components of the tensor  $\hat{a}_i$  for the chain averaged over all configurations. The subscript  $r$  on the left side of equation 54 signifies that the averaging is for the chain with fixed ends.

Combining equations 51 and 52, we obtain for the birefringence of a phantom network,

$$\Delta n_{\text{ph}} = \left( \frac{\xi}{V} \right) kTC \left[ \lambda_x^2 - \frac{(\lambda_y^2 + \lambda_z^2)}{2} \right] \quad (55)$$

Focusing on the birefringence along the two principal axes  $x$  and  $y$  (typical for uniaxial deformation experiments), we obtained

$$\Delta n_{xy} = \left( \frac{2\pi v}{27V} \right) \left( 1 - \frac{2}{\varphi} \right) \left[ \frac{(n^2 + 2)^2 \Gamma_2}{n} \right] (\lambda_x^2 - \lambda_y^2) \quad (56)$$

For the development of equation 56, we have used the expression for the quantity  $C$ , the stress-optical coefficient, which is given by (compare to eq. 47)

$$C = \frac{2\pi}{27kT} \frac{(n^2 + 2)^2}{n} \Gamma_2 \quad (57)$$

and  $n$  is the mean refractive index of the network.

**The Real Network.** The total birefringence for a real network is the linear combination of the contributions resulting from the phantom network and the contributions arising from the constraints (51).

$$\Delta n_{xy} = \Delta n_{xy,\text{ph}} + \Delta n_{xy,\text{c}} \quad (58)$$

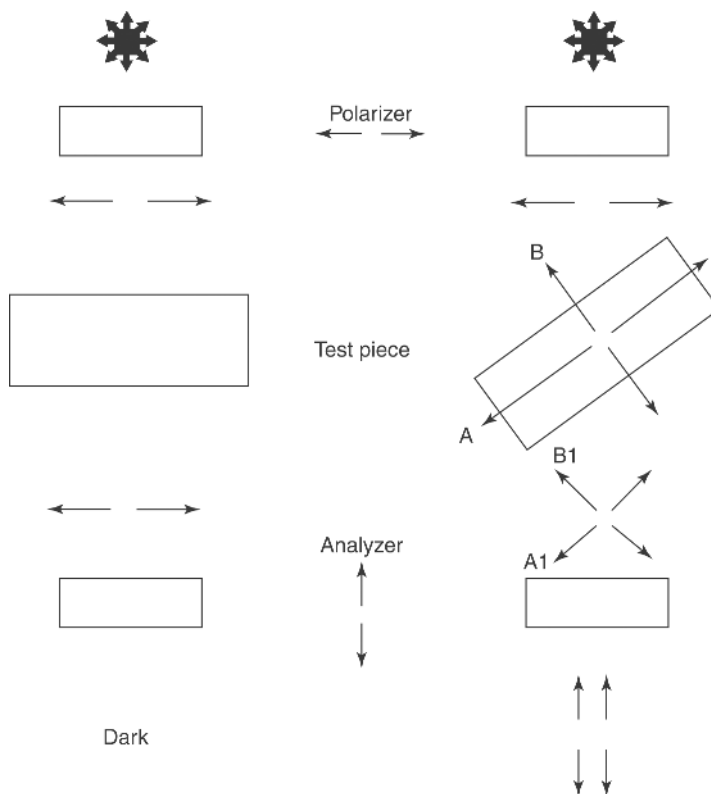


**Fig. 8.** Basis for experimental birefringence setup. From Ref. 54.

Flory has defined a reduced birefringence in a way similar to the reduced stress:

$$[\Delta n_{xy}] = [\Delta n_{xy,ph}] \left[ 1 + \frac{\Delta n_{xy,c}}{\Delta n_{xy,ph}} \right] \quad (59)$$

where

$$[\Delta n] = \Delta n \left( \frac{V}{V_0} \right)^{1/3} (\alpha^2 - \alpha^{-1})^{-1} \quad (60)$$

The contribution from topological constraints is based on the various theories of rubber-like elasticity (52).

**Birefringence Measurements.** Birefringence measurements rely on placing a birefringent object between crossed polarizers (53,54). The basic concept is depicted in Figure 8.

Placing the sample at  $45^\circ$  to the plane of light polarization causes the object to stand out on a dark background. The two components of the polarized light A and B correspond to the principal planes of the sample. These two components travel the sample at different speeds, thus causing the emerging beams A1 and



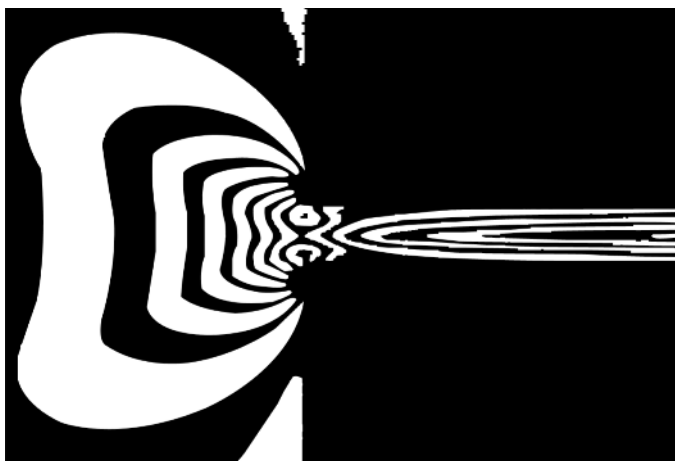


**Fig. 9.** Stress field visualization through birefringence. From Ref. 55.

B1 to be out of phase. Each of these components reaches the analyzer, where they may be resolved into components parallel and perpendicular to the analyzer direction. One can see the interference results since they cause bright colors (typically called interference patterns). A photosensor may also be used to help quantify the results. Advances in technology of photoelastic modulators (PEM) and digitizing image software are helping in the designing of new instruments that measure birefringence.

One application of birefringence related to polymer rheology is stress field visualization. It relies on flow-induced birefringence techniques to examine the spatial and temporal evolutions of stress in a polymer melt (see Fig. 9) (55). In this particular example, the picture shows the isochromatic fringe patterns of a high density polyethylene melt in the entrance region in capillary flow experiment at 200°C. Techniques such as the application of birefringence to polymer flow problems are very useful in understanding the polymer processing.

Extensional flow and structure–property relationships may also be studied by birefringence. A particularly interesting application from transient flow is presented in Figure 10, where phenomena such as overshoot and ringing are observed (55). In this example, we see results for 1.5% polyethylene oxide solution for three different velocity gradients. Birefringence detects the presence of an overshoot, whose magnitude increases with the velocity gradient, while the time needed to attain the maximum has decreased. Phenomena such as these are observed after start-up of an extensional flow in a four-roll mill at various strain rates. Theories of polymer rheology can be improved with the insight provided by such experiments.

## Nonlinear Optical Properties of Polymers

All the properties dealt with up until now involve linear interactions between light and polymer. Interaction of light with polymers in the nonlinear region

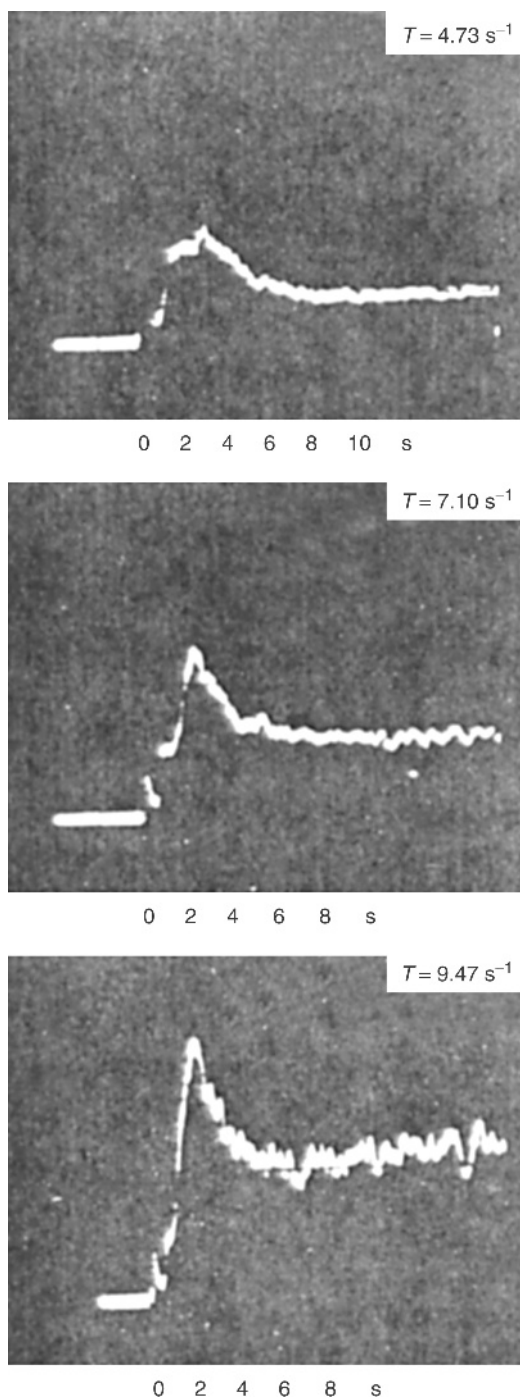


**Fig. 10.** Overshoot and ringing as observed through flow-birefringence experiments. In this example we see results for 1.5% polyethylene oxide solution for three different velocity gradients. From Ref. 55.

involves second- and third-order effects as well as the phenomenon of photo refractivity (56,57). An optical nonlinear optical (NLO) polymer is one that, in response to an externally applied electric field, can either vary the speed of incoming light or alter its frequency. Varying the speed of light involves a change in the refractive index of the material. An optically nonlinear polymer has two components: the polymer itself and an optically nonlinear molecule (chromophore), which is either chemically attached to the polymer or dissolved in it.

The induced polarization  $P$  of a polymer is given by

$$P = \chi^{(1)}E + \chi^{(2)}EE + \chi^{(3)}EEE + \dots \quad (61)$$

Linear optical phenomena involve the first-order susceptibility  $\chi^{(1)}$ , and in that case only the first term in the equation above is important. Higher order susceptibilities are involved in nonlinear optical phenomena. Susceptibilities are a function of wavelength.

An equivalent equation but at the molecular level is the following:

$$\Delta\mu = \alpha E + \beta EE + \gamma EEE + \dots \quad (62)$$

which gives the change in dipole moment  $\mu$  when the field  $E$  is applied. Molecular polarizability is given by the term  $\alpha$ . We saw equation 62 in a similar form earlier as equation 1. Higher order polarizabilities (hyperpolarizabilities) are given by  $\beta$  (second-order),  $\gamma$  (third-order), etc.

In order for the polymer–chromophore system to be optically nonlinear, the chromophores must be aligned so that on average they are all pointing in the same direction within the polymer. This alignment is achieved through a process called poling. The polymer is placed in a strong electric field, and its temperature is raised above its  $T_g$ . Above this temperature, the chromophores become mobile and can orient themselves in the external field. After orientation, the polymer is cooled back down to room temperature and the orientational ordering is “frozen-in.”

Polymer NLOs are easily formed into thin films for guiding light in the optical equivalent of integrated circuits. These can potentially be operated at very high data rates, much higher than those possible for inorganic systems. However, inorganic systems do not need poling to achieve nonlinearity. In polymer systems, orientation degradation occurs as a result of thermal noise. Cross-linking has been considered as an one method to stabilize the orientation of the chromophores. Another method is the use of high  $T_g$  polymer matrices.

The area of applications of nonlinear optics has not matured yet, and the opportunities for creative work, both theoretical and experimental, abound. Here, we have only covered some very introductory concepts.

## BIBLIOGRAPHY

“Optical Properties” in *EPST* 1st ed., Vol. 9, pp. 525–623, by Robert Zand, University of Michigan; in *EPSE* 2nd ed., Vol. 10, pp. 493–540, by N. J. Mills, University of Birmingham, U.K.; in *EPST* 3rd ed., Vol. 7, pp. 293–320, by V. Galiatsatos, Equistar Chemicals, L.P.

## CITED PUBLICATIONS

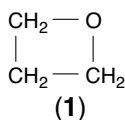
1. G. H. Meeten, ed., *Optical Properties of Polymers*, Elsevier, London, 1986.
2. K. S. Lee, ed., *Adv. Polym. Sci.* **158**, (2002). Special issue, "Polymers for Photonics Applications I"; K. S. Lee, ed., *Adv. Polym. Sci.* **161**, (2003). Special issue, "Polymers for Photonics Applications II."
3. T. Lippert, ed., *Adv. Polym. Sci.* **168**, (2004). Special issue, "Polymers and Light."
4. V. Galiatsatos, in K. B. Lipkowitz, and D. B. Boyd, eds., *Reviews in Computational Chemistry*, VCH Publishers, Inc., New York, 1995, pp. 6, 149.
5. V. Galiatsatos, *Polym. Eng. Sci.* **33**, 285 (1993).
6. P. W. Atkins, *Quanta*, 2nd ed., Oxford University Press, New York, 1991.
7. P. J. Flory, *Statistical Mechanics of Chain Molecules*, Interscience Publishers, New York, 1969.
8. C. P. Wong, ed., *Polymers for Electronic and Photonic Applications*, Academic Press, Inc., San Diego, Calif., 1993.
9. P. N. Butcher and D. Cotter, *The Elements of Nonlinear Optics*, Cambridge University Press, New York, 1990.
10. A. C. Newell and J. V. Moloney, *Nonlinear Optics*, Addison-Wesley Publishing Co., Redwood City, Calif., 1992.
11. S. Sen, V. Galiatsatos, and G. D. Patterson, *J. Chem. Phys.* **103**, 892 (1995).
12. P. Lorrain and D. R. Corson, *Electromagnetic Fields and Waves*, W. H. Freeman and Co., New York, 1970.
13. W. Kauzmann, *Quantum Chemistry*, Academic Press, New York, 1957.
14. L. Onsager, *J. Am. Chem. Soc.* **58**, 1486 (1936).
15. R. W. Christy, *Am. J. Phys.* **40**, 1403 (1972).
16. ISO 31/6 (1980), Quantities and units of light and electromagnetic radiations.
17. G. Ross and A. W. Birley, *Thermoplastics: Properties and Design*, John Wiley & Sons, Inc., London, 1974.
18. H. A. Lorentz, *Wied. Ann. Phys.* **9**, 641 (1880).
19. L. V. Lorenz, *Wied. Ann. Phys.* **11**, 70 (1880).
20. J. C. Seferis, in J. Brandrup and E. H. Immergut, eds., *Polymer Handbook*, 3rd ed., John Wiley & Sons, Inc., New York, 1989.
21. V. Galiatsatos, B. J. Sherman, S. Sen, and R. O. Neaffer, in J. E. Mark, ed., *Physical Properties of Polymers Handbook*, AIP Press, New York, 1996.
22. J. Bicerano, *Prediction of Polymer Properties*, Marcel Dekker, Inc., New York, 1993.
23. J. H. Gladstone and T. P. Dale, *Trans. R. Soc. (London) A* **418**, 518 (1858).
24. P. Debye and A. M. Bueche, *J. Appl. Phys.* **20**, 518 (1949).
25. R. S. Stein, in R. W. Lenz and R. S. Stein, eds., *Structures and Properties of Polymeric Films*, Plenum Publishing Corp., New York, 1973.
26. H. E. Bennet, *Opt. Eng.* **17**, 480 (1978).
27. M. Kerker, *The Scattering of Light*, Academic Press, Inc., Orlando, Fla., 1969.
28. J. M. Elson, H. E. Bennett, and J. M. Bennett, *Applied Optics and Optical Engineering*, Academic Press, Inc., Orlando, Fla., 1979.
29. F. W. Billmeyer, Jr. and Y. Chen, *Color Res Appl.* **10**, 219 (1985).
30. L. Mascia, *Thermoplastics: Materials Engineering*, 2nd ed., Elsevier Applied Science, New York, 1989.
31. H. Bender, *Kunststoffe* **59**, 501 (1969).
32. A. C. Webber, *J. Opt. Soc. Am.* **47**, 785 (1957).
33. R. Clark Jones, *J. Opt. Soc. Am.* **31**, 488 (1941).
34. Ref. 33, p. 493.
35. Ref. 33, p. 500.
36. R. Clark Jones, *J. Opt. Soc. Am.* **32**, 486 (1942).

37. R. Clark Jones, *J. Opt. Soc. Am.* **37**, 107 (1947).
38. R. Clark Jones, *J. Opt. Soc. Am.* **37**, 110 (1947).
39. R. Clark Jones, *J. Opt. Soc. Am.* **38**, 671 (1948).
40. R. Clark Jones, *J. Opt. Soc. Am.* **46**, 126 (1956).
41. H. Mueller, *J. Opt. Soc. Am.* **38**, 661 (1948).
42. H. Poincare, in Georges Carre, ed., *Theorie Mathematique de la Lumiere II*, Paris, 1892.
43. H. Janeschitz-Kriegl, *Polymer Melt Rheology and Flow Birefringence*, Springer-Verlag, Berlin, 1983.
44. V. N. Tsvetkov, *Rigid-Chain Polymers; Hydrodynamic and Optical Properties in Solution*, Consultants Bureau, New York, 1989.
45. K. Nagai, *J. Chem. Phys.* **40**, 2818 (1964).
46. K. Nagai, *J. Chem. Phys.* **47**, 2052 (1967).
47. A. N. Gent, *Macromolecules* **2**, 262 (1969).
48. W. Kuhn, *F. Grun Kolloid Z.* **101**, 248 (1942).
49. L. R. G. Treloar, *The Physics of Rubber Elasticity*, 3rd. ed., Clarendon Press, Oxford, U.K., 1975.
50. R. O. Neaffer and V. Galiatsatos, *Macromolecules* **26**, 4013 (1993).
51. J. E. Mark and B. Erman, *Rubberlike Elasticity, A Molecular Primer*, John Wiley & Sons, Inc., New York, 1989.
52. B. Erman and J. E. Mark, *Structures and Properties of Rubberlike Networks*, Oxford University Press, New York, 1997.
53. C. D. Han, *J. Rheol.* **25**, 139 (1981).
54. R. Brown, ed., *Handbook of Polymer Testing-Physical Methods*, Marcel Dekker, Inc., New York, 1999.
55. G. G. Fuller and L. G. Leal, *J. Polym. Sci., Polym. Phys. Ed.* **19**, 557 (1981).
56. P. N. Prasad and D. J. Williams, *Introduction to Nonlinear Optical Effects in Molecules and Polymers*, John Wiley & Sons, Inc., New York, 1990.
57. S. R. Marder, J. E. Sohn, and G. D. Stucky, eds., *Materials for Nonlinear Optics* (ACS Symposium Series No. 455), American Chemical Society, Washington, D.C., 1991.
58. E. Riande and E. Saiz, *Dipole Moments and Birefringence of Polymers*, Prentice Hall, Inc., Englewood Cliffs, N.J., 1992.

VASSILIOS GALIATSATOS  
Equistar Chemicals, L.P.

## OXETANE POLYMERS

Oxetane is a name commonly used for the unsubstituted cyclic ether with a four-membered ring and the structure (1):



This monomer is also known by other names including trimethylene oxide, oxacyclobutane, and 1,3-epoxypropane. The parent ether polymerizes readily as a result of ring strain associated with the small ring size. A variety of substituted oxetanes have been synthesized and many of them also polymerize readily (Table 1).

The most important chemistry needed to polymerize and understand the mechanisms of polymerization of oxetanes was observed in the late 1930s (5,6) and developed throughout the 1940s. Tetrahydrofuran (THF), the next higher member in the homologous series of cyclic ethers, was used as a model monomer. The first report of the polymerization of an oxetane was that of 3,3-bis(chloromethyl)oxetane (BCMO) (7). This was followed in 1955 by a detailed consideration of a family of 3,3-disubstituted oxetanes (8) and in 1956 by studies of the homopolymerization of oxetane itself (9,10). In each decade since then, interest in these polymerizations and in the resulting polymers has waxed and waned as monomers with different substituents became available and new applications for known polymers have been found.

During the 1950s, Hercules, Inc. developed a commercial synthesis for poly[3,3-bis(chloromethyl)oxetane] (PBCMO) and marketed the polymer for about 15 years, but it has since been withdrawn. Other oxetanes are being copolymerized, mainly with THF, to prepare precursors for use as the soft segment in polyurethanes (qv), polyethers, and poly amide-type elastomers. In the United States, interest has centered on energetic polymers prepared from oxetanes in which one or more of the hydrogen atoms in the 3 position have been replaced by

electron-deficient groups like  $\text{—CH}_2\text{CH}_3$ ,  $\text{—NO}_2$ , and  $\text{—CH}_2\text{OCH}_2\overset{\text{CH}_3}{\underset{|}{\text{C}}}(\text{NO}_2)_2$ . These materials are explored as precursors to polymers that can be used as propellants and other explosives.

## Monomers

**Properties.** More than a hundred different oxetanes have been synthesized; a few selected examples are given in Table 1 (see also Ref. 11). The parent, unsubstituted oxetane is a liquid that boils at  $\sim 48^\circ\text{C}$ . Fully deuterated and fully fluorinated analogues have been prepared (1). Alkyl, cycloalkyl, bridged hydrocarbon, haloalkyl, sulfonyl chloride, ether, ester, hydroxyl, sulfide, mercapto, amino, substituted amino, carboxyl, nitrile, nitro, and azido groups can be introduced at any desired position on the ring or in side chains. Multiple substitution is common. Sometimes the functional groups are attached directly to the ring; most often there is a methylene group between the ring and the functional group. The physical properties of the resulting monomers vary widely with the substituent. Substituted oxetanes can be solids or very high boiling liquids distillable only at reduced pressure.

Many of the oxetanes are polymerizable. Quantitative conversion to polymer is often observed when polymerizations are carried out under proper conditions with suitably purified materials and appropriate initiators (12). The basicity of the monomer and ring strain are important indicators of the polymerizability

**Table 1. Properties of Selected Oxetanes**

Monomer	Structure	Abbrev	Bp, °C <sup>a</sup>	Mp, °C	Polymer $T_m$ , °C	Refs.
oxetane		OX	47.8	-99	35	1,2
2-methyloxetane		2MOX	60		amorphous	1
3-methyloxetane		3MOX	67		amorphous	1
3-azidooxetane		AZOX	120–130 <sup>b</sup>		low mol wt oil	3
3-nitrooxetane		NIOX	77 <sup>c</sup>			3
3,3-dimethyloxetane		DMOX	80		47	1
3,3-dinitrooxetane		DNOX		70, 71	200–202	3
3,3-bis(chloromethyl)-oxetane		BCMO	91 <sup>d</sup>	19	170	1
3,3-bis(azidomethyl)-oxetane		BAMO	liq dec 160–170		75–78	4

<sup>a</sup>At 101.3 kPa unless otherwise noted. To convert kPa to mm Hg, multiply by 7.5.

<sup>b</sup>0.93–1.3 kPa.

<sup>c</sup>0.067–0.13 kPa.

<sup>d</sup>2.3 kPa.

of a given cyclic ether; both are high and favorable for polymerization of many oxetanes. The unsubstituted oxetane is the most basic of the unsubstituted cyclic ethers (13). It has a ring strain of 107 kJ/mol (25.6 kcal/mol), only slightly smaller than that of the readily polymerizable cyclic ether with a three-membered ring (oxirane) and more than 20 times greater than that of the cyclic ether with a six-membered ring, which does not homopolymerize (13).

Basicity and ring strain are not the only factors that determine polymerizability. Some substituted oxetanes do not polymerize under normal conditions because of the nature of their substituents. The usual mechanism by which oxetanes polymerize involves a cationic (oxonium ion) ring-opening reaction. Unless they are suitably protected, amine, hydroxyl, carboxyl, and other simple electron-donating substituents either inhibit polymerization entirely or terminate polymerization after one or two propagation reactions. Ether or formal substituents are known transfer agents and the molecular weight of any polymer formed is consequently reduced (12). Bulky substituents on the 2 and 4 positions may prevent polymerization due to steric inhibition; many electronegative substituents on the ring may prevent formation of a stable oxonium ion. However, copolymerization of such unpolymers with less substituted oxetanes or with tetrahydrofuran and other monomers that polymerize by a similar mechanism may still be possible. Copolymerization of this kind is known to occur with THF (12,14).

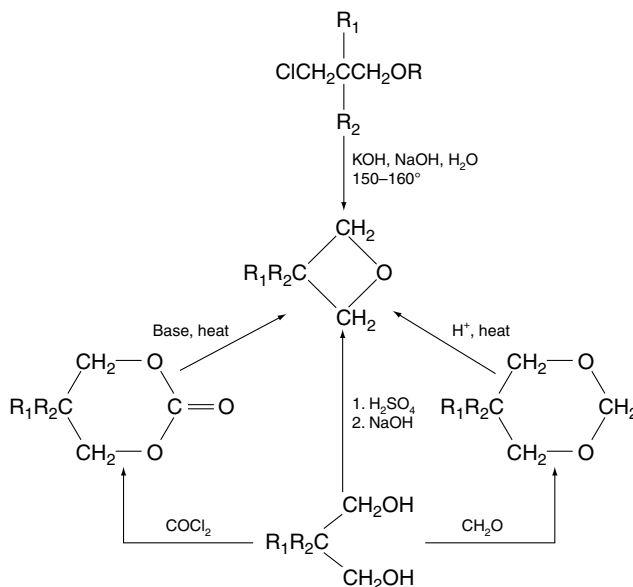
**Preparation.** Syntheses of oxetanes are well established, but side reactions are common and yields are usually not more than 60% (3,15). Purification is often difficult and adds significantly to production expense.

Figure 1 summarizes the methods commonly used to form the oxetane ring (1,3). Treatment of a 3-chloropropanol or 3-chloropropyl acetate with base is by far the most commonly used method. 3-Bromopropanols react in the same way, but treatment of 3-iodopropanols with alkali normally gives different products such as olefins (15). Iodo-derivatives, eg, 3,3-bis(iodomethyl)oxetane, are prepared by exchanging the chlorine or bromine of the corresponding 3,3-bis(halomethyl)oxetane using NaI as the source of iodine (1). Other substituted 3,3-bis(methyl)oxetanes, eg, fluoromethyl or azidomethyl derivatives, are similarly prepared using reagents like KF (1) or NaN<sub>3</sub> (3), respectively. Figure 2 outlines the methods that have been used (3) to prepare a series of oxetanes with other kinds of substituents in the 3 position. The key intermediate for this series of compounds is 3-hydroxyoxetane. The hydroxyl is protected during ring closure. The protecting group can be removed with acid; the hydroxyl group is converted to its *p*-toluenesulfonate (tosylate), and the 3-(tosyl)oxetane is converted by the methods shown to the 3-azido-, 3-amino-, 3-nitro-, and 3,3-dinitrooxetane derivatives.

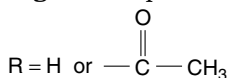
## Polymerization

The ring-opening polymerization (qv) of oxetane (OX) is primarily accomplished by cationic polymerization (qv) methods. Insertion polymerization (16), anionic polymerization (qv) (17), and with certain special oxetanes, a free-radical ring-opening polymerization (18) have also been used. In certain cases, aluminum-based catalysts (18) impose a degree of microstructural control on the





**Fig. 1.** Preparation of oxetanes (1,3).  $R_1, R_2 = \text{H}, \text{CH}_2\text{X}$  or other functional group and



polymerization process that is not obtainable with a pure cationic system. The polyoxetane structure has also resulted from an anionic rearrangement polymerization. A polymer having largely the structure of poly(3-hydroxyoxetane) was obtained from the anionic polymerization of glycidol or its trimethylsilyl ether, both oxirane monomers (19).

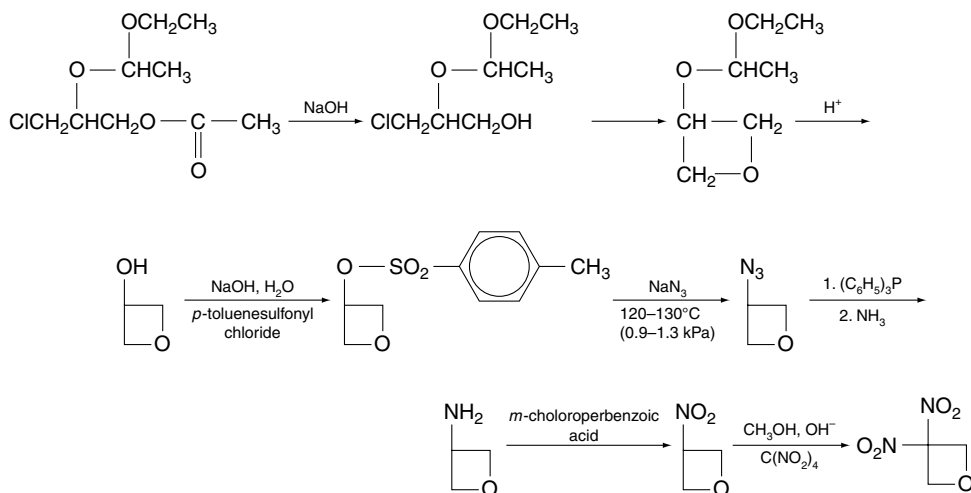
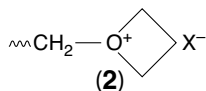
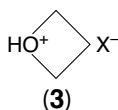


**Fig. 2.** 3-Hydroxyoxetane derivatives (3).

**Initiators.** The initiation of cationic polymerization requires a reagent that generates the propagating tertiary oxonium ion (2):



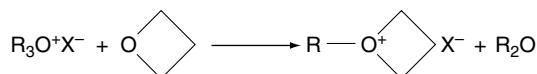
This can be accomplished by a variety of electrophilic reagents such as Lewis acids, preformed trialkyl oxonium ion salts, acylium ion salts, carbocationic salts, etc. Appropriate strong acids may be used, either directly or generated *in situ*, but present the complication that the secondary oxonium ion formed first (3)



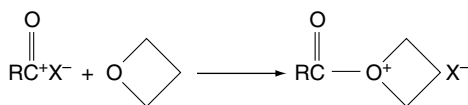
is unreactive relative to the propagating tertiary oxonium ion (2)(10). A counterion  $\text{X}^-$  of rather low nucleophilicity is required in order to generate a propagating oxonium ion species of adequate stability (14). Thus simple anions such as chloride or bromide are not suitable because they collapse immediately to the corresponding haloalkyl ether (or alcohol). The ions used in the earliest studies were commonly  $\text{BF}_4^-$  or  $\text{BF}_3\text{OH}^-$  which allowed for practical polymerizations of the reactive oxetane ring system, but suffered from a degree of instability evident in careful kinetic analyses. Thus more recent studies have tended to use the marginally better  $\text{SbCl}_6^-$  or the superior ions  $\text{PF}_6^-$ ,  $\text{AsF}_6^-$ , or  $\text{SbF}_6^-$  (14,20). The exact nature or structure of the anion formed with the alkyl aluminum–water initiators is not known, but it seems to function as a very stable ion of low nucleophilicity.

**Lewis Acid Types.** The Lewis acids corresponding to the counterions just discussed are suitable initiators for oxetane polymerizations. Thus  $\text{BF}_3$  or  $\text{BF}_3$  etherate was used in classic studies of OX polymerization (9,10). Pure dry monomer will not polymerize with  $\text{BF}_3$  alone (7); an active hydrogen material, generally water or an alcohol, is required and leads to a  $\text{BF}_3\text{OH}^-$  or  $\text{BF}_3\text{OR}^-$  counterion. Some of the stronger Lewis acids such as  $\text{PF}_5$  or  $\text{SbF}_5$  are able to self-initiate and do not require the presence of active hydrogen compounds (21).

**Preformed Trialkyl Oxonium Ion Salts.** The preparation of triethyl and trimethyl tetrafluoroborate has been described (22). The corresponding hexafluorophosphate or hexafluoroantimonate salts can be prepared similarly or a method starting with a commercially available hexafluorophosphoric acid solution can be used (23). Additionally, the salts are often formed *in situ* using the Lewis acid with a so-called epoxide promoter (24). These salts are strong alkylating agents and initiate polymerization by a simple alkyl exchange reaction:

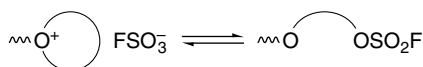


**Acylium Ion Salts.** The acylium ion salts corresponding to the counterions mentioned above are also good initiators:



The acyl dialkyl oxonium ion is about as reactive as a similar trialkyl ion. These salts can also be isolated and used directly, or they can be formed *in situ* from the acid chloride and a silver salt, eg, silver hexafluoroantimonate (25).

**Super Acids and Their Esters.** These compounds are often excellent initiators for cationic polymerization of cyclic ethers. The fluorosulfonates and trifluoromethanesulfonates especially have been exploited. The polymerization kinetics are complicated by an ester ion equilibrium, but proper choice of a solvent with a high dielectric constant



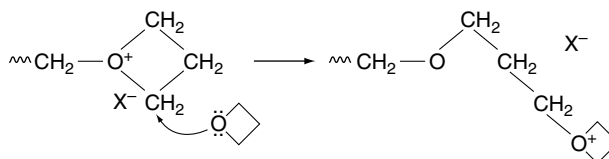
often favors the formation of the reactive ion and produces good polymerization rates (14). However, these initiators have been found to be of little value in oxetane polymerizations. For example, polymerization of BCMO initiated by ethyl trifluoromethanesulfonate proceeds extremely slowly because the above equilibrium is far to the right under polymerization conditions (26); the ester form is virtually unreactive to the cyclic ether and does not participate in the propagation reaction. Moreover, the active oxonium ion, when formed, collapses immediately to the corresponding ester. Thus a suitable mechanism for rapid polymer formation with this otherwise excellent group of initiators does not exist for BCMO and probably not for other oxetanes as well.

**Aluminum Alkyl-based Initiators.** Cationic initiators can be prepared from trialkylaluminum by modification in inert solvent with 0.5–1.0 mol of water per mole of aluminum alkyl (27,28). Initiator efficiencies and rates of initiation are enhanced by the use of epoxide promoters with *in situ* trialkyl oxonium salt formation (24,28). A true cationic polymerization strictly analogous to those obtained with Lewis acid initiators is obtained, but the true nature of the counterion formed is not known and, in fact, is probably not a single species. Furthermore, it is difficult to predict the exact number of active sites that form (29,30). The alkyl aluminum coordination catalysts, developed primarily for oxirane polymerizations, can also be successfully applied to oxetanes (16). These catalysts are prepared by adding one of several coordinating modifiers to a water-modified aluminum alkyl system. The most commonly used modifier appears to be acetone (2,4-pentanedione) (16,31,32).

**Other Initiators.** Cationic polymerization of oxetane has been initiated electrochemically (33), by  $\gamma$ -rays (34), by free-radical systems (18,35), and by uv radiation (36). These methods have not achieved any great importance.

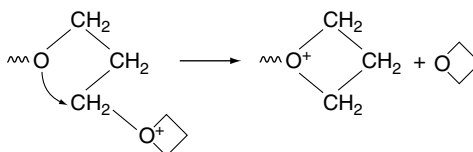
**Mechanistic Considerations.** The cationic ring-opening polymerization of four-membered (and higher) cyclic ethers takes place by a nucleophilic attack

of the incoming monomer oxygen on one of the two-ring,  $\alpha$ -carbon atoms of the active cyclic oxonium ion:

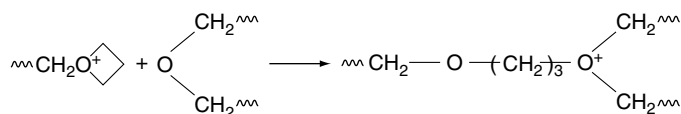


If the oxetane is unsymmetrically substituted, the microstructure of the product differs if attack occurs only at one of the two  $\alpha$ -carbon sites or if both  $\alpha$ -carbon atoms are subject to attack.

The monomer oxygen atom is not the only reactive oxygen atom in the system. All ether oxygen atoms in the backbone, side chains, or additives are potentially reactive. Thus polymer oxygen atoms can attack the active cyclic oxonium ion. Intramolecular attack by polymer oxygen, ie, attack of the oxonium ion end group by a polymer oxygen of the same polymer chain, can lead to either depolymerization (qv) or to formation of cyclic oligomers. Attack by the penultimate oxygen atom ion leads to depolymerization:



Whereas this is an important reaction for tetrahydrofuran, it is energetically unfavored for the highly ring-strained oxetane system and does not need to be considered under ordinary polymerization conditions. Attack of this same oxygen atom at either of the two-ring,  $\alpha$ -carbon atoms leads to an eight-membered ring, which also is energetically unfavored and not found. Attack by oxygen atoms further back on the chain leads to the oxonium ion precursors of larger ring systems that are often found in substantial quantities. Intermolecular attack by polymer oxygen leads to the formation of polymeric acyclic oxonium ions:



Such ions have been invoked to explain various kinetic features, eg, temporary termination as an explanation of the dramatic change from a very rapid to a slow, steady polymerization rate (37). Evidence of polymeric acyclic oxonium ions was inferred from the higher viscosity of an unterminated oxetane polymerization solution compared to the viscosity of the same solution just after amine termination (38). This effect was not observed for a DMOX polymerization where steric inhibition prevents reaction of polymer oxygen. Intermolecular reaction of polymer

oxygen also accelerates broadening of the molecular weight distribution to its most probable value of two.

**Kinetics.** The kinetics of OX and DMOX polymerizations were first considered in 1956 (10). Subsequent analysis has shown that the kinetic expression for these polymerizations can be reduced to

$$\frac{-d[M]}{dt} = k_p[I_0][M]$$

which was thought to describe all oxetane polymerizations adequately regardless of the initiator used (39). Here only the propagation rate constant  $k_p$  is used and  $[I_0]$  represents either the concentration of a fast, 100% efficient initiator or the concentration of active sites as measured directly;  $[M]$  is monomer concentration. Some systems may not be this simple and rate constants obtained from actual measurements of active sites may represent average, overall rate constants encompassing several processes.

The following conclusions for OX polymerizations in methylene chloride at  $-30^\circ\text{C}$  using  $\text{PF}^-$  counterion have been presented (37). Initiation with the trialkyl oxonium ion salt is slow. Initiation with trityl salts is by direct addition of the trityl carbocation to oxetane and the reaction is fast. The polymerization, ie, the propagation reaction, is very fast. A competing fast reaction with polymer oxygen removes active growing sites to form dormant or "sleeping" ions by a process often referred to as temporary termination. The polymeric acyclic oxonium ion so formed is analogous in structure and reactivity to the triethyl oxonium ion and thus reacts only slowly with monomer to reinitiate the fast polymerizing active site. Such participation of polymer oxygen also accounts for the molecular weight distributions which are broader than the anticipated Poisson distribution. Furthermore, such a scheme is also consistent with the proposals that have been made to explain cyclic oligomer formation.

More recent studies with 3MOX, carried out at  $-78^\circ\text{C}$  and using acetyl hexafluorophosphate as initiator, confirm the extremely fast propagation rate (40). Near quantitative conversion to polymer in less than two minutes suggests no involvement of polymer oxygen using this monomer under these conditions. A similar observation was made when DMOX polymerization was qualitatively compared with OX polymerization, both at  $25^\circ\text{C}$  in methylene chloride and both initiated by triethyloxonium hexafluoroantimonate (38). The rate of polymerization of DMOX was much faster than that of OX, and a lack of the viscosity effect upon termination of the DMOX polymerization suggested little, if any, involvement with polymer oxygen in the case of DMOX. Qualitative or quantitative kinetic data bearing on this point have not yet been reported for other substituted oxetanes.

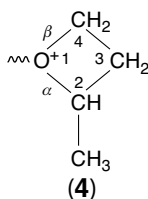
**Cyclic Oligomers.** The formation of high polymer from OX monomers is often accompanied by variable amounts of low molecular weight oligomeric material, eg, the cyclic tetramer, a 16-membered tetraoxacyclic ether (9). The amount of cyclic tetramer that forms varies with polymerization conditions and with monomer structure; OX and DMOX form cyclic tetramer, whereas 2MOX and BCMO do not. Later studies showed that small amounts of a cyclic trimer can form in BCMO polymerizations (41). In more recent studies, in the case

of the unsubstituted OX, both cyclic tetramer and cyclic trimer form (42). The amounts formed vary with counterion, polymerization temperature, and solvent. A more detailed study revealed that an array of cyclic oligomers results for both OX (trimer through octamer) and DMOX (tetramer through nonamer); tetramer is the major one in both cases (43). Oligomers are formed only from polymer (not by a direct reaction) and only in the presence of monomer. First, a "backbiting reaction," ie, an intramolecular reaction of polymer oxygen, forms a macrocyclic oxonium ion. Subsequent reaction with monomer at the exocyclic methylene group releases the free macrocycle and regenerates the active propagating ion (43).

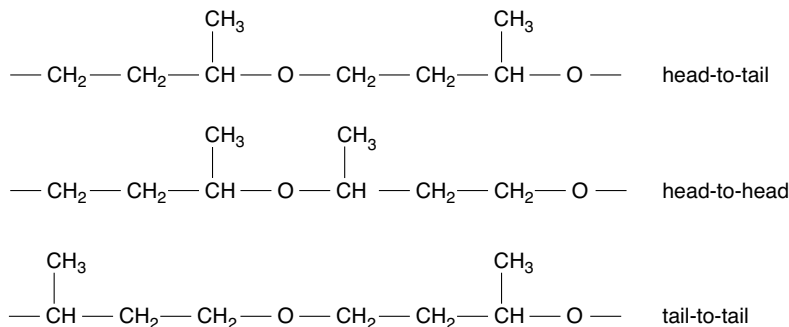
The ease of macrocycle formation is very dependent on stereochemical considerations, such as the preferred conformation of polymer chains. Thus the extent of cyclic oligomer formation varies greatly with oxetane-ring substitution (see also MACROCYCLIC POLYMERS).

**Microstructure.** High frequency nmr instrumentation is useful for studies of the microstructure of unsymmetrically substituted oxetanes and oxetane copolymers. Propagation occurs when monomer attacks either of the two endocyclic  $\alpha$ -carbon atoms of the active cyclic oxonium ion. In the case of the unsubstituted OX or the 3-substituted derivatives, the molecules are symmetrical and no observable differences arise between attack at the two endocyclic  $\alpha$ -carbon atoms.

However, for the 2-substituted oxetane, eg, 2MOX,



attack at C-4 results in  $\beta$ -bond cleavage, opening of the O—CH<sub>2</sub> bond, whereas attack at C-2 results in  $\alpha$  cleavage. Exclusive attack at one position to give only  $\beta$  (or  $\alpha$ ) cleavage results in a regular head-to-tail structure. But even occasional attack at the other position to give  $\alpha$  (or  $\beta$ ) cleavage results in backwards placement of the monomer unit and consequent head-to-head, tail-to-tail structural units:



Furthermore, the head-to-head linkages can have either a meso or a racemic configuration of the two methyl groups.

Cationic polymerization results in both  $\alpha$  and  $\beta$  cleavage. Both head-to-tail and head-to-head, tail-to-tail placement can be detected by  $^{13}\text{C}$  nmr (20,27,44). The extent of mixed cleavage depends on polymerization temperature. Higher temperatures favor more random attack at the two sites. An alkyl aluminum catalyst system coordinated with acetylacetone results in exclusive head-to-tail placement (27,32). Either  $\alpha$  or  $\beta$  cleavage occurs exclusively; this result cannot distinguish between the two modes of cleavage. In addition, the coordinate catalyst exerts steric control, and measurement of isotactic, syndiotactic, and heterotactic triad concentrations showed that syndiotactic placement was somewhat favored over the random placement found in the head-to-tail units produced by cationic catalysts. Further analysis using optically active 2MOX monomer led to pure isotactic structure with coordinate catalysis and showed that  $\alpha$  cleavage occurs primarily with inversion of configuration of the chiral center (45,46).

In the polymerization of *cis*- and *trans*-2,4-dimethyloxetane, the meso *cis* isomer is converted to a polymer that has a largely racemic diisotactic structure (45,47). The racemic *trans* isomer yields a polymer suggesting random placement of the repeating units. Thus the direction of ring opening is influenced by the configuration of the growing oxonium ion only for the *cis* isomer. The anionic and insertion polymerizations of propylene oxide also include some head-to-head monomer placement (31,48).

An oxetane doubly substituted in the 2 position, the 2,2-dimethyloxetane, leads exclusively to head-to-tail structure under cationic conditions (49). Ring opening occurs exclusively by  $\alpha$  cleavage as a result of an equilibrium between the oxonium ion and the corresponding ring-opened tertiary carbocation. It is suggested the propagation in this case is via the carbocation, whereas the oxonium ion easily undergoes transfer to monomer. In this way, the production of only low molecular weight polymer and oligomers with primary hydroxyl and isopropenyl end groups is accounted for (49).

Though symmetrically substituted, the P3MOX can, in theory, show isotactic-syndiotactic-heterotactic placement of the lone methyl along the polymer chain. It is very difficult to detect by  $^{13}\text{C}$  nmr because the isotactic-syndiotactic-heterotactic splitting is only about 0.017 ppm (compared to 0.14 ppm for P2MOX). Though it could not be accurately assessed, the relative areas were consistent with a totally random placement of the methyl groups (40).

**Polyoxetane Glycols.** Relatively low molecular weight polyethers with hydroxy end groups have been the only commercially important products resulting from THF polymerization. Thus as the next lower homologue, with increased potential for functional or modifying ring substitution, the oxetanes offer an enticing extension of this chemistry. However, as has been noted, oxetane polymerization is very fast and control of the polymerization to give low molecular weight products with end-group functionality has, until recently, not been possible. Japanese patents (50,51) describe the preparation of low molecular weight oxetane-tetrahydrofuran copolymers using methods that appear similar to those used to prepare PTHF glycols (52). The preparation of polyoxetanes and oxetane-THF copolymers substituted with energetic groups such as azido or nitro have also been described (4,53-55). The latter methods generally involve

polymerization in the presence of relatively large amounts of organic diols, eg, 1,4-butanediol, or the use of preformed Lewis aciddiol mixtures as polymerization initiators. Butyllithium has been used to cleave high molecular weight polyoxetane (POX) to low molecular weight POX glycols (56). Low molecular weight POX glycols have also been prepared by ozone degradation of a high molecular weight polymer followed by lithium aluminum hydride reduction or by direct polymerization using Lewis aciddiol mixtures as initiator (57). Standard methods and recipes are then used to extend the chain of these glycols into polyurethane networks (58). POX glycols have also been used to prepare a series of block copolymers (qv) (59).

**Copolymers.** Oxetane copolymerizes, often competing effectively with other oxetanes and with other cyclic ethers such as oxiranes or THF or with lactones, dioxanes, or dioxolanes (28). Copolymerization (qv) is often desired in order to modify and adjust crystallinity or crystallization rates. Symmetrical oxetanes generally crystallize readily and for some applications this is not a desirable property, eg, for elastomeric applications. Since BCMO was once commercial and its polymer is highly crystalline and high melting, its copolymerizations have been extensively studied (28). Copolymerization of BCMO with the dioxolane ring of a 1,6-anhydroglucopyranose has also been demonstrated (60). Many pairs of reactivity ratios ( $r_1r_2$ ) covering a wide variety of copolymers of oxetanes have been determined and tabulated (28,61). These values can vary substantially with conditions and need to be critically evaluated before use.

Studies of ionomers have resulted in copolymerizations of oxetane with ethyl glycidate (62) and with ethyl undecanoate (63,64). Ethyl glycidate does not copolymerize readily and only copolymers containing ca 1 mol % ethyl glycidate have been prepared. The copolymerization of DMOX with THF was studied in order to determine the  $T_g$  (see also GLASS TRANSITION) of various compositions (65) and the apparent  $r_1, r_2$  values (66). The latter studies indicated that random copolymers were formed. Random copolymerization was also found for the DMOX–OX pair (67). The study suggested that OX was more reactive than DMOX toward each of the two growing ions. A study of the copolymerization of 2MOX with 2-methyltetrahydrofuran, which does not homopolymerize, showed that copolymerization of 2-methylTHF also does not occur readily. Nmr analysis indicated that both monomers entered the polymer chain in both head-to-tail and head-to-head placement (68), that is, on copolymerization both monomers behave like 2MOX (20).

Copolymerization with carbon dioxide has been demonstrated (69). Reaction with carbon dioxide to give a polycarbonate requires an alkyl tin catalyst modified with a phosphine or an amine.

## Properties of Polymers

A large number of polyoxetanes have been prepared and partially characterized (1). The properties of the polymers vary greatly with the symmetry, bulk, and polarity of the substituents on the chain (Table 1). The polymers range from totally amorphous liquids to highly crystalline, high melting solids. The unsubstituted



oxetane polymer has a melting temperature of 35°C, not far above ambient temperature. A single methyl substituent at either the 2 or 3 position gives a polymer with stereoisomeric possibilities. Only amorphous polymers have been reported for oxetanes with single methyl substituents (1,10). The 3,3-dimethyl derivative gives a crystalline polymer with a melting temperature of 47°C, whereas 3,3-bis(halomethyl)oxetanes melt at 135, 180, 220, and 290°C for fluoro-, chloro-, bromo-, and iodo- derivatives, respectively (1). As usual, the effect of copolymerization is to lower the melting temperature. For example, the random, high molecular weight copolymer of BCMO and THF is a tough, amorphous rubber (12).

Other crystallization parameters have been determined for some of the polymers. Numerous crystal-structure studies have been made (70–77). Isothermal crystallization rates of polyoxetane from the melt have been determined from 19 to –50°C (78,79). Similar studies have been made for PDMOX from 22 to 44°C (80,81).

The pressure dependence of the glass-transition temperature  $T_g$  of BAMO–THF copolymer has been determined by high pressure ( $\leq 850$  MPa or 8.5 kbar) dta and dielectric methods (82).  $T_g$  increases with increasing pressure. The results fit a modified Gibbs–DiMarzio theory. The effect of copolymer composition on  $T_g$  (65) and on dipole moments (83) has been studied over the whole composition range for DMOX–THF copolymer. The copolymers exhibit a  $T_g$  intermediate between those of the parent homopolymers.

Solubility parameters of 19.3, 16.2, and 16.2 (J/cm<sup>3</sup>)<sup>1/2</sup> have been determined for POX, PDMOX, and poly(3,3-diethyloxetane), respectively, by measuring solution viscosities (84). Heat capacities have been determined for POX and compared to those of other polyethers and polyethylene (85,86). The thermal decomposition behavior of poly[3,3-bis(ethoxymethyl)oxetane] has been examined (87).

Properties have been determined for a series of block copolymers based on poly[3,3-bis(ethoxymethyl)oxetane] and poly{[3,3-bis(methoxymethyl)oxetane]-*co*-THF}. The block copolymers had properties suggestive of a thermoplastic elastomer (59) (see THERMOPLASTIC ELASTOMERS).

Extensive physical property measurements have been reported only for PBCMO (88,89) (Table 2). This polymer was commercially available in the United States from Hercules, Inc. for about 15 years under the trade name Penton, but it is not currently produced for commercial sale. It has also been studied extensively elsewhere under the name Pentaplast. The comparatively high heat-distortion temperature combined with a low water-absorption value make PBCMO suitable for articles that require sterilization. It also has excellent electrical properties, a high degree of chemical resistance, and, because of the chlorine in the backbone, is self-extinguishing. PBCMO is resistant to most solvents, specifically to ketones, water, aldehydes, esters, aromatic hydrocarbons, and weak organic bases, eg, aniline, and ammonia, weak acids, weak alkalis, and strong alkalis; it is attacked by strong acids (88). It is reported to be somewhat soluble in hot *o*-dichlorobenzene or cyclohexanone and in hexamethylphosphoramide at room temperature (1). It is attacked by fuming nitric acid and sulfuric acid (88). Most other crystalline oxetane polymers are also insoluble in common organic solvents (71). The amorphous and low melting oxetane polymers, in contrast, are soluble in a wide variety of organic solvents.

**Table 2. Typical Properties of Poly[3,3-bis(chloromethyl)oxetane]**

Property	Value		Refs.
melting temperature, °C	$\alpha$ form, 186	$\beta$ form, 180	90
glass-transition temperature, °C	7–32 <sup>a</sup>		90
density, 25°C, g/cm <sup>3</sup>			
amorphous	1.386		90
crystalline	1.47		90
compression modulus, 6.9 MPa <sup>b</sup>	130		91
tensile strength, MPa <sup>b</sup>	41.4		88,90,91
elongation at break, %	35–150		88,91
heat-distortion temperature, °C			
1.82 MPa <sup>b</sup>	85–93		91
0.48 MPa <sup>b</sup>	149		91
izod impact (notched), 228°C, J/m <sup>c</sup>	27		88,91
Rockwell hardness	R100		91
flexural strength, MPa <sup>b</sup>	34.5		88
thermal expansion, 10 <sup>-5</sup> /°C	8		88
volume resistivity, $\Omega$ ·cm	$1 \times 10^{16}$		88
dielectric strength, V/ $\mu$ m	16		88
dielectric constant, 10 <sup>6</sup> Hz	3		88
power factor, 10 <sup>6</sup> Hz	0.011		88
flammability	self-extinguishing		88
water absorption, % (24 h)	0.1		88
mold shrinkage, cm/cm	0.005		88
crystallographic data	$\alpha$ form	$\beta$ form	71
crystal system	orthorhombic	monoclinic <sup>d</sup>	
space group	D2H-2, D2H-16	CS-1 or CS-2 CS-3	
unit cell			
<i>a</i> , nm	1.785 <sup>e</sup>	0.685, 1.142	
<i>b</i> , nm	0.816 <sup>e</sup>	1.142, 0.706	
<i>c</i> , nm	0.467–0.482	0.475, 0.482	
$\beta$ , degrees		109.8, 114.5	
monomer/unit cell	4	2	
crystal density, g/cm <sup>3</sup>	1.47–1.514	1.472, 1.456	
heat of fusion, kJ/mol	23.0		
chain configuration, N*P/Q	3*1/1	3*1/1	

<sup>a</sup>Depends on method of determination.<sup>b</sup>To convert MPa to psi, multiply by 145.<sup>c</sup>To convert J/m to ftlb/in., divide by 53.38.<sup>d</sup>Two groups of data for a monoclinic cell are given in Table 2. A third group suggests an orthorhombic cell with C2V-12 space group; *a* = 1.301 nm; *b* = 1.171 nm; *c* = 0.467 nm; 4 monomers/unit cell and a crystal density of 1.447 g/cm<sup>3</sup>.<sup>e</sup>One reference reverses *a* and *b*.

## Processing

This discussion is limited to processing of PBCMO because this is the only oxetane polymer that has been commercialized (88). A typical commercial polymer

had a number-average molecular weight of 250,000–350,000. Such PBCMO can be injection-molded in standard machines, using chrome-plated or polished hard-steel dies. As a result of its highly crystalline nature, PBCMO has a fairly low melt viscosity and easily fills molds. Molding cycles of 20 s or less are possible for parts with wall thicknesses of 1.6 mm or less. A stress-free molding with low shrinkage on cooling is obtained. The parts can be machined easily and components with exceptional dimensional stability are produced. PBCMO can also be extruded, using screw designs of the type used for nylon or polyethylene and temperatures of 182–230°C. Because of its low water absorption, predrying of the molding powder is not necessary. Coatings with a homogeneous void-free finish up to 1-mm thick can be applied to a variety of substrates (glass, steel, paper) by water or solvent-dispersion systems or by using the fluidized-bed technique of coating (88).

### Analytical and Test Methods

**Titration.** A rapid method for determining the oxetane content of a sample by titration has been reported (92). The sample (1–2 meq) is refluxed for 3 h with 25 mL of 0.20-*N* pyridinium chloride in anhydrous (<0.01% water) pyridine to convert the oxetane to its 1,3-chlorohydrin. The mixture is cooled and the apparatus is rinsed with 50-mL water. Excess pyridinium chloride is titrated with standard aqueous alkali (0.15-*N* NaOH) using phenolphthalein indicator. A blank determination is carried out on 25 mL of the pyridinium chloride solution. The difference between the blank and the excess is a measure of the oxetane content of the sample:

$$[(B - S) \times N \times 5.806]/w = \% \text{ oxetane-ring content}$$

where *B* = mL of NaOH to titrate blank, *S* = mL of NaOH to titrate sample, *N* = normality of NaOH, and *w* = sample weight in grams.

**Spectroscopy.** Ir and nmr spectroscopy are useful aids in the characterization of oxetanes and oxetane polymers. The CH frequencies of the monomer are generally observed at 2900–3000 cm<sup>-1</sup>. The oxetane ring shows absorption between 960 and 980 cm<sup>-1</sup> regardless of the substituents on the ring (1). An unusually high oxetane-ring ir frequency of 1000 cm<sup>-1</sup> has been reported for DNOX (3). Polymer ether (COC) ir absorptions are typically near 1100 cm<sup>-1</sup>. Proton nmr chemical shifts for oxetane monomer and polymer are typically ~4.0–4.8 δ (CH<sub>2</sub>) and 3.5–4.7 δ (CH<sub>2</sub>), respectively (3,40,44). <sup>13</sup>C nmr increasingly is being used to characterize polyoxetane microstructure (27,69).

**Equivalent Weight of Hydroxyterminated Polymer.** The following procedure has been used for PAZOX (3). Approximately 0.2 g of polyoxetane, 5 mL of 1,2-dichloroethane, 2 mL of 1,1,1,3,3,3-hexamethyldisilazane, and 0.5 mL of chlorotrimethylsilane were added to a 50-mL, round-bottomed flask equipped with a magnetic stirrer, condenser, and drying tube. Volatile materials were removed at 70°C under vacuum. The residue was dissolved in 1-mL deuteriochloroform and the <sup>1</sup>H nmr spectrum was recorded. The hydroxyl equivalent weight was calculated on the basis of the areas of the δ 3.3 signal (5 protons per monomer

unit) and the  $\delta$  0 signal (9 protons per siloxy group). The same method was used for polymers with more complex nmr spectra by using weighed mixtures of silylated polymer and a known amount of a reference such as *p*-dichlorobenzene. In these cases, the equivalent weight was calculated on the basis of the reference and siloxy signals (3).

## Health and Safety Factors

Very little has been reported about the toxicity and hazards of handling the oxetanes and their polymers. Both properties are influenced markedly by the substituents. Oxetane itself is a low boiling flammable organic liquid and should be handled with care like any other low boiling and flammable liquid. Details of its toxicity are unknown, although one report states that it may be narcotic in high concentrations (93). BCMO is reported to be moderately irritating to the respiratory tract with high danger of permanent injury. Animal experiments show irritant and narcotic effects (94). Because of its structure and chlorine content, BCMO can evolve toxic fumes on decomposition and is classified as dangerous in disasters (94). AZOX is one of the monomers designed to yield energetic polymer and, as such, is hazardous. Adiabatic compression tests indicate that the material is a sensitive explosive (3). AZOX can be handled safely by collecting the material directly in methylene chloride at  $-78^{\circ}\text{C}$  as it forms and storing it as a methylene chloride solution (3). Under no circumstances should an energetic monomer be distilled; rather purification of energetic monomers via column chromatography is suggested. Elution of BAMO with methylene chloride through a column packed with basic alumina (95) or elution of 3-nitrato-methyl-3-methyloxetane with 50/50 vol/vol chloroform/hexane through a neutral alumina packed column (96) have been recommended. Methylene chloride-hexane was used to purify DNOX by passing through silica gel (3). The polymers derived from the energetic monomers burn with a great deal of smoke. Special procedures have been developed for disposal of these energetic polymers.

## Uses

Suggested uses for PBCMO include valves, bearings, precision gears, corrosion-free coatings, wedges and slot liners for starters in electric motors, films, adhesives, and even rope. Markets for this high price, high performance material were mainly in the field of chemical processing and precision injection-molded industrial parts. As a lining material PBCMO converts carbon steel tanks into vessels capable of handling high corrosive fluids at elevated temperatures (88). There are a large number of reports of the usefulness of PBCMO in adhesive and coatings applications (97,98). There are a substantial number of reports that describe the use of BCMO and other oxetanes to prepare polyglycols or copolyglycols for use in polyurethanes or polyesters or polyamide-type elastomers (51,99). PBCMO has been used in glass- and metal-filled composites (100,101). Grafting of 2- and 4-vinylpyridine to PBCMO and subsequent quaternization with methyl bromide

give ion-containing membranes that demonstrate significant salt exclusion and are potentially useful as reverse-osmosis membranes (102).

## BIBLIOGRAPHY

"Oxetane Polymers" in *EPST* 1st ed., Vol. 9, pp. 668–701, by S. Okamura, H. Miyake, and N. Shimazaki, Kyoto University; pp. 702–708, by H. Boardman, Hercules, Inc.; in *EPSE* 2nd ed., Vol. 10, pp. 653–670, by M. P. Dreyfuss and P. Dreyfuss, Michigan Molecular Institute.

## CITED PUBLICATIONS

1. E. J. Goethals, *Ind. Chim. Belge*, **30**, 559 (1965).
2. P. Luger and J. Buschman, *J. Am. Chem. Soc.* **106**, 7118 (1984).
3. K. Baum, P. J. Berkowitz, V. Grakauskas, and F. G. Archibald, *J. Org. Chem.* **48**, 2953 (1983).
4. M. B. Frankel, E. R. Wilson, D. O. Woolery, C. L. Hamermesh, and C. McArthur, *JANNAF Propulsion Committee Meeting No. AD-A103 844*, *CPIA Publication No. 340*, Chemical Propulsion Information Agency, Johns Hopkins University, Baltimore, Md., 1981, p. 39.
5. Ger. Pat. 741,478 (June 21, 1939), H. Meerwein (to I. G. Farbenindustrie AG).
6. H. Meerwein, D. Delfs, and H. Morshel, *Angew. Chem.* **72**, 927 (1960).
7. A. C. Farthing and R. J. W. Reynolds, *J. Polym. Sci.* **12**, 503 (1954).
8. A. C. Farthing, *J. Chem. Soc.*, 3648 (1955).
9. J. B. Rose, *J. Chem. Soc.*, 542 (1956).
10. *Ibid.*, p. 546.
11. E. S. Miller, P. A. Miller, T. N. Hall, and R. Reed, Jr., *Off. Nav. Res. U.S. Rev.*, 21 (Spring 1981).
12. M. P. Dreyfuss and P. Dreyfuss, *J. Polym. Sci. Part A-1*, **4**, 2179 (1966).
13. S. Inoue and T. Aida in K. J. Ivin and T. Saegusa, eds., *Ring-Opening Polymerization*, Vol. 1, Elsevier Science Publishing Co., Inc., New York, 1984, Chapt. 4, p. 193.
14. P. Dreyfuss, *Poly(tetrahydrofuran)*, Gordon & Breach, New York, 1982.
15. S. Searles, Jr., R. G. Nickerson, and W. K. Witsiepe, *J. Org. Chem.* **24**, 1839 (1960); S. Searles, D. G. Hummel, S. Nukina, and P. E. Throckmorton, *J. Am. Chem. Soc.* **82**, 2928 (1960).
16. E. J. Vandenberg and A. E. Robinson in E. J. Vandenberg, ed., *Polyethers*, *ACS Symp. Ser.* 6, American Chemical Society, Washington, D.C., 1975, pp. 101–119.
17. T. Hiramio, S. Nakayama, and T. Tsuruta, *Makromol. Chem.* **176**, 1897 (1975).
18. N. L. Sidney, S. E. Shaffer, and W. J. Bailey, *Polym. Prepr. Am. Chem. Soc. Div. Polym. Chem.* **22**(2), 373 (1981).
19. E. J. Vandenberg, *J. Polym. Sci. Polym. Chem. Ed.* **23**, 915 (1985).
20. J. Kops, S. Hvilsted, and H. Spanggaard, *Macromolecules* **13**, 1058 (1980).
21. R. Hoene and K.-H. W. Reichert, *Makromol. Chem.* **177**, 3545 (1976).
22. H. Meerwein, *Org. Synth.* **46**, 113 (1966).
23. U.S. Pat. 3,585,227 (June 15, 1971), M. P. Dreyfuss (to B. F. Goodrich).
24. Ref. 13, pp. 27–29.
25. E. Franta, L. Reibel, J. Lehmann, and S. Penczek, *J. Polym. Sci. Polym. Symp.* **56**, 139 (1976).
26. T. Saegusa and S. Kobayashi in Ref. 16, pp. 150–168.
27. N. Oguni and Y. Hyoda, *Macromolecules* **13**, 1687 (1980).

28. P. Dreyfuss and M. P. Dreyfuss in K. C. Frisch and S. L. Reegen, eds., *Ring Opening Polymerizations*, Marcel Dekker, Inc., New York, 1969, Chapt. 2, pp. 111–158.
29. T. Saegusa and S. Matsumoto, *J. Polym. Sci. Part A-1* **6**, 1559 (1968).
30. K. Brzezinska, W. Chwialkowska, P. Kubisa, M. Matyjaszewski, and S. Penczek, *Makromol. Chem.* **178**, 2491, (1977).
31. E. J. Vandenberg, *J. Polym. Sci. Part A-1* **7**, 525 (1969).
32. J. Kops and H. Spanggaard, *Macromolecules* **15**, 1200 (1982).
33. F. Andruzzi, P. Cerrai, G. Guerra, L. Nucci, A. Pescia, and M. Tricoli, *Eur. Polym. J.* **18**, 685 (1982).
34. K. Hayashi and S. Okamura, *Makromol. Chem.* **47**, 230 (1961).
35. K. Takakura, K. Hayashi, and S. Okamura, *J. Polym. Sci. Part A-1* **4**, 1747 (1966).
36. J. V. Crivello and J. H. W. Lam, *Macromolecules* **10**, 1307 (1977).
37. P. E. Black and D. J. Worsfold, *Can. J. Chem.* **54**, 3325 (1976).
38. A. Bello, E. Perez, and J. M. G. Fatou, *Makromol. Chem.* **185**, 249 (1984).
39. T. Saegusa and S. Kobayashi, *Prog. Polym. Sci. Jpn.* **6**, 107 (1973).
40. E. Riande, J. G. De la Campa, J. Guzman, and J. De Abajo, *Macromolecules* **17**, 1431 (1984).
41. Y. Arimatsu, *J. Polym. Sci. Part A-1* **4**, 728 (1966).
42. P. Dreyfuss and M. P. Dreyfuss, *Polym. J.* **8**, 81 (1976).
43. M. Bucquoye and E. J. Goethals, *Makromol. Chem.* **179**, 1681 (1978).
44. E. Riande, J. G. De la Campa, J. Guzman, and J. De Abajo, *Macromolecules* **17**, 1891 (1984).
45. J. Kops and H. Spanggaard, *Polym. Prepr. Am. Chem. Soc. Div. Polym. Chem.* **26**(1), 52 (1985).
46. A. Leborgne, N. Spassky, and J. Kops in E. J. Goethals, ed., *Cationic Polymerization and Related Processes, Proceedings of the 6th International Cationic Symposium*, Ghent, Belgium, Academic Press, Inc., London, 1984, pp. 227–236.
47. J. Kops and H. Spanggaard in Ref. 46, pp. 219–226.
48. C. C. Price, R. Spectro, and A. C. Tumolo, *J. Polym. Sci. Part A-1* **5**, 407 (1967).
49. J. Kops and H. Spanggaard, *Macromolecules* **15**, 1225 (1982).
50. Jpn. Kokai Tokkyo Koho 58/125718 [83/125,718] (July 26, 1983) (to Daicel Chemical Industries, Ltd.).
51. Ger. Offen. 3,326,178 (Oct. 18, 1984), Y. Toga, I. Okamoto, and T. Kanno (to Daicel Chemical Industries, Ltd.).
52. Ref. 13, pp. 195–205.
53. R. S. Miller, P. A. Miller, T. N. Hall, and R. Reed, Jr., *Off. Nav. Res. U.S. Res. Rev.*, 21 (Spring 1981).
54. U.S. Pat, 4,393,199 (July 12, 1983), G. E. Manser (to SRI International).
55. *Ind. Chem. News*, cover (November 1981).
56. E. J. Vandenberg, *J. Polym. Sci. Polym. Chem. Ed.* **10**, 2887 (1972).
57. S. V. Conjeevaram, R. S. Benson, and D. J. Lyman, *J. Polym. Sci. Polym. Chem. Ed.* **23**, 429 (1985).
58. Ref. 13, pp. 207–211.
59. K. E. Hardenstine, C. J. Murphy, R. B. Jones, L. H. Sperling, and G. E. Manser, *J. Appl. Polym. Sci.* **30**, 2051 (1985).
60. T. Urzu, K. Hatanaka, and K. Matsuzaki, *Makromol. Chem.* **181**, 2137 (1980).
61. G. E. Manser, R. W. Fletcher, and M. R. Knight, *Off. Nav. Res. U.S. Res. Rep. No. N00014-82-0800* (June 1985).
62. D. Tirrell, O. Vogl, T. Saegusa, S. Kobayashi, and T. Kobayashi, *Macromolecules* **13**, 1041 (1980).
63. J. Muggie and O. Vogl, *J. Polym. Sci. Polym. Chem. Ed.* **23**, 649 (1985).
64. D. A. Bansleben and O. Vogl, *J. Polym. Sci. Polym. Chem. Ed.* **23**, 673 (1985).

65. L. Garrido, E. Riande, and J. Guzman, *Makromol. Chem. Rapid Commun.* **4**, 725 (1983).
66. L. Garrido, J. Guzman, E. Riande, and J. de Abajo, *J. Polym. Sci. Polym. Chem. Ed.* **20**, 3377 (1982).
67. M. Bucquoye and E. J. Goethals, *Eur. Polym. J.* **14**, 323 (1978).
68. J. Kops and H. Spanggaard, *Macromolecules* **16**, 1544 (1983).
69. A. Baba, H. Meishou, and H. Matsuda, *Makromol. Chem. Rapid Commun.* **5**, 665 (1984).
70. P. Geil, *Polymer Single Crystals*, Wiley-Interscience, New York, 1963, p. 526.
71. R. L. Miller in J. Brandrup and E. G. Immergut, eds., *Polymer Handbook*, 2nd ed., John Wiley & Sons, Inc., New York, 1975, Chapt. III, p. 1.
72. Y. Takahashi, Y. Osaki, and H. Tadokoro, *J. Polym. Sci. Polym. Phys. Ed.* **18**, 1863 (1980).
73. *Ibid.*, **19**, 1153 (1981).
74. R. Gilardi, C. George, and J. Karle, *Off. Nav. Res. U.S. Res. Rep.*, No. LSM 81-1 (Oct. 15, 1981).
75. B. Moss and D. L. Dorset, *J. Polym. Sci. Polym. Phys. Ed.* **20**, 1789 (1982).
76. E. Perez, M. A. Gomez, A. Bello, and J. G. Fatou, *Colloid Polym. Sci.* **261**, 571 (1983).
77. K. E. Hardenstine, G. V. Henderson, L. H. Sperling, and C. J. Murphy, *Gov. Rep. Announce. U.S. No. AD-A148271/0/GAR* **85**, 172 (1985).
78. E. Perez, A. Bello, and J. G. Fatou, *An. Quim. Ser. A* **80**, 509 (1984); *Chem. Abstr.* **102**, 176755p (1985).
79. E. Perez, A. Bello, and J. G. Fatou, *Colloid Polym. Sci.* **262**, 605 (1984).
80. *Ibid.*, p. 913.
81. E. Perez, A. Bello, and J. G. Fatou, *Makromol. Chem.* **186**, 439 (1985).
82. K. D. Pae, C. L. Tang, and E. S. Shin, *J. Appl. Phys.* **56**, 2426 (1984).
83. L. Garrido, E. Riande, and J. Guzman, *J. Polym. Sci. Polym. Phys. Ed.* **21**, 1493 (1983).
84. E. Perez, M. A. Gomez, A. Bello, and J. G. Fatou, *J. Appl. Polym. Sci.* **27**, 3721 (1982).
85. U. Gaur and B. Wunderlich, *Polym. Prepr. Am. Chem. Soc. Div. Polym. Chem.* **20**(2), 429 (1979).
86. U. Gaur and B. Wunderlich, *J. Phys. Chem. Ref. Data* **10**, 1001 (1981).
87. R. B. Jones, C. J. Murphy, L. H. Sperling, M. Farber, S. P. Harris, and G. E. Manser, *J. Appl. Polym. Sci.* **30**, 95 (1985).
88. D. C. Miles and J. H. Briston, *Polymer Technology*, Chemical Publishing Co., Inc., New York, 1979.
89. P. Dreyfuss and M. P. Dreyfuss in M. Grayson, ed., *Kirk-Othmer Encyclopedia of Chemical Technology*, 3rd ed., Vol. 18, John Wiley & Sons, Inc., New York, 1982, pp. 645-670.
90. D. J. H. Sandiford, *J. Appl. Chem.* **8**, 188 (1958).
91. E. W. Cronin, *Mod. Plast.* **34**(6), 150 (1957).
92. R. T. Keen, *Anal. Chem.* **29**, 1041 (1957).
93. N. Irving Sax, *Dangerous Properties of Industrial Materials*, 4th ed., Van Nostrand Reinhold Co., Inc., New York, 1975, p. 1204.
94. *Ibid.*, p. 456.
95. U.S. Pat. 4,483,978 (Nov. 20, 1984), G. E. Manser (to SRI International).
96. G. E. Manser, *Nitrate Ester Polyether Glycol Prepolymers*, JANNAP Propulsion Committee Meeting, New Orleans, La., Chemical Propulsion Information Agency, Johns Hopkins University, Baltimore, Md., 1984.
97. E. N. Sokolov and A. V. Rogachev, *Vestsi Akad. Navuk B SSR Ser. Fiz. Tekh. Navuk* (2), 54 (1982).
98. N. F. Shumskii and V. I. Galkina, *Deposited. Document of the Solid Propellant Rocket Static Test Panel No. 15Khp-D82*, SPSTL, 1982.

99. Ger. Offen. 3,326,178 (Oct. 18, 1984), Y. Toga, I. Okamoto, and T. Kanno; Jpn. Pat. 83/64,801 (Apr. 13, 1983) (to Daicel Chemical Industries, Ltd.).
100. V. A. Belyi, I. M. Vertyachikh, Yu. L. Voronezhnev, V. A. Gol'dade, and L. S. Pinchuk, *Dokl. Akad. Nauk SSSR* **275**, 639 (1984); *Chem. Abstr.* **101**, 73826n (1984).
101. N. I. Egorenkov, A. I. Kuzavkov, V. V. Evmenov, and D. G. Lin, *J. Therm. Anal.* **24**, 9 (1982).
102. E. Bittencourt, V. Stannett, J. L. Williams, and H. B. Hopfenberg, *J. Appl. Polym. Sci.* **26**, 879 (1981).

M. P. DREYFUSS  
P. DREYFUSS  
Michigan Molecular Institute

## OXIDATIVE POLYMERIZATION

### Introduction

*Oxidative polymerization* is, formally, abstraction of two hydrogen atoms from a monomer to give a polymer, and thus may be classified as polycondensation. The applicable monomers are mainly aromatic compounds. Electrical and chemical oxidation methods are often used, in which catalysis with dioxygen or hydrogen peroxide is the most favorable; the reaction temperature is moderate and the by-product is water only. Oxidative polymerization is one of the cleanest and lowest loading methods in polycondensation. However, the reaction mechanism is unclear in many cases and the coupling selectivity is not generally easy to control.

This article deals with oxidative polymerization of phenols, anilines, thiophenol derivatives, aromatic hydrocarbons, heterocyclic aromatics, and other monomers. The reaction mechanism, the coupling selectivity, and the characteristics of the resulting polymers are discussed.

### 2,6-Disubstituted Phenols

Until the 1950s, oxidation of 2,6-dimethylphenol (2,6-Me<sub>2</sub>P) by an oxidant like benzoyl peroxide (1) or alkaline ferricyanide (2) mainly gave 3,3',5,5'-tetramethyldiphenquinone (DPQ) (Fig. 1). In 1959, oxidative polymerization of 2,6-Me<sub>2</sub>P catalyzed by CuCl/pyridine (Py) under dioxygen leading to poly(2,6-dimethyl-1,4-phenylene oxide) (Poly-2,6-Me<sub>2</sub>P) was discovered (3). Various catalysts such as copper/substituted-ethylenediamine complexes were developed and Poly-2,6-Me<sub>2</sub>P was found completely miscible with polystyrene (4) (see POLYETHERS, AROMATIC).

**Oxidative Coupling Mechanism.** Poly-2,6-Me<sub>2</sub>P is a C—O coupling product and DPQ is a product via C—C coupling. Control of the C—O coupling is a most important question (5). Three possible reaction mechanisms for the C—O coupling selectivity have been proposed as follows: (1) coupling of free phenoxy



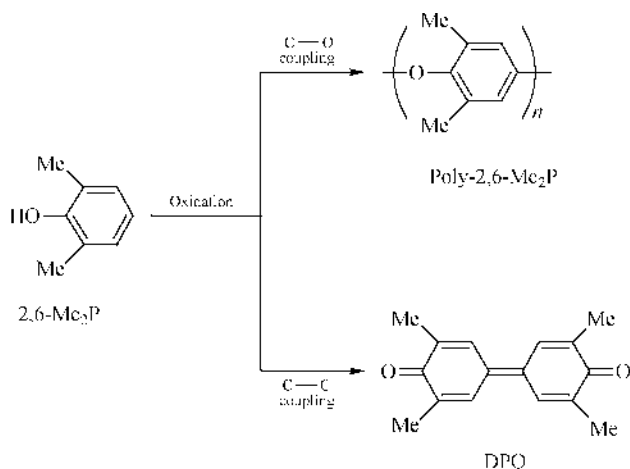


**Fig. 1.** Oxidation of 2,6-dimethylphenol.

(i) Coupling of free phenoxy radicals:

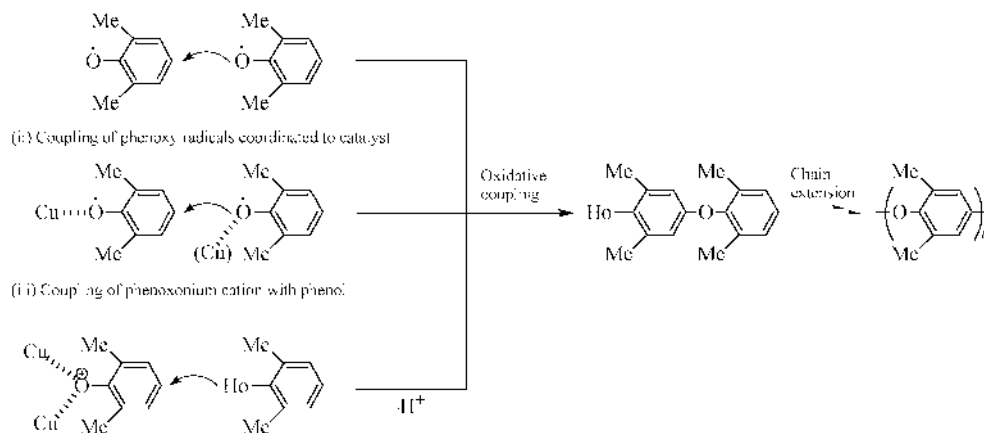


**Fig. 2.** Three possible mechanisms for C—O coupling in the oxidative polymerization of 2,6-dimethylphenol.

radicals resulting from one-electron-oxidation of 2,6-Me<sub>2</sub>P, (2) coupling of phenoxy radicals coordinated to a catalyst complex, and (3) coupling through phenoxonium cation formed by two-electron-oxidation of 2,6-Me<sub>2</sub>P (Fig. 2).

**Coupling of Phenoxy Radicals Coordinated to Catalyst Complex.** Because the oxidative coupling of 2,6-Me<sub>2</sub>P with benzoyl peroxide or alkaline ferricyanide affords DPQ as the main product (1,2), it seems that the free phenoxy radical leads to C—C coupling. C—O coupling results from the phenoxy radical coordinated to the copper complex [(ii) in Fig. 2]. In CuCl/Py catalysis, increasing the amount of Py to copper (6,7) favors the C—O coupling. Substituents at the 2,6-positions of Py (6) or high reaction temperature (8) makes the C—C coupling favorable.

The kinetic study of Cu/Py catalysis showed that the oxidative polymerization proceeded by a Michaelis–Menten-type reaction mechanism and the C–O coupling is preferred when at least one of the radicals is coordinated to copper (9). ESR measurements using a copper(II) acetate/Py complex (10), where Py/Cu = 20, showed two phenoxo-copper(II) complexes, and the oxidative polymerization gave mainly Poly-2,6-Me<sub>2</sub>P. For Py/Cu = 2, none of phenoxo-copper(II) complexes was detected and the major product was DPQ. Thus, these data suggest that coupling via the coordinated phenoxy radicals mainly leads to the C–O coupling.

**Coupling of Phenoxonium Cation with 2,6-Dimethylphenol.** No ESR signals of free phenoxy radicals in the oxidation of 2,6-Me<sub>2</sub>P with a [CuCl(OCH<sub>3</sub>)Py] complex were detected (11). It was assumed that the phenoxy radical was oxidized by the Cu(II) complex (totally two-electron-oxidation from the phenol) to give the phenoxonium cation, which can couple with the phenol leading to C–O coupling [(iii) in Fig. 2]. For a Cu/*N*-methylimidazole (NMI) catalyst, the reaction order in copper changed from 1.22 at NMI/Cu=10 to 1.70 at NMI/Cu=75, and the selectivity for the C–O coupling reached a maximum at the NMI/Cu ratio of at least 30 (12). From the data, the key intermediate may be a  $\mu$ -phenoxo dicopper(II) complex, in which two-electron-transfer from phenoxo moiety to two copper atoms can give a phenoxonium cation.

By ab initio calculation, the atomic charges for the phenol, phenolate anion, phenoxy radical, phenoxonium cations of 2,6-Me<sub>2</sub>P were determined (13). Since the oxygen atoms in all the species were negative, it was considered that the species susceptible to the C–O coupling has positive charge on the *para*-carbon, and therefore, it should be the phenoxonium cation. The coupling of the phenoxy radicals was excluded, because the treatment of 2,6-Me<sub>2</sub>P with benzoyl peroxide yielded DPQ (1). The reaction between the phenoxy radical and phenol was ruled out, because 2,6-dimethylanisole did not react in the oxidative polymerization of 2,6-Me<sub>2</sub>P (14).

If the oxidative coupling of 2,6-Me<sub>2</sub>P proceeds via the phenoxonium cation, in the presence of a nucleophilic reagent in excess to the phenol, the phenoxo cation should react with the nucleophile, and hence, Poly-2,6-Me<sub>2</sub>P cannot be obtained. In fact, it was found that the oxidative polymerization of 2,6-Me<sub>2</sub>P catalyzed by a Cu(tmed) (tmed: *N,N,N',N'*-tetramethylethylenediamine) complex with an excess amount of *n*-pentylamine produced Poly-2,6-Me<sub>2</sub>P in 75% yields (5). The nucleophilicity of *n*-pentylamine toward benzyl chloride was confirmed to be much greater than that of 2,6-Me<sub>2</sub>P. These facts strongly indicate that such electrophilic intermediates as a phenoxonium cation are not involved in the oxidative polymerization.

**Coupling of Free Phenoxy Radicals.** The above two mechanisms [(ii) and (iii) in Fig. 2] are based on the assumption that the coupling via free phenoxy radicals of 2,6-Me<sub>2</sub>P leads to the C–C coupling mainly. With alkaline ferricyanide (2), DPQ was produced in 45–50% but the other half of the oxidized material was a yellow nonketonic polymer, probably Poly-2,6-Me<sub>2</sub>P. On the other hand, the oxidation with benzoyl peroxide afforded the C–C coupling products in total 60% yield (1). However, detailed analysis for this oxidation reaction showed that the reaction mechanism did not involve radical intermediates but rather a benzoyl perester intermediate (15). It was reported that the thermal decomposition of

benzoyl 2,6-dimethylphenyl carbonate, which should generate the phenoxy radical, produced Poly-2,6-Me<sub>2</sub>P and DPQ in 35–38% and 10% yield, respectively (16). From these studies, it seems that some complicated experimental results and different understandings were involved in the above assumption of the C–C coupling selectivity in the free-radical coupling, which was pointed out before (17).

In addition, many studies on the oxidative coupling of 2,6-Me<sub>2</sub>P with inorganic oxidants were performed, and in some cases the free radical was observed. The oxidation with MnO<sub>2</sub>, PbO<sub>2</sub>, and Ag<sub>2</sub>O produced Poly-2,6-Me<sub>2</sub>P in 60–95% yields. For MnO<sub>2</sub> (18) and Ag<sub>2</sub>O (19), the free radicals of 2,6-Me<sub>2</sub>P and Poly-2,6-Me<sub>2</sub>P were detected by ESR measurements. By the addition of increasing amount of triethylamine in oxidative polymerization with PbO<sub>2</sub>, the formation of DPQ was suppressed and the yield of Poly-2,6-Me<sub>2</sub>P was increased (20). On the other hand, the oxidation by hexachloroiridate(IV) anion in an acidic aqueous solution afforded DPQ in 55–65% (21).

It was considered from the above studies (20,21) that the selectivity for the C–O or C–C coupling of 2,6-Me<sub>2</sub>P was much affected by a coexisting base or acid. Recently, oxidative coupling of 2,6-Me<sub>2</sub>P with Ag<sub>2</sub>CO<sub>3</sub> was examined in the presence of excess *n*-pentylamine (nPA) or acetic acid (AcOH) (5). The ratio of the products Poly-2,6-Me<sub>2</sub>P and DPQ was 50/50 without these additives, >99/~0 with nPA, and 0/100 with AcOH. These data indicate that generally in the oxidative coupling of 2,6-Me<sub>2</sub>P the addition of a base would lead to the C–O coupling and that of an acid to the C–C coupling.

The above observations may be explained by the following proposal (22): in basic reaction media, a free phenoxy radical is formed leading to C–O coupling [(i) in Fig. 2], and in acidic reaction media, a phenoxonium cation could be generated to give the C–C coupling. In the electrochemical oxidation of 2,6-Me<sub>2</sub>P, the oxidation above pH 5.2 takes place via two monoelectronic steps, the first of which forms the free phenoxy radical; the oxidation below pH 5.2 undergoes one dielectronic step, which might generate the phenoxonium cation (23). It is still unclear whether or not the phenoxonium cation is really involved as the intermediate in the oxidative coupling; however, at least the phenoxonium cation should be easier to form under acidic conditions than under basic conditions.

To summarize on the above observations about the reaction mechanisms, the C–O/C–C coupling selectivity in the oxidative polymerization of 2,6-Me<sub>2</sub>P appears to be as follows (5).

- (1) The coupling via coordinated phenoxy radicals and the coupling of free phenoxy radicals under basic conditions would mainly lead to the C–O coupling.
- (2) The coupling of free phenoxy radicals under acidic conditions or the coupling of phenoxonium cations from the two electron oxidation with phenol would favor the C–C coupling.

**Chain Extension Mechanism.** The chain extension mechanism in the oxidative polymerization of 2,6-Me<sub>2</sub>P has been almost established (Fig. 3). It has been widely accepted that two dimeric phenoxy radicals couple with each other

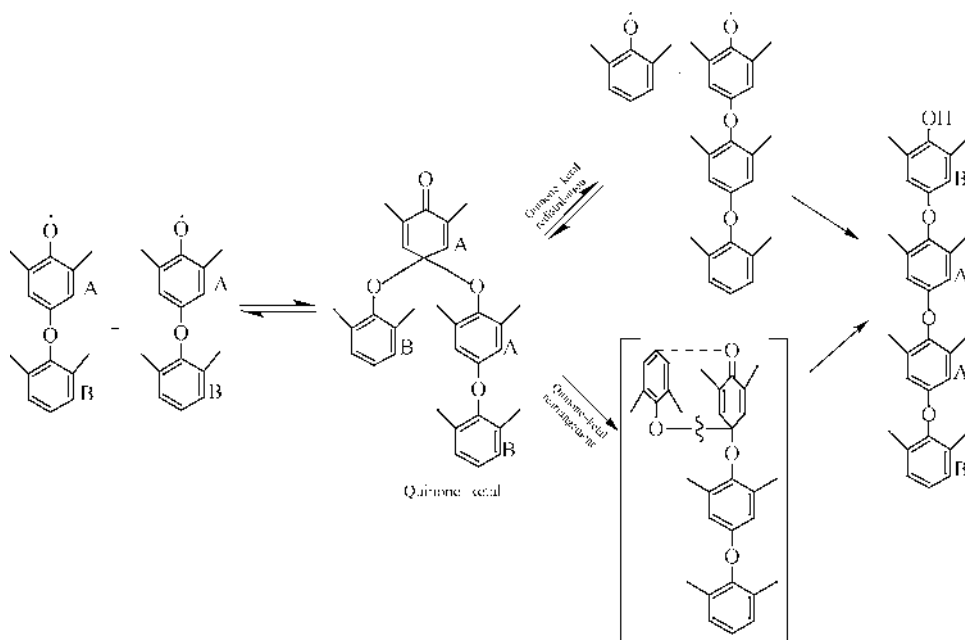


**Fig. 3.** Chain extension in the oxidative polymerization of 2,6-dimethylphenol.

to give a quinone-ketal intermediate, which has not been detected. No reactivity of the tail phenoxy group (marked B in Fig. 3) was observed, because the  $\pi$ -conjugation is cut off by the ether bond (25); ie, the head-tail coupling mechanism, in which the oxygen atom of head phenol unit couples at the *para*-carbon atom of tail phenoxy group (24), is excluded. The oxidation of a 4-phenoxyphenol marked with methyl group (let it be A-B as two distinguishable aromatic rings) yielded none of the dimer through a head-tail coupling (A-B-A-B) but the dimer through a quinone-ketal intermediate (B-A-A-B) (26).

Two reaction routes from a quinone-ketal intermediate to a tetramer were proposed; one is a quinone-ketal redistribution to give a monomer radical and a trimer radical (27), and the other is a quinone-ketal intramolecular rearrangement (28). The oxidative polymerization from 2,6-Me<sub>2</sub>P dimer produced the oligomers of even numbers such as 2,6-Me<sub>2</sub>P itself and the trimer (27,29). From these data, the extension mechanism for the oxidative polymerization of 2,6-Me<sub>2</sub>P definitely involves quinone-ketal redistribution and it is unclear whether or not quinone-ketal rearrangement actually occurs. For 2-methyl substituted and 2,6-unsubstituted 4-phenoxyphenols, only quinone-ketal rearrangement took place at a low temperature; however, at higher reaction temperatures, quinone-ketal redistribution also occurred (26). Application of the redistribution mechanism resulted in the modification (30–32) and depolymerization (33) of Poly-2,6-Me<sub>2</sub>P.

In general, the oxidative polymerization of phenols undergoes a stepwise growth mechanism, although the electrochemical oxidative polymerization has been suggested to be a chain reaction mechanism (34). However, phenolic dimers and higher oligomers have electron-donating phenoxy groups at *p*-positions and

become easier to oxidize (more reactive) than phenolic monomers. Therefore, until the monomer is almost consumed, the reaction mixture consists mainly of the monomer and polymer, and so it often seems to proceed formally via chain reaction mechanism, but it is actually reactive intermediate polycondensation (35).

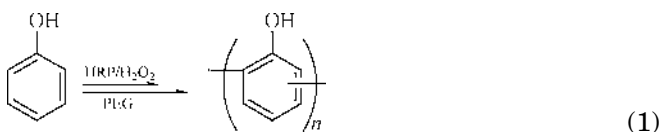
**Other 2,6-Disubstituted Monomers.** Various poly(2,6-substituted-1,4-phenylene oxide)s possessing alkyl, aryl, alkoxyl, and halogen groups have been produced (see POLYETHERS, AROMATIC). Recently, some functional polymers (36–39) were synthesized, one of which was converted to a heterocyclic ladder polymer (39). Poly(2,6-difluoro-1,4-phenylene oxide)s with crystallinity (40) and no crystallinity (41) were synthesized. By enzyme catalysis, oxidative polymerization of 3,5-disubstituted-4-hydroxybenzoic acids, with liberation of carbon dioxide, produced poly(2,6-disubstituted-1,4-phenylene oxide)s (42,43).

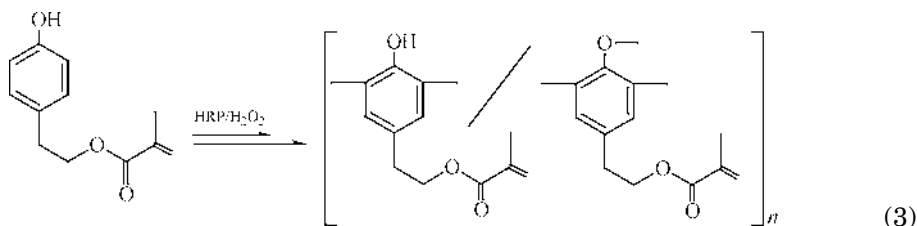
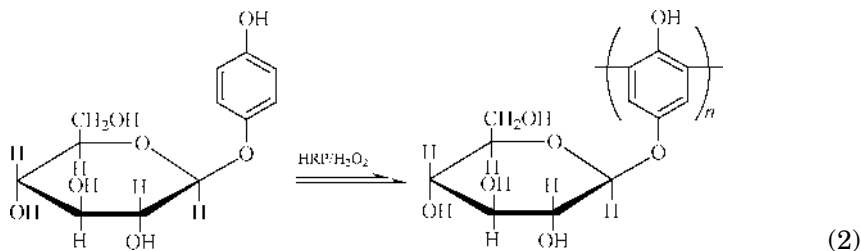
## 2- and/or 6-Unsubstituted Phenols

A phenoxy radical intermediate has four reactive positions: the oxygen and *para*-carbon as well as two *ortho*-carbons. Therefore, for *o*-unsubstituted phenols, it is difficult to regulate the coupling selectivity. Enzyme catalysts and enzyme model catalysts have been studied for the control of the polymerization of 2- and/or 6-unsubstituted phenols.

**Enzyme Catalyst.** Oxidative coupling of phenols is involved in some biological reactions; for example, formation of lignin (qv) or melanin is catalyzed by oxidoreductase enzymes such as peroxidase, oxidase, or oxygenase (44,45). In 1983, horse radish peroxidase (HRP) catalyst was used to remove phenols from waste water, affording water-insoluble low molecular weight phenolic polymers (46). Since HRP was employed as the polymerization catalyst (47–49), the polymerization of various phenols by using HRP with hydrogen peroxide or laccase (an oxidase) with dioxygen has been extensively investigated (50,51). These enzymes show high catalytic activity for generating free radicals from phenols, but are unable to control the coupling selectivity (52).

In oxidative polymerization of phenol by HRP catalyst (53,54), soluble polyphenol was obtained for the first time by controlling the polymer structure and molecular weight (55). Regio-controlled poly(hydroxyphenylene) was synthesized by using poly(ethylene glycol) (PEG) as template (eq. 1) (56). The enzyme-catalyzed oxidative polymerizations of alkylphenols (57–61), biphenols (62–64), and various functional phenols (65–70) were also performed. For glucose- $\beta$ -D-hydroquinone, only C–C coupling at *o*-positions was claimed (eq. 2) (65). Chemos-elective polymerization of a phenolic monomer having a methacryloyl group (eq. 3) (71) and an ethynyl group (72) was achieved and gave the corresponding polyphenol. “Artificial urushi” was prepared by laccase-catalyzed cross-linking reactions of urushiol analogues (73,74). (see ENZYMATIC POLYMERIZATION).





**Peroxidase Model Catalyst.** An *N,N'*-bis(salicylidene)ethylenediamino iron [Fe(salen)] complex was found to be a cheap peroxidase model catalyst for oxidative polymerization of phenols with hydrogen peroxide (75–79). Hematin also polymerized ethylphenol in a reaction mechanism similar to that for HRP (80).

**Tyrosinase Model Catalyst (“Radical-Controlled” Oxidative Polymerization Catalyst).** Conventional copper catalysts were not able to give useful polymers from phenols having at least one *o*-position unsubstituted (26,81,82). Peroxidase (HRP), oxidase (laccase), and peroxidase-model [Fe(salen)] catalysts also showed a limited ability for controlling the coupling selectivity of such phenols (5,53). New copper catalysts were then studied. Copper(I)/diamine complexes, typical conventional catalysts, reacted with dioxygen to give bis( $\mu$ -oxo) dicopper(III) complexes (83). In the reaction of HRP with hydrogen peroxide, Fe(IV)=O intermediates were formed (84). These active oxygen complexes were subjected to the reaction with phenols to afford “free” phenoxy radical species (83,85). These data suggest that the regioselective coupling cannot be achieved by the catalysts generating “electrophilic” or “radical” active oxygen species.

Then, a working hypothesis was made (Fig. 4) (86,87): if a catalyst generates only a “nucleophilic,” strictly speaking “basic,”  $\mu$ - $\eta^2$ : $\eta^2$ -peroxo dicopper(II) complex 1 (88,89), it will abstract a proton (not a hydrogen atom) from phenol to give phenoxo–copper(II) complex 2, equivalent to phenoxo radical–copper(I) complex 3. Intermediate species 2 and/or 3 are not “free” radicals but “controlled” radicals, and therefore regioselectivity of the subsequent coupling will be entirely regulated. The difficulty for conventional catalysts to control the regioselectivity (90,91) is probably due to generation of free radicals. This new concept is characterized by the exclusive formation of controlled phenoxy radicals, and hence the new concept was termed a “radical-controlled” oxidative polymerization (87).

**Oxidative Polymerization of 4-Phenoxyphenol by Tyrosinase Model Catalyst.** “Radical-controlled” oxidative polymerization of 4-phenoxyphenol (PPL) catalyzed by tyrosinase model complexes has been developed (eq. 4) (86,87,92,93).

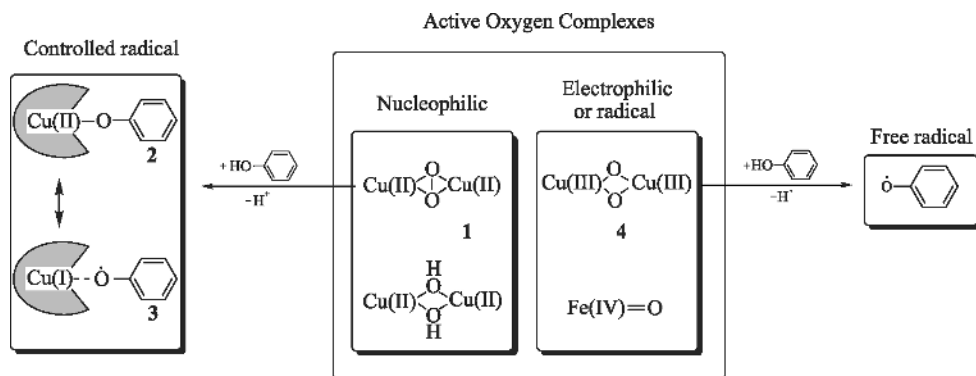
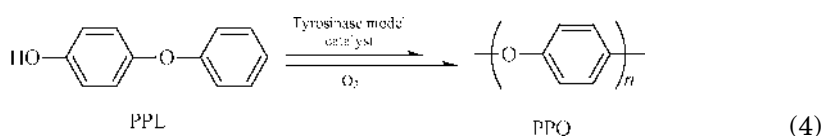
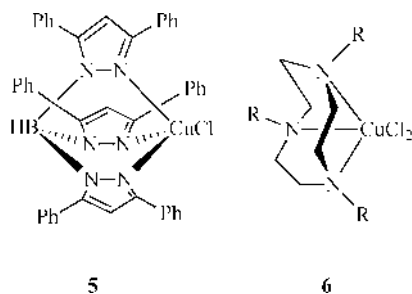


**Fig. 4.** Nucleophilic vs electrophilic active oxygen complexes.



This was the first simple synthesis of crystalline poly(1,4-phenylene oxide) (PPO) having a melting point by the catalytic oxidative polymerization method, although other time-consuming synthesis procedures have been reported (94–96). As the tyrosinase model, (hydrotris(3,5-diphenyl-1-pyrazolyl)borate) copper  $[\text{Cu}(\text{Tpzb})]$  complex (5) and (1,4,7- $\text{R}_3$ -1,4,7-triazacyclononane) copper  $[\text{Cu}(\text{L}^{\text{R}})]$ :  $\text{R}$  = isopropyl (iPr), cyclohexyl (cHex), and *n*-butyl (nBu)] complexes (6) were employed.



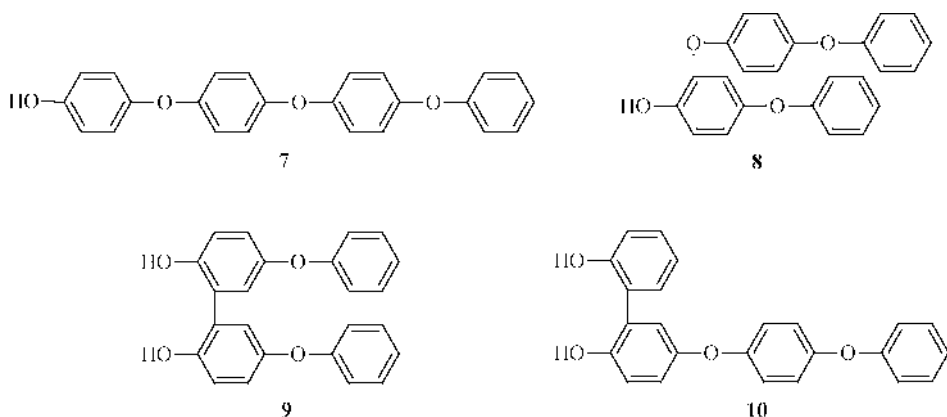
To examine the coupling selectivity, the ratio of oxidative coupling dimers formed at the initial stage of polymerization of PPL was investigated (Table 1) (86,87).  $\text{CuCl}/N,N,N',N'$ -tetraethylethylenediamine (teed), which was the sole catalyst reported for oxidative coupling of PPL (26), was also employed (entry 7). As a model system of free phenoxy radical coupling, an equimolar amount of 2,2'-azobisisobutyronitrile (AIBN) was used for the oxidation of PPL (entry 8). In the case of  $\text{CuCl}/\text{teed}$ , four dimers were detected and the structures of the dimers were identified as 7, 8, 9, and 10. Products 7 and 8 are formed by C–O coupling, and formation of 9 and 10 is based on C–C coupling.

**Table 1. Dimer Ratio at Initial Stage of Oxidative Polymerization of 4-Phenoxyphenol**

Entry	Catalyst	Oxidant	Solvent	Initial dimer ratio, %			
				7	8	9	10
1	Cu(Tpzb)Cl <sup>a</sup>	O <sub>2</sub>	Toluene	91	9	0	0
2	Cu(Tpzb)Cl <sup>a</sup>	O <sub>2</sub>	THF	91	9	0	0
3	Cu(L <sup>iPr</sup> )Cl <sub>2</sub> <sup>a</sup>	O <sub>2</sub>	Toluene	93	7	0	0
4	Cu(L <sup>iPr</sup> )Cl <sub>2</sub> <sup>a</sup>	O <sub>2</sub>	THF	89	7	1	3
5	Cu(L <sup>cHex</sup> )Cl <sub>2</sub> <sup>a</sup>	O <sub>2</sub>	Toluene	95	5	0	0
6	Cu(L <sup>nBu</sup> )Cl <sub>2</sub> <sup>a</sup>	O <sub>2</sub>	Toluene	90	9	0	1
7	CuCl/teed <sup>a</sup>	O <sub>2</sub>	Toluene	79	6	2	13
8	<sup>b</sup>	AIBN	Toluene	82	4	2	12

<sup>a</sup>Polymerization of PPL (0.60 mmol) with Cu complex (0.030 mmol) and 2,6-diphenylpyridine (0.30 mmol) in solvent (1.2 g) under dioxygen (101.3 kPa) at 40°C. CuCl (0.030 mmol) and teed (0.015 mmol) was used as the Cu complex in entry 7.

<sup>b</sup>Oxidized by AIBN (0.60 mmol) under nitrogen at 40°C.



For the CuCl/teed catalyst, considerable amounts of the two C–C coupling dimers of 9 and 10 were detected and 7 selectivity was low (79%). The dimer ratio was very similar to that via free-radical coupling by AIBN oxidation, in which considerable amounts of the C–C coupling dimers were observed. However, for Cu(Tpzb) (5) in toluene and in THF, and for the Cu(L<sup>iPr</sup>), Cu(L<sup>cHex</sup>), and Cu(L<sup>nBu</sup>) (6) in toluene, none or very little of the C–C coupling dimers were detected, showing high regioselectivity of 7. The order of 7 selectivity was Cu(L<sup>nBu</sup>) (90%) < Cu(L<sup>iPr</sup>) (93%) < Cu(L<sup>cHex</sup>) (95%), in good agreement with that of steric hindrance of the substituents (87). These data show that the regioselectivity of phenoxy radical coupling can be controlled by these catalysts. The dimerization catalyzed by the Cu(L<sup>iPr</sup>) in THF gave C–C coupling dimers to some extent.

The resulting polymer was isolated as a methanol-insoluble part. In the cases with little or no C–C dimer formation (entries 1–3,5,6), white powdery polymers with  $M_w$  of 700–4700 were obtained. The IR spectrum patterns of the polymers were very similar to that of PPO synthesized by Ullmann condensation (95). From the DSC analysis, the polymers showed melting points ( $T_m$ ) at 171–194°C. In polymerizations giving considerable amounts of the C–C dimers



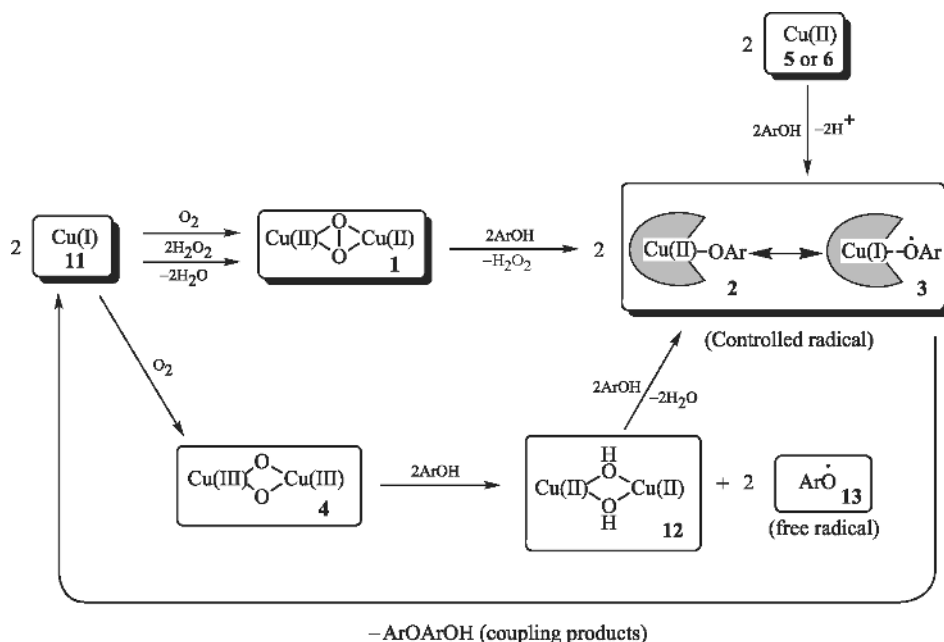


**Fig. 5.** Reaction mechanism for copper complex catalysis of oxidative polymerization.

(entries 4,7,8), the brownish polymers showed no clear melting points in the DSC traces.

**Reaction Mechanism of Catalytic Cycle.** On the basis of the above data, the reaction mechanism for the copper complex catalysis is postulated as follows (Fig. 5). First, the starting copper(II) chloride complex  $\text{Cu}(\text{Tpzb})\text{Cl}$  (5) or  $\text{Cu}(\text{L}^{\text{R}})\text{Cl}_2$  (6) reacts with PPL or oligomers of PPL to give phenoxo-copper(II) complex (2), equivalent to phenoxo radical-copper(I) complex (3). Regioselective coupling takes place between two molecules of 2 and/or 3 to produce copper(I) complexes (11) as well as the phenylene oxide products having *p*-linkage selectively, because the steric hindrance of the catalysts blocks the coupling at *o*-positions.

In case of the  $\text{Cu}(\text{Tpzb})$  complex (5), formation of  $\mu\text{-}\eta^2\text{:}\eta^2\text{-peroxo}$  dicopper(II) complex (1) from 11 was confirmed under dioxygen (89) in both toluene and THF. For the  $\text{Cu}(\text{L}^{\text{iPr}})$  complex as well as the  $\text{Cu}(\text{L}^{\text{cHex}})$  and  $\text{Cu}(\text{L}^{\text{nBu}})$  complexes (6), it was reported that 11 afforded complex 1 in nonpolar solvents such as toluene (97). 1 reacts with phenols to regenerate 2 (98) and hydrogen peroxide (99). Hence, this catalytic system would allow only the regioselective coupling process from 2 and/or 3 and completely exclude free-radical coupling reactions; the present reaction is thus recognized as “radical-controlled” oxidative polymerization.

For the  $\text{Cu}(\text{L}^{\text{iPr}})$  complex under dioxygen in THF, 11 gave bis( $\mu\text{-oxo}$ ) dicopper(III) complex (4) (97). 4 abstracts hydrogen atoms from phenols to give bis( $\mu\text{-hydroxo}$ ) dicopper(II) complex (12) and free phenoxy radical (13). Therefore, this catalytic cycle involves the free-radical coupling with the formation of C–C linkages, although production of 2 from complex 12 also takes place (100). The  $\text{CuCl}/\text{teed}$  complex also reacts with dioxygen to give 4 (83).

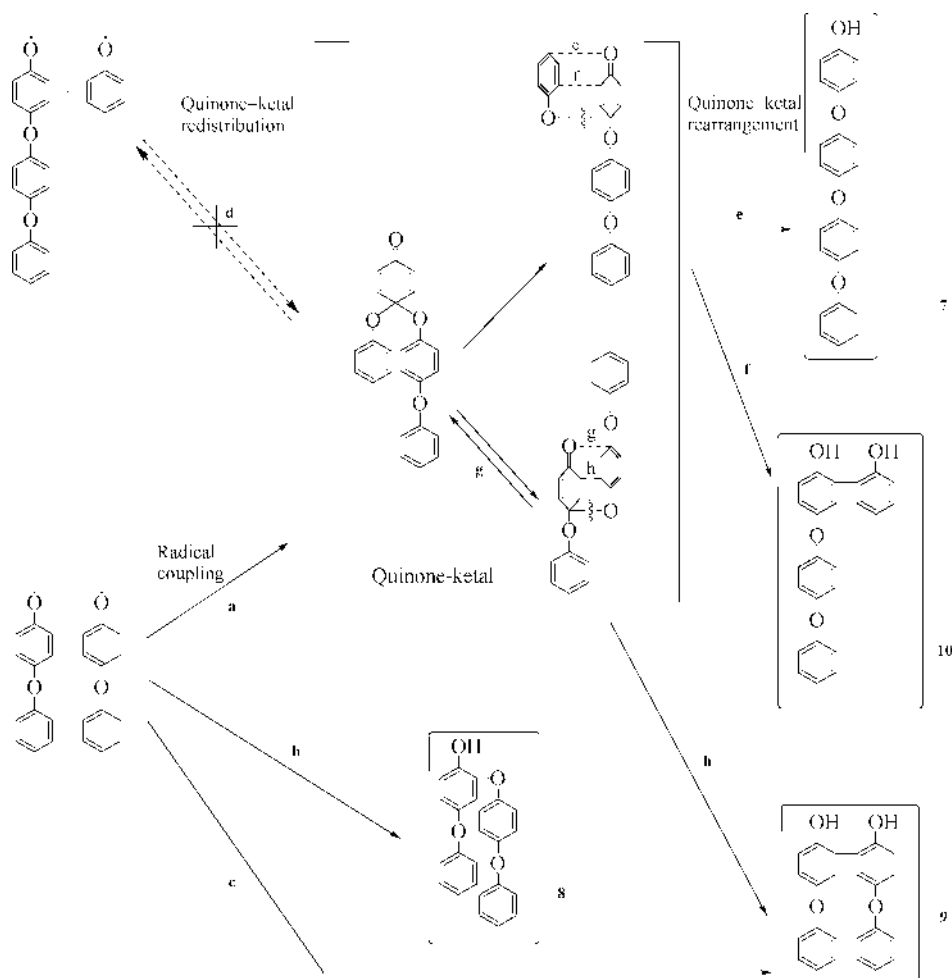


**Fig. 6.** Reaction mechanism for oxidative coupling and chain extension of 4-phenoxyphenol.

Two computational studies have been performed; one disagreed with the above reaction mechanism (101), but the other was in good agreement (102).

**Reaction Mechanism of Oxidative Coupling and Chain Extension.** Figure 6 shows a speculative reaction mechanism for oxidative coupling of PPL to produce dimers (87,92). For simplicity, the mechanism is argued here by expressing intermediate structures in the form of free radical rather than controlled radicals. First, two phenoxy radicals are generated from PPL and couple to each other (radical coupling); then only three reaction routes (**a**, **b**, and **c**) can take place, giving rise to a quinone-ketal intermediate, 8 and 9, respectively. From the quinone-ketal, the redistribution path (quinone-ketal redistribution, **d**) was ruled out, and therefore the rearrangement path (quinone-ketal rearrangement) is proposed in the oxidative coupling of PPL. On cleavage of the ketal C—O bond, synchronous bond formation of route **e** to 7, that of **f** to 10, and that of **h** to 9 can occur, but that of **g** regenerates the quinone-ketal.

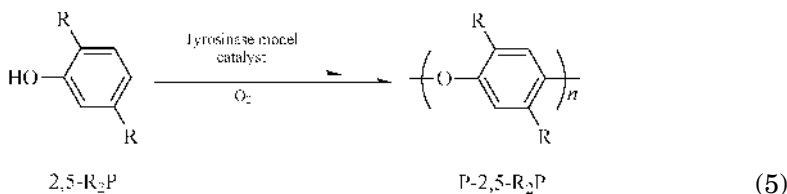
In the “radical-controlled” oxidative coupling of PPL, the radical coupling takes place from controlled phenoxy radical–copper(I) intermediate. Therefore, the steric effect of the catalyst would suppress 8 formation (route **b**) and inhibit 9 formation (route **c**), mainly giving quinone-ketal intermediate (route **a**). Moreover, almost no detection of 10 as well as 9 shows that the catalyst must be kept interacting with the quinone-ketal intermediate during the rearrangement. Probably, the carbonyl group of the quinone-ketal coordinates to the copper(I) atom of the catalyst. Thereby, bond formation at the *o*-position to 10 and 9 via routes **f** and **h**, respectively, would be protected and give 7 predominantly via route **e**. Further chain extension follows in a similar way to that of dimerization.

*Oxidative Polymerization of Other Phenols by Tyrosinase Model Catalyst.*

The substituent effect of phenol monomers on the reaction rates has been investigated (103). For the Cu(tmed) catalyst, the reaction rates were governed by the O–H homolytic bond dissociation energies of the monomers, which are closely related to the electronic effect of substituents. On the other hand, for the Cu(L<sup>iPr</sup>) catalyst, the steric effect of substituents at the *o*-positions depressed the reaction rates.

In the oxidative polymerization of phenol, the Cu(L<sup>iPr</sup>) catalyst showed high selectivity for C–O coupling; however, it did not exclude the formation of C–C coupling (104). The resulting polymer consisted mainly of a 1,4-phenylene oxide unit but contained a considerable amount of C–C coupling structures, showing no crystallinity. The oxidative polymerization of 2- and 3-methylphenol regioselectively produced soluble poly(phenylene oxide)s, showing good thermal stability (105,106).

The polymers obtained from 2,5-dialkylphenols [2,5-R<sub>2</sub>P: R = methyl (Me), ethyl (Et), *n*-propyl (nPr)] are noteworthy (107) (eq. 5). The oxidative polymerization of 2,5-Me<sub>2</sub>P catalyzed by Cu(L<sup>iPr</sup>)Cl<sub>2</sub> in toluene under dioxygen produced a white polymer. The *M<sub>w</sub>* was 19,300 and the structure was composed exclusively of a 2,5-dimethyl-1,4-phenylene oxide unit. The melting temperatures in the first and second scan (*T<sub>m1</sub>* and *T<sub>m2</sub>*) were detected at 308 and 303°C, respectively. Poly-2,5-Me<sub>2</sub>P (eq. 5) showing heat-reversible crystallinity was synthesized for the first time. The isomeric polymer Poly-2,6-Me<sub>2</sub>P (Fig. 1) showed a melting point at 237°C (*T<sub>m1</sub>*), but once the crystalline part had been totally melted, recrystallization never occurred (*T<sub>m2</sub>* not detected) by slow cooling or after annealing (108). Since thermoplastic polymers are mainly used as melt-moldings, Poly-2,6-Me<sub>2</sub>P is generally accepted as an amorphous polymer; however, Poly-2,5-Me<sub>2</sub>P is considered as a crystalline one.



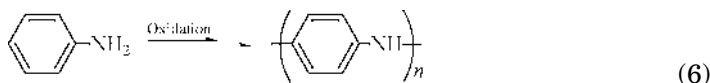
In the oxidative polymerization of 2,5-Et<sub>2</sub>P and 2,5-nPr<sub>2</sub>P (107), white polymers with *M<sub>w</sub>* of 23,100 and 32,200, respectively, possessed only the

1,4-phenylene oxide units. The latter showed heat-reversible crystallinity with  $T_{m2}$  at 276°C, however, the former did not show a detectable  $T_{m2}$ . The recrystallization for poly(alkylated phenylene oxide)s after melting seems to be governed by both the position and nature of alkyl substituents.

**Oxidative Polymerization of Naphthol Derivatives.** Oxidative polymerization of 2-naphthol (109) and 1,5-dihydroxynaphthalene (110) has been done using enzyme catalysts. Solid-state polycondensation of 2,6-dihydroxynaphthalene with  $\text{FeCl}_3$  catalyst (111) has been accomplished. Asymmetric oxidative coupling polymerization of 2,3-dihydroxynaphthalenes and their derivatives was achieved by chiral copper catalysts (112–115).

### Oxidative Polymerization of Anilines

Oxidative polymerization of aniline produces polyaniline (PAN) (eq. 6). This polymer was obtained as aniline black about a century ago (116,117) and has been revived as an electrically conducting polymer (see ELECTRICALLY ACTIVE POLYMERS).



Polyaniline has been synthesized electrochemically (118,119) and with chemical oxidizing agents (120–123); a typical oxidizing agent is ammonium persulfate (120,121). Catalytic oxidative polymerization of aniline using iron salt catalyst (124) or HRP enzyme catalyst (125–129) with hydrogen peroxide, iron salt catalyst with ozone (130), and copper salt catalyst with dioxygen (131) has been done. A photo-induced catalytic system (132,133) and a gas-phase plasma method (134) have also been reported. Strongly acidic reaction conditions in the polymerization are normally selected, because polymer structure and electrical conductivity of PAN depend on the pH of the polymerization reaction (135,136).

The reaction mechanism of oxidative polymerization of aniline has been a big controversy (Fig. 7). The dimerization step is generally proposed as (i), in which aniline is one-electron-oxidized to a cation radical, followed by coupling of two molecules of the cation radical to a dimer. The subsequent steps of chain extension are under discussion; routes involving coupling of cation radicals such as (ii)–(iv) (137–140) and routes via electrophilic attack of a two-electron-oxidized quinodol diiminium ion (v) or nitrenium ion (vi) (141,142) have been proposed. The addition of electron-rich arenes does not inhibit the polymerization, and therefore the route through the nitrenium ion (vi) seems to be rejected (137).

Protonic doping is necessary to convert PAN from an insulator to a conductor (136), and so various dopants such as acid-substituted polymers (143–146) and chiral sulfonic acids (147–149) have been employed. Emulsion polymerization of aniline-afforded PAN particles (150–156) and PAN–silica particles (157,158). Polyaniline nanofibers have been synthesized by template-guided polymerization (159,160) and aqueous/organic interfacial polymerization (161–163). Intercalated PANs in  $\text{V}_2\text{O}_5$  (164),  $\text{VOPO}_4$  (165),  $\text{MoO}_3$  (166), and  $\text{FeOCl}$  (167) have been

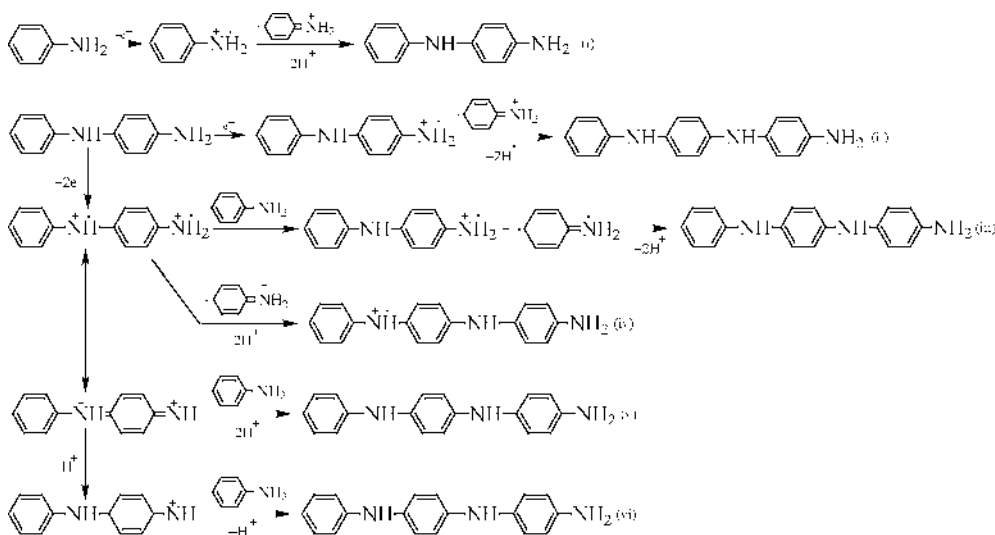


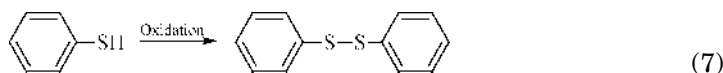
**Fig. 7.** Reaction mechanism for oxidative polymerization of aniline.

obtained, and included PANs in zeolite molecular sieves (168) and mesoporous channel hosts (169).

Many substituted polyanilines were also synthesized (170). Typical examples are self-doping polymers, such as sulfonic acid ring-substituted PANs (171–177), mercaptopropanesulfonic acid substituted PANs (178), *N*-alkylsulfonic acid substituted PANs (179–181), and *N*-phenylsulfonic acid substituted PANs (182,183). Polyanilines having boronic acid for detecting sugar and dopamine (184,185) and for controlling self-doped states (186) have been produced. Long-chain-substituted anilines were polymerized at an air–water interface by the Langmuir–Blodgett technique (138,187,188). (see LANGMUIR-BLODGETT FILMS). Polyanilines with liquid crystalline substituents (189,190) and redox-active disulfide unit (191) were synthesized. Oxidative polymerization of 1-aminonaphthalenes gave PAN-like polymers (192,193).

## Oxidative Polymerization of Thiophenols and Their Derivatives

Thiophenol is oxidatively coupled to give diphenyldisulfide (eq. 7), because formation of an S–S bond, resulting from the coupling of thiophenoxyl radicals, happens more readily than formation of a C–S bond (194). Oxidative polymerization of 1,3-dimercaptobenzene afforded poly(1,3-phenylenedisulfide) (195–197).



Poly(phenylene sulfide) (PPS) has been synthesized by oxidative polymerization of diphenyl disulfide, which was obtained via oxidation of thiophenol

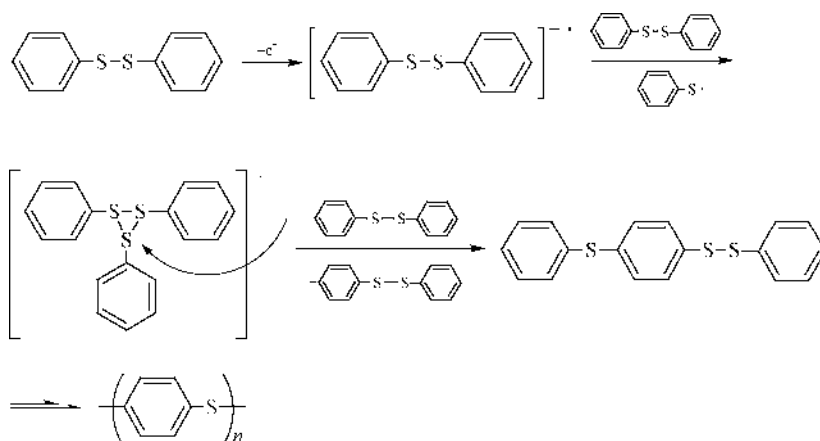
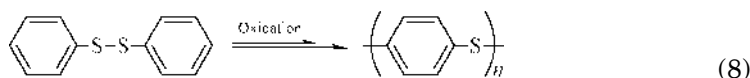


**Fig. 8.** Reaction mechanism for oxidative polymerization of diphenyl disulfide.

(eq. 8) (198–208). PPS is an engineering plastic with a high melting point, which is manufactured by condensation polymerization eliminating a salt.

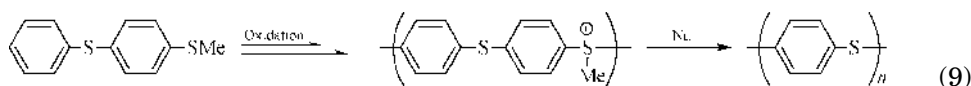


The oxidative polymerization of diphenyl disulfide was carried out in the presence of a strong acid by electrolysis (198) and by reaction with Lewis acids such as  $\text{SbCl}_5$  (199–201) or quinones such as 2,3-dichloro-5,6-dicyano-1,4-benzoquinone (202–205). VO catalysts such as vanadyl acetylacetonate with  $\text{O}_2$  have also been used for the oxidative polymerization (206–208), and the catalytic reaction mechanism involving four-electron reduction of  $\text{O}_2$  has been discussed (209–215).

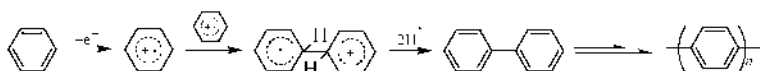
The chain extension mechanism is shown in Figure 8 (201). Diphenyl disulfide is oxidized to a cation radical, which reacts with diphenyl disulfide to give phenylbis(phenylthio)sulfonium cation, followed by electrophilic attack of diphenyl sulfide on the cation.

The use of various diaryl disulfides as the monomer produced PPSs substituted with methyl groups at the 2- or 3-, 2,3-, 2,5-, or 2,6-positions, methoxy at the 2-position, etc. (204,207). Reactive functionalized oligomers (216) and block polymers containing alkylene and perfluoroalkylene groups (217,218) have been obtained. Cyclic hexakis(1,4-phenylene sulfide) was synthesized (219), and ring-opening polymerization of such cyclic oligomers was also found (220).

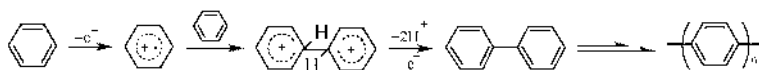
The synthesis of PPS via poly(sulfonium cation) as a soluble precursor (221) was developed through oxidative polymerization of methyl 4-(phenylthio)phenyl sulfide (222), followed by dealkylation (eq. 9) (223–225).



(i) Coupling of two cation radicals



(ii) Coupling of one cation radical with one neutral molecule



(iii) Coupling of one cation radical with many neutral molecules (stair-step mechanism)

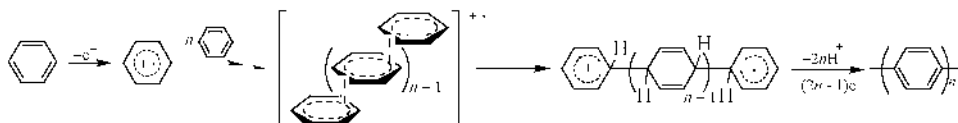
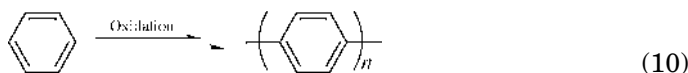


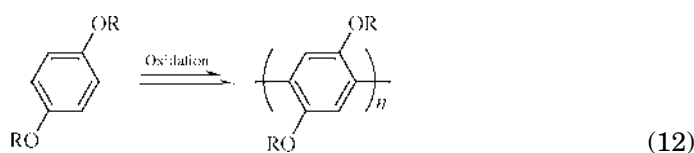
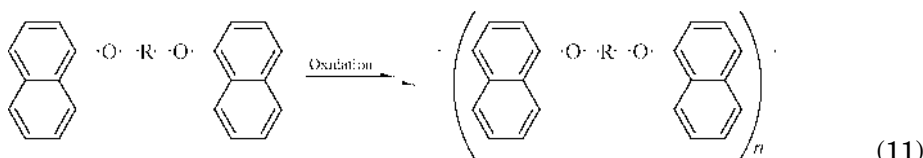
Fig. 9. Reaction mechanism for oxidative polymerization of benzene.

## Oxidative Polymerization of Aromatic Hydrocarbons

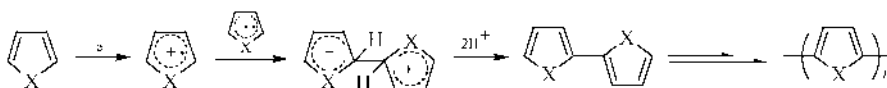
In the 1960s, oxidative polymerization of benzene by  $\text{CuCl}_2\text{-AlCl}_3$  was discovered (eq. 10) (226). Other oxidants such as  $\text{AlCl}_3\text{-MnO}_2$ ,  $\text{FeCl}_3$ , and  $\text{MoCl}_5$  were employed. These systems allowed the polymerization of various monomers such as toluene, chlorobenzene, diphenyl, naphthalene, and phenanthrene (227).



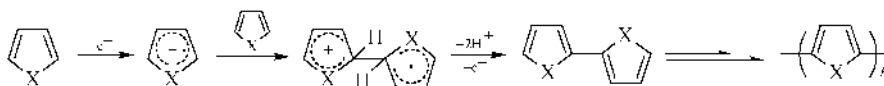
Oxidative polymerization of bis(1-naphthoxy) monomers is known as the Sholl Reaction (eq. 11) (228). 1,4-Dialkoxybenzenes have been polymerized using  $\text{FeCl}_3$  (229,230) and oxovanadium catalyst with dioxygen (231) to give poly(2,5-dialkoxy-1,4-phenylene)s (eq. 12). Poly(4,6-di-*n*-butyl-1,3-phenylene) was also obtained (232).



(i) Coupling of two cation radicals



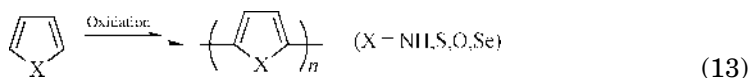
(ii) Coupling of one cation radical with one neutral molecule

**Fig. 10.** Reaction mechanism for oxidative polymerization of heterocyclic aromatics.

Three reaction mechanisms of C—C coupling in oxidative polymerization of benzenes have been reported (Fig. 9). The first step of each mechanism is one electron oxidation of a monomer to give a cation radical. The next step may be (i) coupling of two cation radicals (233,234), (ii) coupling of one cation radical with one neutral molecule (226,228), or (iii) coupling of one cation radical with many neutral molecules (stair-step mechanism) (235).

### Oxidative Polymerization of Heterocyclic Aromatics

Oxidative polymerization of pyrrole (236), thiophene (237), furan (238), and selenophene (239) was performed with electrical methods around two decades ago (eq. 13). More recently, numerous studies on the resulting polymers, particularly polypyrroles and polythiophenes, have been performed in terms of electrical conductivity (see ELECTRICALLY ACTIVE POLYMERS).



For the oxidative polymerization of heterocyclic aromatics, two reaction mechanisms, similar to that of benzenes, have been proposed (Fig. 10). One is coupling of two cation radicals [(i) in Fig. 10] (240,241), and the other is coupling of one cation radical with one neutral molecule [(ii) in Fig. 10] (242,243).

**Oxidative Polymerization of Pyrroles.** The synthesis of pyrrole blacks was performed by chemical oxidative polymerization with a variety of oxidizing agents such as hydrogen peroxide, lead dioxide, quinines, ferric chloride, and persulfates (244) before the electrical method was employed (236). The catalytic oxidative polymerization under dioxygen to give polypyrrole (PPY) has also been developed (245–247).

Various PPYs having 1-substituted (248), 3-substituted (249,250), and 3,4-disubstituted (251–253) groups, and transition metal complex moieties (254–256) have been obtained.

PPY particles were produced by colloidal dispersion method (257–259). Monolayer and multilayer PPYs were obtained by thiol–Au interaction (260,261),



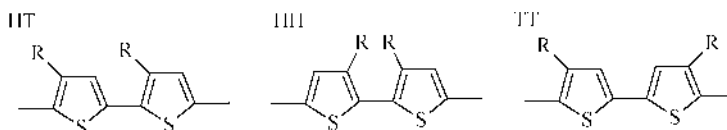


Fig. 11. Regoisomers of 3-substituted polythiophenes.

by deposition on  $\text{YBa}_2\text{Cu}_3\text{O}_{7-\delta}$  (262,263), by intercalation in  $\text{FeOCl}$  (264), and by monomer amphiphilicity (265). PPY wires (266–268), PPY tubes (269–271), and PPY microcontainers (272,273) have also been synthesized.

**Oxidative Polymerization of Thiophenes.** Thiophene is oxidatively polymerized to give polythiophene (PTH) by electrochemical oxidation (237); by chemical oxidation with  $\text{AsF}_5$  (274), NO salts (275), and  $\text{FeCl}_3$  (276); and by catalytic oxidation with dioxygen (277).

PTH can be substituted at the 3- and/or 4-positions (278). 3-Substituted PTHs have regoisomers (Fig. 11), and the regioregularity greatly affects conjugation length and electronic properties. For poly(3-alkylthiophenes), high regioselectivity of 91–98% HT has been obtained by organometallic reaction (279,280); however, a maximum 89% HT (Fig. 11) has been obtained by oxidative polymerization (281,282). In oxidative polymerization of 3-arylthiophenes (283–285) and 3-alkoxy-4-methylthiophenes (286), 94–96% HT contents were achieved. This regioselectivity has been discussed as arising from the spin density of the radical cations (287,288).

Poly(3,4-ethylenedioxythiophene) was developed around 1990, and its combination with poly(styrene sulfonic acid) became practical because of its high film-formability, conductivity, transparency, and stability (289). Many functional PTHs were prepared possessing crown ether (290,291), tetrathiafluvalene-like structures (292,293),  $\text{C}_{60}$ -attachment (294,295), probes for affinity chromism (296–298), and various metal complexes (299–306).

PTH film obtained by electrochemical deposition was stronger than aluminum film (307). PTH fibers were produced by using capillary flow cell (308) and with electrically independent connections (309). PTHs were included in zeolite (310,311) and such PTH wires (312) were obtained. PTH catenanes and rotaxanes have also been synthesized (313,314).

## Oxidative Polymerization of Other Monomers

Treatment of *m*-diethynylbenzene with a copper catalyst and dioxygen gave a poly(phenylene butadiynylene) (315). Use of Cu-incorporated mesoporous materials as the oxidative polymerization catalyst for 1,4-diethynylbenzene produced highly conjugated poly(1,4-phenylene-1,4-butadiynylene) (316).

Bifunctional *p*-tolylcyanoacetic esters (317) and monofunctional phenylcyanoacetic esters (318) were oxidatively polymerized using a copper catalyst with dioxygen.

## BIBLIOGRAPHY

“Oxidative Polymerization” in *EPSE* 2nd ed., Vol. 10, pp. 670–683, by Martin B. Jones, University of North Dakota, and Peter Kovacic, University of Wisconsin-Milwaukee; in *EPST* 3rd ed., Vol. 10, pp. 740–764, by H. Higashimura, Sumitomo Chemical Company, Ltd., and S. Kobayashi, Kyoto University.

## CITED PUBLICATIONS

1. S. L. Cosgrove and W. A. Waters, *J. Chem. Soc.* 388 (1951).
2. C. G. Haynes and co-workers, *J. Chem. Soc.* 2823 (1956).
3. A. S. Hay and co-workers, *J. Am. Chem. Soc.* **81**, 6335 (1959).
4. A. S. Hay, *J. Polym. Sci., Part A: Polym. Chem.* **36**, 505 (1998).
5. S. Kobayashi and H. Higashimura, *Prog. Polym. Sci.* **28**, 1015 (2003).
6. G. F. Endres and co-workers, *J. Org. Chem.* **28**, 1300 (1963).
7. H. Finkbeiner and co-workers, *J. Org. Chem.* **31**, 549 (1966).
8. E. Tsuchida and co-workers, *Makromol. Chem.* **176**, 1349 (1975).
9. E. Tsuchida and co-workers, *Makromol. Chem.* **151**, 221 (1972).
10. E. P. Talsi and co-workers, *J. Mol. Catal.* **57**, 325 (1990).
11. J. Kresta and co-workers, *Makromol. Chem.* **176**, 157 (1975).
12. P. J. Baesjou and co-workers, *J. Mol. Catal., A: Chem.* **110**, 195 (1996).
13. P. J. Baesjou and co-workers, *J. Am. Chem. Soc.* **119**, 12590 (1997).
14. A. S. Hay, *Adv. Polym. Sci.* **4**, 496 (1967).
15. C. Walling and R. B. Hodgdon Jr., *J. Am. Chem. Soc.* **80**, 228 (1958).
16. V. A. Dodonov and W. A. Waters, *J. Chem. Soc.* 2459 (1965).
17. C. C. Price and K. Nakaoka, *Macromolecules* **4**, 363 (1971).
18. E. McNelis, *J. Org. Chem.* **31**, 1255 (1966).
19. W. G. B. Huysmans and W. A. Waters, *J. Chem. Soc. B* 1163 (1967).
20. H. M. van Dort and co-workers, *J. Polym. Sci., Part C* **22**, 431 (1968).
21. R. Cecil and J. S. Littler, *J. Chem. Soc. B* 1420 (1968).
22. W. A. Waters, *J. Chem. Soc. B* 2026 (1971).
23. J.-L. Roubaty and co-workers, *Makromol. Chem.* **179**, 1151 (1978).
24. W. A. Butte Jr. and C. C. Price, *J. Am. Chem. Soc.* **84**, 3567 (1962).
25. D. A. Bolon, *J. Am. Chem. Soc.* **88**, 3148 (1966).
26. W. J. Mijs and co-workers, *Tetrahedron* **23**, 2253 (1967).
27. G. D. Cooper and co-workers, *J. Am. Chem. Soc.* **87**, 3996 (1965).
28. B. Miller, *J. Am. Chem. Soc.* **86**, 1127 (1964).
29. P. J. Baesjou and co-workers, *Macromolecules* **32**, 270 (1999).
30. D. M. White, *J. Org. Chem.* **34**, 297 (1969).
31. H. A. M. van Aert and co-workers, *Macromolecules* **28**, 7967 (1995).
32. H. A. M. van Aert and co-workers, *Macromolecules* **30**, 6056 (1997).
33. K. Saito and co-workers, *Chem.—Eur. J.* **9**, 4240 (2003).
34. E. Tsuchida and co-workers, *Reactive Oligomers*, American Chemical Society, Washington, D.C., 1985, p. 175.
35. W. Koch and co-workers, *Makromol. Chem., Suppl.* **12**, 105 (1985).
36. S.-H. Hyun and co-workers, *Bull. Chem. Soc. Jpn.* **61**, 1319 (1988).
37. E. Tsuchida and co-workers, *Macromolecules* **28**, 7917 (1995).
38. K. Takeshi and coworkers, *Chem. Lett.* **28**, 393 (1999).
39. K. Oyaizu and co-workers, *Macromolecules* **35**, 67 (2002).
40. R. Ikeda and co-workers, *Macromolecules* **33**, 6648 (2000).
41. K. Oyaizu and co-workers, *Macromolecules* **33**, 5766 (2000).
42. R. Ikeda and co-workers, *Macromolecules* **29**, 3053 (1996).

43. R. Ikeda and co-workers, *Polym. Int.* **47**, 295 (1998).
44. K. Sarkanen, *Lignins*, Wiley-Interscience, New York, 1971.
45. H. S. Mason, *J. Biol. Chem.* **172**, 83 (1948).
46. A. M. Klibanov and co-workers, *Science* **221**, 259 (1983).
47. M. Schnitzer and co-workers, *Soil Biol. Biochem.* **16**, 371 (1984).
48. J. S. Dordick and co-workers, *Biotech. Bioeng.* **30**, 31 (1987).
49. J. A. Akkara and co-workers, *J. Polym. Sci., Part A: Polym. Chem.* **23**, **29**, 1561 (1991).
50. S. Kobayashi, *J. Polym. Sci.: Part A: Polym. Chem.* **24**, **37**, 3041 (1999).
51. S. Kobayashi and co-workers, *Chem. Rev.* **101**, 3793 (2001).
52. L. B. Davin and co-workers, *Science* **275**, 362 (1997).
53. H. Uyama and co-workers, *Chem. Lett.* 423 (1994).
54. H. Uyama and co-workers, *Chem. Lett.* 795 (1995).
55. T. Oguchi and co-workers, *Macromol. Rapid Commun.* **20**, 401 (1999).
56. Y.-J. Kim and co-workers, *Macromolecules* **36**, 5058 (2003).
57. H. Uyama and co-workers, *J. Polym. Sci., Part A: Polym. Chem.* **35**, 1453 (1997).
58. F. F. Bruno and co-workers, *Langmuir* **11**, 889 (1995).
59. N. Mita and co-workers, *Chem. Lett.* **31**, 402 (2002).
60. H. Tonami and co-workers, *Macromol. Chem. Phys.* **200**, 2365 (1999).
61. T. Fukoka and co-workers, *Macromolecules* **36**, 8213 (2003).
62. S. Kobayashi and co-workers, *Macromol. Rapid Commun.* **17**, 503 (1996).
63. S. Kobayashi and co-workers, *Macromol. Chem. Phys.* **199**, 777 (1998).
64. T. Fukuoka and co-workers, *Macromolecules* **33**, 9152 (2000).
65. P. Wang and co-workers, *J. Am. Chem. Soc.* **117**, 12885 (1995).
66. H. Tonami and co-workers, *Macromol. Chem. Phys.* **200**, 1998 (1999).
67. P. Wang and J. S. Dordick, *Macromolecules* **31**, 941 (1998).
68. T. Fukuoka and co-workers, *Biomacromolecules* **3**, 768 (2002).
69. W. Liu and co-workers, *Chem. Mater.* **12**, 1577 (2000).
70. W. Liu and co-workers, *Macromolecules* **34**, 3522 (2001).
71. H. Uyama and co-workers, *Macromolecules* **31**, 554 (1998).
72. H. Tonami and co-workers, *Biomacromolecules* **1**, 149 (2000).
73. S. Kobayashi and co-workers, *Chem. Lett.* **29**, 1214 (2000).
74. S. Kobayashi and co-workers, *Chem.—Eur. J.* **7**, 4755 (2001).
75. Jpn. Kokai Tokkyo Koho, JP 08053545 (1996), A. Terahara and H. Higashimura (to Sumitomo-Chemical Co.) (in English); *Chem. Abstr.* **125**, 11750 (1996).
76. H. Tonami and co-workers, *Polym. Bull.* **42**, 125 (1999).
77. T. Tsujimoto and co-workers, *Chem. Lett.* **29**, 1122 (2000).
78. R. Ikeda and co-workers, *Macromol. Rapid Commun.* **21**, 496 (2000).
79. T. Fukuoka and co-workers, *Macromol. Rapid Commun.* **23**, 698 (2002).
80. J. A. Akkara and co-workers, *Macromolecules* **33**, 2377 (2000).
81. A. S. Hay, *J. Polym. Sci.* **58**, 581 (1962).
82. E. Tsuchida and co-workers, *Makromol. Chem.* **164**, 203 (1973).
83. V. Mahadevan and co-workers, *J. Am. Chem. Soc.* **119**, 11996 (1997).
84. J. E. Penner-Hahn and co-workers, *J. Am. Chem. Soc.* **108**, 7819 (1986).
85. M. Valoti and co-workers, *Arch. Biochem. Biophys.* **269**, 423 (1989).
86. H. Higashimura and co-workers, *J. Am. Chem. Soc.* **120**, 8529 (1998).
87. H. Higashimura and co-workers, *Macromolecules* **33**, 1986 (2000).
88. N. Kitajima and co-workers, *J. Am. Chem. Soc.* **111**, 8975 (1989).
89. N. Kitajima and co-workers, *J. Am. Chem. Soc.* **114**, 1277 (1992).
90. A. S. Hay and G. F. Endres, *Polym. Lett.* **3**, 887 (1965).
91. A. S. Hay, *Polym. Eng. Sci.* **16**, 1 (1976).
92. H. Higashimura and co-workers, *J. Polym. Sci., Part A: Polym. Chem.* **38**, 4792 (2000).
93. H. Higashimura and co-workers, *J. Mol. Catal., A, Chem.* **161**, 233 (2000).

94. E. Tsuchida and co-workers, *J. Macromol. Sci., Chem. A* **21**, 1081 (1984).
95. H. M. van Dort and co-workers, *Eur. Polym. J.* **4**, 275 (1968).
96. M. Kubo and co-workers, *Macromolecules* **31**, 3469 (1998).
97. J. A. Halfen and co-workers, *Science* **271**, 1397 (1996).
98. N. Kitajima and Y. Moro-oka, *Chem. Rev.* **94**, 737 (1994).
99. S. Mahapatra and co-workers, *J. Am. Chem. Soc.* **116**, 9785 (1994).
100. K. Fujisawa and co-workers, *Chem. Lett.* **28**, 739 (1999).
101. E. Tkatchouk and co-workers, *Macromolecules* **36**, 5607 (2003).
102. M. Kubota and co-workers, *Bull. Chem. Soc. Jpn.* **77**, 813 (2004).
103. H. Higashimura and co-workers, *Polym. Adv. Tech.* **11**, 733 (2000).
104. H. Higashimura and co-workers, *Polym. Prepr. Jpn.* **48**, 706 (1999).
105. H. Higashimura and co-workers, *Appl. Catal., A: Gen.* **194–195**, 427 (2000).
106. H. Higashimura and co-workers, *J. Mol. Catal., A: Chem.* **155**, 201 (2000).
107. H. Higashimura and co-workers, *Macromol. Rapid Commun.* **21**, 1121 (2000).
108. S. Z. D. Cheng and B. Wunderlich, *Macromolecules* **20**, 1630 (1987).
109. R. S. Premachandran and co-workers, *Macromolecules* **29**, 6452 (1996).
110. L. Wang and co-workers, *J. Polym. Sci., Part A: Polym. Chem.* **31**, 2855 (1993).
111. M. Suzuki and Y. Yatsugi, *Chem. Commun.* 162 (2002).
112. S. Habaue and co-workers, *Macromolecules* **36**, 2604 (2003).
113. S. Habaue and co-workers, *Macromolecules* **35**, 2437 (2002).
114. S. Habaue and co-workers, *Polym. J.* **35**, 592 (2003).
115. X. Xie and co-workers, *Angew. Chem. Int. Ed.* **42**, 2168 (2003).
116. R. Willstätter and S. Dorogi, *Chem. Ber.* **42**, 4118 (1909).
117. A. G. Green and A. E. Woodhead, *J. Chem. Soc.* 2388 (1910).
118. D. M. Mohilner and co-workers, *J. Am. Chem. Soc.* **84**, 3618 (1962).
119. E. M. Geniés and co-workers, *Synth. Met.* **36**, 139 (1990).
120. W.-S. Huang and co-workers, *J. Chem. Soc., Faraday Trans. 1* **82**, 2385 (1986).
121. A. Pron and co-workers, *Synth. Met.* **24**, 193 (1988).
122. M. Inoue and co-workers, *Synth. Met.* **30**, 199 (1989).
123. N. Toshima and H. Yan, *Bull. Chem. Soc. Jpn.* **68**, 1056 (1995).
124. D. K. Moon and co-workers, *Makromol. Chem.* **193**, 1723 (1992).
125. J. A. Akkara and co-workers, *Indian J. Chem.* **31B**, 855 (1992).
126. L. A. Samuelson and co-workers, *Macromolecules* **31**, 4376 (1998).
127. W. Liu and co-workers, *J. Am. Chem. Soc.* **121**, 71 (1999).
128. W. Liu and co-workers, *J. Am. Chem. Soc.* **121**, 11345 (1999).
129. R. Nagarajan and co-workers, *Macromolecules* **33**, 9542 (2000).
130. N. Toshima and co-workers, *Chem. Lett.* **29**, 1428 (2000).
131. N. Toshima and co-workers, *Bull. Chem. Soc. Jpn.* **67**, 1947 (1994).
132. K. Teshima and co-workers, *Chem. Commun.* 829 (1996).
133. K. Teshima and co-workers, *Macromolecules* **31**, 6783 (1998).
134. R. Hernandez and co-workers, *J. Phys. Chem.* **88**, 3333 (1984).
135. F. Lux, *Polymer* **35**, 2915 (1994).
136. A. G. Macdiarmid and co-workers, *Mol. Cryst. Liq. Cryst.* **121**, 173 (1985).
137. Y. Ding and co-workers, *J. Polym. Sci., Part A: Polym. Chem.* **37**, 2569 (1999).
138. R. R. Bodalia and R. S. Duran, *J. Am. Chem. Soc.* **115**, 11467 (1993).
139. K. Tzou and R. V. Gregory, *Synth. Met.* **47**, 267 (1992).
140. E. M. Genies and C. Tsintavis, *J. Electroanal. Chem.* **195**, 109 (1985).
141. Y. Wei and co-workers, *J. Phys. Chem.* **94**, 7716 (1990).
142. E. M. Genies and M. Lapkowski, *J. Electroanal. Chem.* **236**, 189 (1987).
143. N. Kuramoto and co-workers, *J. Chem. Soc., Chem. Commun.* 1478 (1990).
144. K. Shannon and J. E. Fernandez, *J. Chem. Soc., Chem. Commun.* 643 (1994).
145. I. Kulszewicz-Bajer and co-workers, *J. Chem. Soc., Chem. Commun.* 641 (1994).

146. S.-A. Chen and H.-T. Lee, *Macromolecules* **28**, 2858 (1995).
147. P. C. Innis and co-workers, *Macromolecules* **31**, 6521 (1998).
148. W. Li and co-workers, *Macromolecules* **35**, 9975 (2002).
149. G.-L. Yuan and N. Kuramoto, *Macromolecules* **36**, 7939 (2003).
150. S. P. Armes and M. Aldissi, *J. Chem. Soc., Chem. Commun.* 88 (1989).
151. B. Vincent and J. Waterson, *J. Chem. Soc., Chem. Commun.* 683 (1990).
152. N. Gospodinova and co-workers, *J. Chem. Soc., Chem. Commun.* 923 (1992).
153. P. J. Kinlen and co-workers, *Macromolecules* **31**, 1735 (1998).
154. D. Kim and co-workers, *Macromolecules* **35**, 5314 (2002).
155. P. S. Rao and co-workers, *Macromolecules* **35**, 4988 (2002).
156. E. Marie and co-workers, *Macromolecules* **36**, 3967 (2003).
157. M. Gill and co-workers, *J. Chem. Soc., Chem. Commun.* 108 (1992).
158. J. Stejskal and co-workers, *Macromolecules* **29**, 6814 (1996).
159. J.-M. Liu and S. C. Yang, *J. Chem. Soc., Chem. Commun.* 1529 (1991).
160. L. Yu and co-workers, *J. Appl. Polym. Sci.* **88**, 1550 (2003).
161. J. C. Michaelson and A. J. McEvoy, *J. Chem. Soc., Chem. Commun.* 79 (1994).
162. J. Huang and co-workers, *J. Am. Chem. Soc.* **125**, 314 (2003).
163. J. Huang and R. B. Kaner, *J. Am. Chem. Soc.* **126**, 851 (2004).
164. M. G. Kanatzidis and C.-G. Wu, *J. Am. Chem. Soc.* **111**, 4139 (1989).
165. H. Nakajima and G. Matsubayashi, *Chem. Lett.* **22**, 423 (1993).
166. R. Bissessur and co-workers, *J. Chem. Soc., Chem. Commun.* 687 (1993).
167. C.-G. Wu and co-workers, *J. Am. Chem. Soc.* **117**, 9229 (1995).
168. P. Enzel and T. Bein, *J. Phys. Chem.* **93**, 6270 (1989).
169. C.-G. Wu and T. Bein, *Science* **264**, 1757 (1994).
170. M. Leclerc and co-workers, *Macromolecules* **22**, 649 (1989).
171. J. Yue and A. J. Epstein, *J. Am. Chem. Soc.* **112**, 2800 (1990).
172. J. Yue and co-workers, *J. Am. Chem. Soc.* **113**, 2665 (1991).
173. J. Yue and A. J. Epstein, *Macromolecules* **24**, 4441 (1991).
174. X.-L. Wei and co-workers, *J. Am. Chem. Soc.* **118**, 2545 (1996).
175. H. S. O. Chan and co-workers, *Chem. Commun.* 1327 (1998).
176. K. Krishnamoorthy and co-workers, *Chem. Commun.* 240 (2002).
177. T. Yamamoto and co-workers, *Macromolecules* **36**, 7075 (2003).
178. C.-C. Han and co-workers, *Macromolecules* **36**, 7908 (2003).
179. P. Hany and co-workers, *Synth. Met.* **31**, 369 (1989).
180. J.-Y. Bergeron and co-workers, *J. Chem. Soc., Chem. Commun.* 180 (1990).
181. S.-A. Chen and G.-W. Hwang, *J. Am. Chem. Soc.* **116**, 7939 (1994).
182. C. DeArmitt and co-workers, *Polymer* **34**, 158 (1993).
183. M. T. Nguyen and co-workers, *Macromolecules* **27**, 3625 (1994).
184. E. Shoji and M. S. Freund, *J. Am. Chem. Soc.* **124**, 12486 (2002).
185. B. Fabre and L. Taillebois, *Chem. Commun.* 2982 (2003).
186. B. A. Deore and co-workers, *J. Am. Chem. Soc.* **126**, 52 (2004).
187. L. J. Kloeppner and R. S. Duran, *Langmuir* **14**, 6734 (1998).
188. L. J. Kloeppner and co-workers, *Macromolecules* **33**, 8006 (2000).
189. L. I. Gabaston and co-workers, *Chem. Commun.* 429 (1996).
190. H. Goto and K. Akagi, *Macromolecules* **35**, 2545 (2002).
191. J.-S. Cho and co-workers, *Macromolecules* **34**, 2751 (2001).
192. D.-K. Moon and co-workers, *Macromolecules* **26**, 6992 (1993).
193. E. P. Cintra and co-workers, *Macromolecules* **36**, 2079 (2003).
194. F. Magno and co-workers, *J. Electroanal. Chem.* **30**, 375 (1971).
195. U.S. Pat. 3,294,760 (1966), A. S. Hay (to General Electric Co.).
196. C. Della and co-workers, *J. Polym. Sci., Polym. Lett. Ed.* **23**, 323 (1985).
197. E. Shouji and D. A. Buttry, *J. Phys. Chem. B* **102**, 1444 (1998).

198. E. Tsuchida and co-workers, *Macromolecules* **20**, 2315 (1987).
199. E. Tsuchida and co-workers, *Macromolecules* **20**, 2030 (1987).
200. K. Yamamoto and co-workers, *Bull. Chem. Soc. Jpn.* **62**, 3655 (1989).
201. E. Tsuchida and co-workers, *Macromolecules* **23**, 2101 (1990).
202. E. Tsuchida and co-workers, *Macromolecules* **23**, 930 (1990).
203. K. Yamamoto and co-workers, *J. Polym. Sci., Part A: Polym. Chem.* **29**, 1359 (1991).
204. K. Yamamoto and co-workers, *Macromolecules* **25**, 2698 (1992).
205. K. Oyaizu and co-workers, *Bull. Chem. Soc. Jpn.* **67**, 1456 (1994).
206. E. Tsuchida and co-workers, *Macromolecules* **22**, 4138 (1989).
207. K. Yamamoto and co-workers, *Macromolecules* **26**, 3432 (1993).
208. K. Yamamoto and co-workers, *Bull. Chem. Soc. Jpn.* **67**, 251 (1994).
209. E. Tsuchida and co-workers, *Inorg. Chem.* **33**, 1056 (1994).
210. K. Yamamoto and co-workers, *J. Am. Chem. Soc.* **118**, 12665 (1996).
211. K. Oyaizu and co-workers, *Inorg. Chem.* **35**, 6634 (1996).
212. E. Tsuchida and co-workers, *Inorg. Chem.* **38**, 3704 (1999).
213. Z. Liu and F. C. Anson, *Inorg. Chem.* **39**, 274 (2000).
214. Z. Liu and F. C. Anson, *Inorg. Chem.* **40**, 1329 (2001).
215. K. Oyaizu and co-workers, *Inorg. Chem.* **42**, 1070 (2003).
216. E. Tsuchida and co-workers, *Macromolecules* **28**, 409 (1995).
217. K. Yamamoto and co-workers, *Macromolecules* **27**, 4312 (1994).
218. E. Tsuchida and co-workers, *Macromolecules* **27**, 7504 (1994).
219. K. Miyatake and co-workers, *Macromolecules* **30**, 4502 (1997).
220. E. Tsuchida and co-workers, *Macromolecules* **31**, 6469 (1998).
221. K. Yamamoto and co-workers, *J. Am. Chem. Soc.* **115**, 5819 (1993).
222. K. Yamamoto and co-workers, *J. Org. Chem.* **61**, 1912 (1996).
223. E. Tsuchida and co-workers, *Macromolecules* **26**, 7144 (1993).
224. E. Tsuchida and co-workers, *Macromolecules* **27**, 1057 (1994).
225. K. Yamamoto and co-workers, *J. Org. Chem.* **60**, 452 (1995).
226. P. Kovacic and A. Kyriakis, *J. Am. Chem. Soc.* **85**, 454 (1963).
227. P. Kovacic and M. B. Jones, *Chem. Rev.* **87**, 357 (1987).
228. V. Percec and H. Nava, *J. Polym. Sci., Part A: Polym. Chem.* **26**, 783 (1988).
229. K. Mukai and co-workers, *J. Polym. Sci., Polym. Chem. Ed.* **23**, 1259 (1985).
230. M. Ueda and co-workers, *Macromolecules* **25**, 5125 (1992).
231. T. Okada and co-workers, *Macromolecules* **29**, 7645 (1996).
232. T. Okada and co-workers, *J. Polym. Sci., Part A: Polym. Chem.* **35**, 2259 (1997).
233. L. M. Goldenberg and P. C. Lacaze, *Synth. Met.* **58**, 271 (1993).
234. K. Yamamoto and co-workers, *Bull. Chem. Soc. Jpn.* **61**, 1731 (1988).
235. S. A. Milosevich and co-workers, *J. Am. Chem. Soc.* **105**, 1088 (1983).
236. A. F. Diaz and co-workers, *J. Chem. Soc., Chem. Commun.* 635 (1979).
237. A. F. Diaz and co-workers, *J. Electroanal. Chem.* **121**, 355 (1981).
238. G. Tourillon and F. Garnier, *J. Electroanal. Chem.* **135**, 173 (1982).
239. K. Yoshino and co-workers, *Jpn. J. Appl. Phys. Part 2* **22**, L701 (1983).
240. E. M. Genies and co-workers, *J. Electroanal. Chem.* **149**, 101 (1983).
241. Y. Wei and co-workers, *Chem. Mater.* **3**, 888 (1991).
242. T. Inoue and T. Yamase, *Bull. Chem. Soc. Jpn.* **56**, 985 (1983).
243. G. Koßmehl, *Makromol. Chem. Macromol. Symp.* **4**, 45 (1986).
244. G. P. Gardini, *Adv. Heterocycl. Chem.* **15**, 67 (1973).
245. N. Toshima and J. Tayanagi, *Chem. Lett.* **19**, 1369 (1990).
246. S. Izumi and N. Toshima, *Bull. Chem. Soc. Jpn.* **67**, 539 (1994).
247. E. Tsuchida and co-workers, *J. Electroanal. Chem.* **438**, 167 (1997).
248. J. R. Reynolds and co-workers, *Macromolecules* **20**, 958 (1987).

249. J. R  he and co-workers, *Synth. Met.* **28**, C177 (1989).
250. D.-K. Moon and co-workers, *Macromolecules* **28**, 6205 (1995).
251. A. Nazzari and G. B. Street, *J. Chem. Soc., Chem. Commun.* 83 (1984).
252. V. Enkelmann and co-workers, *Synth. Met.* **37**, 79 (1990).
253. P. Schottland and co-workers, *Macromolecules* **33**, 7051 (2000).
254. A. Deronzier and J.-C. Moutet, *Acc. Chem. Res.* **22**, 249 (1989).
255. C. J. Pickett and co-workers, *J. Chem. Soc., Chem. Commun.* 694 (1992).
256. G. Bidan and co-workers, *J. Am. Chem. Soc.* **114**, 5986 (1992).
257. S. P. Armes and B. Vincent, *J. Chem. Soc., Chem. Commun.* 288 (1987).
258. N. Cawdery and co-workers, *J. Chem. Soc., Chem. Commun.* 1189 (1988).
259. M. L. Digar and co-workers, *J. Chem. Soc., Chem. Commun.* 18 (1992).
260. R. J. Willicut and R. L. McCarley, *J. Am. Chem. Soc.* **116**, 10823 (1994).
261. R. L. McCarley and R. J. Willicut, *J. Am. Chem. Soc.* **120**, 9296 (1998).
262. S. G. Haupt and co-workers, *J. Am. Chem. Soc.* **116**, 9979 (1994).
263. R.-K. Lo and co-workers, *J. Am. Chem. Soc.* **118**, 11295 (1996).
264. M. G. Kanatzidis and co-workers, *J. Am. Chem. Soc.* **109**, 3797 (1987).
265. D. M. Collard and M. A. Fox, *J. Am. Chem. Soc.* **113**, 9414 (1991).
266. C. J  r  me and R. J  r  me, *Angew. Chem. Int. Ed.* **37**, 2488 (1998).
267. T. Bein and P. Enzel, *Angew. Chem. Int. Ed.* **28**, 1692 (1989).
268. M. Ikegami and co-workers, *Angew. Chem. Int. Ed.* **42**, 2154 (2003).
269. C. R. Martin and co-workers, *J. Am. Chem. Soc.* **112**, 8976 (1990).
270. C. R. Martin, *Science* **266**, 1961 (1994).
271. M. R. Ghadiri and co-workers, *Nature* **369**, 301 (1994).
272. L. Qu and G. Shi, *Chem. Commun.* 206 (2003).
273. L. Qu and co-workers, *Macromolecules* **36**, 1063 (2003).
274. G. Ko  mehl and G. Chatzitheodorou, *Makromol. Rapid Commun.* **2**, 551 (1981).
275. G. Ko  mehl and G. Chatzitheodorou, *Makromol. Rapid Commun.* **4**, 639 (1983).
276. K. Yoshino and co-workers, *Jpn. J. Appl. Phys.* **23**, L899 (1984).
277. S. Yu and co-workers, *Chem. Lett.* **28**, 559 (1999).
278. J. Roncali, *Chem. Rev.* **92**, 711 (1992).
279. T.-A. Chen and R. D. Rieke, *J. Am. Chem. Soc.* **114**, 10087 (1992).
280. R. D. McCullough and R. D. Lowe, *J. Chem. Soc., Chem. Commun.* 70 (1992).
281. M. Leclerc and co-workers, *Makromol. Chem.* **190**, 3105 (1989).
282. S. Amou and co-workers, *J. Polym. Sci., Part A: Polym. Chem.* **37**, 1943 (1999).
283. M. R. Andersson and co-workers, *Macromolecules* **27**, 6503 (1994).
284. T. Hayakawa and co-workers, *J. Polym. Sci.: Part A: Polym. Chem.* **39**, 2287 (2001).
285. M. Miyasaka and co-workers, *Macromolecules* **33**, 8211 (2000).
286. G. Daoust and M. Leclerc, *Macromolecules* **24**, 455 (1991).
287. M. Fr  chette and co-workers, *Synth. Met.* **84**, 223 (1997).
288. S. Ando and M. Ueda, *Synth. Met.* **129**, 207 (2002).
289. L. B. Groenendaal and co-workers, *Adv. Mater.* **12**, 481 (2000).
290. M. J. Marsella and T. M. Swager, *J. Am. Chem. Soc.* **115**, 12214 (1993).
291. S. Scheib and P. B  uerle, *J. Mater. Chem.* **9**, 2139 (1999).
292. P. J. Skabara and co-workers, *Chem. Commun.* 1005 (2000).
293. P. J. Skabara and co-workers, *Macromolecules* **34**, 2232 (2001).
294. T. Benincori and co-workers, *Angew. Chem. Int. Ed.* **35**, 648 (1996).
295. B. Jousselme and co-workers, *Macromolecules* **36**, 3020 (2003).
296. S. Bernier and co-workers, *J. Am. Chem. Soc.* **124**, 12463 (2002).
297. H. A. Ho and co-workers, *Angew. Chem. Int. Ed.* **41**, 1548 (2002).
298. H. A. Ho and M. Leclerc, *J. Am. Chem. Soc.* **125**, 4412 (2003).
299. R. P. Kingsborough and T. M. Swager, *J. Am. Chem. Soc.* **121**, 8825 (1999).
300. R. P. Kingsborough and T. M. Swager, *Angew. Chem. Int. Ed.* **39**, 2897 (2000).

301. C. L. Kean and P. G. Pickup, *Chem. Commun.* 815 (2001).
302. O. Clot and co-workers, *J. Am. Chem. Soc.* **122**, 10456 (2000).
303. O. Clot and co-workers, *J. Am. Chem. Soc.* **123**, 9963 (2001).
304. D. A. Weinberger and co-workers, *J. Am. Chem. Soc.* **123**, 2503 (2001).
305. D. H. Kim and co-workers, *J. Org. Chem.* **608**, 133 (2000).
306. A. Vigalok and co-workers, *J. Am. Chem. Soc.* **123**, 7917 (2001).
307. G. Shi and co-workers, *Science* **267**, 994 (1995).
308. S. Li and co-workers, *Science* **259**, 957 (1993).
309. C. L. Curtis and co-workers, *Science* **262**, 2014 (1993).
310. P. Enzel and T. Bein, *J. Chem. Soc., Chem. Commun.* 1326 (1989).
311. J. V. Caspar and co-workers, *J. Am. Chem. Soc.* **113**, 600 (1991).
312. G. Li and co-workers, *Angew. Chem. Int. Ed.* **42**, 3818 (2003).
313. D. L. Simone and T. M. Swager, *J. Am. Chem. Soc.* **122**, 9300 (2000).
314. J. Buey and T. M. Swager, *Angew. Chem. Int. Ed.* **39**, 608 (2000).
315. A. S. Hay, *J. Org. Chem.* **25**, 1275 (1960).
316. V. S.-Y. Lin and co-workers, *J. Am. Chem. Soc.* **124**, 9040 (2002).
317. H. A. P. de Jongh and co-workers, *J. Polym. Sci., Polym. Chem. Ed.* **11**, 345 (1973).
318. H. A. P. de Jongh and co-workers, *J. Org. Chem.* **36**, 3160 (1971).

HIDEYUKI HIGASHIMURA  
Sumitomo Chemical Company Ltd.  
SHIRO KOBAYASHI  
Kyoto University

## OXYGEN SCAVENGING SYSTEMS

### Introduction

Oxygen scavengers are mainly used for food and pharmaceutical applications, but can also be used for any product that needs a low oxygen storage atmosphere. Essentially, oxygen scavengers are so named because they preferentially absorb oxygen within the environment, thus, preventing the oxygen from reacting with the product. Many other terms have been used to describe oxygen scavengers, which include the following: antioxidants, interceptors, controllers, and absorbers. According to Brody, the definition of an oxygen scavenger is a material in which a chemical (or combination of reactive compounds) is incorporated into a package structure and may combine with oxygen to effectively remove oxygen from the inner package environment (1). The purpose of an oxygen scavenger is to limit the amount of oxygen available for deteriorative reactions that can lead to reduced functionality of the product. For foods and pharmaceutical products, deteriorative reactions include lipid oxidation, nutritional loss, changes in flavor and aroma, alteration of texture, and microbial spoilage. Typically, oxygen scavengers are used in packages that have air tight seals and are used in conjunction with other means of preservation, such as chemical preservatives, reduced water activity, reduced pH, vacuum packaging, or modified atmosphere packaging.





**Fig. 1.** Mitsubishi ageless sachets.

## History

Research on oxygen scavengers began in the 1920s for enclosed packages using a ferrous sulfate and moisture absorbing mixture (1). A British patent from 1938 used iron, zinc, or manganese to scavenge oxygen from canned foods (2). Research continued throughout the 1940s with the bulk of the work performed in the United Kingdom and by the U.S. Army for military rations. During the 1970s, the first major commercial oxygen scavenger was introduced by Mitsubishi Gas and Chemical Company in Japan, which was available in the United States by the late 1970s. The product eventually became known under the trade name Ageless and functions by using a permeable sachet that contains a reduced iron salt and moisture absorbent material. Toppan Printing Company in Japan also produced a commercially available oxygen scavenging system, but it functioned using an ascorbic acid-based reaction. During the 1970s and 1980s, more oxygen scavenging systems were introduced by Japanese and U.S. companies using several scavenging methods (1,2). During the 1980s, work began on oxygen scavenger development using singlet oxygen reaction by the Commonwealth Scientific Industrial Research Organization (CSIRO) in Australia. (See sachets shown in Figs. 1 and 2).

Oxygen scavengers are the most patented of all active packaging technologies with at least 50 patents through 1989 and 20 issued from 1990 to 1994 (3). In the 1990s, work focused more heavily on technologies to incorporate oxygen scavengers directly into film and other package forms such as closure liners, thermo-formed cups, tubs, and trays rather than sachets. Part of the reason for this change was related to concern over consumers accidentally using the sachets as “flavor packets” and incidents whereupon the contents of the sachet may seep out into the food. These problems can lead to loss of product quality and can also lead to serious consumer safety concerns. For example, iron in concentrated amounts can be toxic to children or pets, because of their small body mass. For this reason, the U.S. Food and Drug Administration mandated that iron-based sachets must be labeled with “Do not eat” on the sachets sold in the United States to avoid accidental ingestion of the contents. (4).

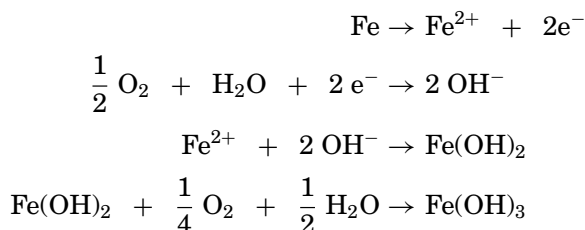


**Fig. 2.** Multisorb Freshpax.

Based on information made available in 2002, oxygen scavengers in bottles made up the largest portion of the market with 43.8% of the market, followed by cap/liner/lidding representing 31.5%, sachets with 22.6%, and oxygen-absorbing film with 2% (5).

## Types and Mechanisms of Action

**Iron-Based Systems.** Iron-based sachets are the type of oxygen-scavenging system that has been used commercially for many years. It generally involves a reaction between iron powder contained in a permeable sachet that also may contain a desiccant. Iron powder reacts with oxygen using the following reactions (6,7):



**Oxygen Scavenging Polymer Materials.** Many polymers have been developed using a wide variety of chemistries (2); however, the most commercially successful materials have been homogeneous blends of reactive substances with polymers. An effective oxygen scavenging polymer was developed in which



**Fig. 3.** Cryovac OS1000 oxygen scavenging film.

dissolved reagents of known chemistry were incorporated into a polymer, and the trigger mechanism was light, which excited the reactive components in the film, thus, influencing oxygen diffusion into the polymer. The oxygen has to be in an excited singlet state, which requires the use of a photosensitizing dye and exposure to visible light. Another approach was based on transition-metal-catalyzed oxidation of an aromatic nylon. The transition metal in this case was cobalt or cobalt salt. This material eventually became known under the trade name, Oxbar. The material easily could be blended with polyester and eventually became important for packaging wine and beer in plastic bottles, because it could effectively prevent oxidation in both products. Amoco Chemicals introduced a material called Amosorb, which blended polyester and polybutadiene and was catalyzed by a transition metal salt. When the catalyst was added late in the injection-molding process, the resulting material became an oxidizable polymer. Another material using light as a triggering mechanism was developed and used a transition metal catalyst and a photosensitizer (8). The reaction was designed in such a way as to prevent the rupture of the polymer backbone as might normally occur through oxidation. The material was composed of unsaturated polymers such as poly(1,2-butadiene), which could scavenge ground-state oxygen as opposed to singlet oxygen. This product is marketed under the trade name OS 1000 or 2000 by Cryovac Division of Sealed Air (Fig. 3).

Other materials that incorporate active components into the polymer include material marketed by Chevron Chemical Company, which works by autooxidation of unsaturated groups on the polymer backbone. Oxidation of aromatic nylons and hydrocarbon polymers with active side groups use light to trigger the oxygen scavenging process. One method that differs from the light-triggering systems involves the light excitation of a photoreducible component such as phenolic compound, which is reduced by oxygen, thereby scavenging oxygen.

Designing an oxygen scavenging system for specific types of packaging is quite complex and still not well understood except by the vendors who specialize in such systems. Most oxygen scavengers are designed for packaging based on the removal of a specified amount of oxygen from the interior of the package over a period of a few days. The oxygen absorption kinetics of six commercial oxygen

scavengers that differed in oxygen scavenging capacity as well as oxygen scavenging methods (ie, iron based and enzyme based) was studied (9). It was determined that the oxygen concentration was the primary limiting factor in the kinetics of oxygen scavengers in atmosphere of less than 500 ppm but other factors such as temperature, capacity, and variation between types of scavengers also occurred. Miltz and Perry (10) studied the performance of iron-based oxygen sachets to improve methods of applying them more effectively since cost and the lack of technical understanding have limited their use. Based on their study, the actual scavenging capacity was higher than the manufacturers specifications. They also found that, in modified atmosphere packages containing carbon dioxide, the sachets also absorbed the carbon dioxide as well as oxygen. Oxygen sachets were found to reduce the transient period time (time to reach equilibrium) for active modified atmosphere packaging by nearly half compared to passive modified atmosphere packaging without a sachet. This effect allowed the shelf life to be extended because of optimal atmosphere as soon as quickly as possible (11).

## Applications

**Current Use.** Oxygen scavengers were initially used by the U.S. military for the meals ready to eat (MRE) rations. Foods with oxygen scavengers for MREs include the following: white and whole wheat bread, pound cake, fudge brownies, wheat snack bread, potato sticks, chow mein noodles, nut raisin mix, pretzels, waffles, and hamburger buns (1). In the retail market, typical uses in the United States include fresh pasta, beef jerky, pepperoni, beer (cap liner and some bottles), ketchup, juice, case-ready meats, prepared foods, and shredded cheese. Use of oxygen sachets is more prevalent and diverse in Japan for products such as seasonings, cheese, aseptically packaged cooked rice, dry pet foods, cough capsules, plant growth hormone, antibiotics, vitamins pills and tablets, medical kits to preserve reagents, kidney dialysis kits, and other products.

### Current Research.

**Meat Packaging.** Oxygen scavengers are used in meat packaging to control color in red meat packages. When the pigment for red meat (myoglobin) is exposed to oxygen, the meat appears as a bright red color, which is associated with freshness and overall acceptability. However, when meat is exposed to too much oxygen over time, the pigment converts to metmyoglobin, which appears as a brown color and is not visually acceptable to consumers. Many studies have used oxygen scavengers in modified atmosphere packages to extend the display life of red meat packages. The conditions under which commercially available scavengers with an oxygen absorbing capacity of 200 mL/sachet could prevent transient discoloration of nitrogen flushed ground beef were studied (12). The rate of oxygen absorption decreased with decreasing oxygen concentration when the oxygen concentration was between 10% and 20%, but the rate of oxygen absorption became exponentially proportional with time when the oxygen concentration was less than 1%. Oxygen concentration in packages needed to be reduced below 10 ppm in 30 min at 2°C or 2 h at 1.5°C to prevent transient discoloration. It was determined that to achieve this, more sachets than were economically feasible would have been required at that time. Continued work on prevention of

transient discoloration of beef was done by Tewari and others (13), who determined that steaks removed from a controlled atmosphere masterpack had less discoloration when packaged with an oxygen scavenger and that the number of sachets had more impact on discoloration prevention than the type of scavenger used. The same research group also studied the effect of oxygen scavengers inside retail trays, lidding and over-wrapped trays, which were all equally effective for extending the acceptable shelf life of modified atmosphere, display ready beef, and pork cuts (14). They also found that eight oxygen scavengers with a capacity sufficient to achieve an oxygen half life of 0.6–0.7 were needed when oxygen concentration could otherwise remain at less than 500 ppm during storage. The redness of meat 96 h after removal from a gas-flushed mother pack was measured (15). It was found that redness of meat packaged in a retail tray containing oxygen scavengers was better than retail trays that did not contain an oxygen scavenger. In another study, researchers found that a tray combined with a controlled atmosphere mother pack (outer bag), double-flushed with 50% carbon dioxide and 50% nitrogen was effective for maintaining the display shelf life of variety of red meat cuts (16). The oxygen scavenger helped maintain a low level of oxygen (0.1%) to prevent formation of metmyoglobin.

Another study involved vacuum-controlled atmosphere packaging with carbon dioxide, carbon dioxide flushed packages containing iron-based oxygen scavenging sachets, and packages that contain oxygen scavengers alone for beef stored for up to 20 weeks at  $-1.5^{\circ}\text{C}$  (17). Beef packaged with oxygen scavenger alone provided the best results with regard to drip loss, microbial, and sensory properties. Fresh pork sausages packaged in a 20% carbon dioxide, 80% nitrogen atmosphere with an iron-based oxygen scavenging sachet, were found to have had reduced psychrotropic aerobic counts and extended shelf life with regard to color and lipid stability for 20 days at  $2^{\circ}\text{C}$  (18). Catfish steaks were packaged in barrier film and vacuum packaged with and without an iron-based sachet. Shelf life was extended 10 days (20 days with sachet vs 10 days without sachet) with the aid of the sachet based on sensory, microbiological, and volatile base nitrogen analysis. The oxygen in the packages containing the sachets reached 0.42% within 24 h of packaging (19). Labels are manufactured that absorb 10–20 mL of oxygen, and larger labels are starting to become available that scavenge 100–200 mL  $\text{O}_2$  (7). Besides labels, oxygen scavengers can also be incorporated into the polymer film. The film is capable of reducing oxygen in the headspace to less than 1 ppm in 4–10 days for products such as dried, smoked meat, as well as processed meat products (20).

**Bakery Products.** Baked goods such as bread, pastries, cakes, and cookies can have an extended shelf life with use of oxygen scavengers combined with modified atmosphere packaging. The low-oxygen condition retard molds and other spoilage bacteria and also reduces lipid oxidation, which can produce off flavors. An advantage over using an oxygen scavenger system compared to modified atmosphere packaging alone was because of the fact that lower oxygen levels could be achieved, and oxygen can be reduced in the case of leakage through defective seals (21). The disadvantages could be cost and possible consumer objection to a packet inserted inside the package that could become loose and cause accidental ingestion by a child or pet. A few studies have reported on the effectiveness of oxygen scavengers for bakery products. Sponge cakes ( $0.8\text{--}0.9 a_w$ ) were packed in

a modified atmosphere package with oxygen absorber sachets of two different absorption capacities (100 and 210 mL). The cakes were analyzed for mold growth over a period of 28 days at 25°C storage. Modified atmosphere package alone provided some benefits regarding mold prevention; however, combining oxygen scavengers (using either 100 or 210 mL) with modified atmosphere (30% CO<sub>2</sub>) prevented mold growth entirely during the 28 days of storage. The results also indicated that a greater benefit existed for cakes with a higher  $a_w$  (0.9) compared to lower  $a_w$  (0.8) (22).

In another study, oxygen absorbers were added to wheat crackers formulated with high levels of oil for storage in hermetically sealed cans used as military rations. The study included storage at 15, 25, and 35°C (23). Shelf life was assessed using sensory panels as well as hexane concentration and headspace oxygen measurements. As storage temperature increased, headspace oxygen decreased within the can. Overall, cans of crackers without oxygen sachets reached unacceptable levels of rancidity within 24 weeks at 25 and 35°C. Cans of crackers with oxygen sachets did not have rancid odors after 44 weeks of storage, regardless of storage temperature. Thus, shelf life of canned crackers was extended for 20 weeks with oxygen absorbers added to the can.

**Other Products.** Orange juice contained in aseptic packages with an oxygen scavenging barrier layer was found to have better retention of ascorbic acid than packages with plain oxygen barrier film (24). Packages that contained oxygen scavengers had less mold growth on cheddar cheese compared to packages without the oxygen scavengers over a 16-week refrigerated storage period (25).

Milk processed using ultra-high temperature processing, was packaged and stored in aseptic pouches that contain an oxygen scavenging film or a pouch without the scavenging film. The milk in the oxygen scavenging pouch had significantly lower levels of dissolved oxygen and levels of volatiles associated with staleness (26). Hazelnuts were packaged under controlled atmosphere conditions with and without iron-based oxygen sachets. The nuts packaged using the sachets were significantly less oxidized compared to the nuts without the sachets. However, when the sachets were analyzed for volatile compounds, other flavor compounds were also scavenged by the sachets (27).

## Regulations

A program was developed by the European Union (EU) Fair R&D program to establish and implement active and intelligent packaging technologies within existing EU regulations, which would enable technologies to be used and allow for products to be globally competitive with other technologies. The program included, inventory, classification, evaluation, and recommendations for regulation of active and intelligent packaging systems. Oxygen scavenging systems were examined as part of the evaluation step and were tested for migration into a variety of food stimulants. It was determined that migration from oxygen scavengers varied significantly depending upon type of system (sachet, cap, crown, or film) and food stimulant (3). For example, migration of oxygen scavenger in water (mg/sample) was 620, 74, 1.0, and 0.2 for sachet, cap, crown, and film, respectively. Migration into liquid, solid, and gelled food stimulants using two different

**Table 1. Oxygen Scavenging Components**

---

Sulfites
Boron
Glycols and sugar alcohols
Unsaturated fatty acids and hydrocarbons
Palladium catalysts
Enzymes
Yeast
Ferrous-iron
Organometallic ligands
Photosensitive dyes
Polydiene block copolymers
Polymer-bound olefins
Aromatic nylon

---

types of oxygen sachets was tested (23). Migration from oxygen scavengers did not exceed E.U. migration limits as long as the sachet was properly located in the package, and the packaging process did not favor the content becoming wet from water released from the food.

## Future Considerations

New methods of producing oxygen scavengers will continue to be developed. For example, the use of aerobic microorganisms as the mechanism for oxygen scavenging has been suggested (29). The microorganisms can be trapped in poly(vinyl alcohol) and used as a coating for high humidity foods. Another use that may see increased application is addition of an oxygen sachet with biopolymer film. Poly(lactic acid) film did not have oxygen barrier properties equal to the polyester film typically used for packaging semihard cheese (30). However, when an oxygen scavenger was added to the package, lipid oxidation of the cheese was significantly reduced and continued to improve with dark storage (Tables 1 and 2).

Another new method may involve radiation treatment of ethyl vinyl alcohol copolymers. Researchers irradiated ethylene vinyl alcohol (29% ethylene) with 30 and 90 kGy dosages and found that as the dosage increased, the longer the polymer was able to react with oxygen (31).

Oxygen scavengers that function better under a variety of temperatures will also be used. A patent was issued for an oxygen scavenging film that acts under ambient and refrigerated conditions and can be incorporated uniformly into a multilayer film (32). Another development involves a patent that indicates that the activation of the oxygen scavenging component of a film can be triggered upon packaging with the product to prevent loss of scavenging capacity in films that may be active while film is in storage (prior to product packaging). The film would receive an initial trigger using actinic radiation, which would not be sufficient to

**Table 2. Commercially Available Oxygen Scavenging Systems**

Trade name	Supplier
Agelessss	Mitsubisihi Gas and Chemical Co., Japan
ATCO	Emco Packaging Systems, UK; Standa Industries, France
Freshlizers series	Toppan Printing, Japan
Freshpax	Multisorb Technologies, Inc. USA
Freshmax	
Bioka	Bioka, Finland
Smartcap	ZapatA Industries, USA
Daraform, Cryovac OS 1000	Cryovac, Division of Sealed Air, USA
Oxyguard	Toyo Seikan Kaisha, Japan
Oxbar	Carnaud Metal Box, UK
Zero <sub>2</sub>	CSIRO, Southcorp Packaging, Australia
Amsorb	Amoco Chemicals, USA

activate the film fully and would receive the total dose necessary to trigger the oxygen scavenging component when desired (33).

An oxygen scavenger that also indicates the level of oxygen present has been developed, which makes it both an active, and intelligent package component. The scavenger is in a pouch form with a layer in the pouch that has a color changing substance that can be viewed through a clear window (34).

## BIBLIOGRAPHY

### CITED REFERENCES

1. A. L. Brody, E. R. Strupinsky, and L. R. Kline, *Active Packaging for Food Applications*, CRC Press, Boca Raton, Fla., 2001.
2. M. L. Rooney, in J. H. Han, ed. *Innovations in Food Packaging*, Elsevier Academic Press, San Diego, Calif., 2005, pp. 123–137.
3. N. de Kruijf, M. van Beest, R. Rijk, T. Spilainen-Malm, P. Paserio Losada, and B. De Meulenaer, *Food Addit. Contam.* **19** (Supp.) 144–162 (2002).
4. M. Ozdemir and J. D. Floros, *Crit. Rev. Food. Sci. Nutr.* **44**, 185–193 (2004).
5. A. Brody, *Active Packaging: Beyond Barriers*, Packaging Strategies, West Chester, Pa and BRG Townsend, Mt. Olive, N.J., 2002.
6. F. Charles, J. Sanchez, and N. Gontard, *J. Food Eng.* **72**, 1–7 (2006).
7. J. P. Kerry, M. N. O'Grady, and S. A. Hogan, *Meat Sci.* **74**, 113–130 (2006).
8. U. S. Pat. 5,211,875 (May 18, 1993), D. V. Speer, W. P. Roberts, and C. R. Morgan (to W. R. Grace & Co.).
9. G. Twari, L. E. Jeremiah, D. S. Jayas, R. A. Holley *Int. J. Food Sci. Technol.* **37**, 199–207 (2002).
10. J. Miltz and M. Perry, *Packag. Technol. Sci.* **18**, 21–27 (2005).
11. F. Charles, J. Sanchez, and N. Gontard, *J. Food. Sci.* **70**, E443–E449 (2005).
12. C. O. Gill and J. C. McGinnis, *Meat Sci.* **41**, 19–27 (1995).
13. G. Twari, D. S. Jayas, E. Jeremiah, and R. A. Holley, *J. Food. Sci.* **66**, 506–510 (2001).
14. G. Twari, D. S. Jayas, L. E. Jeremiah, and R. A. Holley, *Int. J. Food. Sci. Technol.* **37**, 209–217 (2002).



15. E. Isdell, P. Allen, A. Doherty, and F. Butler, *Int. J. Food. Sci. Technol.* **34**, 71–80 (1999).
16. E. Isdell, P. Allen, A. Doherty, and F. Butler, *Int. J. Food. Sci. Technol.* **38**, 623–632 (2003).
17. S. R. Payne, C. J. Durham, S. M. Scott, and C. E. Devine, *Meat Sci.* **49**, 277–287 (1998).
18. L. Martinez, D. Djenane, I. Cilla, J. A. Beltran, and P. Roncales, *Food. Chem.* **94**, 219–225 (2006).
19. C. O. Mohan, C. N. Ravishankar, and T. K. Srinivasagopal, *J. Sci Food. Agric.* **88**, 442–448 (2008).
20. B. Butler, in *Proceedings of Worldpak 2002*, East Lansing, Mich., 2002.
21. I. S. Kotsianis, V. Giannou, and C. Tzia, *Trends Food Sci. Technol.*, **13**, 319–324 (2002).
22. M. E. Guynot, V. Sanchis, A. J. Ramos, and S. Marín, *J. Food Sci.* **68**, 2547–2552 (2003).
23. S. Berenzon and I. S. Saguy *Lebensm.-Wiss. Technol.* **31**, 1–5 (1998).
24. K. Zerdin, M. Rooney, and J. Vermue, *Food. Chem.* **82**, 387–395 (2003).
25. E. Oyugi and E. Mbuy, *Int. J. Dairy Technol.* **60**, 89–95 (2007).
26. M. Perkins, K. Zerdin, M. L. Rooney, B. R. D’Arcy, and H. C. Deeth, *Packag. Technol. Sci.* **20**, 137–146 (2007).
27. S. Pastorelli, S. Valzacchi, A. Rodriguez, and C. Simoneau, *Food Addit. Contam.* **23**, 1236–1241 (2006).
28. J. Lopez-Cervantes, D. I. Sanchez-Machado, S. Pastorelli, R. Rijk, and P. Paserio-Losada, *Food. Addit. Contam.* **20**, 291–299 (2003).
29. C. Altieri, M. Sinigaglia, M. R. Corbo, G. G. Buonocore, P. Falcone, and M. A. Del Nobile, *Lebensm.-Wiss. Technol.* **37**, 9–15 (2004).
30. V. K. Holm, G. Mortensen, M. Vishart, M. A. Petersen, *Int. Dairy J.* **16**, 931–939 (2006).
31. A. Lopez-Rubio, J. M. Lagaron, T. Yamamoto, and R. Gavara. *J. Appl. Polym. Sci.*, **105**, 2676–2682 (2007).
32. U. S. Pat. 7,078,100 B2 (July 18, 2006), C. L. Ebner, A. E. Matthews, and T. O Millwood, (to Cryovac Division of Sealed Air).
33. U. S. Pat. 7,238,300 (July 3, 2007), J. A. Solis, R. Dayrit, S. W. Beckwith, B. L. Butler, R. L. Cotterman, D. V. Speer, and T. D. Kennedy.
34. European Pat. Appl. EP 1 676 790 A1 (2006) W. Yang, Y. Yang, and L. Xiuzhi.

## GENERAL REFERENCES

M. L. Rooney, in M. L. Rooney, ed., *Active Food Packaging*, Blackie Academic Professional, London, UK, 1995, pp. 145–165; F. N. Teumac, pp. 193–202.

G. Robertson, in G. Robertson, ed., *Food Packaging, Principles and Practices*, 2nd ed., CRC Press, Boca Raton, Fla., 2006, pp. 292–293.

V. Daniel, and F. L. Lambert. Available at <http://palimpsest.stanford.edu/waac/wn/wn15/wn15-2/wn15-206.html>. Accessed November 7, 2008.

KAY COOKSEY  
Clemson University  
Clemson, South Carolina

## PACKAGING MATERIAL, MOLECULAR WEIGHT

### Introduction

An important characteristic of packaging polymers is their molecular sizes relative to the much smaller organic or inorganic molecules. The molecular weight of a packaging polymer, a measure of its molecular chain length, can significantly affect the physical properties of the polymer. As molecular weight increases, tensile and impact strengths increase sharply before leveling off, while melt viscosity increases slowly and then sharply (Fig. 1).

When selecting molecular weight for a specific application, the strength and melt viscosity should be compromised. The molecular weight should be high enough to acquire adequate strength, but low enough to avoid high melt viscosity, which makes the polymer difficult to process, such as flowing into a mold or through an extruder die. Typically, the practical molecular weight range for packaging polymers is between 50,000 and 200,000 as mentioned above.

Unlike small molecules such as oxygen or water, a polymer does not have a single molecular weight. This is because polymer molecules of different sizes are formed during the polymerization reaction. The relative fraction of different sizes may be characterized using a plot of frequency versus molecular weight, known as molecular weight distribution (MWD), as shown in Figure 2.

Two average molecular weights are often obtained from the MWD. The number-average molecular weight  $\bar{M}_n$  is defined as

$$\bar{M}_n = \frac{\sum_i N_i M_i}{\sum_i N_i} \quad (1)$$

where  $N_i$  and  $M_i$  are the number and molecular weight of polymer molecule  $i$ , respectively. The weight-average molecular weight  $\bar{M}_w$  is defined as

$$\bar{M}_w = \frac{\sum_i w_i M_i}{\sum_i w_i} = \frac{\sum_i N_i M_i^2}{\sum_i N_i M_i} \quad (2)$$

where  $w_i$  is weight of polymer molecule  $i$ .

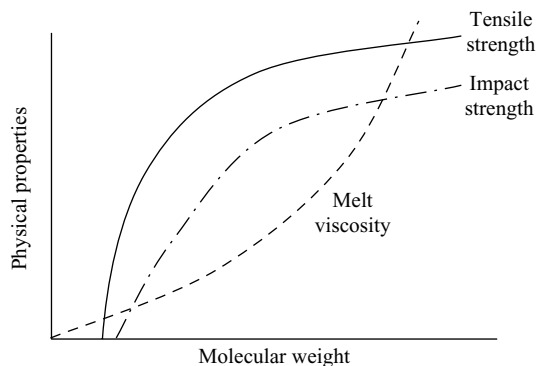


**Fig. 1.** Effects of molecular weight on polymer properties.

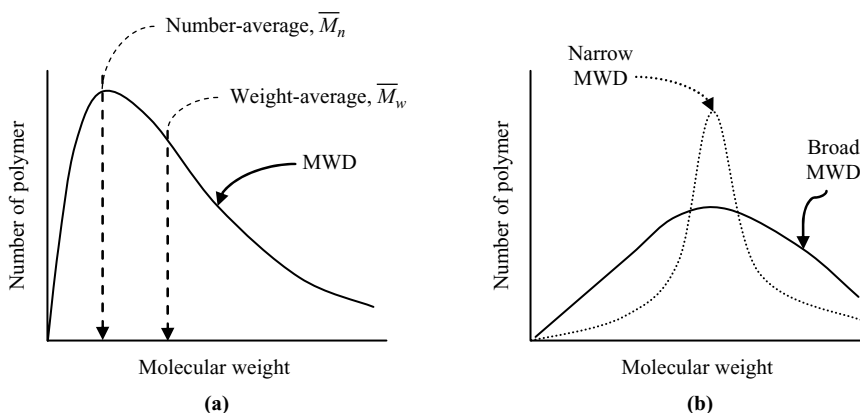


**Fig. 2.** Molecular weight distribution.

The polydispersity index (PDI) is defined as

$$\text{PDI} = \bar{M}_w / \bar{M}_n \quad (3)$$

which is a measure of the spread of the molecular weight distribution. The value of PDI is always  $\geq 1$ . A value of  $\text{PDI} = 1$  means that all the polymer molecules have the same molecular weight and thus  $\bar{M}_n = \bar{M}_w$ . However,  $\text{PDI} = 1$  is difficult if not impossible to achieve; most commercial packaging polymers have  $\text{PDI} > 2$ . A higher PDI is associated with a broader MWD (Fig. 2b), meaning more variation in molecular weights among the polymer molecules.

A broader MWD tends to decrease the tensile and impact strengths of a polymer but to increase its ease of processability, due to the smaller molecules in the distribution acting as a plasticizer or processing aid.

## Chain Entanglement

A unique characteristic associated with large molecular weight of packaging polymers is chain entanglement, the ability of polymer chains to become entangled with one another. The degree of chain entanglement increases with length of the polymer chain or molecular weight of the polymer. Polymers consisting of short chains are weak and brittle, but become strong and ductile above some critical length. A minimum of 1000 to 2000 repeating units, for example, is necessary for polyethylene to acquire the strength adequate for packaging foods.

Chain entanglement is important for packaging polymers. For example, during thermoforming or blow molding of a thermoplastic, the polymer is in molten state with its molecular chains resembling cooked spaghetti tangled up on a plate. Chain entanglement holds the polymer chains together but also allows them to slide pass one other, thereby providing both the necessary strength and the pliability for the polymer to be molded into a film, bottle, or other shapes. After cooling, sliding between polymer chains is more difficult and chain entanglement makes the polymer strong and resilient.

## Summation of Intermolecular Forces

The physical properties of a material are greatly influenced by the forces (such as dipole–dipole forces, hydrogen bonding, and dispersion forces) between its molecules. Although intermolecular forces exist between all molecules, their influences are more pronounced for polymers. Summation of intermolecular forces refers to the total force between neighboring molecules—this total force is particularly significant for packaging polymer molecules due to their long molecular chains.

The effects of summation of intermolecular forces may be observed in the physical states of large and small molecules, for example, polyethylene of solid versus ethane of gas. Except for the difference in size, the chemical structures are the same and weak nonpolar intermolecular forces operate on both compounds. Although weak nonpolar forces are operating in both compounds, the summation of intermolecular forces is much greater for the long polyethylene chains of solid than for ethane gas. However, polyethylene molecules are held more strongly together due to greater summation of intermolecular forces.

Summation of intermolecular forces and chain entanglement can significantly influence the mechanical, thermal, rheological, and other properties of thermoplastics.

KIT L. YAM  
Rutgers University  
New Brunswick, New Jersey

## PACKAGING, FLEXIBLE

### Introduction

Flexible packaging is used to deliver a product from the manufacturer or distributor to the retailer or ultimate consumer and protect that product during shipping, display, and storage. The total North American market for flexible packaging was estimated to be worth approximately \$17 billion in the year 2000 (1). Flexible packaging provides a lightweight, cost-effective means for the transportation, storage, and display of many products. Flexible packaging offers many advantages over competitive rigid packaging including reduced weight and volume of packaging material used, and subsequently discarded, as well as increased consumer convenience. Whatever the application or use, polymer materials are selected, and the entire packaging structure is designed, to meet the performance requirements specific to that particular application.

Performance requirements may include the requirements of all users in the value chain. For consumers this may mean the packaging protects the product, identifies the product, and is easy to open. For retailers the packaging may provide eye-catching graphics that help sell the product and is of the proper physical form for display purposes. For the packager, flexible packaging may need to provide high packaging speeds and low scrap rates, as well as meeting the functional requirements for protecting the product inside the package. Specific performance requirements will vary greatly from one type of package to another. But in every case meeting the performance requirements will help assure proper protection of the goods being packaged.

### Forms of Flexible Packaging

Flexible packaging films may be in the forms of wraps, bags, and pouches of many shapes and sizes. Packages may be as small as a single-serving sugar pouch or as large as a palletized load of mulch bags. Packaging may be supplied to the packaging end-user in the form of premade bags or pouches, or rolls of film. The film may be applied directly to the packaged goods, as in the case of stretch film, or may be formed into a package in-line with the filling machinery, as in the case of a bag formed on a vertical form/fill/seal machine used to package candy. Some packages are formed in a step that occurs well before the product is packaged. Then the product is placed inside the package and the package is secured.

**Key Performance Requirements.** Some of the key performance requirements for high performance flexible packaging include the following. Barrier properties: to keep oxygen, water, light, or grease from entering the package or from leaving the package. Barrier properties may be characterized by measuring the permeation of oxygen and water vapor through the packaging material. Selective permeability: to allow oxygen and carbon dioxide to permeate through the package at a calculated rate, in order to extend the life of fresh-cut produce, for example. Oxygen, carbon dioxide, and water vapor permeability are frequently measured and specified (see BARRIER POLYMERS). Abuse resistance: to prevent damage to the packaging material and its contents during shipping and

storage. Abuse resistance may include puncture resistance, tear strength, impact strength, and modulus. Some packages require good toughness at refrigerated or freezer temperatures. Sealability: to allow packages to be made at high packaging speeds and keep the product secure by preventing the package seams from failing. Sealability may be characterized by heat seal and hot tack strength, heat seal and hot tack initiation temperatures, seal-through-contamination performance, caulkability, and seal integrity. *Hot tack* refers to the strength of the seal while still in the molten state. It is critically important for packages where the product drops into the package while the seal is still partly molten. *Caulkability* refers to the ability of the sealant material to flow, filling in gaps around folds, wrinkles, or product contaminants. Machineability: to allow the packaging films to be easily run on high speed automatic packaging equipment. Machineability is governed largely by film modulus, film thickness, seal properties, and coefficient of friction. Consumer appeal: package appearance is an important factor driving product preference by consumers. Appeal is largely related to print quality and package gloss. Film thickness and modulus may also impact consumer appeal.

**Polymer Materials Frequently Used in Flexible Packaging.** Polymer materials commonly used in flexible packaging include linear low density polyethylene (LLDPE) (ETHYLENE POLYMERS, LLDPE, PROPYLENE POLYMERS (PP)), low density polyethylene (LDPE) (ETHYLENE POLYMERS, LDPE), high density polyethylene (HDPE) (ETHYLENE POLYMERS, HDPE), high molecular weight high density polyethylene (HMW-HDPE), and polypropylene (PP). Higher value, more specialty polymers used include polyolefin plastomers (POP), ultralow density polyethylene (ULDPE) (Ethylene Polymers, VLDPE), metallocene-catalyzed linear low density polyethylene (mLLDPE), enhanced polyethylene (EPE), ethylene vinyl acetate (EVA) copolymers, acid copolymers, (IONOMERS), nylon or polyamide (PA), poly(ethylene terephthalate) (PET), ethylene vinyl alcohol (EVOH), and poly(vinylidene chloride) (PVDC). See POLYAMIDES, PLASTICS; POLYESTERS, THERMOPLASTIC; VINYL ACETATE POLYMERS; VINYL ALCOHOL POLYMERS; VINYLIDENE CHLORIDE POLYMERS (PVDC). See also FILMS AND SHEETING.

These polymers are selected for the specific performance that they provide, and are combined in the final package design to meet all the requirements for the specific application in which they are being used. Often there are many different combinations of materials or film constructions that will meet the minimum performance requirements of an application. In these cases selection of the final packaging structure may be based on considerations such as availability from multiple suppliers and ability to provide differentiation over competitive packaging. For example a combination of a box and an inner liner may be used or a stand-up pouch may be used, each combination providing the minimum requirements for product protection and safety. One manufacturer may select to use a box and inner liner and other manufacturers may elect to package their product in a stand-up pouch for the same product. Or one manufacturer may choose to use a stand-up pouch and another manufacturer may choose to use a pillow pouch for the same product.

Polymers may also be combined with other materials, such as foil or paper, to create a flexible package with performance attributes not achievable by the polymers alone. This is done through the lamination or extrusion coating process, described below.

## Manufacturing Techniques

Polymer films may be manufactured by blown film or cast film extrusion or by extrusion coating of a polymer onto another substrate such as paper or aluminum foil (see FILMS, MANUFACTURE; EXTRUSION). Blown films are made by melting and pumping polymer through an annular die. Cast films are made by melting and pumping polymer through a flat die. The extrusion coating process is similar to the cast film process except that the molten polymer is coated directly onto another material. The selection of manufacturing process is governed by factors such as the size of the job to be run, the type of packaging material to be made, performance requirements for the end-user packaging, and availability of equipment. Cast film extrusion equipment typically operates at much higher output rates than blown film equipment, so it may be advantaged for production of large volumes of film of a single type, such as in the manufacture of stretch film. Blown film extrusion typically runs at a lower rate and may result in film with improved physical properties. Blown film also allows for adjustment of the bubble size and resulting width of the film produced, a key advantage when films of many different widths must be produced on the same machine.

The coextrusion process is used to combine multiple materials into a single film (see COEXTRUSION). Both blown films and cast films may be coextruded in three, five, seven, or more layers. The combination of multiple materials in a single film allows a cost-effective means of combining the performance properties of several polymers in a single film. One example would be the coextrusion of a barrier polymer such as EVOH or PVDC with a sealant resin such as LLDPE, EVA, or a POP. Coextrusion is widely used in producing high performance packaging films such as those used to package foods. It is also widely used to produce industrial films such as stretch film, and is increasingly used in producing other types of industrial films.

Polymer films may be stretched, or oriented, to impart improved properties useful for a variety of packaging applications. Oriented film is produced by a double bubble or tenter frame process. A thick film or sheet is manufactured at a thick gauge, typically 0.254–0.508 mm (10–20 mil) and is subsequently oriented (stretched) in a semisolid state to many times its original dimensions (see FILMS, ORIENTATION). The multiple-step production is normally done in a continuous operation. The stretching of the sheet to make the final film may occur simultaneously in the machine and transverse directions, or the stretching may occur sequentially. After orienting, the films are typically 12.7–25.4  $\mu\text{m}$  (0.5–1.0 mil) thick. The film is typically supplied in roll form. Biaxially oriented polypropylene (BOPP) is most often manufactured using a tenter frame process. Oriented polyethylene films are usually manufactured using a double bubble process. PVC films may also be oriented. Some oriented films are crosslinked to further enhance their performance. Compared to other films, oriented films typically provide improved optical properties, higher stiffness, and increased film shrinkage during packaging, which leads to improved package appearance.

Lamination is used to combine two or more films into a single packaging structure. It allows for the combination of materials that cannot be coextruded. An example would be a lamination of aluminum foil and a polyethylene sealant

film. More complicated laminations may include multiple types of polymer film, paper, and foil. Laminations can be categorized into main types: adhesive laminations and extrusion laminations. In adhesive laminations, the substrates are combined using an adhesive material. In extrusion laminations the substrates are adhered together using a molten polymer, often LDPE, as the adhesive layer. Lamination offers an additional benefit of allowing for the protection of the printing ink between layers of polymer, thus providing superior graphics to packages which are surface printed. Many packages with superior graphics, such as glossy stand-up pouches, have a reverse printed outer layer laminated to structural and sealant materials. Laminations are also used to provide a barrier to oxygen, moisture, or light. The barrier functionality may be provided by foil or a barrier polymer such as EVOH or PVDC. Most high value processed meat and cheese packages are laminations. This allows for both the combinations of various materials into the packaging structure and for the superior graphic properties possible by reverse printing the surface layer of the package and protecting the printing inks within the package itself. Since laminations are more costly than coextruded or monolayer films, laminations are generally reserved for use in higher value applications.

Metallization is used to apply a thin coating of metal, typically a form of aluminum, to a polymer film. This provides improved oxygen and water barrier properties as well as barrier to light. The best known use of metallized film is probably potato chip bags. Metallized films may also be used for nuts and salty snacks. Metallized films may be coated to provide sealability or may be laminated to another polymer film to provide improved properties such as seal integrity. Other types of coatings, whether to provide barrier properties or other functionality, may also be applied to polymer films used in flexible packaging.

**Methods of Producing Packages.** Packages may be formed in-line by a variety of techniques or may be supplied to the packer as preformed pouches or bags. Packaging may be created by wrapping or shrinking a basic film around a bundle of goods. Examples of in-line packaging forming include vertical form/fill/seal (VFFS), horizontal form/fill/seal (HFFS), and thermoform/fill/seal. In VFFS operations, film from a roll is passed through a series of rollers and is shaped by a forming collar into a tube. The film moves in a vertical direction (down) over a filling tube. A vertical seal is made, forming the film into a continuous tube. As the film continues through the machine, a horizontal seal is made, perpendicular to the machine direction of the film, forming the bottom-end seal of the bag. The product is dropped into the partially formed bag and the top-end seal is made. The process may operate in a step-wise or continuous manner. One example of a product normally packaged on VFFS equipment is fresh-cut produce. In HFFS operations, the film moves in a horizontal direction during the packaging step, eliminating the need for high hot tack strength. One application that typically uses HFFS equipment is chunk cheese. In thermoform/fill/seal operations, a bottom web is formed, product is added, and the top web, which is normally flat, is sealed to the bottom web. Thermoform/fill/seal packaging is frequently used for bacon and processed meats. Stand-up pouches and other types of packaging may be formed in-line with the filling equipment, or may be fully or partially prefabricated prior to the filling step.



## Uses and Types of Flexible Packaging

Flexible packaging is used for the packaging of all types of items including food products, medical devices, industrial goods, and consumer goods. The packaging types can be described in terms of the products being packaged, such as bakery goods, or by the type of packaging being used, such as shrink film. Major uses for flexible packaging are described below.

**Food Packaging.** One key use of high performance flexible packaging films is the packaging of food for distribution and retail sale. Food products are increasingly being packaged at the manufacturer end for sale to the ultimate consumer in the original package. This is a change from the traditional distribution system where the product was wrapped for the consumer at the butcher shop.

**Fresh Red Meat.** Fresh red meat is often transported in large pieces from the slaughtering house to local butcher shops in large barrier bags. These bags are designed to provide a barrier to oxygen. As well as oxygen barrier, package toughness and seal integrity are key requirements for these bags. These bags may contain PVDC or EVOH as a barrier material, along with layer of various PE resins for toughness and sealability.

**Processed Meat.** Processed and cook-in meat such as luncheon meat, ham, bologna, and salami are packaged in barrier films that are designed to keep oxygen from entering the package. This extends the shelf-life of the meat product and allows the retailer to display the product for sale for an extended period of time. It also allows the consumer to keep the product in their refrigerator, unopened, for some period of time after purchase. These packages are often printed with eye-catching graphics to increase the likelihood of retail sale. These films may contain a barrier polymer, printing surface such as PET or nylon, toughness layers of LLDPE or ULDPE, and a sealant layer that could be LLDPE, a POP, or an ionomer. In addition to low permeability to oxygen, abuse resistance and seal integrity are critical to maintaining the proper atmosphere inside the package. Optical properties such as high gloss and high clarity are important to create consumer appeal. Barrier requirements for processed meats range from 0.2 to 1.0 cm<sup>3</sup>/(100 in.<sup>2</sup>·day·atm) for oxygen transmission rate (OTR) and 0.2–0.5 g/(100 in.<sup>2</sup>·day) for water vapor transmission rate (WVTR).

**Case-Ready Meat.** An emerging use for plastic packaging is in the packaging of case-ready meats. In this application, a smaller package of fresh meat is packaged immediately after the slaughtering operation and distributed through retail stores directly to consumers. This saves the step of having the local butcher cut and prepare the individual cuts of meat for retail sale. It allows for reduced labor at the retail level and better usage of various cuts of meat. It also provides an improved level of food safety because handling of the raw food is reduced. Pork products such as pork loins and ribs are commonly sold in case-ready flexible packaging. Beef and other meat products are increasingly being sold in case-ready packaging. Different types of case-ready systems operate using different systems for product protection and extension of shelf-life. Some products are packaged in barrier packages, totally excluding oxygen from the package. Some case-ready systems package the food in a high oxygen environment, and these systems also use barrier films. Other systems package the meat in a bag

or tray/lid combination that allows oxygen to permeate the package at the proper time to allow reddening of the meat that is expected by consumers.

**Retortable Pouches.** A growing use of flexible packaging is in the replacement of metal cans with retortable pouches. These pouches are typically laminations containing biaxially oriented nylon for toughness, foil for oxygen barrier, and a PP sealant film. These pouches may contain items like tuna, pet food, and soup. The food items are held at elevated temperature after packaging, so the packages must remain intact at elevated temperatures. A minimum requirement might be the ability to withstand a temperature of 130°F for 20 min. In addition to temperature resistance, toughness, seal strength, and barrier properties are critically important.

**Bakery Products.** Bakery products such as bread, bagels, and tortillas are usually sold in plastic bags. These bags are typically surface printed LDPE or LLDPE and their main functional requirement is to protect the product from drying out or being damaged during distribution. Good machineability is required for high packaging speeds. These films are typically surface printed monolayer structures. A haze of 5% or less is typically required of these high clarity films. Films generally require COF of below 0.2 for fast packaging speeds.

**Candy and Confectionery Packaging.** Candy and other sweets are packaged in flexible packaging. At the smallest level, individual bite-size portions of a candy product may be packaged in a small pouch or a twist-wrap type package. Candy bars are typically wrapped with oriented PP film that has been surface printed. These items may then be packaged in a secondary bag, which may be a laminated structure containing polyethylene and sometimes reverse printed BOPP films. The outer bags must have sufficient toughness to protect the food inside. The films are generally very glossy for maximum consumer appeal. To provide fast packaging speeds the films need to have high hot tack strength combined with low hot tack and heat seal initiation temperatures.

**Cheese.** Most cheese sold in the United States is prepackaged in some type of flexible packaging. Types of cheese packaging include individually wrapped slices of processed cheese, chunk cheese, and shredded cheese. Both chunk cheese and shredded cheese require substantial barrier to oxygen to prevent mold growth and spoilage. Either EVOH or PVDC may provide the oxygen barrier. While EVOH is generally coextruded into the film structure, PVDC may be coated onto the surface of a film via a coating process. They also require excellent seal integrity and abuse resistance to prevent the controlled atmosphere inside the package from being lost. Cheese packages are often laminations made with reverse printed outer webs containing PET or nylon for superior graphical presentation. They may also be extrusion coated structures where the sealant layer has been extrusion coated onto the outer layer. Sealant layers may consist of EVA, an ionomer, or a POP. Low heat seal initiation temperature (90°C or below) and good seal through contamination performance are required of the sealant material used. Processed cheese typically require films with OTR of 0.6–1.0 cm<sup>3</sup>/(100 in.<sup>2</sup>·day·atm) and WVTR of 1.0 g/(100 in.<sup>2</sup>·day).

**Fresh-Cut Produce.** Key performance requirements for fresh-cut produce packaging include proper oxygen and carbon dioxide permeability, seal integrity, machineability, and consumer appeal. Consumer appeal includes both feel and appearance. Feel is generally determined by film thickness and modulus while

appearance is governed by print quality and film optical properties such as clarity, haze, and gloss. In order to extend the shelf-life of the produce being packaged, films must provide a level of oxygen permeability that is properly matched to the respiration rate of the produce inside the package. Cut produce respires after harvesting consuming oxygen and giving off carbon dioxide. By controlling the permeation of gases through the package the environment inside the package is controlled, respiration is slowed, and shelf-life is extended. The bags must have complete seal integrity in order to prevent the unplanned transfer of gases between the bags and the environment. Bags may contain PP, LLDPE, ULDPPE, EVA, or POP. Oxygen transmission rate requirements vary widely depending on the type of produce being packaged, but common items range from about 100  $\text{cm}^3/(\text{100 in.}^2\cdot\text{day}\cdot\text{atm})$  for caesar salad mixes, 150–200  $\text{cm}^3/(\text{100 in.}^2\cdot\text{day}\cdot\text{atm})$  for iceberg salad mixes, and 200–350  $\text{cm}^3/(\text{100 in.}^2\cdot\text{day}\cdot\text{atm})$  for specialty salad mixes such as baby greens and exotic lettuces.

**Frozen Foods (Fruits, Vegetables, IQF Poultry).** Frozen foods are packaged in a variety of packaging types. Examples of frozen foods packaged in flexible packaging include frozen fruits, vegetables, french fries, and individually quick frozen chicken breasts. Many frozen foods are packaged in surface printed polyethylene films. Some higher value added items are packaged in laminations, which may be shaped into stand-up pouches. Most frozen food bags are made on standard VFFS machinery. Low temperature toughness, modulus, high hot tack strength, and high seal strength are key requirements for frozen food packaging. Some packages are clear and require good clarity, while others are pigmented and require good gloss. LLDPE, ULDPPE, EVA, and POP resins are all commonly used in creating frozen food packaging. Stiffness must be adequate for high speed packaging, and packaging films must have tear and puncture strength high enough to prevent package damage during transportation and storage.

**Crackers, Cookies, and Cake Mixes.** Inner Liners are used for packaging products such as cereal, crackers, and cookies inside a box. The key performance requirement for packaging these products is most often moisture barrier. The packaging film selected must be capable of keeping the product dry and in excellent condition upon delivery to the consumer. The packaging must offer seal integrity and machineability as well. Certain products have additional requirements such as puncture resistance—to keep the product from poking through the packaging film—and flavor and aroma barrier for highly flavored cereals. Most inner liners contain HDPE for its moisture barrier properties and a sealant layer which may be EVA or POP. Heat seal initiation temperatures of 90°C and below are commonly required. MVTR of 0.2  $\text{g}/(\text{100 in.}^2\cdot\text{day}\cdot\text{atm})$  or below is often required.

**Salty Snacks.** Salty snacks are frequently high in fat content and may require a package that provides an oxygen barrier in order to prevent the fat in the food from going rancid. They may also require grease resistance to keep the package from leaving an oily spot. Salty snacks may be packaged in barrier films containing foil, a metallized polymer film, or a barrier polymer such as EVOH or PVDC.

**Potato Chips.** Potato chips are often packaged in metallized films. Metallization of a polymer film provides a combination of oxygen barrier, moisture barrier, and light barrier. The use of a clear polymer film would not provide

equivalent light barrier. Seal strength must be optimized to provide a secure package that can be easily opened by the consumer. Seal integrity and consumer appeal are also critical for this type of snack food packaging.

**Ice.** Ice bags are a specific type of carry-out bag used to transport manufactured ice. These bags are typically surface printed monolayer films. EVA copolymer is frequently used for these bags for its combination of sealability, low temperature toughness, and ease of manufacture into a film. Ice bags require good low temperature toughness, especially puncture strength, and adequate seal strength to prevent the bags from bursting. The bags must not, however, be so strong that the consumers cannot easily get to the ice inside the package.

**Medical Device Packaging.** Flexible films are used to package many types of medical devices. These packages must protect the device from contamination. Some medical devices are sterilized after packaging, and for these devices the packaging must be compatible with the sterilization procedure and must then maintain the sterile environment until the package is opened. Seal integrity and abuse resistance are key requirements for medical packaging (see MEDICAL APPLICATIONS).

### **Industrial Packaging.**

**Heavy Duty Shipping Sacks.** Heavy duty shipping sacks are used for the transportation of items such as resin, salt, pet food, fertilizer, chemicals, topsoil, bark mulch, and compressed bales of fiber glass insulation. They typically contain 40 pounds or more of product. Heavy duty shipping sacks may be supplied as preformed bags or as rollstock, which is formed into bags in a continuous VFFS operation. Special machinery is required to form heavy duty shipping sacks on VFFS machinery in a high-speed continuous operation. These bags need moderate COF because they must easily pass through the packaging equipment, but stacked bags must slide off each other. Bags filled with hot products, such as salt, must also be able to withstand the filling temperatures without excessive stretching or dimpling of the film. Film toughness and creep resistance are also of key importance in many heavy duty shipping sack applications.

**Shrink Film.** Shrink film is used to collate bundles of goods. Industrial shrink film is typically manufactured by the blown film process from a blend of LDPE and LLDPE. Specialty polymers may be used to impart specific properties required for specialty applications of industrial shrink film. The use of LDPE, with its long chain branching and high level of molecular entanglement results in a film with a significant amount of molecular orientation locked into the film after fabrication. When the film is subsequently heated the oriented molecules tend to relax and return to an unoriented state. This allows the film to be shrunk around the packaged goods by the application of heat. This is most typically done in a shrink tunnel or sometimes with a hot air gun. Common uses of shrink film include cases of bottled water and soft drinks. Industrial shrink films are typically several mils thick. Shrink films require good shrinkage properties and holding force as well as enough abuse resistance to protect the product being packaged.

**High Clarity Shrink Film (Oriented).** Oriented, high clarity shrink film is used for the protection and display of high value consumer goods. It is distinguished from regular shrink film by its superior clarity and appearance, as well as increased shrinkage properties and higher stiffness. Goods are packaged by wrapping the film loosely around the goods, sealing the film to make a completely enclosed bag, and then shrinking the film by passing the package

through a shrink tunnel or oven. Small holes may be poked in the film before wrapping to allow air to escape from the surface of the package while the film is shrinking. As in industrial shrink film, heat causes the molecules in the film to relax, causing the film return to its original unoriented size, and it shrinks tightly around the packaged goods. Since the polymer molecules in oriented shrink film are much more highly oriented, a greater level of shrinkage may be obtained. Boxed software and stationery products are often wrapped with high clarity shrink film. Ice cream cartons and other food products are also wrapped in high clarity shrink film. Optical properties, seal properties, shrinkage, and holding force are key requirements for oriented shrink film (see FILMS, ORIENTATION).

**Liners.** Liners, called trash bags by most consumers, are used for waste disposal in homes and businesses. Liners range in size from small bags used to line a bathroom wastebasket to large lawn and leaf bags sized to hold 40 gallons or more of waste. Liners may be supplied on a continuous roll, which has been perforated for easy separation of the individual bags, or as separate bags contained in a box or bag. Liners are made from blown film, and the bags may be aligned in either the machine or cross direction. Bags supplied on rolls are aligned with the machine direction of fabrication, and the width of the bag is equal to the layflat obtained during blown film extrusion. Some bags, such as drawstring bags, may be aligned in the cross direction, or transverse to the direction of fabrication. These bags have seals on their sides that run perpendicular to the direction of fabrication. Liners are made primarily from LLDPE. Key properties include tear strength, impact strength, and tensile strength and modulus.

**Storage Bags.** Storage bags are small polyethylene bags, normally containing a plastic zipper or other closure, used by consumers and businesses for storing small quantities of food or other products. They are typically made from LDPE or LLDPE or blends of these two materials. Bag thickness may range from less than 1 mil to more than 3 mils depending on total bag size and intended use. Most bags are unprinted, though some contain a special labeling area on the outside of the bag for use by the consumer in marking the bags with a brief description of the items placed inside the bags. Most bags are clear to allow consumers to see the product inside the bag. Since many bags have zipper closures, the bags must be made from materials that are compatible with the simultaneous extrusion or attachment of the zippers.

**Carry-Out Bags.** Carry-out bags are used by consumers to carry purchased merchandise to their homes or businesses. These bags are typically polyethylene structures. Many are surface printed monolayer films. Some are coextruded films for enhanced performance. Examples include the merchandise bags used by department stores and discount stores and grocery sacks used at supermarkets. Depending on the specific use the bags may be fabricated from high molecular weight HDPE, LDPE, or LLDPE. Tensile strength and toughness are key requirements, although some carry-out bags are highly oriented HMW-HDPE, and consequently have low MD tear strength.

**Stretch Film.** Stretch film, or stretch/cling film, is used in the unitization of goods for transportation. A thin film is stretched, either by machine or by hand, and wrapped around multiple smaller packages to hold the goods together. The film clings to itself and to the pallet, securing the load. In its most common form, stretch/cling film is applied to a pallet of goods using a power prestretch pallet wrapper in an automated operation. In this operation the film is stretched,

typically between 100 and 300% of its original length, by a set of rollers turning at different speeds and is then applied to a pallet of goods, which sit atop a moving turntable. Machine wrap film is typically supplied on rolls that are 20 or 30 in. wide. Hand wrap film is supplied on smaller rolls. Stretch/cling films may be manufactured by either a cast film or blown film process. Most stretch/cling films are coextruded structures, and LLDPE is the primary component of most stretch films. For specialized applications, coextrusions containing minor layers of PP, EVA, POP, or ULDPE may be employed. For most stretch film structures, a resin with good inherent cling is used as one or both surface layers, or a tackifier such as polyisobutylene is added to the structure to provide the proper level of cling force. Stretch film is used to hold entire or partial pallets of goods, such as resin bags, fertilizer bags, cartons of consumer goods or food products, together during shipment. Most stretch film is removed by the retailer prior to the display of the packaged items for sale. Consumers can frequently view pallets of lawn and garden products, such as bark mulch and topsoil, still wrapped with stretch film on display at home improvement warehouses. Stretch films must have good stretchability, load retention, and puncture resistance.

**Stretch Hooder.** Stretch hooder film is used to form a large bag capable of containing an entire pallet of goods. Film is supplied on rolls and formed into a gusseted bag during the packaging operation. The bag is then stretched to increase its circumference and, while under tension, placed over a pallet of goods. The tension on the film is released as the film covers the goods, and the film contracts and secures the load. The main advantage of stretch hooder packaging over regular stretch wrap is that the load is completely covered on the top and sides. The chief disadvantage is that considerably more polymer is required to make a stretch hooder bag than to make enough stretch/cling film to contain the same load. Stretch hooder film is made on blown film extrusion equipment. Stretch hooder films must have good elastic memory and good abuse resistance.

## **BIBLIOGRAPHY**

"Packaging Materials" in *EPST* 1st ed., Vol. 9, pp. 709–714, by S. Sacharow, Reynolds Metals Co.; "Packaging Materials, Flexible Materials" in *EPSE* 2nd ed., Vol. 10, pp. 684–695, by A. L. Brody, Schotland Business Research, Inc.; "Packaging, Flexible" in *EPST* 3rd ed., Vol. 3, pp. 353–363, by J. J. Wooster, The Dow Chemical Company.

## **CITED REFERENCES**

1. L. L. Hoover, *Flexible Packag.* 22–27 (Oct. 2000).
2. W. A. Jenkins and J. P. Harrington, *Packaging Foods with Plastics*, Technomic Publishing Co., Lancaster, Pa., 1991.
3. L. K. Mergenhagen and N. F. Whiteman, in *Polymers, Laminations, and Coatings Conference*, 1993.
4. T. I. Butler, S. Lai, and R. Patel, In *SPI International Plastics Exposition and Conference*, Chicago, 1994.
5. J. J. Wooster, in *Film Pack Conference*, Philadelphia, 1999.
6. T. D. Stirling, in *Future-Pak Conference*, Chicago, 1997.
7. M. F. Simpson and J. L. Presa, in *Future-Pak Conference*, Chicago, 1996.

8. J. S. Brandenburg and M. Davis, in *Specialty Polyolefins Conference (SPO)*, Houston, 1996, pp. 213–229.
9. J. V. Krohn and D. W. Jordy, *Tappi J.* **80**(3), 151–155 (1996).
10. G. Ealer, in *Polymers, Laminations, and Coatings Conference*, 1990, pp. 327–333.
11. N. F. Whiteman, J. A. deGroot, L. K. Mergenhagen, and K. B. Stewart, in *RETEC Conference*, Houston, 1995.
12. B. Lipsitt, *Plast. Eng.* 25–28 (Aug. 1997).
13. C. L. Dawson and J. Tunison, in *Specialty Polyolefins Conference (SPO)*, Houston, 1996, pp. 231–245.
14. K. T. Higgins, *Food Eng.* 46–54 (Nov. 2000).
15. T. Bezigian, *Converting Mag.* 54–57 (Sept. 1997).
16. P. T. DeLassus, *Tappi J.* **77**(1), 109–113 (Jan. 1994).

JEFFREY J. WOOSTER  
The Dow Chemical Company

## PELLETIZING

### Introduction

In the production of thermoplastics, the primary products frequently leave the manufacturing facility in the form of pellets. Incorporation of antioxidants, stabilizers, colors, fillers, reinforcing agents, and other additives requires that the polymer be in the melt stage to assure uniform distribution. After incorporation the melt is pelletized into uniform sizes and shapes to facilitate handling.

Polymerization products are frequently in powder form, with the raw material already compounded. Uniform pelletized form offers the following processing advantages: simpler feeding system with fewer feeders, dust-free handling, and easier cleaning between changes of feedstock; fewer unsatisfactory products because of uniformity of size and homogeneity of feed; and greater extrusion capacity and lower shipping costs as a result of higher feed-bulk density.

Offsetting these advantages may be a higher heat exposure of the product (an additional melting step), as well as the additional manufacturing costs associated with pelletizing. Molten reactor products must be pelletized.

The process involves pressure development for forced flow through a die. The extrudate is cooled to solidification and then cut into pellets, or the molten extrudate is cut as it emerges from the die and the pellets are subsequently cooled. In the latter case, both cutting and cooling may be done in air or water, or cutting may be done in air, followed by quenching in water.

Quenching solidifies the exterior shell of the pellets to prevent reagglomeration. With a water quench, enough residual heat content is left in the pellet interior to evaporate the surface moisture remaining after the excess water has been centrifuged off. The dried pellets are classified to remove both fines and agglomerates. Typical pellets are 2–4 mm maximum dimension. Diced pellets are cubic-, rectangular-, or octahedral-shaped. Strand pellets are approximately cylindrical. Die-face pellets may be cylindrical or oblate spheroids.

## Equipment

Pelletizing equipment can be classified as follows:

<i>Quenching, solidifying, and cutting</i>	<i>Cutting, quenching, and solidifying die-face pelletizers</i>
dicers strand pelletizers	dry-face pelletizers water-ring pelletizers underwater pelletizers centrifugal pelletizers rotary-knife pelletizers

Each type of pelletizer has its function in plastics compounding, depending on the throughput rate required, the kind of compounding equipment used upstream, the material being processed, and the pellet shape required.

Compared to dicers and strand pelletizers, the more expensive die-face pelletizers utilize less space, can be more readily automated, require less supervision, and can handle higher rates. Cutting thermoplastics as a melt rather than as a solid generates fewer fines and less knife wear, but can cause more die wear if the knife must ride on the die face, as for example, with polymers like polypropylene.

**Dicers.** Dicers were first used in the rubber industry and subsequently applied to thermoplastics. Most poly(vinyl chloride) and acrylonitrile–butadiene–styrene copolymers are diced, as well as some other thermoplastics (1,2).

In typical operations after leaving the forming equipment (direct-strip extrusion or sheeting from a two-roll mill), the strip of polymer is quenched before entering the dicer. The strip is fed at a constant rate through nip rolls into the rotating knives operating against a stationary-bed knife. Dicers can be used with the sheet entering straight into the cutting edge or with the cutter rotor offset at a 45° angle to the entering strip. The former method uses either a notched or a ratchet-tooth knife, whereas the latter uses a stair-step knife to produce the individual pellets.

A variation of the notched-knife dicer is the slitter chopper, which first slits the polymer sheet into parallel strips that are then chopped by rotor knives acting against a bed knife. Pellet length is controlled by feed rate and cutter rotation speed.

For strip dicing, very low die pressure is required, which permits stock temperatures to remain low. In comparison to strand cutting, constant operator attention is usually not required. However, dicing systems require extensive space (30 m of water bath for a 3-mm thick strip) and noise levels are high. Frequently, the dicer is isolated in a soundproof chamber.

**Strand Pelletizers.** Strand pelletizers (Figure 1) are the simplest and least expensive pelletizers. An extruder or gear pump forces the molten polymer through a row of small, round orifices. The emerging strands are conveyed through a cooling water bath with grooved rollers to keep the strands separate from each other until they are solidified. After emerging from the water bath,



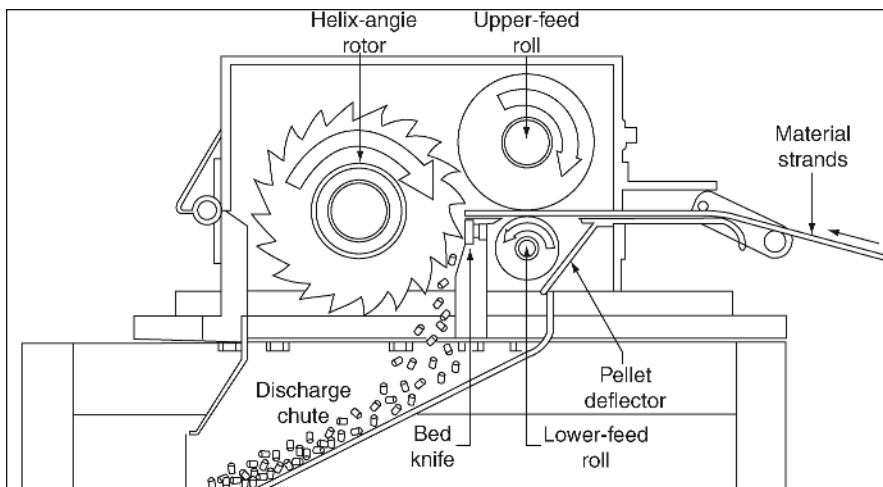


**Fig. 1.** Strand pelletizer. Courtesy of Conair, Inc.

the strands may be air-dried and fed through nip rolls of a multiknife-blade rotor operating against a fixed blade. The strands, 2–4 mm in dia, are chopped into cylinders of round or slightly oval cross sections, 1–5-mm long, as determined by intake roll speed and cutter frequency.

Although strand cutting is technically feasible at very high-capacities, a practical limit for many polymers is ca 2000–3000 kg/h (3). Beyond that rate, the die and bath become very wide and it becomes more difficult to maintain individual strand integrity. Frequent operator attention may be required to restring broken or entangled strands.

Like dicing, stranding requires extensive floor space for quenching the polymer before cutting. Recent housing modifications have considerably reduced the noise associated with strand cutters.

Practically all thermoplastics can be strand-cut, except those that are very brittle or have no melt strength to enable the strand to be pulled through the bath into the cutter. In some instances, this can be overcome by moving a ribbed, endless belt in the bath at the same lineal velocity as the strands. Two belts on either side guide the strands up and down over rollers in a deep bath, thereby conserving floor space.

**Die-face Pelletizers.** Many thermoplastics can be pelletized by moving knives rapidly across a multiple-hole die plate. The multiblade cutter slices the polymer and hurls the pellets away from the die. The pellets are quenched in air alone with a water mist, or by subsequent immersion into a water bath; rates are up to 6000 kg/h (4).

The eccentrically mounted cutter of a typical dry-face pelletizer may have up to six arms and may run at speeds up to 2500 rpm. Knife clearance from the die can be adjusted during operation by axial movement of the cutter spindle with respect to the die face. Band heaters bring the die up to temperature at start-up and offset heat losses during operation. Although not much heat can be transferred between the polymer and die because of the low thermal conductivity of

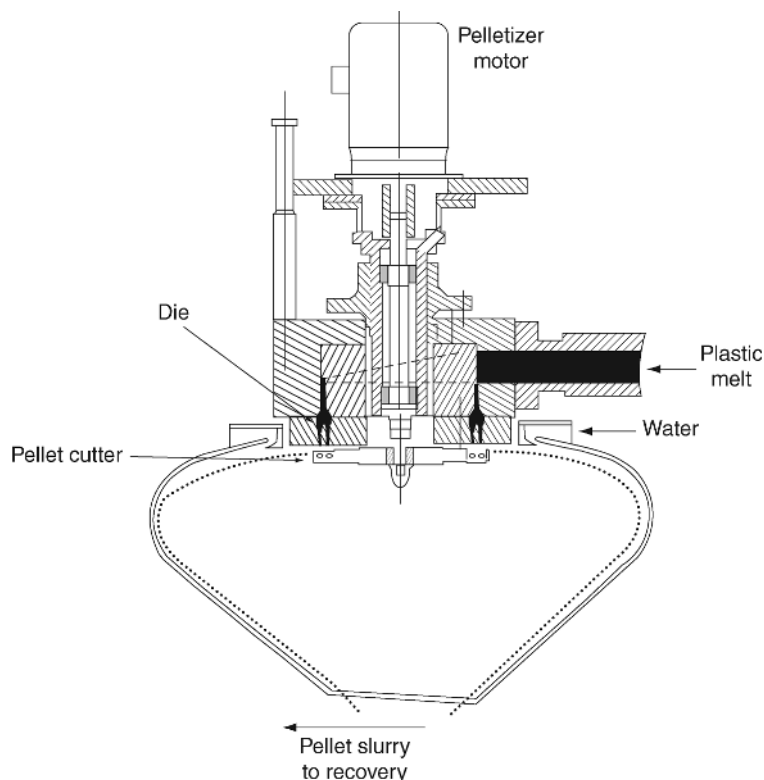


**Fig. 2.** Water-ring pelletizer. Courtesy of Berringer Co.

the polymer and the short time that the polymer is in the lead hole and capillary of the die, it is important to maintain a uniform temperature to provide uniform flow rate per hole. If there is a known temperature gradient in the polymer approaching the die, it is possible to compensate for the variation in viscosity by appropriate changes in the lengths of the capillaries and lead holes.

**Water-ring Pelletizers.** In the water-ring pelletizer, the molten strands emerging from the die are cut with a centrally mounted cutter (Figure 2). The freshly cut hot pellets are thrown into a spirally rotating water stream, ~20-mm deep, surrounding but not touching the die. The pellets are quenched as they rotate with the water. After the pellet slurry leaves the housing, the water is removed by screening and the pellets are dried. In some instances, a water spray near the cutting surface may be used to deposit a skin on the molten pellets to reduce pellet agglomeration.

The water-ring pelletizer is insensitive to process interruptions, has easier start-up, and requires less operator attention. Although usually mounted with the cutter axis vertical, some have a horizontal cutter axis for closer distance between extruder and die plate.

**Underwater Pelletizers.** An underwater pelletizer (Figure 3) operates with the die face immersed in water. The severed pellets are carried away as a slurry in water for further cooling in transit to the dewatering, screening, and drying

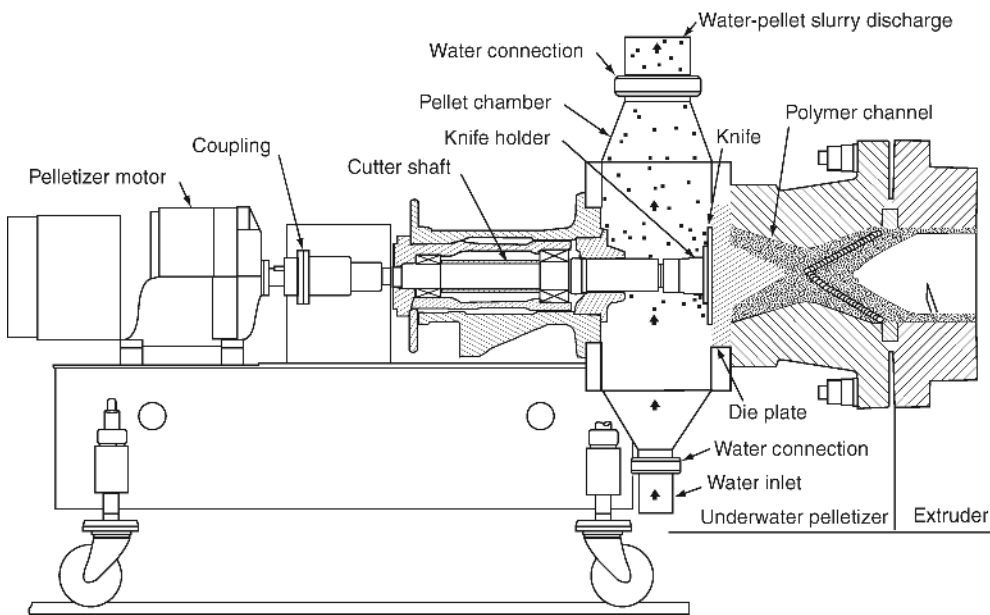


**Fig. 3.** Underwater pelletizer. Courtesy of Farrel Co.

equipment. The die plate may be mounted in such a way that the polymer is extruded horizontally or downward. Underwater pelletizers are available for all capacities up to 24000 kg/h (5).

The critical design areas are the die plate and knife adjustment. The cutter hub is mounted near the center of the die with all the blades continuously riding on, or near, the die. The die frequently is provided with heat channels surrounding each row of holes. High temperature steam or oil heats the polymer channels to supply the large amount of heat lost to the water sink at the die face. Sometimes hardened ceramic inserts around the die holes provide insulation and better wear resistance. If there is a momentary interruption in flow, die freeze-off can be a problem, which can be overcome by adequate die-plate heating. Freeze-off is when the temperature of the polymer falls below its solidification point, thereby plugging the die hole. Start-up requires precise sequencing of polymer and water flows.

**Centrifugal Pelletizers.** The centrifugal pelletizer (Figure 4) differs from all other pelletizers (6,7). The polymer melt is fed into a rotating die chamber at atmospheric pressure. Pressure to extrude the polymer through the die holes is generated by centrifugal force within the die, rather than by an extruder or a melt pump. The die holes are located in the periphery of the rotor. The emerging strands are cut by a single stationary knife, which does not run on the die as the strands are held outward by centrifugal force. The severed pellets fly off on their own momentum into an air- or water-quench system similar to that for a dry-face pelletizer. The die is heated for start-up and for offsetting heat loss to the surroundings by generation of eddy currents within the rotor as it spins between a pair of magnetic fields. In addition, the die is self-emptying upon cessation of flow.

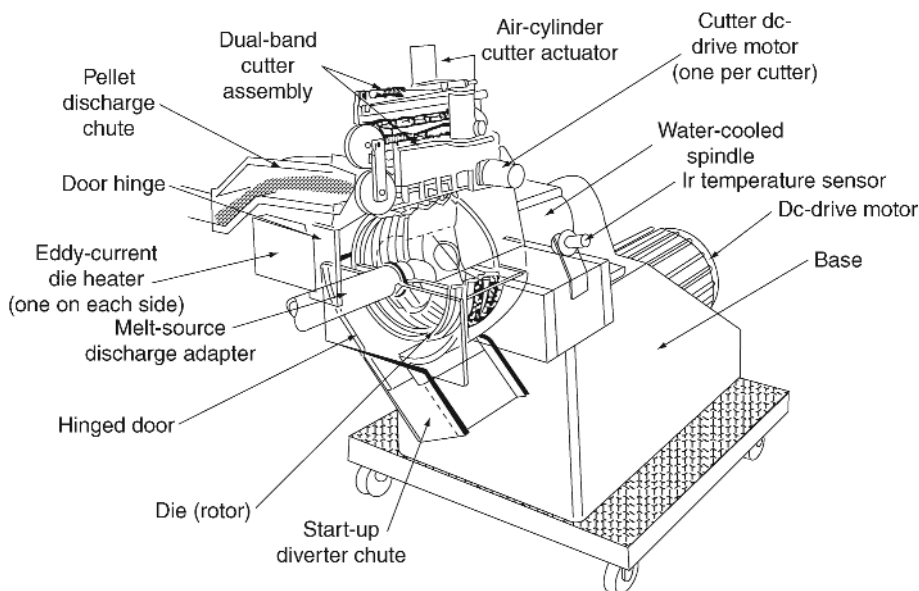


**Fig. 4.** Centrifugal pelletizer. Courtesy of Baker Perkins, Inc.

The centrifugal pelletizer can operate with less heat exposure since the temperature rise associated with pressure generation in an extruder or melt pump is avoided. Cutter life is extended by slow movement in the fixed position. Cutters can be changed without interruption of polymer flow. The main disadvantage of a centrifugal pelletizer is that pressure generation and cutting frequency are both dependent on rotor speed and therefore are not independent of each other.

**Rotary-knife Pelletizers.** The rotary-knife pelletizer (Figure 5) operates with a die similar to a strand die, but with the rotary cutter operating in close proximity to the emerging strands. The cutter is completely enclosed. A water stream may be introduced into the rotor housing to help quench the severed pellets, with the pellets leaving the housing either coaxially with the cutter rotor or at the bottom of the housing. In addition to the simple row die shown in Figure 5, a cylindrical die can be used with several rows of die holes for flow of polymer into the cylinder for severing by a helically grooved cutter.

**Die Design.** Shaping the viscous polymer melt before pelletizing requires external pressure, except for the centrifugal pelletizer or sheeting off a two-roll mill for a dicer. The viscoelastic property of many polymers causes the strand emerging from a capillary to swell in diameter, even if rapidly quenched. Thus for a given desired diameter pellet, the capillary diameter may have to be considerably smaller. Small capillaries lead to high pressure drop (up to 10 MPa or 1500 psig) through the die, and the small holes are more prone to freeze-off. Some polymers coming through a strand die possess enough melt strength so that they can be drawn down by the nip rolls to a diameter smaller than the die orifice.

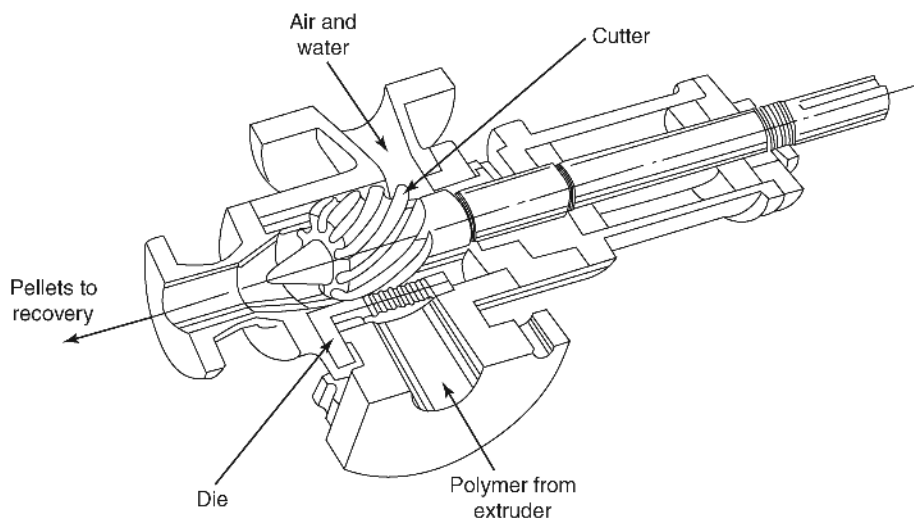


**Fig. 5.** Rotary-knife pelletizer. Courtesy of Welding Engineers, Inc.

The design of die plates is based on the rheological properties of the polymer, which are a function of temperature and shear rate, as well as entrance-loss correction and die-swell behavior. Dies for underwater pelletizers are subjected to high heat losses because of direct contact with water, and critical attention to heating is required to avoid freeze-off. Nonuniform die temperature is the main contributing factor to nonuniform pellet size.

Erosion within the capillaries may cause die wear, particularly with highly filled polymers. Wear is also caused by the knife passing over the die face. Irregular cutting between a rotating knife and the die face in melt cutting, or between a rotating and bed knife in stranding or dicing, can generate undesirable fines or tails on the pellets.

**Pelletizer Selection.** Table 1 provides general guidance for pelletizer selection. Most suppliers can demonstrate their equipment on a pilot scale of ~500 kg/h. Extremes in apparent viscosity create problems that may become acute in any pelletizer. For example, both fractional melt-index and high melt-index (>100), low density polyethylene (LDPE) are very difficult to pelletize, particularly in the same apparatus, even though an average LDPE can be pelletized in any of the described pelletizers.

The choice of pelletizer is also affected by considerations of total feed rate, turn-down-ratio requirements, frequency of feedstock change, operator attention, knife and die wear, and pellet shape (8).

## Energy Requirements

The amount of energy required for pelletizing depends on the starting condition of the polymer, viscosity, and type of pelletizer. For example, the energy required

Table 1. Selection Chart for Pelletizers<sup>a</sup>

Polymer	Pelletizer					
	Dicer	Strand	Dry-face	Water-ring	Underwater	Centrifugal
ABS copolymer	A	A	A	S	S	A
polyacetal	N	A	A	S	A	S
polyamide	A	A	N	N	S	N
polycarbonate	N	S	A	S	S	S
polyester	S	A	S	<b>S</b>	<b>S</b>	<b>S</b>
HDPE	S	S	A	A	A	A
LDPE	A	A	A	A	A	A
LLDPE	S	S	A	S	A	A
poly(methyl methacrylate)	N	S	S	N	A	S
polypropylene	N	<b>S</b>	A	N	A	A
polystyrene	N	A	A	N	A	A
poly(vinyl chloride)						
flexible	A	A	<b>A</b>	<b>S</b>	S	S
rigid	A	S	A	S	N	S
thermoplastic rubber	A	S	S	S	S	S

<sup>a</sup>A = acceptable; S = sometimes acceptable; and N = not acceptable.

to pelletize 4500 kg/h of a low melt-index polyethylene leaving a compounder at 200°C with an underwater pelletizer is:

<i>Energy requirement</i>	<i>kW</i>
extruder power to develop die-head pressure	146
heat loss from extruder	8
heat loss from die	35
underwater pelletizer drive	41
<i>Total</i>	<i>230</i>

Thus the specific energy required would be ca 0.05 kW·h/kg. The energy associated with quenching, drying, and classifying the pellets is additional. With a much lower viscosity, the power required for extrusion is also much lower. Strand cutters, water-ring, and dry-face pelletizers operate with less power, as the cutter rotors are turning in air rather than water. Developing pressure in a centrifugal pelletizer is independent of viscosity, and there is no heat buildup during pressure development. The specific power required for a centrifugal pelletizer in the above case would be <0.015 kW·h/kg.

## Safety

With all pelletizers, there are always inherent hazards due to hot molten polymers, rotating devices, and sharp knives. Standards for the construction, care, and use of dicers and strand pelletizers are contained in ANSI B151.11 (1982).

## BIBLIOGRAPHY

"Pelletizing" in *EPSE* 2nd ed., Vol. 10, pp. 802–810, by D. B. Todd, Baker Perkins, Inc.

## CITED PUBLICATIONS

1. H. Boulay, *Plast. Compound*. 46 (Nov.-Dec. 1980).
2. S. H. Collins, *Plast. Compound*. 64 (Nov.-Dec. 1981).
3. R. R. Lange, *Plast. Compound*. 39 (Mar.-Apr. 1979).
4. J. W. Hunt, *Plast. Compound*. 48 (July-Aug. 1978).
5. E. W. Sehuler, "Advances in High Volume Palletizing Techniques," *SPE ANTEC Technical Papers*, Vol. 21, Society of Plastic Engineers, Greenwich, Conn., 1975, pp. 477–480.
6. D. B. Todd, H. G. Karian, and J. D. Layfield, *Plast. Compound*. 33 (July-Aug. 1983).
7. D. B. Todd and H. G. Karian, *Mod. Plast.* 56 (Dec. 1983).
8. H. Herrmann, ed., *Granulieren von Thermoplastischen Kunststoffen*, VDI-Verlag GmbH, Dusseldorf, FRG, 1974.

D. B. TODD  
Baker Perkins, Inc.

## PERFLUORINATED POLYMERS, PERFLUORINATED ETHYLENE-PROPYLENE COPOLYMERS

### Introduction

Perfluorinated ethylene-propylene (FEP) resin is a copolymer of tetrafluoroethylene (TFE) and hexafluoropropylene (HFP) [116-15-4]; thus, its branched structure contains units of  $-\text{CF}_2-\text{CF}_2-$  and of  $-\text{CF}_2-\text{CF}(\text{CF}_3)-$ . Modified FEP fluorocarbon resins may also contain other fluoromonomers at a level of not more than 2% by weight. FEP retains most of the desirable characteristics of polytetrafluoroethylene (PTFE) but with a melt flow rate (MFR) high enough for conventional melt processing. The introduction of HFP lowers the melting point of PTFE from 325 to about 260°C.

The desire for a resin with PTFE properties yet capable of being fabricated by conventional melt processing led to the discovery of this product (1). It allows melt extrusion of wire insulations or tubing of longer continuous lengths than the batchwise paste extrusion of PTFE. It also allows melt extrusion of films and injection molding of intricately shaped parts. The FEP polymer is melt-fabricable without severe sacrifice in mechanical properties because the perfluoromethyl side groups on the main polymer chain reduce crystallinity, which varies between 30% and 45%. This change in the crystallinity causes FEP and other copolymer particles to behave differently from PTFE particles; they do not fibrillate like PTFE particles and therefore do not agglomerate easily.

As a true thermoplastic, FEP copolymer can be melt-processed by extrusion A compression, injection, and blow molding. Films can be heat bonded and

**Table 1. Properties of Hexafluoropropylene<sup>a</sup>**

Properties	Value
Molecular weight	150.021
Boiling point at 101 kPa <sup>a</sup> , °C	−29.4
Freezing point, °C	−156.2
Critical temperature, °C	85
Critical pressure, kPa <sup>b</sup>	3254
Critical density, g/cm <sup>3</sup>	0.60
Vapor pressure at K, kPa <sup>b</sup> 243.75 < <i>T</i> < 358.15	$\log P \text{ (kPa)} = 6.6938 - 1139.156/T$
Liquid density, g/cm <sup>3</sup>	
60°C	1.105
20°C	1.332
0°C	1.419
−20°C	1.498
Heat of formation for ideal gas at, 25°C, $\Delta H$ , kJ/mol <sup>c,d</sup>	−1078.6
Flammability limits in air at 101 kPa <sup>a</sup>	Nonflammable for all mixtures of air and hexafluoropropylene
Heat of combustion, kJ/mol <sup>c,d</sup>	879
Toxicity, LC <sub>50</sub> (rat), 4 h, ppm <sup>e</sup>	3000

<sup>a</sup>Ref. (4).<sup>b</sup>To convert kPa to mmHg, multiply by 7.5.<sup>c</sup>To convert kJ to kcal, divide by 4.184.<sup>d</sup>Ref. (43).<sup>e</sup>Ref. (44).

sealed, vacuum formed, and laminated to various substrates. Chemical inertness and corrosion resistance make FEP highly suitable for chemical services; its dielectric and insulating properties favor it for electrical and electronic services; and its low frictional properties, mechanical toughness, thermal stability, and nonstick quality make it highly suitable for bearings and seals, high temperature components, and nonstick surfaces.

Mechanical properties are retained up to 200°C, even in continuous service, which is better than with most plastics. At high temperatures, these copolymers react with molten alkali metals. They are commercially available under the DuPont trademark Teflon FEP fluorocarbon resin. A similar product is manufactured by Daikin Kogyo and Dyneon and sold under the trademarks Neoflon and Hostaflon, respectively. FEP products are also manufactured in the People's Republic of China and in Russia. Additional information on specific manufacturers' products can often be obtained by consulting their internet Web sites (eg, [http://www2.dupont.com/Teflon/en\\_US/index.html](http://www2.dupont.com/Teflon/en_US/index.html)).

## Monomers

**Preparation.** The preparation, properties, and uses of TFE have been described. Hexafluoropropylene was initially prepared by pyrolysis of PTFE (2,3) and by fluorination of 1,2,3-trichloropropane followed by dehalogenation (4). A



number of other routes are described in the patent literature (5–10). Hexafluoropropylene can be prepared in high yield by thermally cracking TFE at reduced pressure at 700–800°C (11,12). Pyrolysis of PTFE at 860°C under vacuum gives a 58% yield of HFP (13). Fluorination of 3-chloropentafluoro-1-propene [79-47-0] at 200°C over activated carbon catalyst yields HFP (14). Decomposition of fluoroform [75-46-7] at 800–1000°C in a platinum-lined nickel tube is another route (15). The thermal decomposition of sodium heptafluorobutyrate [2218-84-4],  $\text{CF}_3\text{CF}_2\text{CF}_2\text{CO}_2\text{Na}$  (16,17), and copyrolyses of fluoroform and chlorotrifluoroethylene [79-38-9] (18,19), and chlorodifluoromethane [75-45-6] and 1-chloro-1,2,2,2-tetrafluoroethane [2837-89-0] (20) give good yields of HFP.

**Properties and Reactions.** The properties of HFP are shown in Table 1. It does not homopolymerize easily and hence can be stored as a liquid. It undergoes many addition reactions typical of an olefin. Reactions include preparation of linear dimers and trimers and cyclic dimers (21,22); decomposition at 600°C with subsequent formation of octafluoro-2-butene and octafluoroisobutylene (23); oxidation with formation of an epoxide (24), an intermediate for a number of perfluoroalkyl perfluorovinyl ethers (25,26); and homopolymerization to low molecular weight liquids (27,28) and high molecular weight solids (29,30). Hexafluoropropylene reacts with hydrogen (31), alcohols (32), ammonia (33), and the halogens and their acids, except  $\text{I}_2$  and HI (31,34–36). It is used as a comonomer to produce elastomers and other copolymers (37–41). The toxicological properties are discussed in Reference (42).

## Copolymers

Hexafluoropropylene and tetrafluoroethylene are copolymerized, with trichloroacetyl peroxide as the catalyst, at low temperature (45). Catalytic methods, including irradiation, achieve copolymerization at different temperatures (46,47). Aqueous and nonaqueous polymerizations appear to be the most convenient routes to commercial production (1,48–52). Polymerization conditions are similar to those of TFE homopolymer dispersion polymerization. In recent years, extensive efforts have been made in using supercritical carbon dioxide as the reaction medium to produce FEP (53–55). The copolymer of HFP–TFE is a *random copolymer*; that is, HFP units add to the growing chains at random intervals. The optimal composition of the copolymer is selected such that the mechanical properties are retained in the usable range and that the MFR is high enough for easy melt processing.

Hexafluoropropylene–tetrafluoroethylene copolymers are available in a variety of MFR and composition ranges that allow a selection of physical properties and processing characteristics, which are suited for the particular processing equipment and end use requirements. FEP is available in pellet, flake, and aqueous dispersion form.

The highest MFR grades are used for applications where high extrusion rate or easier flow is required. These grades are more suitable for injection molding by conventional thermoplastic molding techniques (56). The most common application for high MFR grades is for wire coating of small gauge wire with relatively thin coatings such as plenum primaries.

**Table 2. Properties of Teflon FEP Fluorocarbon Resin<sup>a</sup>**

Mechanical property	ASTM method	Teflon 110	Teflon 100	Teflon 140	Teflon 160
Melt flow number, g/10 min	D2116		7.0	3.0	1.5
Specific gravity	D792	2.13–2.17	2.13–2.17	2.13–2.17	2.13–2.17
Tensile strength at 23°C, MPa	D1708	20	23	30	31
Elongation at 23°C, %	D1708	300	325	325	305
Compressive strength, MPa	D695		21	21	23
Flexural strength at 23°C, MPa	D790		18	18	18
Impact strength at 23°C, J/m	D256		No break	No break	No break
Flexural modulus at 23°C, MPa	D790	655	620	620	586
Hardness durometer, Shore D	D2240	55	56	56	57
Coefficient of friction, metal/film	D1894		0.27	0.27	0.235
Deformation under load at 23°C, 6.9 MPa, 23 h, %	D621	1.8	0.5	0.5	0.5
Water absorption, 24 h, %	D570	<0.01	0.004	0.004	0.004
Linear coefficient of expansion, °C	E831				
0–100°C			$13.5 \times 10^{-5}$	$13.9 \times 10^{-5}$	$7.6 \times 10^{-5}$
100–150°C			$20.8 \times 10^{-5}$	$21.2 \times 10^{-5}$	$11.5 \times 10^{-5}$
150–200°C			$26.6 \times 10^{-5}$	$27.0 \times 10^{-5}$	$14.2 \times 10^{-5}$

<sup>a</sup>Compression-molded specimens; property data on extruded wire specimens are similar.

Intermediate MFR grades are suited for applications that require more stress crack resistance. Typical applications include coatings over wire braid constructions such as coaxial cables, insulation of wires larger than AWG 12 (American Wire Gauge) and insulations where high current loads or excessive thermal cycling may occur, such as heater cables. Other applications include cable jacketing, tubing, and films.

The lowest MFR resin is used as liners for process equipment and as thick films. Its MFR is significantly lower than that of other resins, and therefore it is unsuitable for conventional injection molding. Stress-crack resistance and mechanical properties are superior to those of the other three products (57) (Table 2).

Modified HFP–TFE polymers offer a combination of high stress-crack resistance and high extrusion rates. Use of perfluorovinyl ethers as modifiers makes it possible to achieve the superior performance without losing excellent chemical inertness and thermal stability (58–60). Incorporation of functional monomers

provides additional functionality such as adhesion to polymer, metal, and glass substrates (61–64).

Color concentrates are available for pigmenting extruded coatings of FEP resins. The concentrates are prepared for melt dispersion in extrusion applications. The pigments (thermally stable) are purified and carefully selected to meet electrical, mechanical, and thermal end use specifications. Color concentrate pellets are easily dispersed among clear pellets by conventional tumbling. The ratio of concentrate to natural resin varies, depending on the wire size, insulation thickness, and color intensity desired.

Nucleant containing grades are available in both fully letdown and concentrated forms. These are used with a blowing agent to produce foams with carefully controlled void content (65).

An FEP copolymer dispersion is available as a 55-wt% aqueous dispersion containing 6% nonionic surfactant (on a solids basis) and a small amount of anionic dispersing agent. Its average particle size is ca 0.2  $\mu\text{m}$ .

**Properties.** The crystallinity of FEP polymer is significantly lower than that of PTFE (70 vs 98%). The structure resembles that of PTFE, except for a random replacement of a fluorine atom by a perfluoromethyl group ( $\text{CF}_3$ ). The crystallinity after processing depends on the rate of cooling the molten polymer. The presence of HFP in the polymer chain tends to distort the highly crystallized structure of the PTFE chain and results in a higher amorphous fraction.

In the free-radical polymerization of FEP copolymers, chain termination occurs by binary coupling of chain ends, thus contributing to high molecular weights. Linear viscoelastic properties of these polymers in the amorphous melts were measured by dynamic rheometry. The FEP samples had high molecular weights and were found to verify the relation of zero shear viscosity vs (mol wt)<sup>3</sup> predicted by the reptation theory. At lower molecular weights, the empirical relation of viscosity vs (mol wt)<sup>3.4</sup> holds (66).

**Transitions and Relaxations.** Only one first-order transition is observed, the melting point. Increasing the pressure raises the melting point. At low pressures, the rate of increase in the melting point is ca 1.74°C/MPa (0.012°C/psi); at high pressures, this rate decreases to ca 0.725°C/MPa (0.005°C/psi). Melting increases the volume by 8%. In the presence of the HFP comonomer, crystal distortion occurs with an increase in intramolecular distance that, in turn, reduces the melting point (67).

The relaxation temperature appears to increase with increasing HFP content. Relaxation involves 5–13 of the chain carbon atoms. Besides  $\alpha$  and  $\gamma$  relaxations, one other dielectric relaxation was observed below  $-150^\circ\text{C}$ , which did not vary in temperature or in magnitude with comonomer content or copolymer density (68). The  $\alpha$  relaxation (also called Glass I) is a high temperature transition ( $157^\circ\text{C}$ ), and  $\gamma$  relaxation (Glass II) (internal friction maxima) occurs between  $-5$  and  $29^\circ\text{C}$ . The chain conformation and crystal structure of a series of HFP–TFE copolymers containing up to 50 mol% of HFP were studied (69). Increasing HFP content leads to significant departures from the highly ordered crystalline structure of PTFE. The helical conformation of the chain relaxes and untwists to accommodate the  $-\text{CF}_3$  pendant group in the HFP unit.

**Thermal Stability.** The polymer is thermally stable and can be processed at ca  $270^\circ\text{C}$ . Thermal degradation is a function of temperature and time, and the

stability is therefore limited. The melt flow rate (thermal degradation) increases significantly for short periods above 280°C, and degradation occurs at lower temperatures with longer hold times. The hourly weight loss is 0.0004% at 230°C, 0.001% at 260°C, 0.01% at 290°C, 0.02% at 320°C, 0.08% at 340°C, and 0.3% at 370°C. Degradation is not significant if the change in melt flow rate during molding is less than 10%. Physical strength decreases after prolonged exposure above 205°C, which accounts for the lower temperature rating of FEP resins (70).

**Radiation Effects.** The primary effect of radiation is the degradation of large molecules to small molecules. Molecular weight reduction can be minimized by excluding oxygen. If FEP is lightly irradiated at elevated temperatures in the absence of oxygen, cross-linking offsets molecular breakdown (68,71).

The degree to which radiation exposure affects FEP resins is determined by the energy absorbed, regardless of the type of radiation. Changes in mechanical properties depend on total dosage but are independent of the dose rate. The radiation tolerance of FEP in the presence or absence of oxygen is higher than that of PTFE by a factor of 10:1. Vacuum UV irradiation seems to provide a high potential for surface modification as compared to plasma treatment (72).

**Mechanical Properties.** Extensive lists of the physical properties of FEP copolymers are given in References (73–78). Mechanical properties are presented in Table 3. Most of the important properties of FEP are similar to those of PTFE; the main difference is the lower continuous service temperature of 204°C of FEP compared to that of 260°C of PTFE. The flexibility at low temperatures and the low coefficients of friction and stability at high temperatures are relatively independent of fabrication conditions. Unlike PTFE, FEP resins do not exhibit a marked change in volume at room temperature because they do not have a first-order transition at 19°C. They are useful above –267°C and are highly flexible above –79°C (79).

Static friction decreases with an increase in load, and the static coefficient of friction is lower than the dynamic coefficient. The tendency to creep must be considered carefully in FEP products designed for service under continuous stress. Creep can be minimized by suitable fillers. Fillers are also used to improve wear resistance and stiffness. Compositions such as 30% bronze-filled FEP, 20% graphite-filled FEP, and 10% glass-fiber-filled FEP offer high PV values [ $\sim 400(\text{kPacm})/\text{s}$ ] and are suitable for bearings.

Articles fabricated from FEP resins can be made bondable by surface treatment with a solution of sodium in liquid ammonia, or naphthalenyl sodium in tetrahydrofuran (79) to facilitate subsequent wetting. Exposing the surface to corona discharge (80) or amines at elevated temperatures in an oxidizing atmosphere (81) also makes the resins bondable. Some of the more recent work is described in References 82–84.

Vibration dampening properties at sonic and ultrasonic frequencies are excellent. However, the thickness of the resin must be sufficient to absorb the energy produced; this is usually determined experimentally.

**Electrical Properties.** Because of excellent electrical properties, FEP is a valuable and versatile electrical insulator. Within the recommended service temperature range, PTFE and FEP have identical properties as electrical insulators. Volume resistivity, which is more than  $10^{17} \Omega\text{-cm}$ , remains unchanged even after prolonged soaking in water; surface resistivity is more than  $10^{15} \Omega/\text{sq}$ .

**Table 3. Mechanical Properties of FEP<sup>a</sup>**

Property	Value	ASTM method
Specific gravity	2.14–2.17	D792-50
Thermal conductivity, W/(m·K)		Cenco-Fitch
–129–182°C	2.4	
–253°C	1.4	
Water absorption in 24 h, 3.175-mm-thick sample, % wt increase	<0.1	D570-547
Dimensional change at 23°C	None	
Coefficient of thermal expansion per °C		D696-44
>23°C	$9.3 \times 10^{-5}$	
<23°C	$5.7 \times 10^{-5}$	
Specific heat, kJ/(kg·K) <sup>b</sup>		
20°C	1.09	
100°C	1.17	
260°C	1.30	
Heat distortion, °C		D648-56
455 kPa <sup>c</sup>	70	
1820 kPa <sup>c</sup>	51	
Tensile yield strength, av, MPa <sup>d</sup>		D638-527
–251°C	165	
–160°C	131	
–129°C	96	
–73°C	62	
–56°C	27	
0°C	14	
23°C	12	
70°C	7	
121°C	3.5	
Tensile modulus, Pa <sup>e</sup>		
–251°C	57	
–160°C	50	
–129°C	36	
–73°C	24	
23°C	4	
100°C	1	
Tensile elongation, %		D638-527
–251°C	4	
–160°C	10	
–129°C	110	
–73°C	200	
23°C	350	
Flexural modulus, Pa <sup>e</sup>		D747-50
–251°C	53	
–160°C	47	
–101°C	32	
–23°C	6.6	
55°C	3.4	

(Continued)

Table 3. (Continued)

Property	Value	ASTM method
Compressive strength, MPa <sup>d</sup>		D695
-251°C	251	
-160°C	207	
23°C	15	
55°C	11	
100°C	3.4	
Izod impact strength, notched, J/m <sup>f</sup>		D256-56
23°C	No break	
Hardness durometer, shore D		D2240-T
23°C	59	
Taber abrasion, g/MHz, 100-g load CS-17 wheel	7.5	

<sup>a</sup>Measured on Teflon FEP T-100.<sup>b</sup>To convert kJ to kcal, divide by 4.184.<sup>c</sup>To convert kPa to atm, multiply by 0.01.<sup>d</sup>To convert MPa to psi, multiply by 145.<sup>e</sup>To convert Pa to mm Hg, multiply by  $7.5 \times 10^{-3}$ .<sup>f</sup>To convert J/m to ft·lbf/in., divide by 53.38 (see ASTM D256).

At low frequencies, the dielectric constant of FEP remains the same ( $\sim 2$ ). However, at more than 100 MHz the constant drops slightly with increasing frequency. As a true thermoplastic, FEP has a void content of zero and most of the fabricated material has a density of 2.14–2.17 g/cm<sup>3</sup>. The National Bureau of Standards has selected Teflon FEP resins for dielectric reference specimens because of the stability of their dielectric constant. The dissipation factor has several peaks as a function of temperature and frequency ( $3 \times 10^{-4}$  at 100 kHz;  $7 \times 10^{-4}$  at 1 MHz). The magnitude of the dissipation factor peak is greater for FEP than for PTFE because the molecular structure of the former is less symmetrical. The dissipation factor is hardly affected by irradiation annealing (85) and unaffected by humidity. The dielectric strength is high (80 GV/mm for 0.25-mm film at 23°C) and unaffected by thermal aging at 200°C. At high frequencies, the dielectric properties deteriorate in the presence of corona. If the voltage stress is not high enough to cause corona ignition, an infinitely long dielectric life is expected at any frequency. Corona discharges on the surface or in a void initiate dielectric breakdown (86). The FEP resins are recommended for continuous service up to 205°C. Although they begin to melt flow at 270°C, they retain some structural integrity up to 250°C (85).

**Chemical Properties.** The FEP resin is inert to most chemicals and solvents, even at elevated temperatures and pressures. However, it reacts with fluorine, molten alkali metal, and molten sodium hydroxide. Acids or bases are not absorbed at 200°C and exposures of 1 year. The absorption of organic solvents is less than 1% at elevated temperatures and long exposure times. Absorption of chemicals or solvents has no effect on the chemical integrity of the FEP molecule and is a reversible physical process.

Gases and vapors permeate FEP resin at a rate that is considerably lower than that of most plastics. Because FEP resins are melt processed, they are

**Table 4. Permeability of FEP Fluorocarbon Resins to Liquid Vapors and Gases**

Vapor	Permeability constant, <sup>a,b</sup> 10 <sup>15</sup> mol/(m·s·Pa)		
	23°C	35°C	50°C
Acetic acid		9.07	
Acetone	0.37		3.23
Benzene	0.75		
Carbon tetrachloride	0.24	0.41	
Decane	112.18		33.48
Depentene	23.50		10.67
Ethyl acetate	0.27	2.06	4.09
Ethanol	1.61	4.66	
H <sub>2</sub> SO <sub>4</sub> , 98%	21.70		
Toluene	5.38		
Water	8.14	20.32	18.26

<sup>a</sup>Ref. (75) Test method ASTM E96-35T (at vapor pressure; for 25.4  $\mu$ m film thickness). Values are averages only and not for specification purposes.

<sup>b</sup>Original data converted to SI units using vapor pressure data from Ref. (87).

void-free and permeation occurs only by molecular diffusion. Variation in crystallinity and density is limited, except in unusual melt-processing conditions.

Because of its low permeability, FEP polymer is used extensively in the chemical industry. Its permeation characteristics are similar to those of PTFE (Table 4). An inverse relationship between permeability and film thickness applies to FEP.

**Weathering.** Articles fabricated from FEP are unaffected by weather, and their resistance to extreme heat, cold, and UV irradiation suits them for applications in radar and other electronic components. For example, after 15 years of solar exposure in Florida, the tensile strength and light transmission (96%) of a 25- $\mu$ m-thick film was unchanged and the film remained crystal clear (88). Elongation increased slightly for the first 5–7 years of outdoor exposure, probably as a result of stress relaxation. Beyond 10 years, a small decrease was observed.

**Optical Properties.** Teflon FEP fluorocarbon film transmits more ultraviolet, visible light, and infrared radiation than ordinary window glass. The refractive index of FEP film is 1.341–1.347 (89).

## Fabrication

Standard thermoplastic processing techniques can be used to fabricate FEP. Thermal degradation must be avoided, and a homogeneous structure and good surface quality must be maintained.

**Injection Molding.** Even the high MFR, FEP resin has a significantly lower MFR than most other thermoplastic products and therefore requires higher processing temperatures, slower injection rates, special mold design, and corrosion-resistant material of construction. When the flow velocity in melt processing exceeds a critical value, melt fracture occurs. The critical shear rate of

FEP is much lower than that of other thermoplastics. Recommendations for materials of construction and the screw design, valves, smear heads, nozzle, operating conditions, and mold design are given in References 57, 90, 91, and 94.

Pigments (thermally stable at processing temperature) are dry blended with the resin before molding. At loadings of 0.1–1%, pigments have no appreciable effect on the dielectric strength, dielectric constant, or mechanical properties. The dissipation factor of pigmented resin varies with the pigment and its amount (92).

**Extrusion.** Conventional melt-extrusion equipment is used in processing FEP resins. Commercial pigments, nucleant packages, or other fluoropolymers can be mixed with the resin before extrusion into wire coating, tubing, rods, molding, beading channels, and so forth. Coating thicknesses of 0.076–2.54 mm have been extruded over such materials as silicone rubber, poly(vinyl chloride), glass braid, metal-shielded cables, twisted conductors, and parallel multiconductor cables.

For primary insulation or cable jackets, high production rates are achieved by extruding a tube of resin with a larger internal diameter than the base wire and a thicker wall than the final insulation. The tube is then drawn down to the desired size. An operating temperature of 315–400°C is preferred, depending on holdup time. The surface roughness caused by melt fracture determines the upper limit of production rates under specific extrusion conditions (93,94). Corrosion-resistant metals should be used for all parts of the extrusion equipment that come in contact with the molten polymer (95).

Tubing is made in a wide range of sizes and is used as slip-on electrical insulation, instrument tubing, and for hoses. Small tubing, called spaghetti tubing, can be produced by a free-extrusion technique, whereas hose-size tubing is produced by conventional forming-box techniques; FEP also is extruded into films.

**Dispersion Processing.** The commercial aqueous dispersion of FEP contains 55 wt% of hydrophobic, negatively charged FEP particles and ca 6 wt% (based on FEP) of a mixture of nonionic and anionic surface-active agents. The average particle size is ca 0.2  $\mu\text{m}$ . The dispersion is processed by the same technique used for PTFE dispersion. For example, the fabric is coated with FEP dispersion, the water is evaporated from the coating, the wetting agent is removed, and the FEP layer is fused with the fabric.

Dispersion is used as a coating for glass fabric, chemical barriers, and wire-insulating tapes; as adhesive coatings for bonding seals and bearings of PTFE to metallic and nonmetallic components; and as antifriction or antistick coatings for metals. The fusion of FEP to provide a continuous film depends on a time–temperature relationship; 1 min at 400°C or 40 min at 290°C is sufficient to achieve good fusion (96).

**Other Techniques.** The FEP resin is bonded to metal surfaces by the application of heat and pressure; it can be heat sealed or hot-gas welded. Heating FEP at 260°C and allowing it to cool slowly results in stress relieving, or annealing. The FEP film is used to weld PTFE-coated surfaces.

**Effects of Fabrication on Product Properties.** Extrusion conditions have a significant effect on the quality of the product (95). Contamination can be the result of corrosion, traces of another resin, or improper handling. Corrosion-resistant high nickel alloys such as Hastelloy C-276 or Inconel 625 should be used in the extruder. Surface roughness is the result of melt fracture or mechanical



deformation. Melt fracture can be eliminated by increasing the die opening, die temperature, and the melt temperature and by reducing the extrusion rate. Bubbles and discoloration are caused by resin degradation, air entrapment, or condensed moisture. Excessive drawdown, resin degradation, or contamination can result in pinholes, tears, and cone breaks. The blisters are caused by degassing of primary coatings, and loose coatings are caused by rapid cooling and long cones.

**Testing and Standards.** Requirements for extrusion and molding grades are cited in ASTM specifications D2116 (97) and in Federal specification LP-389A of May 1964 (98). For fabricated shapes, FEP film and sheet are covered by Aeronautical Material Specifications (AMS) 3647 and LP-523 (99). Besides the specifications covered by the Fluorocarbons Division of the Society of the Plastics Industry, Inc.(100), other specifications are listed in References 101 and 102.

## Economic Aspects

Because of the high cost of HFP, FEP is more expensive than PTFE. In the United States, in 2009, FEP sold at prices up to \$48/kg, depending on type and grade. Most grades are marketed in a colorless, translucent, extruded pellet form. The dispersion containing about 55% solids is priced at ca \$60/kg.

## Health and Safety

The safety precautions required in handling HFP–TFE copolymers are the same as those applied to handling PTFE (103). Large quantities have been processed safely by many different fabricators in a variety of operations. With proper ventilation, the polymer can be processed and used at elevated temperatures without hazard. The fumes from heated FEP or its thermal decomposition products are toxic in high concentrations, like the fumes or decomposition products of other polymers. Ventilation should be provided in areas where the resin is at processing temperature (270–400°C). At ambient temperatures, FEP resin is essentially inert. Inhalation of fumes given off by heated FEP resin may result in influenza-like symptoms. They may occur several hours after exposure and disappear within 35–48 h, even in the absence of treatment; the effects are not cumulative (57). Such attacks usually follow exposure to vapors evolved from the polymer without adequate ventilation or from smoking tobacco or cigarettes contaminated with the polymer. Toxicology study of the particulates and fumes is reported in Reference (104).

## Applications

The principal electrical applications include hookup wire, interconnecting wire, coaxial cable, computer wire, thermocouple wire, plenum cable, and molded electrical parts. Principal chemical applications are lined pipes and fittings, overbraided hose, heat exchangers, and laboratory ware. Mechanical uses include antistick applications, such as conveyor belts and roll covers. FEP film for solar

collector windows takes advantage of excellent weatherability and high solar transmission. FEP film and coatings are used for a variety of applications that require high temperature performance, good release properties, and excellent chemical or UV resistance.

## BIBLIOGRAPHY

"Tetrafluoroethylene Polymers, Copolymers with Hexafluoropropylene" in *EPST* 1st ed., Vol. 13, pp. 654–670, by D. I. McCane, E. I. du Pont de Nemours & Co., Inc.; "Tetrafluoroethylene Polymers, Tetrafluoroethylene–Hexafluoropropylene Copolymers" in *EPSE* 2nd ed., Vol. 16, pp. 601–613, by S. V. Gangal, E. I. du Pont de Nemours & Co., Inc.; "Perfluorinated Polymers, Perfluorinated Ethylene–Propylene Copolymers" in *EPST* 3rd ed., Vol. 3, pp. 364–378, by S. V. Gangal, E. I. du Pont de Nemours & Co., Inc.

## CITED PUBLICATIONS

1. U.S. Pat. 2946763 (July 26, 1960), M. I. Bro and B. W. Sandt (to E. I. du Pont de Nemours & Co., Inc.).
2. U.S. Pat. 2394581 (Feb. 12, 1946), A. F. Benning, F. B. Dowing, and J. D. Park (to Kinetic Chemicals, Inc.).
3. E. G. Young and W. S. Murray, *J. Am. Chem. Soc.* **70**, 2814 (1949).
4. A. L. Henne and T. P. Waalkes, *J. Am. Chem. Soc.* **68**, 496 (1946).
5. U.S. Pat. 3446858 (May 27, 1969), H. Shinzu and co-workers (to Daikin Kyogo Co.).
6. U.S. Pat. 3459818 (Aug. 15, 1969), H. Ukihashi and M. Hisasue (to Asahi Glass Co.).
7. U.S. Pat. 3873630 (Mar. 25, 1975), N. E. West (to E. I. du Pont de Nemours & Co., Inc.).
8. U.S. Pat. 5043491 (Aug. 27, 1991), J. Webster and co-workers, (to E. I. du Pont de Nemours & Co., Inc.).
9. U.S. Pat. 5057634 (Oct. 15, 1991), J. Webster and co-workers (to E. I. du Pont de Nemours & Co., Inc.).
10. U.S. Pat. 5068472 (Nov. 26, 1991), J. Webster and co-workers (to E. I. du Pont de Nemours & Co., Inc.).
11. U.S. Pat. 3758138 (Aug. 7, 1956), D. A. Nelson (to E. I. du Pont de Nemours & Co., Inc.).
12. B. Atkinson and A. B. Trenwith, *J. Chem. Soc.*, Part II 2082 (1953).
13. U.S. Pat. 2759983 (Aug. 21, 1956), J. S. Waddell (to E. I. du Pont de Nemours & Co., Inc.).
14. U.S. Pat. 3047640 (July 31, 1962), R. F. Sweeny and C. Woolf (to Allied Chemical Corp.).
15. U.S. Pat. 3009966 (Nov. 21, 1961), M. Hauptschein and A. Fainberg (to Pennsalt Chemicals Corp.).
16. L. T. Hals, T. S. Reid, and G. H. Smith, *J. Am. Chem. Soc.* **73**, 4054 (1951).
17. U.S. Pat. 2668864 (Feb. 9, 1954), L. T. Hals, T. S. Reid, and G. H. Smith (to Minnesota Mining and Manufacturing Co.).
18. G. Pass, *J. Chem. Soc.*, Part I 824 (Jan. 1965).
19. U.S. Pat. 3318963 (May 9, 1967), G. Pass (to Imperial Chemical Industries, Ltd.).
20. Ger. Pat. 1236497 (Mar. 16, 1967), W. Oese, H. Dude, and F. Reinke (to VEB Fluorwerke Dohma).
21. U.S. Pat. 2918501 (Dec. 22, 1959), W. J. Brehm and co-workers (to E. I. du Pont de Nemours & Co., Inc.).

22. U.S. Pat. 3316312 (Apr. 25, 1967), D. I. McCane and I. M. Robinson (to E. I. du Pont de Nemours & Co., Inc.).
23. R. A. Matula, *J. Phys. Chem.* **72**, 3054 (1968).
24. U.S. Pat. 3358003 (Dec. 12, 1967), H. S. Eleuterio and R. W. Meschke (to E. I. du Pont de Nemours & Co., Inc.).
25. U.S. Pat. 3180895 (Apr. 27, 1965), J. F. Harris Jr. and D. I. McCane (to E. I. du Pont de Nemours & Co., Inc.).
26. U.S. Pat. 3291843 (Dec. 13, 1966), C. G. Fritz and S. Selman (to E. I. du Pont de Nemours & Co., Inc.).
27. E. V. Volkova and A. E. Skobina, *Vysokomol. Soedin.* **6**, 964 (1964).
28. Fr. Pat. 1524571 (May 10, 1968), S. W. Osborn and E. Broderich (to Thiokol Chemical Corp.).
29. U.S. Pat. 2983764 (May 9, 1961), D. F. Knaack (to E. I. du Pont de Nemours & Co., Inc.).
30. U.S. Pat. 2958685 (Nov. 1, 1960), H. S. Eleuterio (to E. I. du Pont de Nemours & Co., Inc.).
31. I. L. Knunyants, E. I. Mysov, and M. P. Krasuskaya, *Izv. Akad. Nauk. SSSR Otd. Khim. Nauk.* 906 (1958).
32. I. L. Knunyants, A. E. Shchekotikhin, and A. V. Fakin, *Izv. Akad. Nauk. SSSR Otd. Khim. Nauk.* 282 (1953).
33. I. L. Knunyants, L. S. German, and B. L. Dyatkin, *Izv. Akad. Nauk. SSSR Otd. Khim. Nauk.* 1353 (1956).
34. R. N. Haszeldine and B. R. Steele, *J. Chem. Soc.*, 1592 (1953).
35. W. T. Miller Jr., E. Bergman, and A. H. Fainberg, *J. Am. Chem. Soc.* **79**, 4159 (1957).
36. I. L. Knunyants, V. V. Shokina, and N. D. Kuleshova, *Izv. Akad. Nauk SSSR Otd. Khim. Nauk.* 1936 (1960).
37. U.S. Pat. 3467636 (Sept. 16, 1969), A. Nersasian (to E. I. du Pont de Nemours & Co., Inc.).
38. U.S. Pat. 3536683 (Oct. 27, 1970), F. V. Bailor and J. R. Cooper (to E. I. du Pont de Nemours & Co., Inc.).
39. U.S. Pat. 3790540 (Feb. 5, 1974), J. E. Dohany and A. C. Whiton (to Pennwalt Corp.).
40. U.S. Pat. 3817951 (June 18, 1974), D. N. Robinson (to Pennwalt Corp.).
41. U.S. Pat. 3868337 (Feb. 25, 1975), P. Gros (to Society Superflexit).
42. G. L. Kennedy Jr., *Crit. Revs. Toxicol.* **21** (2), 149–170 (1990).
43. H. C. Duus, *Ind. Eng. Chem.* **47**, 1445 (1955).
44. J. W. Clayton, *Occup. Med.* **4**, 262 (1962).
45. U.S. Pat. 2598283 (May 27, 1952), W. T. Miller (to U.S. Atomic Energy Commission).
46. R. A. Naberezhnykh and co-workers, *Dokl. Akad. Nauk SSSR* **214**, 149 (1974).
47. A. S. Kabankin, S. A. Balabanova, and A. M. Markevich, *Vysokomol. Soedin., Ser. A* **12**, 267 (1970).
48. Br. Pat. 781532 (Aug. 21, 1957), C. G. Krespan (to E. I. du Pont de Nemours & Co., Inc.).
49. U.S. Pat. 3132124 (May 5, 1964), M. J. Couture, D. L. Schindler, and R. B. Weiser (to E. I. du Pont de Nemours & Co., Inc.).
50. U.S. Pat. 4380618 (1983), A. Khan and R. Morgan (to E. I. du Pont de Nemours & Co., Inc.).
51. U.S. Pat. 4384092 (1983), J. Herison (to Ugine Kuhlmann).
52. U.S. Pat. 4861845 (1989), E. Slocum, A. Sobrero, and R. Wheland (to E. I. du Pont de Nemours & Co., Inc.).
53. U.S. Pat. 5618894 (Apr. 8, 1997), J. DeSimone and T. Romack (to The University of North Carolina, Chapel Hill, N.C.).

54. U.S. Pat. 6051682 (Apr. 18, 2000), E. Debrabander and P. Brothers (to E. I. du Pont de Nemours & Co., Inc.).
55. Process G Extrusion and Molding Resins, Product Information Bulletin No. H-95608-1, E. I. du Pont de Nemours & Co., Inc., Wilmington, Del., 2007.
56. R. S. Atland, *Modern Plast.* **62**, 200 (1985).
57. Teflon-FEP Fluorocarbon Resin, Techniques for Injection Molding, Information Bulletin 95d, E. I. du Pont de Nemours & Co., Inc., Wilmington, Del., 1969.
58. U.S. Pat. 5677404 (Oct. 14, 1997), L. M. Blair (to E. I. du Pont de Nemours & Co., Inc.).
59. U.S. Pat. 5688885 (Nov. 18, 1997), L. M. Blair (to E. I. du Pont de Nemours & Co., Inc.).
60. U.S. Pat. 5700889 (Dec. 23, 1997), L. M. Blair (to E. I. du Pont de Nemours & Co., Inc.).
61. U.S. Pat. 6107423 (Aug. 22, 2000), R. Wheland and P. Brothers (to E. I. du Pont de Nemours & Co., Inc.).
62. U.S. Pat. 6177196 (Jan. 23, 2001), P. Brothers, M. Hung, M. Michalczyk, and T. Takahashi (to E. I. du Pont de Nemours & Co., Inc.).
63. U.S. Pat. 6300445 (Oct. 9, 2001), M. Hung, P. Brothers and D. Kerbow (to E. I. du Pont de Nemours & Co., Inc.).
64. U.S. Pat. 5780552 (Jul. 14, 1998), D. Kerbow (to E. I. du Pont de Nemours & Co., Inc.).
65. R. T. Young, *Wire J. Int.* **42** (6), 66–70 (2009).
66. S. Wu, *Macromolecules* **18**, 2023–2030 (1985).
67. R. K. Eby, *J. Appl. Phys.* **34**, 2442 (1963).
68. R. K. Eby and F. C. Wilson, *J. Appl. Phys.* **33**, 2951 (1962).
69. M. L. White and co-workers, *J. Polym. Sci., Part B: Polym. Phys.* **36**, 2811–2819 (1998).
70. Safe Handling Guide, Teflon Fluorocarbon Resins, du Pont Materials for Wire and Cable, Bulletin E-85433, E. I. du Pont de Nemours & Co., Inc., Wilmington, Del., 1986.
71. R. Y. M. Huang and P. J. F. Kanitz, *Polym. Prepr. Am. Chem. Soc. Div. Polym. Chem.* **10**, 1087 (1969).
72. V. N. Vasilets and co-workers, *J. Polym. Sci., Part I: Polym. Chem.* **36**, 2215–2222 (1998).
73. R. J. Diamond, *Plastics* **27**, 109 (1962).
74. J. Frados, ed., *Modern Plastics Encyclopedia*, Vol. 46, No. 10A, McGraw-Hill Book Co., Inc., New York, 1969, p. 974.
75. *J. Teflon* **11** (1), 8 (1970).
76. J. A. Brydson, *Plastics Materials*, Iliffe Books, Ltd., London, 1966, Chapt. 10, pp. 203–218.
77. Teflon 100 FEP—Fluorocarbon Resin—Melt Processible Resin, Information Bulletin X-90a, E. I. du Pont de Nemours & Co., Inc., Wilmington, Del., 1960.
78. *Teflon Fluorocarbon Resins, Mechanical Design Data*, 2nd ed., E. I. du Pont de Nemours & Co., Inc., Wilmington, Del., 1965.
79. A. A. Benderly, *J. Appl. Polym. Sci.* **6**, 221 (1962).
80. Brit. Pat. 890466 (Feb. 28, 1962), D. L. Ryan (to E. I. du Pont de Nemours & Co., Inc.).
81. U.S. Pat. 3063882 (Nov. 13, 1962), J. R. Chesire (to E. I. du Pont de Nemours & Co., Inc.).
82. R. R. Rye and G. W. Arnold, *Langmuir* **5**, 1331 (1989).
83. D. T. Clark and D. R. Hutton, *J. Polym. Sci., Polym. Chem. Ed.* **25**, 2643 (1987).
84. R. C. Bening and J. J. McCarthy, *Polym. Prepr.* **29**, 336 (1988).
85. Electrical (*Electronic Design Data for Teflon*, E. I. du Pont de Nemours & Co., Inc., Wilmington, Del.

86. J. C. Reed, E. J. McMahon, and J. R. Perkins, *Insulation (Libertyville, Ill.)* **10**, 35 (1964).
87. D. W. Green, ed., *Perry's Chemical Engineers' Handbook*, 6th ed., McGraw-Hill Book Co., Inc., New York, 1984.
88. DuPont FEP-Fluorocarbon Film, Information Bulletin H55007, E. I. du Pont de Nemours & Co., Inc, Wilmington, DE (Dec. 1996)
89. DuPont FEP-Fluorocarbon Film, Properties Bulletin H55008, E. I. du Pont de Nemours & Co., Inc, Wilmington, DE (Dec. 1996)
90. Injection Molding Guide for Teflon FEP, PFA and Tefzel, Bulletin No. E-96680, E. I. du Pont de Nemours & Co., Inc., Wilmington, Del., July 1987.
91. "Teflon (Tefzel" Injection Moulding Trouble-Shooting Guide, Bulletin No. E-96164 (Rev.), E. I. du Pont de Nemours & Co., Wilmington, Del., Sept. 1991.
92. L. H. Gillespe, D. O. Saxton, and F. M. Chapman, *New Design Data for Teflon*, E. I. du Pont de Nemours & Co., Inc., Wilmington, Del., 1960.
93. *J. Teflon* **18** (1), 8 (1977).
94. Technical Information, Melt Extrusion Guide, Bulletin No. H-45321, E. I. du Pont de Nemours & Co., Inc., Wilmington, Del., Apr. 2001.
95. Teflon FEP—Fluorocarbon Resin—Techniques for Processing by Melt Extrusion, 2nd ed., Information Bulletin X-82, E. I. du Pont de Nemours & Co., Inc., Wilmington, Del., 1960.
96. Properties and Processing Techniques for Teflon 120 FEP—Fluorocarbon Resin Dispersion, Preliminary Information Bulletin No. 20, E. I. du Pont de Nemours & Co., Inc., Wilmington, Del., 1961.
97. ASTM D2116-07, Standard Specification for FEP-Fluorocarbon Molding and Extrusion Materials, American Society for Testing and Materials, West Conshohocken, Pa., 1993.
98. Federal Supply Service Bureau Specification L-P-389A, Section SW, 470E L'Enfant Plaza, Washington, D.C.
99. Technical Data, SAE International, Inc., Warrendale, Pa., 1993.
100. Scos Annual Book of ASTM Standards. Vol. 08.03, American Society for Testing and Materials, Philadelphia, Pa., 1993.
101. Technical Data, Society of the Plastics Industry, Inc., Fluorocarbon Division, Washington, D.C., 1993.
102. *J. Teflon* **15** (1), 10 (1974).
103. *Guide to Safe Handling of Fluoropolymer Resins*, 4rd ed., Fluoropolymers Division of the Society of the Plastics Industry, Inc., Washington, D.C., Nov. 2005.
104. K. P. Lees and W. C. Seidal, *Inhalation Toxicol.* **3**, 237 (1991).

## GENERAL REFERENCE

"Fluorinated Ethylene–Propylene Copolymers," under "Fluorine Compounds, Organic," in *ECT* 4th ed., Vol. 11, pp. 644–656, by S. V. Gangal, E. I. du Pont de Nemours & Co., Inc.

SUBHASH V. GANGAL

PAUL D. BROTHERS

E. I. du Pont de Nemours & Co., Inc.,  
Wilmington, Delaware

## PERFLUORINATED POLYMERS, POLYTETRAFLUOROETHYLENE

### Introduction

Polytetrafluoroethylene (PTFE) [9002-84-0], more commonly known as Teflon (E.I. du Pont de Nemours & Co., Inc.), a perfluorinated straight-chain high polymer, has a most unique position in the plastics industry because of its chemical inertness, heat resistance, excellent electrical insulation properties, and low coefficient of friction over a wide temperature range. Polymerization of tetrafluoroethylene monomer gives this perfluorinated straight-chain high polymer with the formula  $-(CF_2-CF_2)_n-$ . The white to translucent solid polymer has an extremely high molecular weight, in the  $10^6$ – $10^7$  range and consequently has a viscosity in the range of 1–10 GPa·s ( $10^{10}$ – $10^{11}$  P) at 380°C. It is a highly crystalline polymer and has a crystalline melting point. Its high thermal stability results from the strong carbon–fluorine bond and characterizes PTFE as a useful high temperature polymer.

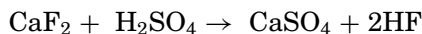
The discovery of PTFE (1) in 1938 opened the commercial field of perfluoropolymers. Initial production of PTFE was directed toward the World War II effort, and commercial production was delayed by DuPont until 1947. Commercial PTFE is manufactured by two different polymerization techniques that result in two different types of chemically identical polymer. Suspension polymerization produces a granular resin, whereas emulsion polymerization produces both the coagulated dispersion that is often referred to as a fine powder and *PTFE dispersion*.

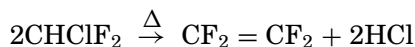
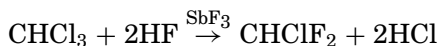
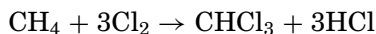
Because of its chemical inertness and high molecular weight, PTFE melt does not flow and cannot be fabricated by conventional techniques. The suspension-polymerized PTFE polymer (referred to as *granular PTFE*) is usually fabricated by modified powder metallurgy techniques. Emulsion-polymerized PTFE behaves entirely differently from granular PTFE. Coagulated dispersions are processed by a cold-extrusion process (like processing lead). Stabilized PTFE dispersions, made by emulsion polymerization, are usually processed according to latex processing techniques.

Manufacturers of PTFE include Daikin Kogyo (Polyflon), DuPont (Teflon), Dyneon, Asahi Glass (Fluon), and Solvay Solexis (Algoflon). Also, the People's Republic of China manufactures many PTFE products and is becoming a significant manufacturing country. Additional information on specific manufacturers' products can often be obtained by consulting their Internet Web sites.

### Monomer

**Preparation.** The manufacture of tetrafluoroethylene (TFE) [116-14-3] involves the following steps (2–9). The pyrolysis is often conducted at a PTFE manufacturing site because of the difficulty of handling TFE. New discoveries have made it somewhat easier to use it at remote places (10).





Pyrolysis of chlorodifluoromethane is a noncatalytic gas-phase reaction carried out in a flow reactor at atmospheric or subatmospheric pressure; yields can be as high as 95% at 590–900°C. The economics of monomer production is highly dependent on the yields of this process. A significant amount of hydrogen chloride waste product is generated during the formation of the carbon–fluorine bonds.

A large number of by-products are formed in this process, mostly in trace amounts; more significant quantities are obtained of hexafluoropropylene, perfluorocyclobutane, 1-chloro-1,1,2,2-tetrafluoroethane, and 2-chloro-1,1,1,2,3,3-hexafluoropropane. Small amounts of highly toxic perfluoroisobutylene,  $\text{CF}_2=\text{C}(\text{CF}_3)_2$ , are formed by the pyrolysis of chlorodifluoromethane.

In this pyrolysis, subatmospheric partial pressures are achieved by employing a diluent such as steam. Because of the corrosive nature of the acids (HF and HCl) formed, the reactor design should include a platinum-lined tubular reactor made of nickel to allow atmospheric pressure reactions to be run in the presence of a diluent. Because the pyrolysate contains numerous by-products that adversely affect polymerization, the TFE must be purified. Refinement of TFE is an extremely complex process, which contributes to the high cost of the monomer. Inhibitors are added to the purified monomer to avoid polymerization during storage; terpenes such as *d*-limonene and terpene B are effective (11).

Tetrafluoroethylene was first synthesized in 1933 from tetrafluoromethane,  $\text{CF}_4$ , in an electric arc furnace (12). Since then, a number of routes have been developed (13–20). Depolymerization of PTFE by heating at ca 600°C is probably the preferred method for obtaining small amounts of 97% pure monomer on a laboratory scale (21, 22.) Depolymerization products contain highly toxic perfluoroisobutylene and should be handled with care.

**Properties.** Tetrafluoroethylene (mol wt. 100.02) is a colorless, tasteless, odorless gas (Table 1). It is stored as a liquid; vapor pressure at –20°C is 1 MPa (9.9 atm). It is usually polymerized above its critical temperature and below its critical pressure. The polymerization reaction is highly exothermic.

Tetrafluoroethylene undergoes addition reactions typical of an olefin. It burns in air to form carbon tetrafluoride, carbonyl fluoride, and carbon dioxide (26). Under controlled conditions, oxygenation produces an epoxide (27) or an explosive polymeric peroxide (26). Trifluorovinyl ethers,  $\text{RO}-\text{CF}=\text{CF}_2$ , are obtained by reaction with sodium salts of alcohols (28). An ozone–TFE reaction is accompanied by chemiluminescence (29). Dimerization at 600°C gives perfluorocyclobutane,  $\text{C}_4\text{F}_8$ ; further heating gives hexafluoropropylene,  $\text{CF}_2=\text{CFCF}_3$ , and eventually perfluoroisobutylene,  $\text{CF}_2=\text{C}(\text{CF}_3)_2$  (30). Purity is determined by both gas–liquid and gas–solid chromatography; the IR spectrum is complex and therefore of no value in determining purity.

**Uses.** Besides polymerizing TFE to various types of high PTFE homopolymer, TFE is copolymerized with hexafluoropropylene (31), ethylene (32),

Table 1. Physical Properties of Tetrafluoroethylene<sup>a</sup>

Property	Value
Boiling point at 101.3 kPa, <sup>b</sup> °C	-76.3
Freezing point, °C	-142.5
Liquid density at <i>t</i> °C, g/mL	
-100 < <i>t</i> < -40	=1.202-0.0041 <i>t</i>
-40 < <i>t</i> < 8	=1.1507-0.0069 <i>t</i> -0.000037 <i>t</i> <sup>2</sup>
8 < <i>t</i> < 30	=1.1325 - 0.0029 <i>t</i> -0.00025 <i>t</i> <sup>2</sup>
Vapor pressure at <i>T</i> K, kPa <sup>c</sup>	
196.85 < <i>T</i> < 273.15	log <sub>10</sub> <i>P</i> <sub>kPa</sub> = 6.4593-875.14/ <i>T</i>
273.15 < <i>T</i> < 306.45	log <sub>10</sub> <i>P</i> <sub>kPa</sub> = 6.4289-866.84/ <i>T</i>
Critical temperature, °C	33.3
Critical pressure, MPa <sup>d</sup>	39.2
Critical density, g/mL	0.58
Dielectric constant at 28°C	
at 101.3 kPa <sup>b</sup>	1.0017
at 858 kPa <sup>b</sup>	1.015
Thermal conductivity at 30°C, m W/(m·K)	15.5
Heat of formation for ideal gas	-635.5
at 25°C, Δ <i>H</i> , kJ/mol <sup>e, f</sup>	
Heat of polymerization of 25°C to solid polymer Δ <i>H</i> , kJ/mol <sup>e, f</sup>	-172.0
Flammability limits in air at 101.3 kPa, <sup>c</sup> vol%	14-43

<sup>a</sup>From Ref. (23), unless otherwise stated.<sup>b</sup>To convert kPa to atm, multiply by 0.01.<sup>c</sup>To convert kPa to psi, multiply by 0.145.<sup>d</sup>To convert MPa to atm, divide by 0.101.<sup>e</sup>To convert J to cal, divide by 4.184.<sup>f</sup>Ref. (24).<sup>g</sup>Ref. (25).

perfluorinated ether (33, 34), isobutylene (35), propylene (36), and in some cases it is used as a termonomer (37). It is used to prepare low molecular weight polyfluorocarbons (38) and carbonyl fluoride (39), as well as to form PTFE *in situ* on metal surfaces (40). Hexafluoropropylene [116-15-4] (41, 42), perfluorinated ethers, and other oligomers are prepared from TFE.

In the absence of air, TFE disproportionates violently to give carbon and carbon tetrafluoride; the same amount of energy is generated as in black powder explosions. This type of decomposition is initiated thermally, and equipment hot spots must be avoided. The flammability limits of TFE are 14-43%; it burns when mixed with air and forms explosive mixtures with air and oxygen. It can be stored in steel cylinders under controlled conditions inhibited with a suitable stabilizer. The oxygen content of the vapor phase should not exceed 10 ppm.

## Manufacture of PTFE

Engineering problems involved in the production of TFE seem simple as compared with those associated with polymerization and processing of PTFE resins.



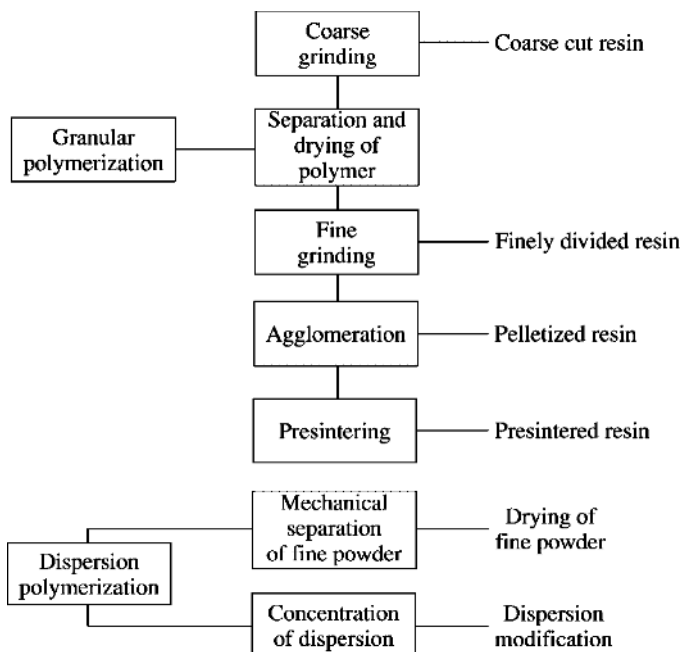


**Fig. 1.** Granular, fine powder, and dispersion PTFE products.

The monomer must be polymerized to an extremely high molecular weight to achieve the desired properties. The low molecular weight polymer does not have the strength needed in end use applications. However, in recent years, some efforts have been made to develop low MW PTFE with desirable properties. (43).

Polytetrafluoroethylene is manufactured and sold in three forms: granular, fine powder, and aqueous dispersion; each requires a different fabrication technique. Granular resins are manufactured in a wide variety of grades to obtain a different balance between powder flows and end use properties (Fig. 1). Fine powders that are made by coagulating aqueous dispersions are also available in various grades. Differences in fine powder grades correspond to their usefulness in specific applications and to the ease of fabrication. Aqueous dispersions are sold in latex form and are available in different grades. A variety of formulation techniques are used to tailor these dispersions for specific applications.

**Polymerization.** In aqueous medium, TFE is polymerized by two different procedures. When little or no dispersing agent is used and vigorous agitation is maintained, a precipitated resin is produced, commonly referred to as granular resin. In another procedure, called *aqueous dispersion polymerization*, a sufficient dispersing agent is employed and mild agitation produces small colloidal particles dispersed in the aqueous reaction medium; precipitation of the resin particles is avoided. The two products are distinctly different, even though both are high molecular weight PTFE polymers. The granular product can be molded in various forms, whereas the resin produced by the aqueous dispersion cannot be molded but is fabricated by dispersion coating or conversion to powder for paste extrusion

with a lubricant medium. Granular resin cannot be paste extruded or dispersion coated.

**Granular Resins.** Granular PTFE is made by polymerizing TFE alone or in the presence of trace amounts of comonomers (44–46). An initiator, a small amount of dispersing agent, and other additives (47) may be present; an alkaline buffer is occasionally used (48). In the early stages of polymerization, an unstable dispersion is formed, but the lack of dispersing agent and vigorous agitation cause the polymer to partially coagulate; the remainder of the process is fairly complex. The polymerized product is stringy, irregular, and variable in shape. The dried granular polymer is ground to different average particle sizes, depending on the product requirements, for example, the flow and other properties. Coarser fabrication of particles leaves a higher void in the sintered article. A better balance between handleability and moldability (ability to mold and sinter in the absence of voids) is achieved by agglomerating the finely divided resin to ca 400–800  $\mu\text{m}$  (49–51). For ram extrusion of granular resin into long tubes and rods, a partially presintered resin is preferred. Granular PTFE resin is nonflammable.

**Fine Powder Resins.** Fine powder resins are made by polymerizing TFE in an aqueous medium with an initiator and emulsifying agents (52). Environmental issues associated with the commercially used emulsifying agent have been discussed extensively (53). Significant work has been conducted to find suitable replacements. In order to obtain unhindered propagation of long PTFE chains, the surfactant needs to be sufficiently inert. Much of the work on alternatives has centered around the use of fluoroether-emulsifying agents (54–67). Replacements suitable for fine powder resins are also applicable to granular as well as TFE copolymer production.

The polymerization mechanism for fine powder is not a typical emulsion type but is subject to some of the principles of emulsion polymerization. The process and ingredients have a significant effect on the product. It is extremely important that the dispersion remains sufficiently stable throughout polymerization, avoiding premature coagulation (68) but unstable enough to allow subsequent coagulation into a fine powder. Gentle stirring ensures dispersion stability. The amount of emulsifying agent in the polymerization process is usually less than its critical micelle concentration.

The rate of polymerization and the particle shape are influenced by the amount of the emulsifying agent (69–72). The particle structure can be influenced by the polymerization process. Most of the particles are formed in the early stages of the polymerization process, and the particles grow as the batch progresses; hence, the radial variation in molecular weight and polymer composition within the dispersion particle can be achieved by controlling the polymerization variables, including ingredients and operating conditions (73–79).

The thin dispersion rapidly thickens into a gelled matrix and coagulates into a water-repellent agglomeration that floats on the aqueous medium as the mechanical agitation is continued. The agglomeration is dried gently; shearing must be avoided.

**Aqueous Dispersions.** Dispersion is made by the same polymerization process used to produce fine powders. Differences lie in the average particle sizes for dispersion products (80). The most common dispersion has an average particle size of about 0.2  $\mu\text{m}$ , probably the optimum particle size for most applications. In

recent years, modified dispersions are also sold. Efforts have been made to reduce the amount of fluorinated emulsifying agents in the dispersion and to recover these agents for reuse (81–83). The raw dispersion is stabilized with a nonionic or anionic surfactant and concentrated to 60–65 wt% solids by electrodecantation, evaporation, or thermal concentration (84). The concentrated dispersion can be further modified with chemical additives. Fabrication characteristics of these dispersions depend on polymerization conditions and additives.

**Filled Resins.** Fillers such as glass fibers, graphite, asbestos, or powdered metals are compounded into all three types of PTFE. Compounding is achieved by intimate mixing. Coagulation of the polymer with a filler produces a filled fine powder.

## Properties

The properties described herein are related to the basic structure of PTFE and are exhibited by both granular and fine powder products. The carbon–carbon bonds, which form the backbone of the PTFE chain, and the carbon–fluorine bonds are extremely strong and are the key contributors in imparting an outstanding combination of properties. The fluorine atoms form a protective sheath over the chain of carbon atoms. If the atoms attached to the carbon-chain backbone were smaller or larger than fluorine, the sheath would not form a regular uniform cover. This sheath shields the carbon chain from attack and confers chemical inertness and stability. It also reduces the surface energy, resulting in low coefficient of friction and nonstick properties.

Polytetrafluoroethylene does not dissolve in any common solvent; therefore, its molecular weight cannot be measured by the usual methods. A number-average molecular weight has been estimated by determining the concentration of end groups derived from the initiator. Earlier estimates, based on an iron bisulfite system containing radioactive sulfur,  $^{35}\text{S}$ , ranged from  $142 \times 10^3$  to  $534 \times 10^3$  for low molecular weight polymer. The same technique applied to polymers of industrial interest gave molecular weights of  $389 \times 10^3$  to  $8900 \times 10^3$  (85, 86). In the absence of a normal molecular weight determination method, an estimated relative molecular weight is used for all practical purposes. It is obtained by measuring the specific gravity (ASTM D792-08), following a standardized fabricating and sintering procedure (ASTM D4894-07, D4895-04, and D4441-04). Because the rate of crystallization decreases with increasing molecular weight, samples prepared from the high molecular weight polymer and cooled from the melt at a constant slow rate have lower standard specific gravities than those prepared from low molecular weight polymer cooled at the same rate (87). The correlation between number-average molecular weight ( $M_n$ ) based on end group estimations and standard specific gravity (SSG) is given by

$$\text{SSG} = 2.612 - 0.058 \log_{10} M_n$$

The SSG procedure assumes the absence of voids (or constant void content). Voids depress the values of the measured specific gravity. The inaccuracies that result from voids can be corrected by applying IR techniques (88).

Melting and recrystallization behavior of virgin PTFE have been studied by DSC (89). A quantitative relationship was found between  $M_n$  and the heat of crystallization ( $\Delta H_c$ ) in the molecular weight range of  $5.2 \times 10^5$  to  $4.5 \times 10^7$ , where  $\Delta H_c$  is heat of crystallization in J/g, which is independent of cooling rates of 4–32°C/min.

$$M_n = 2.1 \times 10^{10} \Delta H_c^{-5.16}$$

At ca 342°C, virgin PTFE changes from white crystalline material to almost transparent amorphous gel. Differential thermal analysis indicates that the first melting of virgin polymer is irreversible and that subsequent remeltings occur at 327°C, which is generally reported as the melting point. Most of the studies reported in the literature are based on previously sintered (ie, melted and recrystallized) polymer; very little work is reported on the virgin polymer. Melting is accompanied by a volume increase of ca 30%. Because the viscosity of the polymer at 380°C is 10 GPa-s ( $10^{11}$  P), the shape of the melt is stable. The melting point increases with increasing applied pressure at the rate of 1.52°C/MPa (0.154°C/atm) (90).

Virgin PTFE has a crystallinity in the range of 92–98%, which indicates an unbranched chain structure. The fluorine atoms are too large to allow a planar zigzag structure, which would permit chain flexibility; therefore, the chains are rigid (91). Electron micrographs and diffraction patterns (92) of PTFE dispersion particles indicate that the rod-like particles present in virgin PTFE dispersions are fully extended chain crystals containing few defects. The spherical particles appear to be composed of similar rod-like entities that are wrapped around themselves in a more or less random fashion.

Between 50 and 300°C, PTFE obeys the relationship between stress  $\tau$  and the apparent shear rate  $\dot{\gamma}$ :  $\tau = K\dot{\gamma}^{1/4}$ . Melting of PTFE begins near 300°C. Above this temperature, the shear stress at constant shear rate increases and the rheological exponent rises from 0.25 to 0.5 at the final melting point (93).

**Transitions.** Transitions observed by various investigators (94–100), their interpretation, and the modes of identification are shown in Table 2. Besides the transition at the melting point, the transition at 19°C is of great consequence because it occurs at ambient temperature and significantly affects the product behavior. Above 19°C, the triclinic pattern changes to a hexagonal unit cell. Around 19°C, a slight untwisting of the molecule from a 180° twist per 13 CF<sub>2</sub> groups to a 180° twist per 15 CF<sub>2</sub> groups occurs. At the first-order transition at 30°C, the hexagonal unit cell disappears and the rod-like hexagonal packing of the chains in the lateral direction is retained. Below 19°C, there is almost perfect three-dimensional order; between 19 and 30°C, the chain segments are disordered; and above 30°C, the preferred crystallographic direction is lost and the molecular segments oscillate above their long axes with a random angular orientation in the lattice.

The dynamic mechanical properties of PTFE have been measured at frequencies from 0.033 to 90 Hz. Abrupt changes in the distribution of relaxation times are associated with the crystalline transitions at 19 and 30°C (101). The activation energies are 102.5 kJ/mol (24.5 kcal/mol) below 19°C, 510.4 kJ/mol (122 kcal/mol) between the transitions, and 31.4 kJ/mol (7.5 kcal/mol) above 30°C.

**Table 2. Transitions in Polytetrafluoroethylene**

Temperature, °C	Region affected	Technique	Reference
1st order			
19	Crystalline, angular, displacement causing, disorder	Thermal methods, x ray, nmr	(95)
30	Crystalline, crystal disordering	Thermal methods, x ray, nmr	(95)
90 (80 to 110)	Crystalline	Stress relaxation, Young's modulus, dynamic methods	(98)
2nd order			
−90 (−110 to −73)	Amorphous, onset of rotational motion around C—C bond	Thermal methods, dynamic methods	(99)
−30 (−40 to −15)	Amorphous	Stress relaxation, thermal expansion, dynamic methods	(98)
130 (120 to 140)	Amorphous	Stress relaxation, Young's modulus, dynamic methods	(98)

Polytetrafluoroethylene transitions occur at specific combinations of temperature and mechanical or electrical vibrations. Transitions, sometimes called *dielectric relaxations*, can cause wide fluctuations in the dissipation factor.

**Mechanical Properties.** Mechanical properties of PTFE depend on processing variables, for example, preforming pressure, sintering temperature and time, cooling rate, void content, and crystallinity. Properties, such as the coefficient of friction, flexibility at low temperatures, and stability at high temperatures, are relatively independent of fabrication. Molding and sintering conditions affect flex life, permeability, stiffness, resiliency, and impact strength. The physical properties of PTFE have been reviewed and compiled (102–104) (Table 3).

A marked change in volume of 1.0–1.8% is observed for PTFE in the transition zone from 18 to 25°C. An article that has been machined on either side of this zone changes dimensions when passing through the transition zone; hence, the final operating temperature of a precision part must be accurately determined. Articles fabricated of PTFE resins exhibit high strength, toughness, and self-lubrication at low temperatures. They are useful from 5 K and are highly flexible from 194 K. They tend to return to their original dimensions after a deformation. At sintering temperature, they rapidly recover their original shapes. For most applications, no special precautions are necessary because decomposition rates below the recommended maximum service temperature of 260°C are very low. Impact strength is excellent over a wide range of temperatures. Static friction decreases with an increase in load. Static coefficient of friction is lower than the dynamic coefficient and therefore reduces stick–slip problems.

**Table 3. Typical Mechanical Properties of Molded and Sintered PTFE Resins<sup>a</sup>**

Property	Granular resin	Fine powder	ASTM method
Tensile strength at 23°C, MPa <sup>b</sup>	7–28	17.5–24.5	D638-61T
Elongation at 23°C, %	100–200	300–600	D628-61T
Flexural strength at 23°C, MPa <sup>b</sup>	Does not break		D790-61
Flexural modulus at 23°C, MPa <sup>b</sup>	350–630	280–630	D747-61T
Impact strength, J/m <sup>c</sup>			
at 21°C	106.7		D256–56
at 24°C	160		
at 77°C	>320		
Hardness durometer, D	50–65	50–65	D1706-59T
Compression stress, MPa <sup>b</sup>			
at 1% deformation at 23°C	4.2		D695-52T
at 1% offset at 23°C	7.0		D695-52T
Coefficient of linear thermal expansion	12 × 10 <sup>-5</sup>		D696-44
12 × 10 <sup>-5</sup> per °C, 23–60°C			
Thermal conductivity, 4.6-mm thickness, W/(m·K)	0.24		Cenco-Fitch
Deformation under load, at 26°C, 24 h, %			D621-59
6.86 MPa <sup>b</sup>		2.4	
13.72 MPa <sup>b</sup>	15		
Water absorption, %	<0.01	<0.01	D570-54T
Flammability	Nonflammable		D635-56T
Static coefficient of friction with polished, steel	0.05–0.08		

<sup>a</sup>Ref. (103).<sup>b</sup>To convert MPa to psi, multiply by 145.<sup>c</sup>To convert J/m to ft-lbf/in., divide by 53.38.

The surface of PTFE articles is slippery and smooth. Liquids with surface tensions below 18 mN/m (= dyn/cm) are spread completely on the PTFE surface; hence, solutions of various perfluorocarbon acids in water wet the polymer (105). Treatment with alkali metals promotes the adhesion between PTFE and other substances (106) but increases the coefficient of friction (107).

**Filled Resins.** Filled compositions meet the requirements of an increased variety of mechanical, electrical, and chemical applications. Physical properties of filled granular compounds are shown in Table 4 (108, 109).

**Chemical Properties.** Vacuum thermal degradation of PTFE results in monomer formation. The degradation is a first-order reaction (110). Mass spectroscopic analysis shows that degradation begins at ca 440°C, peaks at 540°C, and continues until 590°C (111).

**Radiation Effects.** Polytetrafluoroethylene is attacked by radiation. In the absence of oxygen, stable secondary radicals are produced. An increase in stiffness in material irradiated in vacuum indicates cross-linking (112). Degradation is due to random scission of the chain; the relative stability of the radicals in vacuum protects the materials from rapid deterioration. Reactions take place in air of oxygen and accelerated scission and rapid degradation occur.

Table 4. Properties of Filled PTFE Compounds<sup>a</sup>

Property	Unfilled	Glass fiber, wt%		Graphite, 15 wt%	Bronze, 60 wt%
		15	25		
Specific gravity	2.18	2.21	2.24	2.16	3.74
Tensile strength, MPa <sup>b</sup>	28	25	17.5	21	14
Elongation, %	350	300	250	250	150
Stress at 10% elongation, MPa <sup>b</sup>	11	8.5	8.5	11	14
Thermal conductivity, mW/(m·K)	0.244	0.37	0.45	0.45	0.46
Creep modulus, kN/m <sup>c</sup>	2	2.21	2.1	3.4	6.2
Hardness durometer, Shore D	51	54	57	61	70
Izod impact, J/m <sup>d</sup>	152	146	119		
PV <sup>e</sup> for 0.13-mm radial wear in 1000 h, unlubricated, (kPa·m)/s <sup>f</sup>	0.70	106	177	52	281
Wear factor, 1/Pa <sup>g</sup>	$5 \times 10^{-14}$	$28 \times 10^{-17}$	$26 \times 10^{-17}$	$100 \times 10^{-17}$	$12 \times 10^{-17}$
Coefficient of friction					
static, 3.4 MPa <sup>b</sup> load	0.08	0.13	0.13	0.10	0.10
dynamic at PV <sup>e</sup> = 172 (kPa·m)/s <sup>f</sup>		0.15–0.24	0.17	0.15	0.15
V = 900 m/s	0.01		–0.24	–0.18	–0.22

<sup>a</sup>Ref. (108).<sup>b</sup>To convert MPa to psi, multiply by 145.<sup>c</sup>To convert kN/m to lbf/in., divide by 0.175.<sup>d</sup>To convert J/m to ft·lbf/in., divide by 53.38.<sup>e</sup>PV = pressure × velocity.<sup>f</sup>To convert kPa to psi, multiply by 0.145.<sup>g</sup>To convert 1/Pa to (in<sup>3</sup>·min)/(ft·lbf·h), divide by  $2 \times 10^{-7}$ .

Crystallinity has been studied by X-ray irradiation (113). An initial increase caused by chain scission in the amorphous phase was followed (above 3 kGy or  $3 \times 10^5$  rad) by a gradual decrease associated with a disordering of the crystallites. The amorphous component showed a maximum of radiation-induced broadening in the NMR at 7 kGy ( $7 \times 10^5$  rad).

In air, PTFE has a damage threshold of 200–700 Gy ( $2 \times 10^4$  to  $7 \times 10^4$  rad) and retains 50% of initial tensile strength after a dose of  $10^4$  Gy (1 Mrad), 40% of initial tensile strength after a dose of  $10^5$  Gy ( $10^7$  rad), and ultimate elongation of 100% or more for doses up to 2–5 KGy ( $2 \times 10^5$  to  $5 \times 10^5$  rad). During irradiation, resistivity decreases, whereas the dielectric constant and the dissipation factor increase. After irradiation, these properties tend to return to their pre-exposure values. Dielectric properties at high frequency are less sensitive to radiation than are properties at low frequency. Radiation has very little effect on dielectric strength (114).

**Absorption, Permeation, and Interactions.** Polytetrafluoroethylene is chemically inert to industrial chemicals and solvents even at elevated temperatures and pressures (115). This compatibility is due to the strong interatomic

bonds, the almost perfect shielding of the carbon backbone by fluorine atoms, and the high molecular weight of the polymer. Under some severe conditions, PTFE is not compatible with certain materials. It reacts with molten alkali metals, fluorine, strong fluorinating agents, and sodium hydroxide above 300°C. Shapes of small cross section burn vertically upward after ignition in 100% oxygen. Because gases may be evolved, the weight loss during sintering of a blend of PTFE and white asbestos is many times greater than loss from pure PTFE. Finely divided aluminum and magnesium thoroughly mixed with finely divided PTFE react vigorously after ignition or at high temperatures.

Absorption of a liquid is usually a matter of the liquid dissolving in the polymer; however, in the case of PTFE, no interaction occurs between the polymer and other substances. Submicroscopic voids between the polymer molecules provide space for the material absorbed, which is indicated by a slight weight increase and sometimes by discoloration. Common acids or bases are not absorbed up to 200°C. Aqueous solutions are scarcely absorbed at atmospheric pressure. Even the absorption of organic solvents is slight, partially resulting from the low wettability of PTFE. Since absorption of chemicals or solvents has no substantial effect on the chemical bond within the fluorocarbon molecule, absorption should not be confused with degradation; it is a reversible physical process. The polymer does not suffer loss of mechanical or bulk electrical properties unless subjected to severely fluctuating conditions.

Dynamic mechanical measurements were made on PTFE samples saturated with various halocarbons (116). The peaks in loss modulus associated with the amorphous relaxation near -90°C and the crystalline relaxation near room temperature were not affected by these additives. An additional loss peak appeared near -30°C, and the modulus was reduced at all higher temperatures. The amorphous relaxation that appears as a peak in the loss compliance at 134°C is shifted to 45–70°C in the swollen samples.

The sorption behavior of perfluorocarbon polymers is typical of nonpolar partially crystalline polymers (117). The weight gain strongly depends on the solubility parameter. Little sorption of substances such as hydrocarbons and polar compounds occurs.

As an excellent barrier resin, PTFE is widely used in the chemical industry. However, it is a poor barrier for fluorocarbon oils because similarity in the chemical composition of a barrier and a permeant increases permeation. Most liquids and gases (other than fluorocarbons) do not permeate highly crystalline PTFE. Permeabilities at 30°C [in  $10^{15} \times \text{mol}/(\text{ms Pa})$ ] are as follows: CO<sub>2</sub>, 0.93; N<sub>2</sub>, 0.18; He, 2.47; anhydrous HCl, <0.01.

Gases and vapors diffuse through PTFE more slowly than through most other polymers (Table 5). The higher the crystallinity, and the less space between polymer molecules, the slower the permeation. Voids greater than molecular size cause an increase in permeability. However, the permeability of the finished article can be controlled by molding the resin to low porosity and high density. The optimum specific gravity for low permeability and good flexural properties is 2.16–2.195. Permeability increases with temperature as a result of the increase in activity of the solvent molecules and because of the increase in vapor pressure of the liquids. Swelling of PTFE resins and film is very low.



**Table 5. Permeability of PTFE Resin to Vapors**

Permeant	Permeability constant, <sup>a,b</sup> $\times 10^{15}$ mol/(m·s·Pa)	
	23°C	30°C
Benzene	1.81	2.93
Carbon tetrachloride	0.13	
Ethanol	1.88	
HCL, 20%	<0.71	
Piperidine	0.96	
H <sub>2</sub> SO <sub>4</sub> , 98%	54.20	
Water		20.70

<sup>a</sup>Ref. (115). Test method ASTM E96-35T (at vapor pressure; for 25.4- $\mu$ m film thickness). Values are averages only and not for specification purposes.

<sup>b</sup>Original data converted to SI units using vapor pressure data from Ref. (118).

**Table 6. Electrical Properties of Polytetrafluoroethylene<sup>a</sup>**

Property	Granular	Fine powder	ASTM method
Dielectric strength, short time, 2-mm thickness, V/mm	23,600	23,600	D149-55T
Surface arc-resistance, s	>300	>300	D495-55T
Volume resistivity, $\Omega$ ·cm	>10 <sup>18</sup>	>10 <sup>18</sup>	D257-57T
Surface resistivity at 100% Rh, $\Omega$ /sq	>10 <sup>16</sup>		D257-57T
Dielectric constant, at 60 to $2 \times 10^9$ Hz	2.1	2.1	D150-59T
Dissipation factor, at 60 to $2 \times 10^9$ Hz	0.0003		D150-59T

<sup>a</sup>Ref. (103).

**Electrical Properties.** Polytetrafluoroethylene is an excellent electrical insulator because of its mechanical strength and chemical and thermal stability, as well as excellent electrical properties (Table 6).

It does not absorb water, and volume resistivity remains unchanged even after prolonged soaking. The dielectric constant remains constant at 2.1 for a temperature range of -40 to 250°C and a frequency range of 5–10 GHz.

Articles fabricated according to standard practice should have dielectric constants in the range of  $2.05 \pm 0.5$  when tested at room temperature (RT). The dielectric constant varies with density and factors that affect density. Machined components can be fabricated to a predetermined dielectric constant by controlling the rod density during processing by adjusting the preforming pressure on the resin and cooling after sintering. The dielectric constant and the density have a linear relationship. Predictable variations in the dielectric constant result from density changes that accompany thermal expansion occurring with increasing temperature. The dielectric constant did not change over 2–3 years of measurements.

The dissipation factor (the ratio of the energy dissipated to the energy stored per cycle) is affected by the frequency, temperature, crystallinity, and void content of the fabricated structure. At certain temperatures and frequencies, the crystalline and amorphous regions become resonant. Because of the molecular vibrations, applied electrical energy is lost by internal friction within the polymer, which results in an increase in the dissipation factor. The dissipation factor peaks for these resins correspond to well-defined transitions, but the magnitude of the variation is minor as compared to other polymers. The low temperature transition at  $-97^{\circ}\text{C}$  causes the only meaningful dissipation factor peak. The dissipation factor has a maximum of  $10^8$ – $10^9$  Hz at RT; at high crystallinity (93%) the peak at  $10^8$ – $10^9$  Hz is absent.

As crystallinity increases, the internal molecular friction and the dissipation factor decrease. Voids reduce the dissipation factor in proportion to the percentage of microvoids present. Certain extruded shapes utilize air to reduce the effective dielectric constant and dissipation factor of a coaxial cable. The dielectric strength of these resins is high and is unaffected by thermal aging at  $200^{\circ}\text{C}$ . Frequency has a marked effect on the dielectric strength because corona discharge becomes more continuous as frequency increases. If the voltage stress is not high enough to cause corona ignition, a very long dielectric life is anticipated at any frequency. Corona discharges on the surface or in a void initiate dielectric breakdown (119). Surface arc resistance of these resins is high and not affected by heat aging. The resins do not track or form a carbonized conducting path when subjected to a surface arc in air. Polytetrafluoroethylene resins are capable of continuous service up to  $260^{\circ}\text{C}$  and can withstand much higher temperatures for limited periods of time. They do not melt or flow and retain some strength even in the gel state that begins at  $327^{\circ}\text{C}$ .

## Fabrication

**Granular Resins.** These resins are sold in different forms; an optimum balance between handleability and product properties is desired. A free-flowing resin is used in small and automatic moldings. A finely divided resin is more difficult to handle, but it distributes evenly in large moldings and has superior properties in sintered articles; it is used for large billet- and sheet-molding operations. A presintered resin with low crystallinity and superior handleability is highly suitable for ram extrusion.

Virgin PTFE melts at about  $342^{\circ}\text{C}$ ; viscosity, even at  $380^{\circ}\text{C}$ , is 10 GPa-s ( $10^{11}$  P). This eliminates processing by normal thermoplastic techniques, and other fabrication techniques had to be developed: The dry powder is compressed into handleable form by heating above the melting point. This coalesces the particles into a strong homogeneous structure; cooling at a controlled rate achieves the desired degree of crystallinity.

**Molding.** Many PTFE manufacturers give detailed descriptions of molding equipment, and procedures are presented in Reference (120). Round piston molds for the production of solid or hollow cylinders are the most widely used. Because preforming usually takes place below  $100^{\circ}\text{C}$ , carbon steel is a suitable material of construction. The compression ratio (ie, the bulk volume of the

powder to the specific volume of the unsintered molding) for granular resins is 3:1 to 6:1. The powder should be evenly distributed and leveled in the mold; and to ensure adequate compression uniformly throughout the preform, maximum pressure should be maintained for a sufficient length of time and then be released slowly.

Automatic molding permits high speed mass production and can be effective. Automatic presses can be operated mechanically, pneumatically, or hydraulically. The mold is filled by means of a special metering system from a storage hopper containing a free-flowing resin. Loading buckets that shuttle back and forth over the single-cavity mold are also used. Because automatic molding requires short cycles, the powder is usually compressed at high speed with a high preform pressure. Small articles such as rings, bushings, washers, gaskets, and ball-valve seats can be molded by this technique.

Isostatic molding allows uniform compression from all directions. A flexible mold is filled with a free-flowing granular powder and evacuated, tightly sealed, and placed in an autoclave containing a liquid that can be raised to the pressure required for performing. The moldings require subsequent finishing because close tolerance cannot be achieved.

**Sintering.** Electrical ovens with air circulation and service temperatures up to 400°C are satisfactory for sintering. In free sintering—the cheapest and most widely used process—a preformed mold is placed in an oven with a temperature variation of  $\pm 2^\circ\text{C}$ . In pressure sintering, the preform is not removed from the mold; instead the mold containing the preform is heated in an oven until the sintering temperature is reached. During sintering and cooling, the mold is again placed under pressure but lower than the preform pressure. Pressure-sintered products have internal stresses that can be relieved by subsequent annealing. In the pressure-cooling process, pressure is applied on the molded article after it has reached sintering temperature and is maintained throughout the cooling period. The final product has a lower void content than the free-sintered mold.

To improve homogeneity, the preformed article is heated to 370–390°C. The time required for heating and sintering depends on the mold dimensions; cooling, which affects the crystallinity and product properties, should be slow.

Free-sintered articles do not have the same dimensions as the mold cavity because they shrink at right angles to the direction of the preform pressure and grow in the direction of the applied pressure.

For processing after sintering, in the least expensive method for sintered PTFE tape or sheet, a large billet is skived on a lathe after it has been sintered and cooled. High precision articles are machined from ram-extruded rods.

Articles that are too complicated to be made by machining are made by coining. A sintered molding is heated to its melting point, transferred to a mold, and quickly deformed at low pressure, where it is held until it has cooled sufficiently to retain the improved shape. However, the coined molding, if reheated to a high temperature, returns to its original shape, and hence there is a limit on the maximum temperature to which coined moldings can be heated.

**Ram Extrusion.** Compression molding is not suitable for the manufacture of continuous long moldings such as pipes or rods. In ram extrusion, a small charge of PTFE powder is preformed by a reciprocating ram and sintered. Subsequent charges are fused into the first charge, and this process continues to form

homogeneous long rods (121). The die tube, which is made of a corrosion-resistant material, is heated by resistance heating. Good temperature control is essential, and the melted and compacted powder must not pass any constrictions in its path. Thermal expansion and friction produce great resistance to movement, and as a result, a considerable force is required to push the polymer through the tube. A high quality surface finish on the inside of the tube reduces the pressure. If adequate bond strength between successive charges is not developed, the extrudate may break at the interface (poker chipping). Free-flowing powders and presintered resins are preferred for ram extrusion. Ram-extruded rods are used for automatic screw machining. Tubing is used as pipe liners or stock from which seals, gaskets, and bellows are machined.

**Fine Powder Resins.** Fine powder PTFE resins are extremely sensitive to shear. They must be handled gently to avoid shear, which prevents processing. However, fine powder is suitable for the manufacture of tubing and wire insulation for which compression molding is not suitable. A paste-extrusion process may be applied to the fabrication of tubes with diameters from fractions of a millimeter to about a meter, walls from thicknesses of 100–400  $\mu\text{m}$ , thin rods with up to 50-mm diameters, and cable sheathing. Calendering unsintered extruded solid rods produces thread-sealant tape and gaskets.

The paste-extrusion process includes the incorporation of ca 16–25 wt% of the lubricant (usually a petroleum fraction); the mixture is rolled to obtain uniform lubricant distribution. This wetted powder is shaped into a preform at low pressure (2.0–7.8 MPa or 19–77 atm), which is pushed through a die mounted in the extruder at ambient temperature. The shear stress exerted on the powder during extrusion confers longitudinal strength to the polymer by fibrillation. The lubricant is evaporated, and the extrudate is sintered at ca 380°C.

The exact amount of lubricant required for extrusion depends on the design of the extruder, the reduction ratio (ie, ratio of the cross-sectional preform area to the cross-sectional area in the die), and the quality of the lubricant. A low lubricant content results in a high extrusion pressure, whereas a high lubricant content causes a poor coalescence and generates defects in the extrudate.

Fine powder resins can be colored with pigments that can withstand the sintering temperature. The pigment should be thoroughly mixed with the powder by rolling the mixture before adding the lubricant. Detailed design parameters of the paste extruder are given in References (120, 122, and 123).

The extrudate is dried and sintered by passing it through a multistage oven located immediately after the extruder. Pipes and rods may be heated up to 380°C. The throughput rate depends on the length of the sintering oven. Residence time varies from a few seconds for thin-walled insulations on a wire to a few minutes for large diameter tubing. For short residence times, temperatures may be as high as ca 480°C. The extrusion pressure depends on the reduction ratio, the extrusion rate, the lubricant content, and the characteristics of the extruder.

To produce unsintered tape by paste extrusion, the fine powder is lubricated and preformed according to the procedure described earlier. The preform is extruded in the form of rods, which are calendered on hot rolls to the desired width and thickness (124).

Different resins have been developed for use in different reduction–ratio application ranges (125, 126). The powders suitable for high reduction–ratio

applications, such as wire coatings, are not necessarily suitable for the medium reduction–ratio applications, such as tubings, or the low reduction–ratio applications, such as thread-sealant tapes or pipe liners. Applications and processing techniques are being used, which utilize the unique combination of properties offered by PTFE in fine powder form (127–129).

**Dispersion Resins.** Polytetrafluoroethylene dispersions in aqueous medium contain 30–60 wt% polymer particles and some surfactant. The type of surfactant and the particle characteristics depend on the application. These dispersions are applied to various substrates by spraying, flow coating, dipping, coagulating, or electrodepositing (130).

Aqueous dispersion is sprayed on metal substrates to provide chemical resistance, nonstick, and low friction properties. The coated surface is dried and sintered. Impregnation of fibrous or porous materials with these dispersions combines the properties of the materials with those of PTFE. Some materials require only a single dipping, for example, asbestos. The material is usually dried after dipping. For high pressure sealing applications, sintering at 380–400°C increases strength and dimensional stability. For film castings, the dispersion is poured on a smooth surface; the formed film is dried and sintered and peeled from the supporting surface.

Aqueous dispersions are used for spinning PTFE fibers. The dispersion is mixed with a matrix-forming medium (131, 132) and forced through a spinneret into a coagulating bath. The matrix material is removed by heating, and the fibers are sintered and drawn molten to develop their full strength.

**Effects of Fabrication on Physical Properties of Molded Parts.** The physical properties are affected by molecular weight, void content, and crystallinity. Molecular weight can be reduced by degradation but not increased during processing. These factors can be controlled during molding by the choice of resin and fabricating conditions. Void distribution (or size and orientation) also affects properties; however, it is not easily measured.

Preforming primarily affects void content, sintering controls molecular weight, and cooling determines crystallinity. Voids caused by insufficient consolidation of particles during preforming may appear in the finished articles. Densities below 2.10 g/cm<sup>3</sup> indicate a high void content. Electrical and chemical applications require a minimum density of 2.12–2.14 g/cm<sup>3</sup>. Particle size, shape, and porosity are also important in determining void content. Although void content is determined largely by particle characteristics and preforming conditions, sintering conditions can also have an effect. Temperatures too high or too low increase void content. Excessively high sintering temperature can decrease the molecular weight. The final crystallinity of a molding depends on the initial molecular weight of the polymer, the rate of cooling of the molding, and to a lesser extent on sintering conditions. The degree of crystallinity of moldings is affected by the cooling or annealing conditions.

Flexural modulus increases by a factor of 5 as crystallinity increases from 50 to 90% with a void content of 0.2%; however, recovery decreases with increasing crystallinity. Therefore, the balance between stiffness and recovery depends on the application requirements. Crystallinity is reduced by rapid cooling but increased by slow cooling. The stress-crack resistance of various PTFE insulations is correlated with the crystallinity and change in density due to thermal mechanical stress (133).

**Table 7. Applications of Polytetrafluoroethylene Resins**

Resin grade	Processing	Description	Main uses
<b>Granular</b>			
Agglomerates	Molding, preforming, sintering, ram extrusion	Free-flowing powder	Gaskets, packing, seals, electronic components, bearings, sheet, rod, heavy-wall tubing; tape and molded shapes for nonadhesive applications
Coarse	Molding, preforming, sintering	Granulated powder	Tape, molded shapes, nonadhesive applications
Finely divided	Molding, preforming, sintering	Powder for highest quality, void-free moldings	Molded sheets, tape wire wrapping, tubing, gaskets
Presintered	Ram extrusion	Granular, free-flowing powder	Rods and tubes
<b>Fine powder</b>			
High reduction ratio	Paste extrusion	Agglomerated powder	Wire coating, thin-walled tubing
Medium reduction ratio	Paste extrusion	Agglomerated powder	Tubing, pipe, overbraided hose, spaghetti tubing
Low reduction ratio	Paste extrusion	Agglomerated powder	Thread-sealant tape, pipe liners, tubing, porous structures
<b>Dispersion</b>			
General purpose	Dip coating	Aqueous dispersion	Impregnation, coating, packing
Coating	Dip coating	Aqueous dispersion	Film, coating
Stabilized	Coagulation	Aqueous dispersion	Bearings

## Applications

Consumption of PTFE increases continuously as new applications are being developed. Electrical applications consume half of the PTFE produced; mechanical and chemical applications share equally the other half. Various grades of PTFE and their applications are shown in Table 7.

**Electrical Applications.** The largest application of PTFE is for hookup and hookup-type wire used in electronic equipments in the military and aerospace industries. Coaxial cables, the second largest application, use tapes made from fine powder resins and some from granular resin. Interconnecting wire applications include airframes. Other electrical applications include computer wire, electrical tape, electrical components, and spaghetti tubing.

**Mechanical Applications.** Seals and piston rings, basic shapes, and antistick uses constitute two-thirds of the resin consumed in mechanical applications. Bearings, mechanical tapes, and coated glass fabrics also consume a large amount of PTFE resins. Seals and piston rings, bearings, and basic shapes are manufactured from granular resins, whereas the dispersion is used for glass-fabric coating and antistick applications. Most pressure-sensitive mechanical tapes are made from granular resins.

**Chemical Applications.** The chemical processing industry uses large amounts of granular and fine powder PTFE. Soft packing applications are manufactured from dispersions, and hard packings are molded or machined from stocks and shapes made from granular resin.

Overbraided hose liners are made from fine powder resins by paste extrusion, and thread-sealant tapes are produced from fine powder by calendering. Fabricated gaskets are made from granular resins, and pipe liners are produced from fine powder resins. Fibers and filament forms are also available.

Highly porous fabric structures, for example, Gore-Tex, which can be used as membranes, have been developed by exploiting the unique fibrillation capability of dispersion-polymerized PTFE (127).

## Micropowders

The PTFE micropowders, also called waxes, are TFE homopolymers with molecular weights significantly lower than that of normal PTFE (134). The molecular weight for micropowders varies from  $2.5 \times 10^4$  to  $25 \times 10^4$ , whereas that of normal PTFE is of the order of  $10 \times 10^6$ . Micropowders are generally white in color and are friable. The average agglomerate particle size is between 5 and 10  $\mu\text{m}$  and is composed of smaller, "as polymerized" primary particles, which are approximately 0.2  $\mu\text{m}$  in diameter. The DSC curves of lower molecular weight micropowder show a higher heat of crystallization and melting (second heating) than normal PTFE. This is due to the higher crystallinity of the micropowder.

The production of micropowders involves the scission of the high molecular weight PTFE chain by gamma or electron beam irradiation at a variety of dosage levels. An increase in dosage reduces the molecular weight. The irradiated low molecular weight material is ground to a particle size ranging from 1 to 25  $\mu\text{m}$  in the final product.

## Economic Aspects

Polytetrafluoroethylene homopolymers are more expensive than most other thermoplastics because of high monomer refining costs. For extremely high molecular weights, ingredients and manufacturing process must be free of impurities. In the United States, the 2008 list prices from primary producers were between \$21/kg and \$50/kg, depending on the resin type and quantity purchased. For example, granular PTFE resins cost \$21–27/kg supplied in 45.4-kg containers. The coagulated fine powders cost \$32–40/kg packaged in 25-kg containers. Formulated dispersions are \$32–50/kg in 19-L, 113-L, or 1041-L containers.

## Testing and Standards

A description of PTFE resins and their classification are given in ASTM D4894-07 for granular molding and extrusion materials, in ASTM D4895-04 for PTFE fine powders and in ASTM D4441-04 for aqueous dispersion of PTFE. A comprehensive listing of industrial and military specifications covering mechanical, electrical, and chemical applications of PTFE can be found in Reference (135).

## Health and Safety

Exposure to PTFE can arise from ingestion, skin contact, or inhalation. The polymer has no irritating effect to the skin, and test animals fed with the sintered polymer have not shown adverse reactions. Dust generated by grinding the resin also has no effect on test animals. Formation of toxic products is unlikely. Only the heated polymer is a source of a possible health hazard (136, 137).

Because PTFE resins decompose slowly, they may be heated to a high temperature. The toxicity of the pyrolysis products warrants care where exposure of personnel is likely to occur. Above 230°C, decomposition rates become measurable (0.0001% per hour). Small amounts of toxic perfluoroisobutylene have been isolated at 400°C and above; free fluorine has never been found. Above 690°C, the decomposition products burn but do not support combustion if the heat is removed. Combustion products consist primarily of carbon dioxide, carbon tetrafluoride, and small quantities of toxic and corrosive hydrogen fluoride. The PTFE resins are nonflammable and do not propagate flame.

Prolonged exposure to thermal decomposition products causes so-called polymer fume fever, a temporary influenza-like condition. It may be contracted by smoking tobacco that has been contaminated with the polymer. It occurs several hours after exposure and passes within 36–48 h; the temporary effects are not cumulative.

Large quantities of PTFE resins have been manufactured and processed above 370°C. In various applications, they are heated above the recommended use temperatures. No cases of serious injury, prolonged illness, or death have been reported resulting from the handling of these resins. However, when high molecular weight PTFE is converted to micropowder by thermal degradation, highly toxic products result.

Micropowders are added to a wide variety of material used in industry, where they provide nonstick and sliding properties (131). They are incorporated into the product by blending and grinding. To disperse well, the powder must have good flow properties. Conditions that make the powder sticky should be avoided.

The PTFE micropowders are commonly used in plastics, inks, lubricants, and finishes such as lacquer. Lubricants containing micropowders are used for bearings, valve components, and other moving parts where sliding friction must be minimized or eliminated. Nonstick finished that require good release properties, for example, in the food and packaging industry, commonly use PTFE micropowders.



In some applications, the high heat stability of the micropowder can be utilized over a reasonably wide temperature range. A maximum service temperature is normally 260°C, provided the crystalline melting point is between 320 and 335°C. Exposure above 300°C leads to degradation and possible evolution of toxic decomposition products.

The particulate morphology of PTFE micropowder in printing inks provides desirable gloss to the printed product. Its inherent lubricity results in good wear and slip properties and surface smoothness. The chemical resistance of the micropowder is as high as that of high molecular weight PTFE. It is therefore used in applications requiring service in strong or corrosive chemical environments such as concentrated mineral acids and alkalies.

## BIBLIOGRAPHY

"Tetrafluoroethylene Polymers" in *EPST* 1st ed., Vol. 13, pp. 623–654, by D. I. McCane, E. I. du Pont de Nemours & Co., Inc.; "Tetrafluoroethylene Polymers, Polytetrafluoroethylene (homopolymer)" in *EPSE* 2nd ed., Vol. 16, pp. 577–600, by S. V. Gangal, E. I. du Pont de Nemours & Co., Inc.; "Perfluorinated Polymers, Polytetrafluoroethylene" in *EPST* 3rd ed., Vol. 3, pp. 378–402, by S. V. Gangal, E. I. du Pont de Nemours & Co., Inc.

## CITED PUBLICATIONS

1. U.S. Pat. 2230654 (Feb. 4, 1941), R. J. Plunkett (to Kinetic Chemicals, Inc.).
2. J. D. Park and co-workers, *Ind. Eng. Chem.* **39**, 354 (1947).
3. J. M. Hamilton, in M. Stacey, J. C. Tatlow, and A. G. Sharpe, eds., *Advances in Fluorine Chemistry*, Vol. 3, Butterworth & Co., Ltd., Kent, UK, 1963, p. 117.
4. J. W. Edwards and P. A. Small, *Nature* **202**, 1329 (1964); *Ind. Eng. Chem. Fundam.* **4**, 396 (1965).
5. F. Gozzo and C. R. Patrick, *Nature* **202**, 80 (1964).
6. Jpn. Pat. 6015353 (Oct. 14, 1960), M. Hisazumi and H. Shingu.
7. U.S. Pat. 2994723 (Aug. 1, 1961), O. Scherer and co-workers (to Farbwerke Hoechst).
8. Brit. Pat. 960309 (June 10, 1964), J. W. Edwards, S. Sherratt, and P. A. Small (to ICI).
9. U.S. Pat. 3459818 (Aug. 5, 1969), H. Ukahashi and M. Hisasne (to Asahi Glass Co.).
10. U.S. Pat. 5345013 (Sept. 6, 1994), D. J. Van Bramer, M. B. Shiflett, and A. Yokozeki (to E. I. du Pont de Nemours & Co., Inc.).
11. U.S. Pat. 2407405 (Sept. 10, 1946), M. A. Dietrich and R. M. Joyce (to E. I. du Pont de Nemours & Co., Inc.).
12. O. Ruff and O. Bretschneider, *Z. Anorg. Allg. Chem.* **210**, 173 (1933).
13. E. G. Locke, W. R. Brode, and A. L. Henne, *J. Am. Chem. Soc.* **56**, 1726 (1934).
14. O. Ruff and W. Willenberg, *Chem. Ber.* **73**, 724 (1940).
15. L. T. Hals, T. S. Reid, and G. H. Smith, *J. Am. Chem. Soc.* **73**, 4054 (1951).
16. U.S. Pat. 2668864 (Feb. 9, 1954), Inventors: L. Hals, T. Reid and G. Smith (to Minnesota Mining and Manufacturing Co.).
17. U.S. Pat. 3009966 (Nov. 21, 1961), M. Hauptschein and A. H. Fainberg (to Pennsalt Chemical Corp.).
18. U.S. Pat. 3471546 (Oct. 7, 1969), G. Bjornson (to Phillips Petroleum Co.).
19. U.S. Pat. 3662009 (May 9, 1972), W. M. Hutchinson (to Phillips Petroleum Co.).

20. U.S. Pat. 3799996 (Mar. 26, 1974), H. S. Bloch (to Universal Oil Products).
21. E. E. Lewis and M. A. Naylor, *J. Am. Chem. Soc.* **69**, 1968 (1947).
22. U.S. Pat. 3832411 (Aug. 27, 1974), B. C. Arkles and R. N. Bonnett (to Liquid Nitrogen Processing Co.).
23. M. M. Renfrew and E. E. Lewis, *Ind. Eng. Chem.* **38**, 870 (1946).
24. H. C. Duus, *Ind. Eng. Chem.* **47**, 1445 (1955).
25. W. M. D. Bryant, *J. Polym. Sci.* **56**, 277 (1962).
26. A. Pajaczkowski and J. W. Spoors, *Chem. Ind.* **16**, 659 (1964).
27. Brit. Pat. 931587 (July 17, 1963), H. H. Gibbs and J. L. Warnell (to E. I. du Pont de Nemours & Co., Inc.).
28. U.S. Pat. 3159609 (Dec. 1, 1964), J. F. Harris Jr. and D. I. McCane (E. I. du Pont de Nemours & Co., Inc.).
29. F. S. Toby and S. Toby, *J. Phys. Chem.* **80**, 2313 (1976).
30. B. Atkinson and V. A. Atkinson, *J. Chem. Soc. Part II* 2086 (1957).
31. U.S. Pat. 2946763 (July 26, 1960), M. I. Bro and B. W. Sandt (to E. I. du Pont de Nemours & Co., Inc.).
32. U.S. Pat. 3847881 (Nov. 12, 1974), M. Mueller and S. Chandrasekaran (to Allied Chemicals Co.).
33. U.S. Pat. 3528954 (Sept. 15, 1970), D. P. Carlson (to E. I. du Pont de Nemours & Co., Inc.).
34. U.S. Pat. 5760151 (June 2, 1998) R. Aten, C. W. Jones, and A. H. Olson (to E. I. du Pont de Nemours & Co., Inc.).
35. U.S. Pat. 3475391 (Oct. 28, 1969), J. N. Coker (to E. I. du Pont de Nemours & Co., Inc.).
36. U.S. Pat. 3846267 (Nov. 5, 1974), Y. Tabata and G. Kojima (to Japan Atomic Energy Research Institute).
37. U.S. Pat. 3467636 (Sept. 16, 1969), A. Nersasian (to E. I. du Pont de Nemours & Co., Inc.).
38. U.S. Pat. 3403191 (Sept. 24, 1968), D. P. Graham (to E. I. du Pont de Nemours & Co., Inc.).
39. U.S. Pat. 3404180 (Oct. 1, 1969), K. L. Cordes (to E. I. du Pont de Nemours & Co., Inc.).
40. U.S. Pat. 3567521 (Mar. 2, 1971), M. S. Toy and N. A. Tiner (to McDonnell Douglas).
41. U.S. Pat. 3446858 (May 27, 1969), H. Shingu and co-workers (to Daikin Kogyo Co.).
42. U.S. Pat. 3873630 (Mar. 25, 1975), N. E. West (to E. I. du Pont de Nemours & Co., Inc.).
43. U.S. Pat. 6531559 (Mar. 11, 2003), P. Smith, J. Visjager, C. Bastiaansen, and T. Tervoort (to Eidgenossische Technische Hochschule).
44. U.S. Pat. 3855191 (Dec. 17, 1974), T. R. Doughty, C. A. Sperati, and H. Un (to E. I. du Pont de Nemours & Co., Inc.).
45. U.S. Pat. 3655611 (Apr. 11, 1972), M. B. Mueller, P. O. Salatiello, and H. S. Kaufman (to Allied Chemicals Co.).
46. K. Hintzer and G. Lohn, in Scheirs, ed., *Modern Fluoropolymers*, John Wiley & Sons, New York, 1997, pp. 239–255.
47. U.S. Pat. 4189551 (Feb. 19, 1980), S. V. Gangal (to E. I. du Pont de Nemours & Co., Inc.).
48. U.S. Pat. 3419522 (Dec. 31, 1968), P. N. Plimmer (to E. I. du Pont de Nemours & Co., Inc.).
49. U.S. Pat. 3766133 (Oct. 16, 1973), R. Roberts and R. F. Anderson (to E. I. du Pont de Nemours & Co., Inc.).
50. Jap. Pat. WO9905203 (Feb. 4, 1999), A. Funaki and T. Takakura (to Asahi Glass Co., Ltd.).

51. Jap. Pat. WO9906475 (Feb. 11, 1999), M. Asano, M. Sukegawa, and M. Tsuji (to Daikin Industries, Ltd.).
52. U.S. Pat. 2612484 (Sept. 30, 1952), S. G. Bankoff (to E. I. du Pont de Nemours & Co., Inc.).
53. Callie Lyons, *Stain-Resistant, Nonstick, Waterproof, and Lethal: The Hidden Dangers of C8*, Praeger Publishers, Westport, Conn., 2007.
54. U.S. Pat. Appl. 0015864 (Jan. 18, 2007), K. Hintzer and co-workers (to 3M Innovative Properties Company).
55. U.S. Pat. Appl. 0015865 (Jan. 18, 2007), K. Hintzer, M. Jurgens, H. Kaspar, K. Lochhaas, A. Maurer, and T. Zipplies (to 3M Innovative Properties Company).
56. U.S. Pat. Appl. 0015866 (Jan. 18, 2007), K. Hintzer, H. Kaspar, A. Maurer, W. Schwertfeger and T. Zipplies (to 3M Innovative Properties Company).
57. U.S. Pat. Appl. 0200571 (Aug. 21, 2008), S. Higuchi, H. Kamiya, J. Hoshikawa and Y. Matsuoka (to Asahi Glass Co. Ltd.).
58. U.S. Pat. Appl. 0207859 (Aug. 2008), Y. Matsuoka, S. Higuchi, J. Hoshikawa and H. Kamiya (to Asahi Glass Co. Ltd.).
59. U.S. Pat. 6878722 (Apr. 2005), M. Visca, A. Chittofrati, V. Kapeliouchko, and M. Malvasi (to Solvay Solexis S.p.A.).
60. WO Pat. Appl. 003929 (Jan. 14, 2010), G. Marchionni, V. Tortelli, I. Wlassics, and V. Kape-Liouchko (to Solvay Solexis S.p.A.).
61. Jap. Pat. 3900883 (Jan. 12, 2007), Y. Homoto, Y. Negishi, and W. Morimoto (to Daikin Industries, Ltd.).
62. U.S. Pat. Appl. 0176942 (Jul. 9, 2009), T. Ishikawa, N. Tsuda, and Y. Yamamoto (to Daikin Industries, Ltd.).
63. U.S. Pat. 7589234 (Sept. 15, 2009), S. Morita, Y. Tanaka, K. Washino, N. Tsuda and M. Kishine (to Daikin Industries, Ltd.).
64. U.S. Pat. 3271341 (Sept. 6, 1966), W. Garrison (to E. I. du Pont de Nemours & Co., Inc.).
65. U.S. Pat. 7705074 (Apr. 27, 2010), P. Brothers and S. Gangal (to E. I. du Pont de Nemours & Co., Inc.).
66. U.S. Pat. Appl. 0114122 (May. 15, 2008), P. Brothers and S. Gangal (to E. I. du Pont de Nemours & Co., Inc.).
67. U.S. Pat. Appl. 0281261 (Nov. 12, 2009), P. Brothers, L. Leung, and S. Gangal (to E. I. du Pont de Nemours & Co., Inc.).
68. U.S. Pat. 4186121 (Jan. 29, 1980), S. V. Gangal (to E. I. du Pont de Nemours & Co., Inc.).
69. U.S. Pat. 4725644 (Feb. 16, 1988), S. Malhotra (to E. I. du Pont de Nemours & Co., Inc.).
70. T. Folda and co-workers, *Nature* **333**, 55 (1988).
71. B. Luhmann and A. E. Feiring, *Polymer* **30**, 1723 (1989).
72. B. Chu, C. Wu, and W. Buck, *Macromolecules* **22**, 831 (1989).
73. U.S. Pat. 4576869 (Mar. 18, 1986), S. C. Malhotra (to E. I. du Pont de Nemours & Co., Inc.).
74. U.S. Pat. 4363900 (Dec. 14, 1982), T. Shimizu and S. Koizumi (to Daikin Kogyo Co.).
75. U.S. Pat. 4766188 (Aug. 23, 1988), T. E. Attwood and R. F. Bridges (to ICI).
76. U.S. Pat. 4036802 (July 19, 1977), R. V. Poirier (to E. I. du Pont de Nemours & Co., Inc.).
77. U.S. Pat. 4129618 (Dec. 12, 1978), J. M. Downer, W. G. Rodway, and L. S. J. Shipp (to ICI).
78. U.S. Pat. 4840998 (June 6, 1989), T. Shimizu and K. Hosokawa (to Daikin Kogyo Co.).
79. U.S. Pat. 4879362 (Nov. 7, 1979), R. A. Morgan (to E. I. du Pont de Nemours & Co., Inc.).

80. U.S. Pat. 4342675 (Aug. 3, 1982), S. V. Gangal (to E. I. du Pont de Nemours & Co., Inc.).
81. U.S. Pat. 3882153 (May 6, 1975) S. Seki and K. Sato (to Kureha Kagaku Kogyo Kabushiki Kaisha).
82. U.S. Pat. 4282162 (Aug. 4, 1981) Jurgen Kuhls (to Hoechst Aktiengesellschaft)
83. U.S. Pat. 6833403 (Dec. 21, 2004) H. Bladel, K. Hintzer, G. Lohr, W. Schwertfeger, and R. Sulzbach (to 3M Innovative Properties Co.).
84. U.S. Pat. 2478229 (Aug. 9, 1949), K. L. Berry (to E. I. du Pont de Nemours & Co., Inc.).
85. K. L. Berry and J. H. Peterson, *J. Am. Chem. Soc.* **73**, 5195 (1951).
86. R. C. Doban and co-workers, paper presented at 130th Meeting of the American Chemical Society, Atlantic City, N. J., Sept. 1956.
87. C. A. Sperati and H. W. Starkweather, *Fortschr. Hochpolym. Forsch.* **2**, 465 (1961).
88. R. E. Moynihan, *J. Am. Chem. Soc.* **81**, 1045 (1959).
89. T. Suwa, M. Takehisa, and S. Machi, *J. Appl. Polym. Sci.* **17**, 3253 (1973).
90. P. L. McGeer and H. C. Duus, *J. Chem. Phys.* **20**, 1813 (1952).
91. C. W. Bunn, *J. Polym. Sci.* **16**, 332 (1955).
92. H. D. Chanzy, P. Smith, and J. Revol, *J. Polym. Sci. Polym. Lett. Ed.* **24**, 557 (1986).
93. H. W. Starkweather Jr., *J. Polym. Sci. Polym. Phys. Ed.* **17**, 73–79 (1979).
94. U.S. Pat. 4840998 (June 6, 1989), R. H. H. Pierce and co-workers, (to Daikin Kogyo Co.).
95. E. S. Clark, and L. T. Muus, paper presented at 133rd Meeting of the American Chemical Society, New York, Sept. 1957.
96. E. S. Clark, paper presented at Symposium on Helices in Macromolecular Systems, Polytechnic Institute of Brooklyn, Brooklyn, N.Y., May 16, 1959.
97. C. A. Sperati, in J. Brandrup and E. H. Immergut, eds., *Polymer Handbook*, 2nd ed., John Wiley & Sons, Inc., New York, 1975, pp. V-29–V-36.
98. Y. Araki, *J. Appl. Polym. Sci.* **9**, 3585 (1965).
99. N. G. McCrum, *J. Polym. Sci.* **34**, 355 (1959).
100. E. S. Clark, *Polymer* **40** (16), 4659–4665 (1999).
101. H. W. Starkweather Jr., *Macromolecules* **19**, 2541 (1986).
102. J. T. Milek, A Survey Materials Report on PTFE Plastics, AD 607798, U.S. Department of Commerce, Washington, D.C., Sept. 1964.
103. Teflon<sup>®</sup> Fluorocarbon Resins Mechanical Design Data, Bulletin, E. I. du Pont de Nemours & Co., Inc. Wilmington, Del., Sept. 1964.
104. Teflon<sup>®</sup> PTFE Fluoropolymers Resin, Properties Handbook, Bulletin H-37051-4, E. I. du Pont de Nemours & Co., Inc., Wilmington, Del., Jan. 2004.
105. M. K. Burnett and W. A. Zisman, *J. Phys. Chem.* **63**, 1911 (1959).
106. U.S. Pat. 2871144 (Jan. 27, 1959), R. C. Doban (to E. I. Du Pont de Nemours & Co., Inc.).
107. A. J. G. Allan and R. Roberts, *J. Polym. Sci.* **39**, 1 (1959).
108. Filled Compounds of Teflon<sup>®</sup> PTFE, Bulletin E-96215, E. I. du Pont de Nemours & Co., Inc., Wilmington, Del., Mar. 1989.
109. Teflon<sup>®</sup> Fluoropolymer, Technical Information, A Tribological Characterization of Teflon<sup>®</sup> PTFE Compounds, Bulletin H-38205, E. I. du Pont de Nemours & Co., Inc., Wilmington, Del., June 1992.
110. J. C. Siegle and co-workers, *J. Polym. Sci. Part A* **2**, 391 (1964).
111. G. P. Shulman, *Polym. Lett.* **3**, 911 (1965).
112. L. A. Wall and R. E. Florin, *J. Appl. Polym. Sci.* **2**, 251 (1959).
113. W. M. Peffley, V. R. Honnold, and D. Binder, *J. Polym. Sci.* **4**, 977 (1966).
114. *J. Teflon<sup>®</sup>* (DuPont) 10(1) (Jan.–Feb. 1969).
115. *J. Teflon<sup>®</sup>* (DuPont) 11(1) (Jan.–Feb. 1970).

116. H. W. Starkweather Jr., *Macromolecules* **17**, 1178 (1984).
117. H. W. Starkweather Jr., *Macromolecules* **10**, 1161 (1977).
118. D. W. Green, ed., *Perry's Chemical Engineers' Handbook*, 6th ed., McGraw-Hill Book Co., Inc., New York, 1984.
119. J. C. Reed, E. J. McMahon, and J. R. Perkins, *Insulation (Libertyville, III.)* **10**, 35 (1964).
120. S. Ebnesajjad, *Non-melt Processible Fluoroplastics*, Vol. 1, Plastics Design Library, Division of William Andrew, Inc., Norwich, N.Y., 2000. Handbook Series.
121. Teflon<sup>®</sup> PTFE Fluoropolymer Resin, Ram Extrusion Processing Guide, Bulletin H-96545, E. I. du Pont de Nemours & Co., Inc., Dec. 2003.
122. Teflon<sup>®</sup> Fluoropolymer Resin, Processing Guide for Fine Powder Resins, Bulletin 190617D, E. I. du Pont de Nemours & Co., Inc., Dec. 1994.
123. Teflon<sup>®</sup> 62, Hose and Tubing, Bulletin H-11959, E. I. du Pont de Nemours & Co., Inc. Feb. 1991.
124. Teflon<sup>®</sup> PTFE, Thread Sealant Tape Processing Guide, Bulletin H-96515, E. I. du Pont de Nemours & Co., Inc., Jan. 2004.
125. U.S. Pat. 3142665 (July 28, 1964), A. J. Cardinal, W. L. Edens, and J. W. Van Dyk (to E. I. du Pont de Nemours & Co., Inc.).
126. U.S. Pat. 4038231 (July 26, 1977), J. M. Douner, W. G. Rodway, and L. S. J. Shipp (to ICI).
127. U.S. Pat. 3962153 (June 8, 1976), R. W. Gore (to W. L. Gore and Associates).
128. U.S. Pat. 3993584 (Nov. 23, 1976), J. E. Owen and J. W. Vogt (to Kewanee Oil Co.).
129. U.S. Pat. 3704171 (Nov. 28, 1972), H. P. Landi (to American Cyanamid Co.).
130. DuPont Fluoroproducts, Dispersions Properties and Processing Guide, Bulletin H-92067, Oct. 2001.
131. U.S. Pat. 3051545 (Aug. 28, 1962), W. Steuber (to E. I. du Pont de Nemours & Co., Inc.).
132. P. E. Frankenburg, *Ullmann's Encyclopedia of Industrial Chemistry*, 5th ed., Vol. A-10, VCH Publishing, Inc., New York, 1987, p. 649, 650.
133. R. L. Baillie, J. J. Bednarczyk, and P. M. Mehta, paper presented at 35th International Wire and Cable Symposium, Chery Hill, N.J., Nov. 18–20, 1986.
134. Zonyl<sup>®</sup> Fluoroadditives, Bulletin H-81712, E. I. du Pont de Nemours & Co., Inc., Sept. 1995.
135. *J. Teflon<sup>®</sup>* (Du Pont) 8, 6 (Nov. 1967).
136. *Teflon<sup>®</sup> Occupational Health Bull.* **17**(2) (1962) (Published by Information Service Division, Department of National Health and Welfare, Ottawa, Canada).
137. *Guide to the Safe Handling of Fluoropolymer Resins*, 4rd ed., Fluoropolymers Division of the Society of the Plastics Industry, Inc., Washington, D. C., Nov. 2005.

SUBHASH V. GANGAL

PAUL D. BROTHERS

E. I. du Pont de Nemours & Co., Inc.  
Wilmington, Delaware

## PERFLUORINATED POLYMERS, TETRAFLUOROETHYLENE–ETHYLENE COPOLYMERS

### Introduction

Copolymers of ethylene [74-85-1] and tetrafluoroethylene [116-14-3] (ETFE) have been a laboratory curiosity for more than half a century. These polymers were studied in connection with a search for a melt-fabricable polytetrafluoroethylene (PTFE) resin (1–5); interest in them lessened with the discovery of TFE–HFP (FEP) copolymers (6). In the 1960s, however, it became evident that a melt-fabricable fluorocarbon resin with higher strength and stiffness was needed than those of PTFE resins. Earlier studies indicated that ETFE [11939-51-6] might have the right combination of properties. Subsequent research efforts (7) led to the introduction of modified ETFE polymer [25038-71-5] (Tefzel) by DuPont in 1970.

Modified ETFE are the products of real commercial value because they have good tensile strength, moderate stiffness, high flex life, and outstanding impact strength, abrasion resistance, and cut-through resistance. Electrical properties include low dielectric constant, high dielectric strength, excellent resistivity, and low dissipation factor. Thermal and cryogenic performance and chemical resistance are good. These properties, combined with elasticity, make this material an ideal candidate for heat-shrinkable film and tubing. This family of copolymers can be processed by conventional methods such as melt extrusion, injection molding, transfer molding, and rotational molding. The properties of the copolymers vary with composition; polymers containing 40–90% TFE (by weight) soften between 200°C and 300°C, depending on composition (1). The TFE segments of the molecules account for more than 75% of the weight of an approximately 1:1 mole ratio copolymer. The two monomers combine readily into a nearly 1:1 alternating structure. Such polymers exhibit a unique combination of mechanical, chemical, and electrical properties, as well as excellent weatherability. However, thermal stress-crack resistance is poor. The copolymer can be modified with a termonomer that undergoes free-radical polymerization and does not cause undesirable chain transfer or termination during polymerization. The modified copolymer exhibits almost the identical physical, chemical, and electrical properties characteristic of the 1:1 alternating copolymer but retains high ultimate elongation up to 200°C.

Ethylene and TFE are copolymerized in aqueous, nonaqueous, or mixed medium with free-radical initiators. The polymer is isolated and converted into extruded cubes, powders, and beads or into dispersion. This family of products is sold by DuPont, Dyneon, Daikin, Asahi Glass, and Solvay under the trade names of Tefzel, Hostafion ET, Neoflon EP, Aflon COP, and Halon ET, respectively. Additional information on specific manufacturers' products can often be obtained by consulting their Internet Web sites.

### Monomers

Tetrafluoroethylene of purity suitable for granular or dispersion polymerizations is acceptable for copolymerization with ethylene. Polymerization-grade ethylene

is suitable for copolymerization with TFE. Modifying termonomers (e.g., perfluorobutylethylene and perfluoropropylene) are incorporated by free-radical polymerization.

## Manufacture

Tetrafluoroethylene–ethylene copolymers have tensile strengths two to three times as high as the tensile strength of PTFE or of the ethylene homopolymer (1). Because these copolymers are highly crystalline and fragile at high temperature, they are modified with a third monomer, usually a vinyl monomer free of telegenic activity. The termonomer provides the copolymer with side chains of at least two carbon atoms, such as perfluoroalkylvinyl or vinylidene compounds, perfluoroalkyl ethylenes, and perfluoroalkoxy vinyl compounds. For high tensile properties and cut-through resistance, a molar ratio of ethylene and TFE between 60:40 and 40:60 is required (8,9).

Copolymerization is effected by suspension or emulsion techniques under such conditions that TFE, but not ethylene, may homopolymerize. Bulk polymerization is not commercially feasible because of heat-transfer limitations and explosion hazard of the comonomer mixture. Polymerizations typically take place below 100°C and 5 MPa (50 atm). Initiators include peroxides, redox systems (10), free-radical sources (11), and ionizing radiation (12). Mixtures of inert solvent and water can be used, in which the polymerization occurs in the solvent medium whereas the water serves both to lower the viscosity of the mixture and to remove the heat of polymerization (13,14).

Purely aqueous polymerization systems give copolymers that are not wetted by the reaction medium. The products agglomerate and plug valves, nozzles, and tubing and adhere to stirrer blades, thermocouples, or reactor walls. These problems are not as prevalent in organic media or mixtures of these with water.

Aqueous emulsion polymerization is carried out with a fluorinated emulsifier, a chain-transfer agent to control molecular weight, and dispersion stabilizers such as manganic acid salts and ammonium oxalate (15,16).

To obtain a 50:50 molar ratio of monomers in the polymer, a mixture of about 75:25 TFE to ethylene must be initially charged to the reactor, depending on reactor pressure and temperature. Reactivity ratios for this system have been studied (17,18). The effects of temperature, addition of termonomer, and ethylene/TFE ratio on both the degree of alternation and the molecular structure have been studied (19). Melting points of ETFE are higher than would be predicted on the basis of a linear relationship between polyethylene and PTFE melting points. ETFE is unique in this respect. All other common copolymers of TFE exhibit either linear or depressed melting points when compared with a line between the respective homopolymer melting point and that of PTFE. This positive melting point deviation occurs from about 35:65 to 65:35 mole ratios and is at a maximum at the 50:50 alternating copolymer, which melts at about 285°C, compared with about 235°C for the 65:35 TFE/ethylene composition. Melting points are lowered by the incorporation of modifier, but the overall shape of a curve of the positive melting point deviation is unaltered. The ability of adjacent chains to interpenetrate is thought to be responsible for this behavior. For the same reason, stiffness follows

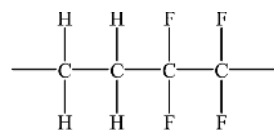
a similar positive deviation, also reaching a maximum at the 50:50 composition. Reactivity ratios of ethylene and TFE are as follows:

Temperature, °C	$r(\text{C}_2\text{F}_4)$	$r(\text{C}_2\text{H}_4)$
-35	$0.014 \pm 0.008$	$0.010 \pm 0.02$
65	$0.045 \pm 0.010$	$0.14 \pm 0.03$

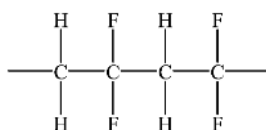
These values indicate strong alternation tendencies that decrease with increasing temperature. Computations show that 1:1 ETFE obtained at -30 and 65°C should have about 97 and 93%, respectively, of alternating sequences (20).

## Properties

The equimolar copolymer of ethylene and TFE is isomeric with poly(vinylidene fluoride) but has a higher melting point (21,22) and a lower dielectric loss (23,24). A copolymer with the degree of alternation of about 0.88 was used to study the structure (25). The unit cell was determined by x-ray diffraction (26,27). Despite irregularities in the chain structure and low crystallinity, a unit cell and structure was derived that gave a calculated crystalline density of 1.9 g/cm<sup>3</sup>. The unit cell is believed to be orthorhombic or monoclinic ( $a = 0.96$  nm,  $b = 0.925$  nm,  $c = 0.50$  nm;  $\gamma = 96^\circ$ ).



Ethylene-tetrafluoroethylene unit



Poly(vinylidene fluoride) segment

The molecular conformation is that of extended zigzag. Molecular packing appears to be orthorhombic, each molecule having four nearest neighbors with the CH<sub>2</sub> groups of one chain adjacent to the CF<sub>2</sub> groups of the next. The x-ray spectrum of a 1:1 copolymer has two main peaks at  $2\theta = 19.63^\circ$  and  $2\theta = 21.00^\circ$ , corresponding to Bragg distances of 0.45 and 0.42 nm, respectively. Compression-molded samples are 50–60% crystalline; however, crystallinity is greatly affected by composition, quench rate, and temperature.

Alternation is usually above 90%. Nearly perfect alternation of isomeric units in an approximately 1:1 monomer ratio has been confirmed by infrared (IR) spectroscopy. Bands at 733 and 721 cm<sup>-1</sup> have an intensity proportional to the concentration of (CH<sub>2</sub>)<sub>n</sub> groups ( $n = 4$  and  $n < 6$ , respectively) present in a



copolymer containing 46 mol% TFE; intensity decreases with increasing concentration of fluorinated monomer.

The molecular weight and its distribution have been determined by laser light scattering, employing a new apparatus for ETFE dissolution and solution clarification at high temperature; diisobutyl adipate is the solvent of choice at 240°C. The molecular weight of molten ETFE is determined by high temperature rheometry (28).

This polymer can be dissolved in certain high boiling esters at temperatures above 230°C (29–31), permitting a weight-average molecular weight determination by light scattering. Solution viscosity data suggest that the polymer exists as a slightly expanded coil under similar conditions (32).

**Transitions.** Samples containing 50 mol% TFE with approximately 92% alternation were quenched in ice water or cooled slowly from the melt to minimize or maximize crystallinity, respectively (24). Internal motions were studied by dynamic mechanical and dielectric measurements and by nuclear magnetic resonance. The dynamic mechanical behavior showed that the  $\alpha$ -relaxation occurs at 110°C in the quenched sample; in the slowly cooled sample, it is shifted to 135°C. The  $\beta$ -relaxation appears near –25°C. The  $\gamma$ -relaxation at –120°C in the quenched sample is reduced in peak height in the slowly cooled sample and shifts to a slightly higher temperature. The  $\alpha$ - and  $\gamma$ -relaxations reflect motions in the amorphous regions, whereas the  $\beta$ -relaxation occurs in the crystalline regions. The  $\gamma$ -relaxation at –120°C in dynamic mechanical measurements at 1 Hz appears, whereas it appears at –35°C in dielectric measurements at  $10^5$  Hz. The temperature of the  $\alpha$ -relaxation varies from 145°C at 100 Hz to 170°C at  $10^5$  Hz. In the mechanical measurement, it is 110°C. There is no evidence for relaxation in the dielectric data.

The activation energy is 318.1 kJ/mol (76 kcal/mol) for the  $\alpha$ -relaxation and 44.3 kJ/mol (10.6 kcal/mol) for the  $\gamma$ -relaxation. These relaxations are attributed to the motion of long and short segments in the amorphous regions, respectively. As ETFE is isomeric with poly(vinylidene fluoride) (23), the  $\gamma$ -relaxation occurs at about the same temperature. Activation energies are similar and are attributed to the motion of short amorphous segments. The  $\beta$ -relaxation in poly(vinylidene fluoride) (PVF2) is considered to be the main-chain amorphous relaxation and is analogous to the  $\alpha$ -relaxation in the ETFE. However, the arrangement of dipoles in the all-*trans* conformation is more symmetrical.

**Physical and Mechanical Properties.** Modified ETFE has a good combination of mechanical properties, including excellent cut-through and abrasion resistance, high flex life, and exceptional impact strength. As wire insulation, it withstands physical tempering during and after installation. Lightweight wire constructions are designed with a minimum diameter and are useful as single, general-purpose insulation and for multiple or composite constructions.

Modified ETFE is less dense, tougher, and stiffer and exhibits a higher tensile strength and creep resistance than PTFE, perfluoroalkoxy (PFA), or fluorinated ethylene propylene (FEP) resins. It is ductile and displays, in various compositions, the characteristic of a nonlinear stress–strain relationship. Typical physical properties of Tefzel products are shown in Table 1 (33,34). Properties such as elongation and flex life depend on crystallinity, which is affected by the rate of crystallization; fabrication conditions, and melt cooling rates.

Table 1. Typical Properties of Tefzel<sup>a</sup>

	ASTM method	Tefzel 200, 280	Tefzel <sup>b</sup> HT-2004
Ultimate tensile strength, MPa <sup>c</sup>	D638	44.8	82.7
Ultimate elongation	D887-64T	200 <sup>d</sup>	8
Compressive strength, MPa <sup>c</sup>	D695	48.9	68.9
Shear strength, MPa <sup>c</sup>		41.3	44.8
Heat deflection temperature, °C	D648		
(at 0.45 MPa)		104	265
(at 1.8 MPa)		74	210
Maximum continuous use temperature, no load, °C		150 <sup>e</sup>	200
Low temperature embrittlement	D746	below -100°C	
Tensile modulus, MPa <sup>c</sup>	D638	827	8270
Flexural modulus, MPa <sup>c</sup>	D790	96.5	6550
Impact strength notched Izod	D256		
°(at -54°C), J/m <sup>f</sup>		>1067	373
°(at 23°C)		No break	485
Deformation under load, 13.7 MPa (at 50°C), %	D621	4.11	0.68
Coefficient of linear expansion per °C	D696-70		
20–30°C		$9 \times 10^{-5}$	$3 \times 10^{-5}$
50–90°C		$9.3 \times 10^{-5}$	$1.7 \times 10^{-5}$
140–180°C		$14 \times 10^{-5}$	$3.2 \times 10^{-5}$
Specific gravity	D792	1.70	1.86
Refractive index ( $n_D$ )		1.4028	
Flammability	UL 94	94V-O	94V-O
	D635	ATB <sup>g</sup> < 5 s; ALB 10 mm	
Melting point, dta peak, °C		270	270
Water absorption at saturation, %	D570	0.029	0.022
Hardness			
Rockwell	D785	R50	R74
Durometer D		D75	
Coefficient of friction <sup>h</sup>			
Dynamic, 689 kPa (at >3 m/min)		0.4	0.3
Static, 689 kPa			0.3

<sup>a</sup>At 23°C and 50% Rh, unless otherwise specified.<sup>b</sup>Reinforced with 25 wt% glass fiber.<sup>c</sup>To convert MPa to psi, multiply by 145.<sup>d</sup>Elongations between 100% and 300% are achieved with varying methods of sample fabrication.<sup>e</sup>Long-term heat-aging tests on Tefzel 280 are in progress. Early data indicate that initial properties are retained after more than 2000 h at 200°C. It is expected that the continuous use temperature of Tefzel 280 will be above 150°C.<sup>f</sup>To convert J/m to ft-lbf/in., divide by 53.38.<sup>g</sup>ATB, average time of burning, to nearest 5 s; ALB, average length of burning, to nearest 5 mm. Test bar thickness = 2.9 mm.<sup>h</sup>Mating material AISI 1018 steel, Rc20, 16AA.

**Table 2. Thermodynamic Properties of Modified ETFE**

Property	Tefzel 200 and 280
Melting point, °C	270
Specific heat	0.46–0.47
Heat of sublimation, kJ/mol	50.2
Heat of fusion <sup>a</sup> , J/g	46.0
Heat of combustion, kJ/g	13.72
Thermal conductivity, W/(m·K)	0.238
Critical surface tension of molten resin, mN/m (= dyn/cm)	22

<sup>a</sup>Little dependence on temperature.

Light transmittance of 25- $\mu$ m films in the visible-to-IR range varies from 91% to 95% for Tefzel 200 and from 89% to 93% for Tefzel 280. In the ultraviolet (UV) range, transmittance increases from 50% at 200 nm to 90% at 400 nm.

**Thermal Properties.** Modified ETFE has a broad operating temperature range up to 150°C for continuous exposure (33). Cross-linking by radiation improves the high temperature capability further. However, prolonged exposure to higher temperatures gradually impairs the mechanical properties and results in discoloration. Thermal and oxidative degradation studies (35,36) suggest that main carbon chain sequences of two or more ethylene links are thought to be a subject of thermal and oxidative degradation. To enhance the thermal stability of ETFE resins, stabilizers may be added for high temperature applications (37). The copolymer will not support combustion in air. Limiting oxygen index (LOI) is about 30–31, depending on monomer ratio. It increases gradually as fluorocarbon content is increased up to the alternating composition. It then increases rapidly to the index of PTFE (38).

The thermodynamic properties of Tefzel 200 and 280 are shown in Table 2; the annual rate of loss of weight with thermal aging for Tefzel 200 ranges from 0.0006 g/g at 135°C to 0.006 g/g at 180°C after an initial loss of absorbed gases of 0.0013 g/g at elevated temperature. The excellent thermal stability of ETFE is demonstrated by aging at 180°C; at this temperature, the annual weight loss of 6 parts per 1000, or a 1% weight loss, takes almost 2 years.

#### **Friction and Bearing Wear of the Glass-Reinforced Copolymer.**

Glass reinforcement improves the frictional and wear properties of modified ETFE resins (HT-2004). For example, the dynamic coefficient of friction [689.5 kPa (100 psi) at >3 m/min] for Tefzel 200 is 0.4, which drops to 0.3 for the 25% glass-reinforced product at these conditions.<sup>33</sup> The wear factor also improves from  $12 \times 10^{-14}$  to  $32 \times 10^{-17}$  1/Pa [ $6000 \times 10^{-10}$  to  $16 \times 10^{-10}$  (in.<sup>3</sup>·min)/(ft·lb·fh)]. These frictional and wear characteristics, combined with outstanding creep resistance, indicate suitability for bearing applications. Glass-reinforced ETFE is less abrasive on mating surfaces than most glass-reinforced polymers. Its static coefficient of friction depends on bearing pressure; for Tefzel HT-2004, the coefficient of friction changes from 0.51 at 68 Pa to 0.34 at 3.43 kPa (0.5 psi).

Dynamic friction depends on pressure and rubbing velocity (PV). The generation of frictional heat depends on the coefficient of friction and the PV factor. For the glass-reinforced product, temperature buildup begins at about PV 10,000 and

**Table 3. Bearing Wear Rate<sup>a</sup>**

		Wear factor $K$ , $10^{17}$ 1/Pa <sup>c</sup>	
Pressure, kPa <sup>b</sup>	Velocity, cm/s	Tefzel	Metal
On steel <sup>d</sup>			
6.8	2.5	32	8
6.8	5.1	28	12
6.8	7.6	38	26
6.8	8.9	60	32
6.8	10.2	fail	
On aluminum <sup>e</sup>			
2.0	5.1	2400	2400
0.68	25.4	960	780

<sup>a</sup>Thrust-bearing tester, no lubricant, ambient air temperature, metal finish 406 nm.

<sup>b</sup>To convert kPa to psi, multiply by 0.145.

<sup>c</sup>To convert 1/Pa to (in.·min)/(ft·lbf·h), divide by  $2 \times 10$ .

<sup>d</sup>AISI 1018.

<sup>e</sup>LM24M (English).

**Table 4. Electrical Properties of ETFE Resins**

	ASTM test	ETFE	Reinforced
Dissipation factor	D150		
$10^2$ Hz		0.0006	0.004
$10^3$ Hz		0.0008	0.002
$10^4$ Hz			0.002
$10^5$ Hz			0.003
$10^6$ Hz		0.005	0.005
$10^9$ Hz		0.005	
$10^{10}$ Hz		0.010	0.012
Volume resistivity, $\Omega \cdot \text{cm}$	D257	$> 10^{16}$	$10^{16}$
Surface resistivity, $\Omega/\text{sq}$	D257	$> 10^{16}$	$10^{15}$
Arc resistance, s	D495	75	110

thermal runaway occurs just below PV 20,000. High wear rates begin above PV 15,000. The wear rate depends on the type of metal rubbing surface and finish, lubrication, and clearances. Lubrication, hard shaft surfaces, and high finishes improve wear rates. Table 3 provides wear factors for steel and aluminum. Because the wear rate of both ETFE and the metal is much higher for aluminum than for steel, an anodized surface is preferred with aluminum.

**Electrical Properties.** Modified ETFE is an excellent dielectric material (Table 4). Its low dielectric constant confers a high corona-ignition voltage. The dielectric constant does not vary with frequency or temperature. Both dielectric strength (ASTM D149) and resistivity are high. The loss characteristics are minimum; the dissipation factor, although low, increases at higher frequencies. Glass reinforcement increases losses and the dielectric constant rises from 2.6 to 3.4 (from  $10^2$  to  $10^{10}$  Hz); the dissipation factor is increased by 10-fold.

Exposure to radiation also increases losses. Dielectric strength is not reduced by thermal aging, unless a physical break occurs in the material. The short-time test of ASTM D149 gives values of 16–20 kV/mm with specimens 3 mm thick to 160–200 kV/mm with films 25–75  $\mu\text{m}$  thick. Tracking resistance is about 70 s by ASTM D495. This is comparable with materials considered to be nontracking; under unusual conditions, tracking occurs. When these resins are foamed, they provide insulation with even lower dielectric constant (39).

**Chemical Resistance and Hydrolytic Stability.** Modified ETFE are resistant to chemicals and solvents (Table 5) that often cause rapid degradation in other plastic materials. Performance is similar to that of perfluorinated polymers (40), which are not attacked by strong mineral acids, inorganic bases, halogens, and metal salt solutions. Organic compounds and solvents have little effect. Strong oxidizing acids, organic bases, and sulfonic acids at high concentrations and near their boiling points affect ETFE to varying degrees.

Physical properties remain stable after long exposure to boiling water. Tensile strength and elongation of Tefzel 200 are unaffected after 3000 h in boiling water. The higher molecular weight ETFE behaves similarly, whereas the glass-reinforced product shows a reduction of 25–35% in tensile strength with loss of reinforcement.

Water absorption of Tefzel is low (0.029 wt%), which contributes to its outstanding dimensional stability as well as to the stability of mechanical and electrical properties regardless of humidity.

High temperature resistance of ETFE and other fluoropolymers in automotive fuels and their permeation resistance have been discussed (41,42).

The ETFE can be cross-linked by radiation (43) despite the high content of TFE units. The recommended upper continuous use temperature for commercial ETFE is 150°C. Physical strength can be maintained at higher temperatures when cross-linking agents are incorporated and cured by peroxide or ionizing radiation (44). The cut-through resistance of thin-wall wire insulation to a physical tempering during installation or use is increased at temperature up to 200°C. Short-term excursions to 240°C are possible for highly cross-linked resins. Cross-linking reduces plasticity but enhances high temperature properties and nondrip performance. The irradiated resin withstands a 400°C solder iron for 10 min without noticeable effect.

Modified ETFE has excellent weather resistance; tensile strength and elongation are not affected. On the other hand, tensile and elongation properties of the glass-reinforced compound show a significant reduction.

Modified ETFE films are used as windows in greenhouses and conservatories because of their high transparency to both UV and visible light and excellent resistance to weathering (45). Pigmented films are applied on white boards and in outdoor advertising laminates. Biaxially oriented films have tensile properties and toughness similar to polyester films (46).

**Vacuum Outgassing and Permeability.** Under vacuum, modified ETFE give off little gas at elevated temperatures. The loss rate is about one-tenth of the acceptable maximum rates for spacecraft uses. Exposing 750- $\mu\text{m}$  specimens for 24 h at 149°C to a high vacuum results in a maximum weight loss of 0.12%; volatile condensable material is less than 0.02%.

Table 5. Tefzel Resistance to Chemicals after 7 Days of Exposure<sup>a</sup>

Chemical	Boiling point, °C	Test temperature, °C	Retained properties, %		
			Tensile strength	Elongation	Weight gain
Organic acids and anhydrides					
Acetic acid (glacial)	118	118	82	80	3.4
Acetic anhydride	139	139	100	100	0
Trichloroacetic acid	196	100	90	70	0
Hydrocarbons					
Mineral oil		180	90	60	0
Naphtha		100	100	100	0.5
Benzene	80	80	100	100	0
Toluene	110	110			
Amines					
Aniline	185	120	81	99	2.7
Aniline	185	180	95	90	
<i>N</i> -Methylaniline	195	120	85	95	
<i>N,N</i> -Dimethyl aniline	190	120	82	97	
<i>n</i> -Butylamine	78	78	71	73	4.4
Di- <i>n</i> -butylamine	159	120	81	96	
Di- <i>n</i> -butylamine	159	160	55	75	
Tri- <i>n</i> -butylamine	216	120	81	80	
Pyridine	116	116	100	100	1.5
Solvents					
Carbon tetrachloride	78	78	90	80	4.5
Chloroform	62	61	85	100	4.0
Dichloroethylene	77	32	95	100	2.8
Methylene chloride	40	40	85	85	0
Freon 113	46	46	100	100	0.8
Dimethylformamide	154	90	100	100	1.5
Dimethyl sulfoxide	189	90	95	95	1.5
Skydrol		149	100	95	3.0
Aerosafe		149	92	93	3.9
A-20 stripper solution		140	90	90	
Ethers, ketones, esters					
Tetrahydrofuran	66	66	86	93	3.5
Acetone	56	56	80	83	4.1
Acetophenone	201	180	80	80	1.5
Cyclohexanone	156	156	90	85	0
Methyl ethyl ketone	80	80	100	100	0
<i>n</i> -Butyl acetate	127	127	80	60	0
Ethyl acetate	77	77	85	60	0
Other organic compounds					
Benzyl alcohol	205	120	97	90	
Benzoyl chloride	197	120	94	95	
<i>o</i> -Cresol	191	180	100	100	
Decalin	190	120	89	95	
Phthalyl chloride	276	120	100	100	

(Continued)

Table 5. (Continued)

Chemical	Boiling point, °C	Test temperature, °C	Retained properties, %		
			Tensile strength	Elongation	Weight gain
Inorganic acids					
Hydrochloric (conc)	106	23	100	90	0
Hydrobromic (conc)	125	125	100	100	
Hydrofluoric (conc)		23	97	95	0.1
Sulfuric (conc)		100	100	100	0
Nitric, 70% (conc)	120	120	0	0	
Chromic	125	125	66	25	
Phosphoric (conc)		100			
Halogens					
Bromine (anhy)	59	23	90	90	1.2
Chlorine (anhy)		120	85	84	7
Bases, peroxides					
Ammonium hydroxide		66	97	97	0
Potassium hydroxide, 20%		100	100	100	0
Sodium hydroxide, 50%		120	94	80	0.2
Hydrogen peroxide, 30%		23	99	98	0
Other inorganic compounds					
Ferric chloride, 25%	104	100	95	95	0
Zinc chloride, 25%	104	100	100	100	0
Sulfuryl chloride	68	68	86	100	8
Phosphoric trichloride	75	75	100	98	
Phosphoric oxychloride	104	104	100	100	
Silicon tetrachloride	60	60	100	100	

<sup>a</sup>Changes in properties of less than 15% are considered insignificant; test performed on 250–1250  $\mu\text{m}$  microtensile bars; tensile strength, elongation, and weight gain determined within 24 h after termination of exposure.

The following permeability values were determined on Tefzel film (100  $\mu\text{m}$ , ASTM D1434) at 25°C [1 nmol (m·s·GPa)]:

	nmol/(m·s·GPa)
Carbon dioxide	500
Nitrogen	60
Oxygen	200
Helium	1800
Water vapor (ASTM E96)	3.3

## Fabrication

Modified ETFE are commercially available in a variety of physical forms (Table 6) and can be fabricated by conventional thermoplastic techniques. Commercial ETFE resins are marketed in melt-extruded cubes, which are sold in

**Table 6. Forms of Modified ETFE Resins**

Tefzel grade	Form	Melt flow, <sup>a</sup> g/10 min	Application
210	Extruded cubes	45	Injection molding, thin coating
200	Extruded cubes	8	General purpose, insulation, tubing, fasteners
280	Extruded cubes	3	Chemical resistance, jacketing, heavy-wall, logging cables
HT-2000	Compacted powder	8	Compounded products
HT-2010	Compacted powder	3	Compounded products, coating lining
HT-2010	Compacted powder	45	Coating

<sup>a</sup>At 297°C and 45 N (5 kg-f) load.

20-kg bags or 150-kg drums. In the United States, the 2008 list price was \$40–\$110/kg, depending on volume and grade; color concentrates are also available.

Like other thermoplastics, they exhibit melt fracture (47) above certain critical shear rates. In extrusion, many variables control product quality and performance (48).

## Melt Processing

Articles are made by injection molding, compression molding, blow molding, transfer molding, rotational molding, extrusion, and coating. Films can be thermoformed and heat sealed (33). Because of high melt viscosity, ETFE resins are usually processed at high temperatures (300–340°C).

Injection-molded articles shrink about 1.5–2.0% in the direction of resin flow and about 3.5–4.5% in the transverse direction under normal molding conditions. A 25% glass-reinforced composition shrinks only about 0.2–0.3% in the flow direction and about 3.0% in the transverse direction. Although shrinkage depends on shape and processing conditions, uniformity is excellent.

Molten ETFE polymers corrode most metals, and special corrosion-resistant alloys are recommended for long-term processing equipment; short-term prototype runs are possible in standard equipment. A technique to reduce the melt processing temperature by using supercritical carbon dioxide to swell the polymer has been developed to permit lower temperature extrusion and molding operations (49).

**Forming and Machining.** Articles can be formed below the melting point with conventional metal-forming techniques. Tetrafluoroethylene–ethylene copolymers are readily machined with the same tools and feed rates as those used for nylon and acetal. For best dimensional stability, the article should be annealed at the expected use temperature before the final machine cut.

**Coloring and Decorating.** Commercial pigments that are thermally stable at the resin processing temperature may be used. Pigments may be dry-blended with the resin, or ETFE pellets may be blended with color concentrates, which are available in pellet form.



Nontreated surfaces can be hot-printed with special foils in a manner similar to that of a typewriter ribbon. The type is heated to about 321°C, and a printing pressure of 172–206 kPa (25–30 psi) is applied for about 0.25 s; no further treatment is required.

Stripes may be applied to wire coated with ETFE fluoropolymer over DuLite 817-5002 fluoropolymer clear enamel or other bases. Thermally stable pigments are required. Stripes may be applied by gravure-wheel-type applicators and oven-cured in-line.

**Assembly.** The success of many applications depends on the ability of ETFE fluoropolymer to be economically assembled.

**Screw Assembly.** Self-tapping screws are used for joining ETFE parts. For maximum holding power, the boss diameter should be about double the screw diameter and the engagement length about 2.5 times the screw diameter; lubricants should be avoided. Threaded inserts can be molded in place, pressed in, or driven in ultrasonically.

**Snap-Fit and Press-Fit Joints.** Snap-fit joints offer the advantage that the strength of the joint does not diminish with time because of creep. Press-fit joints are simple and inexpensive but lose holding power. Creep and stress relaxation reduce the effective interference, as do temperature variations, particularly with materials with different thermal expansions.

**Cold or Hot Heading.** Rivets or studs can be used in forming permanent mechanical joints. The heading is made with special tools and preferably with the rivet at elevated temperatures. Formed heads tend to recover part of their original shape if exposed to elevated temperatures, resulting in loose joints. Forming at elevated temperature reduces recovery.

**Spin Welding.** Spin welding is an efficient technique for joining circular surfaces of similar materials. The matching surfaces are rotated at high speed relative to each other and then brought into contact. Frictional heat melts the interface and, when motion is stopped, the weld is allowed to solidify under pressure.

**Ultrasonic Welding.** Ultrasonic welding has been applied to Tefzel with weld strength up to 80% of the strength of the base resin. Typical conditions include a contact pressure of 172 kPa (25 psi) and 1- to -2-s cycle time. The two basic designs, the shear and butt joints, employ a small initial contact area to concentrate and direct the high frequency vibrational energy.

**Potting.** Potting of wire insulated with Tefzel has been accomplished with the aid of a coating of a colloidal silica dispersion. The pots produced with a polysulfide potting compound meeting MIL-S-8516C Class 2 standards exhibit pull-out strengths of 111–155 N (25–35 lbf).

**Bonding.** Surface treatment, such as chemical etch, corona, or flame treatments, is required for adhesive bonding of Tefzel. Polyester and epoxy compounds are suitable adhesives.

ETFE respond well to melt bonding to untreated aluminum, steel, and copper with peel strengths above 3.5 kN/m (20 lbf/in.). For melt bonding to itself, hot-plate welding is used. The material is heated to 271–276°C, and the parts are pressed together during cooling.

The plasma surface treatment of ETFE to improve adhesion has been studied (50).

## Testing and Standards

A description of modified ETFE and its classification is given by the American Society for Testing and Materials under the designation D3159-83 (51). A comprehensive listing of industrial and military specifications is available (52).

**Applications.** Tefzel 200 is a general-purpose, high temperature resin for insulating and jacketing low voltage power wiring for mass transport systems, wiring for chemical plants, and control and instrumentation wiring for utilities. In injection-molded form, it is used for sockets, connectors, and switch components (53). Because of excellent mechanical properties, it provides good service in seal glands, pipe plugs, corrugated tubing, fasteners, and pump vanes. In chemical service, it is used for valve components, laboratory ware, packing, pump impellers, and battery and instrument components. ETFE is used in coating applications (54–57). It can also be used in membrane electrode assembly (58). ETFE is also suitable for multilayer fuel hose construction (59).

Tefzel 210, the high melt-flow resin, provides a high speed processing product for use in coating of fine wire and injection molding of thin-walled or intricate shapes. It is also used for other fine-wire applications requiring high line speeds and mechanical strength, but in which harsh environmental conditions are not anticipated.

For high temperature wiring with mechanical strength and stress-crack and chemical resistance, Tefzel 280 is preferred. Rated by Underwriters Laboratories, Inc., at 150°C, it is widely used for insulating and jacketing heater cables and automotive wiring and for other heavy-wall application, in which temperatures up to 200°C are experienced for short period of time or in which repeated mechanical stress at 150°C is encountered. It is also suitable for oil-well logging cables and is used in transfer moldings and extrusions for lined chemical equipment. It is injection molded into articles with metal inserts, thick sections, and stock shapes.

## Health and Safety

Large quantities of Tefzel have been processed and used in many demanding service applications. No cases of permanent injury have been attributed to these resins, and only limited instances of temporary irritation to the upper respiratory tract have been reported (60).

As with other melt-processible fluoropolymers, trace quantities of harmful gases, including hydrogen fluoride, diffuse from the resin even at room temperature. Therefore, the resins should be used in well-ventilated areas. Even though the resin is physiologically inert and nonirritating to the skin, it is recommended that spills on the skin be washed with soap and water. These resins are stable at 150°C and are recommended for continuous use at this temperature. Degradation, as measured by weight loss, is insignificant up to the melting point of 270°C. At processing temperatures, sufficient quantities of irritating and toxic gases are generated to require removal of the gases by exhaust hoods over the die and at the hopper heater. For extrusion into water, a quench tank or partially filled container for purging is recommended. In extrusion operations, proper procedures

must be maintained to control temperature and pressure. The weight loss with increasing temperature is as follows:

Temperature, °C	Hourly weight loss, %
300	0.05
330	0.26
350	0.86
370	1.60

To remove all decomposition products, a “total-capture” exhaust hood is recommended.

Under normal processing conditions at 300–350°C, Tefzel resins are not subject to autocatalytic degradation. However, extended overheating can result in “blowbacks” through extruder feed hopper or barrel front.

Prolonged soldering in confined spaces with restricted air circulation requires ventilation. A small duct fan is recommended for hot-wire stripping. Tefzel articles should not be exposed to welding conditions.

The LOI of Tefzel as measured by the candle test (ASTM D2863) is 30%. Tefzel is rated 94 V-0 by Underwriters Laboratories, Inc., in its burning test classification for polymeric materials. As a fuel, it has a comparatively low rating. Its heat of combustion is 13.7 MJ/kg (32,500 kcal/kg) compared with 14.9 MJ/kg (35,000 kcal/kg) for poly(vinylidene fluoride) and 46.5 MJ/kg (110,000 kcal/kg) for polyethylene.

Bulk quantities of Tefzel fluoropolymer resins should be stored away from flammable materials. In the event of fire, personnel entering the area should have full protection, including acid-resistant clothing and self-contained breathing apparatus with a full facepiece operated in the pressure-demand or other positive-pressure mode. All types of chemical extinguishers may be used to fight fire involving Tefzel resins. Large quantities of water may be used to cool and extinguish the fire.

The DuPont Haskell Laboratory for Toxicology and Industrial Medicine has conducted a study to determine the acute inhalation toxicity of fumes evolved from Tefzel fluoropolymers when heated at elevated temperatures. Rats were exposed to decomposition products of Tefzel for 4 h at various temperatures. The approximate lethal temperature (ALT) for Tefzel resins was determined to be 335–350°C. All rats survived exposure to pyrolysis products obtained from Tefzel heated to 300°C for this time period. At the ALT level, death was from pulmonary edema; carbon monoxide poisoning was probably a contributing factor. Hydrolyzable fluoride was present in the pyrolysis products, with concentration dependent on temperature.

## BIBLIOGRAPHY

“Fluorinated plastics, tetrafluoroethylene copolymers with ethylene” in *EPST* 1st ed., Suppl. Vol. 1, pp. 268–278, by R. L. Johnson, E. I. du Pont de Nemours & Co., Inc.; “Tetrafluoroethylene polymers, tetrafluoroethylene–ethylene copolymers” in *EPSE* 2nd

ed., Vol. 16, pp. 626–642, by S. V. Gangal, E. I. du Pont de Nemours & Co., Inc.; Perfluorinated polymers, tetrafluoroethylene–ethylene copolymers” in *EPST* 3rd ed., Vol. 3, pp. 402–418, by S. V. Gangal, E. I. du Pont de Nemours & Co., Inc.

## CITED REFERENCES

1. U.S. Pat. 2,468,664 (Apr. 26, 1949), W. E. Hanford and J. R. Roland (to E. I. du Pont de Nemours & Co., Inc.).
2. U.S. Pat. 2,479,367 (Aug. 16, 1949), R. M. Joyce Jr. (to E. I. du Pont de Nemours & Co., Inc.).
3. Brit. Pat. 1,166,020 (Oct. 1, 1969), M. Modena and co-workers (to Montecatini Edison, SpA).
4. Jpn. Kokai 6,422,586 (Sept. 12, 1964), K. Hirose and co-workers (to Nitto Chemical Industry, Co., Ltd.).
5. Belg. Pat. 725,356 (Feb. 14, 1969), Z. Kenkyusho (to Asahi Glass Co., Ltd.).
6. U.S. Pat. 2,946,763 (July 26, 1960), M. I. Bro and B. W. Sandt (to E. I. du Pont de Nemours & Co., Inc.).
7. D. P. Carlson, Development of Tefzel Fluoropolymer Resins, E. I. du Pont de Nemours & Co., Inc. Wilmington, Del. unpublished paper, 1972.
8. U.S. Pat. 3,624,250 (Nov. 30, 1971), D. P. Carlson (to E. I. du Pont de Nemours & Co., Inc.).
9. U.S. Pat. 4,123,602 (Oct. 31, 1978), H. Ukihashi and M. Yamake (to Asahi Glass Co., Ltd.).
10. Brit. Pat. 1,353,535 (May 22, 1974), R. Hartwimmer (to Farbwerke Hoechst, AG).
11. U.S. Pat. 3,401,155 (Sept. 10, 1986), G. Borsini and co-workers (to Montecatini Edison, SpA).
12. Y. Tabata, H. Shibano, and H. Sobue, *J. Polym. Sci. Part A* **2**, 1977 (1964).
13. U.S. Pat. 4,521,575 (June 4, 1985), S. Nakagawa and K. Ihara (to Daikin Kogyo Co. Ltd.).
14. U.S. Pat. 4,614,276 (Sept. 30, 1986), K. Ihara and T. Nakagawa (to Daikin Kogyo Co., Ltd.).
15. U.S. Pat. 3,960,825 (June 1, 1976), D. N. Robinson and co-workers (to Pennwalt Corp.).
16. U.S. Pat. 4,338,237 (July, 1982), R. A. Sulzbach and co-workers (to Hoechst Aktiengesellschaft).
17. M. Iuliano and co-workers, *Makromol. Chem.* **190**, 827–835 (1989).
18. F. Kostov and A. Nikolov, *J. Appl. Polym. Sci.* **57**, 1545–1555 (1995).
19. R. Naberezhnykh and co-workers, *Vysokomol. Soedin.* **19**(1), 33–37 (1977).
20. M. Modena, C. Garbuglio, and M. Ragazzini, *Polym. Lett.* **10**, 153 (1972).
21. M. Modena, C. Garbuglio, and M. Ragazzini, *J. Polym. Sci. Part B* **10**, 153 (1972).
22. F. S. Ingraham and D. F. Wooley Jr., *Ind. Eng. Chem.* **56**(9), 53 (1964).
23. S. Yano, *J. Polym. Sci. Part A2* **8**, 1057 (1970).
24. H. W. Starkweather, *J. Polym. Sci. Part A2* **11**, 587 (1973).
25. F. C. Wilson and H. W. Starkweather, *J. Polym. Sci. Part A2* **11**, 919 (1973).
26. T. Tanigami and co-workers, *Polymer* **27**, 999–1006 (1986).
27. T. Pieper, B. Heise, and W. Welke, *Polymer* **30**, 1768–1775 (1989).
28. B. Chu and Chi Wu, *Macromolecules* **20**, 93–98 (1987).
29. B. Chu, C. Wu, and W. Buck, *Macromolecules* **22**, 371 (1989).
30. B. Chu and C. Wu, *Macromolecules* **19**, 1285 (1986).
31. B. Chu and C. Wu, *Macromolecules* **20**, 98 (1987).

32. Z. Wang, A. Tontisakis, W. Tuminello, W. Buck, and B. Chu, *Macromolecules* **23**, 1444 (1990).
33. *Tefzel Fluoropolymer, Design Handbook*, E. I. du Pont de Nemours & Co., Inc., Wilmington, Del., 1973.
34. *Tefzel—Properties Handbook*, Bulletin No. E-31301-6, E. I. du Pont de Nemours & Co., Inc., Wilmington, Del., Dec. 1999.
35. J. Morelli and co-workers, *J. Appl. Polym. Sci.* **43**, 601–611 (1991).
36. S. Malkevich, L. Tarutina, and L. Chereshevskiy, *Plasticheskie massy* **6**, 5–7, (1960).
37. U.S. Pat. 4,390,655 (June 28, 1983), J. C. Anderson (to E. I. du Pont de Nemours & Co., Inc.).
38. D. L. Kerbow, in J. Scheirs, ed., *Modern Fluoropolymers*, John Wiley & Sons, Inc., New York, 1997, p. 301.
39. S. K. Randa, C. R. Frywald, and D. P. Reifschneider, in *Proceedings of the 36th International Wire and Cable Symposium*, Arlington, Va., 1987, pp. 14–22.
40. *Technical Information, Tefzel Fluoropolymer Resin, Chemical Use Temperature Guide*, Bulletin 195062E, E. I. du Pont de Nemours & Co., Inc., Wilmington, Del., 1995.
41. M. Carpenter, S. Chillons, and R. Will, in *Proceedings of the International Congress and Exposition*, Detroit, Mich., Feb. 25–Mar. 1, 1991, SAE International Technical Paper Series 910103.
42. D. Goldsberry, S. Chillons, and R. Will, in *Proceedings of the International Congress and Exposition*, Detroit, Mich., Feb. 25–Mar. 1, 1991. SAE International Technical Paper Series 910104.
43. U.S. Pat. 3,738,923 (June 12, 1973), D. P. Carlson and N. E. West (to E. I. du Pont de Nemours & Co., Inc.).
44. U.S. Pat. 4,155,823 (May 22, 1979), A. J. Gotcher and P. B. Gemeraad (to Raychem Corp.).
45. J. Emsley, *New Scientist* **46** (Apr. 22, 1989).
46. U.S. Pat. 4,510,301 (Apr. 9, 1985), S. B. Levy (to E. I. du Pont de Nemours & Co., Inc.).
47. *Technical Information, Jacketing Rate Calculation*, Bulletin No. 10, Fluoropolymers Division Technical Service Laboratory, E. I. du Pont de Nemours & Co., Inc., Wilmington, Del., Aug. 1982.
48. *Extrusion Guide for Melt Processible Fluoropolymers*, Bulletin No. E-41337, E. I. du Pont de Nemours & Co., Inc., Wilmington, Del.
49. U.S. Pat. 6,960,633 (Jan. 11, 2005), K. Wynne, S. Shenoy, S. Irie, T. Ohsaka, and Y. Ohsaka (to Daikin Institute of Advance Chemistry).
50. S. Kaplan, O. Kolluri, G. Hansen, R. Rushing, and R. Warren, in *Proceedings of the Conference on Adhesives*, Society of Manufacturing Engineers, Atlanta, Ga., Sept. 12, 1989.
51. *Modified ETFE-Fluorocarbon Molding and Extrusion Materials*, ASTM D3159-95a, American Society for Testing and Materials, Philadelphia, Pa., 1998.
52. *J. Teflon* **15**(1), 1974.
53. *Tefzel Fluoropolymers, Product Information (DuPont Materials for Wire and Cable)*, Bulletin No. E-81467, E. I. du Pont de Nemours & Co., Inc., Wilmington, Del., May 1986.
54. U.S. Pat. 7,192,638 (Mar. 20, 2007), N. Tomihashi, K. Ogita, T. Miyatani, Y. Nakatani, and H. Torii (to Daikin Co. Ltd.).
55. U.S. Pat. 7,208,227 (Apr. 24, 2007), N. Tomihashi, H. Torii, and K. Ogita (to Daikin Co., Ltd.).
56. U.S. Pat. 6,589,597 (July 8, 2003), M. Ono and T. Takakura (to Asahi Glass Co., Ltd.).
57. U.S. Pat. 6,242,089 (May 6, 2001), A. Buegman (to E. I. du Pont de Nemours & Co., Inc.).

58. U.S. Pat. 7,569,616 (Aug. 4, 2009), S. Kotera, H. Wakabayashi, S. Kinoshita, and H. Shimoda (to Asahi Glass Co., Ltd.).
59. U.S. Pat. 6,656,553 (Dec. 2, 2003), E. Nishi, M. Nagashima, N. Isobe, T. Nishioka, and Y. Iwata (to Asahi Glass Co., Ltd., and UBE Industries).
60. *Guide to the Safe Handling of Fluoropolymer Resins*, 3rd ed., Fluoropolymers Division of the Society of the Plastics Industry, Inc., Washington, D.C., 1998.

SUBHASH V. GANGAL  
PAUL D. BROTHERS  
E. I. du Pont de Nemours & Co., Inc.  
Wilmington, Delaware

## PERFLUORINATED POLYMERS, TETRAFLUOROETHYLENE-PERFLUORODIOXOLE COPOLYMERS

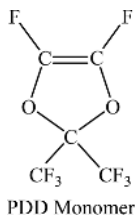
### Introduction

Copolymers of tetrafluoroethylene and 2,2-bistrifluoromethyl-4,5-difluoro-1,3-dioxole (PDD) are perfluorinated amorphous polymers and possess an unusual combination of properties. They retain the outstanding chemical, thermal, and surface properties of perfluorinated polymers, in addition to having excellent electrical and optical properties, and have solubility at ambient temperature in a normal perfluoro solvent. This family of copolymers is manufactured by DuPont and sold under the trade name of Teflon AF, amorphous fluoropolymers.

All tetrafluoroethylene-based homo- and copolymers, described in earlier papers, are semicrystalline with distinct melting points. On the other hand, tetrafluoroethylene-PDD copolymers are totally amorphous and can be tailored for specific glass-transition temperatures ( $T_g$ ) by altering the polymer composition (1). These perfluorinated amorphous polymers exhibit properties derived from their amorphous structure and perfluorinated chains.

### Monomer

**Preparation.** 2,2-Bistrifluoromethyl-difluoro-1,3-dioxole (PDD) monomer is synthesized in four steps (2). In the first step, hexafluoroacetone and ethylene oxide are reacted to form 2,2-bistrifluoromethyl-4,5-dichloro-4,5-difluoro-1,3-dioxolane. This product is then fully chlorinated and subsequently partially fluorinated to difluoro-1,3-dioxolane. In the last step, the fluorinated product is dechlorinated to obtain the final product, PDD. Some of these steps involved in the synthesis of PDD have low yields, as a result the overall yield is low and the cost of manufacturing of this monomer is very high.



**Properties.** PDD is a colorless liquid with the boiling point of  $33^{\circ}\text{C}$  (3). It is very reactive and can homopolymerize and therefore needs to be stored at low temperature with a small amount of free-radical inhibitor. PDD can copolymerize with tetrafluoroethylene or other fluorinated monomers, such as vinylidene fluoride, vinyl fluoride, or chlorotrifluoroethylene.

**Copolymerization.** Copolymers of tetrafluoroethylene and PDD can be synthesized by free-radical initiators in either aqueous or nonaqueous medium (1). The homopolymer of PDD results in an amorphous polymer with the  $T_g$  of  $335^{\circ}\text{C}$ . This polymer is difficult to melt process because of the narrow processing window below its decomposition temperature. Copolymers can be prepared with any proportion of tetrafluoroethylene and PDD. Polymers containing less than 20 mol% PDD tend to be partially crystalline. At 20 mol% PDD, the  $T_g$  of the copolymer is about  $80^{\circ}\text{C}$ . The glass-transition temperature increases with an increase in the PDD content. The commercial Teflon AF products are copolymers of tetrafluoroethylene and PDD and have  $T_g$ s of 160 and  $240^{\circ}\text{C}$  for Teflon AF-1600 and Teflon AF-2400, respectively (4). During aqueous polymerization, small amounts of acid fluoride or carboxylic acid end groups may be produced by a ring-opening process. For many applications, these unstable ends are removed and converted to perfluorinated end groups by first treating the polymer with ammonia, followed by fluorination (5).

**Properties.** Teflon AF copolymers have many characteristics, such as high temperature stability, excellent chemical resistance, low surface energy, low water absorption, and high limiting oxygen index (LOI), similar to those of other copolymers of tetrafluoroethylene. On the other hand, many properties are different because of their amorphous structure. These polymers are soluble at ambient temperature in perfluorinated solvents. They are transparent and have low refractive index. They are significantly stiffer and have high gas permeability. The glass-transition temperature of tetrafluoroethylene-PDD copolymers is sensitive to the structure of the dioxide monomer. It is likely that steric interactions involving the two trifluoromethyl groups lead to a highly congested chain structure with limited mobility (6). The structural study of these polymers indicate that there are microvoids in their structure and probably cause lower than expected polymer density, low dielectric constant, low refractive index, high gas permeability, and low thermal conductivity. Most likely, the origin of these microvoids is loose chain packing caused by the high energy for rotation and reorientation of the dioxole ring containing polymer chain (7).

Table 1 summarizes mechanical, electrical, optical, and thermal properties of Teflon AF-1600 and AF-2400 (10). The dielectric constant for Teflon AF is lower than that for polytetrafluoroethylene (PTFE) and is unaffected by humidity.

Table 1. Properties of Teflon AF-1600 and AF-2400

Property	AF-1600	AF-2400	ASTM method	References
Melt viscosity, Pa·s <sup>a</sup> (at 250°C)	2650		D3835	8
(at 350°C)		540		
Density, g/cm <sup>3</sup>	1.78	1.67	D792	4
Water absorptivity; 1	<0.01	<0.01	D570	9
Contact angle, water, °	104	105		8
Critical surface energy, mN/m (=dyn/cm)	15.6–15.7	15.6–15.7		8
Electrical properties				
Dielectric strength, kV (0.1 mm) <sup>-1</sup>	2.1	1.9	D149	4
Dielectric constant				
1 MHz	1.934	1.904	D150	8
1 GHz	1.93	1.897		
13.6 GHz	1.927	1.89		
Dissipation factor				
1 MHz	0.00012	0.00012	D150	4
1 GHz	0.00018	0.00024		
13.6 GHz	0.00020	0.00035		
Flammability, LOI %O <sub>2</sub>	95	95		9
Hardness, Rockwell	103	97.5	D785	8
Refractive index	1.31	1.29	D542	9
Optical transmissions	>95	>95	D1003	9
Tensile strength at break, MPa <sup>b</sup>			D638	8
23°C	27	26		
150°C	8			
220°C		4		
Elongation at break, %				
23°C	17	8	D638	9
150°C	89			
220°C		8		

<sup>a</sup>To convert Pa·s to P, multiply by 10.<sup>b</sup>To convert MPa to psi, multiply by 145.

The low temperature dielectric properties investigation (11) revealed that the  $\gamma$ -relaxation found at  $-186^\circ\text{C}$  for PTFE is only one-third the intensity for AF-1600 and AF-2400. This relaxation is attributed to the cooperative motion of the four carbon atoms of a TFE dimer unit. The low concentration of such units in AF explains the difference in the intensity of  $\gamma$ -relaxation.

The refractive index of Teflon AF is the lowest known for any solid organic polymer (12). One of the key properties of AF is its solubility in fluorinated solvents, such as Fluorinert FC-72, FC-75, and FC-40, perfluorobenzene, perfluoromethylcyclohexane, perfluorodimethylcyclohexane, perfluorooctane, or perfluorodecalin.

The thermal stability of Teflon AF approaches that of other perfluorinated polymers. At  $260^\circ\text{C}$  after 4 h of exposure, no weight loss was observed. The weight



losses after the exposure at 360, 380, 400, and 420°C were 0.3, 0.5, 1.9, and 8.8%, respectively.

Copolymers of PDD with other fluoromonomers are discussed in Reference 3.

**Fabrication.** Teflon AF is processed by a wide variety of techniques. AF solutions can be used for spin coating, dip coating, spraying, or casting. Melt-processing techniques such as extrusion and injection molding are used. Compression molding has also been used effectively. Spin coating is used to produce very thin and uniform coatings on flat substrates. The film thickness is influenced by the nature of the substrate, the spin speed, and the concentration of the solution. Dip coating is suitable for nonplanar surfaces (13). Compression molding is done about 100°C above  $T_g$  and may require longer heat-up time than other polymers because of its lower thermal conductivity. Laser ablation and vacuum pyrolysis techniques are also used (14,15).

**Health and Safety.** Safe practices employed for handling PTFE and perfluoroalkoxy (PFA) resins are adequate for Teflon AF (16). Adequate ventilation is required for processing above 330°C. Above 360°C, decomposition products HF, COF<sub>2</sub>, CO, and hexafluoroacetone are observed (17).

**Applications and Economic Aspects.** Teflon AF is used for antireflective coatings (18), for low dielectric coatings, for pellicles used in electronic chip fabrication (19,20), as cladding in plastic optical fiber (21,22), as a low dielectric insulator (23,24), for coating gas separation membranes (25–27), as clear hydrophobic layers in optical devices (28,29), and in electrochemical devices (30).

The PDD monomer used for AF is very expensive, which results in making AF products very costly. These polymers in solid form are sold in 25- and 500-g packages, with list prices in 2008 of \$1500 and \$15,000, respectively. The solutions are available in 100-mL and 1-L packages. They contain 1–18% solids, depending on the grade. The prices for solutions range from \$210 for 1% solids of AF-2400 in 100-mL package to \$23,430 for 18% solids of AF-1600 in 1-L package.

## BIBLIOGRAPHY

“Perfluorinated polymers, tetrafluoroethylene–perfluorodioxole copolymers” in *EPST* 3rd ed., Vol. 3, pp. 418–422, by S. V. Gangal, E. I. du Pont de Nemours & Co., Inc.

## CITED REFERENCES

1. U.S. Pat. 3,978,030 (Aug. 31, 1976), P. R. Resnick (to E. I. du Pont de Nemours & Co., Inc.).
2. U.S. Pat. 3,865,845 (Feb. 11, 1975), P. R. Resnick (to E. I. du Pont de Nemours & Co., Inc.).
3. P. R. Resnick and W. H. Buck, in J. Scheirs, ed., *Modern Fluoropolymers*, John Wiley & Sons, Inc., New York, 1997, pp. 397–419.
4. W. H. Buck and P. R. Resnick, *Teflon*® AF, Technical Bulletin no. H-52454-1, E. I. du Pont de Nemours & Co., Inc., Wilmington, Del., 1993.

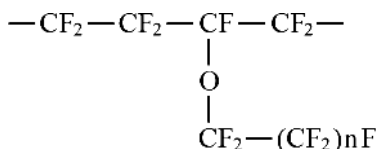
5. U.S. Pat. 4,946,902 (Aug. 7, 1990), P. G. Bekiarian, M. D. Buckmaster, and R. A. Morgan (to E. I. du Pont de Nemours & Co., Inc.).
6. M. Hung, *Macromolecules* **26**, 2829 (1993).
7. W. J. Davies and R. A. Pethrik, *Eur. Poly. J.* **30**, 1289 (1994).
8. P. Gunther, H. Ding, and R. Gerhard-Multhaupt, in *Proceedings of the 1993 IEEE Conf. on Electrical Insulation and Dielectric Phenomena*, 1993, pp. 197–202.
9. M. S. Jahan, D. R. Ermer, and D. W. Cooke, *Radiat. Phys. Chem.* **41**(1/2), 77–83 (1993).
10. D. L. Kerbow and C. A. Sperati, in J. Brandrup, E. H. Immergut, and E. A. Grulke, eds., *Polymer Handbook*, 4th ed., Wiley-Interscience, New York, 1999, pp. V-31–V-58.
11. H. Starkweather and co-workers, *Macromolecules* **24**, 3853 (1991).
12. W. Groh and A. Zimmermann, *Micromolecules* **24**, 6660 (1991).
13. I. M. Thomas and J. H. Campbell, *SPIE* **1441**, 294 (1990).
14. G. B. Blanchet, *Appl. Phys. Lett.* **62**, 479 (1993).
15. J. Griesar and co-workers, *Proc. SPIE* **1330**, 111 (1990).
16. *Guide to the Safe Handling of Fluoropolymer Resins*, 3rd ed., Fluoropolymers Division of the Society of the Plastics Industry, Inc., Washington, D.C., 1998.
17. *DuPont Teflon® Amorphous Fluoropolymer—Safety in Handling and Use, H-75334-1*, E. I. du Pont de Nemours & Co., Inc., Wilmington, Del., 2005.
18. H. G. Floch and P. F. Belleville, *SPIE* **1758**, 135 (1992).
19. U.S. Pat. 5,061,024 (Oct. 29, 1991), D. E. Keys (to E. I. du Pont de Nemours & Co., Inc.).
20. U.S. Pat. 7,416,820 (Aug. 26, 2008), T. Brunner and M. Hibbs (to International Business Machines Corp.).
21. U.S. Pat. 4,530,569 (July 23, 1985), E. N. Squire (to E. I. du Pont de Nemours & Co., Inc.).
22. U.S. Pat. 7,362,429 (Apr. 22, 2008), A. Gilby (to Waters Investments Limited).
23. U. S. Pat. 7,351,653 (Apr. 1, 2008), J. Ahn, K. Lee, and Y. Kim (to Samsung Electronics Co., LTD.).
24. U.S. Pat. 6,726,996 (Apr. 27, 2004), E. Barth, S. Cohen, C. Dziobkowski, J. Fitzsimmons, S. Gates, T. Ivers, S. Purshothaman, D. Restaino, and H. Wildman (to International Business Machine Corp.).
25. C. C. Cho, R. M. Wallace, and L. A. Files-Sesler, *J. Electronic Mater.* **23**, 827 (1994).
26. U.S. Pat. 7,336,875 (Feb. 26, 2008), H. Cho, J. Hwang, J. Choi, S. Cho, and Y. Son, Y. Park (to Samsung Electronics Co., Ltd.).
27. U.S. Pat. 7,150,815 (Dec. 19, 2006), J. Ashmead and S. Tang (to E.I. Du Pont de Nemours & Co., Inc.).
28. U.S. Pat. 7,463,398 (Dec. 9, 2008), B. Feenstra, R. Hayes, and M. Prins (to Liquivista B.B.).
29. U.S. Pat. 7,602,557 (Oct. 13, 2009), B. Berge and J. Peseux (to Varioptic S.A.).
30. U.S. Pat. 6,880,238 (Apr. 19, 2005) S. Kumar and G. Rajendran (to E. I. du Pont de Nemours & Co., Inc.).

SUBHASH V. GANGAL  
PAUL D. BROTHERS  
E. I. du Pont de Nemours & Co., Inc.  
Wilmington, Delaware

## PERFLUORINATED POLYMERS, TETRAFLUOROETHYLENE-PERFLUOROVINYL ETHER COPOLYMERS

### Introduction

Perfluoroalkoxy (PFA) fluorocarbon resins are designed to meet industry's needs in chemical, electrical, and mechanical applications. These melt-processible copolymers contain a fluorocarbon backbone in the main chain and randomly distributed perfluorinated ether side chains:



A combination of excellent chemical and mechanical properties at elevated temperatures results in reliable, high performance service to the chemical processing and related industries. Chemical inertness, heat resistance, toughness and flexibility, stress-crack resistance, excellent flex life, antistick characteristics, little moisture absorption, nonflammability, and exceptional dielectric properties are among the characteristics of these resins.

The introduction of a perfluoromethyl side chain (Teflon FEP) greatly reduces the crystallinity of polytetrafluoroethylene (PTFE). Crystallinity is reduced even further by replacing the short side chain with a long side chain, such as perfluoropropyl ether. In contrast to Teflon FEP, only a small amount of vinyl ether is required to reduce crystallinity and develop adequate toughness.

Tetrafluoroethylene (TFE) [116-14-3] and perfluorovinyl ether are copolymerized in aqueous (1,2) or nonaqueous (3) media. The polymer is separated and converted into various forms, such as extruded cubes, powders, beads, or dispersions. This family of products is sold by DuPont, Daikin, Dyneon, and Asahi Glass under the trade names of Teflon PFA, Neoflon AP, Hostaflon TFA, and Aflon PFA, respectively. Additional information on specific manufacturers' products can often be obtained by consulting their Web sites.

### Monomers

**Preparation.** The preparation of TFE has been described previously. Perfluorovinyl ethers (4–7) are prepared by the following steps. Hexafluoropropylene (HFP) [116-15-4] is oxidized to an epoxide HFPO [428-59-1] (5) which, on reaction with perfluorinated acyl fluorides, gives an alkoxyacyl fluoride.

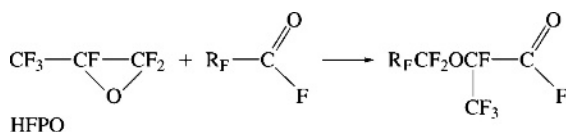
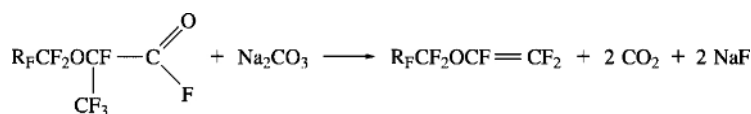


**Table 1. Properties of Perfluoropropyl Vinyl Ether,  $F_3C-CF_2-O-CF=CF_2$** 

Property	Value
Critical temperature, °K	423.58
Critical pressure, MPa <sup>a</sup>	1.9
Critical volume, cm <sup>3</sup> /(g·mol)	435
Surface tension, mN/m (=dyn/cm)	9.9
Boiling point, °C	36
Specific gravity (at 23°C)	1.53
Vapor density (at 75°C), g/cm <sup>3</sup>	0.2
Vapor pressure (at 25°C), kPa <sup>b</sup>	70.3
Solubility in water	0
Odor	None
Color	Colorless
Flash point, °C	-20
Flammable limits in air, <sup>c</sup> vol%	1

<sup>a</sup>To convert MPa to atm, divide by 0.1013.<sup>b</sup>To convert kPa to psi (psia), multiply by 0.145.<sup>c</sup>Extremely flammable.

The alkoxyacyl fluoride is converted to vinyl ethers by treatment with base at approximately 300°C (8).



where  $R_F = F(CF_2)_n$ .

Alkoxyacyl fluorides are also produced by an electrochemical process (9).

The preparation of perfluoromethyl and perfluoroethyl vinyl ethers is described in References 10 and 11.

**Properties.** Properties of perfluoropropyl vinyl ether (PPVE) [1623-05-8], a colorless, odorless liquid (molecular weight 266), are shown in Table 1. Perfluoropropyl vinyl ether is an extremely flammable liquid and burns with a colorless flame. It is significantly less toxic than HFP; the average lethal concentration is 50,000 ppm (12).

## Copolymerization

Tetrafluoroethylene-perfluoropropyl vinyl ether copolymers [26655-00-5] are made in aqueous (1,2) or nonaqueous media (3). In aqueous copolymerizations, water-soluble initiators and a perfluorinated emulsifying agent are used. The products previously manufactured with ammonium perfluorooctanoate as the perfluorinated surfactant can be produced using alternative surfactant systems (reference). Molecular weight and molecular weight distribution are controlled by a chain-transfer agent. Sometimes, a second phase is added to the reaction

medium to improve the distribution of the vinyl ether in the polymer (13); a buffer may also be added. In nonaqueous copolymerization, fluorinated acyl peroxides are used as initiators that are soluble in the medium (14) and a chain-transfer agent may be added for molecular weight control.

Temperatures range from 15 to 95°C and the pressures from 0.45 to 3.55 MPa (65–515 psi). The temperatures used for the aqueous process are higher than those for the nonaqueous process.

Alkyl vinyl ethers tend to rearrange when exposed to free radicals (15). Temperatures must be kept low enough to prevent termination by free-radical coupling. In the aqueous process, temperatures below 80°C minimize the number of acid end groups derived from vinyl ether transfer. In the nonaqueous process, temperature must also be limited to avoid excessive vinyl ether transfer as well as reaction with the solvent. End groups are stabilized by treating the polymer (16) with methanol, ammonia, or amines (17–19). Treatment of PFA with elemental fluorine generates CF<sub>3</sub> end groups and a very low level of contamination (20), which is important for the semiconductor industry (21).

The polymer is separated from the medium and converted to useful forms such as melt-extruded cubes for melt-processible applications. Teflon PFA is also available as a dispersion, fine powder, or in unmelted bead form.

Description and classification of PFA resins are given in Reference 22. Various specifications are given in Reference 23.

A family of copolymers containing TFE and perfluoromethyl vinyl ether modified with PPVE, referred to as MFA, is produced by Ausimont (24). The relatively small pendant group —O—CF<sub>3</sub> seems to have a similar effect on the crystallinity reduction as is exhibited by —CF<sub>3</sub> in FEP (perfluoropropylene-tetrafluoroethylene copolymer); however, the higher reactivity of perfluoromethyl vinyl ether than that of HFP makes the polymerization process more efficient. The performance characteristics are described in References 11 and 25.

A new family of copolymers called Teflon HP Plus has been introduced by DuPont, using perfluoroethyl vinyl ether analogous to PPVE used to produce the standard PFA (26). A significantly higher reactivity of perfluoroethyl vinyl ether has made it possible to produce copolymers with widely different comonomer concentrations on a commercial scale while reducing the tendency to rearrange and form acid end groups from vinyl ether transfer. Even though perfluoroethyl group provides a somewhat shorter pendant group, its effect on the reduction of crystallinity is very similar to that of perfluoropropyl group. This makes the perfluoroethyl vinyl ether an optimum comonomer to produce a versatile family of products.

## Properties

The melting point of commercial Teflon PFA is 305°C, that is, between those of PTFE and FEP. Second-order transitions are at –100, –30, and 90°C, as determined by a torsion pendulum (27). The crystallinity of the virgin resin is 65–75%. Specific gravity and crystallinity increase as the cooling rate is reduced. An ice-quenched sample with 48% crystallinity has a specific gravity of 2.123, whereas the press-cooled sample has a crystallinity of 58% and a specific gravity of 2.157.

Table 2. Properties of Teflon PFA

Property	ASTM method	Teflon 340	Teflon 350
Nominal melting point, °C		302–306	302–306
Specific gravity	D3307	10.6	1.8
Continuous use temperature, °C		260	260
Tensile strength, MPa <sup>a</sup>			
(at 23°C)	D1708	28	31
(at 250°C)		12	14
Tensile yield, MPa <sup>a</sup>			
(at 23°C)	D1708	14	15
(at 250°C)		3.5	4.1
Ultimate elongation, %			
(at 23°C)		300	300
(at 250°C)	D1708	480	500
Flexural modulus, MPa <sup>a</sup>			
(at 23°C)	D790	655	690
(at 250°C)		55	69
Creep resistance <sup>b</sup> tensile, modulus, MPa <sup>a</sup>			
(at 20°C)	D695	270	270
(at 250°C)	D695	41	41
Hardness durometer	D2240	D60	D60
MIT folding endurance, 775–200 $\mu$ m film thickness, cycles		50,000	500,000
Water absorption, %	D570	0.03	0.03
Coefficient of linear thermal expansion per °C	D696		
20–100°C		$12 \times 10^{-5}$	$12 \times 10^{-5}$
100–150°C		$17 \times 10^{-5}$	$17 \times 10^{-5}$
150–210°C		$20 \times 10^{-5}$	$20 \times 10^{-5}$

<sup>a</sup>To convert MPa to psi, multiply by 145.

<sup>b</sup>Apparent modulus after 10 h: stress = 6.89 MPa at 20°C, 6.89 kPa at 250°C.

**Mechanical Properties.** Table 2 shows the physical properties of Teflon PFA (28,29). At 20–25°C, the mechanical properties of PFA, FEP, and PTFE are similar; differences between PFA and FEP become significant as the temperature is increased. The latter should not be used above 200°C, whereas PFA can be used up to 260°C. Tests at liquid nitrogen temperature indicate that PFA performs well in cryogenic applications (Table 3).

Unfilled Teflon PFA has been tested in mechanical applications, using Teflon FEP 100 as a control (30). Tests were run on molded thrust bearings at 689.5 kPa (100 psi) against AISI 1080, Rc 20, 16AA steel, and at ambient conditions in air without lubrication. A limiting PV value of 5000 was found. Wear factors and dynamic coefficients of friction are shown in Table 4.

Hardness is determined according to ASTM D2240 on  $7.6 \times 12.7 \times 0.48$ -cm injection-molded panels (31). Results on the D scale are 63–65 for Teflon PFA and 63–66 for Teflon FEP.

**Chemical Properties.** A combination of excellent chemical and mechanical properties at elevated temperatures results in high performance service in

**Table 3. Cryogenic Properties of Teflon PFA Resins**

Property	ASTM method	At 23°C	At -196°C
Yield strength, MPa <sup>a</sup>	D1708 <sup>b</sup>	15	
Ultimate tensile strength, MPa <sup>a</sup>	D1708 <sup>b</sup>	18	129
Elongation, %	D1708 <sup>b</sup>	260	8
Flexural modulus, MPa <sup>a</sup>	D790-71 <sup>c</sup>	558	5790
Impact strength, notched Izod, J/m <sup>d</sup>	D256-72a <sup>e</sup>	No break	64
Compressive strength, MPa <sup>a</sup>	D695		414
Compressive strain, %	D695		35
Modulus of elasticity, MPa <sup>a</sup>	D695		4690

<sup>a</sup>To convert MPa to psi, multiply by 145.

<sup>b</sup>Crosshead speed B, 1.3 mm/min; used at both temperatures for more direct comparison.

<sup>c</sup>Method 1, procedure B.

<sup>d</sup>To convert J/m to ft-lbf/in., divide by 53.38.

<sup>e</sup>Method A, head weight is 4.5 kg at 23°C and 0.9 kg at 160°C.

**Table 4. Teflon PFA Fluorocarbon Resin Thrust-Bearing Wear-Test Results<sup>a</sup>**

Velocity, m/min	Wear factor <i>K</i> , 10 <sup>17</sup> 1/Pa <sup>6</sup>	Dynamic coefficient of friction	Test duration, h
Teflon PFA TE-9704			
0.91	3.12	0.210	103
3.05	3.67	0.214	103
9.1	1.96	0.229	103
15.24	1.38	0.289	103
Teflon FEP 100			
0.91	3.71	0.341	104
3.05	2.19	0.330	104
9.1	3.16	0.364	104
15.24	1.60	0.296	103

<sup>a</sup>Mating surface: AISA 1018 steel, Re 20, 16AA; contact pressure: 689 kPa; at 20°C in air; no lubricant.

<sup>6</sup>To convert 1/Pa to (in.·min)/(ft-lbf·h), divide by 2 × 10.

the chemical processing industry. Teflon PFA resins have been exposed to a variety of organic and inorganic compounds commonly encountered in chemical service (32). They are not attacked by inorganic acids, bases, halogens, metal salt solutions, organic acids, and anhydrides. Aromatic and aliphatic hydrocarbons, alcohols, aldehydes, ketones, ethers, amines, esters, chlorinated compounds, and other polymer solvents have little effect. However, like other perfluorinated polymers, they react with alkali metals and elemental fluorine.

**Thermal Stability.** Teflon PFA resins are very stable and can be processed up to 425°C. Thermal degradation is a function of temperature and time. A significant increase in melt flow rate indicates degradation after a short time above 425°C; at lower temperatures degradation takes longer. Degradation is not significant if the change in melt flow rate of the resin during molding is below 20%. Degradation is also indicated by the formation of small bubbles or discoloration; however, high stock temperatures may cause slight discoloration without adversely affecting properties.

**Table 5. Electrical Properties of Teflon PFA**

Property	ASTM method	Value
Dielectric strength, <sup>a</sup> kV/m		79
Volume resistivity, $\Omega\cdot\text{cm}$	D257	$10^{18}$
Surface resistivity, $\Omega/\text{sq}$	D257	$10^{18}$
Dissipation factor	D150	
(at $10^2$ Hz)		0.000027
(at $10^6$ Hz)		0.000080
(at $10^7$ Hz)		0.000145
(at $10^9$ Hz)		0.00115
(at $3 \times 10^9$ Hz)		0.00144
(at $1.4 \times 10^{10}$ Hz)		0.00131
(at $2.4 \times 10^{10}$ Hz)		0.00124

<sup>a</sup>Short term, 250  $\mu\text{m}$  thick sample.

Heat aging at 285°C, a temperature slightly below but near the melting point, increases the strength of Teflon PFA. Samples aged in a circulating air oven for 7500 h at 285°C show a decrease in melt flow number as defined by ASTM D2116. A decline in melt flow number indicates an increase in average molecular weight, which is also indicated by a 25% increase in tensile strength and enhanced ultimate elongation. Toughness is also measured by MIT flex life, which improves severalfold on heat aging at 285°C.

When exposed to fire, Teflon PFA contributes little in fuel value and is self-extinguishing when the flame is removed. The fuel value is approximately 5.4 MJ/kg (2324 Btu/lb). It passes the UL-83 vertical-flame test and is classified as 94VE-O according to UL-94. The limiting oxygen index by ASTM D2863 is above 95%.

**Electrical Properties.** The electrical properties of Teflon PFA are given in Table 5. The dielectric constant of PFA resins is about 2.06 over a wide range of frequencies ( $10^2$  to  $2.4 \times 10^{10}$  Hz), temperatures, and densities (ASTM D150). The values for PFA density vary only slightly (2.13–2.17), and the dielectric constant varies only about 0.03 units over this range, among the lowest of all solid materials. Humidity has no measurable effect on the dielectric constant of PFA. The dielectric strength (short-term) of PFA resins is 80 kV/mm (0.25-mm films, ASTM D149); FEP films give similar results, whereas PTFE films are typically measured at 47 kV/mm. Like other fluoropolymer resins, PFA loses dielectric strength in the presence of corona discharge. The dissipation factor at low frequency ( $10^2$ – $10^4$  Hz) decreases with increasing frequency and decreasing temperature. Temperature and frequency have little influence on the dissipation factor over the frequency range  $10^4$ – $10^7$  Hz. As frequencies increase to  $10^{10}$  Hz, there is a steady increase in dissipation factor. Above  $10^7$  Hz, increases measured at room temperature are highest; a maximum at about  $3 \times 10^9$  Hz is indicated. The higher dissipation factor with increasing frequency should be considered in electrical insulation applications at high frequencies. The volume and surface resistivities of fluorocarbon resins are high and are not affected by time or temperature. When tested with stainless steel electrodes (ASTM D495), no tracking was observed for the duration of the test (180 s), indicating that PFA resin does not form a carbonized conducting path (33,34).



**Table 6. Optical Properties of Teflon PFA Film**

Property	ASTM method	Value
Refractive index <sup>a</sup>	D542-50	1.350 ± 0.002
Haze, %	D10003-52	4
Light transmission, %		
Ultraviolet <sup>b</sup> 0.25–0.40 μm		55–80
Visible, 0.40–0.70 μm		80–87
Infrared, 0.70–2.1 μm		87–93

<sup>a</sup>Measured at 546 nm and 20°C.<sup>b</sup>Cary model spectrophotometer.**Table 7. Effects of Radiation on Tensile Strength of PFA<sup>a</sup>**

Exposure, kGy	ASTM D1708	
	Tensile strength, MPa <sup>b</sup>	Elongation, %
0	30.27	358
5	28.20	366
10	24.96	333
20	21.24	302
50	14.55	35
200		<5
500		<5

<sup>a</sup>Sample: 250-μm compression-molded films of Teflon PFA 340. *Source:* G. E. resonance transformer, 2-MeV capacity at a current of 1 mA.<sup>b</sup>To convert MPa to psi, multiply by 145.

**Optical Properties and Radiation Effects.** Within the range of wavelengths measured [ultraviolet (UV), visible, and near-infrared (NIR) radiation], Teflon PFA fluorocarbon film transmits slightly less energy than FEP film (35) (Table 6). In thin sections, the resin is colorless and transparent; in thicker sections, it becomes translucent. It is highly transparent to IR radiation; UV absorption is low in thin sections. Weather-O-Meter tests indicate unlimited outdoor life.

Like other perfluoropolymers, Teflon PFA is not highly resistant to radiation (36). Radiation resistance is improved in vacuum, and strength and elongation are increased more after low dosages (up to 30 kGy or 3 Mrad) than with FEP or PTFE. Teflon PFA approaches the performance of PTFE between 30 and 100 kGy (3–10 Mrad) and embrittles above 100 kGy (10 Mrad). At 500 kGy (50 Mrad), PTFE, FEP, and PFA are degraded. The effect of radiation on tensile strength and elongation is shown in Table 7.

## Fabrication

Teflon PFA resins are fabricated by the conventional melt-processing techniques used for thermoplastics (37). Processing equipment is constructed of corrosion-resistant materials and can be operated at 315–425°C. A general-purpose grade, Teflon PFA 340, is designed for a variety of molding and extrusion applications,

including tubing, shapes, and molded components, in addition to insulation for electrical wire and cables. Because of the excellent thermal stability of Teflon PFA 350, a wide range of melt temperatures can be used for fabrication. Extrusion temperatures are 20–26°C above the melting point.

Teflon PFA 440 HP is a chemically modified form of Teflon PFA 340 that provides additional benefits such as enhanced purity and improved thermal stability. This product is suitable for producing tubing, pipe linings for production of ultrapure chemicals, semiconductor components, and fluid handling systems for high performance filters (38).

**Extrusion.** Like other thermoplastics, Teflon PFA resin exhibits melt fracture above certain critical shear rates. For example, samples at 372°C and 5-kg load show the following behavior:

Teflon PFA	Melt flow, g/10 min	Critical shear rate, s <sup>-1</sup>
340	14	50
310	6	16
350	2	6

Because Teflon PFA melt is corrosive to most metals, special corrosion-resistant alloys, such as Hastelloy C, Monel 400, and Xaloy 306, must be used for the extrusion equipment. Barrels, liners, screws, adapters, breaker plates, and dies are made of corrosion-resistant metals (39). Corrosion is promoted by resin degradation and high processing temperatures, long residence times, or dead spots. Extruders used with Teflon FEP are also suitable for PFA resins. Heaters and controllers capable of accurate operation in the range of 330–425°C are required. Extruder barrels should have three or four independently controlled heating zones, each equipped with its own thermocouple and temperature-indicating control.

The screw consists of a feed section, a rapid transition section, and a metering section; a rounded forward end prevents stagnation. The breaker plate that converts the rotary motion of the melt into smooth, straight flow should have as many holes as possible; both ends of each hole should be countersunk for streamlined flow.

The temperature of the melt downstream from the breaker plate may exceed the front barrel temperature because of the mechanical work transmitted to the resin by the screw; it varies with screw speed and flow rate. The melt temperature is measured by a thermocouple inserted into the melt downstream from the breaker plate. A hooded exhaust placed over the extruder die and feed hopper removes decomposition products when the extrudate is heated.

High melt strength of Teflon PFA 350 permits large reductions in the cross section of the extrudate by drawing the melt in air after it leaves the die orifice (40). At a given temperature, the allowable flow rates are limited at the low end by resin degradation and at the high end by the onset of melt fracture. A broader range of specific gravities (2.13–2.17) may be obtained in articles fabricated from Teflon PFA 350 than from FEP 160. Unlike with PTFE, higher crystallinity in PFA seems to have little effect on flex life.

**Injection Molding.** Any standard design plunger or reciprocating screw injection machine can be used for Teflon PFA 340, although a reciprocating screw machine is preferred (41). Slow injection into mold cavities avoids surface or internal melt fracture, and control of ram speed is important at low speed. Corrosion-resistant metals are used for parts in continuous contact with molten resin; Hastelloy C and Xaloy 306 or 800 are recommended.

Because the mold is usually maintained at temperatures below the melting point of the resin, corrosion on the mold surface is less than in the molding machine. Nonreturn ball check valves and ring check valves are used; the latter is preferred for PFA. A streamlined flow must pass through the valve, preventing areas of stagnant flow or holdup and localized degradation.

A smear head causes less stagnation and overpacking than a nonreturn valve. A conventional-type reverse-tapered nozzle with the bore as large as possible without sudden changes in diameter is preferred. Independently controlled, zone-type heaters for heating the nozzle and at least two zones on the cylinder are used.

At a holdup time longer than 10–15 min at a high temperature, resin degradation is avoided by keeping the rear of the cylinder at a lower temperature than the front. At short holdup times (4,5 min), cylinder temperatures are the same in rear and front. If melt fracture occurs, the injection rate is reduced; pressures are in the range of 20.6–55.1 MPa (3000–8000 psi). Low back pressure and screw rotation rates should be used.

The cycle can usually be estimated on the basis of about 30 s/3 mm of thickness; most of it is devoted to ram-in-motion time (except for very thin sections). The mold temperature used with Teflon PFA 340 is often the highest temperature that allows the part to be ejected undamaged from the mold and retain its shape while cooling.

The resin must be of highest purity for optimum processing characteristics and properties. Degradation results in discoloration, bubbling, and change in melt flow rate.

**Transfer Molding.** Valve and fitting liners are made by a transfer-molding process (42), with the valve or fitting serving as the mold. Melted resin is forced into the fitting at a temperature above the melting point of the resin. The melt may be produced by an extruder or an injection molding machine or melted cubes contained in a melt pot and transferred by applying pressure to a piston in the pot. After the resin transfer is completed, the fitting is cooled under pressure. Stock temperatures of 350–380°C and fitting temperatures of 350–370°C are used to process Teflon PFA 350. A slight adjustment in the cooling cycles may be required for transfer molding Teflon PFA 350 because it has higher melting and freezing points than FEP.

**Rotocasting Teflon PFA Beads.** The resin has sufficient thermal stability for a commercial rotocasting operation; that is, TE-9738 has a melting point of about 303°C. In rotocasting trials, incoming flue gas temperatures of 355–365°C (43,44) and heat cycles of 90–180 min have been used. Conventional rotations for major and minor axes can be applied without modifications; Freecote 33 performs adequately as a mold release agent. Mold release instructions can be followed without modification. Heating cycles, including a preheat stage and a fusion stage, give consistent rotocasting. Preheating at 15–30°C below the fusion

temperature takes 10–25 min. Heat-cycled Teflon PFA rotocastings are translucent white, often with bluish tinge. Rotocastings that have been heated too long may darken to a translucent brown. Uniform cooling is essential for undistorted, stress-free products; combinations of air and water are employed. The rotocasting is cooled below the resin melting temperature with air at ambient temperature, then with a water spray, and finally with a stream of air.

**Dispersion Processing.** A commercial aqueous dispersion of Teflon PFA contains more than 50 wt% PFA particles and about 5 wt% surfactants and fillers. PFA dispersion is processed by the same technique as for PTFE dispersion (45). It is used for coating various surfaces, including metal, glass, and glass fabrics. A thin layer of Teflon PFA coating can also serve as an adhesive layer for PTFE topcoat.

**Powder Coating.** Teflon PFA is also available in a finely divided powder form. It can be used to produce thin layers on various surfaces by heating these surfaces above the melting point of PFA and then bringing the powder in contact with them. This allows a thin layer of the powder to melt on the surface of the substrate.

For some applications, the powder is suspended in an aqueous medium or a solvent with the help of emulsifying agents and then sprayed onto the substrate. The powder is also used as a filler to prepare sprayable compositions of PTFE dispersions, which can then be used to coat various substrates (46).

**Pigmentation.** Commercial color concentrates of Teflon PFA containing approximately 2% pigment can be easily dispersed in clear extruded cubes. The resin can also be dry-blended with stable inorganic pigments. At 0.1–1% of concentration, the pigment has no appreciable effect on the dielectric strength and dielectric constant or mechanical properties. The dissipation factor of pigmented resin varies with the type and concentration of the pigment.

Pigment used for dry blending is dried overnight at 150°C in a vacuum oven to remove absorbed gases and moisture. It is screened through a 149- $\mu\text{m}$  (100-mesh) screen directly onto the cubes, which are rolled or tumbled for at least 15 min. The pigmented resin is stored in an airtight container to prevent absorption of moisture.

## Applications and Economic Aspects

The perfluorovinyl ether comonomer used for PFA is expensive, as is PFA. Most PFA grades are sold as extruded cubes. List prices for 2009 were from \$58.00 to \$80.00/kg depending on grade. Specialty molding grades or conductive products may list for up to \$105/kg. Some PFA types are also marketed in nonextruded forms as powder and dispersions for coatings.

Teflon PFA can be fabricated into high temperature electrical insulation (47,48) and components and materials for mechanical parts requiring long flex life. PFA is used as a liner for chemical process equipment, specialty tubing, and molded articles for a variety of applications (49–55). Teflon PFA 340 is a general-purpose resin for tubing, shapes, primary insulation, wire and cable jacketing, injection- and blow-molded components, and compression-molded articles. Teflon

PFA 440 HP is a chemically modified form of PFA with enhanced purity and improved thermal stability while processing. This resin is suitable in semiconductor manufacturing, fluid handling systems for industry or life sciences (56–59), and instrumentation for precise measurements of fluid systems.

## Health and Safety

Safe practices employed for handling PTFE and FEP resins are adequate for Teflon PFA (60); adequate ventilation is required for processing above 330–355°C. In rotoprocessing, a vacuum (250–750 Pa or 1.8–5.6 mm Hg) in the oven ensures exhaust to the outside (46). Removal of end caps or opening of sealed parts in a well-ventilated area ensures ventilation of decomposition fumes. During rotoprocessing, molds should be vented.

## BIBLIOGRAPHY

“Fluorinated plastics, tetrafluoroethylene copolymers with perfluoroalkoxy pendant groups” in *EPST* 1st ed., Suppl. Vol. 1, pp. 260–267, by R. L. Johnson, E. I. du Pont de Nemours & Co., Inc.; “Tetrafluoroethylene polymers, tetrafluoroethylene-perfluorovinyl ether copolymers” in *EPSE* 2nd ed., Vol. 16, pp. 614–626, by S. V. Gangal, E. I. du Pont de Nemours & Co., Inc.; “Perfluoroethylene polymers, tetrafluoroethylene-perfluorovinyl ether copolymers” in *EPST* 3rd ed., Vol. 3, pp. 422–435, by S. V. Gangal, E. I. du Pont de Nemours & Co., Inc.

## CITED REFERENCES

1. U.S. Pat. 3,132,123 (May 5, 1964), J. F. Harris and D. I. McCane (to E. I. du Pont de Nemours & Co., Inc.).
2. U.S. Pat. 3,635,926 (Jan. 18, 1972), W. F. Fresham and A. F. Vogelpohl (to E. I. du Pont de Nemours & Co., Inc.).
3. U.S. Pat. 3,536,733 (Oct. 27, 1970), D. P. Carlson (to E. I. du Pont de Nemours & Co.).
4. U.S. Pat. 3,358,003 (Dec. 12, 1967), H. S. Eleuterio and R. W. Meschke (to E. I. du Pont de Nemours & Co., Inc.).
5. U.S. Pat. 3,180,895 (Apr. 27, 1965), J. F. Harris and D. I. McCane (to E. I. du Pont de Nemours & Co., Inc.).
6. U.S. Pat. 3,250,808 (Oct. 10, 1966), E. P. Moore, A. S. Milian Jr., and H. S. Eleuterio (to E. I. du Pont de Nemours & Co., Inc.).
7. U.S. Pat. 4,118,421 (Oct. 3, 1978), T. Martini (to Hoechst Aktiengesellschaft).
8. U.S. Pat. 3,291,843 (Dec. 13, 1966), C. G. Fritz and S. Selman (to E. I. du Pont de Nemours & Co., Inc.).
9. U.S. Pat. 2,713,593 (July 1955), T. J. Brice and W. H. Pearlson (to Minnesota Mining and Manufacturing Co.).
10. U.S. Pat. 5,777,179 (July 7, 1998), P. Resnick, B. Liang, and M. Hung (to E. I. du Pont de Nemours & Co., Inc.).
11. P. Pozzoli, G. Vita, and V. Arcella, in J. Scheirs, ed., *Modern Fluoropolymers*, John Wiley & Sons, Inc., New York, 1997, p. 373.

12. A. H. Olson, E. I. du Pont de Nemours & Co., Inc., private communication, 1992.
13. U.S. Pat. 4,499,249 (Feb. 12, 1985), S. Nakagawa and co-workers (to Daikin Kogyo Co., Ltd.).
14. U.S. Pat. 2,792,423 (May 14, 1957), D. M. Young and W. N. Stoops (to Union Carbide and Carbon Corp.).
15. R. E. Putnam, in R. B. Seymour and G. S. Kirshenbaum, eds., *High Performance Polymers: Their Origin and Development*, Elsevier Scientific Publishing, Inc., New York, 1986, p. 279.
16. M. Pianca and co-workers, *J. Fluorine Chem.* **95**, 71–84 (1999).
17. U.S. Pat. 3,674,758 (July 4, 1972), D. P. Carlson (to E. I. du Pont de Nemours & Co., Inc.).
18. U.S. Pat. 4,599,386 (July 8, 1986), D. P. Carlson and co-workers (to E. I. du Pont de Nemours & Co., Inc.).
19. PCT Int. Appl. WO 8,911,495 (1989), M. D. Buckmaster (to E. I. du Pont de Nemours & Co., Inc.).
20. U.S. Pat. 4,943,658 (1988), J. Imbalzano and D. Kerbow (to E. I. du Pont de Nemours & Co., Inc.).
21. C. J. Goodman and S. Andrews, *Solid State Technol.* **65** (July 1990).
22. *PFA-Fluorocarbon Molding and Extrusion Materials*, ASTM 3307-86, American Society for Testing and Materials, Philadelphia, Pa., 1987.
23. *J. Teflon* **15**(1) (1974).
24. U.S. Pat. 5,463,006 (Oct. 31, 1995), J. A. Abusleme and P. Colaianna (to Ausimont, S.p.A.).
25. Ausimont (now Solvey Solexis). *Hyflon<sup>®</sup> MFA, Fluoropolymers 620 and 640, Properties and Applications Selection Guide*.
26. U.S. Pat. 5,760,151 (June 2, 1998), R. M. Aten, C. W. Jones, and A. H. Olson (to E. I. du Pont de Nemours & Co., Inc.).
27. R. A. Darby, E. I. du Pont de Nemours & Co., Inc., private communication, 1992.
28. *PFA Fluorocarbon Resins*, Sales Brochure, E08572, E. I. du Pont de Nemours & Co., Inc., Wilmington, Del.
29. M. I. Bro and co-workers, in *Proceedings of the 29th International Wire and Cable Symposium*, Cherry Hill, N.J., Nov. 1980.
30. *Teflon PFA Fluorocarbon Resins: Wear and Frictional Data*, APD #2 Bulletin, E. I. du Pont de Nemours & Co., Inc., Wilmington, Del., 1973.
31. *Teflon PFA Fluorocarbon Resins: Hardness*, APD #4 Bulletin, E. I. du Pont de Nemours & Co., Inc., Wilmington, Del., 1973.
32. *Teflon PFA Fluorocarbon Resins: Chemical Resistance*, PIB #2 Bulletin, E. I. du Pont de Nemours & Co., Inc., Wilmington, Del., 1972.
33. E. W. Fasig, D. I. McCane, and J. R. Perkins, in *Proceedings of the 22nd International Wire and Cable Symposium*, Atlantic City, N.J., Dec. 1973.
34. *Handbook of Properties for Teflon PFA*, Sales Brochure, E46679, E. I. du Pont de Nemours & Co., Inc., Wilmington, Del., Oct. 1987.
35. *Teflon PFA Fluorocarbon Resins: Optical Properties*, APD #6 Bulletin, E. I. du Pont de Nemours & Co., Inc., Wilmington, Del., 1973.
36. *Teflon PFA Fluorocarbon Resins: Response to Radiation*, APD #3 Bulletin, E. I. du Pont de Nemours & Co., Inc., Wilmington, Del., 1973.
37. K. Hintzer and G. Lohr, in J. Scheirs, ed., *Modern Fluoropolymers*, John Wiley & Sons, Inc., New York, 1997, p. 223.
38. *Teflon PFA 440 HP*, Product information, H-27760, E. I. du Pont de Nemours & Co., Inc., Wilmington, Del., 1990.
39. *Teflon PFA Fluorocarbon Resin: Injection Molding of Teflon PFA TE-9704*, PIB #4 Bulletin, E. I. du Pont de Nemours & Co., Inc., Wilmington, Del., 1973.

40. *Melt Extrusion Guide*, Technical Information, Bulletin No. H-45321, E. I. du Pont de Nemours & Co., Inc., Wilmington, Del., Mar. 1993.
41. *Injection Molding Guide for Teflon® FEP, PFA and Tefzel®*, Bulletin No. E-96680, E. I. du Pont de Nemours & Co., Inc., Wilmington, Del., July 1987.
42. *Transfer Moulding Guide*, Technical Information, Bulletin No. H-34556, E. I. du Pont de Nemours & Co., Inc., Wilmington, Del., Jan. 1972.
43. *Processing Guidelines for Du Pont Fluoropolymer Rotocasting Powders of Tefzel and Teflon PFA*, Technical Information, No. 11, E. I. du Pont de Nemours & Co., Inc., Wilmington, Del., 1982.
44. *Teflon PFA TE-9783 Rotation Molding Powder*, Technical Information, H-26600, E. I. du Pont de Nemours & Co., Inc., Wilmington, Del., June 1990.
45. U.S. Pat. 7,534,825 (May 19, 2009), M. Malvasi and V. Kapeliouchko (to Solvay-Solexis, S.p.A.).
46. Brit. Pat. 2051091B (Feb. 9, 1983), J. E. Bucino (to Fluorocoat Ltd.).
47. U.S. Pat. 7,553,551 (June 2, 2009), C. Park, G. Nam, J. Park, I. Kim, I. Seo, and G. Lee (to LS Cable, Ltd.).
48. U.S. Pat. 7,569,616 (Aug. 4, 2009), S. Kotera, H. Wakabayashi, S. Kinoshita, and H. Shimada (to Asahi Glass Co., Ltd.).
49. U.S. Pat. 7,553,551 (June 30, 2009), M. Chiu and N. Li.
50. U.S. Pat. 7,472,723 (Jan. 6, 2009), P. Marcolin (to Manifattura Tubi Gomma, S.p.A.).
51. U.S. Pat. 7,407,708 (Aug. 5, 2008), M. Amari, Y. Hashimoto, and T. Ogawa (to Entegris, Inc.).
52. U.S. Pat. 7,350,833 (Apr. 1, 2008), L. Bongiorno.
53. U.S. Pat. 7,116,199 (Oct. 3, 2006), D. Hall, H. Hall, D. Pixton, S. Dahlgren, C. Sneddon, J. Fox, and M. Briscoe (to Intelliserv, Inc.).
54. U.S. Pat. 6,577,841 (June 10, 2003), T. Hwang (to Samsung Electronics Co., Ltd.).
55. U.S. Pat. 6,241,393 (June 5, 2001), E. Georges and D. Tourneux (to Stephanois Rech MEC).
56. U.S. Pat. 7,582,100 (Sept. 9, 2009), E. Johnson, T. Fogarty, F. Arko, J. Elkins, and M. Seery (to Crux Biomedical Corp.).
57. U.S. Pat. 7,168,952 (Jan. 30, 2007), A. Karmaker, L. Lopez, B. Alpert, and B. Finnigan (to Pentron Clinical Technologies).
58. U.S. Pat. 6,989,486 (Jan. 24, 2006), P. Lovoi, P. Smith, and L. Lim (to Xoft Microtube, Inc.).
59. U.S. Pat. 6,648,874 (Nov. 18, 2003), M. Parisi, M. Willard, Y. Wang, R. Bianchi, and T. Rubesch (to Scimed Life Systems, Inc.).
60. *Guide to the Safe Handling of Fluoropolymers Resume*, 3rd ed., Fluoropolymers Division of the Society of the Plastics Industry, Inc., Washington, D.C., 1998.

SUBHASH V. GANGAL

PAUL D. BROTHERS

E. I. du Pont de Nemours & Co., Inc.  
Wilmington, Delaware

## PHASE TRANSFORMATION

### Introduction

Phase transformations of polymeric materials, such as unmixing of a polymer solution or polymer blend, or the crystallization of a polymer melt or its glass transition into an amorphous structure, are very common phenomena and have important applications. This article briefly summarizes some key theoretical concepts about these phenomena, discusses the extent to which they differ from related phenomena in other materials (1) and mentions a few typical experiments to introduce the main techniques used to study such phase transitions.

Some transitions that are only known for macromolecules, however, will not be mentioned at all since they are covered elsewhere in this Encyclopedia (see, eg. GEL POINT). Also we shall not be concerned here with the transformations from the molten state to the solid state of polymeric materials, since this is the subject of separate treatments (see CRYSTALLIZATION KINETICS; GLASS TRANSITION; VISCOELASTICITY). Unlike other materials, polymers in the solid state rarely reach full thermal equilibrium. Of course, all amorphous materials can be considered as frozen fluids (see GLASS TRANSITION). Rather perfect crystals exist for metals, oxides, semiconductors etc, whereas polymers typically are semicrystalline, where amorphous regions alternate with crystalline lamellae, and the detailed structure and properties are history-dependent (see SEMICRYSTALLINE POLYMERS). Such out-of-equilibrium aspects are out of the scope of the present article, which rather emphasizes general facts of the statistical thermodynamics (qv) of phase transitions and their applications to polymers in fluid phases.

### Thermodynamics

According to the Gibbs phase rule, a system containing  $z$  "components," ie, chemically different constituents, and  $r$  phases, has  $f = z + 2 - r$  degrees of freedom (such as temperature  $T$ , pressure  $p$ , or relative concentration  $c_i$  of the  $i$ th component (2)). When one applies this formula to systems containing polymers, one usually treats one chemical type of polymer as one component, even if it is polydisperse. Strictly speaking, each fraction with a specific molecular weight needs to be treated as a distinct component (see THERMODYNAMIC PROPERTIES OF POLYMERS). For many practical purposes this complication can be neglected. Special effects on phase transitions (3) due to polydispersity will be mentioned when appropriate.

"Phases" in thermodynamic systems are then macroscopic homogeneous parts with distinct physical properties. For example, densities of "extensive thermodynamical variables," such as particle number  $N_i$  of the  $i$ th species, enthalpy  $U$ , volume  $V$ , entropy  $S$ , and possible order parameters, such as the nematic order parameter for a liquid crystalline polymer etc, differ in such coexisting phases. In equilibrium, "intensive thermodynamic variables," namely  $T$ ,  $p$ , and the chemical potentials  $\mu_i$  have to be the same in all phases. Coexisting phases are separated by well-defined interfaces (the width and internal structure of such interfaces play an important role in the kinetics of the phase transformation (1) and in other



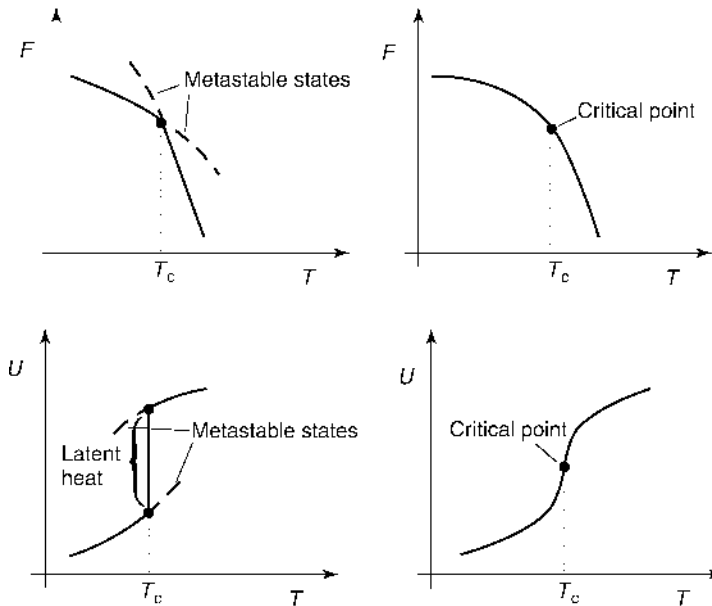


**Fig. 1.** Schematic variation of the Gibbs free energy  $F$  of a single-component system with temperature at constant pressure for a first-order transition (upper part left) and a second-order transition (upper part right). Lower part shows the corresponding behavior of the internal energy  $U$ .

material properties, see eg (4,5)). Phase transformations can be brought about eg by varying parameters such as temperature (Fig. 1) or pressure. In magnetic systems and superconductors also the magnetic field  $H$  is a suitable control parameter, in dielectric materials the electric field  $E$ . These variables will be ignored here throughout, although the switching of block copolymer mesophase structures by electric fields in thin films is of interest (6).

Figure 1 shows that one must distinguish first-order phase transitions [where first derivatives of the appropriate thermodynamic potential  $F$ , such as the enthalpy  $U = [\partial(\beta F)/\partial\beta]_p$ , where  $\beta = 1/k_B T$ ,  $k_B$  being Boltzmann's constant, or volume  $V \equiv (\partial F/\partial p)_T$  exhibit a jump] and second-order transitions, where  $U, V$  are continuous, but second derivatives are singular (1,2,7). The classical example for the latter case is the gas-liquid critical point, where the specific heat  $C_p = (\partial U/\partial T)_p$  or the isothermal compressibility  $\kappa_T = -(1/V)(\partial V/\partial p)_T$  diverge,

$$\kappa_T = \hat{\kappa}_T (T/T_c - 1)^{-\gamma}, \quad p = p_c, \quad T \rightarrow T_c^+ \quad (1)$$

where  $p_c$  is the critical pressure,  $T_c$  the critical temperature,  $\hat{\kappa}_T$  is called a "critical amplitude" and  $\gamma$  a "critical exponent," which has the value  $\gamma_{MF} = 1$  according to van der Waals theory and related mean-field theories (7,8), while  $\gamma_I \approx 1.24$  according to the Ising model "universality class" (7-10). Here we have already invoked the notion that the critical exponents that describe the asymptotic singular behavior as a critical point is approached do not depend upon which specific material is investigated, but are the same for all systems belonging to the same class.

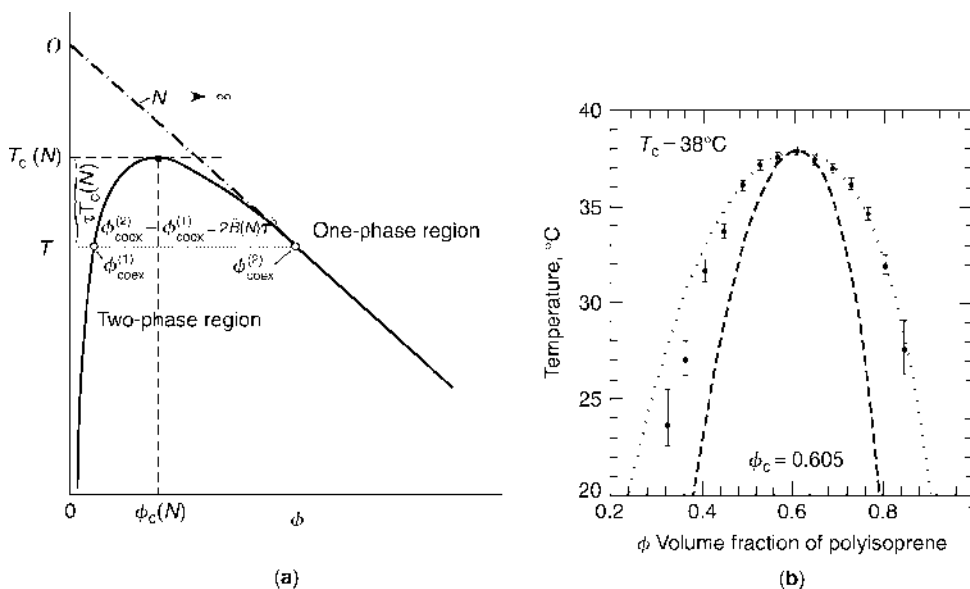


**Fig. 2.** (a) Schematic phase diagram of a polymer solution, at constant pressure, using temperature  $T$  and volume fraction  $\phi$  of the polymer as variables. Phase separation into a dilute or semidilute solution (with volume fraction  $\phi_{\text{coex}}^{(1)}$ ) and a more concentrated solution (with volume fraction  $\phi_{\text{coex}}^{(2)}$ ) occurs for states  $(T, \phi)$  that fall in the two-phase region underneath the coexistence curve (binodal). The binodal ends in the critical point  $\phi_c(N)$ ,  $T_c(N)$ , where  $N$  is the degree of polymerization of the polymer. For  $N \rightarrow \infty$  the critical point merges with the theta point of the dilute solution, ie,  $T = \Theta$ ,  $\phi_c(N \rightarrow \infty) = 0$ . For further explanations cf text. (b) Phase diagram of the partially miscible polymer blend poly(isoprene)–poly(ethylene) with molecular weights of 2000 and 5000, respectively. From Ref. 12. Broken curve inside of the coexistence curve (dotted) is the spinodal as estimated from a Flory–Huggins fit.

There are only a few classes, eg all systems in  $d = 3$  space dimensions, exhibiting for  $T < T_c$  a scalar “order parameter” belong to this same class. Of course, the gas–liquid transition is of little relevance for polymers simply because for high molecular weights  $T_c$  is too high, so that the polymer would chemically degrade already at much lower temperatures. Only for short alkanes gas–liquid critical phenomena can be studied (eg  $T_c = 723$  K for  $\text{C}_{16}\text{H}_{34}$  (11) while for  $\text{C}_{24}\text{H}_{50}$   $T_c$  is no longer available). However, it turns out that the phase diagram of a polymer in a solvent of variable quality (assuming that the quality is controlled by temperature) is isomorphic to the gas–liquid phase diagram of the polymer, see Figure 2a. Also phase diagrams of partially miscible polymer blends (qv) (see also MISCIBILITY) belong to the Ising class. Figure 2b presents an experimental example (12).

In Figure 2a, it was assumed that the pure solvent critical point is much higher than the  $\Theta$  temperature of the solution, so the latter can be approximated as incompressible for simplicity. Then the role of the pressure for the gas–liquid transition is now played by the osmotic pressure of the polymer in solution, and the volume fraction  $\phi$  rather than the density is used to distinguish the phases. In terms of  $t \equiv 1 - T/T_c(N)$  we can introduce another power law for the “order

parameter” of the transition  $\psi$ ,

$$\psi = (\phi_{\text{coex}}^{(2)} - \phi_{\text{coex}}^{(1)})/2 = \hat{B}(N)t^\beta \quad (2)$$

where  $\hat{B}(N)$  is another critical amplitude, and the exponent  $\beta$  takes the values  $\beta_{\text{MF}} = 1/2$  in the mean-field theories and  $\beta_{\text{I}} \approx 0.325$  in the Ising class. Here  $N$  denotes the degree of polymerization or “chain length” of the flexible linear polymer, respectively.

In Figure 1 we have already emphasized that at a first-order transition one typically finds metastable states. In principle, statistical thermodynamics describes systems in thermal equilibrium only, ie, only those branches of  $F$  that are the lower solid ones in the upper part of Figure 1 (left part) can be described, and nothing is said about the dashed continuations describing the metastable states. However, mean-field theories (such as the van der Waals equation of a fluid, or Flory–Huggins theory (13–15) for a polymer mixture) readily yield approximate descriptions of metastable states up to a “limit of metastability” or “spinodal.” Such a “spinodal curve” delineating this boundary between metastable and unstable regions in the  $(T, \phi)$  plane of a binary polymer mixture has been drawn in Figure 2b. It is important to realize, however, that such spinodals are mean-field concepts. They are meaningful objects in statistical thermodynamics in very special limiting cases only. One such limit is realized for polymer blends when the chain lengths  $N_A, N_B$  of the two flexible linear polymers constituting the mixture both tend to infinity (15–17). Then the mean-field spinodal line adopts a well-defined meaning as a sharp dividing line between two distinct kinetic mechanisms of phase separation: Metastable states in between binodal and spinodal (Fig. 2b) decay via nucleation and growth, while “unstable states” underneath the spinodal curve of the binary mixture decay by the spontaneous growth of “concentration waves” with wavelengths exceeding a characteristic critical wavelength  $\lambda_c$ , which diverges at the spinodal curve (Fig. 3). This mechanism of phase separation is called “spinodal decomposition” (15–20). Theory predicts (15–17) that in the limit  $N_A \rightarrow \infty, N_B \rightarrow \infty$  the lifetime of metastable states becomes infinite right up to the spinodal curve, since homogenous nucleation is suppressed. Although there is ample experimental evidence for the occurrence of (nonlinear) spinodal decomposition as a mechanism of phase separation in polymer blends (19), experimental evidence for the specific singularities associated with spinodal lines in the phase diagrams of mixtures is still lacking. Thus, although spinodal curves are often drawn in phase diagrams of real materials, such as in Figure 2b, we caution the reader that these curves are either the result of a mean-field fit or of some extrapolation procedure, and hence of limited validity.

## Phase Diagrams

When one approaches the critical point in the phase diagram (Figs. 2 and 3), the distinction between the two coexisting phases and also the difference  $\phi_{\text{coex}}^{(2)} - \phi_{\text{coex}}^{(1)}$  (cf eq. 2) vanish. Also the two branches of the spinodal curve meet in the critical point of the phase diagram. In Figures 2 and 3, we have assumed that the

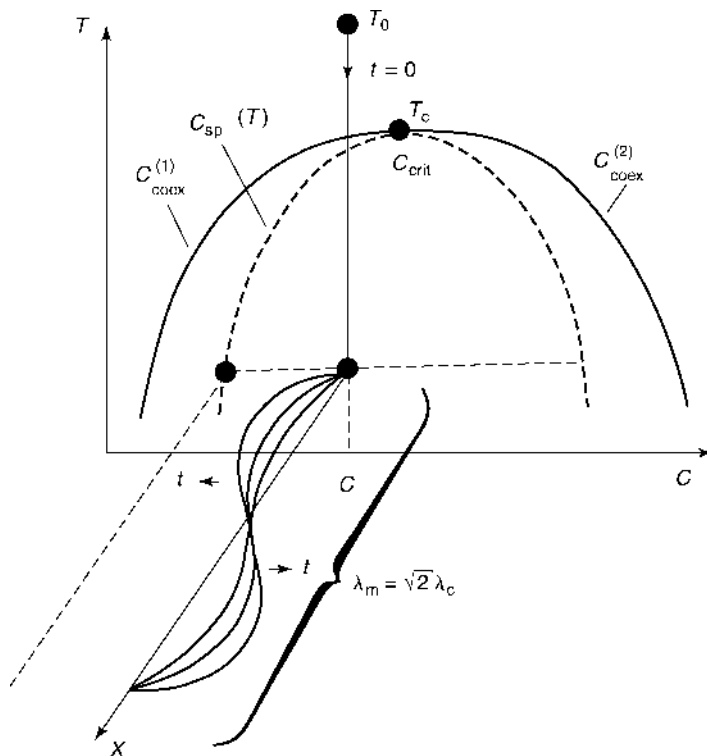


**Fig. 3.** Schematic illustration of a “quenching experiment” of a binary mixture, where phase separation via “spinodal decomposition” is initiated by a sudden reduction of temperature  $T$  from an initial temperature  $T_0$  in the one-phase region to a temperature  $T$  in the two-phase region in the temperature concentration ( $c$ ) plane underneath the spinodal (shown as broken curve) at time  $t = 0$ . While the average concentration  $\bar{c}$  stays constant, of course, in the course of time concentration inhomogeneities spontaneously develop with wavelengths  $\lambda_c < \lambda < \infty$ . Maximum growth occurs at a wavelength  $\lambda_m = \sqrt{2}\lambda_c$ , according to the linearized theory of spinodal decomposition (18). This is symbolically indicated by showing growing waves assuming one spatial coordinate  $x$  only. In practice there is a band of growing wavelengths, and the phases of the waves and the orientations of the wave vectors are randomly distributed, and hence in real space the concentration pattern is not periodic.

phase diagram contains a miscibility gap at low temperatures, ie, an “upper critical solution temperature” (UCST) where  $T_c$ ,  $\phi_c$  is a maximum of both the coexistence curve and the spinodal. In fact, many polymer solutions and polymer blends show the opposite behavior, ie, the phases separate when the temperature is raised, starting at a “lower critical solution temperature” (LCST) (21) and there also are examples of systems that exhibit both LCST and UCST behavior, eg poly(isobutylene) dissolved in benzene (22).

At this point, we mention one important caveat: The assertion that the critical point is at a maximum or minimum of the coexistence curve in the  $(T, \phi)$ -plane is only true if the polymer is strictly monodisperse. One of the characteristic effects of polydispersity is that the critical point no longer coincides with the extremum of the coexistence curve (although it still is an extremum of the

spinodal) (23). An example for this behavior is the LCST mixture of poly(styrene) (PS) and poly(vinylmethylether) (PVME). For example, for molecular weights  $\bar{M}_w = 62700$  and  $\bar{M}_w = 60000$ , obtained from light scattering, one finds the minimum of the binodal at about  $\phi_{\min} \approx 0.38$  PS while  $\phi_c \approx 0.48$  PS (24).

Of course, the concepts of a “limit of metastability” for metastable states at first-order transitions, and the distinction between two mechanisms of phase separation (nucleation and growth of a new phase vs long wavelength instabilities (25,26)) is not only used for solutions or mixtures, but for first-order transitions (Fig. 1) in general. For example, for metallic alloys undergoing order–disorder transitions to ordered superstructures, which in typical cases (such as the Au–Cu system (1)) are of first-order, the concept of “spinodal ordering” was coined (27), and similar phenomena where an order parameter grows spontaneously out of a disordered phase are expected to occur for the order–disorder transition of block copolymers, for instance. As is well known (15,28–36), diblock copolymer melts display an order–disorder transition (ODT; also referred to as “microphase separation transition”) from a disordered melt to mesophases with various types of long-ranged order (Fig. 4) when the product of chain length  $N$  and Flory–Huggins parameter  $\chi$  [that characterizes the degree of incompatibility between the partners A and B of the block copolymer,  $N = N_A + N_B$ ,  $f = N_A/(N_A + N_B)$ ] is large enough. Actually, the phase diagrams of Figure 4 are grossly simplified as they assume perfect symmetry between A and B (same size and shape of the monomers, same chain stiffness, etc), and therefore the phase diagrams are perfectly symmetric around  $f = 1/2$ , which experimentally is known not to be the case (37). Additional phases occur in narrow regions of the phase diagram (such as the gyroid and close-packed spherical phases (33)) which are not displayed in Figure 4. At this point we also mentioned that ordered phases were also observed (37), such as the double diamond and perforated lamellar structure, which are—at least in the idealized mean-field limit—only metastable rather than truly stable phases (33).

While in the mean-field limit the self-assembly of block copolymers into ordered mesophases is only controlled by two parameters,  $\chi N$  and  $f$ , this is no longer true when one goes beyond mean-field theory by including the effect of statistical fluctuations (30). Then the chain length  $N$  enters as a separate parameter, and the topology of the phase diagram changes (Fig. 4b). Only in the limit  $N \rightarrow \infty$  mean-field theory is recovered, but this limit is hard to achieve since even for an effective chain length  $\bar{N} = 10^4$  ( $\bar{N} = [(\sqrt{6}R_g)^3 \rho_c]^2$ ,  $\rho_c$  being the chain density and  $R_g$  the gyration radius) there are appreciable differences between the actual phase diagram (Fig. 4b) and the corresponding mean-field limit (Fig. 4a). While in the mean-field limit for  $f = 1/2$  the ODT is a second-order transition, it is actually weakly of first order. Therefore close to the transition point the ordered phase forms from the disordered one also by nucleation and growth (31). Defining as an order parameter the amplitude  $A$  of a concentration wave

$$\phi(\vec{r}) = 2A \cos(q^* \vec{n} \cdot \vec{r} + \varphi), \quad q^* \approx 1.945/R_g \quad (3)$$

where  $\vec{n}$  is a unit vector perpendicular to the lamellas and  $\varphi$  characterizes the phase of the concentration wave, one can derive an effective free-energy functional  $f_H(A)$  as shown in Figure 5 (31). When  $\chi > \chi_0$ , only the disordered phase

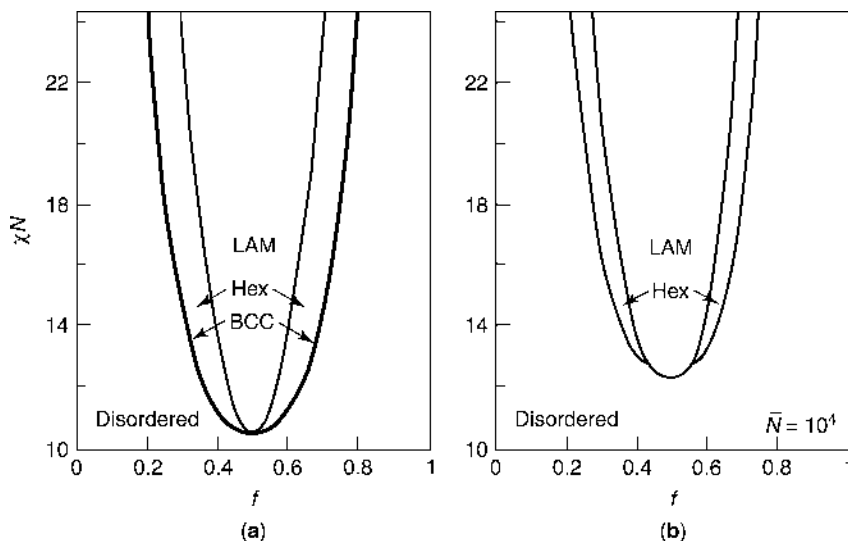


**Fig. 4.** Theoretically predicted phase diagrams of diblock copolymer  $A_f B_{1-f}$  melts in the plane of parameters  $\chi N$  ( $\chi$  = Flory–Huggins parameter,  $N$  = chain length) and composition  $f$  [where  $f = N_A/(N_A + N_B)$ ], according to the Leibler (29) random phase approximation (a) and the Fredrickson-Helfand (30) Hartree approximation (b). Mesophases considered are the lamellar (LAM) phase, the hexagonal (HEX) phase where cylinders rich in the minority component are arranged periodically, a cross section perpendicular through the cylinders yielding a triangular lattice, and the body-centered cubic (BCC) lattice of spherical micelles. From Ref. 32.

is stable (single minimum of  $f_H(A)$  at  $A = 0$ , Fig. 5a), while at  $\chi = \chi_0$  metastable minima with nonzero  $A$  appear, which become degenerate in depth with  $f_H(A = 0)$  at the transition point,  $\chi = \chi_t$ , (see Fig. 5c). Even for  $\chi > \chi_t$  the disordered phase ( $A = 0$ ) is still metastable, since the minimum at  $A = 0$  still persists and is separated by barriers from the stable minima. Note that the point  $\chi = \chi_0$  is a spinodal point of the ordered phase within the region of the phase diagram where the disordered phase is the stable one. Finally, we recall from equation 3 that the characteristic wavelength  $\lambda^* = 2\pi/q^*$  of the ordering is of the same order as the gyration radius of the chains, and hence of a “mesoscopic” scale rather than an atomistic scale. This justifies the name “mesophase” for the ordered structures in Figure 4.

Similar considerations as outlined here for diblock copolymers can be made for other types of orderings (liquid crystals (38,39)) or density functional theory of crystallization (melting transitions (40)). However, we shall not dwell on these topics (rather see LIQUID CRYSTALLINE POLYMERS and CRYSTALLIZATION KINETICS).

## Surfaces

The concept of phase transitions can be carried over from bulk systems also to their surfaces (41–47). To be specific, let us consider a binary polymer blend (A,B)

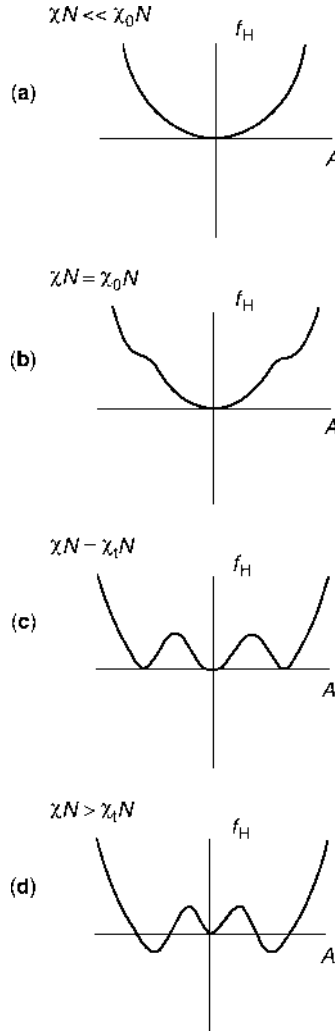


**Fig. 5.** Schematic free-energy functional  $f_H(A)$  of a symmetrical diblock copolymer ( $f = 1/2$ ) plotted vs the amplitude  $A$  of the concentration wave characterizing the lamellar ordering in the weak segregation limit. Cases (a–d) show  $f_H(A)$  for regions above (a) and at (b) the spinodal  $\chi_0$  of the ordered phase, at the order–disorder transition (c) and below it (d). From Ref. 31.

in a thin-film geometry (46,47). We suppose the film has a uniform thickness  $\mathcal{D}$  and is bounded by a substrate on its lower surface and by some other material (or gas or vacuum, respectively) on its upper surface, as is the common situation in the application of thin polymer films (4,5). Then the thermodynamic potential  $F$  needs to be decomposed into bulk and surface terms (41–47)

$$F = F_{\text{bulk}} + \frac{1}{\mathcal{D}} F_s^{(l)} + \frac{1}{\mathcal{D}} F_s^{(u)}, \quad \mathcal{D} \rightarrow \infty \quad (4)$$

where  $F_s^{(l,u)}$  are the surface excess free energies due to the lower (upper) boundary of the thin film. Just as the bulk free energy  $F$  may exhibit singularities (Fig. 1) as a function of external control parameters due to phase transitions, also surface excess free energies  $F_s$  may exhibit singularities due to surface phase transitions. For example, in a binary polymer blend one expects that one species (eg, B) is preferred by a surface, and hence there is an enrichment layer of B at this surface. A surface phase transition (of first order) then physically corresponds to a jump in thickness of this enrichment layer, caused eg by variation of temperature (if the thickness of the layer jumps from a finite value to infinity, this is called a “wetting transition,” while it is called “prewetting transition” if the jump occurs from a smaller to a larger value (48–50). Similar surface-induced ordering can also be considered for block copolymers (46,47,51,52). There is also great interest (both from theory (47,53) and from experiment (54) on surface effects on the kinetics of phase transformations in polymer blends (“surface-directed spinodal decomposition” (55,56). Finally, we mention that related concepts also apply to phase transformations of thin homopolymer films on substrates: If the film is metastable, the dewetting of the substrate starts by the nucleation and growth of holes in the film (57), while for unstable films “spinodal dewetting” (58,59) is predicted. A particular active field is also the study of phase transformations in thin block copolymer films (36,47,60,61).

## Critical Phenomena in Polymer Solutions and Blends

In this section we elaborate further on the phenomena that occur in the vicinity of the critical points (cf phase diagrams Figs. 2a and 2b), since these phenomena were extensively studied in the last decade and a rather definite knowledge about them has been gained.

Of course, a useful starting point of the discussion still is the Flory–Huggins mean-field theory (13–16), where the excess free-energy density of mixing is written as

$$\frac{1}{a^3} \frac{\Delta F_{\text{mix}}}{k_B T} = \frac{\phi_A \ln \phi_A}{N_A} + \frac{\phi_B \ln \phi_B}{N_B} + \chi \phi_A \phi_B \quad (5)$$

where  $a$  is the lattice spacing of the underlying lattice model;  $\phi_A$ , and  $\phi_B = 1 - \phi_A$  are the volume fractions of the two types of (effective) monomers;  $N_A, N_B$  are the chain lengths of the two polymers (formally a polymer solution is obtained putting  $N_A = N, N_B = 1$ ); and the Flory–Huggins parameter  $\chi$  is related to pairwise interaction energies  $\varepsilon_{AA}, \varepsilon_{AB}, \varepsilon_{BB}$  via  $\chi = z [\varepsilon_{AB} - (\varepsilon_{AA} + \varepsilon_{BB})/2]/k_B T = z(\Delta\varepsilon)/k_B T$ ,  $z$  being the coordination number of the lattice.

Neglecting any possible dependence of  $\chi$  on  $\phi$  ( $= \phi_A$ ), the condition of the spinodal  $\chi_s$  becomes

$$\left. \frac{\partial^2 (\Delta F_{\text{mix}}/k_B T)}{\partial \phi^2} \right|_{\phi = \phi_s(\chi)} = 0 \Rightarrow 2\chi_s(\phi) = \frac{1}{\phi N_A} + \frac{1}{(1 - \phi)N_B} \quad (6)$$



For monodisperse polymers, the maximum of the spinodal  $\phi_s(\phi)$  yields the critical point

$$\phi_c^{\text{FH}} = (\sqrt{N_A/N_B} + 1)^{-1}, \quad 1/\chi_c^{\text{FH}} = 2(N_A^{-1/2} + N_B^{-1/2})^{-2} \quad (7)$$

For the special case of a symmetric mixture ( $N_A = N_B = N$ ), we have  $\phi_c = 1/2$  and  $\chi_c = 2/N$ , ie, the critical temperature  $k_B T_c = z(\Delta\varepsilon)/\chi_c = z(\Delta\varepsilon)N/2$  scales linearly with  $N$ . For the other special case of a polymer solution,  $\phi_c \propto 1/\sqrt{N}$  for  $N \rightarrow \infty$ , and  $1/\chi_c \rightarrow 2$ , ie, the theta temperature (Fig. 2a) is  $\Theta = 2z(\Delta\varepsilon)/k_B$ . The two branches of the coexistence curve are obtained as

$$\phi_{\text{coex}}^{(1,2)} - \phi_c = \pm \hat{B}(\chi/\chi_c - 1)^{1/2} \quad (8)$$

where  $\hat{B} = \sqrt{3}/2$  for a symmetric mixture, while  $\hat{B} \propto N^{-1/4}$  for a solution. In the latter case equation 8 holds only for  $x = \frac{1}{2}\sqrt{N}(\chi/\chi_c - 1) \ll 1$  (62). In the opposite limit  $x \gg 1$ , one rather finds (62)

$$\phi_{\text{coex}}^{(1)} \approx \frac{3}{2}(1 - T/T_c) \exp\left[-\frac{3}{8}(1 - T/T_c)^2 N\right], \quad \phi_{\text{coex}}^{(2)} \approx \frac{3}{2}(1 - T/\Theta) \quad (9)$$

For  $N \rightarrow \infty$  (keeping  $1 - T/\Theta$  fixed) one hence finds  $\phi_{\text{coex}}^{(2)} - \phi_{\text{coex}}^{(1)} \propto (1 - T/\Theta)$ , ie, the exponent of the order parameter now is  $\beta_{\text{MF}}^t = 1$ , as expected for a tricritical point (62).

Of course, it is of interest to study how the critical properties of a polymer solution scale with  $N \rightarrow \infty$  (62–68). A standard assumption invokes power laws (66)

$$\hat{B}(N) \propto N^{-x_1}, \quad \phi_c(N) \propto N^{-x_2}, \quad \Theta - T_c(N) \propto N^{-x_3} \quad (10)$$

which have the mean field values  $x_1^{\text{MF}} = 1/4$ ,  $x_2^{\text{MF}} = 1/2$ ,  $x_3^{\text{MF}} = 1/2$ . Assuming that the mean-field-type scaling behavior  $\phi_{\text{coex}}^{(2)} - \phi_{\text{coex}}^{(1)} \propto N^{-1/2} \tilde{\phi}[N^{1/2}(1 - T/T_c)]$  holds generally but in the vicinity of  $T_c$  one must recover equation 2 with the correct Ising universality class exponent  $\beta \approx 0.325$  yields instead  $x_1 = (1 - \beta)/2 \approx 0.34$  (14,62), while the exponents  $x_1, x_3$  would keep their mean-field values. However, the results of many experiments (64,65) and simulations (66,67) agree only with  $x_3 = 1/2$  but suggest instead  $x_2 \approx 0.38$ , if one insists on the simple power laws (eq. 10). The idea involved to explain  $x_2 \approx 0.38$ , namely that the chains at the critical point are already partially collapsed and no longer ideal Gaussian coils (as they should be at the theta point (14)), is also clearly refuted by the simulations. There are several possibilities to explain the problems with equation 10. For example, one expects logarithmic corrections to the simple power laws near a tricritical point (63)

$$\phi_c(N) \propto (\ln N)^{1/2}/N^{1/2}, \quad \Theta - T_c(N) \propto N^{-1/2}(\ln N)^{-3/11}, \quad N \rightarrow \infty \quad (11)$$

It is rather likely, however, that neither experiments nor simulations have reached the regime of sufficiently large  $N$  yet where equation 11 is observed.

Another possibility is that the crossover between mean field and Ising critical behavior, which is spread out over many decades in  $1 - T/T_c$  (68,69), also causes the exponents  $x_1, x_2, x_3$  in equation 10 to be “effective exponents,” which show a significant variation when one studies  $\hat{B}(N), \phi_c(N)$ , etc. over many decades in  $N$ . Usually experiments and simulations have only 1 to 2 decades in  $N$  at their disposal, and therefore all conclusions on the validity of equations 10 and 11 are still preliminary. However, experiments do allow a study of enough decades in  $|1 - T/T_c|$  to confirm the theoretical expectation that the critical exponents  $\beta, \gamma$ , etc. take the values of the Ising universality class.

While the Flory–Huggins mean-field theory is not a good approximation for the description of critical phenomena in polymer solutions, it works much better for (approximately symmetric) polymer blends. To understand this fact, it is useful to consider the scattering from concentration fluctuation within the framework of the “random phase approximation (RPA)” (14). It is based on the assumption that the chain configurations in the blend are unperturbed Gaussian coils, and it reduces the collective scattering function  $S_{\text{coll}}(\vec{q})$ ,  $q$  being the scattering wavevector, to the single-chain factors  $S_A(\vec{q}), S_B(\vec{q})$  as follows,

$$S_{\text{coll}}^{-1}(\vec{q}) = [\phi S_A(\vec{q})]^{-1} + [(1 - \phi) S_B(\vec{q})]^{-1} - 2\chi_{\text{eff}} \quad (12)$$

where  $S_A(q) = N f_D(R_{g,A}^2 q^2)$ ,  $f_D(x)$  being the Debye function  $f_D(x) = (2/x^2)[\exp(-x) - 1 + x]$ ,  $R_{g,A} = \sigma_A \sqrt{N_A/6}$  being the gyration radius of the A chains, and  $\sigma_A$  their segment sizes. A similar notation holds for the B component.  $\chi_{\text{eff}} = \chi$  if  $\chi$  is strictly independent of  $q$ , otherwise (15,16)  $\chi_{\text{eff}} = - (1/2) \partial^2 / \partial \phi^2 [\phi(1 - \phi)\chi(\phi)]$ . The RPA expression is routinely used to extract the Flory–Huggins parameter from small-angle neutron scattering experiments. Unfortunately, the value depends slightly on the system (eg, there are differences between homopolymer blends and block copolymer systems (70)) and on the method (eg, scattering, composition of the coexisting phases and surface enrichment (71)). Expanding equation 12 for small  $q$  yields

$$S_{\text{coll}}(q) = S_{\text{coll}}(0)/(1 + q^2 \xi^2) \quad (13)$$

with  $S_{\text{coll}}^{-1}(0) = (\phi N_A)^{-1} + [(1 - \phi) N_B]^{-1} - 2\chi_{\text{eff}}$ .  $1/S_{\text{coll}}$  vanishes at the spinodal curves (cf eq. 6, and  $\xi$  is the correlation length of the concentration fluctuations. Defining the effective lattice parameter  $a$  of the Flory–Huggins lattice by  $a^2 = \sigma_A^2(1 - \phi) + \sigma_B^2 \phi$ , one finds for  $\phi = \phi_c$ ,  $\chi < \chi_c$  that

$$S_{\text{coll}}(0) = (2\chi_c)^{-1} (1 - \chi/\chi_c)^{-1}, \quad \xi = \frac{a}{6} (4N_A N_B)^{1/4} (1 - \chi/\chi_c)^{-1/2} \quad (14)$$

which are special cases of the relations  $S_{\text{coll}}(0) = \hat{S}(T/T_c - 1)^{-\gamma}$ ,  $\xi = \hat{\xi}(T/T_c - 1)^{-\nu}$  describing the critical singularities of the critical scattering intensity and correlation length, respectively, with  $\gamma_{\text{MF}} = 1$ ,  $\nu_{\text{MF}} = 1/2$ , the corresponding mean-field exponents. Equation 14 shows that the critical amplitude  $\hat{\xi}$  for a symmetrical polymer mixture is of the same order as the gyration radius  $R_g$  (while for a polymer solution it is much smaller,  $\hat{\xi} \propto \sqrt{a R_g}$ ). This large value of  $\hat{\xi}$  is critical for the validity of mean-field theory for  $N \rightarrow \infty$ , as the Ginzburg criterion (72,73)

shows. According to this criterion mean-field theory is valid when the fluctuation of the order parameter in a correlation volume is much less than the mean square order parameter itself. This yields (in  $d$  dimensions)

$$\hat{S}\hat{\xi}^{-d}/\hat{B}^2 \ll |1 - T/T_c|^{(2-d)/2} \quad \text{or} \quad \text{Gi} \ll |1 - T/T_c| \quad (15)$$

where the “Ginzburg number”  $\text{Gi}$  is proportional to  $(\hat{S}\hat{\xi}^{-d}/\hat{B}^2)^{2/(4-d)}$ . For a symmetric polymer mixture,  $\hat{B}$  is of order unity, while  $\hat{S} \propto N$ ,  $\hat{\xi} \propto N^{1/2}$ , and hence  $\text{Gi} \propto N^{(2-d)/(4-d)}$  ( $= 1/N$  in  $d = 3$ ). Thus for large enough  $N$  mean-field theory becomes valid for polymer mixtures in  $d = 3$  (but not in  $d = 2$ , ie, for polymer blends in thin film geometry  $\text{Gi}$  is of order unity). For polymer solutions, where  $\hat{B} \propto N^{-1/4}$ ,  $\hat{S}$  of order unity,  $\hat{\xi} \propto N^{1/4}$ , one rather finds  $\text{Gi} \propto N^{-1/2}$  in  $d = 3$ . Since equation 8 is only supposed to hold if  $\sqrt{N}(1-T/T_c) \ll 1$  but equation 15 requires that  $|1 - T/T_c| \gg 1/\sqrt{N}$ , we see that Flory–Huggins theory must fail in the critical region of a phase-separating polymer solution, and this is confirmed by experiment (65,69).

For polymer blends in  $d = 3$  it then turns out that a crossover scaling description applies (74–76),  $t = |1 - T/T_c|$ ,

$$\phi_{\text{coex}}^{(2)} - \phi_{\text{coex}}^{(1)} \propto t^{1/2} \tilde{B}(t/\text{Gi}), \quad S_{\text{coll}}(0) \propto Nt^{-1} \tilde{S}(t/\text{Gi}) \quad (16)$$

where the scaling functions for small values of their arguments behave as  $\tilde{B}(x) \propto x^{\beta-1/2}$ ,  $\tilde{S}(x) \propto x^{1-\gamma}$ , to reproduce the critical behavior of the Ising universality class. There exists an analytic approximation (74) for  $\tilde{\xi}(x)$  that provides a very good fit to the experimental data (76). However, while the above prediction  $\text{Gi} \propto 1/N$  is confirmed by simulations of an idealized lattice model (75) it is not compatible with the experimental data for polymer blends (76,77). This discrepancy is attributed to the compressibility of the blend (which is completely neglected in eqs. 5, 12 and 13, which gives rise to an anomalous pressure dependence of the Ginzburg number (77).

At this point, it is appropriate to critically reexamine to what extent the Flory–Huggins description (Eqs. 5–7) is valid as a phenomenological model. One important qualitative effect that is neglected completely is the “correlation hole effect” (14): For an effective monomer of a chain it is more likely to have other monomers in the neighborhood that belong to the same chain rather than to other chains. Of course, only interchain interactions and no intrachain interaction contribute to macroscopic phase separation, and hence the “effective coordination number”  $z$  that enters the Flory–Huggins parameter  $\chi$  gets reduced. It turns out (78) that this leads to  $1/\sqrt{N}$  corrections in  $d = 3$ ,  $z = z_\infty + \text{const}/\sqrt{N}$ , and similarly  $\chi_c = \chi_\infty + \text{const}/\sqrt{N}$ ,  $\phi_c = \phi_c^{\text{FH}} + \text{const}/\sqrt{N}$ , etc. In  $d = 2$ , however, this effect is far more drastic, since the chains can interpenetrate only rather little, and hence  $z \propto 1/\sqrt{N} \rightarrow 0$  as  $N \rightarrow \infty$ , and therefore also (79)  $\chi_c \propto 1/\sqrt{N}$  rather than  $\chi_c \propto 1/N$  as in the case of  $d = 3$ . The linear scaling of the critical temperature  $T_c$  with  $N$  in  $d = 3$  has been experimentally verified (80) while no systematic studies of phase separation of polymer blends in ultrathin films so far have been possible.

Of course, polymer blends are fluids, and a more realistic description of the packing of neighboring atomic groups is needed than can be achieved by Flory–Huggins theory (and its extensions that account for compressibility (81)). An approach that attempts to generalize theories of fluid structure and thermodynamics to polymer mixtures is the polymer reference interaction site model (PRISM) (82,83). While this approach is not useful for the critical properties, it clearly is a powerful description of the general interplay between structure and thermodynamics in polymer blends. It shares a disadvantage with the Monte Carlo computer simulation approach (75,78,84,85), namely that extensive numerical computations are mandatory. A complementary approach is the lattice cluster theory of Freed and co-workers (86), which takes better account of asymmetry in size and shape of monomers by using a lattice model with “monomers” occupying several lattice sites. The monomer shape might impart an entropic contribution (87,88) or a composition dependence (88) onto the Flory–Huggins parameter that might result in a significant modification of the phase behavior as a function of temperature and composition. However, there is neither a fully satisfactory approach that could predict the Flory–Huggins parameter (if one uses eq. 5 as an effective description) from atomistic input, nor can one describe the complete phase diagrams of binary and ternary blends and the structure of the coils under the various thermodynamic conditions accurately. Note that the RPA (eq. 12) also is a rough approximation only. In reality, the polymer coils do respond to the conditions of the thermodynamic state in which the system is in; eg, in a polymer blend typically chains of the minority component contract (89,90), while in block copolymer melts pretransitional chain stretching occurs (91,92)—and also is seen in the experiment (93)—because the center of mass of the A block gets separated from that of the B block, so that the polymer coil adopts a dumbbell-like shape. Because of all these limitations, the understanding of more complex phase-separation phenomena—where eg, microphase separation of block copolymers competes with macroscopic phase separation—are much less well understood, and will not be treated here. Such phenomena occur in blends of block copolymers (94) or blends of homopolymers with block copolymers (95).

We only mention, that for homopolymer–block copolymer mixtures RPA predicts that the wavelength  $\lambda^*$  of lamellar ordering may diverge at particular points in the phase diagram, so-called Lifshitz points (96); however, isotropic Lifshitz points are destabilized by statistical fluctuations and hence exist only in the mean field limit, while in reality one expects there a kind of “microemulsion” in the phase diagram. Such microemulsion phases also occur presumably in random copolymer melts (97), interpenetrating polymer networks (98), etc.

Returning now to the phase diagram of polymer solutions, we emphasize also that much more complicated phenomena than envisaged in Figure 2a can occur. For example, considering the solution of short alkane chains (eg hexadecane) in carbondioxide, one encounters a competition between gas–liquid transitions of both polymer ( $C_{16}H_{34}$ ) and solvent ( $CO_2$ ) and liquid–liquid phase separation (99,100). Thus the phase diagram not only contains (in the space of three variables  $p, T$ , and  $\phi$ ) various lines of critical points, but special points such as critical end points, triple points, and tricritical points may also occur. Each system then requires a separate detailed discussion on an atomistic level to understand all the possible phase changes that it can undergo. In this article, we hence have not

emphasized these rather specific aspects, but the general feature of the critical-point phenomena involved.

## Interfaces between Coexisting Phases

There are two methods to extend equation 5 to the inhomogeneous situation where a domain of the phase rich in polymer coexists with solvent or a domain rich in polymer A coexists with another domain rich in polymer B. The simplest approach (15,16,99,101) amends equation 5 with a  $(\nabla\phi)^2$  term; this is appropriate in the “weak segregation limit.” In the opposite case (“strong segregation limit”) one goes from pure A to pure B in a blend and the method of choice is the self-consistent field theory (102–106), which also is a powerful method for the study of the block copolymer phase diagrams in this strong segregation limit (32–36). These theories predict the “interfacial tension”  $f_{\text{int}}$  (= excess free energy due to the interface per unit area) and the “intrinsic width”  $w_0$  of the interface. For a polymer solution in the critical region near  $T_c(N)$ , the mean field theory yields (107)

$$f_{\text{int}} \propto N^{-1/4} [1 - T/T_c(N)]^{3/2}, \quad w_0 = 2\xi \propto N^{1/4} [1 - T/T_c(N)]^{-1/2} \quad (17)$$

while actually the behavior compatible with Ising universality class is (107), with  $\nu \approx 0.63$ ,

$$f_{\text{int}} \propto \xi^{-2} = N^{\nu-1} [1 - T/T_c(N)]^{2\nu}, \quad w_0 \propto N^{(1-\nu)/2} [1 - T/T_c(N)]^{-\nu} \quad (18)$$

Conversely, for the symmetrical polymer blend in the mean field critical regime the corresponding results are (15,16)

$$f_{\text{int}} \propto N^{-1/2} (1 - \chi_c/\chi)^{3/2}, \quad w_0 = 2\xi \propto N^{1/2} (1 - \chi_c/\chi)^{-1/2} \quad (19)$$

while in the Ising critical regime one has

$$f_{\text{int}} \propto \xi^{-2} = N^{2(\nu-1)} (1 - \chi_c/\chi)^{2\nu}, \quad w_0 = 2\xi \propto N^{1-\nu} (1 - \chi_c/\chi)^{-\nu} \quad (20)$$

Finally, we note the behavior in the strong segregation limit (102),  $\rho$  being the monomer density and  $a$  the statistical segment length, and a factor  $(k_B T)^{-1}$  is absorbed in  $f_{\text{int}}$

$$f_{\text{int}} = \rho a \sqrt{\chi/6}, \quad w_0 = a/\sqrt{6\chi} \quad (21)$$

Equation 20 also holds for a strongly segregated polymer solution (but then  $\chi$  is of order unity).

Now interfacial widths can be measured by depth-profiling techniques which eg use a nuclear reaction analysis to obtain the concentration profile through a thin polymer film (108,109) or by total reflection of neutrons (110) or X-rays. However, it should be noted that neither in an experiment nor in a simulation can one ever observe the “intrinsic width” of an interface, which is

an absolutely hypothetical object (106,111). Rather the observed width always results from a convolution of the intrinsic profile with the capillary wave broadening (106,111,112). On a lateral length scale  $L$ , one obtains for the actual mean square width

$$w^2 = w_0^2 + \frac{1}{4f_{\text{int}}}(\ln L - \ln \lambda_0) \quad (22)$$

where  $\lambda_0$  is the short wavelength cutoff of the capillary wave spectrum, and it was assumed that the thickness  $\mathcal{D}$  of the film is large enough such that the finite size effect due to  $\mathcal{D}$  is still negligible. In many circumstances this is not the case (109), and then a much stronger size effect  $w^2 \propto (\text{const } \mathcal{D})$  may result (113). Now the appropriate choice of  $\lambda_0$  is still questionable (104–106,114), and while  $f_{\text{int}}$  can be extracted if one observes the predicted linear variation between  $w^2$  and  $L$ , obviously there is no unique separation between  $w_0^2$  and  $\ln \lambda_0/(4f_{\text{int}})$ . In practice, observations of equation 22 are rare, and  $f_{\text{int}}$  is estimated experimentally by other methods (eg the “capillary rise” method or the “sessile drop” method, see eg Ref. 115).

Since many application properties of amorphous solid polymer blends (which often are phase-separated on a mesoscopic scale) are controlled by the interfaces they contain, a good understanding of the structure and properties of interfaces is very important. Simulations (116) have shown that free volume and chain ends get enriched at the interfaces, and homopolymers become oriented parallel to the interface at strong segregation, while adsorbed block copolymers tend to orient perpendicularly (117). The compatibilizing effect of block copolymers adsorbed to interfaces in unmixed blends is well known.

Once more, we emphasize that our treatment has simplified the topic enormously, and only the most salient features were mentioned. Complications due to the pressure dependence in blends and due to the gas–liquid transitions in polymer solvent-systems may lead to new effects. For example, for the interfaces between gaseous  $\text{CO}_2$  bubbles in a  $\text{C}_{16}\text{H}_{34}$  matrix one obtains interfacial wetting of fluid  $\text{CO}_2$ , which reduces the interfacial tension drastically and hence facilitates nucleation (118). In fact, an understanding of nucleation in polymer blends (119) and solutions (118) is just emerging.

## BIBLIOGRAPHY

“Phase Transformations” in *EPSE* 2nd ed., Vol. 11, pp. 30–45, by L. Leibler, Université Pierre et Marie Curie; in *EPST* 3rd ed., Vol. 10, pp. 766–788, by K. Binder and M. Müller, Institut für Physik, Johannes Gutenberg Universität, Mainz.

## CITED REFERENCES

1. G. Kostorz, ed., *Phase Transformations in Materials*, Wiley-VCH, Weinheim, 2001.
2. L. D. Landau and E. M. Lifshitz, *Statistical Physics*, Pergamon Press, Oxford, 1958.
3. P. Sollich, *J. Phys.: Condens. Matter* **14**, R79 (2002).
4. I. C. Sanchez, ed., *Physics of Polymer Surfaces and Interfaces*, Butterworth-Heinemann, Boston, 1992.

5. S. Granick, ed., *Polymers in Confined Environments* (Advances in Polymer Science, Vol. 138) Springer, Berlin, 1999.
6. T. Thurn-Albrecht, J. De Rouchy, T. P. Russell, and H. M. Jaeger, *Macromolecules* **33**, 3250 (2000).
7. D. Chowdhury and D. Stauffer, *Principles of Equilibrium Statistical Mechanics*, Wiley-VCH, Weinheim, 2000.
8. M. A. Anisimov and J. V. Sengers, in J. S. V. Sengers, R. F. Kayser, C. J. Peters, and H. J. White, eds., *Equations of State for Fluids and Fluid Mixtures*, Elsevier, Amsterdam, 2000, pp. 381–434.
9. M. E. Fisher, *Rev. Mod. Phys.* **46**, 587 (1974).
10. K. Binder and E. Luijten, *Phys. Rep.* **344**, 179 (2001).
11. M. J. Anselme, A. Gude, and A. S. Teja, *Fluid Phase Equilibria* **57**, 317 (1990).
12. A. Cumming, P. Wiltzius, and F. S. Bates, *Phys. Rev. Lett.* **65**, 863 (1990).
13. P. J. Flory, *Principles of Polymer Chemistry*, Cornell University Press, Ithaca, 1953.
14. P. D. de Gennes, *Scaling Concepts in Polymer Physics*, Cornell University Press, Ithaca, 1979.
15. K. Binder, *Adv. Polym. Sci.* **112**, 181 (1994).
16. K. Binder, *J. Chem. Phys.* **79**, 6387 (1983).
17. K. Binder, *Phys. Rev. A: At., Mol., Opt. Phys.* **29**, 341 (1984).
18. J. W. Cahn, *Acta Metall.* **9**, 795 (1961).
19. T. Hashimoto, in E. J. Kramer, ed., *Materials Science and Technology, Vol. 12: Structure and Properties of Polymers*, VCH, Weinheim, 1992.
20. K. Binder and P. Fratzl, in Ref. 1, pp. 409–480.
21. N. P. Balsara, in J. E. Mark, ed., *Physical Properties of Polymers Handbook*, AIP, Woodbury, New York, 1996.
22. J. M. Bardin and D. Patterson, *Polymer* **10**, 247 (1969).
23. R. Koningsveld and L. A. Kleintjens, *Macromolecular Chemistry*, Vol. 1, Butterworth, London, 1973, p. 97.
24. H. L. Snyder, P. Meakin, and S. Reich, *Macromolecules* **16**, 757 (1983).
25. K. Binder and D. Stauffer, *Adv. Phys.* **25**, 343 (1976).
26. J. D. Gunton, M. San Miguel, and P. S. Sahni, in C. Domb, and J. L. Lebowitz, eds., *Phase Transitions and Critical Phenomena*, Vol. 8, Academic Press, London, 1983, p. 267.
27. D. De Fontaine and H. E. Cook, in R. E. Miller, E. Ascher and I. Jaffee, eds., *Critical Phenomena in Alloys, Magnets and Superconductors*, McGraw Hill, New York, 1971, p. 257.
28. E. Helfand and Z. R. Wasserman, *Macromolecules* **9**, 879 (1976).
29. L. Leibler, *Macromolecules* **13**, 1602 (1980).
30. G. H. Fredrickson and E. Helfand, *J. Chem. Phys.* **87**, 697 (1987).
31. G. H. Fredrickson and K. Binder, *J. Chem. Phys.* **91**, 7265 (1989).
32. F. S. Bates and G. H. Fredrickson, *Annu. Rev. Phys. Chem.* **41**, 525 (1990).
33. M. W. Matsen and M. Schick, *Curr. Opin. Colloid Interface Sci.* **1**, 329 (1996).
34. I. W. Hamley, *The Physics of Block Copolymers*, Oxford University Press, Oxford, 1998.
35. J. Noolandi and A.-C. Shi, *Curr. Opin. Colloid Interface Sci.* **3**, 436 (1998).
36. M. J. Fasolka and A. M. Mayes, *Annu. Rev. Mater. Sci.* **31**, 323 (2001).
37. F. S. Bates, M. F. Schulz, A. K. Khandpur, S. Förster, and J. H. Rosedale, *Faraday Discuss.* **98**, 7 (1994).
38. P. G. de Gennes, *The Physics of Liquid Crystals*, Clarendon Press, Oxford, 1974.
39. S. Chandrasekhar, *Liquid Crystals*, Cambridge University Press, Cambridge, 1992.
40. M. Baus, *J. Stat. Phys.* **48**, 1129 (1987).

41. K. Binder, in C. Domb and J. L. Lebowitz, eds., *Phase Transitions and Critical Phenomena*, Vol. **8**, Academic Press, London, 1983, p. 1.
42. P. G. de Gennes, *Rev. Mod. Phys.* **57**, 827 (1985).
43. D. E. Sullivan and M. M. Telo da Gama, in C. A. Croxton, ed., *Fluid Interfacial Phenomena*, John Wiley & Sons, Inc., New York, 1986, p. 45.
44. S. Dietrich, in C. Domb and J. L. Lebowitz, eds., *Phase Transitions and Critical Phenomena*, Vol. **12**, Academic Press, London, 1988, p. 1.
45. M. Schick, in J. Charvolin, J. F. Joanny, and J. Zinn-Justin, eds., *Liquids at Interfaces*, North-Holland, Amsterdam, 1990.
46. K. Binder, *Acta Polym.* **46**, 204 (1994).
47. K. Binder, in Ref. 4, pp. 1–89.
48. J. W. Cahn, *J. Chem. Phys.* **66**, 3667 (1977).
49. I. Schmidt and K. Binder, *J. Phys. (France)* **46**, 1631 (1985).
50. M. Müller, K. Binder, and E. V. Albano, *Int. J. Mod. Phys. B* **15**, 1867 (2001).
51. G. H. Fredrickson, *Macromolecules* **20**, 2535 (1987).
52. K. Binder, H. L. Frisch, and S. Stepanow, *J. Phys. II (Paris)* **7**, 1353 (1997).
53. K. Binder, *J. Nonequil. Thermodyn.* **23**, 114 (1998).
54. G. Krausch, *Mater. Sci. Eng. Rep. R* **14**, 1 (1995).
55. R. A. L. Jones, L. H. Norton, E. J. Kramer, F. S. Bates, and P. Wiltzius, *Phys. Rev. Lett.* **66**, 1326 (1991).
56. S. Puri and K. Binder, *Phys. Rev. A* **46**, R4487 (1992).
57. G. Reiter, *Phys. Rev. Lett.* **68**, 75 (1992).
58. F. Brochard and J. Daillant, *Can. J. Phys.* **68**, 1084 (1990).
59. R. Xie, A. Karim, J. F. Douglas, C. C. Han, and R. A. Weiss, *Phys. Rev. Lett.* **81**, 1251 (1998).
60. T. P. Russell, *Curr. Opin. in Colloid Interface Sci.* **1**, 107 (1996).
61. K. Binder and M. Müller, *Curr. Opin. Colloid Interface Sci.* **5**, 315 (2000).
62. B. Widom, *Physica A* **194**, 532 (1993).
63. B. Duplantier, *J. Phys. (France)* **43**, 991 (1982).
64. I. C. Sanchez, *J. Appl. Phys.* **58**, 2871 (1985).
65. R. Perzynski, A. Delsanti, and M. Adam, *J. Phys. (France)* **48**, 155 (1987).
66. N. B. Wilding, M. Müller, and K. Binder, *J. Chem. Phys.* **105**, 802 (1996).
67. H. Frauenkron and R. Grassberger, *J. Chem. Phys.* **107**, 9599 (1997).
68. A. A. Povodyrev, M. A. Anisimov, and J. V. Sengers, *Physica A* **264**, 345 (1999).
69. Y. B. Melnichenko, M. A. Anisimov, A. A. Povodyrev, G. D. Wignall, J. A. Sengers, and W. A. Van Hook, *Phys. Rev. Lett.* **79**, 5266 (1997).
70. W. W. Maurer, F. S. Bates, T. P. Lodge, K. Almdal, K. Mortensen, and G. H. Fredrickson, *J. Chem. Phys.* **108**, 2989 (1998).
71. J. Klein, T. Kerle, F. Zink, and E. Eiser, *Macromolecules* **33**, 1298 (2000).
72. V. L. Ginzburg, *Sov. Phys. Solid State* **2**, 1824 (1960).
73. P. G. de Gennes, *J. Phys. Lett. (Paris)* **38**, L34 (1997).
74. M. Y. Belyakov and S. B. Kiselev, *Physica A* **190**, 75 (1992).
75. H.-P. Deutsch and K. Binder, *J. Phys. II (France)* **3**, 1049 (1993).
76. D. Schwahn, G. Meier, K. Mortensen, and S. Janssen, *J. Phys. II (France)* **4**, 837 (1994).
77. D. Schwahn, *Macromol. Symp.* **149**, 43 (2000).
78. M. Müller, and K. Binder, *Macromolecules* **28**, 1825 (1995).
79. A. Cavallo, M. Müller, and K. Binder, *Europhys. Lett.* **61**, 214 (2003).
80. M. D. Gehlsen, J. H. Rosedale, F. S. Bates, G. D. Wignall, and K. Almdal, *Phys. Rev. Lett.* **68**, 2452 (1992).
81. I. C. Sanchez and R. H. Lacombe, *Macromolecules* **11**, 1145 (1978).
82. K. S. Schweizer and J. G. Curro, *Adv. Chem. Phys.* **98**, 1 (1997).



83. K. S. Schweizer and A. Yethiraj, *J. Chem. Phys.* **98**, 9053 (1993).
84. K. Binder, in K. Binder, ed., *Monte Carlo and Molecular Dynamics Simulations in Polymer Science*, Oxford University Press, New York, 1995, pp. 356–432.
85. S. K. Kumar, *Macromolecules* **30**, 5085 (1997).
86. K. W. Foreman and K. F. Freed, *Adv. Chem. Phys.* **103**, 335 (1998).
87. J. Dudowicz, K. F. Freed, and J. F. Douglas, *J. Chem. Phys.* **116**, 9983 (2002).
88. M. Müller, *Macromolecules* **28**, 6556 (1995).
89. A. Sariban and K. Binder, *Macromol. Chem.* **189**, 2357 (1988).
90. M. Müller, *Macromolecules* **31**, 9044 (1998).
91. H. Fried and K. Binder, *Europhys. Lett.* **16**, 237 (1991).
92. K. Binder and H. Fried, *Macromolecules* **26**, 6878 (1993).
93. K. Almdal, J. H. Rosedale, F. S. Bates, G. D. Wignall, and G. H. Fredrickson, *Phys. Rev. Lett.* **65**, 1112 (1990).
94. H. Frielinghaus, N. Hermisdorf, K. Almdal, K. Mortensen, L. Messe, L. Corvazier, J. P. A. Fairclough, A. J. Ryan, P. D. Olmsted, and I. W. Hamley, *Europhys. Lett.* **53**, 680 (2001).
95. D. Schwahn, K. Mortensen, H. Frielinghaus, K. Almdal, and L. Kielhorn, *J. Chem. Phys.* **112**, 5454 (2000).
96. D. Broseta and G. H. Fredrickson, *J. Chem. Phys.* **93**, 2927 (1990).
97. J. Houdayer and M. Müller, *Europhys. Lett.* **58**, 660 (2002).
98. S. Stepanow, A. V. Dobrynin, T. A. Vilgis, and K. Binder, *J. Phys. I (Paris)* **6**, 837 (1996).
99. L. G. MacDowell, P. Virnau, M. Müller, and K. Binder, *J. Chem. Phys.* **117**, 6380 (2002).
100. P. Virnau, M. Müller, L. G. MacDowell, and K. Binder, *Comput. Phys. Commun.* **147**, 378 (2002).
101. J. F. Joanny and L. Leibler, *J. Phys. (France)* **39**, 951 (1978).
102. E. Helfand and Y. Tagami, *J. Chem. Phys.* **56**, 3592 (1971).
103. D. Broseta, G. H. Fredrickson, E. Helfand, and L. Leibler, *Macromolecules* **23**, 132 (1990).
104. A. N. Semenov, *Macromolecules* **26**, 6617 (1993).
105. A. N. Semenov, *Macromolecules* **27**, 2732 (1994).
106. A. Werner, F. Schmid, M. Müller, and K. Binder, *Phys. Rev. E* **59**, 728 (1999).
107. B. Widom, *Stat. Phys.* **52**, 1343 (1988).
108. A. Budkowski, *Adv. Polym. Sci.* **142**, 1 (1999).
109. T. Kerle, J. Klein, and K. Binder, *Euro. Phys. J. B* **7**, 401 (1999).
110. M. Stamm and D. W. Schubert, *Annu. Rev. Mater. Sci.* **25**, 325 (1996).
111. K. Binder and M. Müller, *Int. J. Mod. Phys. C* **11**, 1093 (2000).
112. D. Jasnov, *Rep. Prog. Phys.* **47**, 1059 (1984).
113. A. Werner, F. Schmid, M. Müller, and K. Binder, *J. Chem. Phys.* **107**, 8175 (1997).
114. A. Milchev and K. Binder, *Europhys. Lett.* **59**, 8 (2002).
115. K.-Q. Xia, C. Franck, and B. Widom, *J. Chem. Phys.* **97**, 1446 (1992).
116. M. Müller, K. Binder, and W. Oed, *J. Chem. Soc., Faraday Trans.* **91**, 2396 (1995).
117. A. Werner, F. Schmid, K. Binder, and M. Müller, *Macromolecules* **29**, 8241 (1996).
118. M. Müller, L. G. MacDowell, P. Virnau, and K. Binder, *J. Chem. Phys.* **117**, 5480 (2002).
119. S. M. Wood and Z. G. Wang, *J. Chem. Phys.* **116**, 2289 (2002).

KURT BINDER

MARCUS MÜLLER

Institut für Physik, Johannes Gutenberg Universität

## PHENOLIC RESINS

### Introduction

Phenolic resins are a large family of polymers and oligomers, composed of a wide variety of structures based on the reaction products of phenols with formaldehyde. Phenolic resins are employed in a wide range of applications, from commodity construction materials to high technology applications in electronics and aerospace. Generally, but not exclusively, thermosetting in nature, phenolic resins provide numerous challenges in the areas of synthesis, characterization, production, product development, and quality control.

As a family of resins originally developed in the early twentieth century, the nature and potential of phenolic resins have been explored thoroughly to produce an extensive body of technical literature (1–9). A symposium sponsored by the American Chemical Society commemorated 75 years of phenolic resin chemistry in 1983 (10), and in 1987 the Phenolic Molding Division of the Society of the Plastics Industry (SPI) sponsored a conference on phenolics in the twenty-first century (1). Exciting new developments continue as new systems are developed for carbon–carbon composites, aramid honeycombs, and new derivative chemistries such as cyanate esters and benzoxazines. New U.S. patents with phenolic resins in the claims are growing at about 150 patents per year.

Phenolic resins are prepared by the reaction of phenol or substituted phenol with an aldehyde, especially formaldehyde, in the presence of an acidic or basic catalyst. Their thermosetting character and the exotherm associated with the reaction presented technical barriers to commercialization. In 1900, the first U.S. patent was granted for a phenolic resin, using the resin in cast form as a substitute for hard rubber (11).

Work on the first commercially viable product was initiated by Baekeland in 1905. Using phenol and formaldehyde as starting materials, he established not only the differences between acid- and alkali-catalyzed products, but also the importance of excess phenol or formaldehyde made in producing intermediates. However, producing the resin was only part of the challenge. Baekeland also developed the technology to convert the reactive resins, which had a severe tendency to foam and cure to a brittle product, into useful molded articles by adding wood or mineral fibers and molding under heat and pressure. The final molded parts were tough, temperature resistant, and had a low void content (12). The first commercial phenolic resin plant was Bakelite GmbH, started in Germany in 1910; in the same year, the General Bakelite Co. was founded in the United States.

Early phenolic resins consisted of self-curing, resole-type products made with excess formaldehyde, and novolaks, which are thermoplastic in nature and require a hardener. The early products produced by General Bakelite were used in molded parts, insulating varnishes, laminated sheets, and industrial coatings. These areas still remain important applications, but have been joined by numerous others such as wood bonding, fiber bonding, and plywood adhesives. The number of producers in 2001 is approximately 15 in the United States and over 50 worldwide. Overall the number of producers is declining as the industry continues to undergo consolidation.

**Table 1. Properties of Phenol**

Property	Value
mol wt	94.1
mp, °C	40.9
bp, °C	181.8
Flash point, °C	79.0
Autoignition temperature, °C	605.0
Explosive limits, vol%	2–10
Vapor pressure at 20°C, Pa <sup>a</sup>	20

<sup>a</sup>To convert Pa to mm Hg, multiply by  $7.5 \times 10^{-3}$ .

**Table 2. Substituted Phenols Used for Phenolic Resins**

Substituted phenol	Resin application
Cresol ( <i>o</i> -, <i>m</i> -, <i>p</i> -)	Coatings, epoxy hardeners
<i>p</i> - <i>t</i> -Butylphenol	Coatings, adhesives
<i>p</i> -Octylphenol	Carbonless paper, coatings
<i>p</i> -Nonylphenol	Carbonless paper, coatings
<i>p</i> -Phenylphenol	Carbonless paper
Bisphenol A	Low color molding compounds, coatings
Resorcinol	Adhesives
Cashew nutshell liquid	Friction particles

## Monomers

**Phenol.** This is the monomer or raw material used in the largest quantity to make phenolic resins (Table 1). As a solid having a low melting point, phenol, C<sub>6</sub>H<sub>5</sub>OH, is usually stored, handled in liquid form at 50–60°C, and stored under nitrogen blanket to prevent the formation of pink quinones. Iron contamination results in a black color.

The most widely used process for the production of phenol is the cumene process developed and licensed in the United States by Honeywell (formerly AlliedSignal). Benzene is alkylated with propylene to produce cumene (isopropylbenzene), which is oxidized by air over a catalyst to produce cumene hydroperoxide (CHP). With acid catalysis, CHP undergoes controlled decomposition to produce phenol and acetone;  $\alpha$ -methylstyrene and acetophenone are the by-products (13). Other commercial processes for making phenol include the Raschig process, using chlorobenzene as the starting material, and the toluene process, via a benzoic acid intermediate. In the United States, ~35–40% of the phenol produced is used for phenolic resins.

**Substituted Phenols.** Phenol itself is used in the largest volume, but substituted phenols are used for specialty resins (Table 2). Substituted phenols are typically alkylated phenols made from phenol and a corresponding  $\alpha$ -olefin with acid catalysts (14). Acidic catalysis is frequently in the form of an ion-exchange resin (IER) and the reaction proceeds preferentially in the para

Table 3. Forms of Formaldehyde

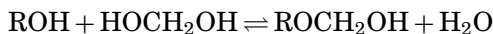
Type	Chemical formula	Resin preparation	
		Advantages	Disadvantages
Gaseous	$\text{CH}_2\text{O}$		Unstable
Formalin			
36%	$\text{HO}(\text{CH}_2\text{O})_n\text{H}^a$	Easy handling, moderate, reactivity, stable at RT	High water content
50%	$\text{HO}(\text{CH}_2\text{O})_n\text{H}^b$	Increased capacity	Elevated temperature storage, formic acid formation
Paraformaldehyde	$\text{HO}(\text{CH}_2\text{O})_n\text{H}^c$	Increased capacity, water-free	Dangerously high reactivity, solids handling
Trioxane	$(\text{CH}_2\text{O})_3$	Water-free	Catalyst requirements, high cost
Hexamethylenetetramine	$(\text{CH}_2)_6\text{N}_4$	Autocatalytic	Amine incorporation

<sup>a</sup> $n \approx 2$ .<sup>b</sup> $n \approx 3$ .<sup>c</sup> $n = 20\text{--}100$ .

position. For example, in the production of *t*-butylphenol using isobutylene, the product is >95% para-substituted. The incorporation of alkyl phenols such as cresol into the resin reduces reactivity, hardness, cross-link density, and color formation, but increases solubility in nonpolar solvents, flexibility, and compatibility with natural oils.

**Formaldehyde.** In one form or another, formaldehyde is used almost exclusively in the production of phenolic resins, regardless of the type of phenol (Table 3). It is frequently produced near the site of the resin plant by either of two common processes using methanol (qv) as the raw material. In the silver catalyst process, the reaction takes place at 600–650°C and produces water and hydrogen as by-products. The more common metal oxide process operates at 300–400°C. The gaseous formaldehyde is absorbed in water, and the final product is a formalin solution containing 36–50% formaldehyde. Of the various chemical forms of formaldehyde, the aqueous form is preferred for making phenolic resins, even though at least half of this form is water. The water serves to moderate the reaction and is readily removed in processing equipment (15).

**Aqueous Formaldehyde.** Water solutions of formaldehyde consist mainly of telomers of methylene glycol having <100 ppm of the formaldehyde as  $\text{CH}_2\text{O}$  (5). Alcohols form hemiformals with aqueous formaldehyde according to the following, where  $n = 1, 2, 3$ , etc.



However, a second mole of alcohol or hemiformal does not add at the ordinary pH of such solutions. The equilibrium constant for hemiformal formation depends on the nature of the R group of the alcohol. Using NMR spectroscopy, a group of alcohols including phenol has been examined in solution with formaldehyde (16,17). The spectra indicated the degree of hemiformal formation in the order of methanol > benzyl alcohol > phenol. Hemiformal formation provides the mechanism of stabilization; methanol is much more effective than phenol in this regard.

The large value for the hemiformal formation constant of methanol and its low molecular weight explains the high efficiency of methanol in stabilizing formalin solutions. Phenol, on the other hand, is inefficient, and phenol hemiformals are only formed by careful removal of water (18).

**Other Aldehydes.** The higher aldehydes react with phenol in much the same manner as formaldehyde, although at much lower rates. Examples include acetaldehyde,  $\text{CH}_3\text{CHO}$ ; paraldehyde,  $(\text{CH}_3\text{CHO})_3$ ; glyoxal,  $\text{OCH}-\text{CHO}$ ; and furfural. The reaction is usually kept on the acid side to minimize aldol formation. Furfural resins, however, are prepared with alkaline catalysts because furfural self-condenses under acid conditions to form a gel.

**Hexamethylenetetramine.** Hexa, a complex molecule with an adamantane-type structure, is prepared from formaldehyde and ammonia, and can be considered a latent source of formaldehyde. When used either as a catalyst or as a curative, hexa contributes formaldehyde-residue-type units as well as benzylamines. Hexa [100-97-0] is an infusible powder that decomposes and sublimes above  $275^\circ\text{C}$ . It is highly soluble in water, up to ca 45 wt% with a small negative temperature solubility coefficient. The aqueous solutions are mildly alkaline at pH 8–8.5 and reasonably stable to reverse hydrolysis.

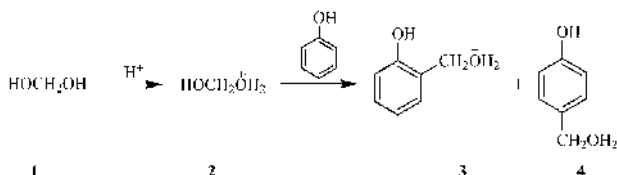
**Other Reactants.** Other reactants are used in smaller amounts to provide phenolic resins that have specific properties, especially coatings applications. Aniline had been incorporated into both resoles and novolaks but this practice has been generally discontinued because of the toxicity of aromatic amines. Other materials include rosin (abietic acid), dicyclopentadiene, unsaturated oils such as tung oil and linseed oil, and polyvalent cations for cross-linking.

## Polymerization

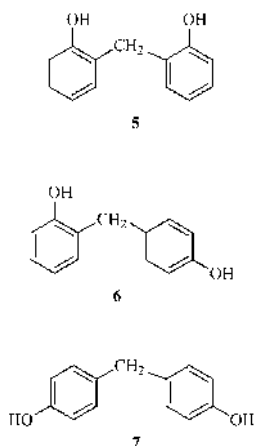
Phenolic resins are prepared with strong acid or alkaline catalysts. Occasionally, weak or Lewis acids, such as zinc acetate, are used for specialty resins.

**Strong-Acid Catalysts, Novolak Resins.** Phenolic novolaks are thermoplastic resins having a molecular weight of 500–5000 and a glass-transition temperature  $T_g$  of  $45\text{--}70^\circ\text{C}$ . The phenol–formaldehyde reactions are carried to their energetic completion, allowing isolation of the resin; formaldehyde–phenol molar ratios are between 0.5:1 and 0.8:1. Methylene glycol [463-57-0] (1) is converted to the corresponding hydrated carbonium ion 2, which adds to the ortho and para positions of phenol with the elimination of water to form the

corresponding ortho (3) and para (4) benzylic ions. The benzylic carbonium ions are in equilibrium with the corresponding benzylic alcohols, observed by NMR as transient species in the formation of novolak resins (16).



In the next step the hydrated benzylic carbonium ions 3 and 4 react with free ortho and para positions on phenols to form methylene-linked bisphenols, 2,2'(5), 2,4'(6), and 4,4'(7).



Continued reaction leads to the formation of novolak polymers having a molecular weight of up to 5000. Acid-catalyzed resins contain 50–75% 2,4' linkages (6). The reaction rate is proportional to catalyst, formaldehyde, and phenol concentrations, and inversely proportional to the concentration of water. The rate of formation of the benzyl alcohol intermediate is 5–10 times lower than the rate to form the methylene-linked bisphenol (3). At typical molecular weights of 500–1000, novolak molecules are essentially linear because of the much lower reactivity of doubly-reacted phenolic units. In higher molecular weight polymers, the low concentration of end groups and unreacted phenol causes branching. Above 1000 molecular weight, branching has been observed by  $^{13}\text{C}$  NMR; about 20% branching has been predicted in computer simulations (14,19,20). In the curing process, end groups are more reactive than the backbone groups. Thus a branched resin having a higher content of end groups than a corresponding linear equivalent may gel sooner and cure faster because of the higher resin functionality. The properties of an acid-catalyzed phenolic resin are shown in Table 4.

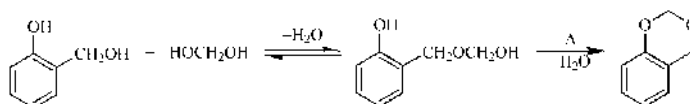
The typical acid catalysts used for novolak resins are sulfuric acid, sulfonic acid, oxalic acid, or occasionally phosphoric acid. Hydrochloric acid, although once widely used, has been abandoned because of the possible formation of toxic

**Table 4. Novolak Resin Properties**

Property	Catalyst	
	Acid	Zn acetate <sup>a</sup>
Formaldehyde/phenol molar ratio	0.75	0.60
NMR analysis, %		
2,2'	6	45
2,4'	73	45
4,4'	21	10
GPC analysis		
Phenol, %	4	7
<i>M<sub>n</sub></i>	900	550
<i>M<sub>w</sub></i>	7300	1800
Water, %	1.1	1.9
<i>T<sub>g</sub></i> , °C	65	48
Gel time, s	75	25

<sup>a</sup>High ortho.

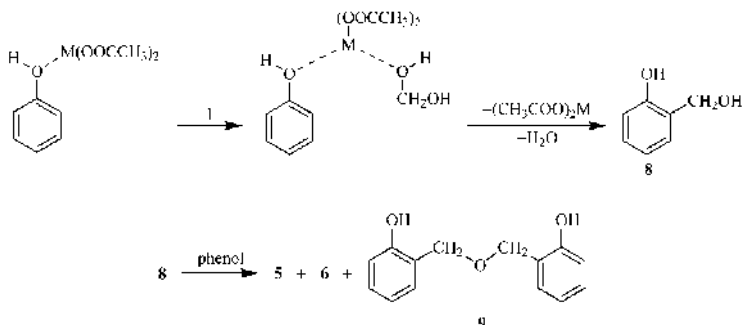
chloromethyl ether by-products. The type of acid catalyst used and reaction conditions affect resin structure and properties. For example, oxalic acid, used for resins chosen for electrical applications, decomposes into volatile by-products at elevated processing temperatures. Oxalic acid catalyzed novolaks contain small amounts (1–2% of the original formaldehyde) of benzodioxanes formed by the cyclization and dehydration of the benzyl alcohol hemiformal intermediates.



Benzodioxane is reasonably stable at neutral pH, but may decompose when the resin is cured, serving as a source of labile formaldehyde. Benzodioxanes are not found in sulfuric or sulfonic acid catalyzed resins, since the stronger acid readily catalyzes the second step in the reaction sequence.

**Neutral Catalysts, High Ortho Novolaks.** In the range of pH 4–7, formaldehyde substitution of the phenolic ring is possible, using divalent metal catalysts containing Zn, Mg, Mn, Cd, Co, Pb, Cu, and Ni; certain aluminum salts are also effective. Organic carboxylates are required as anions in order to obtain sufficient solubility of the catalyst in the reaction medium, as well as to provide a weak base. Acetates are most convenient and economical. Although lead acetate is highly effective because of its excellent solubility properties, it has been largely eliminated because of lead toxicity. Zinc and calcium salts are probably the most widely used catalysts (21).

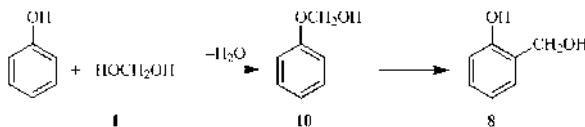
Novolaks produced from these catalysts exhibit a high content of 2,2'-methylene units. The mechanism proposed for the ortho-directing effect involves chelation of the phenolic unit with the metal ion.



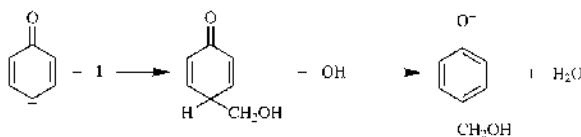
Zinc acetate catalyst produces essentially 100% *o*-methylol phenol (8) in the first step. The second step gives an approximately equal quantity of 2,2'- (5, 45%) and 2,4'-diphenylmethane (6, 45%) bridges, indicating little chelate-directing influence. In addition, a small quantity (10%) of methylene ether units (9) (dibenzyl ether) is observed at moderate reaction temperature.

High ortho novolaks have faster cure rates with hexa. Typical properties of a zinc acetate catalyzed high ortho novolak are also shown in Table 4. The gel time with hexa is one-third of that with a strong acid catalyzed novolak.

**Alkaline Catalysts, Resoles.** Resole-type phenolic resins are produced with a molar ratio of formaldehyde to phenol of 1.2:1 to 3.0:1. For substituted phenols, the ratio is usually 1.2:1 to 1.8:1. Common alkaline catalysts are NaOH,  $Ca(OH)_2$ , and  $Ba(OH)_2$ . While novolak resins and strong acid catalysis result in a limited number of structures and properties, resoles cover a much wider spectrum. Resoles may be solids or liquids, water-soluble or -insoluble, alkaline or neutral, slowly curing or highly reactive. In the first step, the phenolate anion is formed by delocalization of the negative charge to the ortho and para positions. Alkaline catalysts are also effective in the polymerization-depolymerization of methylene glycol. The mechanism of the formaldehyde addition to the phenolate is still not completely understood. The most likely mechanism involves the contribution of phenol hemiformals (10) (5).



Rate studies show that base-catalyzed reactions are second order and depend on the phenolate and methylene glycol concentrations. The most likely path involves a nucleophilic displacement by the phenoxide on 1, with the hydroxyl as the leaving group. In alkaline media, the methylolated quinone intermediate is readily converted to the phenoxide by hydrogen-ion abstraction (22).





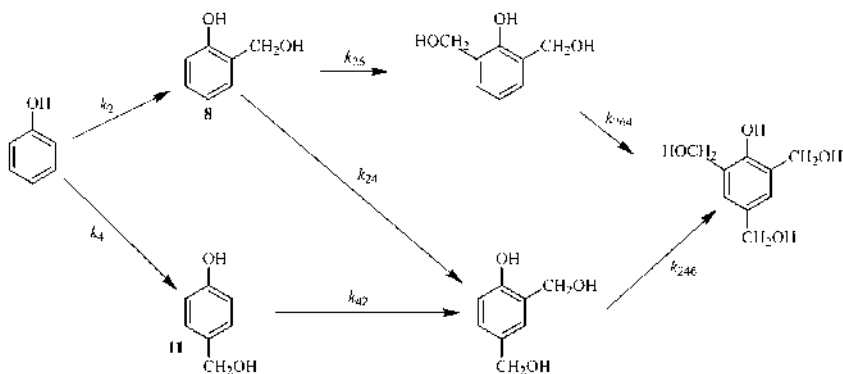


**Fig. 1.** Possible pathways and rate constants for the methylation of phenol.

The ratio of ortho-to-para substitution depends on the nature of the cation and the pH. Para substitution is favored by  $K^+$  and  $Na^+$  ions and higher pH, whereas ortho substitution is favored at lower pH and by divalent cations, such as  $Ba^{2+}$ ,  $Ca^{2+}$ , and  $Mg^{2+}$  (23).

Several extensive kinetic studies on the polymethylation of phenol have been reported (22,24,25). For the reaction scheme shown in Fig. 1, seven different rate constants must be determined. Despite different solution concentration, temperatures, and methods of analysis, comparing reaction rates (26–28) from each study using an NaOH catalyst gave fairly close agreement that rate constants increase with methylol substitution. In fact, dimethylol-substituted phenols react with formaldehyde two to four times faster than phenol. As a result, unreacted phenol remains high in resole resins (5–15%) even though the formaldehyde/phenol ratio is as high as 3:1.

The rate studies show that  $k_{264}$  is by far the fastest reaction (by a factor of 4–6) than  $k_2$  or  $k_4$ , with  $k_{24}$  the second fastest (by a factor of 2–4) (22,25).

Although monomeric methylolated phenols are used in certain applications, such as in fiber bonding, higher molecular weight resins are usually desirable. Molecular weight is increased by further condensation of the methylol groups, sometimes after the initial pH has been reduced. Dibenzyl ether (9) and diphenylmethylene formation are shown in the following. The formation of diphenylmethylene bridges is favored above  $150^\circ C$  and under strongly alkaline conditions; dibenzyl ether formation is favored at lower temperatures and near neutral pH.

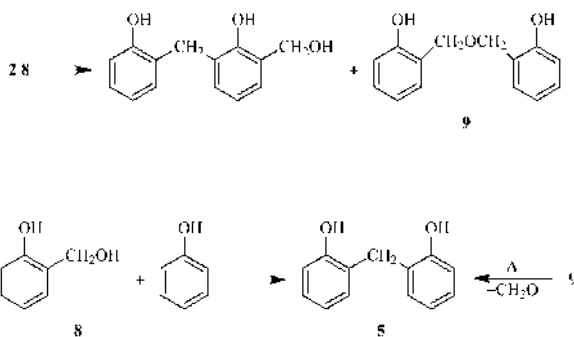
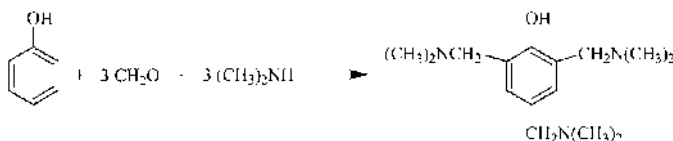


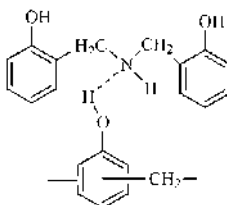
Table 5. Properties of Resole Resins

Property	Catalyst	
	NaOH	Hexa
Concentration, pph	3	10
Formaldehyde/phenol ratio	2.0	1.5
Water solubility, %	100	Swells
GPC analysis		
Phenol, %	6	8
$M_n$	280	900
$M_w$	500	3000
$T_g$ , °C	35	47
Gel time, s	65	110

Special resoles are obtained with amine catalysts, which affect chemical and physical properties because amine is incorporated into the resin. For example, the reaction of phenol, formaldehyde, and dimethylamine is essentially quantitative (29).



In practice, ammonia is most frequently used. With hexa, the initial reaction steps differ, but the final resole resins are identical, provided they contain the same number of nitrogen and CH<sub>2</sub> groups. Most nitrogen from ammonia or hexa is incorporated as dibenzylamine with primary, tertiary, and cyclic amine structures as minor products.



The physical properties of a resole resin prepared with hexa catalyst are shown in Table 5. Compared to the resin catalyzed with NaOH, this resin has higher molecular weight, less free phenol, lower water solubility, and a higher  $T_g$ . This increase in  $T_g$  is higher than that expected if only phenol and formaldehyde were used, and is a result of the hydrogen-bonding interaction between the backbone amine units and the phenolic hydroxyls. Taking advantage of this effect, hexa and ammonia have been frequently used to produce solid, grindable, and water-insoluble resoles for molding compounds.

**Table 6. Methylene Group Distribution, % in Resoles**

Methylene group	Catalyst	
	NaOH	Hexa <sup>a</sup>
2-CH <sub>2</sub> OH	30	24
2-CH <sub>2</sub> OCH <sub>2</sub> OH	24	1
2-CH <sub>2</sub> OR	2	4
4-CH <sub>2</sub> OH	12	9
4-CH <sub>2</sub> OCH <sub>2</sub> OH	16	0
4-CH <sub>2</sub> OR	2	4
2,2'-CH <sub>2</sub>	0	0
2,4'-CH <sub>2</sub>	7	12
4,4'-CH <sub>2</sub>	7	10
2-CH <sub>2</sub> N	0	27
4-CH <sub>2</sub> N	0	7
Benzoxazine	0	2

<sup>a</sup>6 pph.

The methylene-isomer distributions of NaOH and hexa-catalyzed resoles are shown in Table 6. The distribution of amine structures is

secondary > primary  $\approx$  tertiary

and most benzylamines are ortho in the phenol ring from early steps in the reaction sequence.

## Manufacture

The final state of a phenolic resin varies dramatically from thermoplastic to thermoset and from solid to liquid, and includes solutions and dispersions. With a bulk process, resole resins, in neat or concentrated form, must be produced in small batches ( $\approx 2\text{--}10\text{ m}^3$ ) in order to maintain control of the reaction and obtain a uniform product. On the other hand, if the product contains a large amount of water, such as liquid plywood adhesives, large reactors ( $20\text{ m}^3$ ) can be used. Melt-stable products such as novolaks can be prepared in large batches ( $20\text{--}40\text{ m}^3$ ) if the exotherms can be controlled. Some reactors are reportedly as large as  $60\text{ m}^3$  (Ref. 9, p. 83).

Batch processes for most phenolic resins employ the equipment shown in Fig. 2. Liquid reactants are metered into the stirred reaction vessel through weigh tanks, whereas solid reactants such as bisphenol A and  $\text{Ba}(\text{OH})_2$  present handling problems. Facilities are provided to carry out the reaction under vacuum or an inert gas.

**Materials of Construction.** Compatibility of the materials of construction and the process chemicals is extremely important. The reactors are usually made of stainless steel alloys. Copper is avoided because of the possible presence of amines. Glass-lined reactors are occasionally used for nonalkaline resins.

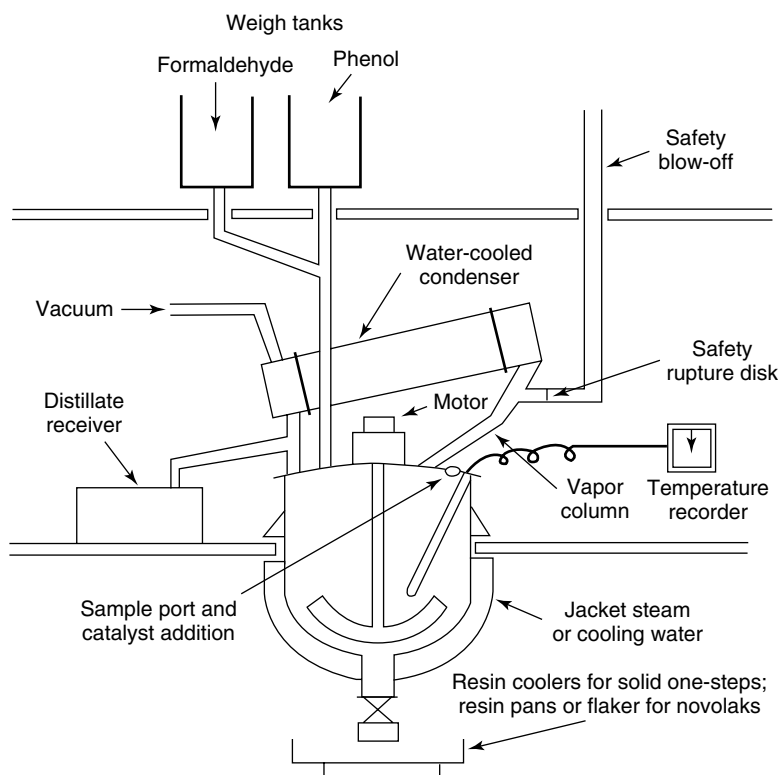


**Fig. 2.** Typical phenolic resin production unit.

Because the use of HCl has been largely discontinued, material requirements are less stringent. The reactor contains a bottom discharge, which for solid heat-reactive resins must be large. Solid resole resins are discharged for rapid cooling in order to quench the thermosetting reactions. Resin coolers are made up of vertical plates with internally circulating water. The product can also be discharged to a large cooled surface. Discharges to belt and drum flakers are highly automated; however they can only be used for less-reactive resins.

Novolak resins can be stored molten in heated holding tanks under nitrogen. Because novolaks are used mainly in pulverized form with hexa and additives, a process that includes belt flaking and feeding directly into the blending and pulverizing system is preferred. Liquid and solution resole resins are cooled in the reactor by using jacket cooling and vacuum refluxing. Discharged products are filtered and pumped to refrigerated intermediate holding areas or packaged for shipping. The stability of liquid resole products varies greatly from product to product and depends on the storage temperature. The viscosity of a liquid resole resin increases but the water miscibility decreases as time and temperature increase. Generally, resoles, both liquids and solids, must be refrigerated.

**Novolak Resins.** In a conventional novolak process, molten phenol is placed into the reactor, followed by a precise amount of acid catalyst. The

formaldehyde solution is added at a temperature near 90°C and a formaldehyde-to-phenol molar ratio of 0.75:1 to 0.85:1. For safety reasons, slow continuous or stepwise addition of formaldehyde is preferred over adding the entire charge at once. Reaction enthalpy has been reported to be above 80 kJ/mol (19 kcal/mol) (30,31). The heat of reaction is removed by refluxing the water combined with the formaldehyde or by using a small amount of a volatile solvent such as toluene. Toluene and xylene are used for azeotropic distillation. Following decantation, the toluene or xylene is returned to the reactor.

The reaction is completed after 6–8 h at 95°C; volatiles, water, and some free phenol are removed by vacuum stripping up to 140–170°C. For resins requiring phenol in only trace amounts, such as epoxy hardeners, steam distillation or steam stripping may be used. Both water and free phenol affect the cure and final resin properties, which are monitored in routine quality control testing by gas chromatography (GC). Oxalic acid (1–2 parts per 100 parts phenol) does not require neutralization because it decomposes to CO, CO<sub>2</sub>, and water; furthermore, it produces milder reactions and low color. Sulfuric and sulfonic acids are strong catalysts and require neutralization with lime; 0.1 parts of sulfuric acid per 100 parts of phenol are used. A continuous process for novolak resin production has been described (32,33). An alternative process for making novolaks without acid catalysis has also been reported (34,35), which uses a peroxidase enzyme to polymerize phenols in an aqueous solution. The enzyme can be derived from soybeans or horseradish.

**High Ortho Novolaks.** The process for high ortho novolaks is similar to the one used for those catalyzed by strong acid. Zinc acetate is used at concentrations higher than the acids, typically 2% or more. The formaldehyde/phenol ratio is similar (0.75–0.85) but yields are 5–10% lower than those produced with strong acids, and reaction times are longer. Problems with gel particles and bulk gelation occur more frequently because small amounts of reactive dibenzyl ether groups are present. Overall, the process is more expensive because of higher raw material costs, lower yields, and longer cycle times.

Another process employs a pH maintained at 4–7 and a catalyst that combines a divalent metal cation and an acid. Water is removed continuously by azeotropic distillation and xylene is recycled. The low water content increases the reaction rate. The dibenzyl ether groups are decomposed by the acid; the yield of 2,2'-methylene can be as high as 97% (36).

**Resoles.** Like the novolak processes, a typical resole process consists of reaction, dehydration, and finishing. Phenol and formaldehyde solution are added all at once to the reactor at a molar ratio of formaldehyde to phenol of 1.2–3.0:1. Catalyst is added and the pH is checked and adjusted if necessary. The catalyst concentration can range from 1 to 5% for NaOH, 3 to 6% for Ba(OH)<sub>2</sub>, and 6 to 12% for hexa. A reaction temperature of 80–95°C is used with vacuum-reflux control. The high concentration of water and lower enthalpy compared to novolaks allows better exotherm control. In the reaction phase, the temperature is held at 80–90°C and vacuum-refluxing lasts from 1 to 3 h as determined in the development phase. Solid resins and certain liquid resins are dehydrated as quickly as possible to prevent overreacting or gelation. The endpoint is found by monitoring the gel time, which decreases as the reaction progresses. Automation includes on-line viscosity measurement, GC, and gel-permeation chromatography (GPC).

**Phenolic Dispersions.** These systems are predominantly resin-in-water systems in which the resin exists as discrete particles. Particle size ranges from 0.1 to 2  $\mu\text{m}$  for stable dispersions and up to 100  $\mu\text{m}$  for dispersions requiring constant agitation. Some of the earliest nonaqueous dispersions were developed for coatings applications. These systems consist of an oil-modified phenolic resin complexed with a metal oxide and a weak solvent.

In the postdispersion process, the solid phenolic resin is added to a mixture of water, cosolvent, and dispersant at high shear mixing, possibly with heating. The cosolvent, frequently an alcohol or glycol ether, and heat soften the resin and permit small particles to form. On cooling, the resin particles, stabilized by dispersant and perhaps thickener, harden and resist settling and agglomeration. Both resole and novolak resins have been made by this process (26).

The *in situ* process is simpler because it requires less material handling (37); however, this process has been used only for resole resins. When phenol is used, the reaction system is initially one-phase; alkylated phenols and bisphenol A present special problems. As the reaction with formaldehyde progresses at 80–100°C, the resin becomes water-insoluble and phase separation takes place. Catalysts such as hexa produce an early phase separation, whereas NaOH-based resins retain water solubility to a higher molecular weight. If the reaction medium contains a protective colloid at phase separation, a resin-in-water dispersion forms. Alternatively, the protective colloid can be added later in the reaction sequence, in which case the reaction mass may temporarily be a water-in-resin dispersion. The protective colloid serves to assist particle formation and stabilizes the final particles against coalescence. Some examples of protective colloids are poly(vinyl alcohol), gum arabic, and hydroxyethylcellulose.

For products intended to remain stable dispersions for an extended period, a particle size of 2  $\mu\text{m}$  or less is desirable. A thickening agent is usually added after the reaction has been completed and the mixture is cooled in order to prevent settling and agglomeration. Examples of thickeners are guar gum, xanthan gum, and hydroxyethylcellulose. The final products are generally between 40 and 50% solids, with a viscosity of 1500–5000 mPa·s (=cP).

Resole dispersions intended for isolation as discrete particles (27) can be used as flattening agents in coatings (28). Particles larger than 1000  $\mu\text{m}$  are used in friction-element compositions. A-stage, thermosetting phenolic particles have been isolated from dispersion (27,38). With a hexa catalyst (6–12 parts) and a formaldehyde/phenol ratio of 1.5:1, the reaction is carried out at 50% solids for  $\approx 90$  min at 85°C. Poly(vinyl alcohol) and gum arabic are the preferred protective colloids. The particles (20–80  $\mu\text{m}$ ) are isolated from the mixture by filtration and, in the patent examples, by fluid-bed drying. These A-stage products (gel time at 150°C, 50–100 s) are suitable in applications where pulverized phenolic resins are being used, as well as in applications that take advantage of their spherical nature. One patent describes a sinter-resistant product for wood-bonding applications (39). In another patented process, both the production of particulate novolak resins and the aqueous dispersions of these resins are described (40).

**Spray-Dried Resins.** Spray drying produces resins in particulate form. Spray-drying a resole solution containing a blowing agent (41) produces phenolic microballoons. Spray drying also produces A-stage resins (42). The resins, prepared with a high NaOH content, are spray dried to give a final particle size

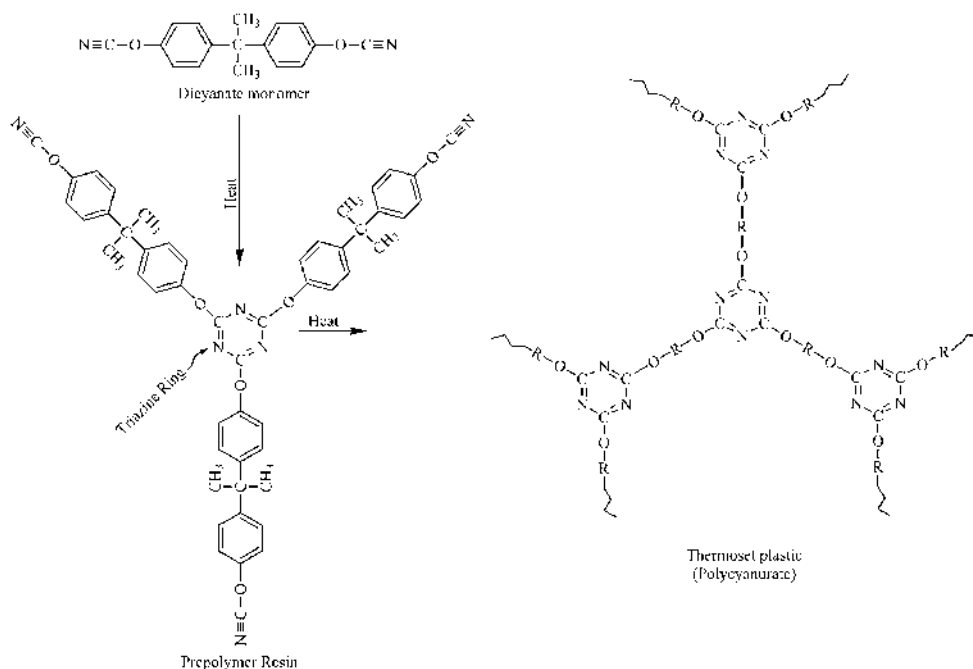


**Fig. 3.** Curing via cyclotrimerization; R = bisphenol unit. From Ref. 43.

of 40–60  $\mu\text{m}$ . The particles are hygroscopic because of the high caustic content, but are sinter-resistant when kept dry. The principal application for this type of product is believed to be wood binding, especially for waferboard applications.

**Cyanate Ester Resins.** Cyanate ester resins, sometimes called triazines or cyanurates after the cured structure that they produce, are derived from phenols and phenolic resins. Specifically the starting phenols are reacted with cyanogen chloride,  $\text{ClCN}$ , and base to give the resins. In the cure step the cyanate groups trimerize to form triazine rings when heated in the range 180–250°C. Performance is generally intermediate between aromatic amine cured epoxides and toughened bismaleimides. Glass transition temperature  $T_g$  is about 250°C and the heat distortion temperature is about 250°C dry and 175°C wet. Electrical properties are excellent due to very low residual chlorine content. Principal applications are printed wiring boards and structural composites (Fig. 3) (43).

**Benzoxazine Resins.** Benzoxazine resins are prepared by the reaction of phenol, formaldehyde, and an amine. In one particular example a benzoxazine is prepared from bisphenol A, formaldehyde, and aniline to give 2,2'-bis(3-phenyl-4-dihydro-1,3,2-benzoxazine) propane. When heated to about 200°C the methylene bond to oxygen breaks and reforms onto the available ortho positions of adjacent moieties to give dibenzylamine structures. Resin formulations have been developed and formulated, in some cases with epoxy and phenolic resins to give ternary systems with  $T_g$  as high as 170°C (Fig. 4) (43–46).

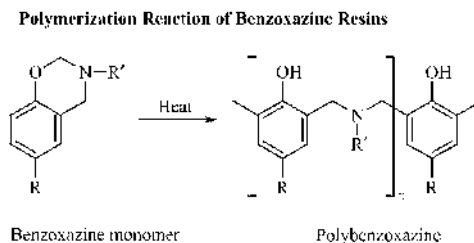


**Fig. 4.** Polymerization reaction of benzoxazine resins.

## Cure

A typical resin has an initial molecular weight of 150 to perhaps 1500. For systems of unsubstituted phenols, the final cross-link density is 150–300 amu per cross-link. In other words, 25–75% of the ring-joining reactions occur during the cure phase.

**Resoles.** The advancement and cure of resole resins follow reaction steps similar to those used for resin preparation; the pH is 9 or higher and reaction temperature should not exceed 180°C. Methylol groups condense with other methylols to give dibenzyl ethers and react at the ortho and para positions on the phenol to give diphenylmethylenes. In addition, dibenzyl ethers eliminate formaldehyde to give diphenylmethanes.

In some resole applications, such as foam and foundry binders, a rapid cure of a liquid resin is obtained at room temperature (RT) with strong acid. The reactions proceed in the same manner as those of novolak resin formation. Methylol groups react at ortho and para phenolic hydrogen to give diphenylmethane units (47).

At pH 4–6, the cure is slower than it is at pH 8 and higher, and much slower than at pH 1–3. Reactions at pH 4–6 resemble those on the more alkaline side, but with a substantial increase in side products. This is partly the result of the low rates of the main reactions and partly the result of stable intermediates at this pH range.

Some resoles contain latent acid catalysts, which on heating generate moderately strong acids. Examples include aryl phosphites such as diphenyl hydrogen phosphite and ammonium sulfate (48,49). The use of latent acid catalysis broadens the range of applications of phenolic resins to include areas such as liquid composite molding and pultrusion. Also resoles, which can contain so-called free formaldehyde, can be formulated with formaldehyde scavengers in form of amines such as melamine.

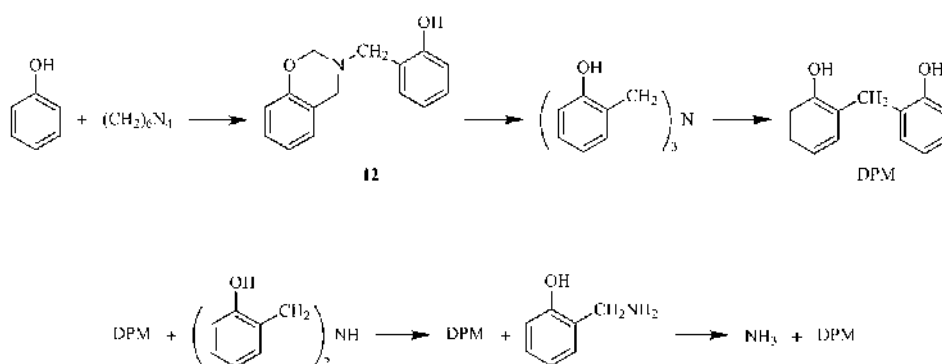
**Novolaks.** Novolak resins are typically cured with 5–15% hexa as the cross-linking agent. The reaction mechanism and reactive intermediates have been studied by classical chemical techniques (3,4) and the results showed that as much as 75% of nitrogen is chemically bound. More recent studies of resin cure (50–53) have made use of TGA, DTA, GC, IR, and NMR (16). They confirm that the cure begins with the formation of benzoxazine (12), progresses through a benzyl amine intermediate, and finally forms (hydroxy)diphenylmethanes (DPM).



**Table 7. Isothermal DMA Results**

Sample	Rate, min <sup>-1</sup>		Activation energy, kJ/mol <sup>a</sup>
	At 150°C	At 185°C	
Hexa-catalyzed resole	0.22	1.00	71.1
Novolak			
6% hexa	0.07	0.09	8.8
12% hexa	0.12	0.19	18.8

<sup>a</sup>To convert kJ to kcal, divide by 4.184.



In the reaction of phenol and bisphenol F with hexa, NMR spectra show the transient appearance of benzoxazine intermediates; after 2 h at 103°C, all the benzoxazine decomposed to the diphenylmethane and benzylamine intermediates (16).

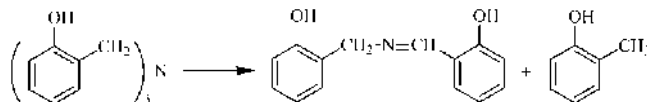
The cure of novolaks with hexa has been studied with differential scanning calorimetry (DSC) and torsional braid analysis (TBA) (54); both a high ortho novolak and a conventional acid catalyzed system were included. The DSC showed an exothermic peak indicating a novolak-hexa reaction  $\approx 20^\circ\text{C}$  higher than the gelation peak observed in TBA. Activation energies were also calculated.

The resin rich in 2,2'-methylene exhibited the lowest activation energy, gel temperature, and DSC exotherm. The high concentration of the slightly acidic 2,2'-diphenylmethane end groups may account for the higher reactivity. These end groups should react with hexa to form benzoxazine intermediates first, which then decompose to react with vacant positions throughout the novolak molecule.

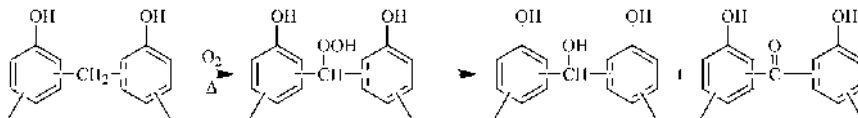
An isothermal method for studying the cure of phenolics employs dynamic mechanical analysis (DMA) (Table 7). The problems associated with programmed heating rates are avoided and mathematical treatment of the results is simplified. Although a more complex treatment is possible, a simple first-order dependence of modulus with time and an Arrhenius-type temperature dependence are sufficient. The rate studies of Table 7 indicate that doubling the amount of hexa doubles the rate at which the modulus approaches its long-term value. The novolak - 12% hexa cures substantially slower than the resole. In addition, they

differ in temperature dependence of cure rates; the resole has an activation energy approximately four times greater than that of the novolak – 12% hexa (55).

**Decomposition of Cured Resoles and Novolaks.** Above 250°C, cured phenolic resins begin to decompose. For example, dibenzyl ethers such as 9 disproportionate to aldehydes (salicylaldehyde) and cresols (*o*-cresol). The aldehyde group is rapidly oxidized to the corresponding carboxylic acid. In an analogous reaction in hexa-cured novolaks, tribenzylamines decompose into cresols and azomethines, which cause yellowing.



Substantial decomposition of phenolic resins begins above 300°C. In the presence of oxygen, the methylene bridging group is converted to a hydroperoxide, which, in turn, yields alcohols and ketones on decomposition.



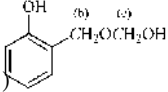
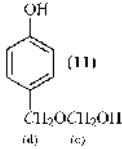
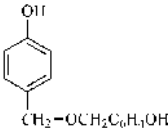
The ketone is especially susceptible to random chain scission. Decomposition continues up to  $\approx 600^\circ\text{C}$ ; the by-products are mostly water, CO,  $\text{CO}_2$ , and phenols. The first stage of decomposition produces a porous structure having minimal shrinkage. The second stage begins near  $600^\circ\text{C}$  and is accompanied by shrinkage and substantial evolution of  $\text{CO}_2$ ,  $\text{H}_2\text{O}$ , methane, and aromatics. The resulting polyaromatic chars represent  $\approx 60\%$  of the original resin when the atmosphere is inert, but this may be substantially less in the presence of air. The char ignites in air above  $900^\circ\text{C}$ .

The controlled decomposition of phenolic resins, in an inert atmosphere, is a method used to make carbon-carbon composites. In this case the resin is combined with other forms of carbon, such as carbon fibers, coke, and synthetic graphite, and cured under heat and pressure. Further heating to about  $900^\circ\text{C}$  converts the resin to a glassy form of carbon that can serve as a binder for the other carbon forms. The carbon yield from the phenolic resins can be in the range of 60–70% of the initial weight.

## Analysis and Characterization

The principal techniques for determining the microstructure of phenolic resins include mass spectroscopy (MS), proton and  $^{13}\text{C}$  NMR spectroscopy, as well as GC, LC, and GPC. The softening and curing processes of phenolic resins are effectively studied by using thermal and mechanical techniques, such as TGA, DSC, and DMA. Infrared (IR) and electron spectroscopy are also employed. Recently matrix-assisted laser desorption-ionization mass spectrometry (MALDI-MS) has

**Table 8. Chemical Shifts of Methylene Carbons in Liquid Resoles**

Structure <sup>a</sup>	Chemical shift, <sup>b</sup> ppm
Methylol C in 8	61.3
	65.4 (b)
	88.0 (c)
Benzyl C in 9	68.9
Methylol C in 11	63.8
	68.5 (d)
	88.0 (e)
	71.5
Methylene C in 5	31.5
Methylene C in 6	35.0
Methylene C in 7	40.4

<sup>a</sup>Designated carbon is shown in italic or described.<sup>b</sup>From tetramethylsilane in *d*<sub>6</sub>-acetone solution.

been used for the determination of molecular weight and end-group analysis (see MASS SPECTROMETRY). MALDI-MS is a soft ionization technique that has been applied to the determination of mass of large biomolecules and synthetics resins. The approach is useful for molecular weight determination and end-group analysis. Both novolaks and resoles have been studied and individual fragments with *m/z* up to about 2000 specifically identified. For resoles the technique is even able to resolve the various hemiformal structures that can occur. (Ref. 9, p. 92; 56–58).

**Spectroscopy.** Infrared spectroscopy (59) permits structural definition, eg, it resolves the 2,2'- from the 2,4'-methylene units in novolak resins. However, the broad bands and severely overlapping peaks present problems. For uncured resins, NMR rather than IR spectroscopy has become the technique of choice for microstructural information. However, Fourier transform infrared (FTIR) gives useful information on curing phenolics (60). Nevertheless, IR spectroscopy continues to be used as one of the detectors in the analysis of phenolics by GPC. (see VIBRATIONAL SPECTROSCOPY)

A great wealth of microstructural information is provided by Fourier transform <sup>13</sup>C NMR. Using the much greater chemical-shift range of this technique, detailed structural information is provided for both the aliphatic and the aromatic carbons (Table 8). Current techniques provide highly reliable quantitative data and relative peak areas (19,61–65) and make possible a quantitative measure of the numbers of branch points and end groups. Branching can cause early gelation in a novolak resin, and end groups usually have greater reactivity in the

thermosetting reaction than do the backbone units. Another important advantage of  $^{13}\text{C}$  NMR is the parametric predictability of the chemical-shift values. As a result, unknown peaks can be assigned to a hypothetical structure with reasonable certainty. At the same time, the process can be reversed and a computer can provide detailed structural analysis.  $^{13}\text{C}$  NMR has been applied to cured phenolic resins (63). (see NUCLEAR MAGNETIC RESONANCE).

**Chromatography.** Gel-permeation chromatography (GPC) is an invaluable technique for determining the molecular size distribution of polymers. Phenolic resins, which have molecular weight components ranging from 100 to rarely more than 5000, require special column arrangements to optimize resolution. By using proper instrument calibration, it is possible to obtain number-average ( $M_n$ ) and weight-average ( $M_w$ ) molecular weight as well as quantitative information on free monomer and certain other low molecular weight species (66–68) (see CHROMATOGRAPHY, SEC).

Many resole resins exist as phenolate salts in solution. Because these ionic species are sparingly soluble in carrier solvents such as tetrahydrofuran, careful neutralization and filtration are required. Although GPC is an excellent technique for examining medium and high molecular weight fractions, GC and high performance LC are more effective for analyzing low molecular weight species.

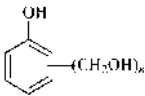
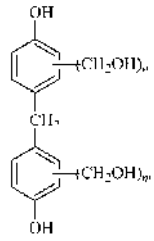
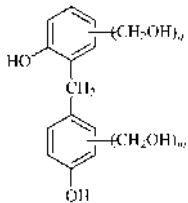
Gas chromatography (GC) has been used extensively to analyze phenolic resins for unreacted phenol monomer as well as certain two- and three-ring constituents in both novolak and resole resins (69). It is also used in monitoring the production processes of the monomers, eg, when phenol is alkylated with isobutylene to produce butylphenol. Usually, the phenolic hydroxyl must be derivatized before analysis to provide a more volatile compound. The GC analysis of complex systems, such as resoles, provides distinct resolution of over 20 one- and two-ring compounds having various degrees of methylation. In some cases, hemiformals may be detected if they have been properly capped (61).

The combined techniques of GC/MS are highly effective in identifying the composition of various GC peaks. The individual peaks enter a mass spectrometer in which they are analyzed for parent ion and fragmentation patterns, and the individual components of certain resoles are completely resolved.

High performance liquid chromatography (HPLC) is extremely effective in separating individual resin components up to a molecular weight of 1000 according to size and polarity. Dilute-solution conditions and low temperatures preserve the structure of unstable components. The resins are usually not derivatized. Gradient solvent elution gives excellent peak separation (69,70). In one study, resoles catalyzed by sodium and barium hydroxide were compared, and the components were separated up to and including methylolated four-ring compounds (61). Resole components resolved by GC and HPLC techniques are shown in Table 9. Like GC, HPLC is most effective when combined with other analytical tools, such as mass and UV spectroscopy. By using preparative-scale HPLC, individual peaks can be analyzed by proton and  $^{13}\text{C}$  NMR spectroscopy.

**Thermal Analysis.** The main thermal analysis techniques applied to phenolic resins are TGA and DSC. In TGA, the sample weight is monitored microanalytically with time and temperature in air or nitrogen. When applied to resins and molding compounds, the scans indicate cure and decomposition temperatures accompanied by a measurable loss in weight. Resoles and novolaks lose from 5 to

**Table 9. Resole Components by HPLC and GC**

Resin <sup>a</sup>	Components
	2; 4; 2,4; 2,6; 2,4,6
	2; 2,6; 2,2'; 2,6,2'; 2,6,2', 6'
	2'; 6; 4; 2', 6'; 6,2'; 4,2'; 4,6; 4,2', 6'; 4,6,2'; 4,6,2',6'

<sup>a</sup>Also, 5, 6, and 7, ie. 2,2'-, 2,4'-, and 4,4'-DPM.

20% of their weight on curing at 100–200°C. Weight loss provides information on shrinkage, void formation, and density change of composites.

Phenolic resins give a high char yield on combustion and TGA provides a measure of the expected yield. Typical values are between 40 and 65% in nitrogen. Decomposition begins at 350°C and continues up to 600°C. Autoignition temperature in air is above 900°C. Thermogravimetric analyses have played an important part in the development of carbon–carbon and carbon–graphite-fiber composites containing phenolic resins. These composites are used in aircraft brake linings and carbon-pipe applications. In DSC and DTA, heat flow and sample temperature are compared to a reference material. Glass-transition temperature  $T_g$  is determined by DSC. The  $T_g$  of liquid resoles is below RT, that of friable novolaks is in the range of 50–75°C, and that of lightly cross-linked phenolics is between 150 and 225°C.

Cure kinetics of thermosets are usually determined by DSC (71,72). However, for phenolic resins, the information is limited to the early stages of the cure because of the volatiles associated with the process. For pressurized DSC cells, the upper limit on temperature is  $\approx 170^\circ\text{C}$ . Differential scanning calorimetry is also used to measure the kinetics and reaction enthalpies of liquid resins in coatings, adhesives, laminations, and foam. Software packages that interpret DSC scans in terms of the cure kinetics are supplied by instrument manufacturers.

**Dynamic Mechanical Analysis.** In DMA, a vibrating or oscillating sample is heated at a programmed rate or held isothermally at elevated temperature. The frequency and damping characteristics of the sample are monitored with time. A change such as gelation or passage through the  $T_g$  causes abrupt

changes in the fundamental oscillation frequency of the sample and the damping ability of the specimen. The oscillation frequency can be related to the storage modulus of the sample, whereas the damping contains information related to the loss modulus.

Softening and cure are examined with the help of a torsional pendulum modified with a braid (73), which supports thermosets such as phenolics and epoxies that change from a liquid to a solid on curing. Another method uses vibrating arms coupled to a scrim-supported sample to measure storage and loss moduli as a function of time and temperature. An isothermal analytical method for phenolic resins provides data regarding rate constants and activation energies and allows prediction of cure characteristics under conditions of commercial use (55).

DSC and DMA scans of a novolac cure are shown in Figures 5a and 5b (74). The sample is a glassy solid initially and the DMA shows the distinctive  $T_g$  at 65°C followed by the appearance of a liquid state. From 110 to 125°C, the resin is a liquid and the chemical curing reactions begin, and it is followed by gelation at 140°C. Further reaction continues until 200°C, when a highly cross-linked, infusible solid is obtained. As the sample is cooled to RT, a slight increase in storage modulus is observed. The peak in the damping curve indicates the  $T_g$  of the cross-linked system at about 185°C.

Dynamic mechanical analysis provides a useful technique to study the cure kinetics and high temperature mechanical properties of phenolic resins. The volatile components of the resin do not affect the scan or limit the temperature range of the experiment. However, uncured samples must be supported by a braid, a scrim, or paper. This does not influence the kinetic results and can be corrected in the calculations of dynamic mechanical properties (qv). Recent DMA work on phenolic resins has been used to optimize the performance of structural adhesives for engineered wood products and determine the effect of moisture in wood product on cure behavior and bond strength (75–77).

**Control Tests.** Numerous chemical and physical tests are used in the manufacture of phenolic resins to ensure correct properties of the finished resins, including the following: refractive index is used to estimate the dehydration during manufacture and is proportional to the solids content; viscosity is used to determine molecular weight and solids content; nonvolatiles content is roughly proportional to polymer content; miscibility with water depends on the extent of reaction in resoles; specific gravity is measured for liquid resins and varnishes; melting point of novolaks and solid resoles affects application performance; gel times determine the reactivity of the resins; resin flow is a measure of melt viscosity and molecular weight; particle size affects performance and efficiency; and flash point and autoignition temperature provide flammability-characteristic measurements required by government agencies regulating safety and shipping. ASTM D4706-93 (1998) describes the standard test method for qualitative determination of methylol group in phenolic resins.

## Health, Safety, and Environmental Factors

The factors contributing to the health and safety of phenolic resin manufacturing and use are those primarily related to phenol (qv) and formaldehyde (qv).

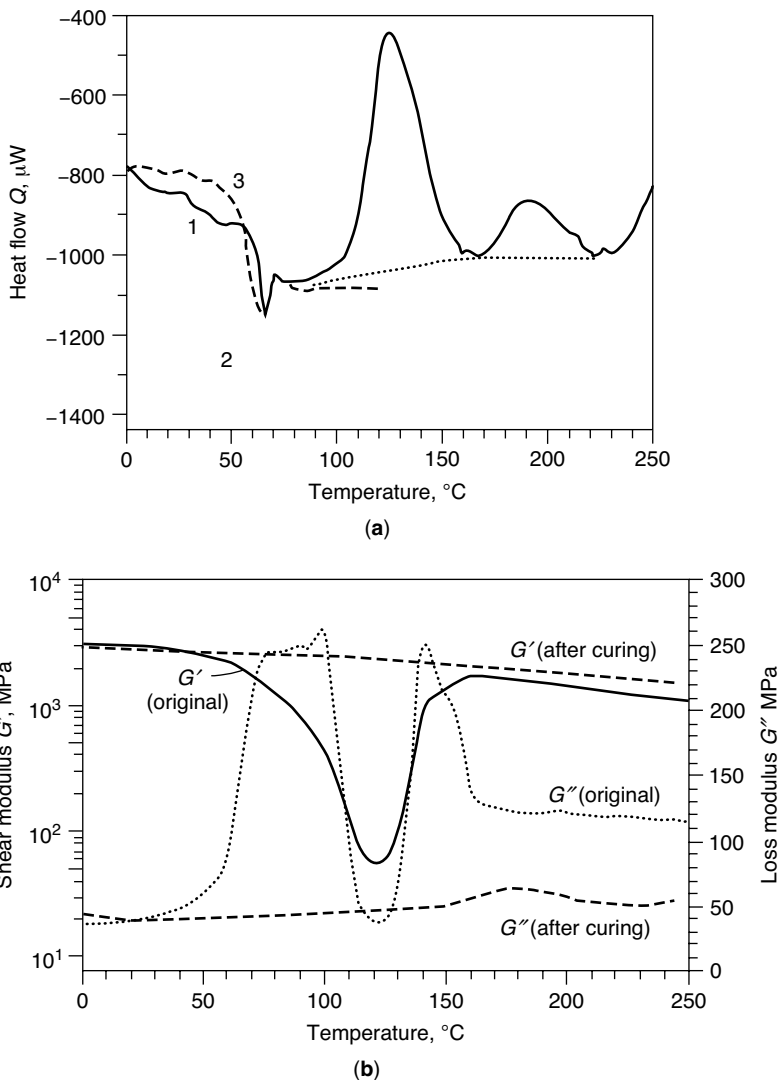


**Fig. 5.** DSC and DMA of novolac resin. (a) DSC Measurement of (1) original PF resin, (2) cured PF resin, and (3) novolac. (b) Torsion pendulum measurement of original and cured PF. To convert MPa to psi, multiply by 145. From Ref. 74.

Unreacted phenol in a resin can range from ~5% for liquid resoles used in impregnation processes to well below 1% for novolaks intended for use as epoxy hardeners. Free formaldehyde can be <1% in liquid adhesives. Novolaks are usually free of formaldehyde. The toxicity of the resins is significantly lower than that of the phenol and formaldehyde starting materials. No detrimental toxicological effects have been reported for cured phenolic resins, which can be used in direct contact with food as in can coatings.

Uncured resins are skin sensitizers and contact should be avoided, as well as breathing the vapor, mist, or dust. Novolak-based pulverized products generally contain hexamethylenetetramine, which may cause rashes and dermatitis. Phenolic molding compounds and pulverized phenolic adhesives must be controlled as potentially explosive dusts. In addition, they contain irritating or toxic additives. ASTM test method D4639-86 (1996) describes the method for volatile content in phenolic resins.

**Phenol.** Phenol is highly irritating to the skin, eyes, and mucous membranes in humans after acute inhalation or dermal exposures. Phenol is considered to be quite toxic to humans via oral exposure, with blood changes, liver and kidney damage, and cardiac toxicity reported. Chronic inhalation exposure to phenol in humans has been associated with gastrointestinal irritation, liver injury, and muscular effects. No data are available on the developmental or reproductive effects of phenol on humans. EPA has classified phenol as a Group D, not classifiable as to human carcinogenicity. The NIOSH threshold limit value (TLV) and Occupational Safety and Health Administration (OSHA) permissible exposure limit for phenol is  $19 \text{ mg/m}^3$  (78). The health and environmental risks of phenol and alkylated phenols, such as cresols and butylphenols, have been reviewed (79).

**Formaldehyde.** Acute and chronic inhalation exposure to formaldehyde in humans can result in eye, nose, and throat irritation and respiratory symptoms. Reproductive effects have been reported in women workers exposed to formaldehyde. Limited human studies have reported an association between formaldehyde exposure and lung and nasopharyngeal cancer. The EPA has classified formaldehyde as a Group B1, probable human carcinogen of medium carcinogenic hazard. The OSHA has set its permissible exposure limit (PEL) at  $4.5 \text{ mg/m}^3$  and the American Conference of Governmental and Industrial Hygienists have set the TLV at  $1.5 \text{ mg/m}^3$  (80).

**Wastewater.** Phenol is a toxic pollutant to the waterways and has an acute toxicity ( $\sim 5 \text{ mg/L}$ ) to fish. Chlorination of water gives chlorophenols, which impart objectionable odor and taste at  $0.01 \text{ mg/L}$ . Biochemical degradation is most frequently used to treat wastewater containing phenol. Primary activated sludge, along with secondary biological treatment, reduces phenol content to below  $0.1 \text{ mg/L}$  (81). ASTM D1783-01 describes the standard test methods for phenolic compounds in water.

**Flammability.** Phenolics have inherently low flammability and relatively low smoke generation. For this reason they are widely used in mass transit, tunnel building, and mining. Fiber-glass reinforced phenolic composites are capable of attaining the 1990 U.S. Federal Aviation Administration (FAA) regulations for total heat release and peak heat release for aircraft interior facings (1,82). They are also used as "fire restricting material" on cruise ships, high speed ferries, and commercial submarines. The self-ignition temperature is about  $600^\circ\text{C}$  and limiting oxygen index (LOI) is in the range 40–49%. (83).

**Recycling.** Thermosets are inherently more difficult to recycle than thermoplastics, and thermosetting phenolics are no exception. However, research in this area has been reported, and molded parts have been pulverized and incorporated at 10–15% in new molding powders. Both German and Japanese groups had instituted this type of practice in 1992 (84,85) (see RECYCLING, PLASTICS).



**Table 10. Long-Term Use of Phenolic Resins,<sup>a</sup> 10<sup>3</sup> t**

End use market	1983	1993	2001
Bonding	295	454	645
Laminating	67	78	111
Plywood	580	687	976
Other	173	173	248
<i>Total</i>	<i>1115</i>	<i>1392</i>	<i>1980</i>

<sup>a</sup>Ref. 91.

A number of alternatives will have to be developed in order to effectively utilize cured phenolic material (86). One approach is the “thermoset recycling pyramid,” a preferred order of execution that includes

- (1) Tier 1: Reintroduction of the used material into the original material at relatively low levels (~10%) in the raw material mix (this approach is used widely to recycle SMC and BMC thermoset polyesters)
- (2) Tier 2: Reuse of the material in a lower performance thermoset product at relatively high levels (40–50%)
- (3) Tier 3: Reuse of the product in alternative materials such as asphalt, roofing materials, concrete, and other construction products
- (4) Tier 4: Pyrolysis of the material to generate raw material feed stocks and incineration for energy recovery. Phenolic molding compounds can yield a caloric value of 14,000–23,000 kJ/kg, depending on the type of filler.

Plenco and other companies have been working with the SPI's Phenolic Division to produce a “Recycling Blueprint” shown in Figure 6 below (87).

**Biomass and Biochemical Processes.** Phenolic resins have been produced from biomass and using biochemical processes in various ways. In Japan biomass from wood waste or waste from the food industry is treated with phenols and strong acid catalysis and heat to produce phenolic resins (88). Research at the National Renewable Energy Laboratory has shown that ablative fast pyrolysis can be used to convert a wide variety of biomass feedstocks into a liquid oil. The phenolic rich component can be extracted from this oil and used as a low cost replacement for synthetic phenol in phenolic resins (89). In another approach, soybean peroxidase enzymes have been used to prepare resins from phenolic moieties without the use of formaldehyde (90).

**Economic Aspects.** In 2000, worldwide consumption of phenolic resins exceeded  $4 \times 10^6$  t; slightly less than half of the total volume was produced in the United States (91). The largest-volume application is in plywood adhesives, an area that accounts for  $\approx 49\%$  of U.S. consumption (Table 10). All wood bonding applications account for about two-third of phenolic resin use. During the early 1980s, the volume of this application more than doubled as mills converted from urea–formaldehyde (UF) to phenol–formaldehyde adhesives because of the release of formaldehyde from UF products.

As a mature industry, U.S. production and application of phenolic resins have paralleled the growth in the GNP and the housing industry. The

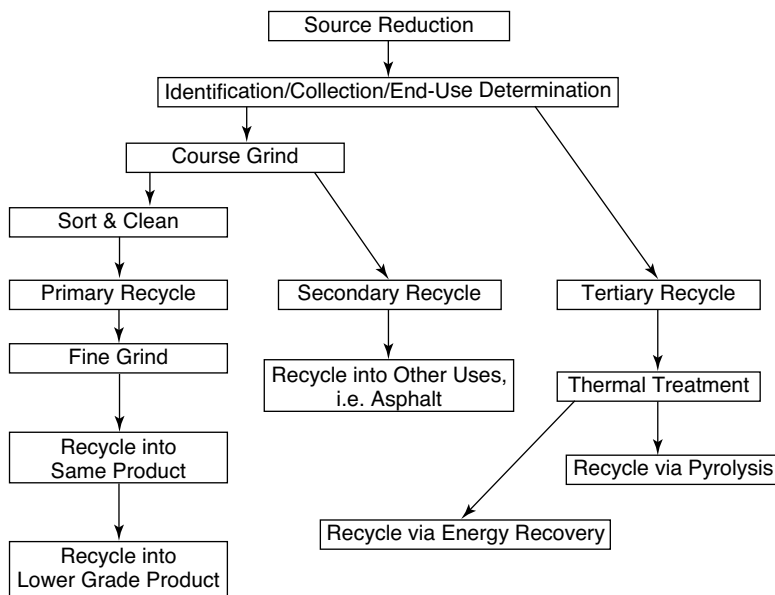


**Fig. 6.** SPI Blueprint for the reclamation of molded phenolics.

consumption of phenolic resins for coatings and molding powders has continued its decrease. The driving force behind coatings has been the need to reduce the volatile organics content (VOC) and the growth in alternative coatings such as waterborne, powder, and radiation-cured coatings. In the area of molding powders, numerous new engineering thermoplastics and alloys having superior properties have been introduced since the 1970s; however, phenolic molding powders continue to be used extensively in electrical, electronic, and machinery and underhood parts applications.

U.S. phenolic resin manufacturers include Ashland, Borden Chemical, Cytec Fiberite, Durez, FiberCote Industries, H.B. Fuller, P.D. George, Georgia-Pacific, International Paper, Lockport Thermosets, Maruzen America, Plastics Engineering, Resinoid, Sumitomo America, TriQuest, and Vantico (92).

Prices of phenolic resins vary substantially depending on the application. In 2001, the price of general-purpose and semisolids was \$1.50–1.80/kg, whereas epoxy-hardener grades can exceed \$2.20/kg. Because raw materials of phenolic resins are derived from crude oil and natural gas, the prices of phenolic resins depend on the prices of these resources.

## Applications

**Coatings.** For coatings applications, phenolic resins are grouped into four classes, depending on heat reactivity and the type of phenol. Substituted phenols are more compatible with oil and hydrocarbons, whereas heat-reactive resins require polar solvents. Depending on its nature, the resin can be used alone or as

a modifying resin that acts as an adhesion promoter, a chemical cross-linker, or a hardening agent. In these cases the primary resin may be an alkyd, polyester, or epoxy (93).

Unsubstituted heat-reactive resins are designed for baked-on coatings and are usually not oil-soluble. They require strong solvents and although most are not water-miscible, their low molecular weight, high formaldehyde content promotes water miscibility. These resins are available as solids, viscous liquids, and solutions. Resins prepared with an alkaline catalyst and a slight excess of formaldehyde over phenol are heat-reactive, but not as much as resole resins designed for fiber bonding and paper impregnation. Recommended cure conditions are 30 min and 150°C.

Heat-reactive resins are more compatible than oil-soluble resins with other polar-coating resins, such as amino, epoxy, and poly(vinyl butyral). They are used in interior-can and drum linings, metal primers, and pipe coatings. The coatings have excellent resistance to solvents, acids, and salts. They can be used over a wide range of temperatures, up to 370°C for short periods of dry heat, and continuously at 150°C. Strong alkalis should be avoided.

The maximum recommended film thickness is 25  $\mu\text{m}$ . At greater thicknesses, volatiles from the curing reaction, mainly water and some formaldehyde and phenol, can cause defects. These coatings have excellent electrical insulation properties, ie, up to 20 V/ $\mu\text{m}$ , because of low moisture absorption and low conductance. The coatings are hard with low flexibility, depending on curing conditions and film thickness.

Phenolic baking coatings can be used for metal, ceramic, and plastic surfaces. Applications include equipment for heating and air conditioning, chemical processing, petroleum refining, and water treatment. Some types are used in oil-well pipes and marine environments (94). Certain coatings can be used in food and beverage processing, subject to regulations.

The largest use of novolak resins in coatings is as a hardener for epoxy resins. The epoxy is frequently based on bisphenol A or epoxidized novolaks. Basic catalysts such as benzyldimethylamine are required for moderate baking conditions, such as 2 h at 180°C. The phenolic/epoxy ratio is adjusted to be stoichiometrically equivalent in order to give a highly cross-linked coating that has moderate flexibility and excellent resistance to chemicals, heat, and moisture. Powder coating of pipes continues to be a growing application, especially when corrosion resistance is required. In solution form, the epoxy-phenolic systems are used as metal primers and in pipe coating.

Substituted heat-reactive resins are most widely used in contact-adhesive applications and, to a lesser extent, in coatings (95,96); *p*-butylphenol, cresol, and nonylphenol are most frequently used. The alkyl group increases compatibility with oleoresinous varnishes and alkyds. In combination with these resins, phenolics reduce water sensitivity. Common applications include baked-on and electrical insulation varnishes, and as modifiers for baking alkyds, rosin, and ester gum systems. Substituted heat-reactive resins are not used for air-dry coatings because of their soft, tacky nature in the uncured state; substituted nonheat-reactive phenolics are the modifying resin of choice in this case.

Substituted nonheat-reactive resins do not form a film and are not reactive by themselves, but are excellent modifier resins for oleoresinous varnishes and

alkyds. Their high  $T_g$  and molecular weight provide initial hardness and reduce tack; oxygen-initiated cross-linking reactions take place with the unsaturated oils.

Early phenolic resin drying-oil varnishes were cooked in order to incorporate the phenolic resin into the formula. These resins have been replaced by cold-cut resins that reduce atmospheric emission by permitting direct incorporation of the phenolic after the oleoresinous varnish has been prepared. High solids systems enable coatings to meet the VOC standards required by regulatory agencies. Newer phenolic varnishes, developed in the 1980s, may contain as high as 80% nonvolatile solids (97).

Oleoresinous phenolic varnishes are excellent coatings that dry in 2–4 h and show exterior durability, corrosion resistance (especially when aluminum-modified), compatibility, solubility, and good package stability. Recoatability and intercoat adhesion are also excellent. The films are sensitive, however, to strong solvents and concentrated acids and alkalies. Unlike systems containing cross-linking phenolics, films containing these resins remain flexible.

Phenolics that are not heat-reactive may be incorporated into both air-dried and baked oleoresinous coatings. Applications vary widely and include clear and pigmented exterior varnishes, aluminum-maintenance paints, zinc-rich primers, can coatings, insulation varnishes, and concrete paints. As modifiers in a great variety of applications, they enhance the performance of oleoresinous and alkyd coatings.

**Dispersions.** In phenolic resin dispersions, the continuous phase is water or a nonpolar hydrocarbon solvent. The resin exists as droplets that have particle sizes of 1–20  $\mu\text{m}$  and are dispersed in the continuous phase. Aqueous dispersions are prepared either *in situ* during the preparation of the resin itself or by high shear mixing (26,37).

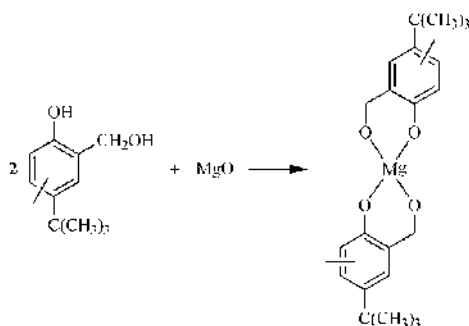
Aqueous dispersions are alternatives to solutions of liquid and solid resins. They are usually offered in 50% solids and may contain thickeners and cosolvents as stabilizers and to promote coalescence. Both heat-reactive (resole) and nonheat-reactive (novolak) systems exist that contain unsubstituted or substituted phenols or mixtures. A related technology produces large, stable particles that can be isolated as discrete particles (52). In aqueous dispersion, the resin structure is designed to produce a hydrophobic polymer, which is stabilized in water by an interfacial agent.

Aqueous dispersions are used in fiber bonding, paper coating, friction and abrasive applications, and laminates and wood bonding. Phenolic dispersions improve the strength of latex-contact adhesive applications. Epoxy-modified phenolic dispersions are prepared by dispersion of the phenolic epoxy resin. The systems are used for baked primer applications and bonding requirements. Minimum baking conditions are 20 min at 150°C (26).

**Adhesives.** Contact adhesives are blends of rubber, phenolic resin, and additives supplied in solvent or aqueous dispersion form; they are typically applied to both surfaces to be joined (98). Evaporation of the solvent leaves an adhesive film that forms a strong, peel-resistant bond. Contact adhesives are used widely in the furniture and construction industries and also in the automotive and footwear industries. The phenolic resins promote adhesion and act as tackifiers, usually at a concentration of 20–40%. In solvent-based contact adhesives,

neoprene is preferred, whereas nitrile is used in specialty applications. The type and grade of phenolic resin selected control tack time, bond strength, and durability.

Neoprene-phenolic contact adhesives, known for their high green strength and peel values, contain a resole-type resin prepared from 4-*t*-butylphenol. The alkyl group increases compatibility and reduces cross-linking. This resin reacts or complexes with the metal oxide, eg, MgO, contained in the formulation, and increases the cohesive strength of the adhesive. In fact, the reactivity with MgO is frequently measured to determine the effectiveness of heat-reactive phenolics in the formulation.



Phenolic resins substantially increase open time and peel strength of the formulation (98). For example, higher methylol and methylene ether contents of the resin improves peel strength and elevated temperature resistance. Adhesive properties are also influenced by the molecular weight distribution of the phenolic; low molecular weight reduces adhesion (99).

Waterborne contact adhesives contain an elastomer in latex form, usually an acrylic or neoprene-based latex, and a heat-reactive, cross-linkable phenolic resin in the form of an aqueous dispersion. The phenolic resin improves metal adhesion, green strength, and peel strength at elevated temperature. A typical formulation contains three parts latex and one part phenolic dispersion (dry weight bases). Although metal oxides may be added, reaction of the oxide with the phenolic resin does not occur readily.

Bonding properties of water-based contact adhesives are similar to those of solvent-based systems, but are free of flammability hazards. However, drying times are longer and the bond is sensitive to moisture.

**Carbonless Copy Paper.** In carbonless copy paper, also referred to as pressure-sensitive record sheet, an acid-sensitive dye precursor, such as crystal violet lactone or *N*-benzoylleucomethylene blue, is microencapsulated with a high boiling solvent or oil within a cross-linked gelatin (94,100,101) or in synthetic mononuclear microcapsules. Microcapsules that have a starch binder are coated onto the back of the top sheet. This is referred to as a coated-back (CB) sheet. The sheet intended to receive the image is treated on the front (coated-front (CF)) with an acid. When the top sheet is mechanically impacted, the dye capsules rupture and the dye solution is transferred to the receiving sheet where the acid developer activates the dye.

**Table 11. CF Coating Slurry Formulation**

Constituent	Parts
Kaolin clay	64
CaCO <sub>3</sub>	3
Colloidal silica	5.4
Hydroxyethyl starch	3
Styrene–butadiene latex	12
Novolak resin dispersion	12

The original acid–clay developers have been largely replaced by phenolic compounds, such as para-substituted phenolic novolaks. The alkyl group on the phenolic ring is typically butyl, octyl, nonyl, or phenyl. The acidity is higher than that of a typical unsubstituted novolak because of the high concentration of 2,2'-methylene bridges.

Color intensity and permanence are improved by metal carboxylate salts, especially zinc salts (100), which catalyze the dye development and stabilize the dye in its colored form. The substituted novolak resin, along with extender and binder, can be applied to the receiving sheet as a solution or aqueous dispersion. Aqueous dispersions are probably the most widely used; they are manufactured by the resin supplier or the user from the base resin.

A typical coating composition for the CF component is shown in Table 11. It is dried in a high velocity air oven at 93°C.

**Molding Compounds.** Molding compounds were among the earliest applications for solid phenolic resins. Molding neat phenolic resin was almost impossible and the strength, especially on impact, was poor without reinforcement. Combining the resin, usually a novolak, with hexa, wood-flour, or asbestos reinforcement, as well as pigments and additives, gave a moldable thermoset. The molded articles exhibit high temperature, flame, and chemical resistance, retention of modulus at elevated temperature, and hardness. Systems that have good electrical properties can be formulated at low cost. Resins can be compounded with a choice of fillers for a variety of applications.

ASTM D4617-96 is the specification that covers phenolic molding compounds. The general-purpose compounds, having good strength and electrical properties, are used in electrical appliances, automotive ignitions, and handles. Impact-resistant grades contain longer glass and textile fibers and rubber modifiers. Applications include pump housing and switches. Heat resistance is improved by incorporating mineral and glass fillers. Electrical-grade compounds contain mica and fiber glass fillers, and are used in specialty switches and cases. Graphite filler reduces the coefficient of thermal expansion. Although phenolic molding compounds compete with a wide variety of thermoset and thermoplastic compounds, they continue to be the preferred material in numerous applications, such as reinforced phenolic pistons in automotive disk brakes and transmission torque converters. Table 12 lists several applications for molded phenolic parts.

Phenolic molding materials are prepared by first blending the pulverized raw materials. In a compounding operation, the blend is passed through heated rolls to form a sheet as the resin melts. The compounded mixture remains on heated rolls until the desired flow and viscosity are reached. At this point, it is

**Table 12. Applications for Molded Phenolic Parts<sup>a</sup>**

Market	Key features	Examples
Appliances	Heat, moisture and chemical resistance; thermal and electrical insulation	Coffee pot handle and base; steam iron parts
Automotive and transportation	Heat, moisture, and hydrocarbon resistance; dimensional stability	Disc brake caliper pistons, transmission parts; water pump parts, torque converters; oil pump covers
Electrical	Heat and wear resistance; thermal and electrical insulation	Circuit breakers; motor control parts; commutators and alternators
Aerospace	Heat and chemical resistance; rigidity	Interior partitions; ablative surfaces
Packaging	Dimensional stability; chemical resistance	Closures

<sup>a</sup>Ref. 102.

discharged as a thin sheet and allowed to cool. The product is then granulated and packaged. Alternatively, a Banbury-type mixer can be used for the initial mixing; the mix is then fed to a roll mill for finishing and sheeting. Compounding extruders are also used and through a continuous process provide a pelletized product.

Phenolic resins used in molding materials are predominantly novolaks with hexa as the curing agent. Oxalic acid catalyzed novolaks and high ortho resins are used. Resole resins may be used in place of hexa as the curing agent in certain electrical applications in which the  $\text{NH}_3$  generated from the hexa can adversely affect metals such as copper and silver. Typically, the compound contains 40–50 wt% resin binder, 40–45% filler, and 5–10% pigment and additive. Fillers and reinforcements include wood flour, nutshell flour, cellulose fiber, mica (qv), wollastonite, mineral wool, mineral flour, glass fiber, organic fiber, carbon fiber, clay, and talc. Additives and pigments are magnesium oxide, graphite, molybdenum sulfide, stearates, calcium carbonate, carbon black, nigrosine, lime, fluoropolymers, and salicylic acid.

Molding materials are fabricated into articles by compression, transfer, and injection molding processes. For compression molding, the powder is poured into the mold cavity or a preform heated prior to molding. Temperature ranges from 140 to 190°C and pressures from 13.8 to 55.5 MPa (2000–8000 psi). Because the material is more fluid in the mold, transfer molding is suitable for molding around inserts or for intricate shapes. In injection molding, cross-linking in the barrel and sprues must be avoided.

**Abrasives.** Abrasive materials are either bonded or coated. Bonded phenolic abrasives have superior strength and shock resistance compared to sintered ceramic compositions. The higher stability permits higher rotational speeds for resin-binder wheels; however, temperatures are lower than with ceramic wheels.

Synthetic aluminum oxide and silicon carbide are the principal inorganic abrasive materials. They are used in grit sizes from 44 or finer to 1680  $\mu\text{m}$

(12–325 mesh). The coarser grit sizes are used for rough work when wheels are as large as 60 cm in diameter and 7.5-cm thick. These wheels are mounted in swinging-frame grinders and used to remove surface imperfections from stainless steel billets. Finer grit (250  $\mu\text{m}$  (60 mesh)) may be used in 45-cm-dia cutoff wheels mounted in automatic grinders. These wheels can slice through a solid 2.5-cm steel bar in 4 s, leaving a clean, shiny cut surface.

In the usual method of manufacture, the grit is first wetted with a low viscosity liquid resole phenolic resin or furfural, using 1–3 wt% of the grit. A dry mixture of phenolic resin and fillers is added and the combination of wet grit and powder is tumbled until each grit particle is coated. The mix is temporarily dry and free-flowing. The powdered phenolic resin varies from 6 to 10% of the weight of the grit. The quantity and type of filler (alumina, cryolite, iron oxide, silicate) depend on the intended use of the wheel, whose grinding characteristics are affected by the filler. The free-flowing grit resin mix is placed into the mold and pressed at RT for 1–2 min at 13.8–34.5 MPa (2000–5000 psi). The dense form is removed and cured for 12–24 h; temperatures are increased gradually to 185°C for 8–12 h. Pressing temperatures may be increased for high density structures.

Heat resistance is an important characteristic of the bond. The strength of typical abrasive structures is tested at RT and at 300°C. Flexural strengths are between 24.1 and 34.4 MPa (3500–5000 psi). An unmodified phenolic resin bond loses about one-third of its RT strength at 298°C. Novolak phenolic resins are used almost exclusively because these offer heat resistance and because the moisture given off during the cure of resole resins results in undesirable porosity. Some novolaks modified with epoxy or poly(vinyl butyral) resin are used for softer grinding action.

Coated abrasives, such as sheets, disks, and drums, are used for polishing and finishing. Here, too, the abrasives, such as aluminum oxide and silicon carbide, have replaced the flint and garnet of common sandpaper. These industrial coated abrasives are manufactured from cloth or tough paper base. First, a coat of medium viscosity liquid resole resin is laid down on a continuous web of the backing. The web passes wet-side-down over a pan of grit, which adheres to it electrostatically and remains embedded in the resin layer. Altering the strength of the applied electrostatic field and the speed of the web can control the amount of grit deposited, which varies from an open to a closed dense mass of abrasive. The uncured coated sheet is partially dried in a low temperature oven at 60°C, and a second, thinner coating of lower viscosity liquid resole resin is applied as a top to anchor the grit thoroughly. The coated web is taken off in rolls to be cured at 107–120°C for 3–4 h.

The resins should dry quickly and cure well at low temperatures. They usually are made at a high pH with high ratios of formaldehyde to phenol and held to fairly low molecular weight. Typical viscosities are 15,000 mPa·s (=cP) at 75% solids content for a first coat and 1000 mPa·s (=cP) at 50% solids for the top resin. For dense backing materials, such as fiber disks, a typical resin has a viscosity of 50,000 mPa·s (=cP) at 80% solids and is cured at 148°C. New opportunities are arising for coated abrasive belts in high pressure grinding. High strength backing has been developed and zirconia media are available for grinding.

**Friction Materials.** Phenolic friction materials are made from molding compounds developed to meet the extraordinary demands required by friction



elements in the transportation industries. Friction materials are used for brake linings, clutch facings, and transmission bands. A moderately high coefficient of friction, which is temperature-independent, is needed. In addition, the material must be high in strength, low in wear and abrasion, and resistant to moisture and hydraulic fluids.

In the 1980s, significant changes occurred in automotive brake elements. Reformation of friction elements eliminated asbestos and increased employment of disk brakes. These developments required binder resins that have higher temperature performance without affecting the coefficient of friction and wear. Alternatives to asbestos include mineral, carbon, aramid, and metal fibers, especially iron. Semimetallic linings contain as much as 70% iron fibers. Other inorganic fillers include barites, alumina, lime, magnesia, and clay. Graphite and molybdenum disulfide are used to reduce scoring.

The resins can be a novolak-hexa or a resole-novolak blend. In some applications liquid resoles are used. Addition of alkylated phenol, oil, or cashew nutshell liquid (CNSL) reduces hardness and increases abrasion resistance. Modification by rubber improves the coefficient of friction and reduces brake fading.

Many friction material formulations contain 5–15 wt% of friction particles, the granulated cross-linked products of the reaction of CNSL, a phenol substituted at the meta position with a  $C_{15}$ , unsaturated side chain, and formaldehyde. Friction particles range in size from 50 to 500  $\mu\text{m}$ . They reduce frictional wear and increase pedal softness (103).

Manufacture of friction elements includes the impregnation of fabrics and subsequent lamination, the wet-dough process, and the dry-mix process. Elements from the last two are prepared by compression-molding the formulation for up to an hour at 150–175°C. Thick brake elements require a carefully controlled heating-and-cooling cycle to minimize stresses created by expansion and contraction.

**Foundry Resins.** In the foundry industry, phenolic resins are used as the binder for sand in the manufacture of shell molds and cores. The two mating halves are joined by clamps or a bonding agent to form a shell mold into which the molten metal is poured for castings. The shell is formed by depositing a resin-sand mix on a hot metal pattern plate. After a certain period the pattern is inverted and the excess resin-sand is removed. The sand particles are bonded by an oven cure, and the shell is ejected from the pattern plate.

Iron is the preferred metal for casting; steel and nonferrous metals are used in smaller amounts. Most castings are made in green sand molds, ie, uncured molds of sand, clay, and water. However, the use of shell moldings is growing, because such moldings permit reproducibility of castings with close dimensional accuracy. In addition, the simplicity of equipment procedures reduces costs.

The shell-molding process, introduced in the United States in 1948, is an important market for phenolic resins. In the original process, dry sand and powdered resin (6–8%) are blended. However, because of the high binder content and the difficulty in obtaining a uniform mix, precoating methods were developed.

Both cold- and warm-coating processes employ solutions of phenolic resins. The principal process used for foundry resins is the hot-coating process. It is the fastest, least expensive, and safest process, and it requires no volatile removal. The sand is heated to 135–170°C in a muller, and solid novolak resin in flake

form is added, which melts quickly and coats the sand. A lubricant may be added at this point. After 1 min of mulling, the batch is cooled by adding water, which evaporates rapidly.

Hexa, which is not supplied with the resin, is usually added either with the water as a solution or just before or immediately after the water addition. By quenching the mix with water, the resin-coated sand is cooled to a point where there is no significant reaction with the curing agent. Any reaction between the resin and the hexa in the muller affects the bonding properties of the coated sand. As the batch cools and begins to break up, more lubricant may be added, which remains on the outside of the coated grains where it is most effective.

The total cycle time for most production batches is 2.5–3.5 min, considerably shorter than the cold- or warm-coating processes. Although a few available units have large capacity per batch, high production rates are possible because of the short cycle. While one batch is being mulled, sand for the next batch can be heated. The typical flake phenolic is an intermediate melting-point novolak containing 4% lubricant.

**Laminates.** Laminate manufacture involves the impregnation of a web with a liquid phenolic resin in a dip-coating operation. Solvent type, resin concentration, and viscosity determine the degree of fiber penetration. The treated web is dried in an oven and the resin cures, sometimes to the B-stage (semicured). Final resin content is between 30 and 70%. The dry sheet is cut and stacked, ready for lamination. In the curing step, multilayers of laminate are stacked or laid up in a press and cured at 150–175°C for several hours. The resins are generally low molecular weight resoles, which have been neutralized with the salt removed. Common carrier solvents for the varnish include acetone, alcohol, and toluene. Alkylated phenols such as cresols improve flexibility and moisture resistance in the fused products.

Industrial laminates are composed of two or more webs in sheet form that have been impregnated with a thermosetting resin and molded under heat and pressure. The web is usually made of cellulose paper, cotton fabric, glass cloth, glass mat, asbestos paper, wood veneer, and similar materials. Laminates are manufactured in sheets, rods, tubes, and special shapes, which can be machined by common methods to produce parts for a wide range of uses. An important example is in printed-circuit applications, which require varnishes that impart electrical properties, punchability, machinability, and hot-solder and solvent resistance to the laminate. General-purpose laminates are used in gears, spacers, cams, ball-bearing retainer rings, and other structural parts requiring machinability as well as moisture, oil, and impact resistance.

A decorative laminate is composed of layers of resin-impregnated paper, which have been molded together under heat and pressure to form a solid homogeneous sheet. The component parts are composed of corestock impregnated with phenolic, print, and overlay. The corestock confers body and strength. The print sheet provides the design characteristic; it is impregnated with melamine resin, as is the overlay sheet that imparts abrasion protection to the print sheet. Approximately seven sheets of phenolic-impregnated corestock are covered with one print sheet, which, in turn, is covered with one overlay sheet. This combination is molded against polished steel plates to obtain the desired finish, usually satin or gloss.

The type of varnish used in the process depends on the kraft paper manufacturer and basis weight of the papers; the machine, temperature, and control (scraper bars, squeeze rolls) used; the method of cutting the paper to size; the laminate being produced (post-forming or regular); and the press-cure cycle.

**Air and Oil Filters.** Liquid resole resins are used to coat and penetrate the cellulose fibers of filters and separators in order to increase strength and stiffness and protect against attack by the environment. The type of phenolic to be used depends on both the final property requirements and the papermaking process.

Air and oil filters are made by a dry-web process in which the filter paper is dried over heated metal drums. The paper is saturated with the phenolic resin solution, either off- or on-line, and dried in an oven advancing the resin to the B-stage (semicured). The sheet, containing 20–30% resin, is rolled and shipped to the filter-unit manufacturer, where the sheet is convoluted and the filter assembled and cured to the C-stage (fully cured).

The resins used in air and oil filters are moderate-to-low molecular weight, catalyzed by caustic in one step; 10–20% alcohol is added; solids content is in the range of 50–60%. These resins are designed to penetrate the sheet thoroughly, yet not to affect the porosity of the paper. In the B-stage, the resin must have sufficient flexibility to permit pleating; the C-stage should have stiffness and resistance to hot oil.

**Wood Bonding.** This application requires large volumes of phenolic resins (5–25% by weight) for plywood, particle board, waferboard, and fiberboard. Initially, phenolic resins were used mainly for exterior applications, whereas UF was used for interiors. However, the concern over formaldehyde emission has caused the replacement of UF by phenol–formaldehyde adhesives.

Different phenolic resins are used for different types of wood; for example, plywood adhesives contain alkaline-catalyzed liquid resole resins. Extension with a filler reduces cost, minimizes absorption, and increases bond strength. These resins have an alkaline content of 5–7% and are low in free phenol and formaldehyde. Because many resins have a high water content and limited storage stability, they are frequently made at or near the mill producing the plywood product. The plywood veneers are dried, coated with resin, stacked for pressing, and cured at 140–150°C.

Particle board and wood chip products have evolved from efforts to make profitable use of the large volumes of sawdust generated annually. These products are used for floor underlayment and decorative laminates. Most particle board had been produced with UF adhesive for interior use; resin demand per board is high due to the high surface area requiring bonding. Nevertheless, substantial quantities of phenol–formaldehyde-bonded particle board are produced for water-resistant and low formaldehyde applications.

The phenolic resins used for particle board are NaOH-catalyzed resoless of low viscosity and high water miscibility, similar to the liquid resole adhesives used in plywood manufacture. The higher resin and caustic content of the board frequently necessitates the addition of hydrophobic agents such as wax emulsions to increase the barrier properties of the board. The adhesive is applied to the particles in thin streams using high agitation to maximize material usage. Boards are cured in presses for 5–10 min at 150–185°C.

Waferboard, a more recent wood construction product, competes more with plywood than with particle board. Waferboard and strand board are bonded with solid, rather than liquid, phenolic resins. Both pulverized and spray-dried, rapid-curing resins have been successfully applied. Wafers are dried, dusted with powdered resin and wax, and formed on a caul plate. A top caul plate is added and the wafers are bonded in a press at  $\approx 180^{\circ}\text{C}$  for 5–10 min. Physical properties such as flexural strength, modulus, and internal bond are similar to those of a plywood of equivalent thickness.

Fiberboard or hardboard is made of low grade wood and wood waste. In the wet production process, a sheet is produced on a papermaking machine, such as a fourdrinier. A liquid resole is usually added to the beater section and precipitated onto the wood fibers by adjusting the pH. The moderately dry felt is further dried and cured in an off-line press.

**Fiber Bonding.** In fiber bonding, the resin is used as a binder in such products as thermal insulation batting, acoustic padding, and cushioning materials. All these materials consist of long fibers (glass or mineral fiber, cotton, polyester) laid down in a randomly oriented, loosely packed array to form a mat. They are bonded with resin to preserve the special insulating or cushioning quality of the mat.

In the dry-bonded process, fibers are reclaimed from woven textile scraps and powdered resin. Automotive acoustical padding (cotton and synthetic organic fiber) and thermal insulation batting (glass fiber) are made by this process. Inorganic and/or organic fibers are picked open to allow distribution of the phenolic resin among individual fibers. The fiber–resin mixture is formed into a blanket by cross-lapping a series of webs or by being blown into a chamber for deposition. The blanket is oven-cured to fuse the resin. Oven temperatures, dwell times, molding temperatures, and cycle times vary, depending on the type of fiber and curing characteristics of the resin.

The wet-bonded process uses virgin fiber spun from molten glass and liquid water miscible resin. High grade, thermal insulation batting is made by this process. The most common wet-bonded process for manufacturing glass or rock-wool, thermal insulation batting employs steam- or air-blowing. A stream of molten glass falls from the melting furnace into a rapidly spinning platinum cylinder. Centrifugal force causes the glass to be extruded through many small holes in the cylinder wall. At the outside, the fibers are attenuated (drawn) by the action of a jet flame from burners located around the spinning cylinder. Spray nozzles located just below this unit apply liquid binder resin to the fibers, which are sucked onto a moving screen to form a continuous mat. The mat is conveyed through a forced hot-air curing oven similar to that used in the dry-bonded process. Curing is followed by cool-down, trimming, slitting, and roll-up.

Fiber bonding resins are marketed in the form of finely pulverized powders of novolak/hexa mixtures or resoles and water-miscible liquids. Resole resins are the standard for the fiber bonding industry. They have excellent curing properties and low content of solvent extractables after curing. Bond strength to the fiber is high and resin usage is low. Solid resole resins must be stored cool to reduce sintering and aging.

Novolak-based resins are primarily used for organic fibers. They require a cross-linking reagent, usually hexa, for cure. Bond strength is good, producing

**Table 13. Mechanical Properties of Composites<sup>a</sup>**

Matrix resin	Flexural strength, <sup>b</sup> MPa <sup>c</sup>	Elongation, %	Notched Izod, J/m <sup>d</sup>	UL-94
Phenolic	228	2	1868	V0
Polyester	276	1.75	960	Burns
Vinyl ester	310	2	1227	Burns

<sup>a</sup>Glass content, 60%.<sup>b</sup>For all three matrix resins, the flexural modulus is 12 GPa ( $1.7 \times 10^6$  psi).<sup>c</sup>To convert MPa to psi, multiply by 145.<sup>d</sup>To convert J/m to ft-lbf/in., divide by 53.38.

bonded mats that have high tensile strengths. The storage stability is also good, so that refrigeration is rarely required. A typical binder mix produced by the customer consists of phenolic resin, urea, hydrocarbon oil or wax emulsion, ammonium sulfate, and occasionally a silane adhesion promoter; it is diluted with water to 5–10% solids content. The urea acts as a scavenger for the free formaldehyde (5–8%) invariably present, both as an inexpensive extender and, owing to its high nitrogen content, as an antimoldering agent. The oil or wax emulsion acts as a fiber lubricant and dust suppressant, the ammonium sulfate as a cure accelerator, and the silane as an adhesion promoter. The large volume of water in the binder mix cools the newly spun fibers, thus preventing premature resin cure, ie, before the mat has been formed and compressed to the proper thickness. All water-miscible resins must be stored under refrigeration.

**Composites.** There has been substantial progress in improving the processability of phenolics in composite materials (104–106) to the point where a variety of materials are available for pultrusion, filament winding, and resin-transfer molding (see COMPOSITES, FABRICATION). More complicated composite systems are based on aramid and graphite fibers.

Epoxy resins are usually superior to phenolics because of better adhesion, lower shrinkage on curing, and a much lower volatile content. Nevertheless, there are many specific applications for phenolic resins, including formable laminates and sheet-molding compounds having low flammability and smoke generation. These systems are suitable for aircraft interiors. Another area is in binders for carbon–carbon composites for applications such as in ablative coatings of reentry vehicle and aircraft brakes. The high char yield and the strength and porosity of the char are important in these applications. Finally, phenolic novolaks are effective curing agents for epoxies, and epoxidized novolaks are being used in applications requiring high functionality and high cross-link density.

**Glass-Reinforced Composites.** These composites are prepared from SMC and by liquid injection molding, (LIM). Phenolic resins are usually not amenable to LIM because of the volatiles generated. However, a resin suitable to LIM has been prepared (107). The properties of the 60% glass-mat-reinforced product obtained from this resin were compared to conventional isophthalic polyester and vinyl ester sheet-molding compounds at equivalent glass loading; the mechanical properties are shown in Table 13 (108,109). The phenolic resin systems have slightly lower strength values but measurably higher impact resistance. In addition, the phenolic glass composite has a UL-94 V0 rating, whereas the polyester SMC burns.

**Table 14. Strength Properties of Phenolic–Carbon-Fiber Composites**

Property	Resin, %		
	Phenolic		Epoxy novolak, 27
	40	35	
Tensile strength, MPa <sup>a</sup>	115	63	64
Flexural strength, MPa <sup>a</sup>	183	126	110
Flexural modulus, GPa <sup>b</sup>	15.8	6.3	6.4

<sup>a</sup>To convert MPa to psi, multiply by 145.

<sup>b</sup>To convert GPa to psi, multiply by 145,000.

A patent describes the glass-reinforced pultrusion of phenolic resin composites (110). In pultrusion, bundles of continuous fiber are wetted with resin and shaped and cured through a series of heated dies. A sulfonic acid accelerates the cure rate, which must be high. The mechanical properties are reported to be equivalent to those obtained from conventional unsaturated polyesters, but the heat-distortion temperature and flammability resistance are superior. An acid-free phenolic pultrusion system has been announced that can produce large panels for buildings, ships, aircraft, and mine ducts. The system involves an injection-type die rather than conventional dip tanks, and up to 70% glass loadings can be attained (111).

Phenolic sheet-molding compound is seeing increased use in interior and exterior applications in mass transit. The trains in service on the English Channel tunnel have several panels made from phenolic SMC, which had to meet the strict European safety standards for fire and smoke generation.

Phenolic resin prepregs on glass fibers are prepared from alcohol solution and occasionally from aqueous solutions. The glass web is dipped in a tank containing resin solution; the resin content in the web is controlled by metering rolls. The wet web is dried in a horizontal or vertical oven arrangement and cured to B-stage of the resin. The dry web is cut, stacked, and stored under refrigeration until used in a laminate. Depending on the application, the prepreg can be rigid, similar to the epoxy-type prepregs used in laminated circuit boards, or soft and flexible, which provides the tack and drape required to conform to a shaped article. Autoclave molding is essential for shaped articles to reduce void formation by trapped air and volatiles. Examples of shaped articles include interior parts of commercial airplanes such as the composite duct assembly, based on wrapped phenolic – fiber glass, being used on the Boeing 737. Although not equal to epoxy-prepreg systems in strength, phenolic resins provide superior flammability resistance and lower smoke toxicity, because antimony and halogens are absent.

**Carbon-Fiber Composites.** Cured laminates of phenolic resins and carbon-fiber reinforcement provide superior flammability resistance and thermal resistance compared to unsaturated polyester and epoxy. Table 14 shows the dependence of flexural strength and modulus on phenolic–carbon-fiber composites at 30–40% phenolic resin (112). These composites also exhibit long-term elevated temperature stability up to 230°C.

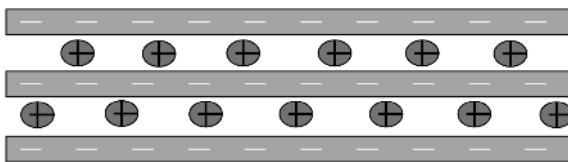
**Carbon–Carbon Composites.** Above 300°C, even such polymers as phenolics and polyimides are not stable as binders for carbon-fiber composites. Carbon–carbon composites are used at elevated temperatures and are prepared by impregnating the fibers with pitch or synthetic resin, followed by carbonization, further impregnation, and pyrolysis (112).

Carbon–carbon composites are used in high temperature service for aerospace and aircraft applications as well as for corrosion-resistant industrial pipes and housings. Applications include rocket nozzles and cases, aircraft brakes, and satellite structures. Carbonized phenolic resin with graphite fiber functioned effectively as the ablative shield in orbital reentry vehicles for many years (113).

Phenolic and furfuryl alcohol resins have a high char strength and penetrate into the fibrous core of the fiber structure. The phenolic resins are low viscosity resoles; some have been neutralized and have the salt removed. An autoclave is used to apply the vacuum and pressure required for good impregnation and sufficient heat for a resin cure, eg, at 180°C. The slow pyrolysis of the part follows; temperatures of 1000–1800°C are recommended for the best properties. On occasion, temperatures above 1800°C are used and constant weight is possible even up to 2760°C (114). A new process for carbon–carbon composite has been developed for engine components using phenolic resin and PAN fiber to produce near netshape parts (115,116).

**Nanocomposites.** Work conducted at Toyota in nylon-6 nanocomposites has generated several commercial products and stimulated substantial interest in a variety of polymer/nanoclay systems (see NANOCOMPOSITES, POLYMER-CLAY). The melt intercalation and curing behavior of phenolic resin were investigated using layered silicates such as montmorillonite and alkyl ammonium modified layered silicates. It was found by X-ray diffraction that the uncured phenolic was effectively intercalated. Depending on the surface treatment, the resulting interaction between organic modifier and phenolic resin played an important role in determining the stable nanostructure and the final morphology of the layered silicate composite (117,118).

The diagram below shows a representation of a polymer–clay, nanocomposite (qv).



**Liquid-Injection Molding.** In LIM, monomers and oligomers are injected into a mold cavity where a rapid polymerization takes place to produce a thermoset article. Advantages of these processes are low cost, low pressure requirement, and flexibility in mold configuration. Conventional systems, such as isocyanate with polyol, release little or no volatiles. The generation of substantial volatiles in the mold is obviously undesirable and has represented a significant obstacle to the development of a phenolic-based LIM system. A phenolic LIM system based on an anhydrous high ortho liquid resole has been reported (119,120).

Formaldehyde is present in the form of both methylol and phenolic hemiformals. A formaldehyde/phenol ratio of  $\approx 1.5$ – $1.0$  is used at a pH of 4–7. Divalent salts catalyze the reaction at 80–90°C for 5–8 h and the water is removed by an azeotropic solvent. Uncatalyzed resoles have excellent storage stability.

An important aspect of this procedure is the use of latent acid catalysts, such as phenyl hydrogen maleate, phenyl trifluoroacetate, and butadiene sulfone. These catalysts reduce the peak exotherm from over 200°C to 130–160°C. The resin catalyst mixture has a working life of up to several days at RT. The elevated temperature of molding these latent catalysts generates the corresponding acids, namely, maleic, trifluoroacetic, and phenolsulfonic, which catalyze the resol reaction. Typically, a cycle time of 1–2 min is required for a mold temperature of  $\sim 150^\circ\text{C}$ .

The water liberated during the cure has no apparent effect on the composite properties. Glass-filled composites prepared in this manner retain mechanical properties at elevated temperatures as well as solvent and flammability resistance (108,109). Phenolic-graphite-fiber composites that exhibit superior mechanical properties have also been prepared by this process.

**Foam.** Phenolic resin foam is a cured system composed of open and closed cells with an overall density of 0.16–0.80 g/cm<sup>3</sup>. Principal applications are in the areas of insulation and sponge-like floral foam. The resins are aqueous resoles catalyzed by NaOH at a formaldehyde/phenol ratio of  $\approx 2$ :1. Free phenol and formaldehyde content should be low, although urea may be used as a formaldehyde scavenger.

The foam is prepared by adjusting the water content of the resin and adding a surfactant (eg, an ethoxylated nonionic), a blowing agent (eg, pentane, methylene chloride, or chlorofluorocarbon), and a catalyst (eg, toluenesulfonic acid or phenolsulfonic acid). The sulfonic acid catalyzes the reaction, while the exotherm causes the blowing agent, emulsified in the resin, to evaporate and expand the foam (121). The surfactant controls the cell size as well as the ratio of open-to-closed cell units. Both batch and continuous processes are employed. In the continuous process, the machinery is similar to that used for continuous polyurethane foam.

The properties of the foam depend mainly on density and the cell character. For insulation, a high content of closed cells, along with an encapsulated fluorocarbon blowing agent, is desired. The foam must have sufficient strength and be able to resist smoldering, ie, a glowing combustion characteristic of early foams. Smoldering is controlled by additives and foam structure. For floral foam, lower density and an open-cell structure having low toughness are desirable. Floral foam usually contains a wetting agent in the formulation to ensure the rapid uptake of water.

An all-phenolic sandwich structure for aircraft interior applications has been developed using syntactic and expandable semisynthetic phenolic foam. The parts have outstanding fire behavior and are moldable to complex sandwich cores (117,118).

When smoldering is eliminated, phenolic foams exhibit excellent flammability resistance. Their LOI is 32–36%, and their smoke density is lower than that of polyisocyanurate foam of similar density. High thermal insulation K values have been obtained on foams of small cell size containing fluorocarbon blowing



**Table 15. Physical Properties of Phenolic Microballoons**

Property	Value
Average particle size, $\mu\text{m}$	43
Typical particle range, $\mu\text{m}$	20–120
Liquid displacement density, $\text{g}/\text{cm}^3$	0.15–0.35
Bulk density, $\text{g}/\text{cm}^3$	0.07–0.15
Toluene flotation, %	~90

agents. Phenolic foams are used for building products and warehouse insulation and ASTM C1126-00 is the standard for faced or unfaced rigid cellular phenolic thermal insulation.

**Honeycombs.** Honeycomb structures usually involve resin-treated papers and fiberglass, sometimes with a core filler and surface skins bonded to the honeycomb. Uses can be in aircraft interior panels as well as more demanding parts. Phenolic resin-impregnated aramid paper honeycomb cores have been developed for fighter aircraft applications. These new honeycomb structures provide greater structural strength than other honeycomb products currently available. One particular part application is the inlet cowl, which incorporates a complex structure, core machining, and core forming (122).

**Spheres.** Hollow spherical fillers have become extremely useful for the plastics industry and others. A wide range of hollow spherical fillers are currently available, including inorganic hollow spheres made from glass, carbon, fly ash, alumina, and zirconia; and organic hollow spheres made from epoxy, polystyrene, UF, and phenol–formaldehyde. Although phenol–formaldehyde hollow spheres are not the largest volume product, they serve in some important applications and show potential for future use.

In an early process by Sohio, a variety of compositions were produced by dissolving a film-forming polymer in a solvent (or water), adding a blowing agent, and spray drying the resulting solution under carefully controlled conditions. The use of spray drying to produce discrete, uniform hollow spheres, organic or inorganic, requires high skills in formulation, process control, and engineering. Some of the organic materials described include phenolic resins, poly(vinyl alcohol), polystyrene, methylcellulose, and protein. In the case of the phenolic resins, water-miscible resoles were used; water was the solvent and ammonium carbonate – ammonium nitrate or dinitrosopentamethylenetetramine was the blowing agent. Hollow phenolic spheres in sizes of 5–50- $\mu\text{m}$  dia were obtained. The principal intended use was as a floating cap on petroleum naphtha and crude oil to retard evaporation.

Emerson & Cumming, Inc., eventually bought the rights to the Sohio process and produced a variety of microspheres. Union Carbide was licensed to produce the phenolic microspheres offered under the name Phenolic Microballoons (Table 15). When Phenolic Microballoons are introduced into a crude-oil storage tank, they form a fluid seal that rises and falls with the level of the oil. A continuous vapor-barrier seal is formed, which reduces evaporational losses up to 90%. Tests have been conducted under various mechanical and weather conditions and with crude oils of varying vapor pressure.

Phenolic Microballoons applications in plastics take advantage of low density, porosity, and surface-to-volume ratio to produce lightweight parts. Probably the most notable example is the syntactic foam.

While a conventional foam uses a blowing agent to form a cellular structure as the resin sets, syntactic foams are made by incorporating hollow spheres into liquid resins, especially epoxy resins in the case of Phenolic Microballoons, although urethanes and polyesters are also used. Having a continuous polymer phase and taking advantage of the high compressive strength of the spheres, syntactic foams can be made much stronger than conventional foams. In addition, they are being formed in place. As a result, syntactic foams have become widely used as a modeling, styling, and structural core material in automotive, marine, and aerospace applications.

A mixture of Phenolic Microballoons and resin binder has a putty-like consistency. It can be molded to shape, trowelled onto surfaces, or pressed into a core. Curing gives a high strength, low density ( $0.144 \text{ g/cm}^3$ ) foam free of voids and dense areas, and without a brittle skin. Syntactic foams are used in widely diverse applications, including boat flotation aids; structural parts in aircraft, submarines, and missiles; structural cores for wall panels; and ablative heat shields for reentry vehicles and rocket test engines.

Microballoons have been used for gap filling, where the spheres dampen sound or vibration in the structure. In the medical area, microballoons have been evaluated as a skin replacement for burn victims and phantom tissue for radiation studies. An important application is in nitroglycerin-based explosives, in which microballoons permit a controlled sequential detonation not possible with glass spheres.

In the 1990s, carbon microbeads have been produced by a proprietary process using phenolic resin. Potential applications are lubricants, adhesives, and conductive fillers for plastics, rubbers, and coatings (123).

**Fibers.** The principal type of phenolic fiber is the novoloid fiber (124). The term novoloid designates a content of at least 85 wt% of a cross-linked novolak. Novoloid fibers are sold under the trademark Kynol, and Nippon Kynol and American Kynol are exclusive licensees. Novoloid fibers are made by acid-catalyzed cross-linking of melt-spun novolak resin to form a fully cross-linked amorphous network. The fibers are infusible and insoluble, and possess physical and chemical properties that distinguish them from other fibers. Applications include a variety of flame- and chemical-resistant textiles and papers as well as composites, gaskets, and friction materials. In addition, they are precursors for carbon fibers.

The fibers are prepared from a high molecular weight novolak resin. Uncured fibers are prepared by melt-spinning the novolak. These fibers are then immersed in aqueous formaldehyde solution containing an acidic catalyst. As heat is applied, curing commences and the novolak resin is transformed into a cross-linked network through the formation of methylene and dibenzyl ether linkages. The final cross-linked structure is free of molecular orientation, and the density of cross-linking is low. The fiber contains  $\approx 5 \text{ wt\%}$  unreacted methylol groups, which can be utilized in the formation of novoloid-fiber composites, or be reduced by heating the cured fiber to  $180^\circ\text{C}$ .

Optimum mechanical properties of the fibers are developed provided the precursor novolak filaments are less than 25  $\mu\text{m}$  in diameter to ensure sufficient diffusion of the formaldehyde and catalyst into the fiber. The individual fibers are generally elliptical in cross section. Diameters range from 14 to 33  $\mu\text{m}$  (0.2–1.0 tex or 2–10 den) and fiber lengths are 1–100 mm. Tensile strength is 0.11–0.15 N/tex (1.3–1.8 g/den) and elongation is in the 30–60% range. Elastic recovery is as high as 96%.

The LOI of novoloid materials varies with the particular structure (fiber, felt, fabric) being evaluated; it is generally in the 30–34% range. By comparison, aramid fiber has a LOI of 28–31 and wool of 24. When exposed to flame, novoloid materials do not melt but gradually char until completely carbonized. The high strength of the phenolic char results in the fiber retaining its original fiber structure, and the char effectively absorbs heat from the materials. When novoloid products are exposed to flame, the products of combustion are principally  $\text{H}_2\text{O}$ ,  $\text{CO}_2$ , and carbon char. Smoke emission is minimal, less than that of any other organic fiber.

Applications for novoloid fibers include a variety of flame-resistant protective clothing, safety accessories, and flame barriers for upholstered furniture. As an asbestos replacement, novoloid fibers have been used in gasketing, packings, brake linings, and clutch facings. In electrical applications, novoloid fibers and papers can be used as flameproof coatings and as wrapping tapes in wire and cable applications.

The novoloid molecular structure includes methylol groups, which are available for cross-linking with reactive sites in the matrix material. The ability of the fibers to react with matrix resins yields synergistic improvements in the properties of the composite. Novoloid fibers have been incorporated into composites with thermoplastic resins such as polypropylene, PVC, and polyamide polyesters. Thermosetting resins include phenolics, epoxies, and melamines. In certain elastomers, the methylol reactivity can be used to upgrade the high temperature performance, for example, in chlorinated polyethylene. A process has been announced that produces carbonized Kynol fiber having extremely high surface area (125).

## BIBLIOGRAPHY

“Phenolic Resins” in *EPST* 1st ed., Vol. 10, pp. 1–73, by W. A. Keutgen, Union Carbide Corp.; in *EPSE* 2nd ed., Vol. 11, pp. 45–95, by Peter W. Kopf, Arthur D. Little, Inc.; in *EPST* 3rd ed., Vol. 7, pp. 322–367, by P. W. Kopf, TIAX, LLC.

## CITED REFERENCES

1. *SPI Phenolic Molding Division Technical Conference*, Cincinnati, Ohio, June 1987.
2. S. R. Sandler and W. Caro, *Phenol Aldehyde Condensation*, Vol. 1, Academic Press, Inc., New York, 1977, Chapt. “2”.
3. R. W. Martin, *The Chemistry of Phenolic Resins*, John Wiley & Sons, Inc., New York, 1956.
4. N. J. L. Megson, *Phenolic Resin Chemistry*, Butterworth & Co. Ltd., Kent, U.K., 1958.

5. J. F. Walker, *Formaldehyde*, Van Nostrand Reinhold Co., Inc., New York, 1974.
6. T. S. Carswell, *Phenoplasts*, Interscience Publishers, New York, 1947.
7. A. Knop and W. Scheilb, *Chemistry and Applications of Phenolic Resins*, Springer, Berlin, 1979.
8. A. Knop and L. Pilato, *Phenolic Resins*, Springer, Berlin, 1985.
9. A. Gardziella, L. A. Pilato, and A. Knop, *Phenolic Resins*, Springer, Berlin, 1999.
10. *ACS Symposium on Phenolic Resins*, Washington, D.C., Aug. 1983.
11. U.S. Pat. 643,012 (Feb. 6, 1900), A. Smith.
12. U.S. Pats. 939,966 (Nov. 15, 1909) and 942,852 (Dec. 12, 1909), L. H. Baekeland.
13. J. B. Flemming, *Hydrocarbon Process.* **55**(1), 185 (Jan. 1976).
14. K. Kamide and Y. Miyakawa, *Makromol. Chem.* **179**, 359 (1978).
15. *Hydrocarbon Process.* 90 (Mar. 1976); 216 (Nov. 1965); 183 (Nov. 1969); 150 (Nov. 1975); 135 (Nov. 1973).
16. P. Kopf and E. Wagner, *J. Polym. Sci., Polym. Chem. Ed.* **11**, 939 (1973).
17. Y. Ihashi, K. Sawa, and S. Morita, *Kogyo Kagaku Zasshi* **68**, 1427 (1965).
18. U.S. Pats. 4,433,119 and 4,433,129 (Feb. 21, 1984), S. W. Chow and G. L. Brode (to Union Carbide Corp.).
19. S. Sojka, *Macromolecules* **12**, 767 (1979).
20. S. Ishida, Y. Tsutsumi, and K. Katsumasa, *J. Polym. Sci., Polym. Chem. Ed.* **19**, 1609 (1981).
21. H. Bender, *Ind. Eng. Chem.* **44**, 1619 (1952).
22. A. Zsavitkas and A. Beaulieu, *Am. Chem. Soc., Div. Org. Coat. Plast. Chem.* **27**, 100 (1967).
23. H. Peer, *Rec. Trat. Chim.* **78**, 851 (1959). *Rec. Trat. Chim.* **79**, 825 (1960).
24. J. H. Freemann and C. Lewis, *J. Am. Chem. Soc.* **76**, 2080 (1954).
25. K. Eapen and L. Yeddanapalli, *Makromol. Chem.* **4**, 119 (1968).
26. U.S. Pat. 4,124,554 (Nov. 7, 1978), J. Fry (to Union Carbide Corp.).
27. U.S. Pat. 4,206,095 (June 3, 1980), J. Wynsta and S. Schultz (to Union Carbide Corp.).
28. U.S. Pat. 3,943,080 (Mar. 9, 1976), M. Wismer (to PPG Industries).
29. H. A. Bruson and C. W. MacMullen, *J. Am. Chem. Soc.* **63**, 270 (1941).
30. T. T. Jones, *J. Soc. Chem. Ind. London* **65**, 264 (1946).
31. O. Vlk, *Plaste Kautsch.* **4**, 127 (1957).
32. U.S. Pat. 3,687,896 (Aug. 29, 1972), S. Vargia and U. Nistri (to Societa Italiana Resine SpA).
33. *Mod. Plast. Int. Ed.* **58**(4), 45 (Apr. 1981).
34. *Chem. Eng.* **99**(6), 19 (June 1992).
35. U.S. Pat. 4,900,671 (1990), A. Pokora (to Mead Corp.); U.S. Pat. 5,153,298 (1992), A. Pokora (to Mead Corp.).
36. U.S. Pat. 4,113,700 (1978), W. Aubertson (to Monsanto Co.).
37. U.S. Pat. 3,823,103 (July 9, 1979), J. Harding (to Union Carbide Corp.).
38. G. Brode, T. Jones, and S. Chow, *Chem. Technol.* **13**, 676 (1983).
39. U.S. Pat. 4,366,303 (Dec. 28, 1982), P. W. Kopf (to Union Carbide Corp.).
40. U.S. Pat. 4,788,236 (Nov. 29, 1988), P. W. Kopf (to Union Carbide Corp.).
41. U.S. Pat. 2,797,201 (July 11, 1957), F. Veatch (to Sohio).
42. U.S. Pat. 4,098,770 (July 4, 1978), A. Berchem, K. Sudan, and E. Gres (to Reichhold Chemicals, Ltd.).
43. R. B. Graver, in S. Lee, ed., *International Encyclopedia of Composites*, 2nd ed., SAMPE Publisher 2000, p. 176.
44. H. Ishida and Y. Rodriguez, *Polymer* **36**, 3151 (1995).
45. H. Ishida and Y. Rodriguez, *J. Appl. Polym. Sci.* **58**, 1751 (1995).
46. U.S. Pat. 6,207,786 (Mar. 27, 2001), H. Ishida and S. Rimdusit (to Edison Polymer Innovation Corp.).

47. K. Hultzs, *Kunststoffe* **37**, 205 (1947).
48. U.S. Pat. 5,334,675 (Aug. 2, 1994), A. Gerber (to Borden, Inc.).
49. U.S. Pat. 5,952,440 (Sept. 14, 1999), W. Walisser and C. Johnson (to Borden, Chemical).
50. E. Orrell and R. Burns, *Plast. Polym.* **68**, 469 (Oct. 1968).
51. V. Pshenitsyna and M. Kotrelev, *Polym. Sci. U.S.S.R.* **11**, 829 (1969).
52. V. Kurachenkov and L. Igonin, *J. Polym. Sci., Part A: Polym. Chem.* **1**, 2283 (1971).
53. M. Yamao, N. Yoshimi, and S. Tanaka, *Kogyo Kagaku Zasshi* **74**, 1938 (1971).
54. J. Gillham, *Polym. Prepr. (Am. Chem. Soc., Div. Polym. Chem.)* **22**(2), 131 (1981).
55. R. Young, P. Kopf, and O. Salgado, *Tappi* **64**(4), 127 (1981).
56. M. Karas and F. Hillenkamp, *Anal. Chem.* **60**, 2299 (1988).
57. H. Paschy, K. Rode, R. Ghahary, and D. Braun, *Die Angew. Makromol. Chemie* **241**, 95 (1996).
58. H. Mandal and A. Hay, *Polymer* **38**, 6267 (1997).
59. H. L. Bender, *Mod. Plast.* **30**, 136 (1953).
60. D. Boeschel, M. Fedtke, and W. Geyet, *Polymer* **38**, 1291 (1997).
61. B. Mechin, D. Hanton, V. Le Geoff, and J. Tanneur, *Eur. Polym. J.* **20**, 333 (1984).
62. J. Shaefer, *J. Am. Chem. Soc.* **98**, 1031 (1976).
63. R. Bryson, G. Hatfield, T. Early, A. Palmer, and G. Maciel, *Macromolecules* **16**, 1669 (1983).
64. C. Fyfe, *Macromolecules* **16**, 1216 (1983).
65. G. Maciel, I. Chuang, and L. Gollob, *Macromolecules* **17**, 1081 (1984).
66. E. Wagner and R. Greff, *J. Polym. Sci., Part A: Polym. Chem.* **1**, 2193 (1971).
67. D. Braun and J. Arnelt, *Angew. Makromol. Chem.* **73**, 133 (1978).
68. A. Rudin, C. Fyfe, and S. Vines, *J. Appl. Polym. Sci.* **28**, 2611 (1983).
69. E. Tesarova and V. Pacakova, *Chromatographia* **17**, 269 (1983).
70. W. Werner and O. Barber, *Chromatographia* **15**, 101 (1982).
71. L. Taylor, *Anal. Chem.* **42**, 297 (1970).
72. M. Kamal and S. Sourour, *Polym. Eng.* **13**, 59 (1973).
73. J. Enns and J. Gillham, *J. Appl. Polym. Sci.* **28**, 2567 (1983).
74. W. Stark, J. Döring, V. Bovtun, and C. Kürten, *NDT. net* **3**(11), 141 (Nov. 1998).
75. L. Lorenz, and A. Christiansen, *Ind. Eng. Chem. Res.* **34**, 4520 (1995).
76. X.-M. Wan, B. Riedl, R. Geimer, and A. Christiansen, *Wood Sci. Technol.* **30**, 423 (1996).
77. R. Geimer and A. Christiansen, *For. Prod. J.* **46**, 67 (1996).
78. U.S. Environmental Protection Agency, Technology Transfer Network, [www.epa.gov](http://www.epa.gov), see phenol (108-95-2), May 17, 2001.
79. H. Babich and D. Davies, *Reg. Tox. Pharm.* **1**(1), 90 (1981).
80. U.S. Environmental Protection Agency, Technology Transfer Network, [www.epa.gov](http://www.epa.gov), see formaldehyde (50-00-0), May 17, 2001.
81. A. Housden, *Water Pollut. Control* **80**, 490 (1981).
82. *Reinforced Plast.* **35**(7/8), 17 (1992).
83. Rogers Corp., Molding Material Division, Manchester, Conn. Product Literature, 2001.
84. *Plast. Week* 2 (Mar. 23, 1992).
85. *Plast. Environ.* 5 (July 10, 1992).
86. B. Olson and H. De Keyser, *Recycling Cured Phenolic Material*, Rogers Corp. Molding Materials Division, Manchester, Conn. Copyright 2001 and SAE International Congress and Exposition, 1992.
87. *Recycling Special Report, Phenolic Division of The Society of the Plastics Industry*, Copyright 2001.
88. *Chem. Eng. News* 21 (Jan. 22, 2001).

89. S. Kelley, M. Myers, D. Johnson, X.-M. Wang, and M. Davis, *Production of Chemicals and Materials from Renewable Resources*, (ACS Symposium Series), American Chemical Society, Washington D.C., 2001, p. 784,
90. U.S. Pat. 5,367,043, J. Butter and R. Brandon (to Enzymol, Inc.).
91. American Plastics Council, 2000 Sales and Production Data, Arlington, Va.
92. *Plastics Technology Online Supplier Directory for Phenolic Resins*, Oct. 2001.
93. G. Bosshard, *Prog. Org. Coat.* **10**, 205 (1982).
94. U.S. Pats. 3,723,156 (Mar. 27, 1973) and 3,732,120 (May 8, 1973), B. Brockett; 3,737,410 (June 5, 1973), H. Mueller; 3,936,573 (Feb. 3, 1976), B. Brockett; and 4,165,102 (Aug. 21, 1979), J. Bodmer (to National Cash Register).
95. W. A. Boyd, C. Merriam, and J. Fry, in R. Tess and G. Behlein, eds., *Applied Polymer Science*, (ACS Symposium Series), 2nd ed., American Chemical Society, Washington, D.C., 1985, pp. 1141–1158.
96. D. M. Berger, *Met. Finish.* **74**(9), 52 (1976).
97. J. Fry, C. Merriam, and G. Misko, *Am. Chem. Soc., Div. Org. Coat. Plast. Chem.* **47**, 540 (1982).
98. B. Barth, in E. Skeist, ed., *Handbook of Adhesive*, Van Nostrand Reinhold Co., Inc., New York, 1977, Chapt. "23", p. 382.
99. H. Kollek, H. Brockmann, and H. Mueller, *Int. J. Adhesion Adhes.* **6**(1), 37 (1986).
100. U.S. Pat. 4,025,490 (May 24, 1977), F. Weaver (to Mead Corp.).
101. J. Perry, *Pulp Pap.* **46**, 93 (Aug. 1973); *Pulp Pap.* **46**, 116 (Oct. 1973).
102. G. Elbe, *Plastics Design Forum*, 66 (Nov./Dec. 1993).
103. U.S. Pats. 4,316,827 (Feb. 23, 1982) and 4,420,571 (Dec. 13, 1983), L. Pacala and J. Blickensderfer (both to Union Carbide Corp.).
104. J. Taylor, *44th International SAMPE Symposium*, Long Beach, Calif., 1999, p. 1123.
105. S. Qureshi, *51st Annual Conference, Composites Institute, SPI*, 1996.
106. K. Yoshioka and J. Seferis, *46th International SAMPE Symposium*, Long Beach, Calif. 2001.
107. U.S. Pat. 4,403,066 (Sept. 6, 1983), G. L. Brode, S. Chow, and W. Hale (to Union Carbide Corp.).
108. *ACS National Meeting*, Washington, D.C., Aug. 1983.
109. G. L. Brode, *Polym. Prepr.* **24**(2), 194 (1983).
110. U.S. Pat. 4,419,400 (Dec. 6, 1983), R. Hindersinn (to Occidental Petroleum).
111. *Plast. World* **47**(6), 42 (1989).
112. J. Delmonte, *Technology of Carbon and Graphite Fiber Composites*, Van Nostrand Reinhold Co., Inc., New York, 1981.
113. E. F'itzer and W. Schafer, *Carbon* **8**, 353 (1970).
114. S. Siebold, *SAMPE Symp.* **20**, 327 (Apr. 1975).
115. W. Kowbel, J. Webb and J. Withers, *44th International SAMPE Symposium*, Long Beach, Calif., 1999, p. 1878.
116. U.S. Pat. 6,051,167 (Apr. 18, 2000), J. Withers, R. Loutfy, W. Kowbel, C. Bruce, and R. Vaidyanathan.
117. M. Chio, I. Chung, and J. Lee, *Chem. Mater.* **12**, 2977 (2000).
118. I. Kleba and E. Haberstroh, *46th International SAMPE Symposium*, Long Beach, Calif., 2001.
119. U.S. Pat. 4,395,521 (July 26, 1983), S. W. Chow (to Union Carbide Corp.).
120. G. L. Brode, S. W. Chow, and M. Michno, *Polym. Prepr. (Am. Chem. Soc., Div. Polym. Chem.)* **24**(2), 192 (Aug. 1983).
121. U.S. Pats. 4,423,163 (Dec. 27, 1983), H. Doerge; 4,165,413 (Aug. 21, 1979), R. Sefton; and 444,912 (Apr. 24, 1984), J. Carlson (to Koppers Co., Inc.).
122. S. Linder and B. Brailsford, Phenolic Resin-Impregnated Aramid Paper Honeycomb Core Program, Navy Mantech Program, Office of Naval Research, FY96-98, 1998.

123. K. Esumi, S. Eshima, Y. Murakami, H. Honda, K. Esumi, and H. Oda, *Colloids Surf.* **108** 113 (1996).
124. U.S. Pats. 3,650,102 (Mar. 21, 1972) and 3,723,588 (Mar. 27, 1973), J. Economy and R. Clark (to Carborundum Co.).
125. *J. Chem. Week*, 5 (Aug. 10, 1989).
126. J. Woodbrey, H. Higginbottom, and H. Culbertson, *J. Polym. Sci., Part A: Polym. Chem.* **3** 1079 (1965).
127. R. Hirst and co-workers, *J. Polym. Sci., Part A: Polym. Chem.* **3**, 2091 (1965).
128. T. Yoshikawa and J. Kumanotani, *Makromol. Chem.* **131**, 273 (1970).
129. T. Sterling and J. Weinkam, *J. Occup. Med.* **30**, 895–901 (Nov. 1988).
130. U.S. Pat. 3,595,821 (July 27, 1971), S. Spector (to PPG Industries).

## GENERAL REFERENCES

- E. Dradi and G. Casiraghi, *Macromolecules* **11**, 1295 (1978).  
T. Liu and S. Rhee, *Wear* **76**, 213 (1978).

PETER W. KOPF  
TIAX, LLC

## PHOSGENE

### Introduction

Phosgene [75-44-5] (carbonyl chloride, carbon oxychloride, chloroformyl chloride),  $\text{Cl}_2\text{CO}$ , is a colorless liquid with a low boiling point. The compound was first prepared in 1812 by J. Davy from the photochemical reaction of carbon monoxide and chlorine. Phosgene may be formed at elevated temperatures by oxidation of chlorinated solvents (1–5). Phosgene has been used in the preparation of a great variety of chemical intermediates. In addition, it is now widely used in the preparation of isocyanates, which are then used in the preparation of Polyurethanes (PUR), in the manufacture of Polycarbonates, and in the synthesis of chloroformates and carbonates, which are used as intermediates in the synthesis of pharmaceuticals and pesticides. Because of phosgene's toxicity, a high level of safety technology has been developed to ensure its safe handling.

### Properties

Some physical properties of phosgene are listed in Table 1. At room temperature and pressure, phosgene is a colorless gas. Impurities may discolor phosgene, transforming it from clear to pale yellow to green. Phosgene has a characteristic odor. At the time of initial exposure, the odor of phosgene gas can be detected only briefly. At ca 0.5 ppm in air, the odor has been described as pleasant and similar to that of newly mowed hay or cut green corn. However, at high concentrations, the odor may be strong, stifling, and unpleasant.

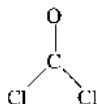
**Table 1. Some Physical Properties of Phosgene<sup>a</sup>**

Properties and characteristics	Value
Molecular weight	98.92
Melting point, °C	−127.84
Boiling point, °C <sup>b</sup>	7.48
Density at 20°C, g/cm <sup>3</sup>	1.387
Vapor pressure at 20°C, kPa <sup>c</sup>	161.68
Vapor density (air = 1.0)	3.4
Critical temperature, °C	182
Density at critical point, g/cm <sup>3</sup>	0.52
Critical pressure, MPa <sup>d</sup>	5.68
Latent heat of vaporization, at 7.5°C, J/g <sup>e</sup>	243
Molar heat capacity of liquid, at 7.5°C, J/K <sup>e</sup>	100.8
Molar heat of formation, kJ <sup>e</sup>	
From elements	218
From CO and Cl <sub>2</sub>	108
Molar entropy, J/K <sup>e</sup>	
At 7°C	280
At 25°C	284
Surface tension, mN/m (=dyn/cm)	
At 0.0°C	34.6
At 16.7°C	20.1
At 34.5°C	17.6
At 46.1°C	15.9

<sup>a</sup>Ref. 6.<sup>b</sup>At 101.3 kPa<sup>c</sup> = 1 atm.<sup>c</sup>To convert kPa to psi, multiply by 0.145.<sup>d</sup>To convert MPa to psi, multiply by 145.<sup>e</sup>To convert J to cal, divide by 4.184.

In general, phosgene is soluble in aromatic and aliphatic hydrocarbons, chlorinated hydrocarbons, and organic acids and esters. It is removed easily from solvents by heating or sparging with air or nitrogen, but because of its toxicity, great care must be taken to control its presence in the atmosphere.

Phosgene is a planar molecule. The interatomic distances are 0.128 nm for C—O and 0.168 nm for C—Cl (1). The Cl—C—Cl angle is 117°. Infrared, ultraviolet, and Raman spectral properties are described in References 7,8–9.



**Reactions.** Phosgene interacts with many classes of inorganic and organic reagents. The reactions are described extensively in the literature, eg, see References 10,11–12. Reaction with sodium takes place at room temperature, but reaction with zinc requires warming.

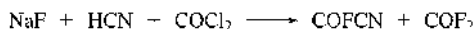
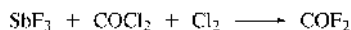
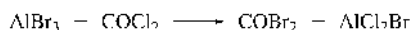
Oxides and sulfides of metals react with phosgene at elevated temperatures, usually yielding very pure chlorides. The reaction of phosgene with cadmium sulfide is a good method for preparing carbonyl sulfide (carbon oxy sulfide), COS.



The reactions of phosgene with calcium, magnesium, tin, and zinc oxide have been described (13–18). The reactions of titanium oxide with phosgene, tungsten trioxide with phosgene, and the chlorination of oxides of interest in the nuclear field, especially uranium oxide, plutonium oxide, and thorium oxide, have also been characterized (19–24).

Phosphates and silicates of metals often react with phosgene at elevated temperatures and yield the metal chloride and phosphorus oxychloride or silicon dioxide. The reaction with ferric phosphate at 300–350°C has been proposed as a synthetic method for phosphorus oxychloride,  $\text{POCl}_3$ .

Anhydrous aluminum chloride forms a variety of complexes with phosgene, eg,  $\text{Al}_2\text{Cl}_6 \cdot 5\text{COCl}_2$  at low temperatures,  $\text{Al}_2\text{Cl}_6 \cdot 3\text{COCl}_2$  at 30°C, and  $\text{Al}_2\text{Cl}_6 \cdot \text{COCl}_2$  at above 55°C. Reaction with aluminum bromide yields carbonyl bromide,  $\text{COBr}_2$ , and aluminum chlorobromide,  $\text{AlCl}_2\text{Br}$ . Reaction of antimony trifluoride with phosgene and chlorine yields carbonyl fluoride (25). Phosgene reacts with sodium fluoride and HCN, yielding phosgene fluorocyanide and carbonyl fluoride (26).



Phosgene reacts slowly with cold water to produce  $\text{CO}_2$  and  $\text{HCl}$ , and more quickly at higher temperatures (27). In the reaction of gaseous phosgene with water, it is difficult to get the necessary intimate mixing of the gas and the water.

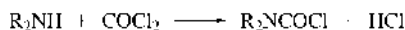


Ammonia reacts vigorously with phosgene. The products are urea, biuret, ammelide (which is a polymer of urea), cyanuric acid, and sometimes cyamelide (which is a polymer of cyanic acid). The secondary products probably arise through the very reactive intermediate carbamyl chloride,  $\text{NH}_2\text{COCl}$ .

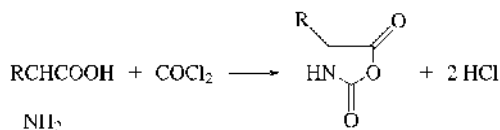
Phosgene reacts with a multitude of nitrogen, oxygen, sulfur, and carbon centers. Reaction with primary alkyl and aryl amines yields carbamoyl chlorides which are readily dehydrohalogenated to isocyanates:



Secondary amines form carbamoyl chlorides:



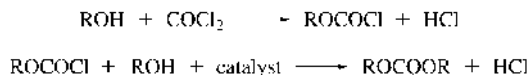
$\alpha$ -Amino acids react readily with phosgene to form oxazolidine-2,5-diones:



Hydrazine reacts with phosgene, yielding carbonylhydrazide:

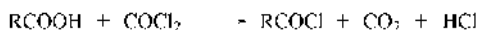


The reaction of phosgene with alcohols yields chloroformates, and with a basic catalyst present, carbonates are formed.

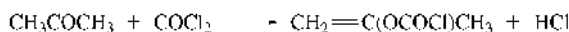


This reaction is commercially important since it serves as a basis for the manufacture of Polycarbonates.

Carboxylic acids react with phosgene to produce acid chlorides (28).



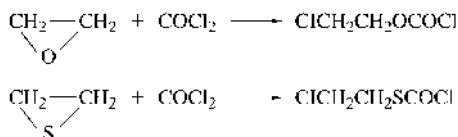
Ketones also react with phosgene:



Amides react with phosgene to yield nitriles (qv).



Phosgene can also initiate ring opening.



Although  $\text{POCl}_3$  is the traditional reagent in the Vilsmeier aldehyde synthesis, phosgene may be employed and its role, as well as that of the intermediates, has been studied extensively (29–31).

## Manufacture

Phosgene is manufactured by the reaction of carbon monoxide with chlorine over activated carbon. However, depending on the quantity of phosgene needed and the availability of the raw materials, numerous variations of this basic synthetic process are being practiced. Continuous processing and a high degree of automation are required for phosgene purification, condensation, and storage. Because of its toxicity, careful and extensive safety procedures and safety equipment are incorporated in plant design and operation. The entire phosgene manufacturing

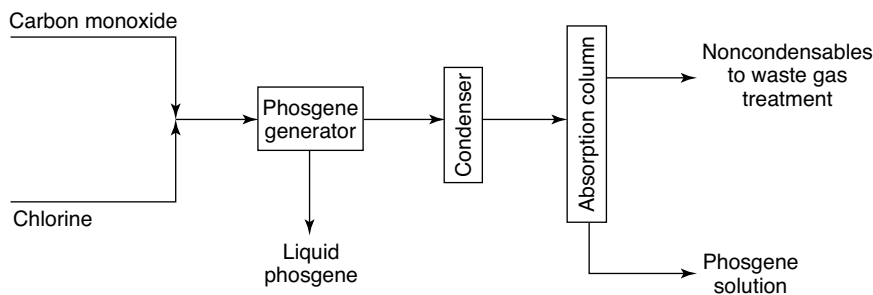


**Fig. 1.** Manufacture of phosgene from carbon monoxide and chlorine.

process consists of preparing and purifying carbon monoxide, preparing and purifying chlorine, metering and mixing of the reactants, reacting the mixed gases over activated carbon, purifying and condensing the resulting phosgene, and recovering trace phosgene to assure worker and environmental safety.

Carbon monoxide may be manufactured according to standard processes from coke, ie, from coal, or by controlled oxidation of hydrocarbon fuels. A carbon monoxide process that yields a gas of the highest possible purity must be chosen. Noncondensable impurities are particularly objectionable since their presence makes the recovery of all the phosgene difficult. Water must be removed from the starting gas to preclude hydrochloric acid formation in the converter. The hydrocarbon and hydrogen content should be minimized because reaction of chlorine with methane or hydrogen could ignite a reaction between chlorine and steel, thereby destroying the equipment. Other impurities might poison the catalyst. Sulfides must be excluded since they produce sulfur chlorides which usually are very undesirable impurities. The chlorine must be as dry and pure as the carbon monoxide so as to avoid corrosion of the equipment and decomposition of phosgene by water and other impurities.

Activated carbon of high adsorptive capacity is suitable for use as a catalyst; it need not be treated with metallic salts or other substances. If starting materials of high purity are employed, excellent and economic catalyst efficiency is obtained. A special carbon catalyst has been shown to give lifetimes that are 5–10 times longer than that of conventional activated carbon and also significantly lower levels of the by-product, carbon tetrachloride (32).

The phosgene generators employed are relatively simple tubular heat exchangers that are filled with granulated activated carbon. Because the reaction is rapid and exothermic, efficient heat removal is important since decomposition of phosgene into its starting materials begins to take place at 200°C. The temperature of the carbon bed in the initial reaction zone of the tubes can reach 400°C, but it rapidly falls to product temperatures of 40–150°C. The reaction is normally run at normal pressure or at a slight excess pressure. A phosgene generation system which monitors the phosgene requirements of a plant and responds by producing only the needed amounts has been developed (33,34).

A flow diagram of the production of phosgene appears in Figure 1. Carbon monoxide and chlorine gas are mixed in equimolecular proportions. A small amount of excess carbon monoxide is used to ensure complete reaction of the

chlorine. The product gases can be condensed to liquid phosgene and uncondensed gases, which are then scrubbed for removal of remaining phosgene. Uncondensed gaseous phosgene can be employed for in-line operations. The solvent used for absorption is typically the solvent used in a later process step. The remaining nonabsorbable gas stream is fed to the waste gas treatment system to be freed from phosgene.

Several methods of decomposing phosgene in waste gas streams are used. These are as follows:

*Decomposition by caustic scrubbing.* The waste gas stream is led through packed towers where a sodium hydroxide solution is introduced at the top of the towers. Venturi scrubbers could also be used. Make-up sodium hydroxide is added under pH control. The efficiency of scrubbing concentrated phosgene gas with caustic decreases significantly at caustic concentration below 4 wt% NaOH (35).

*Decomposition with moist activated carbon.* The waste gas stream is passed through packed activated carbon towers where water is fed at the top of the towers. The water is normally recycled. If the hydrochloric acid concentration in the recycled water exceeds 10%, the decomposition efficiency is greatly reduced. Thus a sufficient supply of fresh water must be assured (36).

*Combustion.* The waste gas stream is burned to convert phosgene to carbon dioxide and hydrochloric acid. An advantage of this method is that all components of the waste gas, such as carbon monoxide and solvent, are burned (37).

The outlet gas from the phosgene decomposition equipment is continuously monitored for residual phosgene content to ensure complete decomposition.

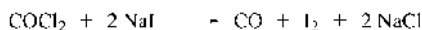
## Analytical and Test Methods

Phosgene in air and in mixture with other gases can be detected by a variety of methods (38). Trace quantities to a lower limit of 0.05  $\mu\text{g/L}$  air can be detected by uv spectroscopy (39). Both ir and gas chromatographies have been used extensively to measure phosgene in air at 1 ppb–1 ppm (7,40,41). Special and multiple-column gas-chromatographic methods have been used for more complex mixtures of gases containing phosgene (42–44). High performance liquid chromatography methods can also be used and offer detection limits of 5- to 10-ppb phosgene (45,46). Absolute determination of phosgene at levels below 100 ppb has been reported using pulsed flow coulometry (47). Laser photoacoustic spectroscopy has been used to detect phosgene at ppb levels (48).

Methods and instruments that are used to monitor phosgene content in air are well developed and have been reviewed (49–51). One detection instrument is a porous tape that measures the concentration of phosgene in air in quantities as small as 6 ppb (52). Fourier transform infrared spectrometry techniques have been used to permit line and area monitoring in the area around phosgene plants (53).

Phosgene dose-indicator badges for personnel exposure monitoring are commercially available and validated (54,55). This is a simple, visually readable, passive sampler based on phosgene indicator paper which is impregnated with a solution of 4-*p*-nitrobenzylpyridine and *N*-benzylaniline. These indicator badges are used at a number of plant sites using phosgene.

Liquid phosgene is assayed by an iodometric method which involves the following reaction (56):



The released iodine is titrated with sodium thiosulfate.

The following specifications and standards have been reported (6):

Assay	Percent
$\text{COCl}_2$ , min	99.0
$\text{Cl}_2$ (free), max	0.1
HCl, max	0.2

## Storage and Handling

All phosgene containers require a Class A, poison-gas label as well as a corrosive label. Phosgene is transported in steel cylinders which conform to rigid safety-design specifications. The cylinders undergo special hydrostatic testing at 5.5 MPa (800 psi), and extension rings are incorporated in the cylinders to protect the valves. Phosgene is shipped in cylinders ranging in size from 43 to 909 kg. Careful testing for leaks is required after filling, and a vapor space must be accommodated in the storage vessel; excessive filling with liquid phosgene must be avoided.

Transportation requirements and classifications for phosgene are as follows:

DOT shipping name	Phosgene
DOT hazard class	2.3
RQ	Yes – 10 pounds
DOT labels	Poison, Corrosive
DOT placards	Poison
Bill of lading description	Phosgene, 2.3, UN1076, RQ (phosgene), inhalation hazard, poison gas and corrosive labels affixed
UN/NA number	UN1076
Additional DOT requirements	Return of empty containers: residue last contained: phosgene, 2.3, UN1076, RQ (phosgene), inhalation hazard, poison gas and corrosive labels affixed

Because phosgene reacts with water, great care must be taken to prevent contamination with traces of water since this could lead to a build up of pressure through the formation of hydrogen chloride and carbon dioxide. Wet phosgene is very corrosive; therefore, phosgene should never be stored with any quantity of water (4).

## Health and Safety Factors

The odor threshold for phosgene is ca 0.5–1 ppm, but varies with individuals. Olfactory fatigue occurs after prolonged exposure (57). Phosgene may irritate the eyes, nose, and throat. The permissible exposure TLV by volume in air is 0.1 ppm (58). The TLV refers to the average airborne concentration at which it is believed nearly all workers may be repeatedly exposed on a daily basis without adverse effect. It is a time-weighted average for an 8-h day or a 40-h week and should be used as a guide for control only. The NIOSH REL (ceiling value) is 0.2 ppm for a 15-min excursion (59). Long-term exposure to phosgene has been reviewed, and potential hazards may exist at <0.2 ppm (60). Medical problems associated with phosgene exposure have been reviewed (61–63), and therapy for phosgene poisoning has also been reviewed (64–67).

When phosgene is inhaled, it reacts very little with the aqueous film on the mucous membranes of the upper respiratory tract. Most of it reaches the pulmonary alveoli, where gas exchange occurs. Here phosgene reacts with  $\text{NH}_2$ ,  $\text{OH}$ , and  $\text{SH}$  groups of the blood–air barrier. This causes the blood–air barrier to lose its function as a membrane between the blood vessels and the pulmonary alveoli. As a result, blood plasma is able to pass from the blood vessels into the pulmonary alveoli, thereby increasingly disturbing the gas exchange.

Breathing phosgene causes pulmonary edema, which may be characterized by a delayed onset. The onset of pulmonary edema is a function of both concentration and length of exposure. Typically exposure above 50 ppm-minutes can lead to pulmonary edema (67). Exposed persons must be removed immediately from the contaminated area and decontaminated. Rescue workers should wear self-contained breathing apparatus. Injured persons should not be allowed any physical activity, and a physician should be consulted immediately. It is advisable to keep an exposed individual under the observation of a physician for 6–24 h, depending on the circumstances of exposure. In some instances this can be accomplished at the plant medical facility, or the exposed individual may require hospitalization.

In handling phosgene, extensive safety precautions and procedures are required to prevent exposure to phosgene. The first point is to design the phosgene system to prevent phosgene emissions from the closed equipment. Chemically resistant, high quality materials are used for plant equipment and lines which are inspected regularly. Pumps that are hermetically sealed to the outside or utilize multiple mechanical seals with buffer fluids are used for phosgene-containing streams. Stringent requirements are set for the quality and design of phosgene process control equipment, and critical areas have redundant control systems. The second point is to quickly detect leaks and contain or decompose escaped phosgene. This includes such measures as continuous alarm systems to monitor the working atmosphere, systems for decomposing escaped phosgene (eg steam-ammonia curtains for gaseous emissions), jacketed pipes, and complete containments for phosgene plants (68,69). Vacuum systems are also used to mitigate phosgene releases. These systems consist of a series of vacuum hoses that can be put near a small leak to draw in escaping phosgene, which is then sent to a decomposition unit. More detailed information on current industrial practices for

safely manufacturing or handling phosgene are available through the Chemical Manufacturers Association Phosgene Panel, Washington, D.C.

In case of extensive leaks or spills, immediate evacuation upwind of the phosgene source is necessary. Phosgene is 3.4 times as heavy as air and may collect in low-lying areas (6). Water should not be used on the source of a phosgene leak as the resulting corrosion enlarges the leak. Suitable personal protective equipment includes eye protection and respiratory equipment. In case of fire, it is essential to cool all phosgene-containing vessels. Leaks of liquid phosgene or phosgene solutions can be effectively combated by covering the phosgene-containing liquid with an absorbent and decomposition agents.

**Waste Disposal.** Because of its low boiling point and high toxicity, measures must be taken to prevent the entrance of phosgene into drains or sewers. If recycle of phosgene is not feasible, phosgene waste can be handled by one of the decomposition methods mentioned in the Manufacture section, ie, caustic scrubbing, moist activated carbon towers, or combustion.

## Uses

Phosgene is an important and widely used intermediate. Practically all phosgene manufacture is captive, ie, it is used in the manufacture of other chemicals within the plant boundary. Only VandeMark (owned by Groupe SNPE) sells phosgene on the merchant market. Phosgene manufacturers with captive consumption in the United States are Aventis, BASF, Bayer, Dow, DuPont, GE Plastics, Huntsman/ICI, Lyondell, PPG, Twin Lake Chemicals, VandeMark, and Zeneca. The U.S. production of phosgene for 1999 was  $1.55 \times 10^6$  t, and for 2000, it was approximately  $1.61 \times 10^6$  t (70). The primary use of phosgene is the manufacture of isocyanates for the polyurethane industry, in which ca 80% of the phosgene output in the United States is consumed. The manufacture of toluene diisocyanate [1321-38-6] accounts for ca 40% of the phosgene consumption, while methylene diphenyl diisocyanate (MDI) [101-68-8] and polymeric MDI [9016-87-9] account for ca 40%. The polycarbonate industry accounts for ca 13% of the phosgene consumption, and the remaining 7% is used to produce aliphatic diisocyanates, monoisocyanates, chloroformates, agrochemicals, and intermediates for pharmaceuticals and dyestuffs. Although several commercial phosgene-free processes for producing polyisocyanates and polycarbonates have been announced, they are not expected to make large inroads into phosgene demand in the near future (71–75).

Phosgene can be employed in a variety of metal-recovery operations, eg, in the recovery of platinum, uranium, plutonium, and niobium (76–80). Phosgene has been proposed for the manufacture of aluminum chloride, beryllium chloride, and boron trichloride (81–83). Phosgene has been patented as a stabilizer, either by itself or in combination with thionyl chloride, for liquid SO<sub>2</sub> (84).

Phosgene is also used in the production of chloroformates, ie, chlorocarbonates, which are intermediates in the production of ore-flotation agents, perfumes, herbicides, and insecticides, and especially in the preparation of pharmaceuticals (85). Chloroalkyl chlorocarbonates have been manufactured as intermediates for

pharmaceuticals and pesticides (86,87). Phosgene is also employed in the manufacture of carbonic esters. Phosgene has been suggested as a starting material for the manufacture of carbon tetrachloride and other chlorinated hydrocarbons (88–92). A number of pesticides have been patented based on the reaction of a thiol or dithiol with phosgene to form thiol chloroformates (93,94). The preparation of aromatic acids using phosgene and detailed process for the manufacture of terephthalic acid from toluene and phosgene have been described (95,96).

An important direct use of phosgene is in the preparation of polymers. Polycarbonates are the most significant and commercially valuable group. However, the use of phosgene has been described for other polymer systems, eg, fiber-forming polymeric polyketones and polyureas (97,98).

## BIBLIOGRAPHY

“Phosgene” in *EPST* 3rd ed., Vol. 3, pp. 435–447, by K. L. Dunlap, Bayer Corporation.

## CITED REFERENCES

1. L. C. Riusema and L. G. Silverstein, *Am. Ind. Hyg. Assoc. J.* **33**(1), 35 (1972).
2. M. H. Noweir, E. A. Pfitzer, and T. F. Hatch, *Am Ind. Hyg. Assoc. J.* **34**(1), 25 (1973).
3. H. F. Anderson, J. A. Dahlberg, and R. Wettstrom, *Ann. Occup. Hyg.* **18**, 129 (1975).
4. H. B. Singh, *Nature* **264**, 428 (1976).
5. M. J. Thomson and co-workers, *Combust. Flame* **98**, 350 (1994).
6. *Chemical Safety, Data Sheet SD-95*, Manufacturing Chemists Association, Washington, D.C., Revised (1978).
7. G. G. Esposito, *Anal. Chem.* **49**, 1774 (Oct. 1977).
8. V. Henri and O. R. Howell, *Proc. R. Soc. London, Ser. A* **128**, 190 (1930).
9. R. Anathakrishnan, *Proc. Indian Acad. Sci. Sect. A* **5**, 285 (1937).
10. H. Babad and A. G. Zieler, *Chem. Rev.* **73**(1), 75 (1973).
11. J.-P. Senet, *The Recent Advance in Phosgene Chemistry*, Group SNPE, Paris, Vol. **1**, 1997; Vol. **2**, 1999.
12. T. A. Ryan, C. Ryan, E. A. Seddon, and K. R. Seddon, *Phosgene and Related Carbonyl Halides*, Elsevier Science B.V., Amsterdam, 1996.
13. A. N. Ketov, V. V. Pechkovskii, and L. P. Kostin, *Issled. Obl. Khim. Tekhnol. Mineral's Solei Okislov, Akad. Nauk SSR Sb. Statei* **202** (1965); *Chem. Abstr.* **65**, 1753a (1966).
14. A. N. Ketov, V. V. Pechkovskii, and L. P. Kostin, *Izv. Vyssh. Uchebn. Zaved., Tsvetn. Met.* **7**(2), 94 (1964); *Chem. Abstr.* **61**, 3894h (1964).
15. A. N. Ketov, V. V. Pechkovskii, and L. P. Kostin, *Zh. Neorg. Khim.* **9**, 467 (1964).
16. Yu. P. Kuznetsov, E. S. Petrov, and A. I. Vakhrusheva, *Izv. Sib. Otd. Akad. Nauk SSSR, Ser. Khim. Nauk* **1**(2), 63 (1969); *Chem. Abstr.* **71**, 1841p (1969).
17. Yu. P. Kuznetsov, E. S. Petrov, and A. I. Vakhrusheva, *Izv. Sib. Otd. Akad. Nauk SSSR, Ser. Khim. Nauk* **1**(3), 60 (1969); *Chem. Abstr.* **71** 116862c (1969).
18. A. N. Ketov, V. V. Pechkovskii, and L. P. Kostin, *Sb. Nauchn. Tr. Permsk. Politekh. Inst.* **14**, 3 (1963); *Chem. Abstr.* **62**, 3642e (1965).
19. A. N. Ketov, V. V. Pechkovskii, and I. M. Kolesov, *Izv. Vyssh. Uchebn. Zaved., Khim. Khim. Tekhnol.* **9**, 570 (1967); *Chem. Abstr.* **66**, 592761k (1967).
20. A. N. Ketov and I. M. Kolesov, *Sb. Nauchn. Tr. Permsk. Politekh. Inst.* **18**, 42 (1965); *Chem. Abstr.* **66**, 7991 (1967).
21. D. Naumann, *Kernenegie* **5**(2), 188 (1962).



22. R. J. Sorenson, U.S. Atomic Energy Commission, HW-79141, 1963, p. 22.
23. D. T. Peterson and D. J. Sundquist, *U.S. Atomic Energy Commission* (IS-917), p. 30 (1964).
24. I. S. Pap and co-workers, *J. Therm. Anal.* **36**, 1765 (1990).
25. R. Hazeldine and H. Iserson, *J. Am. Chem. Soc.* **79**, 5801 (1957).
26. C. W. Tullock and D. D. Coffman, *J. Org. Chem.* **25**, 2016 (1960).
27. R. Mertens and co-workers, *Angew. Chem.* **106**, 1320 (1994).
28. Ger. Pat. 4,028,774 (Dec. 3, 1992), P. Ksoll and co-workers (to BASF A.G.).
29. G. Martin and M. Martin, *Bull. Soc. Chim. Fr.* (8), 637 (1963).
30. H. H. Bosshard and H. Zollinger, *Helv. Chim. Acta* **42**, 1659 (1959).
31. *Chemistry & Industry* 682 (Sept. 21, 1992).
32. L. Abrams, W. V. Cicha, L. E. Manzer, and S. Subramoney, *Studies in Surface Science and Catalysis*, Elsevier Science B.V., Amsterdam, 2000, p. **130**.
33. U. Osterwalder, *Ber. Int. Kolloq. Verhuetung Arbeitsunfaellen Berufskrankh. Chem. Ind.* **10**, 785; *Chem. Abstr.* **104**, 111756 (1985).
34. *Chem. Eng.* 27 (Nov. 10, 1986).
35. *Unpublished papers on the Caustic Scrubbing of Phosgene, Department of Army, Office of the Program for Chemical Demilitarization*, 1975–1978.
36. Ger. Pat. 961681 (1953), H. Wollthan, and W. Groves (to Bayer A.G.).
37. K. Hess and R. Kotkamp, *Chem. Ing. Tech.* **45**, 873 (1973).
38. P. C. Nigam and S. Prasad, *Indian J. Environ. Health* **28**, 218 (1986); *Chem. Abstr.* **105**, 196347 (1986).
39. W. B. Crummett and J. D. Melean, *Anal. Chem.* **37**, 424 (1965).
40. B. B. Baker, *Am. Ind. Hyg. Assoc. J.* **35**, 735 (1974).
41. D. Reichert, U. Splengler, and D. J. Henschler, *Chromatograph* **179**(1), 181 (1979).
42. R. J. Graham and F. D. Stevenson, *J. Chromatogr.* **47**, 555 (1970).
43. P. K. Basu, C. J. King, and S. Lynn, *J. Chromatogr. Sci.* **10**, 419 (1972).
44. H. Geisser and W. Richarz, *J. Chromatogr.* **147**, 453 (1978).
45. W. S. Wu and S. Virindar, *Analyst* **118**, 1285 (1993).
46. R. J. Rando, H. G. Poovey, and S. N. Chang, *J. Liq. Chromatogr.* **16**, 3291 (1993).
47. H. B. Singh, D. Lillian, and A. Appleby, *Anal. Chem.* **47**, 860 (1975).
48. X. Luo, F. Y. Shi, and J. X. Lin, *Int. J. Infrared Millimeter Waves* **12**(2), 141 (1991); *Chem. Abstr.* **115**, 34533 (1991).
49. M. H. Noweir and E. A. Pfitzer, *Am. Ind. Hyg. Assoc. J.* **32**(3), 163 (1971).
50. B. W. Thomas, *Oil Gas J.* **63**(24), 119, 121 (1965).
51. R. M. Tuggle and co-workers, *Ind. Hyg. Assoc. J.* **40**, 387 (1979).
52. N. Nakano, A. Yamamoto, and Y. Kobayashi, *Talanta* **42**, 641 (1995).
53. R. H. Hunt, in *Optical Remote Sensing and Applications to Environmental and Industrial Safety Problems*, Apr. 6–8, 1992, Air and Waste Management Association, Pittsburgh, Pa., 1992, p. 446.
54. *K&M Environmental Safe Air System Validation Report for Phosgene, Virginia Beach, Va.*
55. *Bacharach Inc. Environmental Testing of Colorimetric Phosgene Dosimeter Badges, Pittsburgh, Pa.*
56. C. A. Rush and C. E. Danner, *Anal. Chem.* **20**, 644 (1948).
57. G. Leonardos, D. Kendall, and N. Barnard, *J. Air Pollut. Control Assoc.* **19**, 91 (1969).
58. *Threshold Limit Values for Chemical Substances and Physical Agents*, American Conference of Governmental Industrial Hygienists, Washington, D.C., 1994.
59. *Phosgene Criteria Document*, NIOSH 76-137, Washington, D.C.

60. S. A. Cucinell, *Arch. Environ. Health* **28**, 272 (May 1974).
61. W. F. Diller, *J. Occup. Health* **20**, 189 (Mar. 1978).
62. W. F. Diller, *Toxicol. Ind. Health* **1**(2), 7 (1985).
63. Y. L. Yue and co-workers, *J. Appl. Physiol.* **69**, 1615 (1990).
64. W. F. Diller and R. Zante, *Toxicol. Ind. Health* **1**(2), 117 (1985).
65. *Critical Review of the Medical Management of Acute Phosgene Poisoning*, International Isocyanate Institute; Ref. 11358.
66. *Options for Medical Management of Phosgene Poisoning*, International Isocyanate Institute; Ref. 11359.
67. *Phosgene Pulmonary Exposure Information*, 2nd ed., Chemical Manufacturers Association Phosgene Panel, Sept. 1996
68. *Chem. Week* 34 (May 28, 1986).
69. *Chem. Eng.* **99**(5), 5 (May 1992).
70. *Chemical Economics Handbook Data Summary – Phosgene*, 687.1000E, SRI International, July 2000.
71. S. Fukuoka, M. Chono, and M. Kohno, *J. Org. Chem.* **49**, 1458 (1984).
72. U.S. Pat. 4,146,727 (1979), E. T. Shaw and J. G. Zajane (to Arco).
73. K. A. Henderson Jr. and V. A. Alexanian, *Org. Prep. Proced. Int.* **18**, 149 (1986).
74. U.S. Pat. 5,189,205 (Feb. 23, 1993), W. D. McGhee and T. E. Waldman (to Monsanto Co.).
75. W. McGhee and co-workers, *J. Org. Chem.* **60**, 2820 (1995).
76. Ger. Pat. 1,077,642 (Mar. 17, 1960), G. R. Bond Jr. (to Houdry Process Corp.).
77. U.S. Pat. 2,890,099 (June 6, 1959), H. B. Rhodes, W. F. Pesold, and J. M. Hirshon (to U.S. Atomic Energy Commission).
78. Fr. Pat. 1,472,438 (Mar. 18, 1965) (to Atomic Energy Research Institute).
79. H. L. Brandt, AEC Accession No. 42455, Rept. No. HW-83235, CFSTI, 20, Washington, D.C., 1964.
80. U.S. Pat. 3,212,847 (Oct. 19, 1965), B. J. Lerner (to Dominion Gulf Co.).
81. J. Hille and W. Dürrwächter, *Angew. Chem.* **72**, 850 (1960).
82. U.S. Pat. 3,146,065 (Aug. 25, 1964), R. O. Bach (to Beryllium Metals and Chemical Corp.).
83. R. K. Pearson and co-workers, U.S. Atomic Energy Commission, CCC-1024-TR-234, 1957.
84. U.S. Pat. 3,042,490 (July 3, 1960), T. W. Saults and J. J. Wimberly (to Tennessee Corp.); Brit. Pat. 975,318 (Nov. 18, 1964), R. V. Riley, T. F. Eden, and W. D. Hopkinson (to Stavely Iron & Chemicals Co., Ltd.).
85. U.S. Pat. 3,152,167 (Oct. 6, 1964), M. Sletzinger (to Merck & Co., Inc.).
86. J. V. Swintosky and co-workers, *J. Pharm. Sci.* **55**, 992 (1966).
87. Ger. Pat. 1,179,922 (Oct. 22, 1964), H. Grassner and F. Stolp (to Badische Anilin & Soda Fabrik A.G.).
88. R. N. Haszeldine and H. Iserson, *J. Am. Chem. Soc.* **79**, 5801 (1957).
89. O. Glemser and co-workers, *Angew. Chem.* **75**, 823 (1963).
90. Ger. Pat. 1,188,570 (Mar. 11, 1965), W. Ziegenbein and K. H. Hornung (to Chemische Werke Huels A.G.).
91. U.S. Pat. 3,406,212 (Oct. 15, 1968), K. O. Christie and A. E. Pavlath (to Stauffer Chemical Co.).
92. Ger. Pat. 1,133,716 (July 26, 1962), D. Ludsteck and co-workers (to Badische Anilin & Soda Fabrik A.G.).
93. U.S. Pat. 3,277,143 (Oct. 4, 1966), H. Tilles (to Stauffer Chemical Co.).
94. U.S. Pat. 3,093,537 (June 11, 1963), H. Tilles.
95. U.S. Pat. 2,552,591 (May 15, 1951), W. H. C. Rueggeberg, R. K. Frantz, and A. Ginsburg (to United States Army).

96. F. Runge, H. Reinhard, and G. Kühnhanss, *Chem. Tech. Berlin* **8**, 644 (1956).
97. Ger. Pat. 1,148,073 (May 2, 1963), R. Moroni and E. Dumont (to Collo-Rheincollodium Koeln G.M.b.H.).
98. U.S. Pat. 3,412,072 (Nov. 19, 1968), C. J. Bouboulis and I. Kirschenbaum (to Esso Research & Engineering Co.).

KENNETH L. DUNLAP  
Bayer Corporation

## PHOSPHOLIPID POLYMERS

### Introduction

A cell membrane is mainly composed of phospholipids, membrane proteins, and polysaccharides bound to lipids and proteins. The well-known "fluid-mosaic model," first proposed by Singer and Nicolson (Fig. 1), has been used to explain the structure of the cell membrane (1). According to this model, amphiphilic phospholipid molecules are arranged in a bilayer structure and the membrane proteins are positioned in or upon it. There is always a dynamical flow of phospholipid molecules through the cell membrane, but the membrane maintains its strength through the supporting proteins. The distribution of phospholipid molecules is asymmetric in the bilayered structure of the cell membrane. The neutral, zwitterionic phosphorylcholine (PC) group bearing phospholipids such as phosphatidylcholines are located in the outer layer of the cell membrane, whereas negatively charged phospholipid molecules such as phosphatidylserines are predominantly found on the inner, cytoplasmic side of the membrane (2,3). The PC groups immobilized surface provides an inert surface for biological components including proteins, glycoproteins, and cells (4–6). This fact provides particularly significant information for the development of polymer biomaterials. Thus, the phospholipid polymers bearing the PC group provide a significant interest in polymer science, biomaterials science, and biomedical engineering.

### Cell Membrane Structure

The cell membrane is the medium through which all cells interact with their environment. The behavior of it is modulated by the chemical composition and the physical properties of cell membrane phospholipids. This is due to variations in the hydrophobic (alkyl chain) and hydrophilic (polar head group) portions of these amphiphilic structures of the phospholipids as shown in Figure 2. The alkyl chains of phospholipids provide the hydrophobic environment that is necessary for the function of intrinsic membrane proteins (4). Also, both the balance of the alkyl groups and polar groups in the molecule characterize the physical properties of the phospholipids. For example, a phase transition temperature of alkyl

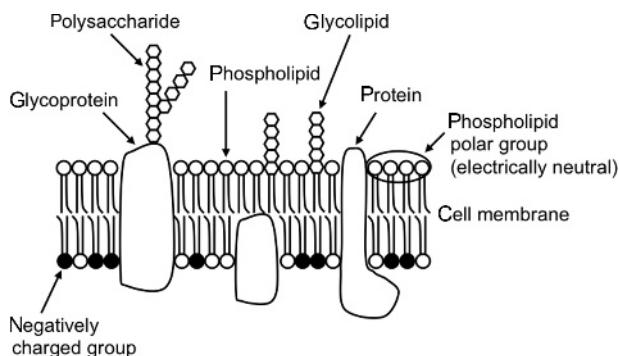


**Fig. 1.** Structure of cell membrane based on the fluid-mosaic model.

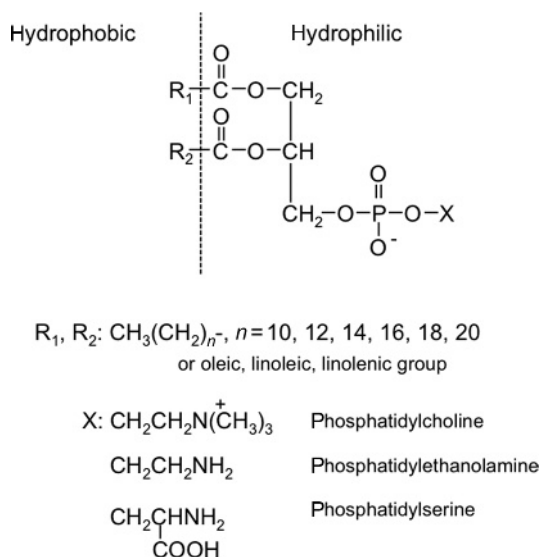


**Fig. 2.** Chemical structure of representative phospholipids.

chains, when it is higher than the normal biological condition, the alkyl chains are in a quasi-crystalline array; on the other hand, it is a phase transition temperature of them is lower than biological temperature; the chains are in a more fluid-like state (7). The polar head groups are in contact with water and therefore contribute largely to the interfacial properties of cell surfaces. From a viewpoint of cellular responses, although the erythrocytes and platelets exhibit high pro-coagulant activities when assayed *in vitro*, their outer surfaces are inactive in coagulation tests. Similarly, no significant prothrombin converting activity can be detected with intact endothelial cells or leucocytes, but such an activity is observed in cell homogenates and phospholipid extracts (4,5).

A new approach to make bioinert and biocompatible surfaces is raised on the basis of the imitation of the natural surfaces of these cells. The simplest common reactive cellular is the high content of the electrically neutral phospholipids,

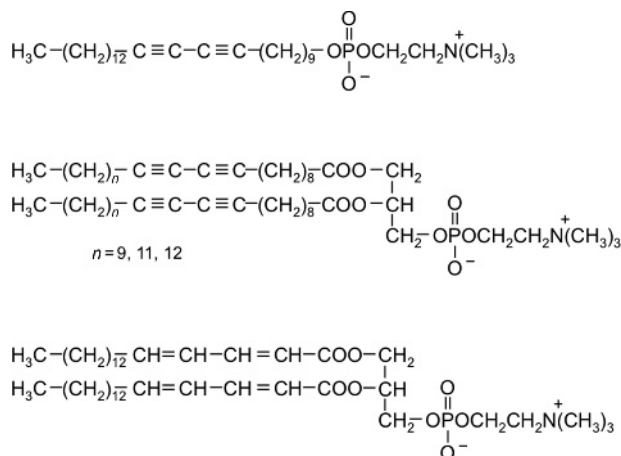


**Fig. 3.** Chemical structure of natural-based polymerizable phospholipids.

which contain the PC group. It has been reported that polymeric materials bearing PC groups as the polar head group form the interface, which mimics the interfacial characteristics of natural cell membrane surfaces.

## Introduction of PC Groups in the Polymer

**Natural-Based Polymerizable Phospholipids.** Some examples of phospholipid molecules with polymerizable groups are examined from the viewpoint of biological science. (8–16). For example, natural phospholipid molecules, which contain diacetylenic groups in their alkyl chains, can form polymers upon irradiation with ultraviolet (UV) light. The UV irradiation results in the two conjugated polymerizable bonds of the monomer that are to be replaced in the polymer by an alternating conjugated double-bonded and triple-bonded structure. The PC molecules were prepared, which contained diacetylenic groups in one (mixed-chains) or both (identical-chain) alkyl chains. The polymerization ability of mixed-chain phosphatidylcholines is greater than that of identical-chain phosphatidylcholines. This difference may be accounted for by the formation of intramolecular linkages in identical-chain lipids (Fig. 3).

It is well known that the natural phospholipid molecules have two solid states that depend on the temperature (7,16). The polymerization of diacetylene groups requires the structural order that is obtained by a solid state. The reactivity of the process, therefore, is dependent upon the preservation of the structural order displayed by the monomeric lattice. That is to say, polymerization proceeds most rapidly when the crystalline phase of the polymer most closely resembles that of the monomer. The polymerization may be induced when the phospholipids are in the solid state, dispersed in aqueous solutions to form vesicles, arranged as a monolayer at an air–water interface, deposited as multilayers on a suitable support, or following the biosynthetic incorporation of phospholipids with a diacetylene group into the membranes of living cells.

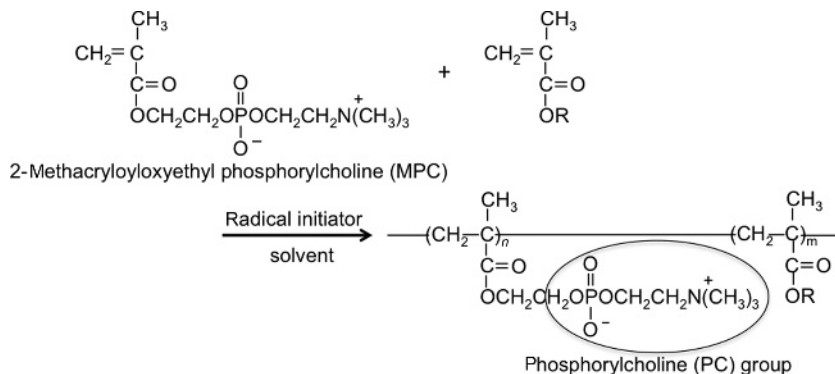


**Fig. 4.** Chemical structure of MPC and its copolymer.

The dynamic properties of the monomeric, phospholipids with the diacetylene group were found to resemble the properties of naturally occurring lipids. These similarities permitted the incorporation of phospholipids with the diacetylene group into the cell membrane and glycolipids of the bacterium *Acholeplasma laidlawii*. When the cells are grown in the presence of phospholipids with the diacetylene group, up to 90% of the diacetylene groups are derived from the cell culture medium. When irradiated at 0°C, up to 97% of the diacetylene groups in the phospholipids can be polymerized, even when those in the living cell membrane. The phospholipids with the diacetylene group pose two significant advantages. The polymerization inhibits the rearrangement and decay evident with multilayers of nonpolymerizable phospholipids. The ability to coat an artificial surface with a stable polymeric phospholipid layer should render the surface a better biomimic, particularly when the polymer is engineered to mimic the surface of host cells. Very recently, some reports have been published for understanding polymerization and the polymerized state of the phospholipids with the diacetylene groups (15,16).

#### Monomers Bearing the PC Group.

**2-Methacryloyloxyethyl Phosphorylcholine.** Much research has been carried out on the synthesis of vinyl monomers bearing phospholipid polar groups. Among these, synthesized monomers-bearing PC groups have strong potential for biomedical applications. The most successful example for this purpose is 2-methacryloyloxyethyl phosphorylcholine (MPC) (Fig. 4) (17). This methacrylate-bearing PC group provides various kinds of polymers to the biomedical fields. The first reported synthesis of MPC was made by Nakabayashi et al. in 1978 (18). They polymerized MPC with methyl methacrylate (MMA) to control the solubility in water and the film formation. They also evaluated the hemolysis of red blood cells. However, owing to the low yield and purity of the obtained MPC, they were unable to characterize the essential properties of poly(MPC) and poly(MPC-co-MMA) from this evaluation, that is, they observed that the poly(MPC) and the copolymer induced hemolysis strongly. In the present time, the poly(MPC) and water-soluble poly(MPC-co-*n*-butyl methacrylate (BMA)) do not induce hemolysis of red blood cells (19,20). Since this first report, several researchers have studied the synthesis of MPC and its polymers (21–23). At that time, the synthesis of

the MPC was very difficult because it indicates the hygroscopic character under atmosphere. Related to this, too low melting point of the MPC, incomprehensible viscosity of aqueous solution of poly(MPC), and unfavorable cell adhesion on the MPC polymer surface were reported. Thus, these early reports failed to illustrate the good performance of MPC polymers.

In 1987, Ishihara and co-workers determined an excellent synthetic route and the purification method for MPC and reported it in 1990 (18,24). By this procedure, a sufficient amount of MPC can be obtained as a white powder. Purification was carried out by recrystallization from absolute acetonitrile. The procedure has been improved much more and transferred to the Japanese chemical company, NOF Co. Ltd., and the MPC has been synthesized on an industrial scale since 1999. Reagent companies throughout the world are now selling the MPC.

Polymerization of and copolymerization with other vinyl compounds are examined, such as those achieved by conventional radical polymerization with a radical initiator, for example, 2,2'-azobisisobutyronitrile (AIBN) or benzoyl peroxide (25–30). Typically, when the MPC is copolymerized in the solution with various alkyl methacrylates, such as *n*-BMA, *n*-hexyl methacrylate (HMA), *n*-dodecyl methacrylate (DMA), or *n*-stearyl methacrylate polymerization progresses very well and a statistically random sequence is obtained. The solubility of the MPC polymers is dependent upon the composition of the MPC, the hydrophobicity of the alkyl methacrylate, and on the molecular weight. As the same procedure, many polymers composed of the MPC units have been synthesized for evaluating their properties as biomaterials. Since MPC is extremely hydrophilic, the swelling of MPC polymer in water increases with an increase in the MPC unit composition, where the polymers with more than 40 unit mol% of MPC unit are soluble in water.

**Polymerization Ability of MPC.** The kinetics of the polymerization of MPC in ethanol is examined by Sato et al. using dimethyl 2, 2'-azobisisobutyrate (MAIB) as the initiator (31). They have shown that the overall activation energy of the homogeneous polymerization is calculated to be 71 kJ/mol. The initial polymerization rate ( $R_p$ ) is expressed by  $R_p = k[\text{MAIB}]^{0.54}[\text{MPC}]^{1.8}$ . The higher dependence of  $R_p$  on the monomer concentration results from the increased propagation due to monomer aggregation by the amphiphilic nature of MPC and also from retardation of the termination due to the viscosity effect of the MPC. Rate constants of propagation ( $k_p$ ) and termination ( $k_t$ ) of MPC are estimated at 60°C using electron spin resonance to be  $k_p = 180 \text{ L}/(\text{mol s})$  and  $k_t = 2.8 \times 10^4 \text{ L}/(\text{mol s})$ , respectively. Because of the much slower termination,  $R_p$  of MPC in ethanol is found to be eight times greater than that of MMA in benzene. The low  $k_t$  value results in the much higher homopolymerization ability of MPC over MMA. Polymerization of MPC with MAIB in ethanol is accelerated by the presence of water and retarded by the presence of benzene or acetonitrile. The radical copolymerization of MPC (M1) and styrene (St) (M2) in ethanol resulted in the following copolymerization parameters, which are similar to those for the copolymerization of typical methacrylate, MMA, and St, that is,  $r_1 = 0.39$ ,  $r_2 = 0.46$ ,  $Q_1 = 0.76$ , and  $e_1 = +0.51$ . These polymerization characteristics are very important for obtaining an MPC polymer suitable for use as biomaterials.

Sato et al. also investigated the kinetics of the homogeneous polymerization of MPC in water with potassium peroxydisulfate (KPS) (32). The overall

activation energy of this polymerization is estimated to be 12.8 kcal/mol. The initial polymerization rate ( $R_p$ ) at 40°C is given by  $R_p = k[\text{KPS}]^{0.98}[\text{MPC}]^{1.9}$ . The presence of alkaline metal halides accelerates the polymerization. The larger the radius of metal cation or halide ion, the larger the accelerating effect observed. The accelerating effect was explained on the basis of interactions of salt ions with ionic moieties of the propagating polymer radical and/or the MPC. A kinetic study is also performed on the polymerization of MPC with KPS in water in the presence of 2.5 mol/L of NaCl, in which  $R_p$  at 40°C is expressed by  $R_p = k[\text{KPS}]^{0.6}[\text{MPC}]^{1.6}$ . A very low value of 4.7 kcal/mol is obtained for the overall activation energy of the polymerization.

**MPC Derivatives.** This successful molecular design of the phospholipid polymer described above encouraged the further development of monomers bearing the PC group. These can be considered as being derivatives of MPC, such as containing different polymerization groups, a variety of spacer units between polymerization groups, and a PC group. Chemical structures of such species are summarized in Figure 5.

Sugiyama et al. reported the synthesis of an acrylate derivative of MPC, 2-acryloyloxyethyl phosphorylcholine (APC) (33). They prepared a series of copolymer microspheres of APC through emulsifier-free emulsion copolymerization with hydrophobic methacrylates such as MMA, ethyl methacrylate, BMA, HMA, and St. The polymerization progresses as well as that found for MPC by radicals. From the kinetics of the copolymerization, it was found that the initial rate of polymerization of St increases in the presence of small amounts of APC. The hydrophilic PC groups are concentrated on the surface of the particles, which was confirmed by X-ray photoelectron spectroscopy (XPS). Ruiz et al. observed the similar tendency of surface enrichment of the PC group (34). They prepared a terpolymer composed of APC, methyl acrylate (MA), and MMA. By blending this polymer to a poly(MA-co-MMA) matrix, the PC groups position themselves at the surface due to their amphiphilic nature. The dynamic surface behavior of the terpolymer also follows the same trend as the organization of its structure in solution. Indeed, as has been shown with XPS and time-of-flight secondary ion mass spectrometry, in an apolar high-vacuum environment, the polar groups are not directly located at the uppermost surface but are rather covered by more hydrophobic polymer chains, thus minimizing the terpolymer surface energy. Thus, in the polar environment, the terpolymer surface rearranges to present the PC groups at the top surface, resulting in a new minimum interfacial energy state. Recently, APC is used to react with generation 5 of poly(amido amine) (PAMAM) dendrimers via the Michael addition reaction between primary amino group of PAMAM dendrimers and an acrylic functional group of APC (35). In this case, APC is used as a reactive compound to introduce PC groups.

Oishi et al. synthesized fumaramate derivatives of MPC, namely isopropyl-2-[2'-(trimethylammonium)ethyl phosphoryl]ethyl fumaramate (IPTPFA) and methyl-2-[2'-(trimethylammonium)ethyl phosphoryl]ethyl fumaramate (MTPFA). The IPTPFA and MTPFA were polymerized and copolymerized with MMA in the presence of radical initiators (36,37). In the case of the homopolymerization, the molecular weight of the polymers was low. The polymerization reactivity of these fumaramate derivatives may be very low because the 1,2-disubstituted ethylene-type motif is sterically hindered by the bulky PC group.



Chemical Structure	Abbreviation	Note and References
$  \begin{array}{c}  \text{CH}_3 \\    \\  \text{CH}_2=\text{C} \\    \\  \text{C}=\text{O} \\    \\  \text{OCH}_2\text{CH}_2\text{O}-\text{P}(=\text{O})(\text{O}^-)-\text{OCH}_2\text{CH}_2\text{N}^+(\text{CH}_3)_3  \end{array}  $	MPC	Ref. 17
$  \begin{array}{c}  \text{CH}_2=\text{CH} \\    \\  \text{C}=\text{O} \\    \\  \text{OCH}_2\text{CH}_2\text{O}-\text{P}(=\text{O})(\text{O}^-)-\text{OCH}_2\text{CH}_2\text{N}^+(\text{CH}_3)_3  \end{array}  $	APC	Refs. 33-35
$  \begin{array}{c}  \text{O} \\     \\  \text{RO}-\text{C}-\text{CH}=\text{CH} \\    \\  \text{C}=\text{O} \\    \\  \text{NH}-\text{CH}_2\text{CH}_2\text{O}-\text{P}(=\text{O})(\text{O}^-)-\text{OCH}_2\text{CH}_2\text{N}^+(\text{CH}_3)_3  \end{array}  $	R:CH(CH <sub>3</sub> ) <sub>2</sub> IPTPFA CH <sub>3</sub> MTPFA	Refs. 36, 37
$  \begin{array}{c}  \text{CH}_2=\text{CH} \\    \\  \text{C}_6\text{H}_4 \\    \\  \text{CH}_2\text{O}(\text{CH}_2)_4\text{O}-\text{P}(=\text{O})(\text{O}^-)-\text{OCH}_2\text{CH}_2\text{N}^+(\text{CH}_3)_3  \end{array}  $	VBOPC	Ref. 38
$  \begin{array}{c}  \text{CH}_3 \\    \\  \text{CH}_2=\text{C} \\    \\  \text{C}=\text{O} \\    \\  \text{O}-(\text{CH}_2)_n\text{O}-\text{P}(=\text{O})(\text{O}^-)-\text{OCH}_2\text{CH}_2\text{N}^+(\text{CH}_3)_3  \end{array}  $	MAPC n=4 MBPC 6 MHPC 10 MDPC	Refs. 39, 40
$  \begin{array}{c}  \text{CH}_3 \\    \\  \text{CH}_2=\text{C} \\    \\  \text{C}=\text{O} \\    \\  \text{O}-(\text{CH}_2\text{CHO})_n\text{O}-\text{P}(=\text{O})(\text{O}^-)-\text{OCH}_2\text{CH}_2\text{N}^+(\text{CH}_3)_3  \end{array}  $	MEO <sub>n</sub> PC n=2 MEO2PC 3 MEO3PC 9 MEO9PC	Refs. 41-45
$  \begin{array}{c}  \text{CH}_3 \\    \\  \text{CH}_2=\text{C} \\    \\  \text{C}=\text{O} \\    \\  \text{OCH}_2\text{CH}_2\text{O}-\text{P}(=\text{O})(\text{O}^-)-\text{OCH}_2\text{CH}_2\text{CH}_2\text{N}^+(\text{CH}_3)_3  \end{array}  $	TPM	Ref. 46
$  \begin{array}{c}  \text{CH}_3 \\    \\  \text{CH}_2=\text{C} \\    \\  \text{C}=\text{O} \\    \\  \text{OCH}_2\text{CH}_2\text{O}-\text{P}(=\text{O})(\text{O}^-)-\text{OCH}(\text{CH}_3)-\text{CH}_2\text{N}^+(\text{CH}_3)_3  \end{array}  $	TMPM	Ref. 47

**Fig. 5.** Chemical structure of MPC derivatives (continued).

Through comparison to the reactivity of alkyl-substituted fumaramate, Oishi et al. concluded that the polymerization reactivity was more heavily influenced by the bulky PC group than by the branched alkyl group. They also prepared, via emulsifier-free emulsion polymerization, microspheres of poly(MMA) containing 1 unit mol% of the IPTPFA unit or MTPFA unit. The fumaramate derivatives formed micelle-like structures in water, the emulsion polymerization proceeded well, and they obtained copolymers with relatively high molecular weights.

Chemical Structure	Abbreviation	Note and references
$  \begin{array}{c}  \text{CH}_3 \\    \\  \text{CH}_2=\text{C} \\    \\  \text{C}=\text{O} \\    \\  \text{NHCH}_2\text{CH}(\text{OCH}_2\text{CH}_2\text{N}^+(\text{CH}_3)_3) \\    \\  \text{CH}_3 \quad \text{O}^-  \end{array}  $	MAPPC	Ref. 48
$  \begin{array}{c}  \text{CH}_2=\text{CH} \\    \\  \text{C}=\text{O} \\    \\  \text{O}-(\text{CH}_2)_{10}-\text{C}(=\text{O})-\text{OCH}_2-\text{CH}_2-\text{O}-\text{P}(=\text{O})(\text{O}^-)-\text{OCH}_2\text{CH}_2\text{N}^+(\text{CH}_3)_3 \\    \\  \text{CH}_3(\text{CH}_2)_{14}\text{COCH}_2\text{CH}_2-\text{C}(=\text{O})-\text{O}-\text{CH}_2-\text{O}-\text{P}(=\text{O})(\text{O}^-)-\text{OCH}_2\text{CH}_2\text{N}^+(\text{CH}_3)_3  \end{array}  $	PADGPC	Ref. 49
$  \begin{array}{c}  \text{CH}_3 \\    \\  \text{CH}_2=\text{C} \\    \\  \text{C}=\text{O} \\    \\  \text{OCH}_2\text{CH}_2\text{NHCOOCH}_2\text{CH}(\text{OH})\text{CH}_2\text{O}-\text{P}(=\text{O})(\text{O}^-)-\text{OCH}_2\text{CH}_2\text{N}^+(\text{CH}_3)_3  \end{array}  $	MCGPC	Ref. 50
$  \begin{array}{c}  \text{CH}_3 \\    \\  \text{CH}_2=\text{C} \\    \\  \text{C}=\text{O} \\    \\  \text{OCH}_2\text{CH}_2\text{N}^+(\text{CH}_3)_2\text{CH}_2\text{CH}_2\text{O}-\text{P}(=\text{O})(\text{O}^-)-(\text{CH}_2)_6\text{O}-\text{C}_6\text{H}_4-\text{C}_6\text{H}_3\text{N}(\text{CH}_3)_2\text{O}  \end{array}  $	MAIP	Ref. 51
$  \begin{array}{c}  \text{CH}_3 \\    \\  \text{CH}_2=\text{C} \\    \\  \text{C}=\text{O} \\    \\  \text{OCH}_2\text{CH}_2\text{N}^+(\text{CH}_3)_2\text{CH}_2\text{CH}_2\text{O}-\text{P}(=\text{O})(\text{O}^-)-(\text{CH}_2)_6\text{O}-\text{C}_6\text{H}_4-\text{N}=\text{N}-\text{C}_6\text{H}_4-\text{OCH}_3  \end{array}  $	MAHP	Ref. 52
$  \begin{array}{c}  \text{CH}_3 \\    \\  \text{CH}_2=\text{C} \\    \\  \text{C}=\text{O} \\    \\  \text{OCH}_2\text{CH}_2\text{N}^+(\text{CH}_3)_2\text{CH}_2\text{CH}_2\text{O}-\text{P}(=\text{O})(\text{O}^-)-\text{OCH}_2\text{CH}_2\text{O}-\text{C}(=\text{O})-\text{C}(\text{CH}_3)=\text{CH}_2  \end{array}  $	MMPC	Ref. 53

Fig. 5. (Continued.)

Kros et al. synthesized a styrene-derivative having a PC group (38). They prepared this compound to develop new coating materials for the poly(St) cell culture plates. The copolymer of 1-(4-vinyl)benzyloxy-4(phosphorylcholine) butane with St shows hydrophilic and high chain mobility compared with those of poly(St). After coating the cell culture plate with this polymer, lower cell growth was observed, even for cells that were alive due to the effect of the PC groups.

Varying the connecting unit between the polymerizable group and PC group is an alternative route to modifying the MPC. In the case of MPC, the ethylene group exists between the methacrylate and PC group. Iwasaki et al. designed MPC derivatives with various alkyl chain lengths ( $\omega$ -methacryloyloxyalkyl phosphorylcholine, MAPC), such as with species containing butyl, hexyl, and decyl

groups (39,40). The procedure for synthesis of these monomers is the same as that used for MPC, and it provides monomers of high purity. Polymerization with BMA in ethanol by radical polymerization proceeds well. Varying the composition of MAPC in the feed solution controls the composition of the MAPC units in the copolymer. For example, rather than introducing alkyl chains, oligooxyethylene chains (MEOnPC) can be used instead (41). The numbers of repeating units of oxyethylene used were 2, 3, and 9. The radical polymerization ability of the MEOnPC does not differ significantly from that of MPC. Copolymerization of MEOnPC with BMA provides polymers whose molecular weights are relatively high, above  $2 \times 10^5$ . The mobility of the PC groups that are connected by the oligooxyethylene chain increases with the increase in the chain length. It was therefore concluded that the MEOnPC is more suited to providing a concentration of PC groups at water-polymer interfaces than is MPC (42–44). This also confirmed the reduction of protein adsorption on the surface (45).

Oishi et al. synthesized various MPC derivatives with different connections between the trimethylammonium and phosphate groups, namely 2-[3'-(trimethylammonium)propylphosphoryl]ethyl methacrylate (TMP) (46) and 2-[2'-(trimethylammonium)-1'-methylethylphosphoryl]ethyl methacrylate (TMPM) (47). Homopolymerization of TMP in water using KPS as an initiator proceeds homogeneously and yields an increase in the viscosity of the polymer solution, despite the short polymerization time. Hence, it can be said that the connection unit in the PC group does not influence the polymerization reactivity. Copolymerizations of TMP with MMA and St provide corresponding polymers. The monomer reactivity is  $r_1 = 0.52$  and  $r_2 = 0.37$  for copolymerization of TPM (M1) and St (M2), and  $r_1 = 1.05$  and  $r_2 = 0.91$  for MMA (M2). The homopolymer of TMPT and copolymer of TMPT with BMA were obtained by using a conventional radical polymerization procedure.

Other MPC derivatives with special functions have been reported (48–52). A photochromic spirobenzopyrane or azobenzene moiety is introduced at the terminus of the PC-like group (51). An optically active monomer, 1-(2-methacryloyloxyethyl)carbamoyl-sn-glycero-3-phosphorylcholine (MCGPC), is synthesized with the reaction between L- $\alpha$ -glycerophosphorylcholine (GPC) and 2-methacryloyloxyethyl isocyanate (50). Copolymerization of the MCGPC with BMA is carried out. A cross-linking monomer (MMPC) with a PC-like linkage in the middle of the molecule is synthesized to prepare new hydrogels (52).

**PC Compounds for Polyaddition and Polycondensation.** Some PC compounds have recently been synthesized for the preparation of polyester and polyurethane (Fig. 6). Diol compounds with the PC group are used for the preparation of polyurethane (53). The first such example was reported by Cooper et al. in 1998, wherein GPC was used. By altering the ratio of GPC to 1,4-butanediol, a series of polymers were obtained, each with a different composition of the PC group. Differential scanning calorimetry and dynamic mechanical analysis showed that the polymer with the highest PC content had the lowest soft segment glass transition temperature ( $T_g$ ) and the highest tensile strength and Young's modulus. This is due to the high degree of microphase separation in the polyurethane as a result of ionic aggregation and hydrogen bonding from the zwitterionic PC group. The measured dynamic contact angle with water showed that these polyurethanes, especially those with high PC content, rearranged

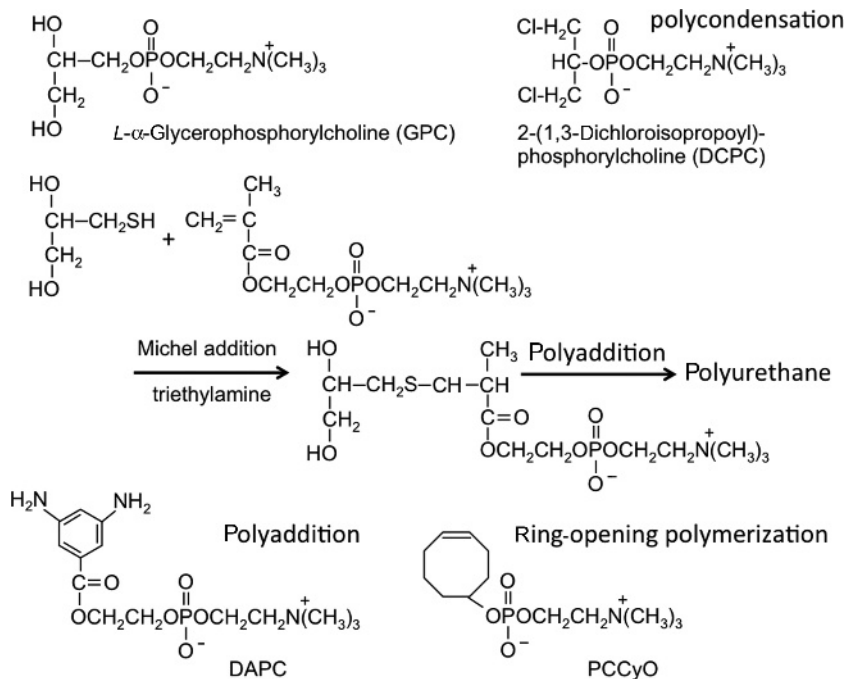


**Fig. 6.** Chemical structure of monomers bearing the phosphorylcholine group for polycondensation, polyaddition, and ring-opening polymerization.

themselves to minimize the interfacial tension upon contact with an aqueous environment, in the same way as found for methacrylate polymers. GPC is a naturally occurring compound. Iwasaki et al. modified the monomer structure (54). The reactivity of secondary functional group is lesser than that of the primary position. Thus, they introduced the PC group connected to the center carbon of glycerol (DCPC). The monomer, DCPC, turns to polycarbonate by a polycondensation reaction. Takami and co-workers determined a more convenient synthesis of these diol compounds, involving the reaction between mercapt compounds and a methacrylate such as MPC (55,56). A Michael addition reaction occurred at the double bond of the methacrylate with the mercapt group of 3-mercaptoputane-1,2-diol, under mild conditions, and in the presence of a ternary amine catalyst. Thus, various diol compounds corresponding to the particular methacrylate were obtained. This diol compound with the PC group can use a monomer for a polyaddition reaction with a diisocyanate compound to provide polyurethane. Nagase et al. produced alternative monomers for this polymerization (57,58). For example, an aromatic diamine compound bearing a PC group (DAPC) was synthesized and an aromatic polyamide prepared by copolymerization of the DAPC and isophthaloyl chloride.

Moreover, a PC monomer for ring-opening polymerization is investigated. Emrick et al. synthesized novel PC-polyolefin polymers and copolymers were prepared by ring-opening metathesis polymerization of PC-substituted cyclooctene, 1,5-phosphorylcholine cyclooctene (59).

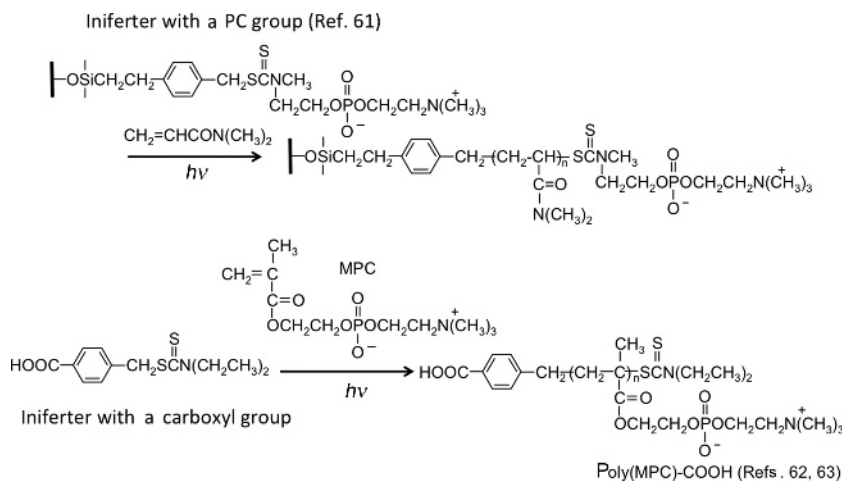


**Fig. 7.** Photoinduced living radical polymerization of MPC with the photoiniferter.

## Living Radical Polymerization of MPC and Derivatives

**Photoinduced Living Radical Polymerization of MPC.** Otsu described that the iniferter polymerizations are of interest because they can be used to produce well-defined block-type copolymers and polymers of relatively low polydispersity (60). The process of the polymerization involves initiation, propagation, and termination steps. The iniferter molecule absorbs UV light and generates a carbon radical and a sulfur-based dithiocarbamyl radical. The carbon radicals produced in these reactions are extremely reactive and initiate the polymerization by reacting with a monomeric double bond, whereas the dithiocarbamyl radical is comparatively less reactive and does not participate significantly in initiating the polymerization. Propagation occurs by the addition of monomers or double bonds to the active centers. In iniferter polymerizations, the carbon radicals constitute the active centers because the dithiocarbamyl radical is stable and relatively unreactive to propagation. Using this polymerization, Matsuda et al. reported a unique system of introducing PC groups at the terminus of the polymer chain (Fig. 7) (61). They prepared a PC group-modified dithiocarbamyl compound as an iniferter and polymerized *N,N*-dimethylacrylamide. A water-soluble polymer terminated with a PC group was thus obtained.

To prepare well-defined MPC polymers, Miyamoto et al. demonstrated the synthesis of water-soluble poly(MPC) with a terminal carboxyl group, (poly(MPC)-COOH), by photoinduced living radical polymerization (62, 63). They used an iniferter that possesses one carboxyl group, 4-(*N,N*-diethyldithiocarbamoylmethyl)benzoic acid. Photopolymerization proceeds in the living manner with a good yield of up to 85% achieved. The molecular weight could be regulated between  $5.0 \times 10^3$  and  $3.7 \times 10^4$  based on the feed composition, and a narrow polydispersity ( $M_w/M_n = 1.23\text{--}1.35$ ) was obtained. They used poly(MPC)-COOH to directly modify the proteins and thus maintained a stable activity in the aqueous medium.

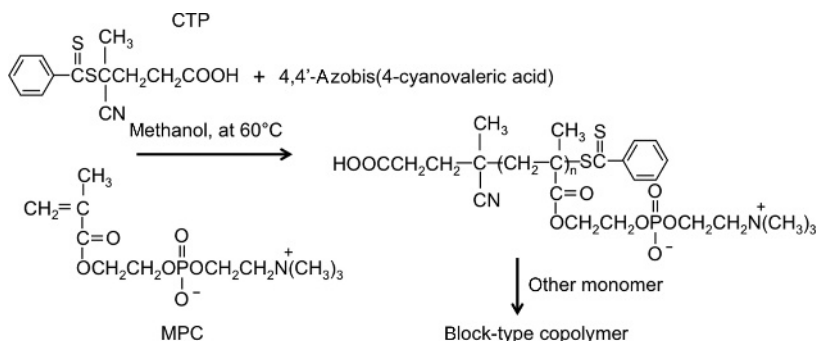


**Fig. 8.** RAFT radical polymerization of MPC.

**Reversible Addition-Fragmentation Chain Transfer Radical Polymerization.** Reversible addition-fragmentation chain transfer (RAFT)-controlled radical polymerization is a metal-free method that uses a chain transfer agent added to an ordinary free radical polymerization system (64). RAFT polymerizations can be carried out under similar conditions to conventional free radical polymerizations, save that a thiocarbonylthio compound is used as the CTA. The polymerization is initiated using thermal decomposition of an azo compound, such as AIBN, although the initiation of the RAFT process has also been investigated using UV initiation. After initiation of the polymerization, the growing macroradical undergoes a transfer process with the RAFT agent to form an intermediate radical. Stenzel et al. reported on the preparation of amphiphilic block copolymers composed of APC and *n*-butyl acrylate (BA) by RAFT polymerization (65). However, methacrylate polymers should be more desirable than acrylate polymers because the former are much more stable toward spontaneous hydrolysis in aqueous media than are the latter, particularly under biological conditions.

A homopolymer of MPC was synthesized in aqueous medium by RAFT polymerization (66–69). The “living” polymerization was confirmed by the fact that the number-average molecular weight increased linearly with monomer conversion, whereas the molecular weight distribution remained narrow and independent of the conversion (Fig. 8). The poly(MPC) thus prepared was end-capped with a dithioester moiety. Using the dithioester-capped poly(MPC) as a macro-CTA, AB diblock-type copolymers composed of poly(MPC) segments and poly(BMA) segments were synthesized (66). Aggregation of the amphiphilic block-type copolymer with various poly(BMA) segment lengths in an aqueous medium was investigated. Lowe and coworkers examined the RAFT polymerization of MPC in water using 4-cyanopentanoic acid dithiobenzoate and 4,4'-azobis(4-cyanovaleric acid) (67). An obtained poly(MPC) segment is employed as a CTA in the synthesis of a range of stimulus-responsive AB diblock-type copolymers in a polar solvent. Well-defined block copolymers of various molar compositions and with narrow polydispersity ( $M_w/M_n = 1.10\text{--}1.24$ ) were prepared with *N,N*-diethylacrylamide, 4-vinylbenzoic acid, *N*-(3-sulfopropyl)-*N*-methacryloyloxyethyl-*N,N*-dimethylammonium betaine, and *N,N*-di-*n*-propylbenzylvinylamine. All block-type polymer chains can be induced to undergo self-assembly in the same aqueous environment, provided that the

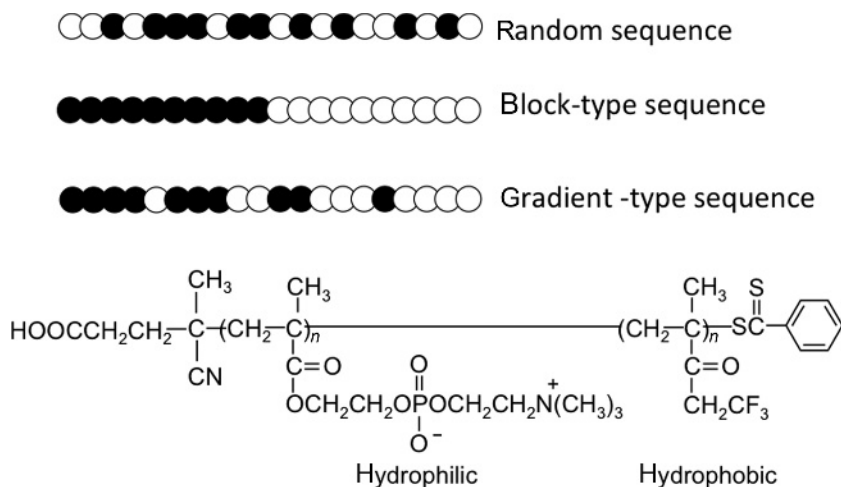


**Fig. 9.** Polymer architecture of the MPC copolymer prepared by RAFT polymerization. An open circle represents MPC unit, and a closed circle represents other monomer units.

correct external stimulus (temperature, pH, or electrolyte concentration) is applied. The polymer aggregates with average sizes in the range of ca. 22–180 nm are formed, most likely due to the formation of polymeric micelles and vesicles.

Narain and coworkers proposed the synthesis of water-soluble and cationic polymers composed of MPC units and 2-aminoethyl methacrylamide hydrochloride (AEMA) units as block and random architectures by RAFT polymerization (68,70,71). They demonstrated that the RAFT polymerization proceeds well in the living radical polymerization manner and that polymers with narrow polydispersity ( $<1.3$ ) are formed, with some even containing primary amine groups. The role of primary amines in gene delivery has been well studied, with the finding that they are superior to tertiary amines. For gene delivery purposes, the cationic polymers composed of MPC units and AEMA units can improve the gene expression by promoting enhanced DNA condensation abilities.

The unique polymer architecture is examined by Inoue et al. using the RAFT polymerization of MPC and other monomers (Fig. 9) (72). They prepared a series of copolymers composed of two monomer units, possessing a polar PC group and an apolar fluorocarbon group with a controlled monomer unit sequence. The MPC and 2,2,2-trifluoroethyl methacrylate were selected as the monomers to investigate the influence of the monomer unit sequence in a polymer chain on the phase-separated structure in the bulk and surface structures. Inoue et al. therefore studied copolymers possessing a continuous change in monomer unit composition along the polymer chain (gradient copolymer), as well as random and block-type copolymers. Analysis of the instantaneous composition revealed that there was a continuous change in the monomer unit composition in the gradient copolymer and also in the statistical monomer unit sequence in the random copolymer. Thermal analysis assumed that the gradient sequence of the monomer unit would make the phase-separated structure in the bulk ambiguous, whereas the well-defined and monodisperse block-type sequence would undergo a distinct phase separation due to the extreme difference in polarity for the component monomer

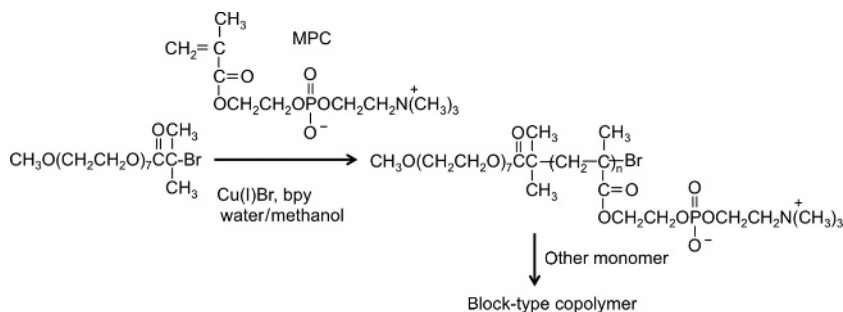


**Fig. 10.** ATRP of MPC.

units. Using a polydimethylsiloxane (PDMS) segment as a macro-CTA, the MPC is polymerized by the RAFT procedure (73). The poly(PDMS-*block*-poly(MPC)) shows good affinity to the PDMS film as a coating material.

The polymer synthesized by the RAFT polymerization can possess a terminal thiol group, which is reactable with a gold substrate. Indeed, Iwasaki et al. synthesized poly(MPC-*co*-methacrylic acid) by the RAFT polymerization and then a terminal dithioester group in the CTA residue is converted to a thiol group with 2-ethanolamine. They showed that the thiol group functioned as an anchor for binding the polymer chain on the gold surface (74).

**Atom Transfer Radical Polymerization.** Atom transfer radical polymerization (ATRP) has been developed by Wang Matyjaszewski in 1995 (75). Reversible chain-end capping using halogen atoms ensures that the instantaneous polymer radical concentration is lower than in conventional radical polymerization, which suppresses termination relative to propagation and hence leads to relatively narrow molecular weight distributions. Efficient block copolymer syntheses can be achieved under optimized conditions, and this pseudoliving free radical chemistry has gained a deserved reputation for its excellent tolerance of both monomer functionality and protic solvents.

Armes et al. reported that MPC can be polymerized with high rates of conversion in both water and methanol at ambient temperature via an ATRP process (Fig. 10). They also reported a more detailed study on the optimization of the ATRP of MPC (76). The results of these studies showed that good conversion from monomer to polymer, first-order monomer kinetics, a linear relationship between conversion and molecular weight, and relatively narrow polydispersities ( $M_w/M_n = 1.15\text{--}1.35$ ) are obtained in both water and methanol media at 20°C. Slower polymerizations and narrower polydispersities were observed when the polymerization was carried out in an alcohol solution. The rate of ATRP was significantly slower in 2-propanol than methanol due to the reduced polarity of the former solvent. The addition of a relatively small amount of water to the solution of alcohol led to significantly faster polymerization. The effect of varying the ligand type on the degree of polymerization was evaluated. It was observed that 2,2'-bipyridine-containing ligands provide good control over the degree of polymerization in the range of 20 and 200. This synthetic advance is expected to allow the preparation of a wide range of polymers, such as AB diblock-type and ABA triblock-type copolymers, for various biomedical applications (76–80).



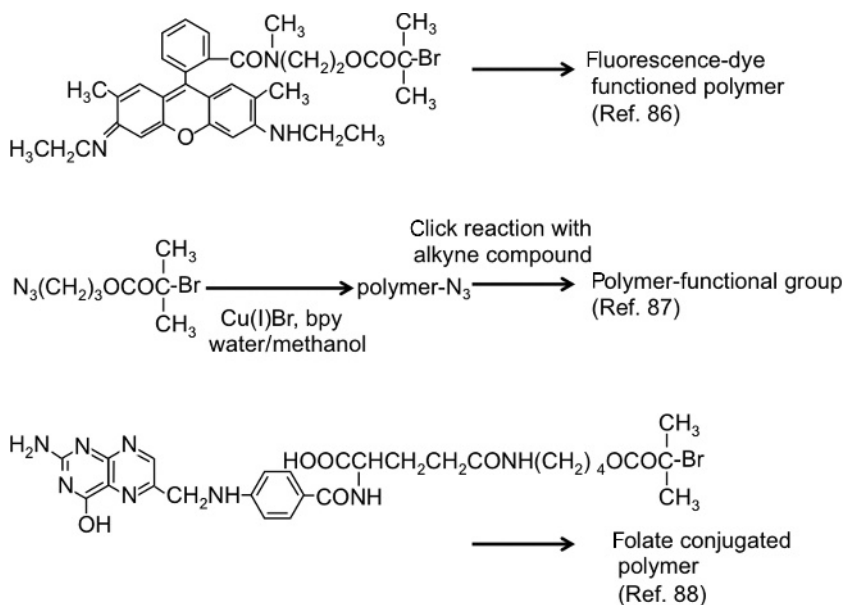


**Fig. 11.** Chemical structure of various ATRP initiators for the preparation of a functional group terminated phospholipid polymer.

### Introduction of Functional Groups at the Terminus of Poly(MPC)

Living polymerization is also useful for introducing a functional group to the terminus of a polymer chain. The functional aliphatic azo compounds were previously used for this purpose (81–85). However, the initiation efficiency is strongly influenced by the functionality of the terminal group in the polymer chain. Furthermore, the presence of some CTAs can result in telomerization occurring during the progress of the polymerization process and introduction of the functional group. Various functionalized poly(MPC)s have been prepared and used to prepare block-type copolymers and graft-type copolymers. From comparison between these methods, living radical polymerization is superior in obtaining a poly(MPC) with a terminal functional group. First, ATRP initiators with the functional group are synthesized and polymerized with MPC (Fig. 11). Fluorescent dye-labeled poly(MPC) is then synthesized to obtain an amphiphilic block-type copolymer (86). The block-type copolymers form polymeric vesicles via hydrophobic interactions in water. These have been applied as carriers of bioactive molecules and as molecular imaging tools. Azide-group functionalized ATRP initiators have been synthesized by Armes et al. (87). The azide functional group is well known for its “click chemistry” with alkyne compounds. After ATRP of MPC with the initiator, they react with propargyl methacrylate to obtain the corresponding macromonomer. Lam et al. prepared folic acid functionalized diblock copolymers based on MPC and either 2-(*N,N*-dimethylamino)ethyl methacrylate or 2-(*N,N*-diisopropylamino)ethyl methacrylate by ATRP using a corresponding initiator (88).

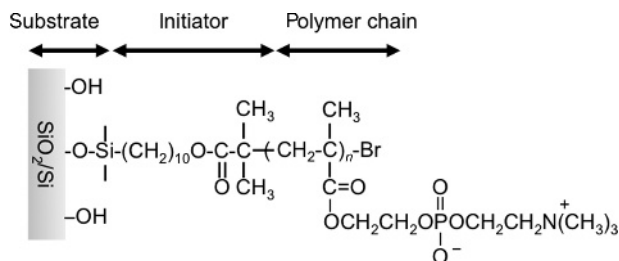


**Fig. 12.** Interfacial structure of poly(MPC) brush surface prepared by ATRP (SI-ATRPs). The BrC10TCS is applied on the surface of Si/SiO<sub>2</sub> as an ATRP initiator.

To prepare an ABA block-type copolymer, macroinitiators for ATRP are synthesized. 2-Bromoisobutyryl bromide is reacted to both terminals of PDMS to obtain a PDMS macroinitiator. Using this method, the poly(PDMS-*block*-poly(MPC)) is obtained (89–91).

### Surface-Initiated ATRP

The poly(MPC)-grafted surface structures known in the literature have been developed using several polymerization methods and substrates (92–97). The thickness and density of the grafted poly(MPC) chains can be controlled using the photoinduced free or living radical polymerization. More particularly, a surface-initiated living radical polymerization method, such as ATRP or RAFT polymerization, provides the polymer brush structure. The polymer brush surface has a dense polymer grafted layer at the surface, and these polymer chains have lengths that exceed 80% of the fully stretched polymer chain. Polymer brush surfaces have been prepared using several kinds of controlled/living radical polymerization. In particular, surface-initiated atom transfer radical polymerization (SI-ATRPs) has been demonstrated to be a versatile technique for the synthesis of well-defined polymers with several types of monomer and organic/inorganic hybrid materials (94–97). The dense and well-defined polymer brush structure could be important for the construction of a biocompatible surface.

A sufficient density of ATRP initiator groups should be immobilized on the surface prior to the graft polymerization of MPC from a silicon wafer (Fig. 12). Surface-attachable initiators with several kinds of silane groups, such as 3-(2-bromoisobutyryl)propyl dimethylchlorosilane (BrC3DMCS) 10-(2-bromo-2-methyl)propionyloxy decyltrichlorosilane (BrC10TCS), and 6-triethoxysilylhexyl 2-bromoisobutylate (BHE), were often used to immobilize the ATRP initiator groups at the silicon wafer through silane-coupling reactions. The primary problem in the preparation of the polymer brush layer is when there is a low concentration of persistent radical on the initiator-immobilized substrate. Two methods are known to solve this problem and control the grafting process: the addition of a persistent radical (deactivator) or the use of a sacrificial initiator at the beginning of the reaction.

The preparation of a poly(MPC) brush layer on the surface using the addition of a deactivator is constructed by Feng et al. (98–101). They performed the ATRP grafting of MPC, with copper(II) bromide ( $\text{CuBr}_2$ ) added as the excess deactivator, and succeeded in the preparation of a 100-nm-thick poly(MPC) brush layer through a precision control of the grafting process. There have also been many cases where a poly(MPC) brush layer was prepared by the addition of a sacrificial initiator. The addition of a sacrificial initiator into the polymerization solution with ATRP initiator-immobilized substrates serves a number of beneficial purposes in terms of both synthesis and characterization of the polymer brush layers. In this regard, the synthesis and characterization of a poly(MPC) brush layer was performed using sacrificial initiators such as ethyl 2-bromoisobutyrate (EBIB) and methoxyoligo(ethylene glycol) 2-bromoisobutyrate (OEGBr). The linear relationship between the MPC concentration and polymerization time is obtained. Also, low polydispersity of the poly(MPC) formed in the solution shows that the MPC can be polymerized in a living radical polymerization manner. The thickness of the poly(MPC) chain in the polymer brush layer, controlled by the ratio of monomer/sacrificial initiator, was in the range of 1–nm. The grafted polymer chain density at the polymer brush layer is also an important feature that determines the characteristics of the polymer brush layer, and it can be easily controlled using the active/inactive initiator-immobilized substrate. For example, the controlled density of poly(MPC) chains from semidiluted to dense brush regions of the silicon wafer has been reported with a mixed self-assembled monolayer of BrC10TCS as the active initiator and decyltrichlorosilane as the inactive initiator. Iwasaki et al. conducted significant work in this field for regulating cell adhesion (102). Surface patterning of poly(MPC) brush is succeeded by UV irradiation of an initiator-immobilized surface and then polymerization was carried out. The pattern area of poly(MPC) can be controlled by using a photomask with 50–100  $\mu\text{m}$  in a square length.

Other kinds of the initiation system for SI-ATRP of MPC are reported (103–107). The ATRP of MPC on cobalt–chromium alloy substrates modified with 11-(2-bromoisobutyrate)-undecyl-1-phosphonic acid was studied (104). After the synthesis of 11-(2-bromoisobutyrate)-undecyl-1-phosphonic acid, which plays the role of the initiator for the SI-ATRP, this molecule was grafted onto the cobalt–chromium alloy substrates. The SI-ATRP of MPC was then achieved on these modified austenitic cobalt–chromium alloy substrates in aqueous media, either at room temperature for 24 h or at 90°C for 1 h. A hydrophilic poly(MPC) graft layer already forms ( $\theta \approx 44^\circ$ ) at room temperature after 24 h of the reaction, but heating is necessary to increase the thickness of the grafted layer, thereby reducing the water contact angle ( $\theta \approx 36^\circ$ ). This process may be applied to the preparation of homopolymer and block-type copolymer brush layers covalently anchored to the oxide layer of metal substrates.

Poly(MPC) brush layers are grown from a macroinitiator coating the mica surface using SI-ATRP of MPC (103,104). Freshly cleaved mica was functionalized through incubation in a 0.2% w/v aqueous solution of cationic macroinitiator, then gently withdrawn from the solution and rinsed thoroughly with pure water. The cationic macroinitiator was derived from a statistical copolymer ( $M_n = 6500$ ,  $M_w/M_n = 1.25$ ) of 2-trimethylammonium iodide ethyl methacrylate and 2,2-bromoisobutyroethyl methacrylate. The polymerization of MPC was conducted

on the macroinitiator-coated mica surface by using ATRP in an oxygen-free aqueous solution at room temperature. With the same concept in mind, a macroinitiator with catechol groups for SI-ATRP has been reported for immobilization on metal substrates (106).

Iwasaki et al. reported the SI-ATRP of MPC from heterogenic surfaces such as nanofibers and nanopores (108,109). For the site-specific dense immobilization of antibodies on a solid support, random copolymer brushes composed of MPC and glycidyl methacrylate (GMA) were prepared on silicone nanofilaments by SI-ATRP. First, the nanofilaments were prepared on the silicon wafer by treatment with trichloromethylsilane ( $\text{MeSiCl}_3$ ). Then,  $\text{O}_2$  plasma was irradiated on the surface to generate Si-OH groups on the nanofilaments and initiators for ATRP were then coupled on the filaments. MPC and GMA were polymerized using SI-ATRP, and pyridyl disulfide groups were introduced into the polymer chains for the immobilization of proteins. The authors were also interested in the preparation of nanoscale holes (nanopores) in tris(trimethylsilane (TMS)) monolayers containing unreacted silanol groups. These silicon-supported mixed tris(TMS)/silanol monolayers further reacted with silane compounds end-functionalized with  $\alpha$ -bromoisobutyrate to yield silicon-supported mixed tris(TMS)/ $\alpha$ -bromoisobutyrate monolayers. Poly(MPC) brushes grew faster from surface-immobilized  $\alpha$ -bromoisobutyrate initiators having hexyl and decyl chains as alkyl spacers than from those with propyl chains. The better mobility and longer alkyl spacers of the initiators allowed them to overcome the steric hindrance of the surrounding tris(TMS), and thus, to reach the monomers more efficiently than those with propyl group spacers. The nanoscopic distribution of the poly(MPC) brushes is only visualized when the grafting density of poly(MPC) brushes in the nanopores is not too high. Under such circumstances, the sizes of the protrusions depend upon both the tris(TMS) coverage and the graft density of the poly(MPC) brushes in the nanopores.

Recently, Kobayashi et al. report very unique SI-ATRP of ionic monomers, which is carried out in fluoroalcohol and ionic liquid as the solvent. The MPC can polymerize in a living polymerization manner even in both solvent conditions (110).

### Characterization of the Poly(MPC) Brush Layer

A kinetic model for the SI-ATRP of MPC has been reported by Brash et al. (111) and Zhou et al. (112). The model was verified with experimental data for the growth of MPC from a silicon wafer, which was carried out by adding either free initiator (Method I) or excess deactivator (Method II) to the solution. It was shown through this modeling that Method II gives better control over the polymer molecular weight and results in a thicker graft layer under similar conditions to Method I. A new mechanism is proposed for the radical termination on the basis of the fact that the rapid activation/deactivation cycle facilitates the "migration" of radical centers on the surface. Zhou et al. considered a simple kinetic model for the SI-ATRP of MPC from silicon (112). They reported that the model describes the development of the polymer layer thickness, as well as the concentrations of radical, dormant, and dead chains. The model accounts for the effects

of the equilibrium constant, activator/deactivator concentration ratio, monomer concentration, grafting density, and rate constants of propagation and termination. Although the radical chains are immobilized, radical centers “migrate” and are terminated through activation and deactivation reactions. The termination rate constant is therefore proportional to the catalyst concentration. The termination is influenced by the chain conformation, and the rate constant is dependent on the grafting density.

The surface properties are drastically changed by the grafting of MPC to generate a poly(MPC) brush layer. The thickness of the polymer brush layer was determined directly using an ellipsometer, and the molecular weight of the grafted poly(MPC) chain was assumed to be the same as that of poly(MPC) produced by a sacrificial initiator in a polymerization solution. Feng et al. reported a graft density of 0.39 chains/nm<sup>2</sup> from the BrC10TCS-immobilized silicon wafer in the presence of the OEGBr as the free initiator (98–101), Kobayashi et al. reported a value of 0.22 chains/nm<sup>2</sup> from a BHE-immobilized silicon wafer using EBIB (113–116), and Iwata et al. (102) and Kitano et al. (117) reported a density of 0.17 chains/nm<sup>2</sup> from a BrC3DMCS-immobilized substrate using EBIB. Inoue et al. showed that the density of poly(MPC) was 0.26 chains/nm<sup>2</sup> using a BrC10DMCS-immobilized surface with EBIB as the free initiator in methanol (118). While there are small differences between the graft densities of the poly(MPC) brush layers prepared by these methods, all the reported values are above 0.1 chains/nm<sup>2</sup>, indicating that dense polymer brush layers were prepared on the silicon wafers.

The poly(MPC) brush surface provides a superhydrophilic surface. Kobayashi and Takahara evaluated the high surface free energy of the poly(MPC) brush layer using static contact angle measurements with air bubbles and various organic liquids such as diiodomethane and hexadecane in water (113–115). The air bubble contact angle measurements in water showed hardly any attachment of air bubble to the surface. They calculated the free energy of the poly(MPC) brush surface, 73 mN/m, which is the same as that of water itself. Thus, the poly(MPC) brush layer has a superhydrophilic nature in water. The conformation of the poly(MPC) chains in the poly(MPC) brush layer in water was analyzed using neutron reflection measurements (116). The poly(MPC) chains with 200 repeating units (the full length of the ethylene groups in the main chain with all-trans conformation was calculated to be 50 nm) were stretched to 60–70 nm in the swelling state, indicating that the tethered polymer chains would have a fairly extended conformation along the direction perpendicular to the surface. The stretched structure of the poly(MPC) does not change even when the ionic concentration in the solution increases. This is because of the unique hydration property of poly(MPC) chains. Kitano et al. revealed that the hydrogen bonding among water molecules in the poly(MPC) aqueous solution is the same as that in native water (119).

## Biomedical Functionalities of the Phospholipid Polymers

**Surface Modification of Biomedical Devices by Grafting of the MPC.**  
An abundance of research on surface modification with MPC polymers has been

carried out due to the versatility and excellent biocompatibility of these systems, and some MPC polymers have already been utilized as surface-modified materials in medical devices (120–126). A biocompatible surface could be obtained via conventional materials, even through a simple coating method. The physical adsorption of MPC polymers to a material surface requires there to be a hydrophobic unit in the polymer chain due to the superhydrophilicity of the MPC unit. However, the high polymerization reactivity of MPC enables the direct synthesis of poly(MPC) chains via photoinduced (living) radical polymerization from conventional initiator-coated materials, such as polyethylene (93,127), parylene (128), poly(dimethylsiloxane) (129,130), and polyetheretherketone (131,132). The immobilization of poly(MPC) chains at the material surface is one of the most promising methods for realizing a remarkably biocompatible surface because of the increasing PC density on the surface. Among these, Kyomoto et al. have researched systemically to produce a new long-life type artificial hip joint (93,127). The basic mechanism of this development is to reduce wear of ultra-high-molecular-weight polyethylene (UHMWPE), which is used at the lubrication interface with an artificial stem made by the metal of ceramics. Hydration lubrication based on the poly(MPC) graft layer is considerable to reduce friction torque and support the stem by strong hydration force. The amount of wear of UHMWPE suppresses more than 99% after grafting of poly(MPC) on the surface compared with that of original UHMWPE, which is used in clinically in the present time.

Of course, these surface modification reduced protein adsorption and following cellular adhesion and activation due to the nature of the poly(MPC) and MPC copolymers. Thus, surface modification with the poly(MPC) chains is effective to provide new medical devices.

**Biomedical Characteristics of the Poly(MPC) Brush Layer.** To understand the biomedical performance of polymer surface, both the protein adsorption resistance and lubricity are interesting properties of the poly(MPC) brush surface. The protein adsorption and cell adhesion repellency have been studied extensively for the poly(MPC) brush layers (98–102,118). The protein adsorption decreased significantly with increasing graft density and/or poly(MPC) chain length and reached to a level of 5 ng/cm<sup>2</sup> at a graft density of more than 0.29 chains/nm and a polymerization degree of more than 100 units, indicating the unprecedented biocompatibility of the poly(MPC) brush layer. Inoue et al. measured adsorption force of protein against the poly(MPC) brush directly and observed a very small value, that is, less than 0.2 nM (118). So, interactions between protein molecules and poly(MPC) brush surface are extremely weak. The high protein adsorption resistance of the poly(MPC) brush layer enables the inhibition of subsequent cell adhesion on this layer.

The poly(MPC) brush layer has been found to provide a novel interface with quite a low friction coefficient (97,104,113–115,117). Kobayashi et al. investigated the macroscopic tribology of the poly(MPC) brush layer using a sliding glass ball. The friction coefficient value was found to decrease with increasing humidity. In general, the lubricity in water is related to the surface hydrophilicity and the conformation of the polymer chains in the polymer brush layer. Considering the surface properties of the poly(MPC) brush layer, Kobayashi et al. concluded that superhydrophilicity results in a low-friction surface. Moreover, Chen et al. reported an extremely high lubricity of the poly(MPC) brush layer under

physiological pressures in pure water, comparable to the levels found in natural joints (97,104).

## Conclusions

This review has summarized the recent research made in bioinspired phospholipid polymers, focusing on the preparation, surface characterization, and biological responses on the surface. In particular, the usefulness of the well-known methacrylate with a PC group (MPC) is emphasized. Various architectures of MPC polymer have been synthesized by using conventional radical polymerization and living polymerization procedures. The living polymerization provides well-defined poly(MPC) and its block-type copolymers. Furthermore, living radical polymerization can commence from the surface of a substrate and a brush-line surface of the poly(MPC) can be obtained. This surface suppresses protein adsorption and the following biological response.

## BIBLIOGRAPHY

### CITED REFERENCES

1. S. J. Singer and G. L. Nicolson, *Science* **175**, 720–731 (1972).
2. R. F. A. Zwaal, P. Cornfurls, and U. M. Van Deenen, *Nature* **268**, 358–360 (1977).
3. R. F. A. Zwaal and H. C. Hemker, *Haemostasis* **11**, 12–39 (1982).
4. J. A. Hayward and D. Chapman, *Biomaterials* **5**, 135–142 (1984).
5. B. Hall, R. R. Bird, M. Kojima, and D. Chapman, *Biomaterials* **10**, 219–224 (1989).
6. F. Bonte, M. J. Hsu, A. Papp, K. Wu, S. L. Regen, and R. L. Juliano, *Biochim. Biophys. Acta* **900**, 1–9 (1987).
7. O. Albrecht, H. Gruler, and E. Sachmann, *J. Phys. (Paris)* **39**, 301–313 (1978).
8. G. Wagner, *Macromol. Chem.* **154**, 35–46 (1972).
9. H. H. Hub, B. Hupfer, H. Koch, and H. Ringsdorf, *Angew. Chem., Int. Ed. Engl.* **19**, 938–940 (1980).
10. S. L. Regen, A. Singh, G. Oehme, and M. Singh, *Biochem. Biophys. Res. Commun.* **101**, 131–136 (1981).
11. E. Lopez, D. F. O'Brien, and T. H. Whitesides, *Biochim. Biophys. Acta* **693**, 437–443 (1982).
12. J. Leaver, A. Alonso, A. A. Durrani, and D. Chapman, *Biochim. Biophys. Acta* **732**, 210–218 (1983).
13. B. M. Peek, J. H. Callahan, K. Namboodiri, A. Singh, and B. P. Gaber, *Macromolecules* **27**, 292–297 (1994) and references cited therein.
14. A. Singh, M. Markowitz, and G. M. Chow, *Nanostruct. Mater.* **5**, 141–153 (1995) and references cited therein.
15. A. Puri, H. Jang, A. Yavlovich, M. A. Masood, T. D. Veenstra, C. Luna, H. Arendas-Espinoza, R. Nussinov, and R. Blumenthal, *Langmuir* **27**, 15120–15128 (2011).
16. J. J. Schaefer, C. B. Foxb, and J. M. Harris, *J. Raman Spectrosc.* **43**, 351–359 (2012).
17. K. Ishihara, T. Ueda, and N. Nakabayashi, *Polym. J.* **23**, 355–360 (1990).
18. Y. Kadoma, N. Nakabayashi, E. Masuhara, and J. Yamauchi, *Kobunshi Ronbunshu (Jpn. J. Polym. Sci. Technol.)* **35**, 423–427 (1978).
19. Y. Iwasaki, M. Ijuin, A. Mikami, N. Nakabayashi, and K. Ishihara, *J. Biomed. Mater. Res.* **46**, 360–367 (1999).

20. M. Kimura, M. Takai, and K. Ishihara, *J. Biomed. Mater. Res. A* **80**, 45–54 (2007).
21. T. Umeda, T. Nakaya, and M. Imoto, *Makromol. Chem. Rapid Commun.* **3**, 475–459 (1982).
22. S. Fukushima, Y. Kadoma, and N. Nakabayashi, *Kobunshi Ronbunshu (Jpn. J. Polym. Sci. Technol.)* **40**, 785–793 (1983).
23. T. Nakaya, H. Toyoda, and M. Imoto, *Polym. J.* **18**, 881–885 (1986).
24. Jpn Pat. 2870727 (1989), K. Ishihara and N. Nakabayashi. Japan Science and Technology Agency (JST).
25. T. Ueda, H. Oshida, K. Kurita, K. Ishihara, and N. Nakabayashi, *Polym. J.* **24**, 1259–1269 (1992).
26. K. Sugiyama and H. Aoki, *Polym. J.* **26**, 561–569 (1994).
27. E. J. Campbell, V. O'Byrne, P. W. Stratfold, I. Quirk, T. A. Vick, M. C. Wiles, and Y. P. Yianni, *Am. Soc. Artif. Internal Organs J.* **40**, M853–M857 (1994).
28. K. Ishihara, Y. Iwasaki, and N. Nakabayashi, *Polym. J.* **33**, 1231–1236 (1999).
29. E. F. Murphy, J. L. Keddie, J. R. Lu, J. Brewer, and J. Russell, *Biomaterials* **20**, 1501–1511 (1999).
30. R. Kojima, M. C. Z. Kasuya, K. Ishihara, and K. Hatanaka, *Polym. J.* **41**, 370–373 (2009).
31. T. Sato, T. Miyoshi, and M. Seno, *J. Polym. Sci., Part A: Polym. Chem.* **38**, 509–515 (2000).
32. H. Wang, A. Miyamoto, T. Hirano, M. Seno, and T. Sato, *Eur. Polym. J.* **40**, 2287–2290 (2004).
33. K. Sugiyama, K. Ohga, and H. Aoki, *Makromol. Chem. Phys.* **196**, 1907–1916 (1995).
34. L. Ruiz, J. G. Hilborn, D. Leonard, and H. J. Mathieu, *Biomaterials* **19**, 987–998 (1998).
35. L. Jia, J.-P. Xu, H. Wang, and J. Ji, *Colloid Surf., B* **84**, 49–54 (2011).
36. T. Oishi, T. Fukuda, H. Uchiyama, F. Kondou, H. Ohe, and H. Tsutsumi, *Polymer* **38**, 3109–3115 (1997).
37. T. Oishi, H. Yamasaki, K. Onimura, T. Fukushima, and S. Morihashi, *J. Appl. Polym. Sci.* **92**, 2552–2557 (2004).
38. A. Kros, M. Gerritsen, J. Murk, J. A. Jansen, N. A. J. M. Sommerdijk, and R. J. M. Nolte, *J. Polym. Sci., Part A: Polym. Chem.* **39**, 468–474 (2001).
39. Y. Iwasaki, K. Kurita, K. Ishihara, and N. Nakabayashi, *J. Biomater. Sci., Polym. Edn.* **6**, 447–461 (1994).
40. Y. Iwasaki, K. Kurita, K. Ishihara, and N. Nakabayashi, *J. Biomater. Sci., Polym. Edn* **8**, 151–163 (1996).
41. K. Ishihara, A. Fujiike, Y. Iwasaki, K. Kurita, and N. Nakabayashi, *J. Polym. Sci., Part A: Polym. Chem.* **34**, 199–205 (1996).
42. Y. Iwasaki, A. Fujiike, Y. Iwasaki, K. Kurita, and N. Nakabayashi, *J. Biomater. Sci., Polym. Edn* **8**, 91–102 (1996).
43. A. Yamasaki, Y. Imamura, K. Kurita, Y. Iwasaki, N. Nakabayashi, and K. Ishihara, *Colloid Surf., B* **28**, 53–62 (2003).
44. Y. Iwasaki, A. Yamasaki, and K. Ishihara, *Biomaterials* **24**, 3599–3604 (2003).
45. T. Oishi, H. Tanaka, H. Yamasaki, and K. Onimura, *J. Appl. Polym. Sci.* **86**, 1092–1105 (2002).
46. T. Oishi, H. Uchiyama, K. Onimura, and H. Tsutsumi, *Polym. J.* **30**, 17–22 (1998).
47. T. Oishi, Y. Yoshimura, H. Yamasaki, and K. Onimura, *Polym. Bull.* **47**, 121–126 (2001).
48. K. Sugiyama, and K. Ohga, *Makromol. Chem. Phys.* **200**, 1439–1445 (1999).
49. K. G. Marra, T. M. Winger, S. R. Hanson, and E. L. Chaikof, *Macromolecules* **30**, 6483–6488 (1997).



50. T. Oishi, M. Yoshikawa, H. Yamasaki, K. Onimura, and H. Tsutsumi, *Polym. Bull.* **47**, 415–420 (2002).
51. K. Sugiyama, H. Nakano, and K. Ohga, *Makromol. Chem. Phys.* **195**, 3915–3928 (1994).
52. Y. Kiritoshi and K. Ishihara, *Polymer* **45**, 7449–7504 (2004).
53. L. Y. L. Yung and S. L. Cooper, *Biomaterials* **19**, 31–40 (1998).
54. Y. Iwasaki, N. Nakabayashi, and K. Ishihara, *Macromol. Rapid Commun.* **21**, 287–290 (2000).
55. R. Matsuno, K. Takami, and K. Ishihara, *Langmuir* **26**, 13028–13032 (2010).
56. K. Takami, R. Matsuno, and K. Kshihara, *Polymer* **52**, 5445–5451 (2011).
57. Y. Nagase, M. Oku, Y. Iwasaki, and K. Ishihara, *Polym. J.* **39**, 712–721 (2007).
58. Y. Nagase, S. Nakajima, M. Oku, Y. Iwasaki, and K. Ishihara, *Polym. J.* **40**, 1149–1152 (2008).
59. K. Kratz, K. Breitenkamp, R. Hule, D. Pochan, and T. Emrick, *Macromolecules* **42**, 3227–3229 (2009).
60. T. Otsu, *J. Polym. Sci., Part A: Polym. Chem.* **38**, 2121–2136 (2000).
61. T. Matsuda, M. Kaneko, and S. Ge, *Biomaterials* **24**, 4507–4515 (2003).
62. D. Miyamoto, J. Watanabe, and K. Ishihara, *Biomaterials* **25**, 71–76 (2004).
63. D. Miyamoto, J. Watanabe, and K. Ishihara, *J. Appl. Polym. Sci.* **95**, 615–622 (2005).
64. J. Chiefari, Y. K. Chong, F. Ercole, J. Krstina, J. Jeffery, T. P. T. Le, R. T. A. Mayadunne, G. F. Meijs, C. L. Moad, G. Moad, E. Rizzardo, and S. H. Thang, *Macromolecules* **31**, 5559–5562 (1998).
65. M. H. Stenzel, C. Barner-Kowollik, T. P. Davis, and H. M. Dalton, *Macromol. Biosci.* **4**, 445–453 (2004).
66. S. Yusa, K. Fukuda, T. Yamamoto, K. Ishihara, and Y. Morishima, *Biomacromolecules* **6**, 663–670 (2005).
67. B. Yu, A. B. Lowe, and K. Ishihara, *Biomacromolecules* **10**, 950–958 (2009).
68. N. Bhuchar, Z. Deng, K. Ishihara, and R. Narain, *Polym. Chem.* **2**, 632–639 (2011).
69. R. Matsuno, Y. Goto, T. Konno, M. Takai, and K. Ishihara, *J. Nanosci. Nanotechnol.* **9**, 358–365 (2009).
70. M. Ahmed, N. Bhuchar, K. Ishihara, and R. Narain, *Bioconjugate Chem.* **22**, 1228–1238 (2011).
71. N. Bhuchar, R. Sunasee, K. Ishihara, T. Thundat, and R. Narain, *Bioconjugate Chem.* **23**, 75–83 (2012).
72. Y. Inoue, J. Watanabe, M. Takai, and K. Ishihara, *J. Polym. Sci., Part A: Polym. Chem.* **43**, 6073–6083 (2005).
73. Y. Iwasaki, M. Takamiya, R. Iwata, S. Yusa, and K. Akiyoshi, *Colloid Surf., B* **57**, 226–236 (2007).
74. P. Akkahat, S. Kiatkamjornwong, S. Yusa, V. P. Hoven, and Y. Iwasaki, *Langmuir* **28**, 5872–5881 (2012).
75. J.-S. Wang and K. Matyjaszewski, *Macromolecules* **28**, 7901–7910 (1995).
76. I. Y. Ma, E. J. Lobb, N. C. Billingham, S. P. Armes, A. L. Lewis, A. W. Lloyd, and J. Salvage, *Macromolecules* **35**, 9306–9314 (2002).
77. Y. Ma, Y. Tang, N. C. Billingham, S. P. Armes, A. L. Lewis, A. W. Lloyd, and J. P. Salvage, *Macromolecules* **36**, 3475–3484 (2003).
78. Y. Ma, Y. Tang, N. C. Billingham, S. P. Armes, and A. L. Lewis, *Biomacromolecules* **4**, 864–868 (2003).
79. Y. Li, Y. Tang, R. Narain, A. L. Lewis, and S. P. Armes, *Langmuir* **21**, 9946–9954 (2005).
80. K. L. Thompson, I. Bannister, S. P. Armes, and A. L. Lewis, *Langmuir* **26**, 4693–4702 (2010).

81. K. Ishihara, T. Tsuji, Y. Sakai, and N. Nakabayashi, *J. Polym. Sci., Part A: Polym. Chem.* **32**, 859–867 (1994).
82. K. Sugiyama, K. Shiraishi, K. Okada, and O. Matsuo, *Polym. J.* **31**, 883–886 (1999).
83. T. Uchida, T. Furuzono, K. Ishihara, N. Nakabayashi, and M. Akashi, *J. Polym. Sci., Part A: Polym. Chem.* **38**, 3052–3058 (2000).
84. T. Oishi, H. Yamasaki, H. Kada, K. Onimura, H. Tsutsumi, and A. Hayashi, *Polym. J.* **32**, 378–380 (2000).
85. N. Tanigawa, K. Shiraishi, T. Abe, and K. Sugiyama, *J. Appl. Polym. Sci.* **113**, 959–965 (2009).
86. J. Madsen, N. J. Warren, and S. P. Armes, *Biomacromolecules* **12**, 2225–2234 (2011).
87. P. D. Topham, N. Sandon, E. S. Read, J. Madson, A. J. Ryan, and S. P. Armes, *Macromolecules* **41**, 9542 (2008).
88. I. K. W. Lam, S. P. Armes, A. L. Lewis, and S. Stolnik, *J. Drug. Target.* **17**, 512–523 (2009).
89. J.-H. Seo, R. Matsuno, T. Konno, M. Takai, and K. Ishihara, *Biomaterials* **29**, 1367–1376 (2009).
90. J.-H. Seo, R. Matsuno, T. Konno, M. Takai, and K. Ishihara, *Biomaterials* **30**, 5330–5340 (2009).
91. J. H. Seo, T. Shibayama, M. Takaia, and K. Ishihara, *Soft Matter* **7**, 2968–2976 (2011).
92. K. Ishihara, Y. Iwasaki, S. Ebihara, Y. Shindo, and N. Nakabayashi, *Colloid Surf., B* **18**, 325–335 (2000).
93. T. Moro, Y. Takatori, K. Ishihara, T. Konno, Y. Takigawa, T. Matsushita, U.-I. Chung, K. Nakamura, and H. Kawaguchi, *Nature Mater.* **3**, 829–836 (2004).
94. J. Pyun, T. Kowalewski, and K. Matyjaszewski, *Macromol. Rapid Commun.* **24**, 1043–1059 (2003).
95. R. Barbey, L. Lavanant, D. Paripovic, N. Schuwer, C. Sugnaux, S. Tugulu, and H.-A. Klok, *Chem. Rev.* **109**, 5437–5527 (2009) and references cited therein.
96. C. J. Galvin and J. Genzer, *Prog. Polym. Sci.* **37**, 871–906 (2012), doi:10.1016/j.progpolymsci.2011.12.001 and references cited therein.
97. M. Chen, W. H. Briscoe, S. P. Armes, H. Cohen, and J. Klein, *Eur. Polym. J.* **47**, 511–523 (2011).
98. W. Feng, J. L. Brash, and S. Shu, *J. Polym. Sci., Part A: Polym. Chem.* **42**, 2931–2942 (2004).
99. W. Feng, S. Zhu, K. Ishihara, and J. L. Brash, *Langmuir* **21**, 5980–5987 (2005).
100. W. Feng, S. Zhu, K. Ishihara, and J. L. Brash, *Biointerphases* **1**, 50–60 (2006).
101. W. Feng, J. L. Brash, and S. Zhu, *Biomaterials* **27**, 847–855 (2006).
102. R. Iwata, P. Suk-In, V. P. Hoven, A. Takahara, K. Akiyoshi, and Y. Iwasaki, *Biomacromolecules* **5**, 2308–2314 (2004).
103. S. Edmondson and S. P. Armes, *Polym. Int.* **58**, 307–316 (2009).
104. M. Chen, M. H. Briscoe, S. P. Armes, and J. Klein, *Science* **323**, 1698–1701 (2009).
105. B. Barthelemy, S. Devillers, I. Minet, J. Delhalle, and Z. Mekhalif, *Appl. Surf. Sci.* **258**, 466–473 (2011).
106. X. Wang, Q. Ye, T. Gao, J. Liu, and F. Zhou, *Langmuir* **28**, 2574–2581 (2012).
107. T. Hoshi, R. Matsuno, T. Sawaguchi, T. Konno, M. Takai, and K. Ishihara, *Appl. Surf. Sci.* **255**, 379–383 (2008).
108. V. P. Hoven, M. Srinanthakul, Y. Iwasaki, R. Iwata, and S. Kiatkamjornwong, *J. Colloid Interface Sci.* **314**, 446–459 (2007).
109. Y. Iwasaki, Y. Omichi, and R. Iwata, *Langmuir* **24**, 8427–8430 (2008).
110. M. Kobayashi, M. Terada, Y. Terayama, M. Kikuchi, and A. Takabara, *Isr. J. Chem.* **52**, 364–374 (2012).
111. X. Gao, W. Feng, S. Zhu, H. Sheardown, and J. L. Brash, *Macromol. React. Eng.* **4**, 235–250 (2010).

112. D. Zhou, X. Gao, W.-J. Wang, and S. Zhu, *Macromolecules* **45**, 1198–1207 (2012).
113. Kobayashi, M., Y. Terayama, N. Hosaka, M. Kaido, A. Suzuki, N. Yamada, N. Torikai, K. Ishihara, and A. Takahara, *Soft Mater.* **3**, 740–746 (2007).
114. M. Kobayashi, H. Yamaguchi, Y. Terayama, Z. Wang, K. Ishihara, M. Hino, and K. Ishihara, *Macromol. Symp.* **279**, 79–87 (2009).
115. M. Kobayashi and A. Takahara, *Chem. Rec.* **10**, 208–216 (2010).
116. M. Kobayashi, Y. Terayama, M. Hino, K. Ishihara, and A. Takahara, *J. Phys.: Conf. Ser.* **184**, 012010 (2009).
117. K. Kitano, Y. Inoue, R. Matsuno, M. Takai, and K. Ishihara, *Colloid Surf., B* **74**, 350–357 (2009).
118. Y. Inoue, T. Nakanishi, and K. Ishihara, *React. Funct. Polym.* **71**, 350–355 (2011).
119. H. Kitano, K. Sudo, K. Ichikawa, M. Ide, and K. Ishihara, *J. Phys. Chem. B* **104**, 11425–11429 (2000).
120. K. Ishihara, *Trend. Polym. Sci.* **5**, 401–407 (1997) and references cited therein.
121. K. Ishihara, *Sci. Technol. Adv. Mater.* **1**, 131–138 (2000) and references cited therein.
122. A. L. Lewis, *Colloid Surf., B* **18**, 261–275 (2000) and references cited therein.
123. Y. Iwasaki and K. Ishihara, *Anal. Bioanal. Chem.* **381**, 534–546 (2005) and references cited therein.
124. K. Ishihara and M. Takai, *J. R. Soc., Interface* **6**, S279–S291 (2009).
125. K. Ishihara, Y. Goto, M. Takai, R. Matsuno, Y. Inoue, and T. Konno, *Biochim. Biophys. Acta: Gen.* **1810**, 268–275 (2010).
126. S. Monge, B. Canniccion, A. Graillot, and J.-J. Robin, *Biomacromolecules* **12**, 1973–1982 (2011).
127. M. Kyomoto, T. Moro, K. Saiga, M. Hashimoto, H. Ito, H. Kawaguchi, Y. Takatori, and K. Ishihara, *Biomaterials* **33**, 4451–4459 (2012) and references cited therein.
128. T. Goda, T. Konno, M. Takai, T. Moro, and K. Ishihara, *Biomaterials* **30**, 5151–5160 (2006).
129. T. Goda, T. Konno, M. Takai, and K. Ishihara, *Colloid Surf., B* **54**, 67–73 (2007).
130. T. Goda, R. Matsuno, T. Konno, M. Takai, and K. Ishihara, *Colloid Surf., B* **63**, 64–72 (2008).
131. M. Kyomoto, T. Moro, Y. Takatori, H. Kawaguchi, K. Nakamura, and K. Ishihara, *Biomaterials* **31**, 1017–1024 (2010).
132. M. Kyomoto and K. Ishihara, *ACS Appl. Mater. Interfaces* **1**, 537–542 (2009).

KAZUHIKO ISHIHARA  
The University of Tokyo, Tokyo, Japan

## PHOSPHORUS-CONTAINING POLYMERS AND OLIGOMERS

### Introduction

The only valid generalization about phosphorus polymers is that they tend to be flame retardant (1–3). The flame-retardant effect depends heavily on the phosphorus content. The mode of action of phosphorus flame retardants can involve both condensed phase (enhanced charring), protective layer formation, and vapor phase physical and chemical action (4,5). Red (polymeric) phosphorus, despite its combustibility, is a commercial flame-retardant additive. Other features of many

phosphorus polymers are adhesion to metals, metal ion-binding characteristics, and increased polarity (1). Flexible P–O–C linkages tend to impart lower glass transition temperatures. Phosphorus polymers with acid groups are used industrially for ion exchange, adhesion, and scale inhibition. Some form water-soluble coatings, that are used as primers in metal protection and for photolithographic plates. The binding properties have led to dental applications. Cellulose phosphates have found some drug and ion-exchange uses. Academic interest has been stimulated by the relationship of certain phosphate polymers to natural products, such as the nucleic acids.

This review gives most attention to those phosphorus polymers which have attained commercial use or which have been (or currently are) the subject of serious development efforts. Another review encompasses phosphorus polymers of mainly academic interest (6). The commercial examples tend to be specialty polymers, and none has attained large volume usage. One reason is cost. In addition, those polymers having P–O links are usually more hydrolyzable than corresponding C–O bonded polymers, and moreover the phosphorus acids, which are liberated, tend to further catalyze hydrolysis. Hydrolytically stable phosphine oxide types are known but are costly. Another hydrolytically stable class, the POLYPHOSPHAZENES, is discussed in a separate article.

Phosphorus-containing oligomers (low polymers) have been included in this article because they have become more important commercially than high polymers, since they can be used as additives or coreactants to introduce sufficient phosphorus for flame retardancy or some other desired property provided by phosphorus such as metal binding (7–9).

The modification of conventional polymers with small amount of phosphorus additives, reactives, or comonomers to impart flame retardancy (1,7,9) or improve other properties has become commercially significant and is discussed separately in connection with the polymer class being modified.

## Phosphorus-Containing Polymers and Oligomers

**Polymeric Forms of Elemental Phosphorus.** Phosphorus occurs in several allotropic forms. The principal commercial form is white (or yellow) phosphorus; the molecule consists of four phosphorus atoms arranged in a tetrahedron. Heating white phosphorus at 270–400°C, preferably with a catalyst, produces red phosphorus, a stable, nontoxic, high melting, insoluble polymeric solid. Red phosphorus (often stabilized by additives) has been used for many decades as the igniting agent for the striking surface of safety matches. It is insoluble, thermally quite stable, and nontoxic; while it can be ignited, it is surprisingly effective as a flame retardant for plastics, and it is now finding commercial use, especially in Europe to flame-retard nylon 6 and 6.6. Red phosphorus provides a certain degree of flame retardancy in polypropylene (UL94, V-2 rating), but it is ineffective in polyethylene (10). It is useful in flame-retarding polyolefin cable covering in combination with magnesium hydroxide, aluminum hydroxide, zeolite and a melamine (11). Other applications and its mode of action have been reviewed in Ref. (12).

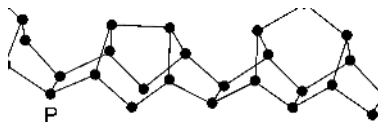


**Fig. 1.** Probable (partial) structure of red phosphorus.

Compounding of red phosphorus is a demanding process, because it requires inert gas blanketing for the whole length of extruder and feeding unit to prevent self-ignition of the powder in contact with high temperature surfaces (13). To prevent decomposition of red phosphorus to the toxic and highly flammable white form, it is stabilized with additives (14) and/or encapsulated with a thermoset resin. Encapsulated grades of red phosphorus have higher autoignition temperature and lower water absorption, and they show better stability in terms of phosphine evolution (15). Even with such stabilization and coating, red phosphorus has been a problem when used as a flame retardant in encapsulated integrated electronic circuits. Its slow reaction with moisture (and probably with air) caused formation of phosphorus acids and eventually electrochemical migration of metal resulting in a short circuit, resulting in device failure (16).

The structure of red phosphorus is not fully established. It is believed (17) to be a cross-linked polymer with chains having fused five- and six-membered rings, as shown in Figure 1.

Two new allotropic “nano-rod” forms of elemental phosphorus consisting of polymeric chains have been isolated from their copper iodide adducts (18).

**Inorganic Phosphorus Polymers.** Inorganic polyphosphates are covalently linked polymers (19,20). Chains of repeating phosphate units are formed by eliminating the elements of water from adjacent orthophosphate units. Such polycondensations take place, for instance, when orthophosphoric acid is heated, producing a broad distribution of linear molecules of various chain lengths corresponding to the general formula  $\text{HO}[\text{P}(\text{O})(\text{OH})\text{O}]_n\text{H}$ . A table showing compositions for various weight percentages of  $\text{P}_2\text{O}_5$  is given in Ref. (21).

Polyphosphoric acid itself has found utility mainly as a supported catalyst in the petroleum industry for alkylation, olefin hydration, polymerization, and isomerization, and for syntheses of fine chemicals and dyes. It is used to phosphorylate alcohol groups, for example, in the production of anionic phosphate surfactants.

Heating of alkali metal or alkaline earth metal dihydrogen phosphates produces cyclic metaphosphates, linear polyphosphates, and cross-linked polyphosphates (ultraphosphates), depending on temperature and the presence of other ingredients (20,21). This complex group of polymers includes materials with crystalline, glasslike, fibrous, or ceramic properties as well as some with thermoplastic and thermoset characteristics; some are useful as binders for metals, ceramics, and dental restorations. Reviews are available on the glasses (21,22), on the crystalline compounds (23), and on polyphosphate fibers (24).

The water-soluble poly- and metaphosphates exhibit chelating properties. Glassy sodium metaphosphate (DP ca (15–20)) is used in water treatment for scale inhibition (25). Long-chain sodium polyphosphates (metaphosphates) are

used as preservatives in red meat, poultry, and fish (25). Long-chain sodium and potassium phosphates are added to sausage meat to improve color and texture (25).

Polyphosphates, even very long chain ones, are produced or found naturally in all classes of organisms. They have been studied especially in prokaryotes where they have many functions including structure and as a stress response agent (26). They have been reviewed in relation to origin and survival of species; it is postulated that polyphosphates may have had a role in prebiotic evolution (27). In yeasts, inorganic polyphosphate may comprise up to 30% of their total phosphate and up to degrees of polymerization of 600 (28). These probably provide energy storage for the yeasts.

Some of the inorganic phosphate polymers possess properties resembling those of glassy organic plastics. Corning has attempted to commercialize low melting phosphate-containing glasses as reinforcing fibers with excellent dimensional stability (29,30). The fibers can be made *in situ* by stirring in a high temperature thermoplastic melt. Phosphate glasses can also be molded at 360–400°C to make high refractive index lenses (31).

Heating of ammonium phosphates under an atmosphere of ammonia or in the presence of urea produces ammonium polyphosphate (32,33). At a high degree of polymerization, the product is a water-insoluble solid. This form of ammonium polyphosphate is used commercially as a flame-retardant additive for plastics and as the latent acid component in intumescent paints, mastics, and caulks (34, 35). The water resistance can be further enhanced by encapsulation with a resin (36).

A melamine salt of polyphosphoric acid is prepared by thermal polymerization of melamine phosphate (37). One such product, MELAPUR 200, developed by DSM in the Netherlands, is now marketed by BASF, one significant use being the flame retarding of polyamides (38).

#### **Polymeric Phosphorus Oxynitrides and Phosphorus Iminoimides.**

Condensed phosphoramides with linear, cyclic, or cross-linked structures are produced by the reaction of  $\text{POCl}_3$  with ammonia. The higher molecular weight products are insoluble in water and on further heating are converted into a cross-linked insoluble polymer, phosphorus oxynitride  $(\text{PON})_x$  (39). Phosphorus oxynitride can be made by prolonged heating of melamine phosphates (40), urea phosphate (40), or ammonium phosphate under conditions where ammonia is retained (41). Phosphorus oxynitride is an effective flame retardant in those polymers such as nylon 6, which can be flame retarded by exclusively char-forming condensed-phase means. However, phosphorus oxynitride is ineffective (at least by itself) in those polymers such as polybutylene terephthalate which are easily pyrolyzed to volatile fuel (42–44).

An imido analog of phosphorus oxynitride, phospham,  $(\text{PN}_2\text{H})_x$ , is also made as the exhaustive self-condensation product of aminophosphazenes but may also be made directly from elemental phosphorus and ammonia or from phosphorus pentasulfide and ammonia (45). Phospham is probably a thermoset phosphazene imide, because it can be also made by heating of hexaminocyclophosphazene (46). It can be amorphous or crystalline. It is also an effective and thermally stable flame retardant, especially for high temperature processed polyamides (47). It was available for a short time as a development product from Japan.

Amorphous polymeric dielectric films of phosphorus nitrides and oxynitrides ("Phoslon") can be prepared on electronic substrates by chemical vapor deposition (48).

### Organic Phosphorus Polymers.

**Phosphines.** Polymeric phosphines exhibit strong metal-binding properties. Nonpolymeric phosphines, in particular triphenylphosphine, are employed as ligands for cobalt and rhodium in hydroformylation catalysts used in plasticizer manufacturing. Extensive efforts have been made to attach phosphine-metal complexes on polymers to facilitate catalyst recovery and enhance selectivity (49). Problems of cost, catalyst life and activity, heat transfer, and mass transfer seem to have prevented their commercialization.

Polymers from diarylphosphinylstyrenes have been prepared as ligands (50). Styryldiphenylphosphine monomer, commercially available in laboratory quantities, is easily polymerized or copolymerized (50,51). Copolymers of styryldiphenylphosphine with divinylbenzene cross-linked with styrene are commercially available in laboratory quantities.

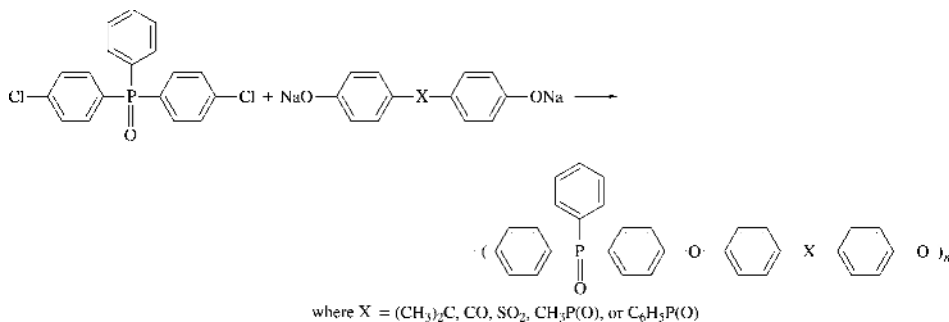
Some polymeric phosphonium salts have been reported to have advantages in reaction rate or ease of separation relative to monomeric phosphonium salts as catalysts for nucleophilic reactions where the large cation favors nucleophilic reactivity of the anion (52).

**Phosphine Oxides.** The outstanding property of polymeric phosphine oxides is their stability. Since the electron pair of the phosphine structure has been donated to an oxygen atom, the phosphine oxide group is unreactive, although it is very polar and is subject to strong hydrogen bonding.

Polymeric phosphine oxides are made by a variety of condensation- and addition-polymerization methods. Radical-initiated copolymerization of compounds with  $\text{RPOCl}_2$  structures and olefins produces polydichlorophosphanes, which on hydrolysis yield polyphosphine oxides (53). Where *p*-xylylene (produced by pyrolysis) is the olefin, this copolymerization affords quite tenacious high temperature thermoplastic phosphine oxides (54).

Polystyrenes with attached phospholene oxide rings are recoverable catalysts for converting isocyanates to carbodiimides (55).

A series of polyesters and polyethers made from aromatic phosphine oxides exhibit stability as well as flame resistance (56,57). Aromatic polyethers containing phosphine oxide structures are made according to the following reaction (57–59):



These polymers show good flame resistance and low smoke, and some have been introduced on a development scale for potential use in graphite composites and as electrical insulation for aircraft. Some polyphosphine oxides have been shown to be suitable for optical applications (60).

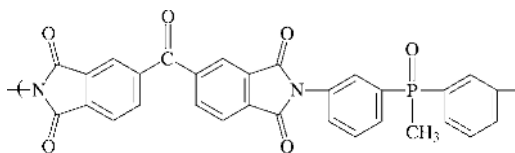
Because of their high thermal and photochemical stability, poly(arylene ethers) with phenylphosphine oxide units in the chain have been proposed for NASA aerospace applications (61).

Aliphatic polyamides with a phosphine oxide unit in the dicarboxylic acid portion or the diamine portion of the polymer chain have been described (62–66). These were intended to have flame resistance while retaining adequate thermal and hydrolytic stability. The effect of the phosphine oxide on softening and heat distortion temperatures of these structures has been studied (67); some show elevated glass transition temperatures ( $T_g$ ) and softening temperatures compared to the phosphorus-free analogues, others show depressed melting behavior and loss of crystallinity. Increasing the content of phosphine oxide depresses the melting point and in most cases the crystallinity. In some cases incorporation of phenylphosphine oxide structures improves thermal properties. Incorporation of triarylphosphine oxide units in the polymer chain improves solubility in aprotic polar solvents (65,66).

Mono-, bis-, and tris(hydroxyaryl)phosphine oxides have been claimed as reactive flame retardants for epoxy composites (68). Bis(*m*-aminophenyl)methyl phosphine oxide was extensively explored in epoxy carbon fiber composites as a curing agent with the intention of use in Airbus airplanes (69). One comparative study showed that the flame retardancy of an aromatic phosphine oxide copolymer was no better than that achieved by a similar amount of phosphine oxide structure as an additive (70).

Aromatic polycarbonates containing diphenylphosphine oxide units attached laterally to the chain (using the diol made by adding diphenylphosphine oxide to benzoquinone) have been shown in a General Electric patent to achieve flame retardancy without loss of  $T_g$  or impact strength (71). The required intermediate, diphenylphosphinous chloride, is commercially available but this application has not been commercialized.

Polyimides (qv) containing phosphine oxide structures have been explored in the quest for highly stable thermoplastics. In the search for flame-retardant, heat-stable composites for aerospace applications, the following structure was prepared:

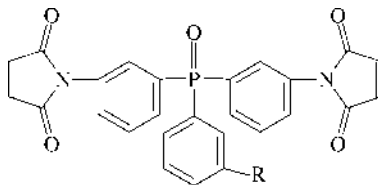


This polymer is stable to 400°C and shows excellent adhesion to glass fiber reinforcement (72,73). Stability is further increased by an ether linkage between the two phosphorus-bonded rings (74).

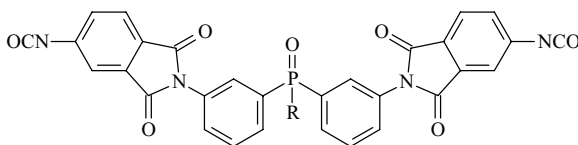
Phosphine oxide containing polyimides were produced at NASA by polymerization of phosphine oxides containing maleimides as illustrated by the following



structure (75):



In an attempt at improving thermal and thermoxidative stability poly-(urethane-imides) as well as obtaining flame retardant properties, phosphine-oxide-containing isocyanates were prepared (76):



where  $R = \text{CH}_3$  or  $\text{C}_6\text{H}_5$

Ammonia cross-linked textile finishes from tetrakis(hydroxymethyl)-phosphonium salts have a primarily phosphine oxide structure and are discussed under the topic of cellulosic textile finishes.

**Phosphinites and Phosphonites.** In common with phosphines, these classes of phosphorus structures have unshared electron pairs on the phosphorus. They tend to be unstable to oxidation and are good metal binders. Consequently, they have been prepared as antioxidant scavengers, catalyst ligands, and ion-extraction reagents, but no commercial applications of polymeric phosphinites or phosphonites are known. A Goodrich patent shows an oligomer made from phenyldichlorophosphine and a dihydric phenol as a polymer stabilizer (77).

**Phosphites.** Phosphites, mostly nonpolymeric, are employed as the peroxide-decomposing components of antioxidant systems for polyolefins and diene rubbers.

Polyphosphites, actually poly(hydrogen phosphonates), have been described as being made by transesterification of dialkyl phosphites with diols, but some examples have been shown to proceed concurrently with dealkylation and formation of acid end groups (78). If the acid end groups are realkylated such as by diazomethane, high molecular weight poly(hydrogen phosphonates) can be made (79). The use of diphenyl hydrogen phosphonate instead of dialkyl hydrogen phosphonate also permits achieving high molecular weight. These phosphite polymers can be oxidized to synthetic analogs of the nucleic acid backbone.

An improved preparation of a poly(alkylene hydrogen phosphonate) by reacting dimethyl hydrogen phosphonate with poly(ethylene glycol) made use of fast heating by microwave (80).

An oligomeric phenyl dipropylene glycol phosphite, averaging eight phosphite groups per mole, is a commercial color stabilizer (Doverphos 12, Dover Chemical Corp.) for rigid and plasticized poly(vinyl chloride). Typical use levels are 0.25–1% in vinyls and polyurethanes.

A lower oligomeric dipropylene glycol phosphite, averaging three phosphite groups and five hydroxyl groups (GE's Weston PTP Phosphite), is used in foamed polyurethanes to control color development and prevent bun scorching.

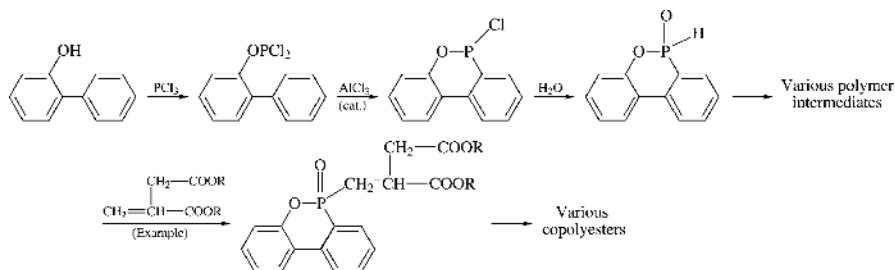
**Phosphinates.** Phosphinate structures confer flame retardancy to polyester fibers, discussed separately later.

Esters of *P*-phenyl-*P*-vinylphosphinic acid can be polymerized to high molecular weight by free-radical initiators. The monomers are prepared from phenylphosphonous dichloride (81).

Oligomeric phosphinic/carboxylic acid copolymers are made by radical-catalyzed polymerization of acrylic and/or maleic acid in the presence of hypophosphorous acid or sodium hypophosphite. The phosphinic unit is incorporated by a chain-transfer reaction (82,83). A phosphonic acid group can be introduced as an end group by chain-transfer polymerization of phosphorous acid with an acrylic acid monomer. Products of this type are effective scale inhibitors for water treatment and are commercially used.

(*P*-Hydroxymethyl)phenylphosphinic acid (an adduct of formaldehyde and phenylphosphinic acid) can be thermally dehydrated to form oligomers, which are useful in flame-retarding polyethylene terephthalate (84). These may have been commercially used in Europe.

A large and varied family of polymers has been made from a cyclic phosphinate, which is made commercially from *o*-phenylphenol by the following reaction sequence:



The key intermediate, a cyclic hydrogenphosphinate, 9,10-dihydro-9-oxa-10-phosphaphenanthrene-10-oxide, has been converted, mostly by Far Eastern manufacturers, to a variety of difunctional polymer intermediates. Addition to itaconic ester produces a dicarboxylic ester commercially used to make thermoplastic polyesters. This technology is discussed later in connection with modified polyester fibers and epoxy resins.

The cyclic hydrogen phosphinate can also be added to benzoquinone to make a substituted hydroquinone and a diglycidyl ether therefrom, discussed later in connection with epoxy resins.

Phosphinates made from acrylic acid and methyl- or phenylphosphonous dichloride are used in small amounts to provide inherent flame retardancy to polyester fibers (see Thermoplastic Polyesters, later).

**Phosphonates.** The principal synthetic routes include addition and condensation methods. Although a large number of vinyl and diene phosphonate monomers have been described in the literature (2,8,12,85), only bis(2-chloroethyl) vinylphosphonate (Akzo-Nobel's now-discontinued Fyrol Bis-Beta monomer), vinylphosphonic acid (Clariant), and dimethyl vinylphosphonate

(Clariant) have been offered commercially. The diethyl vinylphosphonate is available in laboratory quantities.

Vinylphosphonates are slow to homopolymerize. They copolymerize with most common monomers but particularly well with vinyl acetate (86), vinyl chloride, and acrylonitrile (87). The copolymerization  $Q$  and  $e$  values for bis(2-chloroethyl) vinylphosphonate are 0.23 and 1.73, respectively (88), reflecting an electron-poor double bond and low resonance stabilization of the free radical. They are also prone to chain transfer. Representative copolymers have been studied and evaluated for their expected flame-retardant action (89), but cost considerations have generally discouraged commercial use of vinylphosphonate esters for this purpose.

Plasticized vinyl polymers are made by terpolymerization of bis(2-chloroethyl) vinylphosphonate with vinyl chloride and alkyl acrylates (90–93). These terpolymers can be calendered to films and were for a time in commercial development by Stauffer Chemical Co. for use as truck and container decals with permanent plasticity.

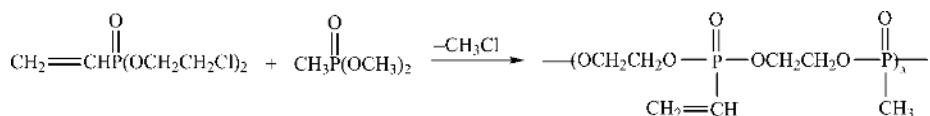
Vinylphosphonic acid is produced in Germany and used, initially by Hoechst later by others, to manufacture a hydrophilic poly(vinylphosphonic acid) prepared by free-radical polymerization in a solvent (94,95). Poly(vinylphosphonic acid) is mainly used for the treatment of aluminum photolithography plates before application of the photosensitive layer (96,97). The coating improves the developing and printing characteristics of the plate. Dental cement applications of cross-linked poly(vinylphosphonic acid) have also been studied (98). Vinylphosphonic acid copolymers with vinylsulfonic acid have been patented as scale inhibitors for water treatment (99).

A study of the binding of various metal cations by a water-soluble poly(vinylphosphonic acid) showed that the polymer-metal interaction was primarily electrostatic (100).

Isopropenylphosphonic acid polymers are water soluble and are believed to have found commercial utility as scale inhibitors (101). A flame-retardant copolymer of alpha-phenylvinylphosphonic acid with styrene has been patented (102).

The tetraethyl ester of 1,1-vinylidenediphosphonic acid has been used to make cross-linked copolymers, which are ion-exchange resins with selective chelation properties for toxic metal cations (103). An alternative method for introducing the diphosphonic acid structure is by the reaction of a methylenediphosphonic ester with chloromethylated styrene copolymer beads (104). At least one such a resin class, Diphonix, also containing sulfonic acid and other functional groups, has shown promise for treatment of radioactive wastes and for iron control in copper electrowinning (105,106). The diphosphonic resins have been reviewed as chelating resins (107).

An oligomeric vinylphosphonate was commercialized in the 1970s as a flame-retardant finish on cotton, principally for children's sleepwear (108).



Upon free-radical initiated curing, usually with a comonomer such as *N*-methylolacrylamide or with an amino resin, this monomer produces a

cross-linked finish for cotton, resistant to laundering (109–111). This product was discontinued in the United States for marketing and cost reasons, but it was later used in Japan for some nonapparel applications.

Vinylbenzylphosphonate diethyl ester was prepared by the Arbuzov reaction of vinylbenzyl chloride with triethyl phosphite, and this monomer was used as a precursor for experimental resins with metal-binding properties (112). The reaction of dialkyl phosphite anions with vinylbenzyl chloride was also used to prepare higher dialkyl *p*-vinylbenzylphosphonates (113). Copolymers of vinylbenzylphosphonate diethyl ester with acrylonitrile and terpolymers with acrylonitrile and styrene were synthesized, and their flame-retardant properties were tested (114). Diphenyl vinylphosphonate, di(2-phenylethyl) vinylphosphonate, and 1,6-phenylene vinylphosphonate were also synthesized and copolymerized with poly(methyl methacrylate) or polystyrene with the purpose of improving flame-retardant performance (115).

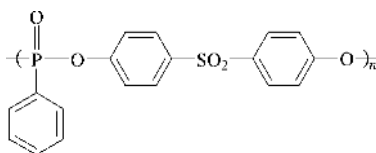
Copolymers of diethyl(methacryloyloxymethyl)phosphonate with methyl methacrylate have recently been shown to have some flame retardancy advantage over phosphorus additives (116). Various acrylate and methacrylate monomers with phosphonic acid groups that aid bonding to dentine have shown promise for dental restoration purposes (117). Various allyl phosphonates (118) have been proposed for these uses, but none appear to have found any application.

Poly(styrene-*co*-diethyl vinylphosphonate) was hydrolyzed and converted to sodium and zinc ionomers. Because of low water absorption, these were unsuitable as exchange membranes (119).

**Condensation Polymerization Routes to Polymeric Phosphonates.** The reaction of a phosphonyl dichloride with an aliphatic diol produces polyphosphonates, which are low melting and hydrophilic. Industrial interest has been focused on the polyphosphonates made from aromatic diols or aromatic phosphonyl dichlorides.

Because of the commercial availability of phenylphosphonyl dichloride (benzene phosphorus oxydichloride, BPOD), much work has been done on this intermediate to make polymeric phosphonates as flame-retardant thermoplastics or as additives for thermoplastics. In an early study, Toy (120) carried out the polycondensation of BPOD and dihydric phenols in a melt. Coover and McConnell added the use of an alkaline earth halide catalyst (121). For enhancement of the flame-retardant effectiveness as fiber additives, tetrabromobisphenols were used to make polyphosphonates (122). Various co-condensed polyesters with both phosphonate ester units and dicarboxylic ester units have been described and patented.

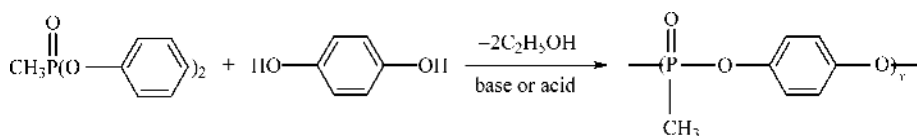
Toyobo in Japan commercially introduced the polymer or oligomer from phenylphosphonic dichloride and 4,4'-sulfonylbisphenol as an additive for polyester fibers, initially to meet the Japanese flame-retardant regulations for home furnishings (123,124).



This oligomer, which seems to have a higher flame-retardant effect than the sulfur-free analogs, has been further studied and piloted in the United States (125–127). Its manufacturing and use has also been developed in China, and it is made there on a commercial scale (128), and its miscibility with poly(ethylene terephthalate) has been studied (129). It was found that this oligomer undergoes partial transesterification when is blended with PET to produce flame-retardant fibers (130).

Interfacial polycondensations for the synthesis of polyphosphonates by the reaction of phosphonyl dichlorides with diols can be very rapid, and under favorable conditions give high molecular weights (131,132).

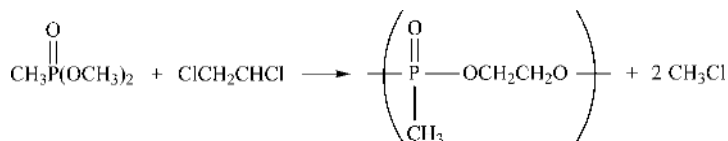
*Transesterification of a Phosphonate with a Diol.* This method proceeds well in the case of *O,O*-dialkyl hydrogen phosphonates (133) but less selectively with *O,O*-dialkyl alkyl- or arylphosphonates. With *O,O*-diaryl alkylphosphonates, ester exchange is an effective route to polymeric phosphonates (134–136):



Process details of a stepwise transesterification have been disclosed (137). A single-step process with catalysis was claimed to produce useful flame-retardant thermoplastics (138). Blends of this polyphosphonate have been claimed with engineering thermoplastics such as poly(butylene terephthalate) with melamine additives to boost flame retardancy (139). Also disclosed were block copolymers of these phosphonates with polyester or polycarbonate blocks (140). Higher molecular weight phosphonate aromatic condensation polymers can be attained by adding tri- or tetrahydric phenols or triaryl phosphates to the reaction mixture (141). A transparent flame-retardant polymethylphosphonate thermoplastic made by this technology was for a time in development by Bayer (135). Mechanical properties were excellent, although resistance to hot water was somewhat deficient. Methylphosphonate aromatic diol higher-molecular-weight polymers are now being further developed as flame-retardant thermoplastics (142). Branched versions are shown to have improved properties (143).

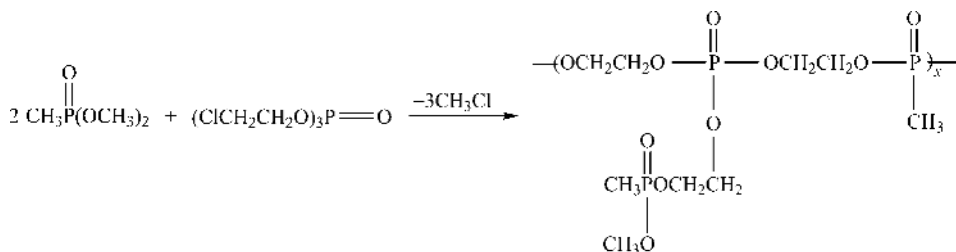
Transesterification has been used to prepare an oligomeric resorcinol methylphosphonate, which shows utility as a reactive flame retardant for epoxy-printed wiring boards (144,145). These are discussed further under Epoxies.

*Transalkylation of a Phosphonate with a Dihalide.* This route is especially useful with *O,O*-dimethyl phosphonates and bis-primary dihalides, for example, in the production of a poly(ethylene methylphosphonate) (146):



The reaction proceeds most readily in the presence of a basic catalyst (12,146). This chemistry was used for the commercial manufacture of a

flame-retardant hydroxyl-terminated oligomer (12,147) suitable for flame-retarding thermoset resins and resin-impregnated paper.

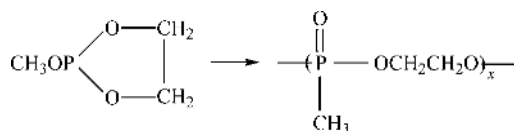


This route was superseded by an alternative halogen-free process using phosphorus pentoxide, as described later.

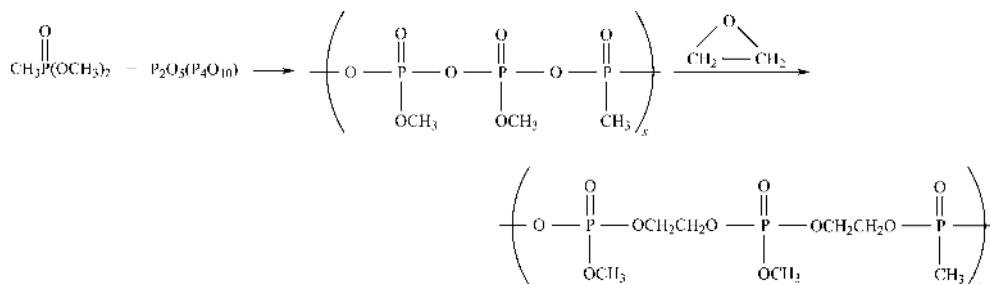
**Arbuzov Polycondensation.** To date industrial applications have been limited to the production of oligomeric flame retardants, such as the conversion of tris(2-chloroethyl) phosphite to a mixture of its intramolecular Arbuzov rearrangement product, bis(2-chloroethyl) 2-chloroethylphosphonate and its oligomeric intermolecular Arbuzov products (148,149).

The detailed structure of the oligomers is open to some question; isomers and branched structures are likely. A product of this reaction, a mixture of monomeric and lower oligomeric compounds, is sold as Antiblaze 78 (A&W, now Albemarle) for flame retardance in urethane foam.

**Arbuzov Cyclopolycondensation.** This versatile reaction and related cyclopolymerizations have been extensively studied (133,150,151). A typical example is the cyclopolycondensation of methyl ethylene phosphite (152):



**Insertion of an Alkylene Oxide into a Phosphonic Anhydride.** A useful route to oligomeric flame retardants is based on the following two-step synthesis (153):



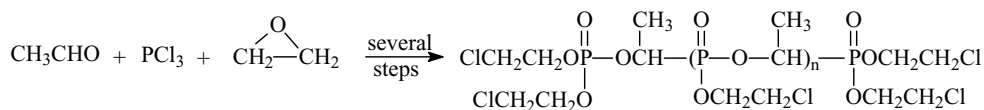
By inclusion of a limited amount of water or alcohol in the synthesis, oligomers of this type can be made with controlled hydroxyl content. Such products are exemplified by Akzo Nobel's Fyrol 51 or Fyrol 58 flame retardants, which

are useful as reactive oligomers in thermosets. In resin-treated automotive air filters, this type of product is chemically linked to the resin and resists leaching by water when the filters are cleaned. Fyrol 51 has also found utility in making flame-retarded polyurethanes. As a wash-resistant textile finish when cured with aminoplasts on cotton or certain blends, it was introduced by Akzo Nobel (Supresta) as FYROLTEX HP (154,155). It later became available from Asheville Lubricants & Chemicals as ALC HP51. Combinations with aminoplasts have been extensively studied at University of Georgia as durable flame-retardant finishes for cotton (156,157) and cotton-nylon blends (158). Formaldehyde-free finishes on cotton were also produced with this phosphonate-phosphate oligomer and, as a coreactant, butane-1,2,3,4-tetracarboxylic acid (159).

*Insertion of a Diepoxide into a Phosphonate Ester.* The insertion reaction of bisphenol-A diglycidyl ether with diaryl aryl- or alkylphosphonates was shown to give polyphosphonates of moderate molecular weight (160).

*Addition of an Olefin to a Hydrogen Phosphonate Oligomer.* As described in a Rhodia patent, transesterification of a dialkyl phosphite (hydrogen phosphonate) with a diol provides a hydrogen phosphonate oligomer, which is then treated with an olefin under peroxide-initiated addition conditions. Thus, oligomeric hexamethylene C<sub>2</sub>-C<sub>10</sub>-alkylphosphonates are described as useful halogen-free flame-retardant additives for polyurethane foams (161).

*Condensation of Phosphites with Aldehydes or Ketones.* A phosphonate flame-retardant oligomer, PHOSGARD C22R (formerly made by Monsanto, possibly still made in Japan) has been used commercially as an additive in acrylics and thermoset plastics (162).



A related product was developed at Rohm and Haas Co. from acetone, ethylene glycol, and PCl<sub>3</sub>, and may have been used in flame-retarded acrylic sheets (163,164).

*Friedel-Crafts Reaction of PCl<sub>3</sub> on Styrenic Polymers, Followed by Oxidation.* Ion-exchange resins with selective affinity for lanthanides and other "hard" cations have been made by the aluminum chloride catalyzed reaction of PCl<sub>3</sub> with macroporous cross-linked styrenic resin beads. The initially formed phosphonous dichloride was hydrolyzed and oxidized to a resin with phosphonic acid groups (165).

*Phosphonylation of a Carboxylic Acid Polymer.* The reaction of a water-soluble polycarboxylic acid with phosphorous acid is said to yield a polymer with hydroxybis(phosphonic acid) structures. These are effective scale inhibiting agents for aqueous systems (166) but not known to have been commercialized. A similar reaction in a Chinese study is said to have resulted in the replacement of carboxyl groups by phosphonic acid groups (167) to produce polymers with similar utility.

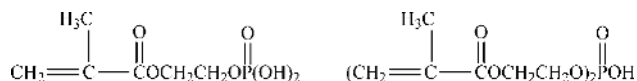
*Phosphates.* Polymeric phosphates are used for the preparation of flame-retardant polymers, ion-exchange resins and models for natural biopolymers such

as nucleic acids, teichoic acids (components of bacterial cell walls) (136), and polynucleotides, which are discussed in a separate article. Synthetic poly(1,3-alkylene phosphates) as mimics of the natural teichoic acids have been studied, particularly in respect to  $\text{Mg}^{2+}$  binding and ion transport (168).

Addition polymerization of unsaturated phosphate monomers has been extensively investigated, but to date only a few industrial applications have been found. Dental anticaries applications of phosphoenol pyruvate polymers and copolymers with acrylic acid have been demonstrated *in vitro* (169).

Monoallyl phosphates undergo chain transfer at the allylic methylene group and polymerize poorly (118). Triallyl phosphate polymerizes with free-radical initiation to a hard, clear cross-linked polymer. This monomer was briefly piloted by the former Marbon Co. but not successfully commercialized.

Acid phosphate monomers made from hydroxyethyl acrylate or methacrylate and  $\text{P}_2\text{O}_5$  are useful acrylic or epoxy coating components and dental adhesives (170), and promote adhesion to metal substrates (171–174). The mono(methacryloxyethyl) phosphate and di(methacryloxyethyl) phosphate are available as Kayamer PM-1 and PM-2 from Nippon Kayaku, or the mixture as Ebecryl 170 from UCB Radcure:



Related monomers with longer polyether chains between the polymerizable group and the acid phosphate and a high monoester to diester ratio are available as Rohm and Haas Sipomer PAM-100 and PAM-200 (methacrylates) and PAM-300 (acrylate). These are useful comonomers for producing coatings and adhesives with improved wet and dry adhesion to metals, as well as scrub resistance and corrosion resistance (175).

**Polycondensation of Phosphoryl Dihalides with Diols.** Poly(arylene aryl phosphates) can be made stepwise by first preparing a phenyl phosphorodichloridate which reacts with a dihydric phenol or in one step by the reaction of phosphorus oxychloride with a mixture of monohydric and dihydric phenols.

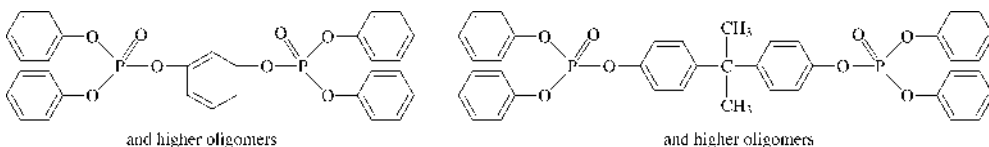
Depending on the reactant ratio, the products can be oligomers or high molecular weight thermoplastic or thermoset polymers. Aromatic phosphate polymers were found to have good transparency, hardness, and adhesion but were too brittle and hydrolytically unstable (176).

Improvements in this process to obtain arylene aryl phosphate polymers with more linear structure and essentially free of chlorine are described by GE inventors (177).

Oligomeric aromatic phosphates have been patented and commercially used as flame-retardant additives mainly for impact-resistant polystyrene blends with polyphenylene oxide and polycarbonate blends with acrylonitrile–butadiene–styrene copolymers (178,179). They have also been shown useful in thermoplastic polyesters (122). The principal commercial examples are based on phenol and resorcinol (Israel Chemical Ltd. Industrial Products (ICL-IP), ex. Akzo-Nobel's Fyrolflex RDP) or phenol and bisphenol A (ICL-IP's Fyrolflex BDP or Albemarle's Ncendx P-30). Although these have the diphosphate as their principal ingredient,



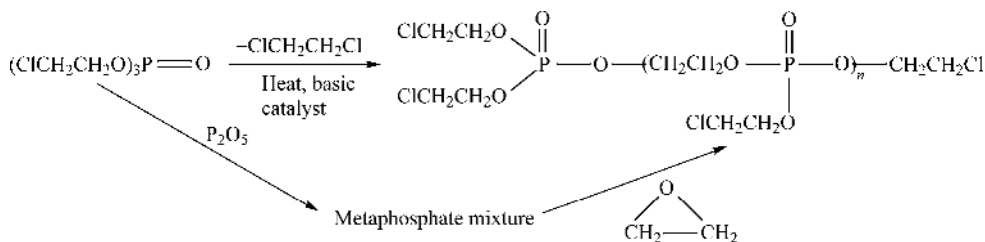
they also contain higher oligomers.



Some patents and publications suggest advantages of flame retardancy for the higher oligomers (180,181). However, some recent patents show the advantage of using of the blend of high molecular weight polyphosphate (10,000) and diphosphate (182) or monophosphate (183). A systematic study of the oligomers and polymers made from alkyl and aryl dichlorophosphates and dihydric phenols showed that their flame retardancy (as expressed by oxygen index) is a function of phosphorus content and thermal stability (184).

A study was made of the comparative hydrolytic stability of eight arylene phenyl phosphate polymers made by interfacial polymerization; the biphenol polymer was found most stable (185).

*Insertion of Phosphorus Pentoxide into a Phosphate Followed by Epoxide Insertion.* The insertion of phosphorus pentoxide into a trialkyl phosphate or a tris(haloalkyl) phosphate produces oligomeric metaphosphoric anhydrides which, upon further insertion of an epoxide into the P-O-P linkages, affords oligomeric phosphates. An older route for the chloroethyl phosphate oligomers used a transalkylation reaction for polycondensation, producing dichloroethane as a by-product.



By inclusion of a proton source, such as  $\text{H}_3\text{PO}_4$ , water, or alcohol, these oligomers can be made with hydroxyl functionality. Thus, a hydroxyl-terminated ethyl ethylene phosphate, Exolit OP 550, is made from triethyl phosphate,  $\text{P}_2\text{O}_5$ , phosphoric acid, water, and ethylene oxide. It was made at Hoechst (186) and has been introduced by Clariant as a reactive flame retardant for polyurethane foams (187); related oligomers were made earlier at Stauffer (188).

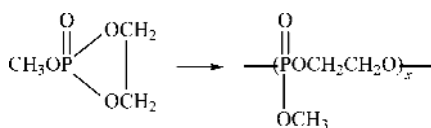
The reaction of triethyl phosphate,  $\text{P}_2\text{O}_5$ , and ethylene oxide, omitting the addition of a proton source unlike the preceding synthesis, produces a substantially nonfunctional oligomer. A product of this type, Supresta's (later, ICL-IP's) Fyrol PNx, has been introduced as a high efficiency flame retardant for flexible or rigid polyurethane and polyisocyanurate foams. Because of its oligomeric character, it has low vapor emission (thus freedom from window fogging) in applications such as automobile seating (173,189). Because of the high percentage of phosphorus (19%), it is quite efficient and as little as 5 parts per 100 parts of polyol is

effective in passing the California 117 test and MVSS 302 in a 1.5–1.8 lb/(cu ft) foam. Marketing in Europe is favored by a trend to nonhalogen-containing flame retardants. Enhanced flame-resistant properties are claimed with blends of this oligomeric phosphate with a monophosphate (190).

**Diepoxide Reaction with Phosphoric Acid.** The reaction of phosphoric acid with diepoxides can produce linear polymers or gels, which can be hydrolyzed to water-soluble poly(alkylene phosphates) (191,192).

**Polycondensation of Compounds Containing a Phosphate Linkage.** Polycondensation of tris(2-chloroethyl) phosphate, preferably in the presence of a nucleophilic catalyst, affords an oligomeric phosphate which was for a time produced by this process as a flame retardant for polyurethane foams, thermoset resins, and air-filter products (193–195). A preferred method, avoiding a chlorinated coproduct, is based on addition to the tris(2-chloroethyl) phosphate of phosphorus pentoxide and ethylene oxide as discussed earlier.

**Cyclopolymerization of Five- or Six-Membered Ring Phosphates.** Poly(ethylene methyl phosphate) is formed from cyclic methyl ethylene phosphate (150).



The reaction is thermally reversible, and consequently, polymers and oligomers with P(O)OCCOP(O)O linkages cannot be used in high temperature applications.

Production of poly(alkylene hydrogen phosphates) can be accomplished by ring-opening polymerization of cyclic hydrogen phosphonates followed by oxidation (eg, by chlorination and hydrolysis). The intermediate chloride can also be converted to esters or amides (151).

An overview of the preparation of alkylene phosphate polymers by ring opening and by transesterification (usually of hydrogen phosphonates followed by oxidation), with an overview of the hydrolytic and metal-binding properties of these polymers, has been published by Penczek and co-workers (196). Poly(alkylene acid phosphates) with two- and three-carbon units, made via diphenyl hydrogen phosphonate transesterification and oxidation of the P(O)H group, have been reviewed in the context of biomimetic molecules and shown to control calcium carbonate crystallization in a process related to biomineralization (197). Bone tissue engineering applications are indicated for related phosphoester polymers (198).

**Phosphorus–Nitrogen Polymers.** The most extensively investigated class of such polymers is the polyphosphazenes which have been reviewed in regard to flame retardancy (199) and which are discussed in a separate article in this Encyclopedia. The phosphazenes, comprising a family of cyclic oligomers (principally trimers and tetramers) and linear polymers of the general formula  $(\text{--N--PRR'})_x$ , usually produced by displacement of chlorines from  $(\text{--N--PCl}_2)_x$ , have been very extensively investigated, with limited practical accomplishment to date. A recent

book with chapters by experts in this field comprises a thorough review (200). Elastomers where R and R' are trifluoroethoxy or aryloxy, such as Ethyl Corporation's EYPEL, were in the market for a time, mostly finding military uses and possibly pipeline sealants where their range of high and low temperature properties and solvent resistance was advantageous and the high price could be tolerated. Some rather promising applications in biocompatible dental prostheses, biodegradable surgical repair, controlled drug release, and selective membranes for gas separation and fuel cells are at the research stage but progress with these uses has been deterred by difficult availability of the phosphazene polymers. Some usage of a mixture of cyclic and oligomeric phenylphosphazenes as flame retardants in electronic plastics and printed wiring boards is known in the Far East (Otsuka's SPB-(100)). Research on polymeric phosphonamides and phosphorimides has not as yet led to commercial use.

**Condensation Polymerization of Phosphonyl Dihalides or Phosphoryl Di-Halides with Diamines.** Polyphosphonamides have been prepared by interfacial reaction of phenylphosphonic dichloride with diamines (131,201); these products have apparently not been commercialized. Polyphosphonic amides have been shown to have useful flame-retardant efficacy in polyolefin formulations with other phosphorus additives (202). Film-forming polyphosphoramides (203) form reverse osmosis membranes impervious to urea and appear to have promise for artificial kidney applications.

**Condensation Polymerization of Phosphonate Esters or Diamides with Diamines and Related Reactions.** Treatment of diphenyl methylphosphonate with diamines produces thermoplastic materials with elemental compositions corresponding to polymeric phosphonamides or imides (134,204,205).

**Phosphorus-Modified Plastics, Resins, and Textiles.** In many cases, only a small quantity of phosphorus is introduced by various means into a polymer to achieve desired properties such as flame retardancy or improved adhesion.

**Polyolefins.** Polyethylene can be phosphorylated with phosphorus trichloride and oxygen by a free-radical chain reaction (206–208). Side reactions include separate oxidation of the phosphorus trichloride and of the polymer. Hydrolysis gives phosphonic acid structures, which can impart flame retardancy and improve adhesion to surfaces. These materials have been explored for dental and bone therapy applications but no commercial use is known.

**Styrenic Resins.** The introduction of phosphorus acid groups into polystyrene gives ion-exchange resins with different selectivities than the usual sulfonated types. In one method  $\text{PCl}_2$  groups are attached to the aromatic ring by the reaction of polystyrene (or cross-linked styrene–divinylbenzene copolymer) with phosphorus trichloride with an aluminum chloride catalyst (209). After hydrolysis and oxidation, the aromatic rings contain  $\text{P}(\text{O})(\text{OH})_2$  groups. Hydrolysis alone gives polystyrenes with phosphinic acid groups (210). Polystyrenes with phosphonic or phosphinic acid groups show selective ion-exchange properties toward metals (211). Low molecular weight polystyrene with chloromethyl phosphonate end groups was obtained by quenching living polymerization of styrene with  $\text{POCl}_3$  and subsequent reaction with methanol (212). This polymer showed surprisingly good flame retardance performance.

A series of phosphorylated ion-exchange resins based on polyols reacted with poly(vinylbenzyl chloride) have been evaluated in detail as bifunctional

coordinating ligands for divalent transition metals (213) (see ION-EXCHANGE RESINS; STYRENE POLYMERS).

A macroporous polystyrene-divinylbenzene with sodium phosphonomethylaminomethyl groups has been marketed as Duolite ES-467 ion-exchange resin (Rohm and Haas Co.), which is highly effective in chelating divalent metal cations. It removes traces of calcium from saturated sodium chloride brine, such as the feed streams to chlorine-caustic electrolytic cells (214). This resin has also high affinity for lead and zinc, and has been used for treating industrial waste streams and cooling-tower waters.

*Vinyl and Acrylic Polymers.* Vinyl and acrylic polymers containing phosphorus are prepared from a phosphorylated monomer or by treating the polymer with a phosphorus compound.

Phosphonate groups are introduced into poly(vinyl chloride) via the Arbuzov reaction with a trialkyl phosphite (206), although this reaction is slow, accompanied by dehydrochlorination of the PVC and by intramolecular Arbuzov rearrangement of the phosphite (215,216). However, this reaction of phosphites may play a role in stabilizing poly(vinyl chloride), where the phosphite may react with stability-impairing reactive chlorines such as allylic chlorines; other mode-of-action hypotheses involve its reducing ability or radical-capturing ability.

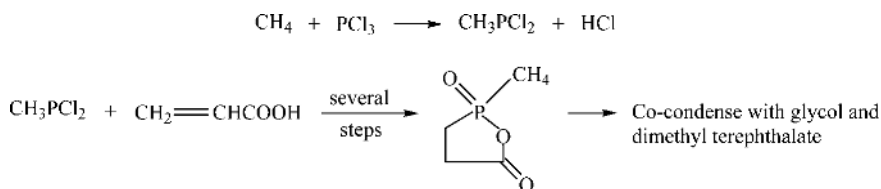
Acrylic dental adhesives have been modified with a phosphate ester linkage by the reaction of a glycidyl methacrylate or hydroxyethyl methacrylate with phosphorus oxychloride (217). One such product, a 3M Scotchbond, adheres to dentine as well as to tooth enamel. Adhesion to enamel can be improved in dental bonding cements by including an acryloxyalkyl- or acryloxyaryl acid phosphate component (218). Japanese products utilize an unsaturated phosphinic acid monomer to improve adhesion (219).

Phosphorus acid groups can be introduced into acrylic acid polymers by the use of chain transfer during polymerization in the presence of phosphorous acid (which provides a phosphonic acid end group) or hypophosphorous acid (which can provide a phosphinic acid middle or end group) (220). Certain water-soluble polymers of the Belclene 700 series (originally Ciba Geigy, later FMC) contain phosphinic or phosphonic acid groups believed to have been made in this manner. These polymers are effective scale inhibitors and can be used in industrial and institutional washing formulations to aid soil removal and dispersion with control of water-hardness deposits.

Dimethyl 2-(methacryloyloxy)ethylphosphonate was commercially used in flame-retardant acrylic coatings (221). Phosphorus-containing polyol with pendant phosphinate groups was made by reacting DOPO-itaconic acid condensate (see below Toyobo product) with ethylene glycol. In the second step this diol was either reacted with an excess of diisocyanate and endcapped with hydroxyalkylacrylate or esterified with acrylic acid. These phosphorus-containing urethane acrylates and ester acrylates were tested in commercial coatings (221).

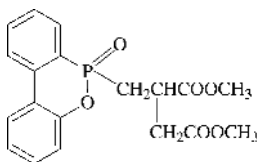
*Thermoplastic Polyesters.* Cocondensation with a phosphorus acid, diol, or diester introduces a small amount of phosphorus into polyesters for flame retardancy, color stability, electrical properties, or antistatic properties. Hoechst and Toyo Spinning (Toyobo) have increased the flame retardancy of poly(ethylene terephthalate) fibers by incorporating small amount of phosphinates.

The Hoechst technology is shown by the following sequence (222,223):



The flame-retardant polyester fiber is marketed (originally by Hoechst, later by Ticona as Trevira CS, now by KoSa as Avora FR) is used for decorative fabrics and curtains, upholstery fabrics, hospital beddings, and sleeping bags. These fibers also exhibit low smoke evolution, good appearance, and light stability.

Technology originally developed at Toyobo for polyester fiber places the phosphinate group on a side chain in a modified poly(ethylene terephthalate) by co-condensation with a phosphinate of the following structure (224–226):



This is an addition product of a hydrogen phosphinate with dimethyl itaconate. Poly(ethylene terephthalate) with this diester reacted with the chain has good textile fiber properties besides flame retardancy (227). It was found that placing the phosphorus ester linkage in the side chain, instead of in the main chain, afforded superior hydrolysis resistance (228) and thermal stability (229,230). A diol with the same ring system can also be used to make other phosphorus-containing thermoplastic polyesters (231).

Numerous patents disclose alternatives for flame-retarding polyester fibers by introducing a small amount, such as less than 1%, of phosphorus. The co-condensation of less than 1% of phenylphosphonic acid into the polyester has been claimed sufficient to flame-retard it to a Japanese standard (232). An Italian development is a polyester fiber made by transesterifying the oligomer of phenyl(hydroxymethyl)phosphinic acid into molten polyethylene terephthalate (233).

**Polyester Resins (Thermoset).** Many patents describe polyesters containing an alkylene oxide reaction product with a phosphonic or phosphoric acid to promote flame retardance; some patents describe transesterifying a neutral or acid phosphate directly into the reaction mixture (234).

Small amounts of phosphorus sufficient to induce flame retardancy are incorporated by transesterification of dimethyl methylphosphonate or other phosphonates with unsaturated polyester resins (235,236).

The phosphorus can also be introduced in the form of vinylphosphonate for copolymerization with styrene in the curing step. Polyesters of this type,

with bis(2-chloroethyl) vinylphosphonate as part of the cross-linking system, were marketed for a time (237). The only use of phosphorus compounds in any significant volume in polyester resins has been that of triethyl phosphate or dimethyl methylphosphonate for viscosity reduction and flame retardancy in filled polyester sheet-molding compositions.

**Polyamides.** Bis(carboxyethyl)alkylphosphine oxide units can be introduced into the backbone of nylon 6,6 to impart flame retardancy with minimal sacrifice of physical properties (57,238). 2-Carboxyethyl phenylphosphinic acid can be incorporated into the backbone of nylon 6,6 during polymerization that provides flame retardancy to carpets manufactured with nylon fibers (239). This phosphinic acid was shortly marketed by Monsanto and then Solutia as a Phosgard. Despite much effort on this approach, these products failed to reach commercialization probably for cost reasons. Small amounts of bis(carboxyethyl)methyl phosphinic acid salts can be introduced into the chain of polyamide 6,6 to impart inherent flame retardancy and stain resistance to carpet fiber (240).

**Epoxy Resins.** In the combustion of epoxy resins, phosphorus inhibits the evolution of fuel gases and increases char (241). Increasing oxidation state of the phosphorus appears to be correlated with increased char (242). For reviews, see Refs. 243–245. Much attention has been given to phosphorus additives or reactives in epoxy resins used as coatings for the purpose of increased adhesion to surfaces (246,247) as well as for fire resistance. The use of phosphorus reactives in epoxy aircraft structures has been surveyed with a comparison of various types (248). Recently, a great deal of effort has been given to phosphorus-containing flame-retarded electrical/electronic laminates and encapsulated electronic parts; here also, both additives and reactives have been investigated.

Some of this effort has been directed to the replacement of tetrabromobisphenol-A, a major reactive component of circuitboards (wiring boards). Extensive development of flame-retarded halogen-free circuit boards has taken place especially in Europe and the Far East to find alternatives to tetrabromobisphenol-A based epoxy circuitboards. This effort is motivated by EU disposal regulations, and halogen avoidance as a marketing tactic. The use of phosphate ester additives usually depresses the thermomechanical properties excessively, so that the use of reactive phosphorus compounds has been the preferred approach.

Phosphorus can be introduced into epoxy resins in diverse ways using reactive means. Diglycidyl phenylphosphonate (249) has been found useful for electronic epoxy products but cost has retarded its commercial development.

Phosphorus can be introduced into epoxy resins by introducing phosphorus halides prior to cure or as a curing step (in either case, a beta-chloroalkoxy phosphorus ester structure is produced), but these reagents are generally too corrosive and labile, and this approach has not been commercialized. Incorporation of phosphoric acid (250) or polyphosphoric acid (251) has shown somewhat more promise. Epoxy resins modified by the reaction with alkyl acid phosphates such as butoxyethyl acid phosphate had development efforts by Dow Chemical Co. (252). Extensive study was done at Ford Co. on epoxy coatings, with alkyl acid phosphates reacted into the epoxy structure (172) for purposes of protective coatings

on steel. The reaction of dialkyl or diphenyl phosphates with epoxy resins and subsequent curing gave products with intumescent flame-retardant properties but diminished thermal stability. The use of diphenyl phosphate raised the glass transition temperature (253) in some epoxy resins. The reaction of epoxy groups with phosphorus acids generates 2-hydroxyalkyl phosphate or phosphonate linkages, along with hydroxy(polyoxyalkylene) phosphates or phosphonates, and also some self-condensation of the epoxy groups. Where self-condensation occurs, gelation may occur.

Oligomeric phosphoric/phosphonic anhydrides can be incorporated into epoxy resins to make prepolymers or used as curing agents (254–256).

The chain extension of epoxy resins can be conducted with dihydric phenolic resins containing phosphate linkages. Bis(3-hydroxyphenyl) phenyl phosphate can be used as a chain extender for epoxy resins and can afford a UL-94 V-0 level of flame retardancy with phosphorus content as low as 1.5% after cure (257). However, the glass transition temperature ( $T_g$ ) is lowered by the flexible phosphate group. Curing with a melamine phenolic novolac can raise  $T_g$  and improve the flame retardancy (258).

Chemtura has patented a series of bis(4-hydroxyphenyl) aryl phosphine oxides, which are incorporated in the epoxy via a chain extension reaction and used to produce flame-retardant epoxy laminates (68). A more cost-efficient mixture of 4-hydroxyphenyl phenyl phosphine oxides is recommended for use in the same application in combination with aluminum hydroxide (259). A mixture of epoxy monomers made by reacting these 4-hydroxyphenylphenyl phosphine oxides with epichlorohydrin was also prepared (260).

The problem of achieving a high  $T_g$  in a circuitboard laminate (to avoid distortion during soldering) is alleviated by the use of a pendant rigid phosphorus-containing ring structure, namely the 9,10-dihydro-9-oxa-10-phosphaphenanthrene 10-oxide (DOPO) group, the synthesis of which was shown earlier. Some mechanism studies suggest that this structure owes its flame-retardant efficiency at least in part to the release of a phosphorus species into the flame with inhibitory consequences (261).

The DOPO ring system has been used in epoxy resins as well as in thermoplastic polyesters (see that topic above). It has been the subject of many patents and publications and is commercially produced in Europe and the Far East. Its original use was in Toyobo's flame-retardant polyester fiber, in the form of the itaconic ester adduct, discussed above.

The hydrogen phosphinate itself can be reacted directly into epoxy resins to produce presumably a beta-hydroxyalkyl phosphinate structure (262,263). However, this consumes epoxy functionality and creates chain ends which will affect mechanical properties.

A more selective means for incorporation of this ring system is to react the hydrogen phosphinate with benzoquinone by reductive addition to produce the phosphinyl-substituted hydroquinone (264). This diol can be used as a chain extension reagent with an epoxy resin to obtain flame retardancy with an improvement of  $T_g$ . A still further elaboration of this cyclic structure is the reaction of the hydroquinone with epichlorohydrin and base to make a diglycidyl ether (265), which can be used as part of the epoxy resin.

The same ring system can also be introduced into a novolac hardener by phosphinylation of one or more of the hydroxyl groups of the novolac, leaving the remaining groups to serve for the cross-linking (266). DOPO can also be reacted with pararosaniline (267) or diaminobenzophenone (268) to produce amine functional curing agents for epoxy.

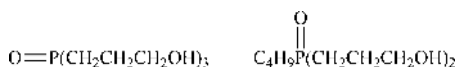
Other stable phosphorus groups can be placed as side chains in epoxy resins. Addition of diphenylphosphinous chloride under hydrolytic conditions to benzoquinone affords (diphenylphosphinyl)hydroquinone, which can also be used as a flame-retardant component in epoxy resins (269).

A cyclic neopentyl hydrogen phosphonate can be added to the epoxy group to impart flame retardancy although the creation of an end group does tend to lower  $T_g$  (270).

A poly(1,3-phenylene methylphosphonate), Supresta's (now ICL-IP) Fyrol PMP, can be reacted with an epoxy resin to afford a flame-retardant cured product suitable for glass-fiber-reinforced electronic circuit boards. The cured product, because of insertion of epoxy groups into the phosphonate ester linkage (271), has a high cross-link density and high  $T_g$ , suitable for lead-free soldering (272–275). Lower levels of the phosphonate can be used if a filler such as ATH, or optionally, a benzoxazine resin, are also added (276).

Phosphonated aromatic diamines (277–279) can serve as flame-retardant curing agents for epoxy resins. Phosphoramides (280–282) and bis(aminophenyl)methylphosphine oxides (283) have been evaluated in the quest for stable, fire-resistant epoxy composites for aerospace applications. Tris(aminophenyl) phosphate, made from *m*-aminophenol and triphenyl phosphate, showed promise in Bayer research for reaching a UL-94 V1 rating with acceptable properties for printed wiring board use (284). A triaminoethylphosphorotriamide as a cross-linking agent for a flame-retardant epoxy has been studied in Hungary (285,286).

Phosphine oxide diols and triols were shown at FMC to be excellent reactive flame retardants or synergists with good thermal and hydrolytic stability in epoxy resins (287).



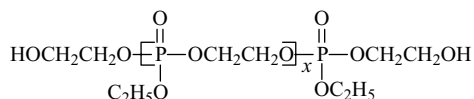
Their cost has retarded commercialization. The diol, where the alkyl group is isobutyl, is available on a development scale from Cytec as Cyagard RF-1243. It has been shown to have the necessary stability to react into an amine-cured epoxy formulation to provide a V0 rating (288).

**Polyurethanes and Isocyanurate-Modified Polyurethanes.** Phosphorus flame retardants, both additive and reactive, are used in large quantities in polyurethanes (qv). Rigid urethane foams employed in thermal insulation must adhere to stringent fire regulations. Flexible foams used in automotive seating must pass the MVSS-302 fire standard; in furniture foam, they must pass the California state standards or other local fire codes, and (if exported), European standards.

Additive flame retardants continue to dominate the flexible foam market despite extensive work on reactive phosphorus compounds (289,290). A



phosphonate-phosphate diol (9) has been used as a component of a blended flame retardant for flexible polyurethanes. A reactive phosphate diol has been introduced by Clariant as Exolit OP-550 (170). This is a mixture, approximately represented by the following formula:

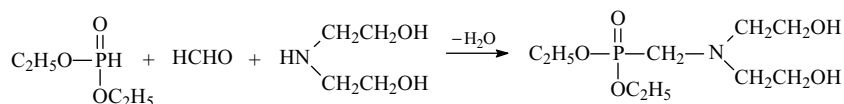


A related structure with low enough hydroxyl content to be considered as an additive, Fyrol PNx (Supresta, now ICL-IP), is also used in flexible polyurethane foams. It is discussed further above, under phosphates (172,173).

Reactive flame retardants have long been used in rigid foams. A successful early example, the diol VIRCOL 82 (Rhodia, now Albemarle), is a phosphate diol made by reaction of dibutyl acid pyrophosphate with propylene oxide (291).

Monohydric alcohols containing phosphorus can also be used to flame-retard polyurethanes. For example, a Daiichi patent shows the use of a cyclic neopentyl hydroxypropyl phosphate used as the reactive flame retardant in flexible foams (292).

A phosphonate diol (Akzo-Nobel's, now ICL-IP's Fyrol (6)) has been used in rigid foams, but is currently used mostly in urethane elastomers. It is a condensation product of diethanolamine with formaldehyde and diethyl phosphonate (293):



The diol structure permits permanent incorporation of the phosphonate group into urethane foams or elastomers. The phosphonate linkage is on a side chain rather than in the backbone of the polyurethane, which increases the hydrolytic stability, and the amino group aids catalysis, a useful feature in spray foam.

A diol containing a phosphine oxide structure (see Epoxy Resins' discussion) was shown to be useful in urethane coatings, adhesives, and rigid foams, as well as in epoxies (260,261,294). Advantages included shelf stability of the amine catalyst-polyol mixture, low smoke, and good resistance to humidity (295).

A phosphorus-containing isocyanate can also be employed, although  $\text{P}(\text{O})\text{N}=\text{C}=\text{O}$  types, in general, are expensive to synthesize and, moreover, give hydrolytically unstable urethanes. The only phosphorus-containing isocyanate currently on the market is Bayer's Desmodur RFE, a solution in ethyl acetate of tris(*p*-isocyanatophenyl) thionophosphate (296). This compound is not employed in urethanes. It is a cross-linking agent for adhesives and is used to increase bonding to rubber and plastic substrates and resistance to heat and solvents. The mode of flame-retardant action of some phosphonate-containing polyurethanes has been shown to involve formulation of a protective phosphorus-containing

layer (297). The mode of degradation of a polyurethane-containing phosphoric acid groups was studied and found to give an enhanced char yield (298).

**Phenolic and Amino Resins.** Numerous patents describe incorporation of phosphorus to increase flame retardancy. Paper impregnated with phenolic resins or amino resins, such as that used in automotive air filters, is treated with oligomeric phosphates or phosphonates (9). Being low in volatility, they are retained during use. Large air filters must retain the flame retardance during washing and reuse; reactive (hydroxyl-terminated) phosphonate-phosphate oligomers are used for this application (299). Such structures presumably become chemically bound to the resin by formation of ether linkages.

Electronic circuitboards based on phenolic resin can be flame retarded by aryl phosphates including oligomeric types made by transesterification of aryl phosphates with novolacs (300). These partially phosphorylated novolacs are then incorporated into the thermoset structure.

**Cellulosic Resins.** In general, phosphorylation of cellulose or treatment of cellulose with phosphorus-containing resins produces a flame-retardant effect by increasing char yield although lowering the decomposition temperature somewhat. The mechanism has been extensively studied (301,302).

The direct phosphorylation of cellulose has been studied extensively, particularly to prepare flame-retardant cotton fabric or paper and ion-exchange materials (303). Heating cellulose with phosphoric acid results in little phosphorylation and much degradation. However, in the presence of urea or dicyandiamide, a sufficient degree of phosphorylation is achieved to impart self-extinguishing properties while allowing retention of useful strength. Such processes have been employed for semidurable, flame-retardant finishing of draperies. Resistance to a few washes and less acid degradation is achieved by using an amino resin such as a methylolurea or methylolated dicyandiamide. Wood has been commercially treated for flame retardancy by aminoplast-phosphoric acid compositions (304).

Cellulose can also be phosphorylated by heating it with polyphosphate salts, such as sodium hexametaphosphate (305). A water-insoluble sodium cellulose phosphate, Selectacel phosphate cation exchanger (Polysciences), is used in chromatography. A more highly substituted version, Selectacel SCP or Calcibind exchanger, is approved by the FDA for binding calcium in the gastrointestinal tract as a treatment of absorptive hypercalciurea (a disease causing recurrent calcium kidney stones) (306) (see CELLULOSE ESTERS, INORGANIC). Cellulose can also be phosphorylated with organic phosphorylating agents, such as pentaerythritol spirobis(chlorophosphate); the product shows enhanced char formation when heated (307). Phosphorylation of cellulose with phosphorous acid in molten urea provides a white water-soluble product with  $\text{OPHO}_2\text{H}$  groups (308,309). The ammonium salt is flame retardant. A variety of phosphorus reagents were shown to react with alkali cellulose to produce phosphorylated celluloses (310).

The strength of paper with calcium carbonate filler was shown to be increased by anionic polymers with acid phosphate or phosphonate groups, such as acid phosphate esters of poly(vinyl alcohol) (311).

**Starches.** Starches are phosphorylated by treatment with sodium orthophosphate, pyrophosphate, metaphosphate, or tripolyphosphate (312). By varying the reagents and conditions, a wide range of properties can be achieved. A phosphate-treated starch swellable in cold water is used in instant puddings.

Water-resistant phosphorylated starch is useful in paper sizing. A hydroxypropyl starch phosphate (Midwest Grain Products' COSMOGEL (46)) is heat and pH tolerant and hydrates to a thick smooth paste useful in skin and hair care products.

Starch can be reacted with phosphoric acid and urea to produce a starch phosphate carbamate of remarkably high swelling ability (313).

*Flame-Retardant Finishes on Cellulosic Fabrics.* The flame retarding of cotton and viscose-rayon fabrics has been the object of a large worldwide effort on phosphorus-containing finishes (314–316). The commercial cotton finishes are based on tetrakis(hydroxymethyl)phosphonium salts, usually the chloride or sulfate (317). These salts are prepared by the reaction of formaldehyde with phosphine in the presence of an acid.



The tetrakis(hydroxymethyl)phosphonium salts, neutralized with base are applied to cellulosic fabric, most commonly as a urea precondensate (Albright & Wilson's, now Rhodia's Proban) and cured with ammonia vapor (318–320). The finish, after oxidation by air or hydrogen peroxide, has phosphine oxide structures in a cross-linked amino resin network, probably also lightly linked to the cellulose. This finish is durable to multiple launderings and is used for industrial cotton garments (321). A prepolymer based on this chemistry was also promising for fire protection of wooden shingles (322).

Other commercial finishes for cotton are less resistant to harsh laundering conditions but can be applied by conventional pad-dry-cure methods. For example, the Ciba Pyrovatex CP flame retardant is based on the methylolated reaction product of dimethyl phosphite with acrylamide, which is condensed on the cotton fabric with an amino resin (323,324) to make a cross-linked amino resin containing a dimethyl phosphonate structure. Pyrovatex CP is  $(\text{CH}_3\text{O})_2\text{P}(\text{O})\text{CH}_2\text{CH}_2\text{C}(\text{O})\text{NHCH}_2\text{OH}$  with related side-reaction products (325,326). The chemistry of the Pyrovatex finish involves linkages both to cellulose directly and to melamine resins which then link to cellulose.

Laboratory development of a durable finish for cotton and cotton-nylon blends at University of Georgia using an OH-functional phosphate-phosphonate and a coreactant was discussed earlier (142–145).

*Phosphorylated Proteins.* Naturally occurring phosphorus containing proteins include such important examples as casein, discussed elsewhere in this Encyclopedia. In living organisms, proteins are often phosphorylated enzymatically on the serine or tyrosine hydroxyl group as an activation or regulation step, and overphosphorylation may play a role in disease; this biochemistry is outside the scope of the present article.

Efforts to manufacture phosphorylated proteins by modification of non-phosphorus proteins have been reviewed (327). Phosphorylation of proteins with phosphorus oxychloride causes cross-linking and insolubilization but improves gel-forming and water-binding properties. Phosphorylation with sodium trimetaphosphate improves functional properties of soybean protein, including water solubility. Nutritional and toxicological investigations are needed before such products can be used in foods (328).

Phosphorylation of wool by spirocyclic pentaerythritol bis(phosphoryl chloride) or other cyclic phosphoryl chlorides has been shown to increase char on fire exposure (329).

## BIBLIOGRAPHY

"Phosphorus-Containing Polymers and Oligomers" in *EPST* 3rd ed., Vol. 3, pp. 447–474, by E. D. Weil, Polytechnic University.

## CITED REFERENCES

1. E. D. Weil, in *Kirk-Othmer Encyclopedia of Chemical Technology*, 4th ed., Vol. 10, Wiley-Interscience, New York, 1993, pp. 976–998.
2. E. D. Weil, in M. Lewin, S. M. Atlas, and E. M. Pearce, eds., *Flame-Retardant Polymeric Materials*, Vol. 2, Plenum Press, New York, 1978, pp. 103–128.
3. S. V. Levchik and E. D. Weil, *J. Fire Sci.* **24**, 345–364 (2006).
4. M. Lewin and E. Weil, in A. Horrocks and D. Price, eds., *Fire Retardant Materials*, Woodhead Publishing Ltd., Cambridge, UK, 2001, pp. 31–68.
5. D. Price, K. J. Bullett, L. K. Cunliffe, T. R. Hull, G. J. Milnes, J. R. Ebdon, B. J. Hunt, and P. Joseph, *Polym. Degrad. Stab.* **88** (1), 74–79 (2005).
6. S. Maiti, S. Banerjee, and S. K. Palit, *Prog. Polym. Sci.* **18**, 227–261 (1993).
7. E. D. Weil, *J. Fire Flammability/Fire Retardant Chem.* **1**, 125 (1974).
8. S. V. Shulyndin, Ya. A. Levin, and B. E. Ivanov, *Russ. Chem. Rev.* **50**, 865 (1981) (Engl. Trans.).
9. E. D. Weil, R. B. Fearing, and F. Jaffe, *J. Fire Retardant Chem.* **9**, 39 (1982).
10. N. Gatti and S. Costanzi, in *Flame Retardants 2004*, Interscience Communications, London, 2004, pp. 133–137.
11. U. S. Pat. 6,797,200 (2004), C. Scelza and A. Zaopo (to Pirelli Cavi i Sistemi).
12. E. D. Weil, Paper presented at 11th Annual BCC Conference on Flame Retardancy, Stamford, Conn., May 22–24, 2000.
13. B. Nass, O. Schacker, E. Schlosser, and W. Wanzke, in *Flame Retardants 2002*, Interscience Communications, London 2002, pp. 63–74.
14. J. J. McCallum and J. F. Alder, *J. Chem. Technol. Biotechnol.* **44**, 121–133 (1989).
15. Q. Wu, J. Lu, and B. Qu, *Polym. Int.* **52**, 1326–1331 (2003).
16. M. Pecht, Y. Deng, *Microelectron. Reliab.* **46** (1), 53–62 (2006).
17. H. Hartl, *Angew. Chem., Int. Ed. Engl.* **34**, 2637–2638 (1998).
18. A. Pfitzner, M. Brau, J. Zweck, G. Brunklaus, and H. Eckert, *Angew. Chem., Int. Ed.* **43**, 4228–4231 (2004).
19. A. D. F. Toy, in J. C. Bailar, H. J. Emeleus, R. Nyholm, and A. F. Trotman-Dickenson, eds., *Comprehensive Inorganic Chemistry*, Vol. 2, Pergamon Press, Oxford, UK, 1973, Chapter 20.
20. N. H. Ray, *Inorganic Polymers*, Academic Press, Inc., London, 1978.
21. A. E. R. Westman, in E. J. Griffith and M. Grayson, eds., *Topics in Phosphorus Chemistry*, Vol. 9, John Wiley & Sons, Inc., New York, 1977, pp. 231–405.
22. R. Brow, ed., Structure, Properties and Applications of Phosphate and Phosphate-Containing Glasses: Proceedings of the 15th University Conference on Glass Science, Elsevier, Amsterdam, June 20–23, 1999, in Rolla, MI; *J. Non-Cryst. Solids* 263 and 264, (2000).
23. M. T. Averbuch-Pouchot and A. Durif, *Topics in Phosphorus Chemistry*, World Science Publishers, Singapore, 1996.

24. E. Griffith, ed., *Phosphate Fibers*, Plenum Publishing Corp., New York, 1995.
25. A. D. F. Toy and E. N. Walsh, *Phosphorus in Everyday Living*, American Chemical Society, Washington, D.C., 1987.
26. M. R. W. Brown and A. Kornberg, *Trends Biochem. Sci.* **33**, 284–290 (2008).
27. M. R. W. Brown and A. Kornberg, *Proc. Nat. Acad. Sci. USA* **101**, 16085–16087 (2004).
28. P. Langen, in H. C. Schroeder and W. E. G. Muller, eds., *Progress in Molecular and Subcellular Biology*, Vol. **23**, Springer-Verlag, Berlin, 1999, pp. 19–26.
29. U.S. Pat. 4,940,677 (July 10, 1990), G. H. Beall and C. J. Quinn (to Corning, Inc.).
30. C. J. Quinn and G. H. Beall, in L. L. Hench and J. K. West, eds., *Chemical Processes and Advanced Materials*, John Wiley & Sons, Inc., New York, 1992, pp. 799–805.
31. U.S. Pat. 5,153,151 (Oct. 6, 1992), B. G. Aitken (to Corning, Inc.).
32. U.S. Pat. 3,723,074 (March 27, 1973), P. G. Sears and H. L. Vandersall (to Monsanto Co.).
33. C. Y. Shen, N. E. Stahlheber, and D. R. Dyroff, *J. Amer. Chem. Soc.* **91**, 62–67 (1969).
34. H. L. Vandersall, *J. Fire Flammability* **2**, 97 (1971).
35. H. Staendeke, in *Flame Retardant Coatings: Problems and Opportunities*, Proceedings of the Meeting of the Fire Retardant Chemicals Association, Pinehurst, N.C., Oct. 27–30, 1985, FRCA, Lancaster, Pa., 1985, pp. 29–50.
36. T. Futterer, in *Proceedings of the Fall FRCA Conference*, Cleveland, Ohio, Oct. 2002, pp. 141–142.
37. U.S. Pat. 6,369,137 (Apr. 9, 2002), J. G. Kersjes and R. H. M. Kierkels (to DSM NV).
38. C. Boelens and R. Grabnax, Paper presented at *BCC Conference on Recent Advances in Flame Retardancy of Polymeric Materials*, Stamford, Conn., May 24–26, 1999.
39. E. Stegor and G. Mildner, *Z. Anorg. Allgem. Chem.* **332**, 314–321 (1964).
40. Brit. Pat. 1,461,615 (1977), K. Sommer (to Benckiser-Knapsack).
41. Fr. Pat. Appl. 2,617,152 (Dec. 30, 1988), R. Marchand, Y. Laurent, and P.-N. Fevennec (to Centre National de la Recherche Scientifique).
42. E. D. Weil, Paper presented at *BCC Conference on Recent Advances in Flame Retardancy of Polymeric Materials*, Stamford, Conn., May 18–20, 1993.
43. E. D. Weil, in *Proceedings of the 2nd Beijing International Symposium / Exhibition on Flame Retardants*, Geological Publishing House, Beijing, People's Republic of China, 1993, pp. 285–290.
44. S. V. Levchik, G. F. Levchik, A. I. Balabanovich, E. D. Weil, and M. Klatt, *Angew. Makromol. Chem.* **264**, 48–55 (1999).
45. Eur. Pat. 1,292, 638 (Jan. 7, 2004) E. Freudenthaler, A. Brand, H.-J. Sterzei, J. Engelmann, and M. Klatt (to BASF).
46. U.S. Pat. 6,093,759 (Jul. 25, 2000) B. Gareiss, H.-M. Schneider, and M. Weber (to BASF).
47. E. D. Weil and N. Patel, *Fire Mater.* **18**, 1–7 (1994).
48. P. C. Li and L. C. Hua, *J. Electrochem. Soc.: Solid State Sci. Technol.* 366–372 (1986).
49. N. L. Holy, in L. H. Pignolet, ed., *Homogeneous Catalysis with Metal Phosphine Complexes*, Plenum Publishing Corp., New York, 1983, Chapt. 14.
50. R. Rabinowitz, R. Marcus, and J. Pellon, *J. Polym. Sci. Part A: Polym. Chem.* **2**, 1241–1249 (1964).
51. W. M. McKenzie and D. C. Sherrington, *J. Polym. Sci., Polym. Chem. Ed.* **21**, 431 (1983).
52. H. J. Cristau and F. Plenat, in F. R. Hartley, ed., *Chemistry of Organophosphorus Compounds*, Vol. 3, John Wiley & Sons, Inc., Chichester, UK, 1994, pp. 159–160.
53. A. Boryniec and B. Laszewicz, *J. Polym. Sci. A* **1**, 1963 (1963).
54. L. A. Errede and N. Knoll, *J. Polym. Sci.* **60**, 33 (1962).
55. U.S. Pat. 4,068,055 (Jan. 10, 1978), C. S. Smith (to Upjohn Co.).

56. U.S. Pats. 4,463,159 (July 31, 1984) and 4,472,570 (Sept. 18, 1984), S. Besecke, G. Schroeder, W. Ude, and W. Wunderlich (both to Roehm GmbH).
57. U.S. Pat. 4,492,805 (Jan. 8, 1985), S. Besecke, G. Schroeder, W. Ude, and W. Wunderlich (to Rohm GmbH).
58. S. Hashimoto, I. Furukawa, and K. Ueyama, *J. Macromol. Sci. Chem. A* **11**, 2167 (1977).
59. D. J. Riley, A. Gungor, S. A. Srinivasan, M. Sankarapandian, C. Tchatchoua, M. W. Muggli, T. C. Ward, and J. E. McGrath, *Polym. Eng. Sci.* **37**, 1501–1511 (1997).
60. U.S. Pat. 6,040,416 (March 21, 2000), V. N. Sekharipuram, B. S. Mecham, A. Bhatnagar, and J. E. McGrath (to Johnson & Johnson Vision Products, Inc. and Virginia Tech Intellectual Properties, Inc.).
61. J. G. Smith Jr., C. M. Thompson, K. A. Watson, and J. W. Connell, *High Perform. Polym.* **14**, 225–239 (2002).
62. S. W. Shalaby, E. A. Turi, M. H. Riggi, and P. J. Harget, *J. Polym. Sci., Polym. Chem. Ed.* **13**, 669 (1975).
63. J. Pellon and W. G. Carpenter, *J. Polym. Sci. A* **1**, 863 (1963).
64. U.S. Pat. 4,032,517 (June 28, 1977), O. A. Pickett Jr. and J. W. Stoddart (to Monsanto Co.).
65. Y. Zhang, J. C. Tebby, and J. W. Wheeler, *J. Polym. Sci., Polym. Chem.* **34**, 1561–1566 (1996).
66. Y. Zhang, J. C. Tebby, and J. W. Wheeler, *J. Polym. Sci.: Polym. Chem. Ed.* **35**, 2865–2870 (1997).
67. J. Pellon, *J. Polym. Sci. A* **1**, 3561 (1963).
68. U. S. Pat. 6,733,698 (May 11, 2004), M. V. Hanson and L. D. Timberlake (to PABU Services).
69. S. V. Levchik, G. Camino, L. Costa, and M. P. Luda, *Polym. Degrad. Stabil.* **54**, 317–322 (1996).
70. T. Kashiwagi, J. W. Gilman, J. E. McGrath, and I.-Y. Wan, in *Proceedings of FRCA Spring Conference*, San Francisco, Calif., Mar. 16–19, 1997, pp. 197–219.
71. U.S. Pat. 5,194,564 (Mar. 16, 1993), G. C. Davis, C. A. A. Claesen, and E. M. A. Gijzen (to General Electric Co.).
72. I. K. Varma and B. S. Rao, *J. Appl. Polym. Sci.* **28**, 2805 (1983).
73. U.S. Pat. 4,433,115 (Feb. 21, 1984), I. K. Varma, G. M. Fohlen, and J. A. Parker.
74. (a) I. K. Varma, G. M. Fohlen, and J. A. Parker, *J. Polym. Sci., Polym. Chem. Ed.* **21**, 2017 (1983); (b) *Contemp. Top. Polym. Sci.* **4**, 115 (1984).
75. I. K. Varma, G. M. Fohlen, and J. A. Parker, *J. Macromol. Sci., Chem. A* **19**, 209 (1983).
76. O. Ozarslan, M. K. Bayazit, and E. Catiker, *J. Appl. Polym. Sci.* **114**, 1329–1338 (2009).
77. U.S. Pat. 4,472,548 (Sept. 18, 1984), P. N. Son and G. Kletecka (to B. F. Goodrich Co.).
78. W. Vogt and S. Balasubramanian, *Makromol. Chem.* **163**, 111 (1973).
79. K. E. Branham, J. W. Mays, and G. M. Gray, *Polym. Prepr.* **40** (1), 78–79 (1999).
80. E. Bezdushna, H. Ritter, and K. Troev, *Macromol. Rapid Commun.* **26**, 471–476 (2005).
81. J. Pretula, K. Kaluzynski, R. Szymanski, and S. Penczek, *Macromolecules* **30**, 8172–8176 (1997).
82. Ger. Pat. 2,344,332 (Jan. 15, 1981), H.-J. Kleiner (to Hoechst AG).
83. U.S. Pat. 5,085,794 (Feb. 4, 1992), J. F. Kneller, V. Narutis, B. E. Fair, and D. A. Johnson (to Nalco Chemical Co.).
84. U.S. Pat. 4,812,502 (Mar. 14, 1989), G. Cipriani and A. Mariano (to Enichem Sintesi S.p.A.).

85. E. L. Gefter, *Organophosphorus Monomers and Polymers* (English transl. by G. Kosolapoff), Assoc. Technical Services, Inc., Glen Ridge, N.J., 1962.
86. Ya. A. Levin, G. B. Fridman, and B. Ye. Ivanov, *Polym. Sci. USSR* **17**, 971 (1975) (*Engl. trans.*).
87. U.S. Pats. 3,725,359 (Apr. 3, 1973) and 3,792,113 (Feb. 12, 1974), P. Kraft and S. Altscher (both to Stauffer Chemical Co.).
88. R. Gallagher and J. C. H. Hwa, *J. Polym. Sci., Polym. Symp.* **64**, 329 (1978).
89. M. Banks, J. R. Ebdon, and M. Johnson, *Polymer* **35**, 3470–3473 (1994).
90. U.S. Pats. 3,725,509 (Apr. 3, 1973); 3,819,770 (Jun. 25, 1974); 3,857,906 (Dec. 31, 1974); 3,943,085 (Mar. 9, 1976); 3,948,842 (Apr. 6, 1976); 3,991,134 (Nov. 9, 1976); 3,992,337 (Nov. 16, 1976); and 3,992,481-2 (Nov. 16, 1976), P. Kraft and S. Altscher (all to Stauffer Chemical Co.).
91. U.S. Pat. 4,210,739 (Jul. 1, 1980), R. E. Gallagher, J. C. Goswami, P. Kraft, and A. Yu (to Stauffer Chemical Co.).
92. U.S. Pat. 4,147,853 (Apr. 3, 1979), J. C. Goswami and R. Querido (to Stauffer Chemical Co.).
93. U.S. Pat. 3,883,463 (May 13, 1975), J. I. Jin and P. Kraft (to Stauffer Chemical Co.).
94. F. Rochlitz and H. Vilcsek, *Angew. Chem.* **74**, 970 (1962).
95. U.S. Pat. 3,297,663 (Jan. 10, 1967), W. Herbst, F. Rochlitz, and H. Vilcsek (to Farbwerke Hoechst AG).
96. U.S. Pat. 4,153,461 (May 8, 1979), G. Berghauser and F. Uhlig (to Hoechst AG).
97. U.S. Pat. 4,448,647 (May 15, 1984), T. N. Gillich, J. E. Walls, S. F. Wanat, and W. J. Rozell (to American Hoechst Corp.).
98. J. Baybrook and J. W. Nicholson, *J. Mater. Chem.* **3**, 361–365 (1993).
99. Eur. Pat. Appl. 0.643.081 (Mar. 15, 1994) (to Hoechst AG).
100. B. L. Rivas, E. Pereira, P. Gallegos, D. Homper, and K. Geckeler, *J. Appl. Polym. Sci.* **92**, 2917–2922 (2004).
101. U.S. Pats. 4,446,028 and 4,446,046 (May 1, 1984), L. W. Becker (both to Betz Laboratories, Inc.).
102. Brit. Pat. Appl. 2,276,388 A (Sept. 29, 1994), A. Archer and M. Zakikhani (to Albright & Wilson).
103. S. D. Alexandratos, A. W. Trochimczuk, D. W. Crick, E. P. Horwitz, R. C. Gatrone, and R. Chiarizia, *Macromolecules* **29**, 1021–1026 (1996).
104. S. D. Alexandratos, A. W. Trochimczuk, E. P. Horwitz, and R. C. Gatrone, *J. Appl. Polym. Sci.* **61**, 273–278 (1996).
105. E. P. Horwitz, R. Chiarizia, S. D. Alexandratos, and M. Gula, in A. H. Bond, M. L. Dietz, and R. D. Rogers, eds., ACS Symposium Series 716, *Metal Ion Separation*, American Chemical Society, Washington, D.C., 1999, pp. 206–215.
106. R. Chiarizia, E. P. Horwitz, S. D. Alexandratos, and M. J. Gula, *Sep. Sci. Technol.* **32** (1–4), 1–35 (1997).
107. S. D. Alexandratos, *Ind. Eng. Chem. Res.*, **48**, 388–398 (2009).
108. U.S. Pats. 3,822,327 (Jul. 2, 1974); 3,855,359 (Dec. 17, 1974); 4,017,257 (Apr. 12, 1977), and 4,067,927 (Jan. 10, 1978); E. D. Weil (all to Stauffer Chemical Co.).
109. B. J. Eisenberg and E. D. Weil, *Text. Chem. Color.* **6** (8), 180 (1974).
110. W. A. Reeves and Y. B. Marquette, *J. Fire Retardant Chem.* **5**, 65 (1978).
111. K. Masuda and M. Tomita, *J. Fire Retardant Chem.* **3**, 53–65 (1976).
112. Z. Yu, W.-X. Zhu, and I. Cabasso, *J. Polym. Sci., Polym. Chem. Ed.* **28**, 227–230 (1990).
113. P. Wyman, V. L. Crook, and J. R. Ebdon, *Designed Monomers Polym.* **7**, 301–309 (2004).

114. P. Wyman, V. Crook, J. Ebdon, B. Hunt, and P. Joseph, *Polym. Int.* **55**, 764–771 (2006).
115. J. R. Ebdon, D. Price, B. J. Hunt, P. Joseph, F. Gao, G. J. Milnes, and L. K. Cunliffe, *Polym. Degrad. Stabil.* **69**, 267–277 (2000).
116. J. B. Ebdon, B. J. Hunt, P. Joseph, C. S. Konkel, D. Price, K. Pyrah, T. R. Hull, G. J. Milnes, S. B. Hill, C. I. Lindsay, and J. McCluskey, *Polym. Degrad. Stabil.* **70**, 425–436 (2000).
117. F. Zeuner, N. Moszner, T. Volkel, K. Vogel, and V. Rheinberger, *Phosphorus, Sulfur Silicon* **144–146**, 133–136 (1999).
118. C. E. Schildknecht, *Allyl Compounds and Their Polymers*, John Wiley & Sons, Inc., New York, 1973, pp. 674–678.
119. Q. Wu and R. A. Weiss, *J. Polym. Sci. B: Polym. Phys.* **42**, 3626–3641 (2004).
120. U.S. Pat. 2,435,252 (1948), A. D. F. Toy (to Victor Chemical Works).
121. H. W. Coover, R. L. McConnell, and M. A. McCall, *Ind. Eng. Chem.* **52**, 409 (1960).
122. U.S. Pat. 3,932,351 (Jan. 13, 1976), H. L. King (to Monsanto Co.).
123. Jpn. Kokai 72 39,154 (Dec. 6, 1972), K. Murayama and R. Yamatera (to Toyobo Co., Ltd.).
124. U.S. Pat. 3,719,727 (Mar. 6, 1973), Y. Masai, Y. Kato, and N. Fukui (to Toyo Spinning Co.).
125. K. S. Kim, *J. Appl. Polym. Sci.* **28**, 1119 (1983).
126. K. S. Kim, *J. Appl. Polym. Sci.* **28**, 2439 (1983).
127. U.S. Pat. 4,206,296 (Jun. 3, 1980), A. J. Yu, S. Altscher, and K. S. Kim (to Stauffer Chemical Co.).
128. Chin. Pat. CN 1167167 A (Dec. 10, 1997), Y. Xia (Qingdao University); Chem. Abst. **132**, 79695 (1998).
129. Y.-Z. Wang, *J. Polym. Sci., Part B: Polym. Phys.* **41**, 2296–2301 (2003).
130. M. Murano, *Polym. J.* **30**, 281–283 (1998).
131. C. E. Carraher Jr., *Inorg. Macromol. Rev.* **1**, 287 (1972).
132. M. Richards, B. I. Dahiyat, D. M. Arm, S. Lin, and K. W. Leong, *J. Polym. Sci., Part A: Polym. Chem.* **29**, 1157–1165 (1991).
133. G. M. Gray, K. E. Branham, L.-H. Ho, and J. W. Mays, in J. F. Harrod and R. M. Laine, eds., *Inorganic and Organometallic Oligomers and Polymers*, Kluwer Academic Publishers, Dordrecht, the Netherlands, 1991, pp. 249–263.
134. U.S. Pat. 4,152,373 (May 1, 1979), M. L. Honig and E. D. Weil (to Stauffer Chemical Co.).
135. M. Schmidt, D. Freitag, L. Bottenbruch, and K. Reinking, *Angew. Makromol. Chem.* **132**, 1 (1985).
136. U.S. Pat. 4,332,921 (Jun. 1, 1982), M. Schmidt, J. Walk, and E. Reese (to Bayer AG).
137. U. S. Pat. Appl. 2008/0051529 (Feb. 28, 2008), R. Kampf.
138. U. S. Pat. Appl. 2007/0129535 (Jun. 7, 2007) by D. Freitag and M. A. Vinciguerra.
139. U. S. Pat. Appl. 2009/0043013 (Feb. 12, 2009) G. Stahl, M. Lebel and D. Freitag (to FRX Polymer).
140. U. S. Pat. Appl. 2007/0129511 (Jun. 7, 2007), D. Freitag.
141. U.S. Pats. 4,331,614 (May 25, 1982) and 4,415,719 (Nov. 15, 1983), M. Schmidt, D. Freitag, L. Bottenbruch, and K. Reinking, H. Rohr, and H.-D. Block (both to Bayer AG).
142. E. Viscarolasaga, *Mass. High Technol. Aug.* **23**, 1, 2009.
143. U. S. Pat. 6,861,499 (Mar. 1, 2005), M. Vinciguerra, D. Freitag, N. Rice, and R. Lusignea (to Triton Systems).
144. S. V. Levchik and E. D. Weil, *J. Fire Sci.* **24**, 345–364 (2006).



145. S. V. Levchik and C. S. Wang, *OnBoard Technol.*, April 2007, 18–20 (2007).
146. U.S. Pat. 3,956,431 (May 11, 1976), M. L. Honig and E. D. Weil (to Stauffer Chemical Co.).
147. U.S. Pats. 4,086,303 (Apr. 25, 1978); 4,152,371 (May 1, 1979); and 4,202,842 (May 13, 1980), E. D. Weil (all to Stauffer Chemical Co.).
148. J. Gloede and H. Gross, *J. Gen. Chem. USSR* **54**, 1285 (1984) (*Engl. trans.*).
149. U.S. Pat. 4,144,387 (Mar. 13, 1979), J. J. Anderson, V. G. Camacho, R. E. Kinney, and F. M. Seger (to Mobil Oil Co.).
150. G. Lapienis and S. Penczek, in K. J. Ivin, ed., *Ring-Opening Polymerization*, Elsevier Science Publishing Co., New York, 1983, Chap. 13.
151. S. R. Sandler and W. Karo, *Polymer Synthesis*, 2nd ed., Academic Press, New York, 1992, pp. 486–493.
152. U.S. Pat. 3,890,411 (June 17, 1975), K. S. Shim (to Stauffer Chemical Co.).
153. U.S. Pat. 4,199,534 (April 22, 1980), R. B. Fearing (to Stauffer Chemical Co.).
154. W. Wu and C. Yang, *Polym. Prepr.* **45**, 803–804 (2004).
155. U. S. Pat. 6,107,507 (Aug. 22, 2000), J. Stowell (to Akzo Nobel NV).
156. C. Q. Yang and X. Qiu, *Fire Mater.* **31** (1), 67–81 (2007).
157. W. Wu and C. Q. Yang, *Polym. Degrad. Stabil.* **92**, 363–369 (2007).
158. H. Yang and C. Q. Yang, *Polym. Degrad. Stabil.* **88**, 363–370 (2007).
159. H. Yang and C. Q. Yang, *J. Fire Sci.* **25**, 425–446 (2007).
160. S. Minegishi, S. Komatsu, A. Kameyama, and T. Nishikubo, *J. Appl. Polym. Sci.: Part A. Polym. Chem.* **37**, 959–965 (1999).
161. Eur. Pat. 0,845,474 (Mar. 3, 2003) C. J. Harris, G. Woodward, A. J. Taylor, and J. S. Manku (to Rhodia).
162. U.S. Pats. 3,014,956 (Dec. 26, 1961) and 3,042,701 (July 3, 1962), G. Birum (both to Monsanto Co.).
163. U.S. Pat. 3,371,131 (Feb. 27, 1968), A. Carson, W. E. Feely, and M. J. Hurwitz (to Rohm & Haas Co.).
164. U.S. Pat. 3,468,980 (Sept. 23, 1969), G. E. Forsyth (to Rohm & Haas Co.).
165. J. Baddiley, *Acc. Chem. Res.* **3**, 98 (1970).
166. U.S. Pat. 4,207,405 (Jun. 10, 1980), W. F. Masler III and D. C. Spaulding (to B. F. Goodrich Co.).
167. Z.-M. Wang and S.-C. Zu, in *Proceedings of the 4th Asian-Pacific Corrosion Control Conference* East China Institute of Chemical Technology, Shanghai, People's Republic of China, 1985, pp. 1020–1028.
168. S. Penczek and P. Klosinski, in C. G. Gebelein, ed., *Biomimetic Polymers*, Plenum Press, New York, 1990, pp. 223–252.
169. A. R. Elmes, E. Khosdel, D. T. Littlewood, and C. A. Taylor, *Eur. Polym. J.* **33**, 1659–1664 (1997).
170. U.S. Pat. 4,499,251 (Feb. 12, 1985), I. Omura, J. Yamauchi, Y. Nagase, and F. Uemura (to Kuraray Co., Ltd.).
171. U.S. Pat. 3,754,972 (Aug. 28, 1973), R. deMajistre, G. M. Parker, and R. Sirkoch (to PPG Industries, Inc.).
172. R. O. Carter III, J. L. Parsons, and J. W. Holubka, *Ind. Eng. Chem. Res.* **26**, 1518–1523 (1987).
173. U.S. Pats. 3,524,903 (Aug. 18, 1970) and 3,574,794 (Apr. 13, 1971), S. R. Hargis Jr. (both to Dow Chemical Co.).
174. M. J. Chen, J. Kiplinger, N. Johnson, E. M. Walsh, and H. Adam, in *International Corrosion Exhibition (ICE)*, Oct. 2000.
175. H. S. Yang, H. Adam, and J. Kiplinger, *JCT Coatings Technol.* **2** (13), 44–52 (2005).
176. B. Helferich and K. G. Schmidt, *Chem. Ber.* **92**, 2054 (2000).

177. U.S. Pat. 6,713,598 (Mar. 30, 2004), I. Selvaraj, J. Gosens and G. De Wit (to GE).
178. U.S. Pat. 4,482,693 (Nov. 13, 1984), V. Serini, P. J. Mayska, H.-D. Block, and D. Freitag (to Bayer AG).
179. Jpn. Kokai Tokkyu Koho 59 24,736 [84 24,736] (Feb. 8, 1984) and 59 45,351 [84 45,351] (March 14, 1984) (both to Adeka Argus Chemical Co., Ltd.).
180. R. Deanin and M. Ali, in G. Nelson, ed., ACS Symposium Series 599, *Fire and Polymers II*, American Chemical Society, Washington, D.C., 1995, pp. 56–64.
181. X. Wang, P. Yang, Q. Qian, Y. Ou, and S. Zhang, *Gaofenzi Cailiao Kexue Yu Gongcheng* **15** (4), 81–83 (1999)(in Chinese); *Chem. Abstr.* **131**, 352076 (2000).
182. U.S. Pat. 6,815,476 (Nov. 9, 2004), Q. Bhatia and R. Howe (to GE).
183. U.S. Pat. 6,684,404 (Feb. 3, 2004), T. Eckel, M. Zobel, D. Wittmann and N. Janke (to Bayer).
184. K. S. Annakutty and K. Kishore, *Polymer* **29**, 756–764, 1273–1276 (1988).
185. N. Narendran and K. Kishore, *J. Appl. Polym. Sci.* **87**, 626–631 (2003).
186. U.S. Pat. 5,608,100 (Mar. 4, 1997), M. Sicken (to Hoechst AG.).
187. U.S. Pat. 5,985,965 (Nov. 16, 1999), M. Sicken and H. Staendek (to Clariant).
188. U.S. Pats. 4,382,042 (May 3, 1983) and 4,458,035 (Jul. 3, 1984), T. Hardy and F. Jaffe (both to Stauffer Chemical Co.).
189. R. Crowell, Paper presented at *FRCA Spring Conference*, Washington, D.C., Mar. 12–15, 2000.
190. U.S. Pat. 7,288,577 (Oct. 30, 2007), L. Bradford, E. Pinzoni, B. Williams, and T. Halchak (to Supresta).
191. S. Penczek, P. Kubisa, P. Klosinski, T. Biela, and A. Nyk, in E. J. Vandenberg and J. C. Salamone, eds., ACS Symposium Series 496, *Catalysis in Polymer Synthesis*, American Chemical Society, Washington, D.C., 1992, pp. 248–257.
192. A. Nyk, P. Klosinski, and S. Penczek, *Makromol. Chem.* **192**, 833–846 (1991).
193. U.S. Pat. 3,513,644 (May 26, 1970), E. D. Weil (to Stauffer Chemical Co.).
194. U.S. Pat. 3,896,187 (Jul. 22, 1975), E. D. Weil (to Stauffer Chemical Co.).
195. U.S. Pat. 4,013,814 (Mar. 22, 1977), E. D. Weil (to Stauffer Chemical Co.).
196. S. Penczek, J. Pretula, and K. Kaluzynski, *Macromol. Symp.* **130**, 305–317 (1998).
197. S. Penczek, J. Pretula, and K. Kaluzynski, *Biomacromolecules* **6**, 547–551 (2005).
198. D.-A. Wang, C. G. Williams, F. Yang, N. Cher, H. Lee, and J. Elisseeff, *Tissue Eng.* **11**, 201–213 (2005).
199. C. W. Allen, *J. Fire Sci.* **11**, 320–328 (1993).
200. M. Gleria and R. De Jaeger, eds., *Phosphazenes: A Worldwide Insight*, Nova Science Publishers, Hauppauge, N.Y., 2004.
201. D. M. Harris, R. L. Jenkins, and M. L. Nielsen, *J. Polym. Sci.* **35**, 540 (1959).
202. U.S. Pat. 5,409,976 (Apr. 25, 1995), A. J. Lindsay (to Minnesota Mining and Manufacturing Co.).
203. M. A. Kraus and M. Nemas, *J. Polym. Sci., Polym. Lett. Ed.* **19**, 617 (1981).
204. U.S. Pat. 4,701,554 (Oct. 20, 1987), H. Kauth, M. Schmidt, D. Freitag, U. Rudolph, and F. Kleiner (to Bayer AG).
205. U.S. Pat. 4,587,362 (May 6, 1986), M. Honig and E. D. Weil (to Stauffer Chemical Co.).
206. A. P. Khardin, O. I. Tuzhikov, and S. N. Bondarenko, *Russ. Chem. Rev.* **52**, 662 (1983) (*Engl. trans.*).
207. J. P. Schroeder and W. P. Sopchak, *J. Polym. Sci. Part A* **1** **47**, 417 (1970).
208. (a) R. A. Weiss, R. W. Lenz, and W. J. MacKnight, *J. Polym. Sci., Polym. Phys. Ed.* **15**, 1409 (1977); (b) *J. Polym. Sci., Polym. Phys. Ed.* **16**, 1101 (1978).
209. R. Bogoczec and J. Surowiec, *J. Appl. Polym. Sci.* **26**, 4161 (1981).

210. S. D. Alexandratos, M. A. Strand, D. R. Quillen, and A. J. Walder, *Macromolecules* **18**, 829 (1985).
211. S. D. Alexandratos, D. L. Wilson, M. A. Strand, D. R. Quillen, A. J. Walder, and W. J. McDowell, *Macromolecules* **18**, 836 (1985).
212. G. Camino, M. Bert, A. Guyot, J. Brossas, and G. Clouet, *Fire Safety J.* **2**, 257–263 (1979).
213. S. D. Alexandratos and X. Zhu, *Macromolecules* **36**, 5981–5986 (2005).
214. J. J. Wolff and R. E. Anderson, in *Adsorption and Ion Exchange*, (AIChE Sym. Series 219), Vol. **78** American Institute of Chemical Engineers, New York, 1982, pp. 46–53.
215. N. A. Mukmeneva, S. I. Agadzhanyan, P. A. Kirpichnov, and K. S. Minsker, *Proc. Acad. Sci. USSR* **233** (3), 174 (1977) (*Engl. trans.*).
216. P. A. Kirpichnikov, N. A. Mukmeneva, and D. G. Pobedimski, *Russ. Chem. Rev.* **52**, 1051 (1983) (*Engl. trans.*).
217. Eur. Pats. 84407A2 (Jul. 27, 1983); 61240 A2 (Sept. 29, 1982); and 58483 A2 (Aug. 25, 1982), J. E. Bunker (all to Minnesota Mining and Manufacturing Co.).
218. U.S. Pat. 4,514,342 (Apr. 30, 1985), R. W. Billington, G. B. Blackwell, and T. E. Prodger (to Dentsply, Ltd.).
219. U.S. Pat. 4,222,780 (Sept. 16, 1980), K. Shibatani, I. Omura, and J. Yamauchi (to Kuraray Co., Ltd.).
220. U.S. Pat. 5,866,664 (Feb. 2, 1999), T. F. McCallum III and B. Weinstein (to Rohm and Haas Co.).
221. Th. Randoux, J.-Cl. Vanovmelt, H. Van den Bergen, and G. Camino, *Progr. Org. Coat.* **45**, 281–289 (2002).
222. U.S. Pat. 4,033,936 (Jul. 5, 1977), U. Bollert, E. Lohmar, and A. Ohorodnik (to Hoechst AG).
223. S. Black and J. Soc. *Dyers Colorists* **108**, 372–373 (1992).
224. V. Freudenberger and F. Jacob, *Angew. Makromol. Chem.* **105**, 203 (1982).
225. U.S. Pat. 4,127,590 (Nov. 28, 1978), S. Endo, T. Kashihara, A. Osako, T. Shizuki, and T. Ikegami (to Toyo Boseki KK).
226. C. S. Wang, J. Y. Shieh, and Y. M. Sun, *Eur. Polym. J.* **35**, 1465–1472 (1999).
227. S. Gyobu, M. Sato, and H. Takeuchi, in *International Fire Safety Conference Proceedings* New Orleans, La., Mar. 9–12, 2003, pp. 157–165.
228. S. Endo, Y. Araki, G. Matsuoka, S. Gyobu, and H. Takeuchi, *J. Appl. Polym. Sci.* **78**, 1134–1138 (2000).
229. S.-C. Yang and J. P. Kim, *J. Appl. Polym. Sci.* **106**, 2870–2874 (2007).
230. S.-C. Yang and J. P. Kim, *J. Appl. Polym. Sci.* **106**, 1274–1280 (2007).
231. C. S. Wang and C. H. Lin, *Polymer* **40**, 747–757 (1999).
232. Jpn. Kokai Tokkyo Koho 59 91,122 (May 24, 1984) (to Japan Exlan Co., Ltd.).
233. U.S. Pat. 4,981,945 (Jan. 1, 1991), G. Landoni and C. Neri (to Enichem Synthesis, S.p.A.).
234. R. C. Nametz, *Ind. Eng. Chem.* **59** (5), 99 (1967).
235. U.S. Pat. 4,360,647 (Nov. 23, 1982), R. E. Hefner Jr. (to Dow Chemical Co.).
236. U.S. Pat. 5,571,888 (Nov. 5, 1996), Y.-N. Cheng, S.-J. Chang, Y.-C. Sheen, and S.-P. Juang (to Industrial Technology Institute).
237. Fr. Pat. 1,584,020 (Dec. 12, 1969), O. Zaske, C. H. Fintelmann, and H. B. Igdaroff (to Vistron Co.).
238. U.S. Pats. 4,032,517 (June 28, 1977) and 4,092,302 (May 30, 1978), O. A. Pickett Jr. and J. W. Stoddard (both to Monsanto Co.).
239. U.S. Pat. 5,750,603 (May 12, 1998), J. Asrar (to Solutia).
240. U.S. Pat. 5,545,833 (Aug. 13, 1996), J. W. Stoddard (to Monsanto Co.).
241. F. J. Martin and K. R. Price, *J. Appl. Polym. Sci.* **12**, 143 (1968).

242. U. Braun, A. I. Balabanovich, B. Schartel, U. Knoll, J. Artner, M. Ciesielski, M. Döring, R. Perez, J. K. W. Sandler, V. Altstadt, T. Hoffmann, and D. Pospiech, *Polymer* **47**, 8495–8508 (2006).
243. S. V. Levchik and E. D. Weil, *Polym. Int.* **53**, 1585–1610 (2004).
244. M. Döring, J. Artner, M. Cielieski, A. Schäfer, and S. Seibold, in *Flame Retardants 2008*, Interscience Communications, London, 2008, pp. 121–132.
245. M. Döring, Paper presented at *European Coatings Conference*, Berlin, Germany, Sept. 18–19, 2008.
246. J. L. Massingill, *J. Coatings Technol.* **63** (797), 47–54 (1991).
247. R. O. Carter III, J. L. Parsons, and J. W. Holubka, *Ind. Eng. Chem. Res.* **26**, 1518–1523 (1987).
248. P. M. Hergenrother, C. M. Thompson, J. G. Smith Jr., J. W. Connell, J. A. Hinkley, R. E. Lyon, and R. Moulton, *Polymer* **46**, 5912–5024 (2005).
249. Eur. Pat. 1,025,141 (Dec. 21, 2005), W. von Gentzkow, D. Heinl, H. Kapitza, and M. Schreyer (to Siemens A.-G.).
250. U.S. Pat. 5,389,704 (Feb. 14, 1995), Y. Yabu (to Dow Chemical Co.).
251. J. A. Mikroyannidis and Z. Nir, *J. Appl. Polym. Sci.* **30**, 83 (1985).
252. U.S. Pat. 4,613,661 (Sept. 23, 1986), H. G. Langer, T. P. Brady, M. A. Paul, and G. A. Doorakian (to Dow Chemical Company).
253. D. Derouet, F. Morvan, and J. C. Brosse, *J. Appl. Polym. Sci.* **62**, 1855–1868 (1996).
254. U.S. Pat. 5,759,691 (Jun. 2, 1998), G. Scholz, S. Hoerold, and W. Pirig (to Clariant AG).
255. U.S. Pat. 5,900,469 (May 4, 1997), H. Kleiner, S. Hoerold, and G. Scholz (to Aventis Research & Development).
256. U.S. Pat. 4,952,646 (Aug. 28, 1990), E. D. Weil, J. Tomko, and F. Jaffe (to Akzo America).
257. C.-S. Wang and J.-Y. Shieh, *Eur. Polym. J.* **36**, 443–452 (2000).
258. X. Wang and J. Lin, *Colloid Polym. Sci.* **283**, 593–603 (2005).
259. U.S. Pat. 6,887,950 (May 3, 2005), L. D. Timberlake, M. V. Hanson, and E. B. Edwards (to PABU Services).
260. U.S. Pat. 6,955,851 (Oct. 18, 2005), M. V. Hanson and L. D. Timberlake (to PABU Services).
261. A. Schäfer, S. Seibold, W. Lohstroh, O. Walter, and M. Döring, *J. Appl. Polym. Sci.* **105**, 685–696 (2007).
262. C.-S. Wang and C. H. Lin, *J. Polym. Sci., Part A: Polym. Chem.* **37**, 3903–3909 (1999).
263. Eur. Pat. 0,806,429 (Dec. 19, 2001), R. Utz (to Schill & Seilacher GmbH).
264. X. Wang and Q. Zhang, *Eur. Polym. J.* **40**, 385–395 (2004).
265. C.-S. Wang and J.-Y. Shieh, *J. Appl. Polym. Sci.* **73**, 353–361 (1999).
266. J.-Y. Shieh and C.-S. Wang, *J. Appl. Polym. Sci.* **78**, 1636–1644 (2000).
267. C. H. Lin, S. X. Cai, and C. H. Lin, *J. Polym. Sci., Polym. Chem. Ed.* **43**, 5971–5986 (2005).
268. Y. L. Liu, *J. Polym. Sci., Polym. Chem. Ed.* **40**, 359–368 (2002).
269. Japan. Kokai Tokkyu Koho JP 2000 265,040 (Sept. 26, 2000), H. Moriyama, Y. Takahashi, and M. Yoshisawa (to Dainippon Ink and Chemicals, Inc.).
270. U.S. Pat. 6,284,869 (Sep. 4, 2001), A. J. Buser and J. A. J. Schutyser (to Akzo Nobel).
271. T. Wu, A. M. Piotrowski, Q. Yao, and S. V. Levchik, *J. Appl. Polym. Sci.* **101**, 4011–4022 (2006).
272. PCT Intl. Pat. Appl. WO 2005/118276, S. V. Levchik, S. Dashevsky, and A. M. Piotrowski (to Supresta U.S.).
273. PCT Intl. Pat. Appl. WO 2004/060957, C. Rottländer, M. Gräfen, H.-G. Reichwein, and S. Krusenbaum (to Bakelite AG).

274. U.S. Pat. 7,449,526, S. V. Levchik, S. Dashevsky, E. D. Weil, and Q. Yao (to Supresta LLC).
275. PCT Intl. Pat. Appl. WO 2004/113411, S. V. Levchik and A. M. Piotrowski (to Akzo Nobel).
276. U.S. Pat. 7,427,652, S. V. Levchik and M. Buczek (to Supresta LLC)
277. J. A. Mikroyannidis and D. A. Kourtidis, in C. K. Riew and J. K. Gillham, eds., *Rubber-Modified Thermoset Resins*, Adv. Chem. Ser., Vol. **208**, American Chemical Society, Washington, D.C., 1984, pp. 351–356.
278. W. Liu, R. J. Varley, and G. P. Simon, *J. Appl. Polym. Sci.* **92**, 2093–2100 (2004).
279. W. Liu, R. J. Varley, and G. P. Simon, *Polymer* **47**, 2091–2098 (2006).
280. U.S. Pat. 3,645,971 (Feb. 29, 1972), R. R. Hindersinn (to Hooker Chemical Co.).
281. R. W. Hunter and R. M. Washburn, in H. Lee, ed., *Epoxy Resins*, Adv. Chem. Ser. Vol. **92**, American Chemical Society, Washington, D.C., 1970, pp. 208–223.
282. U.S. Pat. 3,516,965 (June 23, 1970), R. M. Washburn (to McDonnell Douglas Corp.).
283. S. V. Levchik, G. Camino, M. P. Luda, L. Costa, G. Muller, B. Costes, and Y. Henry, *Polym. Adv. Technol.* **7**, 823–830 (1996).
284. O. Mauerner, *Polym. Degrad. Stabil.* **88**, 70–73 (2005).
285. A. Toldy, P. Anna, I. Csontos, A. Szabó, and Gy. Marosi, *Polym. Degrad. Stabil.* **92**, 2223–2230 (2007).
286. A. Toldy, A. Szabó, Cs. Novák, J. Madarász, A. Tóth, and Gy. Marosi, *Polym. Degrad. Stabil.* **93**, 2007–2013 (2008).
287. E. R. Fretz and J. Green, *Print. Circuit Fabr.* **6** (5), 55 (1983).
288. M. J. Alcón, G. Ribera, M. Galià, and V. Cádiz, *J. Polym. Sci.: Part A: Polym. Chem.* **43**, 3510–3515 (2005).
289. A. J. Papa, *Ind. Eng. Chem. Prod. Res. Dev.* **9**, 478 (1970).
290. W. C. Kuryla and A. J. Papa, eds., *Fire Retardancy of Polymeric Materials*, Vol. **3**, Marcel Dekker, Inc., New York, 1975, pp. 1–133.
291. Brit. Pat. 954,792 (April 8, 1964), C. L. Harowitz (to Virginia-Carolina Chemical Corp.).
292. U.S. Pat. 6,861,452 (Mar. 1, 2005), N. Tokuyasu and K. Kameda (to Daiichi Chemical).
293. U.S. Pat. 3,235,517 (Feb. 15, 1966), T. M. Beck and E. N. Walsh (to Stauffer Chemical Co.).
294. U.S. Pat. 4,456,742-3 (June 24, 1984), F. T. H. Lee and J. Green (to FMC Corp.).
295. J. Green, *Plast. Compound.* (Nov.-Dec.) 30 (1984).
296. U.S. Pat. 3,136,806 (June 9, 1964), H. Holtschmidt (to Farbenfabriken Bayer AG).
297. M. Spirckel, N. Regnier, B. Mortaigne, B. Youssef, and C. Bunel, *Polym. Degrad. Stabil.* **78**, 211–218 (2002).
298. K. Mequanint, R. Sanderson, and H. Pasch, *Polym. Degrad. Stabil.* **77**, 121–128 (2002).
299. E. D. Weil, J. Kearnan, and G. Leitner, in *Phosphorus Flame Retardants for Resin-Treated Paper*, TAPPI Paper Synthetics Conference Papers, TAPPI, Atlanta, Ga., pp. 301–305.
300. Jpn. Kokai Tokyo Koho 60/124630 A2 (July 3, 1985) (to Hitachi Chemical Co.); *Chem. Abst.* **104**, 6623 (1985).
301. A. A. Farooq, D. Price, G. J. Milnes, and A. R. Horrocks, *Polym. Degrad. Stabil.* **44**, 323–333 (1994).
302. B. K. Kandola, A. R. Horrocks, D. Price, and G. V. Coleman, *J. Macromol. Sci., Rev. Macromol. Chem. Phys. C* **36**, 721–794 (1996).
303. E. E. Nifant'ev, *Russ. Chem. Rev.* **34**, 942 (1965) (Engl. trans.).
304. U.S. Pat. 4,461,720 (July 24, 1984), A. G. Lovyet and D. J. Morgan (to Hoover Treated Wood Products, Inc.).

305. M. E. Hall and A. R. Horrocks, *Trends Polym. Sci.* **1**, 55 (1993).
306. (a) C. Y. C. Pak, *Am. J. Med.* **71**, 615 (1981); (b) *FDA Drug Bull.* **13** (1), 1 (1983).
307. R. A. Horrocks and S. Zhang, *Polymer* **42**, 8025–8033 (2001).
308. N. Inagaki, S. Nakamura, H. Asai, and K. Katsuura, *J. Appl. Polym. Sci.* **20**, 2829–2836 (2003).
309. D. M. Suflet, G. C. Chitanu, and V. I. Popa, *React. Funct. Polym.* **66**, 1240 (2006).
310. O. Petreus, G. Cazacu, T. Babulac, and I. Petreus, *J. Appl. Polym. Sci.* **90**, 327–333 (2003).
311. X. Chen, R. Huang, and R. Pelton, *Ind. Eng. Chem. Res.* **44**, 2078–2085 (2005).
312. C.-T. Kim, F. F. Shine, E. T. Champagne, and K. Daigle, *Starch/ Stärke* **51**, 280–286 (1999).
313. U. Heinze, D. Klemm, E. Unger, and F. Pieschel, *Starch/ Stärke* **55** (2), 55–60 (2003).
314. A. R. Horrocks, *Rev. Prog. Coloration* **16**, 62 (1986).
315. E. D. Weil and S. V. Levchik, *Flame Retardants for Plastics and Textiles: Practical Applications*, Hanser Publishers, Munich, Germany/Hanser Publications, Cincinnati, OH, 2009, pp. 197–225.
316. A. R. Horrocks, in D. Heywood, ed., *Textile Finishing*, Vol. **2**, Society of Dyers and Colorists, Bradford, UK, 2003.
317. (a) S. L. Vail, D. J. Daigle, and A. W. Frank, *Text. Res. J.* **52**, 671, 678, 738 (1982); (b) D. J. Daigle and A. W. Frank, *Text. Res. J.* **52**, 751 (1982).
318. U.S. Pat. 4,311,855 (Jan. 19, 1982), R. Cole and J. E. Stephenson (to Albright & Wilson).
319. W. F. Herbes, K. H. Remley, and J. B. Tracek, *Am. Dyest. Rep.* **65** (9), 72–76 (1976).
320. U.S. Pats. 4,078,101 (Mar 7, 1978) and 4,145,463 (Mar 20, 1979), R. Cole (both to Albright & Wilson, Ltd.).
321. E. D. Weil, *Am. Dyest. Rep.* **76** (1), 41 (1987); **76** (2), 40 (1987).
322. G. M. Elgal and G. L. Drake, Jr., *Ind. Eng. Chem. Prod. Res. Dev.* **23**, 441 (1984).
323. R. Aenishanslin, C. Guth, P. Hofmann, A. Maeder, and H. Nachbur, *Text. Res. J.* **39**, 375 (1969).
324. R. Aenishanslin and N. Bigler, *Textilveredlung* **3**, 467 (1968).
325. F. Lohse, in *Proceedings of the International Symposium on Flame Retardants*, Nov. 1–5, 1989, Beijing, China, International Academic Publishers, Beijing, People's Republic of China, 1989, pp. 489–494.
326. A. I. Kapura, *J. Fire Sci.* **12**, 3–13 (1994).
327. A. W. Frank, *CRC Crit. Rev. Biochem.* **16** (1), 51 (1984).
328. F. F. Shih, in S. Magdassi, ed., *Surface Activity of Proteins*, Marcel Dekker, Inc., New York, 1996, pp. 91–113.
329. A. R. Horrocks and S. Zhang, *Textile Res. J.* **74**, 433–441 (2004).

EDWARD D. WEIL

Polytechnic Institute of NYU

Brooklyn, New York

SERGEI V. LEVCHIK

Israel Chemical Ltd. – Industrial Products

Tel Aviv, Israel

## PHOTOPOLYMERIZATION, CATIONIC

### Introduction

*Light-induced polymerization reactions*, commonly known as *photopolymerizations*, are generally chain reactions in which the propagating active centers (free radicals or cations) are produced by a photochemical event. These reactions may be initiated using ultraviolet or visible light, and offer many advantages when compared to the more common thermal polymerizations in which heat is used to produce active centers. For example, photopolymerization uniquely offers spatial control (since the light may be directed to locations of interest in the system) and temporal control (since the light is readily modulated on and off) of the initiation reaction, and the rate of production of active centers is often independent of temperature. In addition, since active centers can be produced rapidly and efficiently using photochemical processes, photocuring offers high production rates, and is highly energy efficient compared to thermal polymerizations in which the entire system must be raised to elevated temperatures. A major application of photopolymerization that exploits these advantages is films and coatings that exhibit high cure rates without the use of volatile solvents, thereby minimizing emissions of organic compounds.

The vast majority of photopolymerizations used in industry are free-radical polymerizations, which have been studied extensively (for reviews, see references 1–5 as well as Photopolymerization, Free Radical (qv)). By far the most widely used classes of monomers for UV-initiated free-radical photopolymerizations are multifunctional acrylates and methacrylates. Several investigations have demonstrated that free-radical polymerizations of these monomers exhibit unusual kinetic behavior, including immediate onset of autoacceleration, the formation of heterogeneous polymers (2,6–11), and the attainment of a maximum conversion significantly less than unity (2,12–15). These monomers polymerize very rapidly, and are easily modified on the ester group, allowing materials with a variety of properties to be obtained (2); and a wide range of acrylates and methacrylates are commercially available. However, free-radical photopolymerizations have a number of problems and drawbacks that have lead scientists to examine other photopolymerization systems. For example, many acrylates are relatively volatile (methacrylates are generally less volatile than acrylates), and have an unpleasant odor. Moreover, there has been a growing concern over potential health hazards associated with the acrylates (3,4,16). Finally, the free-radical photopolymerizations are inhibited by oxygen and must be carried out under an inert atmosphere such as nitrogen or under a protective film or mold to achieve the highest reaction rates and the optimal properties of the film or coating.

UV-initiated cationic photopolymerizations exhibit several advantages when compared with the free-radical photopolymerization discussed above. First of all the cationic photopolymerizations are not inhibited by oxygen. This feature provides a significant practical advantage for industrial processes since it is not necessary to blanket the system with nitrogen to achieve rapid cure rates. Secondly, in contrast to the free-radical photopolymerizations which experience a rapid decrease in polymerization rate when the light source is removed (due to radical–radical termination reactions), the cationic polymerizations proceed long

after the irradiation has ceased, consuming nearly all of the monomer. Finally, cationic photopolymerization is a very versatile technique and may be used to polymerize important classes of monomers, including epoxides and vinyl ethers. Although these classes of monomers cannot cure by free-radical photopolymerizations, they exhibit many desirable properties, including low volatility, good rheological properties, and low toxicity (3). Furthermore, the cured polymer films associated with these monomers exhibit excellent clarity, adhesion, abrasion resistance, and chemical resistance. In addition, the cationic ring-opening polymerizations of epoxides exhibit less shrinkage, as low as 1–2% (17), than do polymerizations of unsaturated monomers such as acrylates and methacrylates, which is typically 5–20%. However, the presence of water vapor may impede the cationic curing, notably if thin films are cured at a low light intensity.

The reaction kinetics are an important aspect of any photopolymerization system under consideration for an application. For some applications, such as coatings on optical fibers, photopolymerization is perhaps the only way in which cure can be achieved fast enough to meet the requirements of the system. The reaction kinetics fundamentally follow from the mechanism by which the reaction takes place, and chain photopolymerization processes generally begin with an initiation step in which active centers are produced photochemically; proceed by the propagation step in which the active center reacts successively with a number of monomer molecules to link them covalently into a polymer chain; and may end in a termination step in which the active centers are consumed by a chemical reaction. Photopolymerization is distinguished by the fact that it is the absorption of a photon (by a specially designed photoinitiator molecule) that results in the production of active centers. Therefore, it is important to understand the photochemical processes by which the active centers are generated. The fundamental nature of the propagation and termination steps is the same for photo- and thermal polymerizations.

This article provides an overview of the important features of the kinetics of cationic photopolymerization, and a valuable resource for any scientist or engineer who is considering these reactions for a study or an application. The article begins with a description of the photoinitiation step, including the compounds and mechanisms by which cationic active centers are produced by a unimolecular process (typically a photo-induced fragmentation of the initiator), or a bimolecular process (typically an energy or electron-transfer process between a photosensitizer and the initiator). Commonly used photoinitiators and photosensitizers have been described and compared. The photoinitiation step is especially important because it is the step that distinguishes these reactions from their thermally initiated counterparts. Next, a description of traditional cationically polymerizable monomers as well as recently developed, highly reactive monomers is provided. Representative kinetic rate expressions have been presented to illustrate the link between the reaction mechanism and a quantitative description of the polymerization rate, and to illustrate the important variables that affect the rate.

## Photoinitiation

Despite the advantages of UV-initiated cationic photopolymerizations discussed above, this technique has received considerably less attention than the



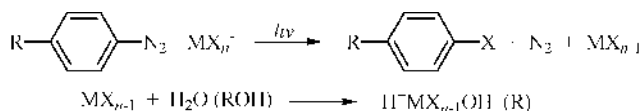


**Fig. 1.** Reaction mechanism for the photolysis of a diazonium photoinitiator. Here, R denotes substituents on the phenyl ring and  $\text{MX}_n^-$  represents a metal halide.

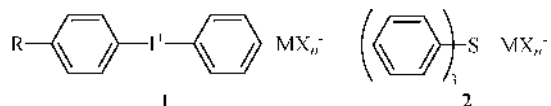
analogous free-radical reactions, and most of the studies in the literature have focused on the photoinitiation step. This fact may be attributed to the lack of suitable UV-sensitive cationic photoinitiators until recent years. In fact, applicable photoinitiators for cationic polymerizations were not developed until the late 1970s, several decades after free-radical photoinitiators had been reported. Until then, photoinitiators developed were specific to particular reaction systems. For example, Asai and co-workers (18–23) investigated the use of numerous metal salts such as sodium chloroaurate, silver salts in aromatic solvents, copper perchlorate, vanadium tetrachloride and titanium tetrachloride, as photoinitiators for cationic polymerization of *N*-vinylcarbazole. Photopolymerizations of isobutylene in the presence of Lewis acids such as vanadium chloride, titanium chloride, and tin chloride have been reported (24) via a radical-cation mechanism. A variety of monoepoxides were polymerized using manganese decacarbonyl (25) and methylcyclopentadienyl manganese tricarbonyl (26). Other examples include photocatalyzed polymerization of epichlorohydrin using bis(cyclopentadienyl) iron complex (27), and polymerization of 2-chloroethyl vinyl ether photosensitized by bis(cyclopentadienyl) titanium chloride (28).

The first more generally applicable cationic photoinitiators that achieved some success were diazonium salts of complex metal halide anions (29–35). These diazonium salts were mainly used for the cationic ring-opening photopolymerization of epoxides. Upon photolysis, these salts produce an aryl halide, molecular nitrogen, and a strong Lewis acid capable of initiating cationic polymerization, as illustrated in Figure 1. The efficiency of the diazonium salt depends on the structure of the phenyl ring, which also affects the spectral sensitivity of the molecule, and the nature of the anion moiety (17,34,36,37).

The use of these diazonium salts, however, was limited because of their poor thermal stability requiring the photoinitiators to be added just before the irradiation, and the release of nitrogen gas as a by-product which caused bubbles and pinholes in the coatings, for which they were mainly used, rendering practical constraint on the film thickness to be less than 15  $\mu\text{m}$  (38). Some attempts have been made to stabilize these salts by adding additives such as nitriles (39), amides (40), sulfoxides (41), and poly(vinyl pyrrolidone) (42); however, these approaches achieved limited success and were not widely adopted.

**Iodonium and Sulfonium Photoinitiators.** A breakthrough in the development of cationic photoinitiators occurred in the late 1970s with the development of the first iodonium salt photoinitiators. These initiators, which were developed independently at the General Electric (43) and 3M (44), avoided the shortcomings of the diazonium photoinitiators. Unlike previous initiators, these salts are remarkably stable in the absence of light, are thermally stable at room temperature, and do not degrade in the presence of moisture. Shortly after the iodonium photoinitiators were introduced, Crivello and Lam (45) reported the

development of the triarylsulfonium salts as a second class of highly efficient cationic photoinitiators that offered many of the same advantages. Representative molecular structures of the diaryliodonium salts and triarylsulfonium salts are shown as structures 1 and 2 respectively. R denotes substituents selected to enhance solubility in organic monomers and to alter the absorbance characteristics of the photoinitiator, and  $\text{MX}_n^-$  represents a metal halide.



The mechanism by which these compounds produce active centers for polymerization is described in detail below; however, at this point it should be noted that in their latent state, the compounds possess a cationic center (situated on the iodine or sulfur atoms), and possess a large anionic counterion. The aromatic rings can generally be functionalized (typically in the ortho and para positions) to enhance solubility in the organic monomers and to alter the absorbance characteristics of the photoinitiator. A number of excellent reviews are available which provide an account of the development of these initiators as well as a comprehensive list of compounds that have been synthesized (36,46,47).

The cation and the anion in the iodonium and sulfonium salts each play an important role in the performance of the photoinitiator. The cation is the light-absorbing component, and adding substituents to the aromatic rings can alter the UV absorption characteristics (for a review of this topic see Ref. 36,47, and 48). Generally, an unsubstituted iodonium salt will exhibit an absorbance maximum in the deep UV region of the spectrum at around 220 nm, and this absorbance maximum can be redshifted to around 270 nm by the addition of substituents such as ether groups, or additional aromatic rings. Sulfonium salts generally exhibit their absorbance maximum at longer wavelengths than do the iodonium salts, and may exhibit notable absorbance peaks between 300 and 320 nm. The structure of the cation also controls the quantum yield (number of molecules of active centers produced per photon absorbed) and the thermal stability of the photoinitiator (46). The iodonium salt exhibits high quantum yield (between 0.7 and 0.9) and these yields are generally higher than those for the sulfonium salts. In summary, the cation of the photoinitiator plays the determining role in the production of active centers, including the wavelengths of light for which the compound will be active, the efficiency with which the light will be used to create active centers, and, as described in more detail below, the ability of the salt to be photosensitized. The cation has very little effect on any of the processes (such as propagation) that occur after the active centers are produced and, as described below, it is the anion that plays a defining role in the rate of the propagation reaction.

Before the active center is produced, the anion serves as the counterion for the iodonium or sulfonium cation, and plays a relatively unimportant role at this stage since it has little effect on the absorbance characteristics of the salt. After the active center is produced, however, the anion serves as the counterion for the propagating active center, and at this stage plays a critical role in the rate

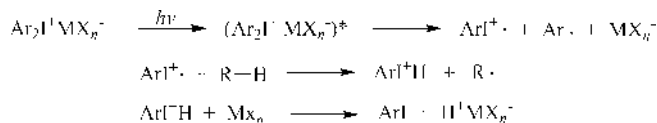


**Fig. 2.** Reaction mechanism for the photolysis of an iodonium photoinitiator. Here, Ar represents aryl group.

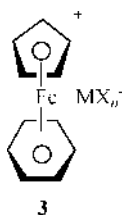
of the propagation reaction and, therefore, ultimately in the performance of the initiator. For the propagation reaction to progress at a high rate the propagating active center must have access to monomer with which it may react; therefore it is important that the active center is not encumbered with a closely associated counterion. This can be achieved if the counterion is large and the negative charge is dispersed over a large volume. This consideration has led to the use of a variety of nonnucleophilic anions such as  $\text{BF}_4^-$ ,  $\text{PF}_6^-$ ,  $\text{AsF}_6^-$ ,  $\text{SbF}_6^-$ ,  $\text{FeCl}_4^-$ , and  $\text{SbCl}_6^-$ . A nucleophilic anion such as  $\text{Cl}^-$  quickly quenches any cationic species generated during the photolysis by forming a closely associated ion pair, which prevents propagation. Based upon the above consideration, the rate of the propagation reaction is directly controlled by the counterion, and for the four most commonly used counterions, polymerization rate follows the order:  $\text{BF}_4^- < \text{PF}_6^- < \text{AsF}_4^- < \text{SbF}_6^-$  (36). Although the use of arsenic and antimony leads to the strongest superacids and the highest polymerization rates, they are toxic heavy metals, and may present problems associated with recycling when used on a large scale. For this reason, Castellanos and co-workers (49) reported a new anion, tetrakis pentafluorophenyl borate, which is as effective as  $\text{SbF}_6^-$ , but does not contain a heavy metal.

The mechanism by which onium photoinitiators produce active centers is very complex and the details are still under investigation by a number of researchers (47,50–56). The generally accepted photoinitiation reaction mechanism for iodonium salts is shown in Figure 2. Upon absorption of a photon the iodonium salt is promoted to an electronic excited state (denoted by an asterisk in the figure), and then undergoes an irreversible photofragmentation in which a carbon–iodine bond is cleaved to produce an arylodonium radical–cation and an aryl radical. It is unclear that precisely which excited state is involved in the fragmentation reaction, as some investigators (47) have concluded that it is a singlet state, while others (52,53) have concluded that it is a triplet state. In any case, it is generally accepted that the result of the fragmentation reaction is the formation of an iodine radical–cation [this has been observed by transient absorption experiments and is highly reactive with a lifetime of approximately  $6 \mu\text{s}$  (36)]. This highly reactive radical–cation will abstract a hydrogen atom from any convenient source, which can be the monomer, water, alcohol, or other impurities; rate constants for this reaction have been measured to be of the order of  $10^6 \text{ M}^{-1} \cdot \text{s}^{-1}$  (36). This hydrogen abstraction step yields an aryl iodine cation and a neutral organic radical, which can initiate radical polymerizations. The aryl iodine cation will quickly expel a proton to form a neutral aryl iodine molecule and a superacid formed by the proton and the counterion. This superacid initiates the cationic polymerization by addition to the monomer. The mechanism for a

sulfonium salt photoinitiator is similar with the cleavage of a carbon–sulfur bond under irradiation.

**Other Onium Salts and Organometallic Photoinitiators.** The success of the iodonium and sulfonium salts as photoinitiators has led to the investigation of a number of analogous onium salts based on the halides and the Group VIA atoms; however, these alternative initiators have not been widely used for various reasons. For example, chloronium and bromonium salts were prepared (57,58) and they were also found to function as cationic photoinitiators, but these salts are difficult to prepare and they have low thermal stability. Similarly, triarylselenonium salts have also been investigated and found to function as cationic initiators (59); however their preparation has been found to be expensive (60). Other onium salts such as phosphonium and arsonium salts, developed by Abu-Abdoun and co-workers for the photopolymerization of *p*-methylstyrene and styrene, have also been reported (61–63) as successful cationic photoinitiators. Photopolymerization of carbazolyloxiranes with sulfonium and tropylium salts has been reported (64). Dialkylphenacyl sulfonium photoinitiator (65–67) has been reported with excellent solubility in both polar and nonpolar monomers. Pyridinium and isoquinolinium salts have also been reported and they were found useful for polymerizing both the epoxide and vinyl ether monomers (68).

Organometallic compounds which can act as highly efficient photoinitiators for epoxide monomers have been described in the literature (25–27,69–71). The most commonly used organometallic compounds are the photoinitiators based on iron arene complex developed by the investigators at the Ciba-Geigy Corp. (37,69–71). These salts are generally prepared from ferrocene, as reviewed by Lohse and Zweifel (37). The molecular structure of a typical iron–arene complex is shown as 3.



Upon irradiation with an appropriate light source, the iron–arene complex loses the uncharged tridentate arene ligand and the positive charge moves to iron, which in association with the anion acts as a Lewis acid capable of polymerization (37). One drawback of these photoinitiators is that they are known to polymerize only the ring-opening monomers and may not be suitable for monomers with unsaturated bonds such as vinyl ethers (46).

**Bimolecular Photoinitiation and Photosensitization.** As mentioned above, the iodonium and sulfonium photoinitiators generally absorb light in the wavelength range of 200–300 nm. The effective initiating wavelength may be expanded by the use of photosensitizers or co-initiators, which shift the effective spectral window to well above 300 nm (into the near-UV and visible regions of the spectrum). The near-UV region of the spectrum is particularly convenient for initiating polymerizations because most monomers and resins absorb negligibly

at these wavelengths, yet industrial medium and high pressure mercury lamps exhibit strong emission bands in this region. In addition, use of a large fraction of the available light contributes to an overall more efficient photolysis of the initiator and, as a consequence, acceleration in the polymerization rate. A variety of compounds can be used as photosensitizers, including heterocyclic and fused-ring aromatic hydrocarbons, organic dyes, and aromatic ketones.

In general, photosensitization results from a direct interaction between an excited photosensitizer molecule (the first excited singlet state or the lowest energy triplet state that takes place due to the absorption of photon by these molecules) and the initiator. This interaction can be either an energy transfer or an electron transfer process. In the energy transfer mechanism the excited-state photosensitizer interacts with a ground-state initiator molecule to form an exciplex. In the exciplex, the excited-state energy is transferred to the initiator by vibrational relaxation that fragments the initiator to create active centers. According to this mechanism, the photosensitizer functions essentially as a catalyst and is regenerated in its ground state. For this energy transfer to be thermodynamically feasible, the excited-state energy of the photosensitizer must be greater than that of the initiator (47), a condition which is rarely met for onium salt photoinitiators.

A second possible mechanism for photosensitization involves electron transfer from the excited state of the photosensitizer to the initiator within the exciplex (47,54,72,73). Figure 3 (73) shows the important photochemical and electron transfer steps in the reaction between anthracene (the photosensitizer) and an iodonium salt. As shown in the figure, when an anthracene molecule is exposed to light it absorbs photons and goes into the first excited singlet state. From this excited state a fraction of anthracene molecules undergoes intersystem crossing to go to the lowest triplet state, where they form an excited-state complex with the initiator molecules. There has been some ambiguity as to whether the exciplex is formed in the triplet state of the sensitizer or the singlet state. Recently, on the basis of a series of fluorescence and phosphorescence lifetime studies, combined with the photochemical rate calculations and triplet state quencher studies, Nelson and co-workers (73) reported that electron transfer occurs predominantly from the triplet excited state of anthracene to the initiator. In this exciplex anthracene may undergo electron transfer to the initiator, forming a radical cation which is capable of initiating cationic polymerization.

For the electron transfer mechanism, the thermodynamic feasibility is governed by the excited-state energy of the photosensitizer (the state that participates in the electron transfer step), the oxidation potential of the excited-state photosensitizer, and the reduction potential of the initiator. It has generally been accepted that the photosensitization of diaryliodonium initiators most often proceeds by the electron transfer mechanism and a number of researchers have studied these reactions (38,47,54,74–77). Moorjani and co-workers (78) showed that the reaction system viscosity has an important effect on the overall rate of the photosensitization of diaryliodonium salts. As the reaction proceeds and the viscosity of the mixture increases because of polymerization, the rate of photosensitization will decrease substantially. It is therefore expected that the rate of initiation will become extremely low after a certain degree of polymerization, and that any further reaction will be almost exclusively from the propagation of

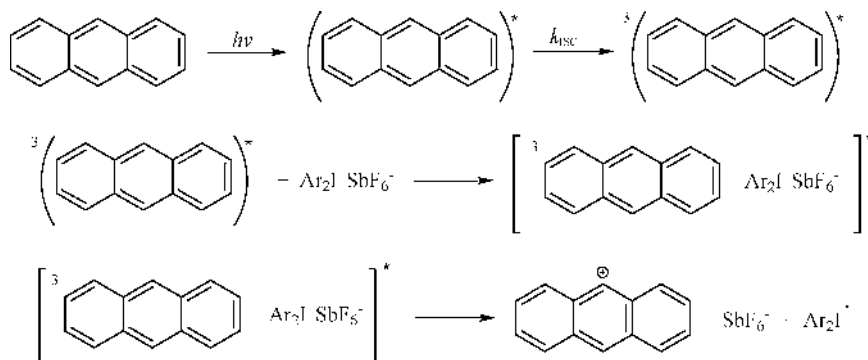


**Fig. 3.** Photosensitization mechanism based on electron transfer from triplet-state anthracene to the iodonium initiator (see reference 73).

existing active centers. This applies especially to the monomers that form glassy polymers. A number of references are available reporting the use of a variety of sensitizers with iodonium photoinitiators (68,79–85).

**Three-Component Photoinitiator Systems.** Three-component initiator systems are flexible and versatile photoinitiators that were initially developed for free-radical photopolymerizations, but may, with careful selection of the components, be used for cationic photopolymerizations. These systems generally contain a light absorbing component (often called a dye), an electron donor (typically an amine), and a third component, which is typically an iodonium salt. These initiator systems offer a number of advantages that have been demonstrated in free-radical photopolymerizations, and are also relevant for cationic photopolymerizations. For example, a wide variety of dyes may be used with the same electron donor and iodonium salt, thereby providing tremendous flexibility in selection of the initiating wavelength and therefore the light source. Indeed, effective visible-light-sensitive systems may allow use of very inexpensive light sources such as halogen and tungsten incandescent lamps. In addition, three-component systems have consistently been found to be faster, more efficient, and more sensitive than other photoinitiator systems. A variety of mechanistic investigations of free-radical three-component initiators have been reported, and the results are generally applicable to the cationic systems as well. For a review of the literature on free radicals literature including a comprehensive list of dyes and electron donors that have been used, as well as a discussion of the mechanisms by which these reaction may proceed, see Reference 86.

Care must be taken to properly design a three-component initiator system for cationic photopolymerizations. Specifically, most of the amine electron donors that are used in free-radical initiator systems are not applicable for cationic polymerizations because they are highly nucleophilic and will terminate the cationic active center. In addition, the iodonium salt must have a nonnucleophilic anion (note that for free-radical initiation, a chloride counterion is commonly used, but is clearly inappropriate for cationic polymerizations). Fewer guidelines have been provided for selection of dyes to initiate cationic photopolymerizations. Bi and Neckers (87) demonstrated cationic photopolymerizations of epoxides

initiated using a three-component initiator system containing a variety of xanthene dyes, amines with low basicity, and iodonium salts with a nonnucleophilic anion. Using this system, the polymerization was initiated by a tungsten lamp equipped with filters that eliminated light below 520 nm (where the iodonium salt does not directly absorb light). The authors further reported that presence of all the three components is required for photopolymerization above this wavelength. The authors attributed the reaction to a mechanism with three primary steps: absorption of light by the dye; production of radicals by reaction of the photoexcited dye with the amine; and production of initiating carbocations by oxidation of the radicals by the iodonium salt.

Detailed guidelines for the design of three-component initiator systems for cationic photopolymerizations were provided by Oxman and co-workers (88–91). These investigators studied a variety of electron donors, including a series of amines with systematically varying basicity (characterized by the  $pK_b$ ), and varying oxidation potential (characterized by the oxidation potential relative to a saturated calomel electrode). They found that to achieve appreciable conversion of epoxide monomer the electron donor should have an oxidation potential less than 1.34 V (to achieve desired photo-induced electron transfer between the electron donor and the onium salt to produce both the cations and the radicals) and a  $pK_b$  value greater than 8 (so that the basicity of the reaction system is low enough for the Lewis acid to proceed with the cationic polymerization without getting completely consumed). These authors used the blue-light absorbing dye camphorquinone in their studies. In addition, since these photoinitiator systems produce both radicals and cations, Oxman and co-workers demonstrated their utility for controlled sequential free-radical/cationic photopolymerization of hybrid systems consisting of methacrylates and epoxides.

## Monomers for Cationic Photopolymerization

A variety of classes of monomers undergo cationic chain polymerization, including epoxides, vinyl ethers, propenyl ethers, siloxanes, oxetanes, cyclic acetals and formals, cyclic sulfides, lactones, and lactams. Any monomer that undergoes cationic polymerization is a candidate for cationic photopolymerization, and a suitable monomer may be selected based upon the specific requirements of the application. Note that these cationically polymerizable monomers include both unsaturated monomers that undergo a chain polymerization through the carbon–carbon double bond, and cyclic ethers that undergo ring-opening polymerizations. An unsaturated monomer is capable of cationic polymerization only if a carbon atom that participates in the double bond also has an electron-releasing substituent such as an alkoxy, phenyl, vinyl, or 1,1-dialkyl group (92). Presence of any of these substituents produces an electron-rich double bond susceptible to electrophilic attack by the propagating cation. Cyclic ethers undergo cationic polymerization because of the presence of the accessible ether electron lone pairs, which are also susceptible to electrophilic attack by the propagating cation, as described in more detail below.

**Cationic Ring-Opening Photopolymerization.** A number of cyclic monomers can be polymerized by the ring-opening process, including ethers

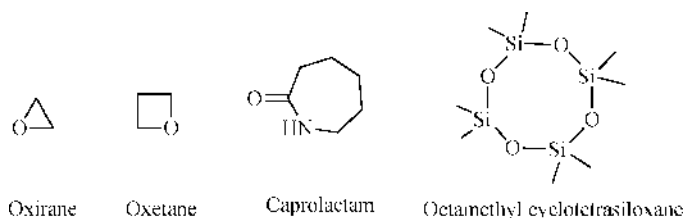


**Fig. 4.** Molecular structures of representative monomers which undergo cationic ring-opening polymerization.

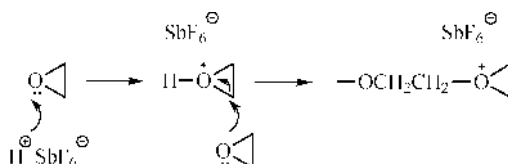


**Fig. 5.** Propagation step for cationic polymerization of an ethylene oxide monomer.

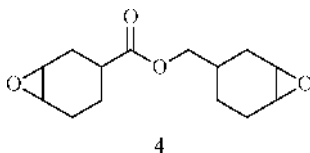
(oxiranes, oxetanes, etc), acetals, amides (lactams), esters (lactones), siloxanes, and sulfides (92). Thermodynamically, ring-opening polymerization of cyclic ethers is favored for all except the six-membered ring (the Gibbs free energy is positive for opening a six-membered ring), and the three- and four-membered rings (oxiranes and oxetanes, respectively) exhibit the most strain and therefore the most rapid polymerizations. Copolymerization of oxirane and oxetane has also been studied (93,94) and presence of oxetane has been reported to increase the overall polymerization rate. Figure 4 shows representative molecular structures of some prominent classes of monomers which undergo ring-opening polymerization. By far the most widely used and thoroughly studied monomers are the oxiranes or epoxides and therefore these monomers provide the basis for most of our discussion. Historically, the epoxide monomers were developed for condensation polymerization with other nucleophilic species such as amines and anhydrides, but they were found to be suitable for cationic ring-opening polymerization as well.

The generally accepted propagation mechanism for cationic ring-opening polymerization for ethylene oxide is shown in Figure 5. According to this mechanism, the proton of the superacid (produced from the initiation step as explained in an earlier section) undergoes an electrophilic addition to the oxygen atom present in the epoxide ring, resulting in the formation of an oxonium ion, which is the propagating species. The  $\alpha$ -carbon of the oxonium ion is electron deficient because of its proximity to the positively charged oxygen, and is therefore subject to nucleophilic attack by a monomer unit. This nucleophilic attack opens the epoxide ring (by breaking the carbon-oxygen bond) and produces a new oxonium ion, thereby propagating the active center to the new monomer unit. This process is repeated a number of times to make a polymer chain, and the polymer chain length is determined by the number of propagation steps that occur before the active center undergoes chain transfer or termination. The kinetics of the



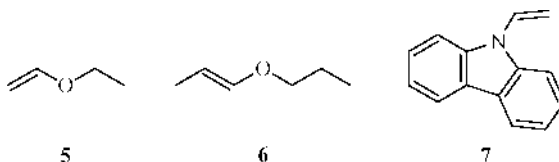
propagation reaction and the reaction parameters affecting it are examined in more detail in the next section.

Commercial epoxide monomers can be generally categorized into two classes: glycidyl ether resins and cycloaliphatic epoxides. An industry standard cycloaliphatic epoxide is 3,4-epoxycyclohexylmethyl-3,4-epoxycyclohexane carboxylate 4.



The structure of an epoxide plays an important role in the polymerization reactivity, as characterized in a number of papers including References 95 and 96. In general, cycloaliphatic epoxides exhibit shorter cure times than do the glycidyl ether resins because of the enhanced epoxy ring strain, which promotes the ring opening of the oxonium ion during the propagation step (17). In addition, viscosity of the cycloaliphatic epoxides is generally lower than that of the glycidyl ethers and hence they may be used as reactive diluents with the latter.

**Cationic Photopolymerization of Unsaturated Monomers.** Prominent classes of cationically polymerizable unsaturated monomers include vinyl ethers 5, propenyl ethers (6), and *N*-vinylcarbazole (7).



Although a number of unsaturated monomers theoretically may undergo cationic photopolymerizations, there have been few studies of these photopolymerization systems reported in the literature. In the last decade some systematic studies of the cationic photopolymerization of vinyl ethers have been reported; therefore these systems are the focus of our discussion. Vinyl ether and propenyl ether monomers are among the most reactive monomers (which polymerize by a cationic mechanism) and they exhibit low vapor pressure, low toxicity, and relatively low viscosity. Hence, these monomers may be used as reactive diluents to enhance the effective cure rates of epoxide photopolymerizations.

The propagation mechanism for cationic polymerization of a vinyl ether monomer is shown in Figure 6. According to this mechanism, proton of the superacid (produced from the initiation step as explained in an earlier section) breaks the carbon-carbon double bond by attaching itself to one carbon atom, making the other carbon atom electron deficient. This carbocation is subjected to a nucleophilic attack by another monomer molecule which results in the formation of a carbon-carbon bond and transfer of the positive charge to the other carbon atom. This process is repeated a number of times to produce the polymer chain (again, the polymer chain length is determined by the number of

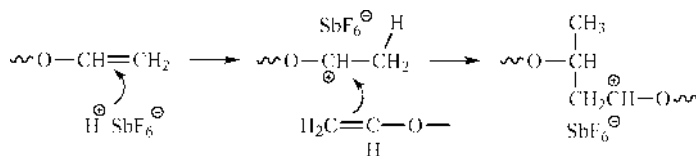


**Fig. 6.** Propagation step for cationic polymerization of a vinyl ether monomer.

propagation steps that occur before the active center undergoes chain transfer or termination).

**Development of New Monomers.** In the past decade, several new cationically polymerizable monomers exhibiting enhanced reaction rates and desirable film properties have been reported, most notably by Crivello and collaborators. These monomers may not be commercially available; however, a synthetic scheme for preparation of such monomers is usually provided. A detailed account of the utility of each monomer is beyond the scope of this article; however, a list of references that may be useful to the interested reader is provided here. Examples of novel cationically polymerizable monomers include epoxide monomers based on benzyl, allyl, propargyl acetal, and propargyl ether groups (97); epoxide monomers based on  $\alpha$ -terpineol (98); difunctional epoxide monomers (99); epoxide monomers based on bisvinyl ethers or propenyl ethers (16,100); monomers based on 1-butenyl ethers (101,102) or 1-butenyl glycidyl ether (103); 1-propenyl ethers (104–107) or 1-propenyl glycidyl ethers (108); aromatic monomers bearing two, three, four, and six cationically polymerizable vinyl, isopropenyl, or propenyl functional groups (109); novel silicon-containing epoxy resins (110–113), oxetanes (114), and 1-propenyl ethers (115,116); novel cycloaliphatic epoxide monomers (117); multifunctional monomers bearing a combination of either epoxy, vinyl ether, cycloaliphatic epoxy, or 1-propenyl ether groups (118,119); ketene acetals (120); epoxy norbornane monomers (121,122); mono-, bi-, and trifunctional oxetanes (123); alkoxy allene monomers (124); monomers based on nopol (125); and dicyclopentadiene (126,127); monomers bearing two, four, and six aryl 2-propenyl groups prepared by isomerization of corresponding allyl groups (128); monomers based on isopropylphenoxy groups (129,130); carbazolyl containing epoxy monomers (131); and novel cycloaliphatic epoxide monomers bearing benzyl ether groups (132). Finally, it should be noted that a wide variety of cationically polymerizable epoxide monomers have been prepared from inexpensive and biorenewable sources such as linseed oil and soybean oil (133–135). In addition, epoxidized soybean oil has also been studied as a reactive diluent with other monomers and the polymerization rate of the reaction system has been characterized (135–137).

## Kinetics of Cationic Photopolymerization

Cationic polymerizations, like other chain polymerizations, begin with the initiation step (which results in the production of active centers); then proceed by the propagation step in which the active center reacts successively with a number of monomer molecules to link them covalently into a polymer chain; and finally may

end in a termination step in which the active centers are consumed by a chemical reaction. The photoinitiation step, as described in detail in the preceding section, is the only step that is dependent on light. Once the active centers are produced the propagation and termination steps generally proceed by the normal cationic polymerization processes and are subject to the usual reaction variables and kinetic considerations, although the typical counterions for cationic photopolymerization may be different than those used in thermal cationic polymerizations. This may be important since the counterions generally have a marked effect on both the propagation and termination reactions. Finally, in the presence of a Lewis base such as water or alcohols, a growing cationic polymer chain may undergo a chain transfer reaction, which results in the termination of one growing chain and the generation of a proton capable of initiating a new chain. This reaction can have a significant effect on the structure of the polymer, especially in cross-linked systems. In thin coatings exposed to humid air, polymerization may even be suppressed.

The polymer chain length (the number of repeat units per chain, or degree of polymerization) is determined by the number of propagation steps that occur before the active center undergoes chain transfer or termination. In contrast, the kinetic chain length corresponds to the total number of propagation steps that occur during the lifetime of the active center, and therefore corresponds to the number of propagation steps that occur before termination. If no chain transfer occurs the polymer chain length is equal to the kinetic chain length, however, trace amounts of nucleophiles such as water or alcohol are typically present and active center chain transfer is common in cationic polymerization. For this reason the degree of polymerization in cationic photopolymerization is typically significantly lower than the kinetic chain length.

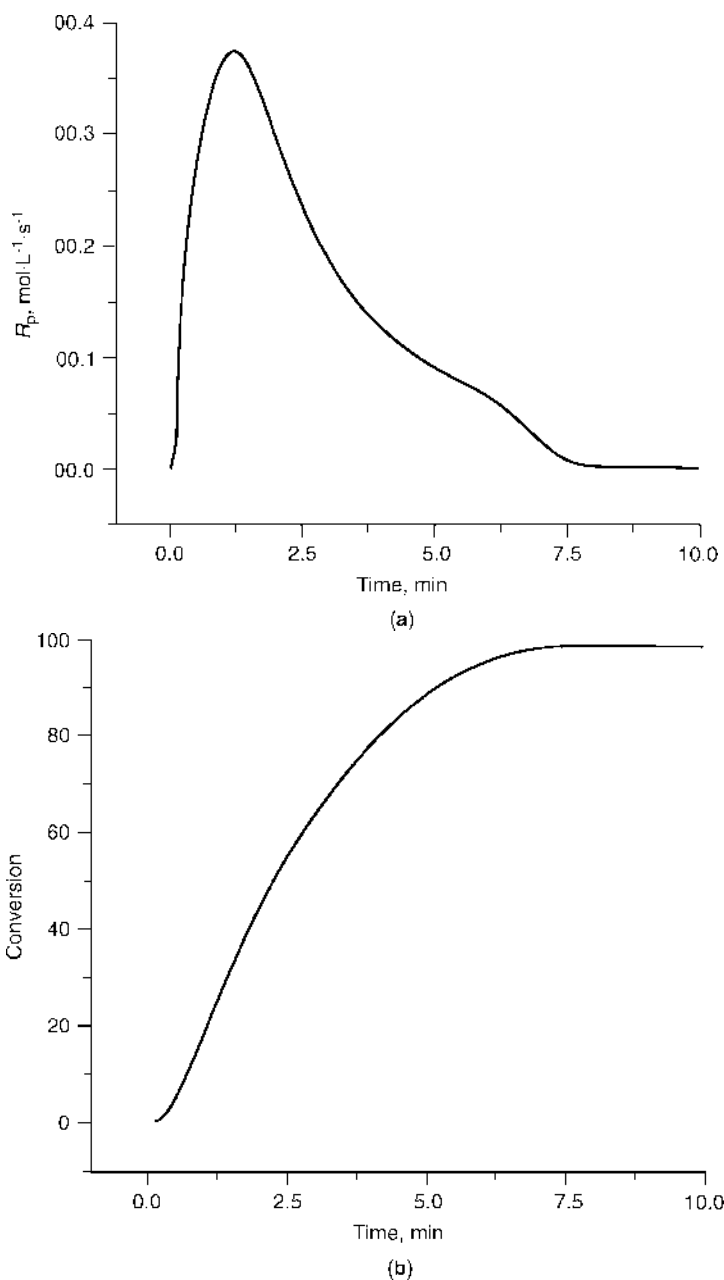
The kinetics of cationic polymerizations are considerably more complex than those of the free-radical polymerizations, and kinetic data is difficult to interpret because of several reasons (92,138–140). For example, in cationic polymerizations the identity and proximity of the counterion has a marked effect on the reactivity of the active center. An active center that is encumbered by a closely associated counterion has a dramatically lower reactivity (typically an order of magnitude lower) than an active center that is separated from the counterion. As described in the section on photoinitiation, this consideration has led to the development of large, nonnucleophilic counterions; however the reactivity of a cationic active center still depends on the proximity of the counterion. Therefore, at any given time, a variety of propagating species may exist, ranging from ion pairs to separated ions. For this reason, an effective propagation rate constant which includes contributions from all propagating species is usually adopted, as described below. Secondly, unlike free-radical polymerizations, the steady-state approximation for active center concentration is not valid since the cationic active centers are not reactive toward one another, and the rate of active center generation through initiation is typically much higher than the rate of consumption of active centers through termination. Therefore, the active center concentration generally increases continuously until the photoinitiator is completely consumed, and must be either measured experimentally (which is extremely difficult) or calculated using unsteady-state species balances. Photosensitized polymerizations are further complicated by the fact that the rate of generation of active centers depends upon

the system viscosity (which changes appreciably during the course of the reaction). With these general considerations in mind, in this section we provide an overview of the propagation and termination reactions in cationic photopolymerization, focusing on the aspects that will be of greatest value to scientists and engineers considering these systems for studies or applications.

***In Situ* Characterization of the Rate of Cationic Photopolymerization.** Before an examination of the propagation and termination reactions individually, a brief overview of the methods that have been used to obtain profiles of the polymerization rate as a function of time is provided. The photopolymerization rate can be monitored by any technique that measures a physical quantity which changes as the reaction progresses. In theory, a wide variety of analytical techniques could be used for this purpose (139–148), and new methods are continuously being developed (149). The commonly used methods for obtaining complete polymerization rate profiles are differential scanning calorimetry, fluorescence spectroscopy, and vibrational spectroscopies such as Raman and infrared.

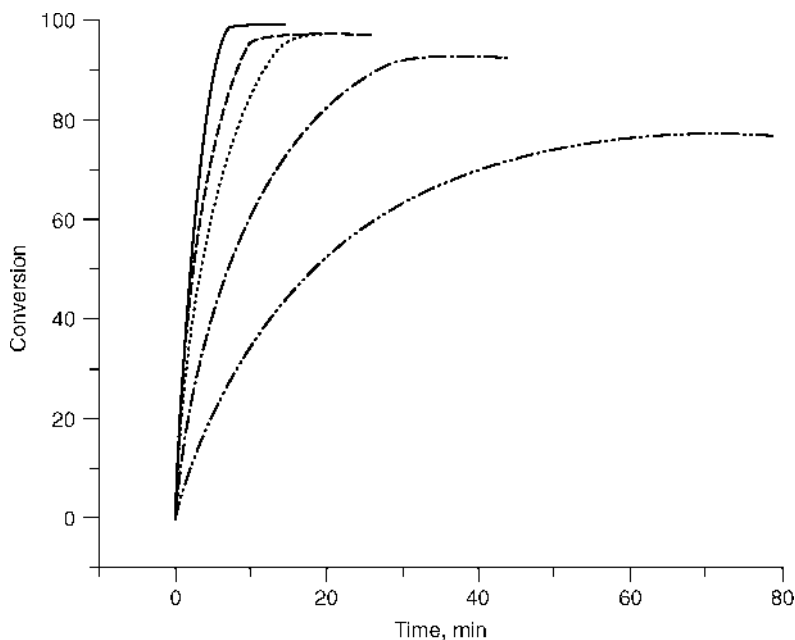
Differential scanning calorimeter (DSC) has, perhaps, become the most widely used instrument for studying the kinetics of polymerization reactions (139,141,142). In this calorimetric technique, the reaction rate is monitored by measuring the heat released during the exothermic polymerization. For homopolymerizations, the rate at which heat is released is directly proportional to the polymerization rate, and conversion profiles can be obtained by integrating the reaction rate profiles. The DSC response time is relatively slow (of the order of 2–3 s); therefore this technique cannot be used for rapid photopolymerization systems. Real-time infrared (RTIR) spectroscopy was developed by Decker and Moussa in the early 1990s (143) to investigate the polymerization of acrylates. This technique has also been used to investigate the polymerization of epoxides (144) by simultaneously monitoring the monomer consumption and the polymer formation by using two IR detectors at the wavelengths of 790 and 1100  $\text{cm}^{-1}$ , respectively. Infrared spectroscopy (both FTIR and RTIR) has sufficient time resolution to monitor rapid polymerizations. For example, FTIR instruments generally allow spectra to be collected every 40 or 50 ms. Raman spectroscopy has also been used for *in situ* monitoring of photopolymerizations of vinyl ether, acrylates, etc. Raman spectroscopy involves the inelastic scattering of photons rather than their direct absorption or emission by a material; therefore the intrinsic time scale of this method is extremely fast (of the order of femtoseconds). The practical time resolution is determined by the signal intensity, and generally several usable spectra can be acquired in a second (140,145). Fluorescence spectroscopy has been used for real-time monitoring of polymerizations and generally the monitoring schemes are based upon fluorescence probes which exhibit enhanced fluorescence intensity with change in variables such as system viscosity with the progress of polymerization due to decreased nonradiative energy transfer (72,146–148).

Figure 7 (150) contains profiles of the polymerization rate and conversion as function of time for cationic photopolymerization of an epoxide monomer obtained using a photo-DSC. As shown in the figure, the reaction rate profile has a general shape that is characteristic of cationic photopolymerizations. Immediately upon illumination, cationic active centers are produced and they react with the surrounding monomer molecules to form a growing polymer chain. The reaction rate increases monotonically because of the increase in the concentration



**Fig. 7.** Polymerization rate (a) and percentage conversion (b) vs time profiles for photopolymerization of phenyl glycidyl ether initiated using 8.86 mM of iodonium tetrakis pentafluorophenyl borate salt at 50°C and light intensity of  $25 \text{ mW} \cdot \text{cm}^{-2}$  (see reference 150).

of active centers, reaches a peak, and then decreases, primarily because of the decrease in the concentration of monomer. Typically, as the conversion reaches a high value, the polymerization rate will slow because of diffusional limitations



**Fig. 8.** Profiles of percentage conversion vs time for various illumination times for photopolymerizations of phenyl glycidyl ether initiated using 8.86 mM of iodonium tetrakis pentafluorophenyl borate salt at 50°C and light intensity of 25 mW·cm<sup>-2</sup> (see reference 150). — Full illumination; - - 90-s illumination; - - - 60-s illumination; - · - 30-s illumination; · · · 15-s illumination.

and may ultimately stop at a limiting conversion below 100% if the system turns glassy and vitrification occurs.

One important characteristic of cationic photopolymerization is that the reaction continues for a long time even after the light has been shuttered off. This is strikingly different from free-radical photopolymerization where the reaction stops in a very short time in dark. Figure 8 (150) shows the reaction rate as a function of time for photopolymerization of an epoxide monomer for various illumination times. The figure contains profiles of the conversion as a function of time for five identical reaction systems illuminated for different periods of time ranging from 15 s to the duration of the experiment (full illumination) and it shows that the polymerization reaction proceeds long after the illumination has ceased, often consuming all of the monomer. For example, the sample that was illuminated for only 15 s continues to react for more than an hour in the dark.

**Rate Constants for Propagation and Termination.** For cationic chain polymerizations, the rate of polymerization is generally accepted to be proportional to the product of the monomer concentration and the active center concentration, with the proportionality constant being the effective propagation rate constant  $k_p$ , as shown in equation 1:

$$R_p = k_p [M] [M^+] \quad (1)$$

The propagation rate constant  $k_p$  includes contributions from a variety of propagating species ranging from ion pairs to separated ions. The value of  $k_p$  depends, of course, on the monomer being polymerized (the previous section contained a description of attempts to create new, highly reactive monomers), and for a given monomer the value of  $k_p$  also depends upon the temperature, the photoinitiator anion, and the proximity of the counterion to the active center, as described below. The propagation rate constants for vinyl ether and epoxide monomers have been studied extensively using techniques such as differential scanning calorimetry and Raman spectroscopy (139,140,150,151).

An interesting hypothesis that has been reported in the literature (139,140) is that the value of  $k_p$  can change appreciably during the course of the reaction because of a change in the proximity of the counterion and the active center. According to this hypothesis,  $k_p$  initially increases sharply, then levels off at a plateau value, and finally as the limiting conversion is reached the value of  $k_p$  decreases. At the beginning of the polymerization reaction, it is hypothesized that the active center and the counterion are relatively close to one another since the viscosity is relatively low, and the diffusional mobility of the counterion allows it to move with the cation. As the polymerization progresses there is an increase in the system viscosity, which reduces diffusional mobility of all the species present in the reaction system. The active center retains considerable mobility through propagation since the cation effectively moves through the reaction mixture by reacting with the monomer units (which is termed *reaction diffusion*). The counterion, however, experiences a decrease in mobility as the system viscosity increases, since it has to physically diffuse through the reaction mixture. During this process, the counterion and the active center separate, and since the separated ions are much more reactive than the ion pairs, it leads to a large increase in the value of  $k_p$ . Finally, the value of  $k_p$  decreases because of the trapping of the active centers. Therefore, a limiting conversion at which the reaction ceases is observed despite the presence of active centers and unreacted monomer.

The rate of termination and, consequently, the active center lifetime for the cationic and radical polymerizations are notably different. Free radicals, which are highly reactive toward one another, have very high termination rate constants (of the order of  $10^5 \text{ L}\cdot\text{mol}^{-1}\cdot\text{s}^{-1}$ ) and have correspondingly short active center lifetimes (typically less than a second). In contrast, for cationic polymerizations the rate of consumption of active centers is very slow, and generally takes place by some type of nucleophilic attack on the propagating cation. The precise nature of this chemical termination may be system specific, and is generally not well understood. In some cases, termination may occur by combination of the propagating active center with the anion. For example an active center may combine with the metal halide ion such as  $\text{PF}_6^-$  (the photoinitiator anion), abstract a fluorine atom, and expel a proton, thus regenerating a Lewis acid. Although it has been relatively unstudied, the average cationic active center lifetime has been found to be of the order of tens of minutes (139,140,150).

In addition to this termination by a chemical reaction, the active center may stop propagating owing to trapping. In this case, although the active centers are still present (they have not terminated per se), they are no longer propagating because the surrounding monomer molecules have polymerized and the active centers are unable to access the unreacted monomer. If the "termination"

reaction is studied by investigating the reduction of the polymerization rate in the dark, then trapping cannot be distinguished from chemical termination. The termination/trapping of the active centers is commonly modeled as first order, which results in the following equation:

$$\frac{d[M^+]}{dt} = -k_{t/t}[M^+] \quad (2)$$

Here,  $[M^+]$  corresponds to the concentration of propagating (untrapped) active centers, while  $k_{t/t}$  represents the first-order kinetic rate constant for termination/trapping of active centers.

**Effect of Light Intensity.** The rate of a cationic photopolymerization depends upon the incident light intensity (radiant flux or photon flux) since an increasing light intensity increases the rate of production of active centers. The rate constants for propagation and termination are independent of light intensity. Therefore, in equation 1, the effect of light intensity is contained within the active center concentration  $[M^+]$ . The relationship between the light intensity and the active center concentration can be captured within a rate constant for absorbance,  $k_{\text{abs}}$ , defined as the product of the incident photon flux and the photoinitiator absorption cross section summed over all incident wavelengths (150). The concentration of cationic active centers produced by the photolysis of a photoinitiator (unimolecular initiation) is given by equation 3:

$$[M^+] = \phi I_0(1 - e^{-k_{\text{abs}}t}) \quad (3)$$

Here,  $\phi$  is the quantum yield of the photoinitiator cleavage (the number of active centers formed per photon absorbed), and  $I_0$  is the photoinitiator concentration at time  $t = 0$ . This equation illustrates that the active center concentration is not at steady state, but rather grows with time until the photoinitiator is consumed. Note that this equation accounts only for production of active centers by photolysis. To completely describe the active center concentration, equations 2 and 3 should be combined to account for both the production and the consumption of active centers. It is important to note that while the incident light intensity does affect the rate of polymerization, it generally has no impact on the final limiting conversion (if the temperature is held constant).

**Effect of Temperature and Photoinitiator Anion.** The polymerization temperature has a significant effect on both the rate of polymerization and the final limiting conversion. For example, Figure 9 contains a series of plots of reaction rate as a function of time for photopolymerization of an epoxide monomer. This figure illustrates that as the temperature is increased, the peak reaction rate increases and the reaction time decreases. The increase in reaction rate with increasing temperature ultimately arises from the effect of temperature on the propagation rate constant (which increases with increasing temperature as described by the Arrhenius equation for the rate constants). The rate of photoinitiation is generally independent of temperature (for unimolecular photoinitiation the activation energy is zero since the initiating energy comes from light rather than heat). In addition, as the temperature is increased the final limiting conversion invariably increases because of enhanced mobility of the active centers and



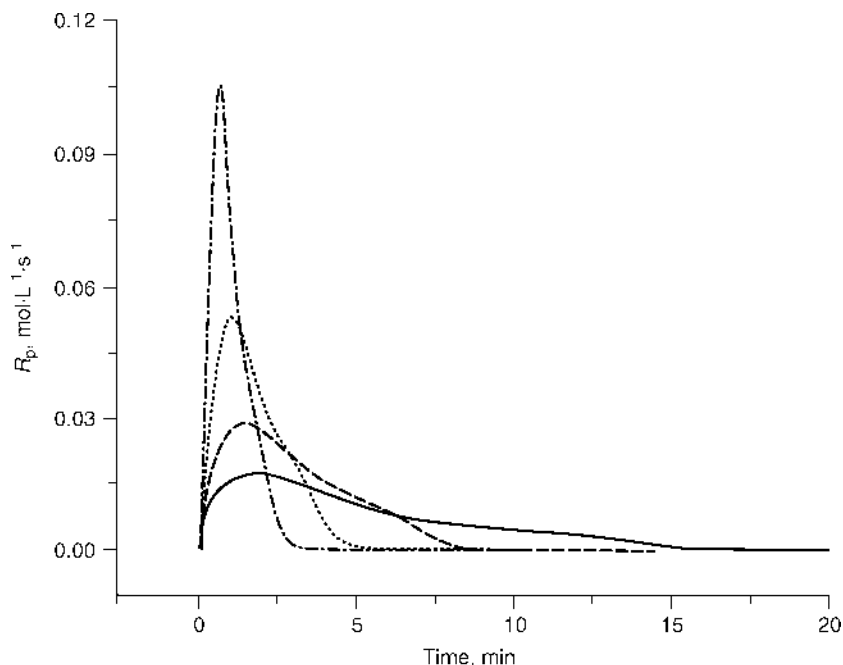


**Fig. 9.** Effect of temperature on the reaction rate as a function of time for photopolymerizations of phenyl glycidyl ether initiated using 8.86 mM of iodonium tetrakis pentafluorophenyl borate salt at light intensity of  $25 \text{ mW}\cdot\text{cm}^{-2}$ . — 40°C; - - - 50°C; ..... 60°C; - · - · - 70°C.

**Table 1.** Effect of the Temperature and the Photoinitiator Counterion on the Termination and Propagation Rate Constants<sup>a</sup>

Temperature, °C	Iodonium tetrakis pentafluorophenyl borate salt		Iodonium hexafluoroantimonate salt	
	$k_t, \text{s}^{-1}$	$k_p, \text{L}\cdot\text{mol}^{-1}\cdot\text{s}^{-1}$	$k_t, \text{s}^{-1}$	$k_p, \text{L}\cdot\text{mol}^{-1}\cdot\text{s}^{-1}$
50	$4.5 \times 10^{-4}$	0.6	$6.8 \times 10^{-4}$	0.4
60	$5.5 \times 10^{-4}$	1.4	$11.3 \times 10^{-4}$	0.8

<sup>a</sup>For photopolymerizations of phenyl glycidyl ether monomer at 50°C and  $25 \text{ mW}\cdot\text{cm}^{-2}$  light intensity and at 8.86 mM concentration of photoinitiators (see reference 150).

diminishing effect of vitrification. The effect of temperature on the propagation and termination rate constants for cationic photopolymerizations of a few vinyl ether and epoxide monomers have been reported (140,150). For example, propagation and termination rate constants for photopolymerization of an epoxide monomer are shown in Table 1 (150).

The data in Table 1 also illustrate the effect of the size of the counterion on the values of the propagation and termination rate constant (150,151). This table illustrates that the tetrakis pentafluorophenyl borate anion, which is 14 times more voluminous than the hexafluoroantimonate anion, results in a higher propagation rate constant and lower termination rate constant for the

photopolymerization. These are the expected trends since the larger counterion will result in a more weakly associated ion pair.

## BIBLIOGRAPHY

"Photopolymerization and Photocross-linking" in *EPST* 1st ed., Vol. 10, pp. 145–156, by G. Oster, Mount Sinai School of Medicine; "Photopolymerization" in *EPSE* 2nd ed., Vol. 11, pp. 186–212, by S. P. Pappas, North Dakota State University; "Photopolymerization, Cationic" in *EPST* 3rd ed., Vol. 10, pp. 784–807, by V. Sipani and A. B. Scranton, University of Iowa.

## CITED REFERENCES

1. A. Reiser, *Photoreactive Polymers*, John Wiley & Sons, Inc., New York, 1989.
2. J. G. Kloosterboer, *Adv. Polym. Sci.* **84**, 1 (1988).
3. C. G. Roffey, *Photopolymerization of Surface Coatings*, John Wiley & Sons, Inc., New York, 1981.
4. S. P. Pappas, *UV Curing, Science and Technology*, Vol. 2, Technology Marketing Corp., Norwalk, Conn., 1985.
5. M. Kaur and A. K. Srivastava, *J. Macromol. Sci. C: Polym. Rev.* **42**, 481 (2002).
6. H. M. J. Boots, J. G. Kloosterboer, G. M. M. Van de Hei, and R. B. Pandey, *Br. Polym. J.* **17**, 219 (1985).
7. H. Galina, B. N. Kolarz, P. P. Wiczorek, and M. Wojczynska, *Br. Polym. J.* **17**, 215 (1985).
8. W. Funke, *Br. Polym. J.* **21**, 107 (1989).
9. J. Bastide and L. Leibler, *Macromolecules* **21**, 2647 (1988).
10. A. Matsumoto, H. Matsuo, H. Ando, and M. Oiwa, *Eur. Polym. J.* **25**, 237 (1989).
11. J. Baselga, M. A. Llorente, I. Hernandez-Fuentes, and I. F. Pierola, *Eur. Polym. J.* **25**, 471 (1989).
12. D. T. Turner, Z. U. Haque, S. Kalachandra, and T. W. Wilson, *Polym. Mater. Sci. Eng.* **56**, 769 (1987).
13. G. P. Simon, P. E. M. Allen, D. J. Bennett, D. R. G. Williams, and E. H. Williams, *Macromolecules* **22**, 3555 (1989).
14. J. G. Kloosterboer, G. F. C. M. Lijten, and C. P. G. Zegers, *Polym. Mater. Sci. Eng.* **60**, 122 (1989).
15. P. E. M. Allen, D. J. Bennett, S. Hagias, A. M. Hounsflow, G. S. Ross, G. P. Simon, D. R. G. Williams, and E. H. Williams, *Eur. Polym. J.* **25**, 785 (1989).
16. S. C. Lapin, in C. E. Hoyle and J. F. Kinstle, eds., ACS Symposium Series, Vol. 417, American Chemical Society, Washington, D.C., 1990, p. 363.
17. J. V. Crivello and K. Dietliker, in G. Bradley, ed., *Photoinitiators for Free Radical Cationic & Anionic Photopolymerisation Volume III*, SITA Technology Ltd., London, 1998, p. 355.
18. M. Asai, K. Kameoka, Y. Takeda, and S. Tazuke, *J. Polym. Sci., Polym. Lett. Ed.* **9**, 247 (1971).
19. M. Asai, S. Tazuke, and S. Okamura, *J. Polym. Sci., Polym. Chem. Ed.* **12**(1), 45 (1974).
20. M. Asai and S. Tazuke, *Macromolecules* **6**, 818 (1973).
21. M. Asai, Y. Takeda, S. Tazuke, and S. Okamura, *Polym. J. (Tokyo)* **7**(3), 359 (1975).
22. Y. Takeda, M. Asai, and S. Tazuke, *Polym. J. (Tokyo)* **7**(3), 366 (1975).
23. M. Asai, H. Matsui, and S. Tazuke, *Bull. Chem. Soc. Jpn.* **47**(4), 864 (1974).
24. M. Marek, L. Toamn, and J. Pilar, *J. Polym. Sci., Polym. Chem. Ed.* **13**(7), 1565 (1975).
25. W. Strohmeier, and P. Hartman, *Z. Naturforsch.* **20b**, 513 (1965).

26. W. S. Anderson, *J. Appl. Polym. Sci.* **15**, 2063 (1971).
27. K. Kaeriyama, *J. Polym. Sci., Polym. Chem. Ed.* **14**, 1547 (1976).
28. K. Kaeriyama, and Y. Shimura, *J. Polym. Sci., Polym. Chem. Ed.* **10**, 2833 (1972).
29. U.S. Pat. 3,708,296 (Jan. 2, 1973), S. I. Schlesinger (to American Can Co.).
30. U.S. Pat. 3,205,157 (1965), J. J. Licari and P. C. Crepeau (to North American Aviation, Inc.).
31. U.S. Pat. 3,829,369 (Aug. 13, 1974), J. H. Feinberg (to American Can Co.).
32. G.B. Pat. 1,404,242 (1975), J. H. Feinberg (to American Can Co.).
33. U.S. Pat. 3,960,684 (1976), J. H. Feinberg (to American Can Co.).
34. S. I. Schlesinger, *Polym. Eng. Sci.* **14**, 513 (1974).
35. M. P. Dreyfuss, J. C. Westfahl, and P. Dreyfuss, *Macromolecules* **1**, 437 (1968).
36. J. P. Fouassier, *Photoinitiation, Photopolymerization, and Photocuring: Fundamentals and Applications*, Hanser/Gardner Publication, Inc., Cincinnati, 1995.
37. F. Lohse and H. Zweifel, *Adv. Polym. Sci.* **78**, 62 (1986).
38. S. P. Pappas, *Prog. Org. Coat.* **13**, 35 (1985).
39. U.S. Pat. 3,721,616 (1974), W. R. Watt (to American Can Co.).
40. U.S. Pat. 3,721,617 (1973), W. R. Watt (to American Can Co.).
41. U.S. Pat. 3,711,391 (1973), J. H. Feinberg (to American Can Co.).
42. U.S. Pat. 3,816,281 (June 11, 1974), J. H. Feinberg (to American Can Co.).
43. J. V. Crivello and J. H. W. Lam, *Macromolecules* **10**(6), 1307 (1977).
44. U.S. Pat. 4,394,403 (July 19, 1983), G. H. Smith (to Minnesota Mining and Manufacturing Co.).
45. J. V. Crivello and J. H. W. Lam, *J. Polym. Sci., Polym. Chem. Ed.* **17**, 977 (1979).
46. J. V. Crivello, *J. Polym. Sci., Part A: Polym. Chem.* **37**, 4241 (1999).
47. J. V. Crivello, *Adv. Polym. Sci.* **62**, 1 (1984).
48. J. V. Crivello, *Dev. Polym. Photochem.* **2**, 1 (1981).
49. F. Castellanos, J. P. Fouassier, C. Priou, and J. Cavezzan, *J. Appl. Polym. Sci.* **60**, 705 (1996).
50. R. S. Davidson and J. W. Goodin, *Eur. Polym. J.* **18**, 589 (1982).
51. J. P. Fouassier, D. Burr, and J. V. Crivello, *J. Macromol. Sci., A: Pure Appl. Chem.* **31**, 677 (1994).
52. R. J. Devoe, M. R. V. Sahyun, N. Serpone, and D. K. Sharma, *Can. J. Chem.* **65**, 2342 (1987).
53. J. L. Dektar and N. P. Hacker, *J. Org. Chem.* **53**, 1835 (1988).
54. J. L. Dektar and N. P. Hacker, *J. Org. Chem.* **55**, 639 (1990).
55. J. L. Dektar and N. P. Hacker, *J. Org. Chem.* **56**, 1838 (1991).
56. V. Jancovicova, V. Brezova, M. Ciganek, and Z. Cibulkova, *J. Photochem. Photobiol., A* **136**, 195 (2000).
57. J. V. Crivello and J. H. W. Lam, *J. Polym. Sci., Polym. Lett. Ed.* **16**, 563 (1978).
58. G. A. Olah, T. Sakakibara, and G. Asensio, *J. Org. Chem.* **43**, 463 (1978).
59. J. V. Crivello and J. H. W. Lam, *J. Polym. Sci., Polym. Chem. Ed.* **17**, 1047 (1979).
60. J. V. Crivello and J. H. W. Lam, *J. Org. Chem.* **43**, 3055 (1978).
61. I. I. Abu-Abdoun and A. Ali, *Macromol. Rep., A* **30**, 327 (1993).
62. D. C. Neckers and I. Abu-Abdoun, *Macromolecules* **17**, 2468 (1984).
63. I. I. Abu-Abdoun and A. Ali, *Eur. Polym. J.* **29**, 1439 (1993).
64. J. V. Gražulevičius, R. Kavaliūnas, R. Lazauskaite, V. M. Getautis, and M. Daškevičienė, *J. Photochem. Photobiol., A* **110**, 85 (1997).
65. J. V. Crivello and S. Kong, *Macromolecules* **33**, 825 (2000).
66. J. V. Crivello and S. Kong, *Macromolecules* **33**, 833 (2000).
67. J. V. Crivello, *Des. Monomers Polym.* **5**, 141 (2002).
68. W. Schnabel, *Makromol. Rapid Commun.* **21**, 628 (2000).
69. Eur. Pat. 094915 (1984), K. Meier, N. Buehler, H. Zweifel, G. Berner, and F. Lohse (to Ciba-Geigy A.-G.).

70. Eur. Pat. 126712 (1984), K. Meier, G. Eugster, F. Schwarzenback, and H. Zweifel (to Ciba-Geigy A.-G.).
71. K. Meier and H. Zweifel, *J. Imaging Sci.* **30**, 174 (1986).
72. E. W. Nelson, T. P. Carter, and A. B. Scranton, *Macromolecules* **27**, 1013 (1994).
73. E. W. Nelson, T. P. Carter, and A. B. Scranton, *J. Polym. Sci., Part A: Polym. Chem.* **33**, 247 (1995).
74. G. Manivannan and J. P. Fouassier, *J. Polym. Sci., Part A: Polym. Chem.* **29**, 1113 (1991).
75. S. P. Pappas, B. C. Pappas, L. R. Gatechair, and W. Schnabel, *J. Polym. Sci., Polym. Chem. Ed.* **22**, 69 (1984).
76. J. P. Fouassier, D. Burr, and J. V. Crivello, *J. Photochem. Photobiol., A* **49**, 317 (1989).
77. R. J. Devoe, M. R. V. Sahyun, and E. Schmidt, *J. Imaging Sci.* **33**, 39 (1989).
78. S. Moorjani, B. Rangarajan, and A. B. Scranton, in A. B. Scranton, C. N. Bowman, and R. W. Peiffer, eds., *ACS Symposium Series*, Vol. 673, American Chemical Society, Washington, D. C., 1997, p. 95.
79. Y. Toba, *J. Polym. Sci., Part A: Polym. Chem.* **38**, 982 (2000).
80. J. V. Crivello and M. Sangermano, *J. Polym. Sci., Part A: Polym. Chem.* **39**, 343 (2001).
81. J. V. Crivello and F. Jiang, *Chem. Mater.* **14**, 4858 (2002).
82. Y. Toba, Y. Usui, M. Alam, and O. Ito, *Macromolecules* **31**, 6022 (1998).
83. Y. Toba, M. Saito, and Y. Usui, *Macromolecules* **32**, 3209 (1999).
84. J. L. Jacobs, E. W. Nelson, and A. B. Scranton, *Polym. Mater. Sci. Eng.* **70**, 74 (1993).
85. H. J. Timpe, H. Rautschek, and C. Mueller, *J. Photographic Sci.* **39**, 19 (1991).
86. K. S. Padon and A. B. Scranton, *Recent Res. Dev. Polym. Sci.* **3**, 369 (1999).
87. Y. Bi and D. C. Neckers, *Macromolecules* **27**, 3683 (1994).
88. U.S. Pat. 5,998,495 (Dec. 7, 1999), J. D. Oxman and D. W. Jacobs (to 3M Innovative Properties Co.).
89. U.S. Pat. 6,025,406 (Feb. 15, 2000), J. D. Oxman and D. W. Jacobs (to 3M Innovative Properties Co.).
90. U.S. Pat. 6,187,836 (Feb. 13, 2001), J. D. Oxman, M. C. Trom and D. W. Jacobs (to 3M Innovative Properties Co.).
91. J. D. Oxman, D. W. Jacobs, and M. C. Trom, *Polym. Mater. Sci. Eng.* **88**, 239 (2003).
92. G. Odian, *Principles of Photopolymerization*, John Wiley & Sons, Inc., New York, 1991.
93. H. Sasaki, J. M. Rudzinski, and T. Kakuchi, *J. Polym. Sci., Part A: Polym. Chem.* **33**, 1807 (1995).
94. H. Sasaki, in K. D. Belfield and J. V. Crivello, eds., *ACS Symposium Series*, Vol. 847, American Chemical Society, Washington, D.C., 2003, p. 296.
95. J. V. Crivello and V. Linzer, *Polimery (Warsaw)* **43**, 661 (1998).
96. B. L. Podlogar and D. J. Raber, *J. Org. Chem.* **54**, 5032 (1989).
97. J. V. Crivello and R. A. Ortiz, *J. Polym. Sci., Part A: Polym. Chem.* **39**, 2385 (2001).
98. J. V. Crivello and S. Liu, *Chem. Mater.* **10**, 3724 (1998).
99. J. V. Crivello and A. M. Carter, *J. Polym. Sci., Part A: Polym. Chem.* **31**, 2663 (1993).
100. J. V. Crivello and D. A. Conlon, *J. Polym. Sci., Polym. Chem. Ed.* **21**, 1785 (1983).
101. J. V. Crivello and B. Yang, *J. Polym. Sci., Part A: Polym. Chem.* **33**, 1381 (1995).
102. S. Kaur, J. V. Crivello, and N. Pascuzzi, *J. Polym. Sci., Part A: Polym. Chem.* **37**, 199 (1999).
103. J. V. Crivello and S. S. Liu, *J. Polym. Sci., Part A: Polym. Chem.* **36**, 1179 (1998).
104. J. V. Crivello, K. D. Jo, W. G. Kim, and S. Bratslavsky, in M. K. Mishra, ed., *Macromolecular Engineering: Recent Advances*, Plenum Press, New York, 1995, pp. 85–99. *Proceedings of the International Conference on Advanced Polymers via Macromolecular Engineering.*
105. J. V. Crivello and G. Löhden *J. Polym. Sci., Part A: Polym. Chem.* **34**, 2051 (1996).

106. J. V. Crivello and W. G. Kim, *J. Macromol. Sci., A: Pure Appl. Chem.* **31**, 1105 (1994).
107. J. V. Crivello and S. A. Bratslavsky, *J. Macromol. Sci., A: Pure Appl. Chem.* **31**, 1927 (1994).
108. J. V. Crivello and W. G. Kim, *J. Polym. Sci., Part A: Polym. Chem.* **32**, 1639 (1994).
109. J. V. Crivello, A. Carter, A. Ramdas, and D. H. Suh, *J. Macromol. Sci., A: Pure Appl. Chem.* **31**, 1807 (1994).
110. J. V. Crivello and J. L. Lee, in Ref. 16, p. 398.
111. J. V. Crivello and J. L. Lee, *J. Polym. Sci., Part A: Polym. Chem.* **28**, 479 (1990).
112. R. P. Eckberg and K. D. Riding, in Ref. 16, p. 382.
113. J. V. Crivello, D. Bi, and M. Fan, *J. Macromol. Sci., A: Pure Appl. Chem.* **31**, 1001 (1994).
114. J. V. Crivello and H. Sasaki, *J. Macromol. Sci., A: Pure Appl. Chem.* **30**, 173 (1993).
115. J. V. Crivello, B. Yang, and W. Kim, *J. Polym. Sci., Part A: Polym. Chem.* **33**, 2415 (1995).
116. J. V. Crivello and G. Löhden, *Macromolecules* **28**, 8057 (1995).
117. J. V. Crivello and U. Varlemann, *J. Polym. Sci., Part A: Polym. Chem.* **33**, 2463 (1995).
118. M. Sangermano, G. Malucelli, R. Bongiovanni, A. Priola, U. Annby, and N. Rehnberg, *Polym. Int.* **50**, 998 (2001).
119. S. K. Rajaraman, W. A. Mowers, and J. V. Crivello, *Macromolecules* **32**, 36 (1999).
120. J. V. Crivello, Y. L. Lai, and R. Malik, *J. Polym. Sci., Part A: Polym. Chem.* **34**, 3103 (1996).
121. J. V. Crivello and R. Narayan, *Macromolecules* **29**, 433 (1996).
122. J. V. Crivello and R. Narayan, *Macromolecules* **29**, 439 (1996).
123. O. Nuyken and M. Ruile, *NATO Sci. Ser., Ser. E* **359**, 117 (1999).
124. J. V. Crivello, T. Yoo, and J. A. Dougherty, *J. Polym. Sci., Part A: Polym. Chem.* **33**, 2493 (1995).
125. J. V. Crivello and S. S. Liu, *J. Polym. Sci., Part A: Polym. Chem.* **37**, 1199 (1999).
126. J. V. Crivello and S. Song, *Chem. Mater.* **12**, 3674 (2000).
127. J. V. Crivello and S. Song, *J. Polym. Sci., Part A: Polym. Chem.* **37**, 3427 (1999).
128. J. V. Crivello and D. H. Suh, *J. Polym. Sci., Part A: Polym. Chem.* **31**, 1847 (1993).
129. J. V. Crivello and Y. L. Lai, *J. Polym. Sci., Part A: Polym. Chem.* **33**, 653 (1995).
130. J. V. Crivello and A. Ramdas, *J. Macromol. Sci., A: Pure Appl. Chem.* **29**, 753 (1992).
131. J. V. Gražlevičius, R. Kavaliūnas, R. Lazauskaitė, V. M. Getautis, M. Daškevičienė, *Chemija* **1**, 89 (1997).
132. J. V. Crivello and R. A. Ortiz, *J. Polym. Sci., Part A: Polym. Chem.* **39**, 3578 (2001).
133. C. Venturello and R. D'Aloisio, *J. Org. Chem.* **53**, 1553 (1988).
134. J. V. Crivello and R. Narayan, *Chem. Mater.* **4**, 692 (1992).
135. J. Chen, M. D. Soucek, W. J. Simonsick, and R. W. Celikay, *Polymer* **43**, 5379 (2002).
136. C. Decker, T. N. T. Viet, and H. P. Thi, *Polym. Int.* **50**, 986 (2001).
137. A. M. Mathur, V. Narayanan, and A. B. Scranton, in *RadTech '98 North Am. UV/EB Conf. Proc. 1998*, 1998, p. 486.
138. J. P. Kennedy and E. Marechal, *Carbocationic Polymerization*, John Wiley & Sons, Inc., New York, 1982.
139. E. W. Nelson, J. L. Jacobs, A. B. Scranton, K. S. Anseth, and C. N. Bowman, *Polymer* **36**, 4651 (1995).
140. E. W. Nelson, and A. B. Scranton, *J. Polym. Sci., Part A: Polym. Chem.* **34**, 403 (1996).
141. J. M. Barton, *Adv. Polym. Sci.* **72**, 111 (1985).
142. H. Ito, N. Kidokoro, and H. Ishikawa, *J. Photopolym. Sci. Technol.* **5**, 235 (1992).
143. C. Decker and K. Moussa, *J. Coat. Technol.* **62**, 55 (1990).
144. C. Decker and K. Moussa, *J. Polym. Sci., Part A: Polym. Chem.* **28**, 3429 (1990).
145. E. W. Nelson and A. B. Scranton, *J. Raman Spectrosc.* **27**, 137 (1996).
146. J. C. Song and C. S. Sung, *Polym. Prepr. (Am. Chem. Soc., Div. Polym. Chem.)* **32**, 362 (1991).

147. B. Strehmel, J. H. Malpert, A. M. Sarker, and D. C. Neckers, *Macromolecules* **32**, 7476 (1999).
148. B. Strehmel, V. Strehmel, and M. Younes, *J. Polym. Sci., Part A: Polym. Chem.* **37**, 1367 (1999).
149. B. Falk, S. M. Vallinas, and J. V. Crivello, *J. Polym. Sci., Part A: Polym. Chem.* **41**, 579, 2003.
150. V. Sipani and A. B. Scranton, *J. Polym. Sci., Part A: Polym. Chem.* **41**, 2064 (2003).
151. V. Sipani and A. B. Scranton, *J. Photochem. Photobiol., A* **159**, 189 (2003).

VISHAL SIPANI  
ALEC B. SCRANTON  
University of Iowa

## PHOTOPOLYMERIZATION, FREE RADICAL

### Introduction

Photopolymerizations, which use light energy (photons) to initiate chain reactions to form polymer materials, are the basis for a growing, billion-dollar industry (1,2). Applications in which photopolymerization is used include films and coatings, inks, adhesives, fiber optics, and dentistry (2–5). Each of these industries has benefited from the high productivity and lower costs afforded by photopolymerization systems.

Photopolymerization has many advantages over thermal and redox polymerizations in which the reaction system is heated to produce active centers. The solvent-free systems used in photopolymerizations eliminate emissions of volatile organic compounds and reduce material costs. Spatial and temporal control of the polymerization is achieved through control of the initiating light. Photopolymerizations also use less energy to effect cure than do thermal means. They produce a more rapid through-cure so that more films and coatings can be processed in less time. Furthermore, photocuring systems are more compact than thermal curing systems and operate at room temperatures. All these characteristics of photopolymerizations translate into lower production costs for industry.

Photopolymerization systems, like thermally initiated systems, contain initiator, monomer, and other additives that impart desired properties (color, strength, flexibility, etc) (6). The reaction is initiated by active centers that are produced when light is absorbed by the photoinitiator. One important class of active centers includes free-radical species, which possess an unpaired electron (5,7). The highly reactive free-radical active centers attack carbon–carbon double bonds in unsaturated monomers to form polymer chains. Although the kinetic treatment of photopolymer systems is similar to that in thermal systems, significant differences arise in the description of the initiation step, which in turn affect the description of the rate of polymerization. An overview of the components, kinetics, and applications of these free-radical photopolymerization systems is

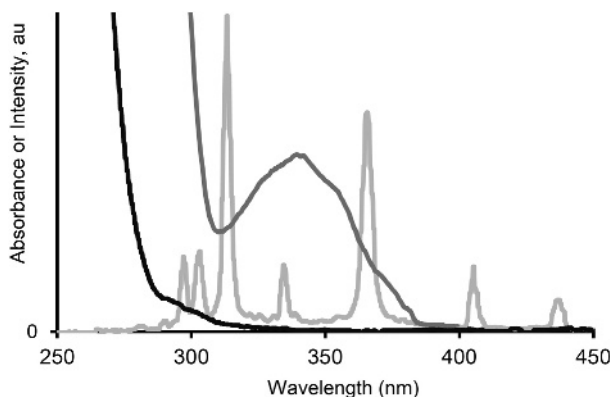


**Fig. 1.** UV-visible absorption spectra of dimethoxyphenylacetophenone (DMPA) (photoinitiator) and 2-hydroxyethyl methacrylate (HEMA) (monomer) in dichloromethane overlaid with the spectral output of a 200-W Hg(Xe) lamp. — DMPA; — HEMA; and — Hg(Xe) Lamp.

given in this article. More detailed information may be obtained in the references cited.

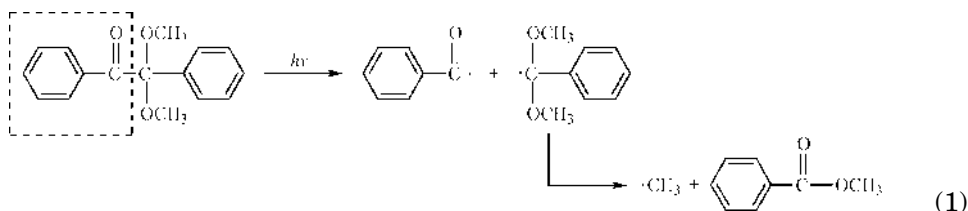
## Photoinitiators

In order to produce free radicals that initiate polymerization, photoinitiators absorb light of a certain frequency. Upon absorption, the photoinitiator molecule is promoted from the ground electronic state to either a singlet or triplet excited electronic state. This excited molecule then undergoes either cleavage or reaction with another molecule to produce initiating free radicals. Numerous photoinitiators have been developed to meet the needs of a variety of photopolymerization systems, as described in a number of recent papers and reviews (3–6,8–12).

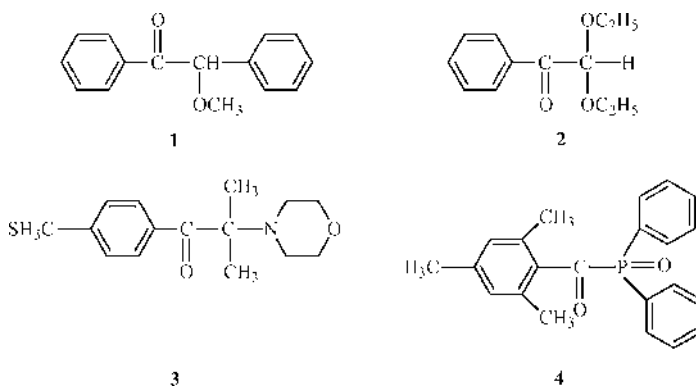
In selecting an appropriate photoinitiator system, several key criteria must be fulfilled. First, the absorption spectrum of the initiator must overlap with the emission spectrum of the light source, be it polychromatic (eg, arc lamp) or monochromatic (eg, laser). Good engineering of the system involves optimizing the light absorption of the initiator and, in many cases, minimizing emission lines that do not coincide with the initiator absorption spectrum (ie, are wasted through absorption by other system components). By matching the absorption of the photoinitiator to the light source output, the initiation efficiency can also be optimized. However, the overlap between the initiator and light source must preferably not coincide with the absorption peaks of other components in the photopolymerization system (monomer, pigments, additives, etc.). In systems where there is overlap, such as highly pigmented systems, higher light intensities and photoinitiator concentrations are often used (13). Figure 1 demonstrates a good match of a photoinitiator with a light source and monomer in that there is a clear optical window for the photoinitiator to absorb light in the 300–400-nm region without competition from the monomer.

Many free radical photoinitiators are based on the benzoyl chromophore (highlighted in eqs. 1 and 2), which produces free radicals when irradiated with light of the appropriate wavelength. Judicious choice of substituents (R groups) and their placement can alter the absorption spectrum, so that more freedom is available in the choice of lamp (and initiating wavelength) and system components. Secondly, the impact of residual photoinitiator and its photoproducts upon the final products must be considered. This becomes most important in thick films and coatings that must be of a certain color. If the photoinitiator fragments absorb at the same wavelength as the photoinitiator, then light cannot penetrate to the bottom of a thick sample, and full conversion of the monomer will not be attained. Also, some photoinitiator fragments, such as aromatic amines, will "yellow" initially colorless and white coatings and films, especially after long exposure times to sunlight or fluorescent lights (13).

**Unimolecular Photoinitiators.** Photoinitiators termed unimolecular are so designated because the initiation system involves only one molecular species interacting with the light and producing free-radical active centers. One type includes photoinitiators that form radicals via the cleavage of the initiator molecule. This cleavage may take place at the  $\alpha$  or  $\beta$  position with respect to the carbonyl group. Upon illumination, the photoinitiator molecule is excited and undergoes cleavage. In  $\alpha$ -cleavage or Norrish Type I, the bond adjacent to the carbonyl is broken to produce two free radicals. Equation 1 demonstrates the  $\alpha$ -cleavage of a representative benzyl ketal photoinitiator dimethoxyphenylacetophenone (the dashed box highlights the benzoyl chromophore).

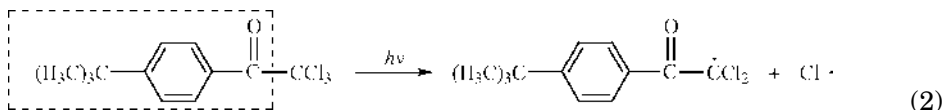


In this case, the benzoyl radical and a methyl radical produced through the fragmentation of  $\alpha,\alpha$ -dimethoxy benzyl radical both initiate polymerization. Other families include benzoin ethers, acetophenone derivatives, amino ketones, and phosphine oxide derivatives (1–4) (3,11).

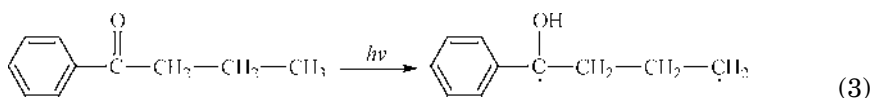




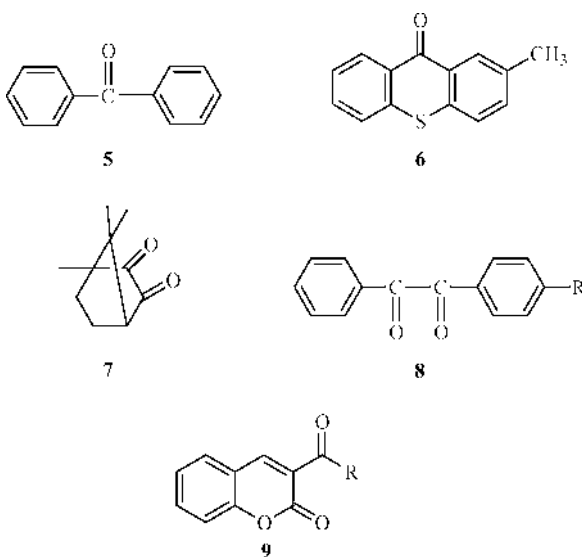
$\beta$ -Cleavage occurs predominately in  $\alpha$ -halogenoacetophenones; however, it is also seen in photoinitiators with a C-S or C-O bond adjacent to the benzoyl chromophore, such as  $\beta$ -ketosulfoxides (3,11). Equation 2 demonstrates this cleavage mechanism for the photoinitiator 2,2,2-trichloro-4'-*tert*-butylacetophenone (the dashed box highlights the benzoyl chromophore).



A second type of unimolecular photoinitiators, also called Norrish Type II, includes those that form biradicals through intramolecular hydrogen abstraction. This occurs in ketones with a  $\gamma$ -hydrogen and is shown in equation 3 for intramolecular H-abstraction of the photoinitiator 1-phenyl-butan-1-one (14). The resulting ketyl radical participates in termination, while the other radical grows the polymer chain.



**Bimolecular Photoinitiator Systems.** Bimolecular photoinitiators are so-called because two molecular species are needed to form the propagating radical: a photoinitiator that absorbs the light and a co-initiator that serves as a hydrogen or electron donor. Photoinitiator families include benzophenone derivatives, thioxanthenes, camphorquinones, benzyls, and ketocoumarins (5–9) (3).



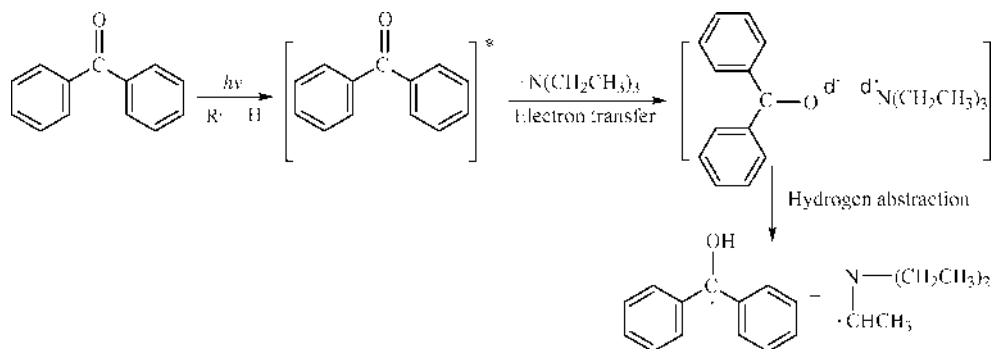
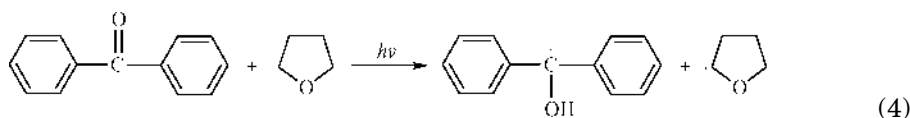


**Fig. 2.** Electron-transfer reaction with subsequent proton-transfer reaction between the photoinitiator benzophenone and the co-initiator triethylamine.

The abstraction of a hydrogen molecule from the co-initiator or the transfer of an electron between the two initiating molecules takes place once the photoinitiator is in the excited state. In both cases, free radicals result, one or more of which may actually begin the photopolymerization. Initiation by hydrogen transfer is common in diaryl ketones. The co-initiator is usually an ether or an alcohol with an abstractable  $\alpha$ -hydrogen, such as 2-propanol. Equation 4 demonstrates the H-abstraction reaction between the photoinitiator benzophenone and the hydrogen donor tetrahydrofuran. In this case, the ether radical initiates polymerization, and the ketyl radical only participates in termination.



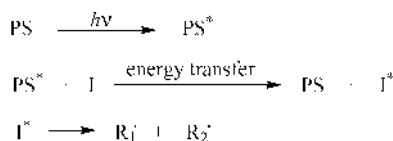
In photoinitiation by electron transfer, the photoinitiator, after absorption of the initiating light, forms an excited-state complex (exciplex or charge-transfer complex) with the co-initiator, typically an amine. Electron transfer from the amine to the photoinitiator occurs in this exciplex, immediately followed by proton transfer of an  $\alpha$ -hydrogen from the amine to the photoinitiator. This results in two radicals: an amine radical that will initiate polymerization and a ketyl-type radical that will most likely terminate by coupling with another free radical species. Figure 2 demonstrates this type of photoinitiation process between benzophenone and an amine co-initiator (3,15).

Bimolecular photoinitiator systems utilize longer wavelengths (thereby requiring less energy) than the unimolecular systems, which are typically constrained to use in the ultraviolet (UV) because of the absorption characteristics of the benzoyl chromophore. However, the production of active centers in bimolecular photoinitiator systems decreases in vitrifying systems (ie, systems in the later stages of conversion where the reaction temperature is less than the glass transition temperature) because diffusion of the initiator and co-initiator molecules

is strongly suppressed. During this stage in the polymerization, formation of the polymer chains occurs through reactive diffusion.

**Photosensitizers.** In the bimolecular initiation reactions described above, the co-initiator will not absorb light to initiate polymerization. In contrast, photosensitizers are able to absorb light and are used to enhance the photopolymerization (ie, the photoinitiator is normally able to function without the photosensitizer) (3,4,16). A visible light photosensitizer may be chosen when ultraviolet light is undesirable, such as when working with biological systems or white pigmented systems. If pigments or monomers absorb in the same region as the photoinitiator, a photosensitizer may be used to extend the optical window of the system. A photosensitizer may also be used to improve initiation efficiency by absorbing photons from the light source that the photoinitiator cannot absorb or may do so with a low efficiency.

Two mechanisms have been identified to describe the interaction between photosensitizers and photoinitiators: *energy transfer* and *electron transfer*. In the energy transfer process, the photosensitizer absorbs the light and transfers that energy to the photoinitiator which will then go through either a unimolecular or bimolecular scheme to produce initiating free radicals.



In this case, the photosensitizer is not consumed by the reaction and reverts back to its ground state upon transferring its excitation energy to the photoinitiator. For example, the photoinitiator 2-methyl-1-[4-(methylthio)phenyl]-2-morpholinopropane-1-one (TPMK) absorbs light in the 275–325-nm region, where the photosensitizer 3-ethylacetate-2'-methylthioxanthone (ETX) exhibits an absorption peak between 380–420 nm (3). Thus, ETX absorbs light in the visible region of the spectrum and transfers that energy to TPMK, which then undergoes  $\alpha$ -cleavage to form the free-radical active centers. In order for this process to occur, the triplet excited electronic state of the photosensitizer must be higher than that of the photoinitiator. Because these states are difficult to match, the energy transfer mechanism is not extensively used.

In the electron transfer mechanism, which is more common, the photosensitizer becomes excited upon illumination and forms an excimer with the photoinitiator. Electron transfer from the photoinitiator to the photosensitizer then occurs, with a subsequent proton transfer. This results in the formation of two radicals. The photosensitizer radical is capable of initiating polymerization, while the photoinitiator radical may not unless it undergoes further reaction (3,13,17). Figure 3 demonstrates this for a representative  $\alpha$ -amino ketone photoinitiator and a thioxanthone being used as a photosensitizer.

**Specialty Photoinitiators.** Photoinitiator systems continue to be developed to meet the needs of industrial applications. Driving forces include increasing reaction speed with higher quantum yields and higher active center reactivities, improving shelf life with greater solubility and stability in the formulations,

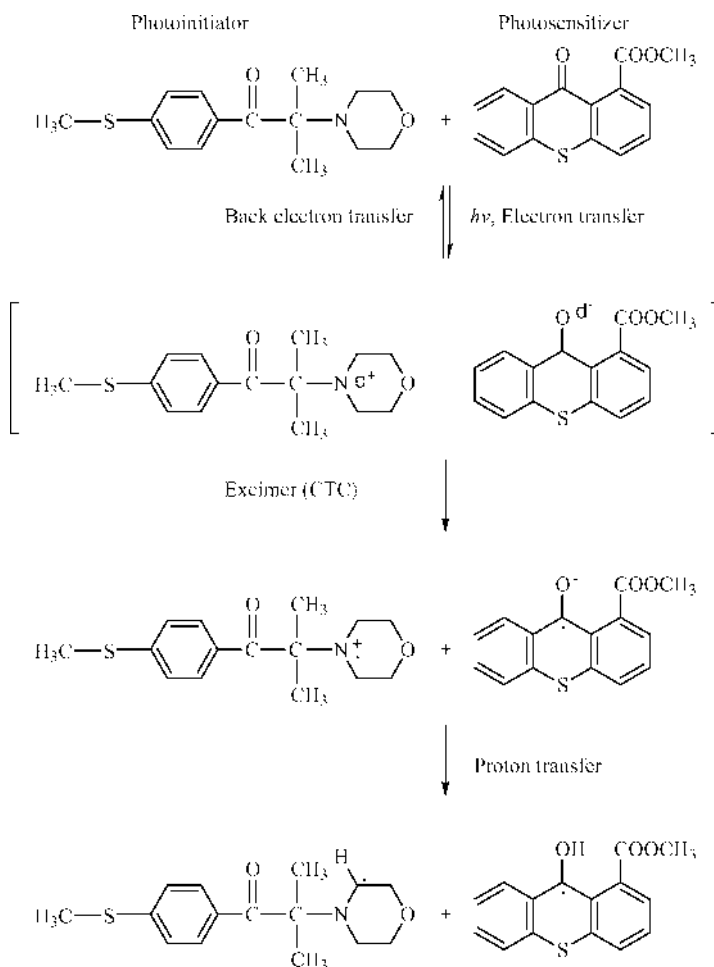


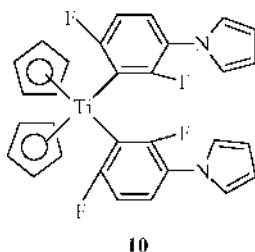
**Fig. 3.** Electron transfer reaction between the photoinitiator 2-methyl-1-[4-(methylthio)-phenyl]-2-morpholinopropane-1-one and the photosensitizer 9-oxo-9H-thioxanthene-1-carboxylic acid methyl ester.

and optimizing the absorption spectrum to meet the requirements of the light source and application. Minimizing toxicity of the initiators and yellowing due to photoproducts and sunlight exposure also is important for many applications.

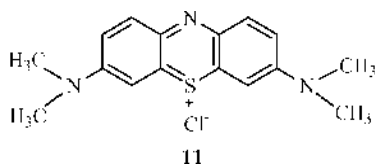
**Visible Light Photoinitiators.** Visible light photoinitiators are desirable for many applications. Visible light is safer than UV light in that it does not cause cell damage in biological systems. Many common, inexpensive light sources, such as halogen or fluorescent lamps, have strong lines in the visible, which could be used for efficient and cost-effective photoinitiation. In addition, visible lasers are used in photoimaging applications, such as lithography and holography (5). Visible light photoinitiators can also enhance polymerization in systems with pigments, fillers, and UV absorbers (18).

Visible light photoinitiators based on metal salts and complexes have been explored (3,10,12). Some systems generate ionic active centers unless

combined with another molecule (such as a dye or halogenated compound) that will react to produce the initiating free radical. Titanocene complexes, an example of which is bis( $\eta^5$ -2,4-cyclopentadien-1-yl)-bis-[2,6-difluoro-3-(1*H*-pyrrol-1-yl)phenyl]titanium 10, are metal-based photoinitiators that undergo cleavage upon illumination in the 400–550-nm region, with the aryl radical initiating polymerization (12).

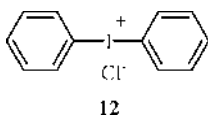


Dyes comprise a large fraction of visible light photoinitiators because their excited electronic states are more easily attained. Co-initiators, such as tertiary amines, iodonium salts, triazines, or hexaarylbisimidazoles, are required since dye photochemistry entails either a photoreduction or photo-oxidation mechanism. Numerous dye families are available for selection of an appropriate visible initiation wavelength; an example of a thiazine dye (with an absorption peak around 675 nm) is methylene blue (11).



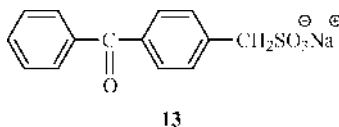
Other examples include acridine dyes (with absorption peaks around 475 nm), xanthene dyes (~500–550 nm), fluorone dyes (~450–550 nm), coumarin dyes (~350–450 nm), cyanine dyes (~400–750 nm), and carbazole dyes (~400 nm) (12,19–21). The oxidation or reduction of the dye is dependent on the co-initiator; for example, methylene blue can be photoreduced by accepting an electron from an amine (22) or photo-oxidized by transferring an electron to benzyltrimethylstannane (12). Either mechanism will result in the formation of a free-radical active center capable of initiating a growing polymer chain. For a more detailed discussion of the mechanisms, see Reference 12.

Three-component visible light photoinitiator systems exhibit faster polymerization rates than those seen in the dye-electron donor systems mentioned above. The third component is usually a sulfonium or iodonium salt (an example is diphenyliodonium chloride) 12, but may also be a bromocompound, ferrocenium salt, or thiol derivative (3,12,21–24).

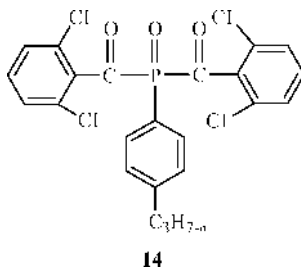


The incorporation of the third component has been shown to provide pathways to scavenge oxygen molecules that inhibit free-radical polymerization, to regenerate the dye photoinitiator, and to produce a free-radical active center in place of a terminating dye radical (3,12,13,21). In addition, the wide selection of dyes available for use in three-component systems allows more flexibility in initiating wavelength selection, and the photopolymerization of thick parts is possible if a photobleaching dye is chosen (21).

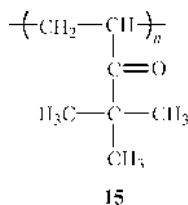
**Water-Soluble Photoinitiators.** Water-soluble photoinitiators are needed for systems such as printing inks and emulsion processes, where the reaction system is an aqueous solution rather than simply a monomer. Since free radical photoinitiators are based on the aromatic benzoyl chromophore, the molecules are generally nonpolar and therefore incompatible with water. Research has focused on developing photoinitiators with hydrophilic substituents that increase water solubility (3,25). Both unimolecular and bimolecular systems have been successfully demonstrated. An example of a unimolecular photoinitiator is sodium 4-benzoylbenzenesulfonate 13.



**Photobleaching Initiators.** Photobleaching initiator systems are designed such that the absorption of the photoinitiator byproducts is lower than that of the photoinitiator (13,26). Thus, as the active centers are formed, more light may pass through the system. This is crucial in thick films, where light penetration to the bottom of the sample is hindered by the absorption characteristics of the upper layers. Insufficient light penetration will result in low conversions at the bottom, wrinkling of the surface, and decreased production speeds. Photobleaching is also necessary for colorless or white films and coatings to prevent yellowing. Acylphosphine oxides and bisacylphosphine oxides 14, which undergo  $\alpha$ -cleavage, are examples of photobleaching initiators widely used today. These photoinitiators absorb well into the visible spectrum; however, once cleavage occurs, the absorption peaks in the visible spectral region disappear.

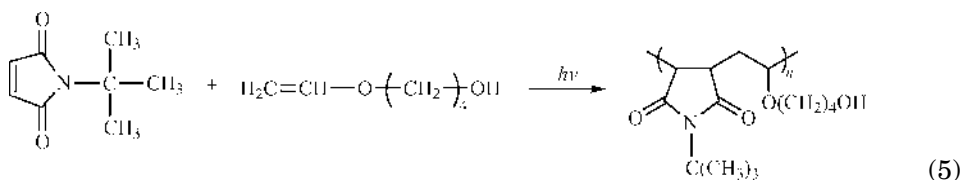


**Polymerizable and Polymeric Photoinitiators.** Growing interest in polymerizable and polymeric photoinitiators is seen in several industries. An example is poly(4,4-dimethyl-1-penten-1-one) 15.



In the food-packaging industry, species that migrate from a film or coating may contaminate foods. In the film and coating industries, migrating species may cause yellowing at film surfaces. Thus, tethering or incorporating the photoinitiator on the main polymer chain is an effective means of reducing migration by photoproducts and unreacted photoinitiator (27). These types of photoinitiators exhibit other practical benefits, such as improved compatibility with monomers, longer shelf life, increased reactivity, and reduced volatile emissions (28,29). Polymeric photoinitiators have been synthesized by grafting the initiator molecule onto the backbone of the polymer chain (3,27,30). They have also been created by terminating polymer chains with the initiator molecules (3,27,29,31,32). Polymeric photoinitiators may become entangled within the polymer product or attached to the main polymer chain or network, depending on whether the active center cleaves from or is part of the polymeric photoinitiator chain (27). Polymerizable photoinitiators may be formed by attaching the photoinitiator on a polymeric or oligomeric chain that has one or more functional groups that can enter into the polymerization as well (3). Thus, the photoinitiators become copolymerized with the main polymer chain or network.

In some cases, a monomer may function as a photoinitiator and become incorporated into a copolymer chain. This has been shown for styrene and other conjugated monomers when exposed to deep-UV light; however, the initiation efficiency in these systems is substantially less than when a photoinitiator is present (p. 223 of Ref. 33, and Ref. 34). A better polymerizable initiator scheme is illustrated by the acceptor-donor chemistry of maleimide-donor systems (35–37). Maleimide acts as both photoinitiator and comonomer in the presence of hydrogen donors such as vinyl ethers or vinyl esters (38,39); an example of this copolymerization is shown in equation 5. It shows the molecular structure of the acceptor *tert*-butylmaleimide (left), the donor 4-hydroxy-butyl vinyl ether (right), and their corresponding copolymer repeat unit.



In these systems, illumination with a subsequent hydrogen abstraction or electron/proton transfer process results in the production of two radicals, both of

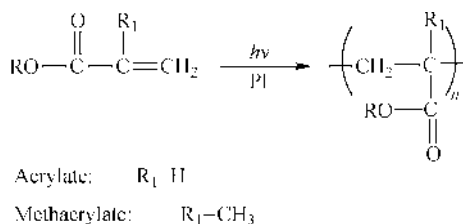
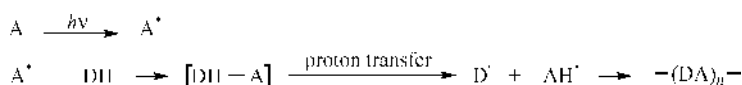


**Fig. 4.** Molecular structure of a generalized acrylate monomer and its corresponding polymer repeat unit.

which may start a propagating chain by adding either monomer (35–37):



These systems have the added advantage of being photobleaching, as well as less inhibited by oxygen.

## Monomers

Unsaturated monomers, which contain a carbon–carbon double bond ( $\text{C}=\text{C}$ ), are used extensively in free radical photopolymerizations. The free-radical active center reacts with the monomer by opening the  $\text{C}=\text{C}$  bond and adding the molecule to the growing polymer chain. Most unsaturated monomers are able to undergo radical polymerization (qv) because free-radical species are neutral and do not require electron-donating or electron-withdrawing substituents to delocalize the charge on the propagating center, as is the case with ionic polymerizations. Commercial consideration in formulation development is therefore given to the final properties of the polymer system, as well as the reactivity of the monomer.

**(Meth)acrylate Systems.** Acrylate and methacrylate monomers are by far most widely used in free-radical photopolymerization processes. The generalized structure of these monomers and their corresponding polymer is shown in Figure 4.

These monomers have very high reaction rates, with acrylates having an even faster reaction rate than their methacrylate counterparts (4). This makes them especially amenable for high speed processing needed in the films and coatings industry. (Meth)acrylate systems are also easily tailored using the ester linkage to obtain the desired chemical, mechanical, and optical properties for a variety of applications (see ACRYLIC ESTER POLYMERS; METHACRYLIC ESTER POLYMERS). Monoacrylates, which have only one  $\text{C}=\text{C}$  group, are generally used as reactive diluents with multiacrylates, which have two or more  $\text{C}=\text{C}$  groups per molecule (Fig. 5). Multiacrylates increase the mechanical strength and solvent resistance of the ultimate polymer by forming cross-linked networks rather than linear polymer chains, whereas monoacrylates reduce the viscosity of the prepolymer mixture for ease of processing (4,6).

One of the drawbacks of acrylate and methacrylate systems is their relatively large polymerization shrinkage. Shrinkage is caused by the formation of



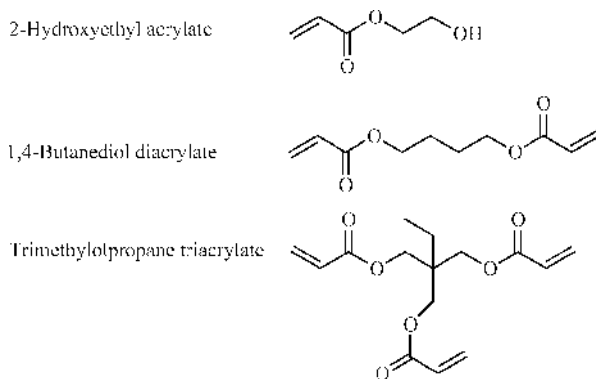
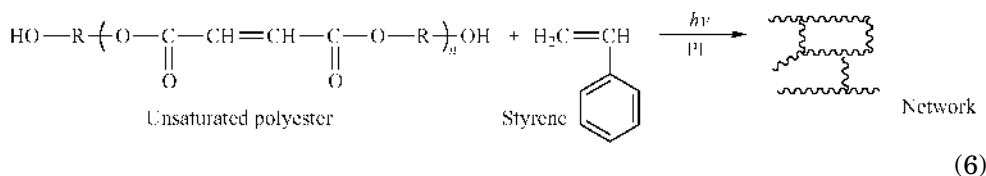


**Fig. 5.** Molecular structures of monomers with a varying number of acrylate reactive groups: a monoacrylate (top), diacrylate (middle), and triacrylate (bottom).

covalent bonds between monomer molecules. When a covalent bond is formed between two monomer molecules, the distance between them is approximately half as much as that between two molecules experiencing van der Waal's forces in solution. In addition, because the number of conformations that a polymer chain can achieve is less than that for the individual monomer molecules, monomer conversion results in a negative entropy of polymerization and less free volume. Thus, volume shrinkage of 5–25% is observed in these systems (4,40–42). This shrinkage causes stresses in the polymer parts, which can affect their ultimate performance, especially in applications such as stereolithography, dentistry, and coatings. One way to overcome this disadvantage is to develop oligomeric acrylates. These oligomers contain 1 to 12 repeat units formed through step-growth polymerization; the ends are then capped with two or more (meth)acrylate functional groups. Commercially available oligomeric families are shown in Figure 6.

In addition to reducing shrinkage, oligomeric acrylates offer improved properties of wear resistance and chemical and moisture resistance. They also enable the use of these functional groups in rapid processing applications, which would not be possible using the slower step-growth polymerization mechanism. Because of their size, these oligomers must be combined with other monomers to reduce the resin viscosity. Examples of coating formulations incorporating multi-acrylates and oligomeric acrylates are shown in Table 1.

**Unsaturated Polyester Systems.** Coatings in the furniture industry rely heavily upon resin formulations containing unsaturated polyesters, styrene, and photoinitiator (3,4,13,43,44). The unsaturated polyesters are synthesized using step-growth polymerization (see POLYESTERS, UNSATURATED). Upon illumination, the carbon-carbon double bond in the unsaturated polyester and styrene copolymerize to form a cross-linked network (eq. 6). Equation 6 shows a generalized reaction scheme for an unsaturated polyester system.



(6)

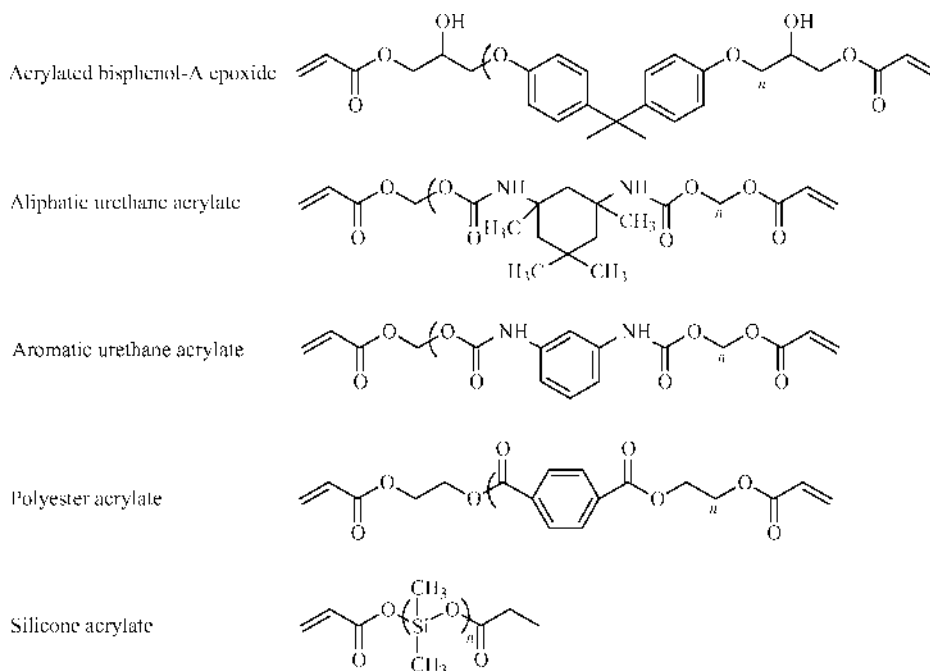


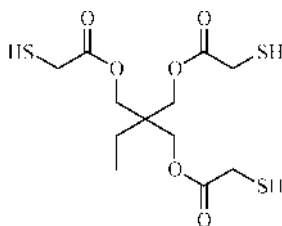
**Fig. 6.** Molecular structure of some generic acrylated oligomers.

**Table 1. Sample (Meth)acrylate Formulations**

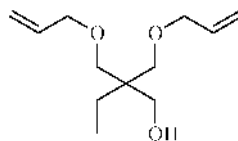
Basic coating	Wood-flooring topcoat	Adhesive resin for dentistry	Resin composite for dentistry
Acrylated epoxy oligomer, 45%	Urethane acrylate, 60%	Dimethacrylated epoxide, 60–70%	Silica filler, 77–87%
Triacrylate, 20%	Diacrylated polyether, 24%	Monomethacrylate, 30–40%	Dimethacrylated epoxide, 5–9%
Diacrylate, 20%	Polyester tetraacrylate, 10%	Camphorquinone, <1%	Dimethacrylated polyether, 5–9%
Amine, 10%	Amine, 10%	Amine, <1%	Camphorquinone, <1%
Benzophenone, 5%	$\alpha$ -Hydroxyketone, 5%		Amine, <1%

Although these systems polymerize much slower than the acrylate systems, they are low cost and can still polymerize at ambient temperatures.

**Thiol–Ene Systems.** Systems that combine thiols [such as a trithiol (16)] with ene comonomers, such as allyl ethers [like trimethylol propane diallyl ether (17)] or acrylates, were first considered in the 1970s; however, because of their unpleasant odor, thiols were abandoned, and acrylates became the monomer of choice for industrial implementation.

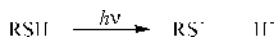


16



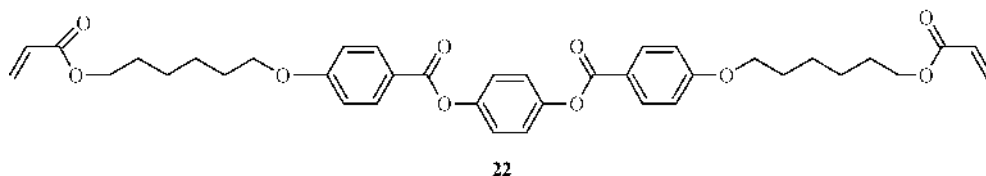
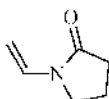
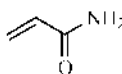
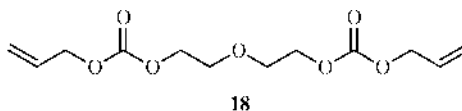
17

Several factors have led to renewed interest in thiol systems. First, the systems require little or no photoinitiator in order to polymerize (45,46). This reduces the cost of formulations (since the photoinitiator is generally the most expensive component), as well as decreases toxicity and purity concerns. In addition, photoinitiator fragments do not interfere with the physical properties of the polymers, such as color and strength. The thiol functions as photoinitiator by producing a thiyl and a hydrogen radical pair through a sulfur-hydrogen bond cleavage when exposed to light (47,48):



Thiol systems are also less sensitive to inhibition by oxygen, a major disadvantage of free-radical polymerizations. The inactive peroxy radical formed through interaction of oxygen and a growing chain end can undergo chain transfer to the thiol to regenerate the active thiyl radical. However, this still results in the incorporation of oxygen into the polymer, which will affect its performance properties. Because most of the double-bond conversion occurs in the liquid state, these systems undergo less volume shrinkage and establish an infinite network (gel point) later in the reaction so that higher conversions, even in systems with multiple functional groups on each monomer, may be reached (49). This is a result of extensive chain transfer during the free-radical chain polymerization, which leads to the formation of very short chains. Long polymer chains and networks are formed through a step-growth mechanism (46–48,50).

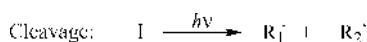
**Other Monomer Systems.** The above sections are by no means an exhaustive list of monomers that are used in free radical photopolymerizations. Diallyldiglycolcarbonate 18 has been used for many years in optical components such as lenses (51). Acrylamide (19) is used in stereolithography and to prepare holographic materials (52–54). *N*-vinylpyrrolidinone (20) is copolymerized with acrylates and methacrylates for cosmetic and biomedical applications (55). Norbornene (21) is copolymerized with thiols for optical fiber coatings (56). Liquid crystal polymers (22) based on acrylates and thiol-enes are being developed to produce mirror coatings, polarizing films, and liquid crystal displays (57,58).



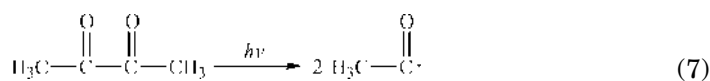
## Kinetics

The description of free-radical chain polymerization kinetics must take into account four basic steps: *initiation*, which creates free-radical active centers; *propagation*, which grows the polymer chains; *termination*, which destroys the active centers and ends chain growth; and *chain transfer*, which ends a growing chain and begins another. These classical steps also describe thermal polymerizations; however, different descriptions are required for thermal- and photoinitiation.

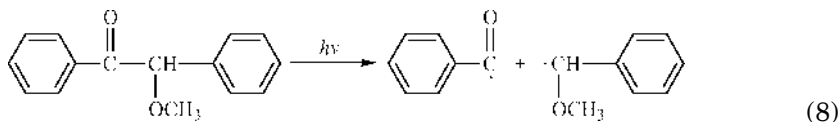
**Initiation.** In both thermal- and photopolymerizations, the rate of initiation depends on two processes: the *dissociation* of the initiator and the *initiation* of the propagating chain. The decomposition rate ( $k_d$ ) of thermal initiators strongly depends on temperature, with the half-life of many thermal initiators at the reaction temperature on the order of minutes or hours. In contrast, for photopolymerizations, the rate at which photons are absorbed at a specific wavelength will determine the decomposition rate of photoinitiators. This process is not temperature-dependent. Thus, in the classic initiation mechanism, the interaction between light of a specific wavelength and a photoinitiator molecule is considered. For a unimolecular photoinitiator, this reaction step can be written as follows:



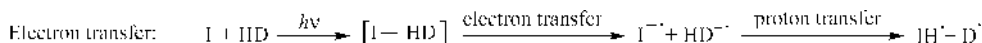
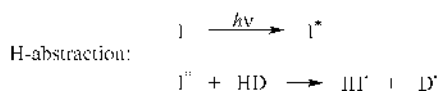
Either one or both of the radicals may then initiate polymerization. Biacetyl is an example of a photoinitiator that generates two identical free-radical groups (eq. 7) (59).



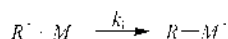
Benzoin methyl ether is an example of a photoinitiator that generates two dissimilar free radicals, each with a different initiation efficiency (ie, benzoyl radical is more likely to start a propagating chain than the ether radical) (eq. 8) (60).



A similar mechanism may be developed for radical production by electron transfer or hydrogen abstraction:



Generally, the donor radical (such as an amine or alcohol) is the initiating species. The reactive radical species ( $\text{R}^\bullet$ ) then goes on to attack a nearby monomer molecule, thereby starting a propagating chain ( $\text{R}-\text{M}^\bullet$ ):



where  $k_i$  is the initiation rate constant, usually expressed in L/mol.s. Taking into account these two reactions (production of the free-radical active centers and initiation of the propagating chain), the rate of photoinitiation ( $R_i$ ), which describes the change in propagating center concentration with respect to time, may be expressed as (33)

$$R_i = \frac{d[\text{R}-\text{M}^\bullet]}{dt} = 2f\varphi I_a$$

Here,  $I_a$  is the amount of photons absorbed by the photoinitiator molecules expressed in mol photon/L.s or Einstein/L.s;  $f$  is the photoinitiator efficiency calculated by determining the moles of propagating chains ( $\text{R}-\text{M}^\bullet$ ) started per mole of free-radical active centers ( $\text{R}^\bullet$ ) generated; and  $\varphi$  is the photoinitiator quantum yield which relates the moles of active center pairs ( $\text{R}^\bullet$ ) produced per moles photons absorbed ( $\varphi$  is defined such that it is  $\leq 1$ ). The integer 2 is included in the expression when both radical species initiate polymerization. If only one of the radical species is active, it is omitted.

Beer's Law, which relates the absorption of light to the concentration of the absorbing species, is used to define  $I_a$  for a specified wavelength of light. It is derived from the partial differential equation used to describe the change in

amount of photons as the light passes through an absorbing medium of thickness  $b$ :

$$\frac{dI}{db} = -kI \quad (9)$$

where  $I$  is the amount of photons in mol photon/(L·s) and  $k$  is the absorption coefficient ( $\text{cm}^{-1}$ ), which can also be expressed in terms of the absorbing species concentration and its molar absorptivity as shown below. A bulk-averaged  $I_a$  may be obtained by integrating equation 9 over the sample depth:

$$I_a = I_0 - I_t = I_0(1 - e^{-2.3\epsilon b[I]}) \quad (10)$$

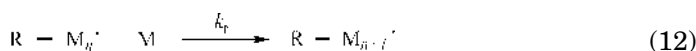
where  $I_0$  is the amount of photons incident upon the sample [mol photon/(L·s)];  $I_t$  is the amount of photons transmitted through the sample [mol photon/(L·s)];  $\epsilon$  is the molar absorptivity of the photoinitiator [L/(mol·cm)];  $b$  is the thickness of reaction system (cm); and  $[I]$  is the photoinitiator concentration (mol/L). If the quantity  $\epsilon b[I]$  is small ( $<0.01$ ), then equation 10 may be approximated by the first term of its Taylor series expansion (61):

$$I_a = 2.3I_0\epsilon b[I] \quad (11)$$

In systems where the quantity  $\epsilon b[I]$  is not small, typically in thick systems, equation 10 must be used such that  $R_i$  increases proportionally with  $I_0$ , but not with  $[I]$ . Thus, simply increasing  $[I]$  does not result in a homogeneous reaction rate: the upper layers will absorb the largest fraction of the incident light, limiting initiation near the bottom of the system. Therefore, in these systems, conversion at the bottom of the sample is generally much less than at the top unless the initiator concentration and initiating wavelength have been properly chosen.

Several groups have developed models to describe photoinitiation and photopolymerization in thick films or films with high optical densities (62–66). The latest models (62,63) take into account variations in the initiator concentration by solving partial differential equations that describe  $[I]$ ,  $I_a$ , and photolysis product concentration as a function of depth and time. If the molar absorptivity, photoinitiator quantum yield, and diffusion properties are known for an initiator system, then these equations can be solved to describe the light intensity gradient in a thick sample and to determine the effects of the initiator absorption characteristics on the efficiency of active center generation for different wavelengths of initiating light.

**Propagation.** Since chain polymerization kinetics are usually followed for free radically photoinitiated polymerizations, the propagation mechanism involves the addition of monomer to the growing polymer chain:



The rate of polymerization ( $R_p$ ) obtained from this mechanism is as follows:

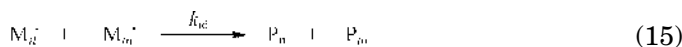
$$R_p = \frac{d[M]}{dt} = k_p [M] [R - M_n^\bullet] \quad (13)$$

where  $k_p$  is the propagation rate constant [L/(mol·s)] and is generally assumed independent of chain length  $n$ .  $[M]$  is the reactive group concentration (mol/L), which is equal to the monomer concentration if only one reactive group is present on the monomer molecule.

**Termination.** Termination of the free-radical active centers may occur either by combination or by disproportionation. In termination by combination, two propagating chains unite to form one long polymer molecule:



In termination by disproportionation, one propagating chain abstracts a hydrogen atom from a neighboring propagating chain, resulting in two polymer molecules, one of them having a terminal double bond:



When developing a rate expression for termination, the rate constants for these mechanisms are often lumped in a single termination rate constant,  $k_t$  [L/(mol·s)]. The rate of termination, which is generally assumed independent of chain length  $n$ , equals the rate of destruction of the propagating active centers ( $M^\bullet$ ):

$$R_t = -\frac{d[M_n^\bullet]}{dt} = 2k_t [M_n^\bullet]^2 \quad (16)$$

**Rate of Polymerization.** The concentration of growing chains ( $R - M_n^\bullet$ ) is difficult to measure experimentally; thus, for simplicity, it is often assumed that the change in the concentration of propagating chains over time is very small in comparison to the change in the monomer concentration. According to this pseudo-steady-state assumption, ( $d[M_n^\bullet]/dt$ ) is approximated as zero, and the rate of initiation is then equal to the rate of termination. When this is invoked, the rate of polymerization may be written as:

$$R_p = k_p [M] \sqrt{\frac{f \varphi I_a}{k_t}} \quad (17)$$

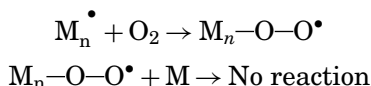
Similarly, the kinetic chain length ( $\nu$ ), which describes the average number of monomer molecules (or reactive groups for multifunctional monomers) that are consumed per initiating radical, can be calculated as follows:

$$\nu = \frac{R_p}{R_i} \approx \frac{R_p}{R_t} = \frac{k_p [M]}{2\sqrt{k_t f \varphi I_a}} \quad (18)$$

The actual chain length will be shorter if chain transfer reactions occur.

Autoacceleration, where the rate of polymerization increases with conversion in isothermal conditions, is observed in both thermal- and photoinitiated free-radical polymerizations because the termination mechanisms are the same for both. As the chains grow longer, it becomes more difficult for the active centers to diffuse and undergo bimolecular termination; thus, termination frequency decreases and active centers at the chain ends can become trapped. In cases where termination is controlled by diffusion, the pseudo-steady-state assumption is no longer valid and chain length dependent termination (CLDT) may occur (67). As is discussed for chain cross-linking photopolymerizations below, more complicated kinetic treatments must then be considered, including unsteady-state kinetics.

**Inhibition.** One of the major disadvantages of free-radical photopolymerization is its susceptibility to oxygen inhibition. This is especially troublesome in thin-film and coating applications where oxygen diffusion plays a significant role in increasing cure times and results in incomplete conversion on the surface. When oxygen, which is essentially a biradical in its electronic ground state, reacts with a free-radical active center, it forms a peroxy radical, which is much less reactive (Refs. 3,4, and p. 264 of Ref. 33):



Thus, oxygen effectively acts as a chain terminator and reduces the rate of polymerization until the oxygen in the system has been consumed.

The cost of preventing or minimizing oxygen inhibition is high. In industry, an inert gas such as nitrogen or carbon dioxide may be used to blanket the system. Waxes or shielding films may also be used to prevent oxygen from entering the system. Other methods involve adding oxygen scavengers, dye sensitizers, or antioxidants to capture oxygen and prevent it from reacting with the propagating chains. High photoinitiator concentrations or increased light intensity may also be used to produce a larger number of active centers in order to consume the oxygen in the system faster. However, very close to the surface, it is difficult to consume the oxygen faster than it diffuses into the sample, which can result in tackiness (or incomplete cure) in the surface layers.

**Techniques for Measuring Rates and Reactive Intermediates.** Kinetic parameters for photopolymerizations may be measured using many different methods or combinations of methods (9,68). Photodifferential scanning calorimetry (PDSC) is a standard technique for obtaining the rate of polymerization ( $R_p$ ) and conversion (69–73). The conversion of monomer C=C bonds to polymer C–C bonds is an exothermic reaction. The heat flow from the sample ( $\Delta H$  in W/g) is directly proportional to  $R_p$ :

$$R_p = \frac{\rho \Delta H}{\Delta H_p}$$

where  $\rho$  is the density of the monomer (g/L) and  $\Delta H_p$  is the heat of polymerization for the reactive group of the monomer (J/mol). The conversion of the sample is



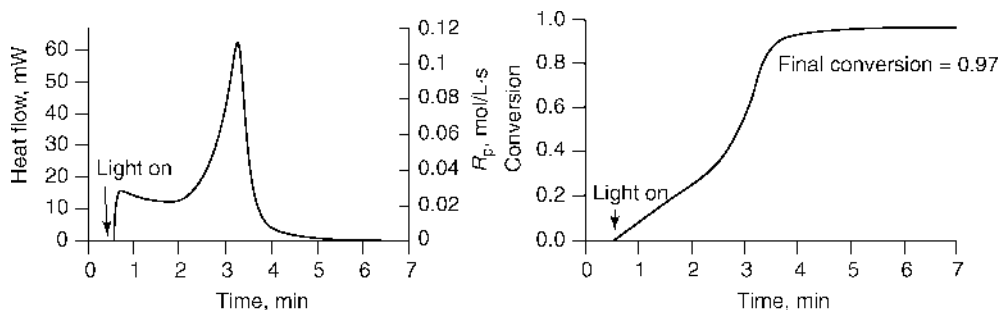


**Fig. 7.** Photodifferential scanning calorimetry profiles for photopolymerization of 2-hydroxyethyl methacrylate initiated with 2 mmolal dimethoxyphenylacetophenone at 50°C and light intensity of 60 mW/cm<sup>2</sup> with nitrogen purge: polymerization rate (left) and degree of conversion (right).

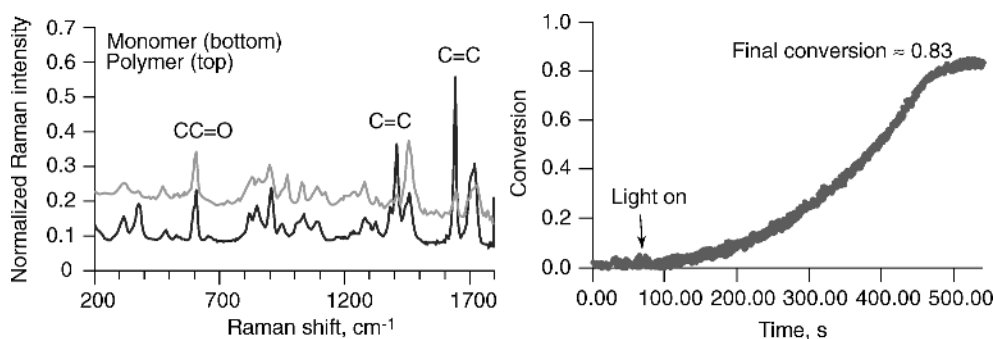


**Fig. 8.** Raman spectra for photopolymerization of 2-hydroxyethyl methacrylate initiated with 2 mmolal dimethoxyphenylacetophenone at 50°C and light intensity of 75 mW/cm<sup>2</sup>: Raman spectra of the monomer and its polymer (left) and degree of monomer conversion based on monitoring the C=C bond depletion at 1640 cm<sup>-1</sup> (in this system, the internal reference band at 605 cm<sup>-1</sup> is constant throughout the reaction and cancels out in the conversion ratio) (right).

calculated by integrating the area under the  $R_p$  versus time curve, as shown in Figure 7.

Conversion and  $R_p$  data may also be obtained using spectroscopic techniques such as Raman spectroscopy (73–75) and infrared spectroscopy (15,50,73,75–77). Here, peaks in these spectra correlate to functional groups within a molecule. As the monomer is converted to polymer, the peaks associated with the C=C bonds decrease. The conversion in the system may be calculated by ratioing this peak height or area at any point in time to the initial peak height or area, as shown in Figure 8:

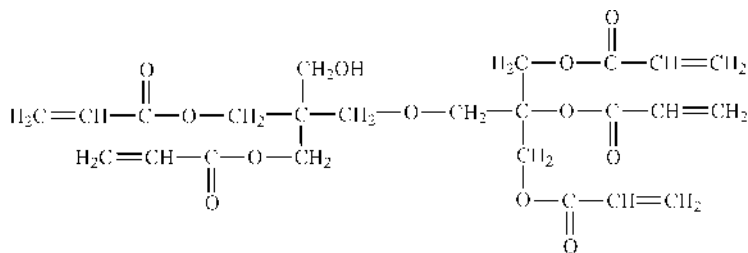
$$Conversion = 1 - \frac{[M]}{[M]_0} = 1 - \frac{P_{rxn}(t)/P_{ref}(t)}{P_{rxn}(0)/P_{ref}(0)}$$

where  $P_{rxn}$  is the peak height or area associated with the reactive functionality and  $P_{ref}$  is the peak height or area associated with an internal reference.  $R_p$  is then calculated by differentiating the conversion curve over time.

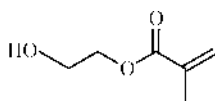
Fluorescence spectroscopy has been used to measure conversion by adding fluorescent molecules to the system that are sensitive to physical parameters (such as polarity or viscosity) that can be correlated to conversion (78–80). Both fluorescence (23) and absorption (35) spectroscopy have been used to follow changes in the photoinitiator spectrum as it absorbs light and produces free radicals. More complicated techniques are used to observe the free-radical active centers generated during polymerization. Since the lifetime of a free-radical active center is very short (typically  $10^{-1}$ – $10$  s) (p. 274 of Ref. 33), sensitive techniques are needed to determine the structure and concentration of initiating or propagating free radicals. These include the addition of trapping agents that ensnare the free radicals through radical combination or hydrogen abstraction, as well as electron spin resonance (ESR) spectroscopy that allows differentiation of radical species, environment, and concentration during reaction (71,81). Other specialized methods include laser flash photolysis (82–84) and photo-chemically induced dynamic nuclear polarization (photo-CIDNP), which provide information on excited state lifetimes and free-radical intermediates (17,84).

**Complex Photopolymerization Systems.** Kinetic modeling of free-radical photopolymerizations becomes more complicated as comonomers are added to the reaction system and as different polymerization methods are used to tailor the polymer properties. Although free-radical reaction mechanisms still hold true, rates of propagation and termination must be reconsidered to account for variables such as differences in double bond reactivities, reaction diffusion, and chain transfer.

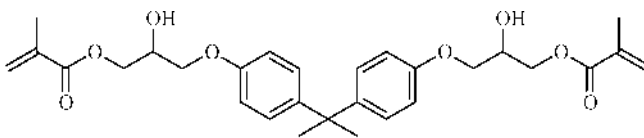
**Chain Cross-Linking Photopolymerizations.** In many applications, polymer networks rather than linear chains are desired. The conversion of double bonds in cross-linked systems is often lower because a fraction of the functional groups becomes trapped in areas inaccessible to the active centers. However, polymer networks show improved strength and chemical resistance because degradation of the polymer requires breaking multiple bonds. In order to achieve these types of structures, multifunctional monomers are needed to connect polymer chains together. The monomer itself may then have more than one functional group, as shown in the example (70). Dipentaerythritol pentaacrylate 23, a cross-linking monomer, has five reactive sites and is used in protective coating formulations.



the chains. For example, 2-hydroxyethyl methacrylate 24 and bisphenol A glycidyl methacrylate (25) are used in adhesive resins for dental composites:

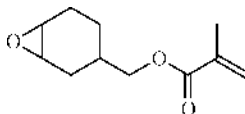


24



25

Cross-linked systems may also be developed in stages. These monomers have one reactive group that undergoes free-radical polymerization and a second reactive group that undergoes cross-linking by another mechanism, such as cationic photopolymerization. One example is the hybrid monomer (3,4-epoxycyclohexyl) methyl methacrylate 26 where the acrylate moiety forms the polymer chains first using free-radical photopolymerization and the epoxy moiety forms the cross-links second using cationic photopolymerization (85):



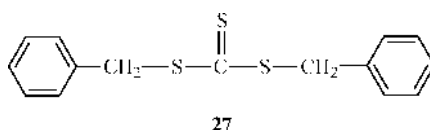
26

The properties of these cross-linked photopolymers are strongly influenced by the cross-link density (ie, the length of the polymer chain between cross-links and the length of the cross-linking molecule itself) (p. 521 of Ref. 33). As the cross-link density increases, hardness and solvent resistance increases, while flexibility decreases (43). The cross-link density can be adjusted by the choice and concentration of the monomers. If different reactive groups are present, then the reactivity ratios of the monomers will determine the rate at which one monomer will react with itself versus the other monomer(s). This will dictate how often a monomer capable of forming a cross-link is added to the main chain. However, in most commercial formulations, mono- and multifunctional monomers with the same type of reactive group (eg, acrylates) are mixed to obtain desired performance properties. Thus, the concentration and number of reactive groups for each monomer will determine the cross-link density.

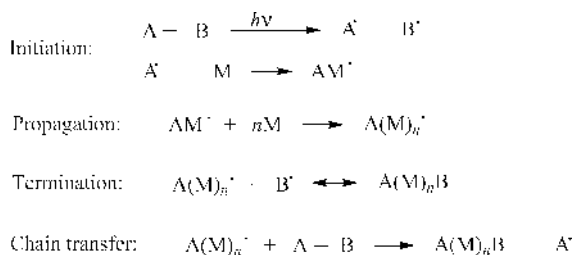
Kinetic modeling of cross-linked systems is significantly more difficult than for linear systems. Termination mechanisms are more complex because active center trapping (first order or unimolecular termination) and effects of reaction-diffusion must be considered (69,86). Monomers with multiple reactive groups used in highly cross-linking systems may exhibit increased rate of consumption for the pendant reactive groups after the molecule has been included in the polymer chain, resulting in the formation of microgel regions. These structural inhomogeneities are manifested by densely cross-linked regions within a looser polymer network. Other differences include delayed volume shrinkage with respect to reaction rate (leading to excess free volume) and immediate autoacceleration in the polymerization rate (leading to an increase in radical

concentration). Modeling efforts have focused on simulating termination in these systems through incorporating chain-length-dependent termination (67,75,87), combining unimolecular and bimolecular termination equations (69), and considering the impact of diffusion-controlled behavior on the rate constants (72,88,89).

**"Living" Free-Radical Photopolymerizations.** The ability to control polymer architecture, molecular weight, polydispersity, and end groups enables the development of polymers with improved and specified properties. Living polymerizations, in which propagating chains do not undergo termination or chain transfer reactions and continue to grow until the monomer supply is exhausted, is one way to gain such control (90). Living polymerizations have been successful in systems with ionic active centers; however, bimolecular termination reactions make this difficult to achieve in free-radical polymerizations. Processes such as atom transfer radical polymerization (ATRP) are used in free-radical thermal polymerizations to produce living polymers (91–93) (see LIVING RADICAL POLYMERIZATION). Light-initiated free-radical living polymerizations can be accomplished using iniferters (94). An iniferter participates in the polymerization by serving as an initiator, chain transfer agent, and chain terminator. Photoiniferters generally contain a carbon–sulfur linkage, which cleaves upon illumination to produce a carbon radical and a sulfur radical. Dibenzyl trithiocarbonate 27 is an example of such an iniferter (93):



The carbon radical ( $A^\bullet$ ) is more reactive and serves as the initiation radical, while the sulfur radical ( $B^\bullet$ ) is less reactive and serves only as the termination radical (95):



Since termination and chain transfer are still present in iniferter-assisted photopolymerizations, these systems are sometimes described as controlled, rather than living, free-radical polymerizations. Regardless, this approach enables control of bulk free-radical photopolymerizations that is not otherwise obtainable. Examples of applications include surface modification of substrates (91), three-dimensional nanoscopic patterns (96), and block copolymers (93,97).

**Photopolymerization in Microemulsion Systems.** Free-radical photopolymerization in microemulsion systems can be used to form stable microlatexes with controlled molecular weight and polydispersity. Microemulsions are

two-phase systems, usually consisting of monomer droplets in an aqueous solvent (termed *oil-in-water*) (98,99). Acrylates, methacrylates, and styrenes are typical monomers for microemulsion photopolymerizations. Surfactant molecules are used to stabilize the monomer droplets in solution and to prevent their coalescence. In microemulsions, co-surfactants such as alcohols are often needed to reduce the surface tension of the monomer droplets. This enables further curvature, producing droplets with diameters on the order of 10–50 nm (100). Because of their small size, they do not scatter visible light as do macroemulsions, which are opaque since they contain droplets on the order of 100–1000 nm (101). Thus, microemulsion systems are transparent and allow light to penetrate throughout the system to initiate polymerization within the droplets. Traditional photoinitiators such as benzophenone (102) may be used to generate the free-radical active centers, as well as photoinitiators developed to function as surfactants (103). The kinetics of microemulsion photopolymerizations deviate from the classical bulk kinetics discussed above. Although kinetic expressions for macroemulsions have been developed, a general understanding of microemulsions has not been attained. The surfactant concentration plays an important role in determining the rate of polymerization, along with the light intensity and monomer and photoinitiator concentrations. Termination reactions are suppressed because of the low radical concentration in the droplets and because of diffusional limitations within the droplets, resulting in higher molecular weight polymers (104,105).

**Hybrid Photopolymerizations.** Hybrid resin systems consist of monomers possessing two different functional groups—one that photopolymerizes by a free-radical active center (such as an acrylate) and the other by a cationic active center (such as an epoxide) (85,106–109). The two functional groups may be combined in one formulation either as separate monomers or as one monomer with both functionalities. If the functional groups are on different molecules, entangled chains or interpenetrating networks will be produced; cross-linked structures will result if the functional groups are on the same molecule because the polymer chains can be connected via either reactive bond.

The systems are designed in order to improve the reaction rate of the mixture and the physical properties of the photopolymer. The flexibility of the two photoinitiation schemes in one system allows for numerous possibilities in achieving greater control of viscosity, conversion, shrinkage, adhesion, and ultimate strength. The kinetics of hybrid photopolymerization systems are more difficult because two reactive systems (free-radical and cationic) must be resolved from one another. Cationic photopolymerization kinetics are more difficult to analyze than free-radical kinetics because the pseudo-steady-state assumption is often not valid for the cationic active center concentration, and the nature and concentration of the cationic active centers is difficult to determine (p. 376 of Ref. 33, see also PHOTOPOLYMERIZATION, CATIONIC).

## Applications

Free-radical photopolymerizations have been traditionally applied to thin films and coatings where the light penetration is less of an issue ( $\epsilon b[I]$  is more likely to be small), high production speeds can be achieved, and formulations free from

volatile emissions are desirable. In this way, the disadvantages of free-radical photopolymerization, such as poor conversion in thick or strongly absorbing systems, in the presence of oxygen, and in vitrifying systems at ambient temperatures, may be minimized. Despite these limitations, applications of free-radical photopolymerization are far-reaching and encompass the automotive, electronic, medical, optical, graphic arts, flooring, and furniture industries, to name a few. Photopolymerizations continue to expand into previously un contemplated areas such as topcoats for automobiles, thick parts and composite structures, and biomedical implants as more industries begin to appreciate the advantages these light-induced reactions have over traditional, thermal polymerization methods (1,2,110,111).

**Films, Coatings, and Adhesives.** Photopolymers may be used as coatings (qv) for a wide range of substrates, including wood, glass, paper, metals, and plastics (2–4,44,110,112–115). These coatings serve to protect surfaces from scratches and chemical exposure, to provide decoration and color, and to allow modification of surface properties. At present, most coatings are applied as a liquid monomer formulation and then photopolymerized; however, photocurable powder coatings are being developed and are expected to have a huge impact in metal-, paper-, and wood-coating applications (2,4). Free radically photopolymerized adhesives provide bonding between laminates, such as glass panes or plastic films. Pressure-sensitive adhesives and release coatings are used to make tapes, labels, and stickers (116,117). Photocurable inks are used on packaging materials and magazines, and photocurable varnishes provide glossy coatings for graphic media.

**Optics and Photoimaging.** Advanced applications of free-radical photopolymerizations include development of optical devices (118–120). The rapid reaction rates afforded by free-radical photopolymerizations have been able to incorporate liquid crystal order in polymers used for displays, waveguides, and holographic gratings (121,122). Films and coatings for optical components, optical fibers, and eyeglasses also benefit from the flexibility and transparency of these photopolymer materials. In the optical fiber industry alone, several photopolymer coatings are used (123–126). A soft, rubbery primary coating is applied to glass fibers as a cushion against stresses and as a barrier against moisture. A hard secondary coating is applied over the primary coating to prevent damage to the fiber during use. Photoimaging techniques are based on the advantage of spatial control over photoinitiation. This has led to tremendous growth in holographic and lithographic applications and even to rapid prototyping of three-dimensional parts through stereolithography (3,127,128). Patterns for gratings, printed circuit boards, and integrated circuits may be created in photoimageable or photoresist materials using photomasks or computer-controlled lasers (129,130). Microlithography can also be used to develop photopolymer membranes on microfluidic chips to perform chemical separations (131,132).

**Biomaterials.** In recent years, photopolymerizations have become more prominent in biological applications because these systems can provide superior products with rapid reaction rates at room temperature. Photopolymerizations for biological applications are more challenging because of the numerous considerations with regard to safety and health. For example, resin formulations and final products must have zero toxicity when introducing these systems into a biological system. Since the migration of small molecules may cause health

problems, high conversions of monomer and low concentrations of residual photoinitiator are desirable. When photopolymerizations are conducted *in vivo*, the formulations must be polymerizable by visible light (to prevent cellular damage), and the reactions must not be hampered by atmospheric oxygen or high water concentrations. If the polymers are designed to biodegrade, then the degradation products themselves must not cause health complications (see BIODEGRADABLE POLYMERS, MEDICAL APPLICATIONS). In addition, polymers that will be used *in vivo* must be biocompatible, as well as sterilizable (133). Scaffolding for bone and tissue engineering (qv), bioadhesives for wound closure, and microchips for biochemical analysis are examples of biomaterials produced using free-radical photopolymerizations (134,139).

**Hydrogels.** Free-radical photopolymerization can be used to produce cross-linked hydrophilic polymer networks that have numerous applications as biomaterials. These hydrogels (qv) are insoluble, but can swell with water to produce soft polymers that have mechanical integrity. Biomedical applications of hydrogels include delivery systems for drugs, enzymes and proteins (140–143); wound dressings (133); and biosensors for detection of glucose and other bioproducts (144). Soft contact lenses are optically transparent hydrogels produced by photopolymerization of mono- and dimethacrylates in a mold (145,146).

**Dental Composites.** Photopolymers are quickly replacing traditional amalgams for the repair of tooth caries and defects (147) (see DENTAL APPLICATIONS). The photopolymers may be matched to the color of the tooth, and treatment does not require the cutting away of natural tooth structures for bonding. A resin adhesive, which contains a mono-(meth)acrylate as a reactive diluent and a multi-(meth)acrylate as a cross-linker, is applied to the prepped tooth to provide a bond between the tooth and filling. The resin composite, which contains multi-(meth)acrylates for cross-linking and silica fillers to reduce shrinkage stresses, is photopolymerized in incremental layers upon the adhesive base to form the tooth filling. Both the adhesive and composite resins use a visible light free-radical photoinitiator system (camphorquinone with an amine co-initiator) with a blue light source (139,148). Photopolymerization of each layer takes place in less than one minute.

## BIBLIOGRAPHY

“Photopolymerization and Photocross-linking” in *EPST* 1st ed., Vol. 10, pp. 145–156, by G. Oster, Mount Sinai School of Medicine; “Photopolymerization” in *EPSE* 2nd ed., Vol. 11, pp. 186–212, by S. P. Pappas, North Dakota State University; “Photopolymerization, Free Radical” in *EPST* 3rd ed., Vol. 10, pp. 807–837, by Y. Cai and J. L. P. Jessop, University of Iowa.

## CITED REFERENCES

1. A. B. Scranton, *RadTech Rep.* **13**(6), 36 (1999).
2. K. Lawson, *RadTech Rep.* **13**(6), 32 (1999).
3. J. P. Fouassier, *Photoinitiation, Photopolymerization, and Photocuring: Fundamentals and Applications*, Hanser Publishers, New York, 1995.
4. J. V. Koleske, *Radiation Curing of Coatings*, ASTM International, West Conshohocken, Pa., 2002.

5. C. Decker, *Macromol. Rapid Commun.* **23**, 1067 (2002).
6. C. G. Roffey, *Photopolymerization of Surface Coatings*, John Wiley & Sons, Inc., New York, 1982.
7. M. Kaur and A. K. Srivastava, *J. Macromol. Sci., Polym. Rev. C* **42**, 481 (2002).
8. N. S. Allen, *J. Photochem. Photobiol. A* **100**, 101 (1996).
9. H. J. Hageman, *Prog. Org. Coat.* **13**, 123 (1985).
10. B. M. Monroe and G. C. Weed, *Chem. Rev.* **93**, 435 (1993).
11. H. F. Gruber, *Prog. Polym. Sci.* **17**, 953 (1992).
12. J. Jakubiak and J. F. Rabek, *Polimery* **44**, 447 (1999).
13. K. Dietliker, in J. P. Fouassier and J. F. Rabek, eds., *Radiation Curing in Polymer Science and Technology, Vol. II: Photoinitiating Systems*, Elsevier Applied Science, New York, 1993.
14. M. Hamity and J. C. Scaiano, *J. Photochem.* **4**, 229 (1975).
15. J. Segurola, N. Allen, M. Edge, A. Parrondo, and I. Roberts, *J. Photochem. Photobiol. A* **122**, 115 (1999).
16. J. P. Fouassier, D. Ruhlmann, B. Graff, and F. Wieder, *Prog. Org. Coat.* **25**, 169 (1995).
17. G. Rist, A. Borer, K. Dietliker, V. Desobry, J. P. Fouassier, and D. Ruhlmann, *Macromolecules* **25**, 4182 (1992).
18. T. L. Marino, D. Martin, and D. C. Neckers, *Adhes. Age* **38**, 22 (1995).
19. M. Bendyk, B. Jedrzejewska, J. Paczkowski, and L. Linden, *Polimery* **47**, 654 (2002).
20. K. Kawamura, Y. Aotani, and H. Tomioka, *J. Phys. Chem. B* **107**, 4579 (2003).
21. K. S. Padon and A. B. Scranton, *Recent Res. Dev. Polym. Sci.* **3**, 369 (1999).
22. K. S. Padon and A. B. Scranton, *J. Polym. Sci., Part A: Polym. Chem.* **38**, 2057 (2000).
23. K. S. Padon and A. B. Scranton, *J. Polym. Sci., Part A: Polym. Chem.* **39**, 715 (2001).
24. C. Grotzinger, D. Burget, P. Jacques, and J. P. Fouassier, *Polymer* **44**, 3671 (2003).
25. R. S. Davidson, *J. Photochem. Photobiol., A* **73**, 81 (1993).
26. A. B. Scranton, G. A. Miller, L. Gou, and M. El-Maazawi, in *RadTech 2002 Conference Proceedings*, Indianapolis, IN, Apr. 2002, p. 130.
27. C. Carlini and L. Angiolini, *Adv. Polym. Sci.* **123**, 127 (1995).
28. T. Corrales, F. Catalina, C. Peinado, and N. S. Allen, *J. Photochem. Photobiol., A* **159**, 103 (2003).
29. N. Kizilcan and A. Akar, *J. Appl. Polym. Sci.* **85**, 500 (2002).
30. A. M. Sarker, K. Sawabe, B. Strehmel, Y. Kaneko, and D. C. Neckers, *Macromolecules* **32**, 5203 (1999).
31. R. Francis and A. Ajayaghosh, *Macromolecules* **33**, 4699 (2000).
32. N. Kizilcan, *J. Appl. Polym. Sci.* **72**, 927 (1999).
33. G. Odian, *Principles of Polymerization*, 3rd ed., John Wiley & Sons, Inc., New York, 1991.
34. H. S. Taylor and A. A. Vernon, *J. Am. Chem. Soc.* **53**, 2527 (1931).
35. C. W. Miller, E. S. Jönsson, C. E. Hoyle, K. Viswanathan, and E. J. Valente, *J. Phys. Chem. B* **105**, 2707 (2001).
36. S. Jönsson, K. Viswanathan, C. E. Hoyle, S. C. Clark, C. Miller, F. Morel, and C. Decker, *Nucl. Instrum. Methods Phys. Res., Sect. B* **151**, 268 (1999).
37. S. Jönsson, P. E. Sundell, M. Shimose, S. Clark, C. Miller, F. Morel, C. Decker, and C. E. Hoyle, *Nucl. Instrum. Methods Phys. Res., Sect. B* **131**, 276 (1997).
38. C. Decker, F. Morel, S. Jönsson, S. Clark, and C. Hoyle, *Macromol. Chem. Phys.* **200**, 1005 (1999).
39. P. Kohli, A. B. Scranton, and G. J. Blanchard, *Macromolecules* **31**, 5681 (1998).
40. M. P. Patel, M. Braden, and K. W. M. Davy, *Biomaterials* **8**, 53 (1987).
41. J. Stansbury, and J. Ge, *RadTech Rep.* **17**(3), 56 (2003).
42. W. D. Cook, D. R. Derrick, and M. J. Tyas, *Biomaterials* **6**, 362 (1985).
43. C. Decker, *Prog. Polym. Sci.* **21**, 593 (1996).



44. U.S. Pat. 4,999,216 (Aug. 21, 1989), J. Gaske, J. J. Krajewski, and G. K. Noren (to Desoto, Inc.).
45. N. B. Cramer, J. P. Scott, and C. N. Bowman, *Macromolecules* **35**, 5361 (2002).
46. N. B. Cramer, T. Davies, A. K. O'Brien, and C. N. Bowman, *Macromolecules* **36**, 4631 (2003).
47. N. B. Cramer and C. N. Bowman, *J. Polym. Sci., Part A: Polym. Chem.* **39**, 3311 (2001).
48. L. Lecamp, F. Houllier, B. Youssef, and C. Bunel, *Polymer* **42**, 2727 (2001).
49. L. V. Natarajan, C. K. Shepherd, D. M. Brandelik, R. L. Sutherland, S. Chandra, V. P. Tondiglia, D. Tomlin, and T. J. Bunning, *Chem. Mater.* **15**, 2477 (2003).
50. B. Chiou and S. A. Khan, *Macromolecules* **30**, 7322 (1997).
51. I. R. Bellobono and M. Zeni, *Makromol. Chem., Rapid Commun.* **7**, 733 (1986).
52. L. Villegas, M. V. Encinas, A. M. Rufs, C. Bueno, S. Bertolotti, and C. M. Previtali, *J. Polym. Sci., Part A: Polym. Chem.* **39**, 4074 (2001).
53. C. Garcia, A. Fimia, and I. Pascual, *Appl. Phys. B: Lasers Opt.* **72**, 311 (2001).
54. H. Yao, M. Huang, Z. Chen, L. Hou, and F. Gan, *Mater. Lett.* **56**, 3 (2002).
55. L. A. White, C. E. Hoyle, S. Jonsson, and L. J. Mathias, *J. Polym. Sci., Part A: Polym. Chem.* **40**, 694 (2002).
56. U.S. Pat. 5,459,175 (Oct. 17, 1995), J. G. Woods, M. A. Rakas, A. F. Jacobine, L. M. Alberino, P. L. Kropp, D. M. Sutkaitis, D. M. Glaser, and S. T. Nakos (to Loctite Corp.).
57. J. Lub, D. J. Broer, and P. van de Witte, *Prog. Org. Coat.* **45**, 211, 2002.
58. D. J. Broer, J. A. M. M. van Haaren, P. van de Witte, and C. Bastiaansen, *Macromol. Symp.* **154**, 1 (2000).
59. J. Jakubiak and J. F. Rabek, *Polimery* **45**, 485 (2000).
60. H. J. Hageman, F. P. B. van der Maeden, and P. C. G. M. Janssen, *Makromol. Chem.* **180**, 2531 (1979).
61. J. D. Ingle Jr., and S. R. Crouch, *Spectrochemical Analysis*, Prentice Hall, New Jersey 1988, pp. 21.
62. G. A. Miller, L. Gou, V. Narayanan, and A. B. Scranton, *J. Poly. Sci., Part A: Polym. Chem.* **40**, 793 (2002).
63. G. Terrones and A. J. Pearlstein, *Macromolecules* **34**, 8894 (2001).
64. M. D. Goodner and C. N. Bowman, *Chem. Eng. Sci.* **57**, 887 (2002).
65. E. A. Lissi and A. Zanoeco, *J. Polym. Sci., Part A: Polym. Chem.* **21**, 2197 (1983).
66. A. R. Shultz and M. G. Joshi, *J. Polym. Sci., Part B: Polym. Phys.* **22**, 1753 (1984).
67. K. A. Berchtold, B. Hacıoğlu, L. Lovell, J. Nie, and C. N. Bowman, *Macromolecules* **34**, 5103 (2001).
68. J. F. Rabek, in J. P. Fouassier and J. F. Rabek, eds., *Radiation Curing in Polymer Science and Technology, Vol. I: Photoinitiating Systems*, Elsevier Applied Science, New York, 1993.
69. E. Andrzejewska, M. B. Bogacki, and M. Andrzejewski, *Macromol. Theory Simul.* **10**, 842 (2001).
70. I. V. Khudyakow, J. C. Legg, M. B. Purvis, and B. J. Overton, *Ind. Eng. Chem. Res.* **38**, 3353 (1999).
71. Q. Yu, S. Nauman, J. P. Santerre, and S. Zhu, *J. Appl. Polym. Sci.* **82**, 1107 (2001).
72. L. Lecamp, B. Youssef, C. Bunel, and P. Lebaudy, *Nucl. Instrum. Methods Phys. Res., Sect. B* **151**, 285 (1999).
73. M. Jöhnck, L. Müller, A. Neyer, and J. W. Hofstraet, *Polymer* **40**, 3631 (1999).
74. G. Mailhot and M. Bolte, *J. Photochem. Photobiol. A* **56**, 387 (1991).
75. B. Hacıoğlu, K. A. Berchtold, L. G. Lovell, J. Nie, and C. N. Bowman, *Biomaterials* **23**, 4057 (2002).
76. L. Cokbaglan, N. Arsu, Y. Yagci, S. Jockusch, and N. J. Turro, *Macromolecules* **36**, 2649 (2003).

77. C. Decker, F. Masson, and R. Schwalm, *Macromol. Mater. Eng.* **288**, 17 (2003).
78. S. M. Keeny III, J. M. Antonucci, F. W. Wang, and J. A. Tesk, in S. W. Shalaby, Y. Ikada, R. Langer, and J. Williams, eds., *Polymers of Biological and Biomedical Significance*, American Chemical Society, Washington, D. C., 1994.
79. W. F. Jager, A. A. Volkers, and D. C. Neckers, *Macromolecules* **28**, 8153 (1995).
80. J. Paczkowski and D. C. Neckers, *Macromolecules* **25**, 548 (1992).
81. M. V. Encinas, A. M. Rufs, E. Norambuena, and C. Giannotti, *J. Polym. Sci., Part A: Polym. Chem.* **35**, 3095 (1997).
82. A. Wrzyszczyński, P. Filipiak, G. L. Hug, B. Marciniak, and J. Paczkowski, *Macromolecules* **33**, 1577 (2000).
83. M. V. Encinas, A. M. Rufs, S. Bertolotti, C. M. Previtali, *Macromolecules* **34**, 2845 (2001).
84. H. Dreeskamp and W. U. Palm, in J. P. Fouassier and J. F. Rabek, eds., *Lasers in Polymer Science and Technology: Applications*, Vol. II, CRC Press, Inc., Fla., 1990.
85. U.S. Pat. 6,187,836 (Feb. 13, 2001), J. D. Oxman, M. C. Matthew, and D. W. Jacobs (to 3M Innovative Properties Co.).
86. J. Jakubiak and J. F. Rabek, *Polimery* **46**, 10 (2001).
87. J. S. Young and C. N. Bowman, *Macromolecules* **32**, 6073 (1999).
88. D. L. Kurdikar and N. A. Peppas, *Macromolecules* **27**, 4084 (1994).
89. T. M. Lovestead, A. K. O'Brien, and C. N. Bowman, *J. Photochem. Photobiol., A* **159**, 135 (2003).
90. C. J. Hawker, *Acc. Chem. Res.* **30**, 373 (1997).
91. B. de Boer, H. K. Simon, M. P. L. Werts, E. W. van der Vegte, and G. Hadzioannou, *Macromolecules* **33**, 349 (2000).
92. R. Krishnan and K. S. V. Srinivasan, *Macromolecules* **36**, 1769 (2003).
93. Y. You, C. Hong, R. Bai, C. Pan, and J. Wang, *Macromol. Chem. Phys.* **203**, 477 (2002).
94. J. H. Ward, A. Shahar, and N. A. Peppas, *Polymer* **43**, 1745 (2002).
95. T. Otsu, *J. of Polym. Sci., Part A: Polym. Chem.* **38**, 2121 (2000).
96. T. A. von Werne, D. S. Germack, E. C. Hagberg, V. V. Sheares, C. J. Hawker, and K. R. Carter, *J. Am. Chem. Soc.* **125**, 3831 (2003).
97. A. Ajayaghosh and R. Francis, *J. Am. Chem. Soc.* **121**, 6599 (1999).
98. G. David, F. Özer, B. C. Simionescu, H. Zareie, and E. Pişkin, *Eur. Polym. J.* **38**, 73 (2002).
99. P. Kuo, N. J. Turro, C. Tseng, M. S. El-Aasser, and J. W. Vanderhoff, *Macromolecules* **20**, 1216 (1987).
100. I. Capek, *Eur. Polym. J.* **36**, 255 (2000).
101. N. K. Pokhriyal, P. G. Sanghvi, D. O. Shah, and S. Devi, *Langmuir* **16**, 5864 (2000).
102. I. Capek, *Polym. J.* **28**, 400 (1996).
103. L. Wang, X. Liu, and Y. Li, *Macromolecules* **31**, 3446 (1998).
104. I. Capek and J. P. Fouassier, *Eur. Polym. J.* **33**, 173 (1997).
105. C. L. Lester, C. D. Colson, and C. A. Guymon, *Macromolecules* **34**, 4430 (2001).
106. A. Stohr and P. Strohrriegl, *Macromol. Chem. Phys.* **199**, 751 (1998).
107. R. Vabrik, I. Czajlik, G. Túry, I. Rusznák, A. Ille, and A. ViG, *J. Appl. Polym. Sci.* **68**, 111 (1998).
108. C. Decker, T. Nguyen Thi Viet, D. Decker, and E. Weber-Koehl, *Polymer* **42**, 5531 (2001).
109. S. Peeters, in J. P. Fouassier and J. F. Rabek, eds., *Radiation Curing in Polymer Science and Technology*, Vol. III: Photoinitiating Systems, Elsevier Applied Science, New York, 1993.
110. C. Bradford, *RadTech Rep.* **13**(6), 19 (1999).
111. D. Harbourne, *RadTech Rep.* **13**(6), 16 (1999).

112. U.S. Pat. 5,888,649 (Aug. 15, 1997), B. S. Curatolo and T. J. Fox (to Avery Dennison Corp.).
113. U.S. Pat. 2002/0143078 A1 (Apr. 3, 2001), M. Awokola, C. Flosbach, H. Loeffler, and V. Paschmann (to E. I. du Pont de Nemours & Co.).
114. U.S. Pat. 2002/0164434 A1 (Sep. 13, 1999), M. Tarvin and M. A. Rau.
115. R. J. Modjewski, *RadTech Rep.* **13**(3), 45 (1999).
116. T. Ozawa, S. Ishiwata, and Y. Kano, *Furukawa Rev.* **20**, 83 (2001).
117. J.-M. Frances, S. Kerr III, and O. Pinto, *Radiat. Curing* **45**(1), 30 (2002).
118. P. Cheben, *Appl. Phys. Lett.* **78**, 1490 (2001).
119. A. Pu and D. Psaltis, *Appl. Opt.* **35**, 2389 (1996).
120. M. L. Schilling, V. L. Colvin, L. Dhar, A. L. Harris, F. C. Schilling, H. E. Katz, T. Wysocki, A. Hale, L. L. Blyler, and C. Boyd, *Chem. Mater.* **11**, 247 (1999).
121. K. Saravanamuttu, X. M. Du, S. I. Najafi, and M. P. Andrews, *Can. J. Chem.* **76**, 1717 (1998).
122. R. Bachelot, C. Ecoffet, D. Deloeil, P. Royer, and D. Loughnot, *Appl. Opt.* **40**, 5860 (2001).
123. J. Zhang, G. Windall, and I. W. Boyd, *Appl. Surface Sci.* **186**, 568 (2002).
124. U.S. Pat. 5,985,952 (Mar. 23, 1998), A. C. Levy (to Alvin C. Levy & Associates, Inc. and Master Adhesives, Inc.).
125. U.S. Pat. 20030100627 A1 (Oct. 9, 2001), T. E. Bishop, P. E. Snowwhite, T. Norlin, J. J. Schouten, J. Southwell, and A. Toussaint (to Pillsbury Winthrop, LLP).
126. U.S. Pat. 6,326,416 (Dec. 30, 1999), C. Chien, E. J. Fewkes, G. F. Jacobs, K. R. Jones, E. H. Urruti, and M. J. Winningham (to Corning, Inc.).
127. U.S. Pat. 5,972,563 (Jul. 28, 1997), B. Steinmann and A. Schulthess (to Ciba Specialty Chemicals Corp.).
128. U.S. Pat. 6,207,347 (Apr. 29, 1999), D. L. Lundy and N. J. Negandhi (to Nichigo-Morton Co. Ltd.).
129. J. Sturge, V. Walworth, and A. Shepp, eds., *Imaging Processes and Materials, Neblette's*, 8th ed., Van Nostrand Reinhold, New York, 1989.
130. U.S. Pat. 5,952,154 (May 29, 1998), R. Barr, D. Lundy, and S. Wheeler (to Morton International, Inc.).
131. C. Yu, M. Xu, F. Svec, and J. M. J. Fréchet, *J. Polym. Sci., Part A: Polym. Chem.* **40**, 755 (2002).
132. C. Yu, F. Svec, and J. M. J. Fréchet, *Electrophoresis* **21**, 120 (2000).
133. J. M. Rosiak and F. Yoshii, *Nucl. Instrum. Methods Phys. Res., Sect. B* **151**, 56 (1999).
134. D. L. Elbert and J. A. Hubbell, *Biomacromolecules* **2**, 430 (2001).
135. A. K. Burkoth and K. S. Anseth, *Biomaterials* **21**, 2395 (2000).
136. J. Elisseff, W. McIntosh, K. Anseth, S. Riley, P. Ragan, and R. Langer, *J. Biomed. Mater. Res.* **51**, 164 (2000).
137. R. S. Benson, *Nucl. Instrum. Methods Phys. Res., Sect. B* **191**, 752 (2002).
138. M. N. Cooke, J. P. Fisher, D. Dean, C. Rimnac, and A. G. Mikos, *J. Biomed. Mater. Res. Part B: Appl. Biomater.* **64B**, 65 (2002).
139. J. A. Burdick, A. J. Peterson, and K. S. Anseth, *Biomaterials* **22**, 1779 (2001).
140. D. N. Robinson and N. A. Peppas, *Macromolecules* **35**, 3668 (2002).
141. N. P. Desai, A. Sojomihardjo, Z. Yao, N. Ron, and P. Soon-Shiong, *J. Microencapsul.* **17**, 677 (2000).
142. M. Kurisawa, Y. Matsuo, and M. Yui, *Macromol. Chem. Phys.* **199**, 705 (1998).
143. P. Ulanski, I. Janik, S. Kadlubowski, M. Kozicki, P. Kujawa, M. Pietrzak, P. Stasica, and J. M. Rosiak, *Polym. Adv. Technol.* **13**, 951 (2002).
144. K. Sirkar and M. V. Pishko, *Anal. Chem.* **70**, 2888 (1998).
145. EP Pat. 0447169 (Sep. 18, 1991), V. McBrierty, J. Magan, and W. Blau (to Bausch & Lomb (US)).

146. U.S. Pat. 6,031,059 (Feb. 29 2000), D. G. Vanderlaan, F. Molock, and G. Fruzzetti (to Johnson & Johnson Vision Products, Inc.).
147. L. G. Lovell, H. Lu, J. E. Elliott, J. W. Stansbury, and C. N. Bowman, *Dent. Mater.* **17**, 504 (2001).
148. J. Nie, L. Å. Lindén, J. F. Rabek, J. P. Fouassier, F. Morlet-Savary, F. Scigalski, A. Wrzyszczyński, and E. Andrzejewska, *Acta Polym.* **49**, 145 (1998).

YING CAI  
JULIE L. P. JESSOP  
University of Iowa

## PHOTOREFRACTION

### Introduction

This article introduces the field of photorefractive materials and the photorefractive effect in polymer composites. The photorefractive effect is expected to play a significant role in the development of all-optical information processing techniques. Photorefractive materials, including polymers, have been proposed for use in high density optical data storage; associative image processing techniques, including dynamic holography, novelty filtering and image amplification; spatial light modulation, such as beam fanning, optical limiters, phase conjugators, self-induced optical resonators, programmable interconnections in integrated optics; and simulations of neural networks and associative memories with parallel signal processing (1–8).

The photorefractive effect requires a specific mechanism for the spatial modulation of the index of refraction of a material arising from an intensity modulation of the incident light (as in a diffraction pattern or hologram). The specific mechanism is the generation, transport, and trapping of charge through photoconduction in the illuminated regions to set up space-charge fields between the light and dark regions. These space-charge fields cause the modulation of the index of refraction acting through electro-optic and molecular orientation effects (9–11).

**Scope of Article.** The Photorefractive Process section describes the photorefractive process in detail, including theoretical models for photorefractive materials that are used to determine optimized material properties for applications using polymers. That section also describes how photorefractive materials can be distinguished from other photo-induced refractive index changes. Composition of Polymeric Photorefractive Materials section describes many of the ways polymeric composite materials have been formulated for their photorefractive properties, primarily by incorporating different functionalities via doping with electro-optic chromophores, photo-charge generation and transport agents, and plasticizers. Test Methods section briefly describes important experimental techniques for studying photorefractive materials, including four-wave mixing, two-beam coupling, and ellipsometry. Test Methods section also highlights several techniques for

studying photoconductivity specifically for the photorefractive response. Finally, Applications section discusses recent progress in developing polymeric photorefractive devices.

Because of the extensive overlap with electro-optics and nonlinear optics, the reader is referred to separate articles on these topics in this encyclopedia. See ELECTROOPTICAL APPLICATIONS for a discussion of the changes in the optical response of polymers due to an applied AC or DC electric field from the so-called Pockels or Kerr effects. Also see, for an overview, NONLINEAR OPTICAL PROPERTIES. Similarly, because photoconductivity is essential to photorefraction, readers may refer to CONDUCTIVE POLYMER COMPOSITES.

In addition to those cited above, many other helpful review articles have appeared in the archived research literature, for example, References 12–18.

### **History and Advantages of Polymeric Photorefractive Materials.**

The research literature on photorefraction dates back to its discovery as optical damage in the inorganic ferroelectric crystal, lithium niobate in 1966 (19). The first reports on photorefraction in an organic crystal appeared in 1990 (20) and in a polymeric material in 1991 (21). Application of crystalline photorefractive materials has been limited due to (1) the difficulty of crystal growth and processing and (2) fundamental limits on the maximum possible variation in the index of refraction of inorganic crystals in which large optical nonlinearities, measured by the electro-optic coefficient,  $r_e$ , are generally accompanied by large dielectric constants,  $\epsilon_r$ , leading to screening of the space-charge distribution through polarization effects (1). For the linear electro-optic contribution, the relevant figure of merit is defined by  $Q = n^3 r_e / \epsilon_r$ , where  $n$  is the index of refraction.  $Q$  values for organic photorefractive materials can exceed those of inorganic materials by more than an order of magnitude. The electro-optic mechanism in polymers is intrinsically different from that in inorganic crystals. In ferroelectric crystals, acoustic and optical phonons contribute significantly to the electro-optic effect, where the polarizability is largely ionic. The linear electro-optic response in organic polymers is primarily due to the electronic excitations of individual molecules and/or molecular units, thus yielding low dielectric constants and minimizing dispersion over DC to optical frequencies (22).

Because of these advantages as well as orientational enhancement effects and the superior compositional flexibility of polymers, the number of studies of polymers for photorefraction grew rapidly during the 1990s and into the current decade. It is now common to see a chapter on polymeric photorefraction in treatises that once emphasized only inorganic crystalline materials (for example, see References 23–27) and to see specific sections on photorefraction in overviews of nonlinear optical properties of polymers (for example, See references 28–31).

## **The Photorefractive Process**

The essential property of photorefraction is the writing of a refractive index grating due to a nonuniform incident optical field, typically through interference and/or diffraction of the incident light beam(s). The photorefractive effect can be understood as four distinct sequential steps, shown schematically in Figure 1. (1) The incident light generates mobile charges, usually positively charged “holes” in

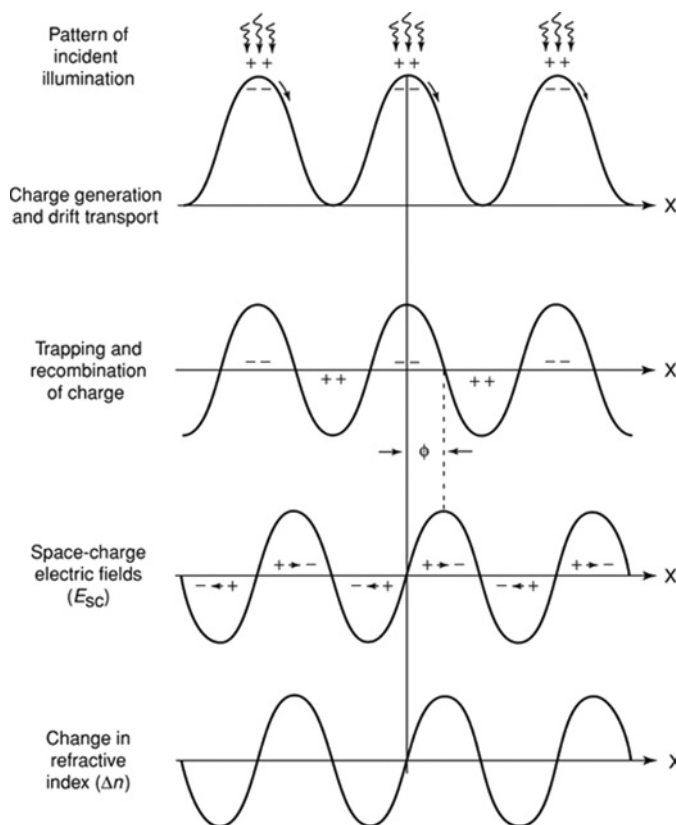


**Fig. 1.** Schematic of the photorefractive process. Note the phase shift,  $\phi$ , between the incident intensity grating and the resulting photorefractive grating in the material. Depending upon the trapping depth and depth of modulation of the intensity of light incident on the material, the phase shift can vary between 0 and  $\pi/2$ . The absence of this phase shift indicates that mechanisms of photoinduced refractive index change other than photorefraction are involved. Many photorefractive applications require phase shifts approaching  $\pi/2$ .

polymeric materials, through the photoionization of light sensitive constituents called sensitizers or photocharge generation agents (32). (2) The photo-induced charge carriers (holes) drift away due to an applied electric field,  $E_B$ , separating the positive from the negative charges by the charge-transfer photoconducting properties of the material, while the negative charges generally remaining localized (33). Other transport mechanisms including diffusion and photovoltaic processes are possible and, though significant in inorganic materials, they have not been found significant in photorefractive polymers. These first two steps show the importance of the photoconductivity of the material which must provide for the transport of the charge over distances many times greater than the wavelength of the illumination. (3) Because the photorefractive material does not generate mobile charge in dark regions (where destructive interference occurs), the third step in the process is the trapping of the mobile charges at suitable charge

trapping sites. These trapped charges establish charge density gradients in the material that produce a patterned internal (“space-charge”) electric field, shifted from the incident light pattern by the migration of the mobile charges into dark regions. (4) Lastly, the space-charge field arising between the dark and light regions modulates the index of refraction of the material via the electro-optic effect and reorientation of the molecular dipoles in the space-charge field (11,34–36). The resulting index-of-refraction pattern then stores the information in the original illumination pattern. This index-of-refraction grating will diffract an incoming reference beam to reproduce the pattern that created it as in a hologram.

Not surprisingly, different material functions are required for each of the steps in the formation of a photorefractive grating, leading to development of multifunctional composite materials and the search for optimal combinations of material properties as discussed in Composition of Polymeric Photorefractive Materials section.

One of the most important results of these processes is that a phase shift  $\phi$  appears between the index of refraction grating and the incident light intensity pattern, ideally by as much as  $90^\circ$  when the centers of mobile and fixed charge density correspond to the regions of minimum and maximum light intensity, respectively (as shown in Fig. 1). As discussed further in Test Methods section and Applications section, this phase shift makes possible an energy exchange between two incident crossed beams (two-beam coupling) necessary for many optical data processing applications requiring optical gain, amplifying one beam at the expense of another.

**Refractive Index Modulation by  $E_{sc}$ .** Photorefractive behavior in polymers can be very roughly modeled by assuming a one-dimensional index of refraction change caused by the vector sum of the applied “bias” field  $E_B$  and a space-charge field resulting from separated, trapped charges within the material  $E_{sc}$ ,  $E_T(x) = E_{sc} + E_B$  (4,37),

$$\Delta n(x) \approx -\frac{n^3 r_e}{2} E_T(x) + \frac{3r_K}{2n} E_T^2(x) \quad (1)$$

where  $n$  is the index of refraction,  $r_e$  is the effective Pockels (linear) electro-optic coefficient, and  $r_K$  is the effective Kerr (quadratic) coefficient due to chromophore reorientation. As further discussed below,  $E_{sc}$  is inversely proportional to the relative permittivity  $\epsilon_r$  (as seen in eq. 3).

For a common alternate representation of the quadratic field dependence, see equation 2.

Refractive index modulations on the order of  $\Delta n \sim 10^{-2}$  have been suggested with known materials at field strengths of only 28 V/ $\mu\text{m}$  (38).

**Orientational Enhancement Effect.** In addition to a strictly electronic and linear (Pockels) electro-optic response given by the first term on the right side of equation 1, the quasi-one-dimensional nonlinear optical chromophores incorporated into the polymer for their electro-optic response often exhibit large differences in the polarizability parallel versus perpendicular to the chromophore long axis (36,39–42). This so-called “polarization anisotropy” ( $\Delta\alpha \approx \alpha_{\parallel} - \alpha_{\perp}$ , where  $\alpha_{\parallel}$  and  $\alpha_{\perp}$  are the linear polarizabilities along and perpendicular, respectively, to the long molecular axis) typically arises from strong light absorption

and a large ground state dipole moment  $\mu_g$  (14) as found in highly colored nonlinear optical chromophores. In fact, reorientation of these chromophores in the space-charge field usually plays the dominant role in determining the depth of the index-of-refraction grating in polymeric composite materials (4). The orientational effect can be interpreted either in terms of the optical Kerr effect (4) as in the second term on the right in equation 1 or as a polarization anisotropy appearing with a quadratic dependence on the space-charge field (14,43). In the latter case, the quadratic dependence is often represented using the following expression based upon an oriented gas model (14).

$$\Delta n_{\text{orient}}(x) \approx \frac{N(\alpha_{\parallel} - \alpha_{\perp})}{45n} \left( \frac{\mu_g E_T}{k_B T} \right)^2 \quad (2)$$

where  $N$  is the density of reorienting nonlinear optical molecules,  $k_B$  is the Boltzmann constant and  $T$  is the temperature.

To understand the significance of the orientational enhancement effect and how it increases the depth of the refractive index change beyond that of the linear electro-optic effect found in crystalline materials, it is helpful to recall that the bulk linear electro-optic effect can only occur when the material lacks inversion symmetry (see ELECTROOPTICAL APPLICATIONS). To induce the asymmetric order in amorphous polymers, the polymer is typically subject to electric-field poling to align the dipoles. In this poling process (see NONLINEAR OPTICAL PROPERTIES), the polymer is heated above its glass-transition temperature ( $T_g$ ) (see GLASS TRANSITION) and then cooled during the application of the poling field to freeze in polar order.

In room-temperature experiments with low  $T_g$  polymers ( $<100^\circ\text{C}$ ), it is found that the polymers will not maintain the polar order needed for the linear electro-optic effect when the poling field is turned off. These materials must therefore be poled *in situ* for the requisite asymmetry to appear. At the same time, an external electric field (also called the bias or drift field) must be applied across the photorefractive polymer *in situ* to enable the mobile charges to move efficiently into the dark regions. Thus, the requisite external poling field is already present for polymeric photorefractive materials. This applied bias field serves two purposes: (1) The dominant mechanism for charge transport is drift of the holes in the direction of the applied field (as further discussed below). (2) The external field strengthens the alignment of the polymer polar order required for the linear electro-optic effect and for the electric-field-induced birefringence.

The applied bias field is not the only field experienced by the molecules, however. The creation of space-charge fields  $E_{sc}$  will also modulate the orientation of the nonlinear chromophores. This so-called orientational enhancement effect was discovered by Moerner and co-workers when they found that the measured diffraction efficiency of a low  $T_g$  photorefractive polymer required  $E_{sc}$  to be an order of magnitude larger than should have been permitted by the projection of  $E_B$ , using only the linear electro-optic effect (11). In effect, the sinusoidal space-charge grating produced a sinusoidal variation in the electro-optic  $r_e$  coefficients and a sinusoidal birefringence of the polymer. Additional enhancements were



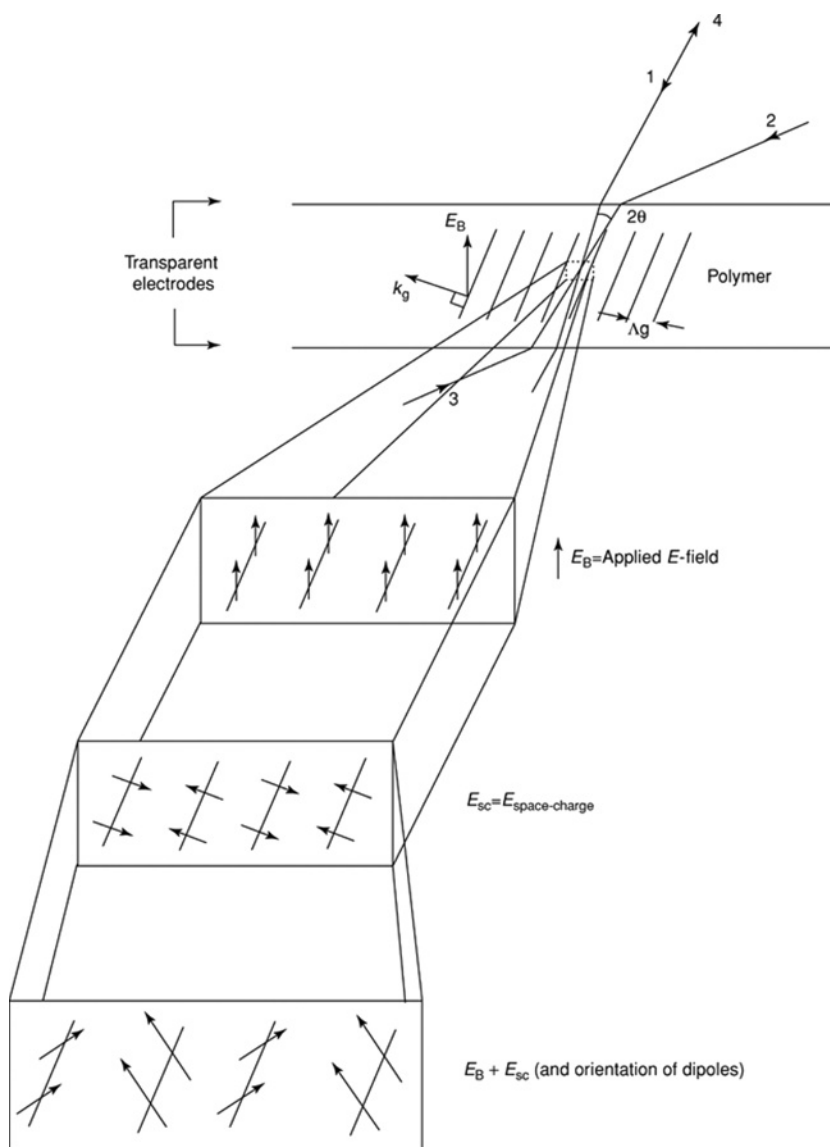


**Fig. 2.** Oblique geometry typically used for characterizing bulk photorefractive polymers. The magnified portion illustrates the orientational enhancement effect described in the text due to the modulated poling of the electro-optic chromophore in the combined  $E_B + E_{sc}$  fields. The beam and grating geometry applies for both four-wave mixing (beams 1–4) and two-beam coupling (beams 1 and 2).

obtained upon adding a plasticizer to the composite in order to further reduce  $T_g$  (44).

A schematic of the typical oblique transmission experimental geometry used to measure the diffraction efficiency of a photorefractive polymer this way is shown in Figure 2. The sample must be tilted with respect to the bisector of

the two beams because the applied field must have a component parallel to the grating wavevector in order to move charges along the grating. This experimental geometry complicates analysis of the relationship between the vector fields and the tensor elements of the resulting refractive index change. A more complete treatment, including the tensorial nature of the index of refraction modulation, as well as figures of merit, may be found in Reference 45.

Understanding the effects of orientational enhancements has been made more complex, however, by the need to account for supramolecular interactions such as dipolar aggregation, the tendency of dipoles to adopt align antiparallel with their neighbors (38). Several studies have explored the effects of glass transition temperature on polymeric photorefractive properties (46–48).

**Origin of the Space-Charge Field  $E_{sc}$ .** For a photorefractive index grating, the space-charge field  $E_{sc}$  can be described approximately by (49)

$$E_{sc} \approx \left( \frac{\Phi}{h\nu} \right) (eL_{eff}) \left( \frac{mI_0\alpha}{\varepsilon_0\varepsilon_r} \right) \quad (3)$$

where  $\Phi$  is the photocarrier generation efficiency,  $h\nu$  the photon energy,  $e$  the electronic charge,  $L_{eff}$  the effective transport length traveled by the mobile charge,  $\alpha$  the absorption coefficient, and  $\varepsilon_0$  the vacuum permittivity. The modulation index  $m$  is a function of the grating geometry and is given by  $m = 2\sqrt{I_1 I_2}/I_0$ , where the interference arises from two crossed beams of combined irradiance  $I_0 = I_1 + I_2$ . For this elementary hologram, the resulting irradiance distribution is

$$I(x) = I_0[1 + m\cos(k_g x)] \quad (4)$$

where  $k_g$  is the wavevector defined by the spacing  $\Lambda_g$  between adjacent irradiance maxima in the incident grating (the grating “wavelength”). Thus,  $k_g = 2\pi/\Lambda_g = 4\pi n \sin \theta/\lambda_g$ , where  $\lambda_g$  and  $\theta$  are the incident optical wavelength (assuming the interfering beams are the same wavelength) and the crossing half-angle between those beams inside the sample. For visible wavelengths,  $\Lambda_g$  ranges from 0.3 to 20  $\mu\text{m}$ , due to the limited range of accessible angles between the two beams (see Fig. 2).

**Photoconduction.** The generation, transport, and trapping of charge necessary to create  $E_{sc}$  and the resulting index-of-refraction modulation are each steps in the process of photoconduction in the photorefractive material (50). The literature on photoconductivity in polymers is voluminous and the variety of effects to be accounted for mirrors the variety of applications to which polymers may be adapted (see, for example, References 51–53). The original rate equations developed by Kukhtarev for inorganic materials (54) are inadequate for polymers due to the electric-field dependence of the charge photogeneration efficiency (55) and the complexities of charge trapping in the transport of charge (56). Unlike the photoconductive effects in inorganic materials, photoconduction in polymers is generally modeled using temperature-activated hopping mechanisms, not the standard band transport model used for inorganic ferroelectric crystals (57–59). In high-mobility polymers, however, the transport involves both traps associated with polymer transport and the conduction band associated with the ordered phase of the material. These combined effects require a hybrid model for

the transport, and its dependence on field (60–62). The hopping model assumes conductivity is controlled not by the size and accessibility of the conduction band, but by the presence and location of suitable trapping and recombination centers between which charges move via electric-field dependent or thermally activated jumps. In polymeric photoconduction, the charge hopping is between traps which are sensitized by the presence of a drift (DC) electric field across the sample as in the Poole–Frankel model (21,33,63–66). Traps are parametrized by their “depth,” ie, by the likelihood that charge may be released from the trap thermally as well as optically (a “shallow” trap) or may only be released, if at all, by absorption of a photon (a “deep” trap, either active or inactive depending upon its photoionizability) (67). Traps may be shallow or deep based on their thermal ionizability and photoionizability and are distinguished from recombination centers by the relative likelihood of the charge either being released from a *trap* to participate further in conduction or being neutralized through *recombination* with a carrier of the opposite sign. Thus, photoconductivity is also an increasing function of incident photon energy.

The time evolution of the charge generation and trapping process has been the subject of particular study because of significant interest in the development of photorefractive materials with a faster response. Notable recent developments include the numerical simulation of the kinetics of  $E_{sc}$  as a function of the light intensity, grating vector, electric field and density of deep inactive traps (68), the introduction of both shallow and deep traps with different, nonzero, excitation rates into the theory (69), and the experimental study of rise, decay, and steady-state photocurrents with pulsed light (70). The rate limiting step in the photorefractive process varies between materials, primarily being due to either the photocarrier generation efficiency or the charge mobility (1,69). Preillumination of the sample has been shown to affect the timing of the response significantly (69–72).

**Photocarrier Generation Efficiency.** The photocarrier generation efficiency  $\Phi_g$  depends upon the applied electric field, and is usually approximated as having a power-law dependence of  $\Phi_g \sim E^p$ , where  $p$  varies between 1.5 and 3.5, depending upon the material (1,50,73). The reason for this dependence is that even if the initial quantum yield from the incident photons is large, the photogeneration efficiency is limited by geminate recombination or back electron transfer due to the small thermalization radius of many polymers, ie, freed carriers cannot separate sufficiently so that the energy of their Coulombic attraction is less than  $k_B T$  (55). A strong applied field will help to separate the charge carriers and so improve the effective carrier generation efficiency (34). Typically, the field dependence of the charge generation and the effects of geminate recombination are understood using the Onsager model (74,75). That model is inadequate, however, in accounting for the slow recombination rate of electron–hole pairs in polymeric materials and has been augmented by the Marcus theory of electron transfer in more recent treatments to model slow recombination rates found in photoconductive polymers (76).

**Charge Transport, Mobility and Free Charge Lifetime.** An important parameter for understanding charge transport in photorefractive polymers is the quantity  $L_{eff}$ , which describes the transport length of the generated photocarriers.  $L_{eff}$  depends on the presence of applied fields, the grating geometry, and the

intrinsic mechanisms of carrier transport (77). It is important to maximize  $L_{\text{eff}}$ , which is defined so as to be always less than the inverse grating wavevector (on the order of 0.1–2.0  $\mu\text{m}$ ) (35). In its simplest form for one carrier and only drift transport, we can represent  $L_{\text{eff}}$  in terms of the grating wavevector  $k_g$  and the average drift length  $L_E$

$$L_{\text{eff}} = \frac{L_E}{[1 + (k_g L_E)^2]^{\frac{1}{2}}} \quad (5)$$

where  $L_E = \mu\tau|\mathbf{E}_B + \mathbf{E}_{\text{sc}}|$  is the transport length due to the combined fields. Here,  $\mu$  is the effective carrier mobility (also a strongly increasing function of  $E_B$ ) and  $\tau$  is the effective free lifetime of the carrier over distances large compared to the distances between traps.

From equation 5, it can be seen that maximization of  $L_{\text{eff}}$  for a given grating spacing requires maximization of the  $\mu\tau$  product or application of a large external field. Because of the dispersive nature of the transport,  $\mu$  and  $\tau$  are not easily defined quantities in polymers (78). The mobilities are field dependent, often in a highly nonlinear way, and the presence of significant trapping in a polymer complicates their determination (33,79). Furthermore,  $\tau$  in many polymers may be effectively limited by the presence of “deep traps” from which further photoionization is inhibited.

A major trade-off in the development of poled polymers for photorefraction arises from the need both to maximize the mobility for photoconductive transport and yet to minimize the dark conductivity to allow poling and subsequent storage of the photorefractive grating (80). Unfortunately, because poling introduces charge carriers into the sample, if the mobility of carriers in the photoconducting polymer is appreciable, the sample will short-circuit in the presence of a large applied poling or drift field before the molecules have adequately aligned (4).

On the other hand, another advantage of polymers over inorganic photorefractives is that the space-charge fields attainable are not generally limited by the trap density, so that large diffraction efficiencies have been realized by the application of large external fields. Thin-film polymers are amenable to the application of large external field, which has led to large efficiencies by compensating for small values of the  $\mu\tau$  product. Destruction of samples due to dielectric breakdown remains a problem and materials with large  $\Delta n$  in a relatively small applied field are of significant interest (38).

One potential benefit of using high mobility polymers is in reducing the response time of the materials in the cases when neither charge generation (69) nor rotational mobility (81) of the chromophores are the rate limiting factors in the PR process. Unlike diffraction efficiency, which can be increased by application of a stronger external field, the application of a strong external field cannot fully compensate for slow speed due to low mobility. While the mobility in some polymeric photorefractives has been found generally to be an increasing function of applied field, negative-field dependence has been predicted and observed in other cases (75,79).

Perhaps a better model for describing the disorder in charge generation and transport in molecularly doped polymers is the so-called "disorder formalism" proposed by Bässler for xerographic photoreceptors (82). In this model, transport occurs through hopping between localized states with a Gaussian distribution of energies and separation distances. A random distribution of permanent dipoles due to the nonlinear optical chromophores produces a local variation of the electrostatic potential and an increasing energy width, and position disorder appears with increasing dipolar molecule concentration. Increasing concentrations of molecules with large dipole moments led to increased disorder and reduced carrier mobility and photorefractive speed (79).

**Distinguishing Photorefraction from Other Photoinduced Refractive Index Changes.** A variety of photoinduced effects, such as photochromism, thermochromism, thermorefractive, conventional electronic  $\chi^{(3)}$  effects and photochemical changes, may lead to changes in the refractive indices of a polymer in ways other than photorefractive, or even so-called, pseudo-photorefractive (83–86). Each of these lacks the physical separation of internal space-charge that leads to a phase shift between the incident light intensity and the refractive index modulation. Though not always experimentally simple, there are many ways to distinguish true photorefractive from competing mechanisms, such as cis–trans isomerization, which lead to refractive index changes (75,87).

**Two Beam Coupling via a Phase Shift of the Index Grating.** The most unmistakable sign of photorefractive (and one of its most promising features) is asymmetric two-beam coupling (88). A critical element in this coupling is the nonzero phase shift between the phase grating and the incident interference pattern (indicated by  $\phi$  in Fig. 1). For absorption gratings from photochemical or photochromic effects, the index and intensity gratings are in phase. Two-beam coupling techniques for measuring the grating phase are discussed in (88) and in Test Methods section. Two-beam coupling in the absence of a moving grating (89) or an AC applied field is the strongest evidence of photorefractive. Its absence, however, does not alone signify the absence of photorefractive (21,90).

**Hologram Erasability.** The photorefractive effect is reversible. The traps that lead to the space-charge fields in photorefractive materials must themselves be photoionizable. If so, the photorefractive diffraction grating is erased simply by bathing the material in a uniform field of the proper photon energies. For photochemical effects, reversibility generally requires heating or other chemical treatment. Photochromic gratings tend to be only partially erasable under uniform illumination.

**Enhancement by External Fields.** The photoconductive response generally increases at least as the square root of the applied drift field. Application of an external field enhances photocarrier generation both by reducing the barrier to charge release and, as previously discussed, by assisting the separation of photogenerated charges to lessen the effects of geminate recombination.

**Correlation with Photoconductivity.** To confirm that the refractive index grating is due to the photoconduction of mobile charges into dark regions, comparisons between the absorption spectrum and the wavelength dependence of the photoconductivity and photorefractivity of a material help identify the underlying

photoconduction mechanism and resultant charge density gradients (33). These comparisons are complicated by the fact that the mobility and photocharge generation efficiency of photorefractive materials can be orders of magnitude lower than those properties appearing in materials developed solely for photoconduction. Some of the difficulties in quantifying relevant photoconductivity parameters in polymeric photorefractives are discussed in Reference 91 and in Test Methods section.

*Polarization Anisotropy of the Grating Readout.* The photorefractive response is dependent upon the polarization of the incident beam. If pure *s*- or *p*-polarized light is used in writing the grating, the depth of the index grating and thus the diffraction efficiency will be different depending upon whether the polarization of the beam has components parallel to the poling field (75). As discussed in Test Methods section, the writing beams in a four-wave mixing configuration usually are *s*-polarized beams to limit the coupling between the illuminating interference pattern and the diffraction of one beam into the other, which is maximized when the reading beam is *p*-polarized to sample the refractive index change parallel to the applied poling field. In addition, the polarization of the writing beams will change the energy-transfer direction in two-beam coupling measurements due to the orientational enhancement effect (11).

## Composition of Polymeric Photorefractive Materials

In this section, in addition to reviewing common ingredients for photorefractive polymeric materials, some of the problems that are being overcome in the formulation of useful multifunctionality in multicomponent polymers are explored. Current polymeric materials are limited in some cases by their slow response times and short wavelengths of operation (44,92) and in other cases by the need for large external electric fields and tendencies towards dielectric breakdown and other material instabilities. Typically, photorefractive polymers require the application of fields around 40–100 V/ $\mu\text{m}$ , severely limiting sample thicknesses to under 100  $\mu\text{m}$ . Higher speed operation is required for data processing using these materials. Also, further work is needed to develop polymeric photorefractives with a longer wavelength response for compatibility with current optical communications standards (for example, typical near infrared telecommunications operate at 1550  $\mu\text{m}$ ).

Formulation of the ideal photorefractive polymer requires finding or mixing materials that combine necessary photogeneration, charge transport and trapping response with electro-optic and orientational anisotropy properties. With respect to the electro-optic response in organic materials, the largest nonlinearities have been in polymers that combine an extended system of highly mobile  $\pi$ -electrons with electron donor and acceptor groups at para positions. To make these materials photorefractive, it is necessary to include one or more additional functionalities, usually by doping after polymerization. Charge generation, transport and trapping properties can be tailored by attaching molecules to the polymer structure with the appropriate ionization energy or electron affinity (63). For instance, charge transfer complexing is accomplished by adding donor sensitizers to acceptor polymers, or vice versa, so that the charge released by the

donor is taken by the acceptor to create an absorption band corresponding to the difference between the donor and acceptor energies. Also, because many other-wise appropriate polymers tend to absorb primarily in the ultraviolet spectrum, dye sensitization of these polymers leads to greater absorption of visible light or longer through the release of photocarriers in the dye (4,33).

When combining functions by adding plasticizers, sensitizers, charge transport agents, and other functional groups, one may be limited to having less than the optimum amount of the nonlinear response to accommodate these functionalities. Also, doping of materials often leads to an increase in phase segregation, which causes undesirable light scattering and can severely limit the useful lifetime of the polymer and/or its processability (21). In the trade-off between using fully-functionalized polymers with better stability and the improved responsiveness of guest–host systems, guest–host systems currently lead in terms of the depth of the index grating, the achievable two-beam coupling gain, and, surprisingly, even in the speed of grating dynamics (4).

**Electro-Optic and Electric-Field-Induced Birefringent Materials.** As can be seen from the analysis of The Photorefractive Process section, one material parameter to be optimized is the electro-optic and orientational response. This can be accomplished either by finding compatible materials with large linear electro-optic coefficients or by optimizing the orientational effects using materials with large birefringence (polarization anisotropy). One major difference in these approaches is the response speed of the photorefractive effect in that the orientational approach is expected to be slower, but submillisecond responses of low  $T_g$  materials have been demonstrated (93–96).

Optimizing the nonlinear response of the polymer usually requires saturating the polymer with the appropriate chromophore, typically 25–35 wt% (38). The most common electro-optic molecules used with these polymers are azo-dyes, such as ethyl-hexyloxy-dimethyl-nitrophenylazo benzene (EHDNPB) (61,97–102), and dimethyl-*p*-nitrophenylazo anisole (DMNPAA) (103–105), and dicyanostyrene (DCST) derivatives, such as diethylaminodicyanostyrene and (DDCST) (106), though the range of molecules used includes simple donor–acceptor units and complex oligomers (107). The chromophore unit is the most common distinguishing factor among demonstrably photorefractive materials. The photorefractive response tends to decrease with an increase in the size of the chromophore (5,108).

**Plasticizers.** To optimize the reorientational effects, either polymers with low glass transition temperature ( $T_g$ ) values (after incorporating other material properties, as discussed below) are used or a plasticizer is added to depress the  $T_g$  value and enable molecular rotations (109), which may or may not be desirable depending upon the need to better fix the grating in the polymer with a high  $T_g$  or to deepen the index-of-refraction modulation through orientation of the chromophores in the space-charge field (11,48).

The most common plasticizer used is ethylcarbazole (ECZ), typically added at 15–30 wt% (110–114). One trade-off in the use of inert plasticizers is the accompanying decreased concentration of other active ingredients. Thus, the use of functionalized plasticizers or materials that fulfill dual roles is preferred (115). However, others used include benzyl butyl phthalate (BBP) (40,110,112, 116), polybutylacrylate (PBA) (117), and diphenyl phthalate (DPP) (118), and

several systems have been developed in which the amount of plasticizer needed is either decreased significantly (119) or eliminated entirely (59,60,106,120,121), using triphenylamine units.

**Photogeneration Sensitizers.** As discussed in Origin of the Space-Charge Field  $E_{sc}$  section, charge generation is often the rate limiting step in achieving the fastest photorefractive response. Though only a small amount is required, typically from 0.1 to 1 wt%, the sensitizer's role is critical. When adding a photogeneration sensitizer, it is important that it absorbs at a longer wavelength than the nonlinear optical chromophore so that attenuation of the beam by the sensitizer is minimized. Obviously, this requires careful balancing of functions that compete for absorbance within the polymer. Sensitizers for photogeneration are available throughout the visible and near infrared spectra that may permit tuning of the photorefractive effect for an otherwise identical polymer (4,58,65).

Charge-generation agents are typically variations on C60 (see, for example, References 116,122–125) or trinitrofluorenone (TNF) derivatives (see, for example, References 126–130), although squaraines, phthalocyanines (131), difluorobenzonitrile (FTCN) (113), and others have also been used. TNF is a charge-transporting molecule/sensitizer, long wavelength photosensitizer. Addition of this charge-generating agent increases the absorption of the material at wavelengths larger than 550 nm as well as increasing the shallow trap concentration. The absorption coefficient increases approximately linearly as a function of concentration of charge-generation agent.

Also, in order to increase the sensitivity of polymer photorefractives, researchers have also investigated the effects of incorporation of nanoparticles (99,132,133). For example, CdSe quantum dots (99,102,133) have come into favor as sensitizers because of their nanoscale and ability to be made to suit specific applications with wavelength sensitivity.

**Charge-Transport Agents.** The charge-transport agents in a photorefractive polymer must provide a closely-spaced network or oxidizable molecules for charge hopping. For the backbone of the photorefractive composite material, poly(*N*-vinylcarbazole) (PVK) is the most common polymer used because of its excellent charge-transport properties and because the photocharge generation efficiency can be improved by adding acceptor molecules that form a charge transfer complex with the carbazole moiety (16,134). Other common transport agents include hydrozanones, such as diethylaminobenzaldehyde-diphenylhydrazone (DEH), polyphenylvinylene (PPV), and arylamines, such as tritolylamine (TTA) (1,71). Typically, the photoconductive polymer requires 40–60 wt% to provide sufficient density of transport sites (1).

The most common reasons for not using polyvinylcarbazole (PVK) are phase separation and higher glass transition temperature ( $T_g$ ), and therefore the need for high amounts of plasticizer, as discussed above. As previously mentioned, the use of a fully-functionalized polymer helps to minimize phase separation while significantly reducing orientational enhancement effects and requiring higher temperature electric field poling. In a fully-functionalized polymer, a polymer main chain or side chains are linked to the chromophore, charge generator, and sensitizer, thereby providing all the necessary photorefractive components in one polymer (17,135–144). Another recent technique to overcome the



limitations of PVK systems is to dope polyimides with dyes that form nanocrystalline J-aggregates. Such systems exhibit high third-order macroscopic polarizability (145,146). Sol-gel glasses with low  $T_g$  have also been used (147,148). For any of these materials, the highest occupied energy level of the transporting agent must be higher than that of the photogenerating agent (1).

**Combinations with Liquid Crystals.** Because polymeric photorefraction is greatly enhanced by the fast reorientation of the nonlinear optical component, many researchers have investigated the use of liquid crystals as ingredients in polymer-composite photorefractives (149–152). Readers looking for a more detailed understanding of liquid crystalline polymers should also see LIQUID CRYSTALLINE POLYMERS, MAIN-CHAIN. A major advantage with these materials is that the liquid crystal alignment can be accomplished with very low fields, on the order of  $\sim 1 \text{ V}/\mu\text{m}$  (153). One of the most common liquid crystals used as the nonlinear optical material is pentylcyanobiphenyl (5CB) (154). It has been used either doped with a photoionizable dye sensitizer, but without a photoconducting polymer or mixed into either polymer-disperse liquid crystal form (155) or a homogeneous photorefractive polymer/nematogen composite (120) to take advantage of photoconducting properties of the polymer.

The resolution of gratings in bulk nematic liquid crystals is too low for most applications leading researchers to develop polymer-dispersed liquid crystal (PDLC) photorefractives. In these materials, liquid crystal domains are dispersed throughout a solid polymer matrix (156). One of the largest two-beam coupling gains recorded,  $3700 \text{ cm}^{-1}$ , was obtained from a mixture of a commercial liquid crystal mixture in a PVK/TNF complex (157). For many liquid crystal polymer composites, the use of PVK is not as common; other polymers such as poly(methyl methacrylate) (PMMA) (89,158–161), poly(vinyl alcohol) (PVA) (162–164), photocross-linkable polymers (PCP) (165), and phenylenevinylene (PPV) (166) are more commonly used than PVK, often requiring additional photoconducting agents (122,149,163). The polymer PMMA is also used in a number of related holographic data storage applications (103,158,167) because of its ease of fabrication and thus low cost, as well as its low index of refraction and high melting point.

## Test Methods

The two most common techniques for characterizing the photorefractive efficiency of a material are degenerate four-wave mixing (DFWM) and two-beam coupling (2BC), both of which use similar configurations, as shown in Figure 3. Ellipsometric techniques are used to measure the electric-field-induced birefringence. Standard time-of-flight and xerographic discharge methods are used to measure photoconductivity, as well as specialized techniques that take advantage of the holographic gratings in photorefractive materials.

**Four Wave Mixing.** In a DFWM experiment, a refractive index grating is recorded by two interfering writing beams (beams 1 and 2 in Fig. 3), which is then read by a weaker third beam (beam 3, which diffracts as beam 4). A maximum index change is obtained when the writing beams are *s*-polarized and the reading beam is *p*-polarized (158). This technique is particularly useful in evaluating the

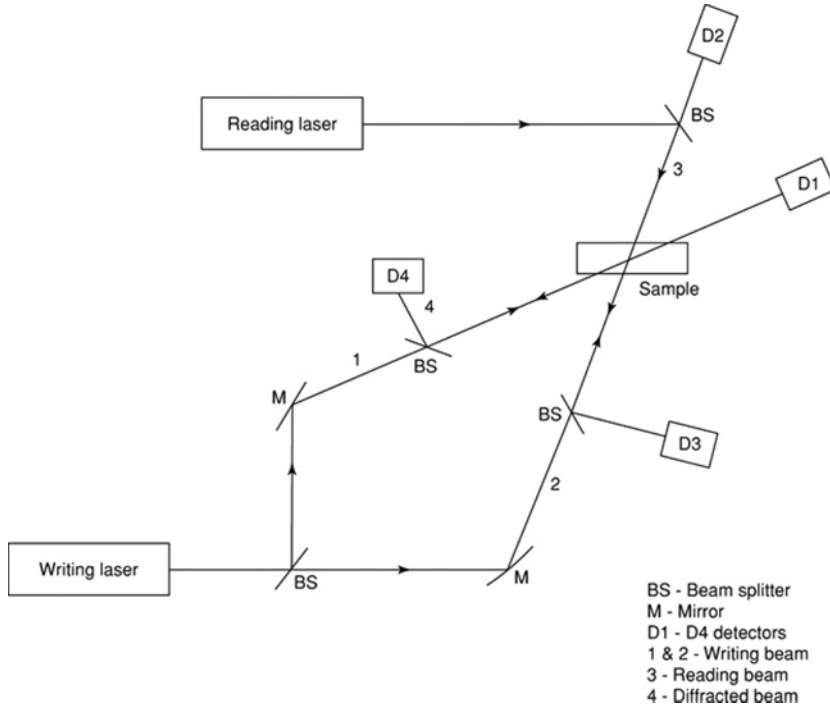


**Fig. 3.** Experimental schematic for four-wave mixing. The diffraction grating is written by beams 1 and 2 and read by beam 3, which need not be of the same wavelength as the writing beams. In the absence of a reading beam, the same geometry may be used to measure two-beam coupling between the writing beams.

rise time or decay time of hologram formation (168). Different times may be seen, however, depending upon whether or how long the bias electric field is applied before the beams are incident on the sample or whether one of the two writing beams is applied well before the other. Theoretical evaluation of the rise time or the decay time is also complicated by the use of different analytical functions to fit the time dependence of the diffraction efficiency (1,4).

One figure of merit in DFWM is given by the energy required to achieve a specified diffraction efficiency in a given thickness of material. The diffraction efficiency is the ratio of the diffracted beam intensity  $I_{\text{diffracted}}$  to the incident reading beam intensity  $I_{\text{reading}}$ . This criterion may be difficult to compare for different device structures such as waveguide versus bulk materials. The theoretical diffraction efficiency can be expressed as (35)

$$\eta = \frac{I_{\text{diffracted}}}{I_{\text{reading}}} = e^{-\alpha d / \cos \theta} \sin^2 \left( \frac{\pi G d \Delta n}{\lambda} \right) \quad (6)$$

where  $\alpha$  is the absorption coefficient,  $d$  is the interaction length of the beams and  $G$  is function of the geometry and polarization of the incident and reading beams on the material (for example,  $G = 1/\sqrt{\cos \theta_1 \cos \theta_2}$  in a simplified quasi-one-dimensional model, where  $\theta_1$  and  $\theta_2$  are the internal angles of the

intersecting beams (37,75). For thin films or materials where the absorption is small, it is usually sufficiently accurate to drop the exponential decay factor and even to approximate the sine function by its argument (35). Using the measured diffraction efficiency to determine  $\Delta n$  and combining with equation 1, one can determine the magnitude of the space-charge field  $E_{sc}$  in the material. Diffraction efficiencies of nearly 100% have been reported at applied electric fields as low as 58 V/ $\mu\text{m}$  in polymeric photorefractives (44,161,169) or even lower fields for polymer-dispersed liquid crystals (170).

In some cases it is important to also compare diffraction efficiency to the diffraction sensitivity of the sample. Sensitivity is a measure of the depth of the refractive index change as a function of the incident power. A material may be sensitive for very low intensities yet not diffract sufficient power for device needs. The sensitivity may be important in that the change in the index of refraction may saturate at a specific laser power density (49).

**Two-Beam Coupling.** In a 2BC experiment, the additional reading beam is not used. Instead, the transmitted intensities of the two writing beams are monitored as a function of the applied external electric field. The writing beams will be deflected or diffracted with respect to the original beams, interfering constructively with one, destructively with the other. Sometimes a piezo transducer is used to measure the phase shift by causing a time-varying energy transfer between beams. These energy shift oscillations depend on the spatial phase shift  $\phi$  of the incident diffraction pattern and the refractive-index grating (171–173).

One important figure of merit in the case of 2BC is the optical gain coefficient  $\Gamma$ , which can be determined by comparing the energies of the two beams when the other is momentarily blocked. If  $\gamma_i$  represents the ratio of the incident powers in front of the sample and  $\gamma_f$  the ratio behind the sample, then the gain is given by

$$\Gamma = \frac{1}{L} [\ln(\gamma_i \gamma_f) - \ln(\gamma_i + 1 - \gamma_f)] \approx \frac{4\pi n_1}{\lambda \cos \theta} \sin \phi \quad (7)$$

where  $L$  is the interaction length within the sample,  $\theta$  is the half-angle between the beams,  $\phi$  is the phase shift, and  $n_1$  is the nonlinear refractive index (4,174). Gains in polymer photorefractives as large as  $\sim 400 \text{ cm}^{-1}$  have been reported, a factor of 10 larger than seen in inorganic crystals (175,176). The actual transferred power, given by  $\exp(\Gamma d)$ , is limited in polymers due to the small sample thickness  $d$  required to attain large applied fields. The 2BC experiment is also used to characterize the response time of the photorefractive polymer, with the fastest responses being around 5 ms at relatively high powers of  $1 \text{ W/cm}^2$  (177).

Two beam coupling measurements can be complicated by the presence of beam fanning, by which additional coupling to randomly scattered light in the sample leads to loss of energy to the scattered light (178). Though not a measurement technique, it is a potentially important application of photorefractive polymers and is discussed further in Applications section.

**Ellipsometry.** Because of the importance of the orientational enhancement effect, the electric-field-induced birefringence is independently measured using a transmission ellipsometry technique. In this experiment, the photorefractive polymer is placed between two crossed polarizers with the normal to the

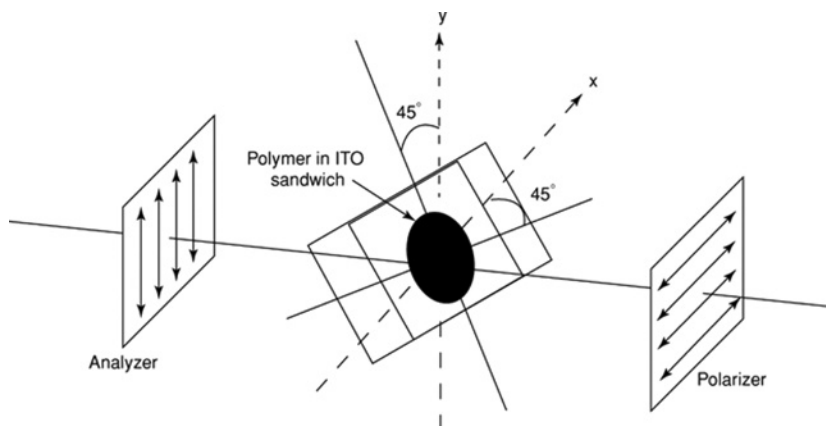


**Fig. 4.** Schematic for ellipsometry measurements.

sample tilted  $45^\circ$  from the  $x$ -axis of the propagating laser beam, as shown in Figure 4. Any change in the refractive index of the sample will result in a change of the polarization state of the laser beam, allowing light to emerge through the polarizers. The index change is then measured by observing the transmittance of the plane-polarized light after passing through both polarizers and the sample (179). Use of ellipsometry is further discussed in Reference 180. Transient ellipsometry techniques are discussed in Reference 46.

**Photoconductivity.** As outlined in Introduction section, the first three steps of the photorefractive process are related to photoconduction, which controls the rate of grating formation and the amplitude of the charge grating, as well as the rate of erasure under uniform illumination. Therefore, to understand and optimize the physical processes involved in photorefractive polymers, it is important to measure their photoconductivity. The most common methods for characterizing the photoconductivity and the hole mobility and effective trapping of photorefractive polymers are conventional DC techniques, xerographic discharge, and time-of-flight mobility measurements (65,181,182).

In the conventional DC technique, a direct comparison is made between the current through the sample under the drift field both in the dark and under uniform illumination. The photoconductivity  $\sigma_{ph}$  is related to the charge mobility  $\mu$  when the absorption is low by  $\sigma_{ph} = pe\mu = [\Phi \alpha I \tau_{eff} / h\nu] e\mu$ , where  $p$  is the density of mobile holes produced at intensity  $I$ ,  $e$  the elementary charge,  $h\nu$  the photon energy,  $\Phi$  the quantum efficiency of charge generation, and  $\alpha$  the absorption coefficient. Recall that the mobility, together with the effective carrier lifetime, determine the speed of response of the material (the effective carrier lifetime  $\tau$  is then controlled by recombination and trapping processes).

The photoconduction sensitivity is usually determined by using a xerographic discharge technique that is applicable to thin films under low intensity illumination, because the measurement of small magnitudes might be confused by sample heating effects. In this experiment one charges the sample using a corona poling apparatus similar to that used for poling, then views the thin film sample as a discharging capacitor and measures the rate of decay of the surface

potential with an electrometer and transparent probe under a high light source, using filters or the monochromator to control the range of wavelengths illuminating the sample. This method can be used with even very low conductivity samples by monitoring the decay rate over long times (91).

One difficulty with bulk photoconductivity measurements is the analysis of the effects of different electrode materials. Comparisons are needed to determine the effects of Ohmic (free supply of charges) versus blocking electrodes (1). To determine the carrier mobilities and the effects of trapping, a relatively unusual approach used for photorefractive polymers is to supplement conventional time-of-flight mobility measurements, during which the flow of photoinduced charge across the bulk sample is monitored on an oscilloscope, with holographic time-of-flight (HTOF) measurements (183). In these measurements, an interference pattern from two short laser pulses in a four-wave mixing geometry creates a sinusoidal distribution of charge carriers that can drift in the presence of an external field (66). As the charge separation advances, the space-charge field is probed with a cw laser through the electro-optic effect. The diffraction efficiency is a function then of the coincidence and anti-coincidence of the mobile carriers with the stationary charge. From the plot of the diffraction efficiency versus time one can determine the drift mobility and the degree of charge transport disorder due to the highly dispersive transport that appears in amorphous polymeric materials. Dispersive transport leads to a length-dependent mobility in these materials (66). A significant advantage of HTOF over conventional time-of-flight measurements is the ability to vary the drift length by varying the angle between the writing beams and between the beams and the applied field and to monitor the motion of charge internally, rather than across the bulk sample (184).

## Applications

**Data Storage.** When a reference beam intersects with the scattered light from an object in a photorefractive material, a hologram is recorded, stored in the form of a refractive index pattern in the material. The image can then be reconstructed by diffracting a third beam on this hologram (in the same manner as DFWM as shown in Figure 3, except that the reading beam need not be of the same wavelength). The use of a photorefractive material in the recording of a hologram eliminates the need for chemical processing in the development of the hologram. Digital data storage is one of the earliest applications of photorefractive polymers (4,185,186).

The high optical damage threshold, low dielectric constants, high photosensitivity, and low cost of photorefractive polymers make them more efficient than inorganic materials (129). Optical data storage in PMMA-based photorefractive polymers has been demonstrated as a cheap and compact way improve data storage on compact discs and digital versatile discs (103). Polysiloxane-based photorefractive polymers have demonstrated the highest optical clarity and lowest optical scattering to date (105).

A significant drawback to the use of photorefractive polymers for data storage is the lack of easy fixing mechanisms and the resulting volatility of the recording. Dark lifetimes and the grating growth rate tend to be inversely

proportional to each other (4). Using high  $T_g$  materials, the grating can be written above the glass transition temperature and frozen-in by cooling the sample during writing, but this scheme has not yet proved practical (187). Other photoinduced refractive index change mechanisms may be preferable for long-term holographic storage where optical gain is not required.

Another drawback of many photorefractive polymer composites is the need to use a thin film geometry that is not as amenable to high storage density as a bulk crystalline material. Multiple holograms have many applications including parallel holographic memory, template matching, and optical neural networks, interconnects, and correlators (188). Additionally, various types of multiplexing including angular and rotation (189,190) multiplexing allow for the storage of many holograms on the same material. A nonmechanical angular multiplexed holographic memory system has been demonstrated in liquid crystalline materials using a moving LCD window that is controlled electronically (191). Using these techniques, each hologram is recorded in the photorefractive polymer using a uniquely oriented setup; the individual holograms can be similarly read using a unique read setup. In this manner, several thousand data pages may be stored in the same element. Polymers are advantageous because large samples can be fabricated, allowing a larger recording volume to hold more holograms.

Materials combining photopolymers with liquid crystals are ideal for wavelength tunable storage devices. Such polymer-dispersed liquid crystal composites (PDLCs) provide a medium for switchable holograms; when the refractive index of the polymer is matched to one of two principal refractive indices of the liquid crystal (LC) an applied electric field alters the orientation of the LC molecules, turning the recorded grating on or off (3,104). As previously mentioned, liquid crystals have the advantage of only requiring a few volts to induce an index grating because of their high nonlinearities (192).

To overcome volatility problems, two-photon absorption (TPA) is the most promising long-term data storage technique to date. TPA can be observed in all materials and lacks the noncentrosymmetric symmetry requirements of even-order nonlinear optical effects. Nevertheless, in centrosymmetric polymers two-photon absorption is allowed between states that have the same parity according to parity selection rules (112). Such a system has been demonstrated with non-destructive readout (113). Additionally, use of two-photon absorption on photorefractive polymer dispersed liquid crystals has been used to record a high 3D data density of 204.8 Gbits/cm<sup>3</sup> (158).

The formation of thick phase holograms has been demonstrated by fabricating photorefractive polymers by injection molding (193).

Adding fluorescent molecules to photopolymers also provides a method for optical data storage. In such a system, the fluorescent molecules bond to the polymer matrix and become more concentrated in the polymerized regions causing the required refractive index pattern (194).

**Optical Correlation, Imaging through Scattering Media, and Novelty Filtering.** Using a photorefractive polymer, optical correlation can be made all-optical, eliminating the need for a computer or any other such devices. Such a device was demonstrated in a 100- $\mu$ m-thick photorefractive polymer using a low power laser. The document is optically encoded and authenticity is validated by correlating the encoded information with a master copy. Such a setup

is used in such applications as the identification of individual pupils and fingerprints, searching of large databases and navigation. Spatial correlation is accomplished by creating a hologram by recording the interference pattern of the optical wavefront of the object with a reference beam in the material. Optical correlation is performed by overlapping the Fourier transform of the master copy with the hologram in the polymer. If the two optical codes match, a correlation peak can be observed and the document under test may be considered valid (4,195,196).

One common application of optical correlation in photorefractive polymers is in edge enhancement, a form of high pass image filtering which uses a Fourier transform holographic operation with a photorefractive composite. Two beams, the more intense one containing the image, interfere in a photorefractive material. The resulting interference pattern is stronger at the edges due to a closer matching of intensities at the edges. Thus, the refractive index change is greatest at the edges and more of the readout beam is deflected or diffracted. A third beam recovers the reconstructed image with enhanced edges. The reconstructed image is an exact copy of the object only if the signal beam intensity is less than that of the reference beam. Violating this condition produces an image only at the edges of the object where the largest index modulation occurs (149,192).

Time-gated holographic imaging through scattered media has been demonstrated at wavelengths appropriate for medical imaging. In these demonstrations, the hologram is formed by the temporal overlap of direct light from the object that has been temporally stretched (without scattering) and a reference pulse (197).

In vibration analysis, or novelty filtering, the hologram acts as an adaptive beam splitter with exact wavefront matching: a plane-wave reference beam is diffracted into the signal beam that is reflected from the surface of the object. The applied field is reversed so that the exponential gain coefficient becomes negative, thus transferring energy from the signal beam to the reference beam, reducing the signal intensity. Only objects moving faster than approximately the inverse of the response time of the photorefractive material are observed. The fast moving parts are constantly changing in time and do not interact long enough with the reference beam to lead to the recording of a hologram. An image amplification configuration may be used build a device to observe an object under low light levels (116,198). This technique can also be used to visualize the mode patterns of a vibrating object; the mode patterns can reveal defects and areas under particular stress. Such devices have typically been made with PVK (199). Applications include remote sensing and inspection, especially in hazardous environments.

**Beam Fanning.** Beam fanning is the spontaneous amplification of scattered light in a photorefractive material arising from an energy exchange between the incident beam and light randomly scattered from impurities or defects (178). It results from a redistribution of charges in the nonlinear material and can complicate two-beam coupling measurements or provide promise for novel applications, such as self-pumped phase conjugation (200) and some forms of optical limiting (201,202). The effect of beam fanning is the depletion of the pump beam and the appearance of a fanned beam that is swept to one side of the material.

**Waveguides.** Utility in waveguides generally imposes additional restrictions on the polymer composition. The geometry required to couple an

external static drift field to the optical field in the waveguide dictates the use of channel waveguides to reach maximum efficiency so that the poling direction has a component along the space-charge field. The bias field is then applied across the width of the channel. Narrow channels are preferred although coupling into the channels becomes more difficult in this case. Problems with the use of waveguides in the study of photorefractive effects also include the presence of thermo-optic changes in the guide and/or coupling mechanism, whereby small temperature changes may significantly change the coupling angles. Thus, temperature control may be imperative in practical applications. All polymer dopants, of course, should be soluble in an appropriate spin-coating solvent for making thin films ( $\approx 1 \mu\text{m}$ ) and of sufficiently high molecular weight so as not to evaporate with the solvent. Waveguides may be utilized in optical data storage applications (203–206).

To summarize, the benefits from the development of photorefractive polymers are many but there are still significant problems to overcome before these benefits can be realized (1). Foremost among the problems may be balancing the competing needs for both steady-state performance and fast response speed, as well as the often competing factors of stability, high mobility and fast orientational response to attain fast, highly sensitive, and efficient response. It will be necessary to better understand the trade-off between dark and photoconductivity and the effects of preillumination history (207). Better understanding is also needed of the nature and depth of charge trapping sites in polymers to optimize the dark lifetimes of the gratings.

## BIBLIOGRAPHY

### CITED REFERENCES

1. O. Ostroverkhova and W. E. Moerner, *Chem. Rev.* **104**, 3267–3314 (2004).
2. L. Solymar, D. J. Webb, and A. Grunnet-Jepson, *The Physics and Applications of Photorefractive Materials*, Clarendon Press, Oxford, 1996.
3. C. Gu, Y. Xu, Y. Liu, J. J. Pan, F. Zhou, and H. He, *Opt. Mater.* **23**, 219–227 (2003).
4. S. J. Zilker, *Chem. Phys. Chem.* **1**, 72–87 (2000).
5. W. E. Moerner and S. M. Silence, *Chem. Rev.* **94**, 127–155 (1994).
6. K. Meerholz, B. Kippelen, and N. Peygambarian, in D. L. Wise, G. E. Wnek, D. J. Trantolo, T. M. Cooper, and J. D. Gresser, eds., *Photonic Polymer System: Fundamentals, Methods, and Applications*, Marcel Dekker, Inc., New York, 1998, pp. 571–631.
7. D. M. Pepper, J. Feinberg, and N. V. Kukhtarev, *Sci. Am.* 63–74 (1990).
8. K.-S. Lee, ed., *Polymers for Photonics Applications II: Nonlinear Optical, Photorefractive and Two-Photon Absorption Polymers*, Springer-Verlag, Berlin, 2003.
9. P. Günter and J.-P. Huignard, in P. Günter and J.-P. Huignard, eds., *Photorefractive Materials and Their Applications I*, Springer-Verlag, Berlin, 1988.
10. P. Yeh, *Introduction to Photorefractive Nonlinear Optics*, John Wiley & Sons, Inc., New York, 1993.
11. W. E. Moerner, S. M. Silence, F. Hache, and G. C. Bjorkland, *J. Opt. Soc. Am. B* **11**, 320–330 (1994).



12. S. R. Marder, B. Kippelen, A. K.-Y. Jen, and N. Peyghambarian, *Nature* **388**, 845–851 (1997).
13. Ch. Bosshard, K. Sutter, Ph. Pretre, J. Hulliger, M. Florsheimer, P. Kaatz, and P. Gunter, *Organic Nonlinear Optical Materials*, Gordon & Breach, Basil, Switzerland, 1995, pp. 193–241.
14. W. E. Moerner, A. Grunnet-Jepson, and C. L. Thompson, *Annu. Rev. Mater. Sci.* **27**, 585–623 (1997).
15. B. Kippelen, K. Meerholz, and N. Peyghambarian, in H. S. Nalwa and S. Miyata, eds., *Nonlinear Optics of Organic Molecules and Polymers*, CRC Press, Inc., Boca Raton, Fla., 1997, pp. 465–513.
16. T. Wada and H. Sasabe, *J. Mater. Chem.* **8**, 809–828 (1998).
17. J. V. Grazulevicius, P. Stroehriegl, J. Pielichowski, and K. Pielichowski, *Prog. Polym. Sci.* **28**, 1297–1353 (2003).
18. Q. Wang, L. Wang, and L. Yu, *Macromol. Rapid Commun.* **21**, 723–745 (2000).
19. A. Ashkin, G. D. Boyd, J. M. Dziedzic, R. G. Smith, A. A. Ballman, J. J. Levinstein, and K. Nassau, *Appl. Phys. Lett.* **9**, 72–74 (1966).
20. K. Sutter and P. Günter, *J. Opt. Soc. Am. B* **7**, 2274–2278 (1990).
21. S. Ducharme, J. C. Scott, R. J. Twieg, and W. E. Moerner, *Phys. Rev. Lett.* **66**, 1846–1849 (1991).
22. Y. Shuto, M. Amano, and T. Kaino, *Jpn. J. Appl. Phys.* **30**, 320–326 (1991).
23. H. S. Nalwa, ed., *Handbook of Advanced Electronic and Photonic Materials and Devices, Vol. 9: Nonlinear Optical Materials*, Academic Press, Inc., San Diego, Calif., 2001.
24. G. S. He, and S. H. Lui, *Physics of Nonlinear Optics*, World Scientific, Singapore, 1999, Chapt. 6.
25. G. Motemazzani, C. Medrano, and M. Zgonik, in P. Gunter, ed., *Nonlinear Optical Effects and Materials*, Springer-Verlag, Berlin, 2000, pp. 301–374.
26. L. Wang, M.-K. Ng, and Q. Wang, in V. Ramamurthy, K. S. Schanze, eds., *Optical Sensors and Switches*, Marcel Dekker, Inc., New York, 2001, pp. 257–319.
27. B. Kippelen, in H. J. Coufal, D. Psalis, and G. Sincerbox, eds., *Holographic Data Storage*, Springer-Verlag, Berlin, 2000, pp. 159–170.
28. N. Peyghambarian, B. Kippelen, K. B. Ferio, J. Herlocker, J. L. Maldonado, E. Hendrickx, S. Mery, A. Golemme, and S. R. Marder, in S. Miyata and H. Sasabe, eds., *Light Wave Manipulation Using Organic Nonlinear Optical Materials*, Gordon & Breach, Amsterdam, the Netherlands, 2000, pp. 223–232.
29. M. Blanchard-Desce, M. Barzoukas, F. Chaput, B. Darracq, M. Mladenova, L. Ventelon, K. Lahlil, J. Reyes, J.-P. Boilot, and Y. Levy, in F. Kajzar and M. V. Agronovich, eds., *Multiphoton and Light Driven Multielectron Processes in Organics: New Phenomena, Materials and Applications*, Kluwer Academic Publishers, Amsterdam, the Netherlands, 2000, pp. 183–198.
30. B. Kippelen, H. S. Kackritz, and R. O. Claus, eds., *Organic Nonlinear Optical Materials and Devices*, Materials Research Society, Warrendale, Pa., 1999.
31. M. Pope and C. E. Swenberg, *Electronic Processes in Organic Crystals and Polymers*, Oxford University Press, New York, 1999, Chaps. XVIII and XX.
32. Cf. K. Okamoto, T. Momura, S.-H. Park, K. Ogino, and H. Sato, *Chem. Mater.* **11**, 3279–3284 (1999).
33. P. J. Reucroft, in A. V. Patsis and D. Z. Seanor, eds., *Photoconductivity in Polymers: An Interdisciplinary Approach*, Technomic Publishing, Co., Inc., Westport, Conn., 1976.
34. J. Feinberg, D. Heiman, Jr, A. R. Tanguay, and R. W. Hellwarth, *J. Appl. Phys.* **51**, 1297–1305 (1980); *Erratum*, **52**, 537 (1980).
35. A. M. Glass and J. Strait, in P. Günter and J.-P. Huignard, eds., *Photorefractive Materials and Their Applications I*, Springer-Verlag, Berlin, 1988, pp. 237–262.

36. W. E. Moerner, S. M. Silence, F. Hache, and G. C. Bjorkland, *J. Opt. Soc. Am. B* **11**, 320–330 (1994).
37. A. M. Glass, I. P. Kaminow, A. A. Ballman, and D. H. Olson, *Appl. Opt.* **19**, 276–281 (1980).
38. F. Wurthner, R. Wortmann, and K. Meerholz, *Chem. Phys. Chem.* **3**, 17–31 (2002).
39. G. Cipparrone, A. Mazzulla, and P. Pagliusi, *Opt. Commun.* **185**, 171–175 (2000).
40. O. Ostroverkhova, A. Stickrath, and K. D. Singer, *J. Appl. Phys.* **91**, 9481–9486 (2002).
41. Th. G. Pedersen, K. Jespersen, and P. M. Johansen, *Opt. Mater.* **18**, 95–98 (2001).
42. I. C. Khoo, *IEEE J. Quantum. Electron.* **32**, 525–534 (1996).
43. M. G. Kuzyk, J. E. Sohn, and C. W. Dirk, *J. Opt. Soc. Am. B* **7**, 842–858 (1990).
44. K. Meerholz, B. L. Volodin, Sandalphon, B. Kippelen, and N. Peyghambarian, *Nature* **371**, 497–500 (1994).
45. R. Wortmann, C. Poga, T. J. Twieg, C. Geletneky, C. Moylan, P. M. Lindquist, R. G. DeVoe, P. M. Cotts, H. Horn, J. E. Rice, and D. M. Burland, *J. Chem. Phys.* **105**, 10637–10647 (1996).
46. R. Bittner, C. Bräuchle, and K. Meerholz, *Appl. Opt.* **37**, 2843–2851 (1998).
47. H. Chun, I. K. Moon, D.-H. Shin, S. Song, and N. Kim, *J. Mater. Chem.* **12**, 858–862 (2002).
48. D. V. Steenwinckel, E. Hendrickx, C. Samyn, C. Engels, and A. Persoons, *J. Mater. Chem.* **10**, 2692–2697 (2000).
49. K. D. Singer and J. H. Andrews, in J. Zyss, ed., *Molecular Nonlinear Optics: Materials Physics, and Devices*, Academic Press, Inc., San Diego, Calif., 1994, Chapt. 6.
50. T. K. Däubler, R. Bittner, K. Meerholz, V. Cimrová, and D. Neher, *Phys. Rev. B* **61**, 13515–13527 (2000).
51. M. Biswas, A. Mukherjee, and V. Mylnikov, *Photoconducting Polymers/Metal-Containing Polymers*, Springer-Verlag, Berlin, 1994.
52. N. A. Davidenko and A. A. Ishchenko, *Theor. Exp. Chem.* **38**, 88–108 (2002).
53. R. H. Bube, *Photoelectronic Properties of Semiconductors*, Cambridge University Press, Oxford, 1992.
54. N. V. Kukhtarev, V. B. Markov, S. G. Odulov, M. S. Soskin, and V. L. Vinetskii, *Ferroelectrics* **22**, 949–964 (1979).
55. A. Twarowski, *J. Appl. Phys.* **65**, 2833–2837 (1991).
56. J. S. Schildkraut and A. V. Buettner, *J. Appl. Phys.* **72**, 1888–1893 (1992).
57. H. Scher and E. W. Montroll, *Phys. Rev. B* **12**, 2455–2477 (1975).
58. J. Mort and G. Pfister, in J. Mort and G. Pfister, eds., *Electronic Properties of Polymers*, John Wiley & Sons, Inc., New York, 1982.
59. M. Thelakkat, *Macromol. Mater. Eng.* **287**, 442–461 (2002).
60. J. Ostrauskaite, H. R. Karickal, A. Leopold, D. Haarer, and N. Thelakkat, *J. Mater. Chem.* **12**, 58–64 (2001).
61. M. Thelakkat, J. Ostrauskaite, A. Leopold, R. Bausinger, and D. Haarer, *Chem. Phys.* **285**, 133–147 (2002).
62. P. Stroehriegl and J. V. Grazulevicius, *Adv. Mater.* **14**, 1439–1452 (2002).
63. B. E. Jones, S. Ducharme, M. Liphardt, A. Goonesekera, J. M. Takacs, L. Zhang, and R. Athalye, *J. Opt. Soc. Am. B* **11**, 1064–1072 (1994).
64. J. S. Schildkraut, *Appl. Phys. Lett.* **58**, 340–342 (1991).
65. W. D. Gill, in J. Mort and D. Pai, eds., *Photoconductivity and Related Phenomena*, Elsevier, Amsterdam, the Netherlands, 1976.
66. G. G. Malliaras, V. V. Krasnikov, H. J. Bolink, and G. Hadziioannou, *Appl. Phys. Lett.* **66**, 1038–1040 (1995).

67. J. S. Schildkraut and Y. Cui, *J. Appl. Phys.* **72**, 5055–5060 (1992).
68. B. H. Yuan, X. D. Sun, Y. Y. Jiang, C. F. Hou, and Z. X. Zhou, *J. Mod. Opt.* **48**, 1161–1170 (2001).
69. O. Ostroverkhova and K. D. Singer, *J. Appl. Phys.* **92**, 1727–1743 (2002).
70. L. Kulikovskiy, D. Neher, E. Mecher, K. Meerholz, H.-H. Horhold, and O. Ostroverkhova, *Phys. Rev. B* **69**, 125216-1-11 (2004).
71. E. Mecher, F. Gallego-Gomez, H. Tillmann, H. H. Horhold, J. C. Hummelen, and K. Meerholz, *Nature* **418**, 959–964 (2002).
72. J. Wolff, S. Schlöter, U. Hofmann, D. Haarer, and S. J. Zilker, *J. Opt. Soc. Am. B* **16**, 1080–1086 (1999).
73. K. Khand, D. J. Binks, and D. P. West, *J. Appl. Phys.* **89**, 2516–2519 (2001).
74. S. C. Freilich, *Macromolecules* **20**, 973–978 (1987).
75. W. E. Moerner, C. Walsh, J. C. Scott, S. Ducharme, D. M. Burland, G. C. Bjorklund, and R. J. Twieg, *SPIE Proc.* **1560**, 148–161 (1991).
76. Y. Wang and A. Suna, *J. Phys. Chem. B* **101**, 5627–5638 (1997).
77. A. Leopold, M. Grasruck, U. Hofmann, M. A. Kol'chenko, and S. J. Zilker, *Appl. Phys. Lett.* **76**, 1644–1646 (2000).
78. T. Jakob, S. Schlöter, U. Hofmann, M. Grasruck, A. Schreiber, and D. Haarer, *J. Chem. Phys.* **111**, 10633–10639 (1999).
79. A. Goonesekera, S. Ducharme, and J. M. Takacs, *Proc. SPIE* **3144**, 195–206 (1997).
80. O. Ostroverkhova, M. He, R. J. Twieg, and W. E. Moerner, *Chem. Phys. Chem.* **4**, 732–744 (2003).
81. J.-C. Ribierre, L. Mager, A. Fort, and S. Méry, *Macromolecules* **36**, 2516–2525 (2003).
82. H. Bassler, *Phys. Status Solidi B* **175**, 15 (1993).
83. A. Ohshima, A. Momotake, and T. Arai, *J. Photochem. Photobiol., A: Chem.* **162**, 473–479 (2004).
84. S. Anguille, P. Brun, and R. Guglielmetti, *Appl. Organomet. Chem.* **18**, 68–70 (2004).
85. M. Levitus and P. F. Aramendia, *J. Phys. Chem. B* **103**, 1864–1870 (1999).
86. E. H. Chung, J. Shim, and W. K. Chae, *J. Photochem. Photobiol., A: Chem.* **129**, 43–48 (1999).
87. G. H. Brown, ed., *Photochromism*, Vols. I–III, Wiley InterScience, New York, 1971).
88. C. A. Walsh and W. E. Moerner, *J. Opt. Soc. Am. B* **9**, 1642–1647 (1992).
89. J. Mun, J. W. Lee, J. K. Park, K. S. Lee, and C. S. Yoon, *Opt. Mater.* **21**, 379–383 (2003).
90. J.-W. Lee, J. Mun, C. S. Yoon, K.-S. Lee, and J.-K. Park, *Adv. Mater.* **14**, 144–147 (2002).
91. J. C. Scott, L. T. Pautmeier, and W. E. Moerner, *J. Opt. Soc. Am. B* **9**, 2059–2064 (1992).
92. M. Liphardt, A. Goonesekera, B. E. Jones, S. Ducharme, J. M. Takacs, and L. Zhang, *Science* **263**, 367–369 (1994).
93. J. A. Herlocker, K. B. Ferrio, E. Hendrickx, B. D. Guenther, S. Mery, B. Kippelen, and N. Peyghambarian, *Appl. Phys. Lett.* **74**, 2253–2255 (1999).
94. D. V. Steenwinckel, E. Hendrickx, A. Persoons, K. Van den Broeck, and C. Samyn, *J. Chem. Phys.* **112**, 11030–11037 (2000).
95. J. C. Ribierre, G. Cheval, F. Huber, L. Mager, A. Fort, R. Muller, S. Méry, and J. F. Nicoud, *J. Appl. Phys.* **91**, 1710–1712 (2002).
96. D. Wright, M. A. Diaz-Garcia, J. D. Casperson, M. DeClue, and W. E. Moerner, *Appl. Phys. Lett.* **73**, 1490–1492 (1998).
97. D. J. Binks and D. P. West, *J. Chem. Phys.* **115**, 6760–6765 (2001).
98. D. J. Binks and D. P. West, *Appl. Phys. B: Lasers Opt.* **74**, 279–282 (2002).
99. D. J. Binks, D. P. West, S. Norager, and P. O'Brien, *J. Chem. Phys.* **117**, 7335–7341 (2002).

100. M. Thelakkat, *Macromol. Mater. Eng.* **287**, 442–461 (2002).
101. D. P. West, M. D. Rahn, C. Im, and H. Bässler, *Chem. Phys. Lett.* **326**, 407–412 (2000).
102. J. G. Winiazar and P. N. Prasad, *Opt. Lett.* **27**, 1330–1332 (2002).
103. D. Day, M. Gu, and A. Smallridge, *Adv. Mater.* **13**, 1005–1007 (2001).
104. D. Day and M. Gu, *Appl. Phys. Lett.* **80**, 2404–2406 (2002).
105. C. Poga, P. M. Lundquist, V. Lee, R. M. Shelby, R. J. Twieg, and D. M. Burland, *Appl. Phys. Lett.* **69**, 1047–1049 (1996).
106. O.-P. Kwon, S.-H. Lee, G. Montemezzani, and P. Günter, *Adv. Funct. Mater.* **13**, 434–438 (2003).
107. W. E. Douglas, A. Kuzhelev, S. Alexandar, I. Yurasova, O. L. Antipov, L. G. Klapshina, V. V. Semenov, G. A. Domrachev, T. I. Lopatina, and D. M. H. Guy, *Phys. Chem. Chem. Phys.* **4**, 109–114 (2002).
108. H. Cun, I. K. Moon, D.-H. Shin, S. Song, and N. Kim, *J. Mater. Chem.* **12**, 858–862 (2002).
109. L. Li, R. J. Jeng, J. Y. Lee, J. Kumar, and S. K. Tripathy, *SPIE Proc.* **1560**, 243–250 (1991).
110. A. V. Afanas'ev, O. L. Antipov, R. E. Benfield, B. A. Bushuk, S. B. Bushuk, G. A. Domrachev, W. E. Douglas, Zh. Fominikh, R. G. Jones, L. G. Klapshina, A. S. Kuzhelev, T. I. Lopatina, A. Mustafa, A. N. Rubinov, V. V. Semenov, I. V. Yurasova, and A. P. Zinoviev, *Silicon Chem.* **1**, 145–154 (2002).
111. P. A. Blanche, B. Kippelen, A. Schlzgen, C. Fuentes-Hernandez, G. Ramos-Ortiz, J. F. Wang, E. Hendrickx, N. Peyghambarian, and S. R. Marder, *Opt. Lett.* **27**, 19–21 (2002).
112. W. E. Douglas, A. S. Kuzhelev, I. V. Yurasova, O. L. Antipov, L. G. Klapshina, V. V. Semenov, G. A. Domrachev, T. I. Lopatina, and D. M. H. Guy, *Phys. Chem. Chem. Phys.* **4**, 109–114 (2002).
113. B. Kippelen, P. A. Blanche, A. Schülzgen, C. Fuentes-Hernandez, G. Ramos-Ortiz, and co-workers, *Adv. Funct. Mater.* **12**, 615–620 (2002).
114. I. V. Yurasova and O. L. Antipov, *Opt. Commun.* **224**, 329–336 (2003).
115. Z. Zhang and K. D. Singer, *Appl. Phys. Lett.* **72**, 2948–2950 (1998).
116. A. Goonesekera, D. Wright, and W. E. Moerner, *Appl. Phys. Lett.* **76**, 3358–3360 (2000).
117. Z. Rui-Zhi, Z. You-Yuan, M. Ke, W. Chang-Chun, and L. Fu-Ming, *Chin. Phys. Lett.* **19**, 795–797 (2002).
118. D. J. Suh, O. O. Park, T. Ahn, and H.-K. Shim, *Opt. Mater.* **21**, 365–371 (2003).
119. C. Castè, V. Castelvetro, F. Ciardelli, A. Colligiani, A. Mazzotta, D. Michelotti, G. Ruggeri, and C. A. Veracini, *Synth. Met.* **138**, 341–345 (2003).
120. J. Zhang and K. D. Singer, *Appl. Phys. Lett.* **72**, 2948–2950 (1998).
121. S.-H. Park, K. Ogino, and H. Sato, *Polym. Adv. Technol.* **11**, 349–358 (2000).
122. Y. Bai, X. Chen, X. Wan, Q.-F. Zhou, H. Liu, B. Zhang, and Q. Gong, *Appl. Phys. B: Lasers Opt.* **73**, 35–37 (2001).
123. Y. Bai, X. Chen, X. Wan, Q. Zhou, H. Liu, B. Zhang, and Q. Gong, *Appl. Phys. Lett.* **80**, 10–12 (2002).
124. D. J. Binks and D. P. West, *J. Opt. Soc. Am. B* **19**, 2349–2356 (2002).
125. O. Ostroverkhova, D. Wright, U. Gubler, W. E. Moerner, M. He, A. Sastre-Santos, and R. J. Twieg, *Adv. Funct. Mater.* **12**, 621–629 (2002).
126. Y. Chen, Q. Gong, F. Wang, B. Zhang, and Z. Chen, *Mater. Lett.* **57**, 4372–4377 (2003).
127. L. Zhang, G. Zhang, G. O. Carlisle, and G. A. Crowder, *J. Mater. Sci.* **11**, 229–234 (2000).
128. S. Wu, F. Zeng, F. Li, and J. Li, *React. Funct. Polym.* **46**, 225–231 (2001).

129. P. Wang, Z. Feng, Y. Chang, C. Ye, F. Wang, and Q. Gong, *J. Appl. Polym. Sci.* **75**, 447–451 (2000).
130. A. Leopold, M. A. Kol'chenko, U. Hofmann, and S. J. Zilker, *J. Lumin.* **86**, 371–374 (2000).
131. Z. Peng, A. R. Gharavi, and L. Yu, *J. Am. Chem. Soc.* **119**, 4622–4632 (1997).
132. R. Termine, I. Aiello, D. Dattilo, M. Ghedini, and A. Golemme, *Adv. Mater.* **15**, 723–726 (2003).
133. K. R. Choudhury, J. G. Winiarz, M. Samoc, and P. N. Prasad, *Appl. Phys. Lett.* **82**, 406–408 (2003).
134. V. S. Mylnikov, *Photoconducting Polymers/Metal-Containing Polymers, Advances in Polymer Science*, Vol. 115, Springer-Verlag, Berlin, Heidelberg, 1994.
135. Z. Bo, L. Hui, G. Qi-Huang, J. Sohn, J. Hwang, S. Y. Park, J. K. Lee, J.-H. Lee, J.-S. Chang, and G. J. Lee, *Chin. Phys. Lett.* **19**, 66–68 (2002).
136. K. D. Belfield, O. Najjar, and S. R. Sriram, *Polymer* **41**, 5011–5020 (2000).
137. F. Brustolin, V. Castelvetro, F. Ciardelli, G. Ruggeri, and A. Colligiani, *J. Polym. Sci., Part A: Polym. Chem.* **39**, 253–262 (2001).
138. Y. Chen, Z. Chen, Q. Gong, and M. Schroers, *Mater. Lett.* **57**, 2271–2276 (2003).
139. Y.-W. Chen, Y.-K. He, H.-Y. Chen, F. Wang, Z.-J. Chen, and Q.-H. Gong, *J. Appl. Polym. Sci.* **77**, 189–194 (2000).
140. J. V. Grazulevicius, P. Stroehriegel, J. Pielichowski, and K. Pielichowski, *Prog. Polym. Sci.* **28**, 1297–1353 (2003).
141. H. Tang, J. Li, and J. Qin, *React. Funct. Polym.* **48**, 193–199 (2001).
142. Q. Wang, L. Wang, J. Yu, and L. Yu, *Adv. Mater.* **12**, 974–978 (2000).
143. Z. Li, J. Luo, J. Li, C. Zhan, and J. Qin, *Polym. Bull.* **45**, 105–111 (2000).
144. C. Jung, T. Aoyama, T. Wada, H. Sasabe, M. Jikei, and M. Kakimoto, *High Perform. Polym.* **12**, 205–212 (2000).
145. A. V. Vannikov, A. D. Grishina, B. I. Shapiro, L. Y. Pereshivko, T. V. Krivenko, V. V. Savel'ev, V. V. Savel'ev<sup>1</sup>, V. I. Berendyaev<sup>3</sup>, and R. W. Rychwalski, *High Energy Chem.* **36**, 38–43 (2002).
146. A. V. Vannikov, A. D. Grishina, B. I. Shapiro, L. Y. Pereshivko, T. V. Krivenko, V. V. Savelyev, V. I. Berendyaev, and R. W. Rychwalski, *Chem. Phys.* **287**, 261–271 (2003).
147. W. J. Kuo, G. H. Hsiue, and R. J. Jeng, *Macromol. Chem. Phys.* **202**, 1782–1790 (2001).
148. D. H. Choi, W. Jun, K. Y. Oh, and J. H. Kim, *Polym. Bull.* **49**, 173–180 (2002).
149. G. P. Wiederrecht, *Annu. Rev. Mater. Res.* **31**, 139–169 (2001).
150. L. Hui, Z. Bo, G. Qi-Huang, B. Yao-Wen, C. Xiao-Fang, W. Xin-Hua, and Z. Qi-Feng, *Chin. Phys. Lett.* **18**, 909–911 (2001).
151. H. Ono, T. Kawamura, N. Mocam Frias, K. Kitamura, N. Kawatsuki, H. Norisada, and T. Yamamoto, *J. Appl. Phys.* **88**, 3853–3858 (2000).
152. H. Ono, T. Kawamura, N. M. Frias, L. Kitamura, N. Kawatsuki, and H. Norisada, *Adv. Mater.* **12**, 143–146 (2000).
153. P. G. de Gennes, *The Physics of Liquid Crystals*, Clarendon Press, Oxford, 1974.
154. I. C. Khoo, H. Li, and Y. Liang, *Opt. Lett.* **19**, 1723–1725 (1994).
155. A. Golemme, B. L. Volodin, B. Kippelen, and N. Peyghambarian, *Opt. Lett.* **22**, 1226–1228 (1997).
156. N. Peyghambarian, in I. Khan and J. Harrison eds., *ACS Symposium Series*, Vol. 726, American Chemical Society, Washington, D.C., 1999, Chapt. 14, pp. 204–225.
157. S. Bartkiewicz, K. Matczyszyn, A. Miniewicz, and F. Kajzar, *Opt. Commun.* **187**, 257–261 (2001).
158. D. McPhail and M. Gu, *Appl. Phys. Lett.* **81**, 1160–1162 (2002).
159. H. Ono, A. Emoto, F. Takahashi, N. Kawatsuki, and T. Hasegawa, *J. Appl. Phys.* **94**, 1298–1303 (2003).

160. H. Ono, H. Shimokawa, A. Emoto, and N. Kawatsuki, *J. Appl. Phys.* **94**, 23–30 (2003).
161. C. Engels, D. V. Steenwinckel, E. Hendrickx, M. Schaerlaekens, A. Persoons, and C. Samyn, *J. Mater. Chem.* **12**, 951–957 (2002).
162. J. E. Hall and D. A. Higgins, *Rev. Sci. Instrum.* **73**, 2103–2107 (2002).
163. J. Mun, C. S. Yoon, H.-W. Kim, S.-A. Choi, and J.-D. Kim, *Appl. Phys. Lett.* **79**, 1933–1935 (2001).
164. P. Pagliusi and G. Cipparrone, *J. Appl. Phys.* **92**, 4863–4869 (2002).
165. N. Kawatsuki, T. Kawakami, and T. Yamamoto, *Adv. Mater.* **13**, 1337–1339 (2001).
166. M. J. Fuller, C. J. Walsh, Y. Zhao, and M. R. Wasielewski, *Chem. Mater.* **14**, 952–953 (2002).
167. U. Gubler, D. Wright, W. E. Moerner, and M. B. Klein, *Opt. Lett.* **27**, 354–356 (2002).
168. J. A. Herlocker, C. Fuentes-Hernandez, K. B. Ferrio, E. Hendrickx, Y. Zhang, J. F. Wang, P. A. Blanche, S. R. Marder, N. Peyghambarian, and B. Kippelen, *Appl. Phys. Lett.* **77**, 2292–2294 (2000).
169. S. Schlöter, U. Hofmann, P. Strohriegel, H. W. Schmidt, and D. Haarer, *J. Opt. Soc. Am. B* **15**, 2473–2475 (1998).
170. A. Golemme, B. Kippelen, and N. Peyghambarian, *Appl. Phys. Lett.* **73**, 2408–2410 (1998).
171. J. E. Hall and D. A. Higgins, *Rev. Sci. Instrum.* **73**, 2103–2107 (2002).
172. Z. Bo, L. Hui, G. Qi-Huang, J. Sohn, J. Hwang, S. Y. Park, J. K. Lee, J.-H. Lee, J.-S. Chang, and G. J. Lee, *Chin. Phys. Lett.* **19**, 66–68 (2002).
173. A. Grunnet-Jepsen, C. L. Thompson, and W. E. Moerner, *J. Opt. Soc. Am. B* **15**, 905–913 (1998).
174. K. Kuroda, ed., *Progress in Photorefractive Nonlinear Optics*, Taylor & Francis, London, 2002, pp. 4–6.
175. D. Wright, U. Gubler, Y. Roh, W. E. Moerner, M. He, and R. J. Twieg, *Appl. Phys. Lett.* **79**, 4274–4276 (2001).
176. D. J. Suh, O. O. Park, T. Ahn, and H. K. Shim, *Jpn. J. Appl. Phys., Part 2* **41**, L428–L430 (2002).
177. D. Wright, M. A. Diaz-Garcia, J. D. Casperson, M. DeClue, and W. E. Moerner, *Appl. Phys. Lett.* **73**, 1490–1492 (1998).
178. A. Grunnet-Jepsen, C. L. Thompson, R. J. Twieg, and W. E. Moerner, *J. Opt. Soc. Am. B* **15**, 901–904 (1998).
179. J. D. Shakos, M. D. Rahn, D. P. West, and K. Khand, *J. Opt. Soc. Am. B* **17**, 373–380 (2000).
180. Sandalphon, B. Kippelen, K. Meerholz, N. Peyghambarian, *Appl. Opt.* **35**, 2346–2354 (1996).
181. V. S. Mylnikov, *Photoconducting Polymers/Metal-Containing Polymers, Advances in Polymer Science* vol. 115, Springer-Verlag, Berlin, 1994.
182. A. Rose, *Concepts in Photoconductivity and Allied Problems*, Interscience Publishers, New York (1963).
183. G. G. Malliaras, V. V. Krasnikov, H. J. Bolink, and G. Hadziioannou, *Phys. Rev. B* **52**, R14324–R14327 (1995).
184. S. J. Zilker, M. Grasruck, J. Wolff, S. Schlöter, A. Leopold, M. A. Kol'chenko, U. Homann, A. Schreiber, P. Strohriegel, C. Hohle, and D. Haarer, *Chem. Phys. Lett.* **306**, 285–290 (1999).
185. H. Chun, W. J. Joo, N. J. Kim, I. K. Moon, and N. Kim, *J. Appl. Polym. Sci.* **89**, 368–372 (2003).
186. P. M. Lindquist, C. Poga, R. G. DeVoe, Y. Jia, W. E. Moerner, M.-P. Bernal, H. Coufal, R. K. Grygier, J. A. Hoffnagle, C. M. Jefferson, R. M. Macfarlane, R. M. Shelby, and G. T. Sincerbox, *Opt. Lett.* **21**, 890–892 (1996).

187. N. Cheng, B. Swedek, and P. N. Prasad, *Appl. Phys. Lett.* **71**, 1828–1830 (1999).
188. H.-W. Kim, K.-S. Choi, J. Mun, S. Jung, C.-S. Yoon, and J.-D. Kim, *Opt. Mater.* **21**, 657–662 (2003).
189. G. J. Steckman, R. Bittner, K. Meerholz, and D. Psaltis, *Opt. Commun.* **185**, 13–17 (2000).
190. K. Curtis, A. Pu, and D. Psaltis, *Opt. Lett.* **19**, 993–994 (1994).
191. S. G. Kim, H. S. Lee, K. T. Kim, E. S. Kim, and B. Lee, *Opt. Quantum. Electron* **32**, 419–430 (2000).
192. H. Ono, T. Kawamura, N. Kawatsuki, and H. Norisada, *Appl. Phys. Lett.* **79**, 895–897 (2001).
193. J. A. Herlocker, C. Fuentes-Hernandez, J. F. Wang, N. Peyghambarian, B. Kippelen, Q. Zhang, and S. R. Marder, *Appl. Phys. Lett.* **80**, 1156–1158 (2002).
194. M. M. Wang and S. C. Esener, *Appl. Opt.* **39**, 1826–1834 (2000).
195. B. L. Volodin, B. Kippelen, K. Meerholz, B. Javidi, and N. Peyghambarian, *Nature* **383**, 58–59 (1996).
196. D. Vacar, A. J. Heeger, B. Volodin, B. Kippelen, and N. Peyghambarian, *Rev. Sci. Instrum.* **68**, 1119–1121 (1997).
197. D. D. Steele, B. L. Volodin, O. Savina, B. Kippelen, N. Peyghambarian, H. Rockel, and S. R. Marder, *Opt. Lett.* **23**, 153–155 (1998).
198. M. B. Klein, G. D. Bacher, A. Grunnet-Jepsen, D. Wright, and W. E. Moerner, *Opt. Commun.* **162**, 79–84 (1999).
199. E. Hendrickx, D. Van Steenwinckel, C. Engels, E. Gubbelmans, K. Van den Broeck, D. Beljonne, J.-L. Bredas, C. Samyn, and A. Persoons, *Mater. Sci. Eng., C* **18**, 25–35 (2001).
200. W.-J. Joo, N.-J. Kim, H. Chun, I. K. Moon, and N. Kim, *Polymer* **42**, 9863–9866 (2001).
201. M. R. Leahy, and D. J. McGee, *Opt. Commun.* **187**, 277–282 (2001).
202. A. N. Simonov, A. V. Larichev, V. P. Shibaev, and A. I. Stakhanov, *Opt. Commun.* **197**, 175–185 (2001).
203. S. Mookherjea and A. Yariv, *Phys. Rev. E* **64**, 066602(6) (2001).
204. T. Sassa, T. Wada, H. Sasabe, M. Yokoyama, and S. Umegaki, *Opt. Lett.* **26**, 995–997 (2001).
205. Y. Hayasaki, N. Ishikura, H. Yamamoto, and N. Nishida, *Rev. Sci. Instrum.* **74**, 3693–3696 (2003).
206. Z. Chen, M. Asaro, O. Ostroverkhova, W. E. Moerner, M. He, and R. J. Twieg, *Opt. Lett.* **28**, 2509–2511 (2003).
207. J. Obrzut, M. J. Obrzut, and F. E. Karasz, *Synth. Met.* **29**, E103–E108 (1989).

## FURTHER READING

In addition to previously cited materials, the reader interested in ongoing developments may also want to consider regular topical symposia on organic photorefractives sponsored by, among others, the Materials Research Society, The Optical Society of America, and the Society of Photo-Optical Instrumentation Engineers (SPIE). Recent related proceedings of SPIE include

- K. Meerholz, *Organic Photorefractive and Photosensitive Materials for Holographic Applications*, 4802 SPIE, Bellingham, Wash., 2002.
- S. Ducharme and J. W. Stasiak, *Organic Photorefractive Materials and Xerographic Photoreceptors*, 2850 SPIE, Bellingham, Wash., 1996.
- S. Ducharme and J. W. Stasiak, *Xerographic Photoreceptors and Organic Photorefractive Materials II*, 3144 SPIE, Bellingham, Wash., 1997.

- S. Ducharme and J. W. Stasiak, *Xerographic Photoreceptors and Organic Photorefractive Materials IV*, 3471 SPIE, Bellingham, Wash., 1998.
- C. M. Lawson and K. Meerholz, *Nonlinear Optical Transmission Processes and Organic Photorefractive Materials*, 4462 SPIE, Bellingham, Wash., 2002.
- G. V. Klimusheva and A. G. Iljin, eds., *Eighth International Conference on Nonlinear Optics of Liquid and Photorefractive Crystals*, 4418 SPIE, Bellingham, Wash., 2001.
- G. V. Klimusheva and A. G. Iljin, *Nonlinear Optics of Liquid and Photorefractive Crystals*, 2795 SPIE, Bellingham, Wash., 1996.
- G. V. Klimusheva, *Nonlinear Optics of Liquid and Photorefractive Crystals II*, 3488 SPIE, Bellingham, Wash., 1998.

JAMES H. ANDREWS  
KAREN ZREBIEC  
Youngstown State University

## **PIEZOELECTRIC POLYMERS**

### **Introduction**

Piezoelectric polymers have been known for more than 40 years, but in recent years they have gained reputé as a valuable class of “smart materials.” There is no standard definition for smart materials, and terms such as intelligent materials, smart materials, adaptive materials, active devices, and smart systems are often used interchangeably. The term “*smart material*” generally designates a material that changes one or more of its properties in response to an external stimulus.

The most popular smart materials are piezoelectric materials, magnetostrictive materials, shape-memory alloys, electrorheological fluids, electrostrictive materials, and optical fibers. Magnetostrictives, electrostrictives, shape-memory alloys, and electrorheological fluids are used as actuators; optical fibers are used primarily as sensors (see SHAPE MEMORY POLYMERS)

Among these active materials, piezoelectric materials are most widely used because of their wide bandwidth, fast electromechanical response, relatively low power requirements, and high generative forces. A classical definition of piezoelectricity, a Greek term for “pressure electricity,” is the generation of electrical polarization in a material in response to mechanical stress. This phenomenon is known as the direct effect. Piezoelectric materials also display the converse effect: mechanical deformation upon application of an electrical charge or signal. Piezoelectricity is a property of many noncentrosymmetric ceramics, polymers, and biological systems. Pyroelectricity is a subset of piezoelectricity, whereby the polarization is a function of temperature. Some pyroelectric materials are ferroelectric, although not all ferroelectrics are pyroelectric. Ferroelectricity is a property of certain dielectrics that exhibit spontaneous electric polarization (separation of the center of positive and negative electric charge that



**Table 1. Comparison of Properties of Standard Piezoelectric Polymer and Ceramic Materials**

	$d_{31}^a$ , pm/V	$g_{31}^a$ , (mV·m)/N	$k_{31}$	Salient features
Poly(vinylidene fluoride) (PVDF)	28	240	0.12	Flexible, lightweight, low acoustic and mechanical impedance
Lead zirconium titanate (PZT)	175	11	0.34	Brittle, heavy, toxic

<sup>a</sup>Values shown are absolute values of constants.

makes one side of the crystal positive and the opposite side negative) that can be reversed in direction by applying an appropriate electric field. Ferroelectricity is named by analogy with ferromagnetism, which occurs in materials such as iron. Traditionally, ferroelectricity is defined for crystalline materials, or at least in the crystalline region of semicrystalline materials. More recently, however, a number of researchers have explored the possibility of ferroelectricity in amorphous polymers, that is, ferroelectricity without a crystal lattice structure (1).

**Characteristics of Piezoelectric Polymers.** The properties of polymers are very different from those of inorganics (Table 1), and they are uniquely qualified to fill niche areas where single crystals and ceramics cannot perform as effectively. As noted in Table 1, the piezoelectric strain constant ( $d_{31}$ ) for the polymer is lower than that of the ceramic. However, piezoelectric polymers have much higher piezoelectric stress constants ( $g_{31}$ ) which indicates that they are much better sensors than ceramics. Piezoelectric polymeric sensors and actuators offer the advantage of processing flexibility because they are lightweight, tough, readily manufactured in large areas, and can be cut and formed into complex shapes. Polymers also exhibit high strength and high impact resistance (2). Other notable features of polymers are low dielectric constant, low elastic stiffness, and low density, which result in high voltage sensitivity (excellent sensor characteristic) and low acoustic and mechanical impedance (crucial for medical and underwater applications). Polymers also typically possess high dielectric breakdown and high operating field strength, which means that they can withstand much higher driving fields than ceramics. Polymers offer the ability to pattern electrodes on the film surface and pole only selected regions. Based on these features, piezoelectric polymers possess their own established area for technical applications and useful device configurations.

**Structural Requirements for Piezoelectric Polymers.** The piezoelectric mechanisms for semicrystalline and amorphous polymers differ. Although the differences are distinct, particularly with respect to polarization stability, in the simplest terms, four critical elements exist for all piezoelectric polymers, regardless of morphology. These essential elements are (1) the presence of permanent molecular dipoles, (2) the ability to orient or align the molecular dipoles, (3) the ability to sustain this dipole alignment once it is achieved, and (4) the ability of the material to undergo large strains when mechanically stressed (3).

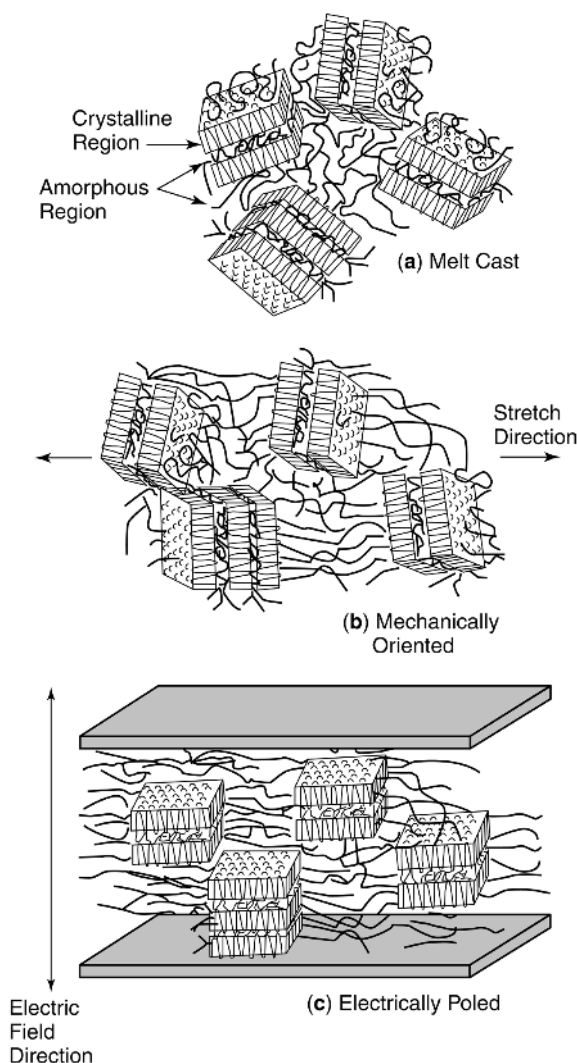


**Fig. 1.** Schematic illustration of random stacks of amorphous and crystal lamellae in the PVDF polymer: (a) the morphology after the film is melt cast; (b) after orientation of the film by mechanically stretching several times its original length; and (c) after depositing metal electrodes and poling through the film thickness.

## **Semicrystalline Polymers**

**Mechanism of Piezoelectricity in Semicrystalline Polymers.** Semicrystalline Polymers must have a polar crystalline phase to render them piezoelectric. The Morphology of such polymers consists of crystallites dispersed within amorphous regions, as shown in Figure 1a. The amorphous region has a glass-transition temperature that dictates the mechanical properties of the polymer, and the melting temperature of the crystallites dictates the upper limit of

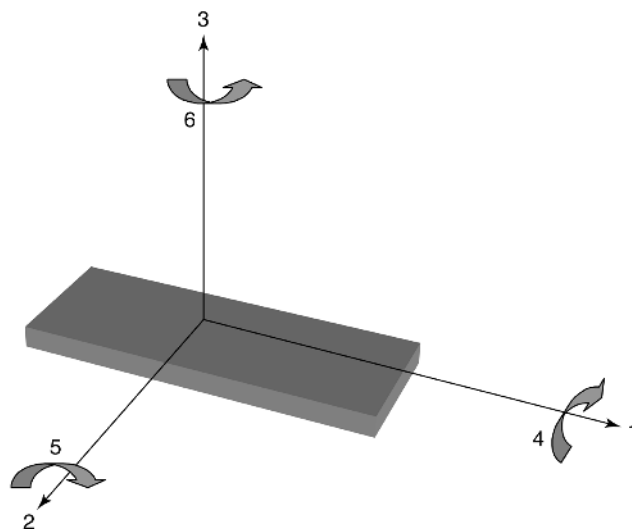


**Fig. 2.** Tensor directions for defining the constitutive relationships.

the use temperature. The degree of crystallinity in such polymers depends on the method of preparation and thermal history. Most semicrystalline polymers have several polymorphic phases, some of which may be polar. Mechanical orientation, thermal annealing, and high voltage treatment are all, it has been shown, effective in inducing crystalline phase transformations. Stretching the polymer aligns the amorphous strands in the film plane, as shown in Figure 1b, and facilitates uniform rotation of the crystallites by an electric field. Depending on whether stretching is uniaxial or biaxial, the electrical and mechanical properties (and therefore the transduction response) are either highly anisotropic or isotropic in the plane of the polymer sheet. Electrical poling is accomplished by applying an electric field across the thickness of the polymer, as depicted in Figure 1c. An electric field of the order of 50 MV/m is typically sufficient to effect crystalline orientation. Polymers can be poled by using a direct contact method or corona discharge. The latter is advantageous because contacting electrodes is not required and samples of large area can be poled continuously. This method is used to manufacture commercial poly(vinylidene fluoride) (PVDF) film (see VINYLIDENE FLUORIDE POLYMERS (PVDF)). Some researchers have also successfully poled large areas of polymer films by sandwiching them between polished metal plates under a vacuum. This method eliminates electrical arcing of samples and the need for depositing metal electrodes on the film surface. The amorphous phase of semicrystalline polymers supports the crystal line orientation, and polarization is stable up to the Curie temperature. This polarization can remain constant for many years if it is not degraded by moisture uptake or elevated temperatures.

**Piezoelectric Constitutive Relationships.** The constitutive relationships that describe piezoelectric behavior in materials can be derived from thermodynamic principles (4). A tensor notation is adopted to identify the coupling between the various entities through mechanical and electrical coefficients. The common practice is to label directions as depicted in Figure 2. The stretch

**Table 2. Definitions of Piezoelectric Constants**

Equations	Units
$d = (dD/dX)_E = (dS/dE)_X$	C/N or m/V
$e = (dD/dS)_E = -(dX/dE)_S$	C/m or N/Vm
$g = (dE/dX)_D = (dS/dD)_X$	Vm/N or m <sup>2</sup> /C
$h = (dE/dS)_D = -(dX/dD)_S$	V/m or N/C

direction is denoted as “1.” The “2” axis is orthogonal to the stretch direction in the plane of the film. The polarization axis (perpendicular to the surface of the film) is denoted “3.” The shear planes, indicated by the subscripts “4,” “5,” and “6,” are perpendicular to the directions “1,” “2,” and “3,” respectively. By reducing the tensor elements and using standard notations (5), the resulting equations can be displayed in matrix form as follows:

$$\begin{pmatrix} S_1 \\ S_2 \\ S_3 \\ S_4 \\ S_5 \\ S_6 \end{pmatrix} = \begin{pmatrix} d_{11} & d_{12} & d_{13} \\ d_{21} & d_{22} & d_{23} \\ d_{31} & d_{32} & d_{33} \\ d_{41} & d_{42} & d_{43} \\ d_{51} & d_{52} & d_{53} \\ d_{61} & d_{62} & d_{63} \end{pmatrix} \begin{pmatrix} E_1 \\ E_2 \\ E_3 \end{pmatrix} + \begin{pmatrix} s_{11}^E & s_{12}^E & s_{13}^E & s_{14}^E & s_{15}^E & s_{16}^E \\ s_{21}^E & s_{22}^E & s_{23}^E & s_{24}^E & s_{25}^E & s_{26}^E \\ s_{31}^E & s_{32}^E & s_{33}^E & s_{34}^E & s_{35}^E & s_{36}^E \\ s_{41}^E & s_{42}^E & s_{43}^E & s_{44}^E & s_{45}^E & s_{46}^E \\ s_{51}^E & s_{52}^E & s_{53}^E & s_{54}^E & s_{55}^E & s_{56}^E \\ s_{61}^E & s_{62}^E & s_{63}^E & s_{64}^E & s_{65}^E & s_{66}^E \end{pmatrix} \begin{pmatrix} X_1 \\ X_2 \\ X_3 \\ X_4 \\ X_5 \\ X_6 \end{pmatrix} \quad (1)$$

$$\begin{pmatrix} D_1 \\ D_2 \\ D_3 \end{pmatrix} = \begin{pmatrix} \varepsilon_{11}^T & \varepsilon_{12}^T & \varepsilon_{13}^T \\ \varepsilon_{21}^T & \varepsilon_{22}^T & \varepsilon_{23}^T \\ \varepsilon_{31}^T & \varepsilon_{32}^T & \varepsilon_{33}^T \end{pmatrix} \begin{pmatrix} E_1 \\ E_2 \\ E_3 \end{pmatrix} + \begin{pmatrix} d_{11} & d_{12} & d_{13} & d_{14} & d_{15} & d_{16} \\ d_{21} & d_{22} & d_{23} & d_{24} & d_{25} & d_{26} \\ d_{31} & d_{32} & d_{33} & d_{34} & d_{35} & d_{36} \end{pmatrix} \begin{pmatrix} X_1 \\ X_2 \\ X_3 \\ X_4 \\ X_5 \\ X_6 \end{pmatrix} \quad (2)$$

Piezoelectricity is a cross coupling among the elastic variables, stress  $X$  and strain  $S$ , and the dielectric variables, electric charge density  $D$  and electric field  $E$ . Note that  $D$  is named in analogy to the  $B$  field in ferromagnetism, although some authors also refer to it as dielectric or electric displacement. There does not seem to be a standard nomenclature; however, it is the opinion of the authors of this article that electric charge density is a better description of this property. The combinations of these variables define the piezoelectric strain constant  $d$ , the material compliance  $s$ , and the permittivity  $\varepsilon$ . Other piezoelectric properties are the piezoelectric voltage constant  $g$ , stress constant  $e$ , and strain constant  $h$  given by the equations in Table 2. For a given constant, the first definition in the table refers to the direct effect, and the second refers to the converse effect. The piezoelectric constants are interrelated through the electrical and mechanical properties of the material. Electric field strength and displacement charge density are related through the dielectric constant,  $\varepsilon\varepsilon_0$  (where  $\varepsilon_0$  is the permittivity of free space), and stress and strain are related through the compliance according to

$$d_{ij} = \varepsilon_0 \varepsilon_i g_{ij} \quad (3)$$

$$e_{ij} = s_{ij} d_{ij} \quad (4)$$

The polarization  $P$  is a measure of the degree of piezoelectricity in a given material. In a piezoelectric material, a change in polarization  $\Delta P$  results from an applied stress  $X$  or strain  $S$  under conditions of constant temperature and zero electric field. A linear relationship exists between  $\Delta P$  and the piezoelectric constants. Because of material anisotropy,  $\mathbf{P}$  is a vector that has three orthogonal components in the 1, 2, and 3 directions. Alternatively, the piezoelectric constants can be defined as

$$\Delta P_i = d_{ij} X_j \quad (5)$$

$$\Delta P_i = g_{ij} S_j \quad (6)$$

The electrical response of a piezoelectric material is a function of the electrode configuration relative to the direction of the applied mechanical stress. For a coefficient  $d_{ij}$ , the first subscript is the direction of the electric field or charge displacement, and the second subscript gives the direction of the mechanical deformation or stress. The  $C_{2v}$  crystallographic symmetry typical of synthetic oriented, poled polymer film leads to cancellation of all but five of the  $d_{ij}$  components ( $d_{31}$ ,  $d_{32}$ ,  $d_{33}$ ,  $d_{15}$ , and  $d_{24}$ ). If the film is poled and biaxially oriented or unoriented,  $d_{31} = d_{32}$  and  $d_{15} = d_{24}$ . Most natural biopolymers possess  $D_\infty$  symmetry which yields a matrix that possesses only the shear piezoelectricity components  $d_{13}$  and  $d_{25}$ . Because the  $d_{33}$  constant is difficult to measure without constraining the lateral dimension of the sample, it is typically determined from equation 7 which relates the constants to the hydrostatic piezoelectric constant,  $d_{3h}$ .

$$d_{3h} = d_{31} + d_{32} + d_{33}. \quad (7)$$

The electromechanical coupling coefficient  $k_{ij}$  represents the conversion of electrical energy into mechanical energy and vice versa. The electromechanical coupling can be considered a measure of transduction efficiency and is always less than unity as shown here:

$$k^2 = \frac{\text{Electrical energy converted to mechanical energy}}{\text{Input electrical energy}} \quad (8)$$

$$k^2 = \frac{\text{Mechanical energy converted to electrical energy}}{\text{Input mechanical energy}} \quad (9)$$

Some  $k$  coefficients can be obtained from a measured  $d$  constant as follows:

$$k_{31} = \frac{d_{31}}{\sqrt{s_{11}^E \varepsilon_3^T}} \quad (10)$$

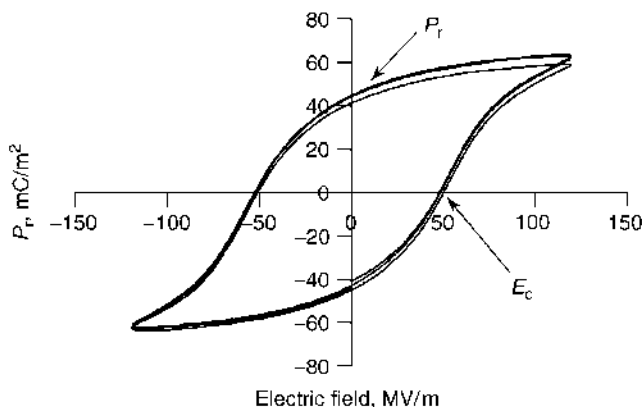


**Fig. 3.** Typical ferroelectric hysteresetic behavior for PVDF.

**Ferroelectricity in Semicrystalline Polymers.** At high electric fields, the polarization in semicrystalline polymers such as PVDF is nonlinear with the applied electric field. This nonlinearity in polarization is defined as hysteresis. The existence of spontaneous polarization together with polarization reversal (as illustrated by a hysteresis loop) is generally accepted as proof of ferroelectricity. Figure 3 is an example of the typical hysteresetic behavior of PVDF. Two other key properties typically reported for ferroelectric materials are the coercive field and the remanent polarization. The coercive field  $E_c$ , which marks the point where the hysteresis intersects the horizontal axis, is about 50 MV/m at room temperature for many ferroelectric polymers. The remanent polarization  $P_r$  corresponds to the point where the loop intersects the vertical axis. The values of  $E_c$  and  $P_r$  depend on temperature and frequency. The Curie temperature  $T_c$  is generally lower than but close to the melting temperature of the polymer. Below  $T_c$ , the polymer is ferroelectric and above  $T_c$ , the polymer loses its noncentrosymmetric nature.

Although ferroelectric phenomenon has been well documented in ceramic crystals, the question of whether polymer crystallites could exhibit dipole switching was debated for about a decade after the discovery of piezoelectricity in PVDF. Inhomogeneous polarization through the film thickness that yielded higher polarization on the positive electrode side of the polymer led to speculations that PVDF was simply a trapped charge electret. These speculations were dispelled when x-ray studies (6) demonstrated that polarization anisotropy vanishes because of high poling field strengths and that true ferroelectric dipole reorientation occurs in PVDF. One researcher used infrared to attribute the polarization reversal in PVDF to  $180^\circ$  dipole rotation (7). Others documented the same via x-ray pole analysis and infrared techniques for odd-numbered nylons (8).

**State of the Art.** Pioneering work in the area of piezoelectric polymers (9) led to the development of strong piezoelectric activity in poly(vinylidene fluoride) (PVDF) and its copolymers with trifluoroethylene (TrFE) and tetrafluoroethylene (TFE). These semicrystalline fluoropolymers represent the state of the art in piezoelectric polymers and are currently the only commercial piezoelectric

**Table 3. Comparison of Piezoelectric Properties of Some Semicrystalline Polymeric Materials**

Polymer	Structure	$T_g, ^\circ\text{C}$	$T_m, ^\circ\text{C}$	Max. use temp., $^\circ\text{C}$	$d_{31}$ , pC/N	Reference
PVDF	$\left( \begin{array}{c} \text{F} \\   \\ -\text{C}-\text{CH}_2- \\   \\ \text{F} \end{array} \right)_n$	-35	175	80	20–28	2
PTrFE	$\left( \begin{array}{cc} \text{F} & \text{F} \\   &   \\ -\text{C}- & \text{CH}- \\   & \\ \text{F} & \end{array} \right)_n$	32	150	90–100	12	2
Nylon-11	$\left( \begin{array}{c} \text{O} \\    \\ -\text{NH}-(\text{CH}_2)_{10}-\text{C}- \\    \\ \text{O} \end{array} \right)_n$	68	195	185	3 at 25°C, 14 at 107°C	22
Polyurea-9	$\left( \begin{array}{c} \text{O} \\    \\ -(\text{CH}_2)_9-\text{HN}-\text{C}-\text{NH}- \\    \\ \text{O} \end{array} \right)_n$	50	180	—	—	28

polymers. Odd-numbered nylons, the next most widely investigated semicrystalline piezoelectric polymers, have excellent piezoelectric properties at elevated temperatures but have not yet been embraced in practical application. Other semicrystalline polymers including polyureas, liquid crystalline polymers, biopolymers, and an array of blends have been studied for their piezoelectric potential and are summarized in the following section. The chemical repeat unit and piezoelectric constants of several semicrystalline polymers are listed in Table 3.

**Poly(vinylidene fluoride) (PVDF).** Interest in the electrical properties of PVDF began in 1969 when it was shown (9) that poled thin films exhibit a very large piezoelectric coefficient, 6–7 pC/N, a value about 10 times larger than had been observed in any other polymer. As seen in Table 3, PVDF is inherently polar. The spatially symmetrical disposition of the hydrogen and fluorine atoms along the polymer chain gives rise to unique polar effects that influence the electromechanical response, solubility, dielectric properties, and crystal morphology and yield an unusually high dielectric constant. The dielectric constant of PVDF is about 12, which is four times greater than that of most polymers, and makes PVDF attractive for integration into devices because the signal-to-noise ratio is smaller for higher dielectric materials (see DIELECTRIC RELAXATION). The amorphous phase in PVDF has a Glass Transition that is well below room temperature ( $-35^\circ\text{C}$ ); hence, the material is quite flexible and readily strained at room temperature. PVDF is typically 50–60% crystalline, depending on thermal and processing history, and has at least four crystal phases ( $\alpha$ ,  $\beta$ ,  $\gamma$ , and  $\delta$ ); at least three are polar. The most stable, nonpolar  $\alpha$  phase results upon casting PVDF from a melt and can be transformed into the polar  $\beta$  phase by mechanical

stretching at elevated temperatures or into the polar  $\delta$  phase by rotating the molecular chain axis in a high electric field ( $\sim 130$  MV/m) (10). The  $\beta$  phase is most important for piezoelectricity and has a dipole moment perpendicular to the chain axis of  $7 \times 10^{-30}$  C·m (2.1 D). After poling PVDF, the room temperature polarization stability is excellent; however, polarization and piezoelectricity degrade as temperature increases and are erased at its Curie temperature. Previously, it was believed that polarization stability was defined only by the melting temperature of the PVDF crystals. Recently, however, some researchers suggest that the polarization stability of PVDF and its copolymers is associated with coulombic interactions between injected, trapped charges and oriented dipoles in the crystals (11). It has been hypothesized that the thermal decay of the polarization is caused by the thermally activated removal of the trapped charges from the traps at the surface of the crystals. The role of trapped charges in stabilizing orientation in both semicrystalline and amorphous polymers is still a subject that needs further study. The electromechanical properties of PVDF have been widely investigated. For more details, the reader is referred to the wealth of literature that exists on the subjects of piezoelectric, pyroelectric, and ferroelectric properties (2,6,12,13), and the morphology (14–16) of this polymer (see VINYLIDENE FLUORIDE POLYMERS).

*Poly(vinylidene fluoride–trifluoroethylene and tetra fluoro ethylene) Copolymers.* Copolymers of vinylidene fluoride with trifluoroethylene (TrFE) and tetrafluoroethylene (TFE) also exhibit strong piezoelectric, pyroelectric, and ferroelectric effects. These polymers are discussed together here because they behave similarly when copolymerized with PVDF. An attractive morphological feature of the comonomers is that they force the polymer into an all-trans conformation that has a polar crystalline phase, which eliminates the need for mechanical stretching to yield a polar phase. P(VDF–TrFE) crystallizes to a much greater extent than PVDF (up to 90% crystalline) and yields a higher remanent polarization, a lower coercive field, and much sharper hysteretic loops. TrFE also extends the use temperature by about 20°C to close to 100°C. Conversely, copolymers with TFE exhibit a lower degree of crystallinity and a suppressed melting temperature, compared to the PVDF homopolymer. Although the piezoelectric constants for the copolymers are not as large as those of the homopolymer, the advantages of P(VDF–TrFE) in processibility, enhanced crystallinity, and higher use temperature make it favorable for applications.

Researchers have recently reported that highly ordered, lamellar crystals of P(VDF–TrFE) can be made by annealing the material at temperatures between the Curie temperature and the melting point. This material is referred to as a “single crystalline film.” A relatively large single crystal of P(VDF–TrFE) 75/25 mol% copolymer was grown that exhibits a room temperature  $d_{33} = -38$  pm/V and a coupling factor  $k_{33} = 0.33$  (17).

The result of introducing defects into the crystalline structure of P(VDF–TrFE) copolymer on electroactive actuation has been studied using high electron irradiation (18). Extensive structural investigations indicate that electron irradiation disrupts the coherence of polarization domains (all-trans chains) and forms localized polar regions (nanometer-sized, all-trans chains interrupted by trans and gauche bonds). After irradiation, the material exhibits behavior analogous to that of relaxor ferroelectric systems in inorganic materials. The resulting material is no longer piezoelectric, but rather exhibits a large electric field-induced



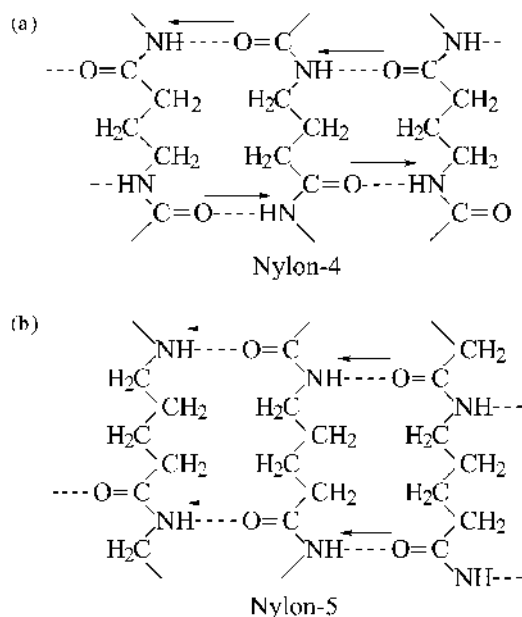


**Fig. 4.** Schematic depiction of hydrogen-bonded sheets showing dipole directions in the crystal lattices of (a) even (nylon-4) and (b) odd polyamides (nylon-5).

strain (5% strain) because of electrostriction. The basis for such large electrostriction is the large change in the lattice strain as the polymer traverses the ferroelectric to paraelectric phase transition and the expansion and contraction of the polar regions. Piezoelectricity can be measured in these and other electrostrictives when a dc bias field is applied. Irradiation is typically accomplished in a nitrogen atmosphere at elevated temperatures using irradiation dosages up to 1,200 kGy (120 Mrad).

**Polyamides.** A low level of piezoelectricity was first reported in polyamides (also known as nylons) in 1970 (19). A systematic study of odd-numbered nylons, however, initiated in 1980 (20) and served as the impetus for more than 20 years of subsequent investigations of piezoelectric and ferroelectric activity in these polymers. The monomer unit of odd nylons consists of even numbers of methylene groups and one amide group whose dipole moment is  $12.3 \times 10^{-30}$  C·m (3.7 D). Polyamides crystallize in all-trans conformations and are packed to maximize hydrogen bonding between adjacent amine and carbonyl groups, as seen in Figure 4 for an even-numbered and an odd-numbered polyamide. The amide dipoles align synergistically in the odd-numbered monomer, resulting in a net dipole moment. The amide dipole cancels in an even-numbered nylon, although remanent polarizations have been measured for some even-numbered nylons, as discussed later in this article. The unit dipole density depends on the number of methylene groups present, and polarization increases from 58 mC/m<sup>2</sup> for nylon-11 to 125 mC/m<sup>2</sup> for nylon-5 as the number of methylene groups decreases (8).

Polyamides are hydrophilic. Because water absorption is associated with hydrogen bonding to the polar amide groups, the hydrophilicity increases as the

density of amide groups increases. Water absorption in nylon-11 and nylon-7 has been shown to be as high as 4.5% (by weight) and more than 12% for nylon-5 (21), whereas it is less than 0.02% for PVDF and its copolymers. Studies have shown that water absorption can have a dramatic effect on the dielectric and piezoelectric properties of nylons; however, water does not affect the crystallinity or orientation in thermally annealed films (21). Thus, films can be dried to restore their original properties.

At room temperature, odd-numbered nylons have lower piezoelectric constants than PVDF; however, when examined above their glass-transition temperatures, they exhibit comparable ferroelectric and piezoelectric properties and much higher thermal stability. The piezoelectric  $d$  and  $e$  constants increase rapidly as temperature increases. Maximum stable  $d_{31}$  values of 17 pC/N and 14 pC/N are reported for nylon-7 and nylon-11, respectively. Corresponding values of the electromechanical coupling constant  $k_{31}$  are 0.054 and 0.049. Studies have also shown that annealing nylon films enhances their polarization stability because it promotes denser packing of the hydrogen-bonded sheet structure in the crystalline regions and hinders dipole switching because of lowered free volume for rotation (22).

Though widely studied, piezoelectric polyamides have not been widely used in applications partly because of their low room temperature piezoelectric response and the problem of moisture uptake.

**Liquid Crystalline Polymers.** Liquid crystals consist of highly ordered rod-like or disk-like molecules. At their melting points they partially lose crystalline order and generate a fluid but ordered state. They can form layered structures called smectic phases or nematic phases that have an approximately parallel orientation of the molecular long axis. It was first predicted in 1975 that spontaneous polarization could be achieved in liquid crystals based on symmetry arguments (23). Subsequently, it has been shown that liquid crystalline molecules whose chiral carbon atoms link a mesogenic group and end alkyl chains may exhibit ferroelectric behavior in the smectic C phase ( $\text{SmC}^*$ ) (24). In this phase, the molecular axis tilts from the normal to the layer plane, and the molecular dipoles align in the same direction, yielding a net polarization. If such liquid crystalline molecules are introduced into the backbone or as a side group on a polymer, a ferroelectric liquid crystalline polymer can be obtained. There are three requirements for spontaneous polarization in a liquid crystal: a center of chirality, a dipole moment positioned at the chiral center that acts transverse to the molecular long axis, and a tilted smectic phase (25).

**Polyureas.** Polyureas are thermosets, long used as insulators in a number of applications. Until a few years ago, ureas were available mostly as insoluble powders or highly cross-linked resins. In 1987, a vapor deposition polymerization method was successfully developed that was later applied to synthesizing polyureas (26,27). Typically, a vapor deposition technique is used by evaporating  $\text{OCN-R}_1\text{-NH}_2$  and  $\text{H}_2\text{N-R}_2\text{-NH}_2$  monomers simultaneously on a substrate (where  $\text{R}_1$  and  $\text{R}_2$  are various aliphatic or aromatic groups). This prevents cross-linking and allows processing thicknesses in the hundreds of nanometers to tens of micrometers.

An exploration (27) of the dielectric and pyroelectric properties of polyurea films led to the discovery of their piezoelectricity. From the early 1990s to the

present, various aromatic and aliphatic polyureas were synthesized, and it was shown that they are piezoelectric (28,29). Aromatic polyureas were the first polyurea structures identified as piezoelectric. They exhibit a piezoelectric  $e$  constant of  $15 \text{ mC/m}^2$  and have high temperature stability, which remains independent of temperature up to  $200^\circ\text{C}$ . Their pyroelectric coefficient is high because of their low dielectric loss compared to other polymers. The  $d$  constant is about  $5 \text{ pC/N}$  at room temperature and increases as temperature increases (28).

Owing to their structures, aliphatic polyureas possess higher flexibility in their molecular chains. Similarly to polyamides, hydrogen bonds play a large role in stabilizing the orientation polarization that is imparted. Polyureas that have an odd number of methyl groups exhibit overall nonzero polarization. Polyurea-9 was synthesized and processed first, and an  $e$  constant of  $5 \text{ mC/m}^2$  was reported (29). Then, polyureas that have a smaller number of carbons were attempted because it was surmised that they should lead to a higher density of urea bond dipoles. Toward that end, polyurea-5 was synthesized, and it was found that the  $e$  and  $d$  constants are twice those of polyurea-9. Aliphatic polyureas exhibit ferroelectric hysteresis and in addition, are piezoelectric when they have odd numbers of methyl groups. Their thermal stability and piezoelectric coefficients depend highly on the poling temperature (typically  $70\text{--}150^\circ\text{C}$ ) but are lower than those of aromatic polyureas.

**Biopolymers.** Piezoelectricity of biopolymers was first reported in keratin in 1941 (30). When a bundle of hair was immersed in liquid air, an electric voltage of a few volts was generated between the tip and the root. When pressure was applied on the cross section of the bundle, an electric voltage was generated. Subsequently, piezoelectricity has been observed in a wide range of other biopolymers including collagen (31,32), polypeptides like poly( $\gamma$ -methylglutamate) and poly( $\gamma$ -benzyl-L-glutamate) (33,34), oriented films of DNA (35), poly(lactic acid) (36), and chitin (37). Most natural biopolymers possess  $D_\infty$  symmetry and so they exhibit shear piezoelectricity. A shear stress in the plane of polarization produces an electric displacement perpendicular to the plane of the applied stress and results in a  $-d_{14} = d_{25}$  piezoelectric constant. The piezoelectric constants of biopolymers are small relative to synthetic polymers; they range in value from  $0.01 \text{ pC/N}$  for DNA to  $2.5 \text{ pC/N}$  for collagen. The electromechanical effect in such polymers is attributed to the internal rotation of polar atomic groups linked to asymmetrical carbon atoms. Keratin and some polypeptide molecules assume an  $\alpha$ -helical or a  $\beta$ -sheet crystalline structure in which the CONH dipoles align synergistically in the axial direction.

Currently, the physiological significance of piezoelectricity in many biopolymers is not well understood, but it is believed that such electromechanical phenomena may have a distinct role in biochemical processes. For example, it is known that electric polarization in bone influences bone growth (38). In one study, a piezoelectric PVDF film was wrapped around the femur of a monkey. Within weeks, a remarkable formation of new bone was observed. The motion of the animal caused deformation of the film, which produced a neutralizing ionic current in the surrounding tissue. This minute fluctuating current appears to stimulate the metabolic activity of bone cells and leads to the proliferation of bone.

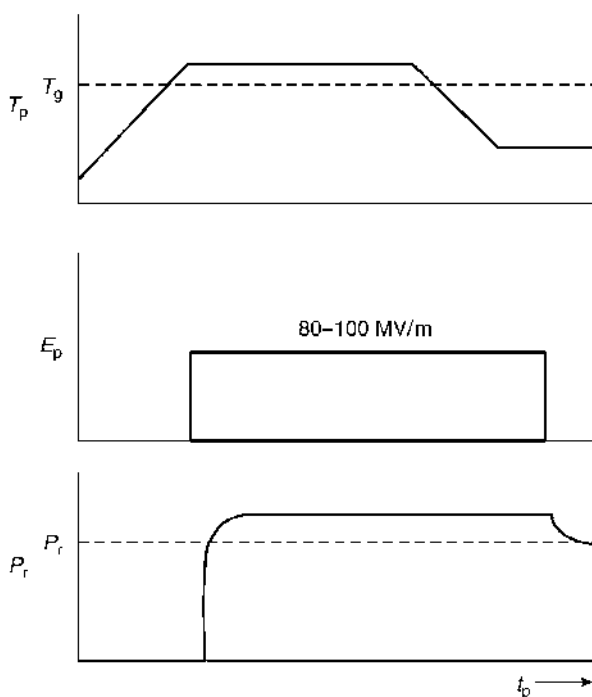


**Fig. 5.** Poling profile of an amorphous polymer.

### Amorphous Polymers

The purpose of this section is to explain the mechanism and key components required for developing piezoelectricity in amorphous polymers and to present a summary of the polarization and electromechanical properties of the amorphous polymers currently under investigation.

**Dielectric Theory.** The piezoelectricity in amorphous polymers differs from that in semicrystalline polymers and inorganic crystals in that the polarization is not in a state of thermal equilibrium, but rather a quasi-stable state because of the freezing-in of molecular dipoles. The result is a piezoelectric-like effect. A theoretical model for polymers that have frozen-in dipolar orientation was presented to explain piezoelectricity and pyroelectricity in amorphous polymers such as poly(vinyl chloride) (39).

One of the most important properties of an amorphous piezoelectric polymer is its Glass Transition temperature because it dictates use temperature and defines the poling process conditions.  $T_g$  is (the temperature below which the material exhibits glass-like characteristics, and above which it has rubber-like properties). Orientation polarization of molecular dipoles is responsible for piezoelectricity in amorphous polymers. It is induced, as shown in Figure 5, by applying an electric field  $E_p$  at an elevated temperature ( $T_p \geq T_g$ ) where the molecular chains are sufficiently mobile and allow dipole alignment with the electric field. Partial retention of this orientation is achieved by lowering

the temperature below  $T_g$  in the presence of  $E_p$ , resulting in a piezoelectric-like effect. The remanent polarization  $P_r$  is directly proportional to  $E_p$  and the piezoelectric response. The procedure used to prepare a piezoelectric amorphous polymer clearly results in both oriented dipoles and space or real charge injection. The real charges are usually concentrated near the surface of the polymer, and they are introduced because of the presence of the electrodes. Interestingly, some researchers (40,41) have shown that the presence of space charges does not significantly affect piezoelectric behavior. The reason is twofold. The magnitude of space charges is usually not significant with respect to polarization charges. Secondly, space charges are essentially symmetrical with respect to the thickness of the polymer; therefore, when the material is strained uniformly, the contribution to the piezoelectric effect is negligible.

In what follows, the origins of the dielectric contribution to the piezoelectric response of amorphous polymers are addressed. The potential energy  $U$  of a dipole  $\mu$  at an angle  $\theta$  with the applied electric field is  $U = \mu \mathbf{E} \cos \theta$ . Using statistical mechanics and assuming Boltzman's distribution of dipole energies, the mean projection of the dipole moment  $\langle \mu \rangle_E$  in the direction of the applied electric field is obtained:

$$\frac{\langle \mu_E \rangle}{\mu} = \coth \frac{\mu E_p}{kT} - \frac{kT}{\mu E} \quad (11)$$

This is the Langevin equation that describes the degree of polarization in a sample when an electric field  $E$  is applied at temperature  $T$ . Experimentally, a poling temperature in the vicinity of  $T_g$  is used to maximize dipole motion. The maximum electric field that may be applied, typically 100 MV/m, is determined by the dielectric breakdown strength of the polymer. For amorphous polymers,  $\mu E/kT$  is much less than 1; this places these systems well within the linear region of the Langevin function. The remanent polarization  $P_r$  is simply the polarization during poling minus the electronic and atomic polarizations that relax at room temperature, once the field  $E_p$  is removed. The following linear equation for remanent polarization results when the Clausius–Mossotti equation is used to relate the dielectric constant to the dipole moment (42):

$$P_r = \Delta \varepsilon \varepsilon_0 E_p \quad (12)$$

It can be concluded that remanent polarization and hence the piezoelectric response of a material are determined by  $\Delta \varepsilon$ ; this makes it a practical criterion to use when designing piezoelectric amorphous polymers. The Dielectric relaxation strength  $\Delta \varepsilon$  may be the result of either free or cooperative dipole motion. Dielectric theory yields a mathematical approach for examining the dielectric relaxation  $\Delta \varepsilon$  due to free rotation of the dipoles. The equation incorporates Debye's work based on statistical mechanics, the Clausius–Mossotti equation, and the Onsager local field and neglects short-range interactions (43):

$$\Delta \varepsilon_{\text{calculated}} = \frac{N \mu^2}{3kT \varepsilon_0} \left( \frac{n^2 + 2}{3} \right)^2 \left[ \frac{3\varepsilon(0)}{2\varepsilon(0) + n^2} \right]^2 \quad (13)$$

where  $N$  is the number of dipoles per unit volume,  $k$  is the Boltzmann constant,  $\varepsilon(0)$  is the static dielectric constant, and  $n$  is the refractive index. One way to measure  $P_r$  in amorphous polymers is the thermally stimulated current (TSC) method (refer to section on characterization).  $P_r$  can be calculated from the liberated charge during TSC, and by reconciling that with the Onsager relationship, the dipole density can be calculated:

$$P_r = \frac{N\mu^2 E_p}{3kT_p} \left( \frac{\varepsilon_\infty + 2}{3} \right)^2 \left[ \frac{3\varepsilon(0)}{2\varepsilon(0) + \varepsilon_\infty} \right] \quad (14)$$

The piezoelectric constants are related to the polarization. From basic thermodynamics,

$$d_{3i} = \left( \frac{\partial P}{\partial \sigma_i} \right)_{\gamma, T} \quad (15)$$

A molecular theory of the direct piezoelectric effect in poled amorphous piezoelectric polymers has been developed. An expression for the hydrostatic coefficient appears in the original paper (41). Later, this theory was extended, and an equation for  $d_{31}$  was obtained (44,45). By differentiating equation 14 and modifying it to account for dimensional effects such as stretching (44,46),

$$d_{31} = P_r(1 - \gamma)S_{11} + \frac{P_r(1 - \gamma)}{3}(\varepsilon_\infty - 1)S_{11} \quad (16)$$

where  $\gamma$  is Poisson's ratio,  $\varepsilon_\infty$  is the permittivity at high frequencies, and  $S_{11}$  is the compliance of the polymer. The first term accounts for dimensional effects, and the second term gives the contribution of the local field effect.

**Polarizability and Poling Conditions.** Designing an amorphous polymer that has a large dielectric relaxation strength and hence piezoelectric response requires the ability to incorporate highly polar groups at high concentrations and cooperative dipole motion. A study of the relationship between relaxation times, poling temperatures, and poling fields is crucial to achieving optimal dipole alignment. Theoretically, the higher the electric field, the better the dipole alignment. The value of the electric field is limited, however, by the dielectric breakdown of the polymer. In practice, 100 MV/m is the maximum field that can be applied to these materials. Poling times need to be of the order of the relaxation time of the polymer at the poling temperature.

During poling, the temperature is lowered to room temperature, while the field is still on, to freeze-in the dipole alignment. In a semicrystalline material, however, locking-in the polarization is supported by the crystalline structure of the polymer, and it is therefore stable above the glass-transition temperature of the polymer. Because the remanent polarization in amorphous polymers is lost in the vicinity of  $T_g$ , their use is limited to temperatures well below  $T_g$ . This means that the polymers are used in their glassy state, where they are quite stiff and thus limit the ability of the polymer to strain as stress is applied. A piezoelectric amorphous polymer may be used at temperatures near its  $T_g$  to optimize its mechanical properties, but not too close so as to maintain the remanent polarization.

Although there are few data that address the stability of piezoelectric activity in amorphous polymers, it is clear that time, pressure, and temperature can contribute to dipole relaxation in these polymers. For a given application and use temperature, the effect of these parameters on the stability of the frozen-in dipole alignment should be determined.

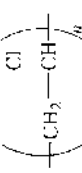
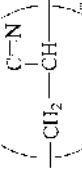
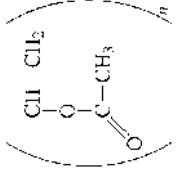
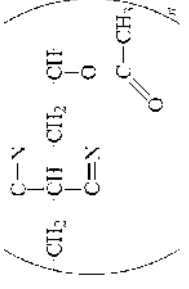
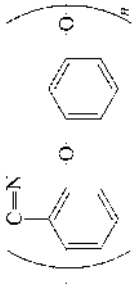
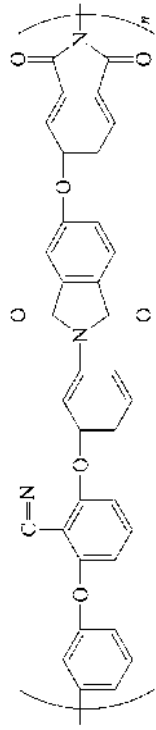
**Examples of Amorphous Piezoelectric Polymers.** The literature on amorphous piezoelectric polymers is much more limited than that for semicrystalline systems. This is in part because no amorphous piezoelectric polymers have responses high enough to attract commercial interest. Much of the previous work on amorphous piezoelectric polymers was in nitrile-substituted polymers, including polyacrylonitrile (PAN) (47–49), poly(vinylidene cyanide–vinyl acetate) (PVDCN/VAc) (50–54), poly(phenyl ether nitrile) (PPEN) (55,56), and poly(1-bicyclobutanecarbonitrile) (57). Weak piezoelectric activity in poly(vinyl chloride) (PVC) and poly(vinyl acetate) (PVAc) has also been found (11,41,58,59). The most promising of these materials are vinylidene cyanide copolymers that exhibit large dielectric relaxation strengths and strong piezoelectricity. Table 4 shows the molecular structures of the most commonly encountered amorphous piezoelectric polymers.

**Poly(vinylidene chloride).** The carbon–chlorine dipole in poly(vinylidene chloride) (PVDC) has been oriented to produce a low level of piezoelectricity. The piezoelectric and pyroelectric activities generated in PVDC are stable and reproducible. PVDC has been used as a basis for understanding and studying piezoelectricity in amorphous polymers (39). The piezoelectric coefficients  $d_{31}$  of PVDC are reportedly in the range of 0.5–1.3 pC/N. This response was improved by simultaneous stretching and corona poling of film (44). The enhanced piezoelectric coefficient  $d_{31}$  ranged from 1.5–5.0 pC/N (see VINYLIDENE CHLORIDE POLYMERS (PVDC)).

**PVDCN Copolymers.** In 1980, exceptionally strong piezoelectric activity was found (50) in the amorphous copolymer of VDCN and VAc. The copolymer was poled at 150°C (20°C below its  $T_g$ ) and cooled to room temperature in the electric field. A  $P_r = 55$  mC/m<sup>2</sup> was obtained in a poling field of 50 MV/m. That is comparable to the  $P_r$  of PVDF. When local ordering, or paracrystallinity, is inherent in the polymer or is induced by mechanical stretching, an increase in the value of the remanent polarization is observed. For example, some researchers (51) assert that the large discrepancy between the measured and calculated  $\Delta\epsilon$  for PVDCN/VAc may be attributed to locally ordered regions in the polymer.  $\Delta\epsilon_{\text{calculated}} = 30$  for the copolymer PVDCN/VAc, and  $\Delta\epsilon_{\text{measured}} = 125$  (51). This large discrepancy in the values of  $\Delta\epsilon$  is indicative of cooperative motion of several nitrile dipoles within the locally ordered regions of the polymers. Cooperativity means that multiple nitrile dipoles respond to the applied electric field in a unified manner, instead of each dipole acting independently. Although the existence of cooperative dipole motion clearly increases the piezoelectric response of amorphous polymers, the mechanisms by which cooperativity can be systematically incorporated into the polymer structure remain unclear at this time (59).

The large relaxation strength exhibited by PVDCN/VAc gives it the largest value of  $P_r$  and hence  $d_{31}$  of all of the amorphous polymers. A number of authors have suggested that PVDCN/VAc also exhibits ferroelectric-like behavior (51–53) because of switching of the nitrile dipoles in an a.c. field. The switching time is long compared to that of a normal ferroelectric polymer.

**Table 4. Structure, Polarization, and  $T_g$  of Piezoelectric Amorphous Polymers**

Polymer	Structure	$T_g$ , °C	$d_{31}$ , pC/N	$P_r$ , mCm <sup>2</sup>	Reference
PVC		80	5	16	44
PAN		90	2	25	49
PVAc		30	—	5	59
P(VDCN/VAc)		170	10	50	51
PPEN		145	—	12	55
( $\beta$ -CN) APB/ODPA		220	5 at 150°C	20	59



**Other VDCN Polymers.** The homopolymer of vinylidene cyanide is thermally unstable (60) and highly sensitive to moisture, but VDCN can be polymerized with a variety of monomers in addition to VAc, such as vinyl benzoate (VBz), methyl methacrylate (MMA), and others that form highly alternating chains. All of these copolymers show some degree of piezoelectricity although lower than PVDCN/VAc, which is explained by different activation energies for dipole orientation in the glassy state and different chain mobility that depends on the side group.

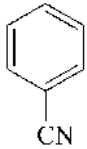
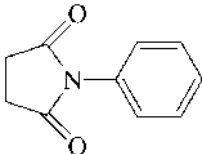
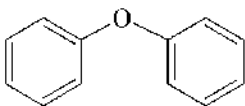
**Polyacrylonitrile.** Polyacrylonitrile (PAN) is one of the most widely used polymers (see ACRYLONITRILE POLYMERS). Shortly after it was shown that the PVDCN/VAc system is piezoelectric, researchers turned their attention to PAN because of its similarity to the aforementioned polymers. The presence of the large nitrile dipole in PAN indicated that it can be oriented by an applied electric field. PAN presented some challenges not encountered in other nitrile-substituted polymers, however. Although theoretical calculations predicted strong piezoelectric behavior, it was difficult to pole. Several investigators (47–49) proposed that the difficulty of poling PAN in the unstretched state is related to the strong dipole–dipole interaction of nitrile groups of the same molecule that repel each other, and thus prevent normal polarization. Upon stretching, the intermolecular dipole interactions facilitate packing of the individual chains and give rise to ordered zones. The remanent polarization of both unstretched and stretched PAN has been measured using the TSC method, and a twofold increase in remanent polarization (TSC peak at 90°C) was observed for PAN that was stretched to four times its original length (47). Another approach is the copolymerization of PAN with another monomer. Researchers have reported reduction of the hindering effect of the dipole–dipole interactions and enhancement of the internal mobility of the polymer segments when PAN is copolymerized with PA(polystyrene) or MMA. Ferroelectric behavior has been observed in P(AN–MMA), where, for given temperature and field conditions, a characteristic hysteretic loop is obtained (49). It was concluded that it may be one rare example where both ferroelectric and frozen-in dipole orientations are superimposed.

**Nitrile-Substituted Polyimide.** Amorphous Polymers that contain polar functional groups were synthesized (61–63) and investigated for use as high temperature piezoelectric sensors. ( $\beta$ -CN) APB/ODPA polyimide is one such system. The ( $\beta$ -CN) APB/ODPA polyimide possesses the three dipole functionalities shown in Table 5. Typically, the functional groups in amorphous polymers are pendent to the main chain. The dipoles, however, may also reside within the main chain of the polymer, such as the anhydride units in the ( $\beta$ -CN) APB/ODPA polyimide. The nitrile dipole is pendent to a phenyl ring ( $\mu = 4.2$  D), and the two anhydride dipoles ( $\mu = 2.34$  D) are within the chain, resulting in a total dipole moment of  $29.4 \times 10^{-30}$  C·m (8.8 D) per repeat unit.

The remanent polarization  $P_r$  of the ( $\beta$ -CN) APB/ODPA polymer found by the TSC method was approximately 20 mC/m<sup>2</sup> when poled at 80 MV/m above the  $T_g$  for 1 h (64). Excellent thermal stability was observed up to 100°C, and no loss of the piezoelectric response was seen after aging at 50°C and 100°C for as long as 500 h.

Partially cured films of the ( $\beta$ -CN) APB/ODPA system were simultaneously corona-poled and cured to enhance dipolar orientation and minimize localized

**Table 5. Values of Dipole Moments Within Nitrile-Substituted Polyimide**

Dipoles	Dipole identity	Dipole moment, C·m <sup>a</sup>
	Pendent nitrile group	$1.39 \times 10^{-29}$
	Main-chain dianhydride group	$7.8 \times 10^{-30}$
	Main-chain diphenyl ether group	$4.33 \times 10^{-30}$

<sup>a</sup>To convert C·m to Debye, multiply by  $2.997 \times 10^{29}$ .

arc during poling. The aligned polar groups should be immobilized by additional imidization and subsequent cooling in an electric field. Both the  $T_g$  and the degree of imidization increase almost linearly as the final cure temperature is increased (64). The value of  $P_r$  was higher for films cured at lower temperatures. The mobility of the molecules in a partially imidized state should be higher than that in the fully cured state and therefore produce a higher degree of dipole orientation.

The importance of dipole concentration in ultimate polarization is evident from a comparison of PAN and the ( $\beta$ -CN) APB/ODPA polyimide. PAN has a single nitrile dipole per repeat unit ( $\mu = 3.5$  D) resulting in a dipole concentration of  $1.34 \times 10^{28}/\text{m}^3$ . This translates into an ultimate polarization of  $152 \text{ mC}/\text{m}^2$  (20). The ( $\beta$ -CN) APB/ODPA polyimide, on the other hand, has a total dipole moment of 8.8 D per monomer. The dipole concentration of ( $\beta$ -CN) APB/ODPA, however, is only  $0.136 \times 10^{28}/\text{m}^3$ , resulting in an ultimate polarization of  $40 \text{ mC}/\text{m}^2$ , which is less than a fourth of that of PAN. As a result, similar polyimides that have increased nitrile concentrations were synthesized and characterized. Studies of these polymers show that polarization is significantly increased by increasing dipole concentration. Structure-property investigations designed to assess the effects of these dipoles on  $T_g$ , thermal stability, and overall polarization behavior are currently being pursued.

**Even-Numbered Nylons.** Nylon 6I and 6I/6T exhibit a *D-E* hysteretic loop across a temperature range of 30–65°C at a fixed maximum field of 168 MV/m (65). The remanent polarization increases as the temperature increases. Note that nylon 6I and 6I/6T are completely amorphous. The  $P_r$  is about  $30 \text{ mC}/\text{m}^2$  (see POLYAMIDES, AROMATIC).

**Aliphatic Polyurethane.** Some researchers (1) have suggested that aliphatic polyurethane systems exhibit ferroelectricity that stems from the amorphous part at temperatures above the glass-transition temperature. This “liquid

state” ferroelectricity is very peculiar, seems to exist, and is supported by the hydrogen bonds present.

## Characterization and Modeling

Most piezoelectric characterization methods were developed for crystalline ceramics and had to be adapted for piezoelectric polymers. Methods based on resonance analysis and equivalent circuits that can be used to characterize semicrystalline PVDF and its copolymers are outlined in IEEE standards (66). Details for applying resonance analysis to piezoelectric polymers have recently been explored (67). Because of the lossy nature of some polymers, the IEEE standards are not adequate, and other techniques are needed to describe piezoelectric properties more accurately.

Quasi-static direct methods are both versatile and well suited to investigating fully the piezoelectric response of polymers. Direct methods of this type are especially appropriate for amorphous polymers. TSC measurements (68) are used to measure the remanent polarization imparted to a polymer, and direct strain or charge measurements are used to investigate the piezoelectric coefficients with respect to the electric field, frequency, and stress.

TSC is a valuable tool for characterizing piezoelectric polymers. After poling a polymer, a measure of the current dissipation and the remanent polarization as a function temperature can be obtained by TSC. As the sample is heated through its glass-transition temperature (or Curie temperature for a semicrystalline polymer) at a slow rate (typically 1–4°C/min), the depolarization current is measured by an electrometer. The remanent polarization is equal to the charge per unit area and is obtained from the data by integrating the current with respect to time and plotting it as a function of temperature:

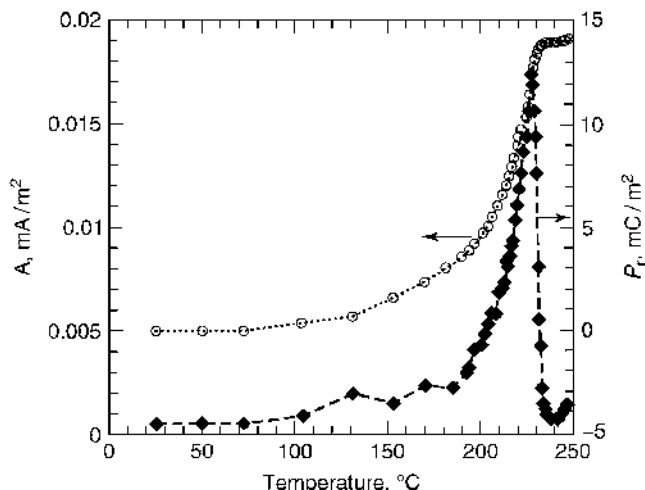
$$P_r = \frac{Q}{A} = \frac{1}{A} \int I(t) - dt. \quad (17)$$

Figure 6 illustrates a typical TSC result. Because permanent dipoles are immobile at temperatures well below  $T_g$ , the current discharge remains low in this temperature range. As temperature increases to and beyond the  $T_g$ , however, the onset of dipole mobility contributes to a significant increase in the current peak. The peak in the current and the subsequent polarization maximum usually occurs in the vicinity of the  $T_g$ .

Direct methods for measuring the strain that results from applying a field or vice versa, applying a strain, and measuring the accumulated charge are abundant. Interferometers, dilatometers, fiber-optic sensors, optical levers, linear variable displacement transducers, and optical methods are employed to evaluate the piezoelectric strain (converse effect) (69–72). The “out-of-plane” or thickness piezoelectric coefficient  $d_{33}$  can be ascertained as a function of the driving field and frequency. The coefficient is measured based on the equation

$$S_{33} = d_{33} E_3, \quad (18)$$

where  $S_{33}$  is the strain and  $E_3$  is the applied electric field.



**Fig. 6.** Plot of thermally stimulated current for a typical amorphous poled polymer.

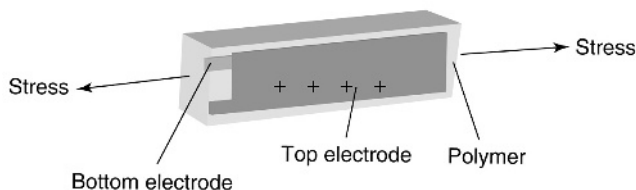


**Fig. 7.** Direct effect in polymers.

A modified Rheovibron, or similar techniques, have been used to measure the direct piezoelectric effect, where charges accumulated on the surfaces of the polymer are measured (59). The piezoelectric coefficient  $d_{31}$  can be obtained by straining the polymer in the direction of applied stress using a force  $F$  as depicted in Fig. 7. A charge  $Q$  is generated on the surface of the electrodes. A geometric factor is used to produce a geometrically independent parameter, surface charge density per unit applied stress:

$$d_{31} = \frac{Q/(WL)}{F/(Wt)}, \quad (19)$$

which has units of pC/N.  $W$ ,  $L$ , and  $t$  are the width, length, and thickness of the sample, respectively.

**Modeling.** The methodology for modeling piezoelectric behavior in polymers varies, depending on the targeted properties. Approaches cover the range from macroscale to micro and atomistic scales. A detailed review of computational methods applied to electroactive polymers has been published (73).

In some cases, modeling can predict behavior where experiments cannot. Using molecular dynamics, the orientation polarization of the ( $\beta$ -CN) APB/ODPA polymer was assessed by monitoring the angle  $\theta$  that the dipoles make with an

applied electric field (74). The bulk  $P_r$  was calculated, and the results agreed extremely well with experimental results (61). Computational modeling, however, gave insight into the contributions of the various dipoles present in a way experimental results could not. The model predicted that 40% of the orientation polarization was due to the dianhydride within the backbone of the ODPA monomer and demonstrated the importance of the flexible ether linkage (oxygen atom) in facilitating dipole alignment. Modeling insight of this kind is invaluable in guiding the synthesis of new materials.

Modeling of PVDCN/VAc can also play a role in understanding the cooperative motion responsible for the high dielectric relaxation strength of this class of polymers, not possible experimentally (75). Mesoscale simulation has been used to describe polarization reversal in PVDF films (76).

**Applications and Future Considerations.** The potential for applying piezoelectric and other electroactive polymers is immense. To date, ferroelectric polymers have been incorporated into numerous sensing and actuating devices for a wide array of applications. Typical applications include devices in medical instrumentation, robotics, optics, computers, and ultrasonic, underwater, and electroacoustic transducers. One important emerging application area for electroactive polymers is the biomedical field where polymers are being explored as artificial muscle actuators, as invasive medical robots for diagnostics and microsurgery, as actuator implants to stimulate tissue and bone growth, and as sensors to monitor vascular grafts and to prevent blockages (77,78). Such applications are ideal for polymers because they can be made biocompatible, and they have excellent conformability and impedance that match body fluids and human tissue. The intent of this article is not to detail specific applications; the interested reader may consult excellent sources on applications of piezoelectric and ferroelectric polymers (79–81).

In the future, we believe that fertile research areas for piezoelectric polymers will include work to enhance their properties, to improve their processibility for incorporation in devices, and to develop materials that have a broader use temperature range. Fundamental structure–property understanding has enabled the development of numerous semicrystalline and amorphous polymers. Based on this knowledge, future research that focuses on property enhancement via new chemistries that have higher dipole concentrations and incorporate dipole cooperativity may yield improved materials. Property enhancements may also be gained from processing studies to alter polymer morphology such as those used to make “single crystalline” fluoropolymers. Development of materials that can operate in extreme environments (high temperature and subambient temperature) is also important for expanding the use of piezoelectric polymers. Piezoelectric and pyroelectric constants of polymers are considerably lower than those of ferroelectric inorganic ceramics. Improvements in properties by incorporating polymers in composites with inorganics to obtain higher electromechanical properties and better mechanical properties are also valuable. To date, piezoelectric polymer–ceramic composites have been made wherein the polymer serves only as an inactive matrix for the active ceramic phase. This is due to the mismatch in permittivity between the polymer and ceramic which makes it difficult to pole both phases. Research that results in active polymer and ceramic phases could yield interesting electromechanical properties.

**BIBLIOGRAPHY**

"Piezoelectric Polymers" in *EPST* 3rd ed., Vol. 3, pp. 474–498, by J. S. Harrison, NASA Langley Research Center and Z. Ounaies, Virginia Commonwealth University.

**CITED REFERENCES**

1. T. Yuki, K. Shida, T. Koda, and S. Ikeda, *10th Int. Symp. Electrets*, 1999, pp. 675–677.
2. G. T. Davis, in C. P. Wong, ed., *Polymers for Electronic and Photonic Applications*, Academic Press, Boston, Mass., 1993, p. 435.
3. M. G. Broadhurst and G. T. Davis, in G. M. Sessler, ed., *Electrets*, Vol. **33**, Springer-Verlag, New York, 1980, p. 283.
4. W. P. Mason, *Physical Acoustics and the Properties of Solids*, Van Nostrand, Princeton, N.J., 1958.
5. J. F. Nye, *Physical Properties of Crystals*, Clarendon Press, Oxford, 1957.
6. R. G. Kepler and R. A. Anderson, *J. Appl. Phys.* **49**, 1232–1235 (1978).
7. J. P. Luongo, *J. Polym. Sci. A-2* **10**, 1119–1123 (1972).
8. B. Z. Mei, J. I. Schienbeim, and B. A. Newman, *Ferroelectrics* **144**, 51–60 (1993).
9. H. Kawai, *Jpn. J. Appl. Phys.* **8**, 975 (1969).
10. K. Tashiro, H. Tadokoro, and M. Kobayashi, *Ferroelectrics* **32**, 167 (1981).
11. T. Furukawa, *IEEE Trans. Electr. Insul.* **24**, 375–393 (1989).
12. G. M. Sessler, *J. Acoust. Soc. Am.* **70**, 1596–1608 (1981).
13. A. J. Lovinger, *Science* **220**, 1115–1121 (1983).
14. J. B. Lando and W. W. Doll, *J. Macromol. Sci.-Phys. B2* 205 (1968).
15. A. J. Lovinger, in D. C. Bassett, ed., *Developments in Crystalline Polymers*, Vol. **1**, Applied Science, London, 1982, p. 242.
16. G. T. Davis and co-workers, *J. Appl. Phys.* **49**, 4998 (1978).
17. K. Omote, H. Ohigashi, and K. Koga, *J. Appl. Phys.* **81**, 2760 (1997).
18. Q. M. Zhang, V. Bharti, and X. Zhao, *Science* **280**, 2101–2104 (1998).
19. H. Kawai and I. Henji, *Oyo Buturi* **39**, 413 (1970).
20. B. A. Newman and co-workers, *J. Appl. Phys.* **51**, 5161–5164 (1980).
21. B. A. Newman, K. G. Kim, and J. I. Scheinbeim, *J. Mater. Sci.* **25**, 1779–1783 (1990).
22. Y. Takase and co-workers, *Macromolecules* **24**, 6644–6652 (1991).
23. R. B. Meyer and co-workers, *J. Phys. Lett. (Paris)* **36**, 69 (1975).
24. P. Le Barny and J. C. Dubois, in C. B. McArdle, ed., *Side Chain Liquid Crystal Polymers*, Blackie, New York, 1989, p. 130.
25. G. Scherowsky, in H. S. Nalwa, ed., *Ferroelectric Polymers, Chemistry, Physics and Application*, Marcel Dekker, New York, 1995, p. 435.
26. Y. Takahashi and co-workers, *J. Vac. Sci. Technol. A* **5**, 2253 (1987).
27. Y. Takahashi, M. Iijima, and E. Fukada, *Jpn. J. Appl. Phys.* **28**, L408–L410 (1989).
28. T. Hattori and co-workers, *J. Appl. Phys.* **79**, 1713–1721 (1996).
29. E. Fukada, *IEEE Trans. Ultrasonics Ferroelectrics Frequency Control* **47**, 1277–1290 (2000).
30. A. J. P. Martin, *Proc. Phys. Soc.* **53**, 183 (1941).
31. E. Fukada, in Ref. 25, p. 393.
32. H. Maeda and E. Fukada, *Biopolymers* **21**, 2055 (1982).
33. M. Date, S. Takashita, and E. Fukada, *J. Polym. Sci. A-2* (8), 61 (1970).
34. T. Furukawa and E. Fukada, *J. Polym. Sci., Polym. Phys. Ed.* **14**, 1979 (1976).
35. Y. Ando and E. Fukada, *J. Polym. Sci., Polym. Phys. Ed.* **14**, 63 (1976).
36. E. Fukada, *Rep. Prog. Polym. Phys. Jpn.* **34**, 269 (1991).

37. Y. Ando, E. Fukada, and M. J. Glimcher, *Biorheology* **14**, 175 (1977).
38. E. Fukada, in R. O. Becker, ed., *Mechanisms of Growth Control*, Charles C. Thomas, Springfield, Ill., 1981, p. 192.
39. M. G. Broadhurst, C. G. Malmberg, F. I. Mopsik, and W. P. Harris, in M. M. Perlman, ed., *Electrets: Charge Storage and Transport in Dielectrics*, The Electrochemical Society, Princeton, N.J., 1973, pp. 492–504.
40. M. G. Broadhurst and co-workers, *Polym. Prepr.* **14**, 820 (1973).
41. F. I. Mopsik and M. G. Broadhurst, *J. Appl. Phys.* **46**, 4204–4208 (1975).
42. B. Hilezer and J. Malecki, in *Electrets* (Studies in Electrical and Electronic Engineering, Vol. 14). Elsevier, New York, 1986, p. 19.
43. H. Frohlick, *Theory of Dielectrics (Monographs on the Physics and Chemistry of Materials, No. 42)*, Oxford, U.K., 1958, p. 15.
44. V. Bharti, T. Kaura, and R. Nath, *IEEE Trans. Dielectr. Electr. Insul.* **2**(6) (1995).
45. H. Stefanou, *J. Appl. Phys.* **50**, 1486–1490 (1979).
46. R. Meyrueix and O. Lemonnier, *Phys. D Appl. Phys.* **27**, 379–386 (1994).
47. R. J. Comstock, S. I. Stupp, and S. H. Carr, *J. Macromol. Sci. Phys.* **3** **13**(1), 101–115 (1977).
48. H. Ueda and S. H. Carr, *Polym. J.* **16**, 661–667 (1984).
49. H. von Berlepsch and co-workers, *IEEE Trans. Electr. Insul.* **24**, 357–362 (1989).
50. S. Miyata and co-workers, *Polym. J.* **12**, 857–860 (1980).
51. T. Furukawa and co-workers, *Jpn. J. Appl. Phys.* **25**, 1178–1182 (1986).
52. I. Seo, *Ferroelectrics* **171**, 45–55 (1995).
53. P. A. Mirau and S. A. Heffner, *Polymer* **33**, 1156–1161 (1992).
54. M. Sakurai and co-workers, *Polym. Commun.* **32**, 397–399 (1991).
55. S. Tasaka, T. Toyama, and N. Inagaki, *Jpn. J. Appl. Phys.* **33**, 5838–5844 (1994).
56. T. Takahashi and co-workers, *Polymer* **36**, 3803–3808 (1995).
57. H. K. Hall and co-workers, *Polym. Bull.* **17**, 135–136 (1987).
58. V. Bharti and R. Nath, *J. Appl. Phys.* **82**, 3488–3492 (1997).
59. Z. Ounaies, J. A. Young, and J. S. Harrison, in I. M. Khan and J. S. Harrison, eds., *An Overview of the Piezoelectric Phenomenon in Amorphous Polymers*, American Chemical Society, Washington, D.C., 1999.
60. S. Tasaka and co-workers, *Polymer* **30**, 1639–1642 (1989).
61. Z. Ounaies, J. A. Young, J. O. Simpson, and B. L. Farmer, *Mater. Res. Soc. Proc.: Mater. Smart Syst. II*, Vol. 459, Materials Research Society, Pittsburgh, Pa., 1997, p. 59.
62. J. O. Simpson, Z. Ounaies, and C. Fay, *Mater. Res. Soc. Proc.: Mater. Smart Syst. II*, Vol. 459, Materials Research Society, Pittsburgh, Pa., 1997, p. 53.
63. Z. Ounaies, C. Park, J. S. Harrison, J. G. Smith, and J. Hinkley, *SPIE Proc., Electroactive Polym. Actuators Devices*, Vol. 3669, Newport Beach, Calif., 1999, p. 171.
64. C. Park, Z. Ounaies, J. Su, J. G. Smith Jr., and J. S. Harrison, *Mater. Res. Soc. Proc.: Electroactive Polym.*, Vol. 600, 1999.
65. Y. Murata, K. Tsunashima, and N. Koizumi, *8th Int. Symp. Electrets (ISE 8)*, 1994, pp. 709–714.
66. IEEE Standard on Piezoelectricity (IEEE Standard 176-1987), Institute of Electrical and Electronic Engineers, New York, 1989.
67. S. Sherritt and Y. Bar-Cohen, in Y. Bar-Cohen, ed., *Electroactive Polymer (EAP) Actuators as Artificial Muscles: Reality, Potential and Challenges*, SPIE Press, Bellingham, Wash., 2001, p. 405.
68. J. van Turnhout, *Polym. J.* **2**, 173–191 (1971).
69. J. T. Dawley, G. Teowee, B. J. J. Zelinski, and D. R. Uhlmann, *Piezoelectric Characterization of Bulk and Thin Film Ferroelectric Materials Using Fiber Optics*, MTI Instruments Inc., Application Note.
70. W. Y. Pan, H. Wang, and L. E. Cross, *Jpn. J. Appl. Phys.* **29**, 1570 (1990).

71. Q. M. Zhang, W. Y. Pan, and L. E. Cross, *J. Appl. Phys.* **63**, 2429 (1988).
72. T. L. Jordan, Z. Ounaies, and T. L. Turner, *Mater. Res. Soc. Symp. Proc.* **459**, 231 (1997).
73. K. E. Wise, in Ref. 67, pp. 267–284.
74. J. A. Young, B. L. Farmer, and J. A. Hinkley, *Polymer* **40**, 2787 (1999).
75. K. E. Wise, *3rd SIAM Conf. Math. Aspects Mater. Sci.*, Philadelphia, Pa., May 21–24, 2000.
76. T. Koda, K. Shibasaki, and S. Ikeda, *Comp. Theor. Polym. Sci.* **10**, 335–343 (2000).
77. Y. Bar-Cohen, in Ref. 67, p. 615.
78. D. DeRossi and P. Dario, in P. M. Galletti, D. E. DeRossi, and A. S. DeReggi, eds., *Medical Applications of Piezoelectric Polymers*, Gordon & Breach, New York, 1988, p. 83.
79. G. M. Garner, in T. Wang, J. Herbert, and A. Glass, eds., *The Applications of Ferroelectric Polymers*, Blackie, London, 1988, p. 190.
80. T. R. Meeker, in Ref. 79, p. 305.
81. E. Yamaka, in Ref. 79, p. 329.

J. S. HARRISON  
NASA Langley Research Center  
Z. OUNAIES  
Virginia Commonwealth University